Advanced Imaging for Physicists

Introduction

Uulke van der Heide

Radiotherapy before image guidance

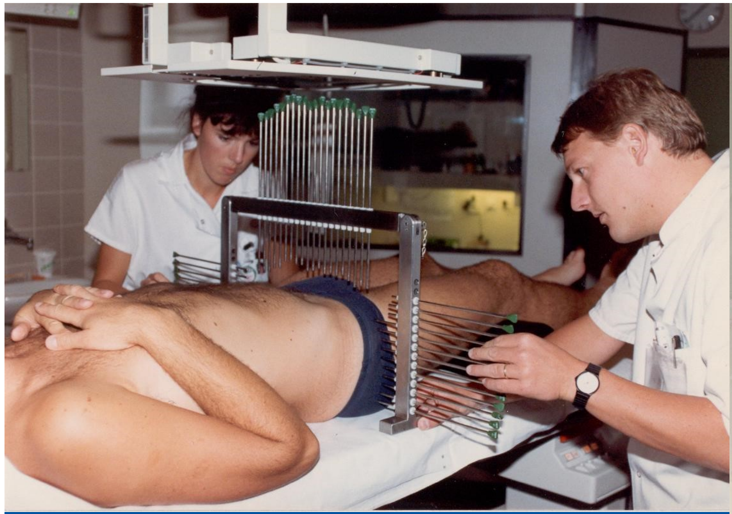

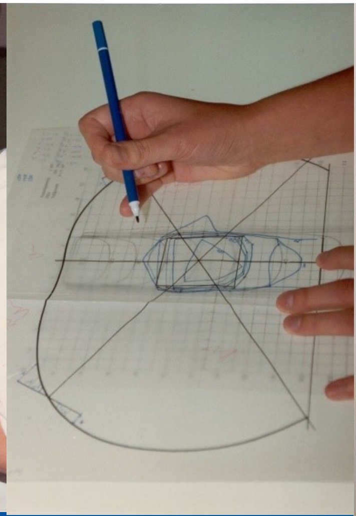

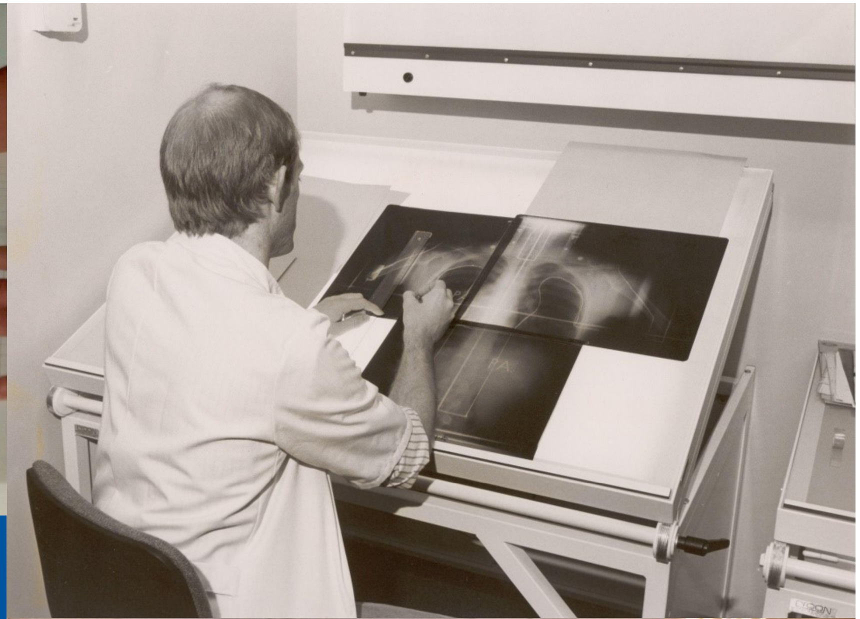

- Radiotherapy was essentially not image based
- Delineation on 2D X-rays

Radiotherapy before image guidance

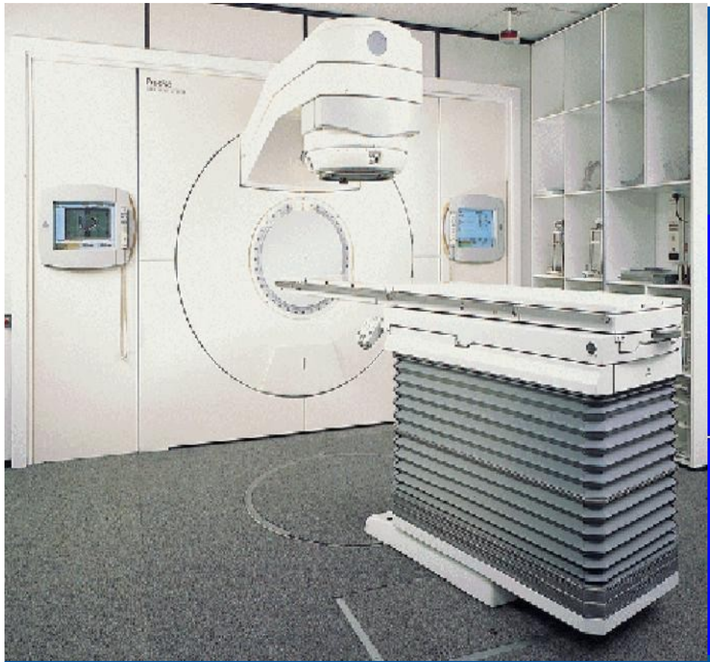

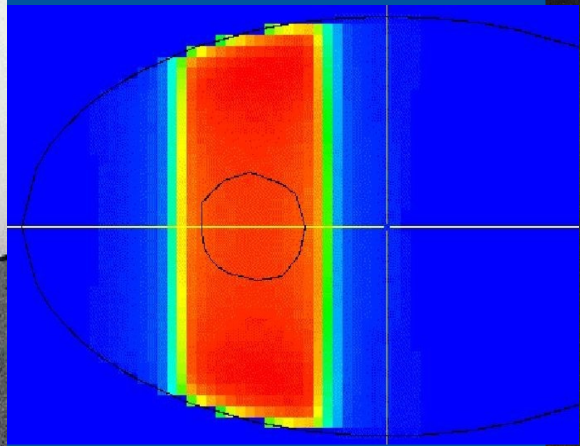

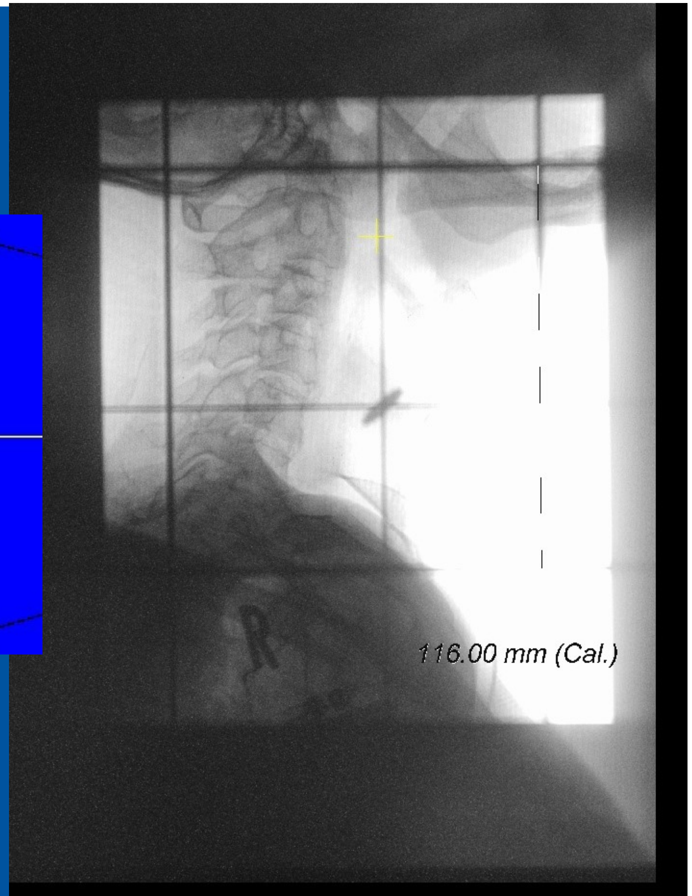

Classical paradigm in radiotherapy

- Treat a large volume of normal tissue with a tumour somewhere inside
- Dose is limited by normal tissue tolerance

A revolution in radiotherapy

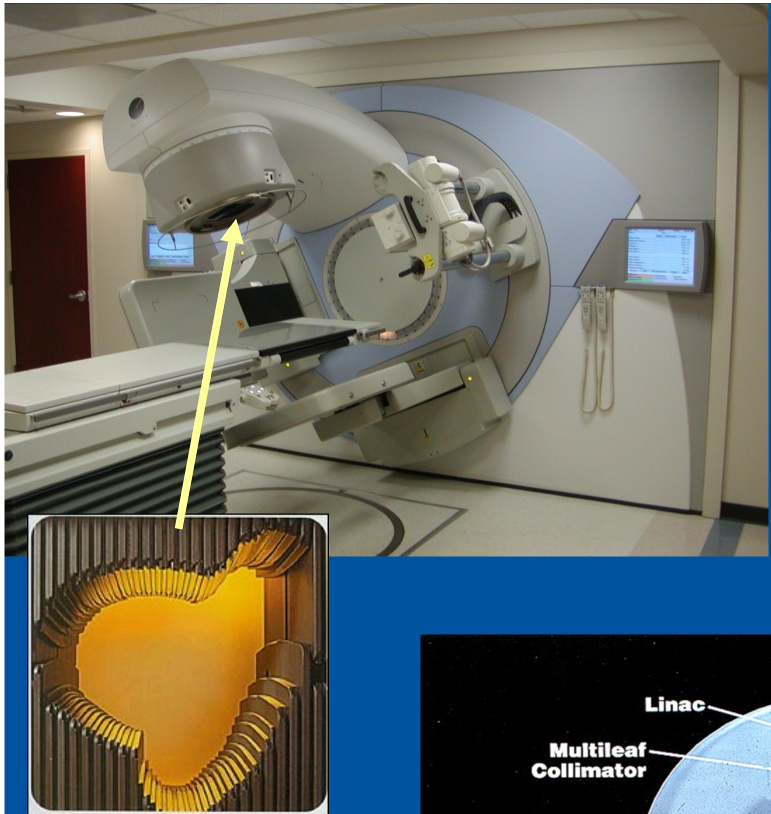

Linac with MLC

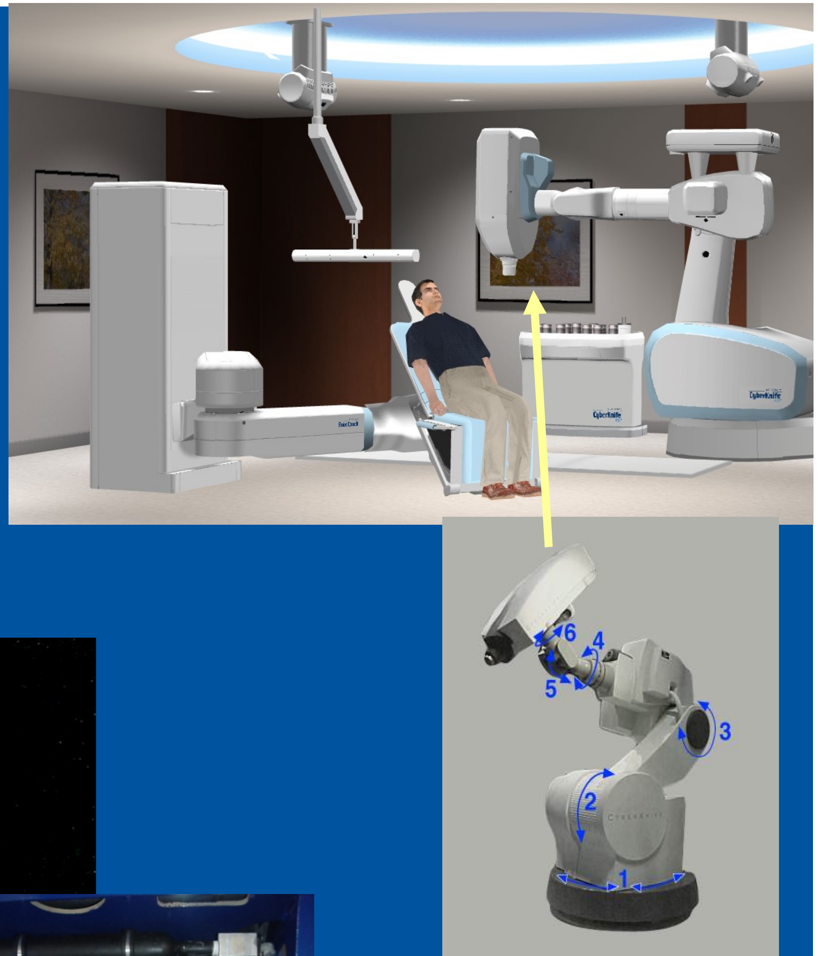

Cyberknife

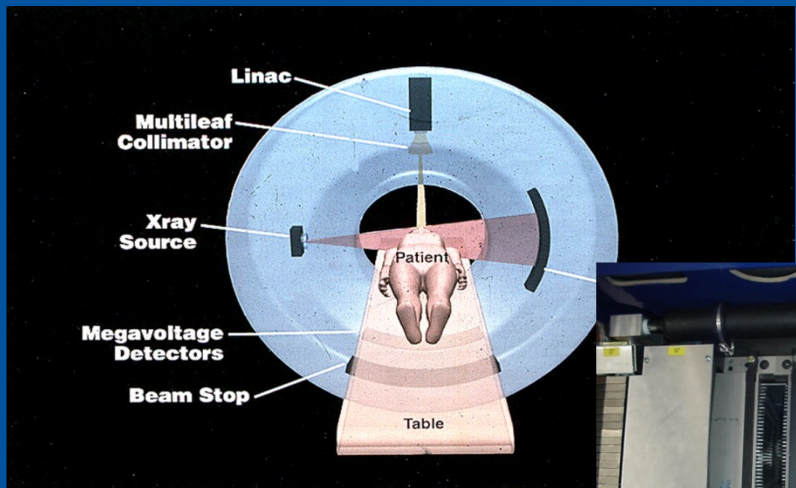

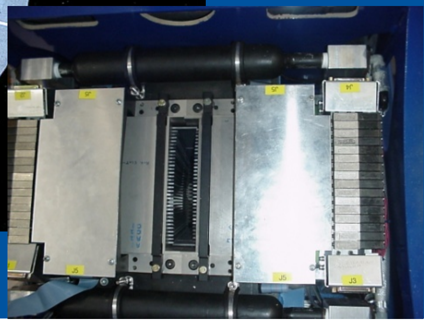

Tomotherapy

Imaging in the treatment room

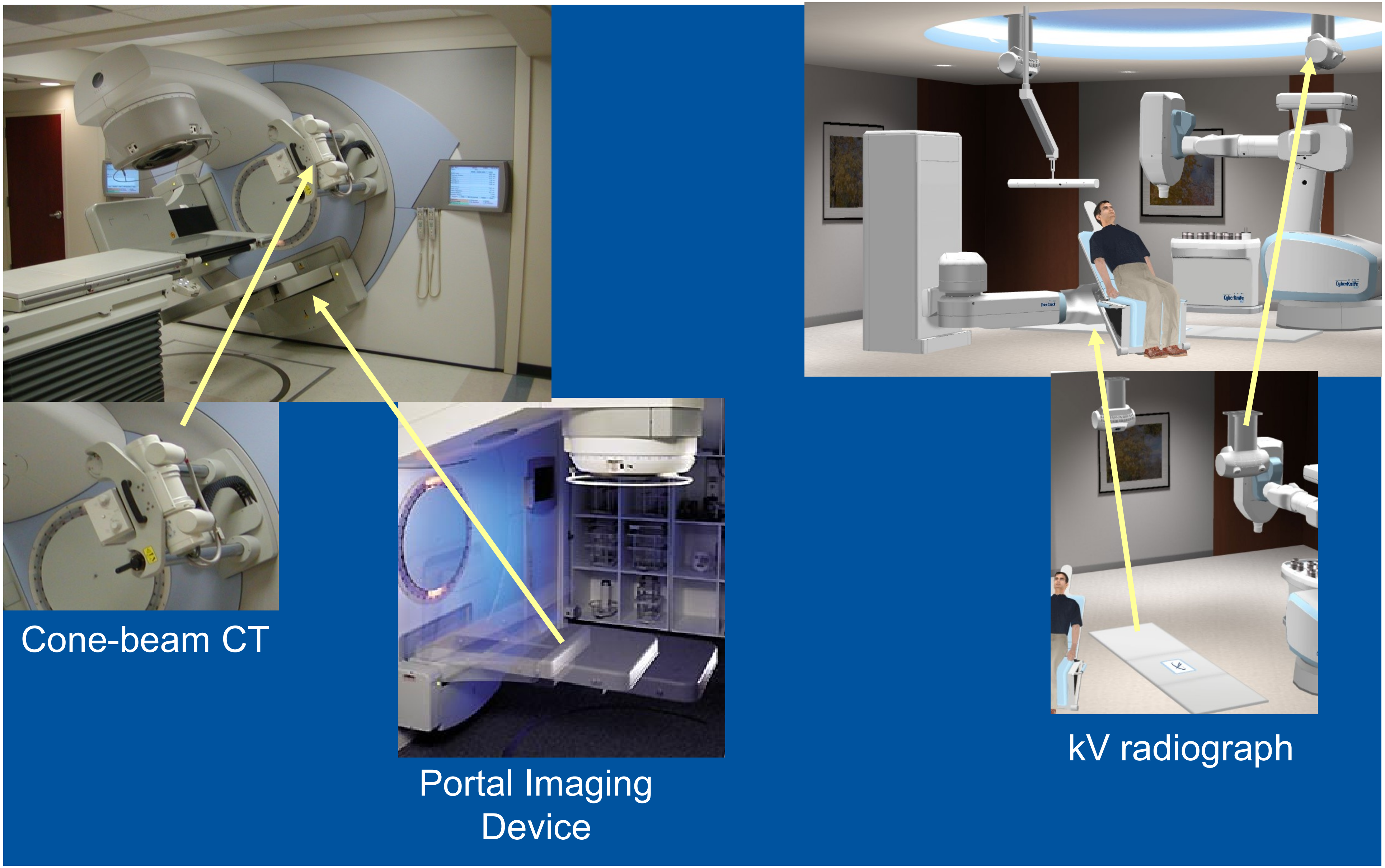

Radiotherapy in the era of advanced delivery techniques and image guidance

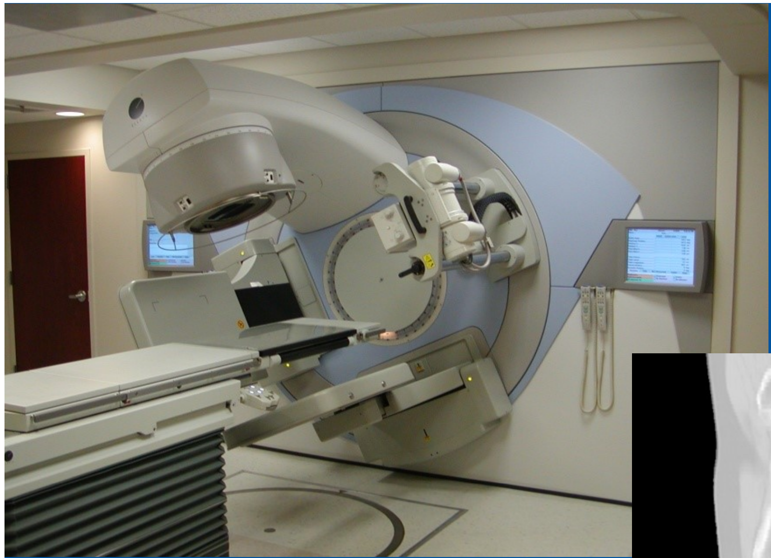

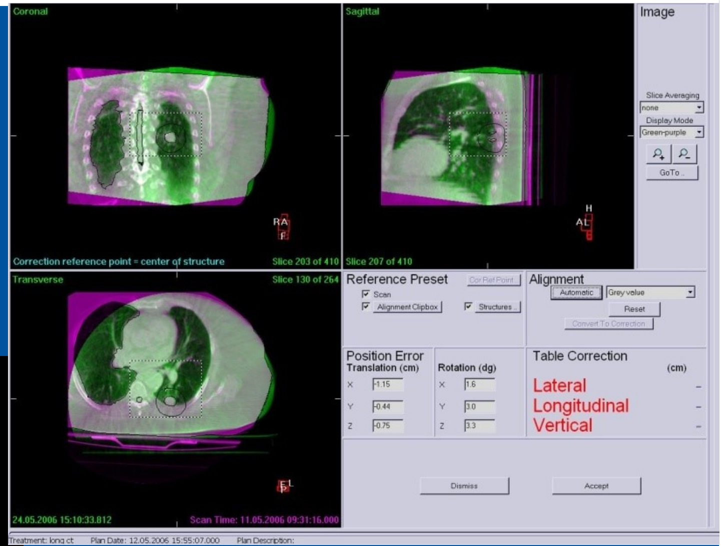

New paradigm in radiotherapy

- Extremely conformal treatment of the tumor
- Dose is determined by characteristics of the tumor

Target is defined on a planning CT scan

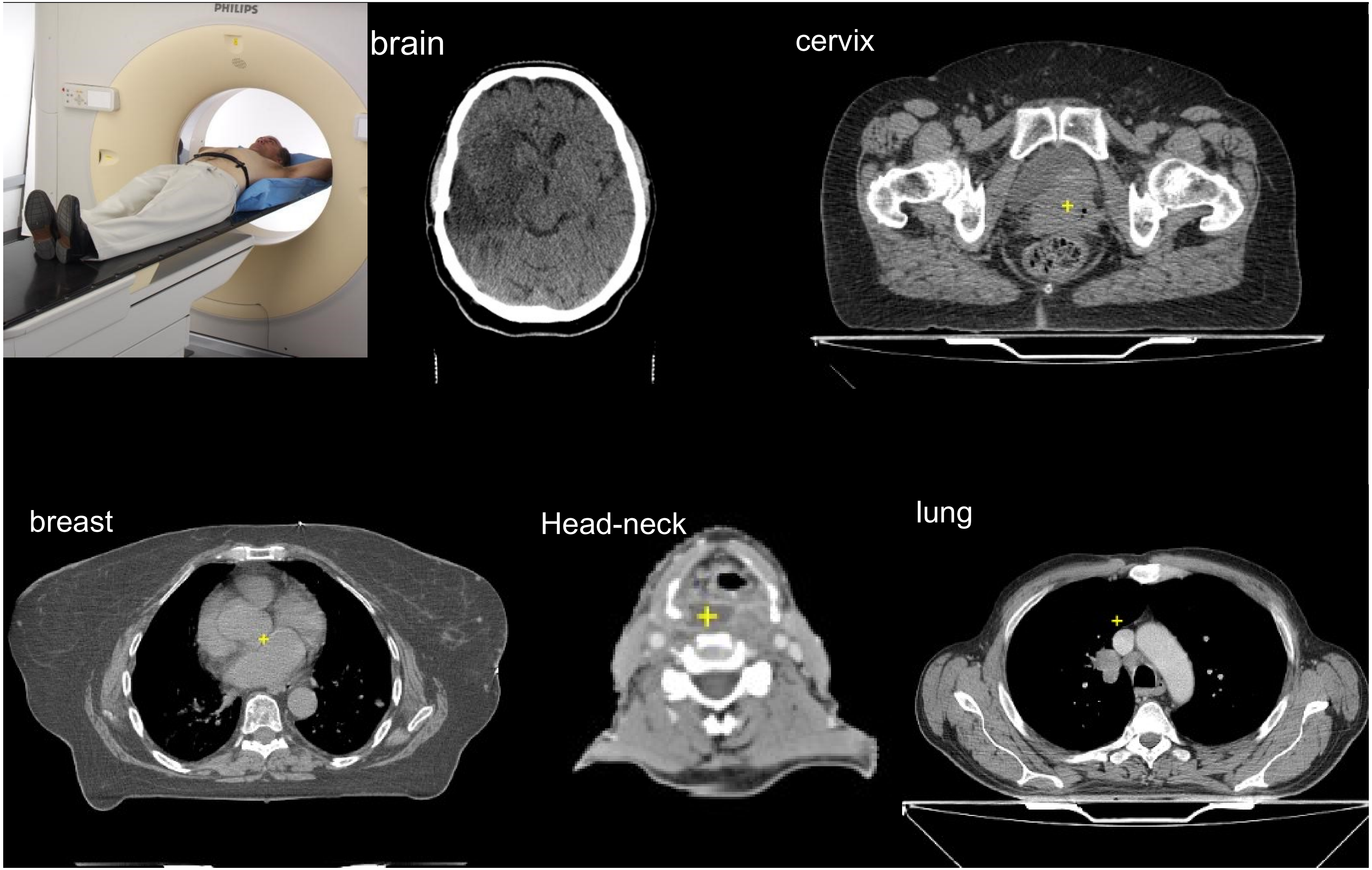

Imaging for radiotherapy

- Imaging for radiotherapy is primarilly CT-based
- CT scanners specifically developed for radiotherapy treatment planning
  - Big bore CT scanners
  - Flat table tops
  - Laser systems
- Cone-beam CT for imaging in the treatment room
  - kV and MV
- Hybrid devices combining imaging and treatment
  - tomotherapy

Inter-observer variations in delineation due to limited soft-tissue contrast

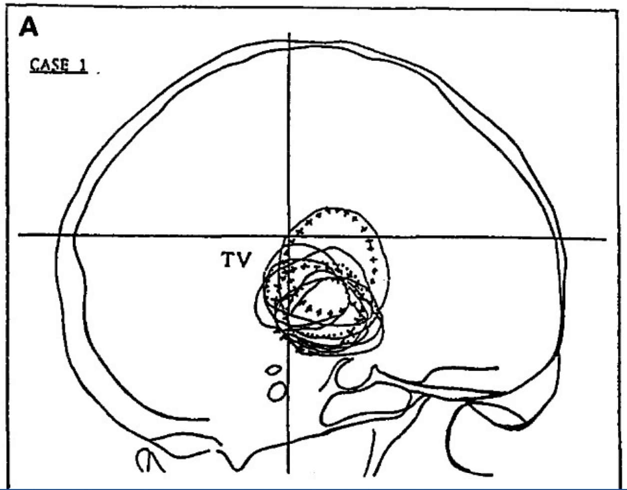

Leunens et al. 1993; Radiother. Oncol. 29:169-175

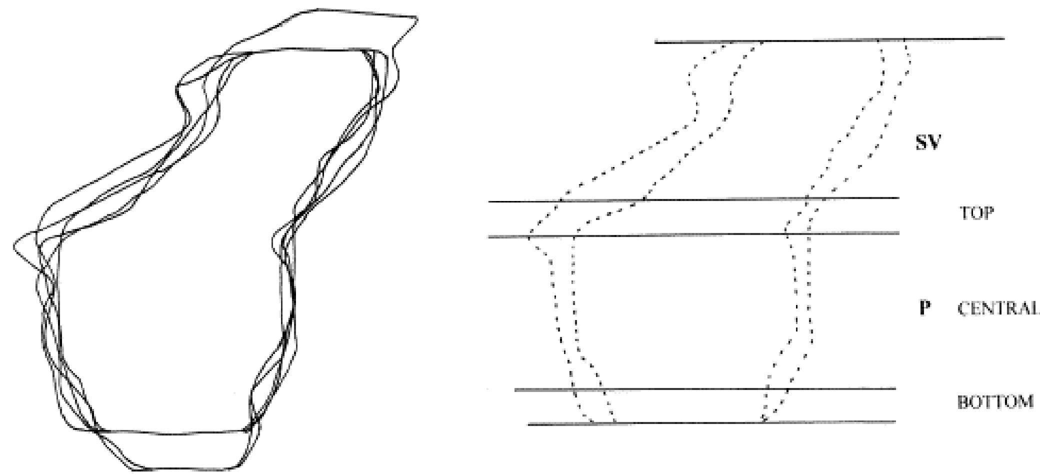

Fiorino et al. 1998; Radiother. Oncol. 47:285-292

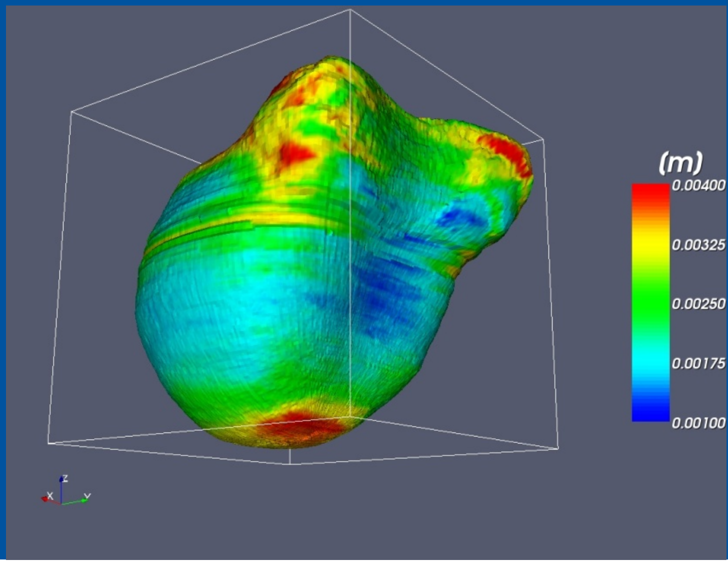

UMC Utrecht data:
5 observers delineate prostate on CT; standard deviations of up to 4 mm

Soft-tissue contrast of cone-beam CT limits registration accuracy

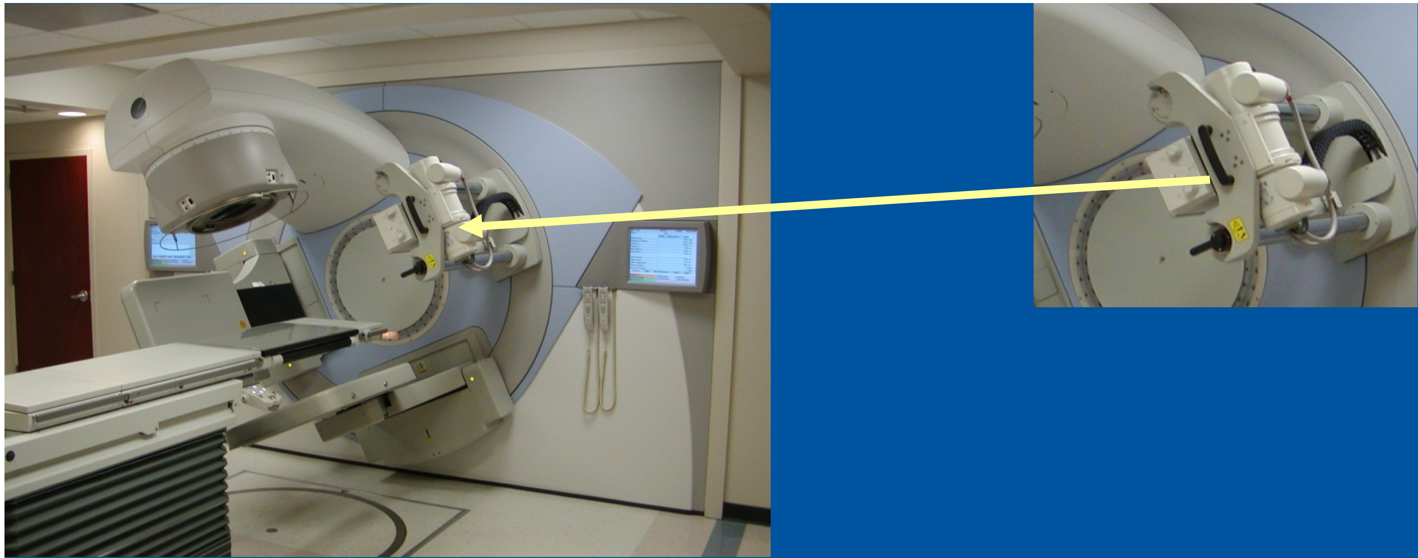

Cone-beam CT

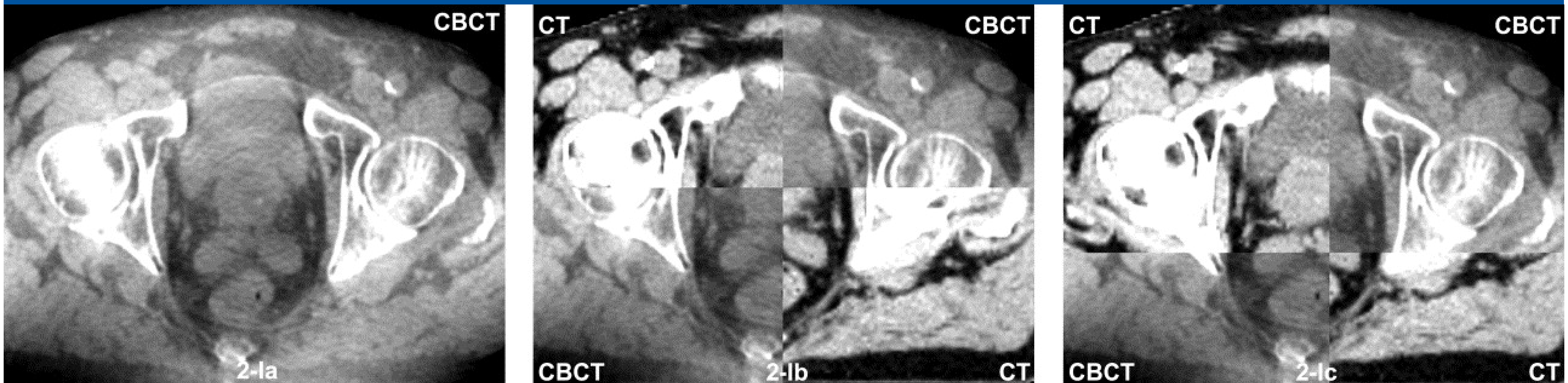

Smitsmans et al. 2005; Int J Radiat Oncol Biol Phys. 63:975-984

MRI has superior soft tissue contrast

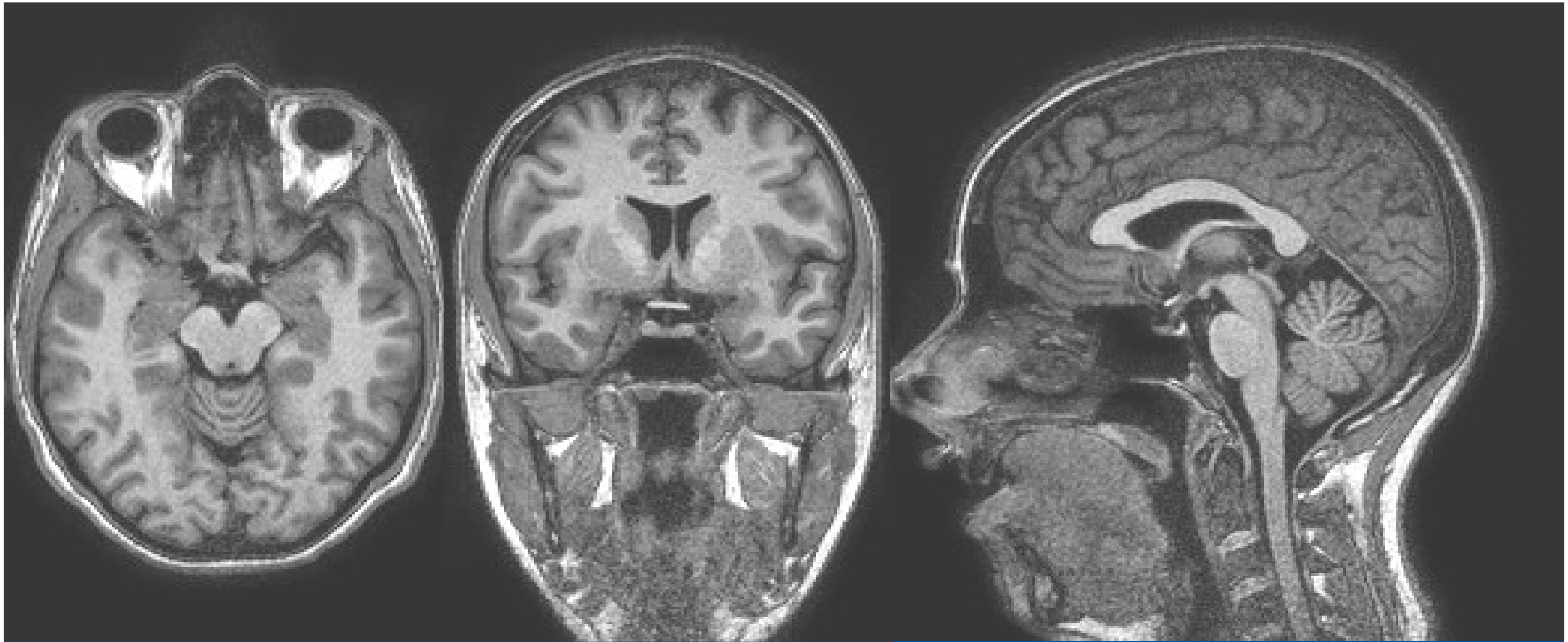

T1 3D-TFE sequence of healthy volunteer

A wide variety of contrasts

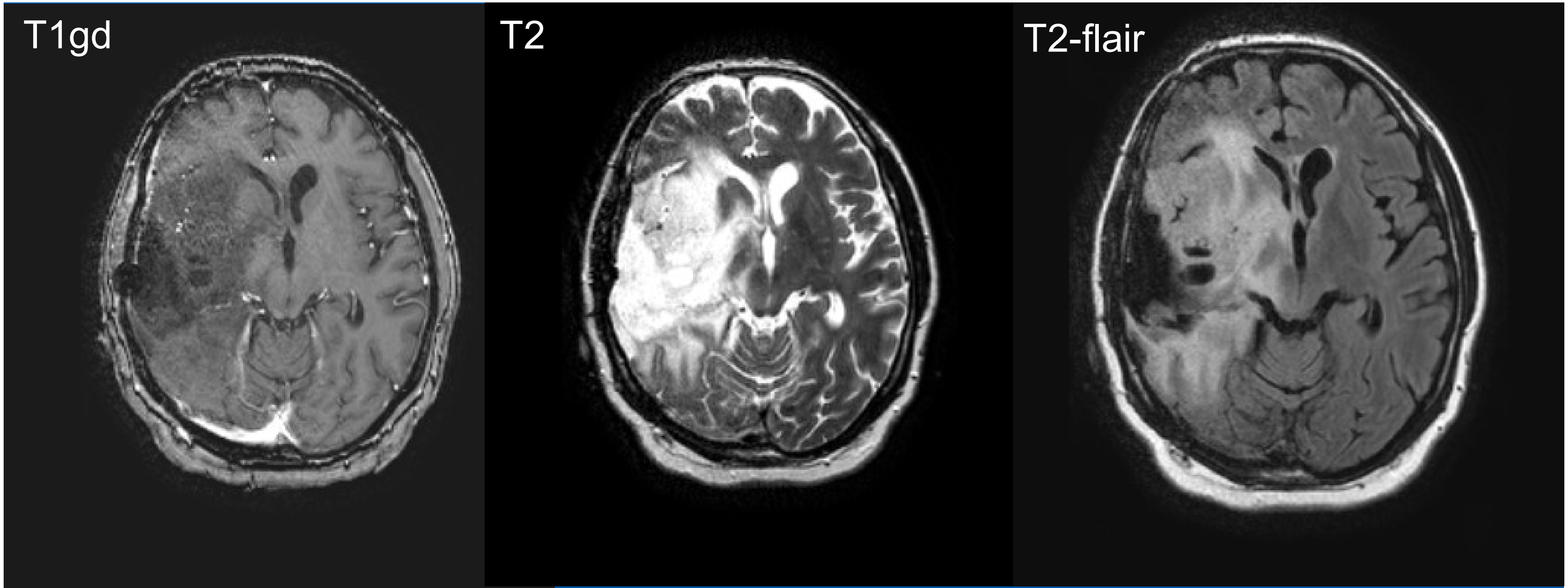

patient with glioblastoma multiforme

Imaging of function with MRI and PET

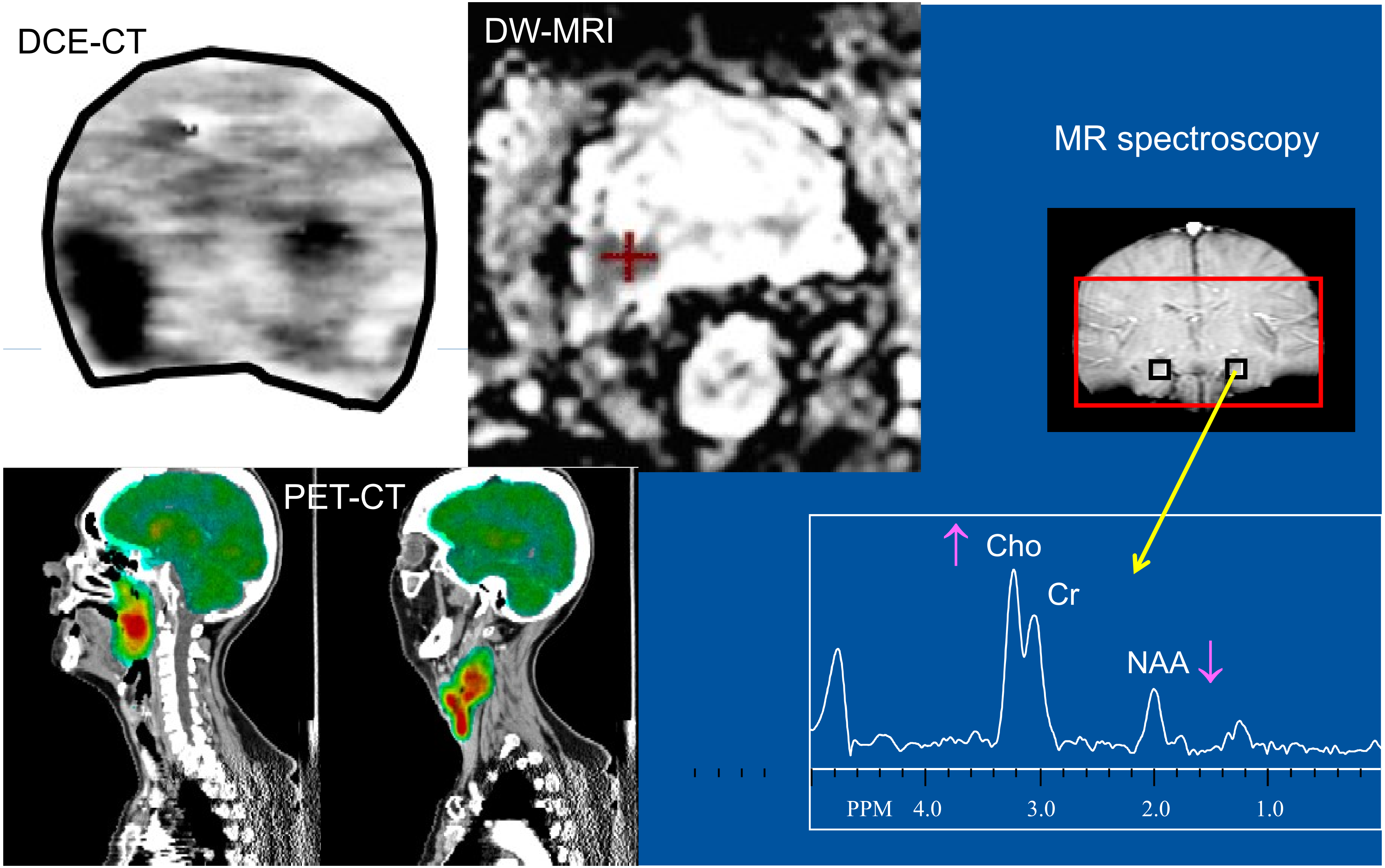

Outline

- What can we do with imaging in radiotherapy?
- Why should medical physicists in radiotherapy worry about imaging technology?

- Structure of the course

The potential of advanced imaging for radiotherapy

- Target definition
- Tissue characterization
- Image guidance
- Treatment monitoring

Impact of MRI on target definition

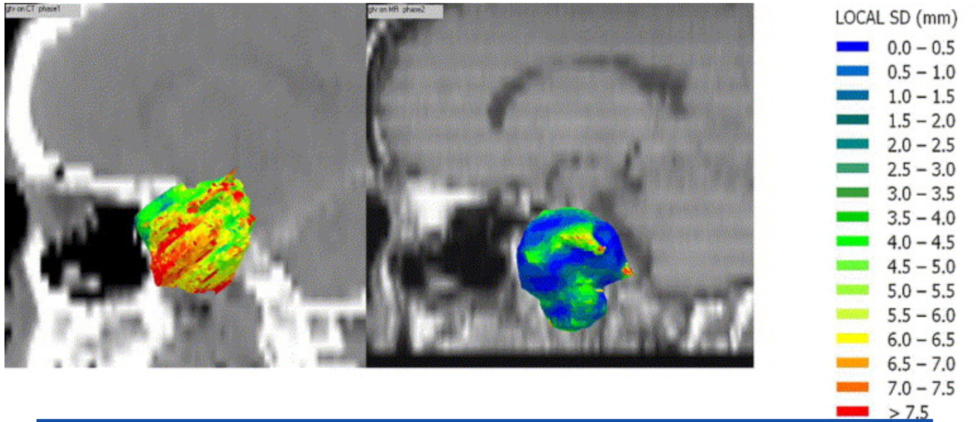

Inter-observer variation

Delineation of nasopharynx tumor
Left: CT, with MRI available, not fused
Right: CT, with fused MRI

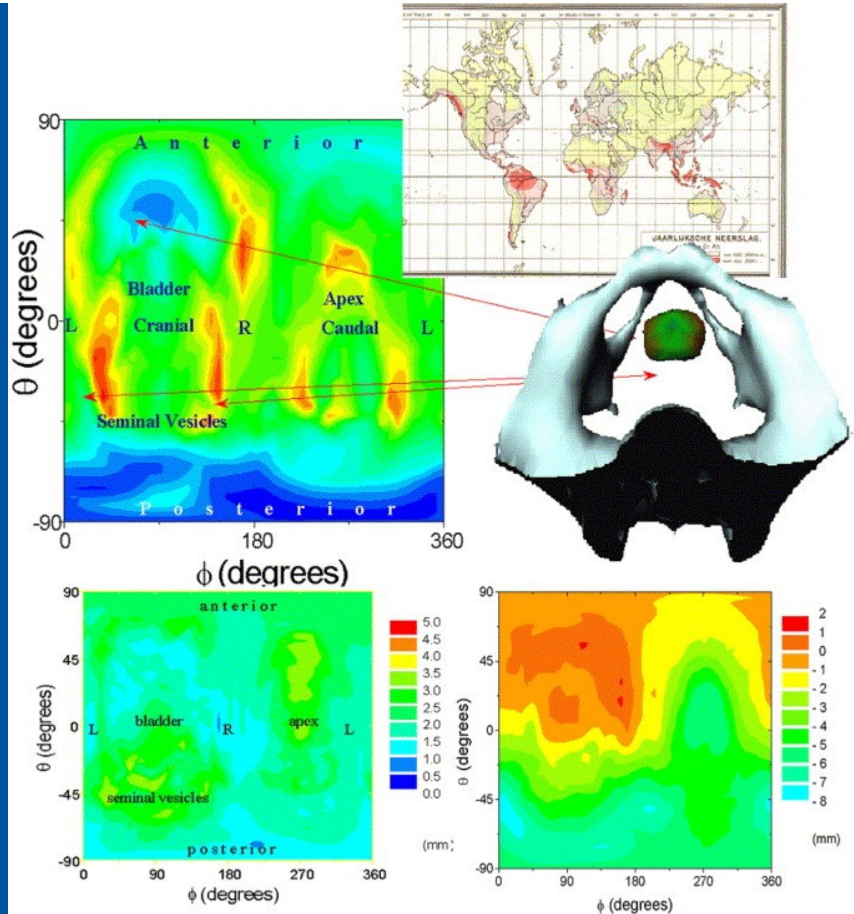

Significant differences in delineation of prostate on CT and MRI

Rasch et al. 2005; Semin. Radiat. Oncol. 15:136-145

Impact of MRI on target definition

Direction	Scalar difference (mm)		Vector difference (mm)	
	Mean ± 1SD	Range	Mean ± 1SD	Range
Left	6.0 ± 7.0	0.6–29.7	3.3 ± 8.5	(−)9.1–29.7
Right	3.3 ± 2.5	0.7–13.1	(−)0.3 ± 3.8	(−)13.1–10.3
Anterior	4.9 ± 3.9	0.6–19.8	1.1 ± 5.8	(−)11.2–19.8
Posterior	4.5 ± 5.0	0.5–24.6	1.5 ± 6.4	(−)10.4–24.6

(−) indicates the extent of the MR outline is less than that of the CT outline.

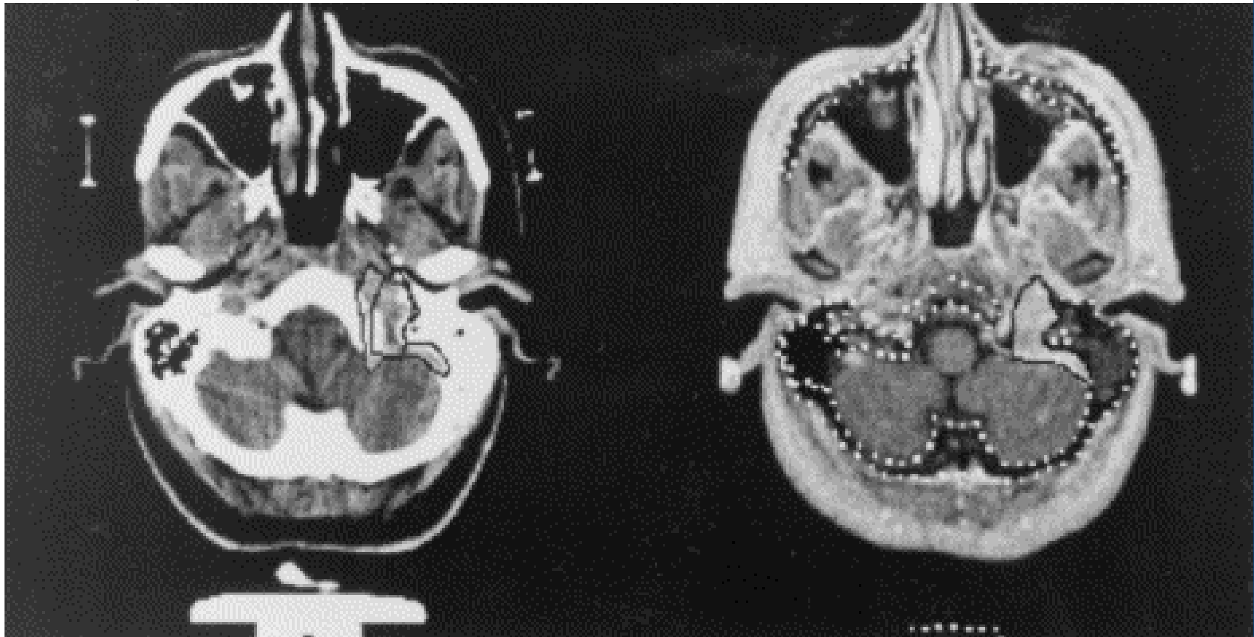

CT MRI

Comparison of delineation of meningioma on CT and MRI

Improved visualization of tumor in bone leads to larger volumes on MRI

Khoo et al. 2000; Int. J. Radiat. Oncol. Biol. Phys. 46:1309-1317

FDG-PET for tumor delineation

- FDG-PET provides a more reliable GTV than CT in laryngeal tumors

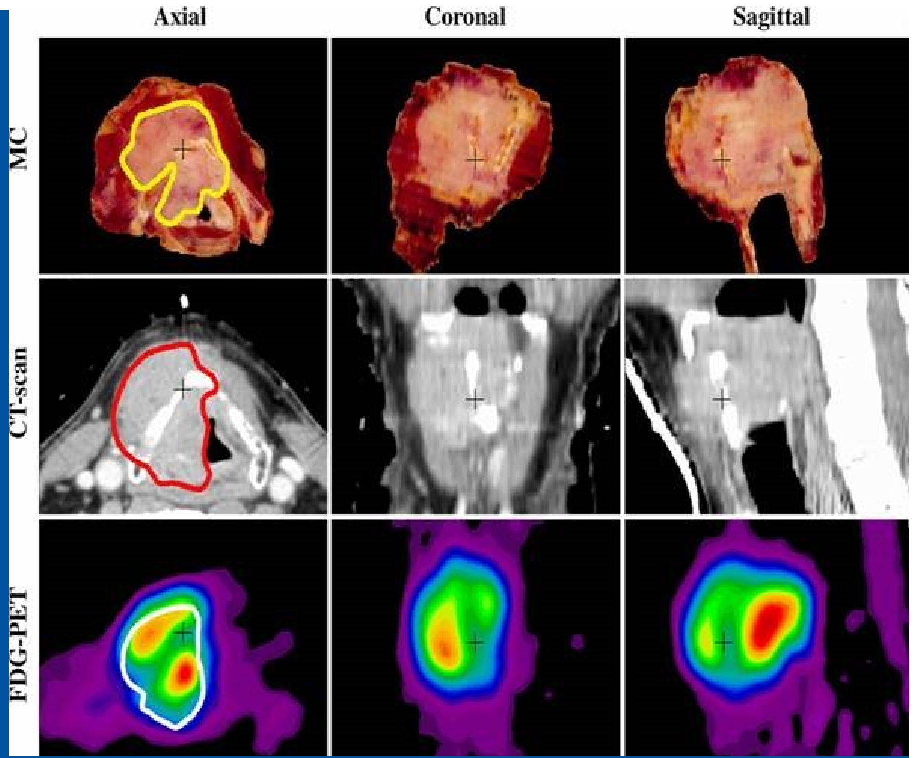

Baardwijk et al. 2007; Int J Radiat Oncol Biol Phys. 68:771-778

Daisne et al. 2004; Radiol. 233:93-100

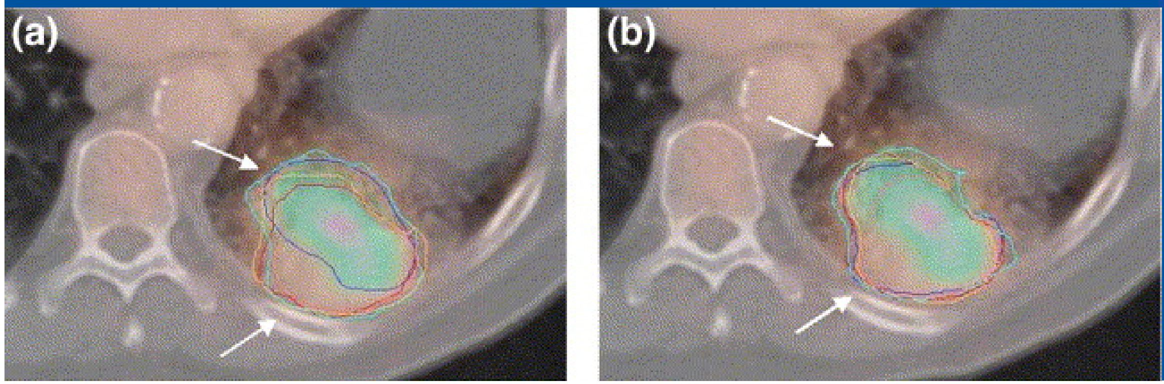

The potential of advanced imaging for radiotherapy

- Target definition
- Tissue characterization
- Image guidance
- Treatment monitoring

Tissue characterization

- improved visualization of anatomy and pathology allows better targeting of the tumor
- visualization of biological function may help defining the right dose for the tumor

- What properties can be imaged?

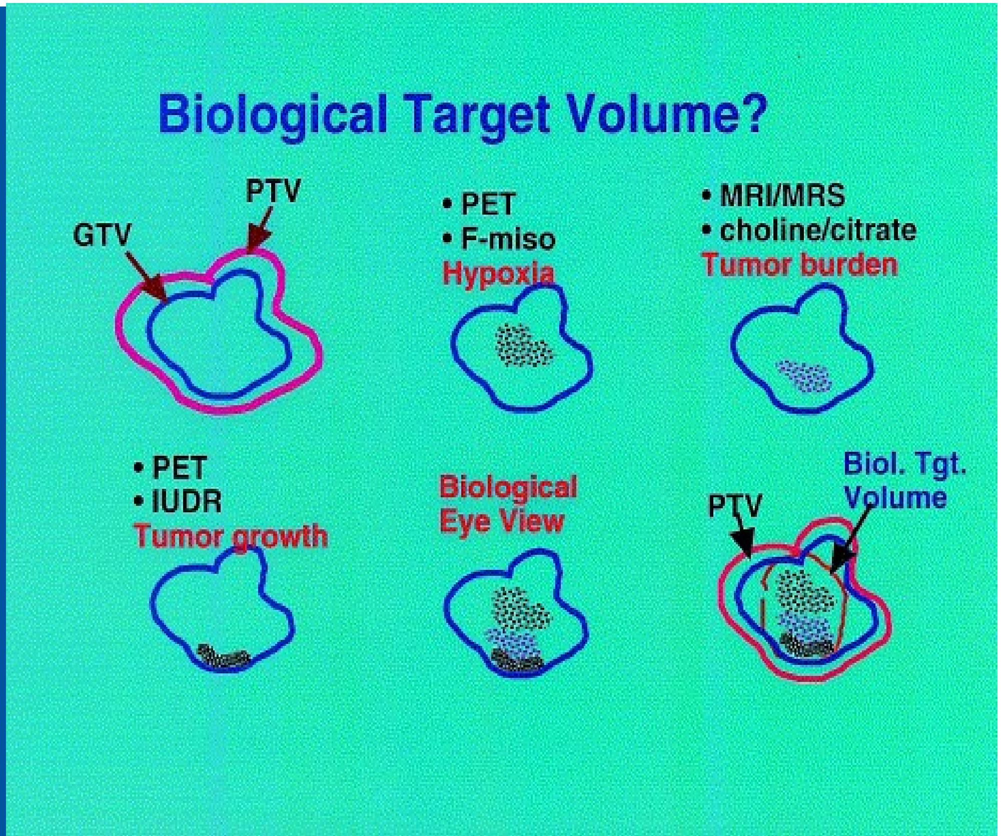

Ling et al. 2000, Int. J. Radiat. Oncol. Biol. Phys. 47:551-556

Cell density

- increase in cell density
- reduction interstitial space
- reduction in water diffusion

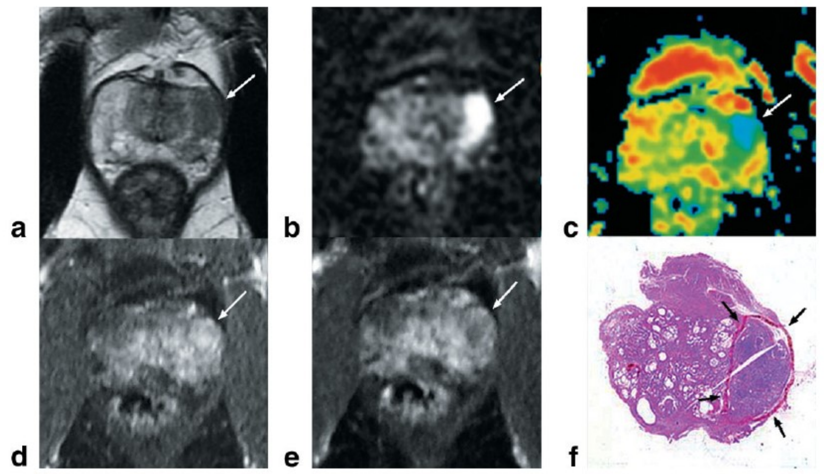

Figure 3. A 59-year-old male with prostate cancer (moderately differentiated adenocarcinoma, Gleason's score 3 + 4 = 7, capsule invasion (→)). When T2W was used, a low intensity area is noted in the left lobe of the prostate (**a**, arrow). DWI (**b**, arrow) and ADC map (**c**, arrow) clearly demonstrate decreased diffusion. The lesion is well enhanced in the early phase of dynamic study (**d**, arrow). In delayed phase, the lesion showed washout (**e**, arrow). The minimum ADC of the lesion is 0.60×10^{-3} mm^2/second. During image interpretation sessions, a rank of 5 was assigned for all three protocols. A histopathological H&E stain section showed the cancerous area corresponding to the MR image findings (**f**, arrows).

Tanimoto et al. 2007, JMRI 25:146-152

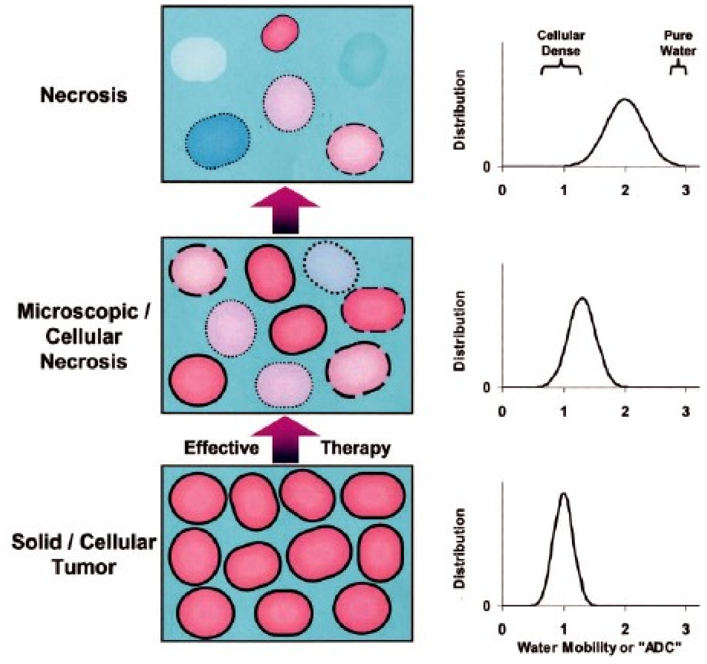

Ross et al. 2003, Mol. Canc. Ther. 2:581-587

Characteristics of capillary bed

- Micro-vessel density
- Organization / regularity of capillary
- Permeability

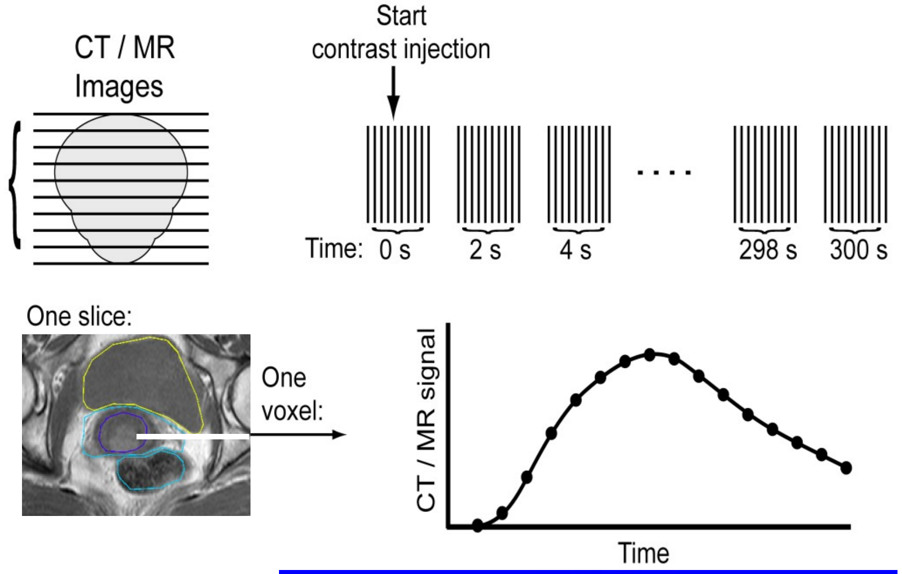

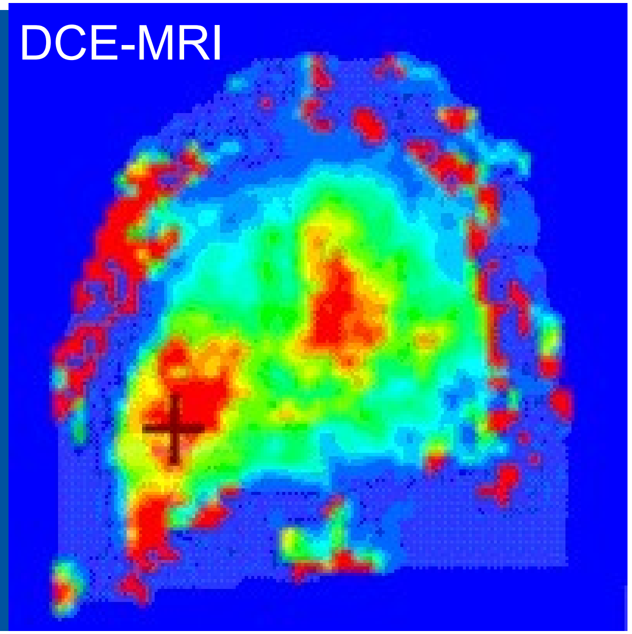

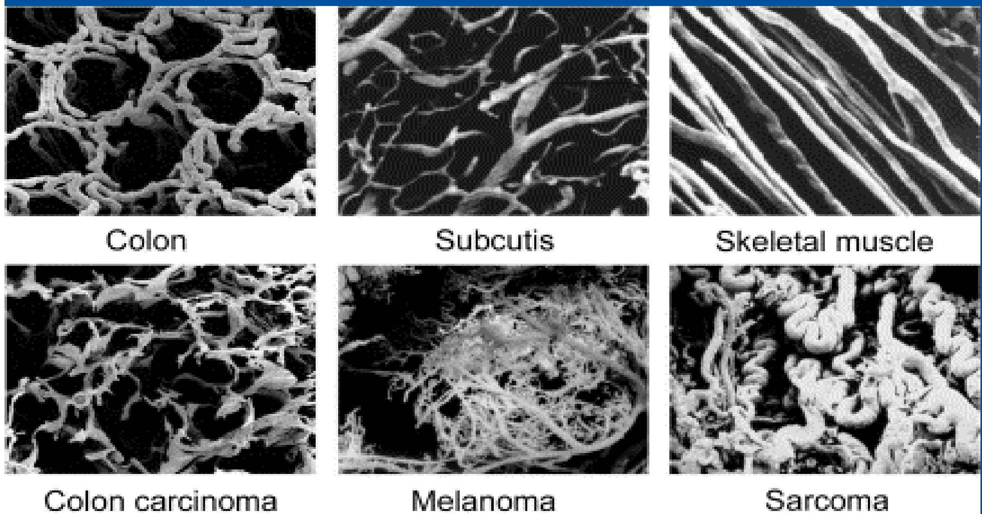

Vaupel, 2004; Semin. Radiat. Oncol. 14:198-206

Hypoxia

Head-neck tumor imaged with

FDG-PET F-Miso-PET

normoxic

hypoxic

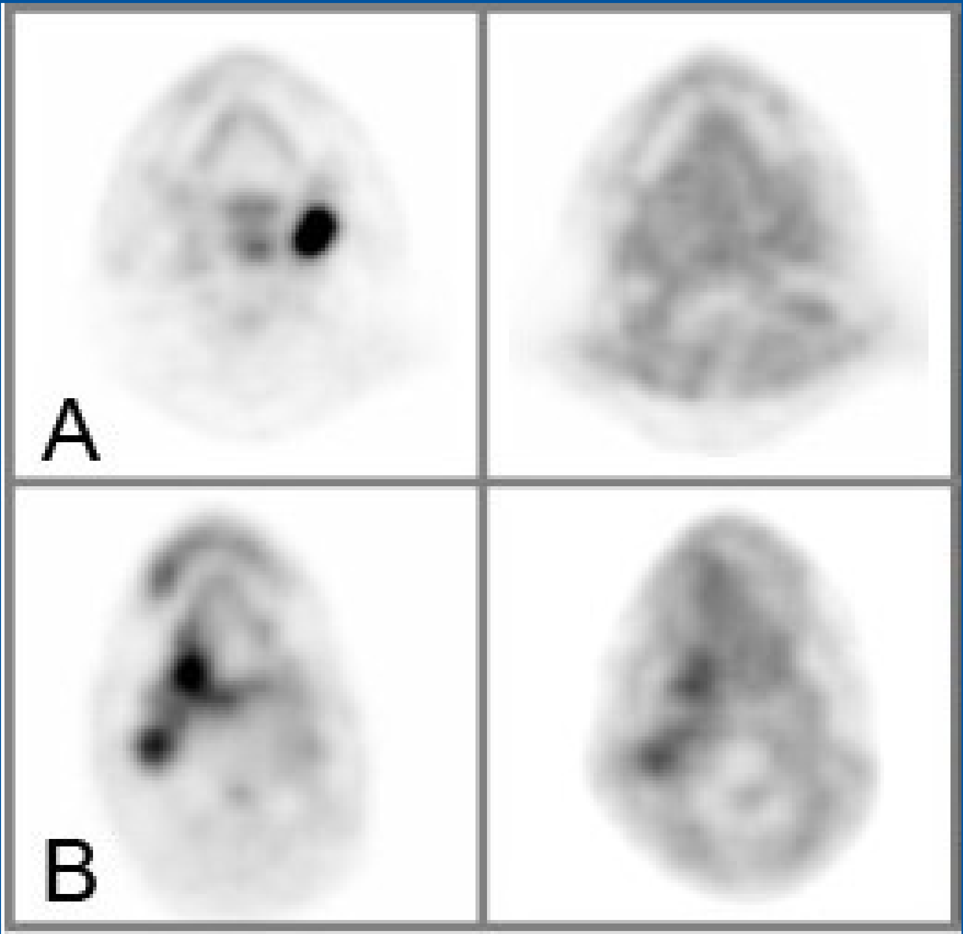

Gagel et al. 2007; BMC Cancer 7:113

Oxygenation

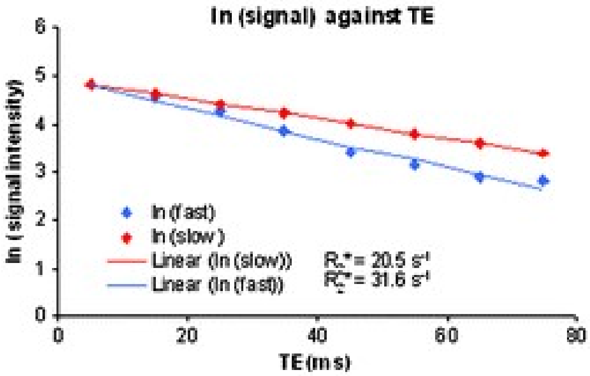

R_2*=20.5 sec^{-1}
R_2*=31.5 sec^{-1}

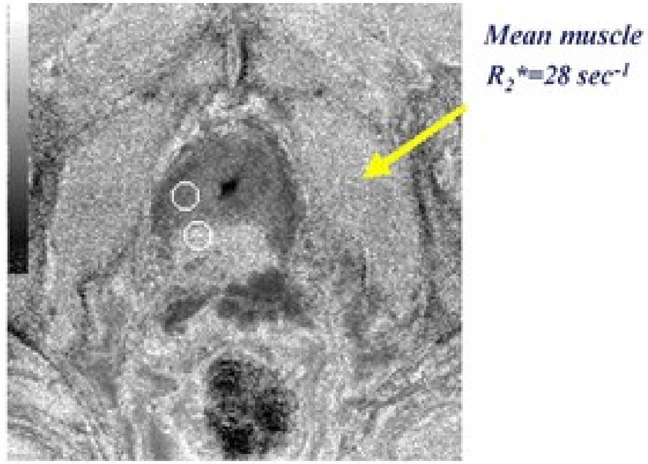

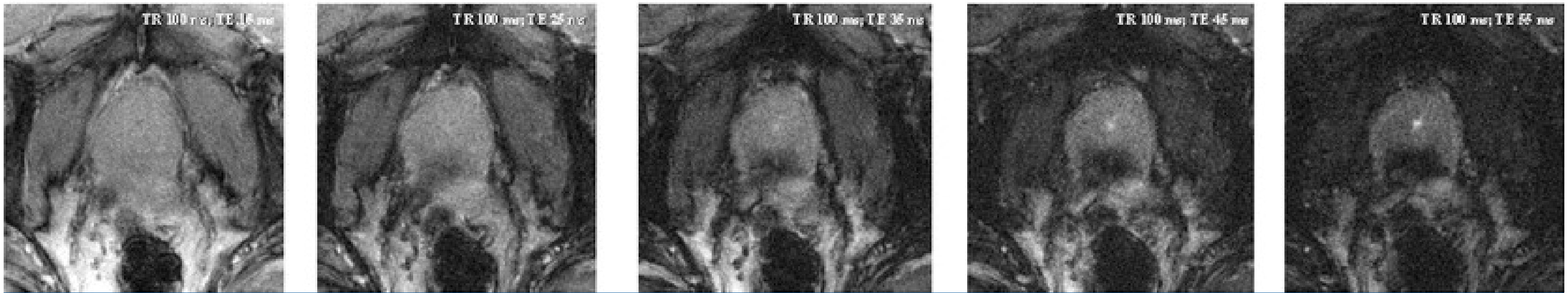

Blood Oxygen Level Dependent (BOLD) MRI

Hoskin et al. 2007, Int. J. Radiat. Oncol. Biol. Phys. 68:1065-1071

The potential of advanced imaging for radiotherapy

- Target definition
- Tissue characterization
- Image guidance
- Treatment monitoring

Cone-beam CT on the linac

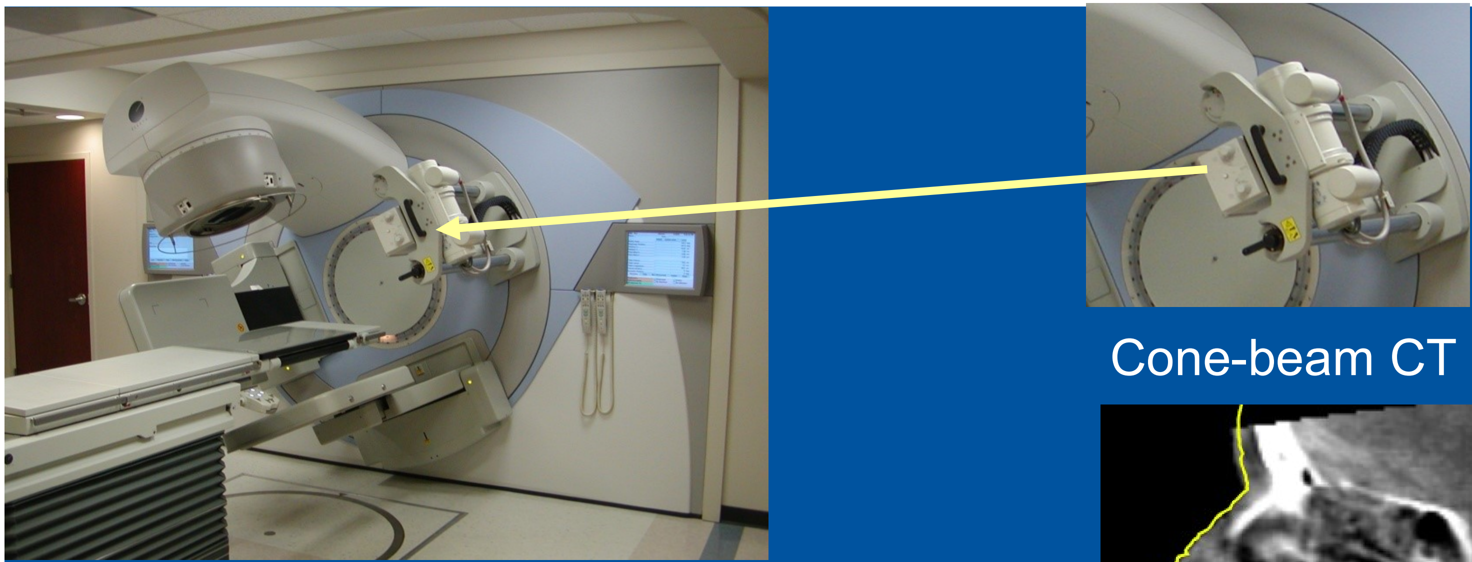

Cone-beam CT

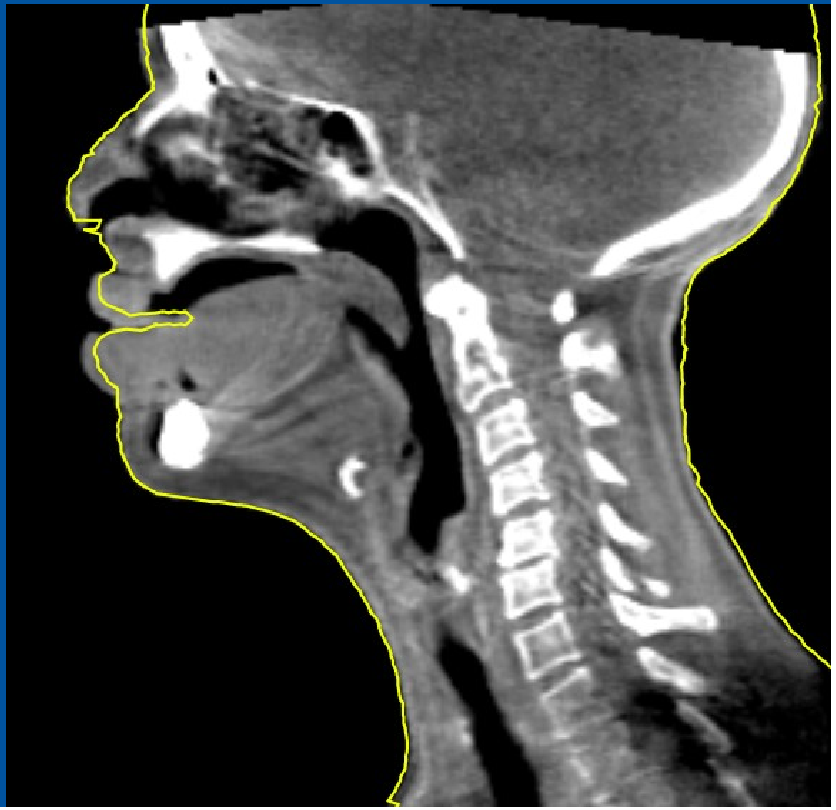

Integrated MRI-linac

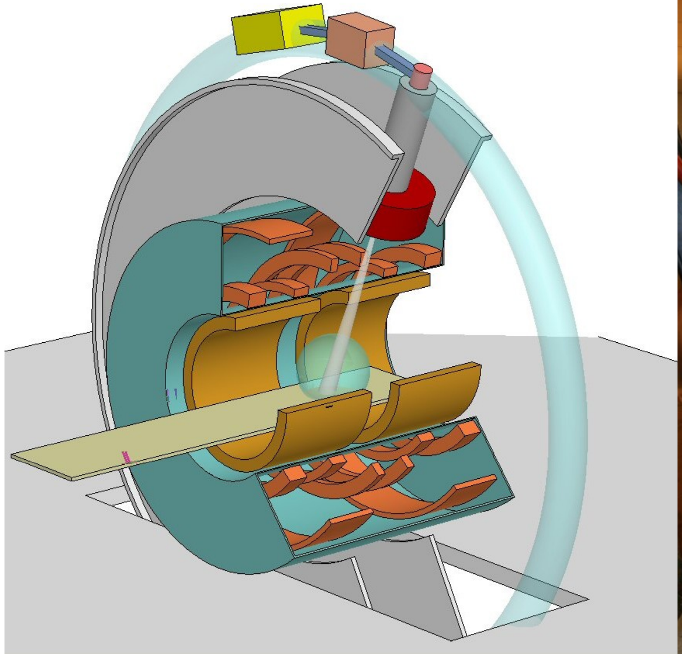

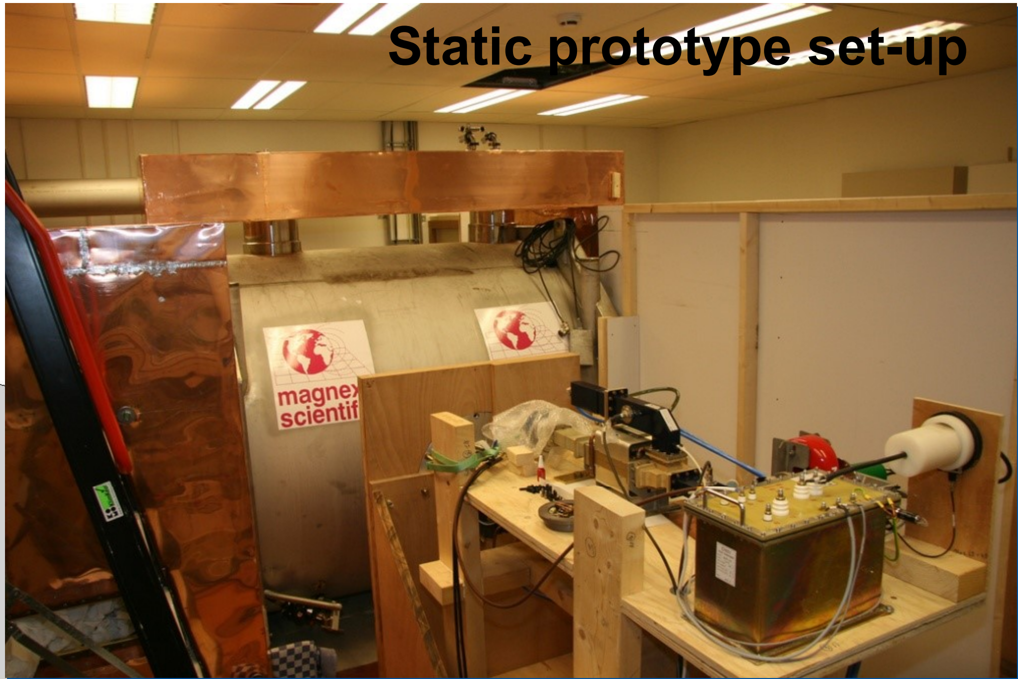

Raaymakers et al., 2009; PMB 54:N409-15

MRI-guided brachytherapy

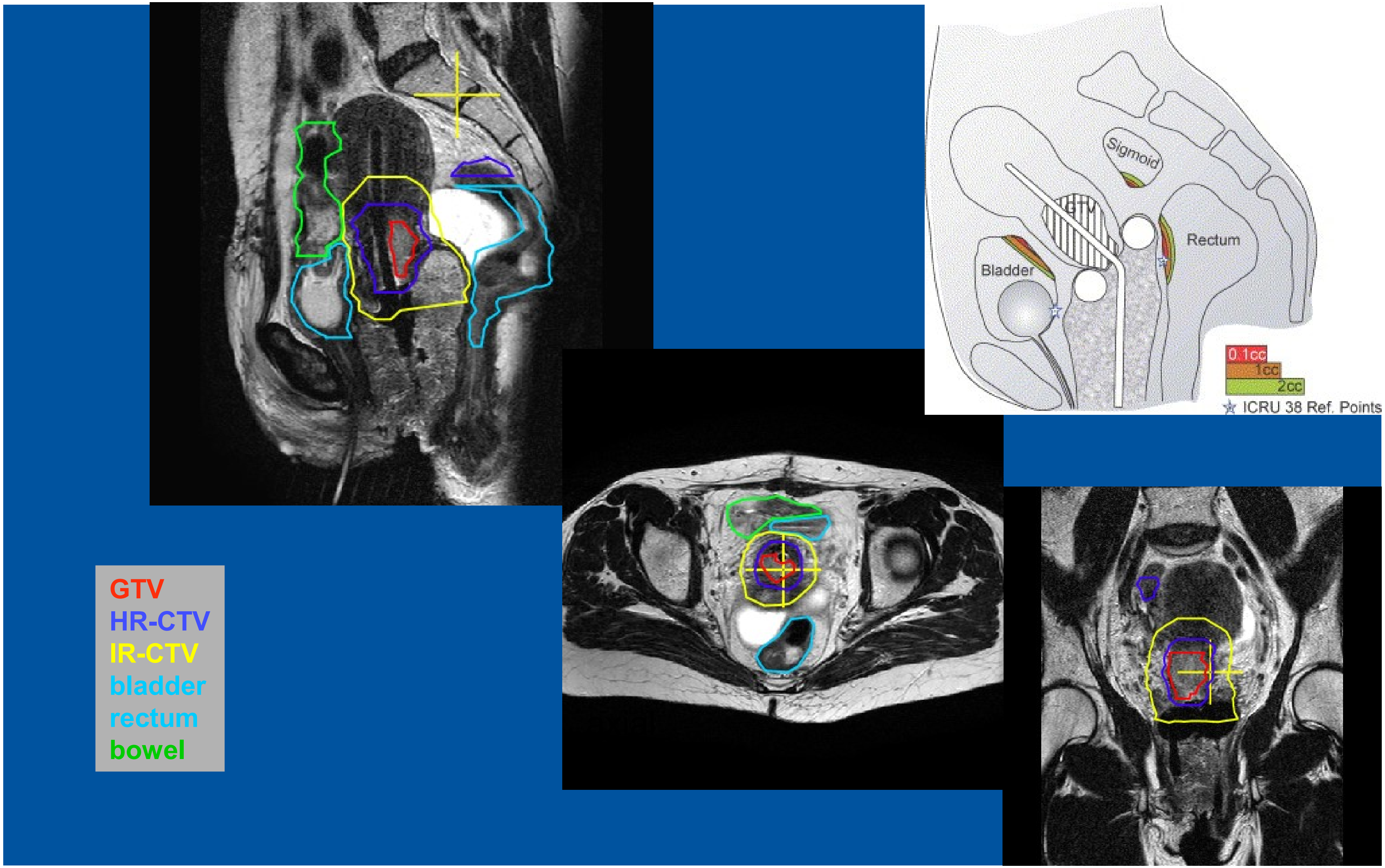

The potential of advanced imaging for radiotherapy

- Target definition
- Tissue characterization
- Image guidance
- Treatment monitoring

Treatment monitoring

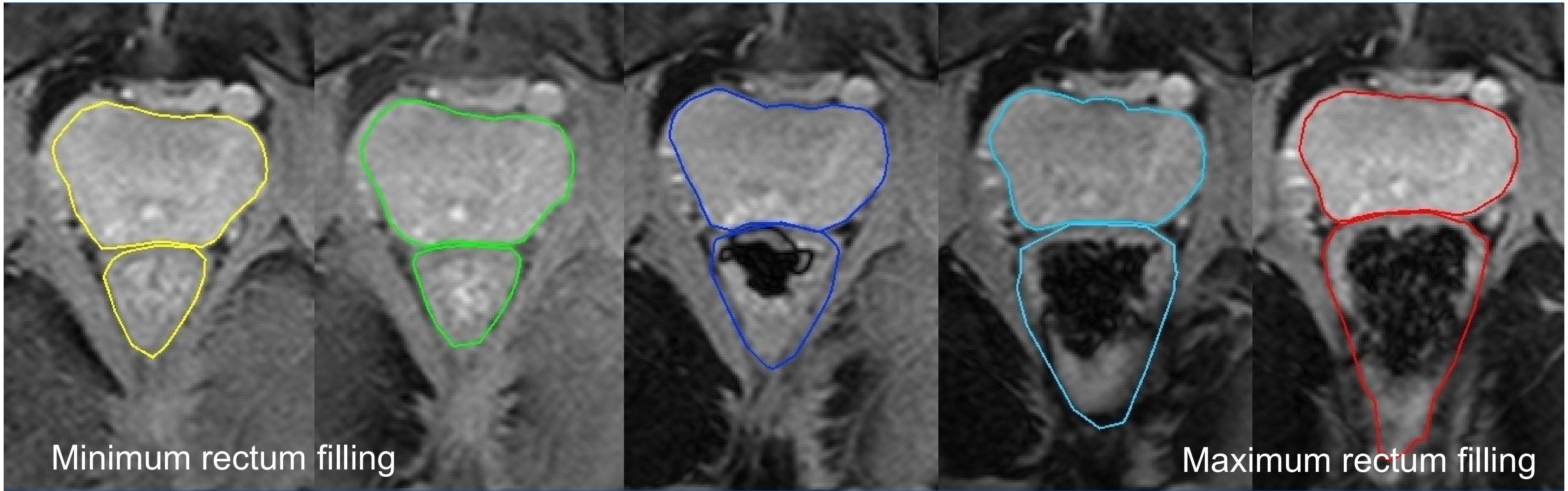

5 successive MRI scans of the prostate in volunteers

Kerkhof et al. 2008, Phys. Med. Biol., 53:5623-5634

Treatment monitoring

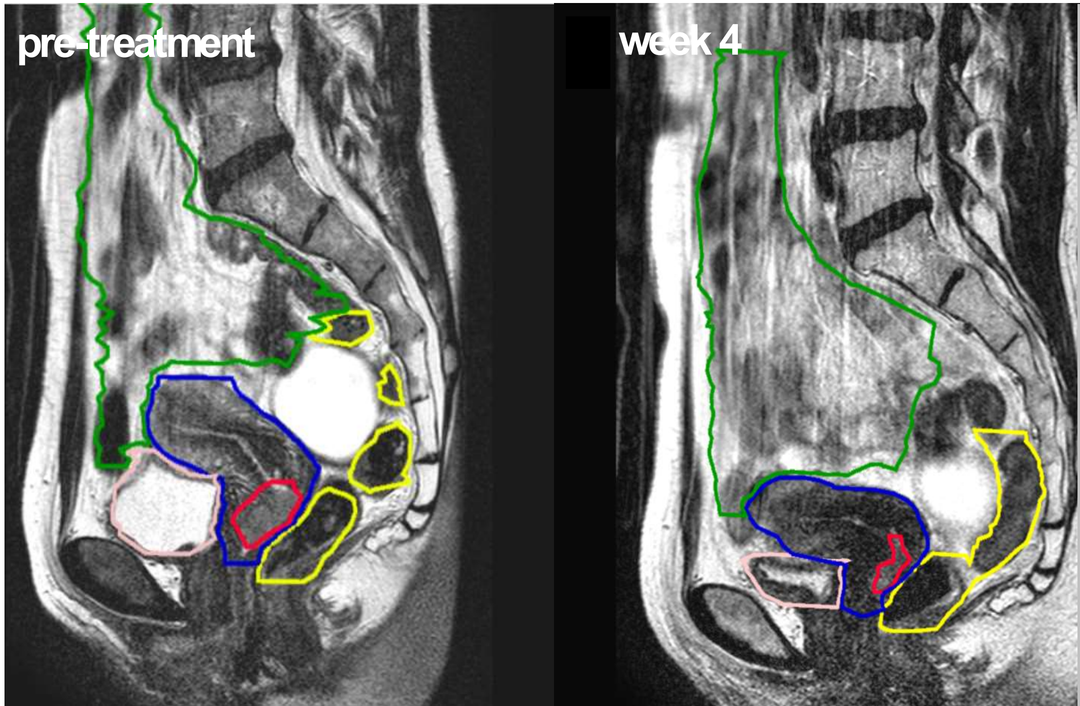

weekly MRI scans of the cervix and uterus in patients with cervical cancer

Van de Bunt et al. 2008. Radioth. Oncol 88:233-240

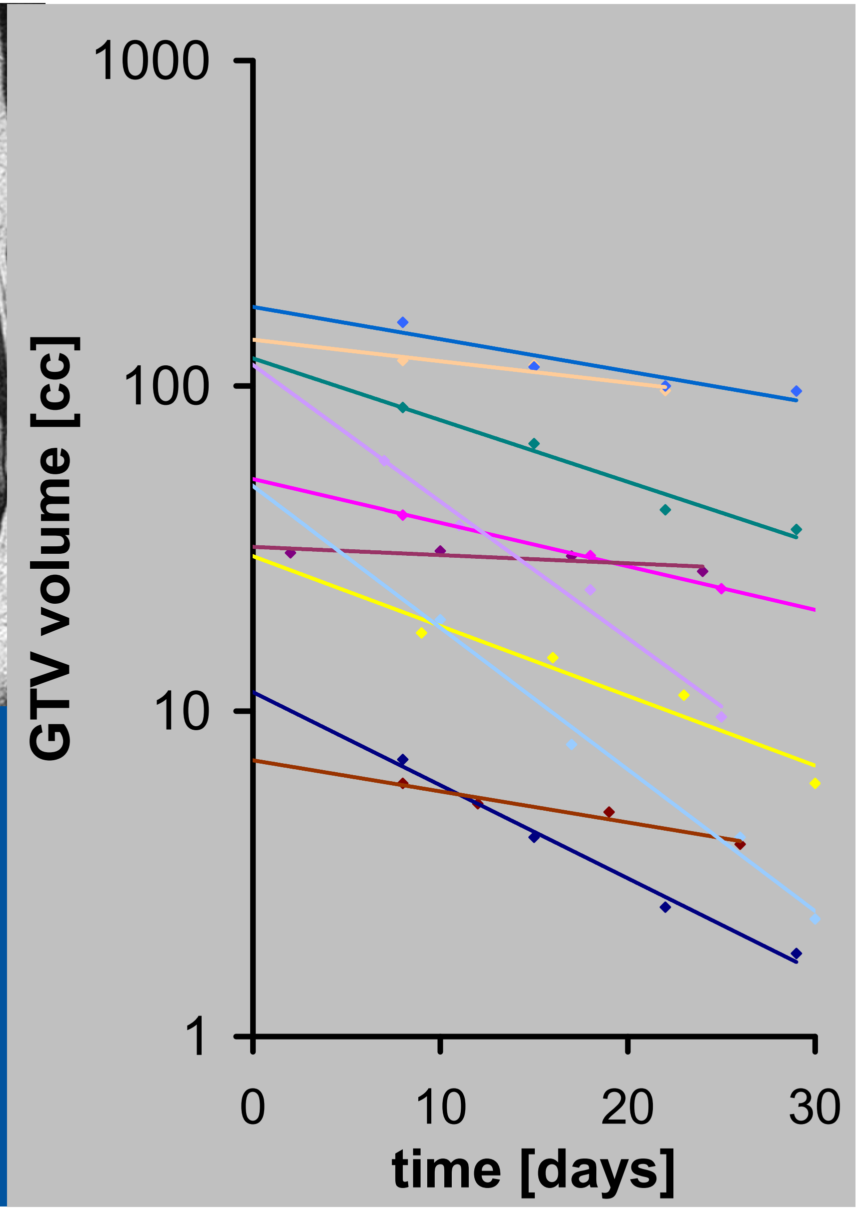

PET for identifying residual disease

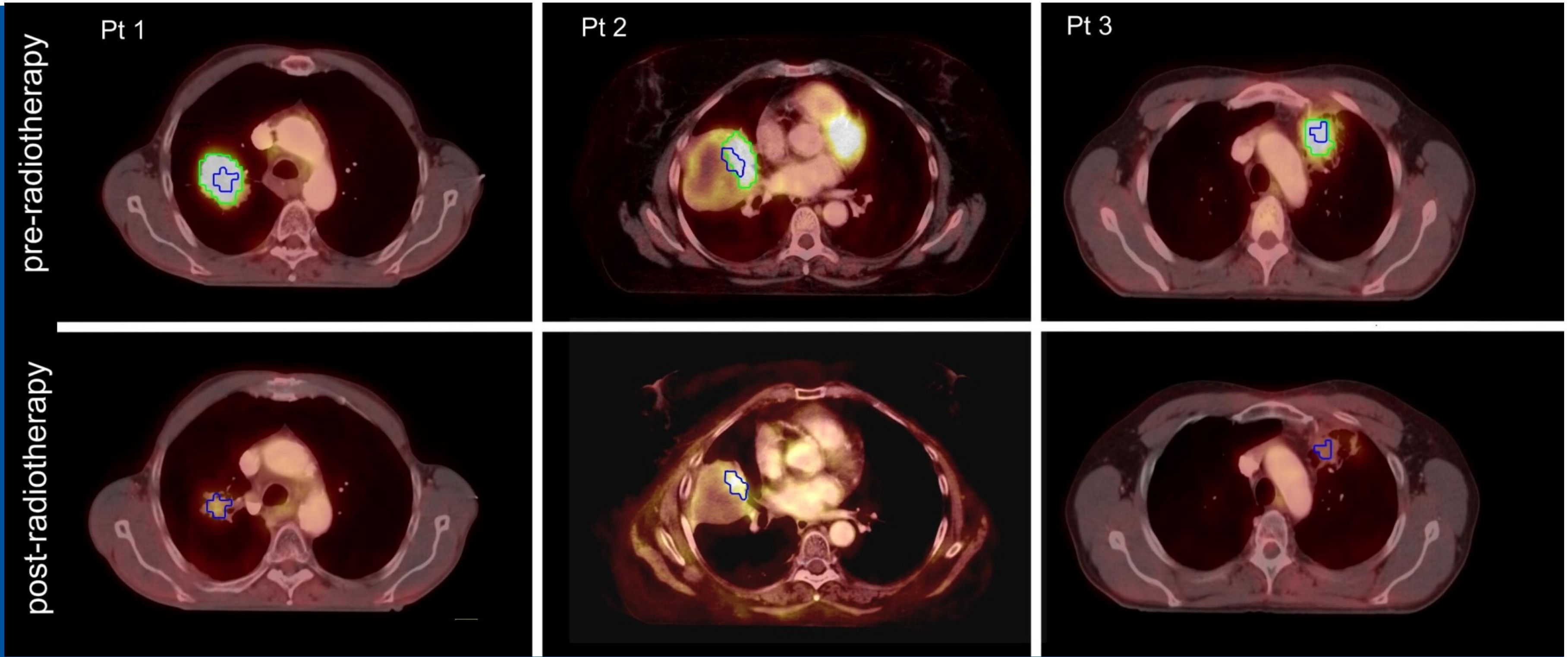

- FDG-PET-CT images pre- and post-radiotherapy

Aerts et al. 2009; Radioth. Oncol. 91:386-392

We can do many things with imaging in radiotherapy!

- Target definition
- Tissue characterization
- Image guidance
- Treatment monitoring

Why should medical physicists in RT worry about imaging technology?

- Radiotherapy asks other questions than standard diagnostics:
  - Not if a patient has cancer, but where the tumor starts and ends
- Radiotherapy poses specific demands on imaging
  - Patient positioning
  - High resolution imaging
  - Geometrical accuracy
- The use of MRI poses specific demands on radiotherapy
  - How to deal effectively with all the images during delineation
  - How to deal with conflicting information
  - How to deal with changes during treatment

Adaptation of scan protocols: patient positioning

- Positioning devices must be MRI compatible
- Regular RF coils may not be compatible with positioning devices
- Position must fit in narrow PET bore

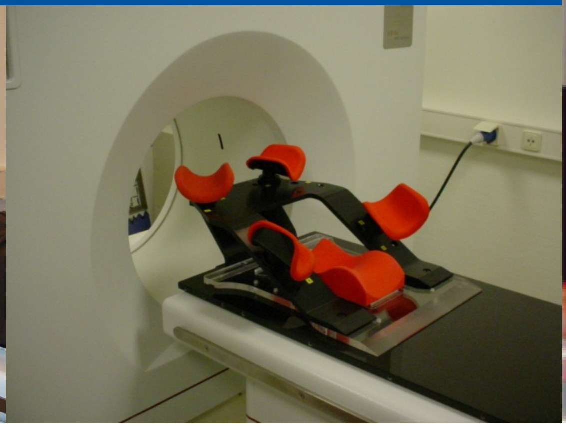

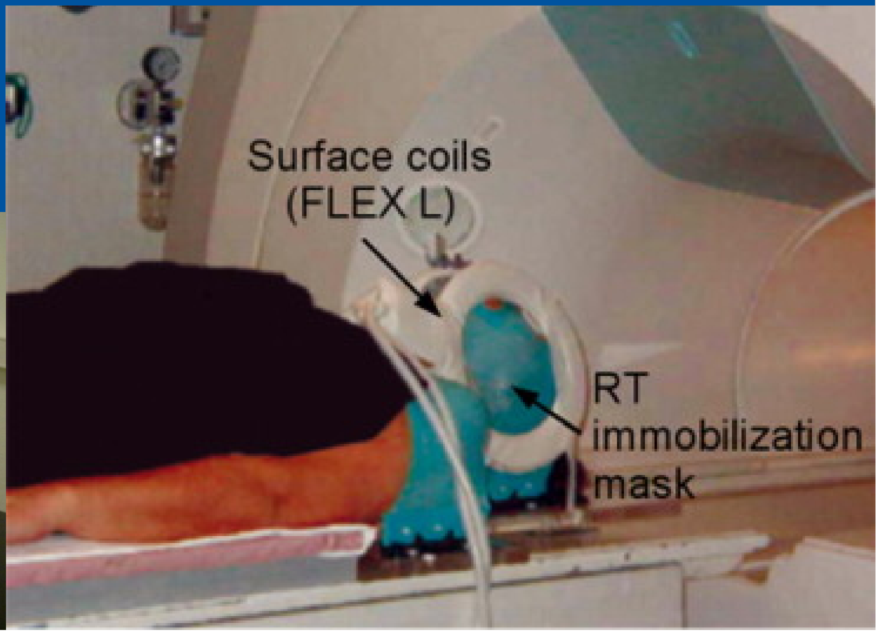

Selection of coils for MRI

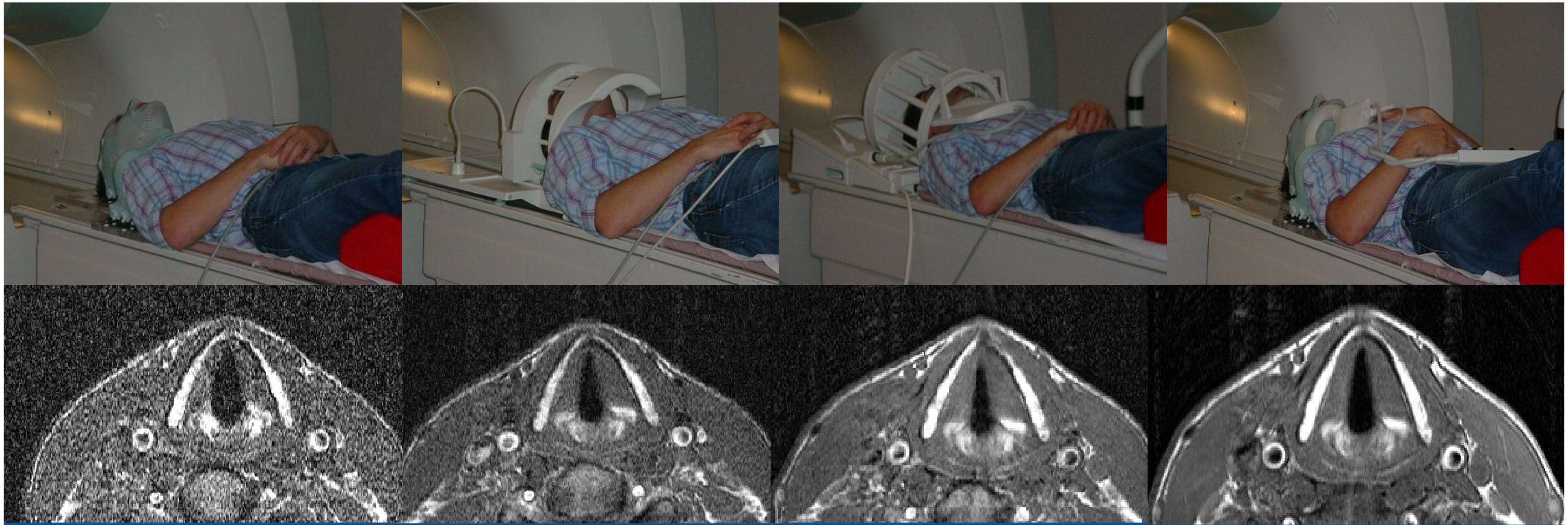

Integrated body coil | quadrature head coil | multi-element hn-coil | two-element flexible surface coil

T1-weighted MRI of healthy volunteer

Verduijn et al. 2009; Int. J. Radiat. Oncol. Biol. Phys. 74:630-636

Diagnostic protocols are not always the best for radiotherapy

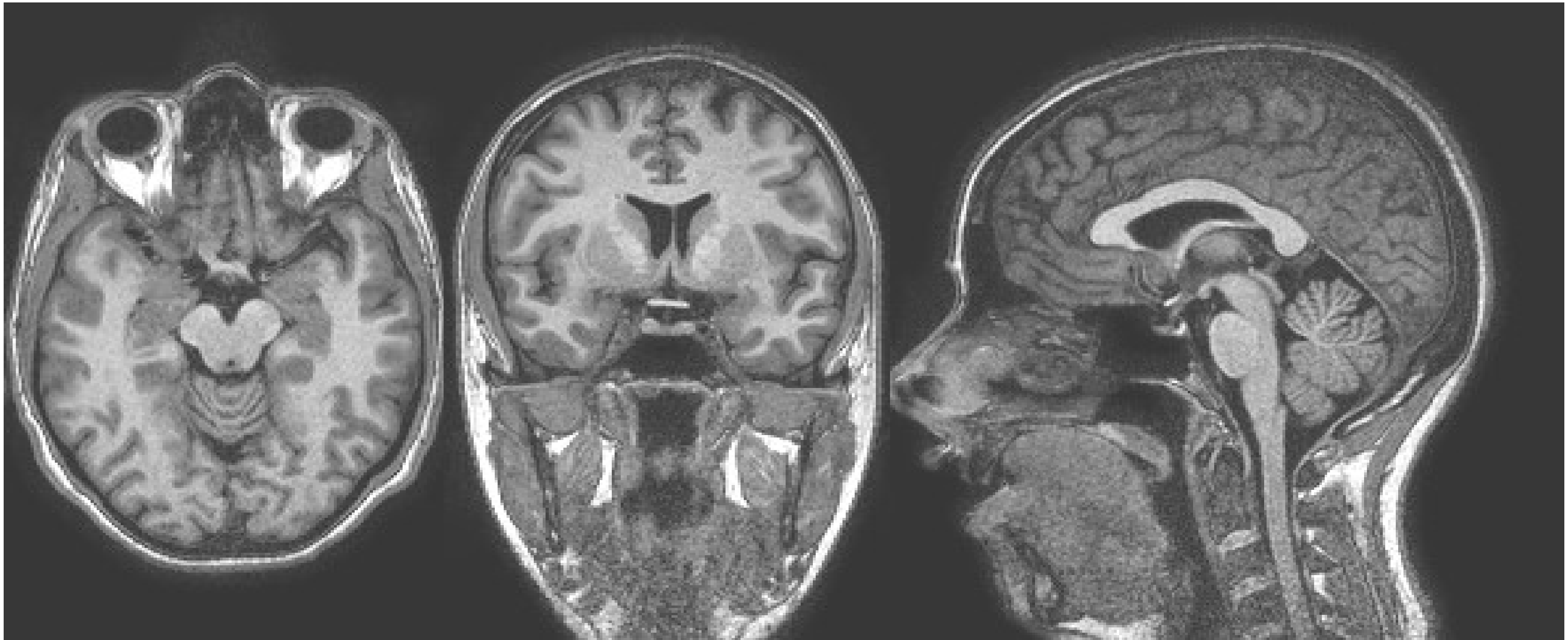

Geometrical distortions

Image distortion and correction on a 0.23 T open MRI scanner

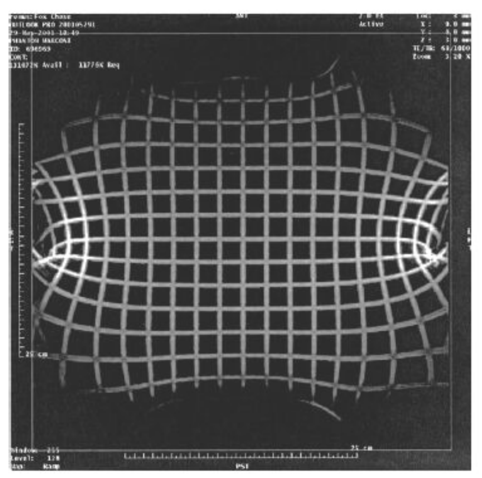

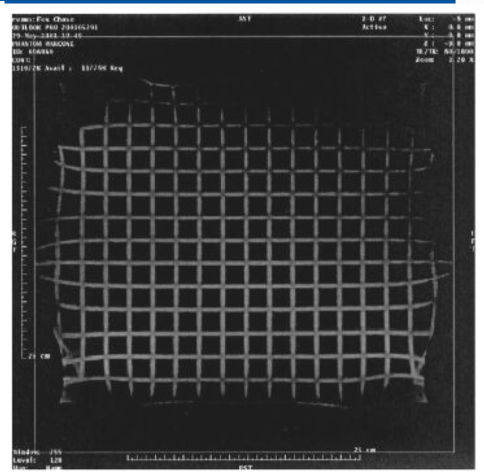

Mah et al. 2002 Int. J. Radiat. Oncol. Biol. Phys. 53 (3), 757-765

Impact of imaging artifacts in radiotherapy

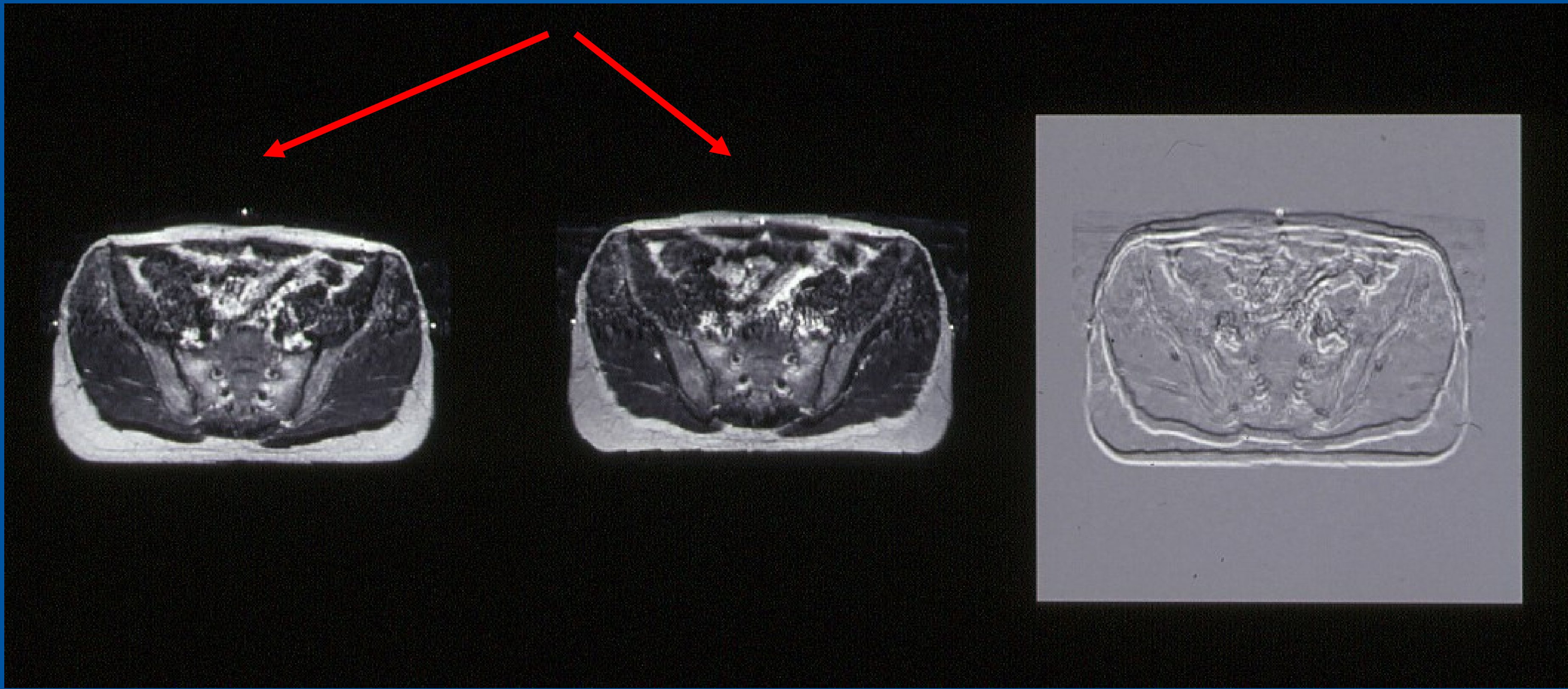

Read-out gradient 0.54 and -0.54 mT/m

WFS = 9 and -9 mm

Combining multiple imaging modalities

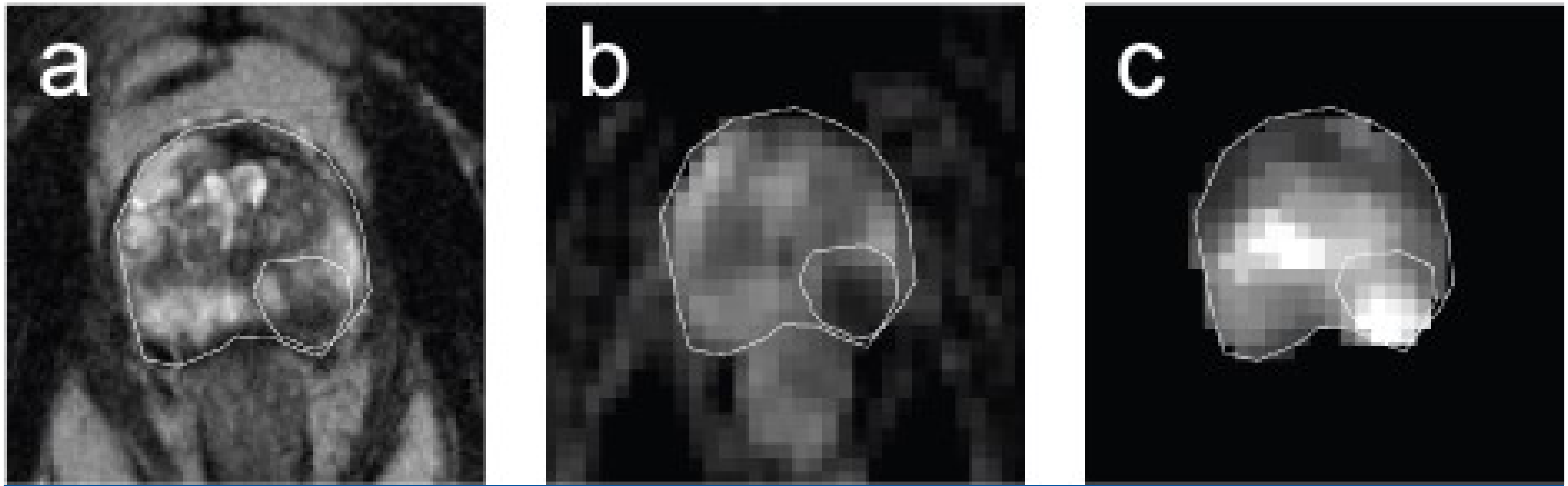

T2w ADC K^{trans}

- Combining multiple imaging modalities tends to increase sensitivity and specificity of an exam
- Do the techniques identify the same voxels as target?
- Identification of volumes depends on threshold setting
- Is there a combination of thresholds for which overlap between ADC and K^{trans} is high?

Groenendaal et al. Radiother Oncol; 2010; 95:185-190

Treatment monitoring

DCE-MRI of cervix cancer during external-beam radiotherapy

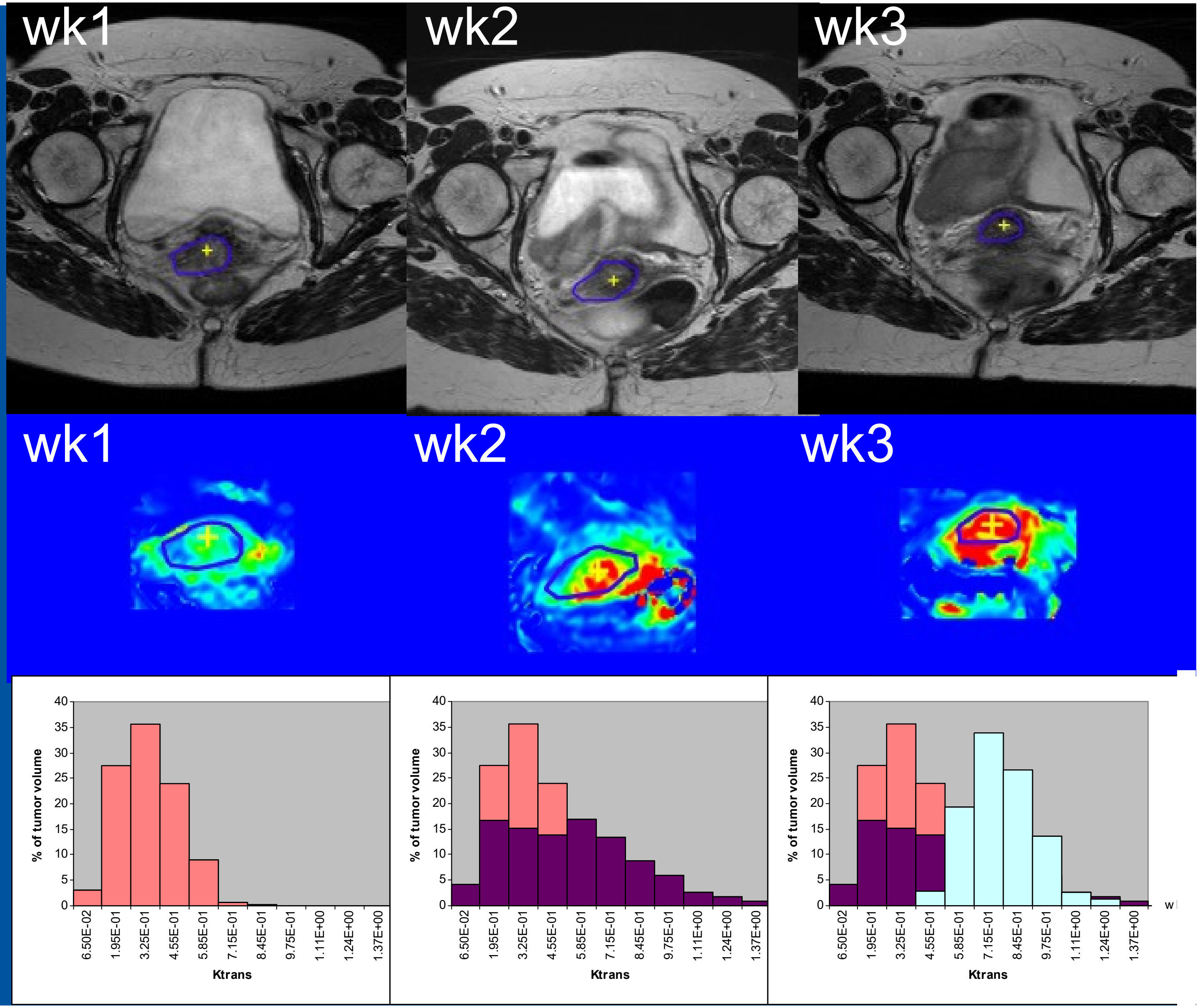

Follow-up

- DCE-MRI of patient with PSA relapse after radiotherapy (top), compared with similar patient without PSA relapse (bottom)

- Changes in imaging characteristics after radiotherapy
  – Normal tissue reaction
  – Recurrence

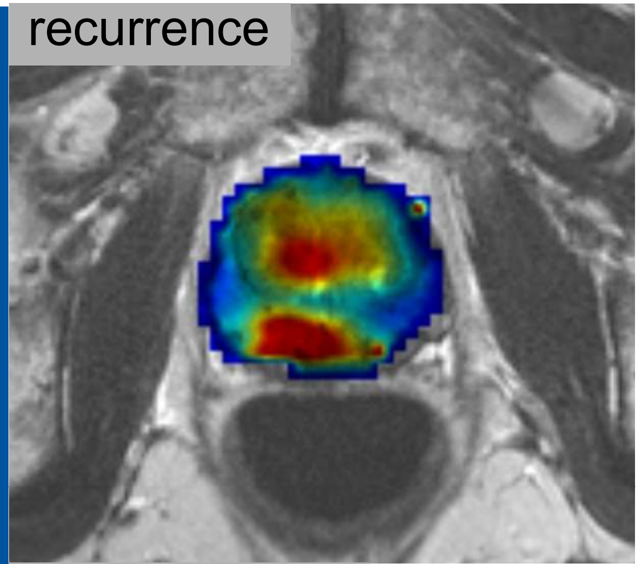

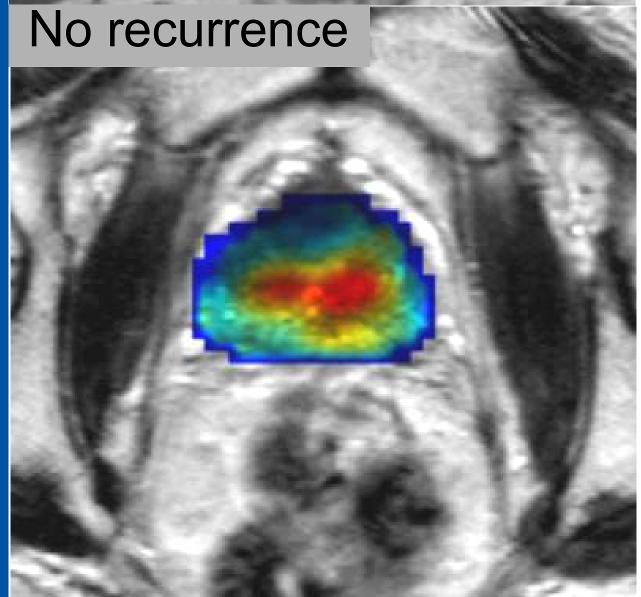

Learning objectives

- Generate sufficient knowledge to be able to work effectively with experts in radiology and nuclear medicine
- Improve the understanding of physics principles of MRI, PET and CT
- Understand the key technical challenges and solutions unique to the application of these imaging techniques in radiotherapy
- Explore the potential of the imaging techniques in clinical practice
- Explore the potential and challenges of biological imaging methods in radiotherapy treatment planning and follow-up

Physics principles of MRI, PET and CT

- MRI physics:
  - Basic principles, contrast formation, space encoding
  - Equipment
  - Fast scanning, volume sequences
- PET physics:
  - Basic principles
  - Image reconstruction, SUV, thresholding
- CT physics:
  - Basic principles
  - 4D, dynamic acquisitions, cone-beam CT
- Case studies: MRI contrast formation
- Case studies: PET
- Case studies: MRI artifacts

Issues specific to application in radiotherapy

- MRI geometrical accuracy
  - Theory
  - Experimental procedures
- In-room imaging
  - Physics of the MRI accelerator
  - Physics of cone-beam CT
- MRI interventions

Potential of (functional) imaging for radiotherapy

Physics of functional imaging on MRI

- Diffusion-weighted imaging
- Dynamic contrast-enhanced imaging
- MRI spectroscopy

PET with other tracers than FDG

Clinical applications

- brain
- gynecology
- head-neck
- lung

Voting system

Question 1: What is your current job?

1: medical physicist

2: resident (trainee) medical physicist

3: physician

4: RTT

5: student

6: other

Access to scanning equipment

Question 2: How does your department use MRI in the radiotherapy workflow?

1. have no access to MRI
2. use standard MRI scans from other departments
3. use dedicated MRI scans from the radiology department
4. the department has its own dedicated scan slots on an MRI in the radiology department
5. the department has its own MRI scanner

Access to scanning equipment

Question 3: How does your department use PET or PET-CT in the radiotherapy workflow?

1. have no access to PET
2. use standard PET scans from other departments
3. use dedicated PET scans from the nuclear medicine department
4. the department has its own dedicated scan slots on a PET in the nuclear medicine department
5. the department has its own PET scanner

Prior knowledge

Question 4: Do you have had earlier training/courses on

1. MRI
2. PET
3. both

More courses on imaging physics

ESTRO — Application of imaging to radiotherapy

EANM European Association of Nuclear Medicine — PET physics and clinical application

ISMRM ONE Community for Clinicians and Scientists — MRI physics and clinical application

Imaging has a bright future in radiotherapy

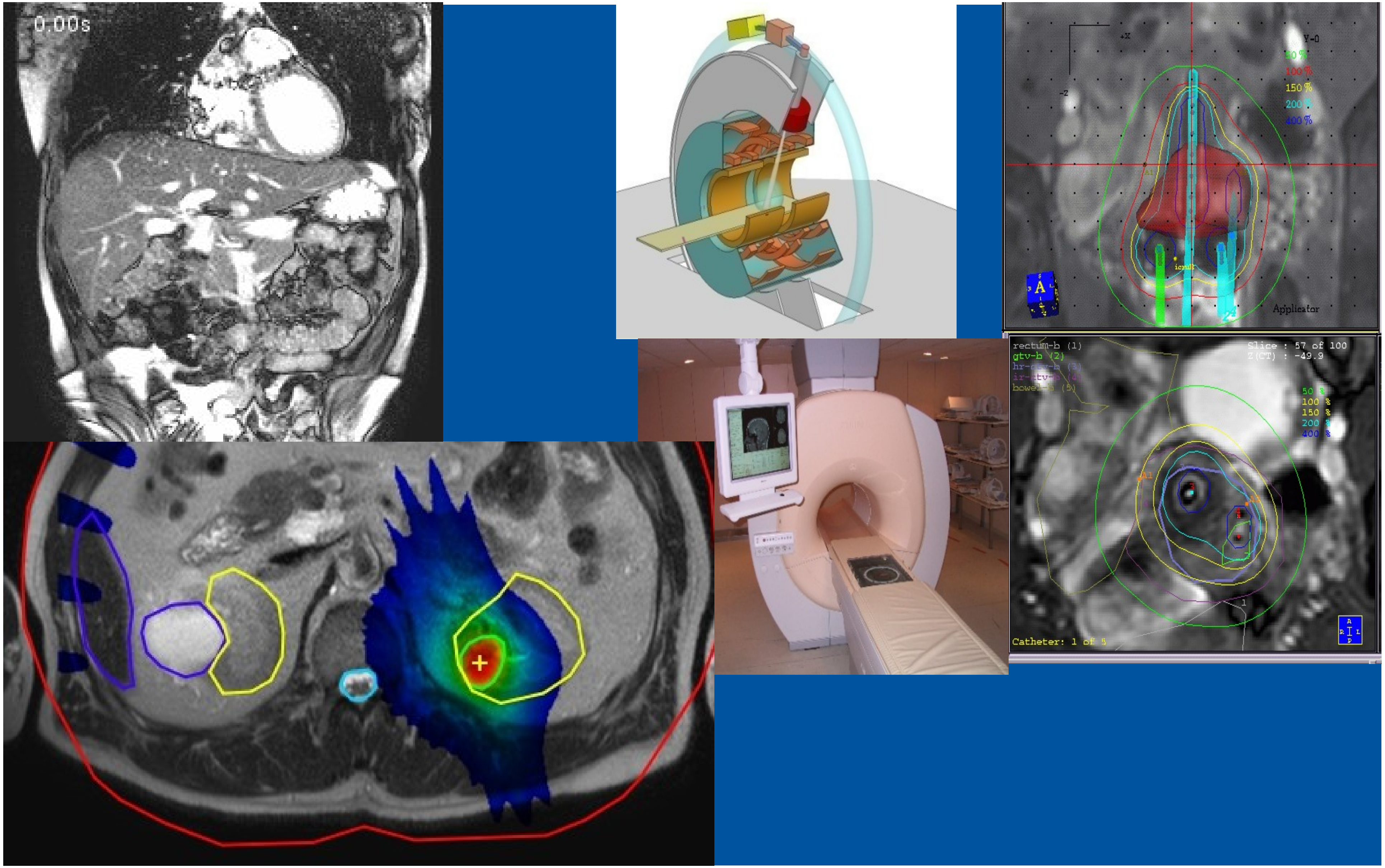

Imaging has a bright future in radiotherapy

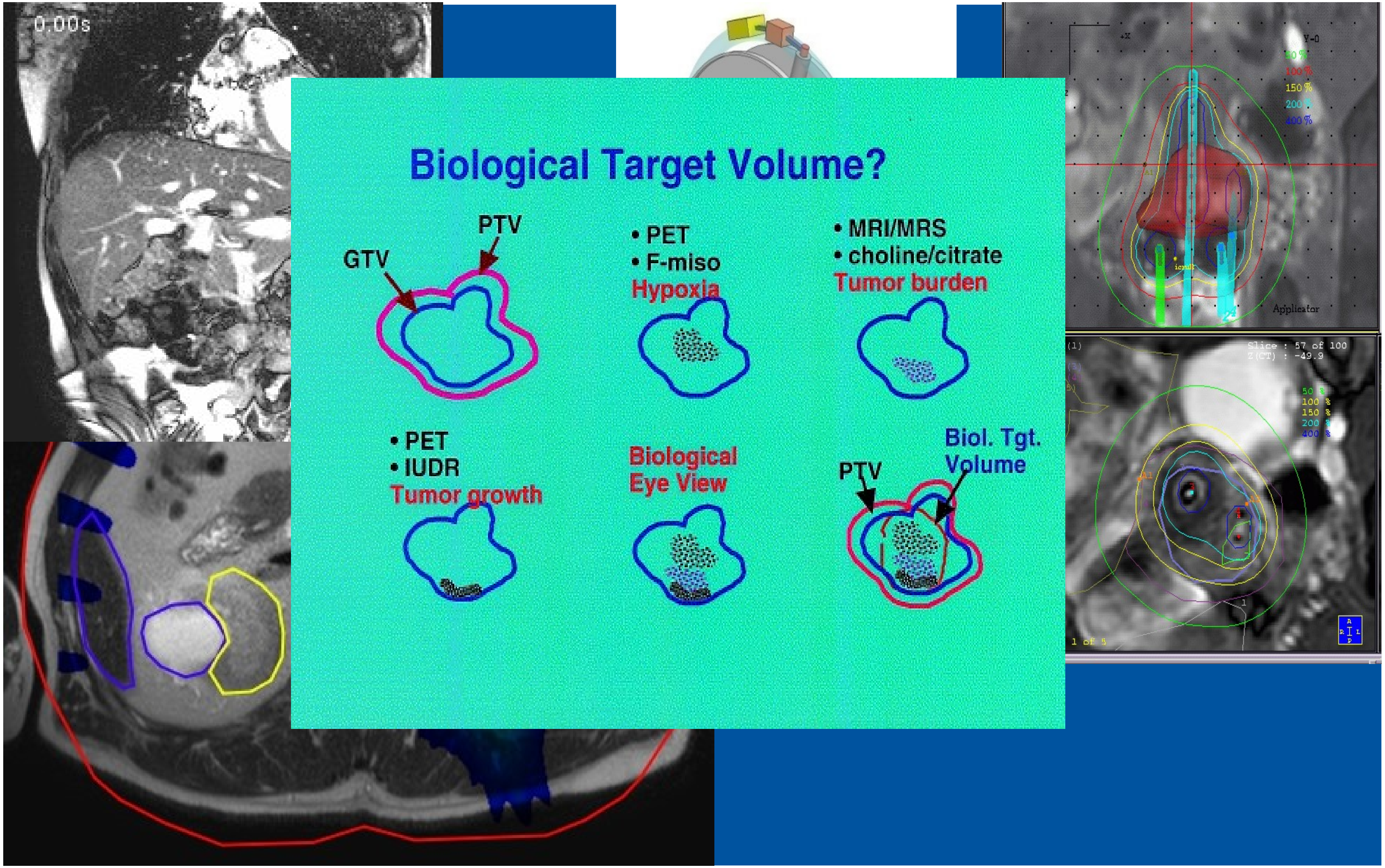

The future is NOW!

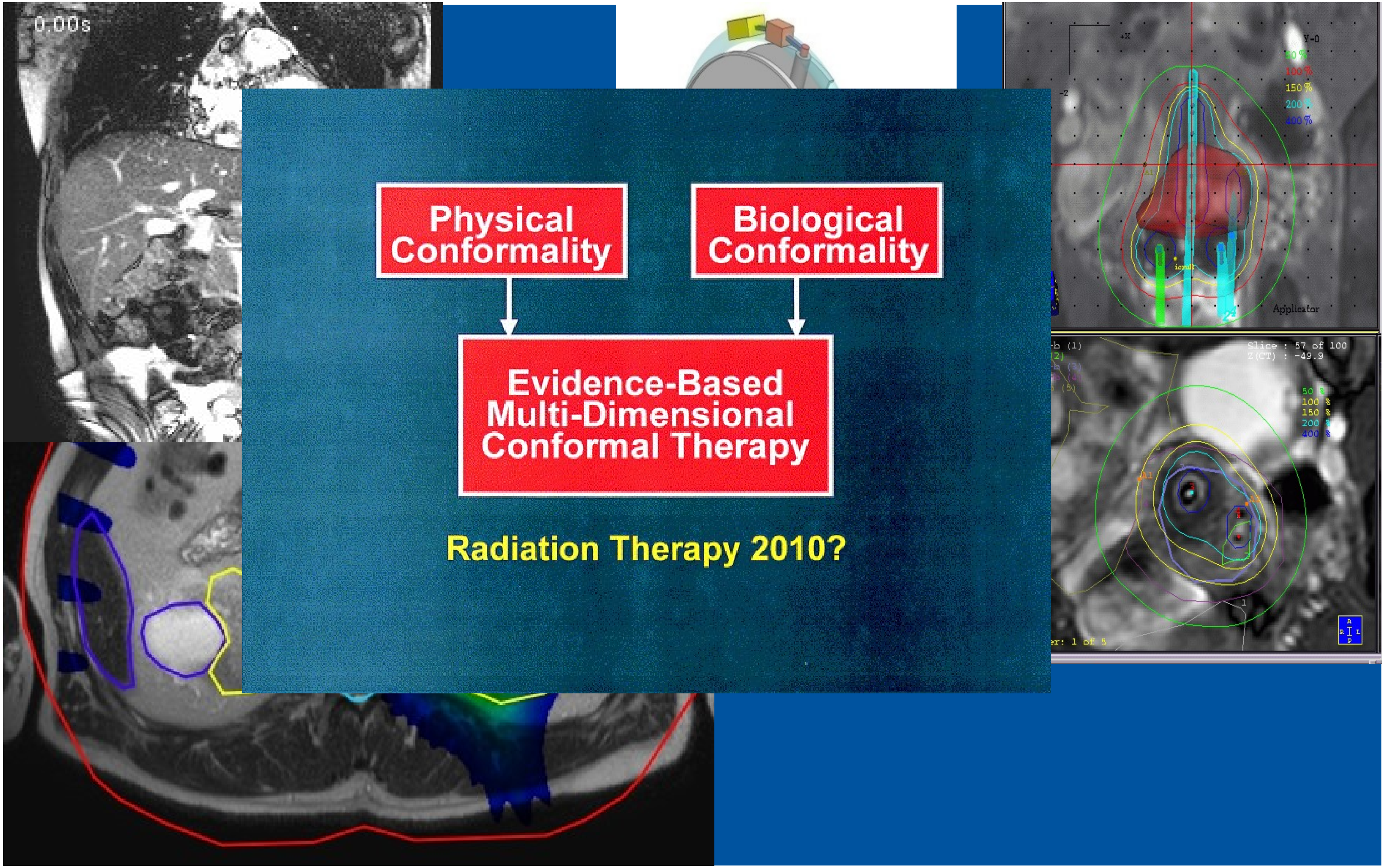

UiO : Department of Physics
University of Oslo

Oslo University Hospital

MRI physics - basic principles

Eirik Malinen

Background

- All clinical applications of MRI today are based on magnetic properties of the hydrogen nucleus
- Body tissues contains lots of water and fat, and hence hydrogen

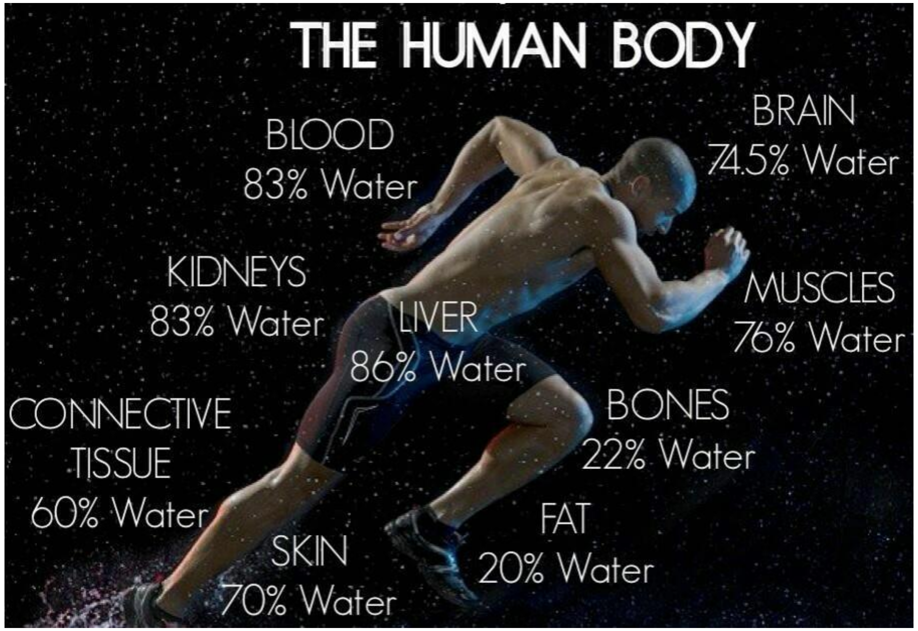

Nuclear magnetic moment

- Stern-Gerlach experiment:

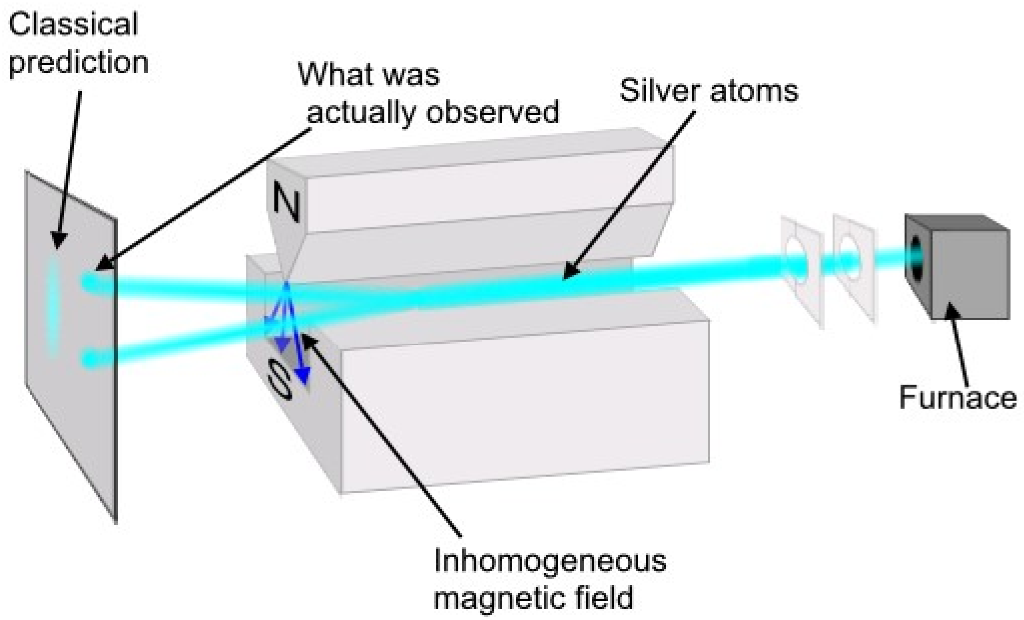

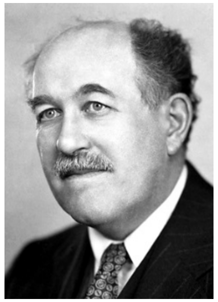

Otto Stern

Walter Gerlach

→ Atomic nuclei has a quantized magnetic moment

Magnetic moment and spin

- Consider charge *q* in circular motion:

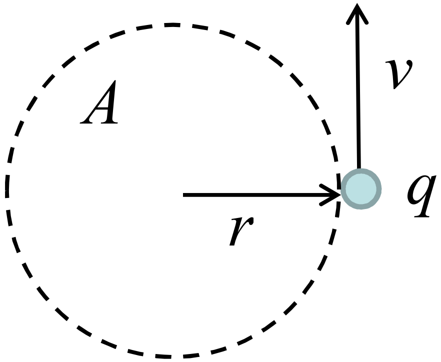

Current:

$$i = \frac{\Delta q}{\Delta t} = \frac{qv}{2\pi r}$$

Magnetic moment:

$$\mu = iA = \frac{q}{2m} L \quad , \quad L = mvr$$

- Rotating charged sphere with uniform charge:

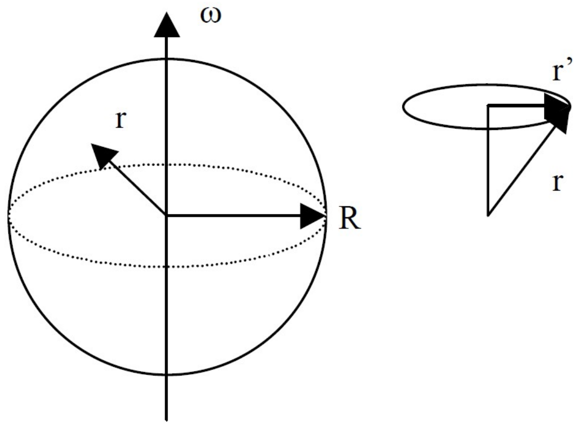

$$\mu = \frac{q}{2m} S$$

Spin!

Quantized nuclear spin

- Nuclear spin is a form of angular momentum
- Nuclear spin, $\mathbf{I}$, is quantized in units of $\hbar$
- Nuclear quantum number depends on nuclear configuration; I=1/2, 1…
- Hydrogen has spin I=1/2, with spin projection numbers m_I=+1/2 , -1/2; spin 'up' or 'down'
- Magnetic moment is $\boldsymbol{\mu}=\gamma\mathbf{I}$

↖ Gyromagnetic ratio

Unpaired nucleons, spin and γ

Nucleus	Unpaired Protons	Unpaired Neutrons	Spin	γ (MHz/T)
^{1}H	1	0	1/2	42.58
^{2}H	1	1	1	6.54
^{31}P	1	0	1/2	17.25
^{23}Na	1	2	3/2	11.27
^{14}N	1	1	1	3.08
^{13}C	0	1	1/2	10.71
^{19}F	1	0	1/2	40.08

Potential energy in magnetic field

- In an external magnetic field, the potential energy is:

$$E_{pot} = -\mu \cdot \mathbf{B}$$

$$= -\gamma\hbar m_I B = \mp\frac{1}{2}\gamma\hbar B$$

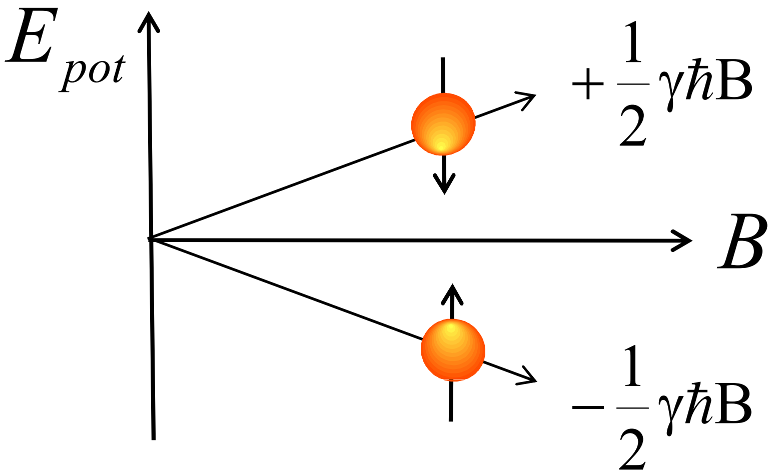

→ Two energy states are possible

- *Zeeman effect*

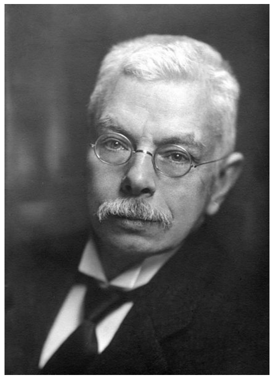

Pieter Zeeman

Magnetic resonance

- Spin system under an external magnetic field exposed to electromagnetic radiation

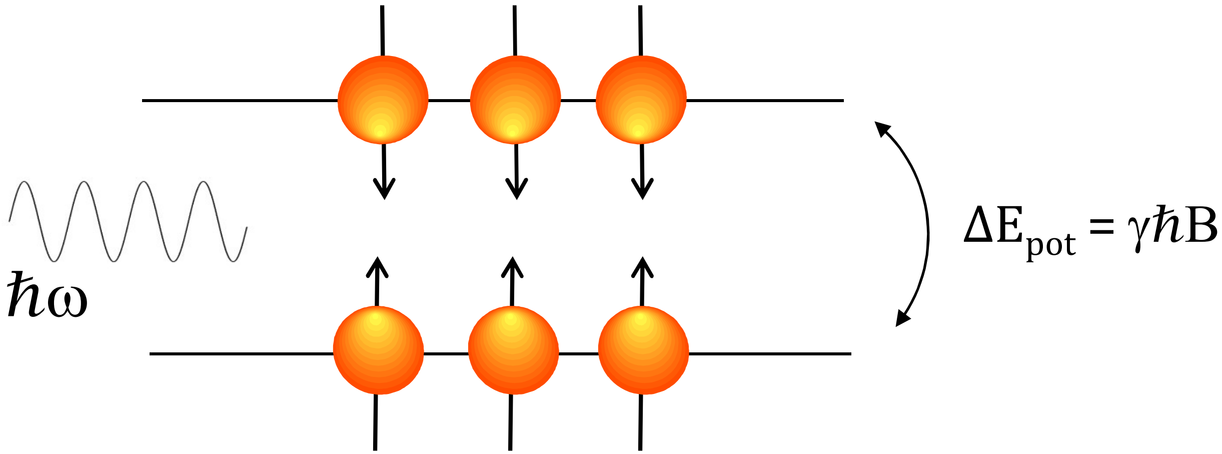

Isidor Isaac Rabi

- Transitions from spin down to spin up or vice versa may occur if $\hbar\omega = \Delta E_{pot} = \gamma\hbar B$

Magnetic resonance

- $\hbar\omega = \gamma\hbar B \rightarrow \omega=\gamma B$; *resonance condition*

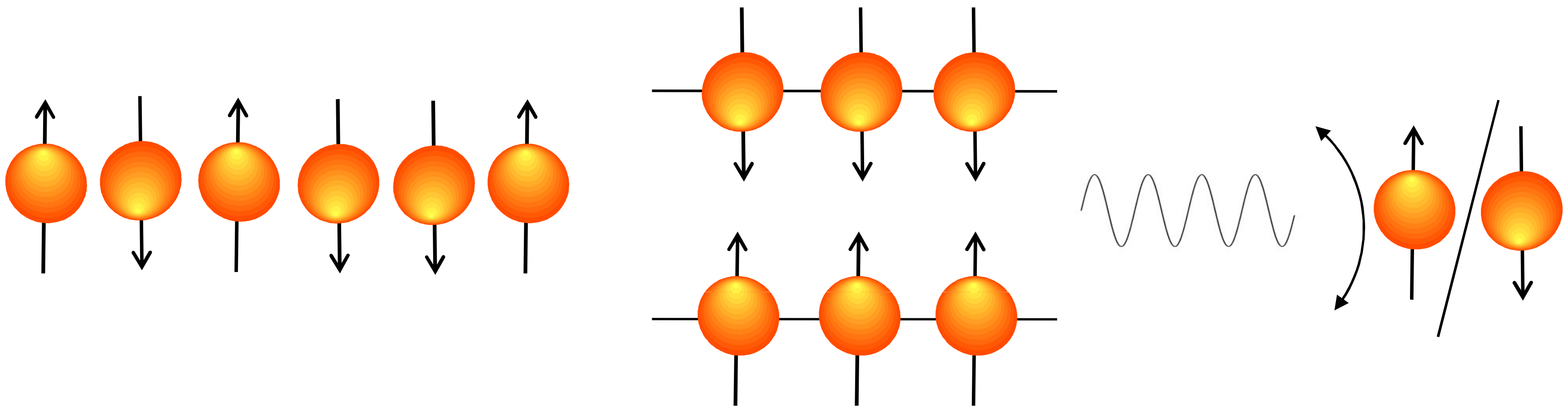

Without external field

With external field

With external field + electromagnetic radiation

- Resonance frequency, ^{1}H, B=1T: $\omega \approx 43$ MHz
  $\rightarrow$ radiofrequency !

Macroscopic considerations

- Spin transition probability is equal for *up*→*down* and *down*→*up*

- How can a net energy absorption be observed?

- Distribution of spins follows Boltzmann:

$$\frac{N_{\downarrow}}{N_{\uparrow}} = e^{-\Delta E_{pot}/kT} = e^{-\hbar\gamma B/kT}$$

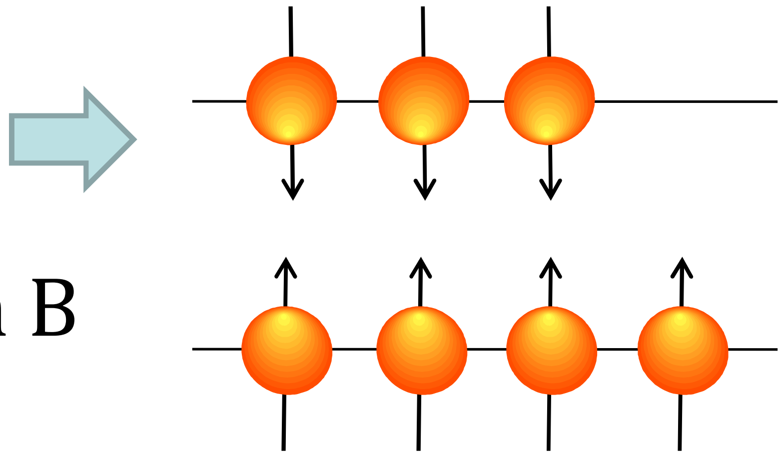

- Difference increases with B and decreases with T

Macroscopic magnetization

- Population difference generates a net magnetization

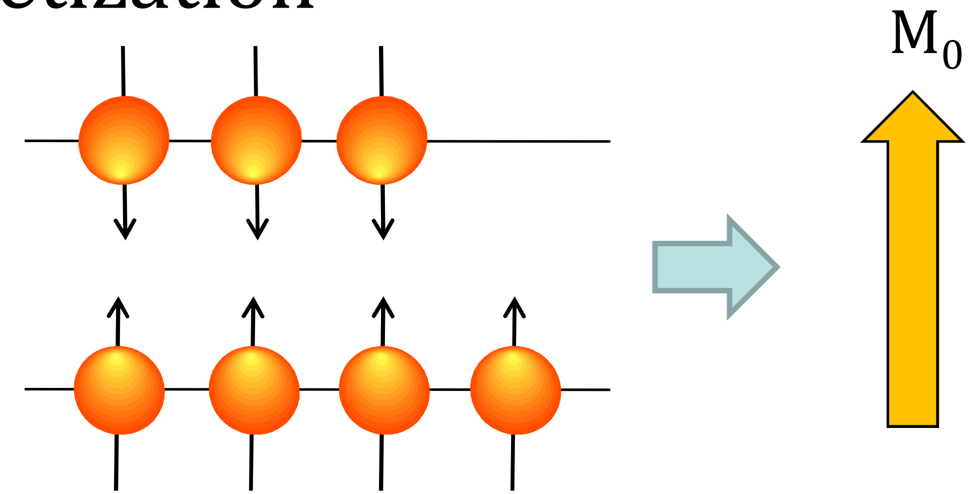

- The more spins, the stronger the magnetization

- Torque exerted on a magnet by a magnetic field:

$$\boldsymbol{\tau} = \frac{d\mathbf{M}}{dt} = \gamma \mathbf{M} \times \mathbf{B}$$

Bloch equations

$$\boldsymbol{\tau} = \frac{d\boldsymbol{M}}{dt} = \gamma \boldsymbol{M} \times \boldsymbol{B}$$

$$\Rightarrow \frac{dM_x}{dt} = \gamma B M_y \quad , \quad \frac{dM_y}{dt} = -\gamma B M_x \quad , \quad \frac{dM_z}{dt} = 0$$

$$\Rightarrow$$

$$M_x(t) = M_x^0 \cos(\omega_L t) \ , \ M_y(t) = M_y^0 \sin(\omega_L t)$$

$$M_z(t) = M_0$$

- $\omega_L = \gamma B$; *Larmor frequency*
- Set of equations describing a *precession* around the axis defined by ***B*** (z-axis)

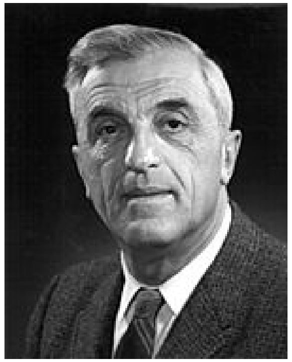

Felix Bloch

Joseph Larmor

Spin precession

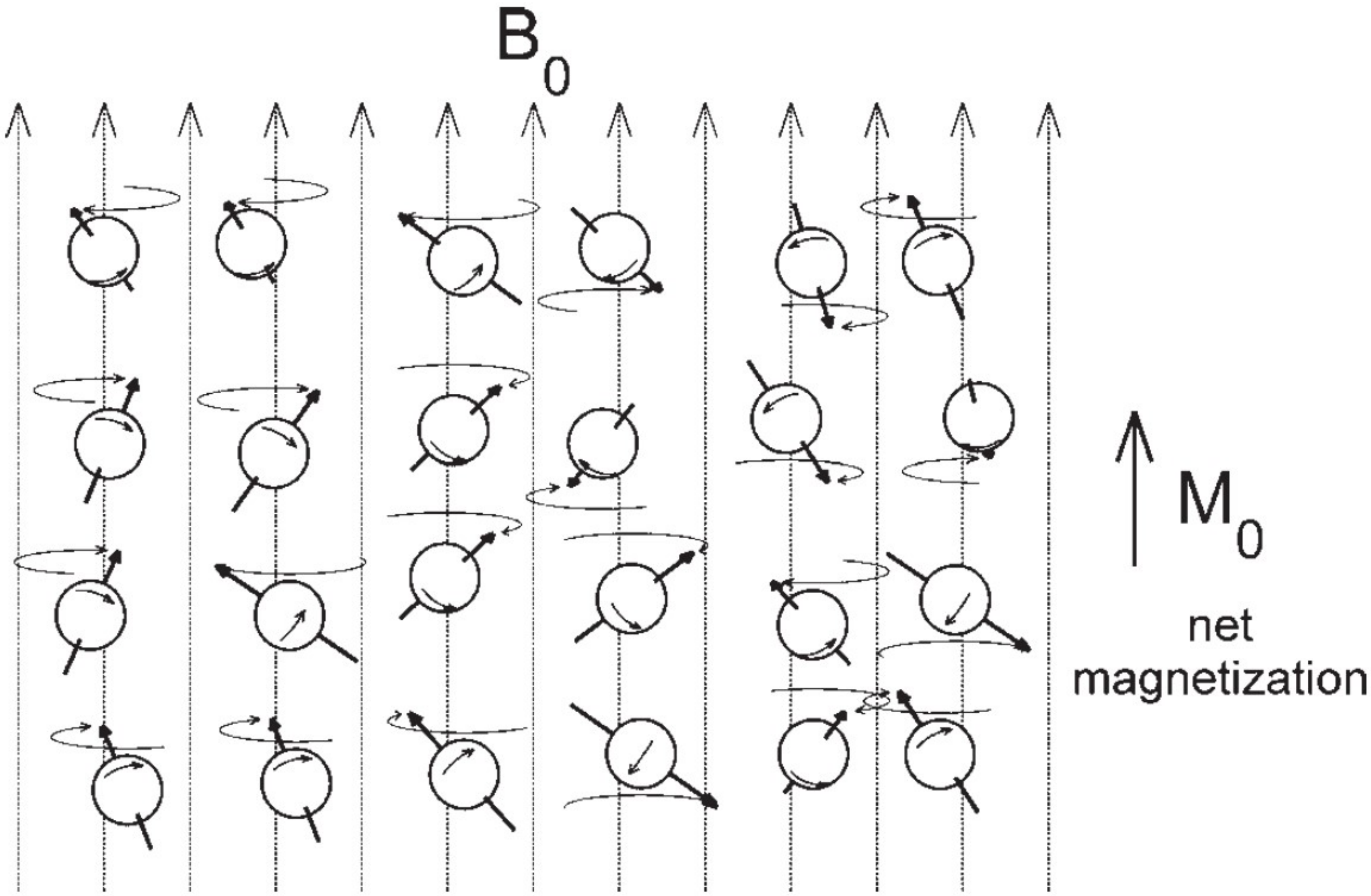

Spin precession

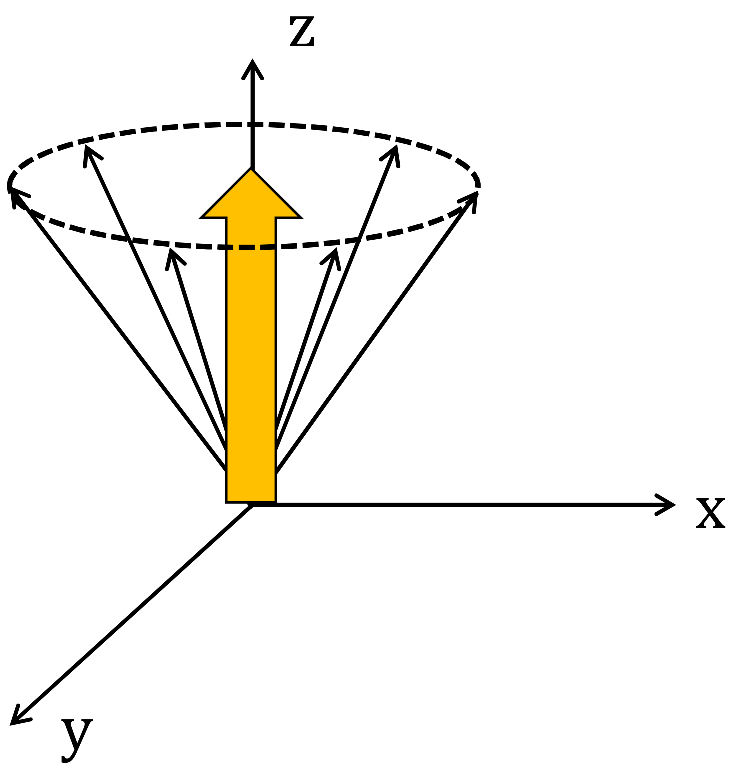

Spins out of phase

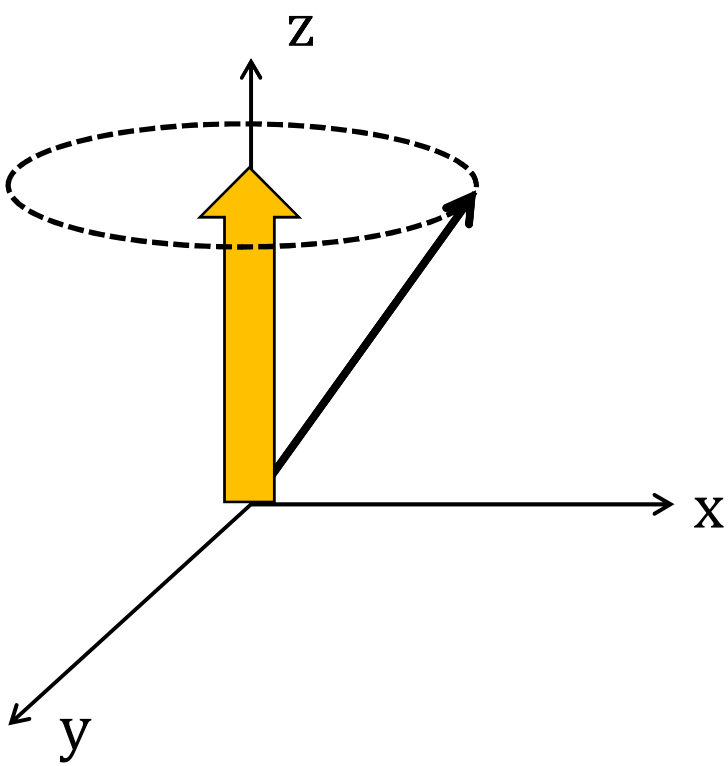

All spins in phase with same Larmor frequency

Introducing the RF field

- How can the magnetization be altered?
- Introduce oscillating (RF) magnetic field in the xy-plane

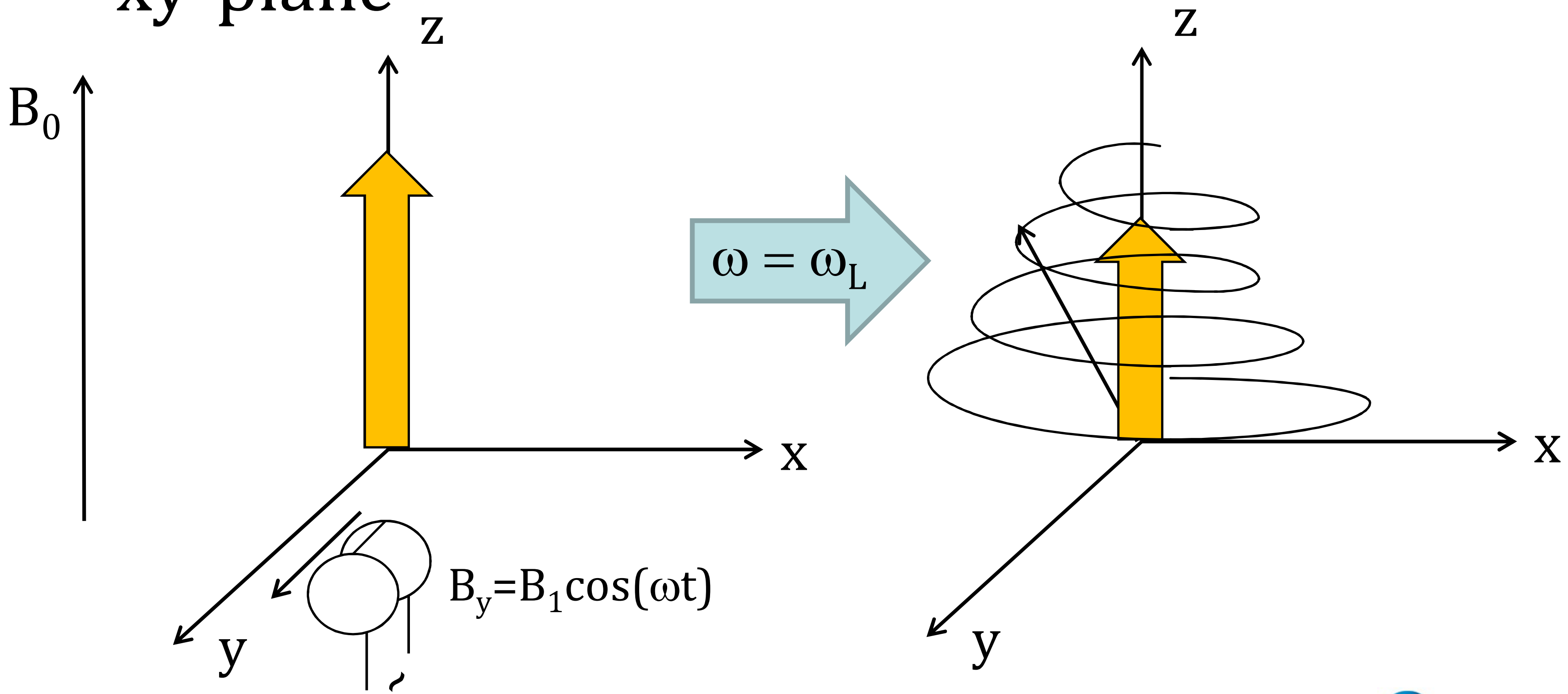

Flip angle

- The degree of which the magnetization is tipped relative to B_0 due to an excitation pulse
- From Bloch's considerations:

$$\theta = 2\pi\gamma\tau B_1$$

- t: duration of pulse
- B1: ~RF power

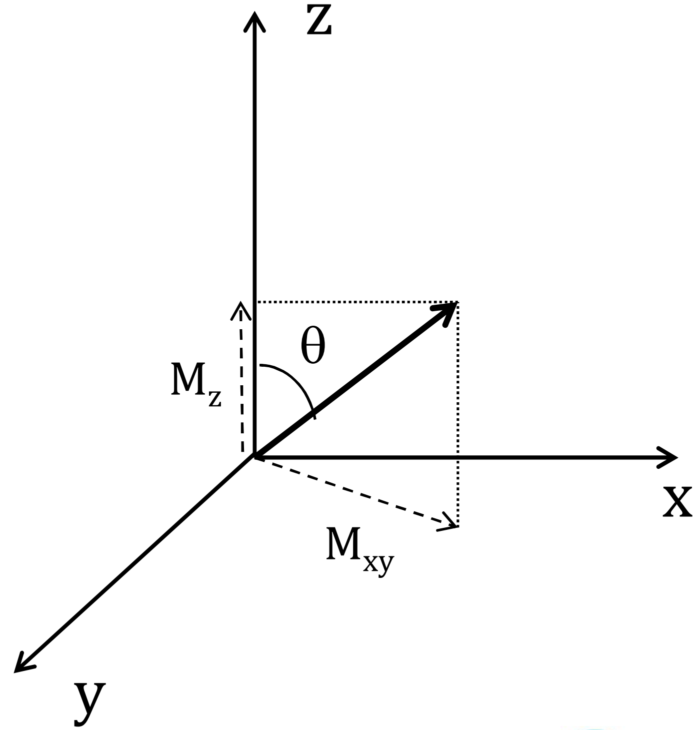

T1 relaxation

- Fluctuating magnetic fields from the molecular environment may have Larmor frequency→ stimulated transitions may occur
- After an RF-pulse, the z-component of M relaxes back to equilibrium via such stimulated transitions
- Longitudinal relaxation, Spin lattice relaxation, T1 relaxation
- Rate of relaxation: R1=1/T1

↑ Varies between tissues

T2 relaxation

- The *transverse* component of the magnetization also decays
- Local, microscopic field inhomogeneities causes each spin to precess with a frequency slightly different from ω_L
- An excitation pulse initially causes all spins to precess in phase, but a dephasing then occurs
- transverse- or spin-spin relaxation; T2
- T2<T1

T2 relaxation cont'd

- However, transverse relaxation is also caused by B_0 inhomogeneities and tissue magnetic susceptibility
- Actual T2 time is denoted T2*:

$$\frac{1}{T2^*} = \frac{1}{T2} + \gamma \Delta B_0$$

- T2*<T2

Relaxation

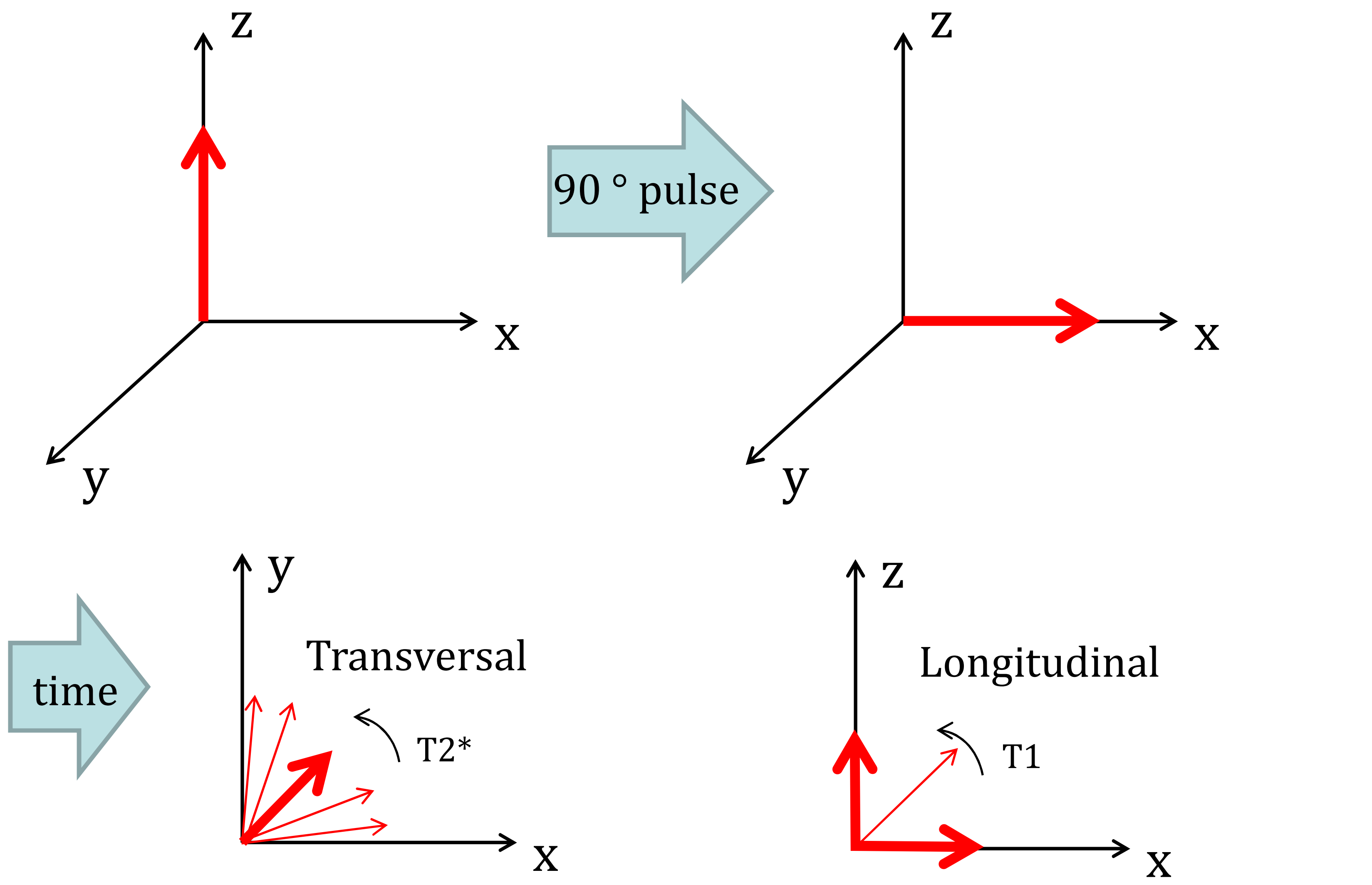

Relaxation – 90° pulse and T1

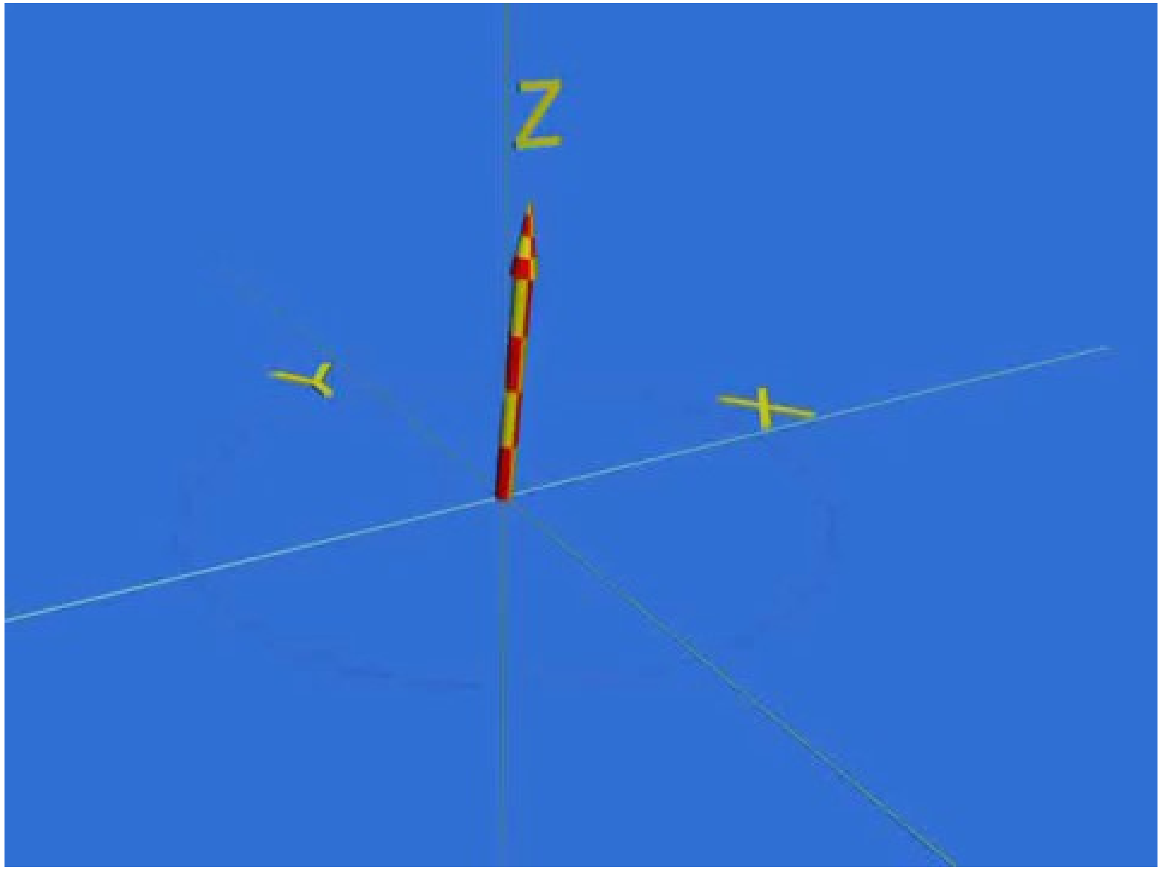

Relaxation - 90° pulse and T2

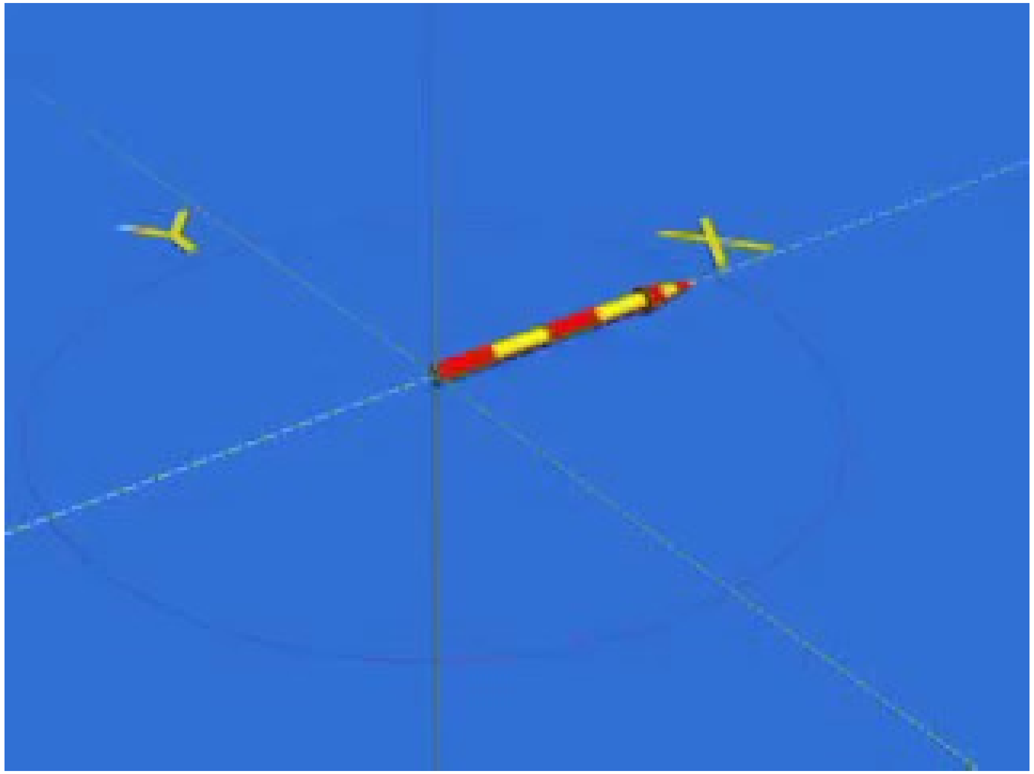

Relaxation dynamics

- Bloch's equations expanded with relaxation components; $M_{xy}/T2^*$ and $(M_z-M_0)/T1$
- May be shown that:

$$M_z(t) = M_0(1 - e^{-t/T1})$$

$$t = T1 \Rightarrow M_z = 0.63 M_{z,\infty}$$

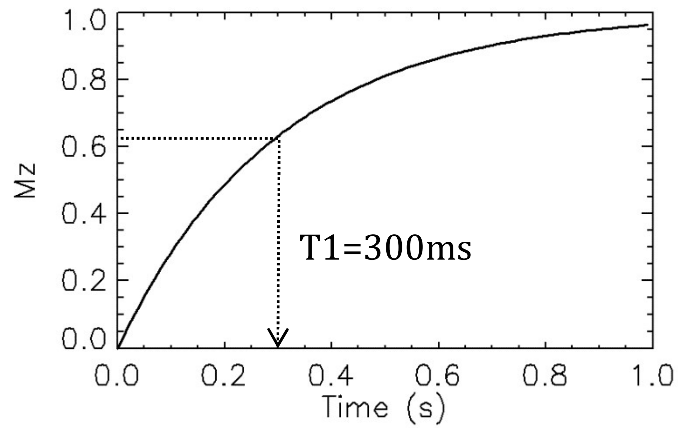

$$M_{xy}(t) = M_{xy,0} e^{-t/T2^*}$$

$$t = T2^* \Rightarrow M_{xy} = 0.37 M_{xy,0}$$

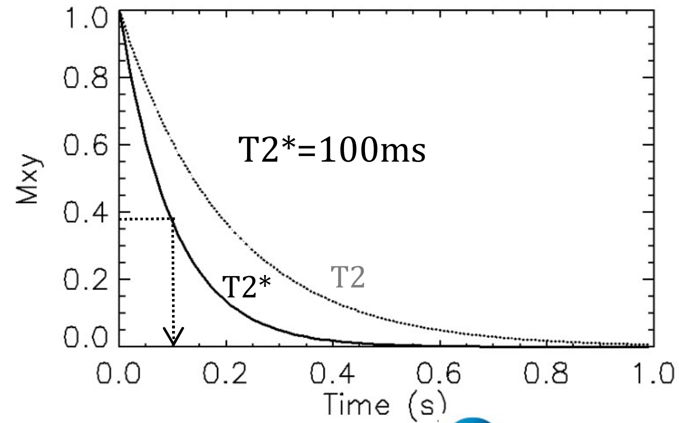

Relaxation times

Tissue	T1 (msec)	T2 (msec)
Water/CSF	4000	2000
Gray matter	900	90
Muscle	900	50
Liver	500	40
Fat	250	70
Tendon	400	5
Proteins	250	0.1- 1.0
Ice	5000	0.001

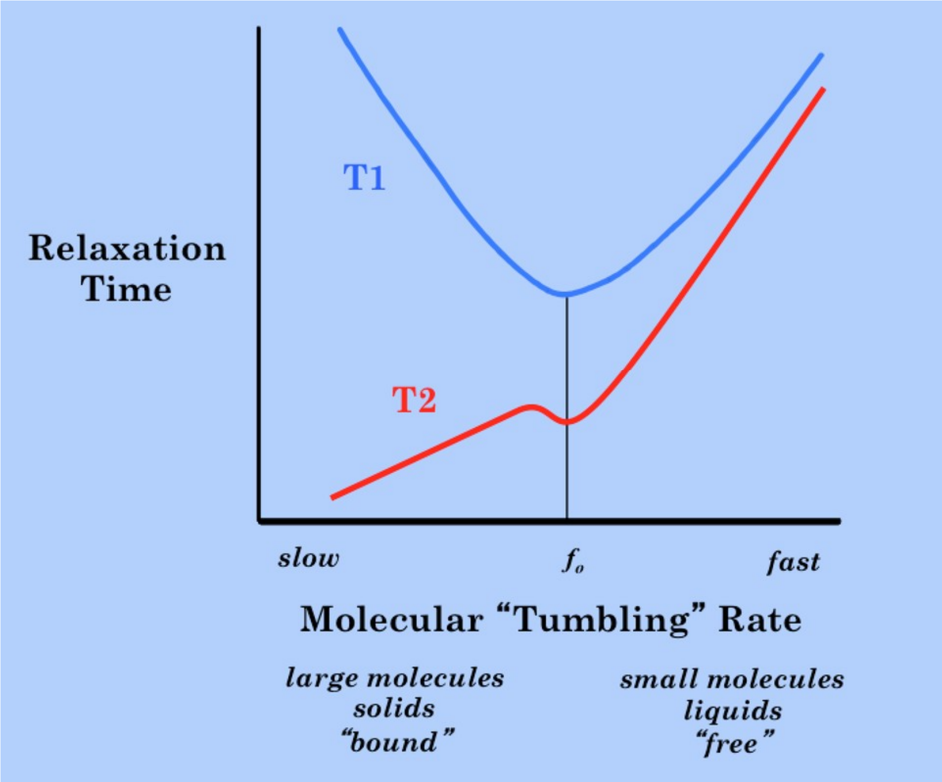

Relaxation dynamics and contrast

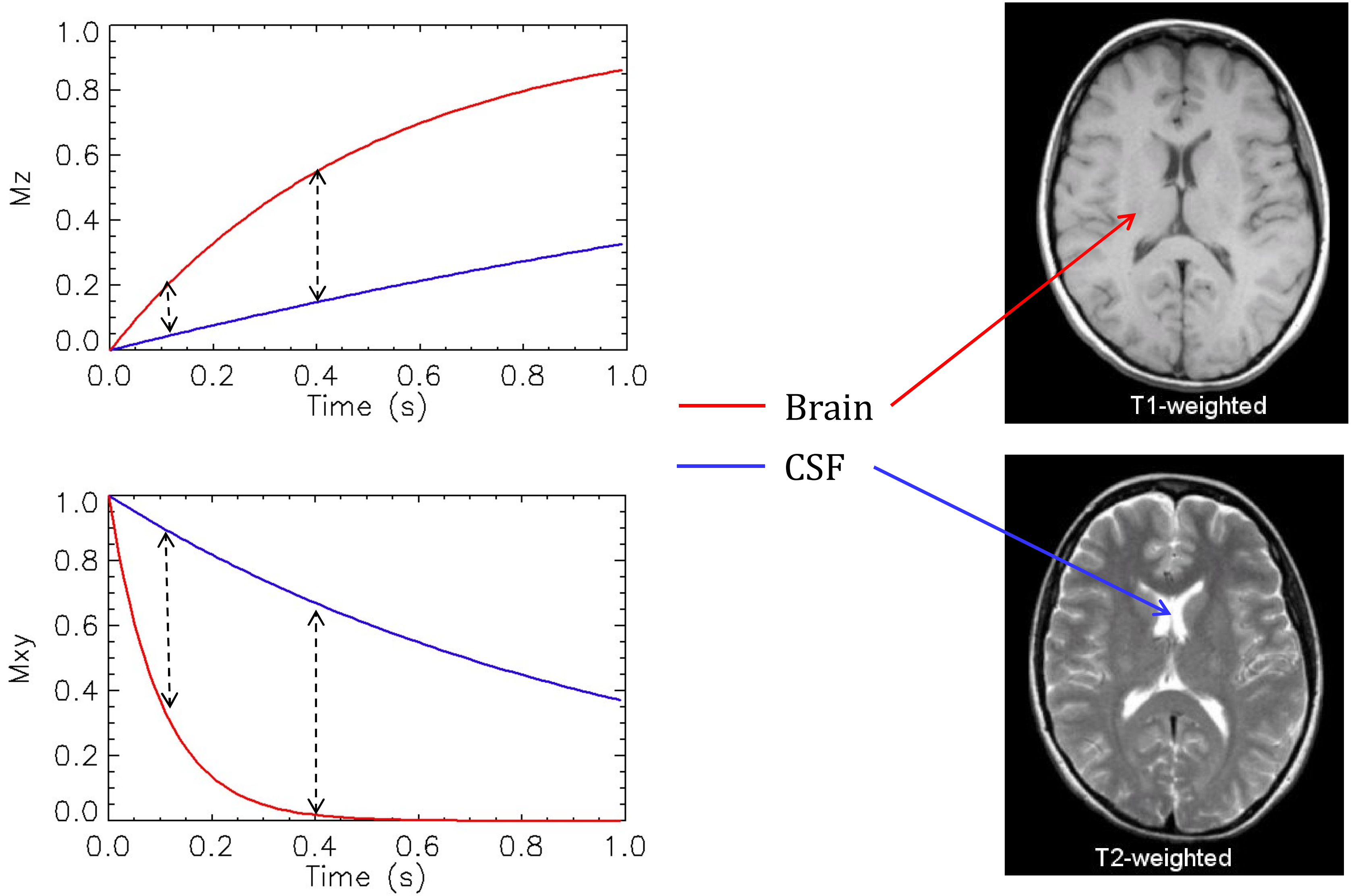

Detection

- Changes in magnetization give rise to a current in a wire loop (Faraday's law of induction)
- Receiver coil perpendicular to B_0:

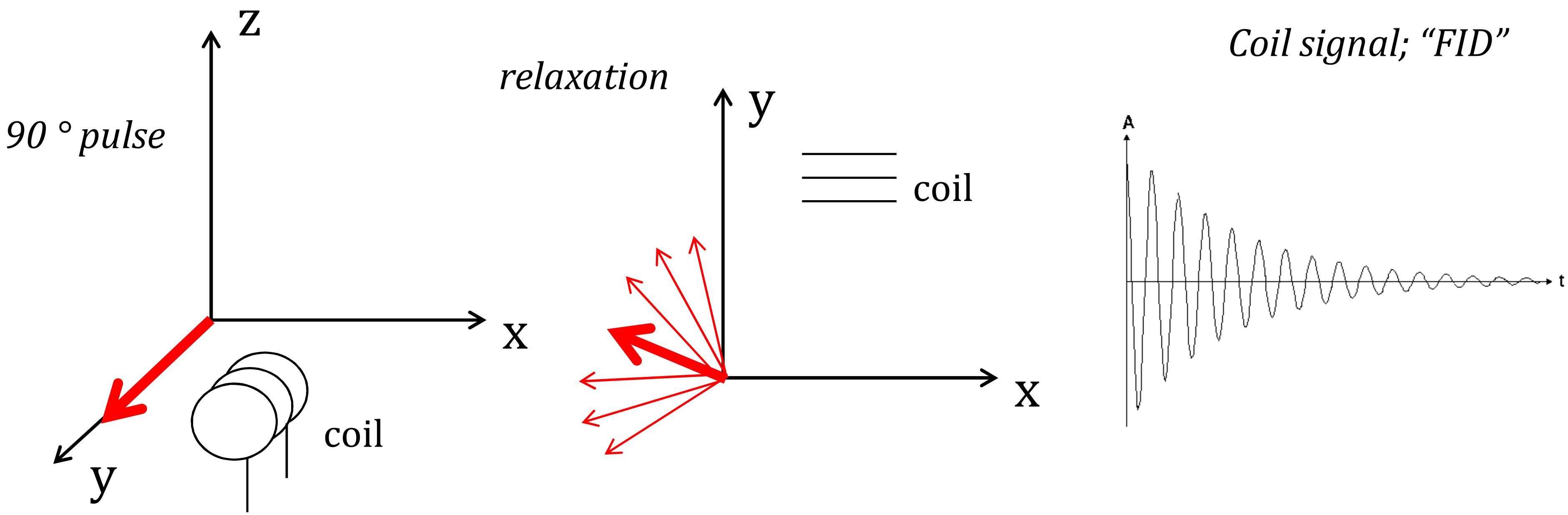

Free induction decay

- Envelope of FID describes the T2*-decay:

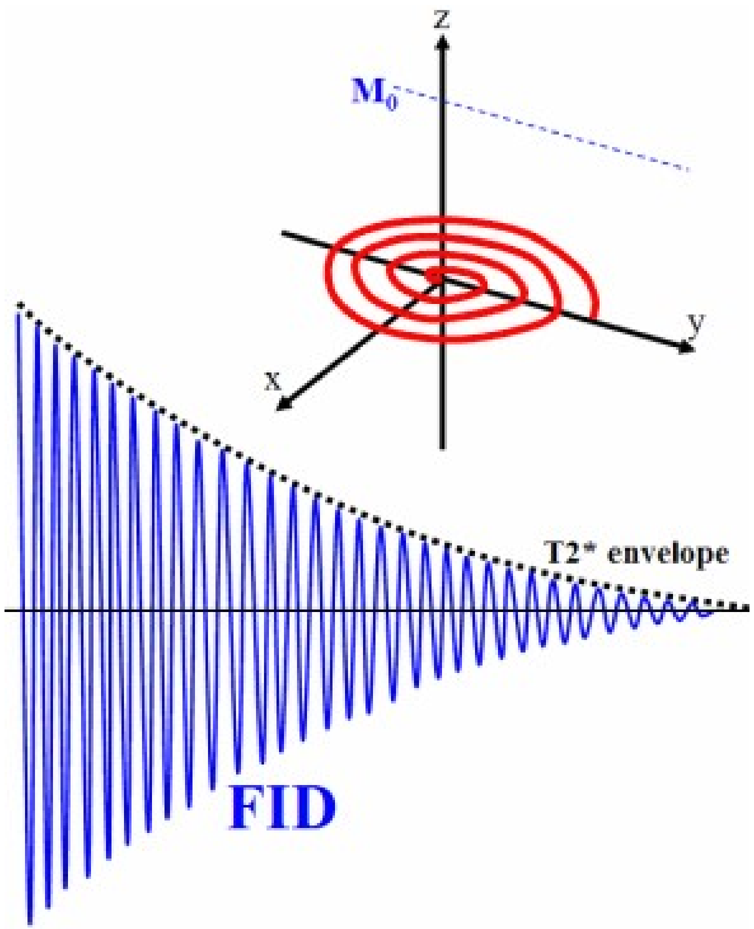

Fourier transform

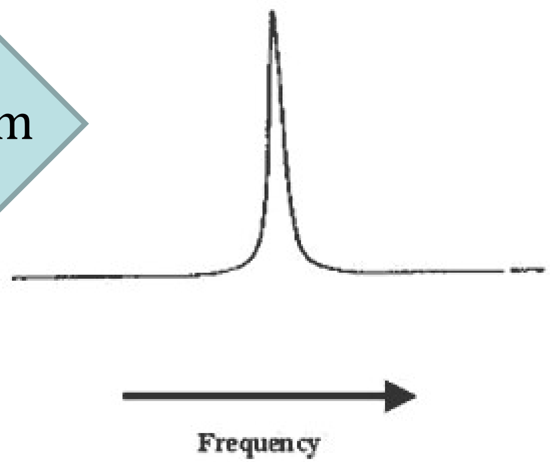

Summary

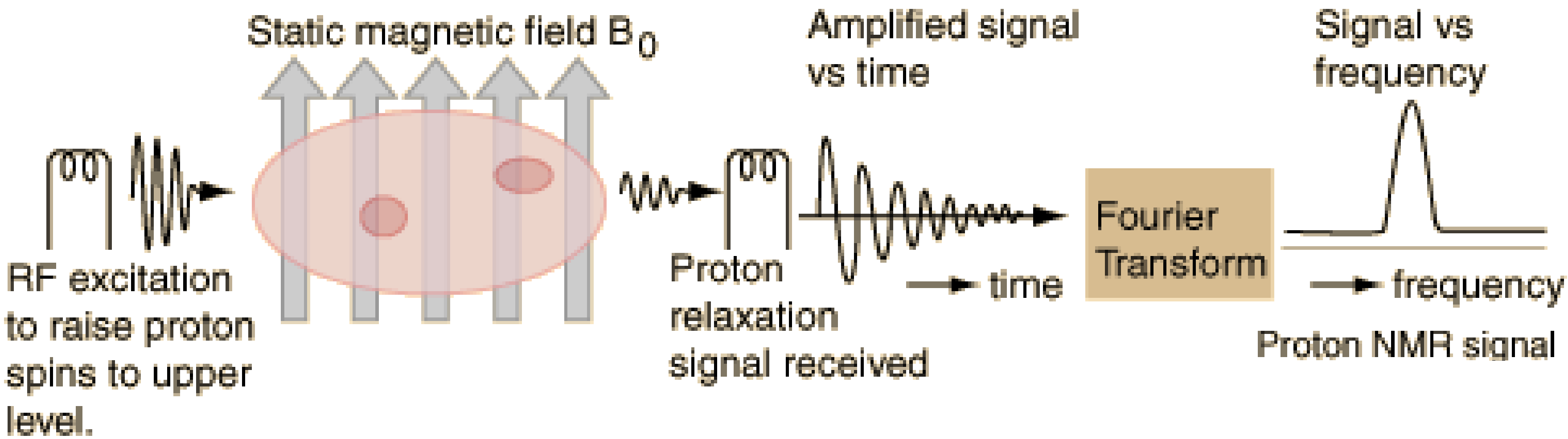

Static magnetic field B_0
Amplified signal vs time
Signal vs frequency
RF excitation to raise proton spins to upper level.
Proton relaxation signal received
time
Fourier Transform
frequency
Proton NMR signal

VÄSTERBOTTENS LÄNS LANDSTING

MRI physics: Contrast formation

Tufve Nyholm

UMEÅ UNIVERSITET

Precession

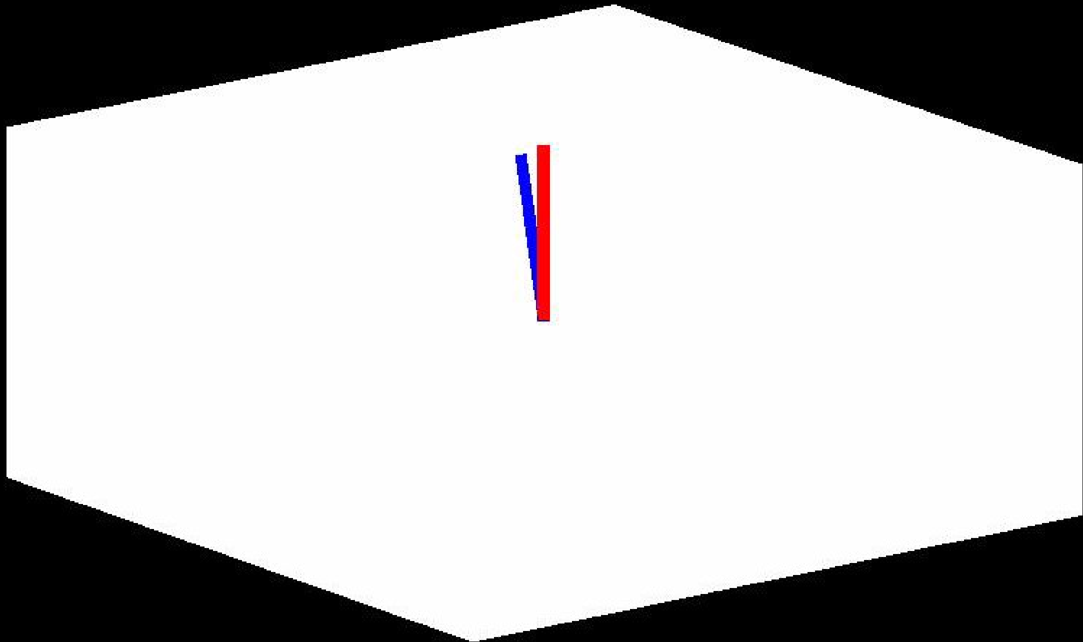

Spin's precession around the local magnetic field:

Larmor frequency

$$\omega = -\gamma B$$

42.576 MHz/T (γ)

Magnetic field (B)

Flip

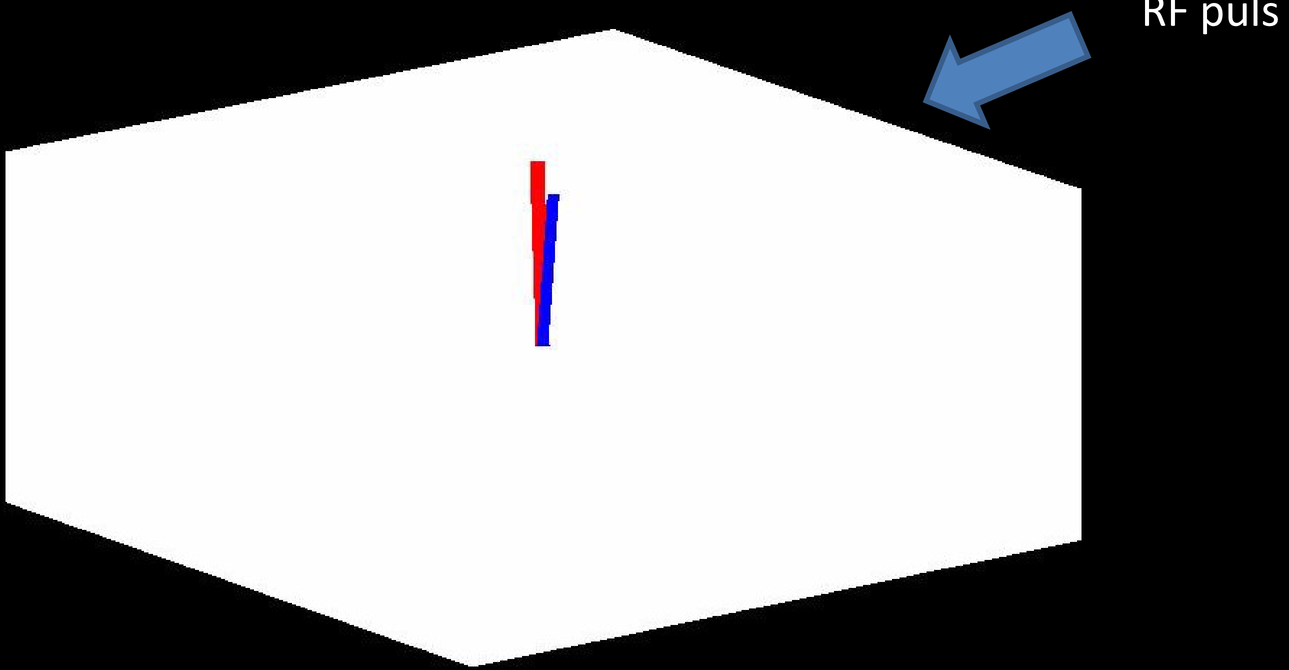

Spin's precession around the local magnetic field:

Larmor frequency

$$\omega = -\gamma B$$

42.576 MHz/T

Magnetic field

Relaxation

T1 relaxation
Parallel plane

Rotating coordiante system

T2 relaxation
Transversial plane

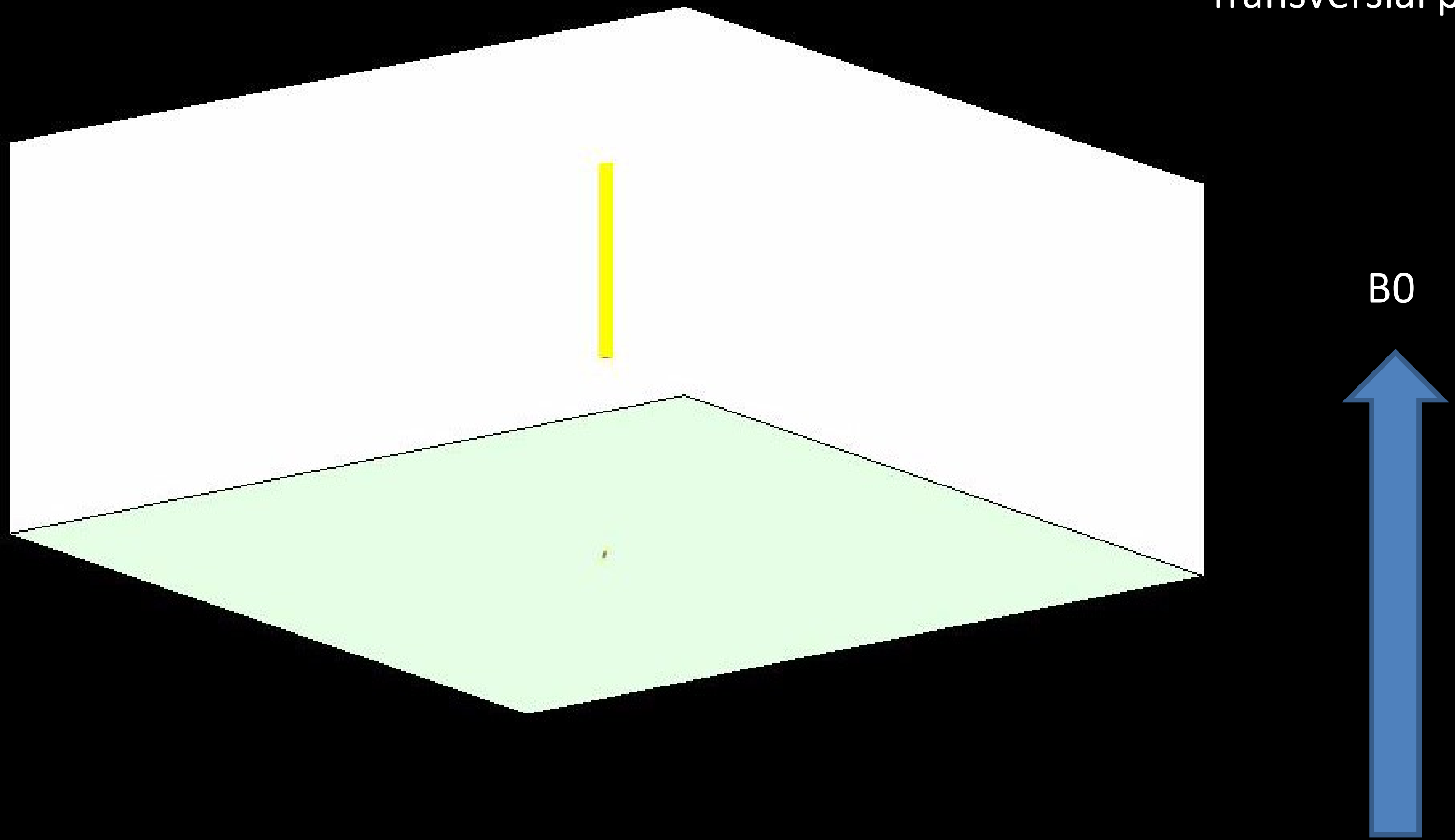

The transversal component gives signal

T1 relaxation

- Spin-lattice or longitudinal relaxation
- Restoring longitudinal magnetization after RF excitation
- T1 – Time until 63% of the initial magnetization M0 is restored

Adipose tissue – 240ms
Spinal fluid – 4300ms
Gray matter – 980ms
White matter – 780ms
Muscles – 880ms

Larmor frequency

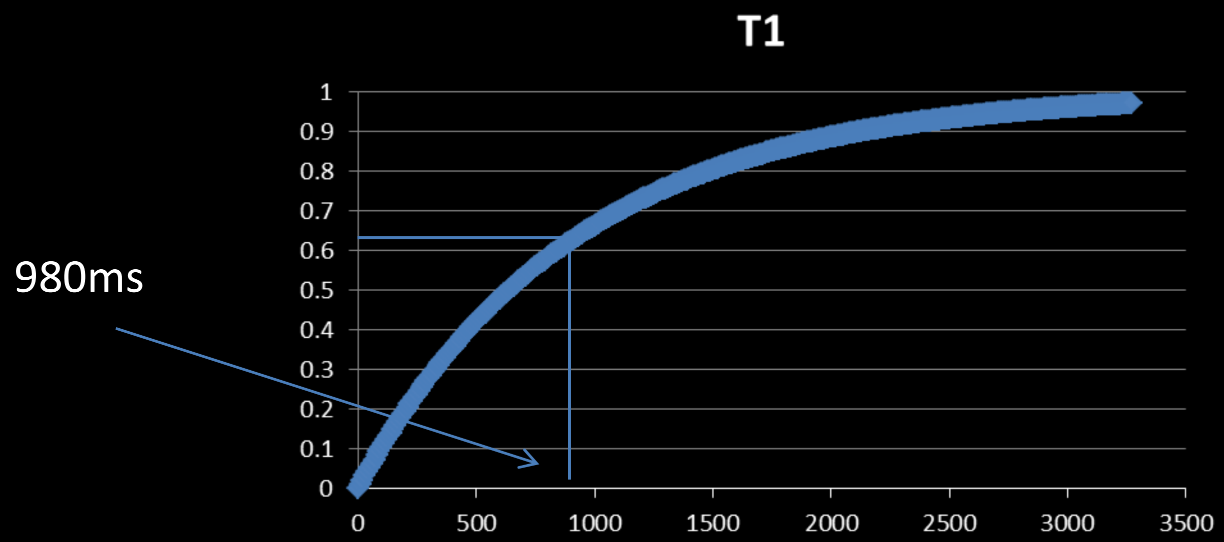

T2 relaxation

- Spin-spin or transversial relaxation
- Loss of transversial magnetization after RF excitation
- T2 – time until 63% of the transversal magnetization is lost

Adipose tissue – 70ms
Spinal fluid – 2200ms
Gray matter – 100ms
White matter – 90ms
Muscles – 50ms

$$M(t)_r = M_{r,t=0}e^{-t/T2}$$

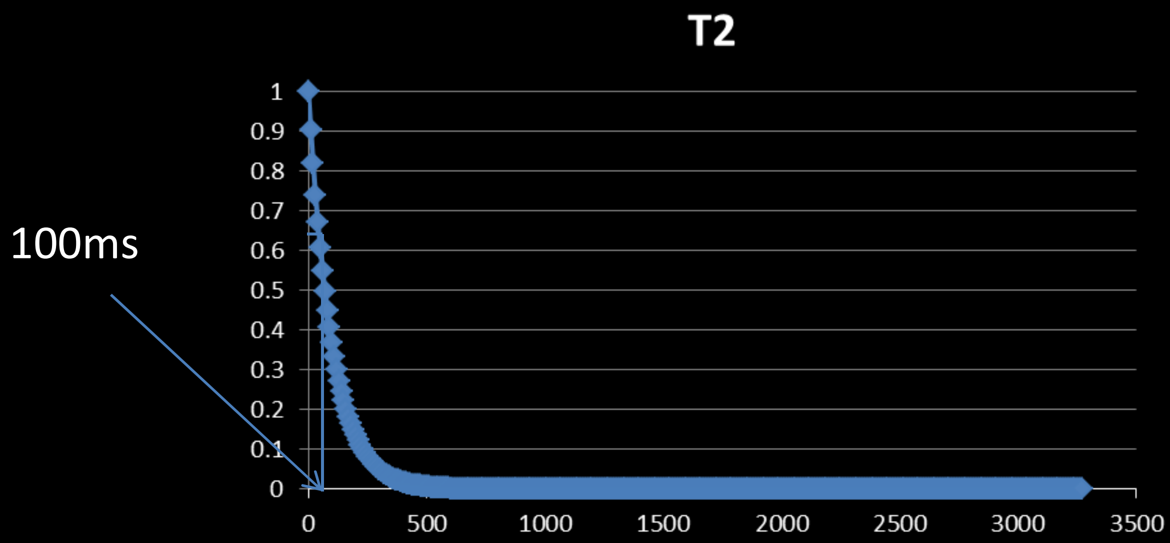

T2* relaxation

$$M(t)_r = M_{r,t=0} e^{-t/T2^*}$$

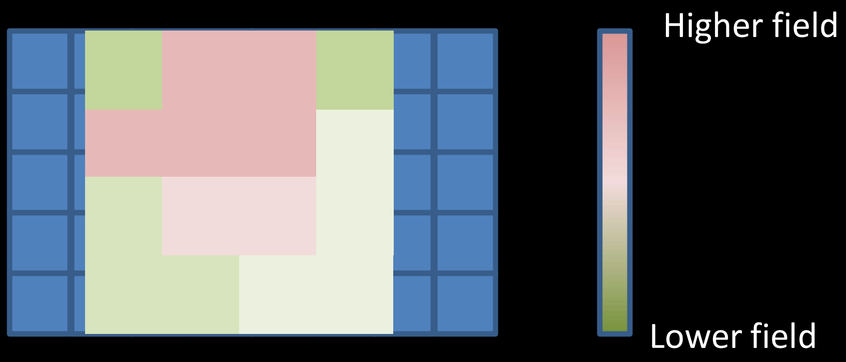

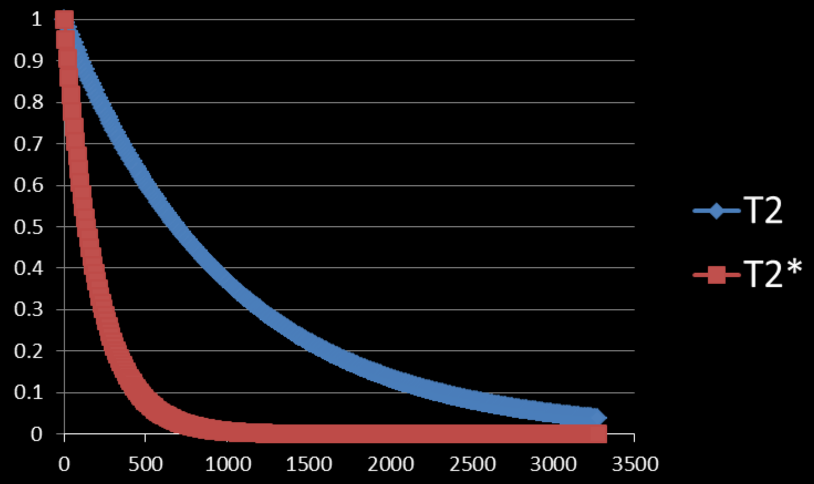

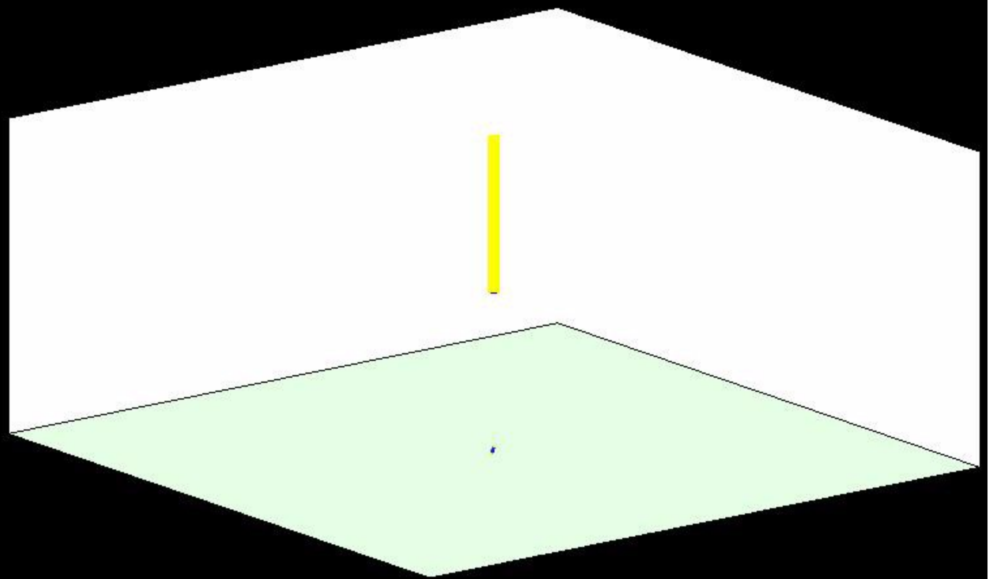

Spin-Echo sequence

- 180 degree pulse refocus the spins
- Signal independent of T2*

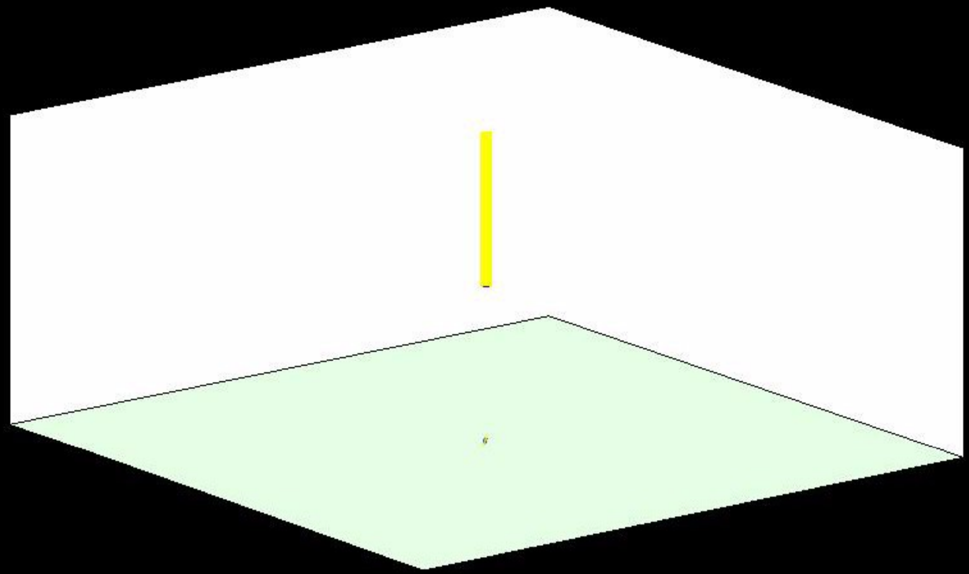

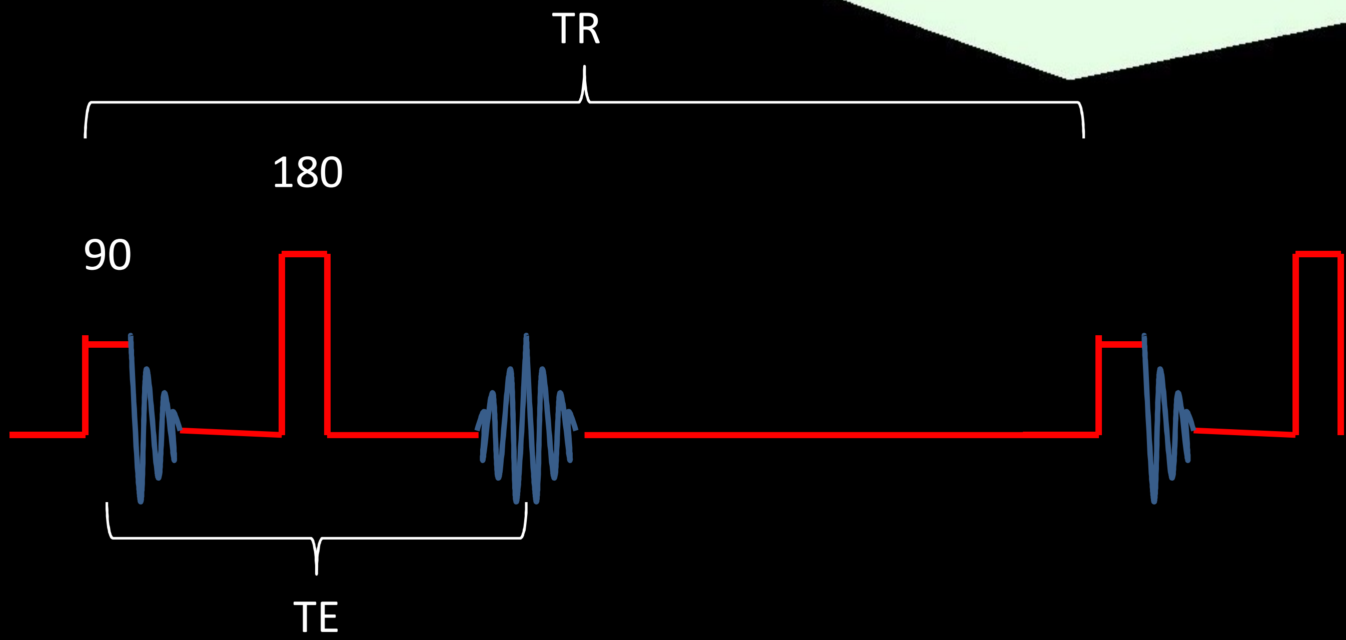

Spin-Echo sequence

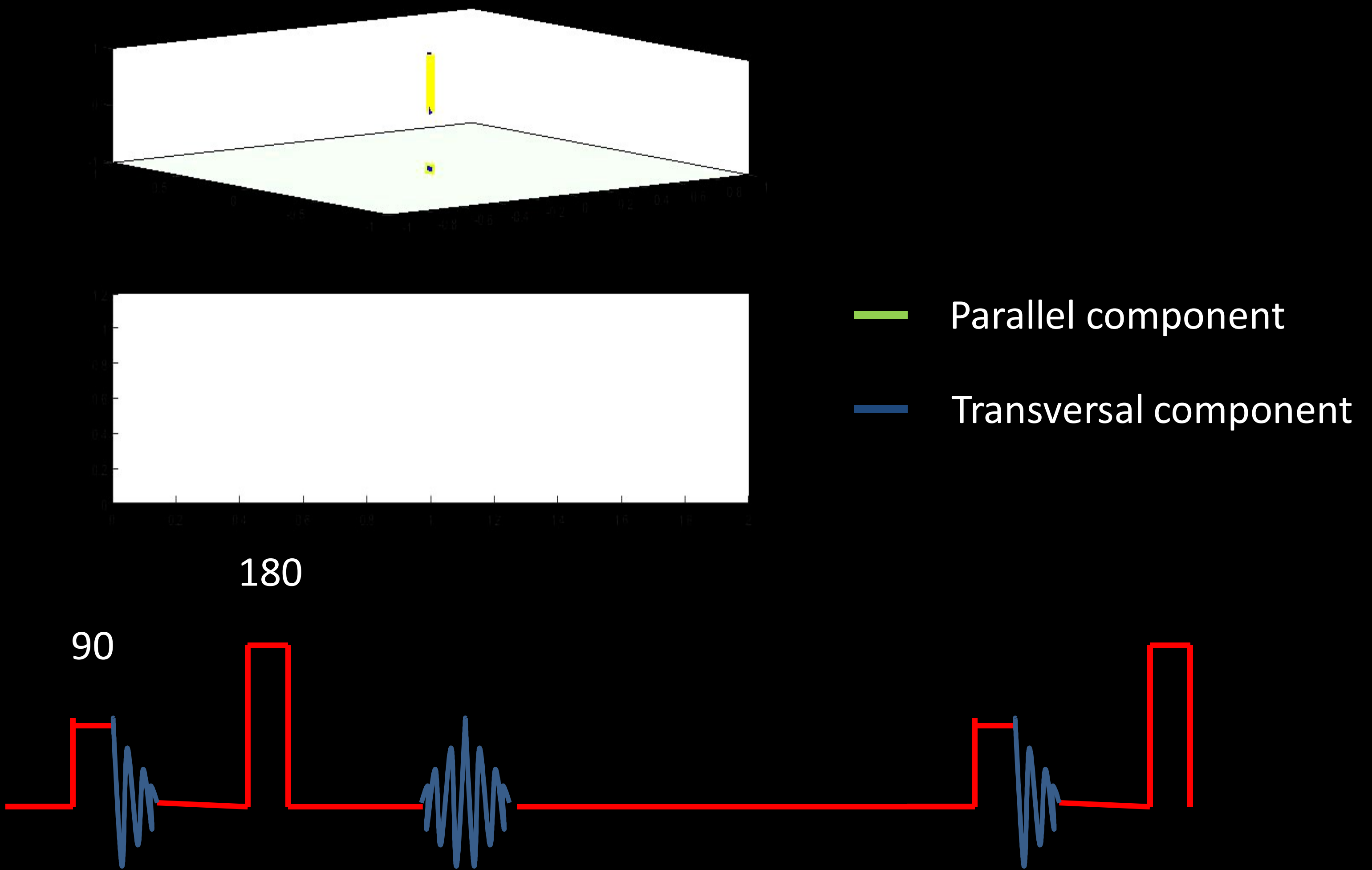

Spin-Echo sequence

T1 relaxation

$$M(t)_z = M_0\left[1 - e^{-t/T1}\right]$$

T2 relaxation

$$M(t)_r = M_{r,t=0}e^{-t/T2}$$

Signal equation

$$S = k\rho\left(1 - e^{-TR/T1}\right)e^{-TE/T2}$$

Constant depending on

- Coils
- Temperature
- etc

Proton density

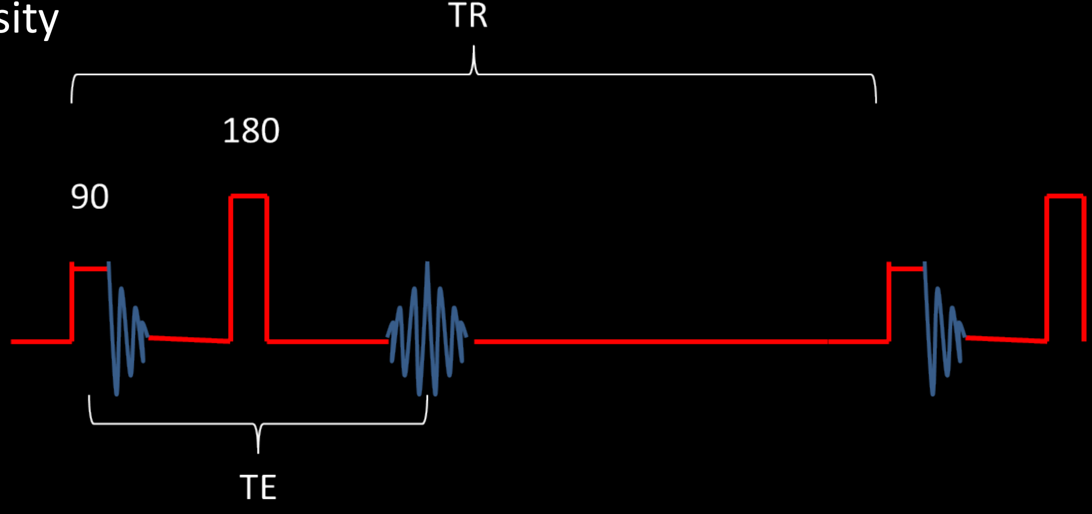

T2 contrast

$$S = k\rho\left(1 - e^{-TR/_{T1}}\right)e^{-TE/_{T2}}$$

Minimize influence i.e. Long TR

Focus

Transversal component

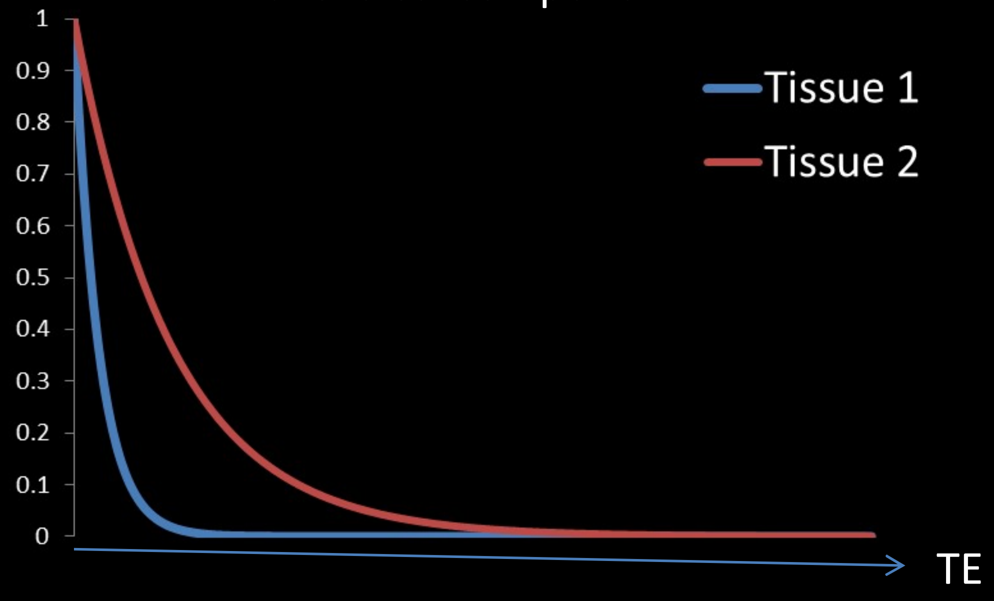

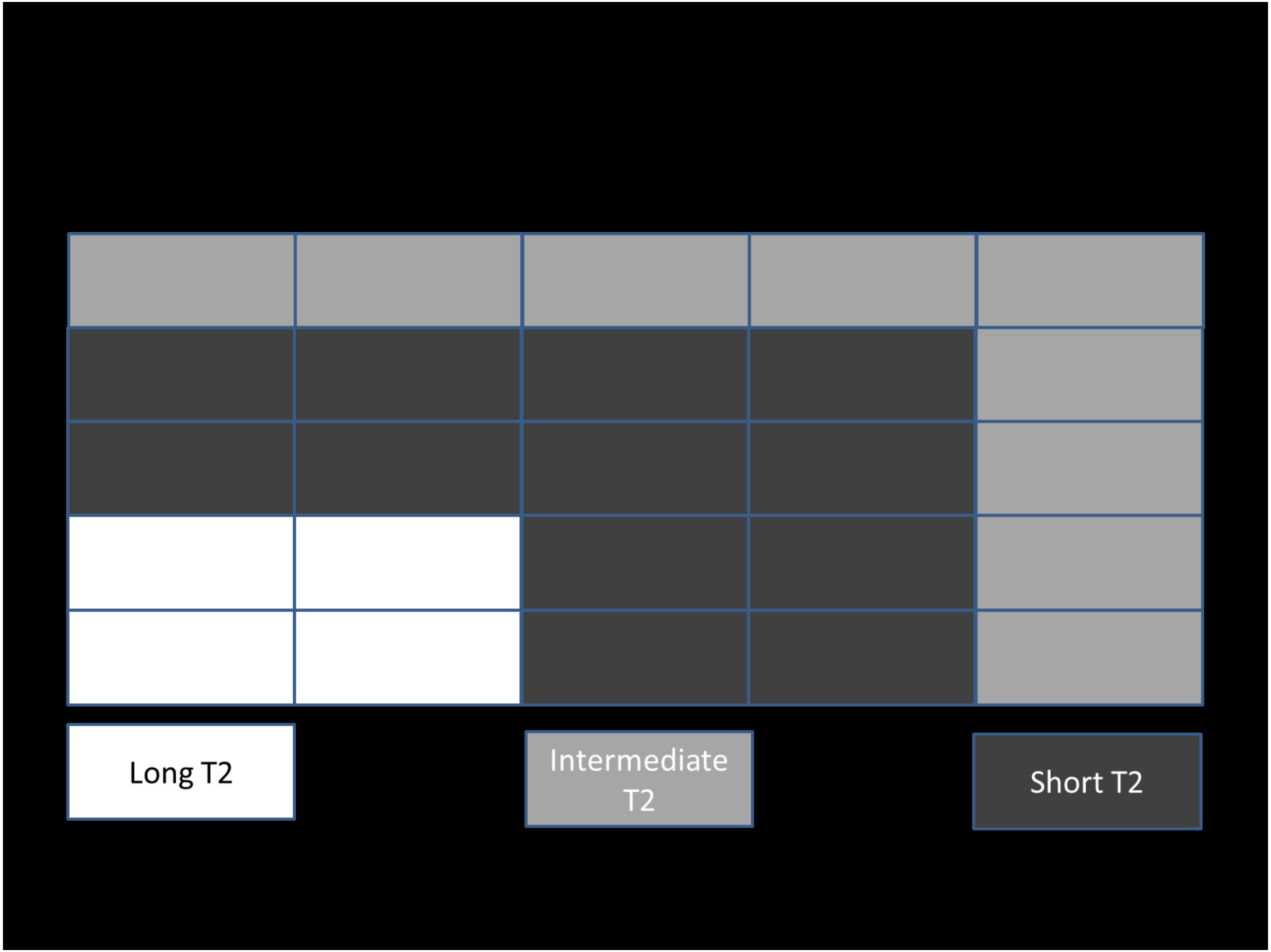
Long T2
Intermediate T2
Short T2

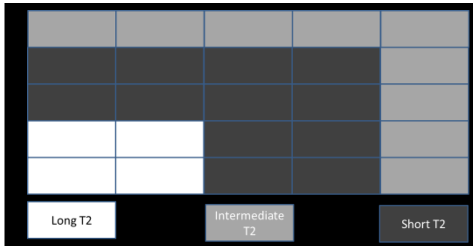

T2 contrast

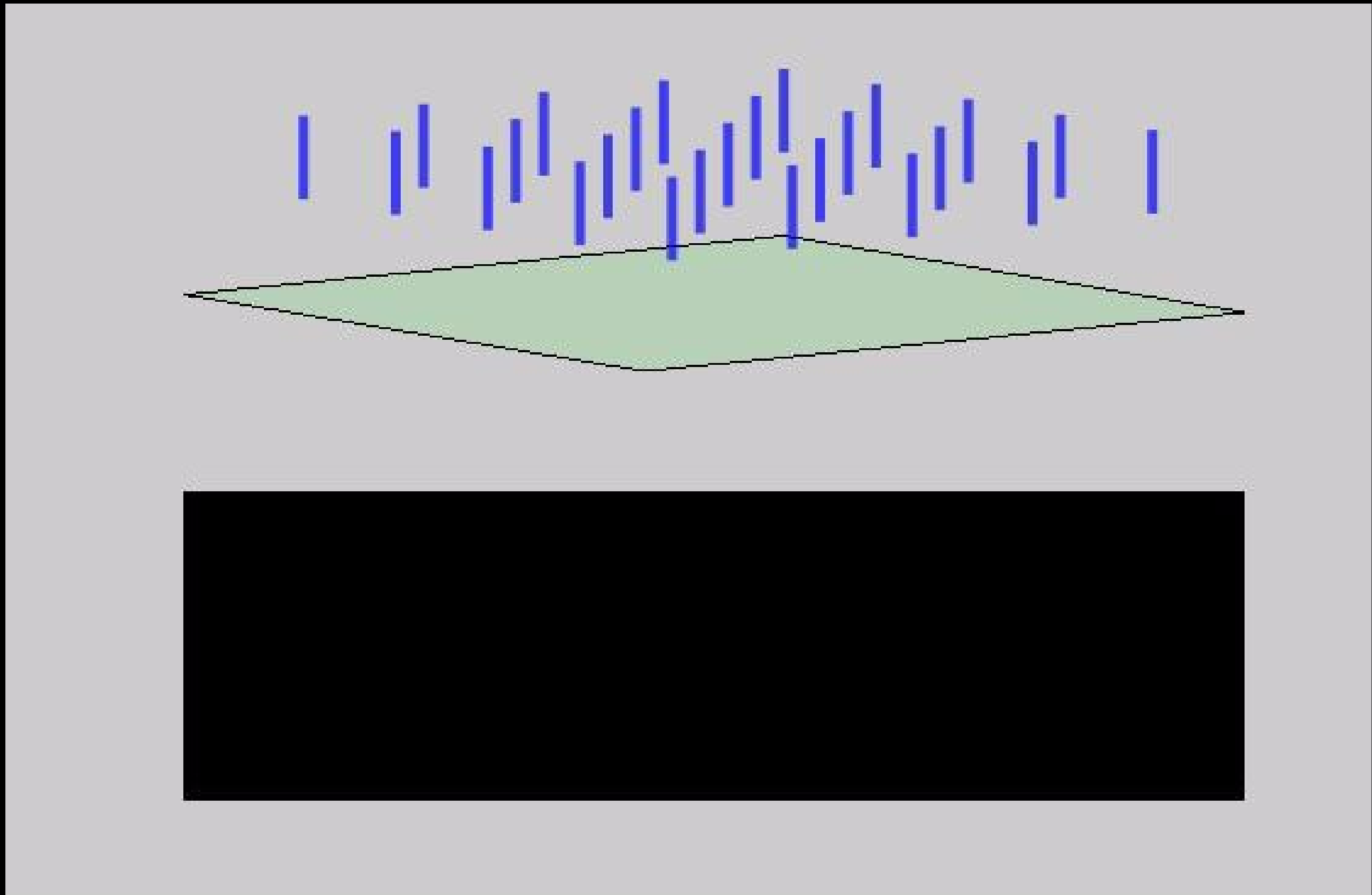

Examples
T2 Contrast

Adipose tissue – 70ms
Spinal fluid – 2200ms
Gray matter – 100ms
White matter – 90ms
Muscles – 50ms

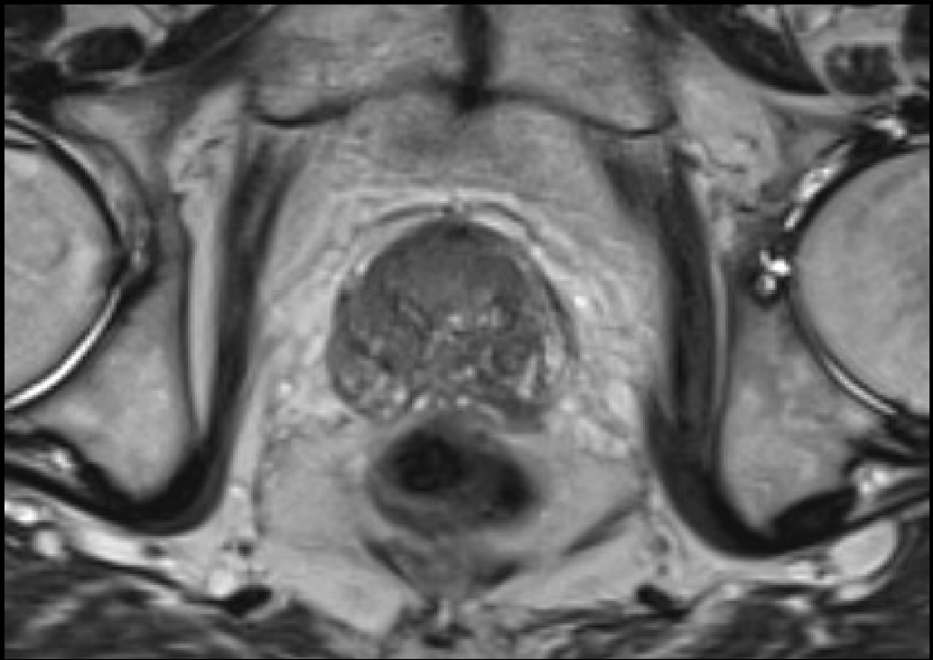

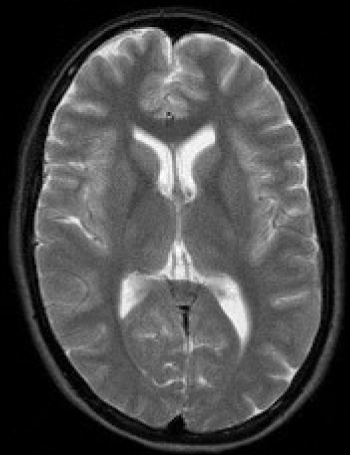

TE=90ms

T1 contrast

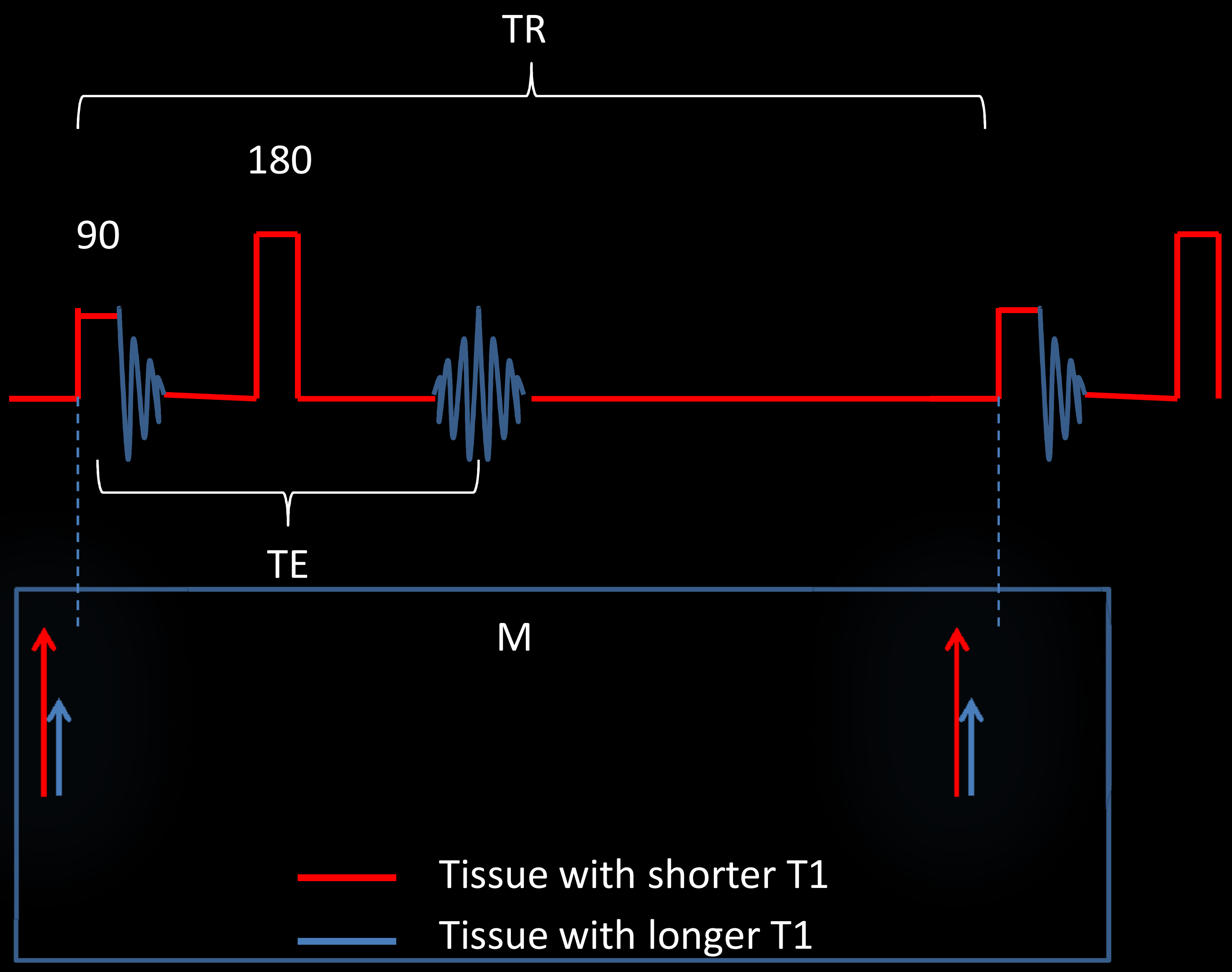

T1 contrast

Long T1

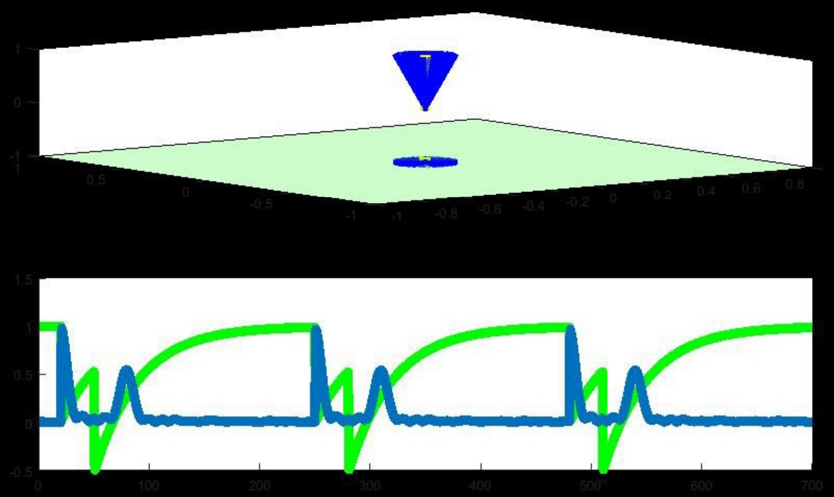

Short T1

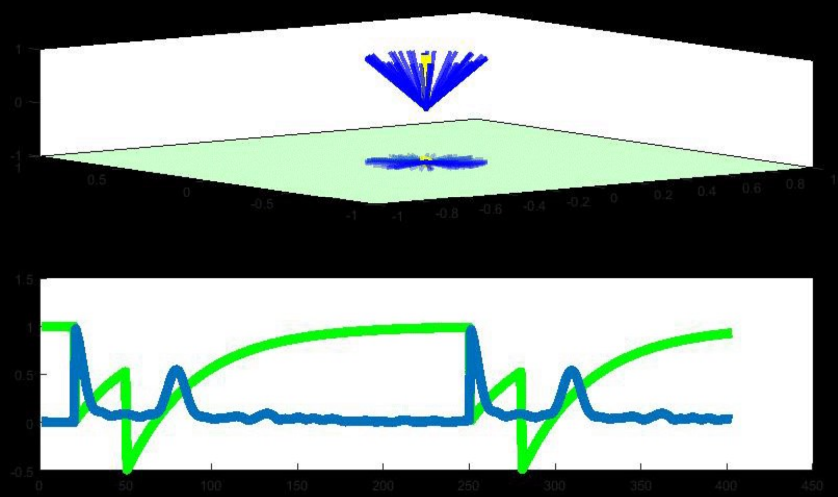

Parallel component

Transversal component

T1 Contrast

$$S = k\rho\left(1 - e^{-TR/T1}\right)e^{-TE/T2}$$

Focus

Minimize influence
i.e. Short TE

Parallel component

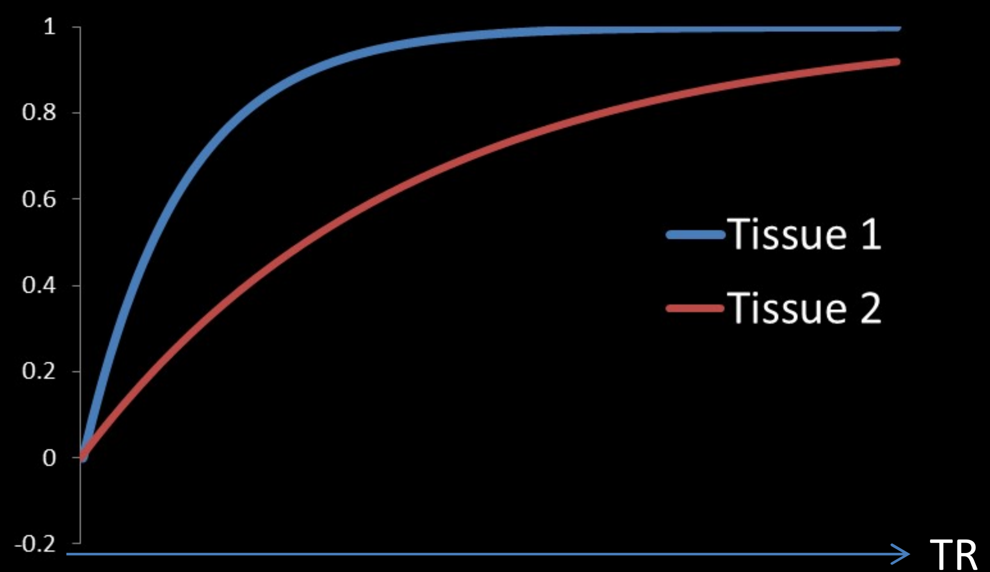

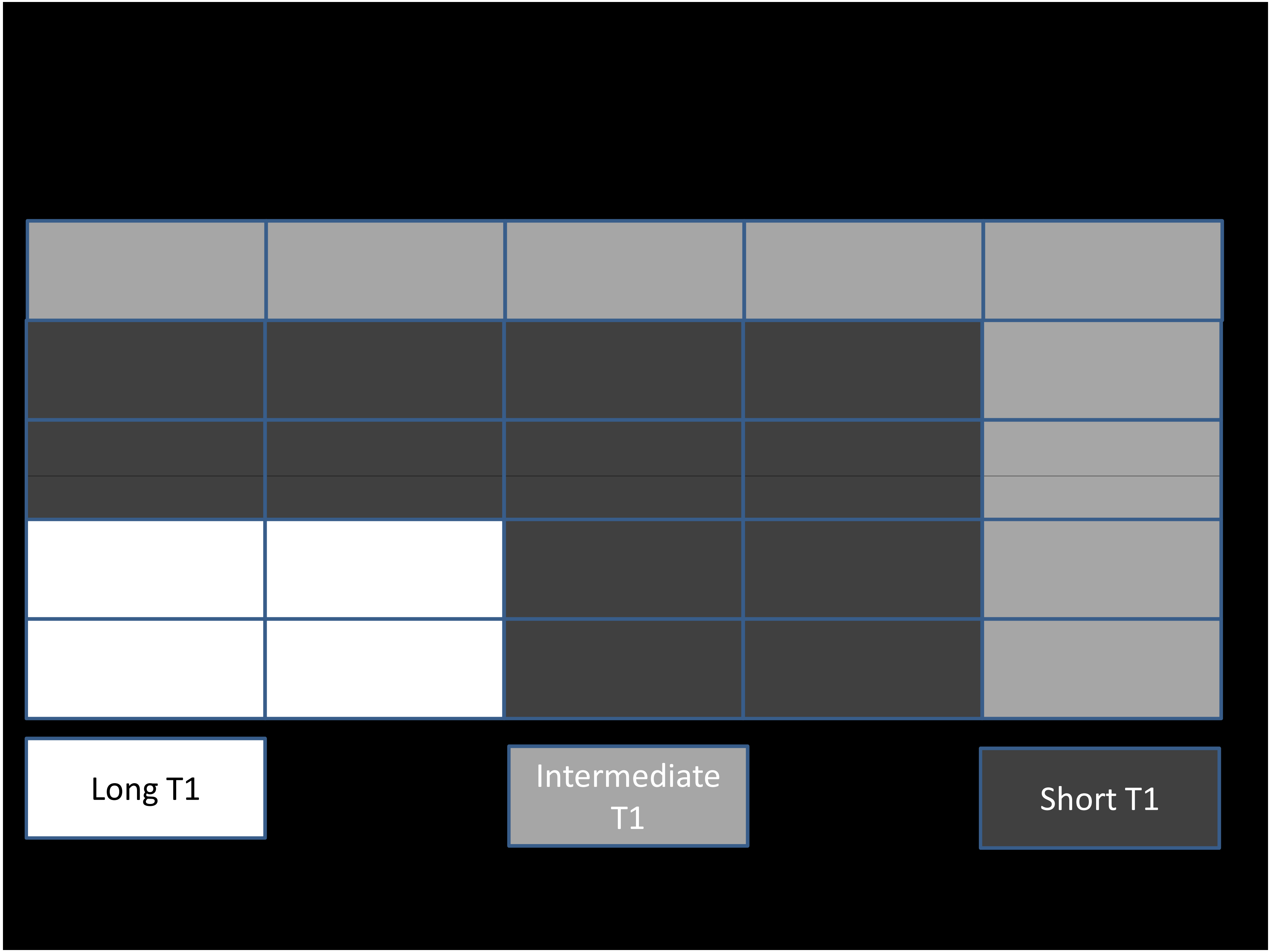
Long T1
Intermediate T1
Short T1

T1 contrast

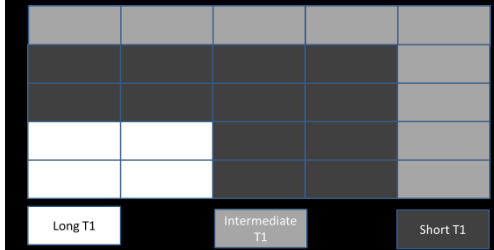

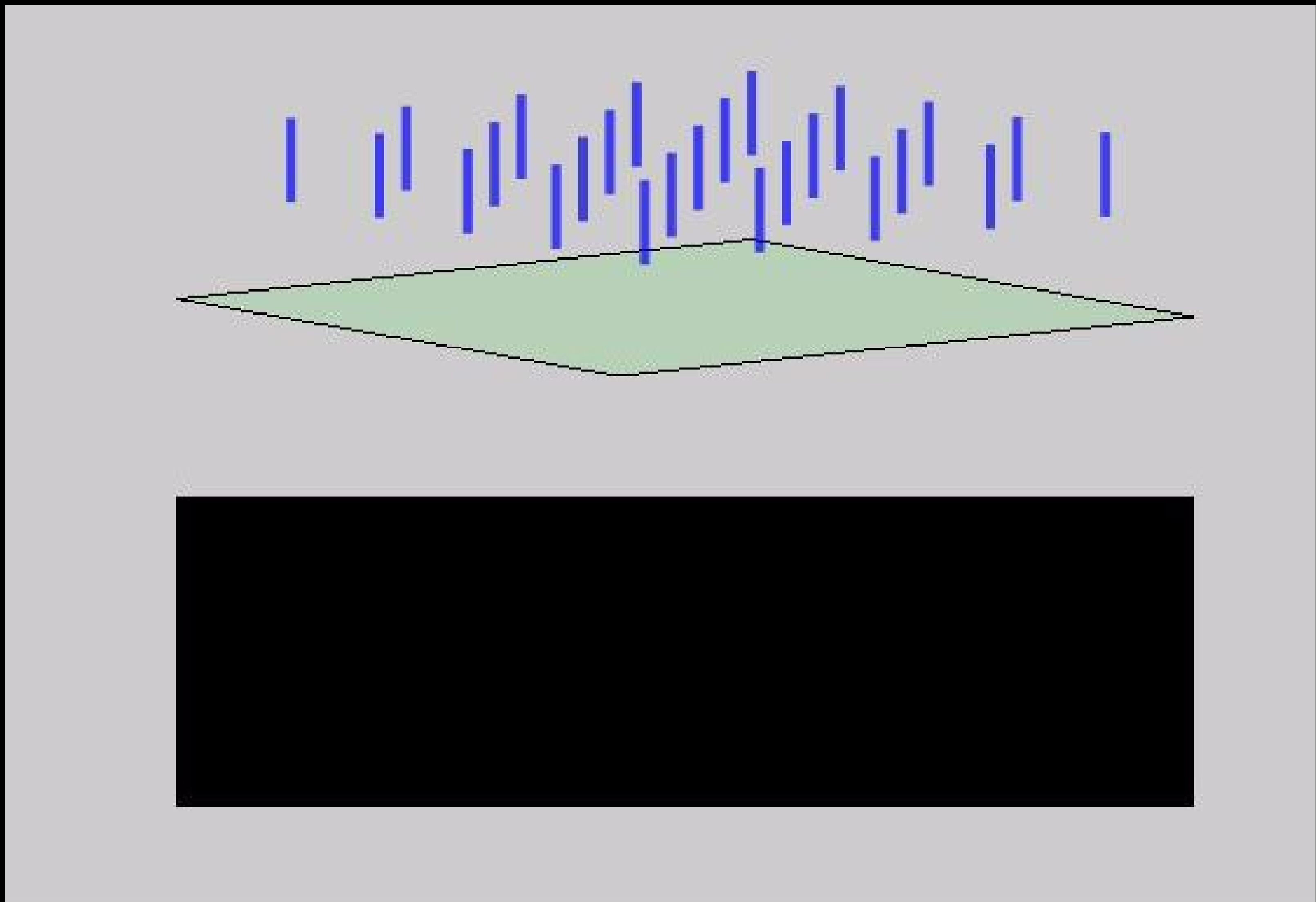

Examples

T1 contrast

Adipose tissue – 240ms
Spinal fluid – 4300ms
Gray matter – 980ms
White matter – 780ms
Muscles – 880ms

TR=450ms

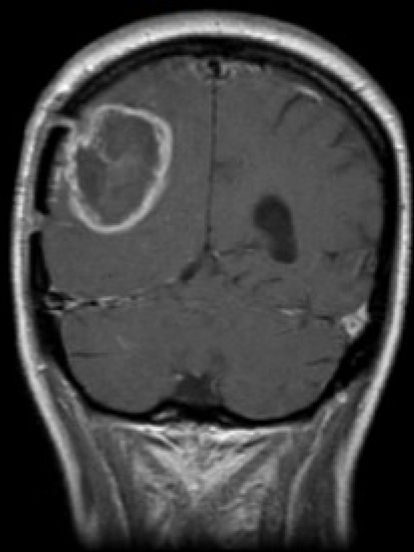

Inversion-recovery (IR)

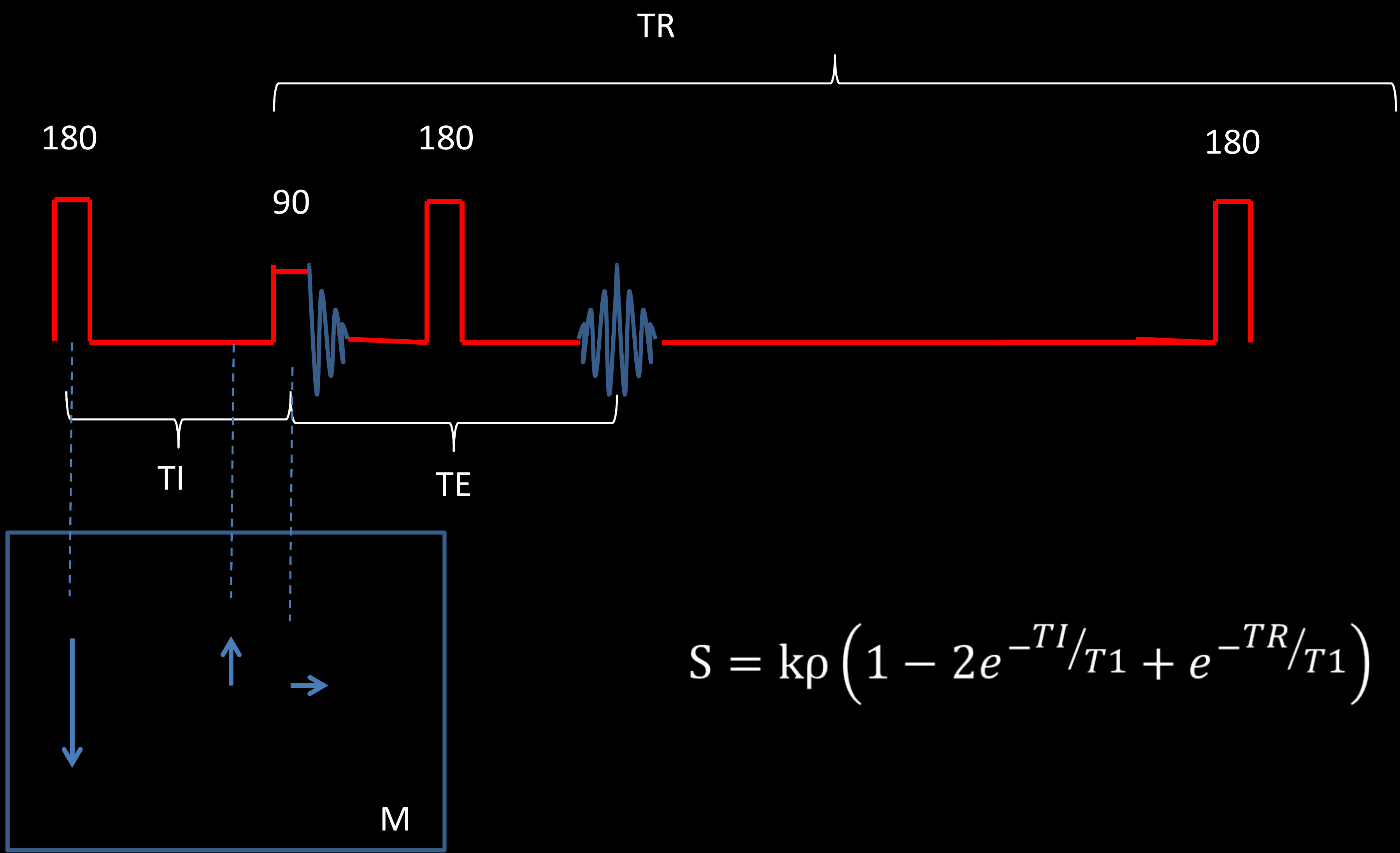

$$S = k\rho\left(1 - 2e^{-TI/T1} + e^{-TR/T1}\right)$$

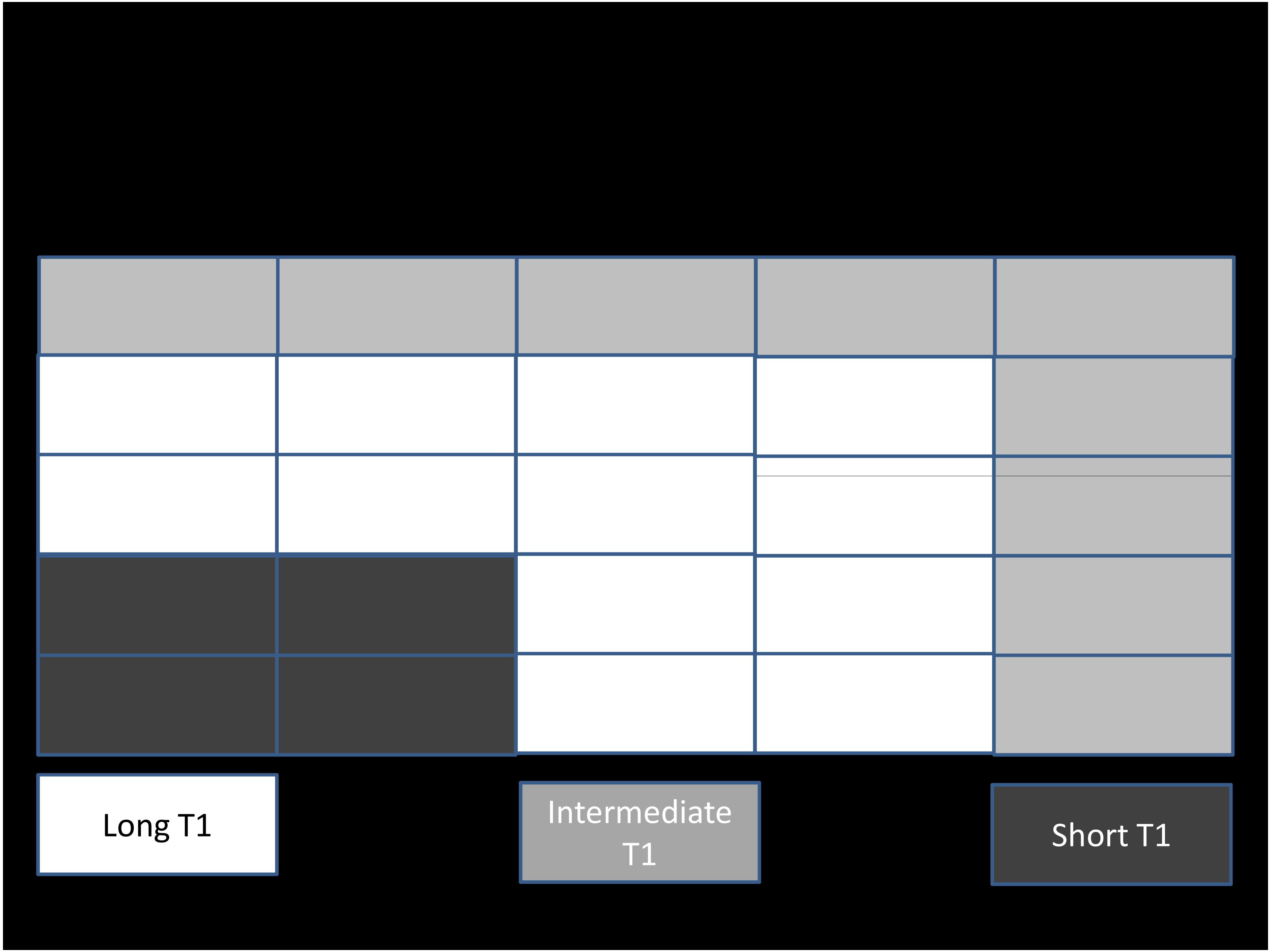

Long T1
Intermediate T1
Short T1

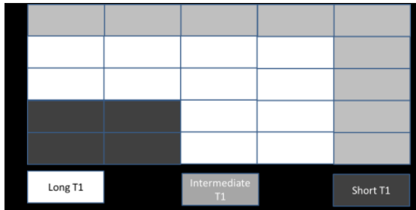

IR

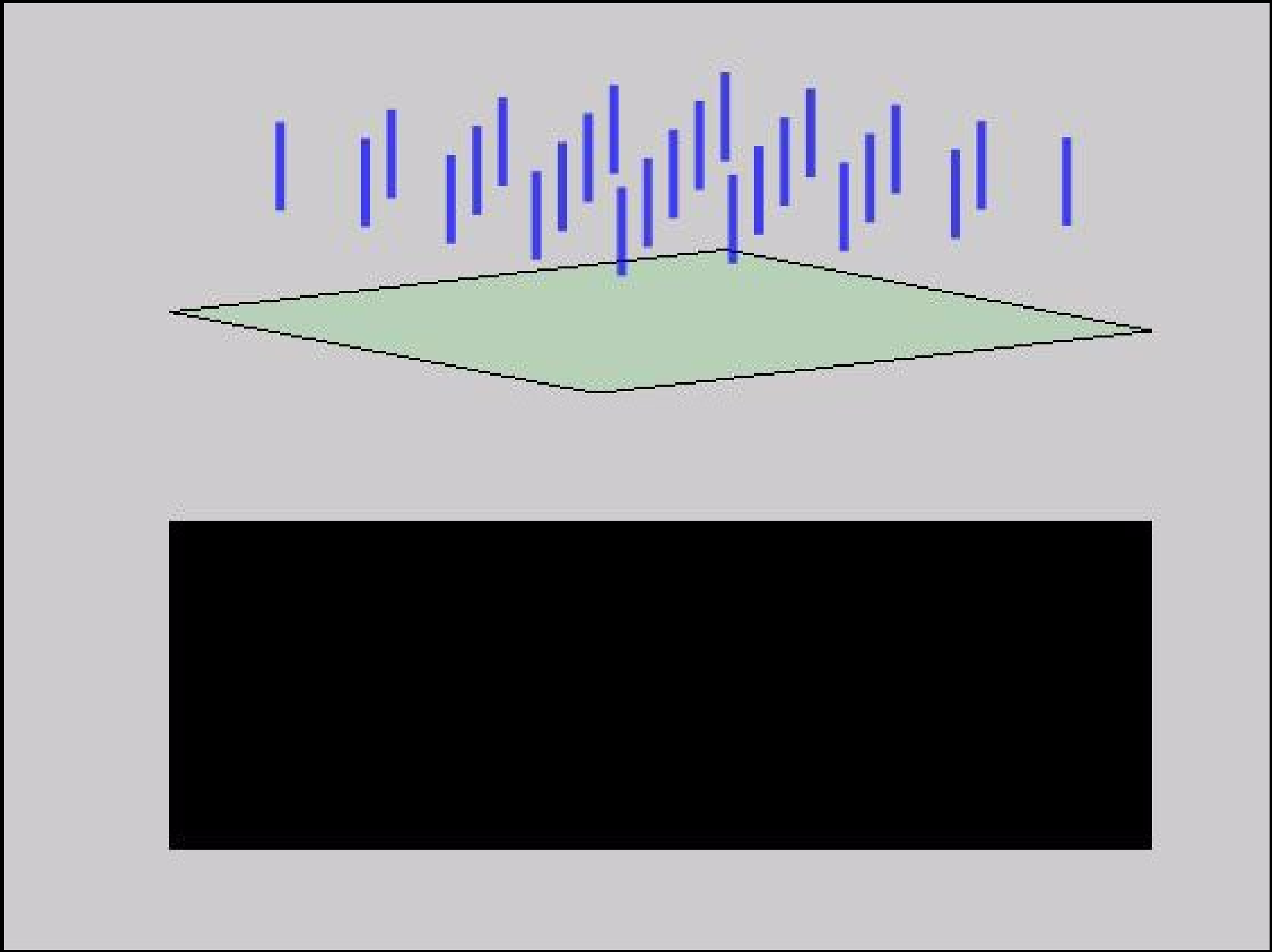

IR

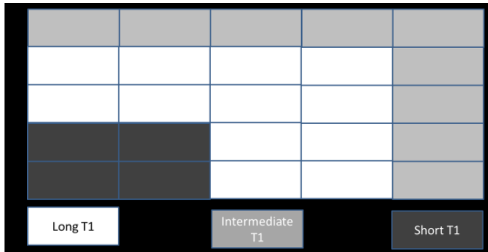

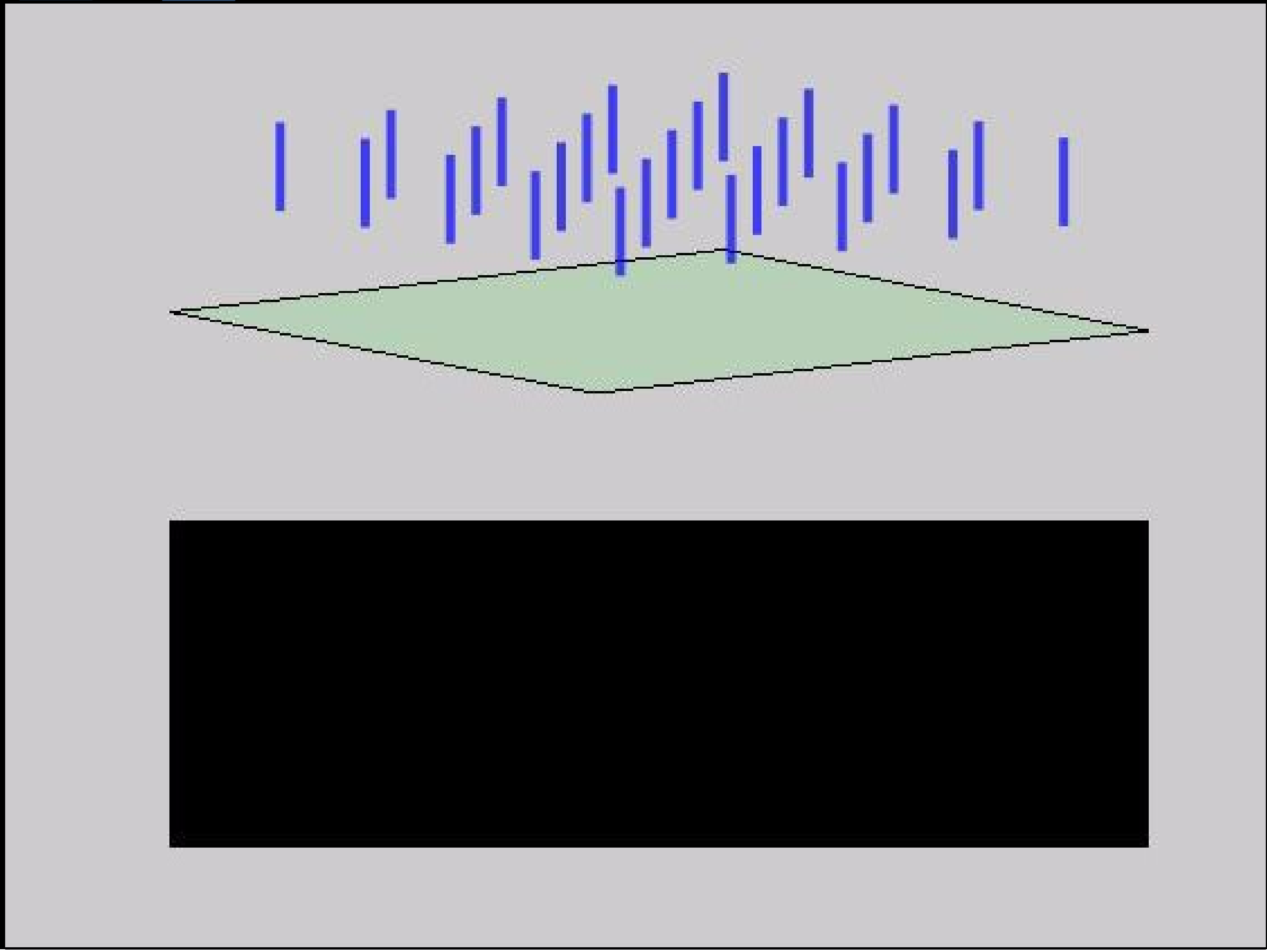

Example Inversion recovery

FLAIR

Dark fluid

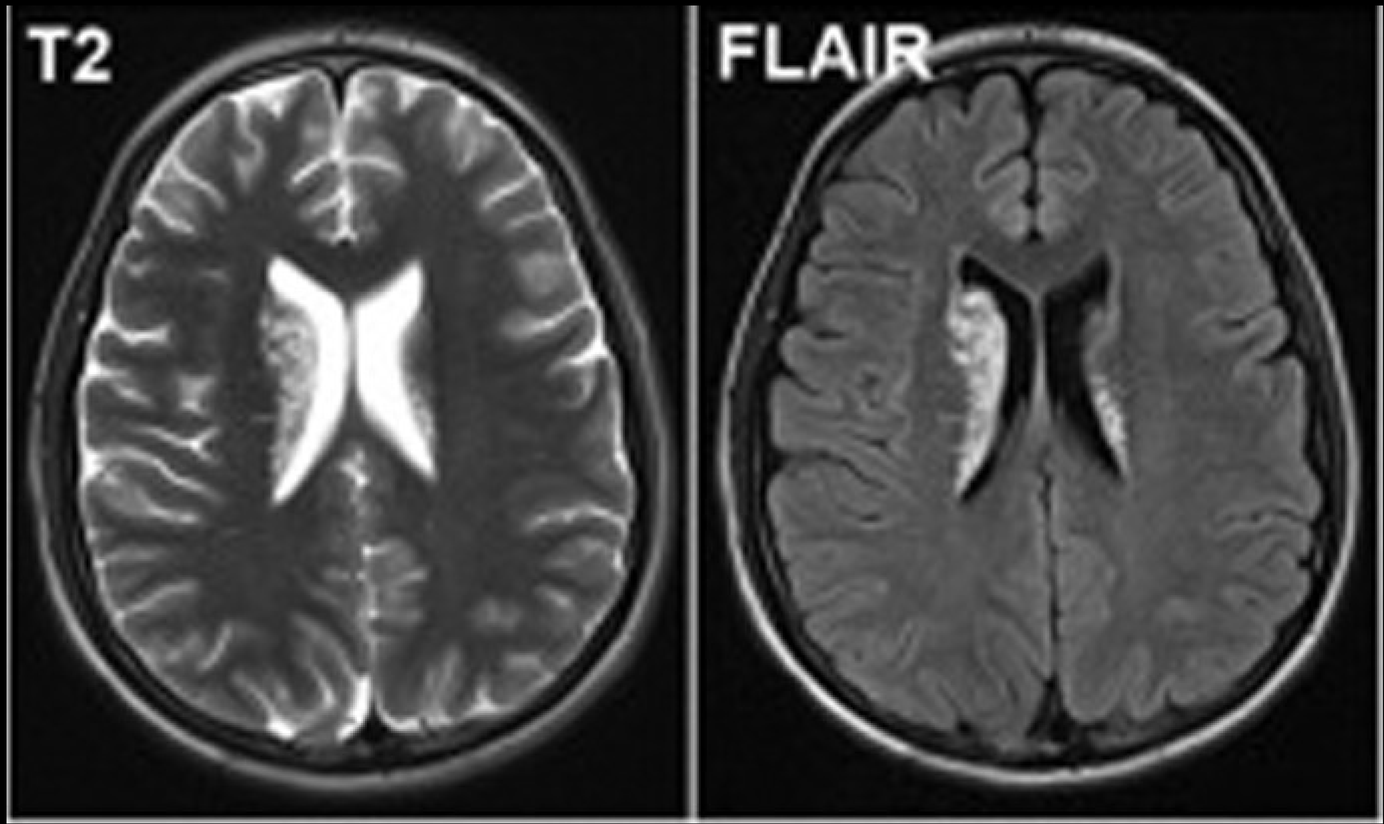

Summary

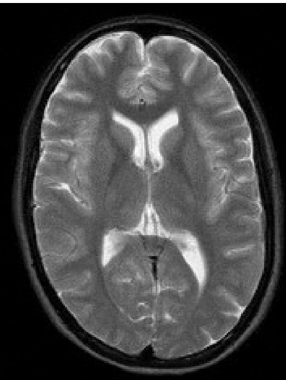

T1 contrast

T2 contrast

TE - Short
TR – Optimized

Inversion recovery
TI - Optimized

- Use for anatomical imaging
- For pathology together with contrast agent

TE - Optimized
TR – Long

- Use for pathology
- Use for anatomical imaging

Proton contrast

$$S = k\rho\left(1 - e^{-TR/T1}\right)e^{-TE/T2}$$

Focus

Minimize infludence
i.e. Long TR

Minimize influence
i.e. Short TE

Turbo spin echo
Fast spin echo

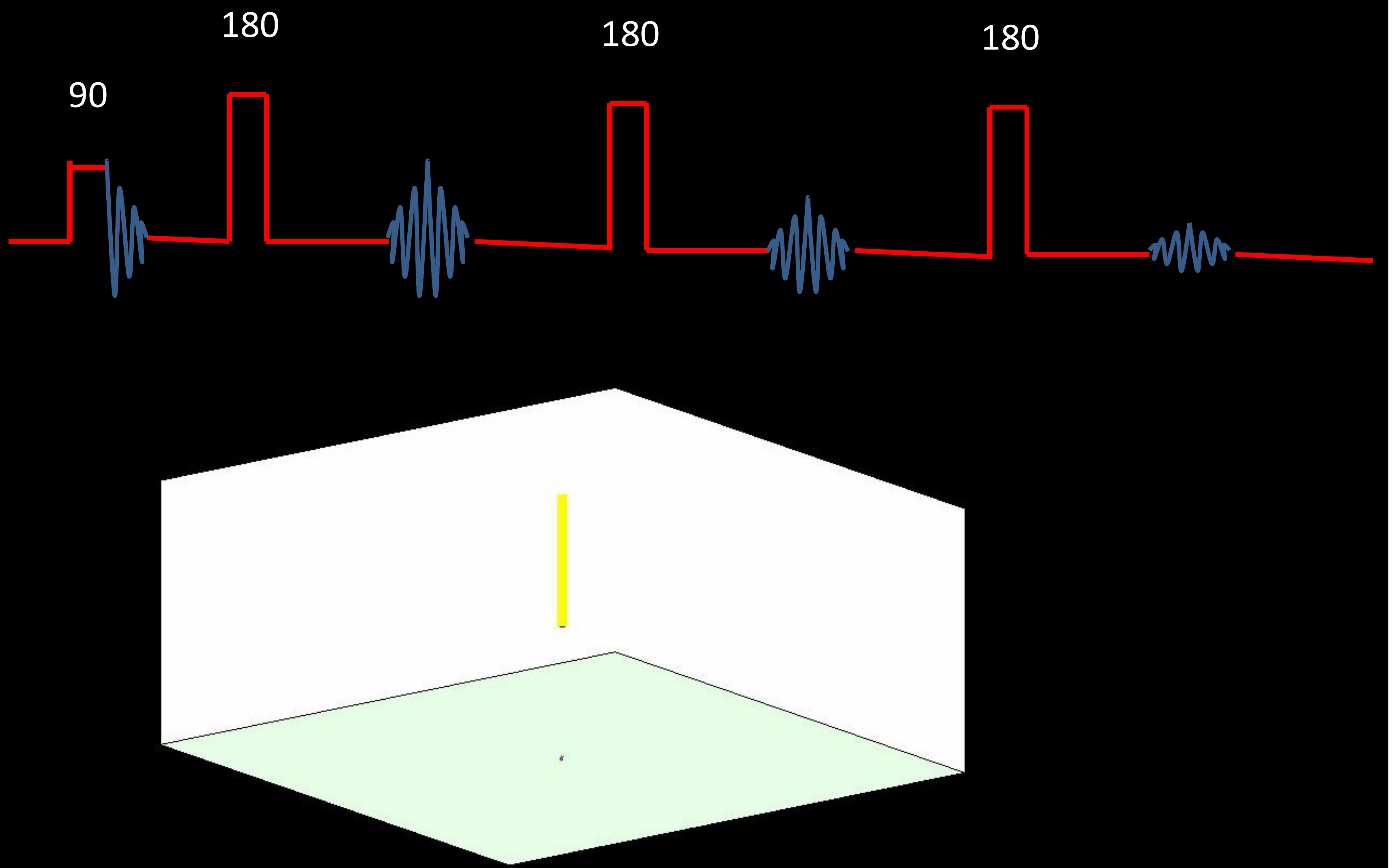

Gradient echo sequences

- No refocusing puls → sensitive to T2*
- Gradients used to generate an echo
- Main benefit: Faster than Spin-Echo

Gradient echo (T2*)

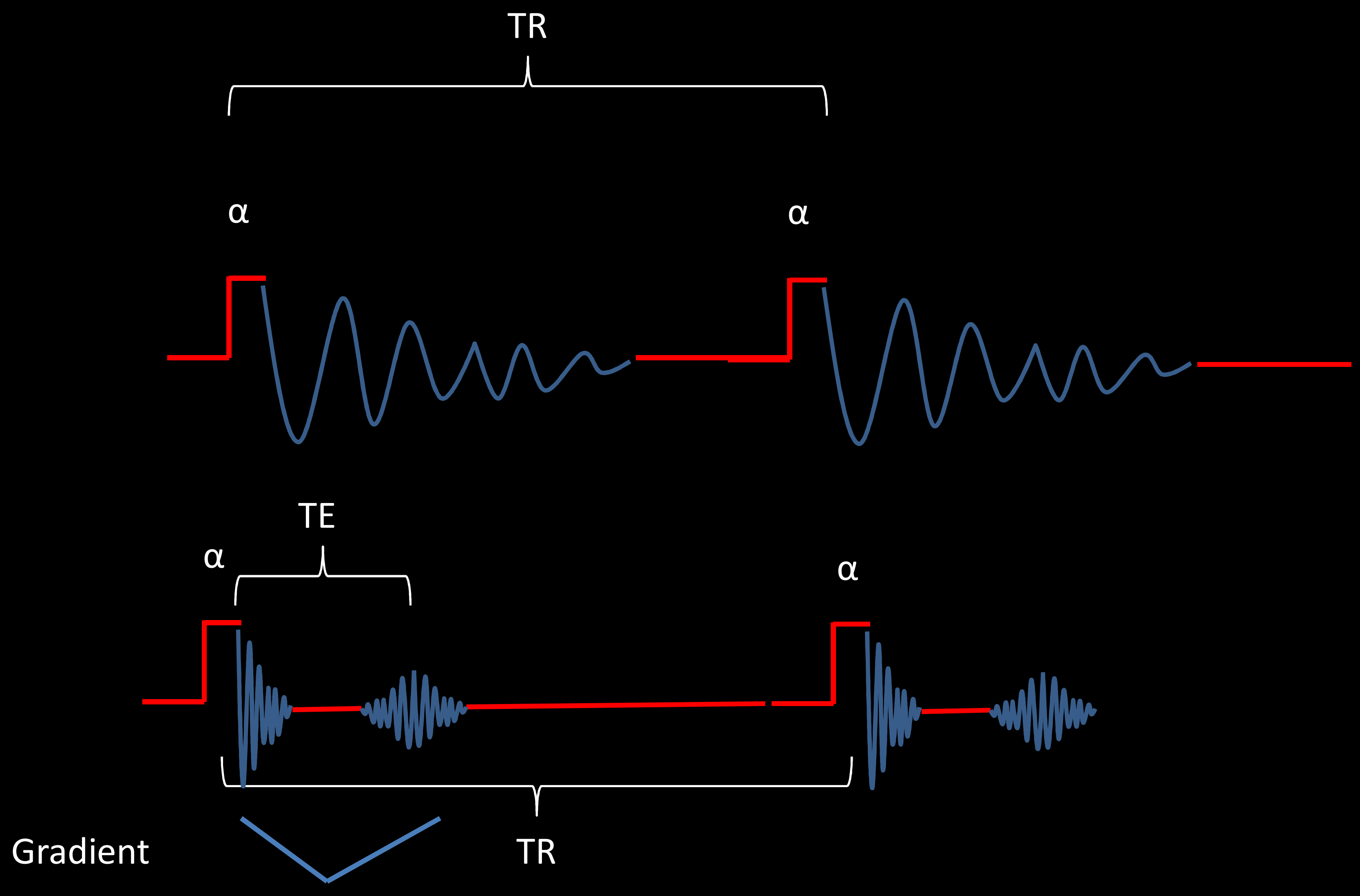

Gradient echo (T2*)

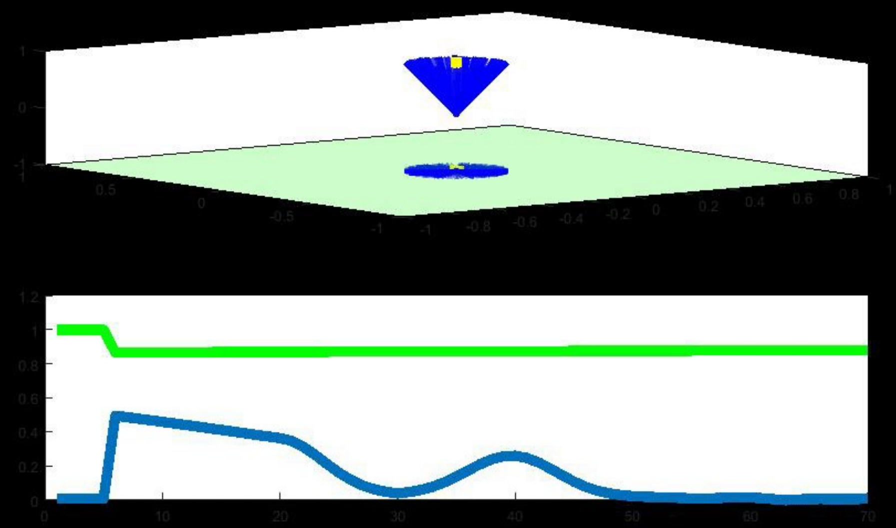

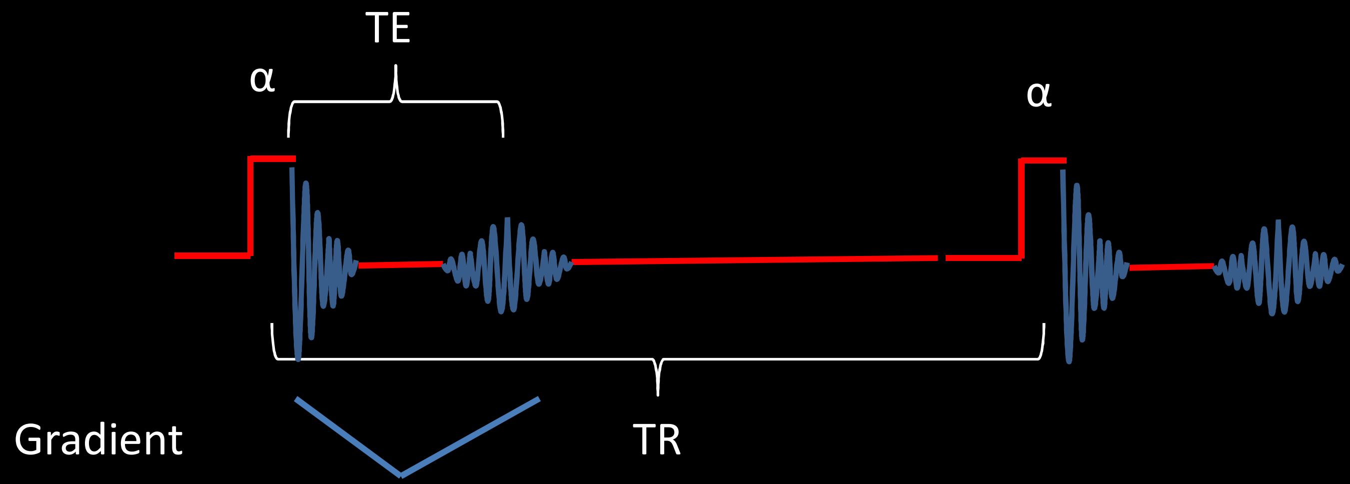

Spooling

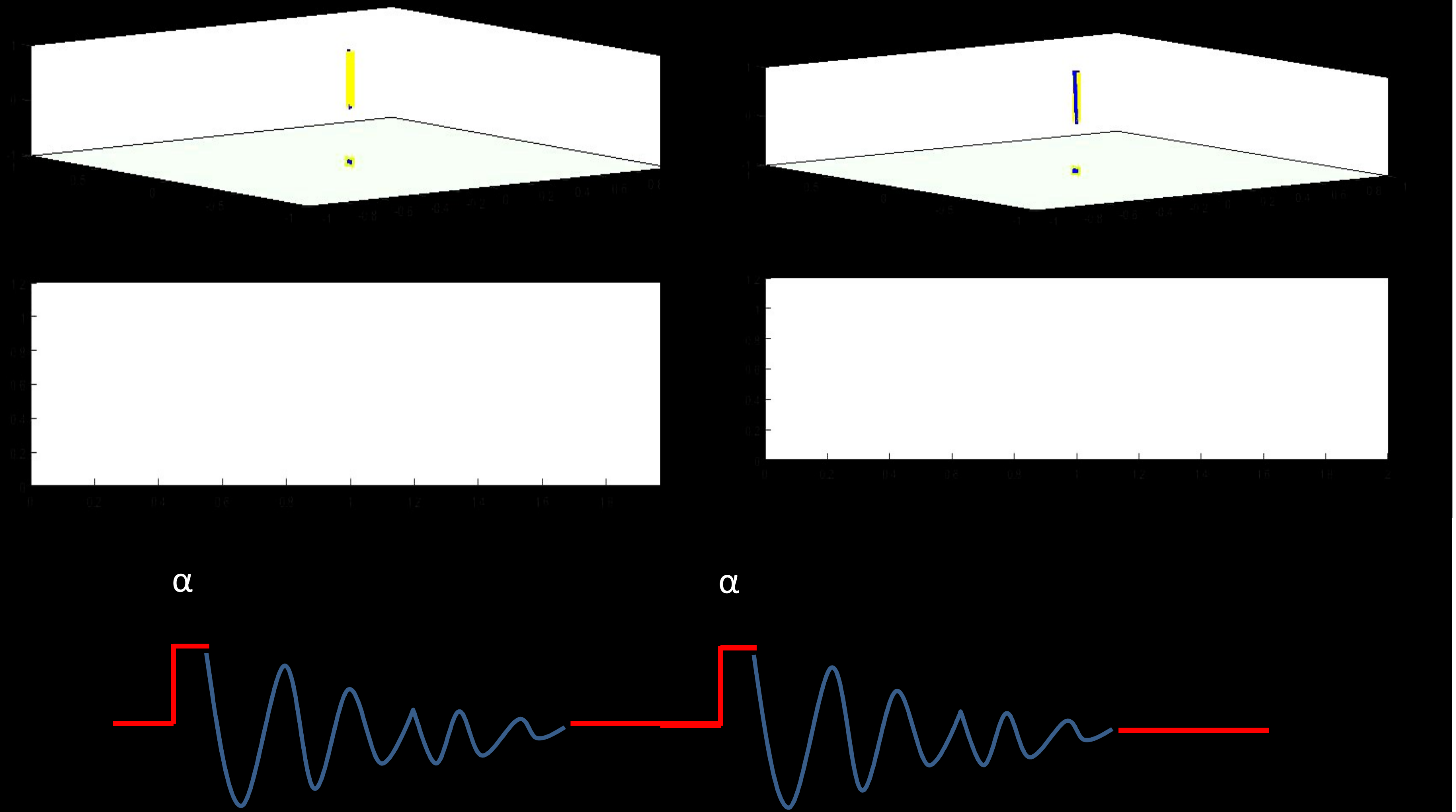

Spooling

- Gradient spooling: Apply a strong gradient to dephase the spins
- RF spooling: Make the flip in different directions every time

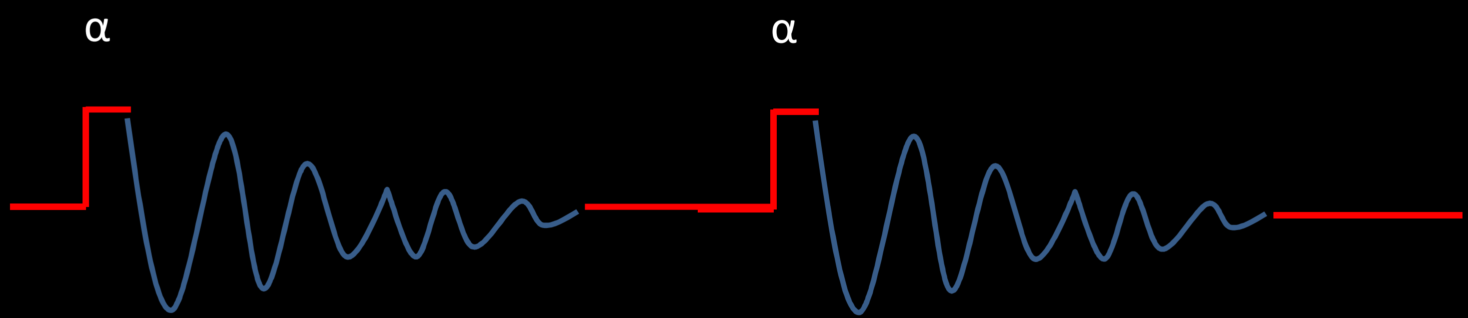

Gradient echo

$$S \sim \rho\left(\sin(\theta) e^{-TE/_{T2*}}\right) \frac{1-e^{-TR/_{T1}}}{1-\cos(\theta) e^{-TR/_{T1}}}$$

Small angle - reduces T1 weighting and yielding proton density weighting
Large flip - yields T1 weighting
Short TR - increases T2* weighting (residual transverse magnetization is dominant)
Long TR - enhances T1 weighting
Short TE - reduces T2* weighting and increases T1 or PD weighting
Long TE - enhances T2* weighting

$$\theta_{Ernst} = \cos^{-1}\left(e^{-TR/_{T1}}\right)$$

Optimal flip angle

Parallel component

Transversal component

Very small angle

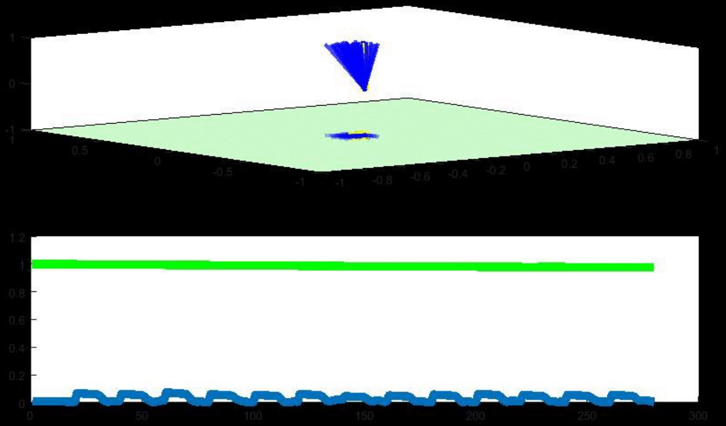

Small angle

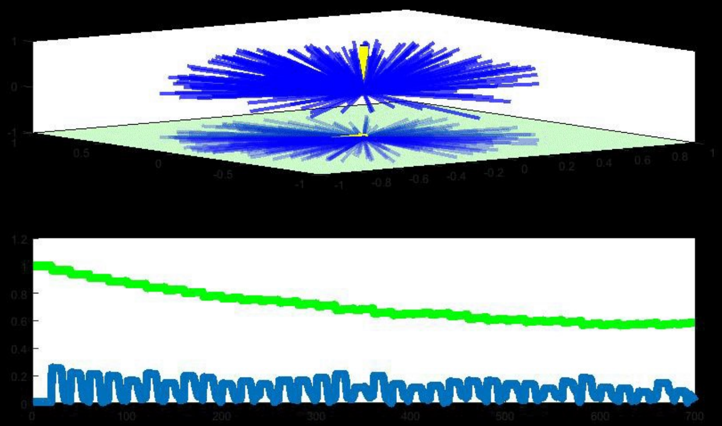

Large angle

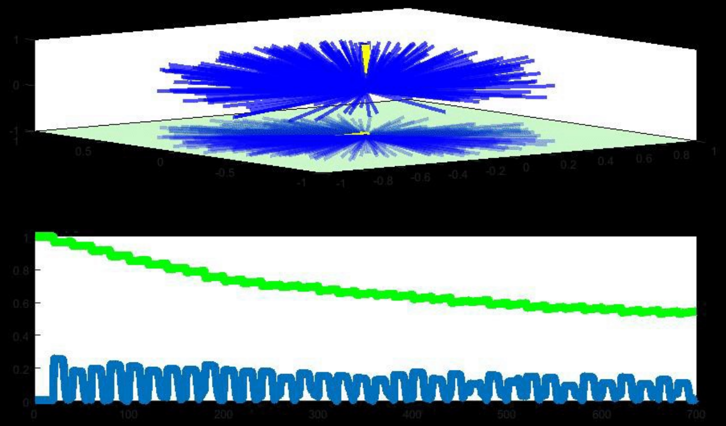

Very large angle

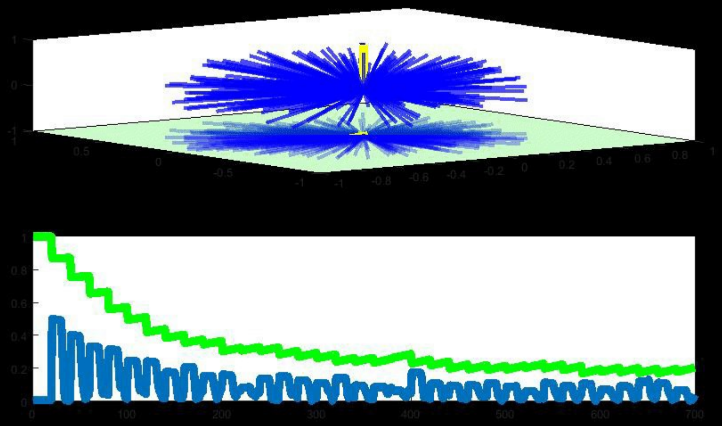

Phase contrast

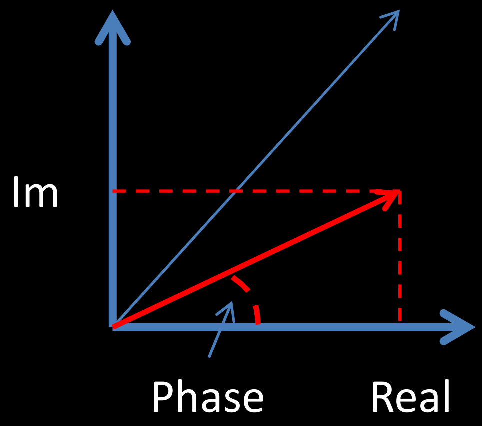

$$Phase \sim TE * \Delta B$$

A little bit more about phase in the DCE lecture

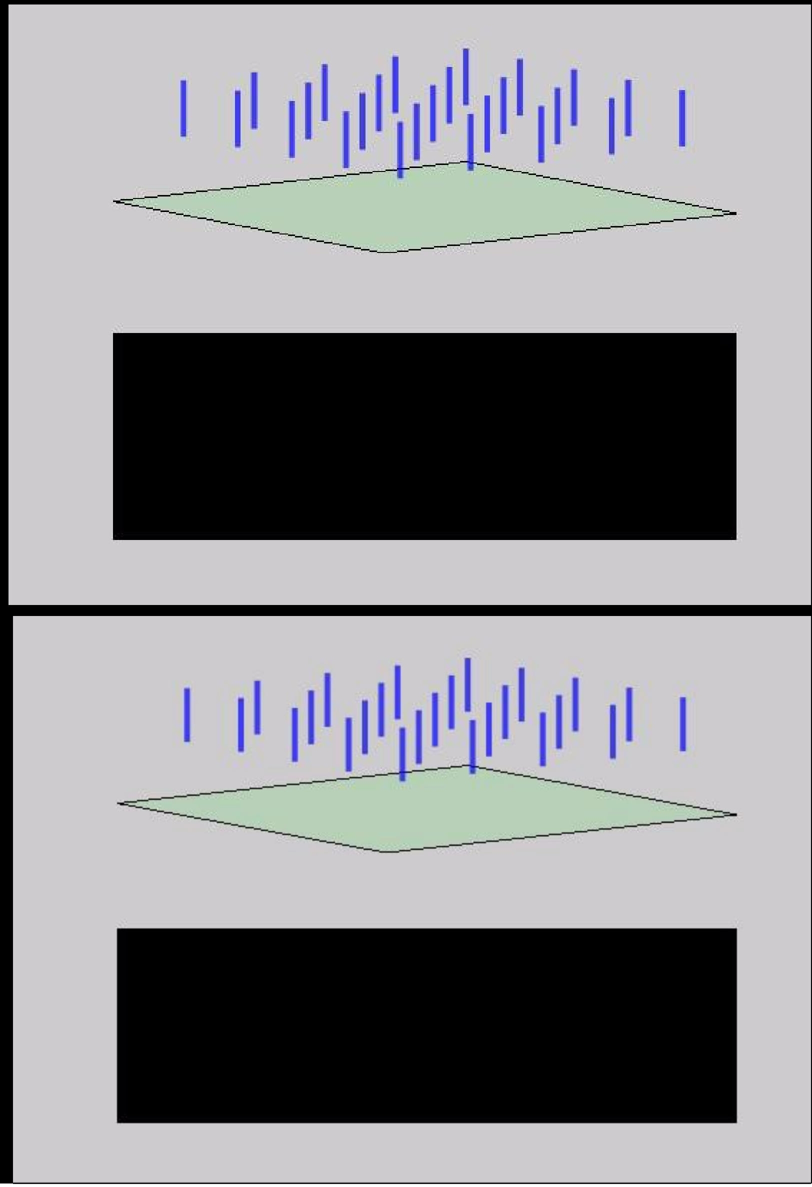

Summary again

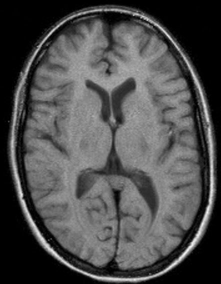

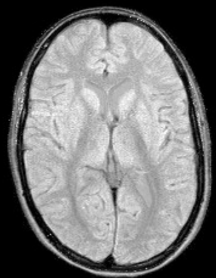

- T1 Weighting
  - Maximizing T1 → short TR
  - Minimizing T2 → short TE
- T2 Weighting
  - Maximizing T2 → long TE
  - Minimizing T1 → long TR
- Proton weighting
  - Minimizing T2 → short TE
  - Minimizing T1 → long TR

Thank you

MRI Physics: Space Encoding

A/Prof Gary Liney

18th September 2016

ESTRO Imaging for Physicists

Introduction

- MRI extremely flexible spatial localisation
  - Orientation easily altered
- Gradients used to modulate phase and frequency
  - In-plane directions always ‘phase’ and ‘frequency’
- Signal is reconstructed with 2D or 3D Fourier Transformation

Spin Echo Sequence

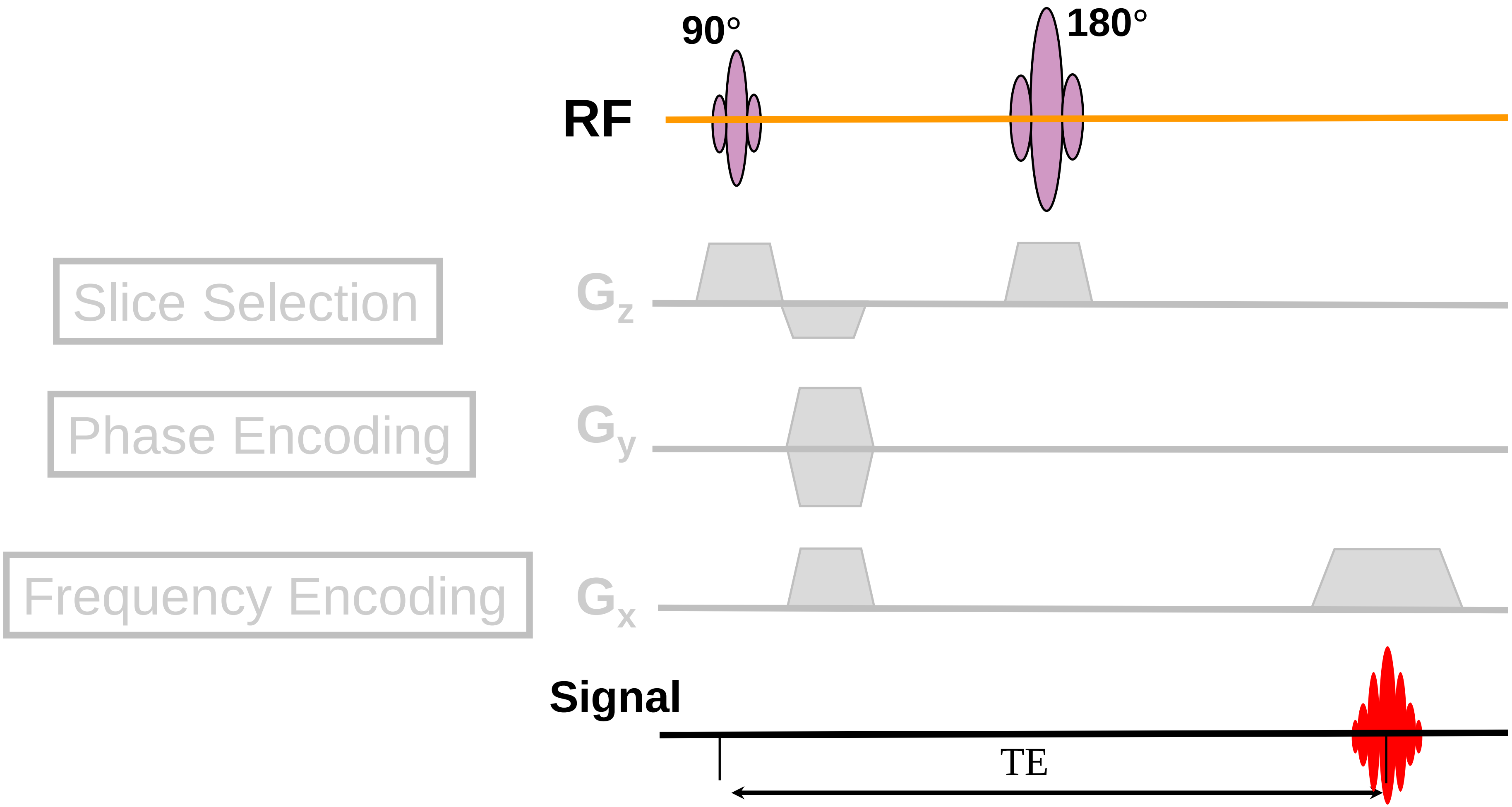

The Image So Far..

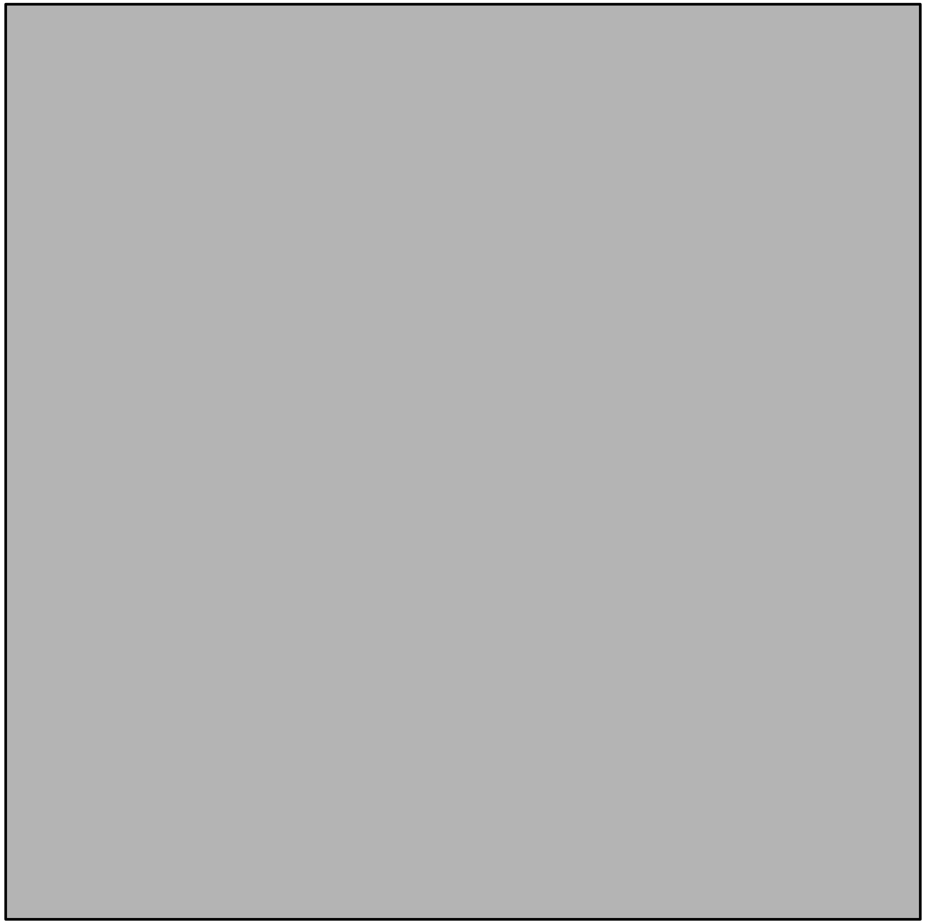

Spin Echo Sequence

Slice Selection

Phase Encoding

Frequency Encoding

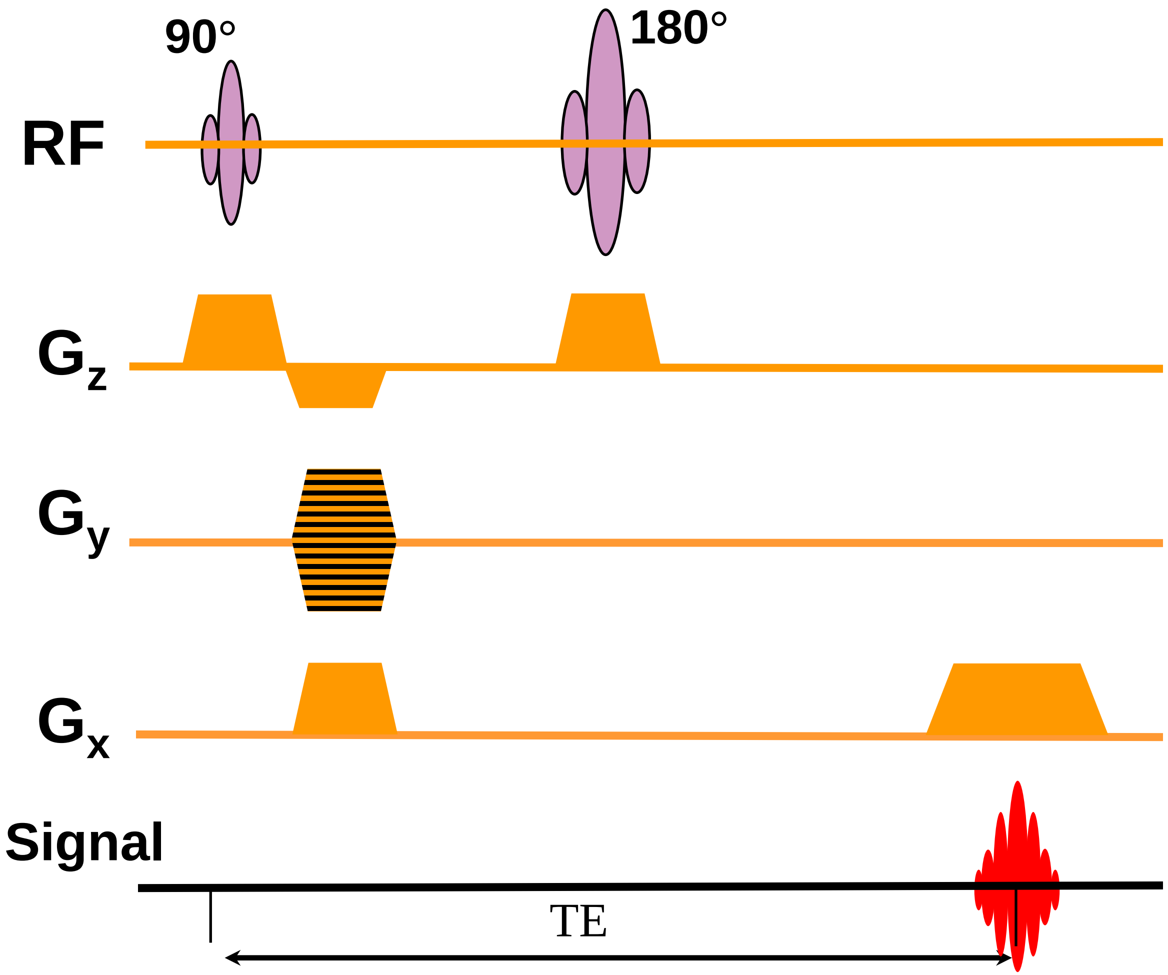

An axial image..

ESTRO School

Fourier Transform (FT)

- Time signal can be decomposed into sum of sinusoids of different frequencies, phases and amplitudes

$$s(t) = a_0 + a_1\sin(\omega_1 t + \varphi_1) + a_2\sin(\omega_2 t + \varphi_2) + \ldots$$

- Fourier series may be represented by frequency spectrum
- Time and frequency domain data can be thought of as FT pairs

Fourier Transform (FT)

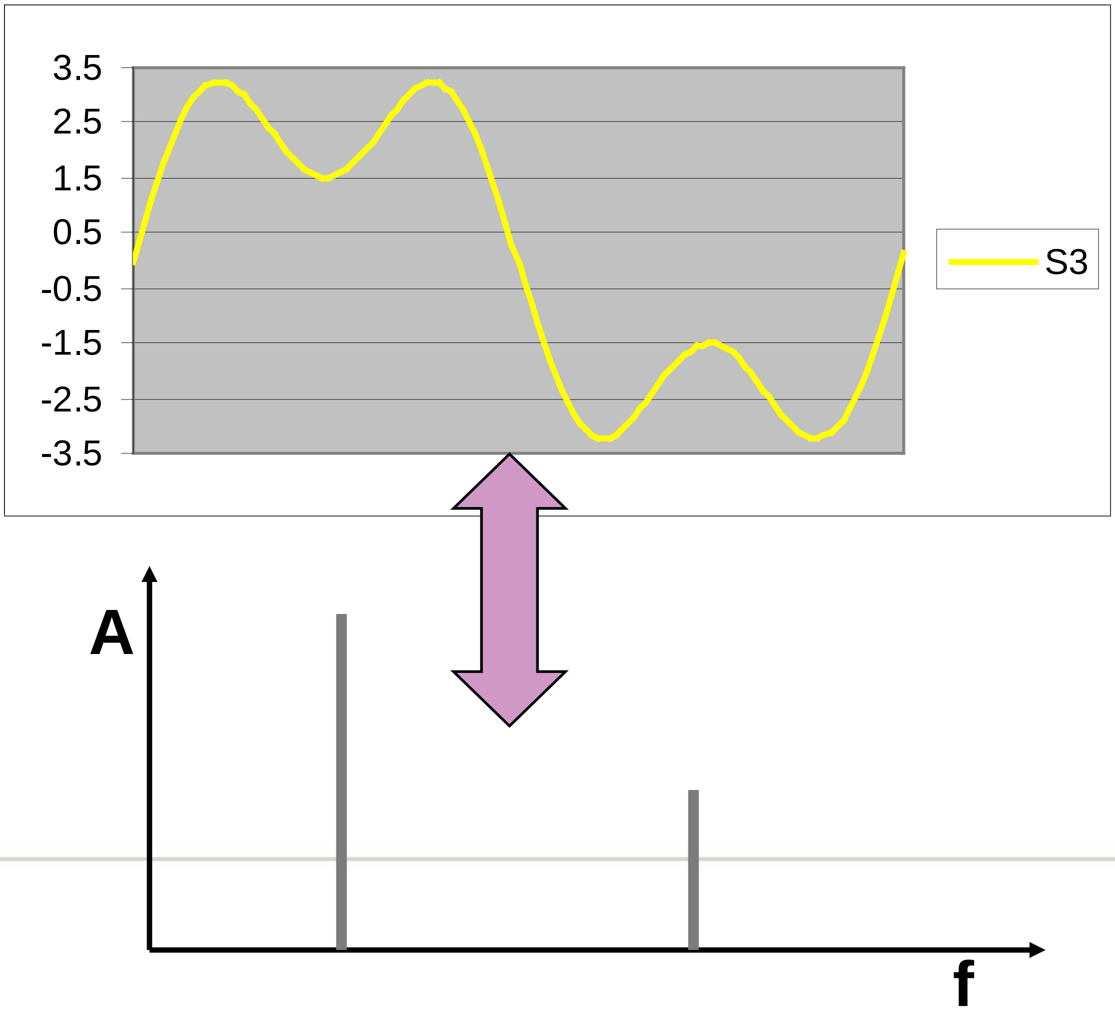

- S1 has amplitude *a* and frequency *f*
- S2 has *a*/2 and 3*f*
- S3 = S1 + S2
- S3 is two sine waves of different *frequency* and *amplitude*

The FT is shown

FT Pairs

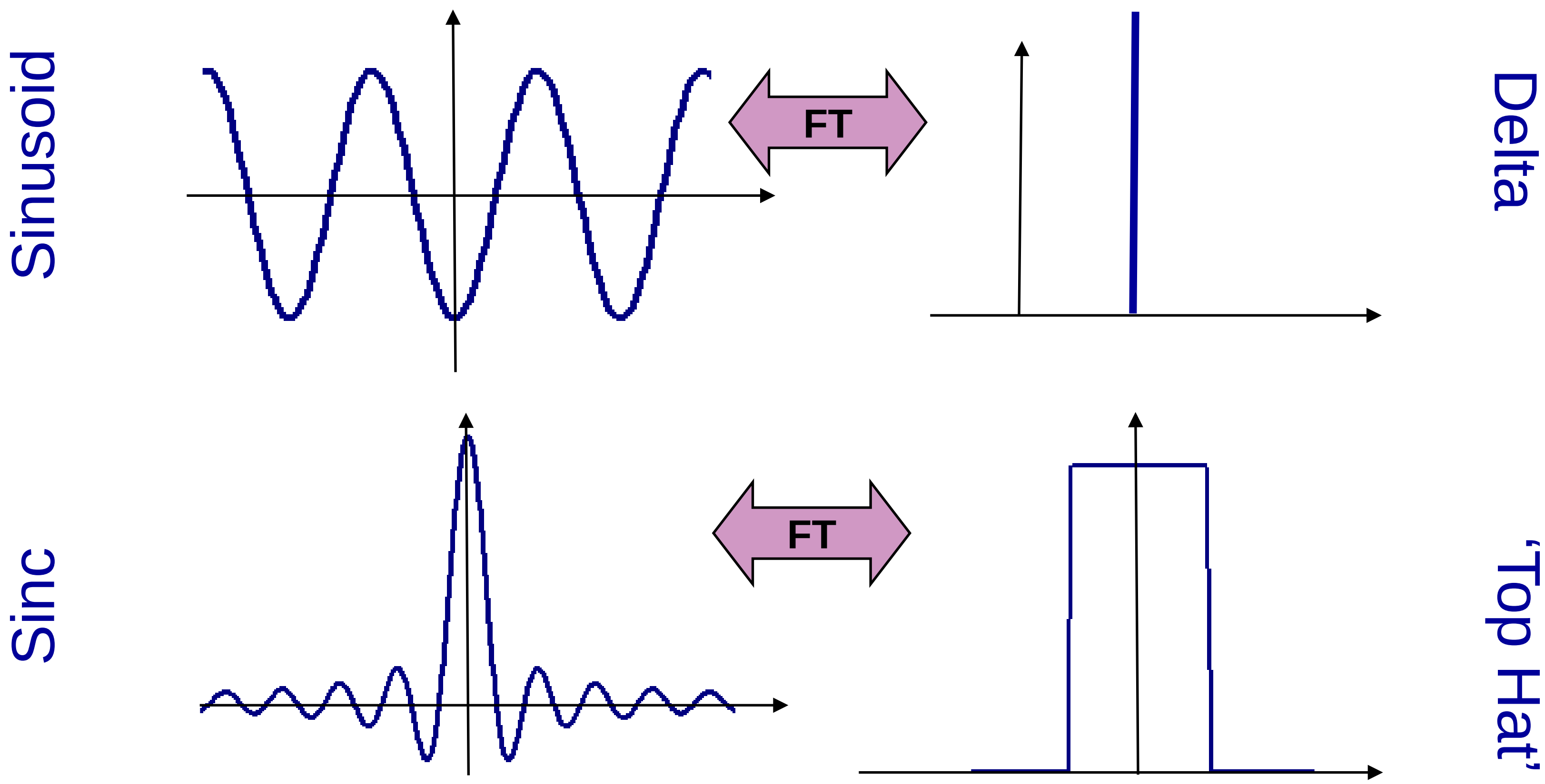

Time

Frequency

FT Pairs

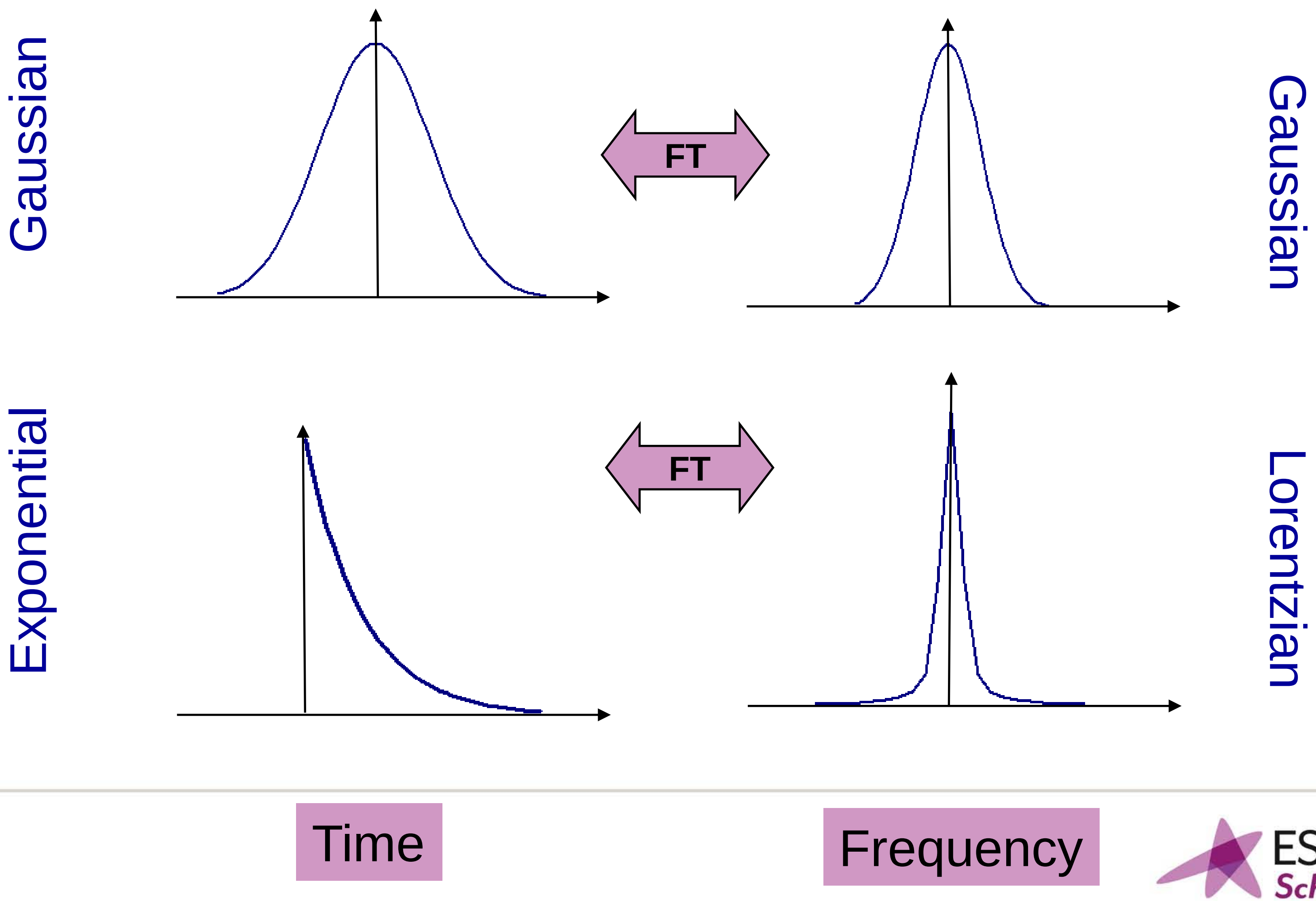

Gaussian
FT
Gaussian
Exponential
FT
Lorentzian
Time
Frequency

Gradients

- Recall that the resonant frequency is proportional to field strength

$$\omega_0 = \gamma B_0$$

- Magnetic gradient changes B_0 field strength over distance
- In MRI a linear gradient changes the resonant frequency in a given direction

$$\omega = \gamma (B_0 + xG_x)$$

$$G_x = dB_0 / dx$$

$$G_y = dB_0 / dy$$

$$G_z = dB_0 / dz$$

Slice Selection

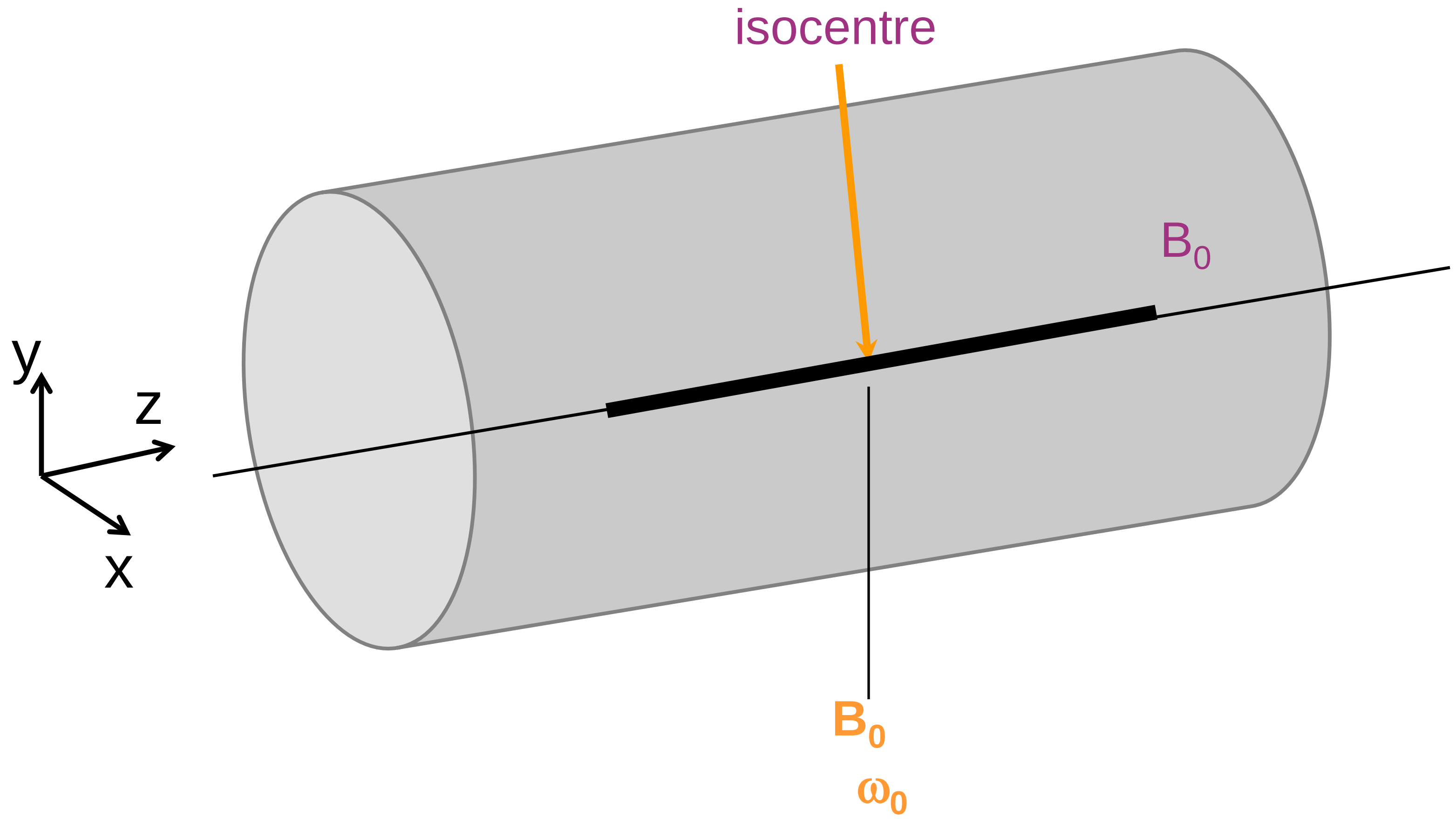

Slice Selection

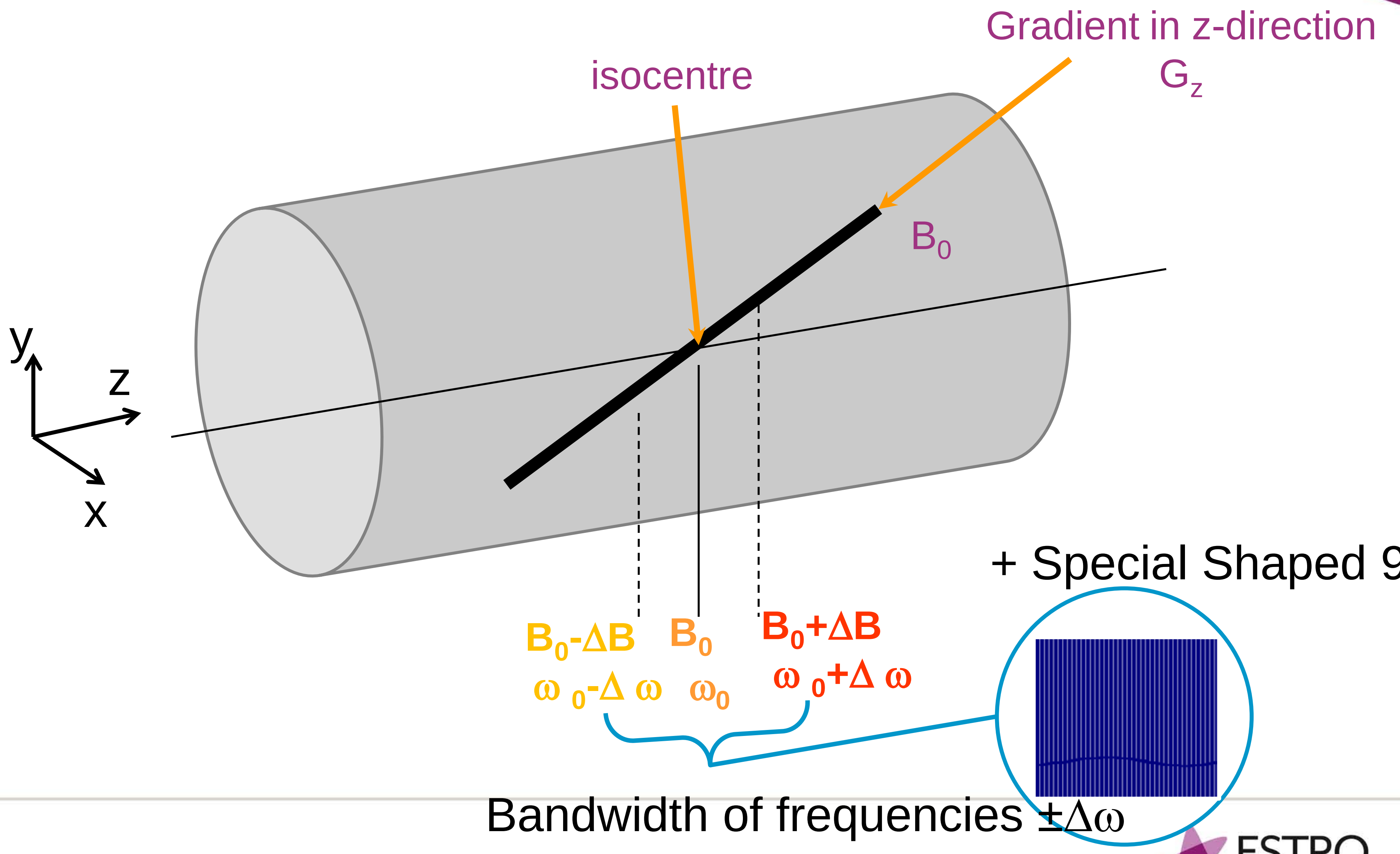

Slice Selection

Only this section can be 'seen' by the coil

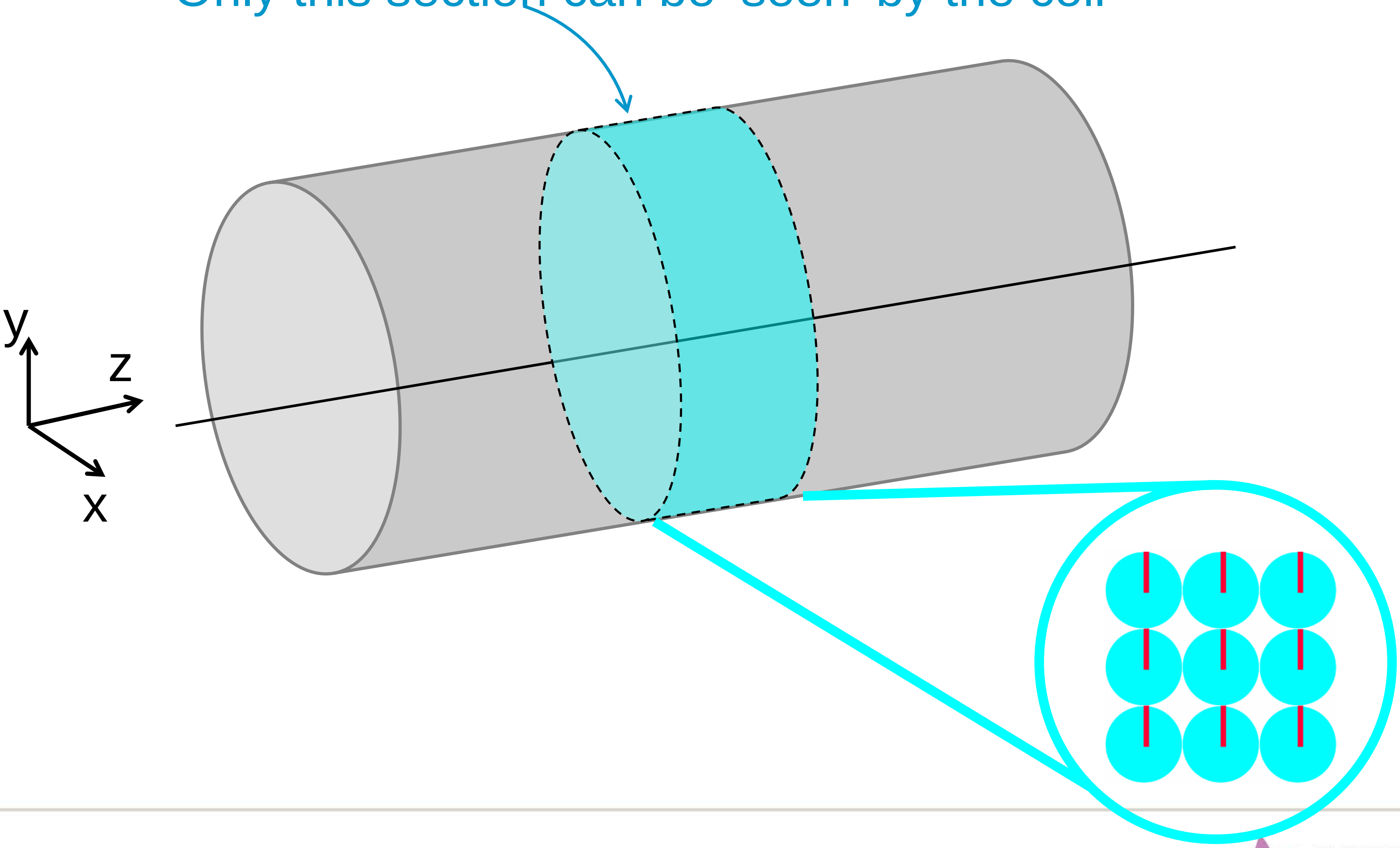

Slice Selection

- Gradient used to change resonant frequency in slice direction
- Excite spins using (*sinc-shaped*) 90° RF pulse containing a bandwidth of frequencies
- Only a particular section of spins are excited into transverse plane
- Signal has been discriminated in one dimension
- Can change orientation, slice thickness and position

Slice Selection

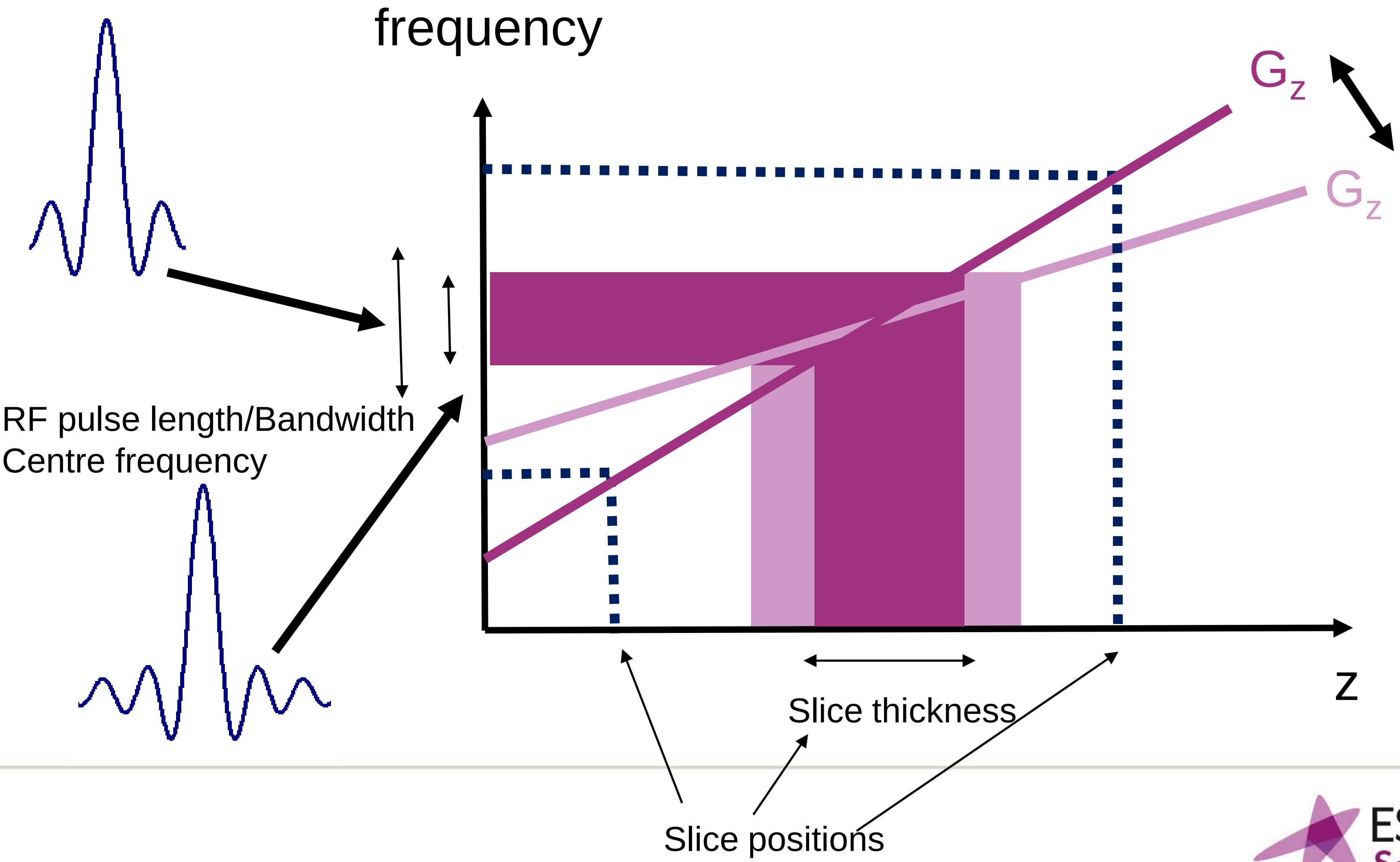

Phase & Frequency Encoding

- Need to still encode signal in remaining directions (x & y)
  - Use changes of frequency & phase
- When a gradient is applied the spins will be at different phases once the gradient has been turned off
- This is the role of the phase encoding gradient
- Used in combination with frequency encoding gradient in the 2nd direction...

In-plane Encoding

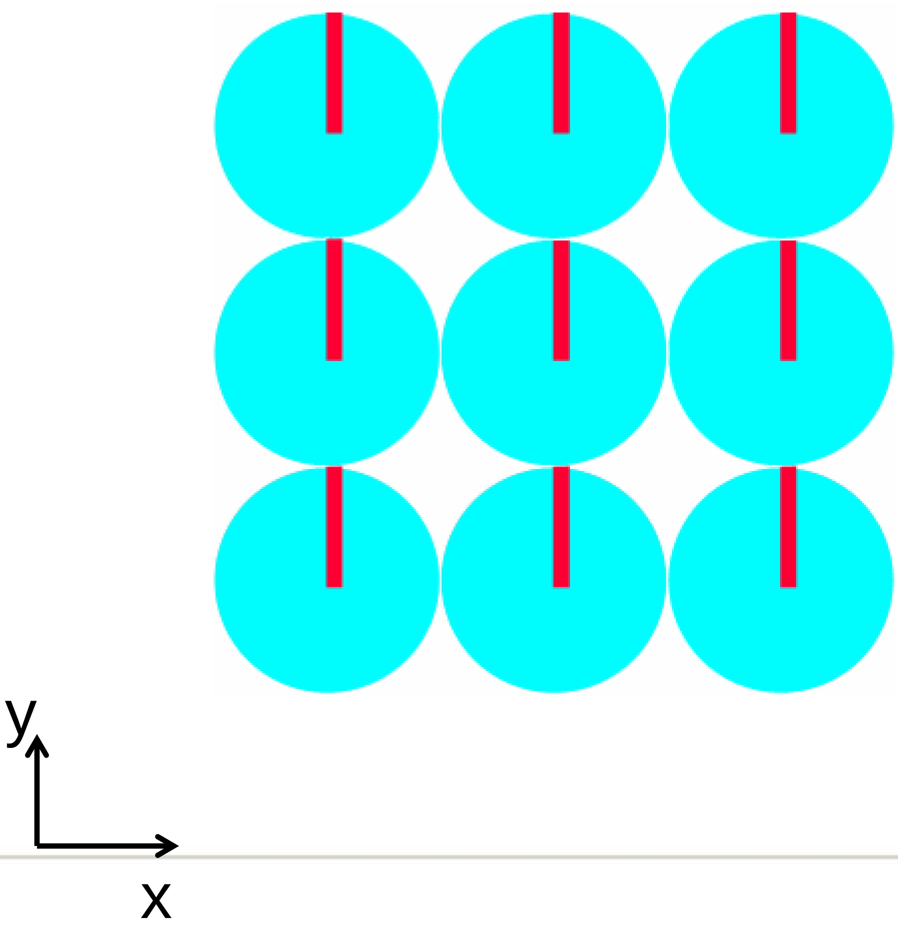

Initially, all spins have **same frequency**

In-plane Encoding

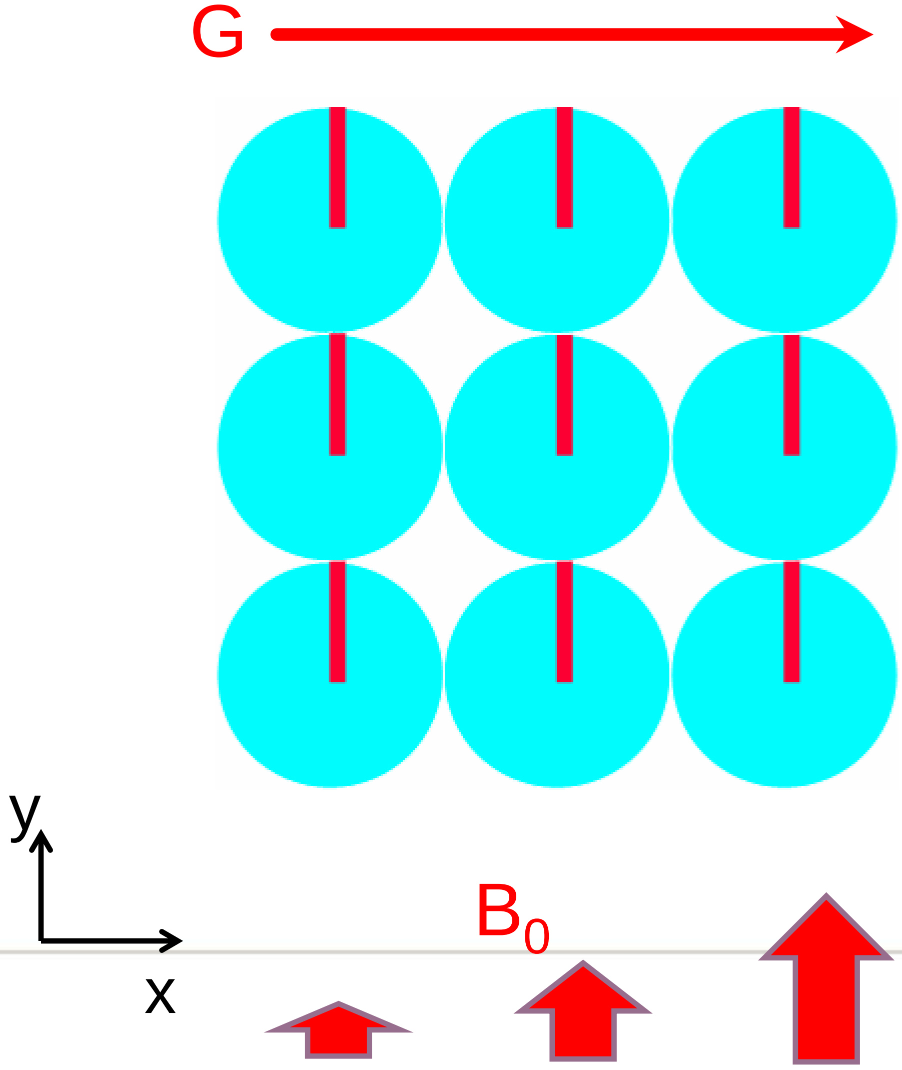

- Apply a gradient left to right
- Linear change in B_0

In-plane Encoding

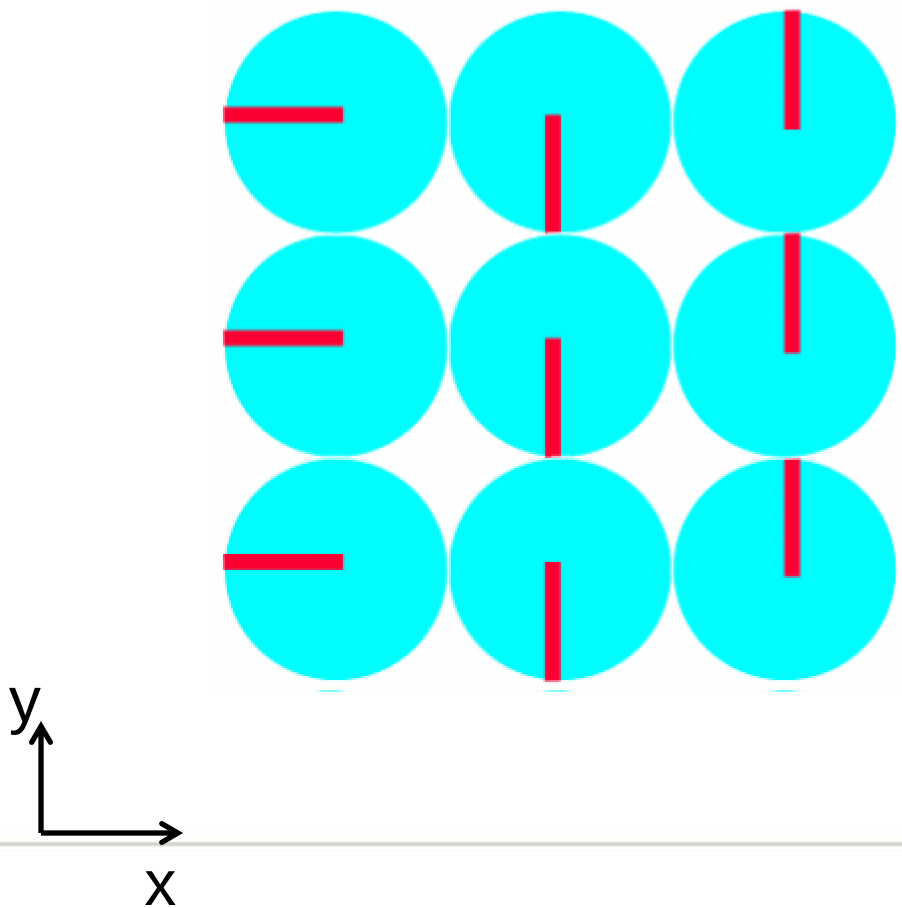

- After gradient is removed
- Spins revert to same frequency
- Phase is different between columns
- This gradient is applied n times with different amplitudes

In-plane Encoding

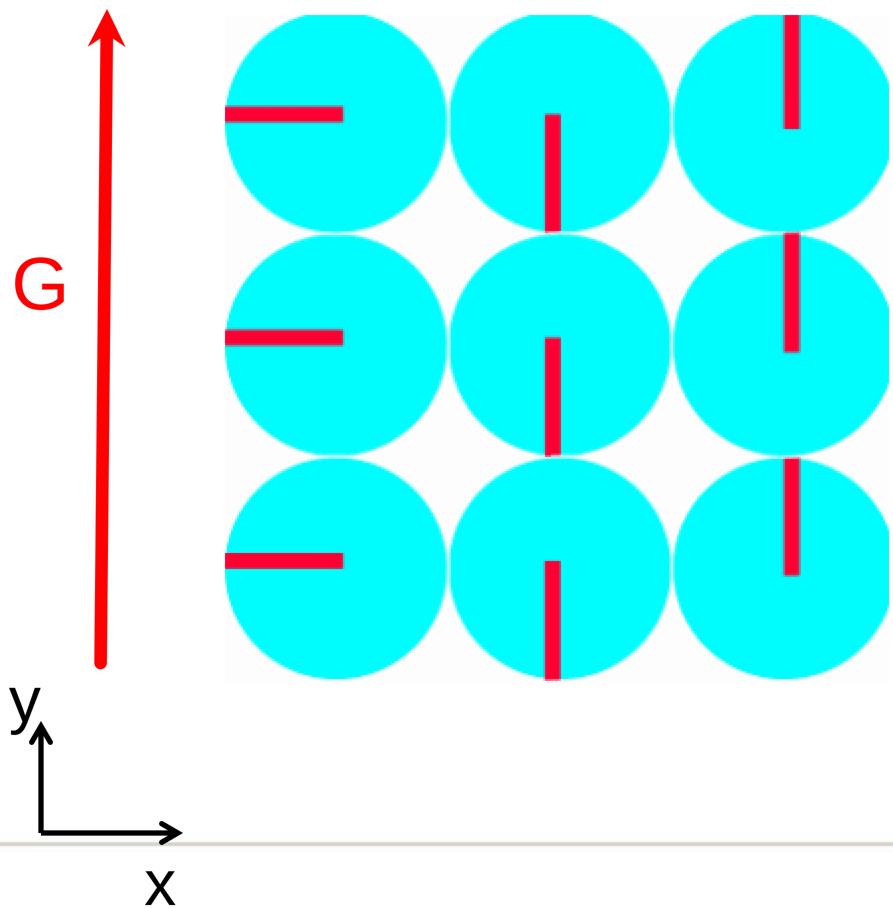

- Apply a further gradient bottom to top
- This gradient is applied once
- Sample the data m times
- Create m×n pixel image

Phase Encoding

- Each pixel is assigned a unique phase and frequency
- FT decodes unique frequency but only measures summation of phase
- Individual phase contributions cannot be detected
- Need multiple increments of PE gradient to provide enough information about phase changes
- Number of PE increments depends on image matrix

Spin Echo Sequence

Resonance condition

$\omega = \gamma\,(B_0 + zG_z)$

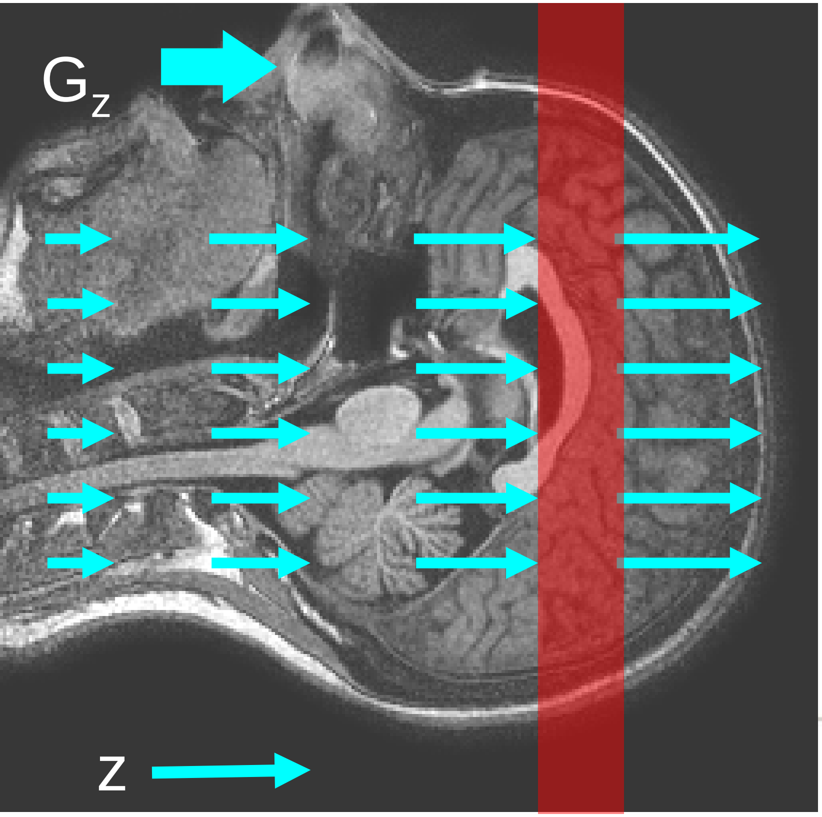

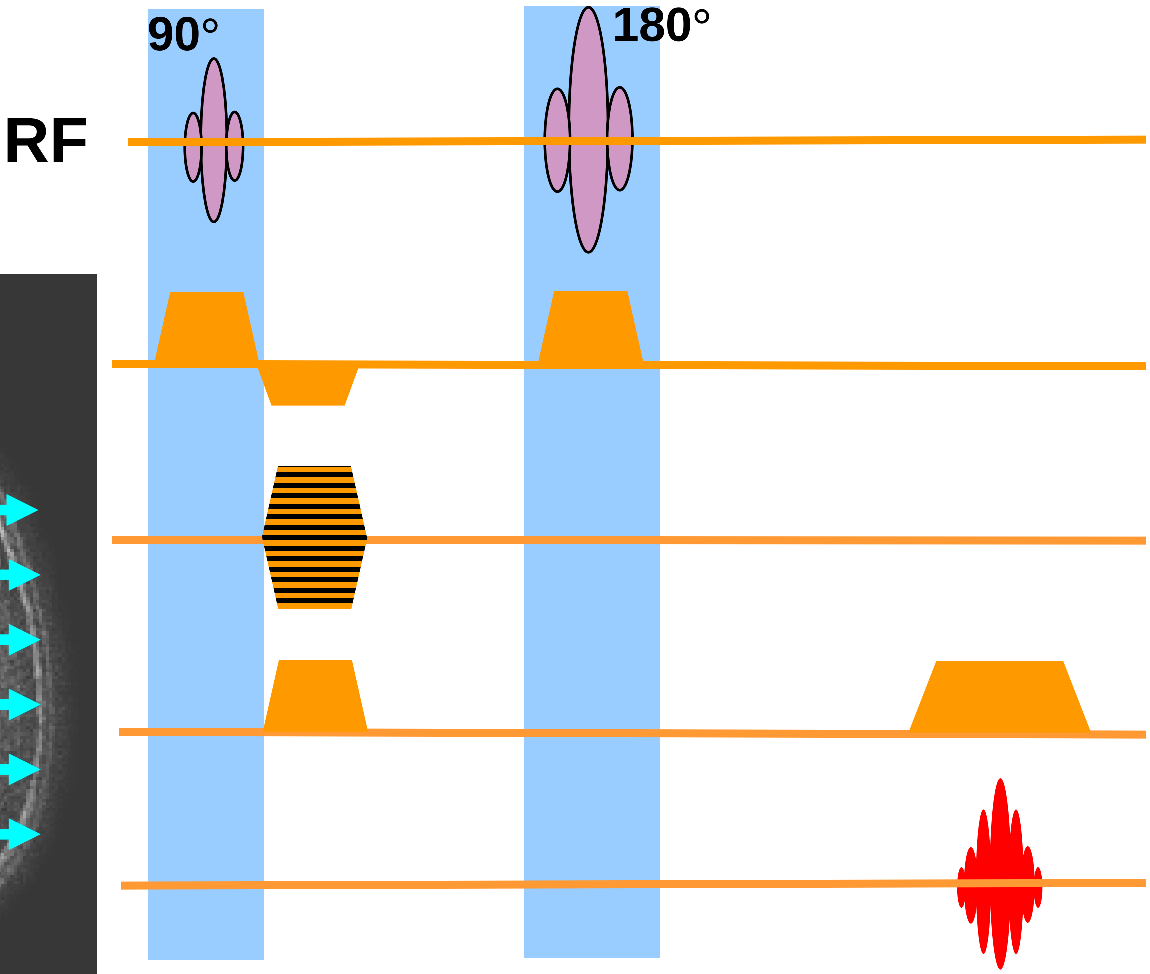

Spin Echo Sequence

Increment gradient after RF pulse and before read-out

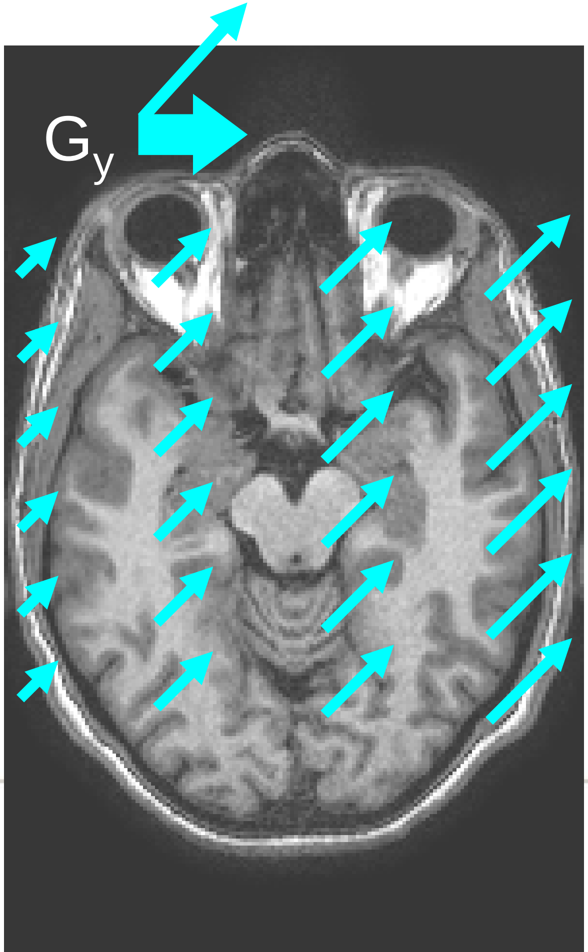

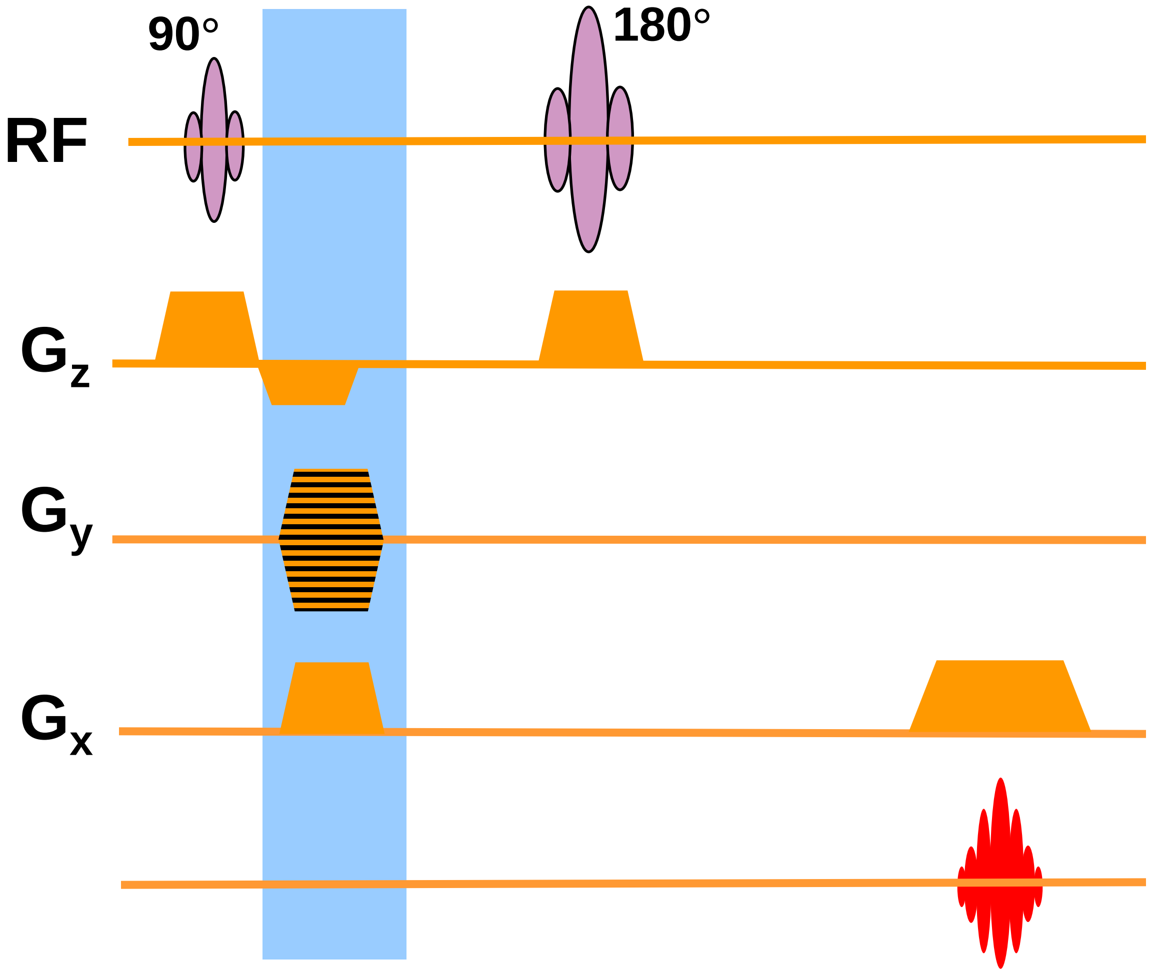

Spin Echo Sequence

Apply gradient during read-out

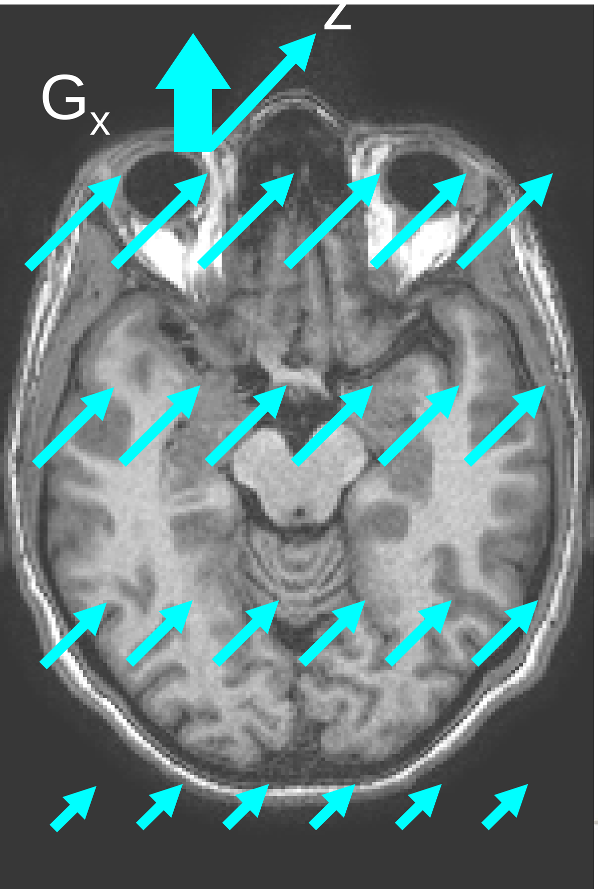

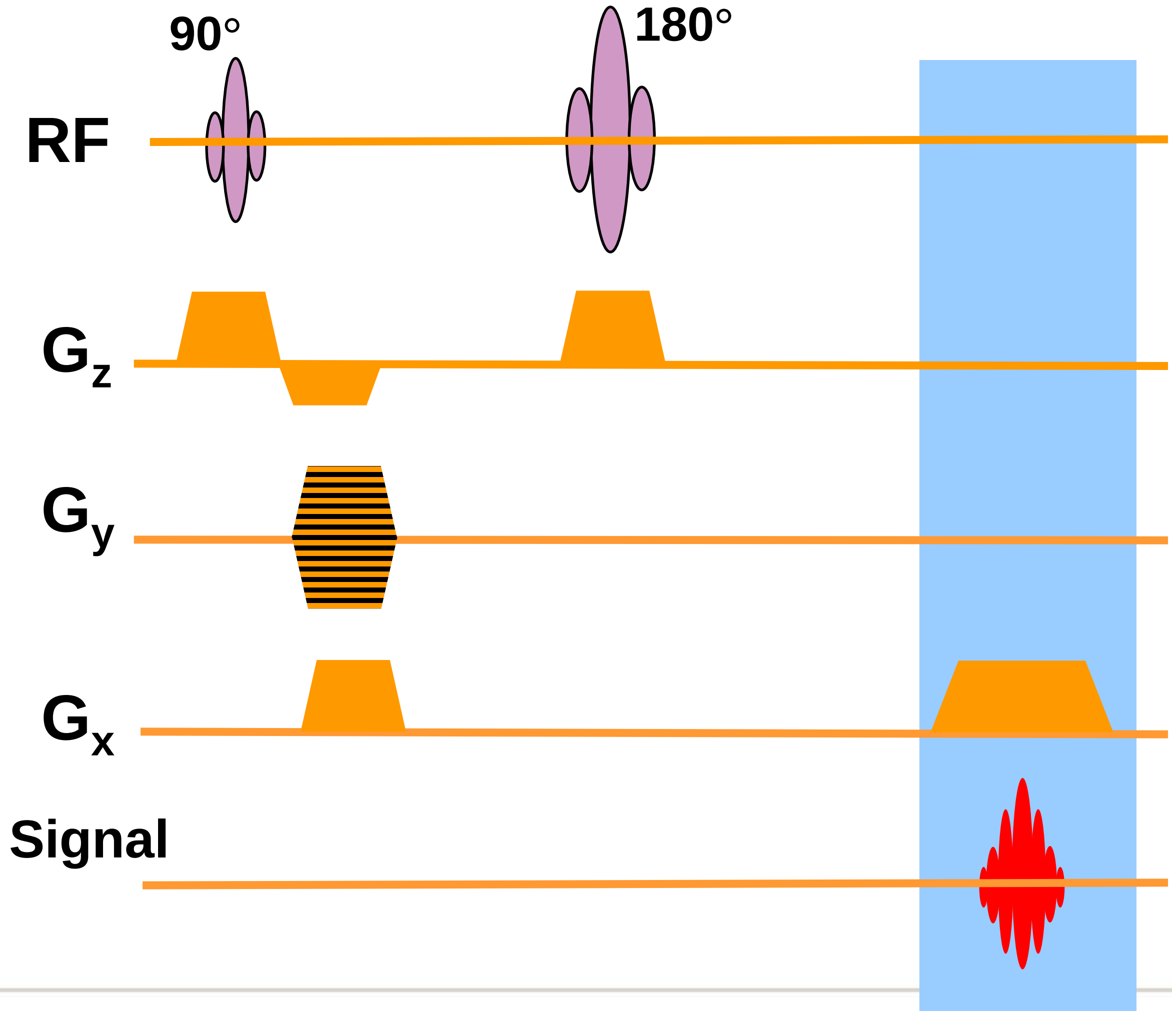

Multi-Slice Imaging

- Period between the echo and the next RF pulse is called *dead time*
- Used to excite a separate slice
- Multiple slices are acquired in each TR
- Slice profiles are not rectangular leading to cross-excitation
- Slices are acquired with gaps or interleaved

Scan Time

- Frequency encoding done at time of echo
- Phase encoding done over many TRs
- Time between TR-TE is dead time

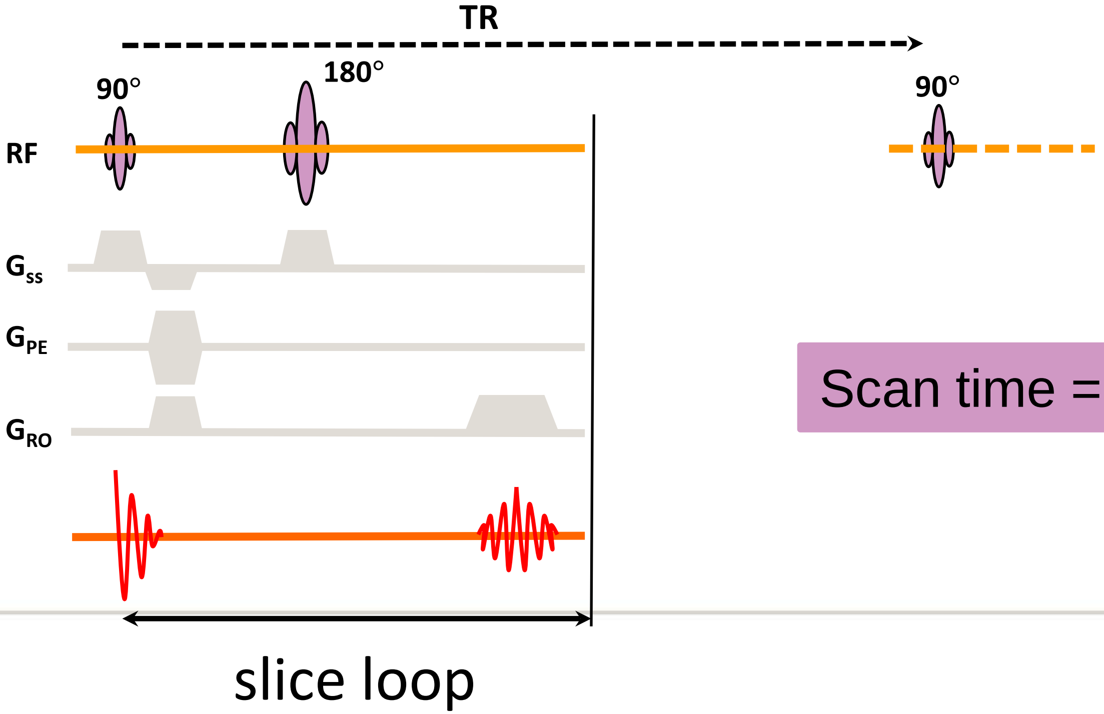

Scan time = TR $\times$ N_{av} $\times$ N_{PE}

‘3D’ Sequences

- True 3D volume rather than multiple 2D slices
- A slab or multiple-slabs are selected
- Phase encoding also in the ‘slice’ dimension
  - Through-plane resolution can be comparable to in-plane
  - Phase wrap in ‘slice’ direction
- SNR is improved, scan time longer:

$$N_{PE} \times TR \times NEX \times N_s$$

Volumetric Imaging

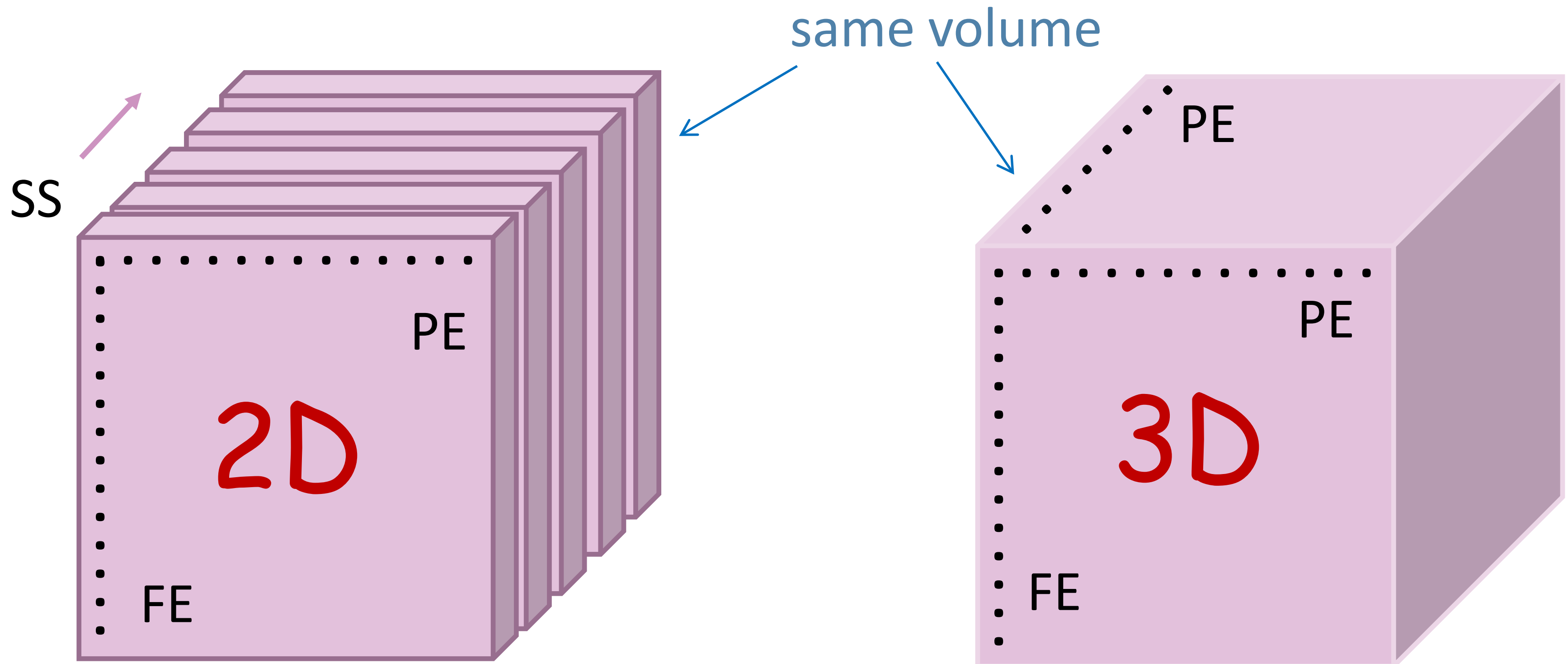

Scan time = TR × N_{av} × N_{PE}

Scan time = TR × N_{av} × N_{PE1} × N_{PE2}

Typical gradient resolution parameters (45 mT/m):
(2D) in-plane 0.012 mm; slice thickness 0.1 mm
(3D) partition 0.05 mm

What is k-space?

- 'k' is wave-number: number of cycles per unit distance
  - Spatial analogue to 'cycles per second' (frequency)
- k-space is the raw data
  - An array of numbers whose FT is the MR image
- Each row in k-space corresponds to the echo data obtained from a single application of the PE gradient
  - Rows near centre correspond to low-order PE steps (small gradients)
  - Rows at edges correspond to high-order steps

What is k-space?

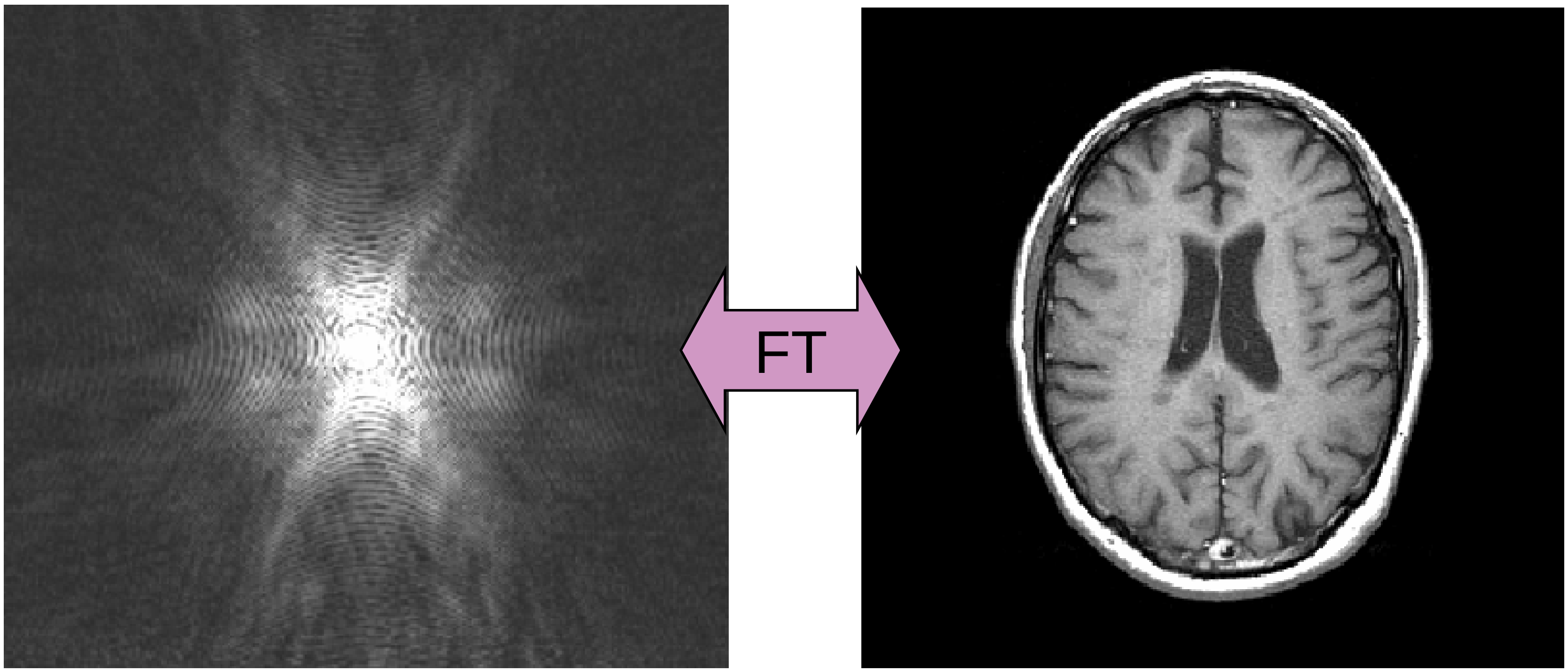

k-space and image-space of the brain

What is k-space?

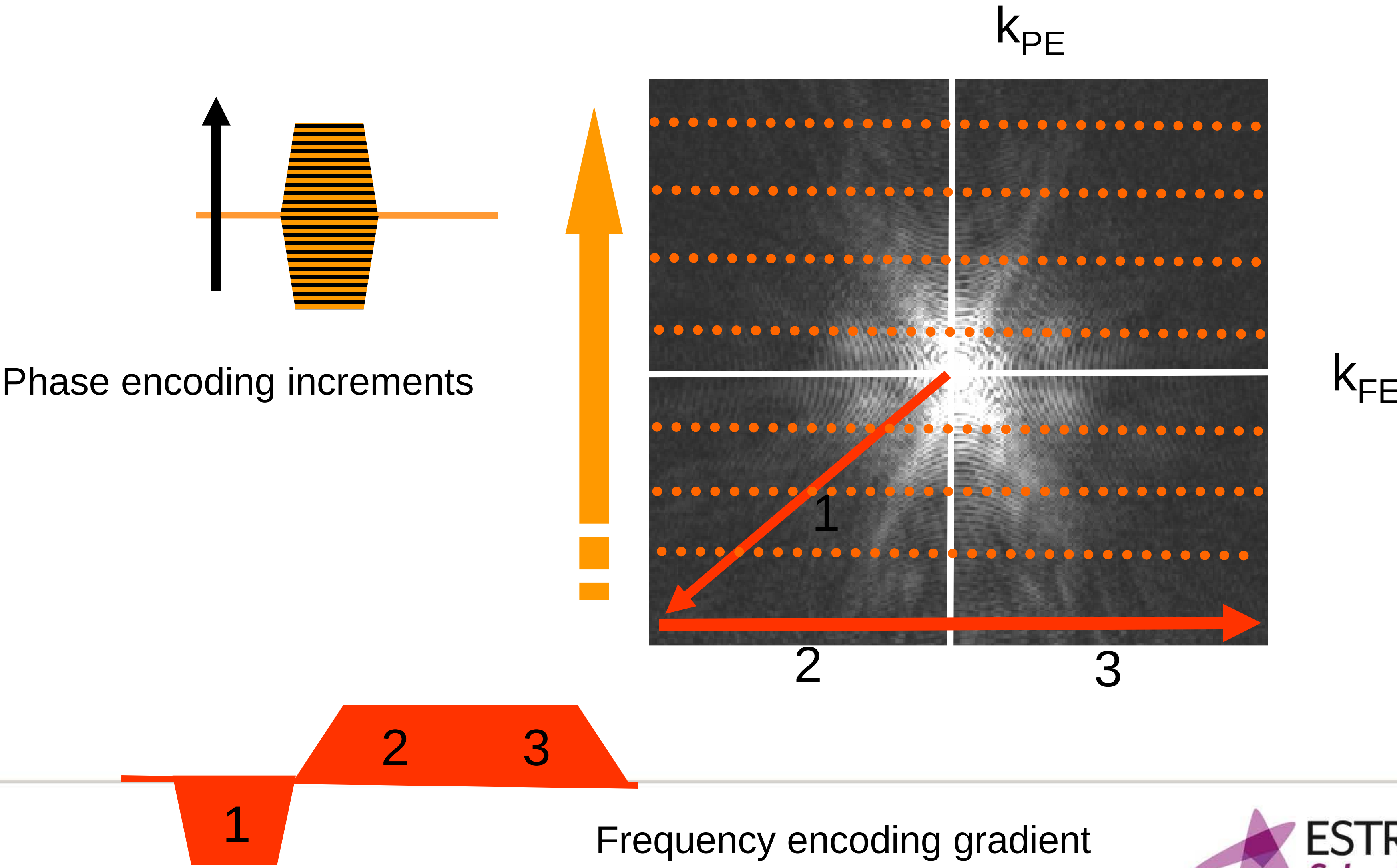

k-space

- All of k-space needs to be filled to create an image
  - ✓ Centre: bulk signal/contrast information
  - ✓ Edge: image detail
- Individual cells do not correspond one-to-one with individual pixels in image
- Each cell has information about every image pixel: *explains why motion artefacts propagate through whole image*

k-space

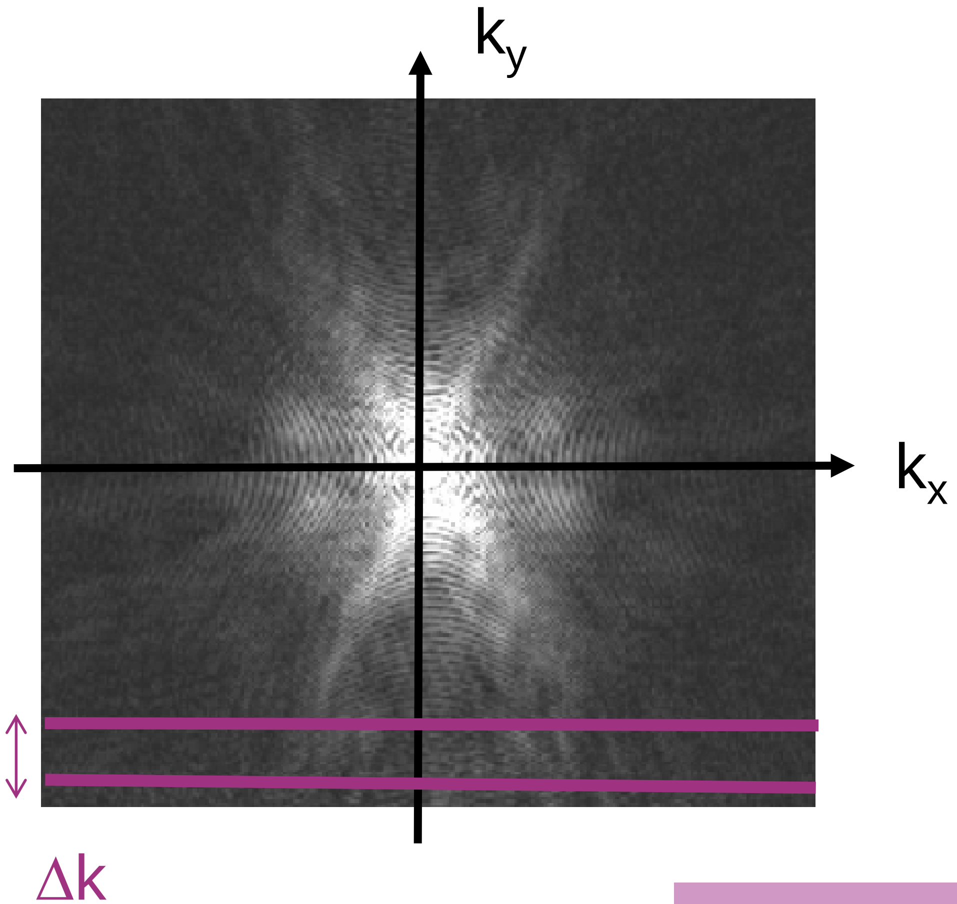

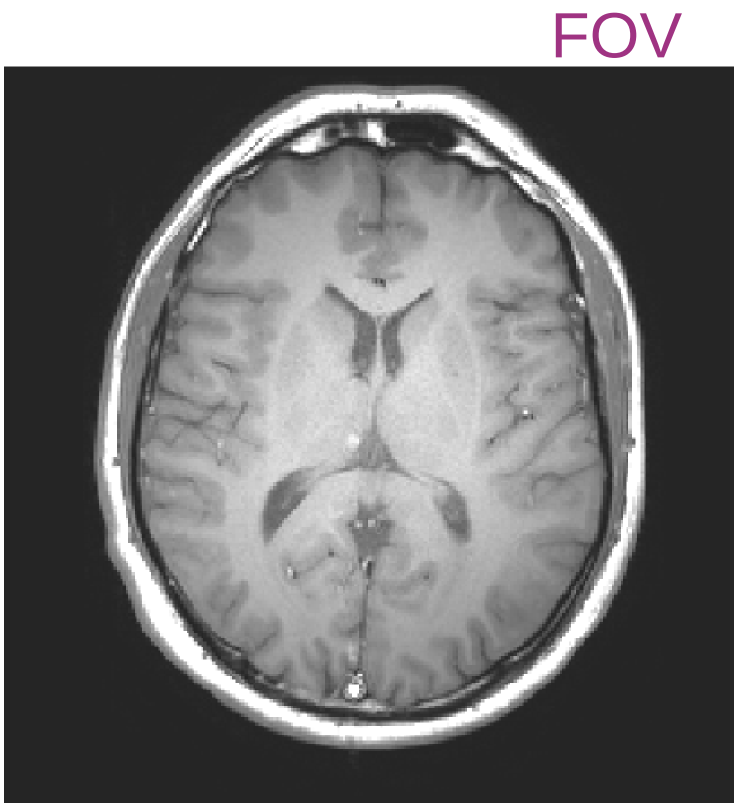

$$FOV = 1/\Delta k$$
$$\Delta x = 1/FOV_k$$

k-space

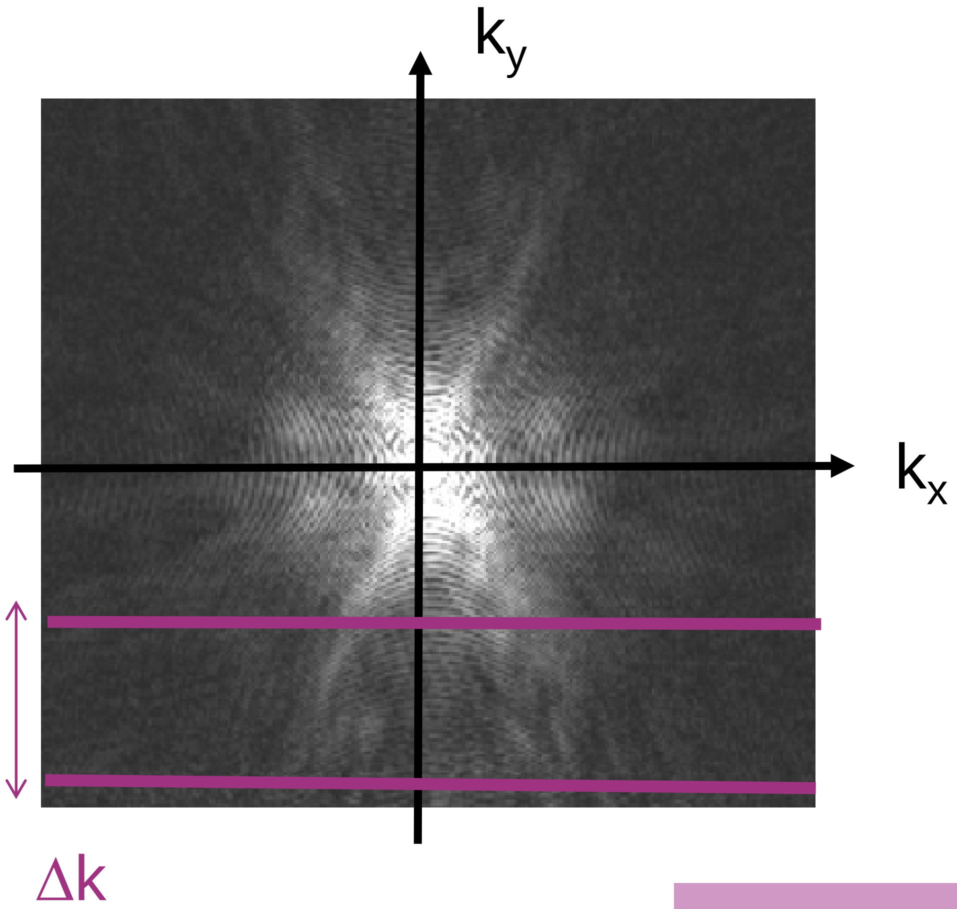

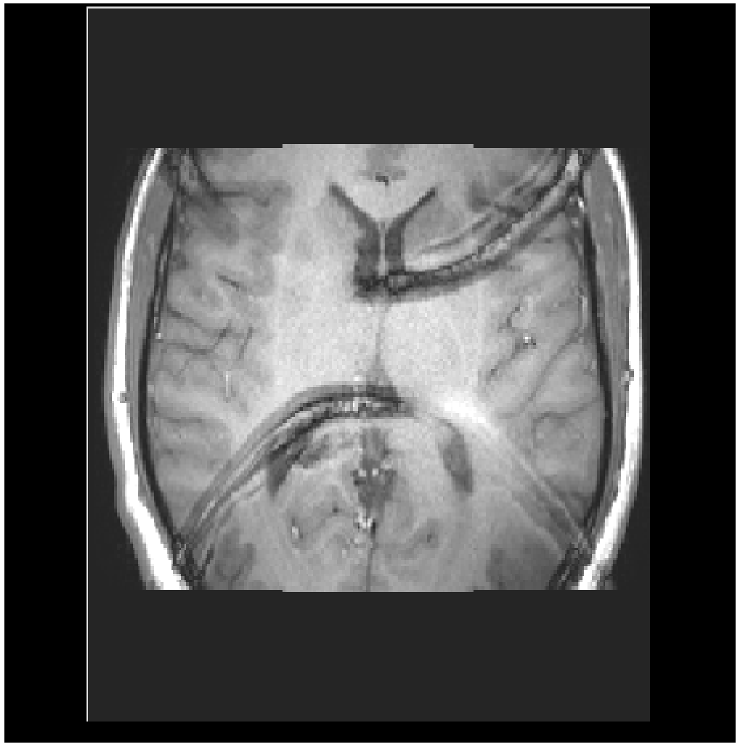

$FOV = 1/\Delta k$

$\Delta x = 1/FOV_k$

k-space

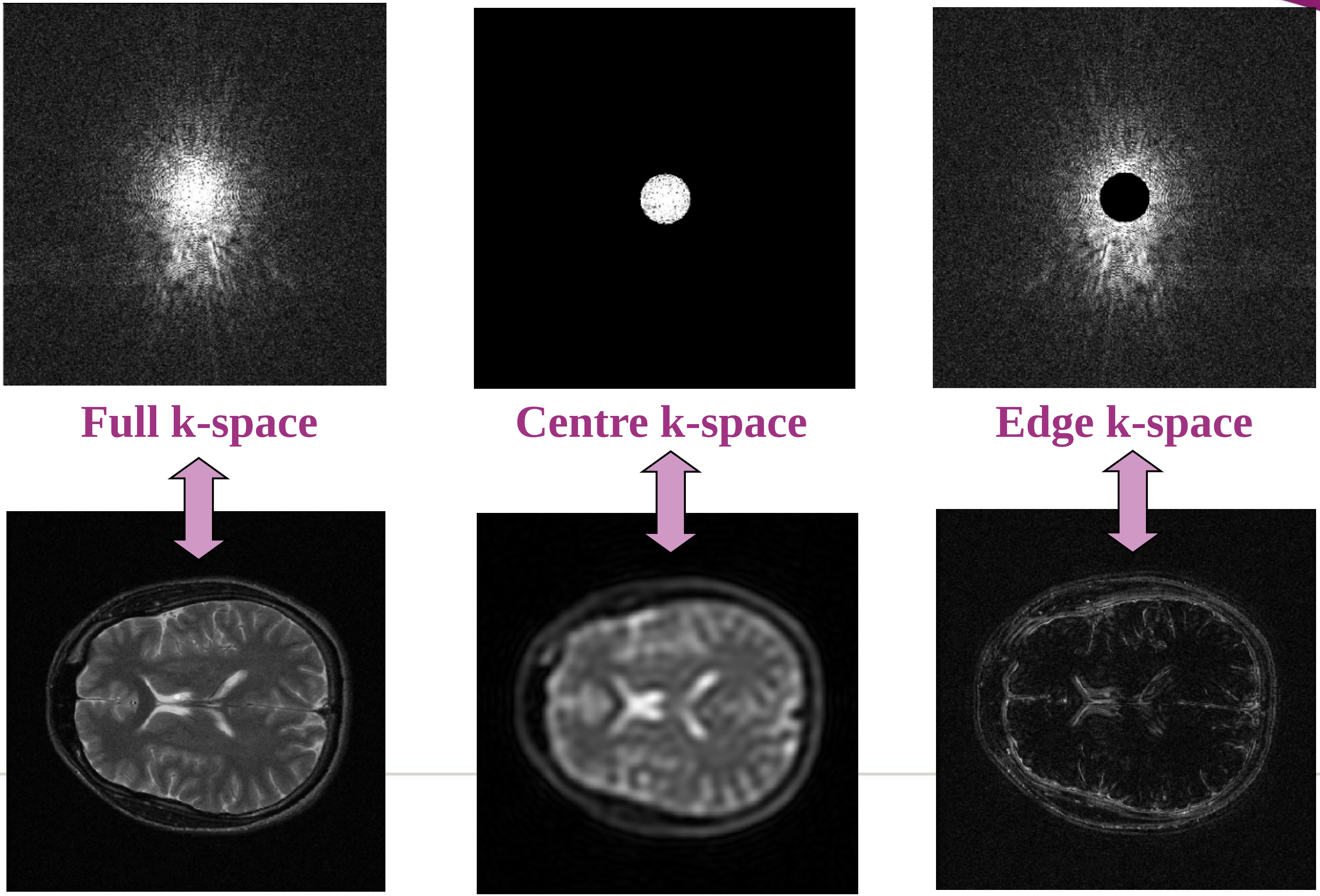

k-space: Acquisition strategies

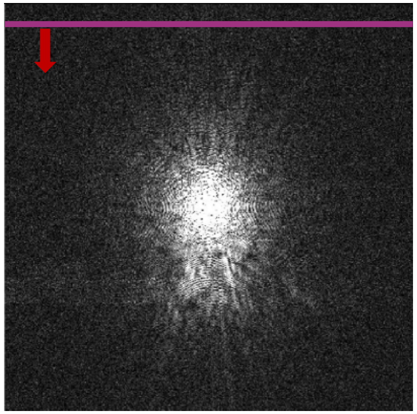

One line per TR

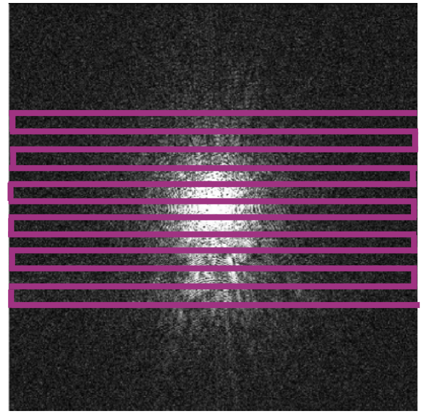

Single-Shot

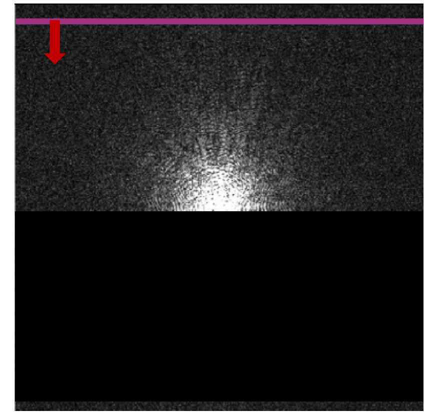

Partial Data

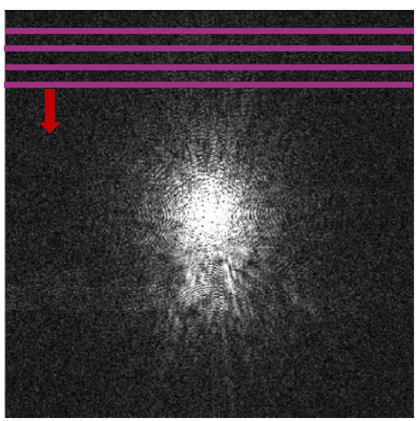

Multiple lines per TR

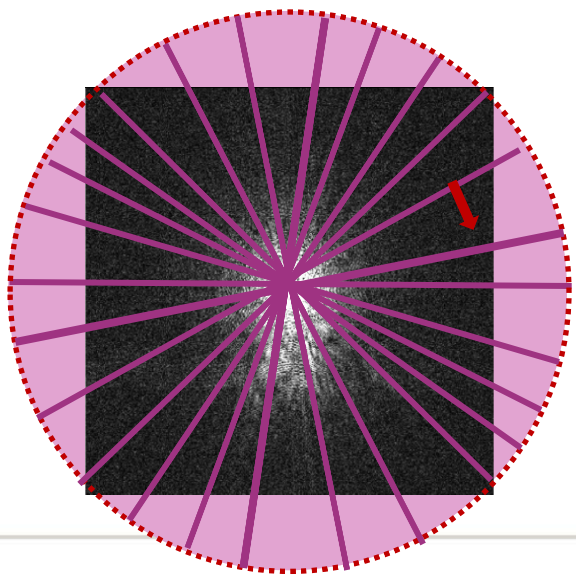

Radial

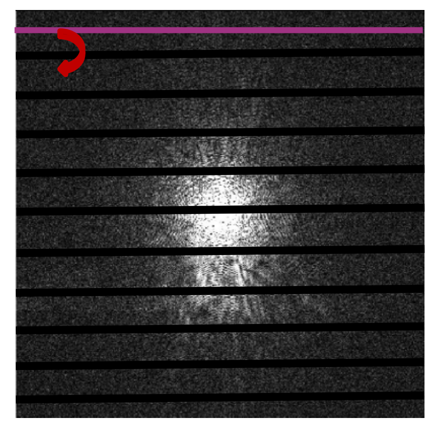

Skip lines

ESTRO School

k-space: Acquisition strategies

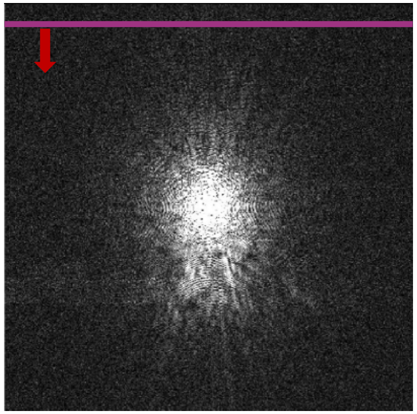

One line per TR

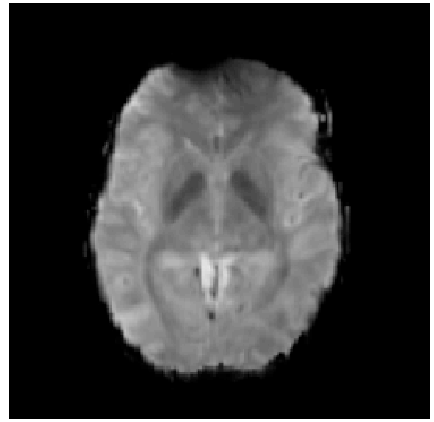

Single-Shot

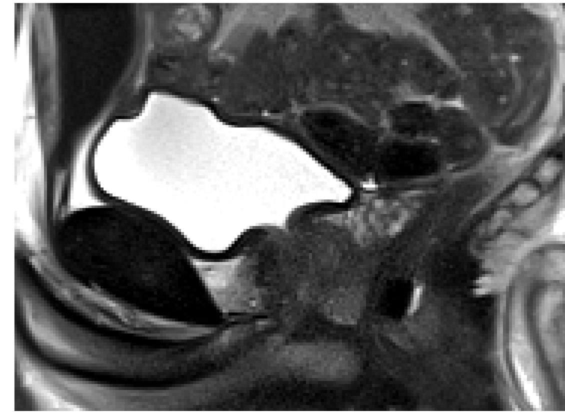

Partial Data

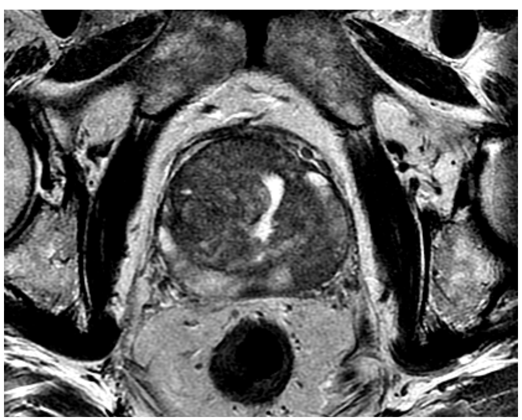

Multiple lines per TR

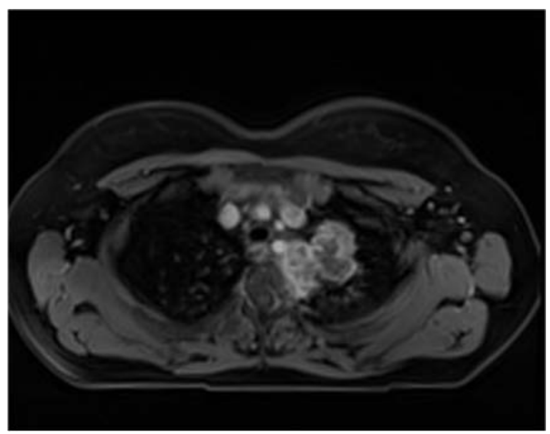

Radial

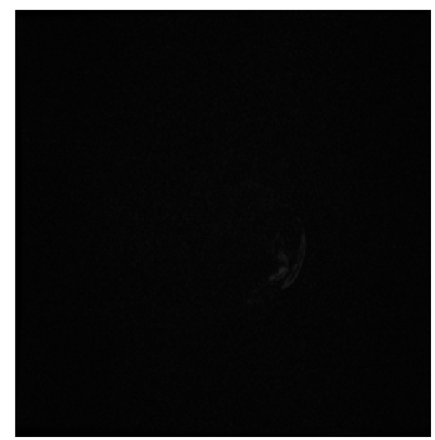

Skip lines

5th MR in RT Symposium 2017

www.mrinrt2017.com

ESTRO School

MRI Physics: Equipment

A/Prof Gary Liney

18th September 2016

ESTRO Imaging for Physicists

ESTRO School

Installation of New Scanner

ESTRO School

RF Cage

- MRI inherently low (RF) signal technique
- Faraday cage
  - All 6 sides enclosed in copper
  - Electromagnetic shielding
  - Examples microwave oven, coax cable
- Integrity must be maintained

  Penetration panel

  Mesh window, waveguide

  Closed scan room door, no fluorescent lights

RF Cage Construction

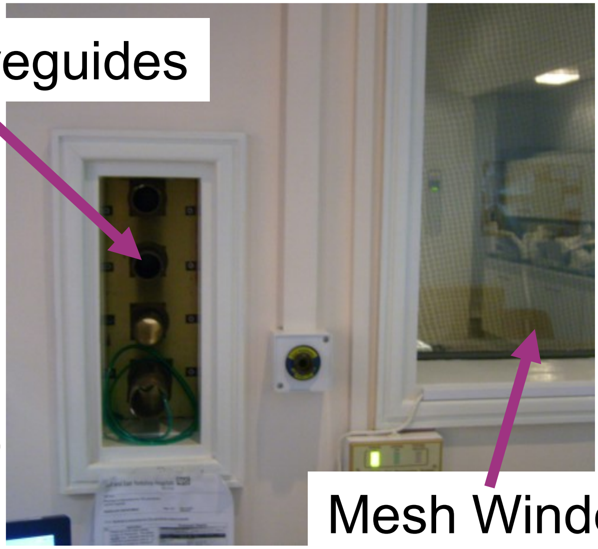

The MRI Controlled Area

Quench pipe

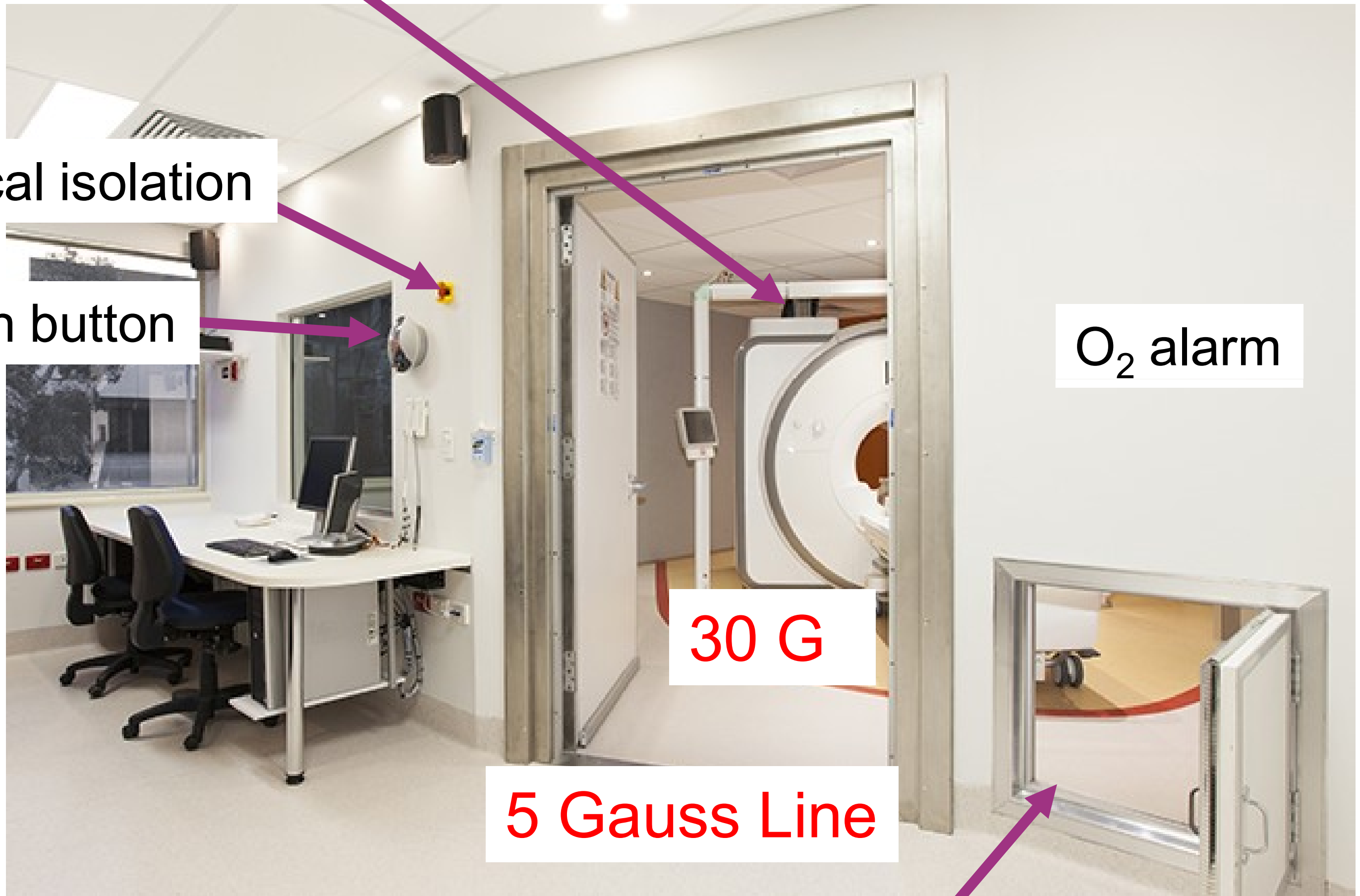

Control Room

Pressure release hatch

ESTRO School

The Inner Controlled Area

Scan Room

30 Gauss

Cabinet (Equipment) Room

Heat Exchanger

RF

Gradients

MNS

MRI Equipment: Overview

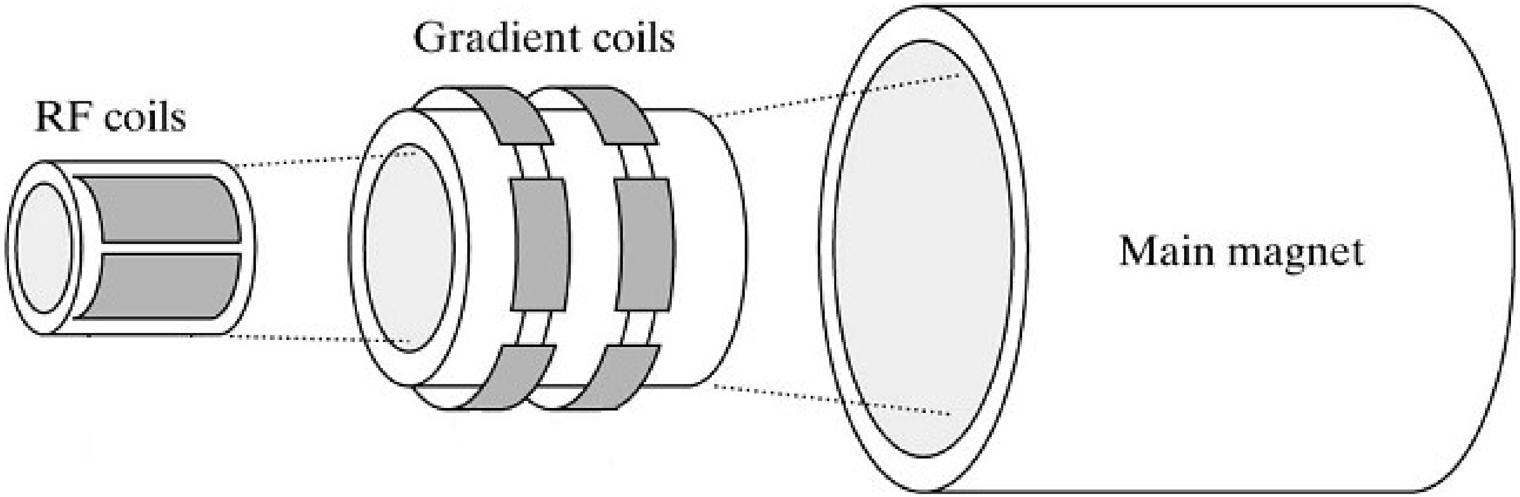

Plus:

Peripheral equipment

RT Specific equipment

Test Objects

Patient Bore

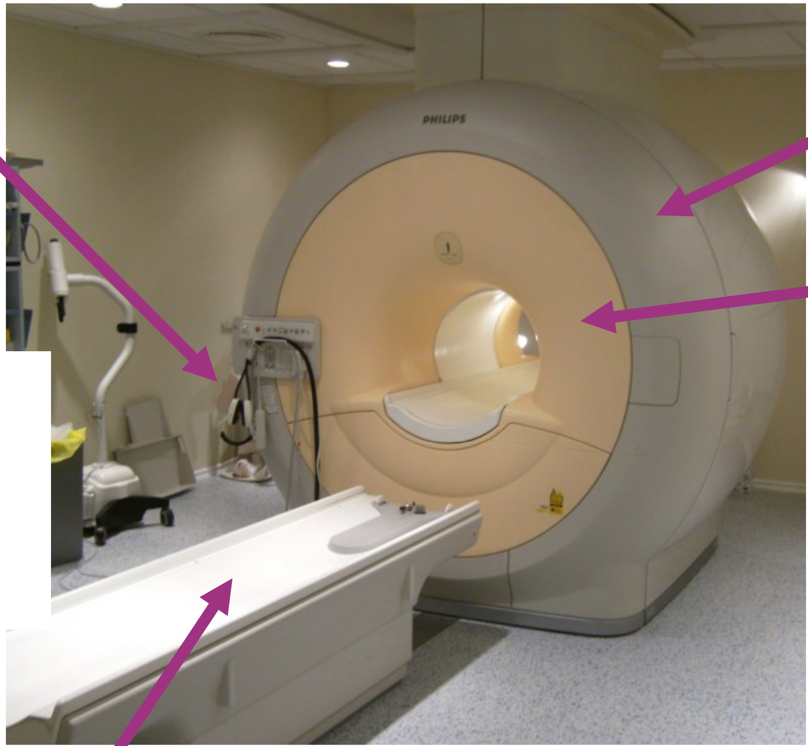

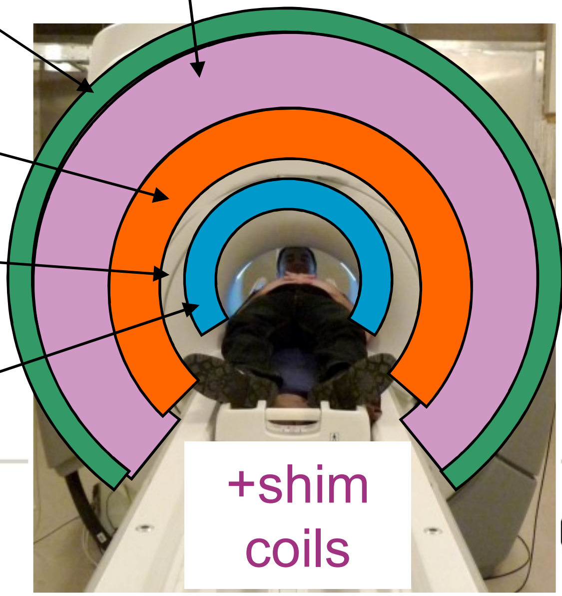

Example Specifications

Shielding	Passive and active
Homogeneity (ppm)	0.2 (40 cm DSV)
Field stability (ppm/hr)	<0.1
Cooling	Liquid helium only
Boil-off (l/hr)	0
Helium refill	10 years
Shim plates	16 x 15
Active shim	3 linear terms (20 coils) 5 2nd order (32 coils)
Mass (tonnes)	5.5
Radial (x,y) 5 Gauss	2.5
Axial (z) 5 Gauss	4.0
Minimum area (m^2)	<30

Example Specifications

RF channels	8,18,32
Bandwidth (MHz)	1
Gradient amplitude (mT/m)	33, 40, 45
Slew rate (mT/m/ms)	125-200

Host computer	2 x Pentium IV
Memory (GB)	2
Hard drive (GB)	73 GB (images)
Image processor speed	2.2 GHz
Reconstruction (ips 256^2 matrix)	1002

Magnet

- Application
  - Whole body (head only) & peripheral systems
- Type
  - Permanent, resistive, superconducting
- Orientation
  - Horizontal, vertical field
- Design
  - Tunnel-short & wide bore
  - Open

1987: Elscint's Gyrex System

Philips' vertical HFO System

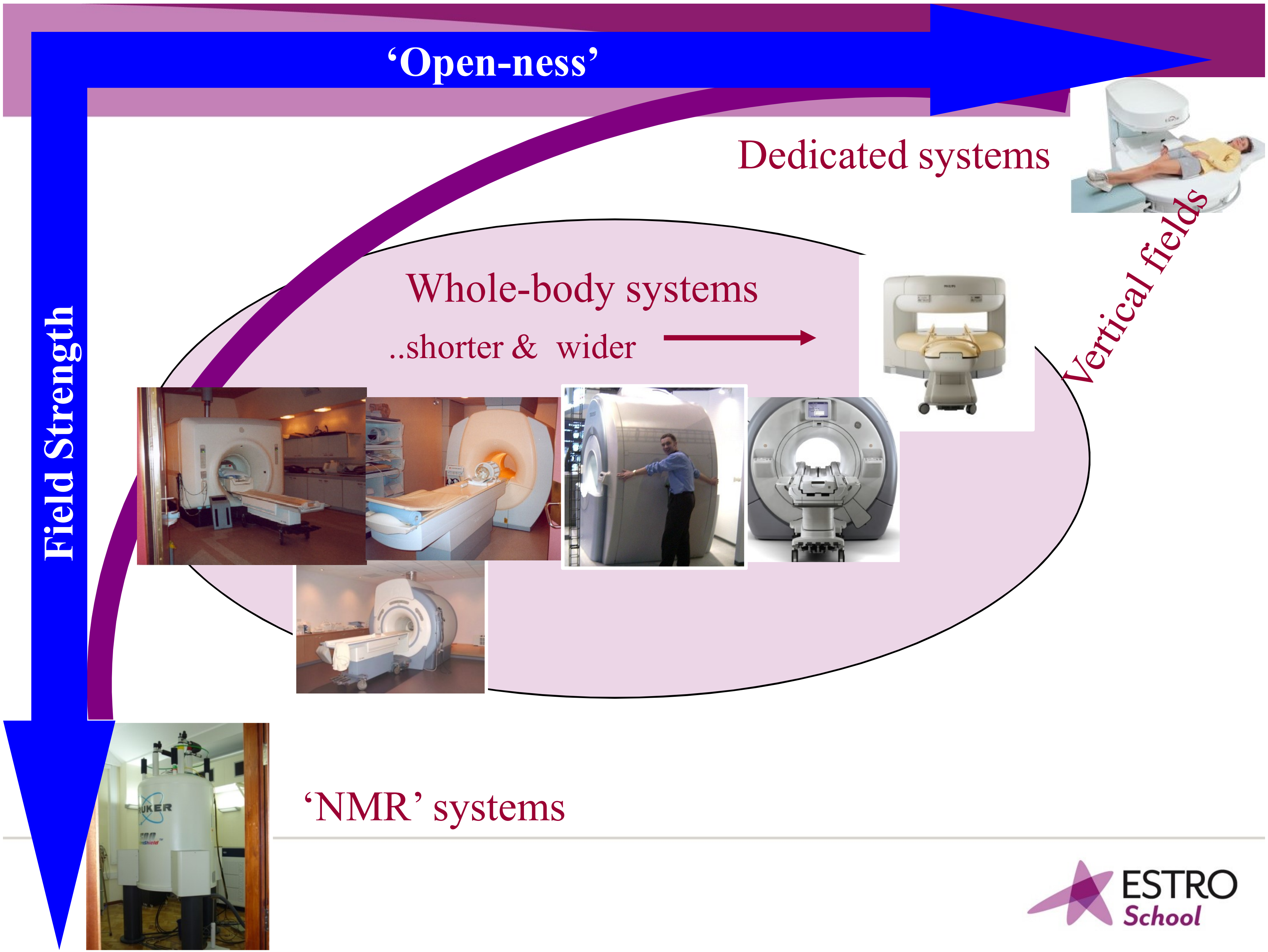

'Open-ness'
Field Strength
Dedicated systems
Vertical fields
Whole-body systems
..shorter & wider
'NMR' systems
ESTRO
School

Static Field (B_0)

- Low sensitivity requires high field
- 1 Tesla = 10,000 Gauss

  0.3-0.7 G Earth's field
- Projectile effect
- Mostly superconductors

  field decay: 5-10 G y^{-1}

  field stability: <0.1 ppm h^{-1}

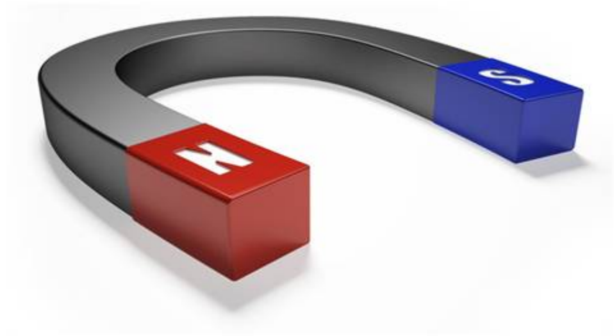

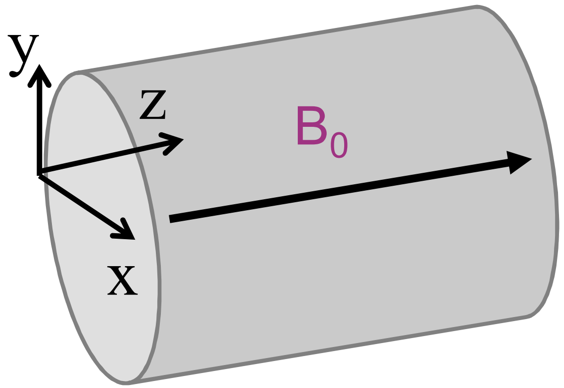

Superconductors

- Niobium-Titanium
- Cryostat
  - Double dewar with nitrogen/helium
  - Cryoshielding helium only
- Cryogens
  - Replenish due to Boil off
  - zero boil off/cryogen free
- Quench
  - Expensive & safety risk!
  - Vent pipe, oxygen monitor

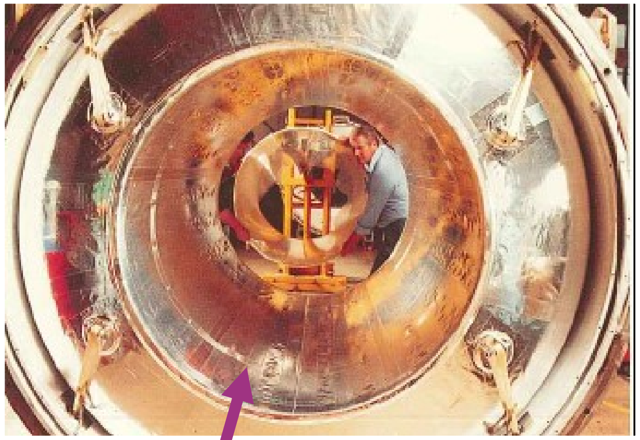

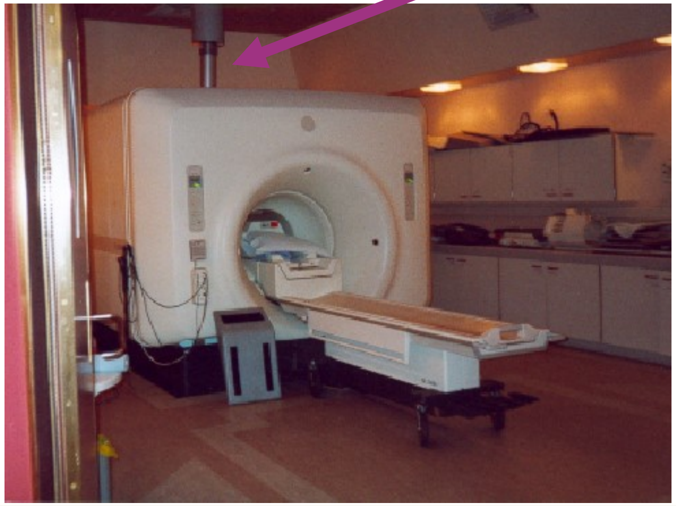

Homogeneity

Uniform imaging volume at isocentre

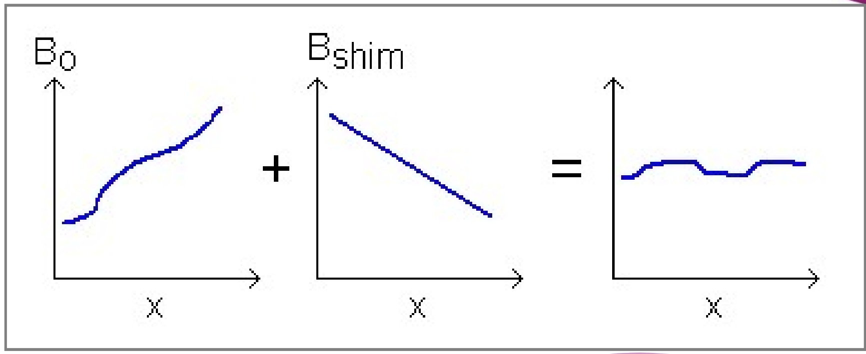

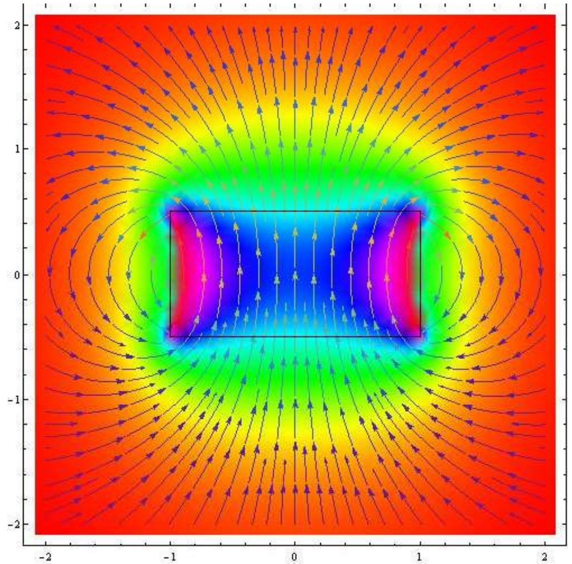

http://en.wikipedia.org/wiki/File:Finite_Length_Solenoid_field_radius_1_length_1.jpg#/media/File:Finite_Length_Solenoid_field_radius_1_length_1.jpg

Off-centre imaging? RT Planning?

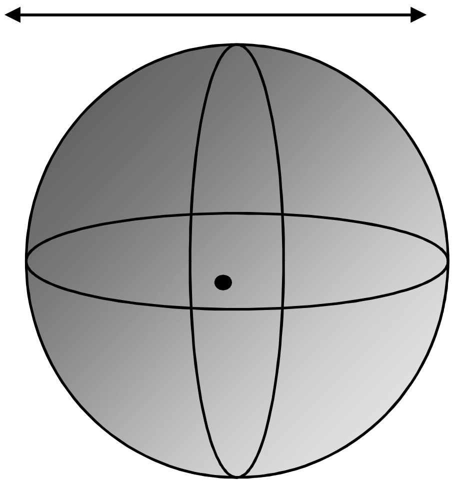

e.g. DSV_{40cm} = 0.2 ppm

(at 1.5 T):
0.2 x 63.87 MHz = 12.8 Hz

- Magnet is shimmed at installation- additional (dynamic) shimming may be required

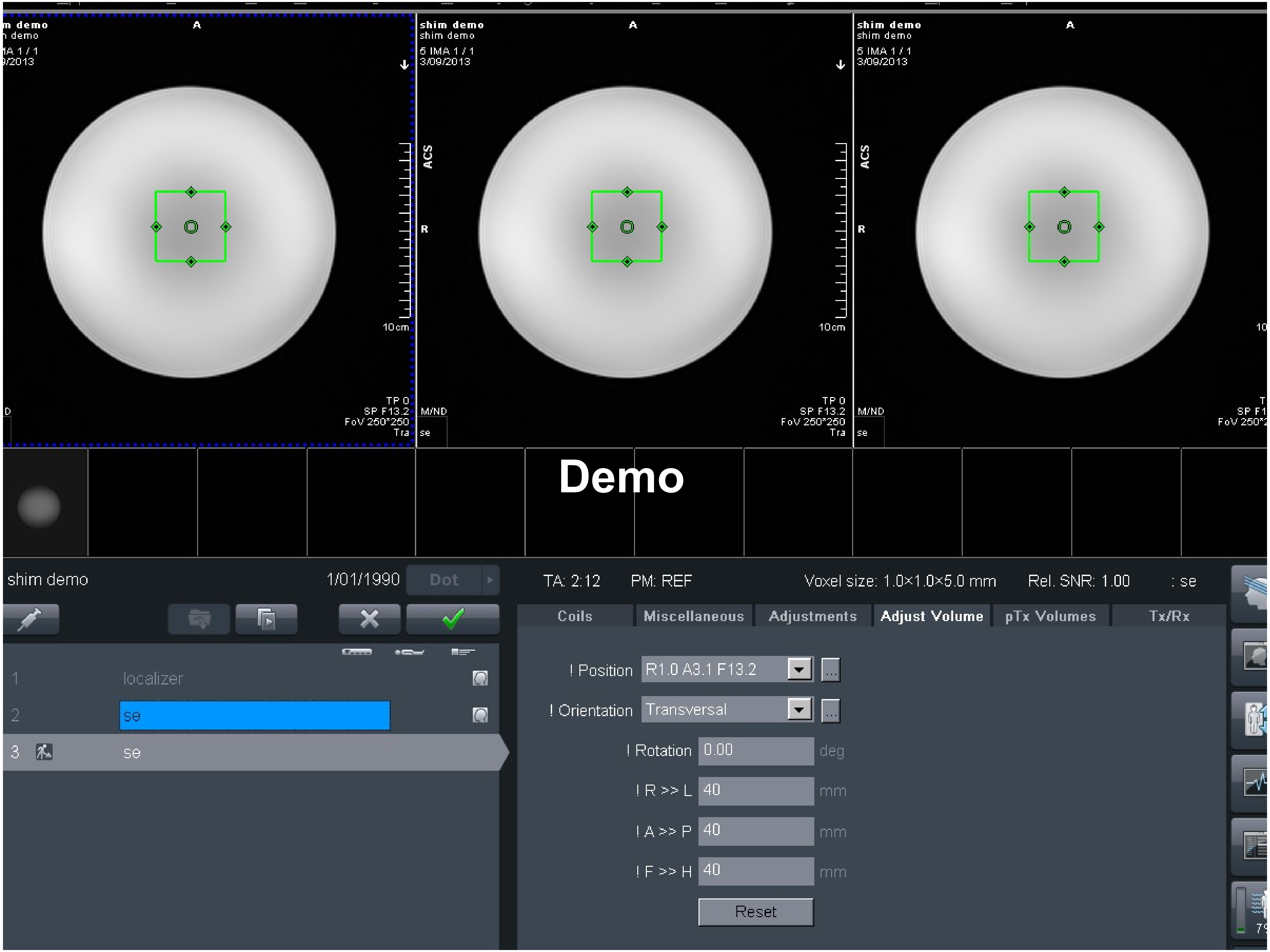

shim demo
A
5 IMA 1 / 1
3/09/2013
ACS
R
10cm
TP 0
SP F13.2
FoV 250*250
Tra
M/ND
se
Demo
shim demo
1/01/1990
Dot
TA: 2:12
PM: REF
Voxel size: 1.0×1.0×5.0 mm
Rel. SNR: 1.00
: se
Coils
Miscellaneous
Adjustments
Adjust Volume
pTx Volumes
Tx/Rx
1 localizer
2 se
3 se
! Position R1.0 A3.1 F13.2
! Orientation Transversal
! Rotation 0.00 deg
! R >> L 40 mm
! A >> P 40 mm
! F >> H 40 mm
Reset

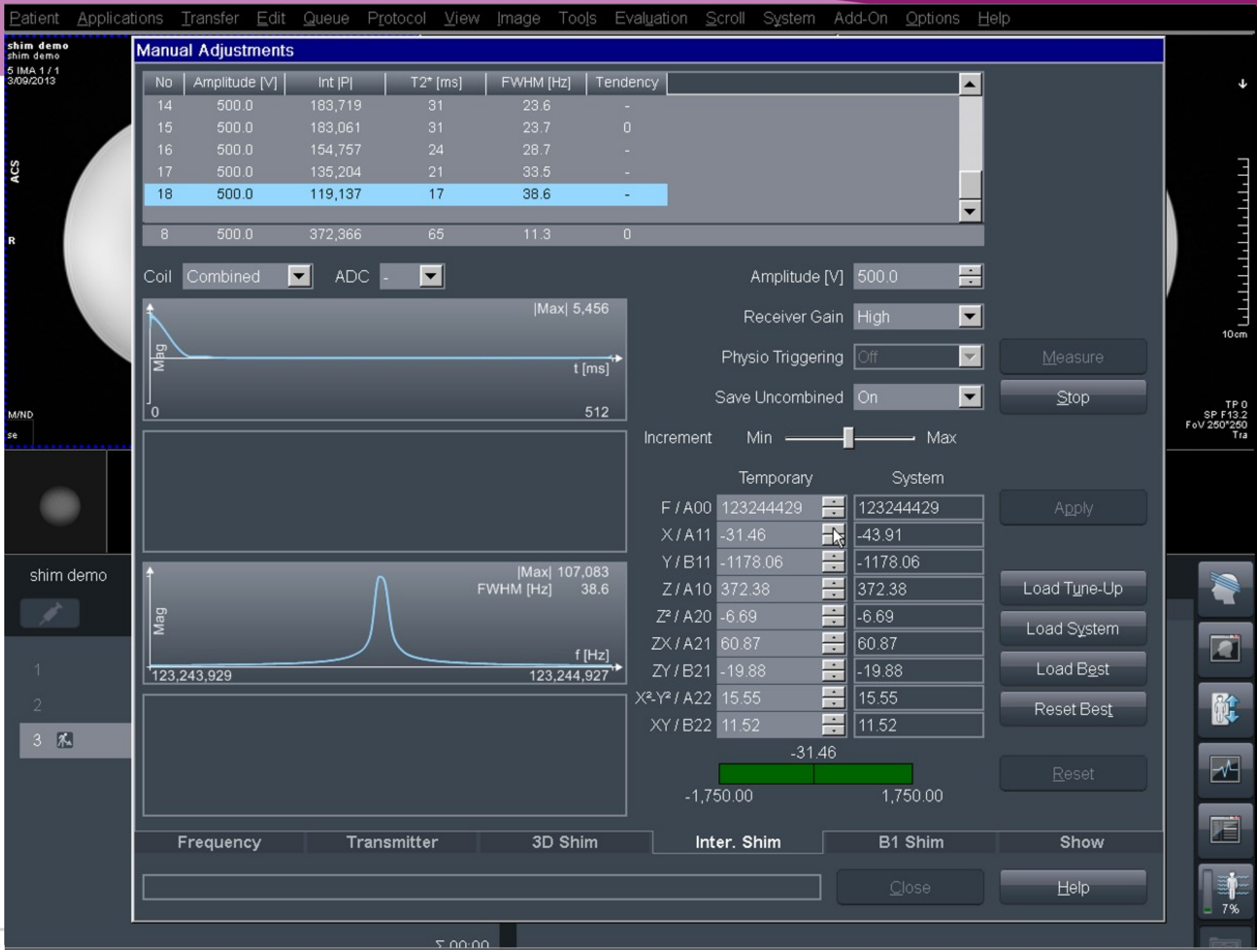

ESTRO School

Fringe (stray) Field

- Scanner 'footprint'
  - Credit cards erased at 10 G
  - Safety limit is 'five gauss line'
- 7 Tesla scanner has 23 m 5 G line
  - Passive & Active shielding
- Radial & axial components
  - Typically axial 1.6 times larger
- May be measured with handheld gaussmeter

> 30 G	Stainless steel, non-ferromagnetic objects
< 30 G	ECG monitors, unrestrained ferromagnetic objects
< 10 G	Credit cards, x-ray tubes
< 5 G	Pacemakers, general public
< 3 G	Moving cars etc
< 1 G	TVs, CT & PET scanners
< 0.5 G	Railways, gamma cameras

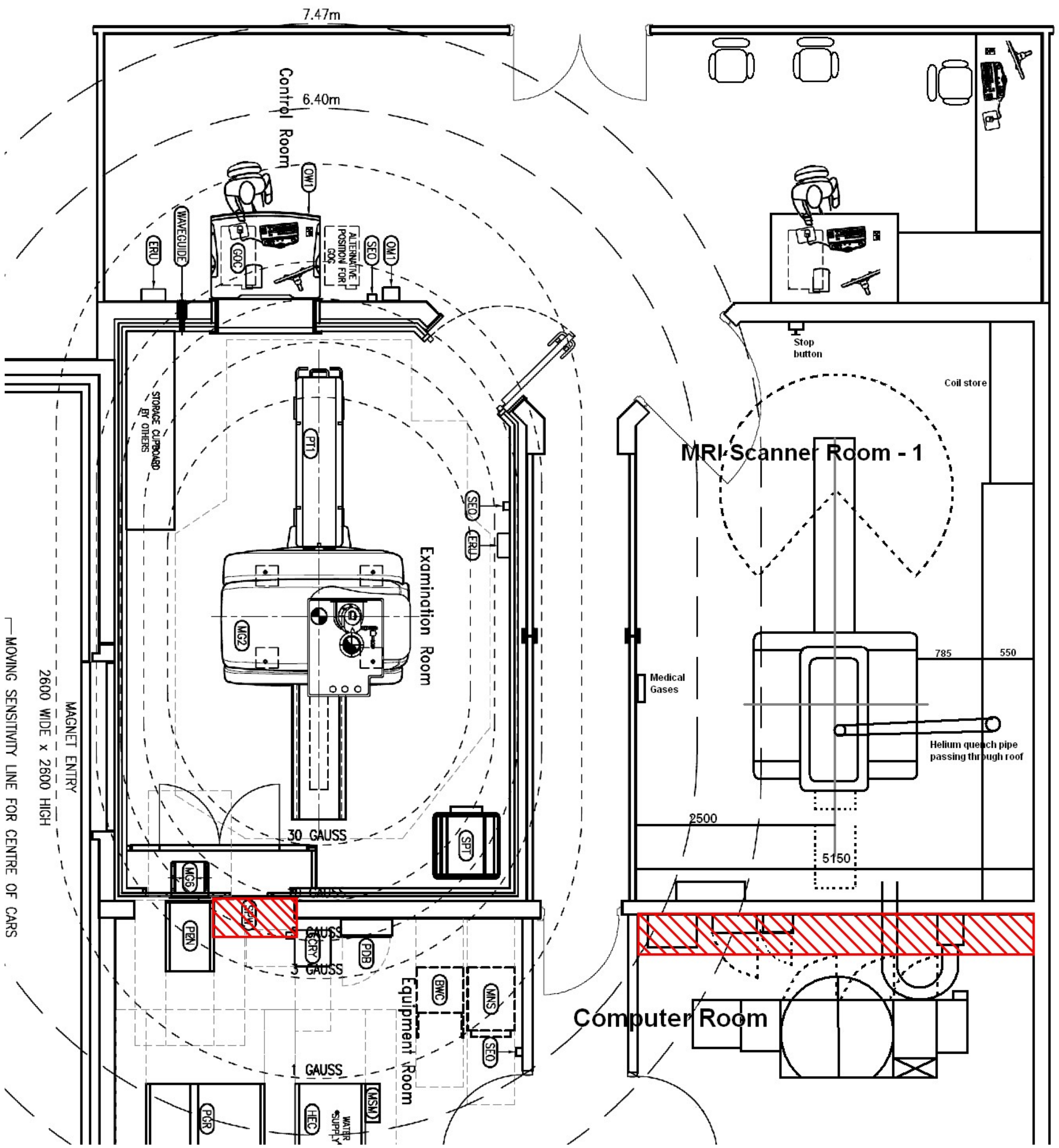
7.47m
6.40m
Control Room
Examination Room
MRI Scanner Room - 1
Stop button
Coil store
Medical Gases
Helium quench pipe passing through roof
785
550
2500
5150
30 GAUSS
3 GAUSS
1 GAUSS
Equipment Room
Computer Room
MAGNET ENTRY
2600 WIDE x 2600 HIGH
MOVING SENSITIVITY LINE FOR CENTRE OF CARS
STORAGE CUPBOARD BY OTHERS
WAVEGUIDE
ALTERNATIVE POSITION FOR GOC


WARNING

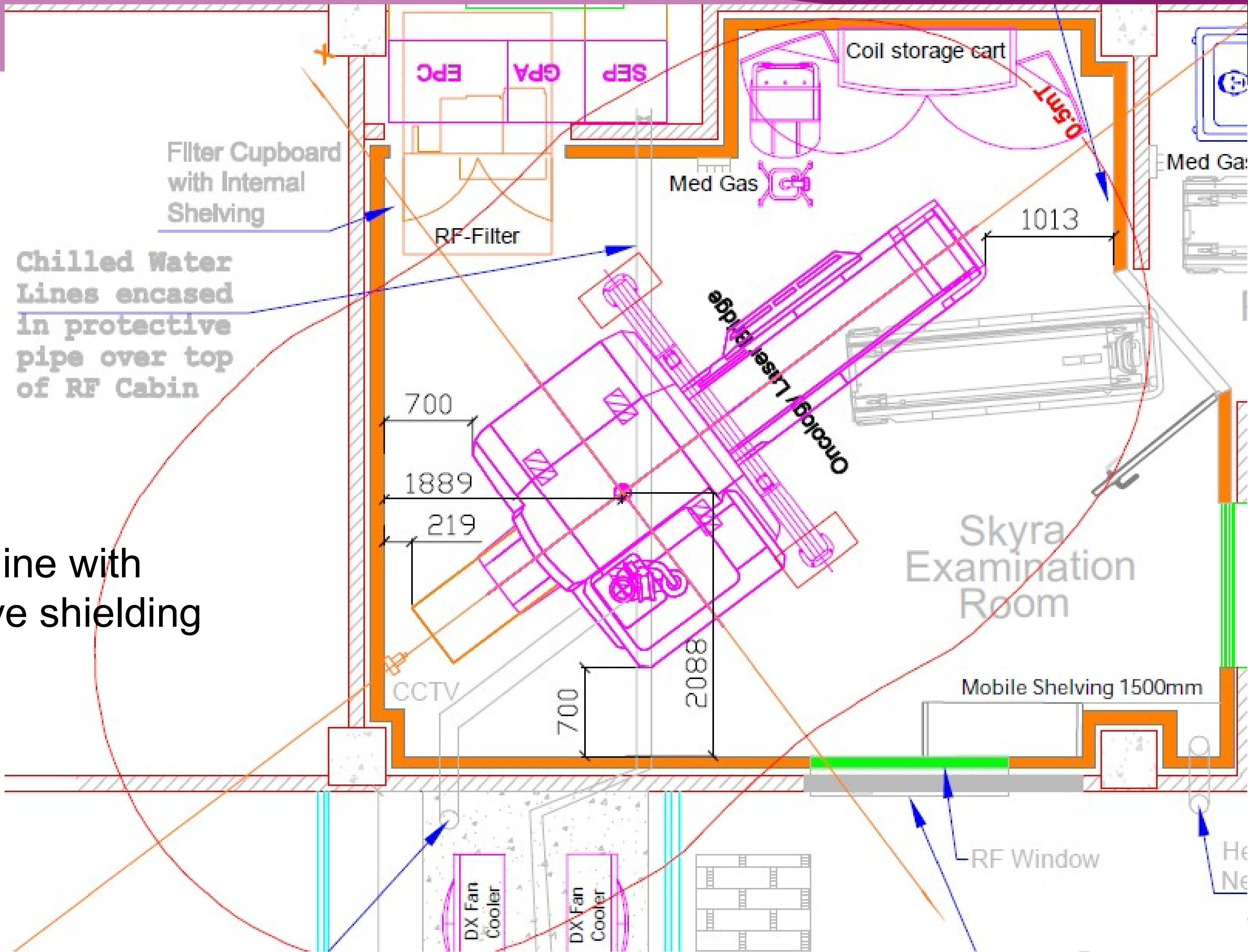

5 G line with Active shielding

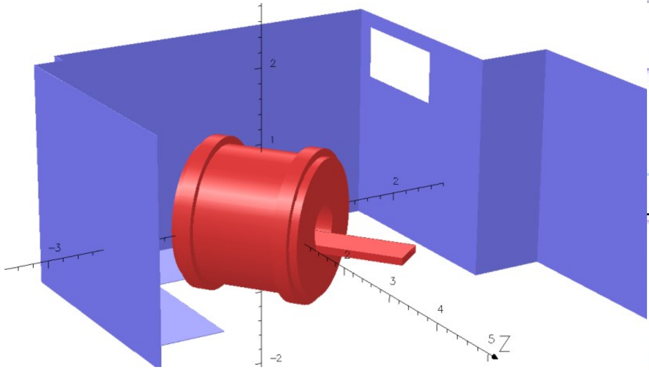

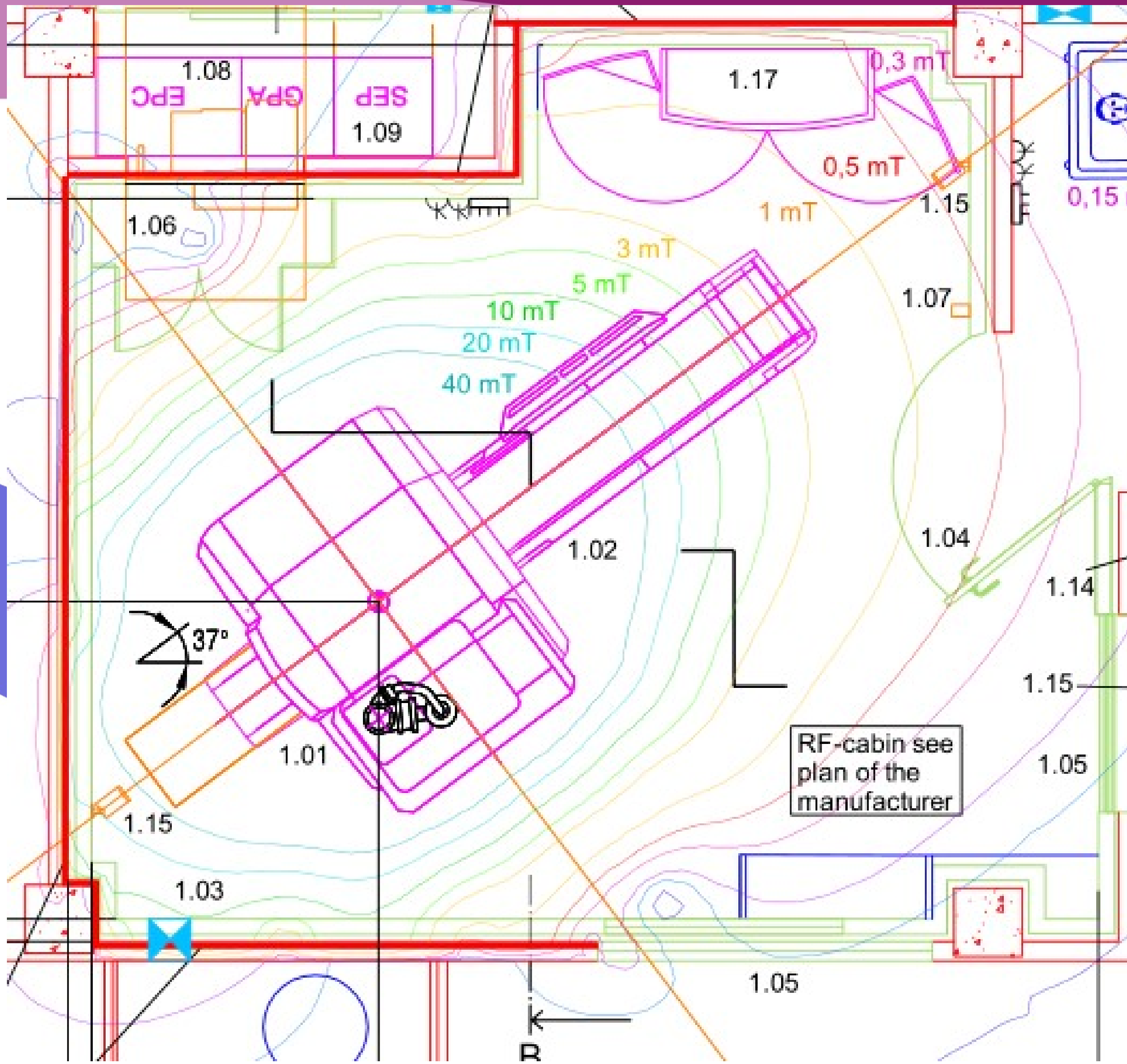

+ Passive shielding

Gradients (db/dt)

- 3 orthogonal or in combination
- High amplitudes
  - -Resolution
  - -DTI
- Fast switching rates
  - -Faster scans

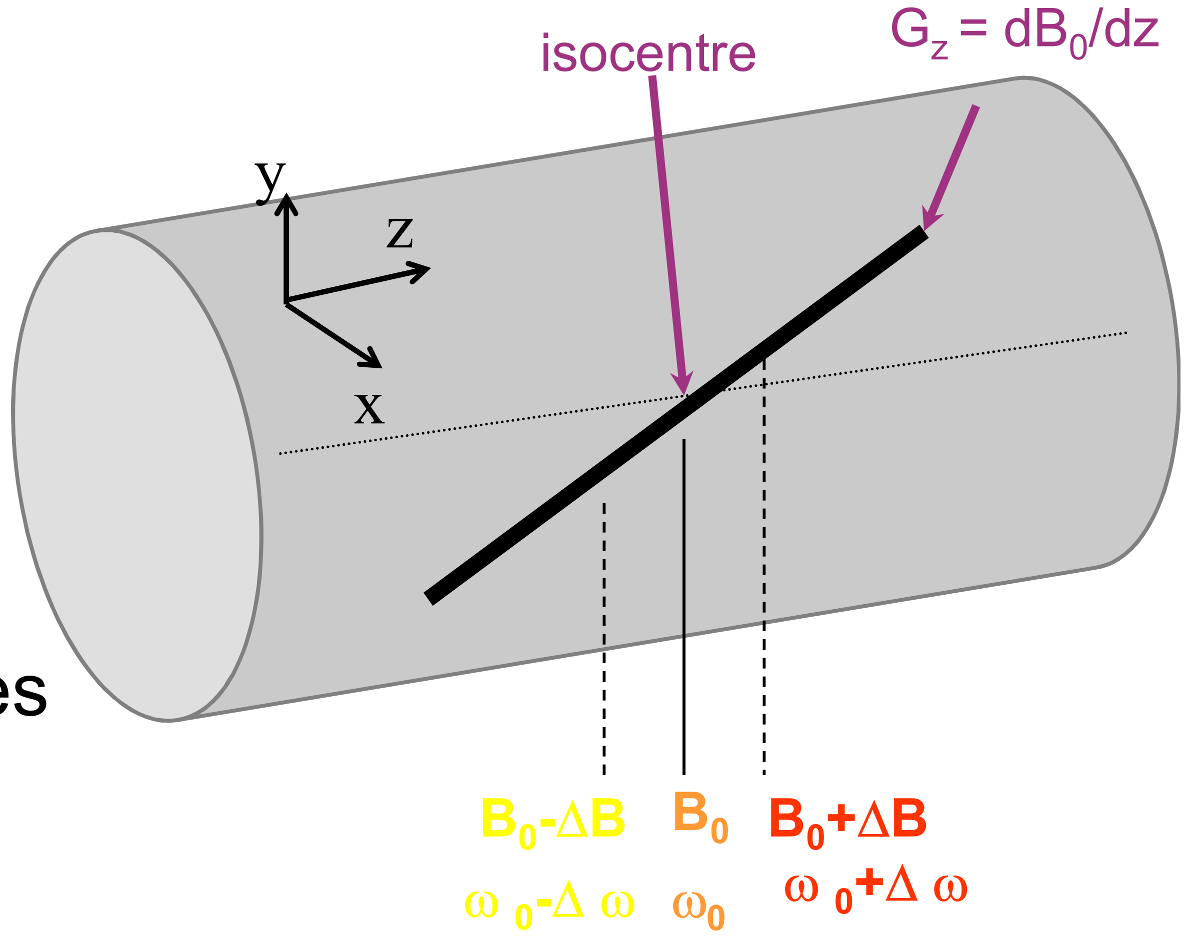

Gradients

- Gradient waveform trapezoidal
- Amplitude, Rise time, Slew rate
  e.g. 10-50 mT/m, 200 μs & 20-150 T/m/s
- Linearity
  Distortion for RT planning?
  GradWarp or similar in 2D/3D

$$\text{Slew Rate (T/m/s)} = \frac{\text{Amplitude (mT/m)}}{\text{Rise Time }(\mu s)}$$

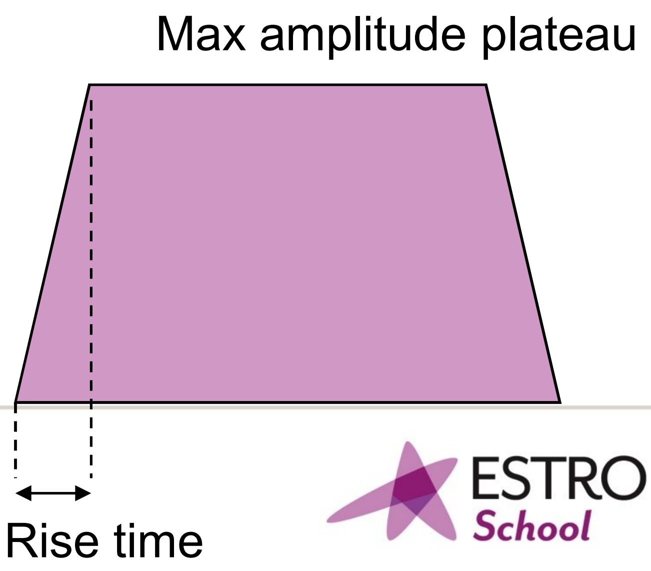

Gradients

Maxwell Pair

Separation = $r\sqrt{3}$

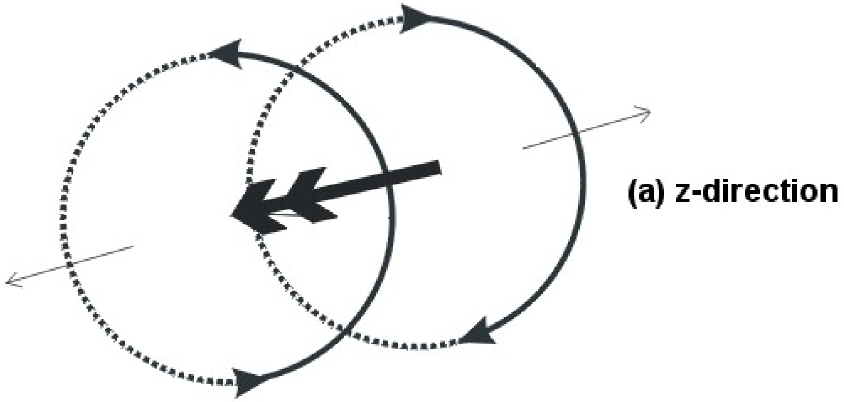

Golay Coils

Linear between central arcs

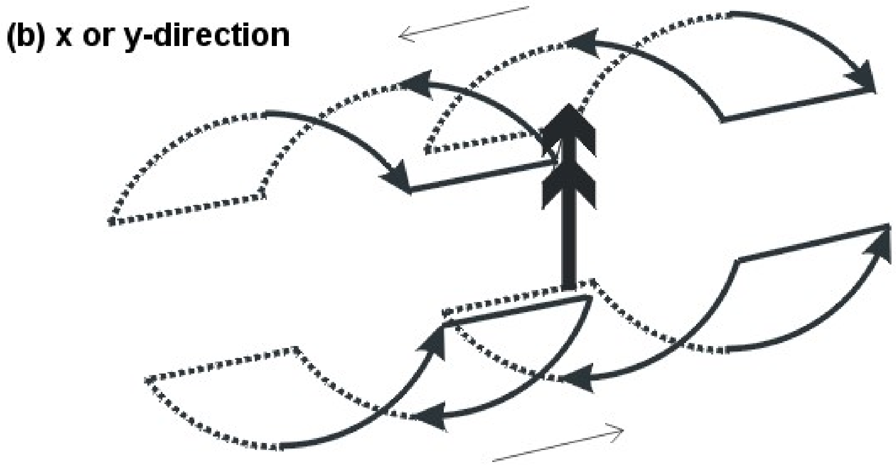

Optimised inductance 'fingerprint' coils

ESTRO School

Gradients

- Eddy currents degrade imaging
  - pre-emphasis (compensation)
  - Active shielding
- Lorentz force causes vibrations
  - Noise & reduction methods

Manufacturer	Field Strength (T)	SPL (dB(A))
Philips	1.5	112
Siemens	1.5	106
GE	1.5	110
Varian	3.0	118
Bruker	3.0	113

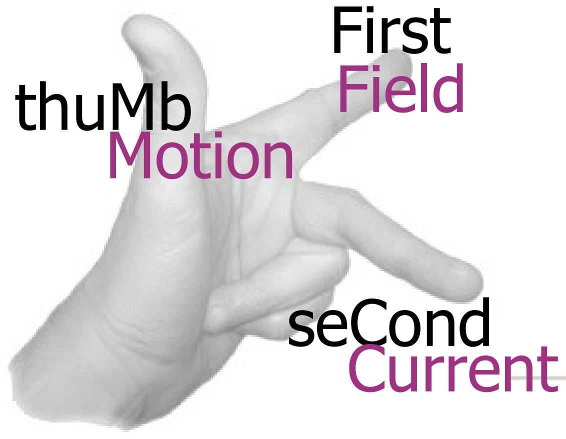

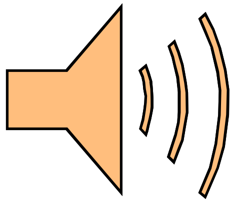

Peripheral Nerve Stimulation (PNS)

- Faster switching = faster imaging
- Stimulation real issue
- Reilly estimates (right)
- Solutions:

  Parallel imaging ('Coil Encoding')

  Twin gradients

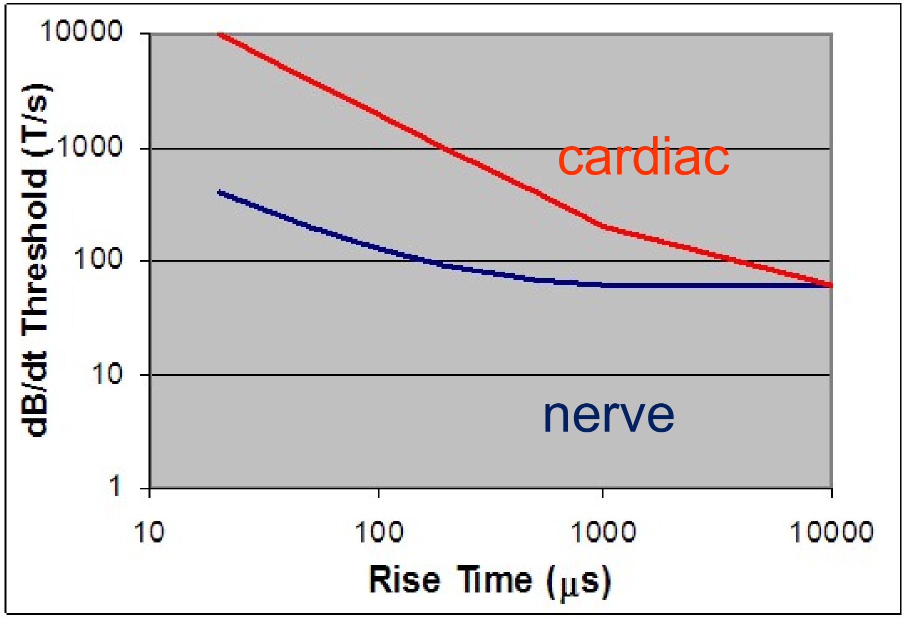

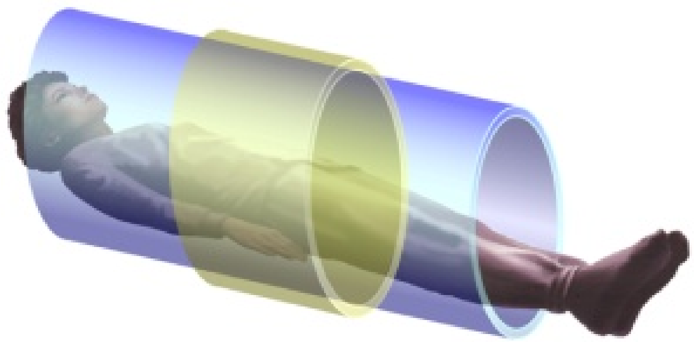

ESTRO School

RF Coils (B_1)

- Coil Usage:

  Transmit and/or receive at resonance

- Properties

  Cable loss, loading

  Q factor ($\omega/\Delta\omega$)

  Efficiency $1\text{-}Q_L/Q_0$

  Filling factor

- RF heating effects (SAR)

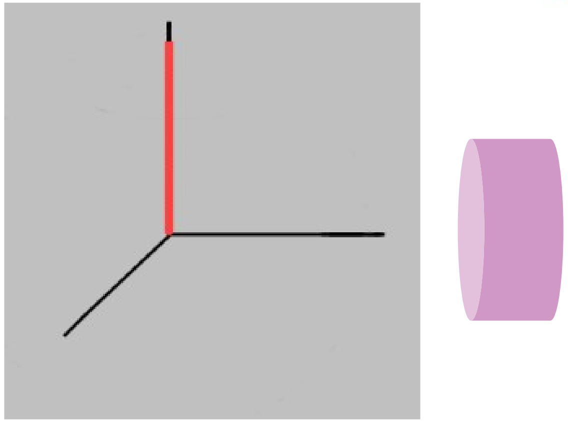

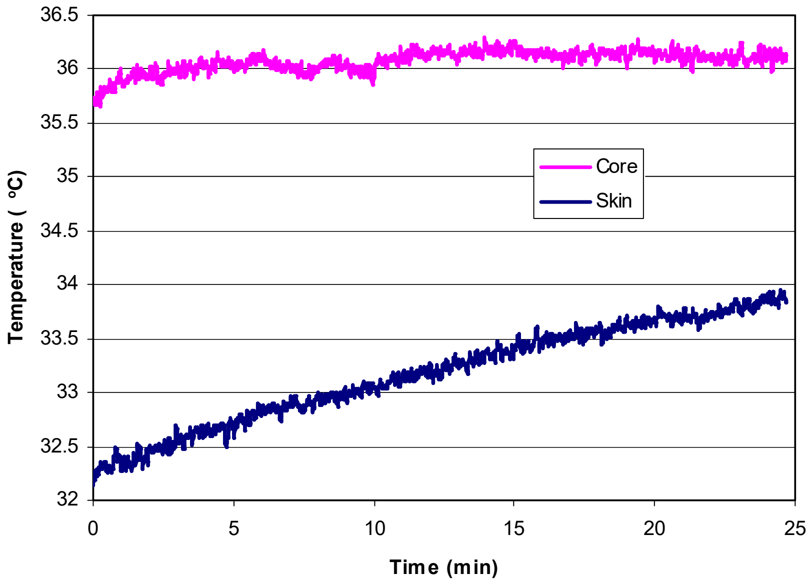

RF Chain

- DAC

  Turns digital signal to analogue for RF transmission
- Double balanced mixer

  Produces amplitude modulated RF waveform
- RF power amplifier
- RF Coil(s) transmit/receive signal
- Pre-Amp
- Phase sensitive demodulator

  Removes RF waveform from detected signal
- Low Pass Filter
- ADC

  Digitisers signal to be processed by computer

RF Coils: Signal Characteristics

$$B = \frac{\mu_0 I 2\pi a^2}{\left(\;\right)^{3/2}}$$

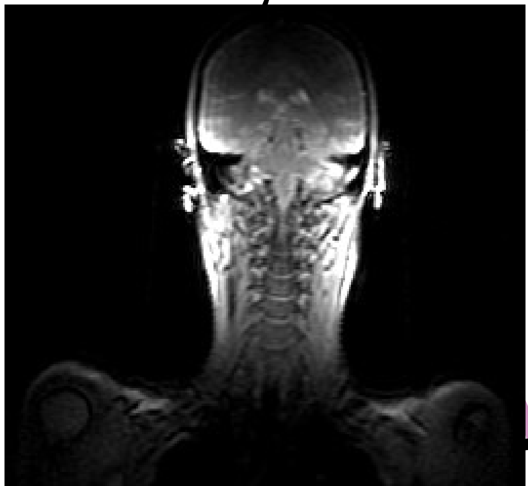

Surface Coil:
Excellent SNR close to coil

Poor uniformity

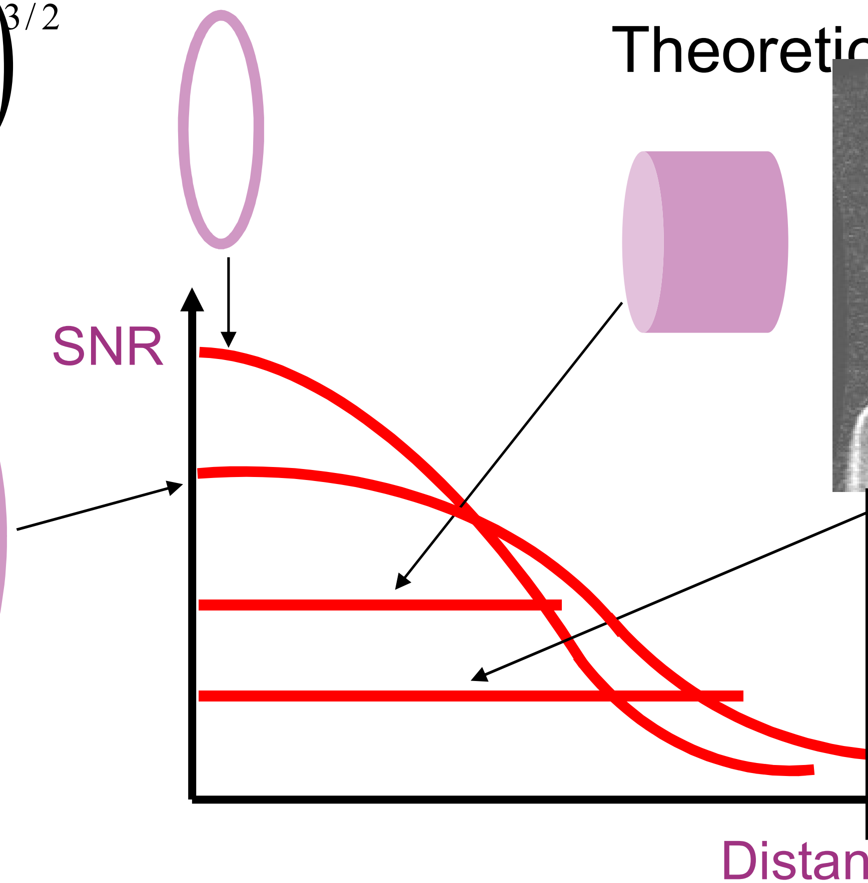

Theoretical cylinder coils

Body Coil:
Poor SNR

Excellent uniformity

Finite Element Modelling used for complicated designs

RF Coil Designs

- Surface coils
- Cylindrical coils
  - Sinusoidal currents around surface gives homogenous B_1
  - Saddle, birdcage ('distributed capacitance') with more conductors approximate this
- Solenoid useful in vertical fields (Philips HFO)

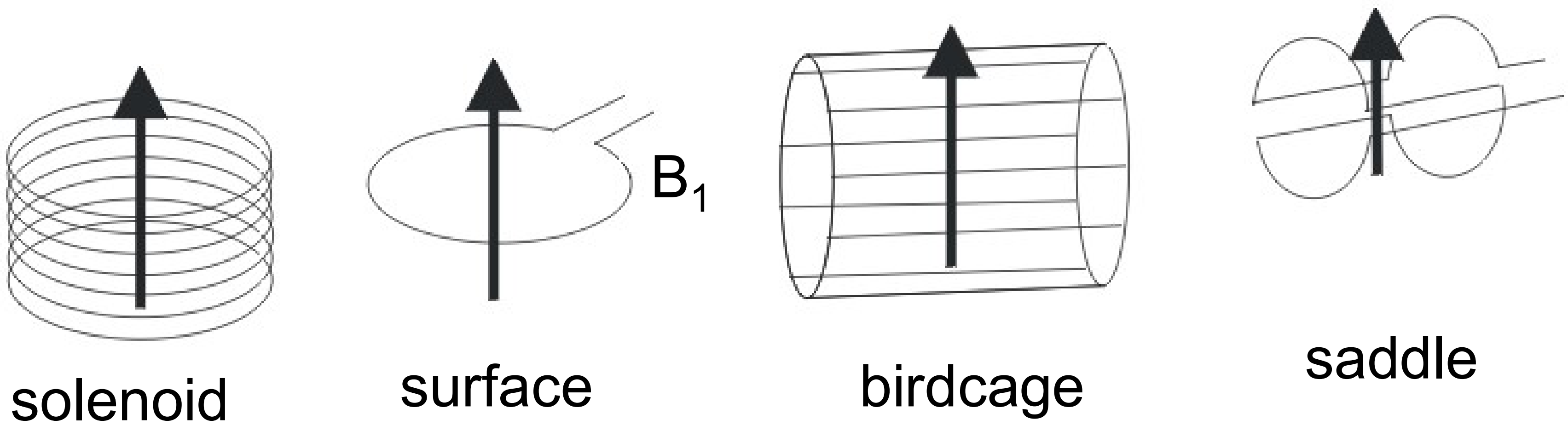

RF Coils

- Typical Scanner Configuration:
  - ✓ Integrated body coil
  - ✓ Head coils (linear for QA)
  - ✓ Torso Coil
  - ✓ Surface coil
  - ✓ Specialist coils e.g. wrist, breast

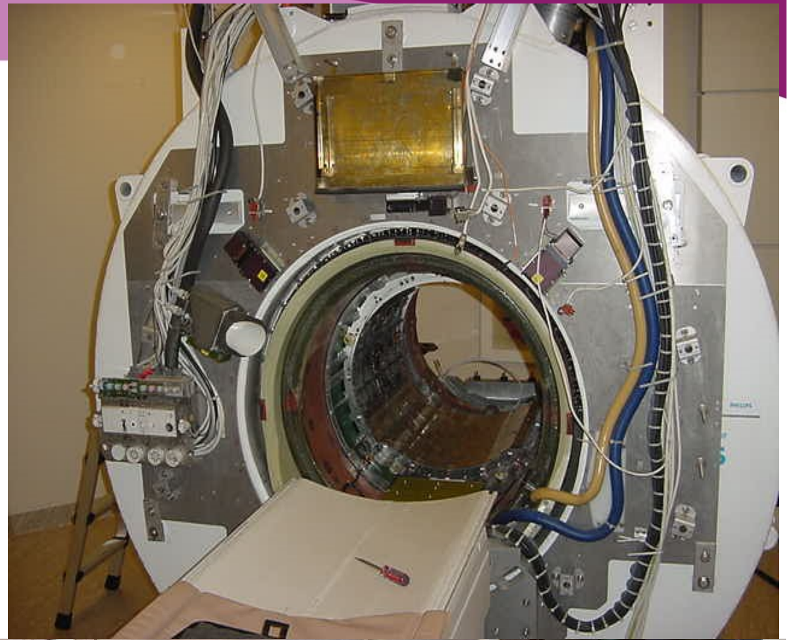

Coil Arrays

- Extend surface coil coverage
  Small coil excellent SNR
- Overlap to prevent mutual inductance
- Separate Rx channels
  Noise not correlated, further increase SNR
- Can be used in parallel imaging*

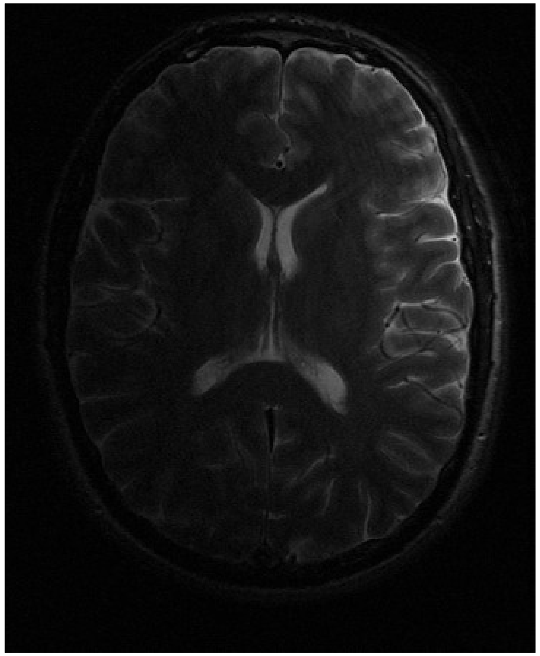

**Covered in 'fast scanning, volume sequences'*

Quadrature Coils

- Linear polarisation- only half RF power effective
- Circularly polarised
  Orthogonal coils at 90° phase
- Efficient transmission
  Power halved (RF heating)
- Receiver coils
  SNR increases $\sqrt{2}$

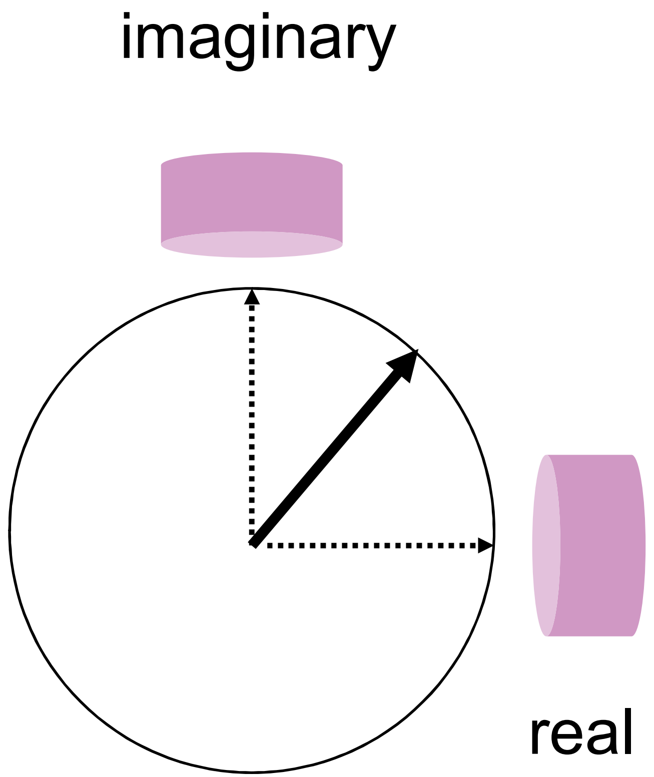

RF Coils: Other

- Dual Tuned
  - Multi-nuclear spectroscopy
  - proton MRI & other MRS
  - Broadband amplifier
- Optical RF Chain
  - e.g. GE's OpTix system
  - Digitised in scan room, optical transmission
  - SNR increase by 27%

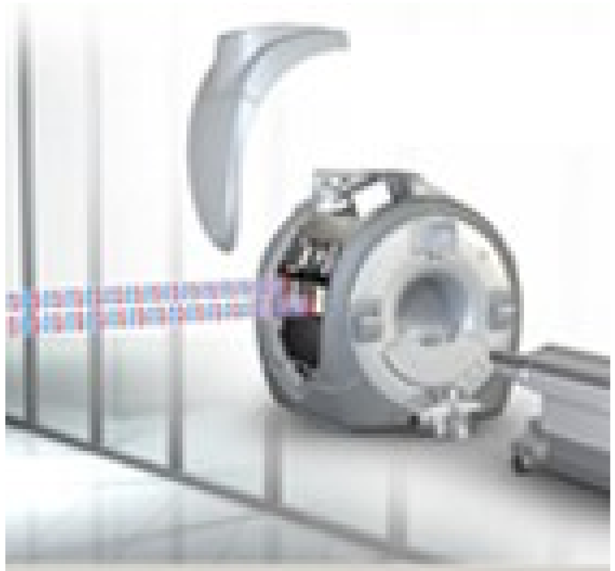

B_1 Uniformity

- Surface coil uniformity problematic (ER coil prostate)
- Commercial correction methods (e.g. SCIC)
- In-house method: PD-W image to divide out inhomogeneites

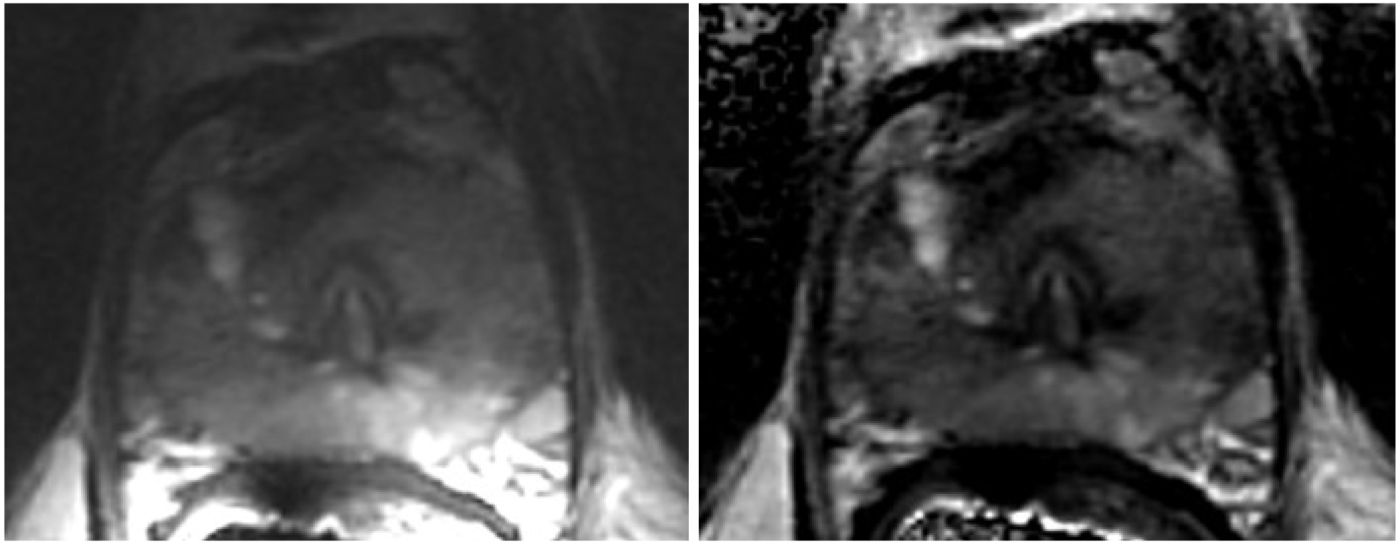

original corrected

Dielectric Effect

- At 3T λ ≈ 26 cm, comparable to patient
- Conductive/resonance effect

  ‘B_1 Doming’
- Dielectric pad, test objects

  Body imaging restored (right)
- Dual transmit body coil

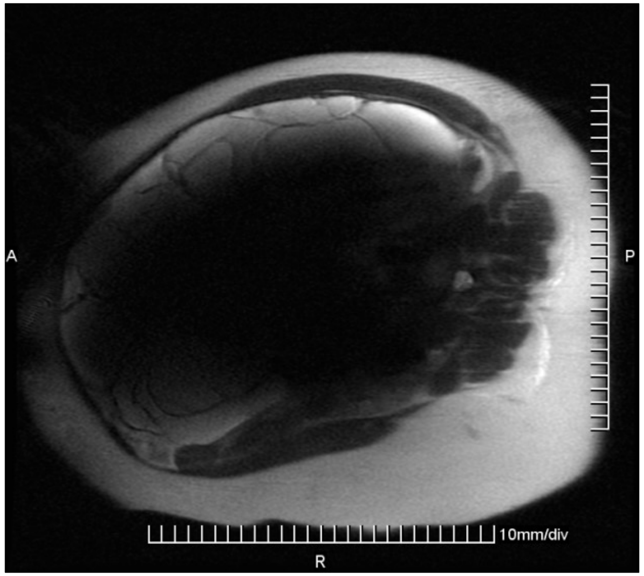

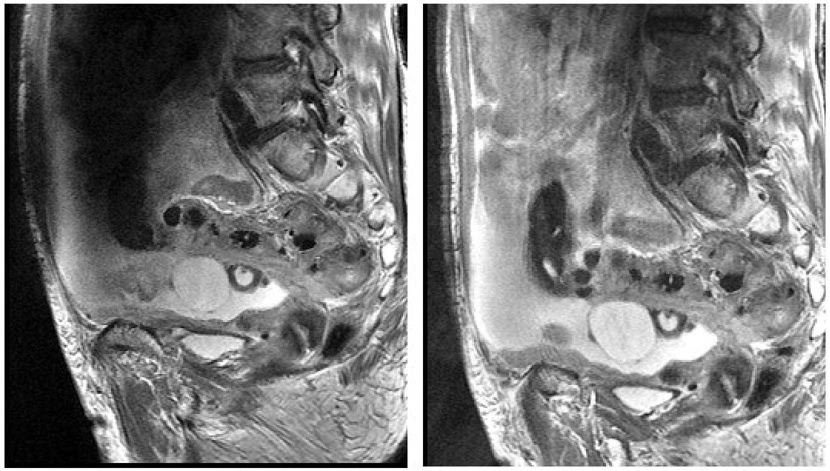

RT Specific Equipment

- Increase in sophistication from ‘making do’ to dedicated equipment

Couch: Flat table-top (?RF coil in table)

Magnet: wide bore

RF coils: Use of diagnostic and/or dedicated equipment

External lasers in MRI room

Associated devices- markers, MR applicators…

RT Planning Scans

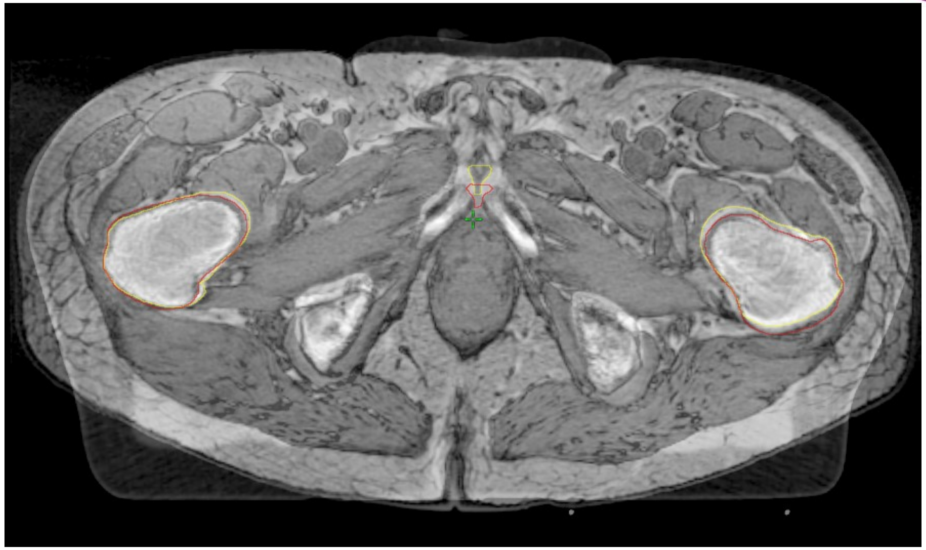

MRI often compromised by available equipment

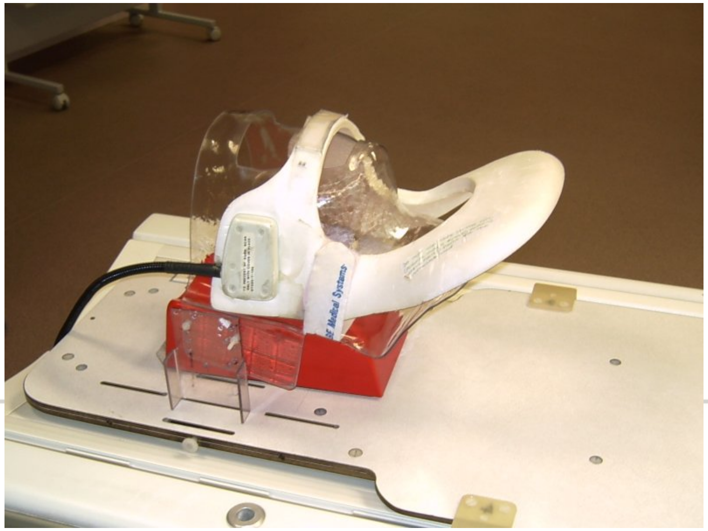

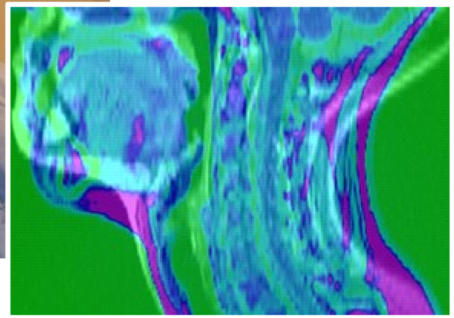

Dedicated System (MR Simulator)

Laser bridge, Wide bore
Flat table top, Coils in bed

ESTRO School

H&N

Flex coils (2 x 4), table coil (32)
plus long cabled body coil (18)

Improved SNR & coverage

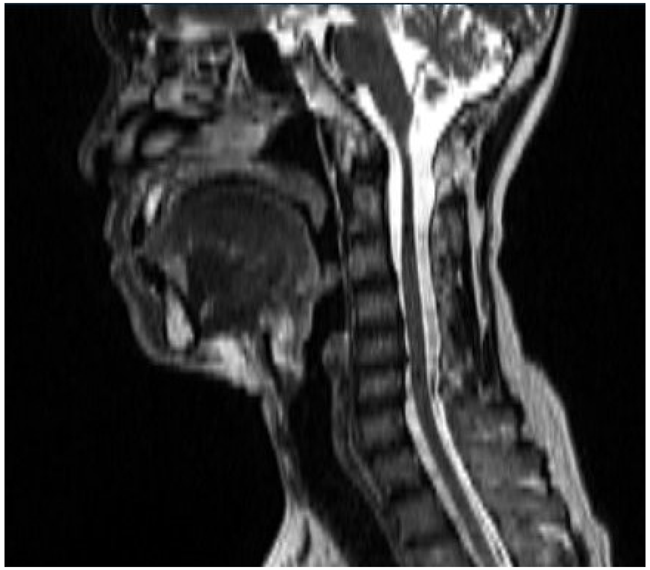

ESTRO School

The Future

- Higher field strength
- More RF channels
- Increase in MR-Simulators
- Hybrid MR-Linac systems

7 Tesla system

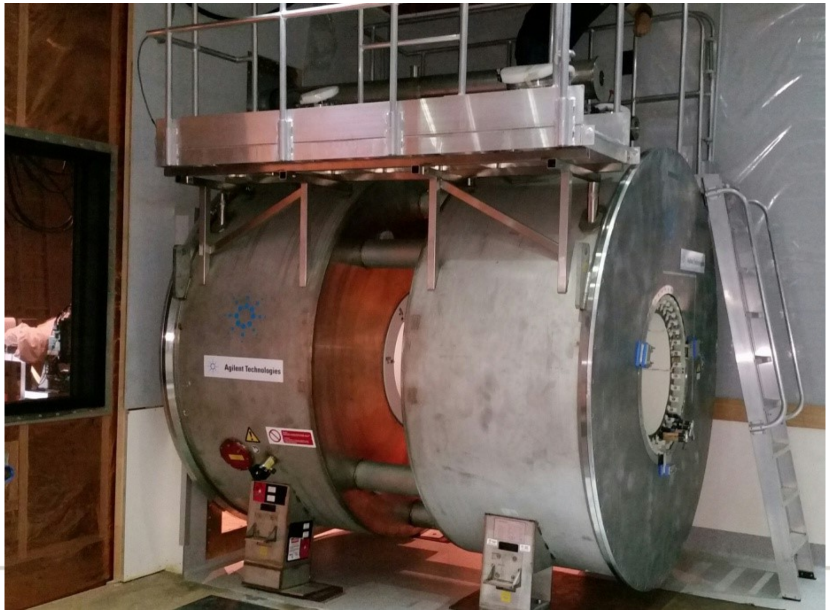

The Australian MR-Linac

64 channel H&N coil

Sydney 2017

5th MR in RT Symposium 2017

www.mrinrt2017.com

ESTRO School

Positron Emission Tomography

Physics - Basic Principles

ESTRO Teaching Course on Advanced Imaging Technologies

September 18-22, 2016 in Florence, Italy

Daniela Thorwarth
Section for Biomedical Physics,
University Hospital for Radiation Oncology, Tübingen

Eberhard-Karls-Universität
UKT
Universitätsklinikum Tübingen

Molecular Imaging with Positron Emission Tomography (PET)

PET imaging adds molecular information to morphology and function imaged with CT and/or MRI.

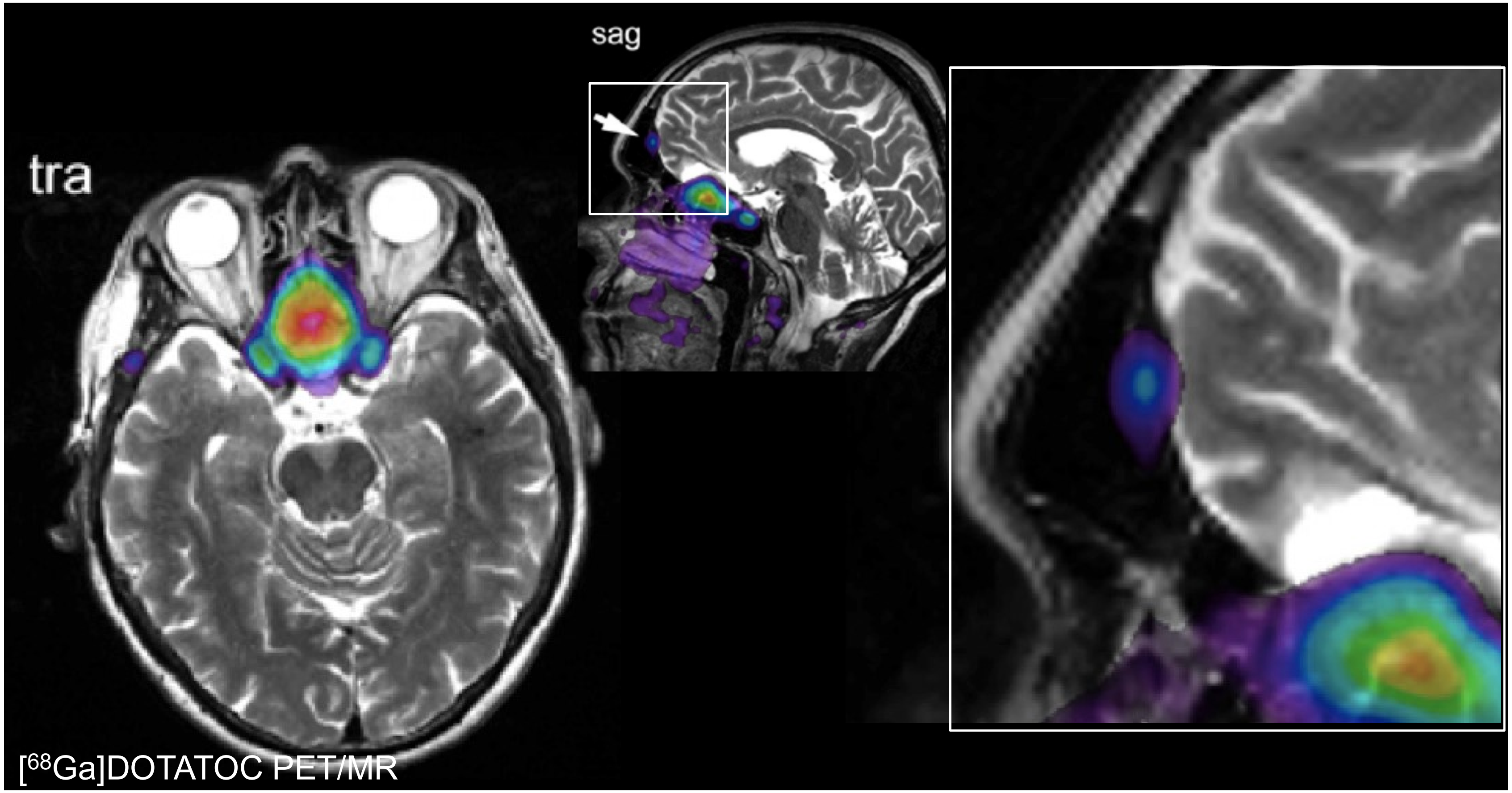

T2w MRI and PET (BrainPET) show small satellite in dorsal area of frontal sinus (detected on PET).

Boss et al, JNM 2010; 51.

Basic principle of PET

- Positron emitters (β+) used as biomarkers
- Positron-electron annihilation
  ⇒ Two γ-quanta with 511 keV each are emitted under approx. 180°

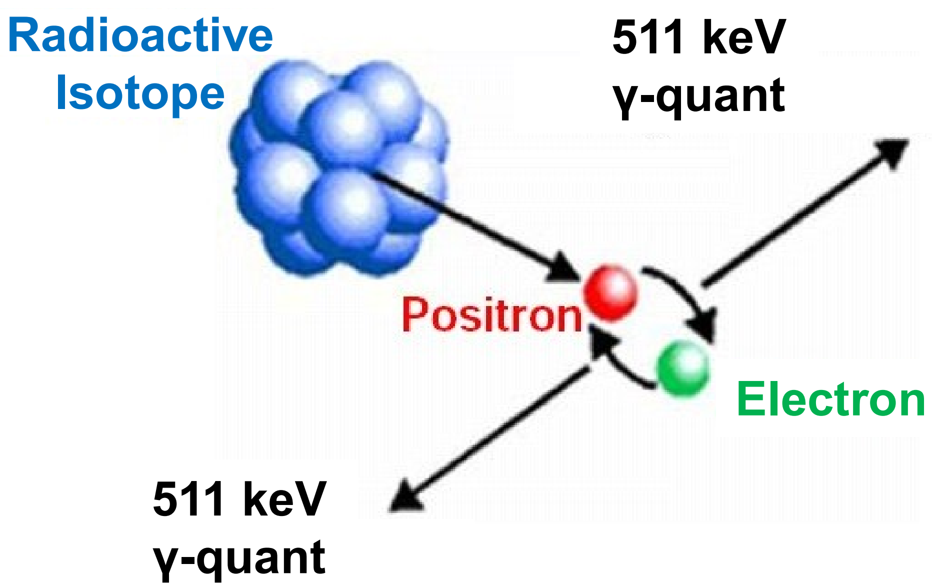

- Coincidence detection in a detector ring

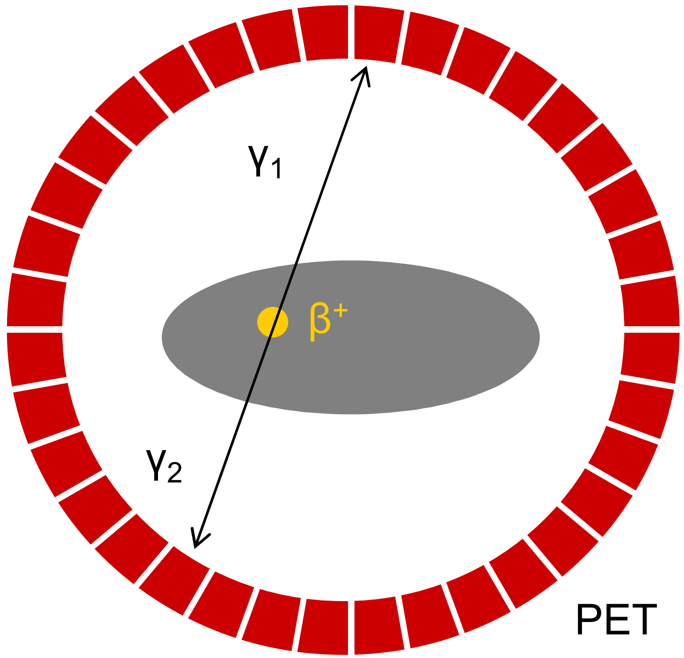

Today: Combined PET/CT

PET/CT: combination of structure and function

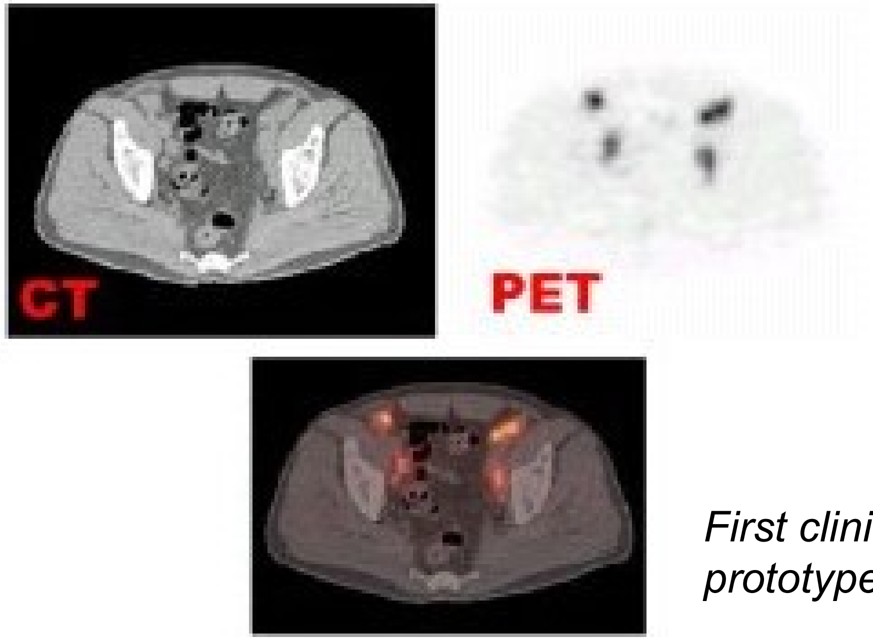

First clinical PET/CT prototype (mid 1990s) [3]

State-of-the-art PET/CT Designs

(a)

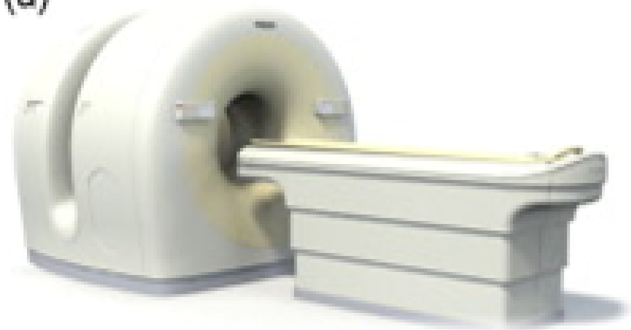

Gemini series, Philips Healthcare Systems

(b)

Biograph series, Siemens Healthcare Solutions

(c)

Discovery series, GE Healthcare

(d)

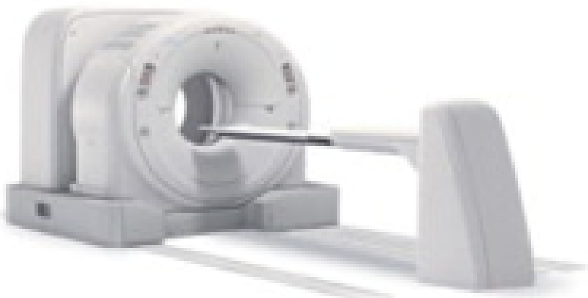

Aquiduo series, Toshiba Medical Systems

(e)

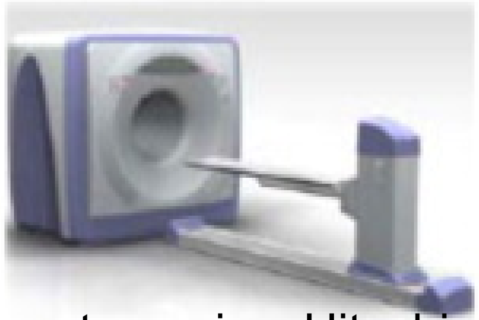

Sceptre series, Hitachi Medical Systems

(f)

Anyscan series, Mediso

! All PET/CT tomographs combine diagnostic PET and CT components and a dedicated patient support system. **!**

Courtesy T. Beyer, cmi-experts Zürich

PET/CT

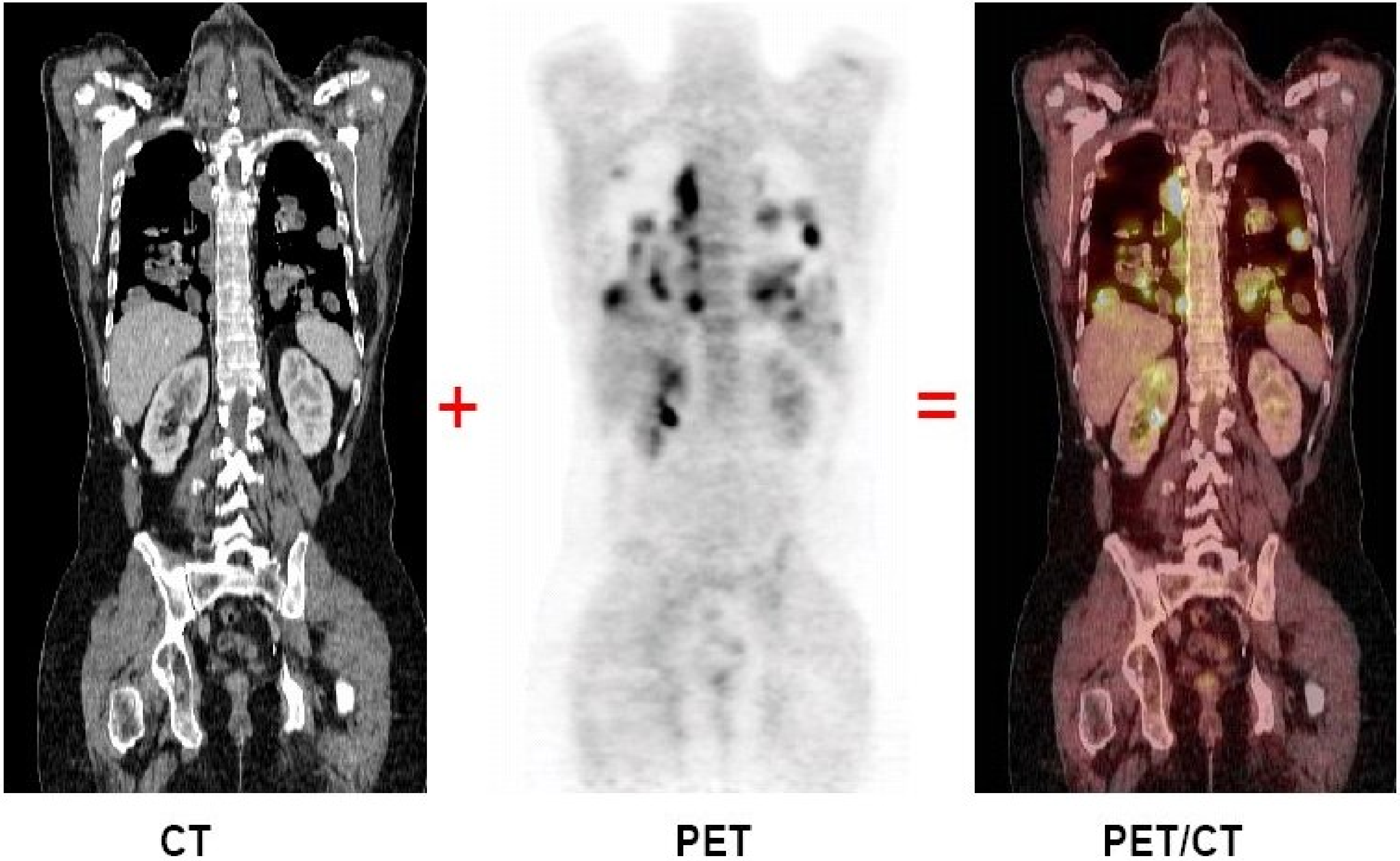

Raw data stored in sinograms

Sinograms:
Measurement of the activity distribution of a radioactive tracer.

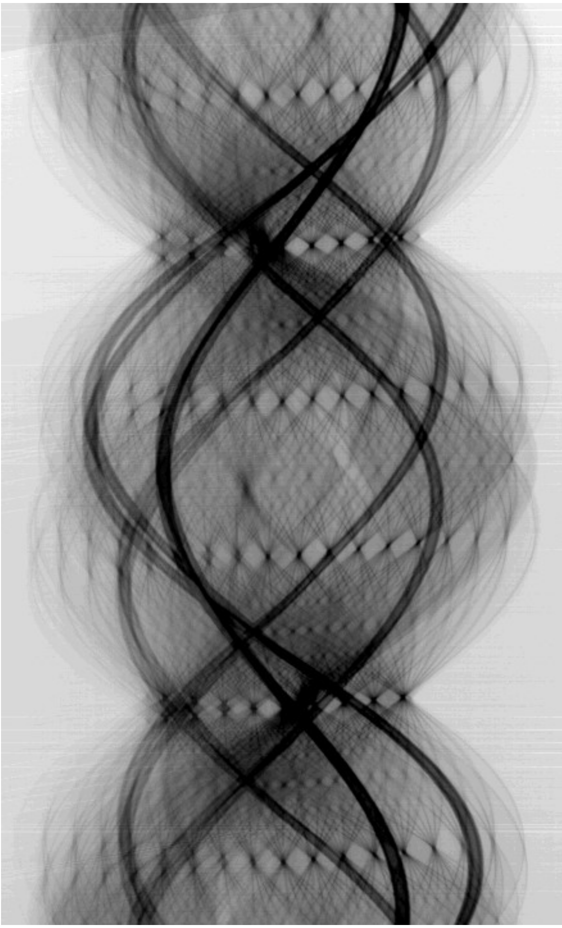

y = φ

x = offset

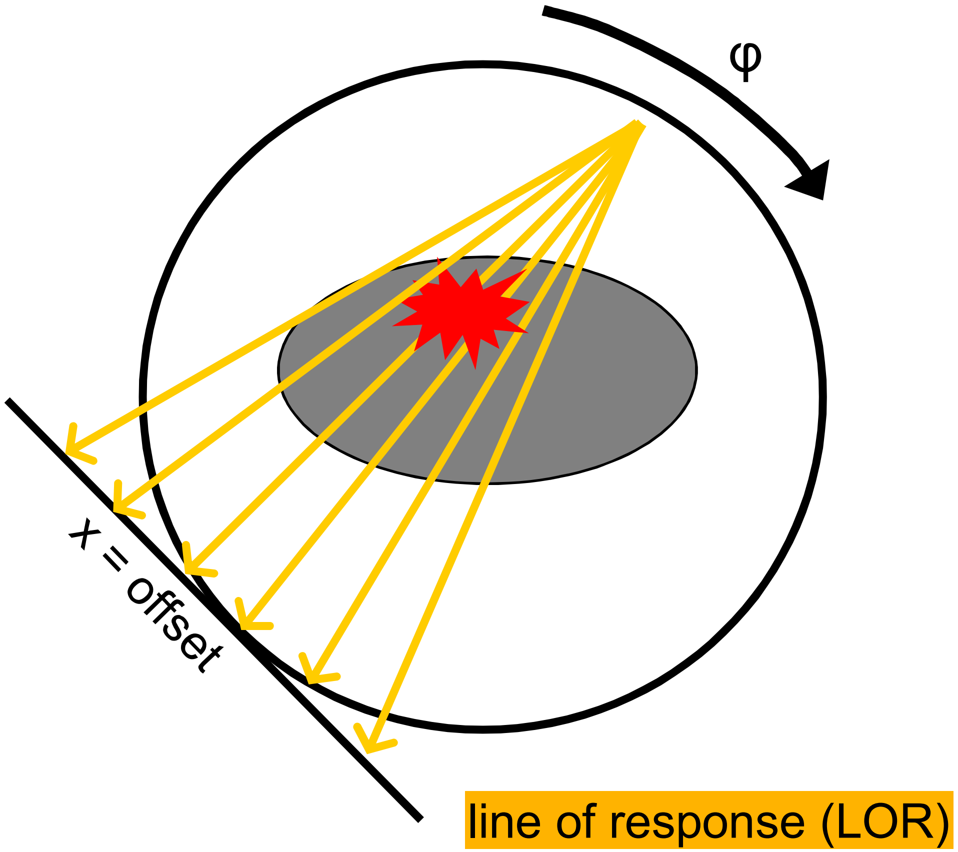

Radial Sampling

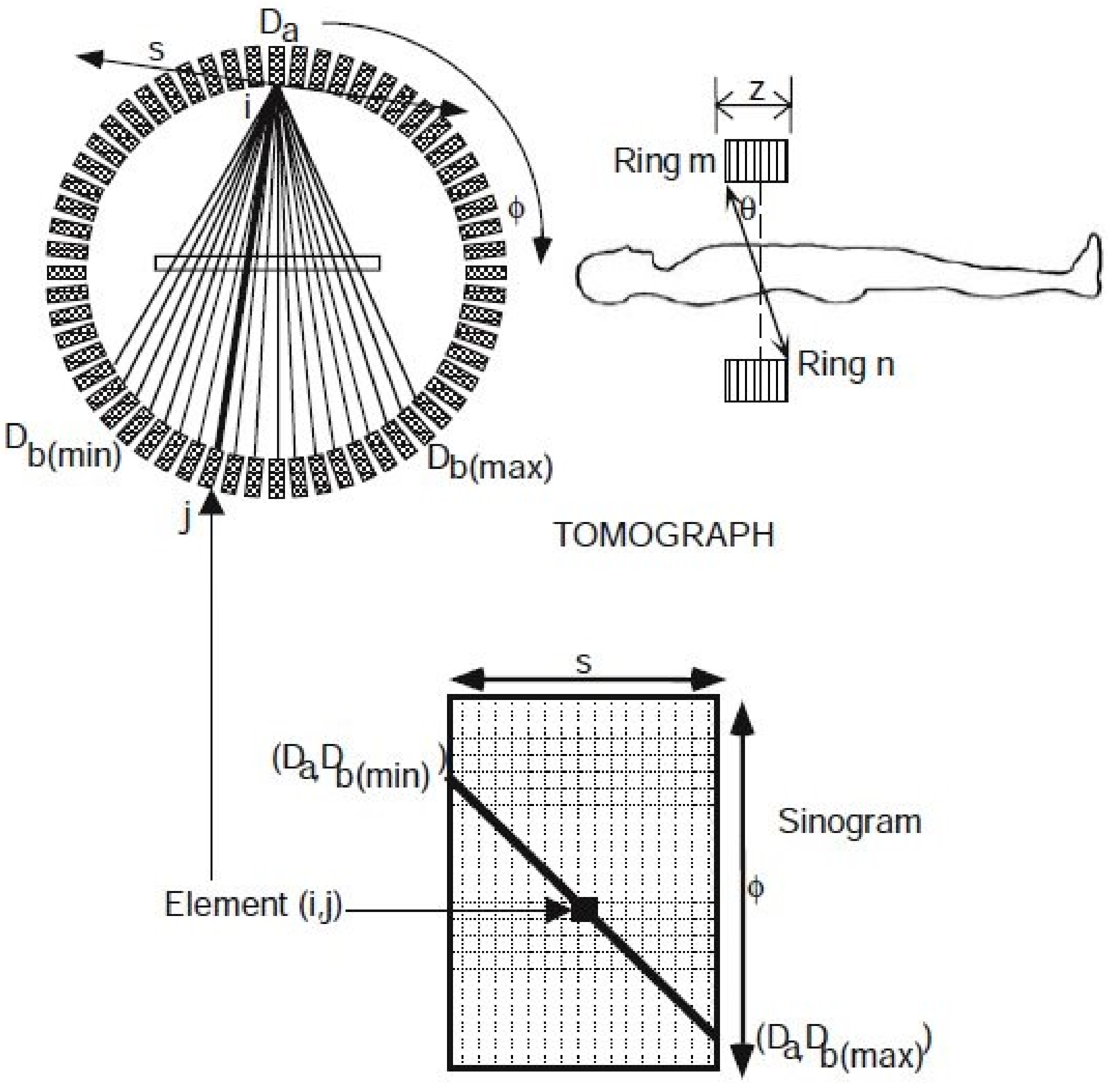

Mapping from sampling projections to sinograms [2].

Transaxial field of view of a PET tomograph is defined by the acceptance angle in the plane.

2D-/3D-PET

2D-PET

- Geometric collimation with septa
- Data sampling only with θ=0°
- Lower overall sensitivity
- Lower fraction of scattered photons

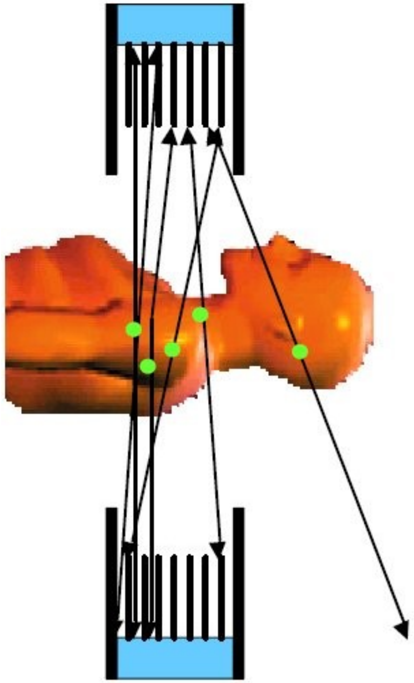

3D-PET

- Projections at polar angles θ>0° measured
- Increased sensitivity
- Higher scatter fraction
- Special reconstruction algorithms are necessary

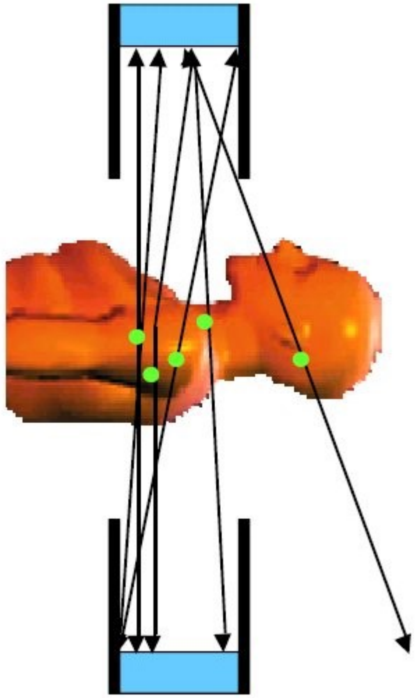

2D/3D-PET acquisition

2D acquisition: the entire FOV is sampled.

3D acquisition: truncation of projections occurs for θ > 0°.
This results in loss of data corresponding the ends of the tomograph [2].

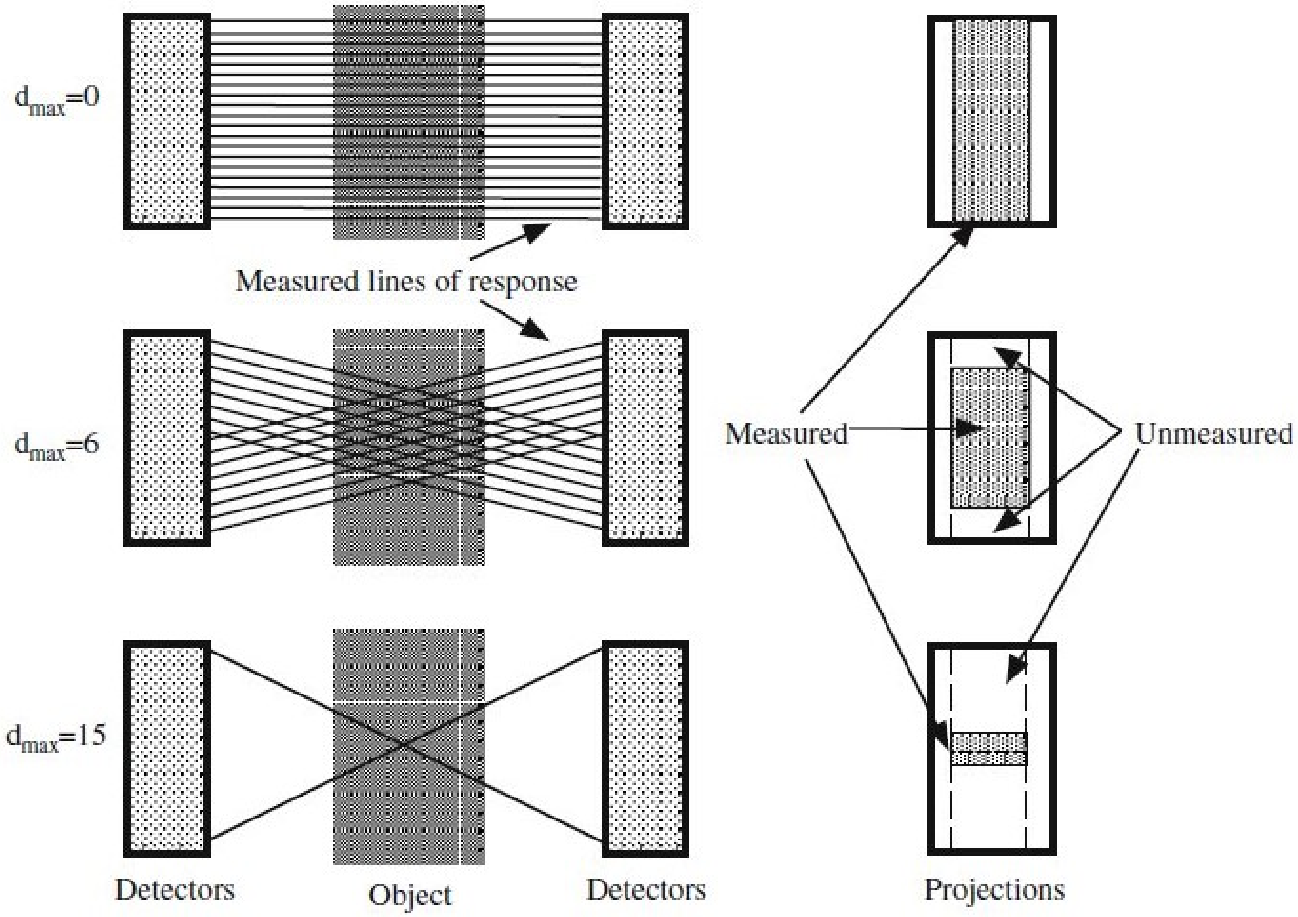

Axial Sensitivity

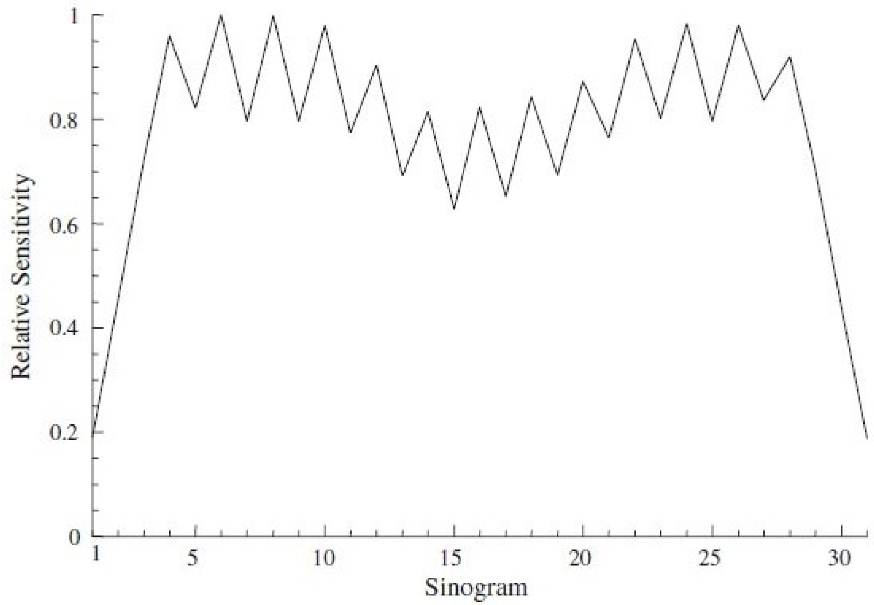

2D axial sensitivity profile for a line source in air in a 16-ring tomograph [2].

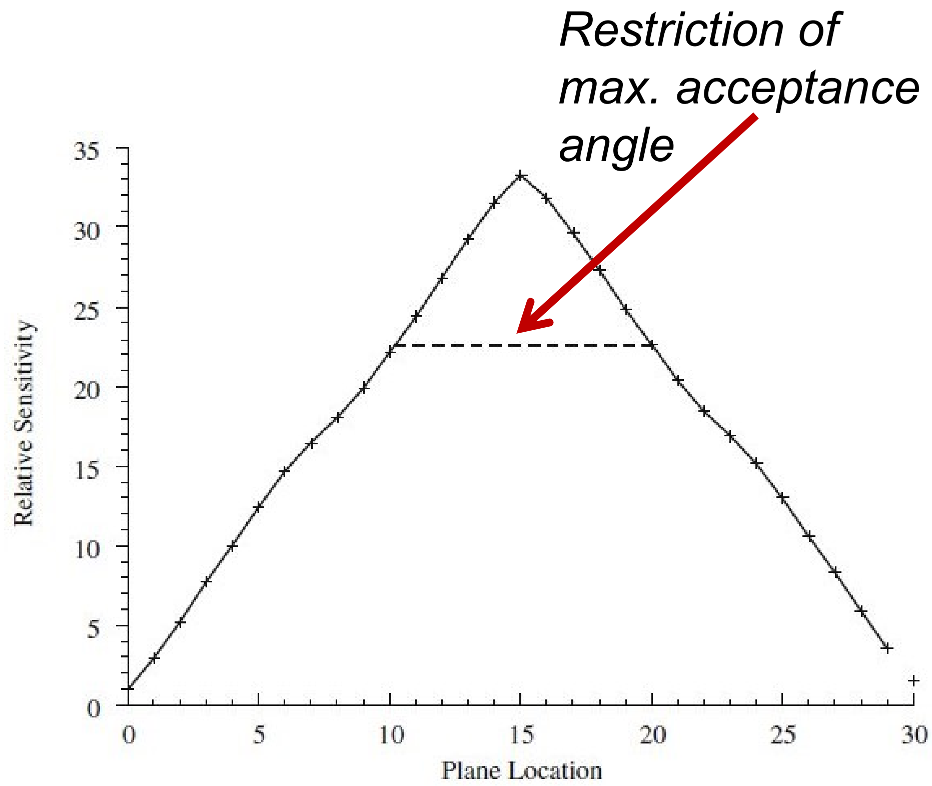

Axial sensitivity variation for 3D acquisition in a 16-ring tomograph [2].

Image Formation

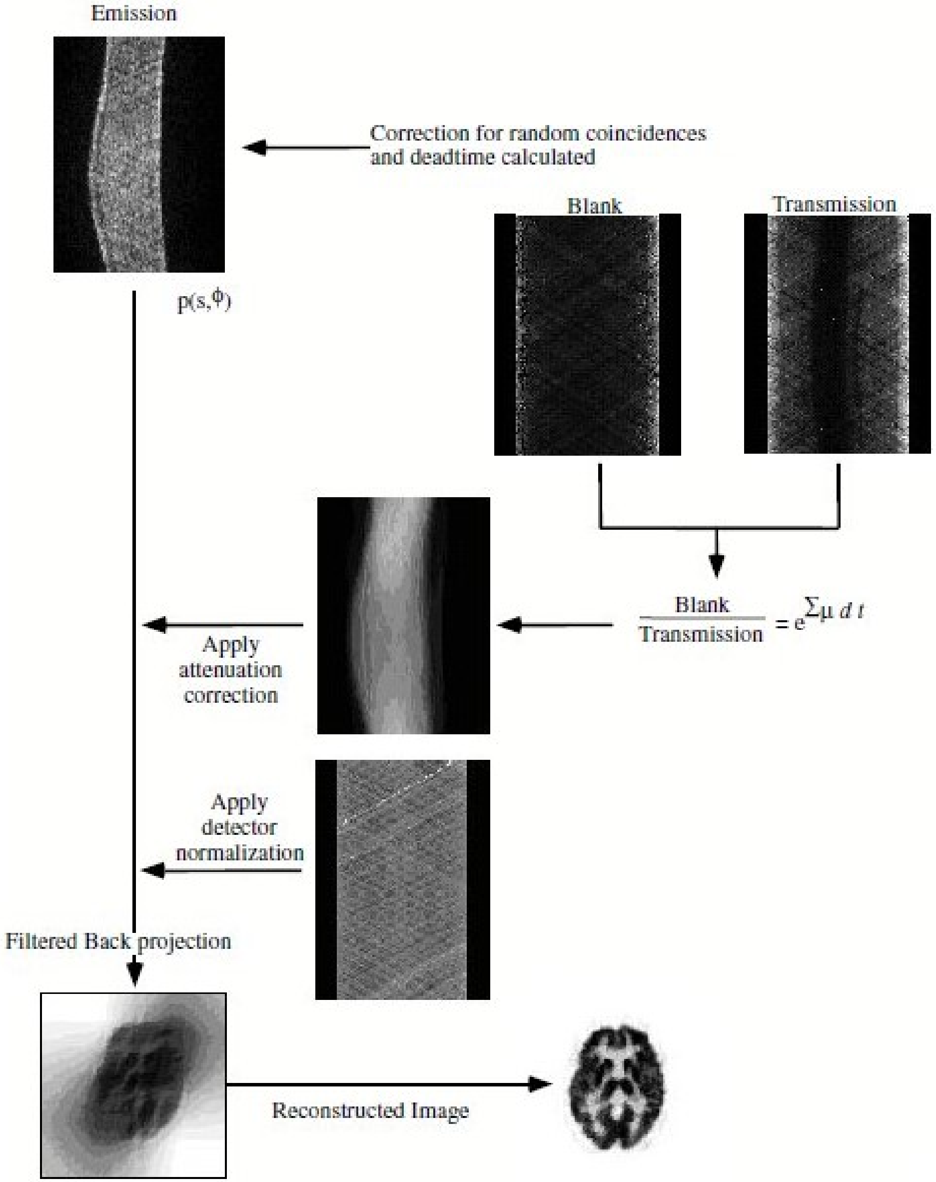

(1) Emission scan

(2) Normalization scans (one per plane in 2D) to correct for differential detector efficiencies and geometric effects related to the detector ring

(3) Set of sinograms of attenuation correction factors to correct of photon attenuation (self-absorption or scattering) by the object

Radiation detection

Desired for PET:

1. High stopping efficiency
2. Good energy resolution

➡ **Scintillation detectors**

- Inorganic crystal that emits visible light photons after interaction of photons with detector.
- # of scintillation photons is proportional to the energy deposited in the crystal.
- Important properties for application in PET:
  - Stopping power for 511 keV photons
  - Signal decay time
  - Light output
  - Intrinsic energy resolution

Properties of scintillaton detectors applied in PET

Property	NaI(Tl)	BGO	LSO	YSO	GSO
Density (g/cm³)	3.67	7.13	7.4	4.53	6.71
Effective Z	50.6	74.2	65.5	34.2	58.6
Attenuation length	2.88	1.05	1.16	2.58	1.43
Decay constant (ns)	230	300	40	70	60
Light output (photons/keV)	38	6	29	46	10
Relative light output	100%	15%	75%	118%	25%
Wavelength λ(nm)	410	480	420	420	440
Intrinsic ΔE/E (%)	5.8	3.1	9.1	7.5	4.6
ΔE/E (%)	6.6	10.2	10	12.5	8.5
Index of refraction	1.85	2.15	1.82	1.8	1.91
Hygroscopic?	Yes	No	No	No	No
Rugged?	No	Yes	Yes	Yes	No
μ (cm^{-1})	0.3411	0.9496	0.8658	0.3875	0.6978
μ/ρ(cm^2/gm)	0.0948	0.1332	0.117	0853	0.104

NaI(Tl): sodium iodide deoped with thallium
BGO: bismuth germanate ($Bi_4Ge_3O_{12}$)
LSO: lutetium oxyorthosilicate doped with cerium(Lu_2SiO_5:Ce)
YSO: yttrium oxyorthosilicate doped with cerium(Y_2SiO_5:Ce)
GSO: gadolinium oxyorthosilicate doped with cerium(Gd_2SiO_5:Ce)

New: LYSO

Photo-multiplier tubes (PMTs)

PMTs: photo-detectors used in scintillation detectors for PET

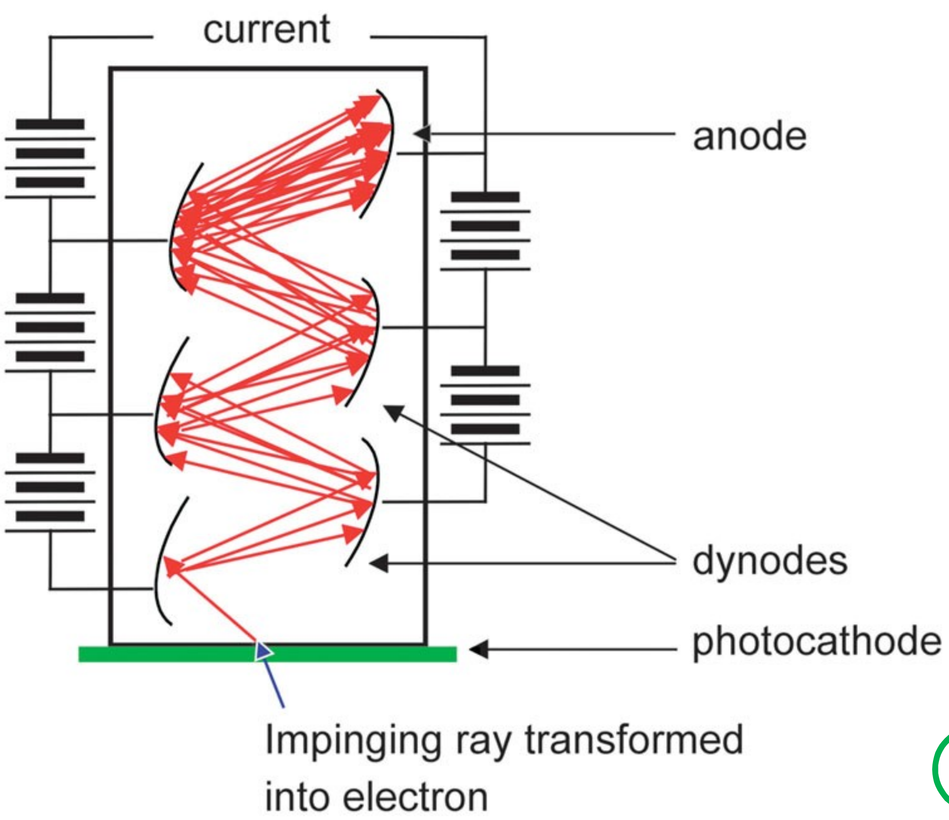

(1) Incoming photon deposits its energy at the photocathode, release of a photo-electron
(2) Applied electric field accelerates the electron to the first dynode
(3) Emission of multiple secondary electrons due to increased electron energy
(4) …

☺ **Good signal-to-noise ratio (SNR)**

☹ **Low quantum efficiency (QE) ~ 25%**

Detector Designs used in PET

One-to-one coupling:

- Single crystals glued to individual photo-detector
- Spatial resolution limited by discr crystal size

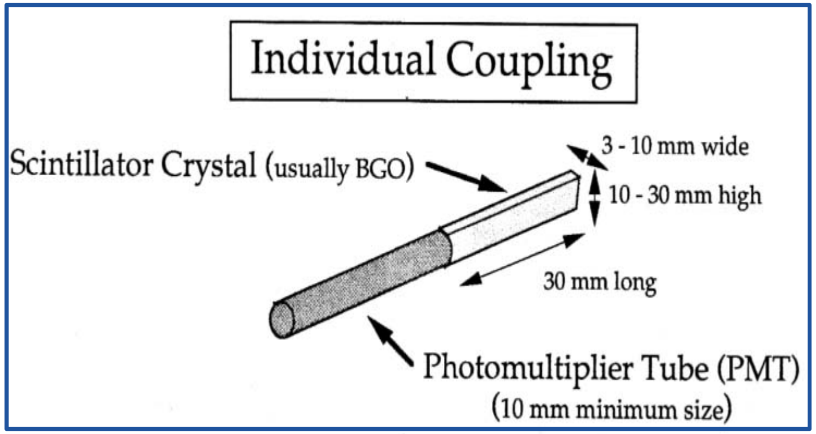

Block detector design:

- Rectangular scintillator block sectioned by partial saw cuts of different depth into discrete elements
- Usually 4 attached PMTs
- Anger positioning

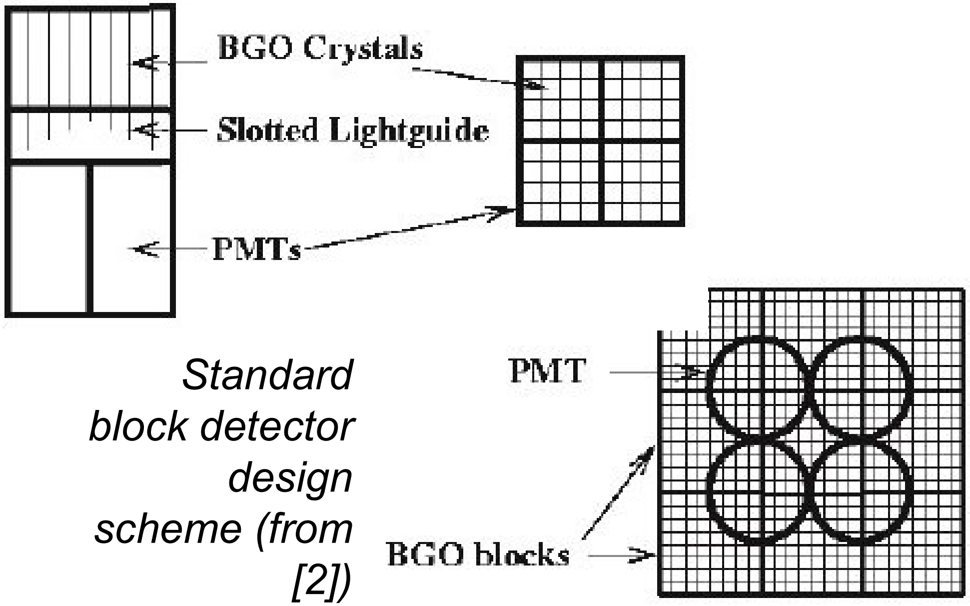

Standard block detector design scheme (from [2])

Detector Designs used in PET

Anger detector:

- Large scintillator crystal glued to array of PMTs
- Weighted centroid positioning algorithm used to estimate interaction position within the detector

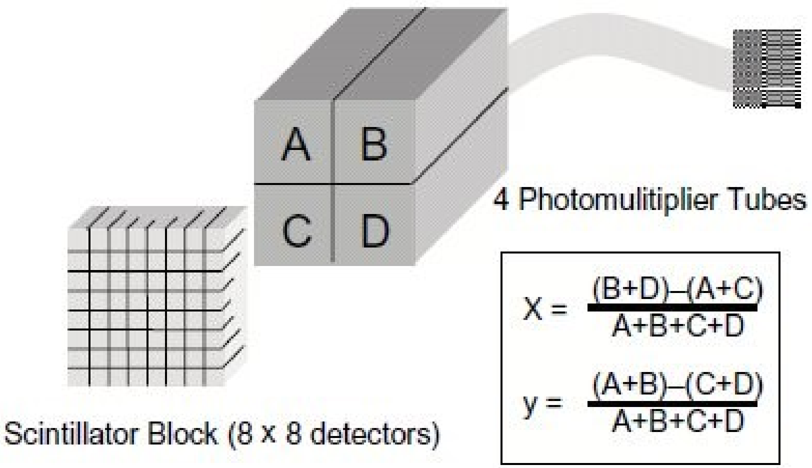

$$X = \frac{(B+D)-(A+C)}{A+B+C+D}$$

$$y = \frac{(A+B)-(C+D)}{A+B+C+D}$$

Block detector system + Anger logic [3]

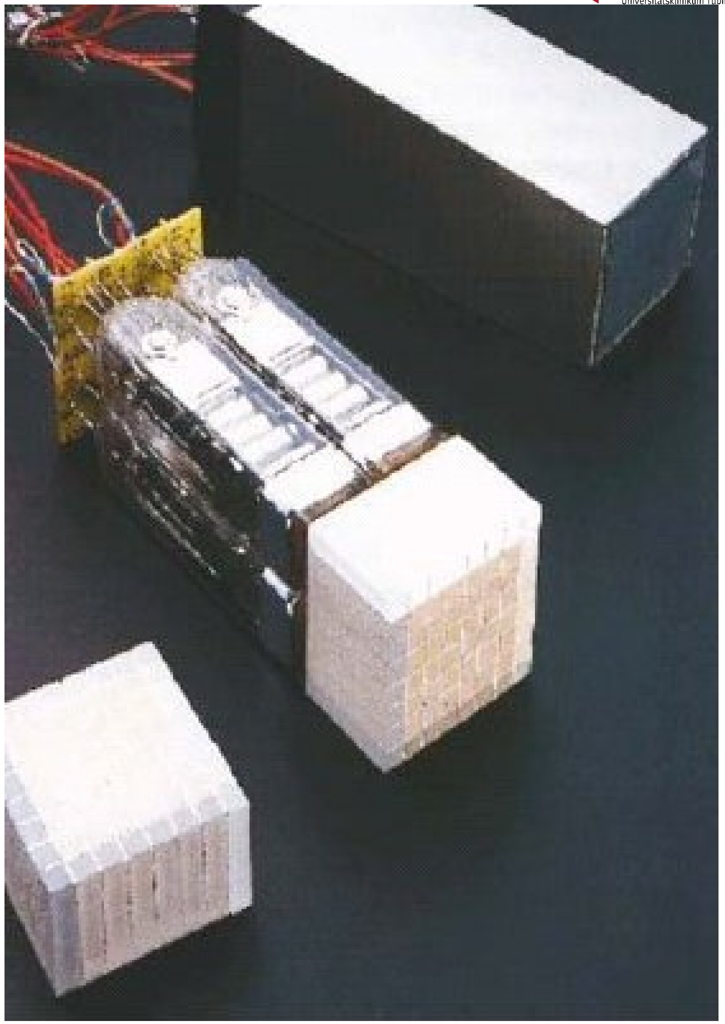

Block detector Siemens-CTI ECAT 951, 8x8 block BGO with 4 PMTs (from [2])

Timing Resolution and Coincidence Detection

Coincidence time window: 2τ

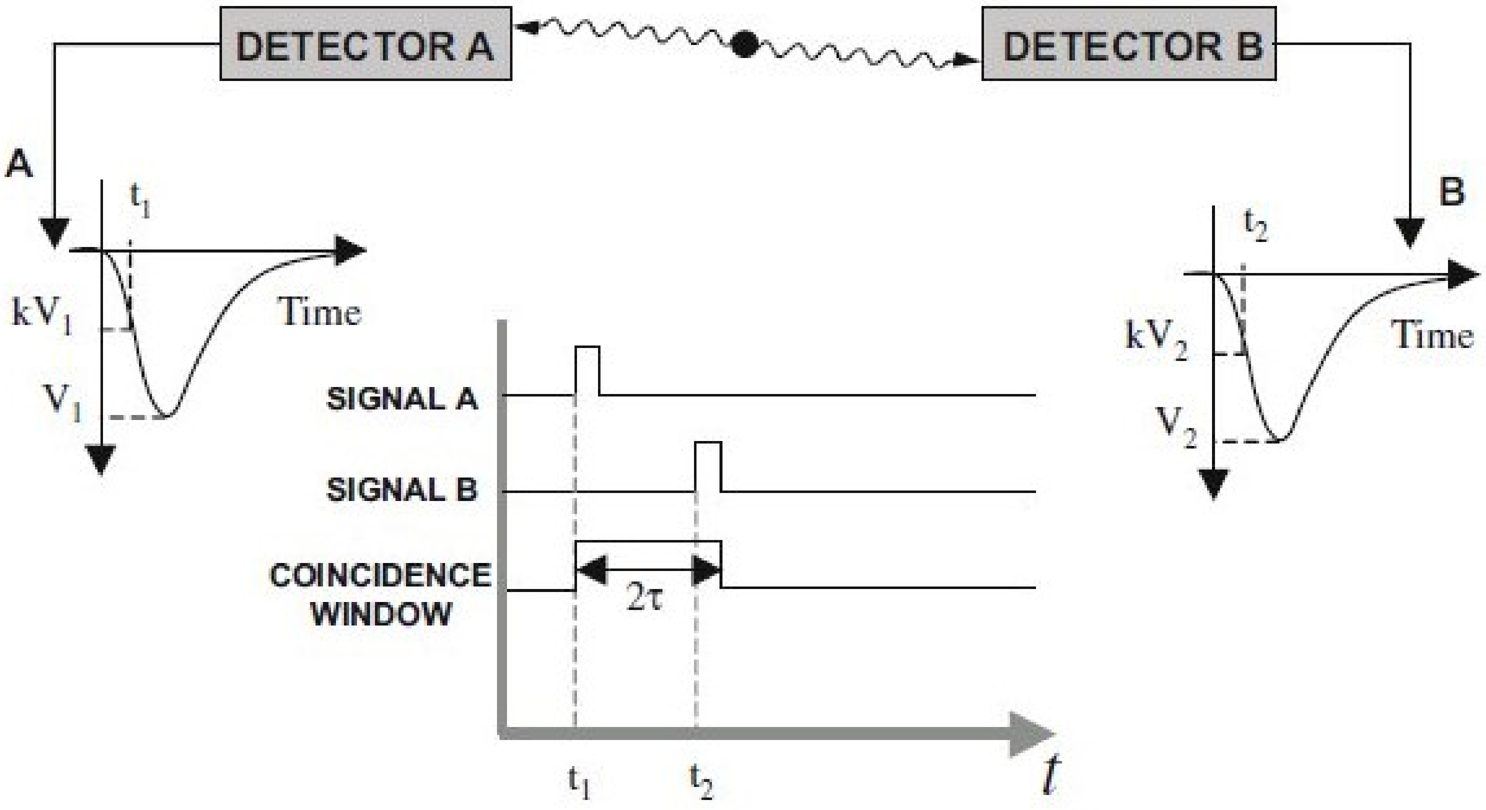

Time-of-flight (TOF) PET

- In addition to the coincidence information, the difference in flight time is registered

$$\Delta t = \frac{2\Delta x}{c}$$

- Better SNR

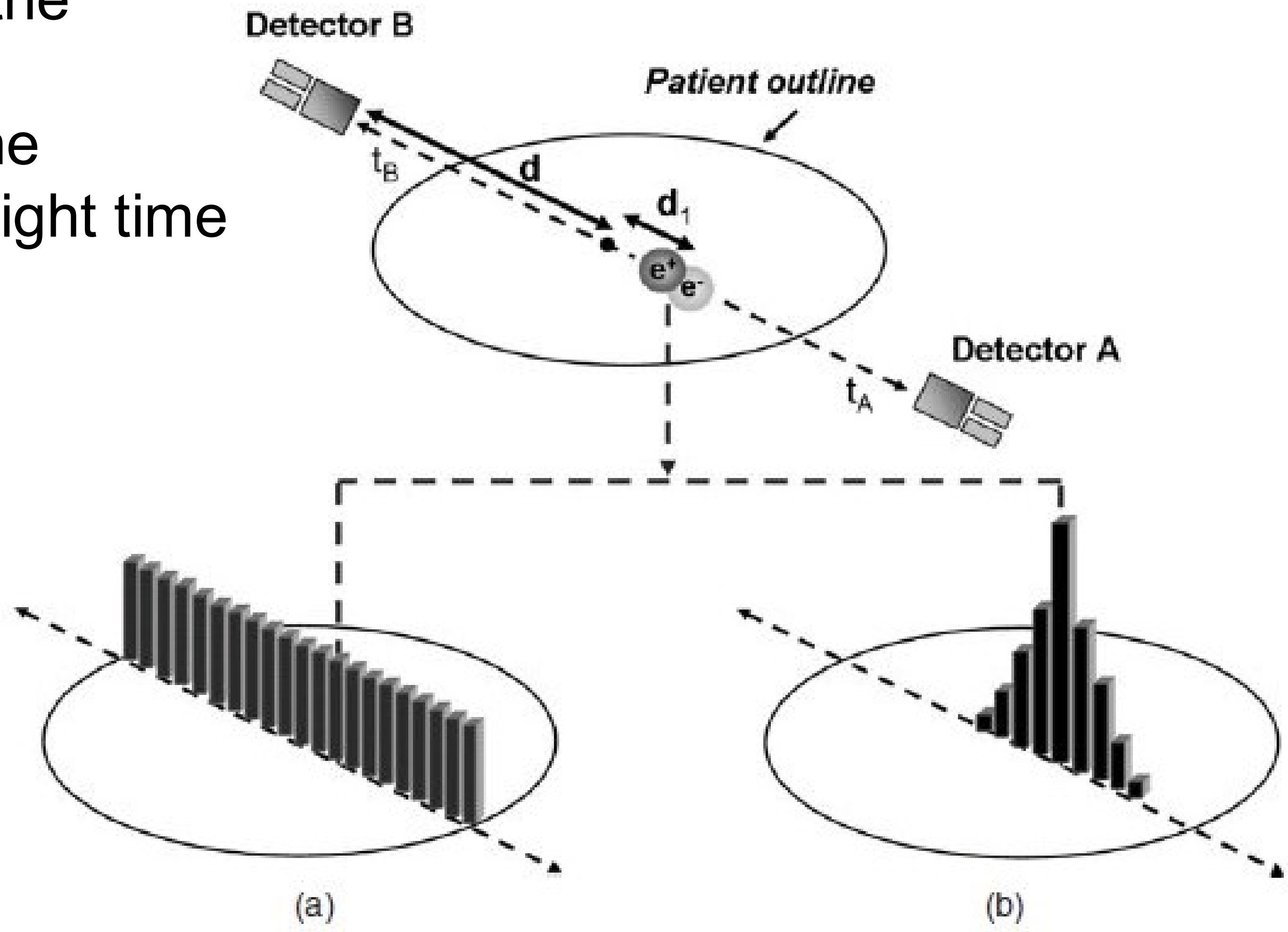

(a) Localization without TOF,
(b) with TOF. Townsend, PMB 2008 [3]

Detected Events in PET

- Detection event is valid (= **prompt** event) if
  - Two photons are detected in coincidence window
  - LOR is within valid acceptance angle
  - Energy of both photons within selected energy window

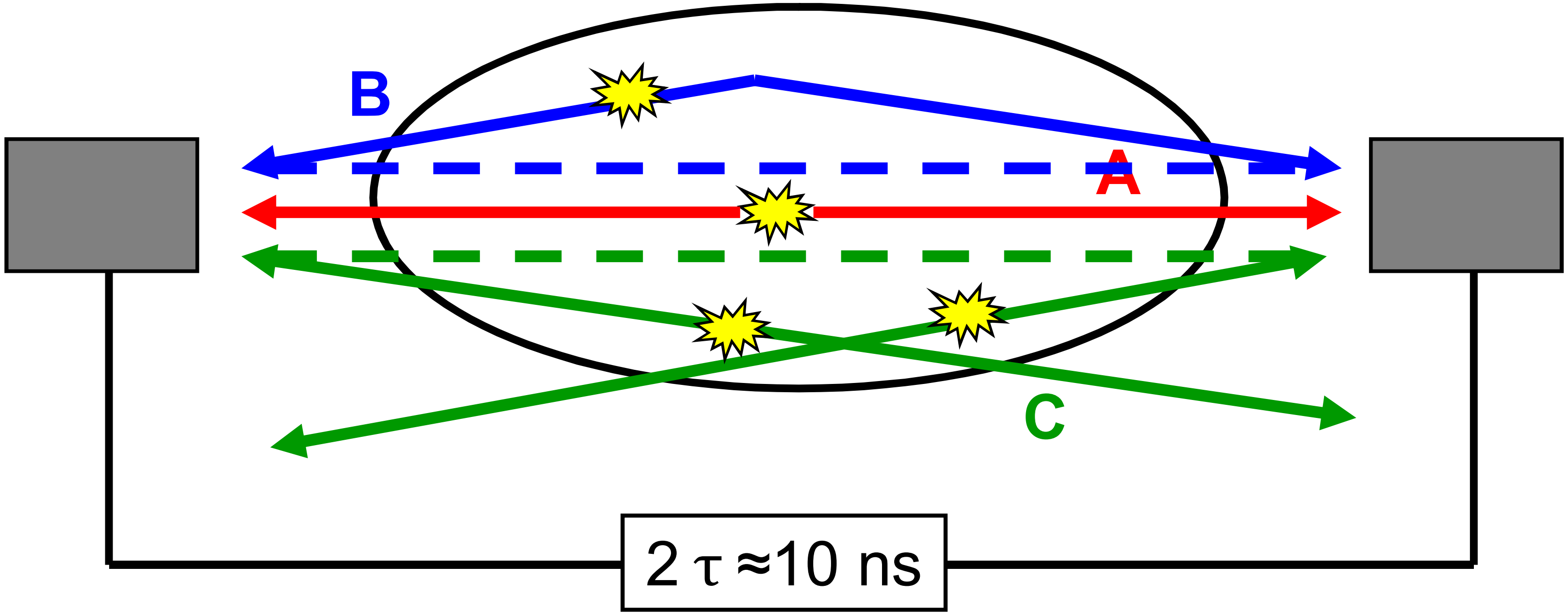

True coincidence (A) , scattered coincidence (B), random coincidence (C)

Prompt Events

- **Single** event
  - single photon is counted by detector (1-10%)
- **True** coincidence
  - event derives from single positron-electron annihilation
  - both photons reach tomograph without interaction
- **Random** coincidence
  - two nuclei decay at approximately the same time
  - random event count rate (R_{ab}) between two detectors *a* and *b*:

$$R_{ab} = 2\tau \cdot N_a N_b \propto N^2$$

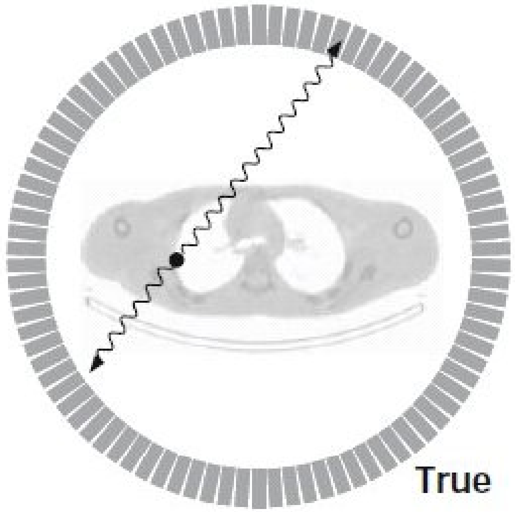

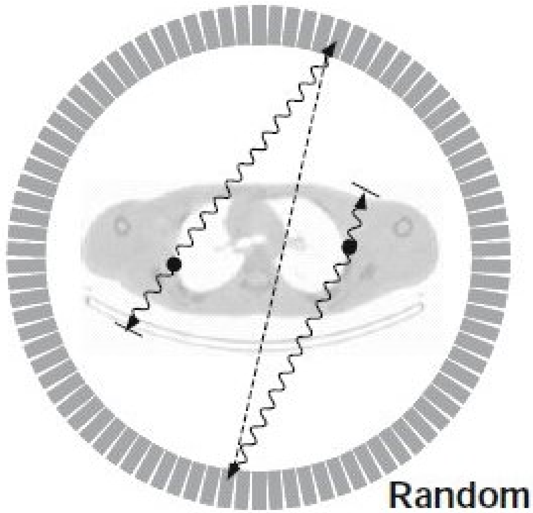

Prompt Events (II)

- **Scattered** events
  - One or both photons detected have undergone a Compton interaction
  - Loss in energy and change in direction
  - Due to poor energy resolution, many scattered photons cannot be discriminated
  - Wrong LOR assigned
- **Multiple** (triple) events
  - Three events from two annihilations detected
  - Event is disregarded
  - Proportional to count rate

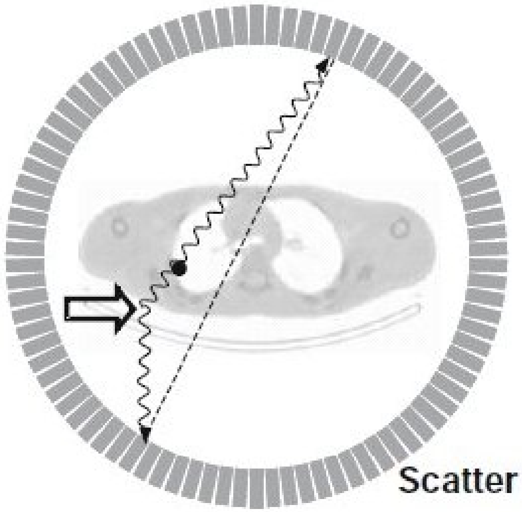

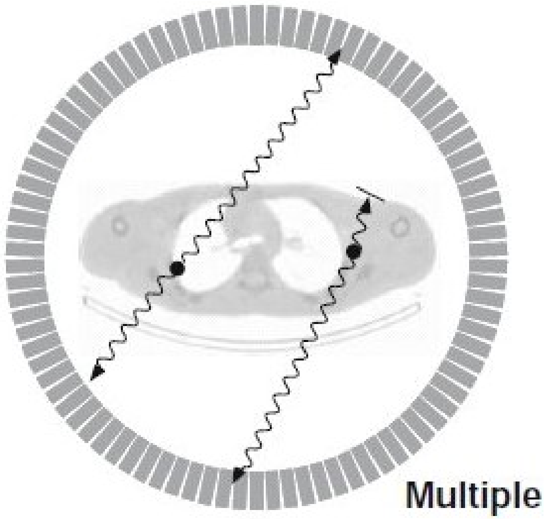

Performance of PET Systems

- Sensitivity

$$S = \frac{c}{t \cdot A} = \left[\frac{\text{counts}}{\sec \cdot kBq} \right]$$

  - Good systems reach *S=7-9 counts/(sec.kBq)*
- Spatial Resolution
- Energy Resolution
- Count Rate Performance
- Scatter Fraction

Performance of PET Systems: Spatial Resolution

- Determined by *full width half maximum* (FWHM) of *point spread function* (PSF): $FWHM = \sqrt{8\ln(2\sigma)}$

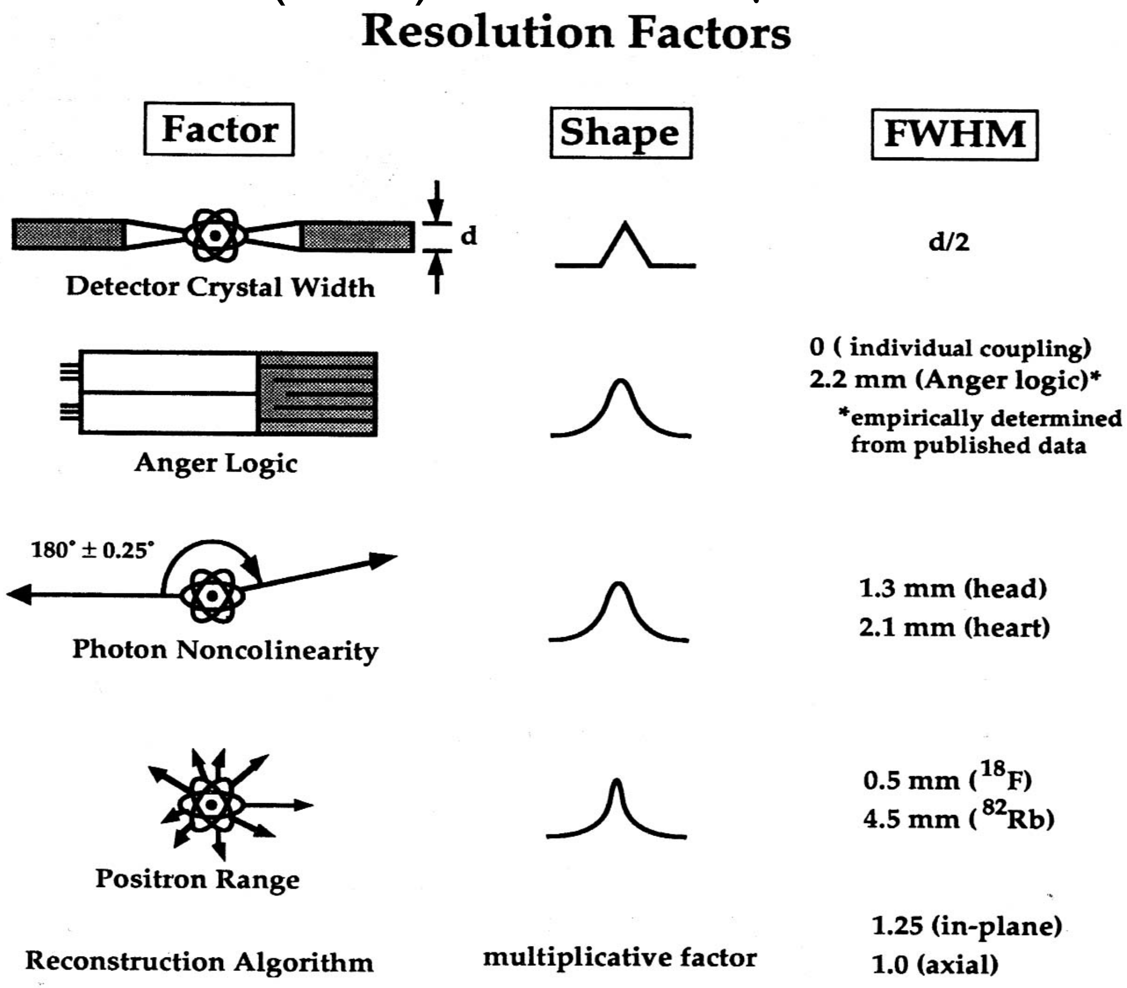

Performance of PET Systems: Energy Resolution

- Statistical uncertainty of energy determination due to limited light yield of scintillator crystal
- Two methods for determination of energy resolution:
  - *Single event* energy resolution
  - *Coincidence* (i.e. both events) energy resolution

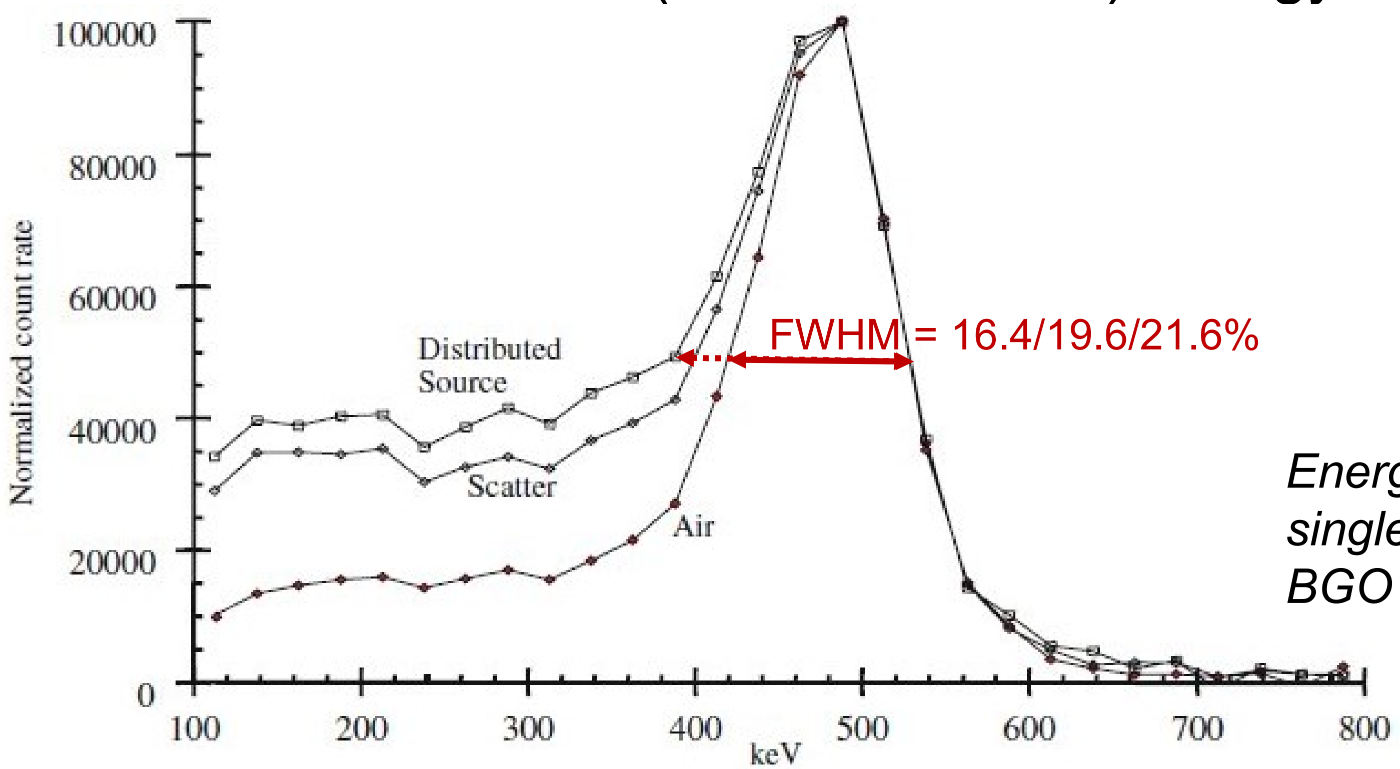

Energy spectra for single photons for a BGO PET system [2].

Performance of PET Systems: Count Rate Performance

- Ratio Trues/Randoms unbalanced for high Activities
- Processing of detected photons takes finite time
- Noise Equivalent Count Rate:

$$NECR = \frac{T^2}{T + S + 2fR}$$

T: trues
S: scattered
R: randoms
f: rel. area of object on proj. surface

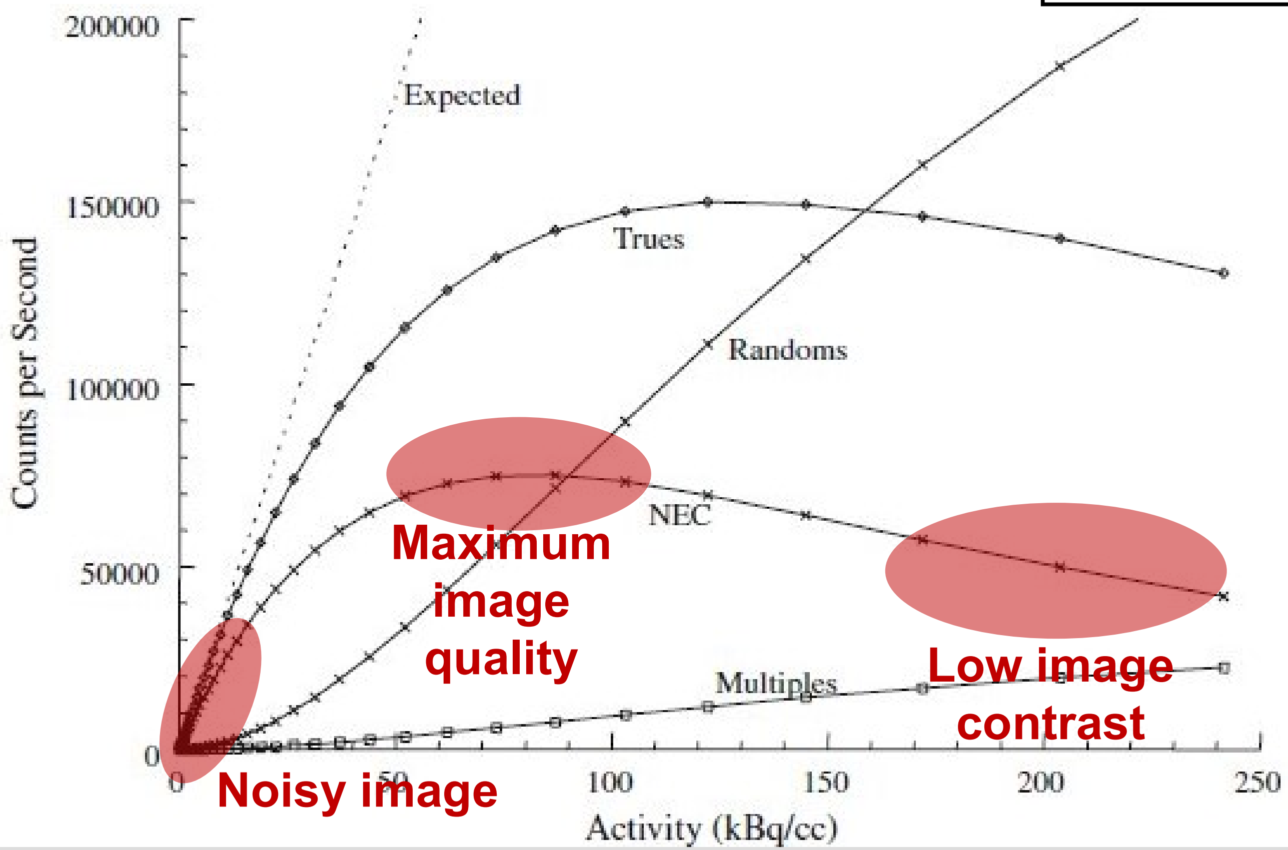

Count rate curves for true, random and multiple coincidences. Derived curves for expected and noise equivalent count rate [2]. Data recorded on a CTI ECAT 953B PET using a ^{11}C-filled cylinder in water.

Performance of PET Systems: Scatter Fraction

- Fraction of the total coincidences recorded in the photopeak window that have been scattered
- Sources of scattering
  - Scattering within the object containing the radionuclide
  - Scattering off the gantry components (lead septa/side shields)
  - Scattering within the detectors

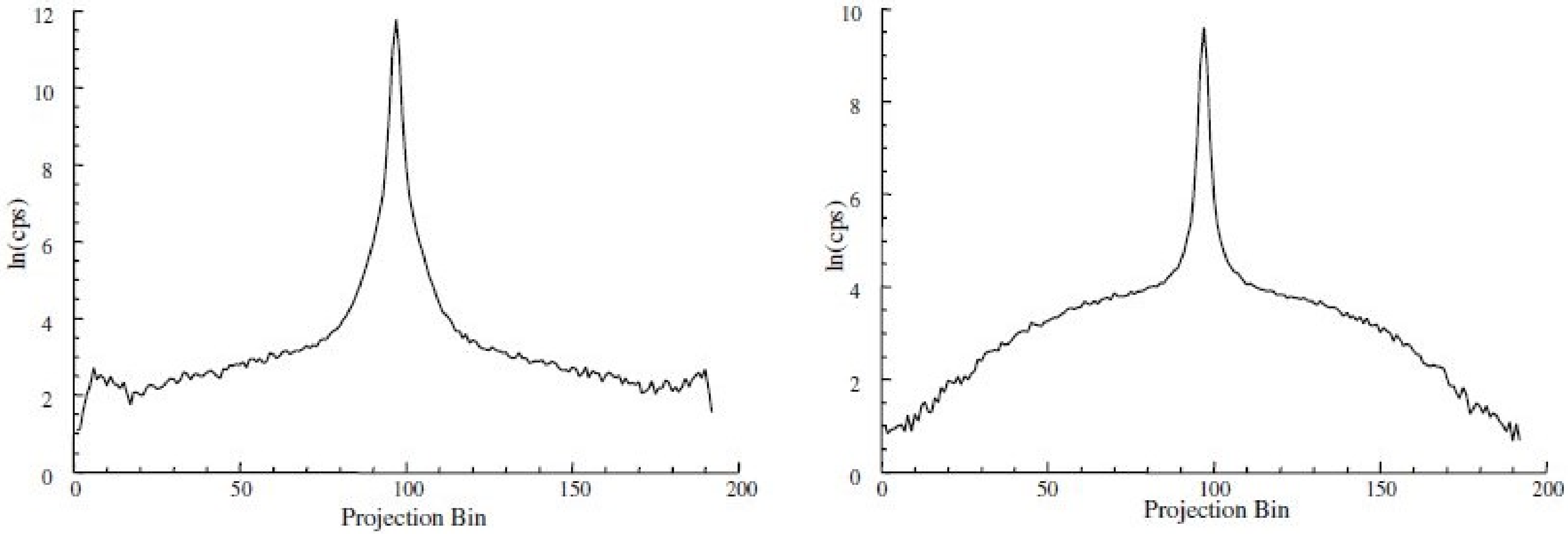

Log-lin count rate profiles of line source in air/water show additive scatter component outside of central peak [2].

Performance of PET Systems: Scatter Fraction

- Fraction of the total coincidences recorded in the photopeak window that have been scattered
- Sources of scattering
  - Scattering within the object containing the radionuclide
  - Scattering off the gantry components (lead septa/side shields)
  - Scattering within the detectors

- Scatter fraction can be reduced by
  - TOF
  - Usage of a powerful iterative reconstruction method
  - Shielding of scattered photons by septa and endshiels
  - Small coincidence window
  - Good energy resolution

Summary

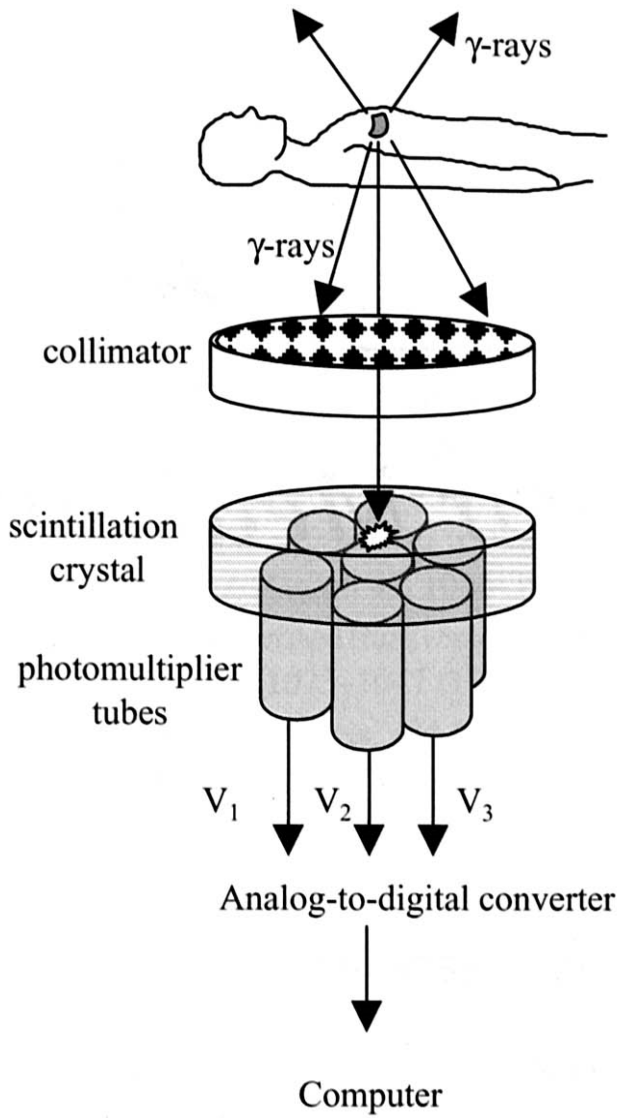

- Positron emitter used as radioactive tracer in the patient
- Use of collimators to generate ‚image slices'
- Detection of γ-quanta in scintillation crystal
- Better resolution due to Anger logic
- Signal amplification using PMTs
- Image reconstruction

Literature

[1] DL Bailey, JS Karp, S Surti. Physics and Instrumentation in PET. In: Positron Emission Tomography: Basic Science and Clinical Practice. Editors: PE Valk, DL Bailey, DW Townsend, MN Maisey. Springer London 2003, pp. 13-39.

[2] DL Bailey. Data Acquisition and Performance Characterization in PET. In: Positron Emission Tomography: Basic Science and Clinical Practice. Editors: PE Valk, DL Bailey, DW Townsend, MN Maisey. Springer London 2003, pp. 41-61.

[3] DW Townsend. Multimodality imaging of structure and function. Phys Med Biol 2008; 53: R1-R39.

[4] B Sattler, JA Lee, M Lonsdale, E Coche. PET/CT (and CT) instrumentation, image reconstruction and data transfer for radiotherapy planning. Radiother Oncol 2010; 96: 288-297. Review.

Imaging for Physicists

Artifacts 1

Uulke van der Heide

Artifacts in MRI

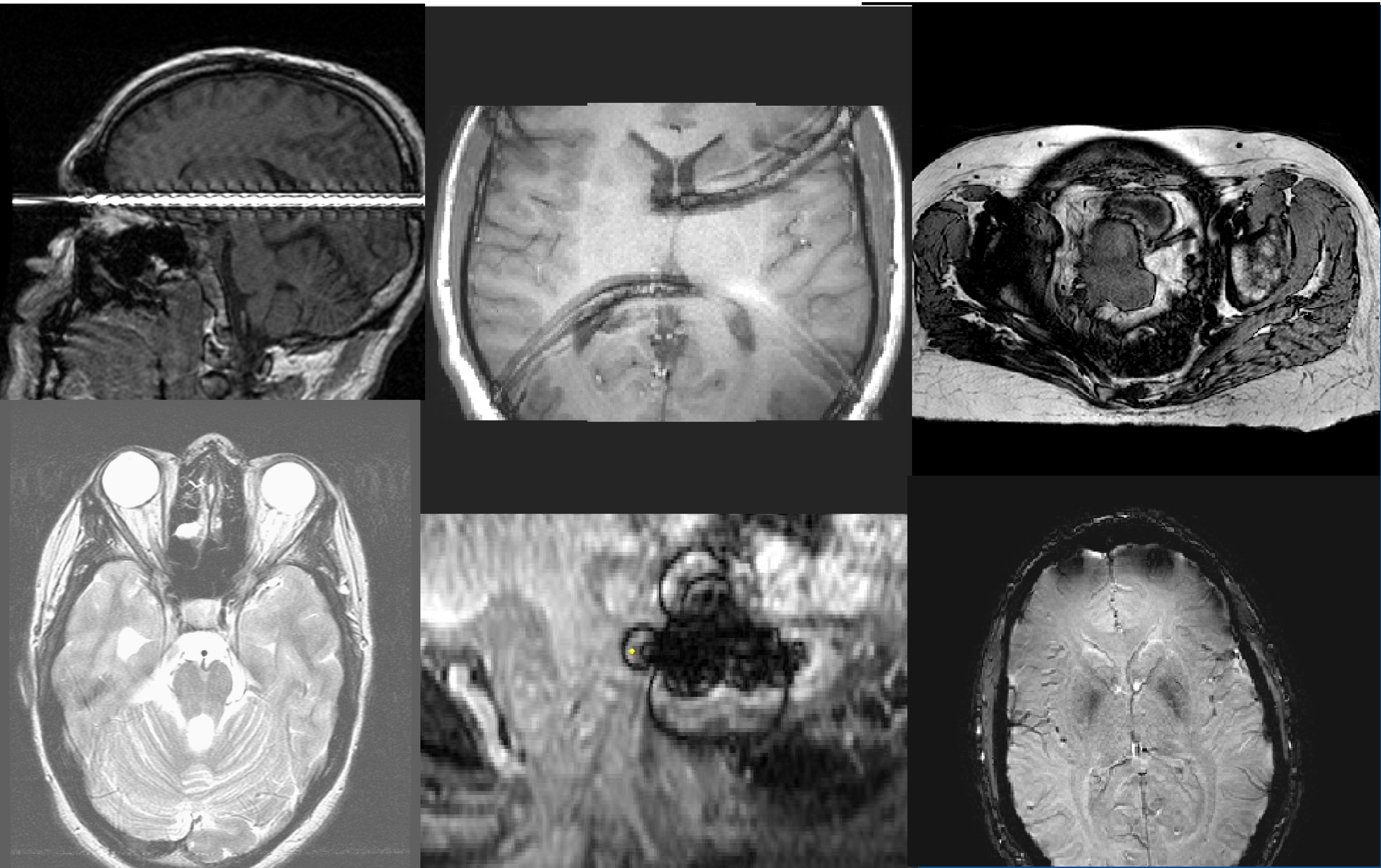

Artifacts in MRI

- An image artifact is any property or effect observed in an image that does not appear in the original object

- Images can be distorted in many ways
  - Signal loss
  - Deformations
  - Poor resolution
  - Ghosting
  - Aliasing
  - .....

- Consequences for use
  - Interpretation is difficult
  - Geometrical accuracy may be compromised

Outline

Lecture 1

- Origin of geometrical artifacts
  - Fold-over artifacts
  - Ringing
  - Impact of field distortions

Lecture 2

- Measurements for characterizing geometrical accuracy
  - Phantom design
  - Characterizing gradient errors
- Examples
- Practical consequences
- Summary

Origin of various artifacts

- Sampling of k-space
  - Sample k-space in too large steps
  - Don’t sample high k-values
- Magnetic field errors
  - Inhomogeneous B_0 field
  - non-linear gradients
  - Susceptibility
  - Chemical shift
- Motion

Imaging artifact

- T_1-weighted SE image of a brain
- What is wrong?

Sampling the MR signal

- Nyquist criterium: signal must be sampled at at least twice the rate of the highest frequency component

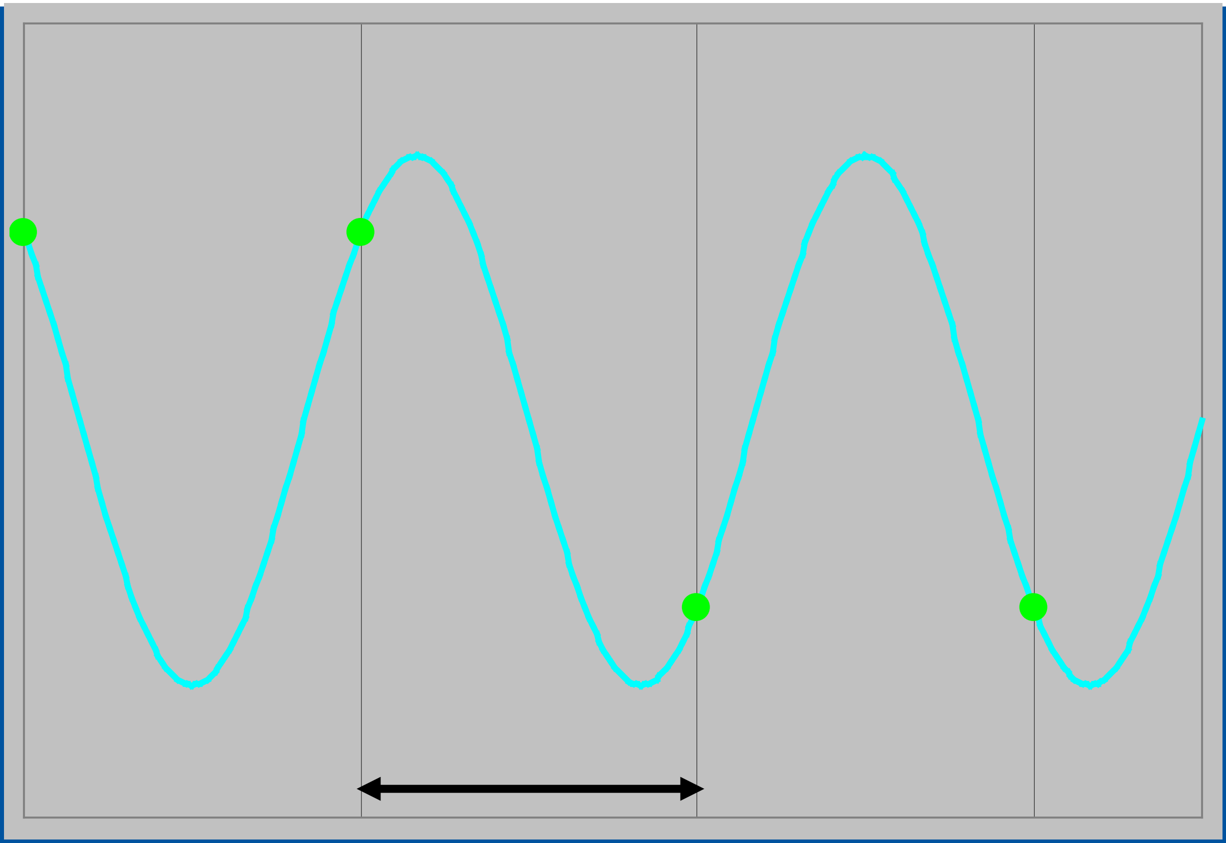

Sampling the MR signal

- Nyquist criterium: signal must be sampled at at least twice the rate of the highest frequency component

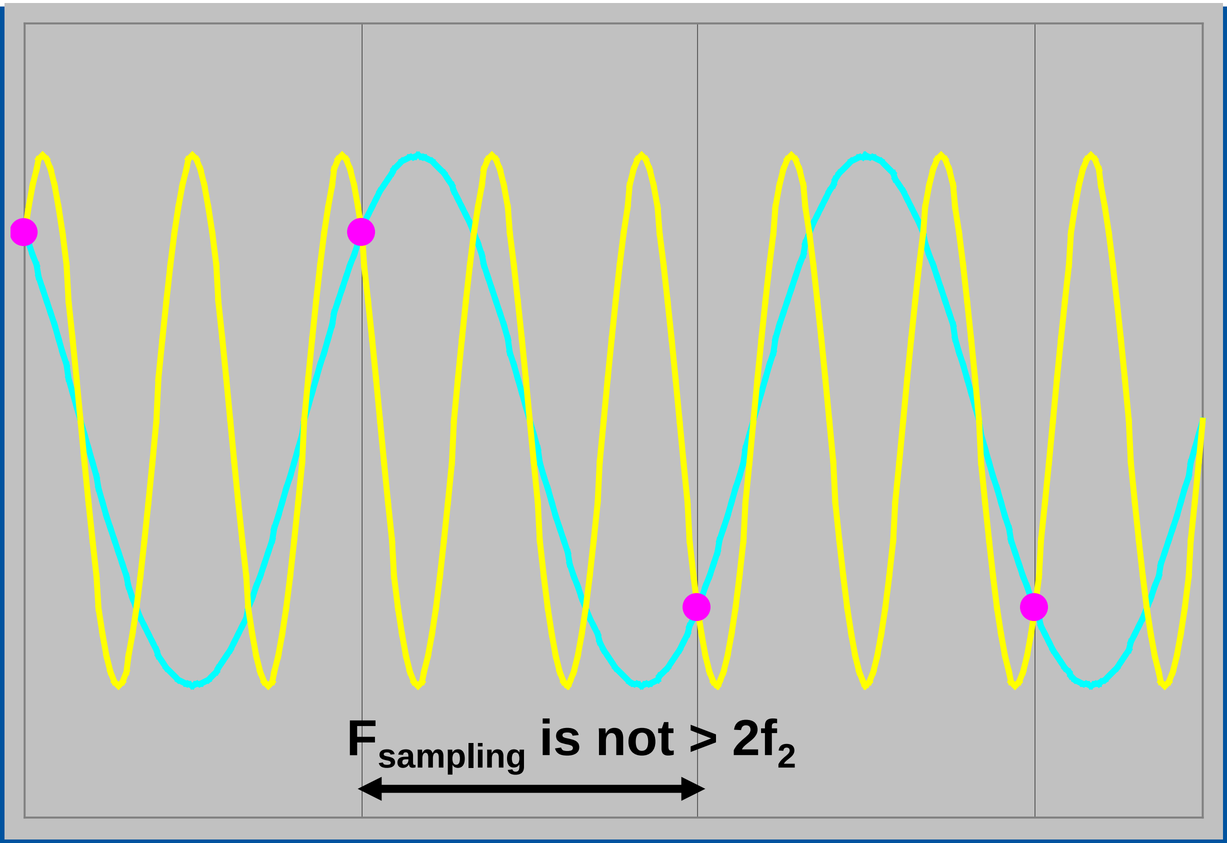

- If the signal contains higher frequency components, aliasing occurs

Resolve aliasing by increasing sampling frequency

- Nyquist criterium: signal must be sampled at at least twice the rate of the highest frequency component

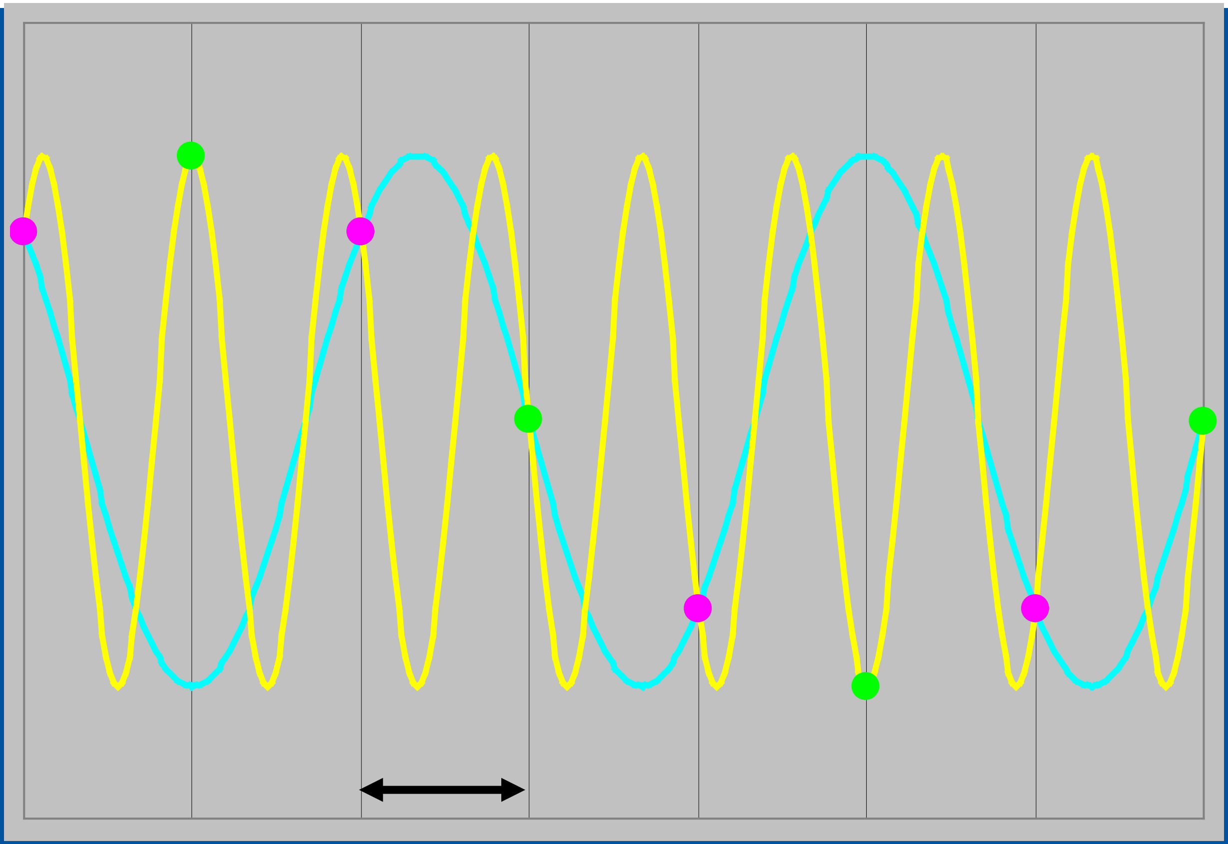

- By increasing the sample frequency, the higher frequency components can be resolved and aliasing is avoided

Field Of View covers entire object: no fold-over

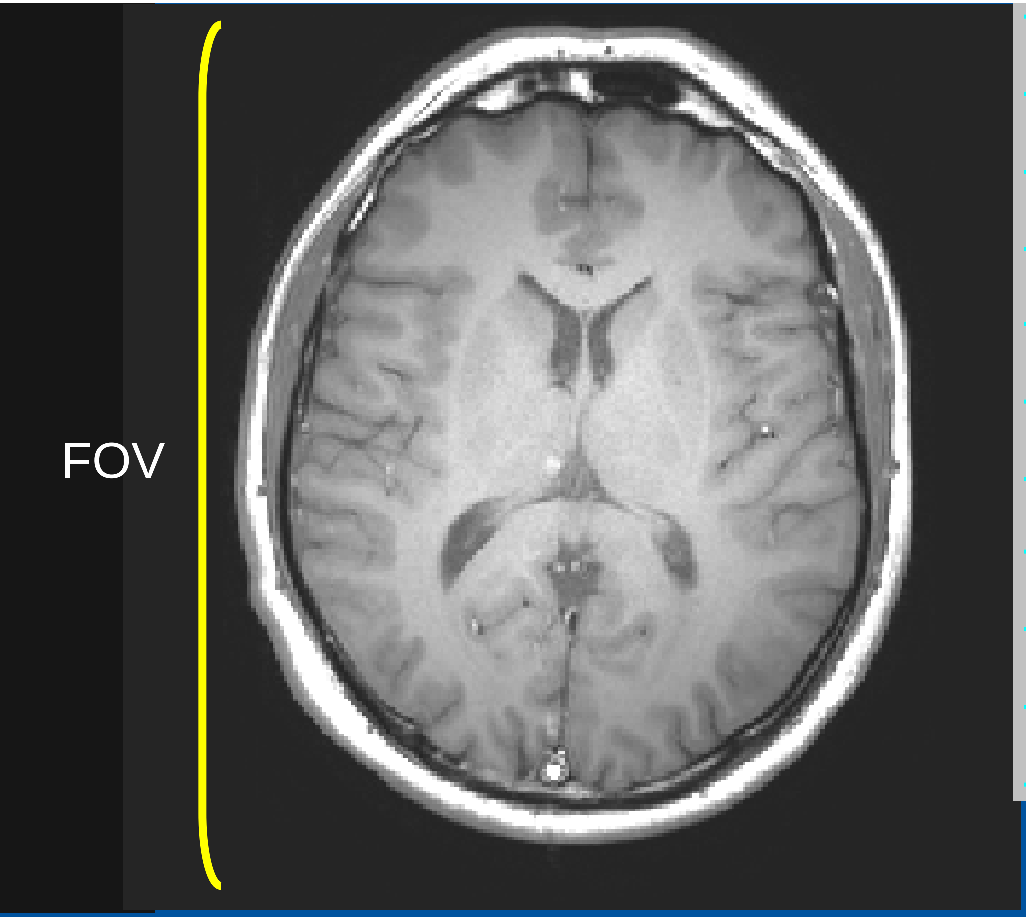

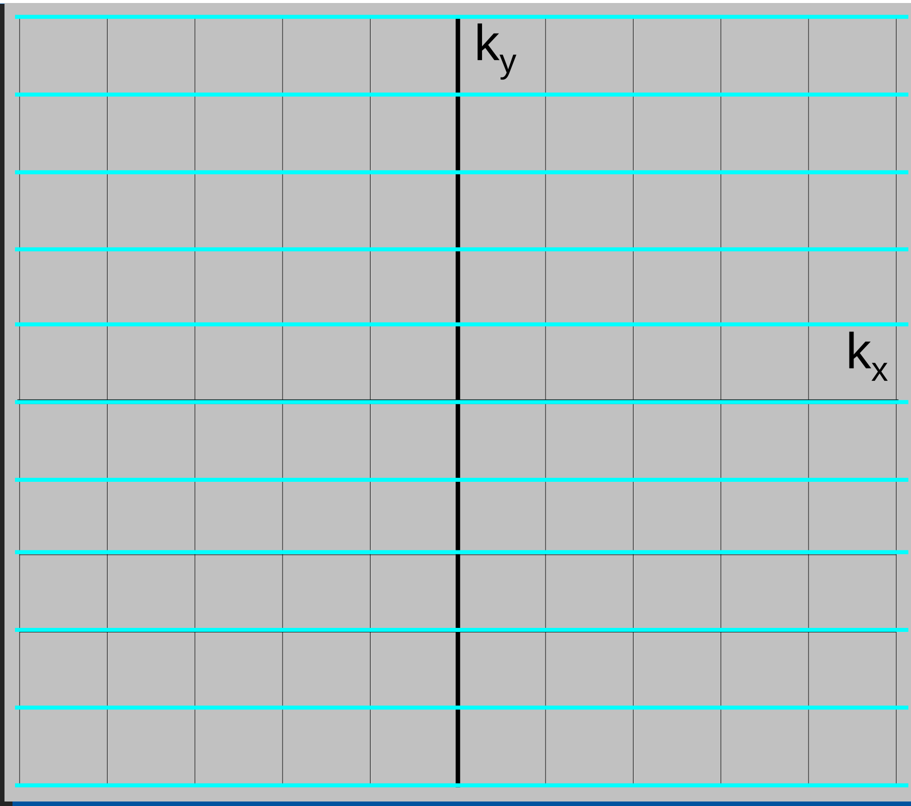

Question: field of view

- What happens with the distance between lines in k-space, if you reduce the field of view by a factor of 2?

1. The distance between k-lines is increased by a factor of 2
2. The distance between k-lines is reduced by a factor of 2
3. The distance between k-lines remains the same (but the extent of k-space is reduced by a factor of 2

Field Of View covers entire object: no fold-over

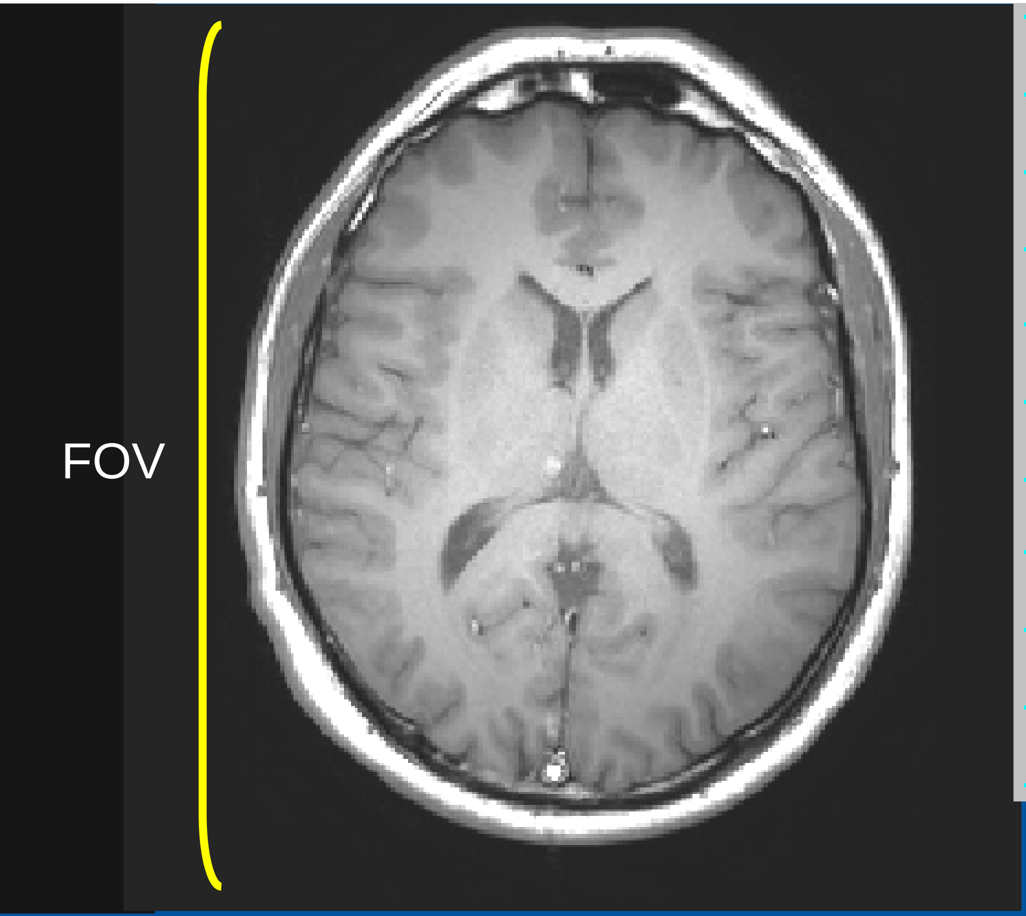

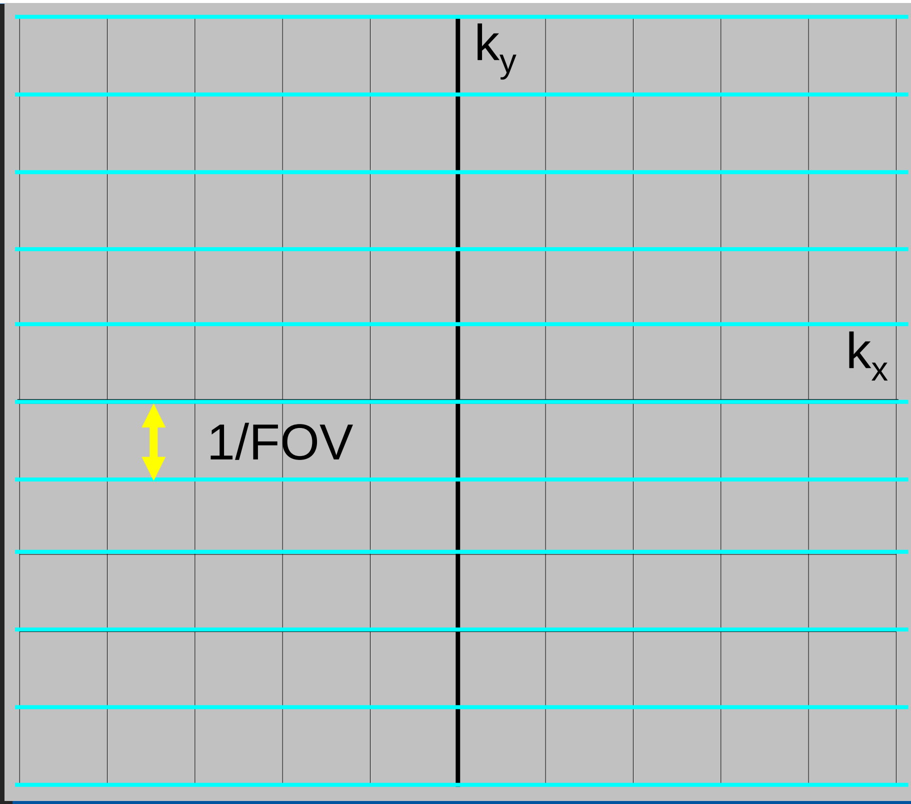

FOV too small: fold-over

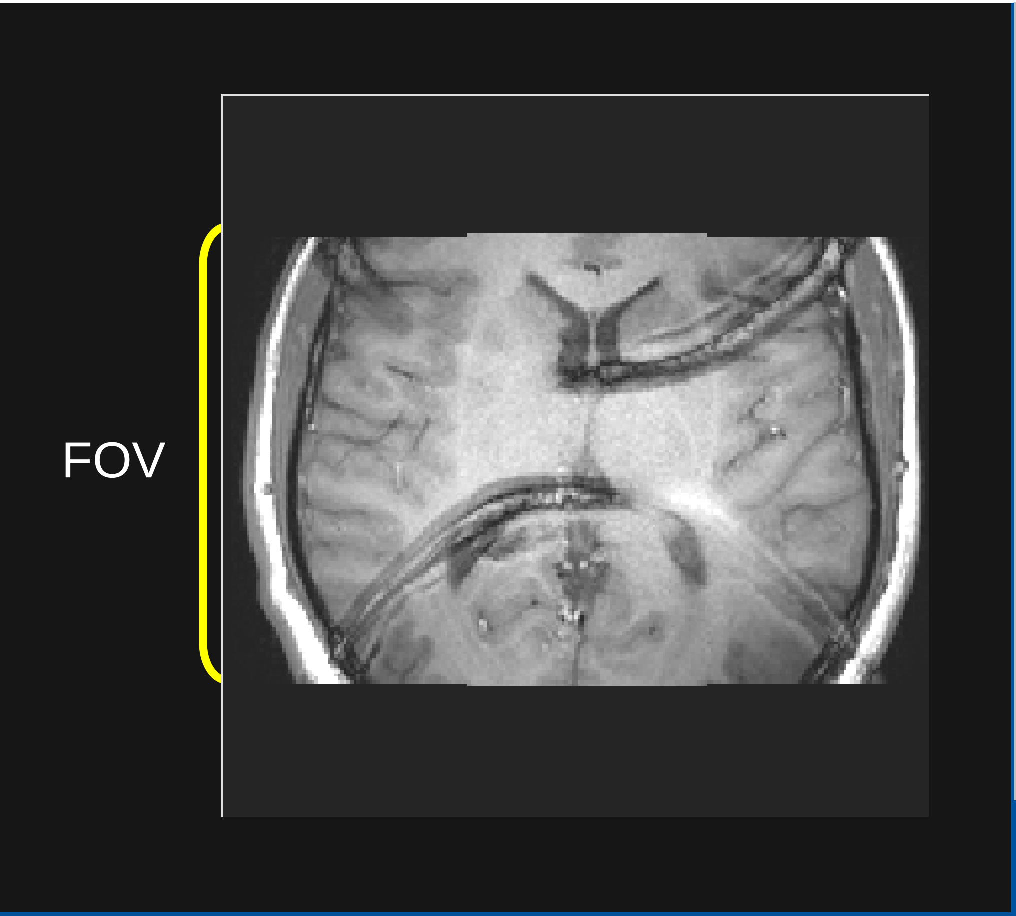

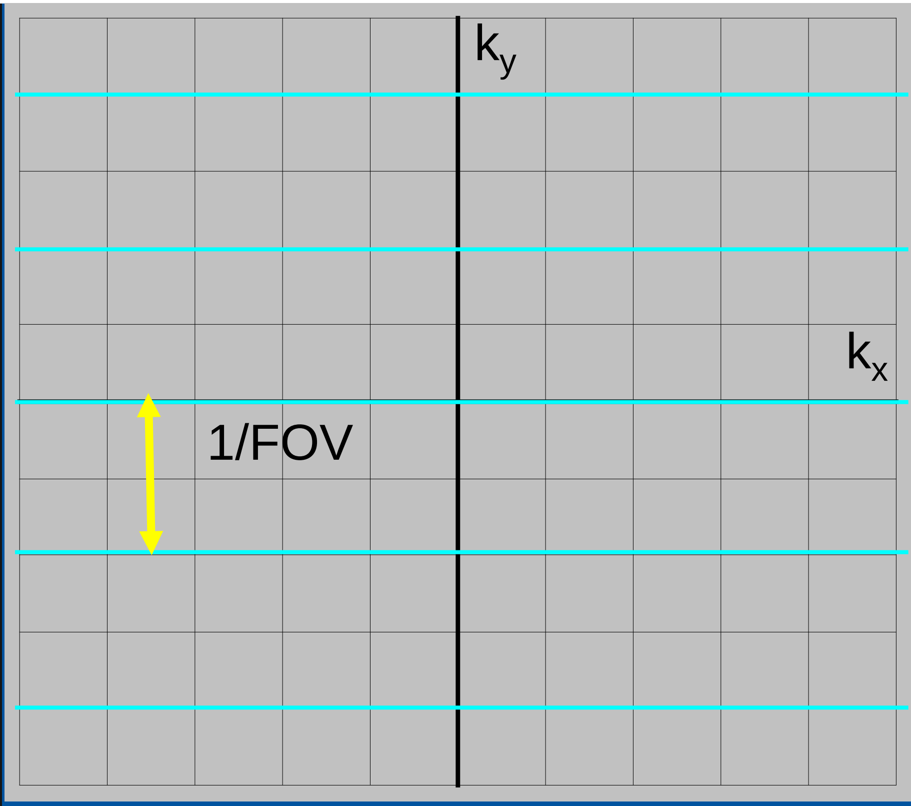

How to suppress fold-over artifacts?

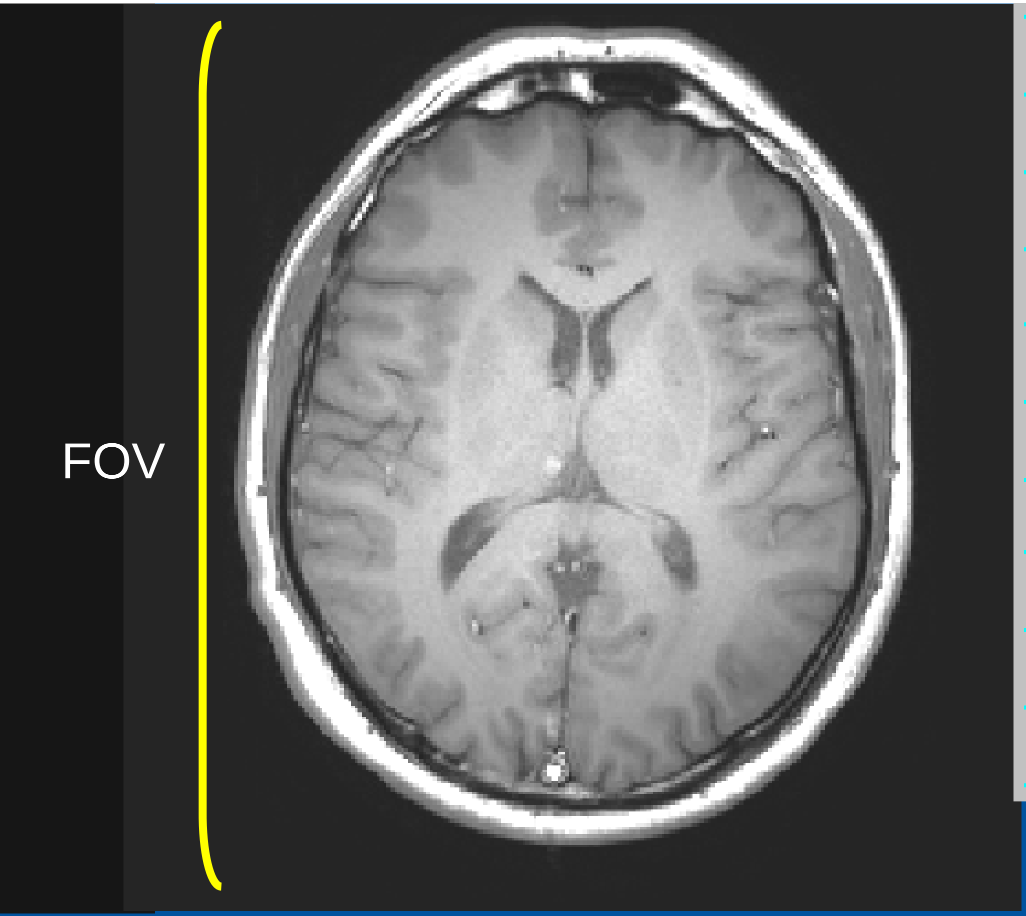

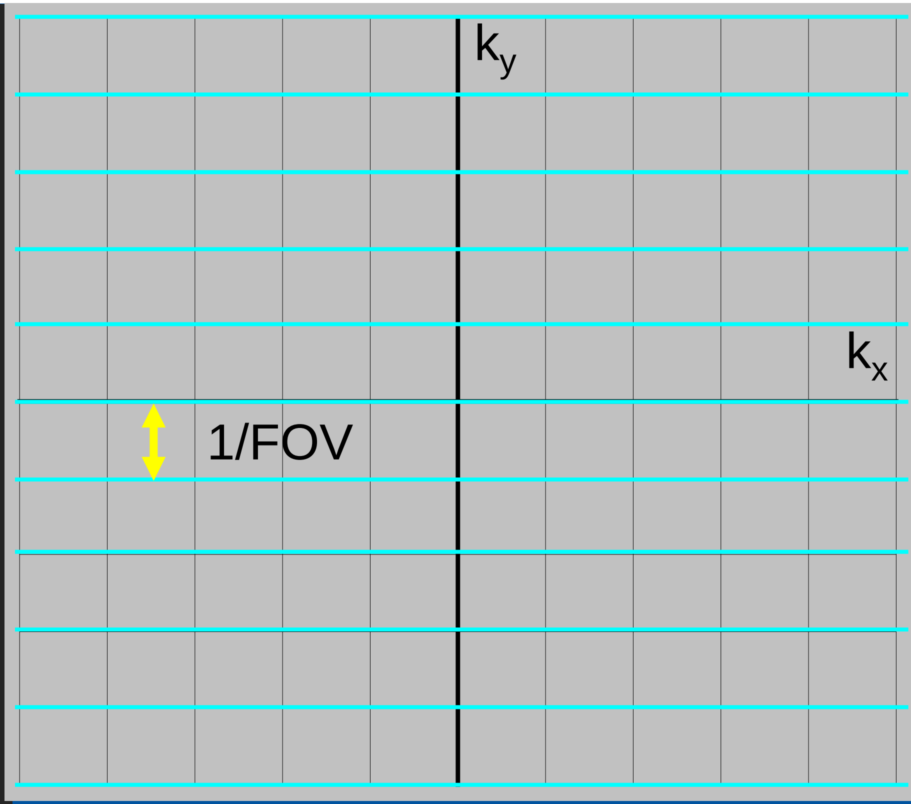

- If NSA>1: Measure all k-lines (full FOV), but reconstruct only half of the image

How to suppress fold-over artifacts?

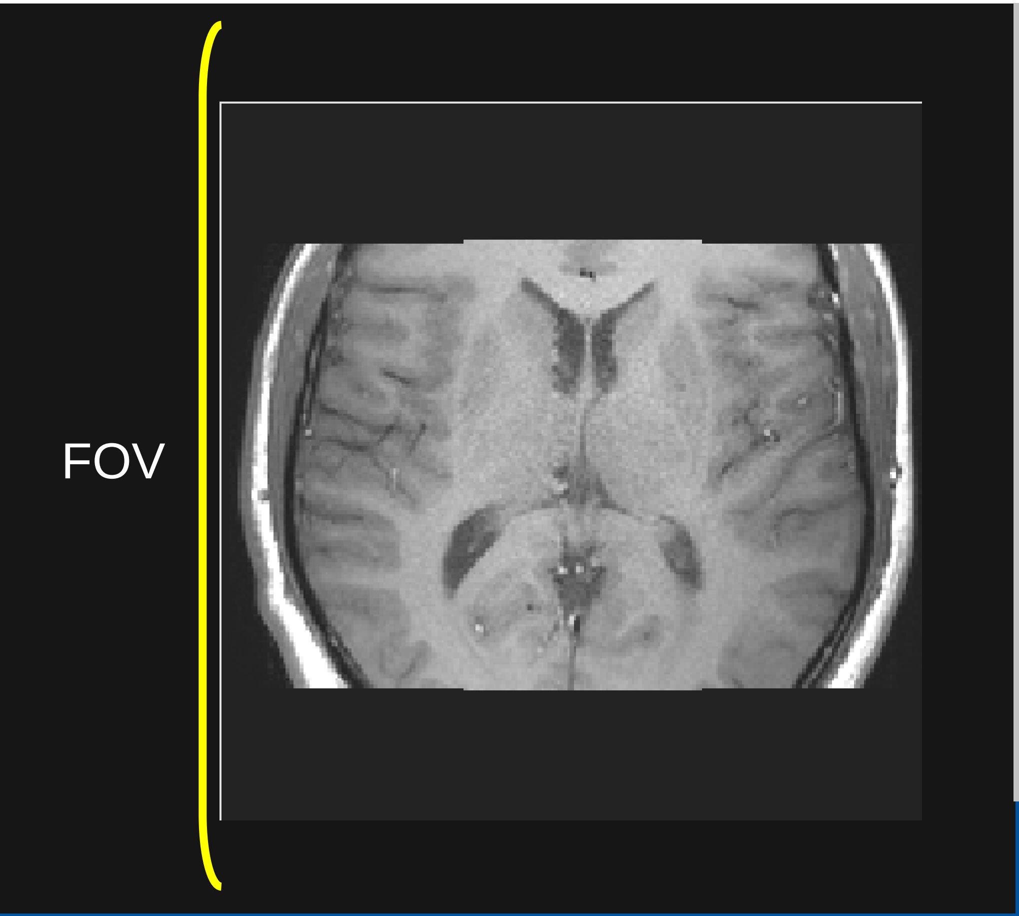

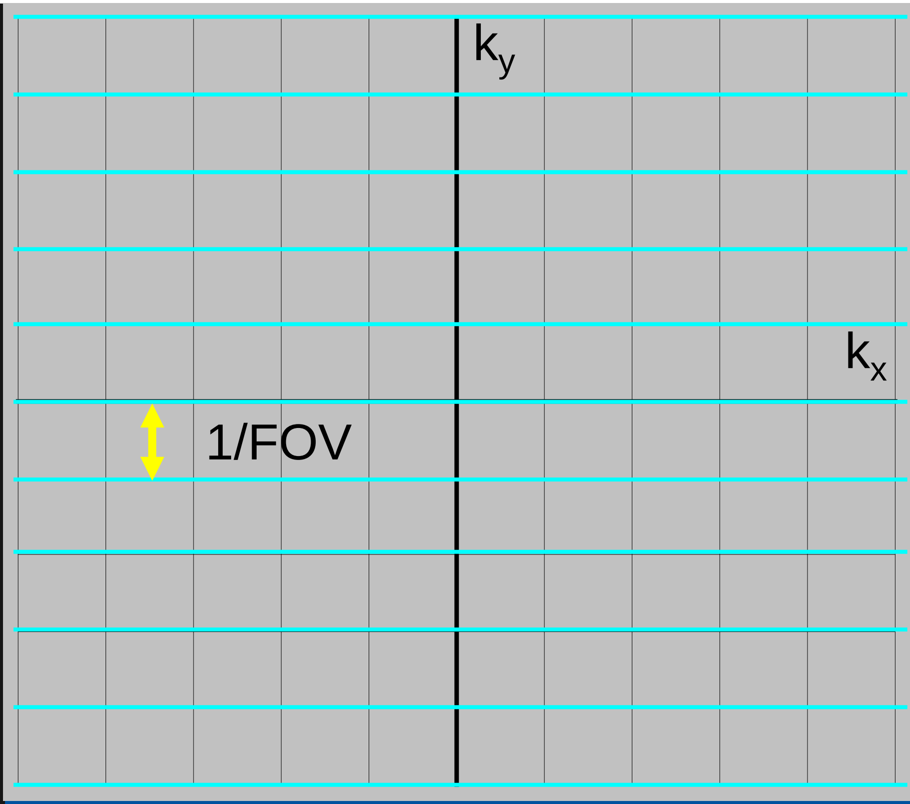

- If NSA>1: Measure all k-lines (full FOV), but reconstruct only half of the image

How to suppress fold-over artifacts?

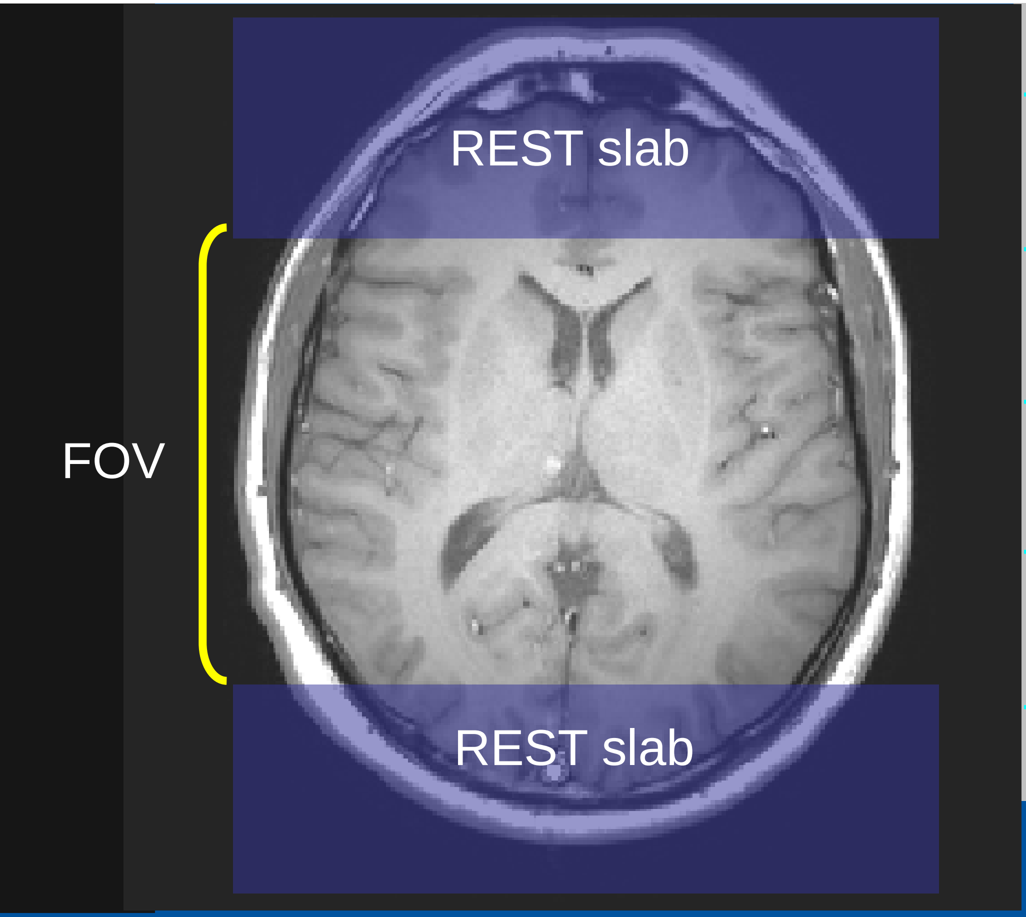

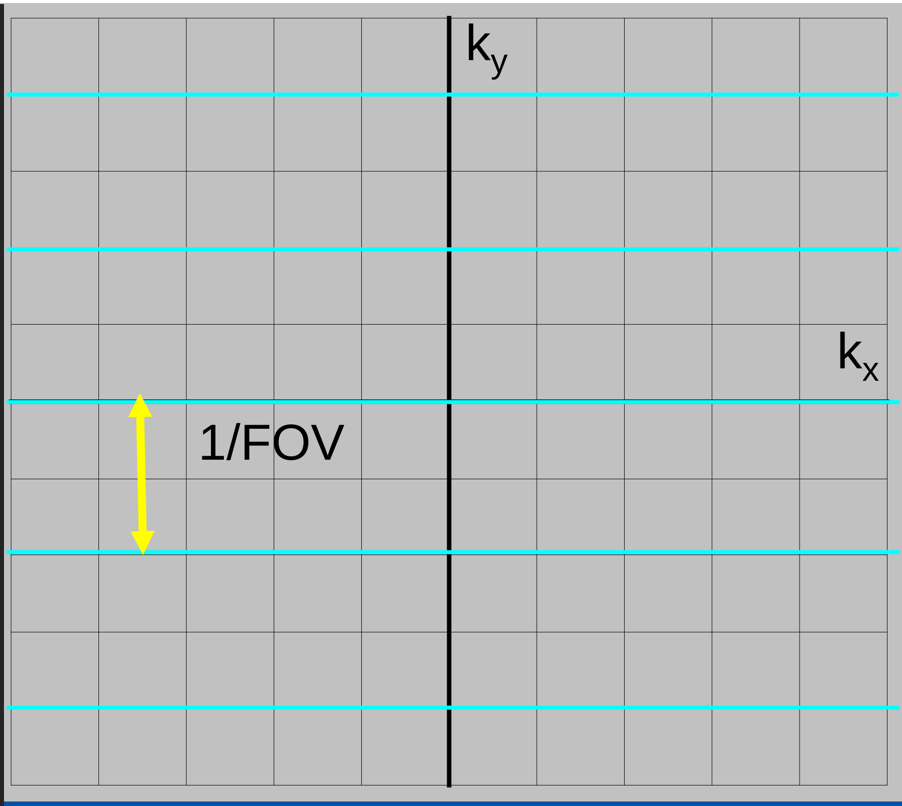

- If NSA=1: Saturate the signal from outside the field-of-view with REST slabs

Saturate signal from outside FOV

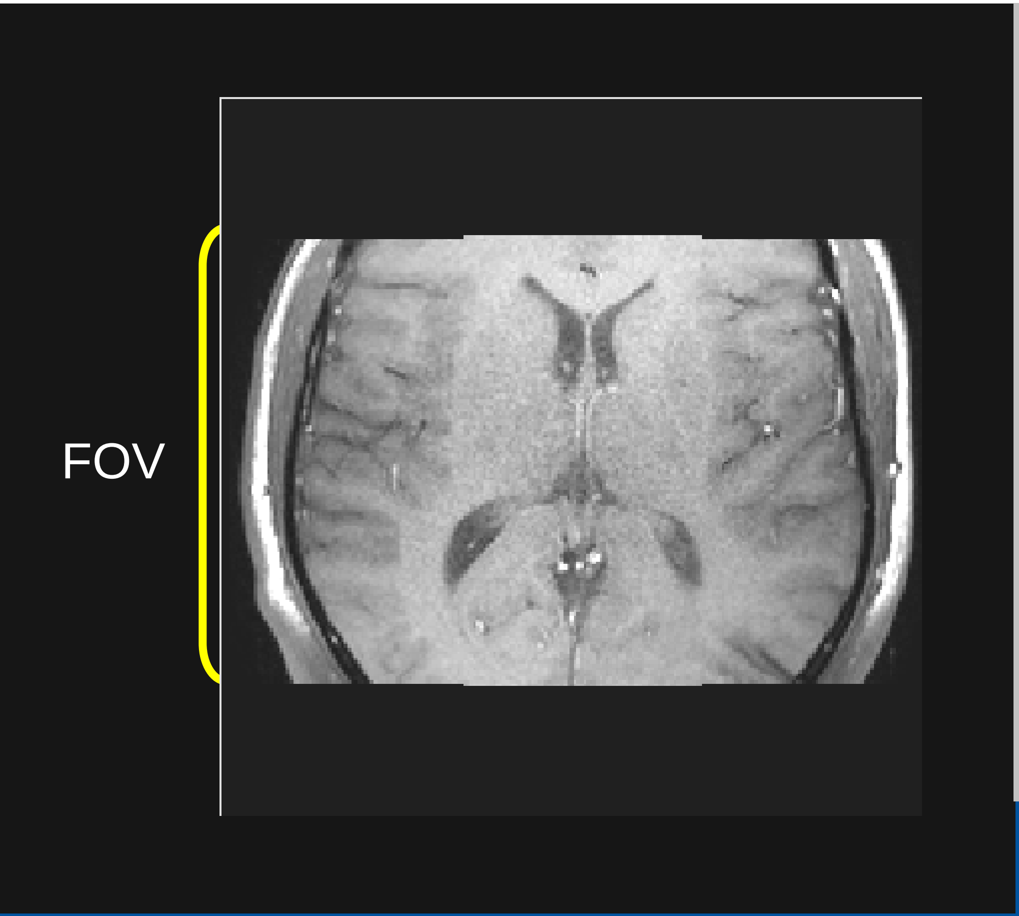

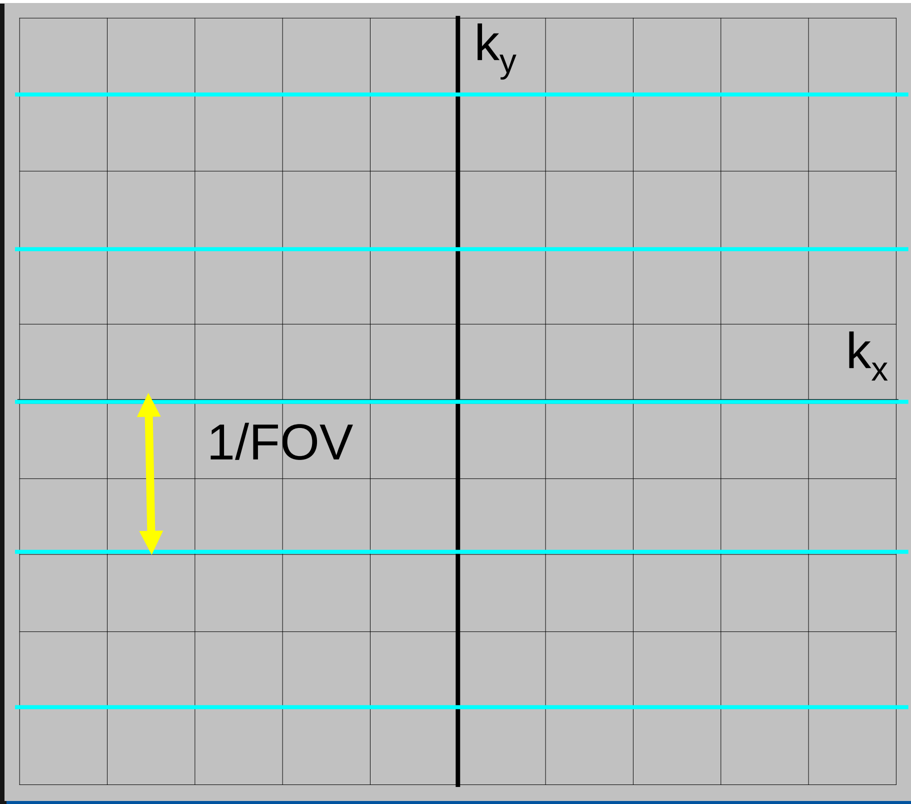

Imaging artifact

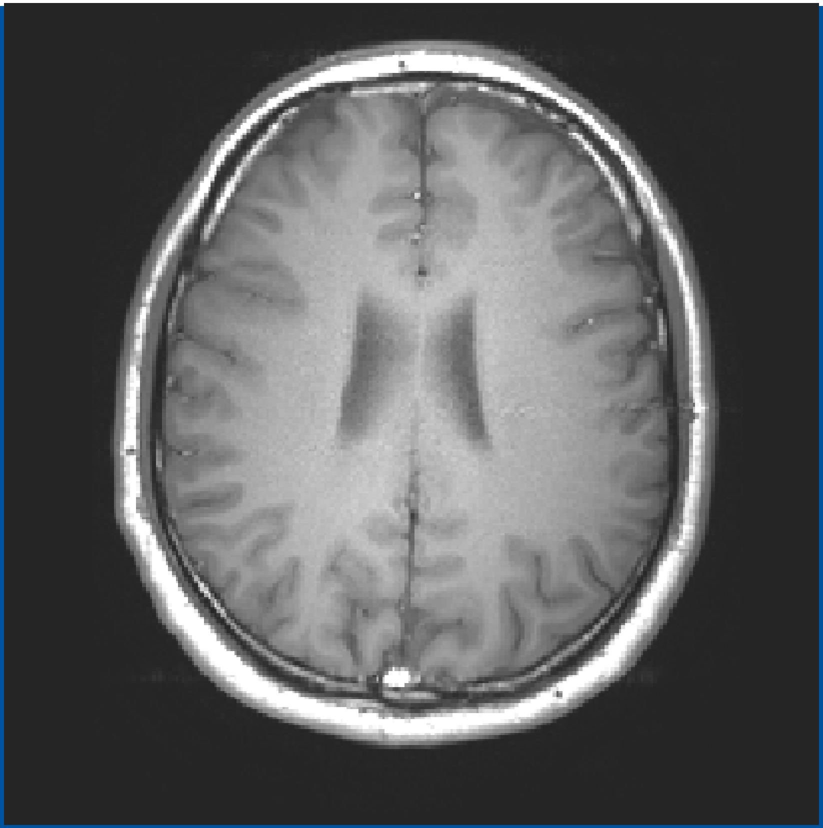

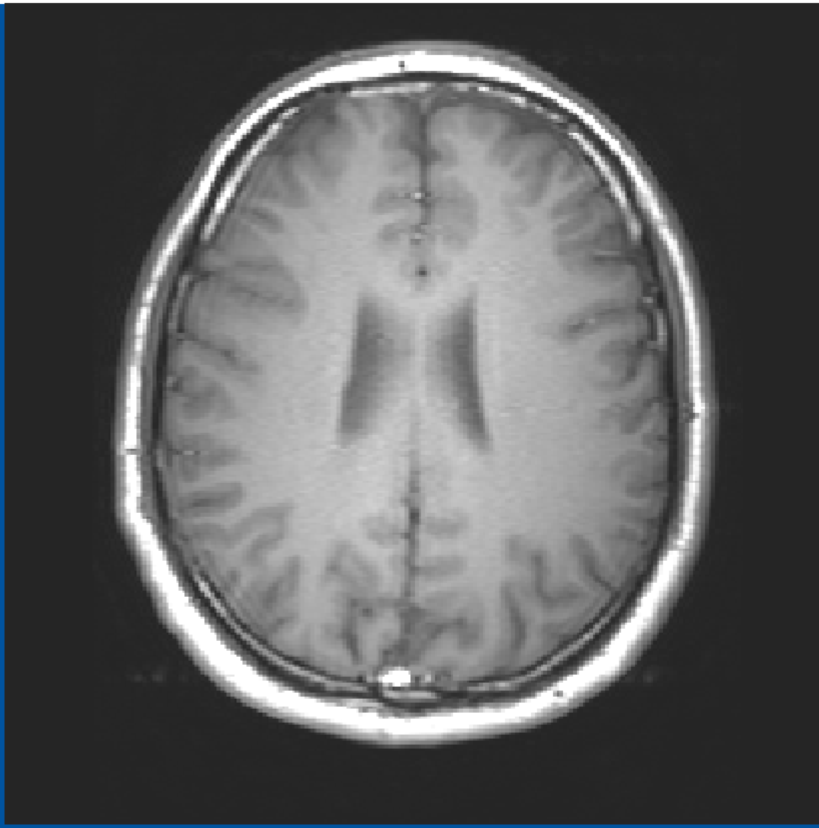

- T_1-weighted SE image of a brain
- What is the difference between the left and right image?

Imaging artifact

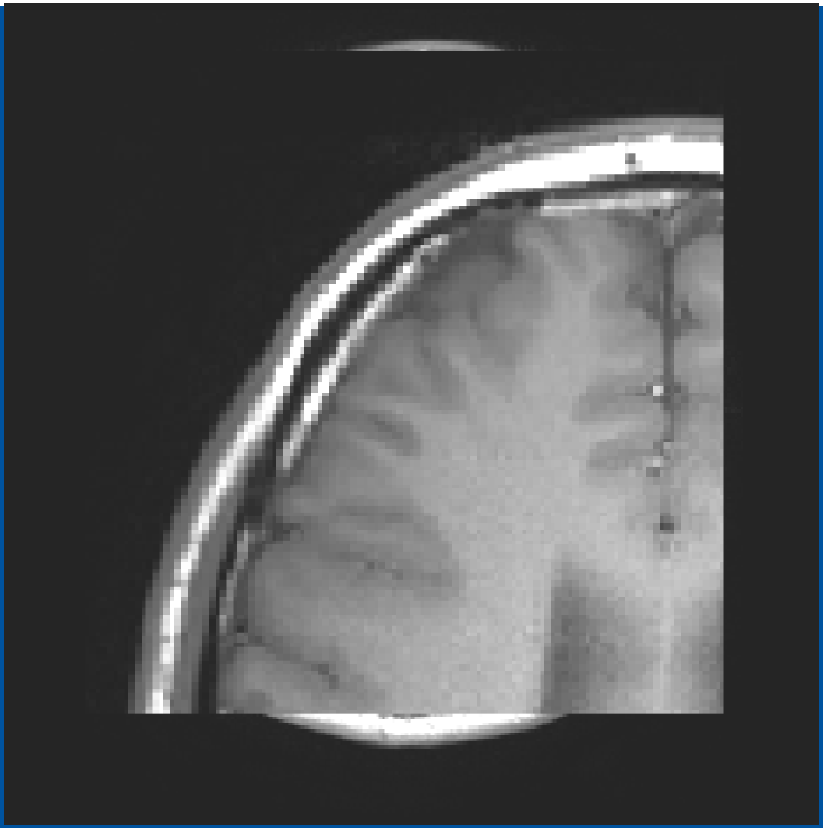

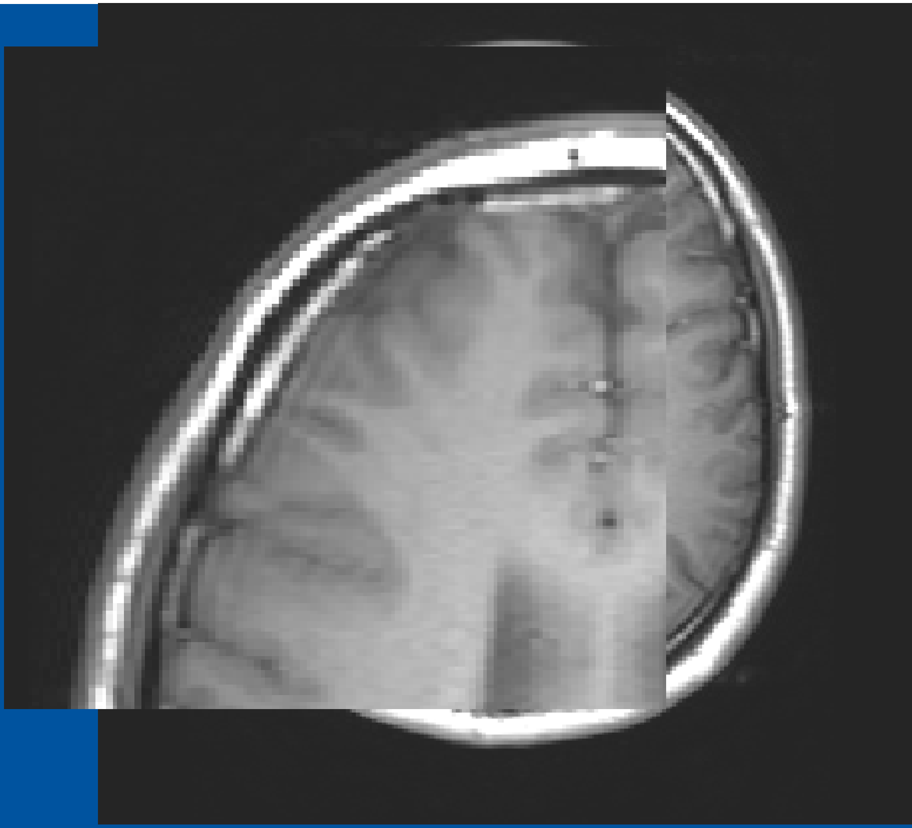

- T_1-weighted SE image of a brain
- What is the difference between the left and right image?

Truncation errors (ringing)

- Imaging sharp edges requires high frequency components in k-space
- Cutting off the high-frequency k-lines causes oscillations in the image

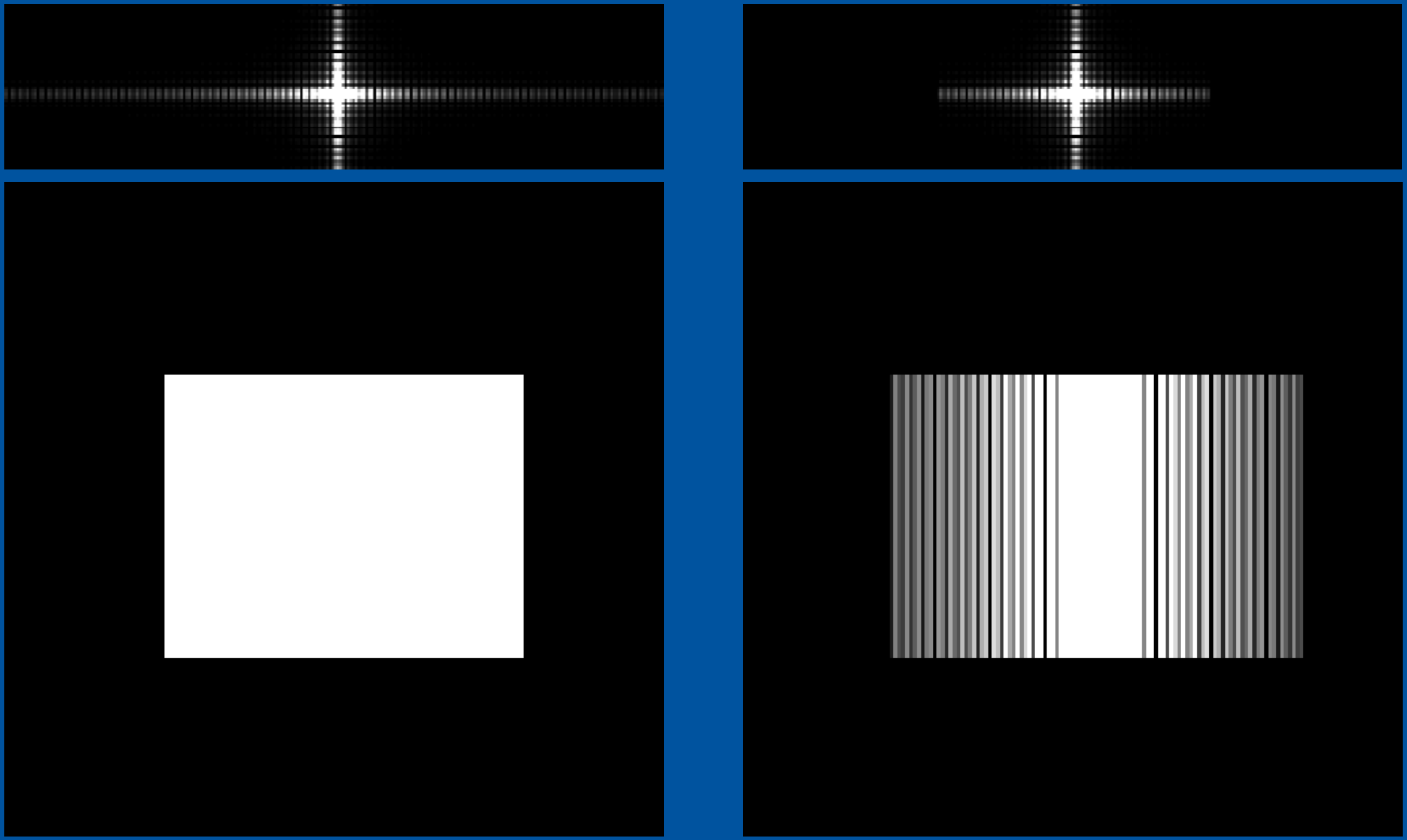

How to avoid truncation errors (Ringing)

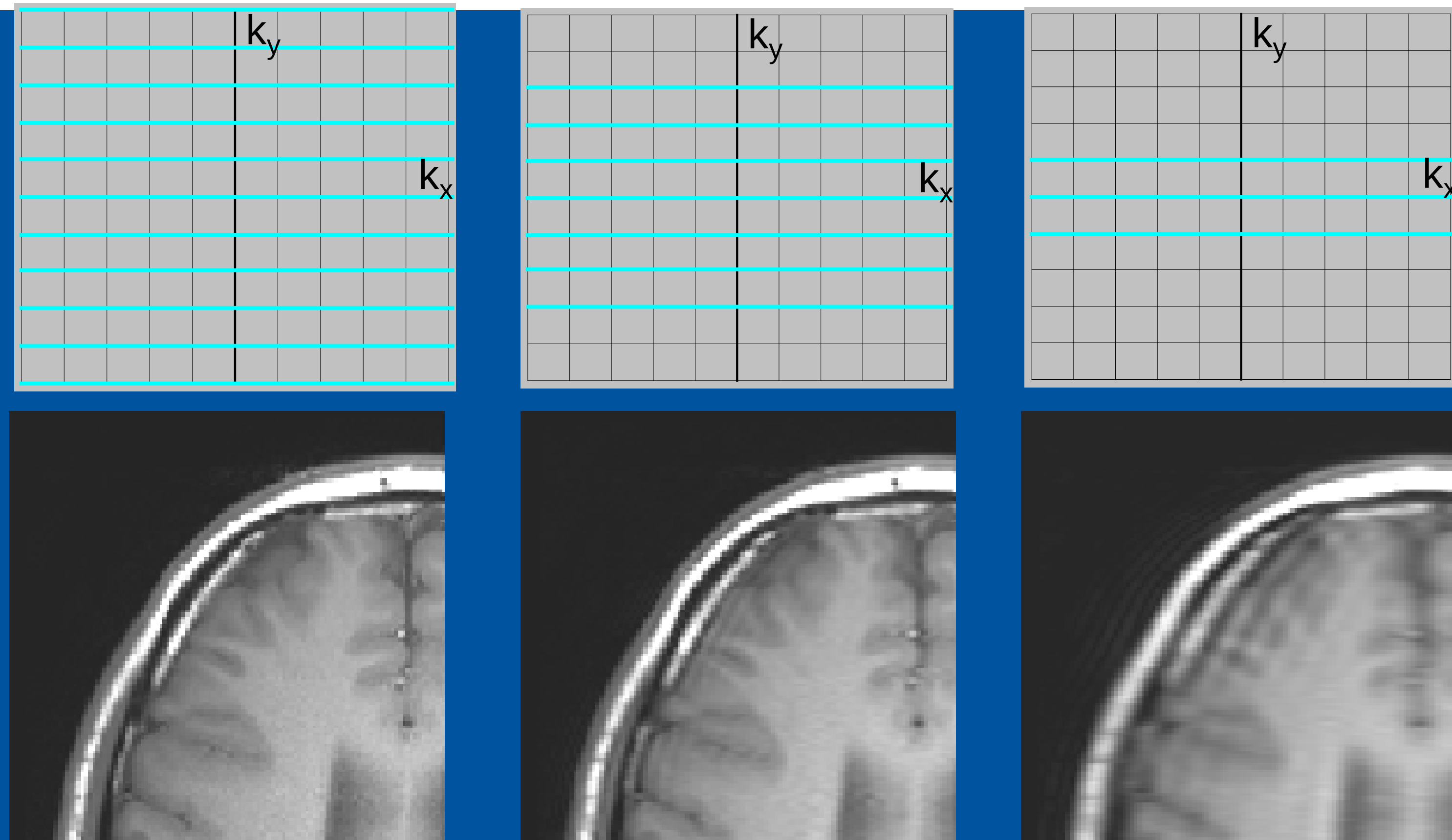

- sample k-space up to sufficiently high frequencies (use sufficiently small voxels during acquisition)
- filtering; the ringing may disappear, but the spatial resolution of the image, and sharpness of edges tends to be compromised

Sampling of k-space

Aliasing/Fold-over artifact:

- Fold-over of signal from outside field-of-view into the image
- Appears in phase-encoding direction

What to do about it:

- Increase FOV in phase-encoding direction
  - (decrease the distance between k-lines)
- Suppress signal from outside FOV

Sampling of k-space

Ringing artifact:

- Oscillating pattern next to sharp edges in an image

What to do about it:

- Decrease voxel size
  - (sample higher k-values)
- Filter the image

Sampling k-space in practice

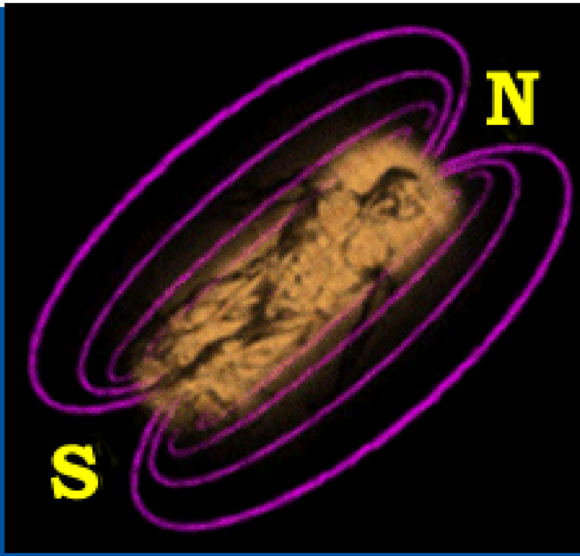

- Let’s assume we sample k-space well. Do we really sample, what we thought we sampled?
- Spatial encoding occurs by switching gradients to modulate frequency and phase
- How can this process lead to artifacts?

$$\omega = \gamma \boldsymbol{B}_0$$

Linear magnetic gradient fields (x, y, z) create spatial differentation of the signals

$\rightarrow$ 3D images

Position encoding in a spin-echo sequence

RF pulse

Slice selection gradient

Phase encoding gradient

Frequency encoding gradient

Signal detection

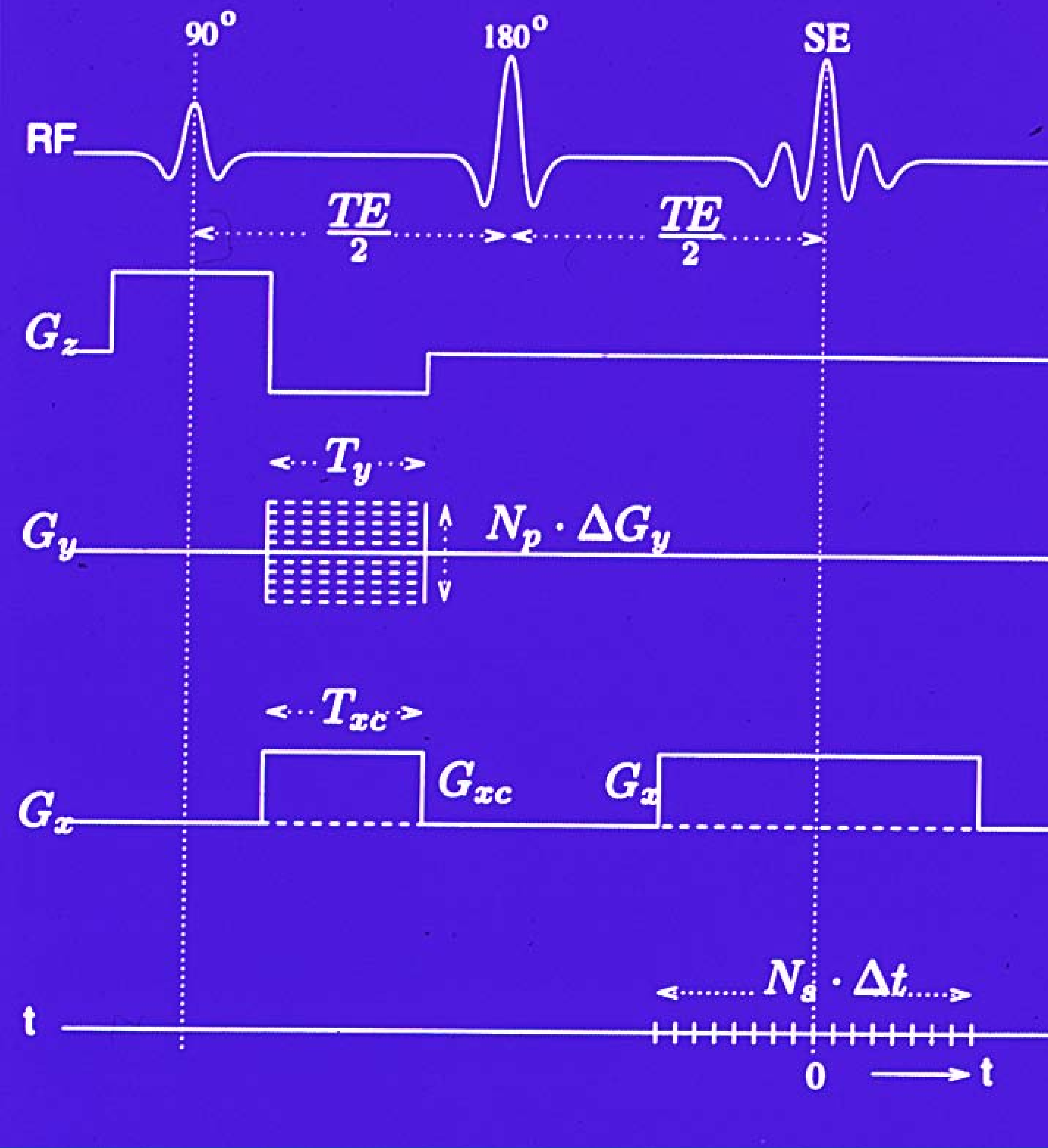

Slice selection: transversal

Resonance condition

$$\omega = \gamma (B_0 + zG_z)$$

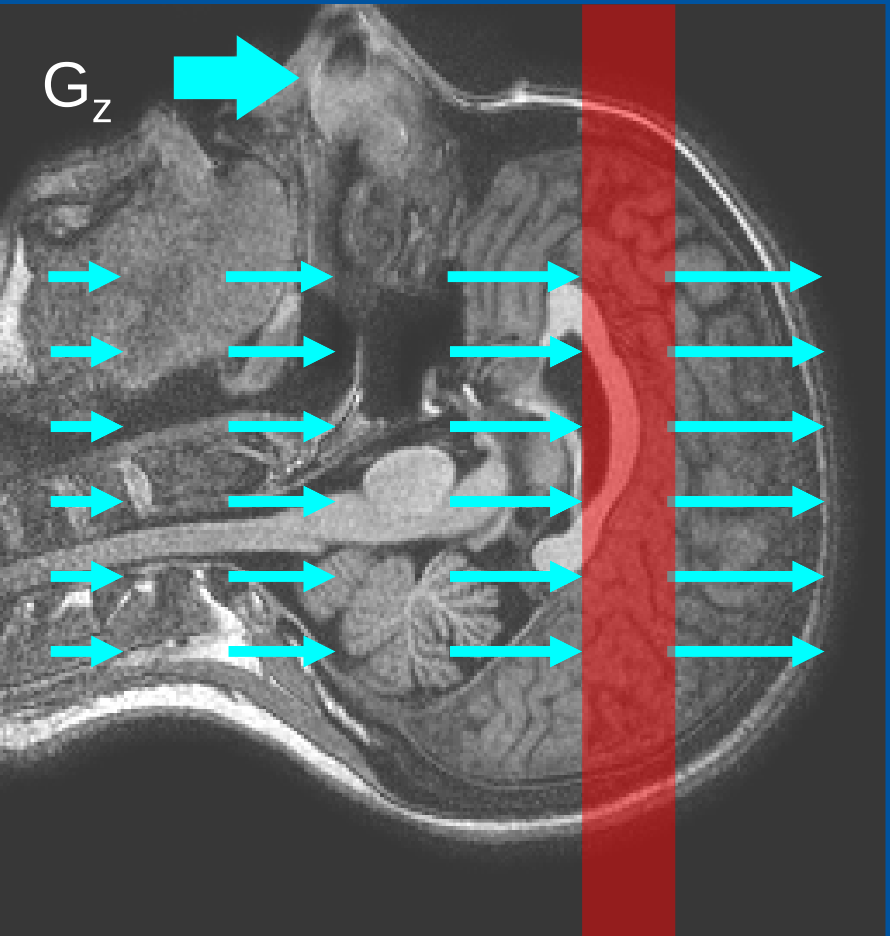

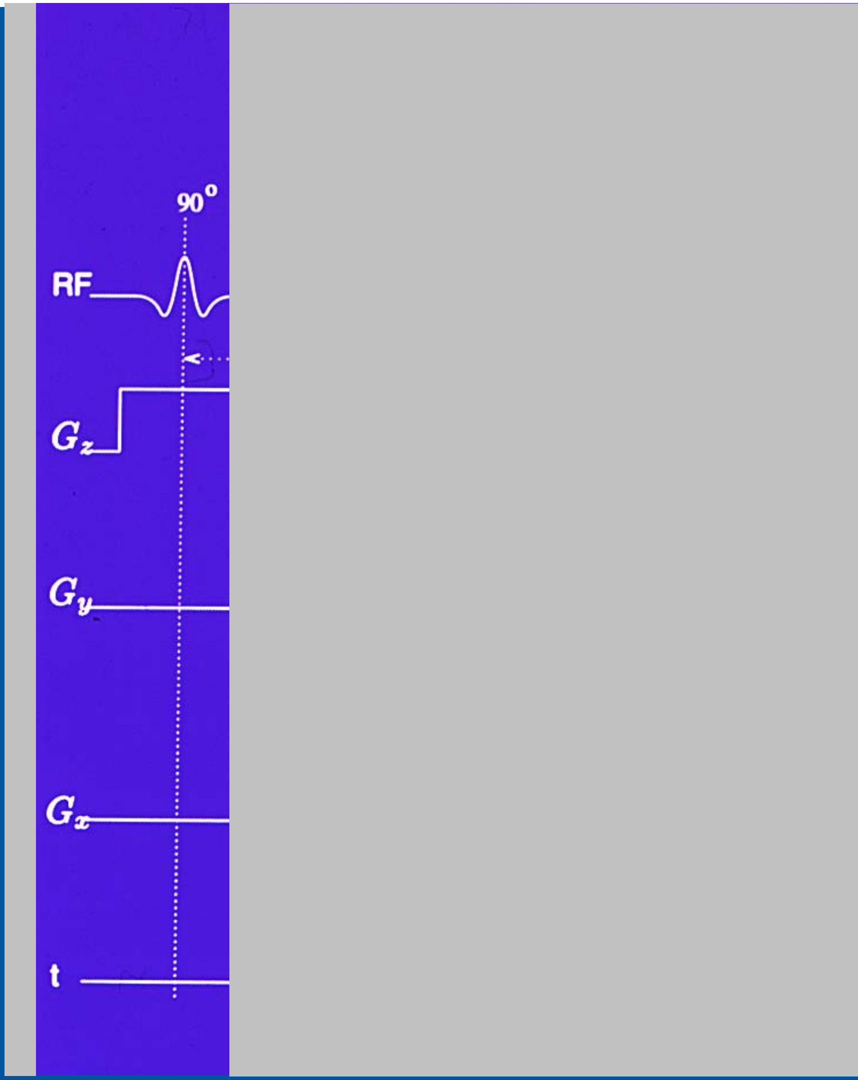

Phase encoding

Apply gradient after RF pulse and before read-out

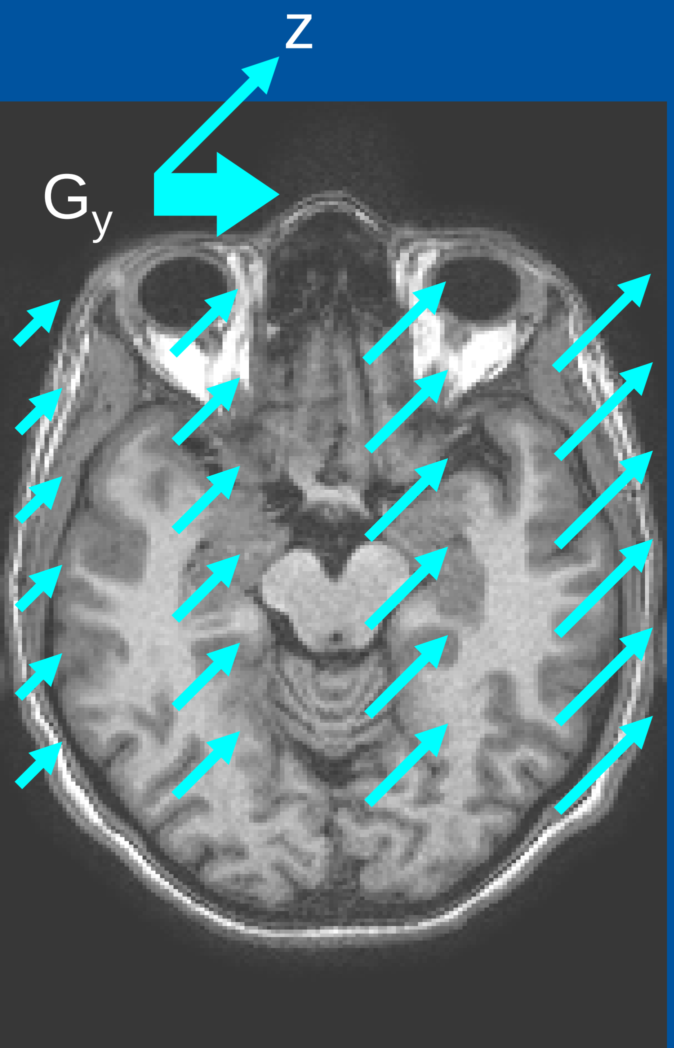

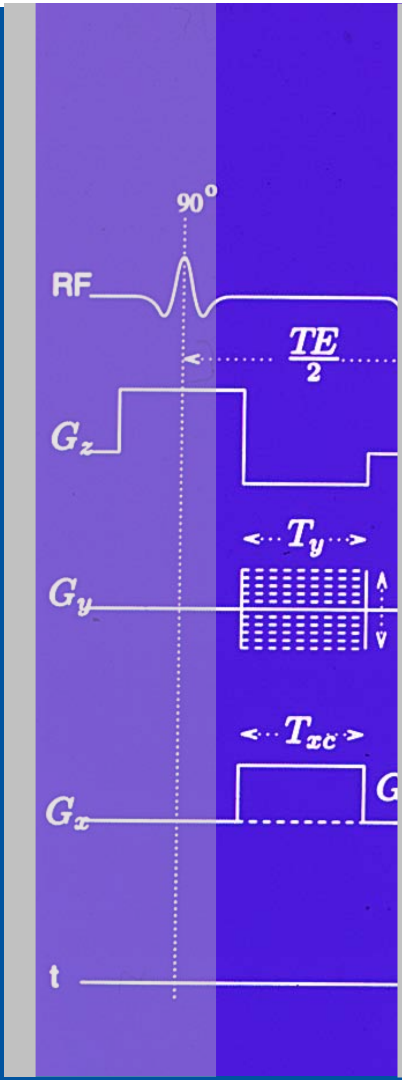

Phase encoding

$$\omega = \gamma B_0$$

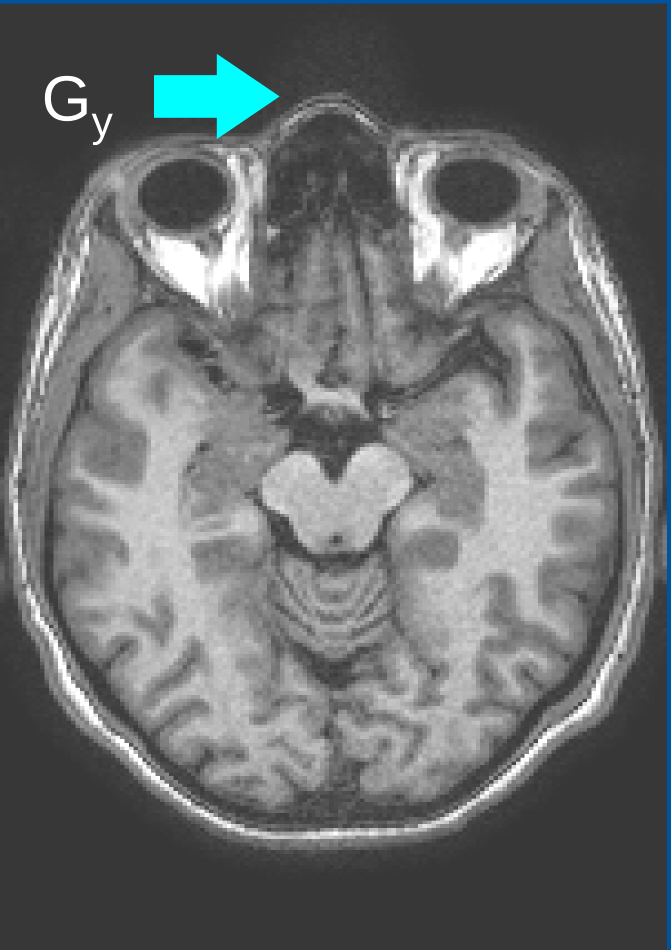

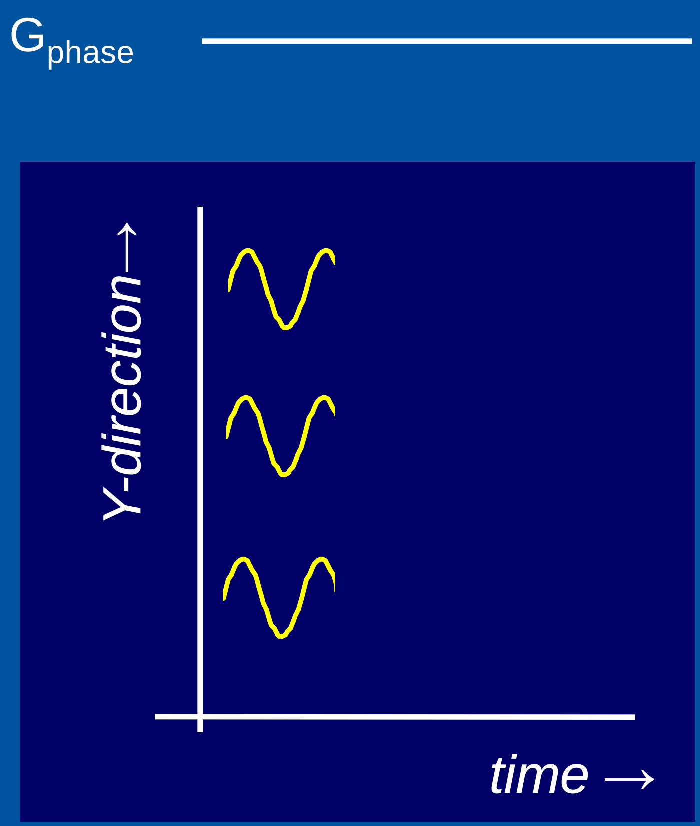

Phase encoding

$$\omega = \gamma\,(B_0 + yG_y)$$

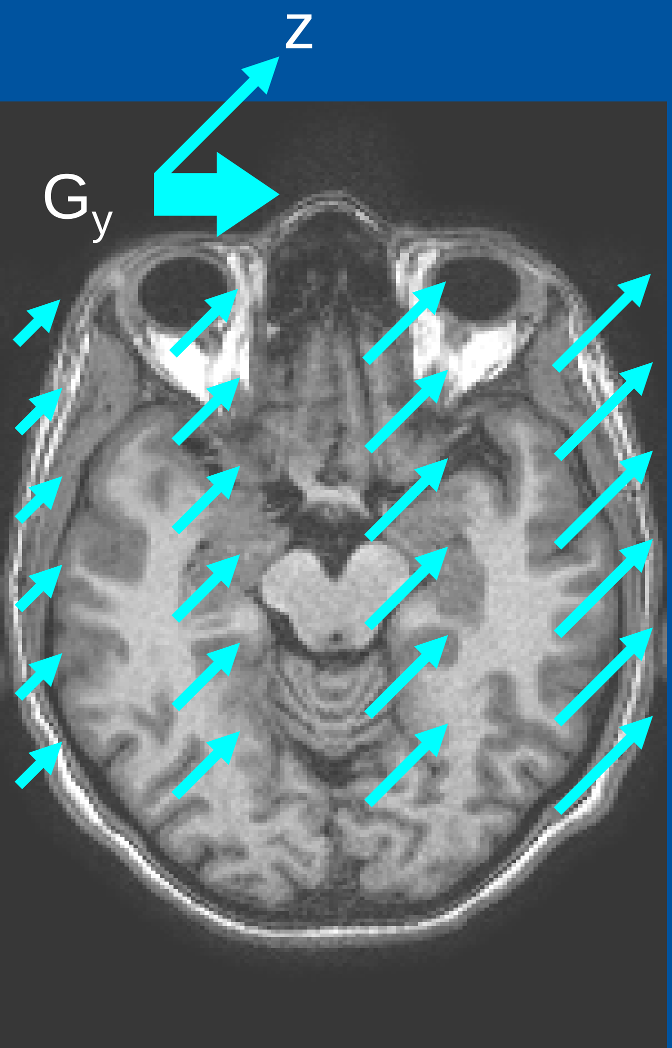

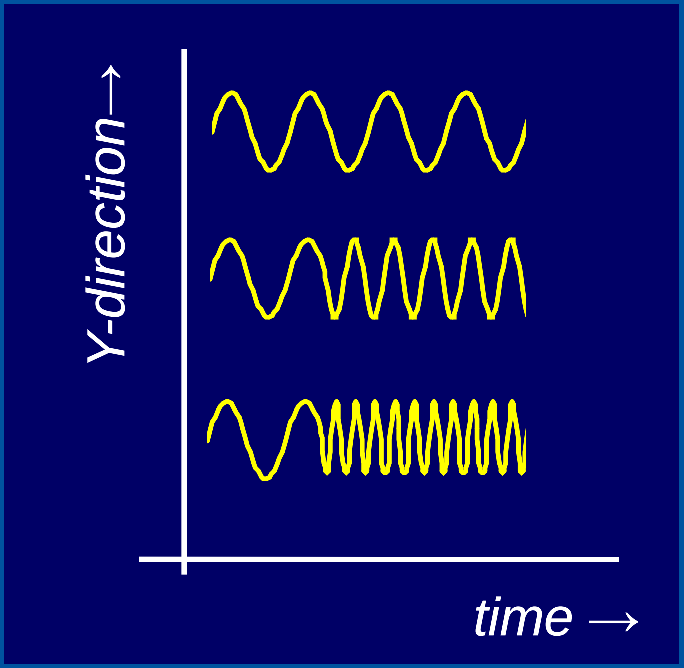

Phase encoding

$$\omega = \gamma B_0$$

G_{phase}

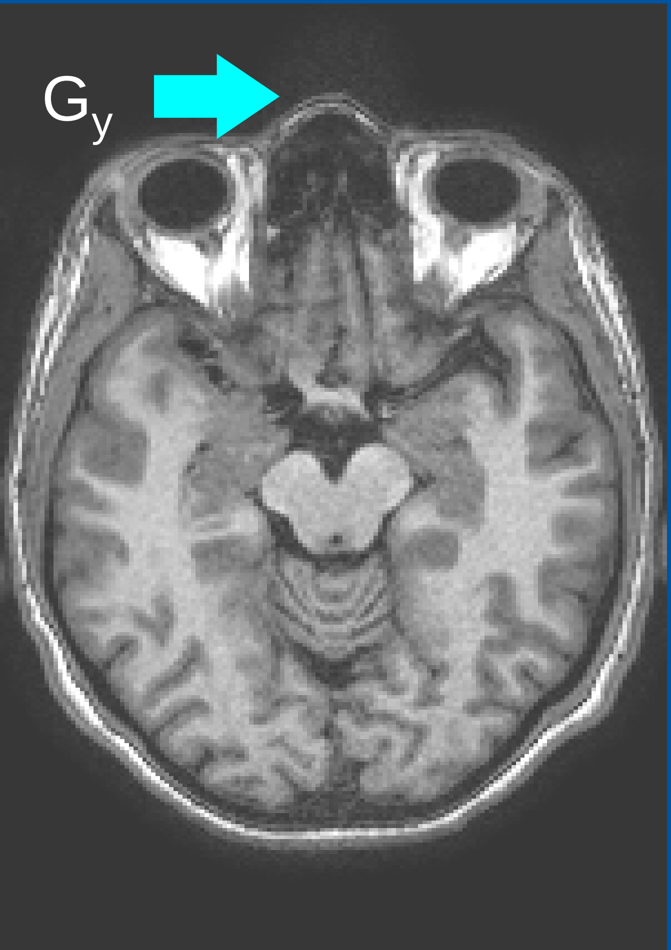

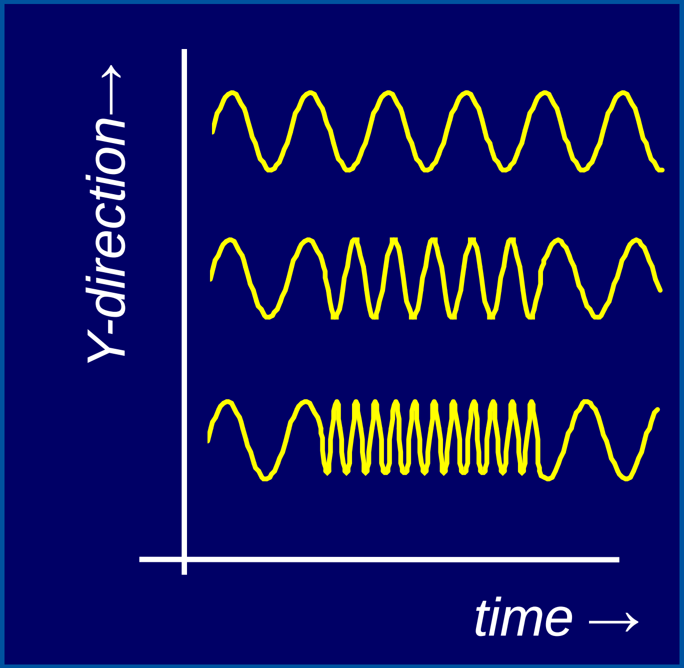

Frequency encoding (read-out)

Apply gradient during read-out

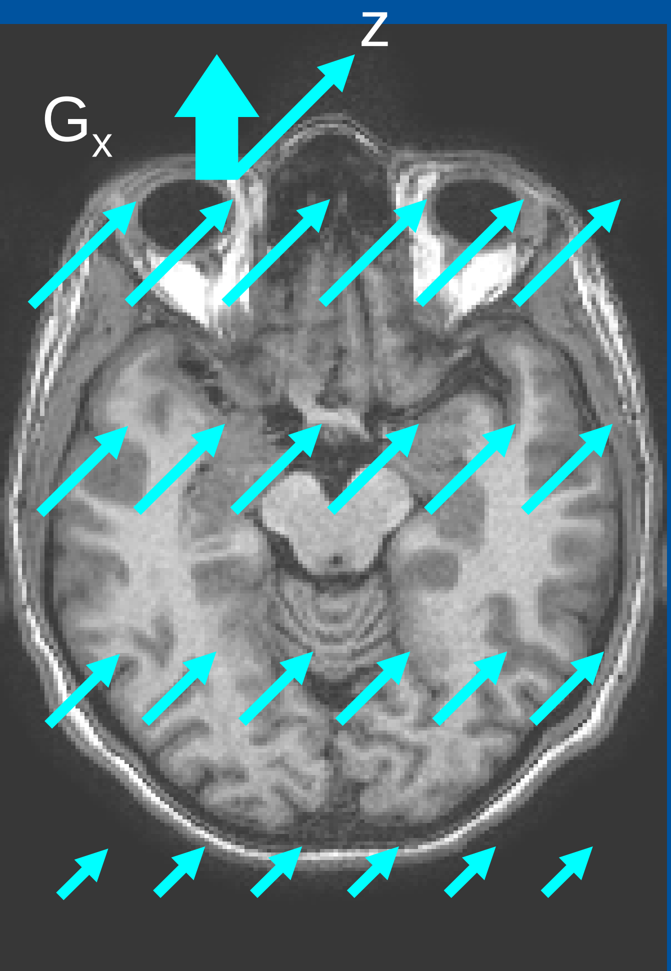

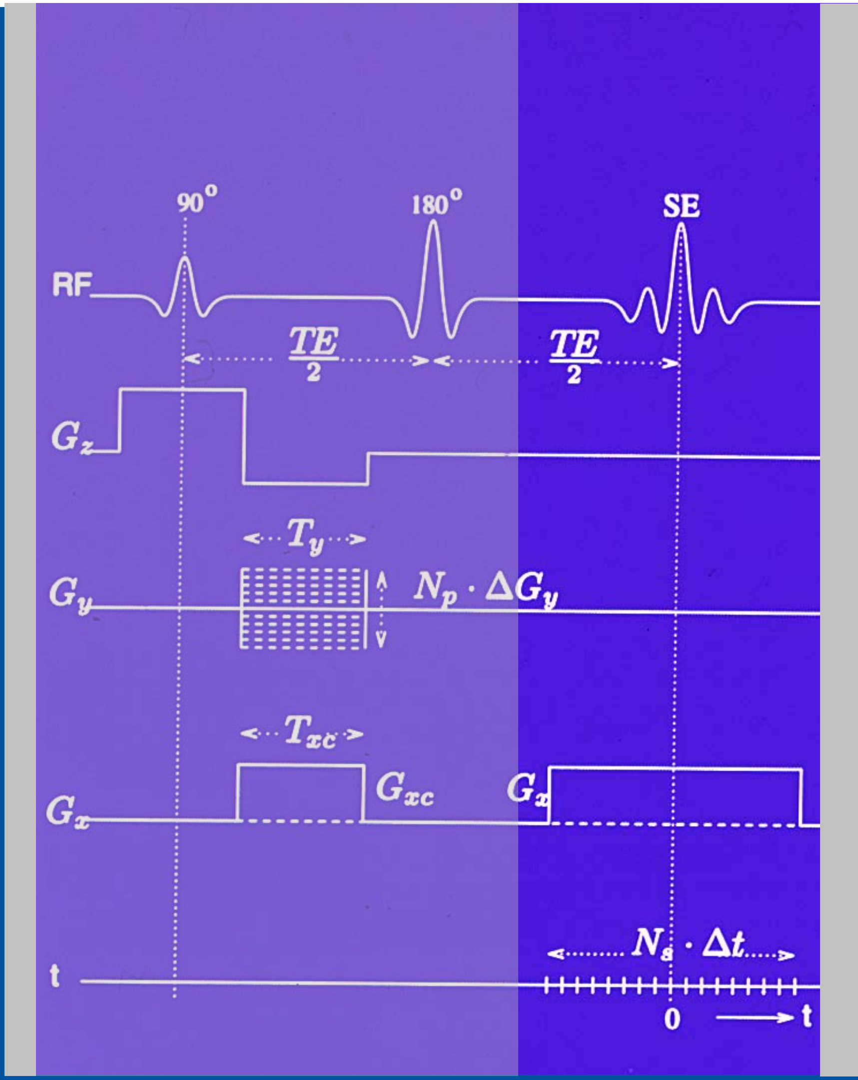

Frequency encoding (read-out)

$$\omega = \gamma (B_0 + xG_x)$$

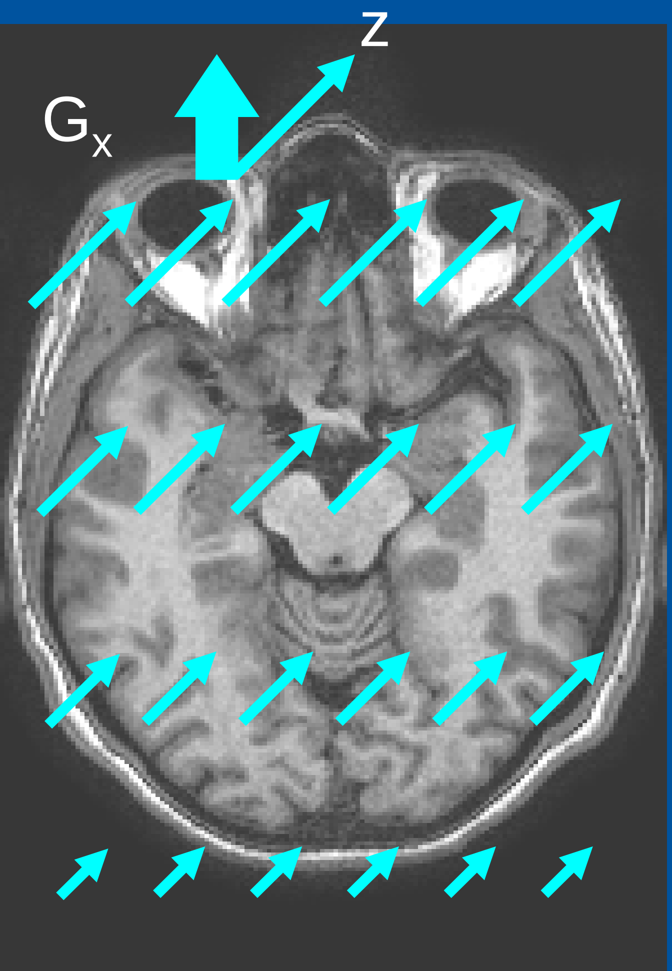

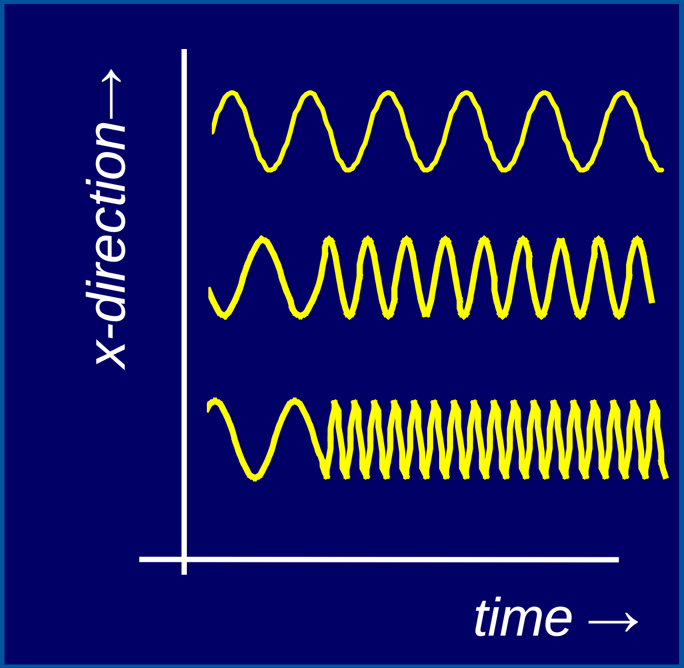

Position encoding in a spin-echo sequence

2D Fourier transform imaging

n^{th} time sample of the signal after the m^{th} phase encoding step:

$$S(n,m) = \int_{-\infty}^{\infty}\int_{-\infty}^{\infty}\int_{-\infty}^{\infty} A(x,y,z)\, e^{i\Phi(x,y,z,n,m)}\, \mathrm{d}x\, \mathrm{d}y\, \mathrm{d}z,$$

Discrete 2D inverse Fourier transformation:

$$A'(u,v) = \sum_{n=-\frac{N_s}{2}}^{\frac{N_s}{2}-1} \sum_{m=-\frac{N_p}{2}}^{\frac{N_p}{2}-1} S(n,m)\, e^{-i\Phi(u,v,n,m)},$$

with

$$n \in [-\tfrac{N_s}{2}, \tfrac{N_s}{2} - 1] \text{ and } m \in [-\tfrac{N_p}{2}, \tfrac{N_p}{2} - 1].$$

gives complex image *A'(u,v).*

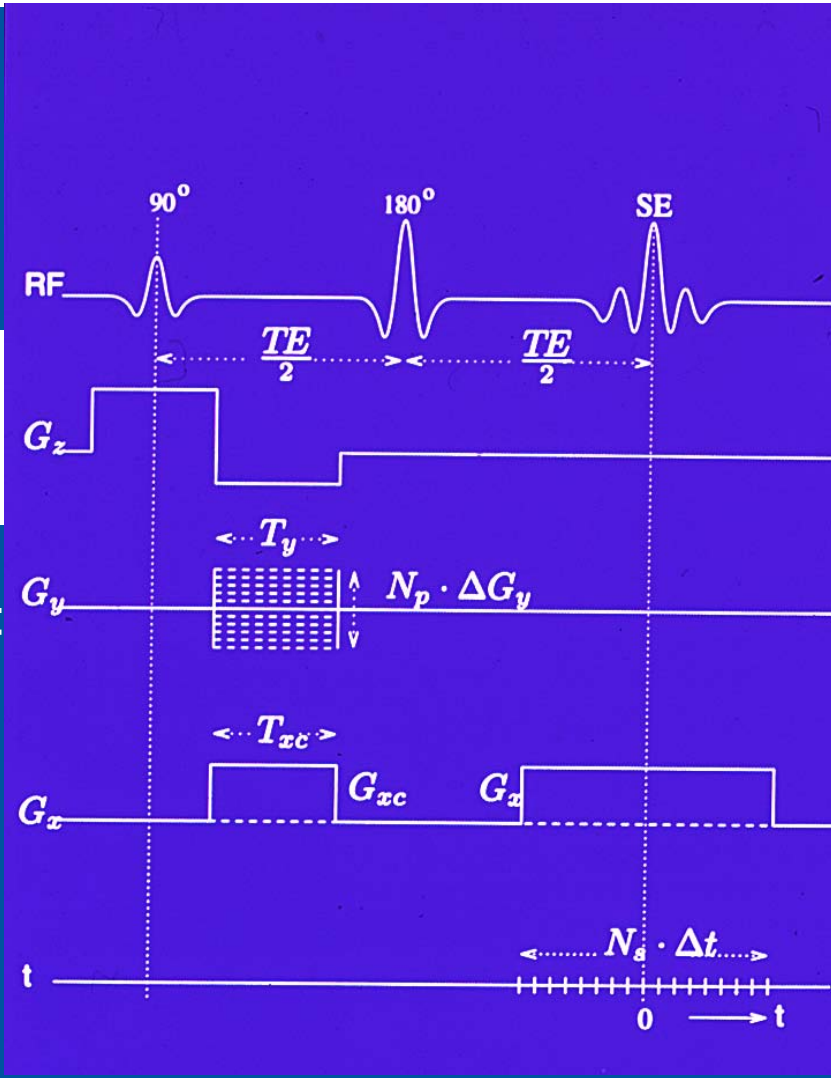

A spin-echo sequence in k-space

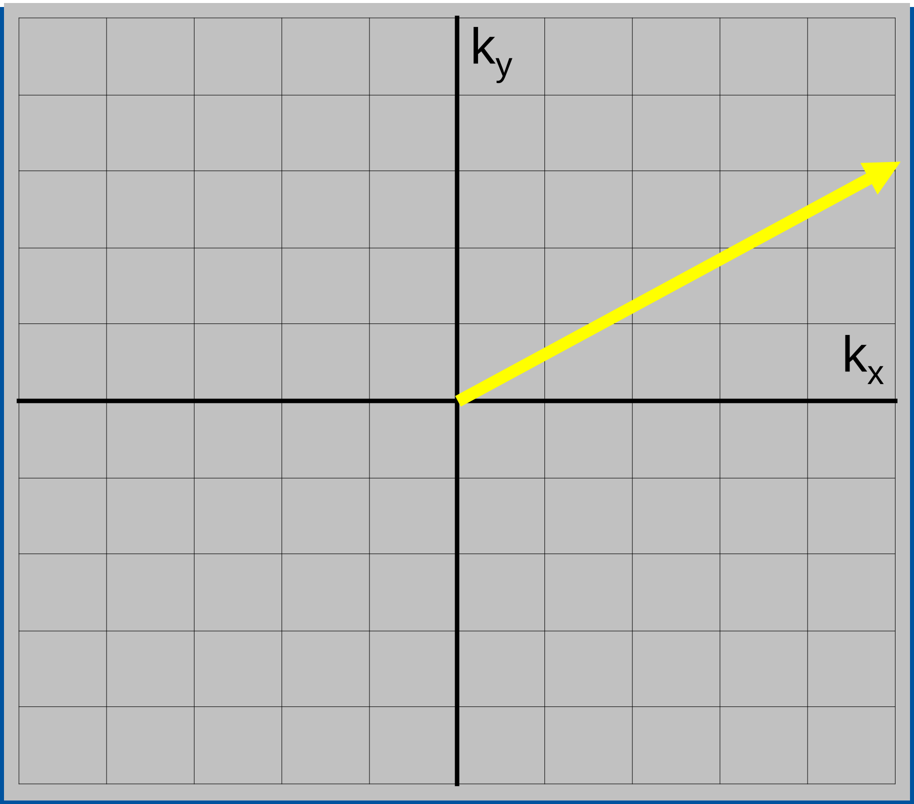

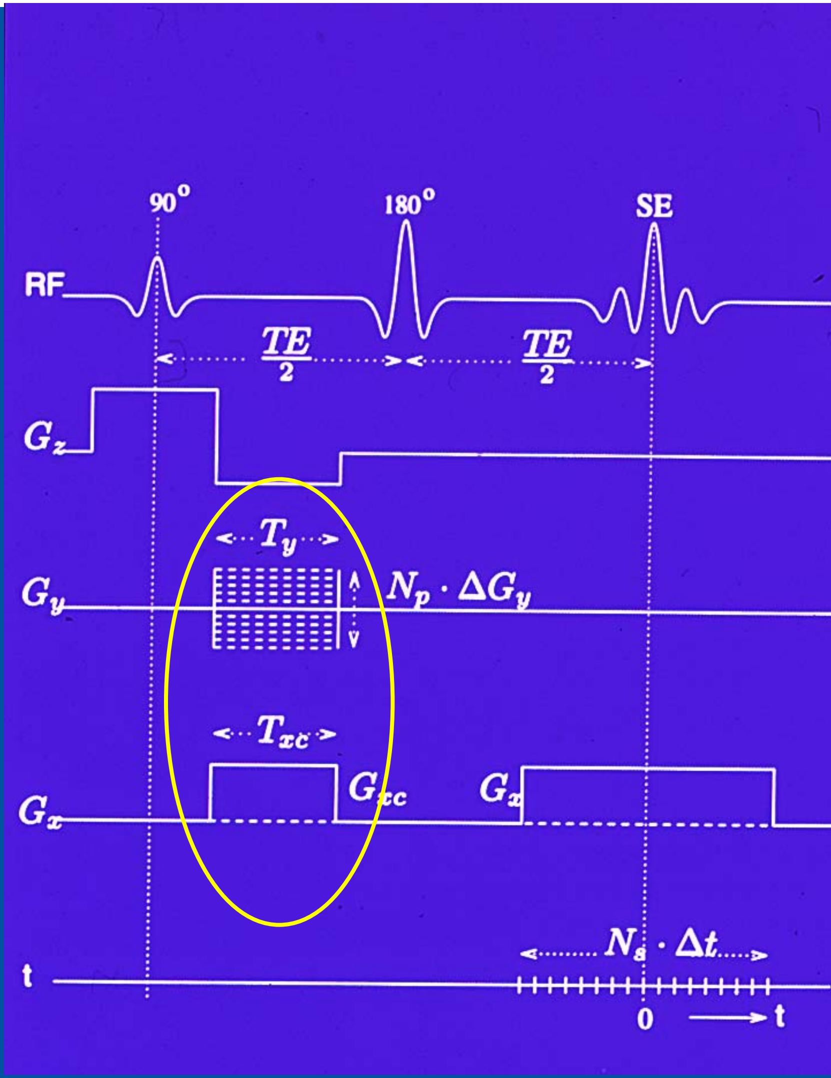

A spin-echo sequence in k-space

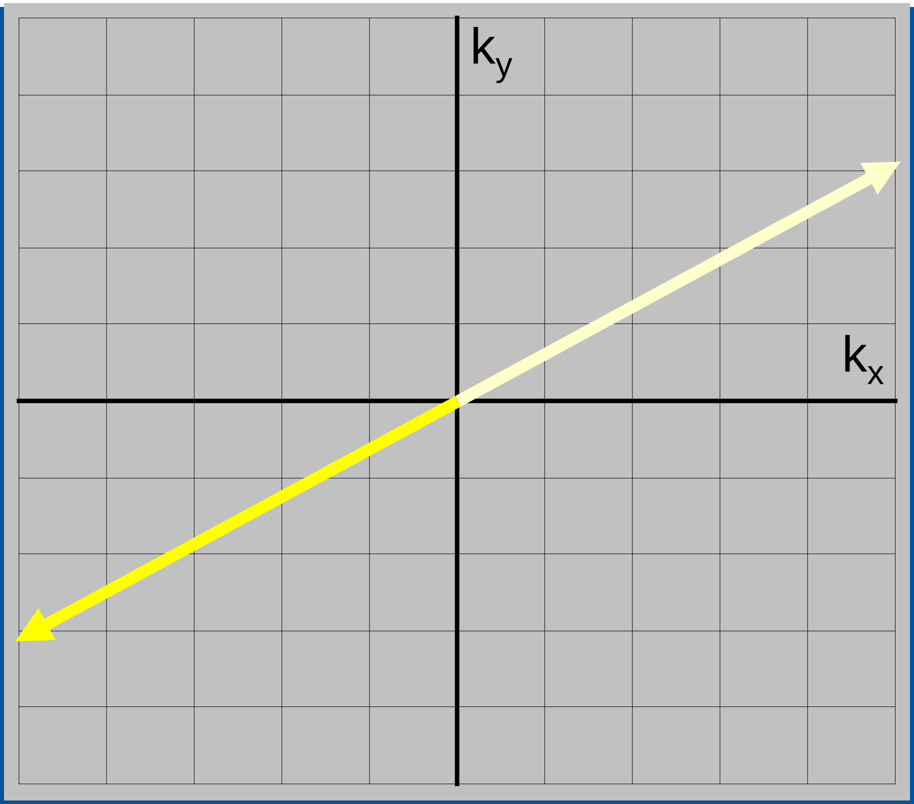

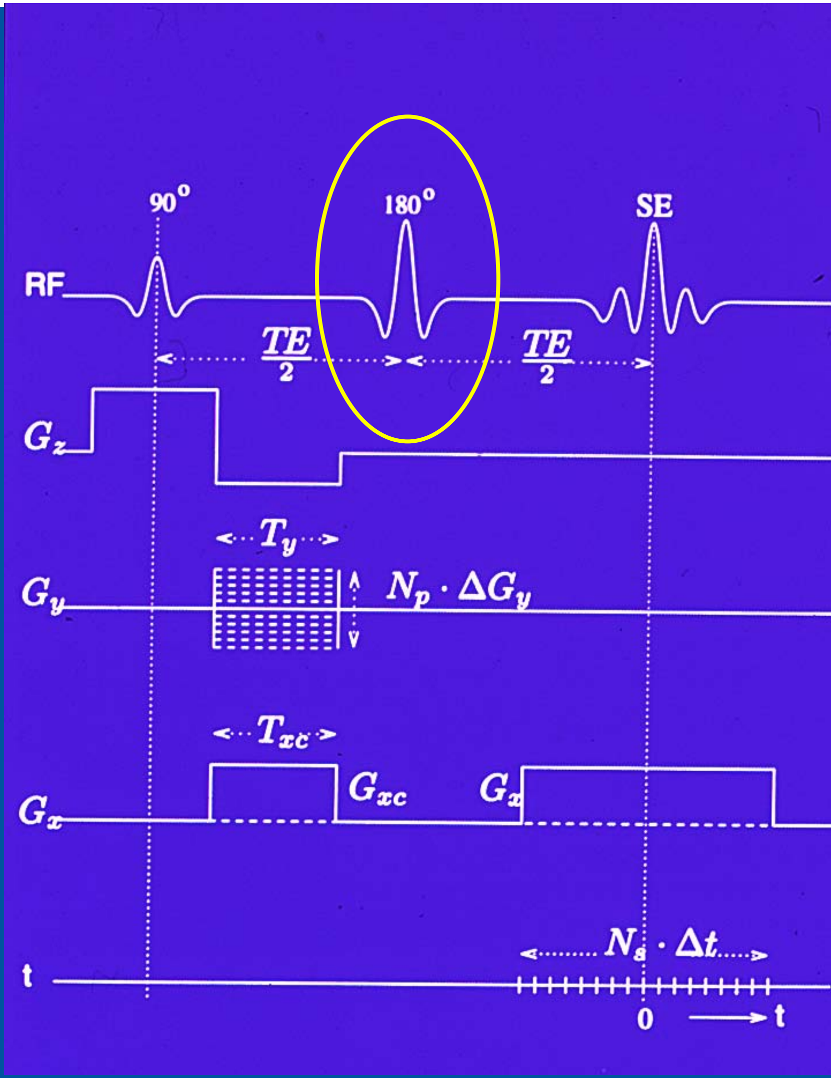

A spin-echo sequence in k-space

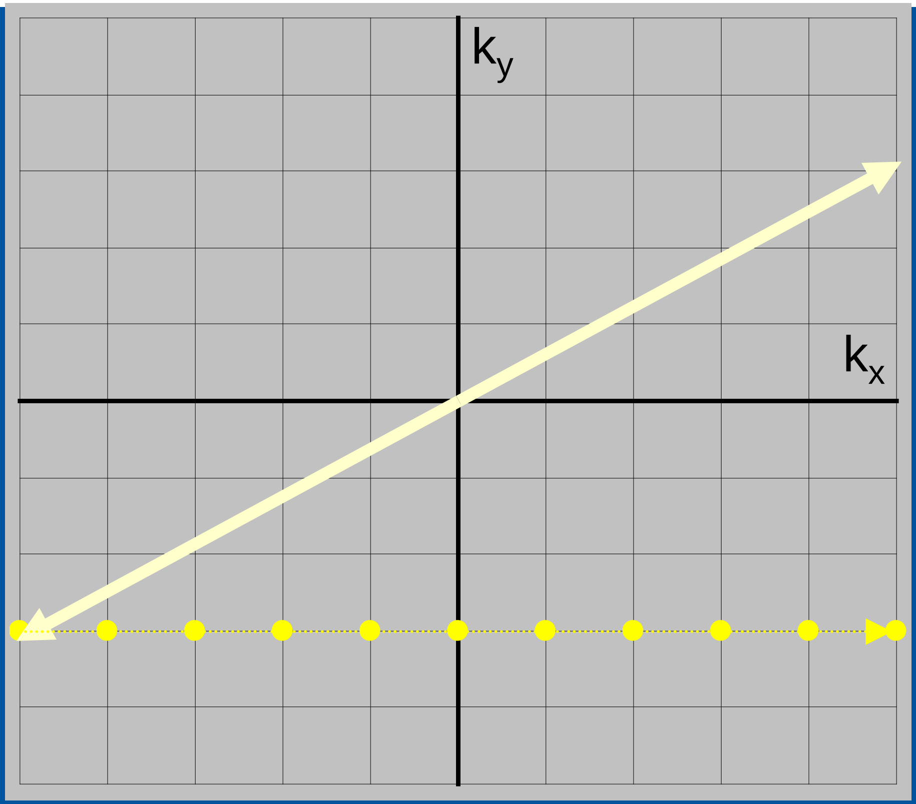

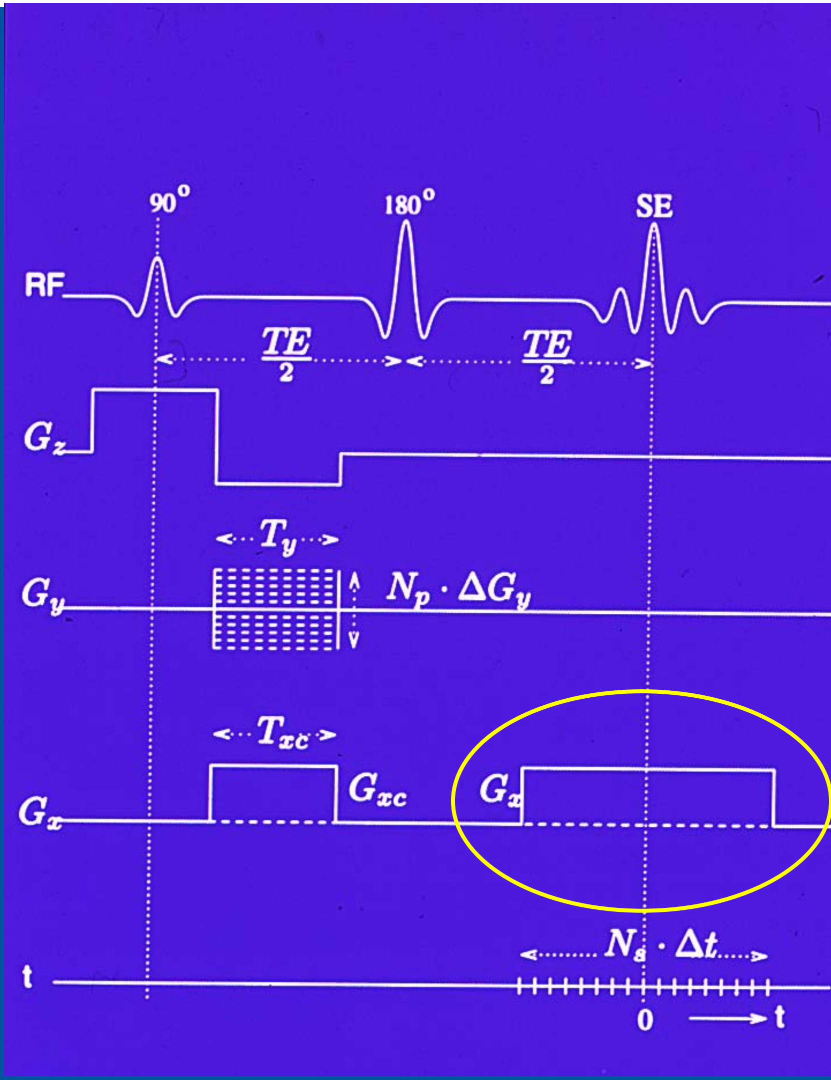

Phase evolution

$$\Phi_0(t) = \omega_0 t$$

- The phase shift depends on the strength and duration of the gradient applied;

$$\Delta\Phi(T) = \Delta\omega T = \gamma \Delta B T$$

- For the phase-encoding (y) and read-out (x) gradients, this means:

$$\Delta\Phi_m = \gamma\, y m \Delta G_y T_y$$ and $$\Delta\Phi_n = \gamma\, x G_x n \Delta T_x$$

- In a spin-echo sequence, the spins flip 180° during the 180° pulse. Thus, a phase difference created before the 180° pulse has the opposite effect during read-out

Phase evolution

$$\Phi(x,y,z,n,m) = -\gamma x G_{xc} T_{xc} + \gamma x G_x \left(n + \frac{N_s}{2}\right)\Delta t - \gamma y m \Delta G_y T_y.$$

With a balanced read-out gradient:

$$-G_{xc}T_{xc} + G_x \Delta t \tfrac{N_s}{2} = 0,$$

And in the absence of field inhomogeneities:

$$\Phi(x,y,z,n,m) = \gamma x G_x n \Delta t - \gamma y m \Delta G_y T_y.$$

with

$$n \in [-\tfrac{N_s}{2}, \tfrac{N_s}{2} - 1] \text{ and } m \in [-\tfrac{N_p}{2}, \tfrac{N_p}{2} - 1].$$

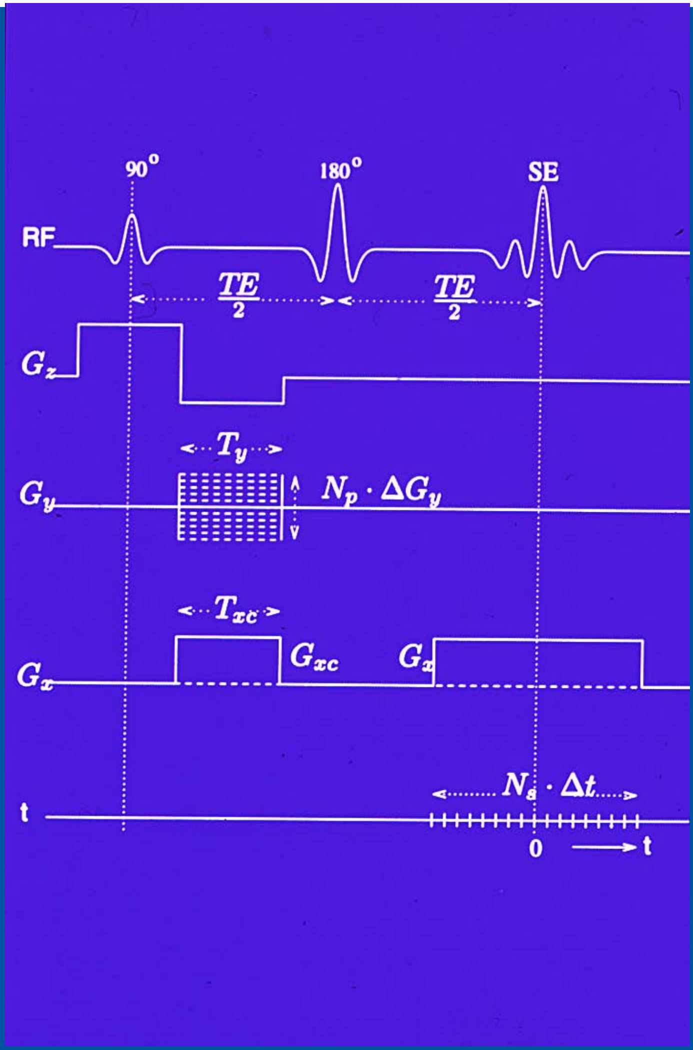

echo centered in the acquisition window at *t=0* (*n=0, m=0*)

A spin-echo sequence in k-space

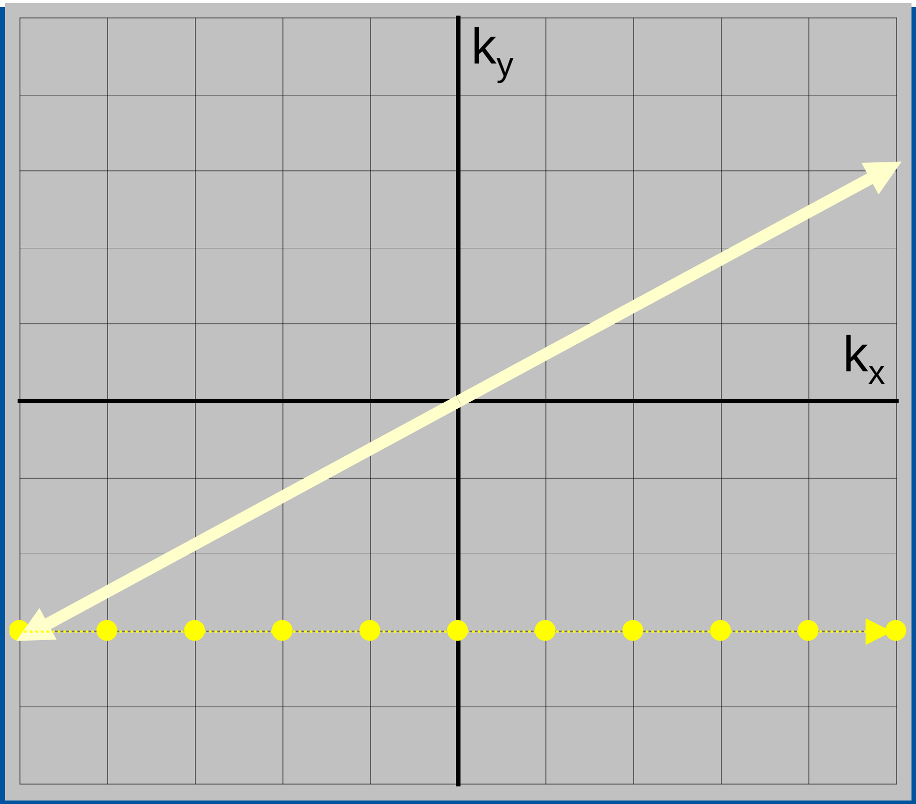

$$k_y = \gamma y m \Delta G_y T_y$$

$$k_x = \gamma x G_x n \Delta T_x$$

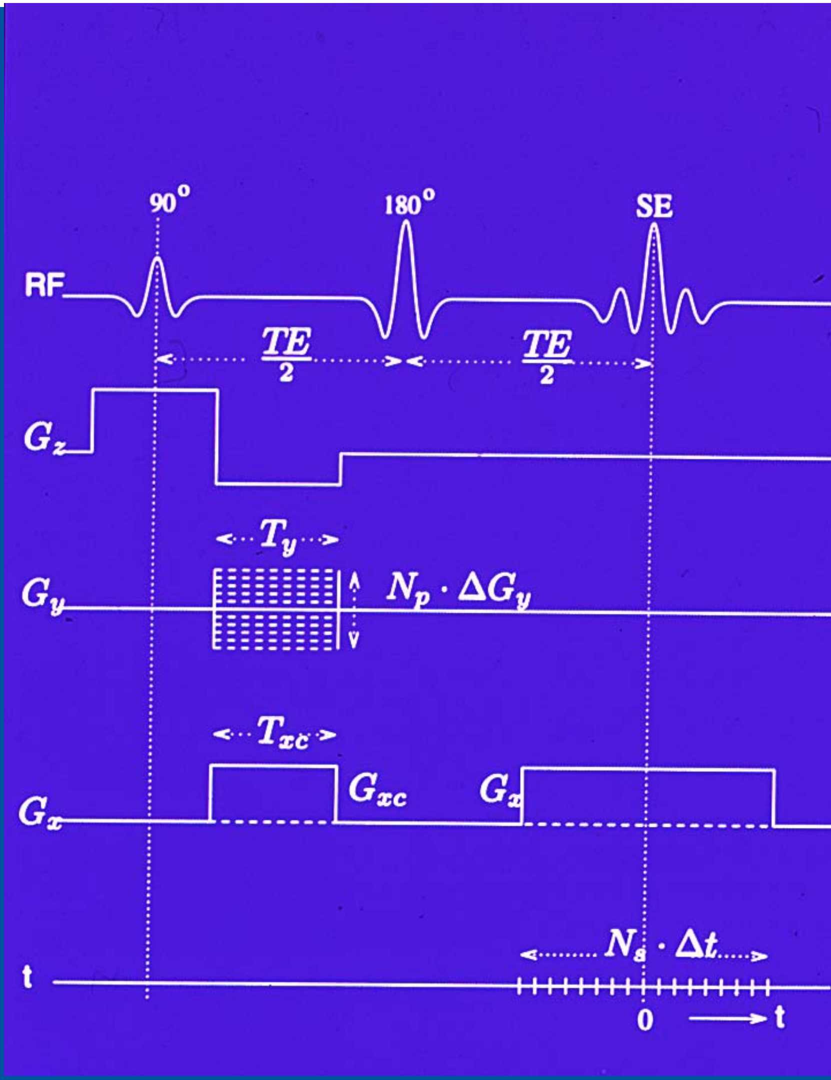

Do we really sample k-space the way we think we do?

Many reasons why the phase evolution can be distorted

- Hardware
  - non-linear gradients
- Patient
  - chemical shift
  - Susceptibility

Imperfections of B_0 and gradient fields

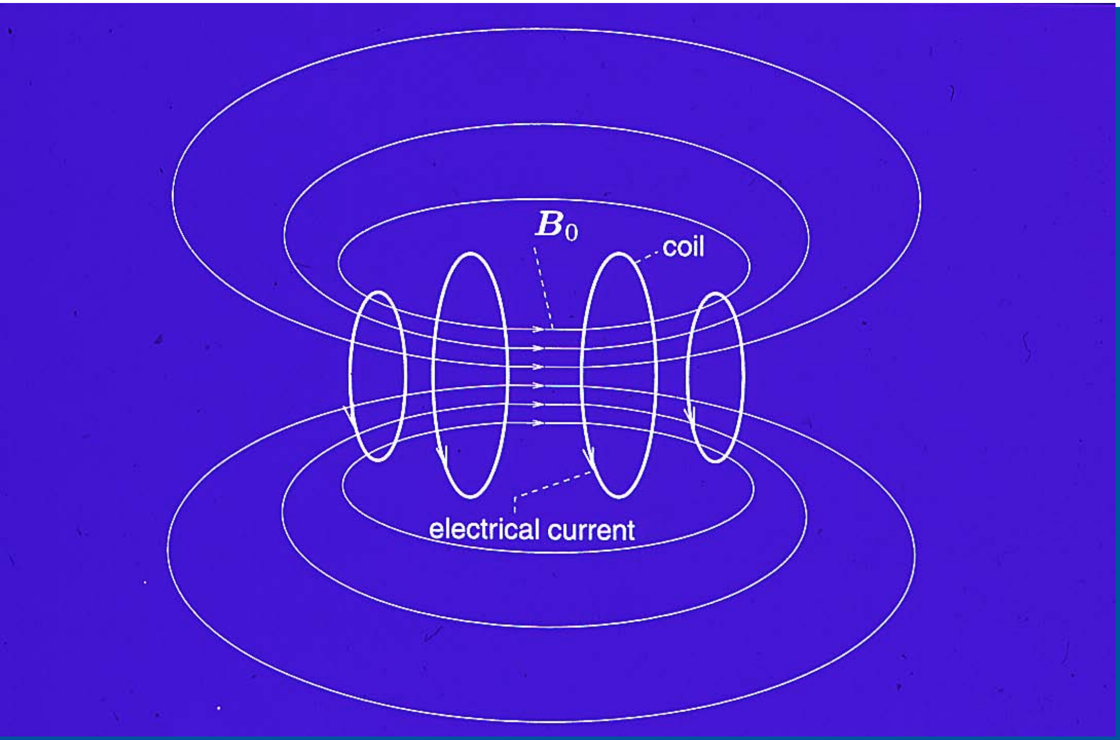

Imperfect magnetic field homogeneity:

- divergence of the magnetic field lines at the end of the coil
- imperfect winding the superconducting wire
- variations of current densities in the wire
- Distortion of the magnetic field by metal close to the scanner

Non-linear gradients cause position distortions

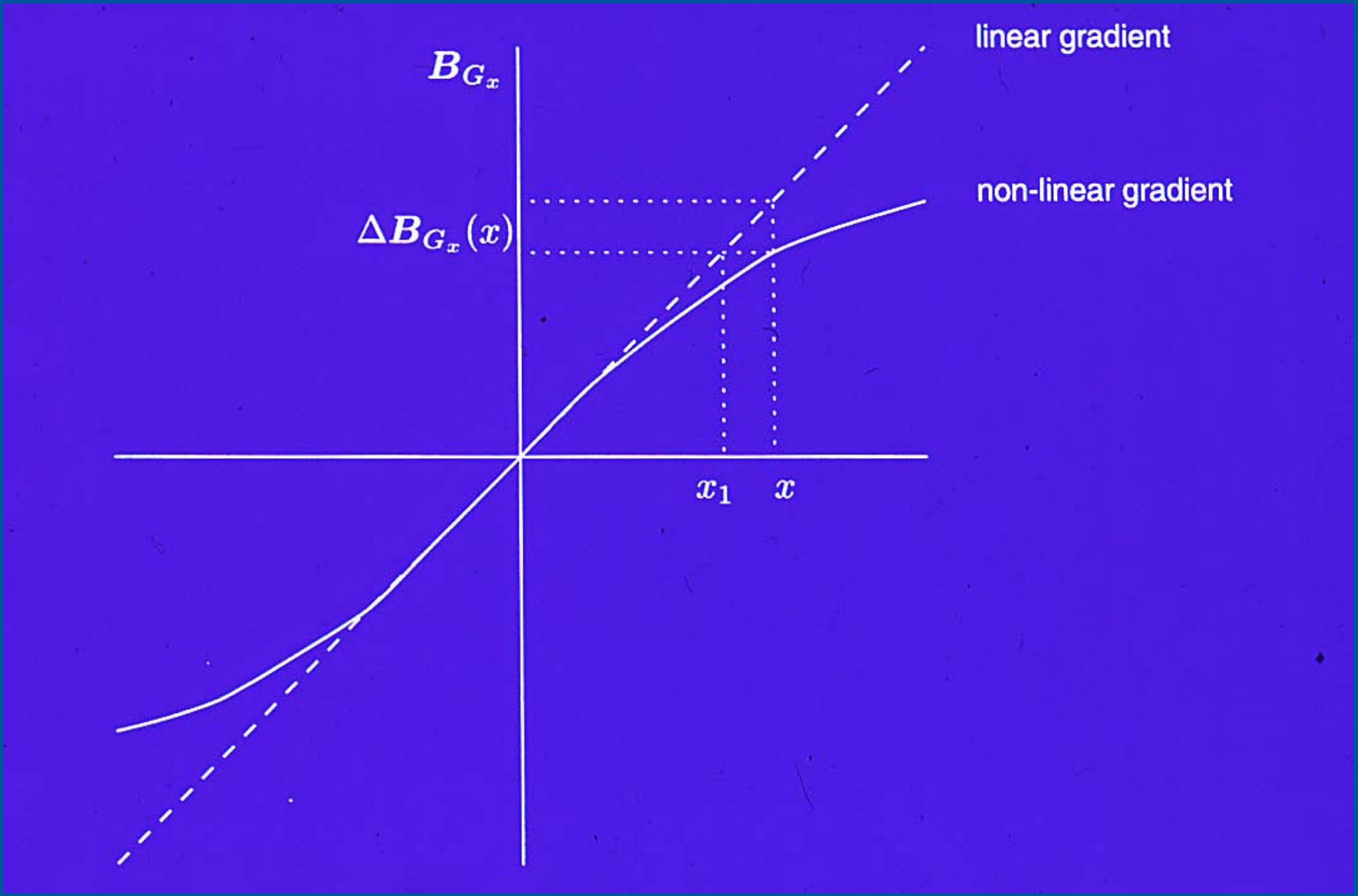

Magnetic susceptibility

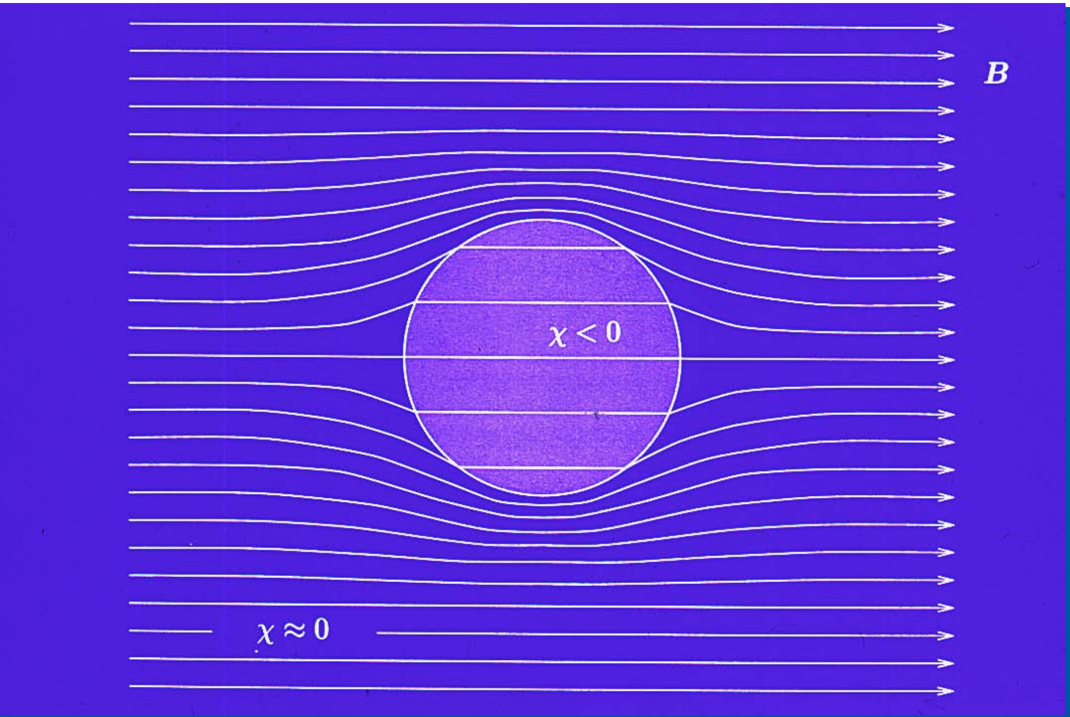

Magnetic susceptibility χ : $M=\chi H$

M = magnetization, H = magnetic field

- diamagnetic materials: $\chi< 0$ (tissues ca. -9.10^{-6})
- paramagnetic materials: $\chi > 0$
- ferromagnetic materials: very large susceptibility
- air: $\chi = 0$

Water-fat shift

Magnetic field at the nucleus depends on magnetic shielding of surrounding electron clouds, depends on molecular environment

example:
resonant frequencies of protons in fat and water differ by 3.4 ppm

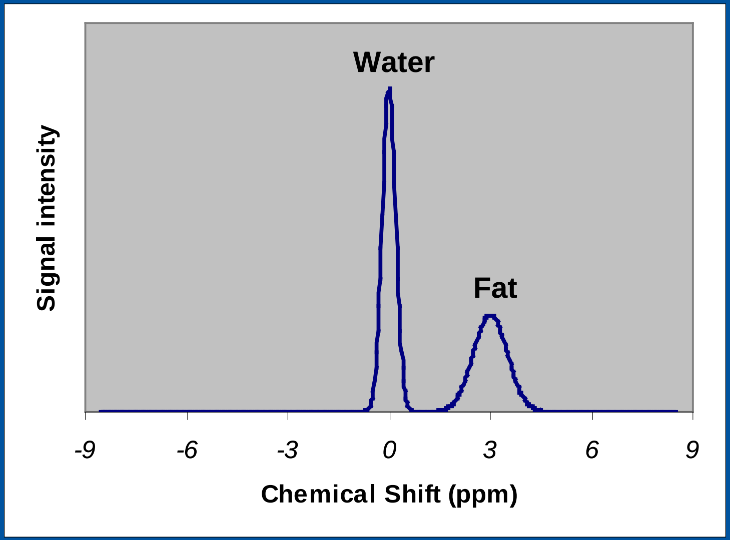

Erroneous sampling of k-space

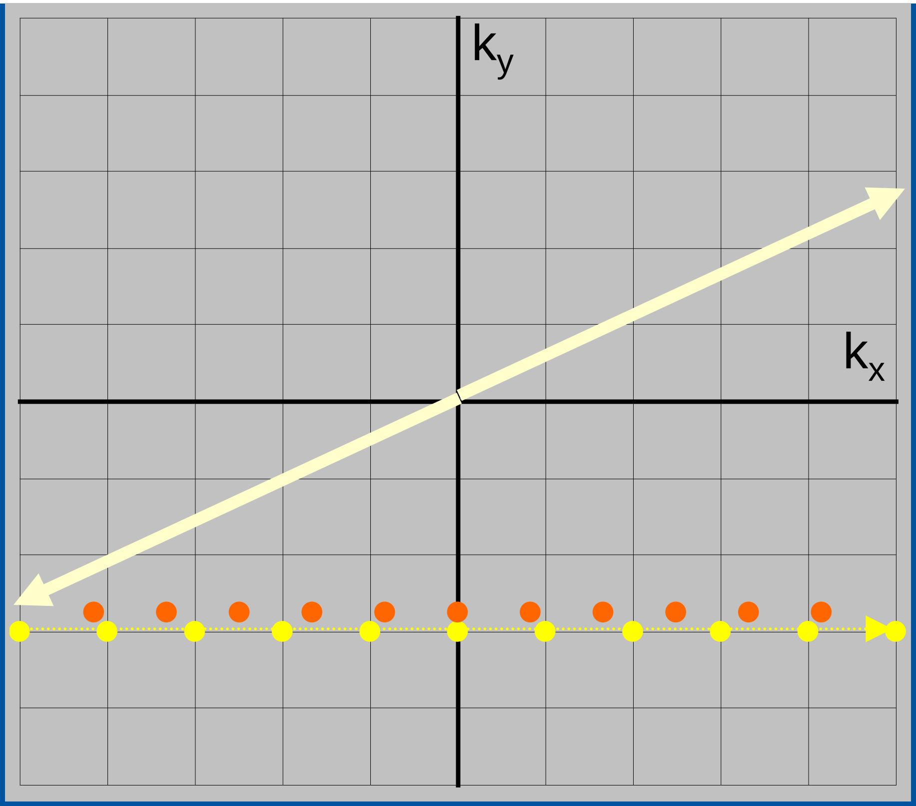

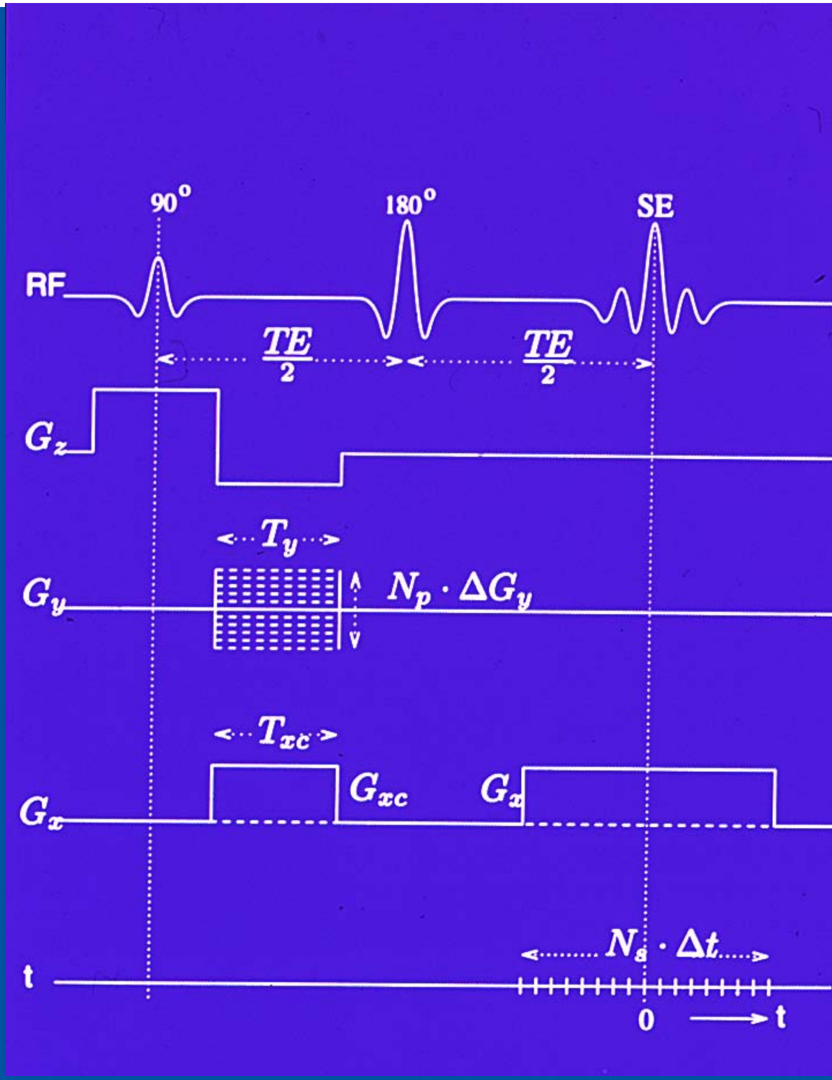

Position errors: slice selection

A deviation of the magnetic field during the 90° pulse results in a shift in the selected slice:

$$z_1 = z - \frac{\Delta B_0}{G_z} - \frac{\Delta B_{G_z}}{G_z}$$

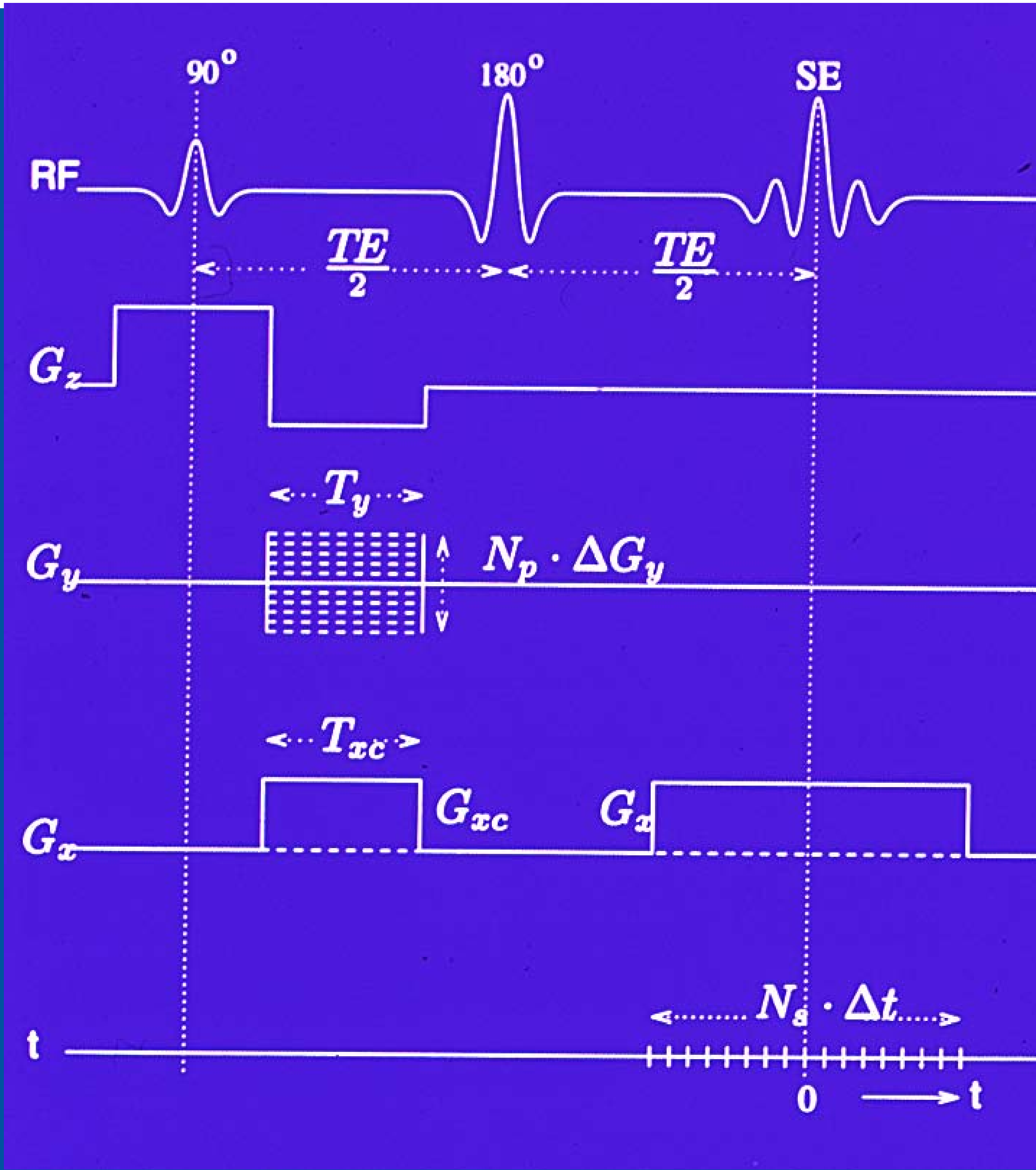

Distortion of phase evolution

$$\Phi^{distorted}(x,y,z,n,m) = \Phi(x,y,z,n,m) + \gamma\Delta B_0(x,y,z)n\Delta t + \gamma\Delta B_{G_x}(x,y,z)n\Delta t - \gamma m\Delta B_{\Delta G_y}(x,y,z)T_y$$

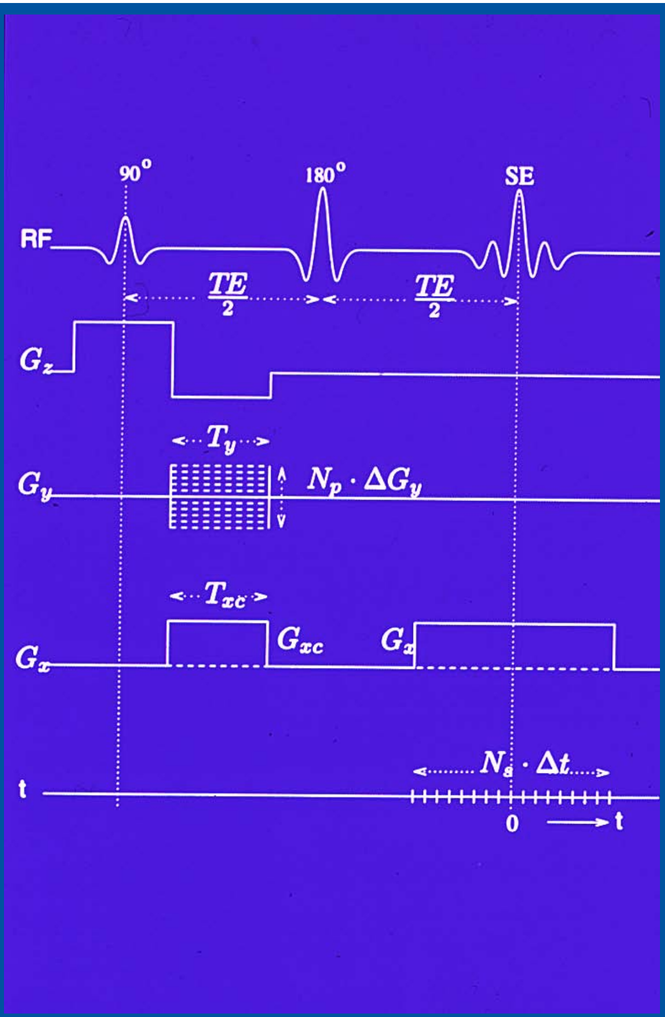

With:

$\Phi^{distorted}$ the distorted phase evolution

Φ the ideal phase evolution:

$$\Phi(x,y,z,n,m) = \gamma x G_x n\Delta t - \gamma y m\Delta G_y T_y$$

Impact on geometrical accuracy

Interpretation of the effect of disturbances:

$$\Phi^{distorted}(x, y, z, n, m) = \Phi(x_1, y_1, z_1, n, m)$$

Group x-terms for distortions in read-out direction:

$$\gamma x G_x n\Delta t + \gamma \Delta B_0(x, y, z) n\Delta t + \gamma \Delta B_{G_x}(x, y, z) n\Delta t = \gamma x_1 G_x n\Delta t$$

and solve for x_1

$$x_1 = x + \frac{\Delta B_0(x, y, z)}{G_x} + \frac{\Delta B_{G_x}(x, y, z)}{G_x}$$

Impact on geometrical accuracy

Group y-terms for distortions in fase-encoding direction:

$$-\gamma y m \Delta G_y T_y - \gamma m \Delta B_{\Delta G_y}(x,y,z) T_y = -\gamma y_1 m \Delta G_y T_y$$

and solve for y_1

$$y_1 = y + \frac{\Delta B_{\Delta G_y}}{\Delta G_y}$$

Assuming that the errors in the gradient are independent of the gradient step, this is equal to

$$y_1 = y + \frac{\Delta B_{G_y}}{G_y}$$

Result: geometrical distortion in spin-echo imaging

$$x_1 = x + \frac{\Delta B_0(x,y,z)}{G_x} + \frac{\Delta B_{G_x}(x,y,z)}{G_x}$$

In the frequency-encoding direction, both the non-linearity of the frequency-encoding gradient and static field inhomogeneity cause geometric distortions

$$y_1 = y + \frac{\Delta B_{G_y}}{G_y}$$

In the phase-encoding direction, distortions are solely caused by the non-linearity of the phase-encoding gradient

Question: water-fat shift

Water and fat have a slightly different resonance frequency. This results in a shift between the water and the fat in an image, called 'water-fat shift'

- In what direction does this shift occur?

1. Slice direction
2. Phase-encoding direction
3. Read-out direction

Result: geometrical distortion in spin-echo imaging

$$x_1 = x + \frac{\Delta B_0(x,y,z)}{G_x} + \frac{\Delta B_{G_x}(x,y,z)}{G_x}$$

frequency-encoding (read-out) direction:

- non-linearity of the gradient
- static field inhomogeneity
  (= static difference in resonance frequency)

$$y_1 = y + \frac{\Delta B_{G_y}}{G_y}$$

phase-encoding direction:

- non-linearity of the gradient

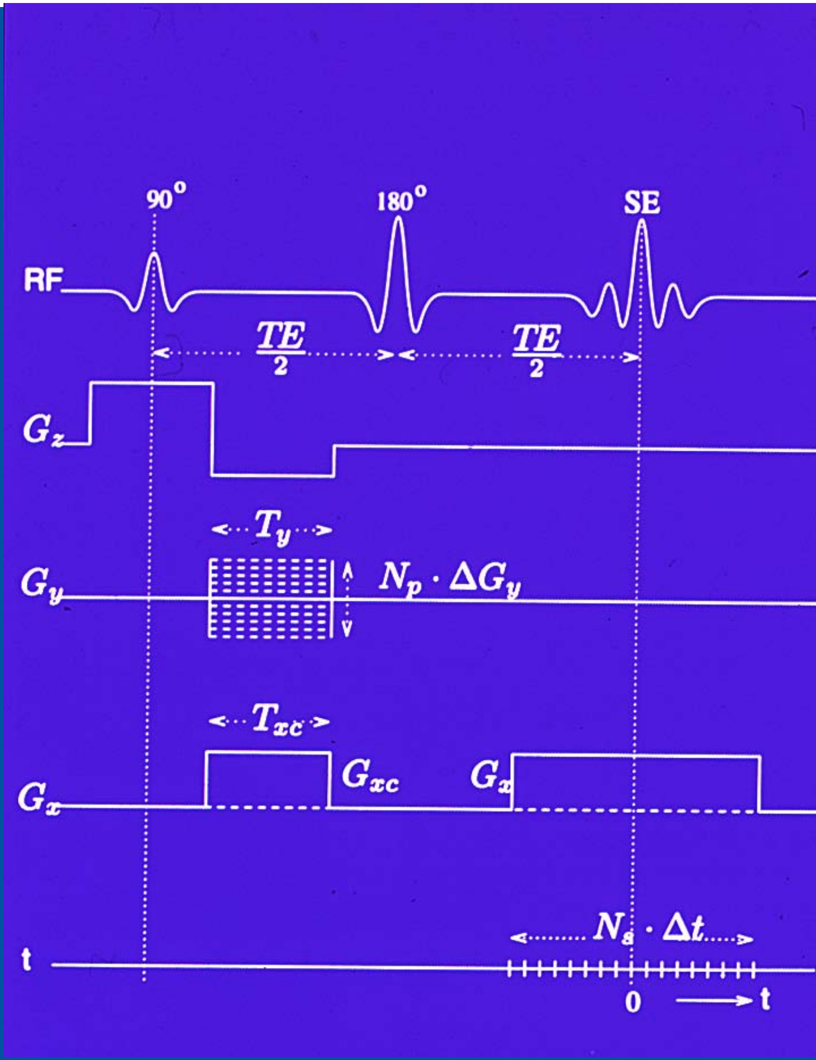

Distortions in a Gradient Echo sequence

In Gradient Echo imaging, the same distortions occur.

However, in the frequency-encoding direction also dephasing occurs, resulting in signal loss:

$$\Delta\Phi(x, y, z) = \gamma TE \Delta B_0 (x, y, z)$$

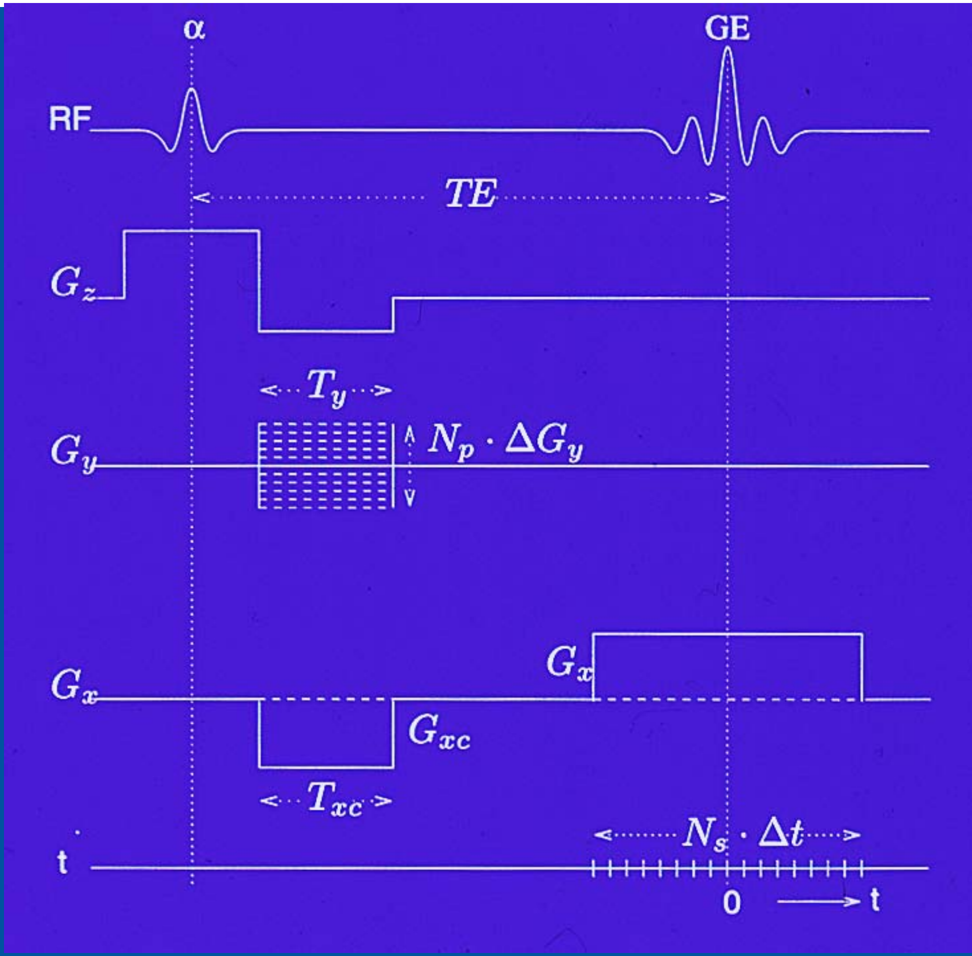

Dephasing due to static field inhomogeneities

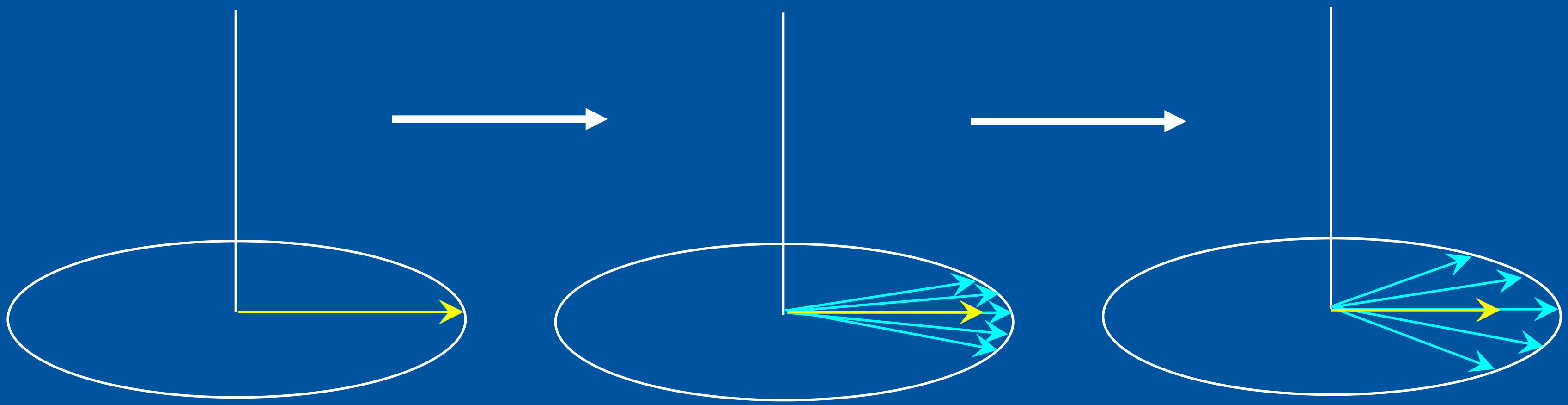

Rephasing in a Spin Echo sequence

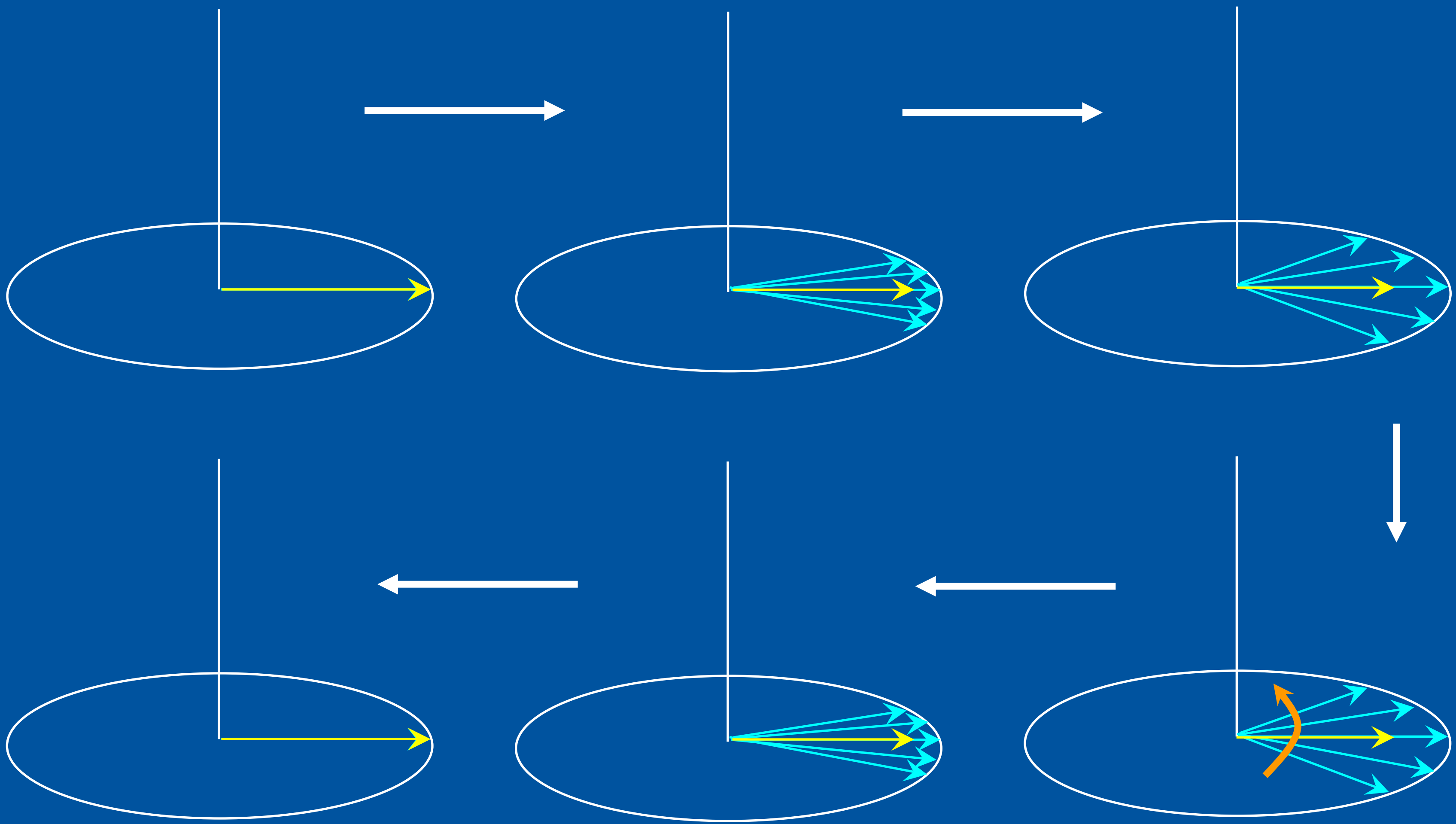

Continued dephasing in a Gradient Echo sequence

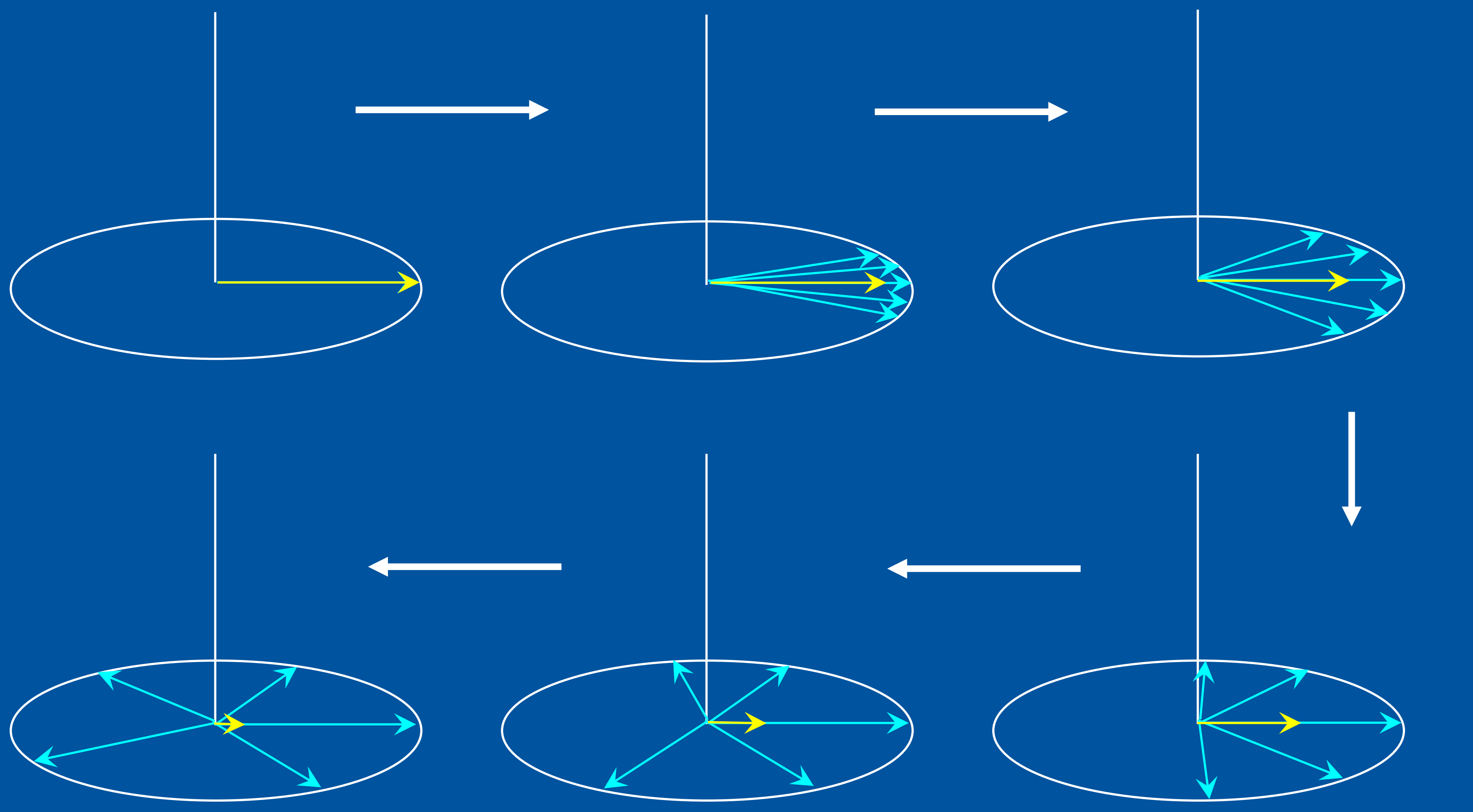

Phantom experiments

Some qualitative experiments with coaxial cylinder (water air susceptibility difference):

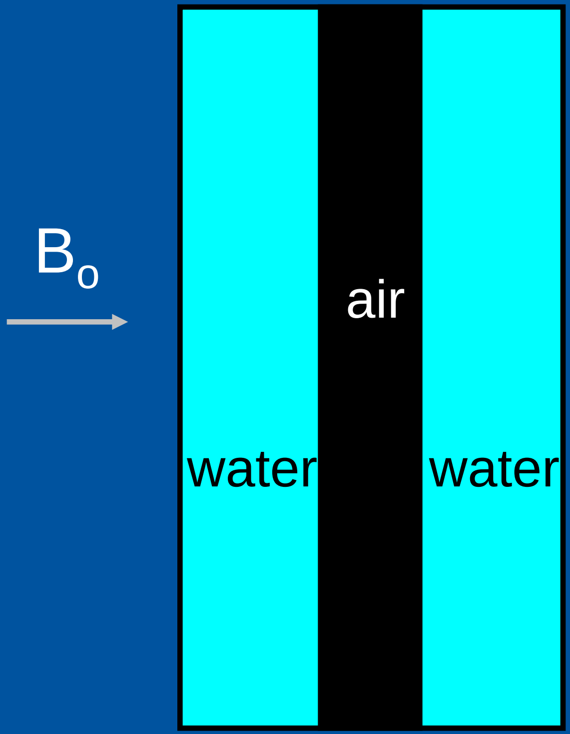

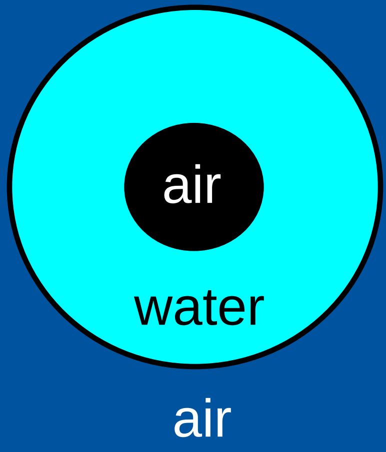

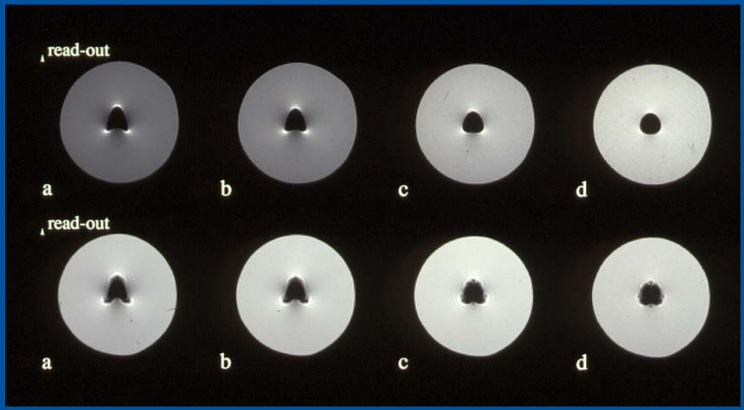

air: $\chi \approx 0$

water: $\chi \approx -9.10^{-6}$

Dephasing effects increase with TE in gradient echo imaging

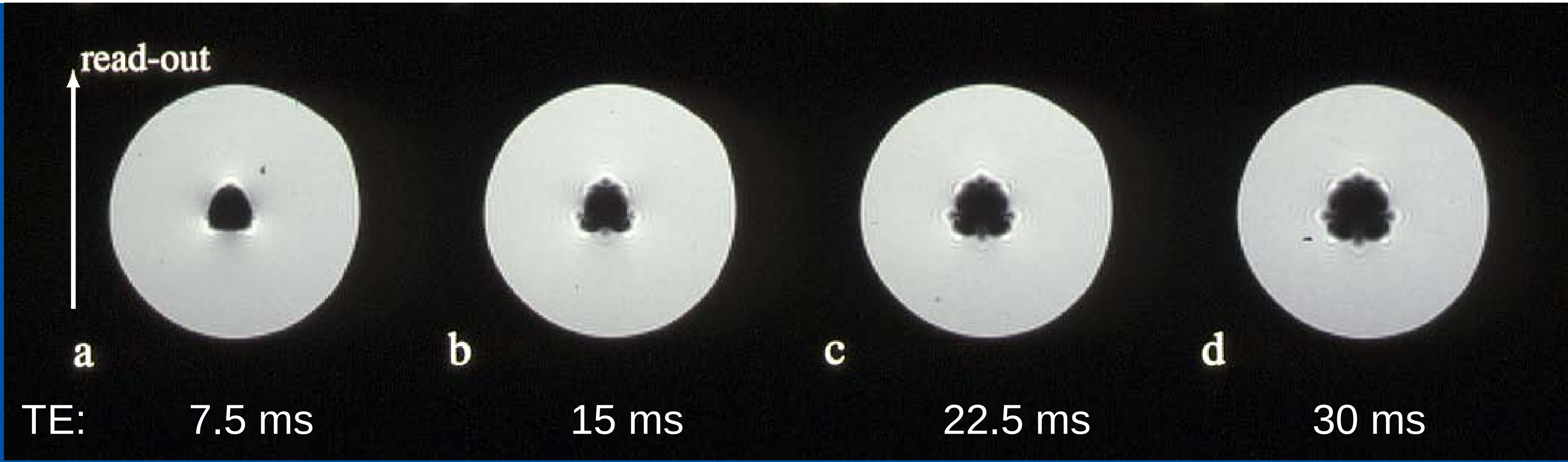

- Dephasing artifacts increase with Echo Time

Dephasing effects increase with TE in gradient echo imaging

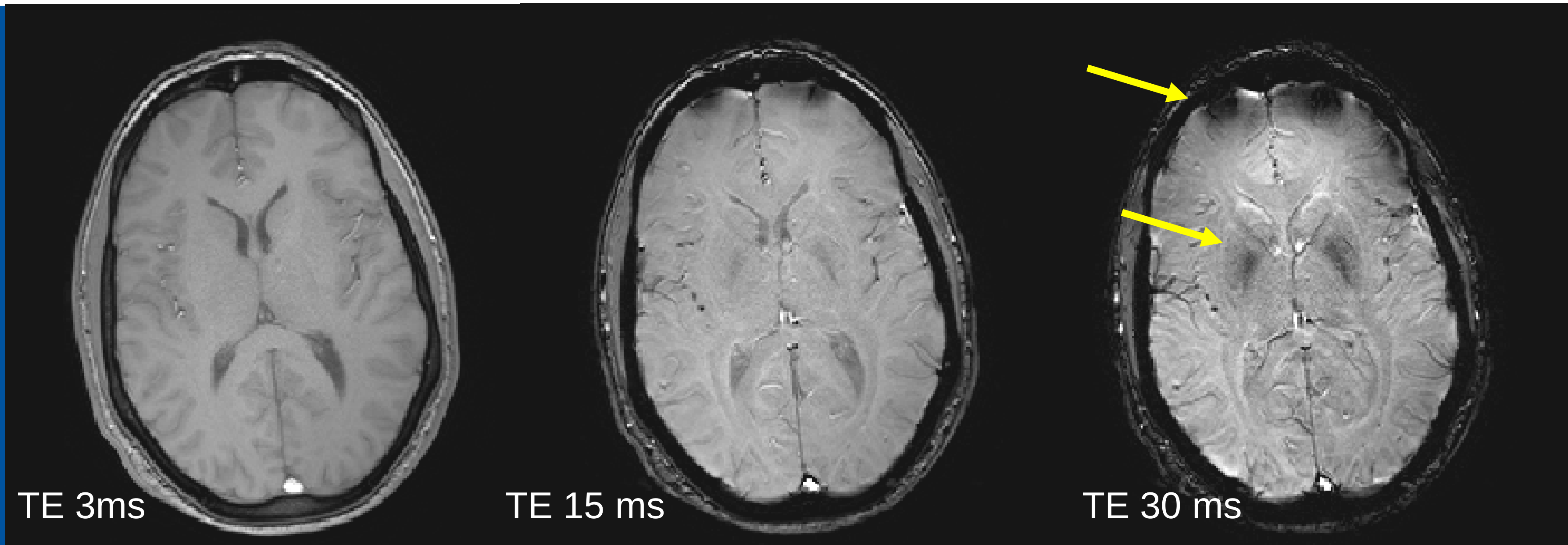

- 3T scanner
- FFE sequence; TR = 100 ms, FA 45º

Summary 1

- Many reasons exists for artifacts in images
  - Erroneous sampling of k-space
    - Aliasing
    - Ringing
  - Magnetic field errors
    - Gradient artifacts
    - Susceptibility artifacts
    - Water-fat shift

- Geometrical artifacts show up in a particular direction
  - Phase encoding direction: aliasing
  - Read-out direction: susceptibility, water-fat shift

- Dephasing results in signal loss in gradient echo sequences

Outline lecture 2

- Measurements for characterizing geometrical accuracy
  - Phantom design
  - Characterizing gradient errors
- Examples
- Practical consequences
- Summary

Imaging For Physicists

Artifacts 2

Uulke van der Heide

Many reasons for artifacts

Erroneous sampling of k-space

- Aliasing
- Ringing

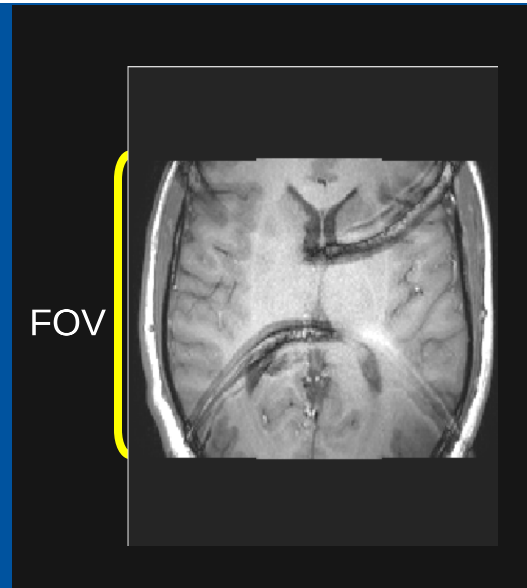

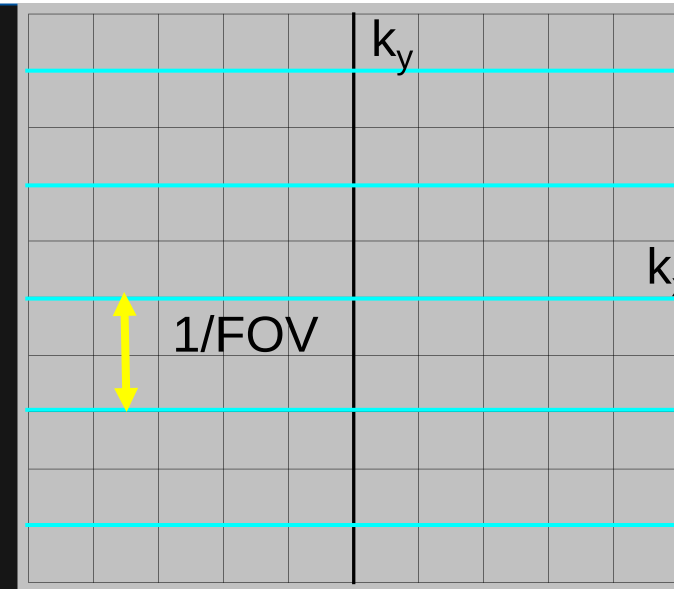

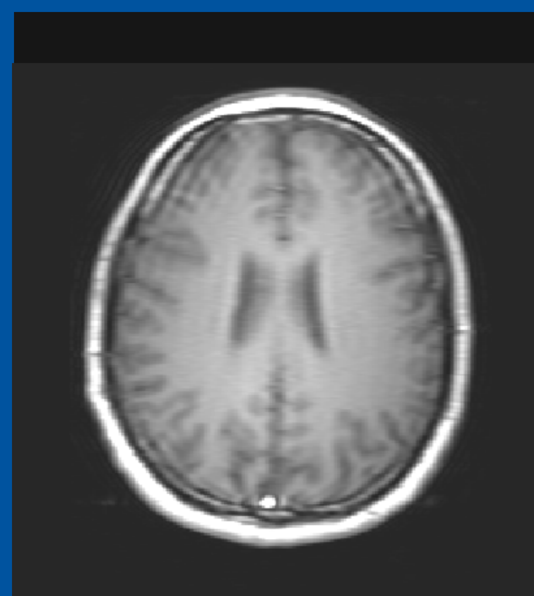

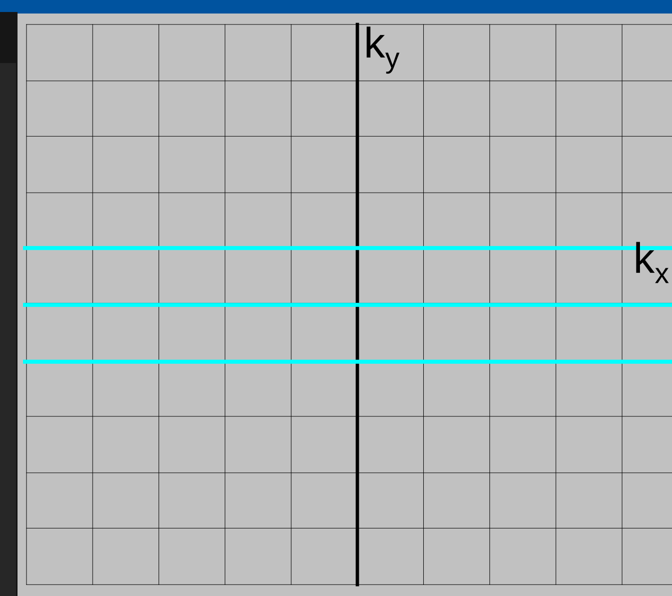

Many reasons for artifacts

- Magnetic field errors
  - Gradient artifacts
  - Susceptibility artifacts
  - Water-fat shift

- Geometrical artifacts show up in a particular direction

$$x_1 = x + \frac{\Delta B_0(x, y, z)}{G_x} + \frac{\Delta B_{G_x}(x, y, z)}{G_x}$$

$$y_1 = y + \frac{\Delta B_{G_y}}{G_y}$$

Many reasons for artifacts

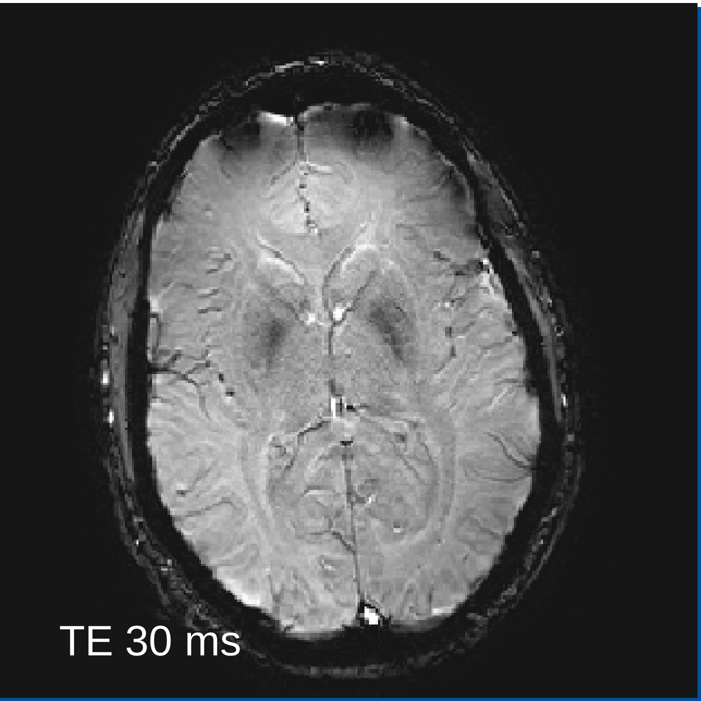

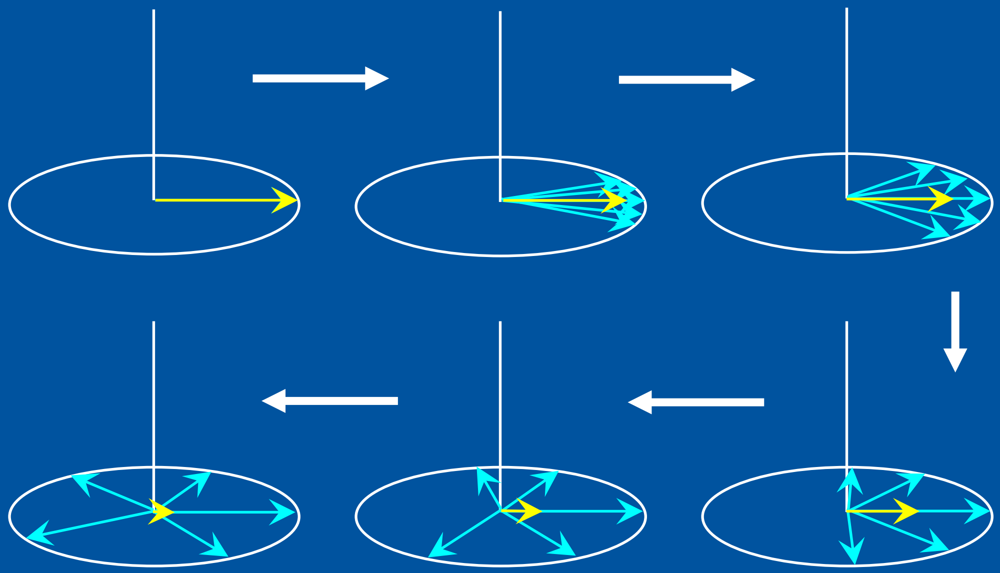

- Field distortions lead to signal loss in gradient echo sequences due to dephasing
- Dephasing is proportional to echo time

Outline lecture 2

- Measurements for characterizing geometrical accuracy
  - Phantom design
  - Characterizing gradient errors
- Examples
- Practical consequences
- Summary

Homogeneity of the main magnetic field

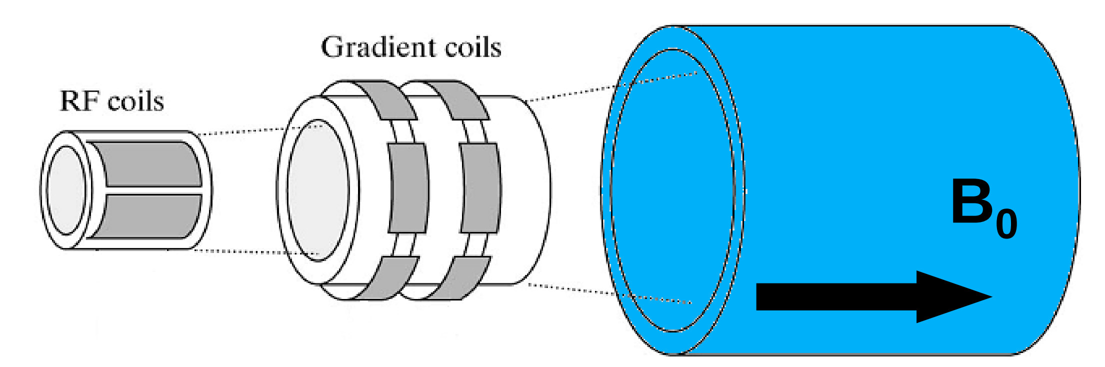

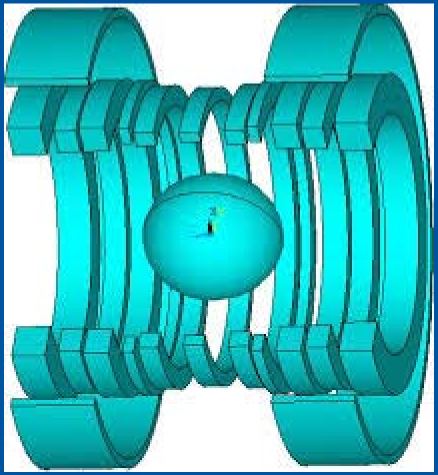

e.g. uniformity in diameter of spherical volume DSV_{40cm} = 0.2 ppm

(at 1.5 T):
0.2 x 63.87 MHz = 12.8 Hz

- Magnet is shimmed at installation- additional (dynamic) shimming may be required

Gradient fields

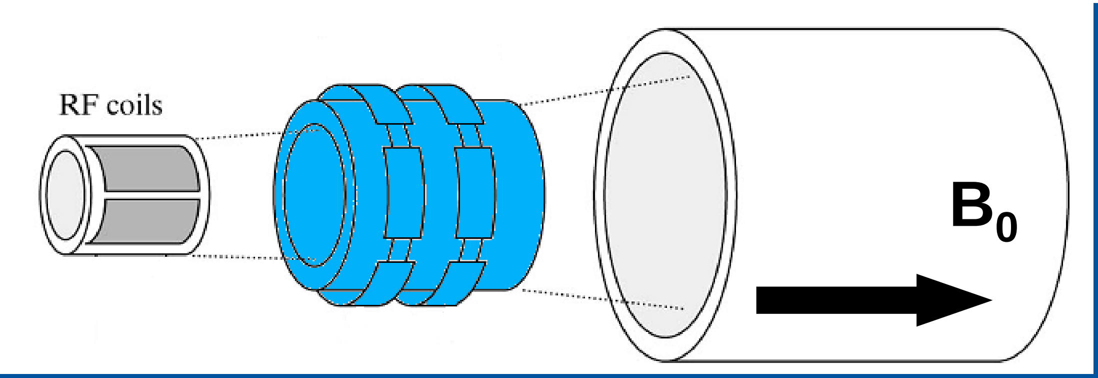

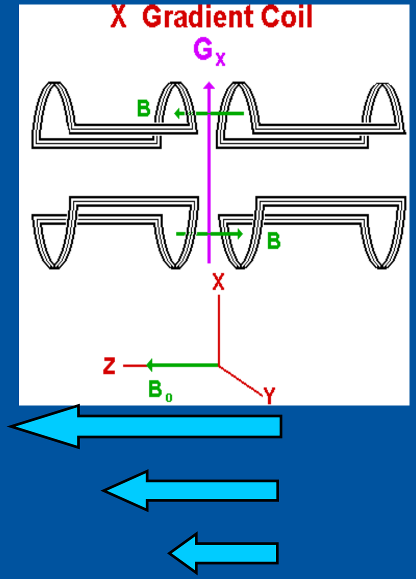

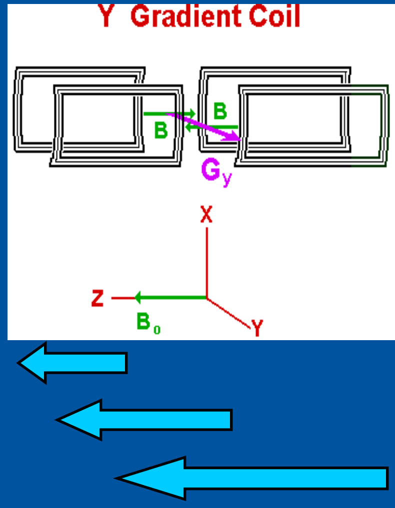

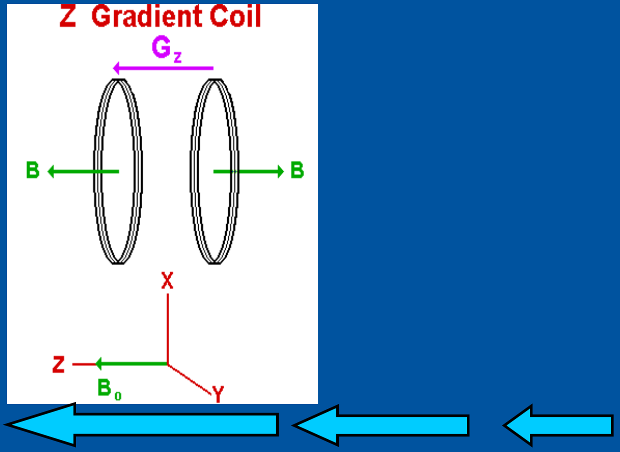

Linear changes in B_0 in each orthogonal direction

Correction of imperfect B_0 and gradient fields

Image distortion and correction on a 0.23 T open MRI scanner

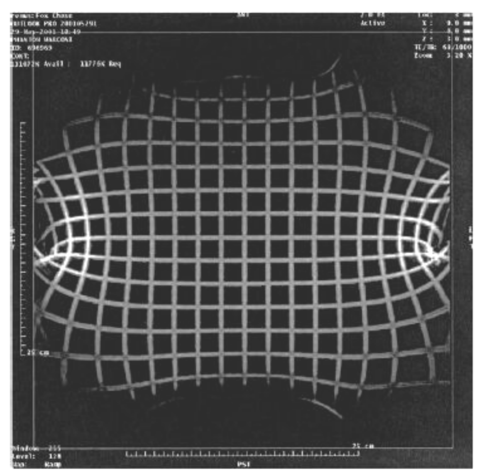

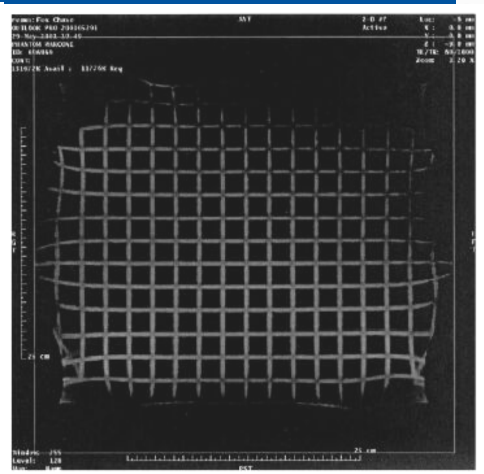

Mah et al. 2002 Int. J. Radiat. Oncol. Biol. Phys. 53 (3), 757-765

Phantoms

Vermandel 2014

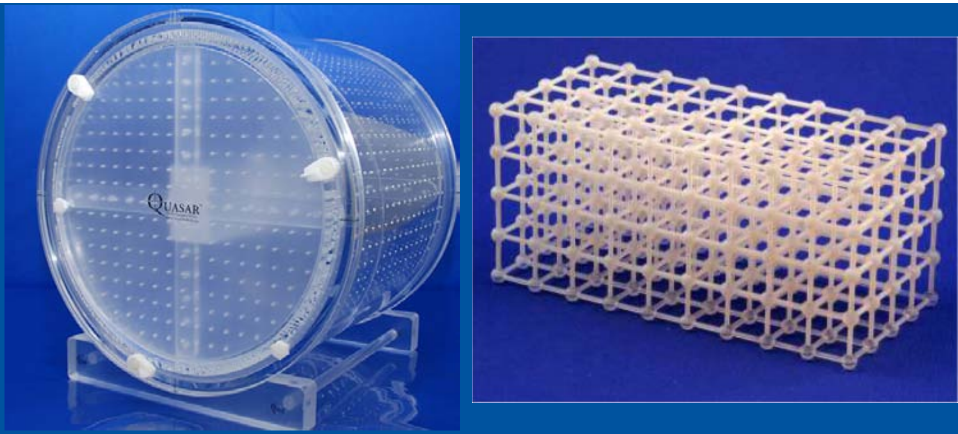

Commercial: Quasar, Modus

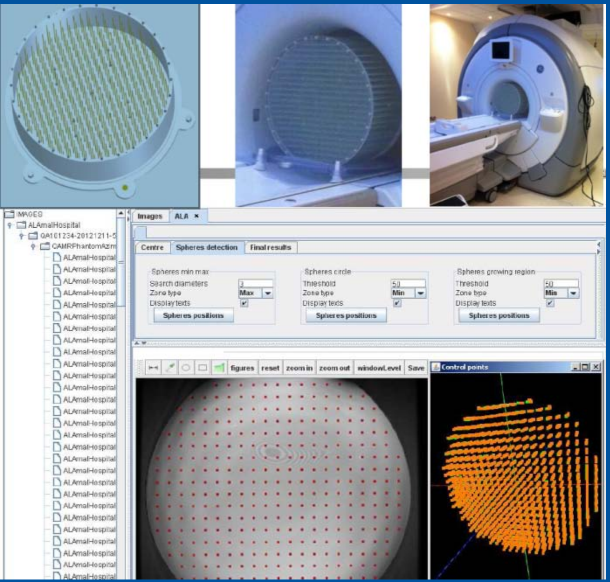

Torfeh 2015

Walker 2015

Vendor: GE

Design of a phantom for field-error measurements

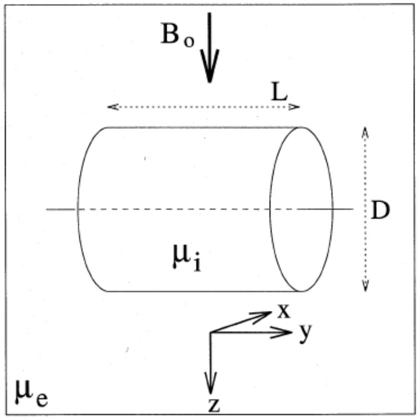

A schematic overview of the cylinder with respect to B_0 (D is the diameter and L the length).

- Use tubes that are long relative to their diameter

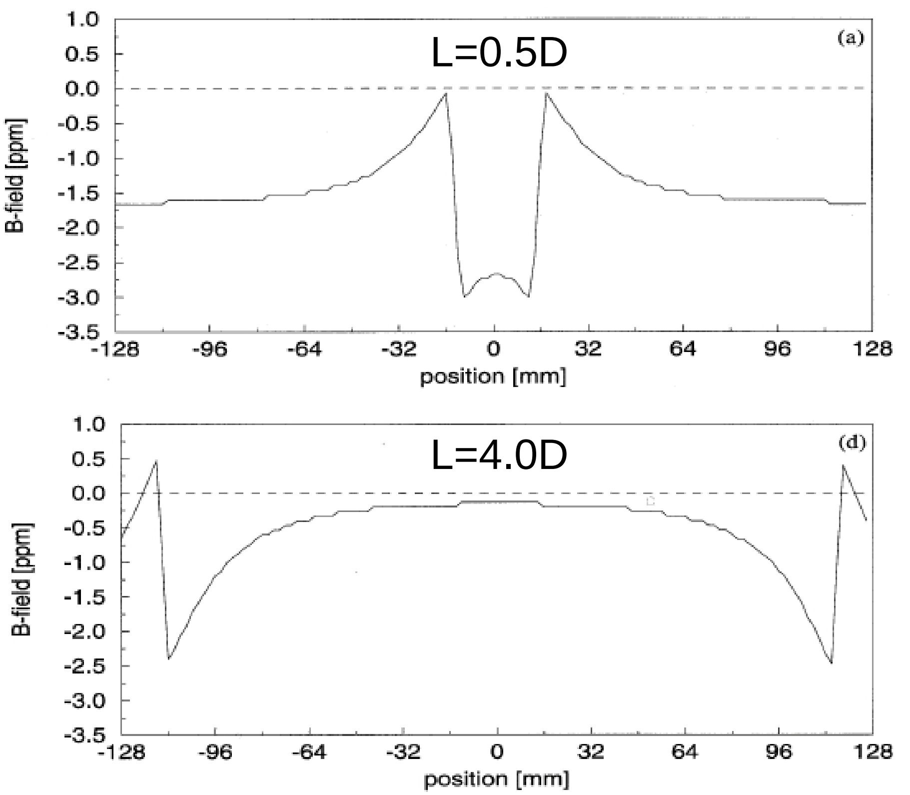

Cross-section of calculated B-field in ppm along the cylinder axis

Baghwandien et al. 1994 Magn. Res. Imag. 12:101-107

Setup of experiments to characterize magnetic field inhomogeneity and gradient non-linearity

Experiment 1:

- phase encoding along y
- Frequency encoding along x

$$x_1 = x + \frac{\Delta B_0(x,y,z)}{G_x} + \frac{\Delta B_{G_x}(x,y,z)}{G_x}$$

$$y_1 = y + \frac{\Delta B_{G_y}}{G_y}$$

Experiment 2:

- phase encoding along x
- Frequency encoding along y

$$x_2 = x + \frac{\Delta B_{G_x}}{G_x}$$

$$y_2 = y + \frac{\Delta B_0(x,y,z)}{G_y} + \frac{\Delta B_{G_y}(x,y,z)}{G_y}$$

Distortion mapping

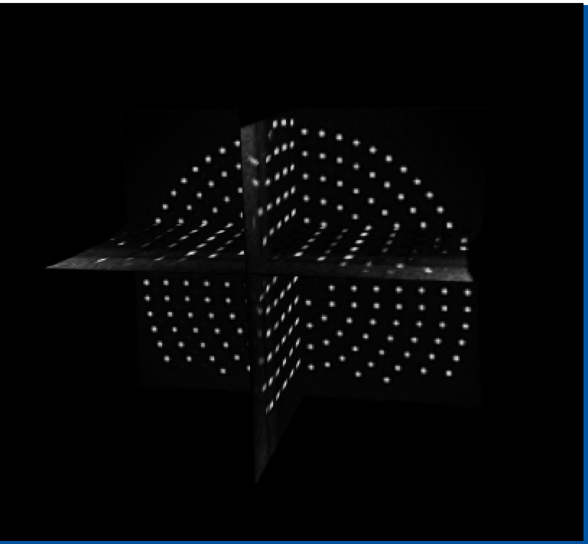

Frequency encoding:

$$x' = x + \frac{\Delta B_0}{G_x} + \frac{\Delta B_{G_x}}{G_x}$$

Phase encoding:

$$y' = y + \frac{\Delta B_{G_y}}{G_y}$$

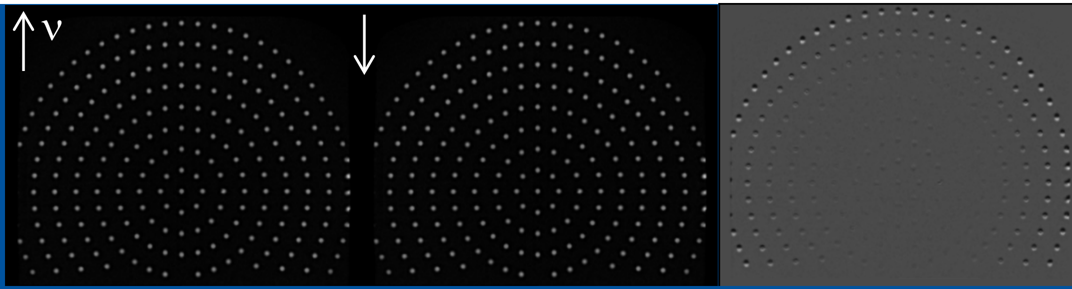

Gradient reversal and subtraction

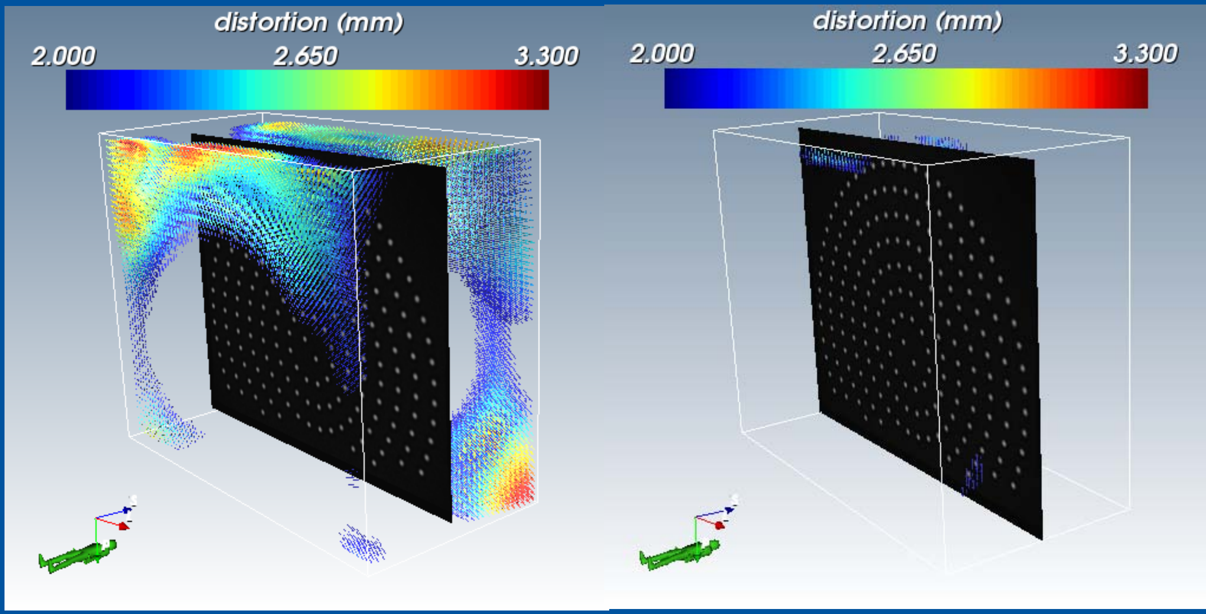

Residual gradient

B_0 component

Walker et al. Med Phys 2015;42:1982-1991

Continuous or stepped table measurement

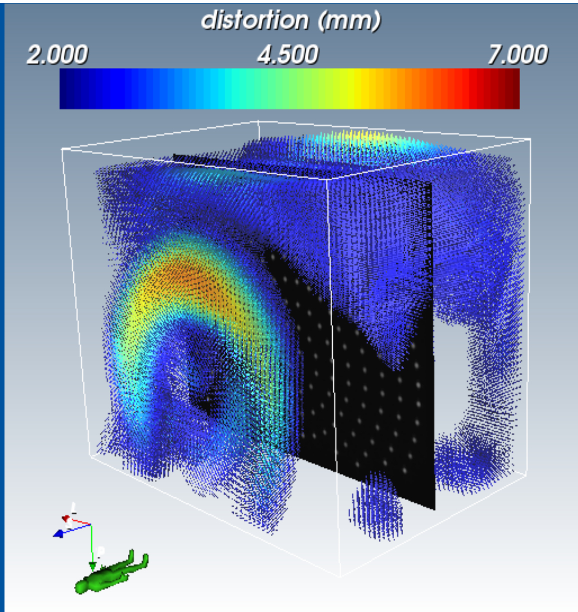

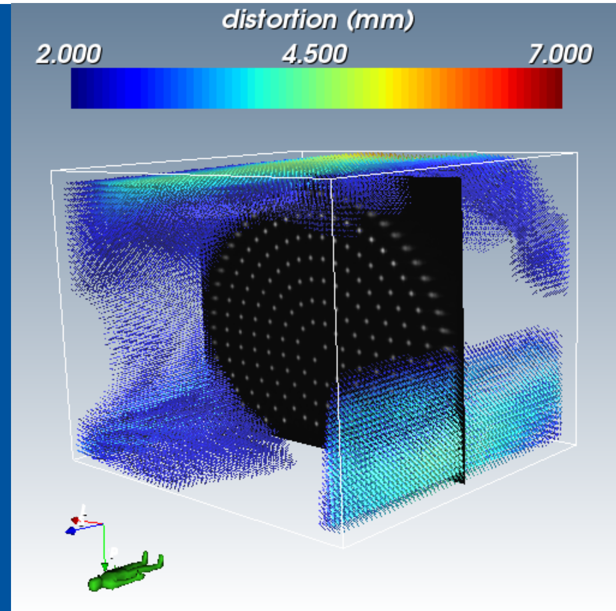

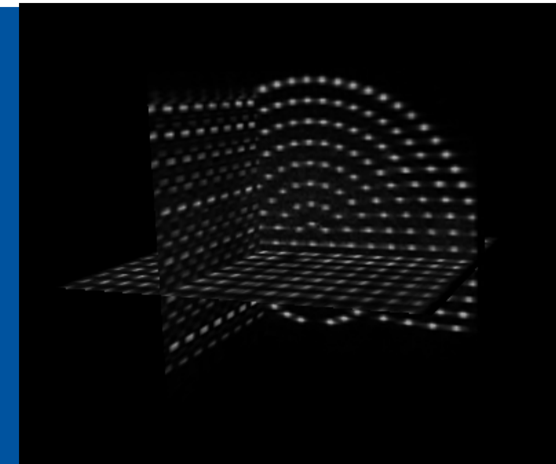

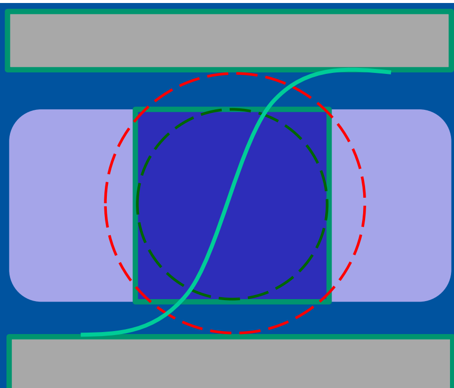

Restrict volume

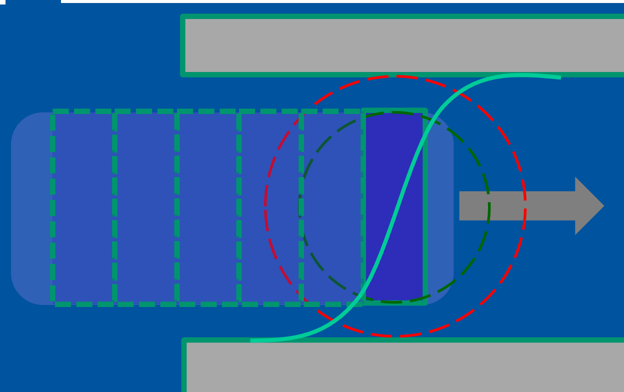

Move table through isocentre

Walker et al. Med Phys 2015;42:1982-1991

Gradient corrections

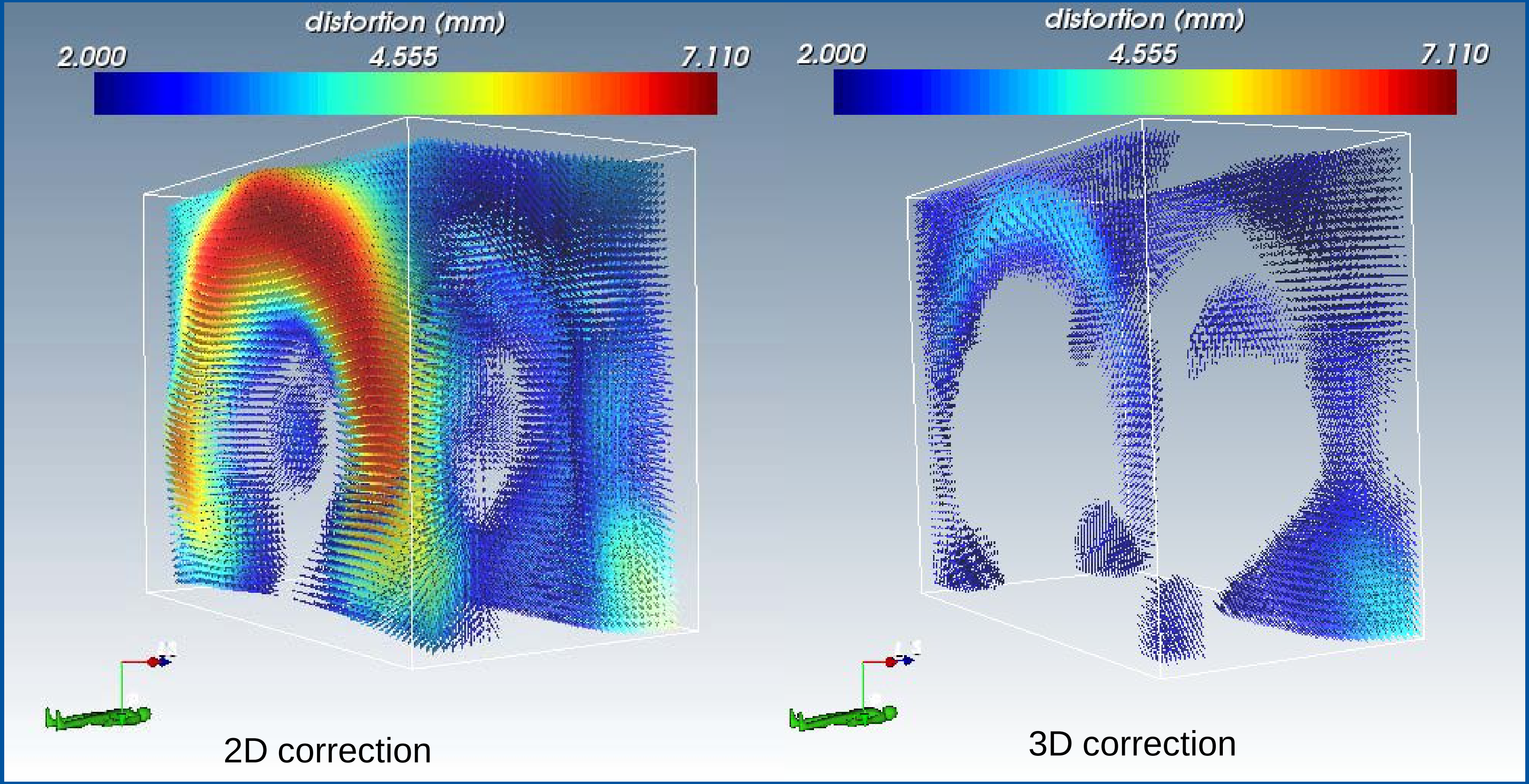

2D correction

3D correction

- 3D correction introduced circa 2006 and adopted by vendors

System measurements

Paper	Year	Phantom size	System	Error
Vermandel	2014	(Head) 24 cm	Various 3.0T & 1.5T	Mean 1 mm uncorrected, 0.5 mm corrected
Glide-Hurst	2014	2500 points, 40 x 40 x 40 cm	1.0T Panorama	24% > 3mm at 150-200 mm radius
Balter	2014	4689 points, 46 x 35 x17 cm	3.0T Skyra	<1 mm at 17 cm radius (60 mm z)
Walker	2015	5830 points, 50 x 38 x 51 cm	3.0T Skyra	250 mm radial, 200 mm z 29-87% of phantom <2mm
Torfeh	2015	357 rods, 40 x 40 x 19 cm	1.5T GE 450w	95% <1mm at 200 mm radial

Characterizing geometrical distortions

- Currently no standard phantom/QA
- Good resolution of points
- Large coverage (x,y,z)
- Flexible design (weight)
- CT compatible
- Rods v points (susceptibility)
- Positive/negative signal material
- Semi-automated measurements

Magnetic susceptibility

Paramagnetic
$\chi > 0$

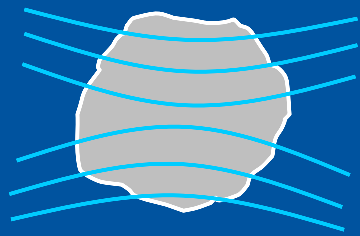

ΔB_0

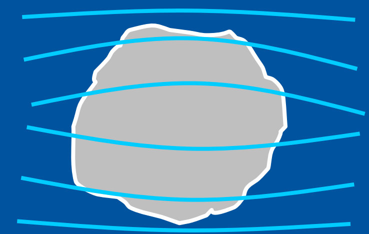

Diamagnetic
$\chi < 0$

Local field variation ΔB_0 superimposes linear gradient

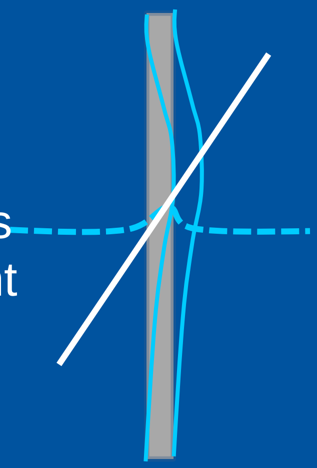

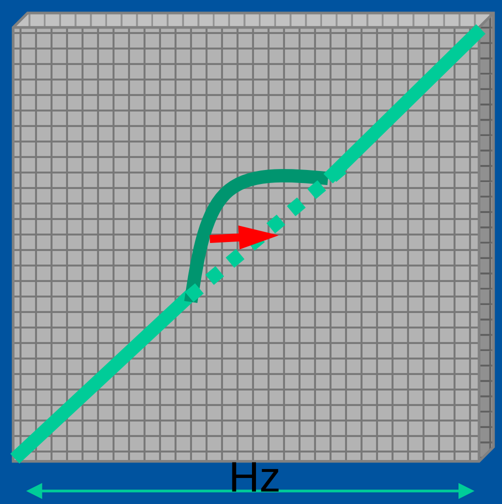

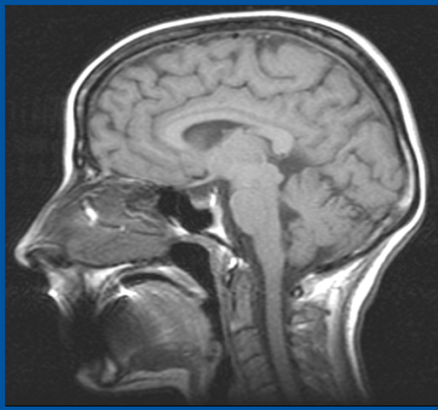

- Off-resonance effects: distortion and signal variations (voids & hyperintensity)
- Ferromagnetic material ($\chi >> 0$) has severe effect

Susceptibility artifacts

- Markers around head

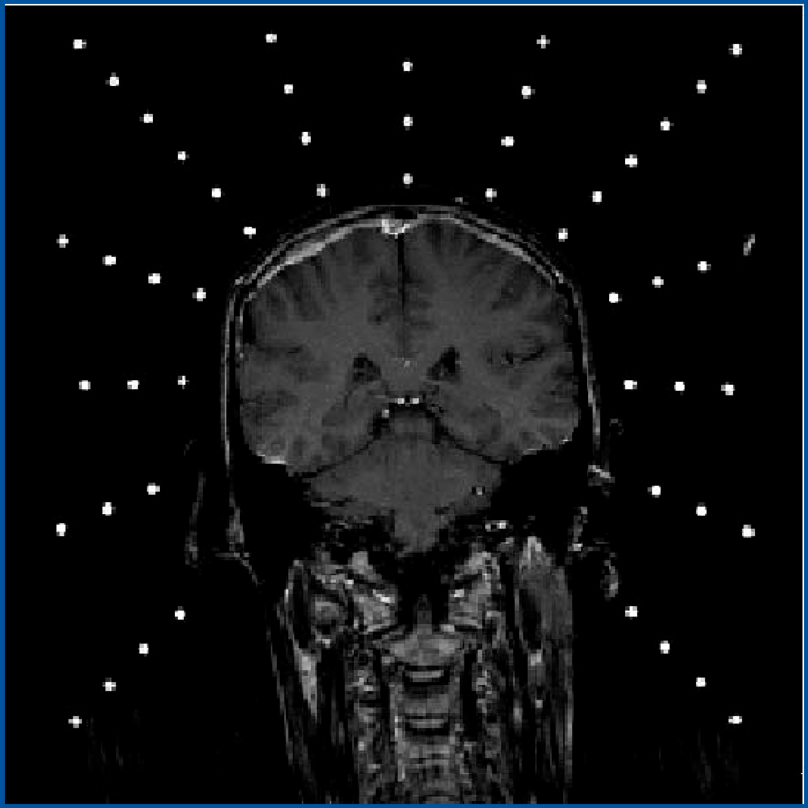

Moerland, PhD thesis 1996

Susceptibility artifacts

- Markers without head

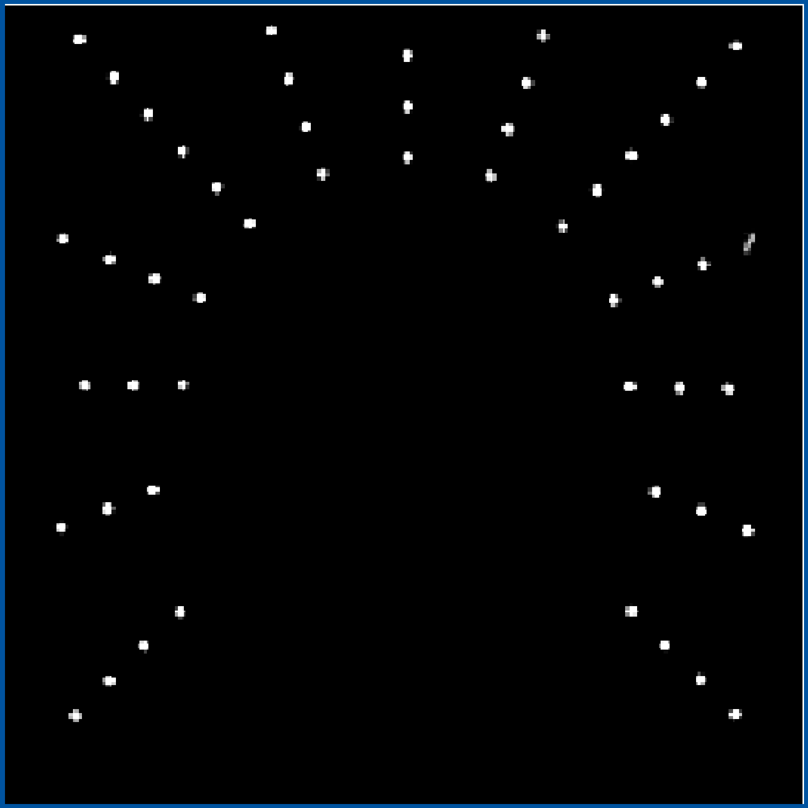

Moerland, PhD thesis 1996

Susceptibility artifacts

- Overlay of images

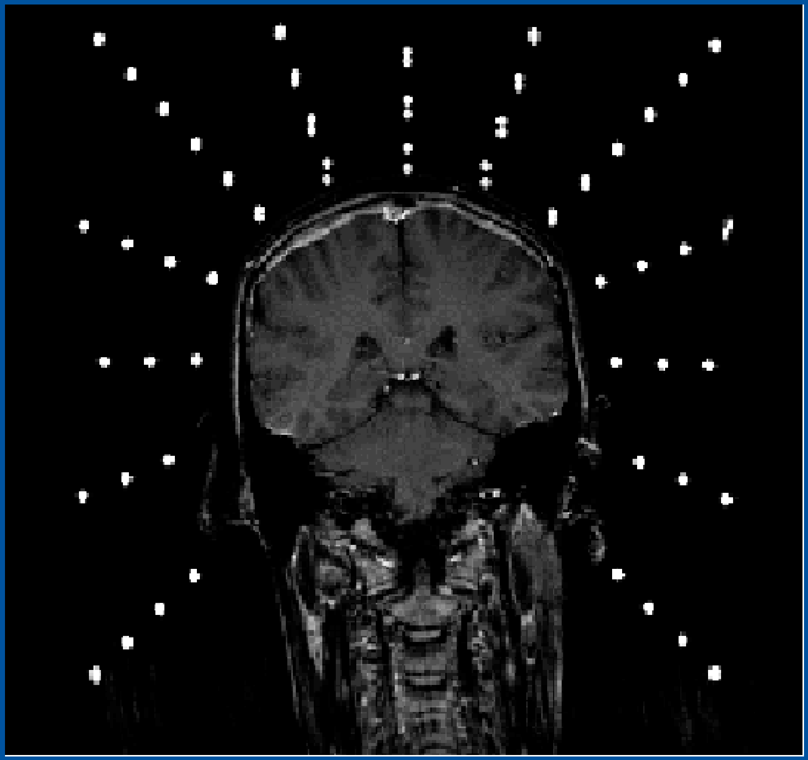

Moerland, PhD thesis 1996

Calculation of field distortions

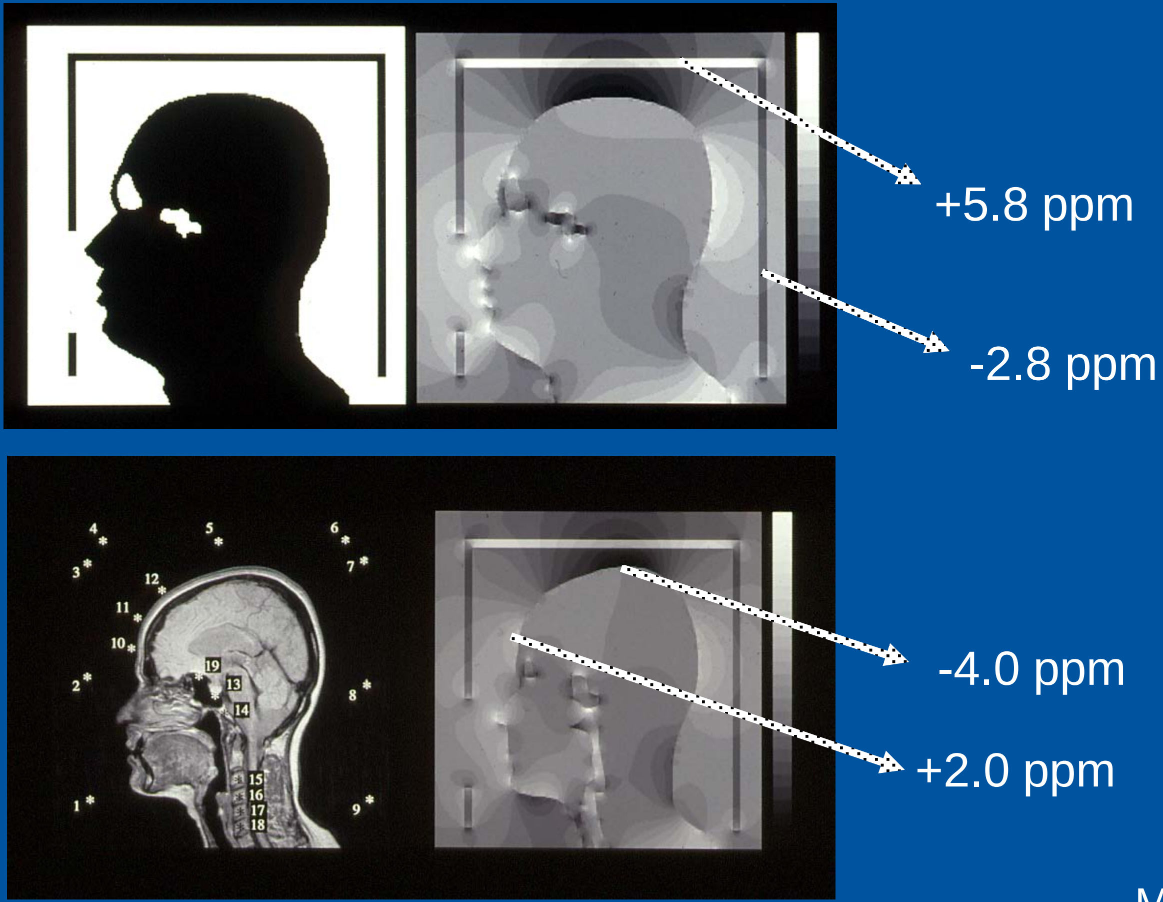

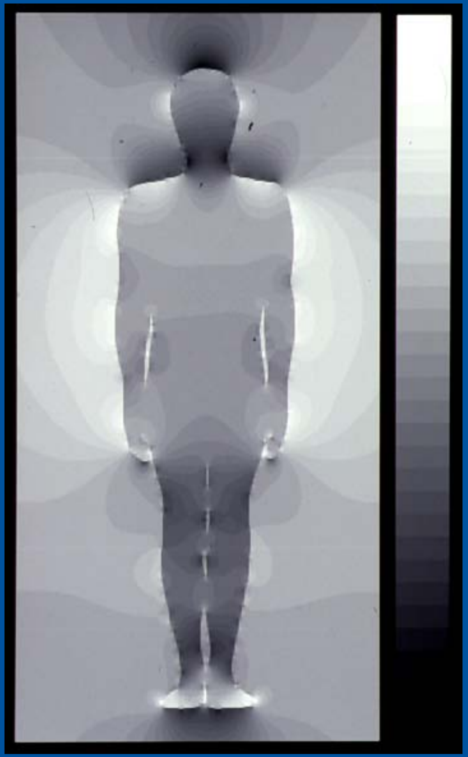

Moerland et al. 1996; Phys. Med. Biol. 40:1651-1664

Susceptibility artifact in read-out direction

$$x_1 = x + \frac{\Delta B_0(x,y,z)}{G_x} + \frac{\Delta B_{G_x}(x,y,z)}{G_x}$$

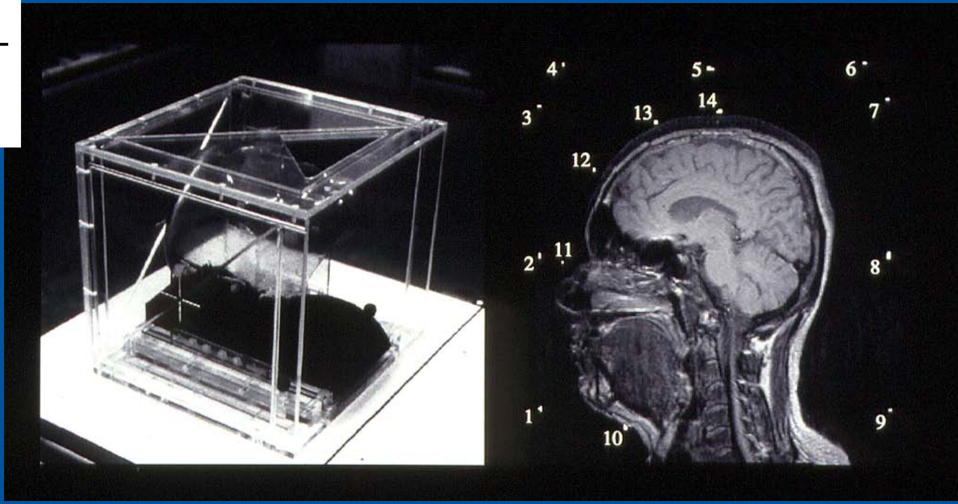

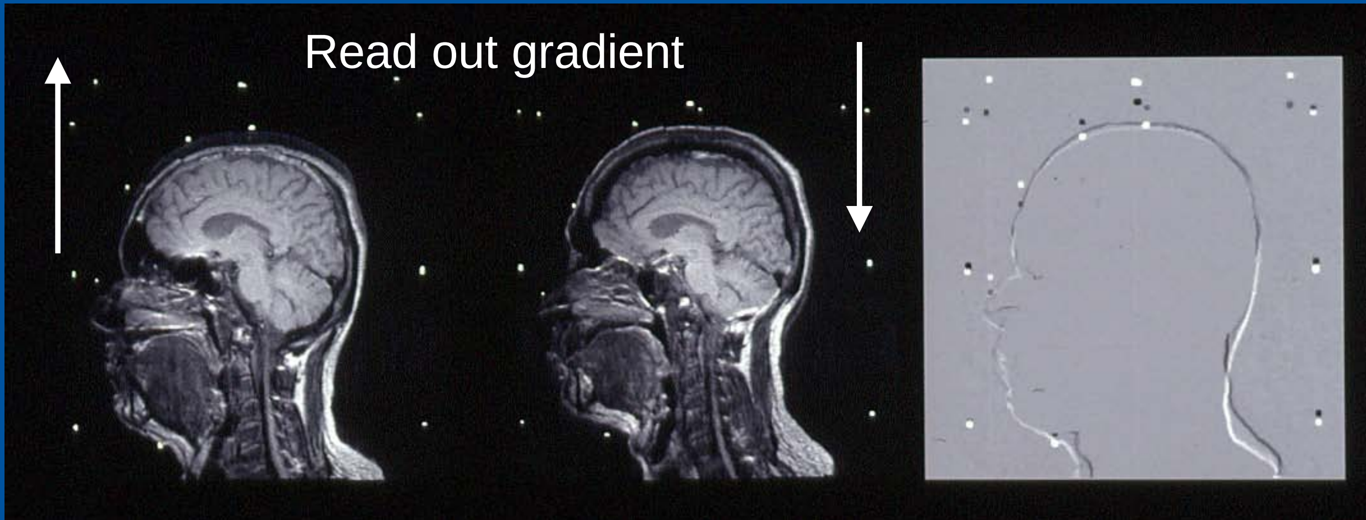

Moerland et al. 1996;
Phys. Med. Biol. 40:1651-

Shimming

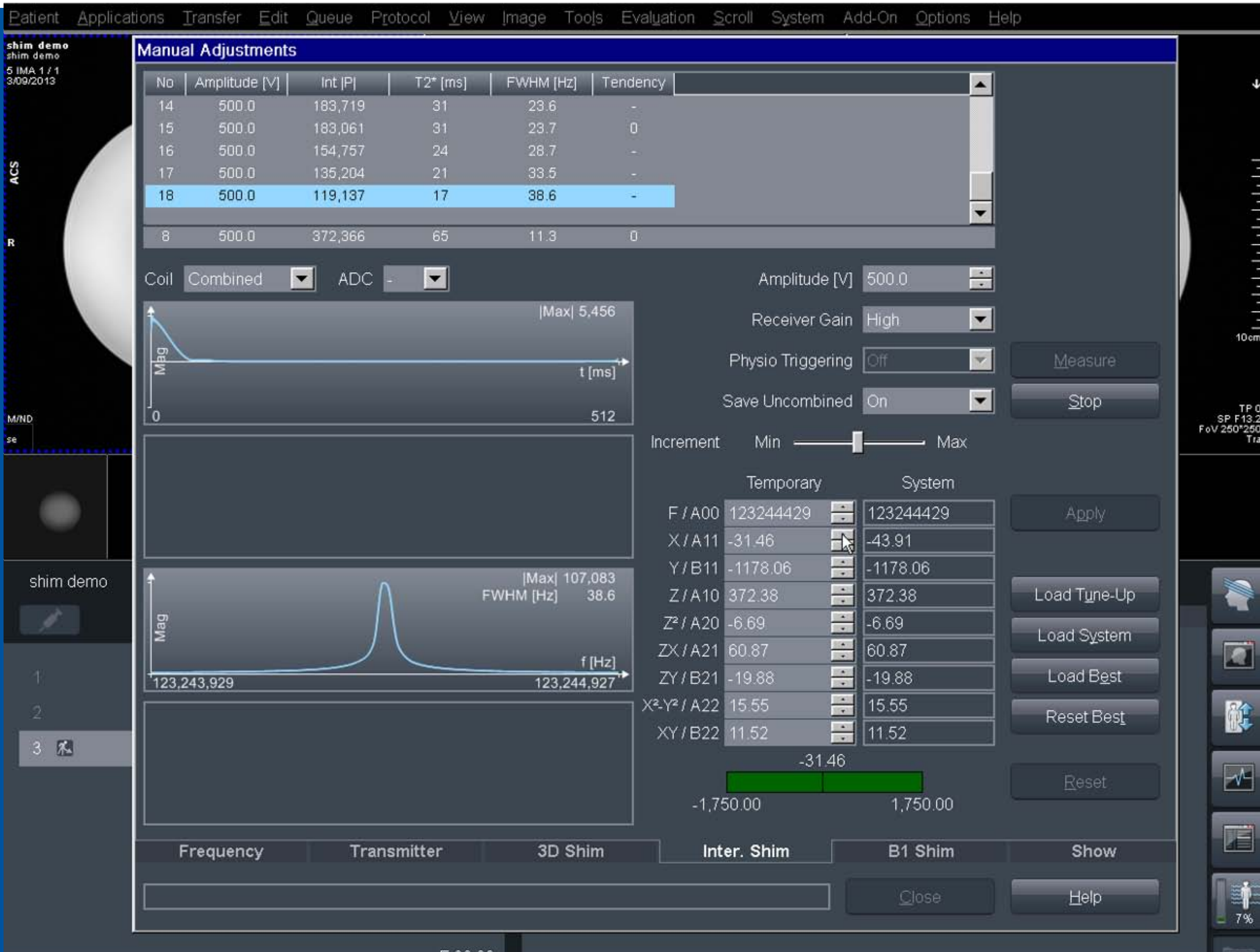

Patient Applications Transfer Edit Queue Protocol View Image Tools Evaluation Scroll System Add-On Options Help
Manual Adjustments
No Amplitude [V] Int |P| T2* [ms] FWHM [Hz] Tendency
14 500.0 183,719 31 23.6 -
15 500.0 183,061 31 23.7 0
16 500.0 154,757 24 28.7 -
17 500.0 135,204 21 33.5 -
18 500.0 119,137 17 38.6 -
8 500.0 372,366 65 11.3 0
Coil Combined
ADC -
|Max| 5,456
Mag
t [ms]
0
512
|Max| 107,083
FWHM [Hz] 38.6
f [Hz]
123,243,929
123,244,927
Amplitude [V] 500.0
Receiver Gain High
Physio Triggering Off
Save Uncombined On
Increment Min Max
Measure
Stop
Temporary System
F / A00 123244429 123244429
X / A11 -31.46 -43.91
Y / B11 -1178.06 -1178.06
Z / A10 372.38 372.38
Z² / A20 -6.69 -6.69
ZX / A21 60.87 60.87
ZY / B21 -19.88 -19.88
X²-Y² / A22 15.55 15.55
XY / B22 11.52 11.52
-31.46
-1,750.00
1,750.00
Apply
Load Tune-Up
Load System
Load Best
Reset Best
Reset
Frequency
Transmitter
3D Shim
Inter. Shim
B1 Shim
Show
Close
Help
shim demo
1
2
3
10cm
7%

B0 mapping

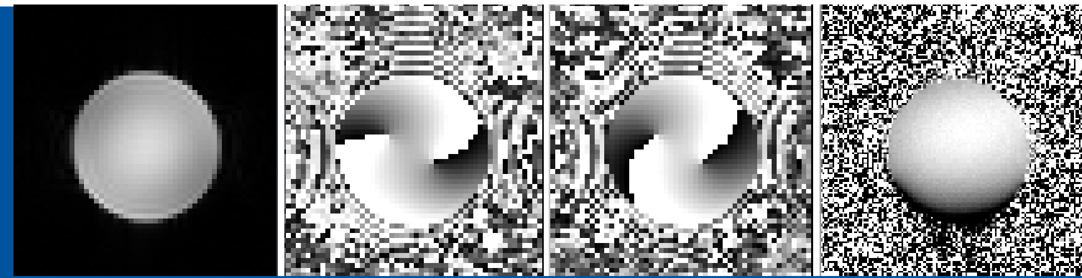

Magnitude Phase (TE1) Phase (TE2) Difference

- Air/tissue interfaces problematic
- Dynamic & HO shimming
- May be measured/corrected:
  - Image at two different TEs
  - Reconstruct phase difference
- Bhagwandien measured -5 to +6ppm i.e. nearly twice WFS

$$\Delta B_0 = \frac{\Delta\varphi}{\gamma \Delta TE}$$

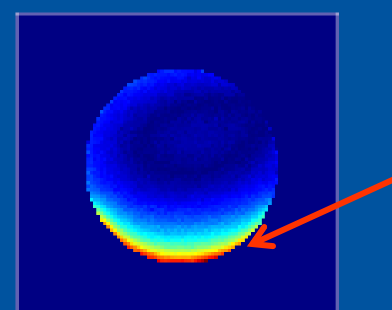

Maximum 34 Hz (0.3 ppm)

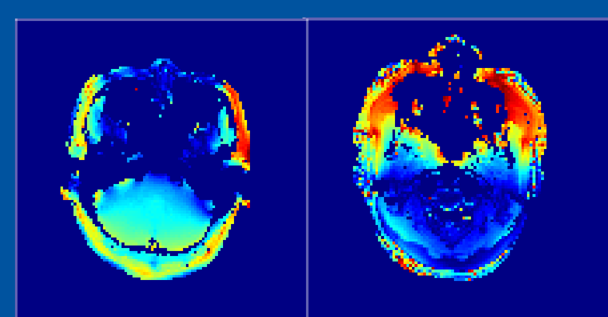

Maximum 203 Hz (1.6 ppm @ 3T)

B0 mapping

Male volunteer. Notice B_0 variations near the rectum due to susceptibility effects of rectal gas

Such a map can be used to calculate the distortion of the image, and in some cases correct for it

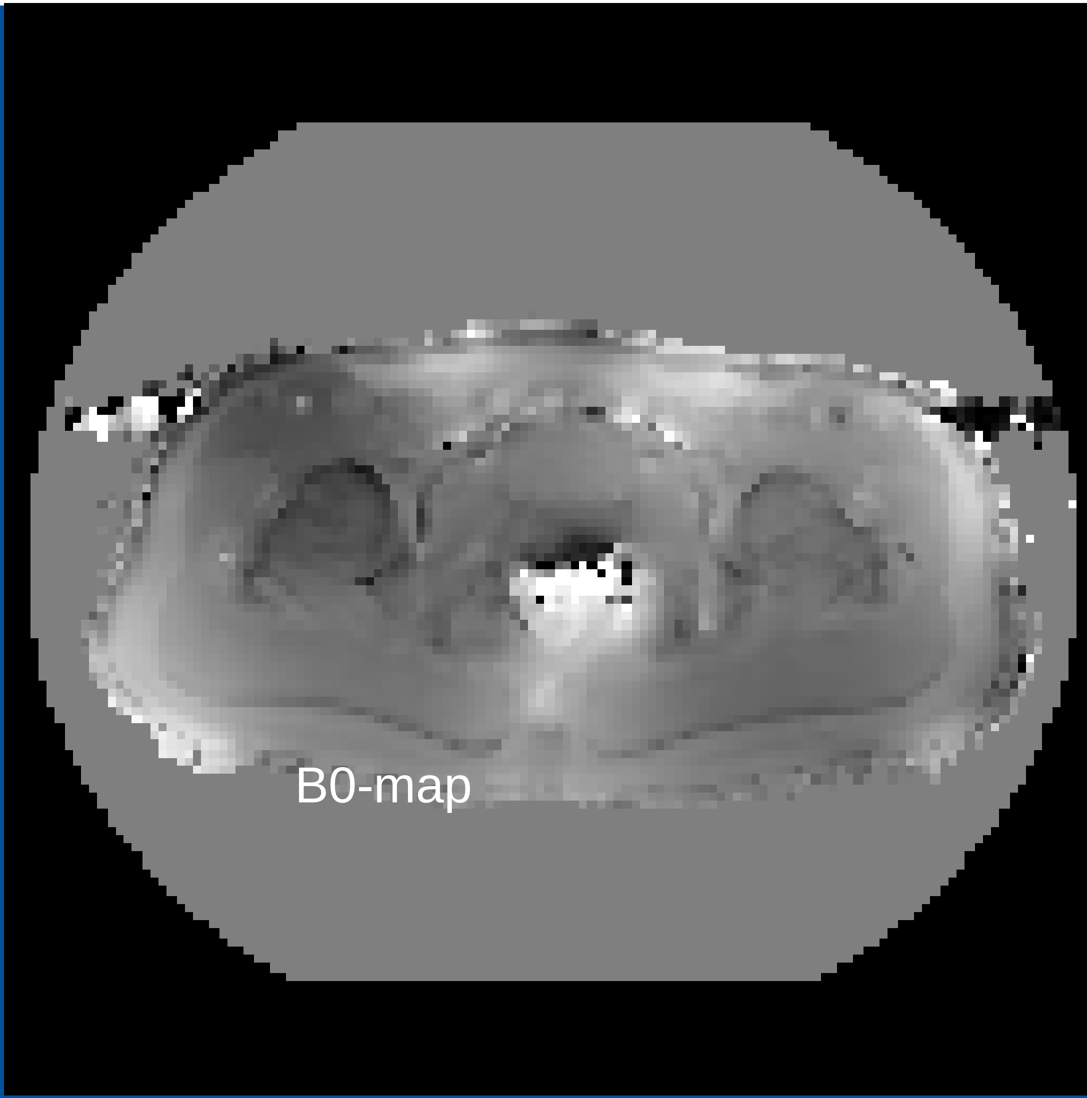

Examples of artifacts

- Susceptibility artifacts
- Water-fat shift
- Motion
- bSSFP artifacts (bTFE, bFFE, trueFISP)
- EPI artifacts

Example from clinical practice. What is wrong?

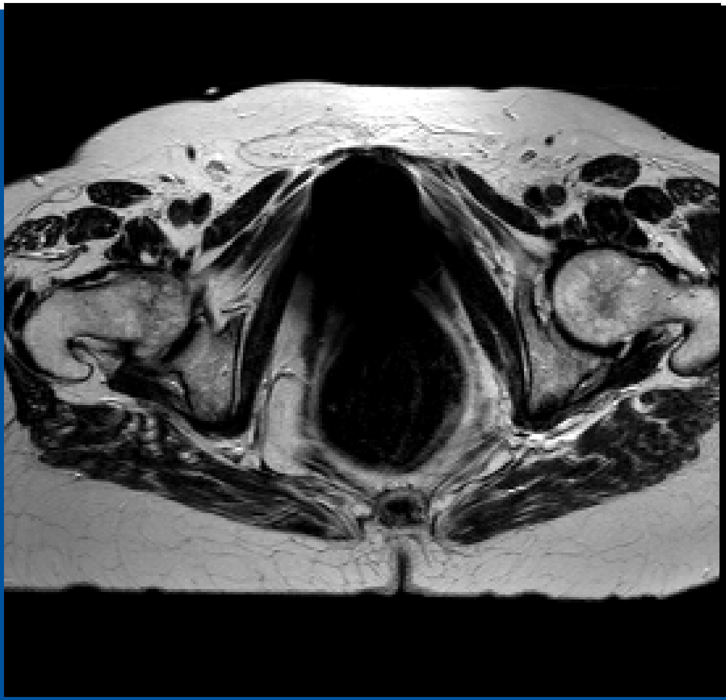

- MRI exam of patient with cervical cancer
- T2-SE sequences shows large area with signal loss
- T1w-THRIVE sequence shows dark ring

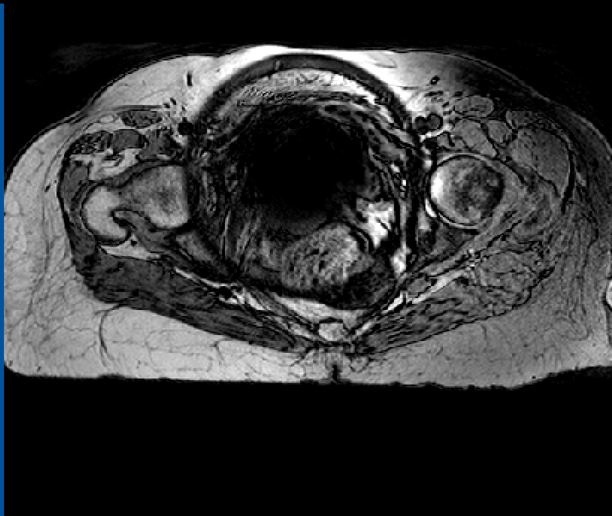

CT scan of same patient

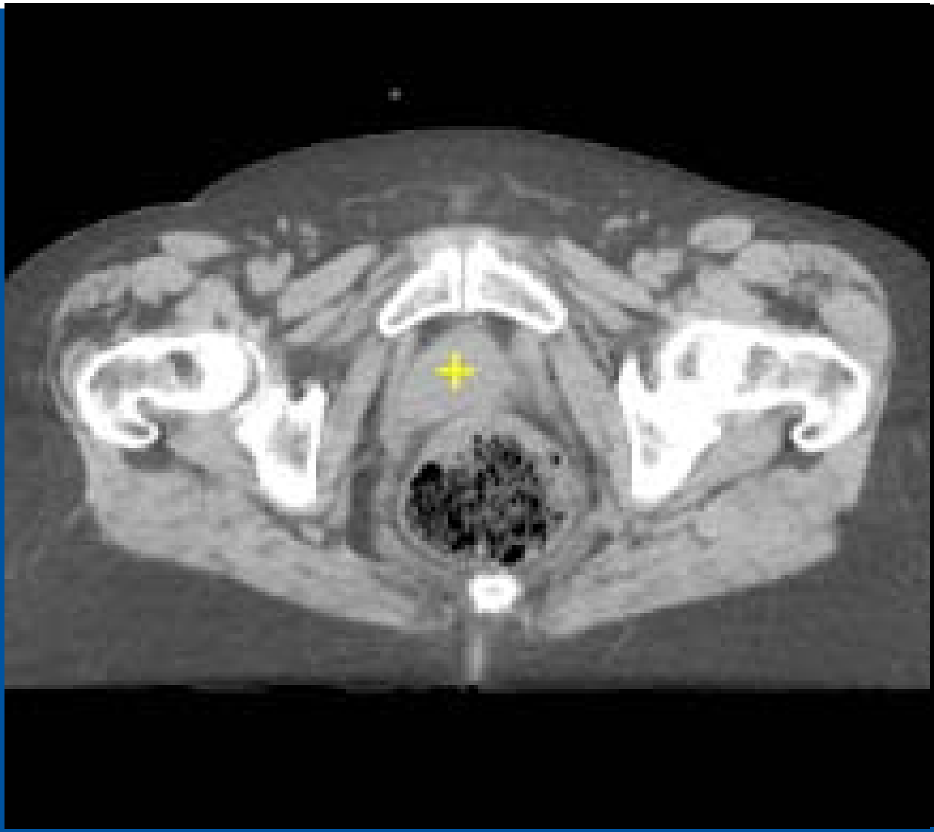

- No obvious metal
- However: a small ferro-magnetic button in her clothes
- Solution: remove metal

Patient with hip prosthesis

- A metal hip prosthesis (titanium)
- Verified that it is safe for the patient
- Big artifact on bSSFP sequence

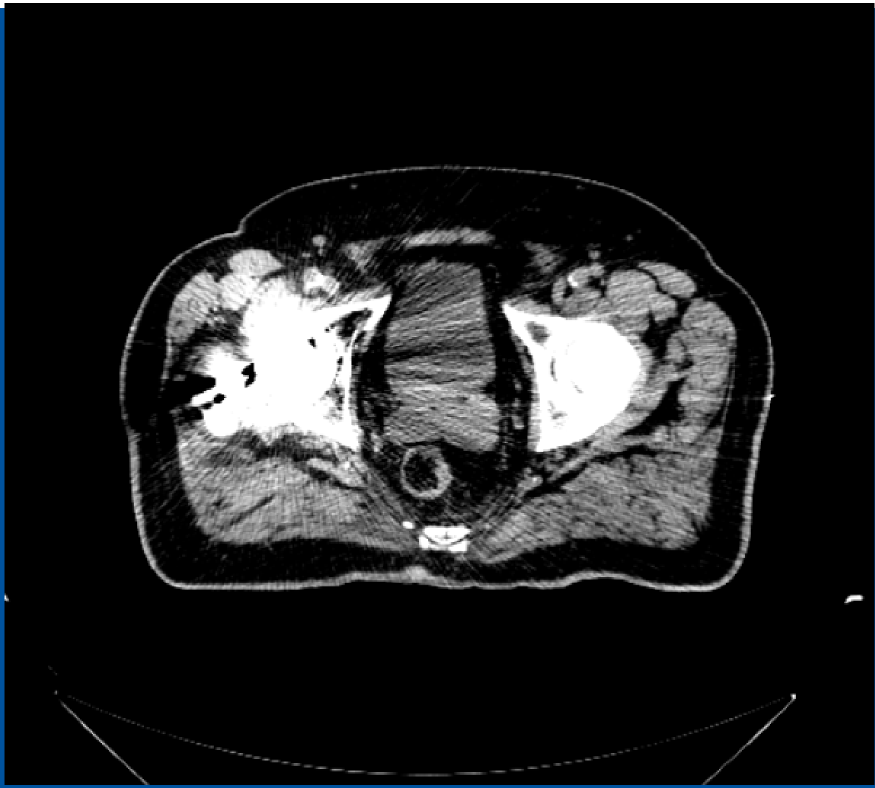

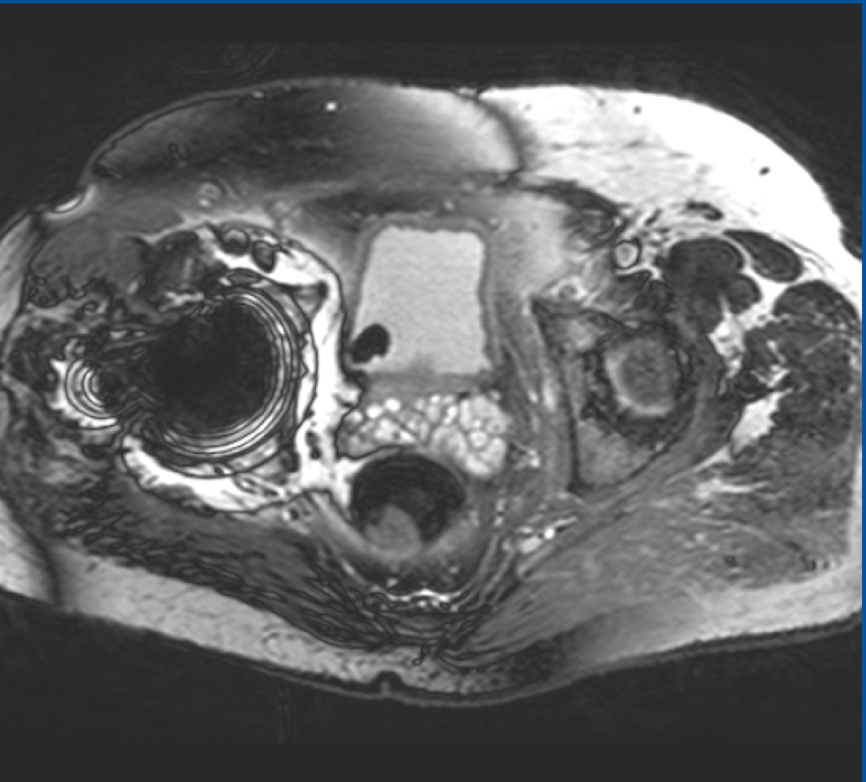

Patient with hip prosthesis

- The T_1-SE sequence and T_2-TSE sequence show a void a the location of the hip, but minimal distortions

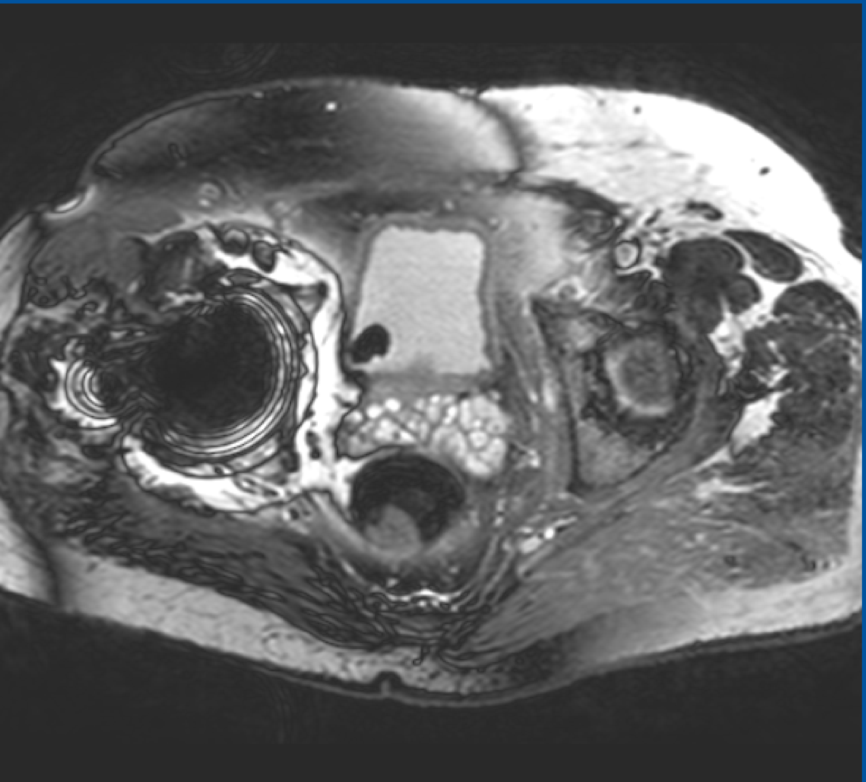

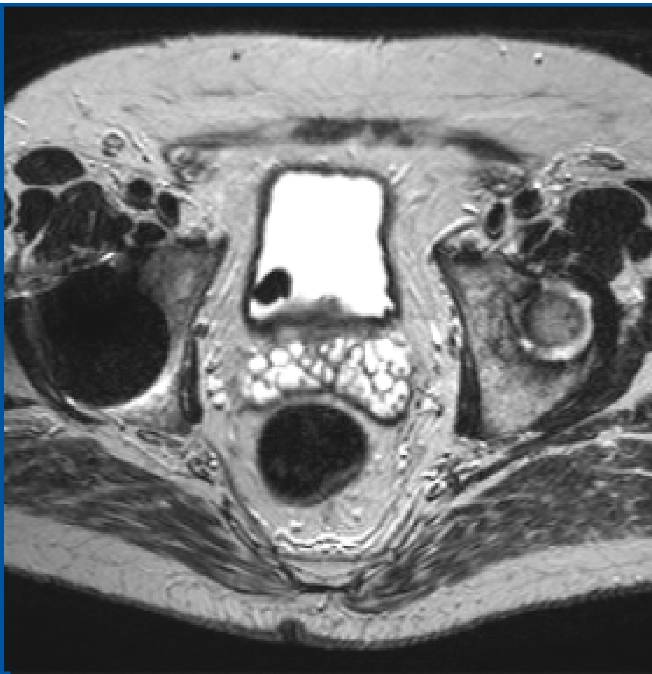

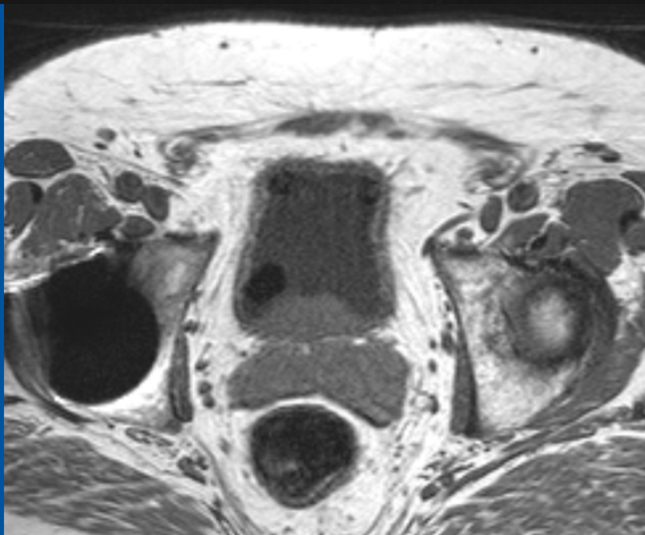

Susceptibility artifact

Artifact:

- Geometrical distortions
- Signal loss

What to do about it:

- Avoid metal, as much as you can
- Minimize pockets of air if possible
- minimize band-width (maximize gradient strength)
- Avoid GE sequences, use SE
- Use short echo times

Water-Fat Shift

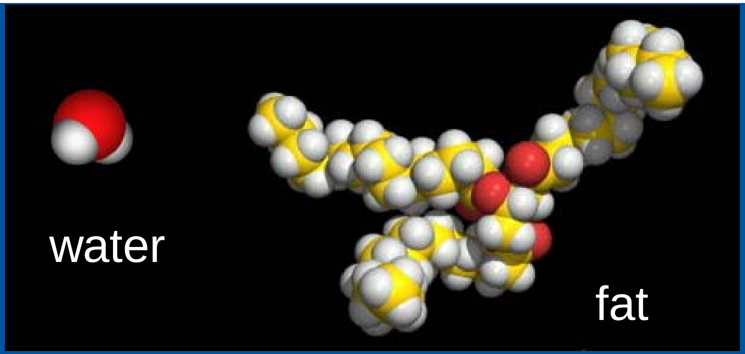

Electron shielding different between molecules

$$B' = B \times (1 - \sigma)$$

Water-fat shift (WFS) = 220 Hz at 1.5 T

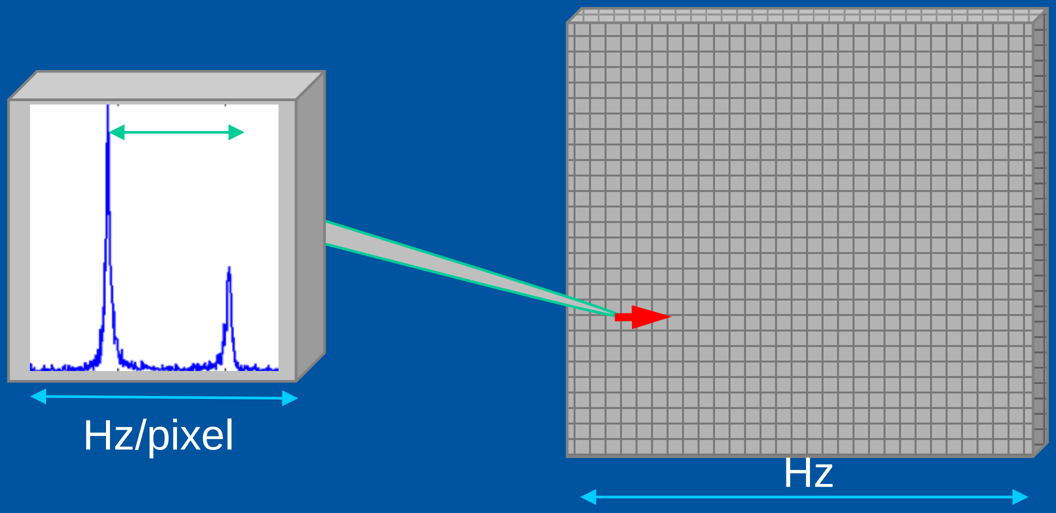

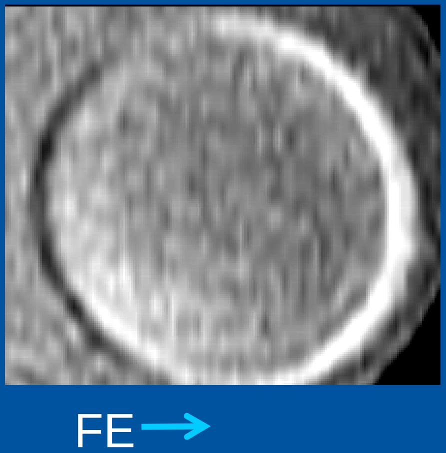

- Produces characteristic signal misregistration
- Assign enough ‘Hz’ across each pixel..increase BW

Water-fat shift

Magnetic field at the nucleus depends on magnetic shielding of surrounding electron clouds, depends on molecular environment

example:
resonant frequencies of protons in fat and water differ by 220 Hz

220 Hz = 3.4 ppm at 1.5 T

$3.4\ 10^{-6} \cdot 1.5T = 5.1\ \mu T$ at 1.5 T

$= 5.1\ \mu T / 3\ mT/m = 1.7\ mm$ at 1.5 T and read out gradient 3 mT/m

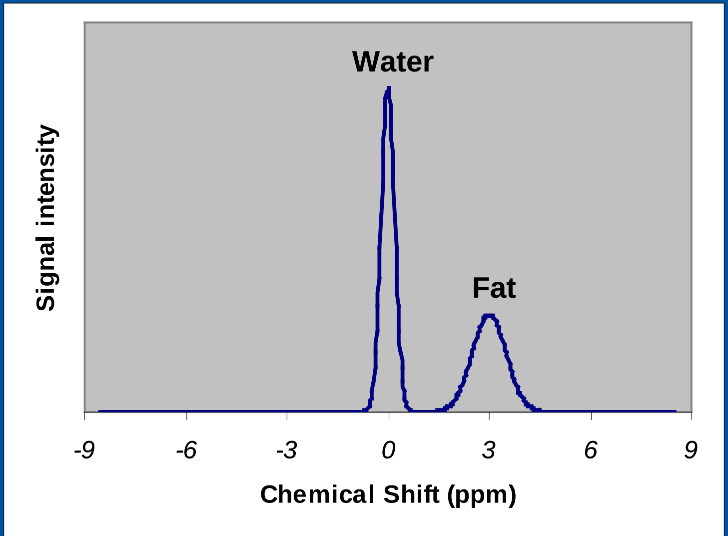

- artifact
  - increases with B_0
  - decreases with gradient strength

Water-fat shift

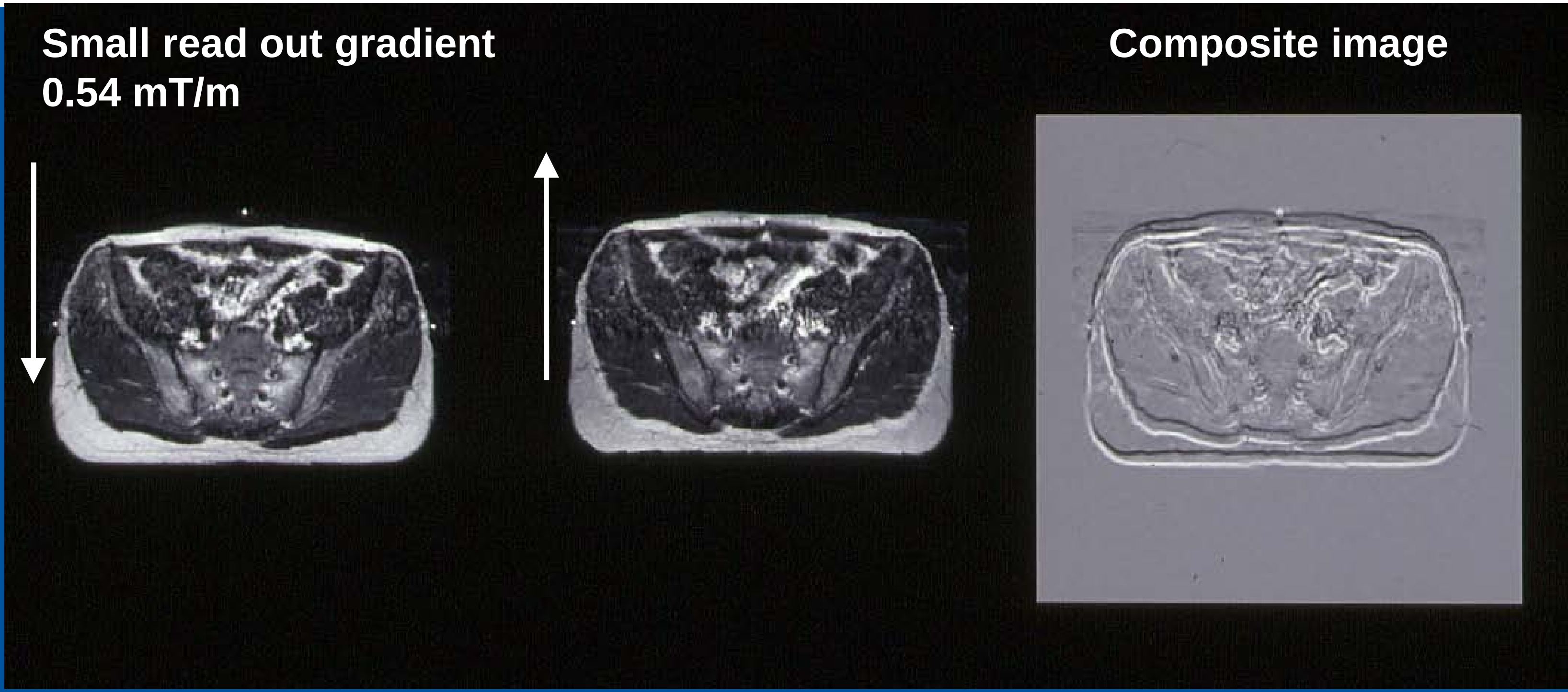

Water-fat shift $\approx$ 9 mm
Contour distortions
marker position error

Distortions due to ΔB_0 (water fat shift, susceptibility) can be reduced to < 1mm by increasing gradient strength, However: gradient errors remain!

Water-fat shift

Artifact:

- Geometrical distortions
- Signal loss

What to do about it:

- Minimize band-width (maximize gradient strength)
- Fat suppression

Question: motion artifacts

- Motion of a patient in the MRI scanner results in an artifact. What is the appearance of this artifact?

1. Blurring of the image in each slice
2. Ghost images in each slice, overlaying the ‘true’ image
3. Shifts between the slices

Motion artifacts

Ghost images

- Interference at periodical intervals along phase encoding axis
- A small motion may result in large offsets

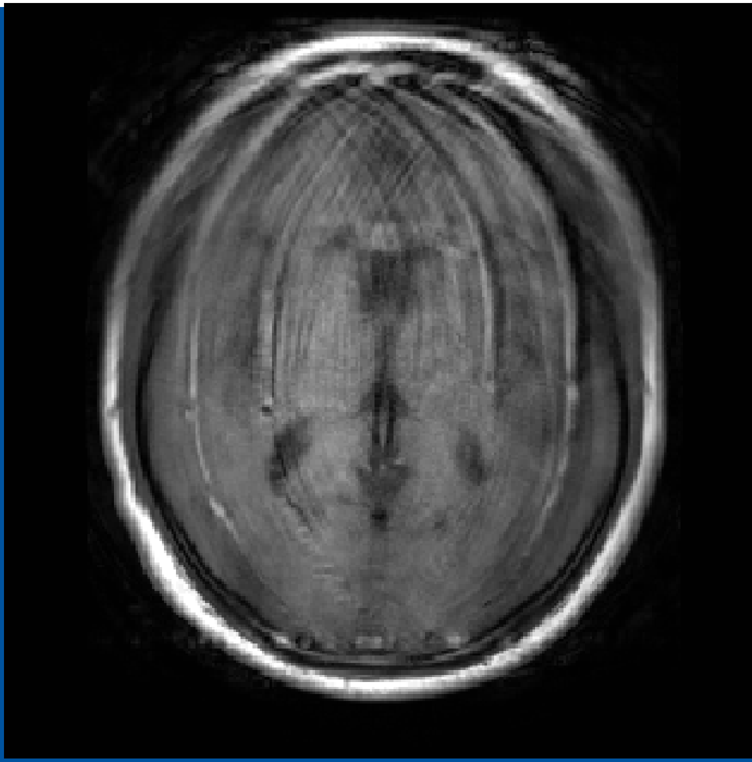

Motion artifacts

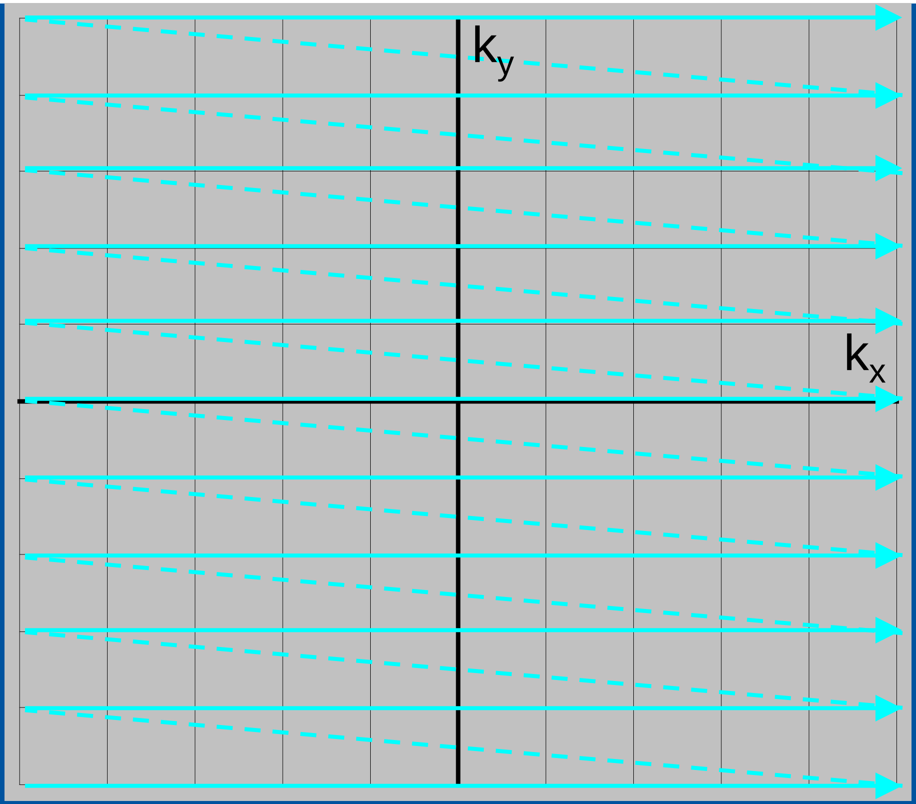

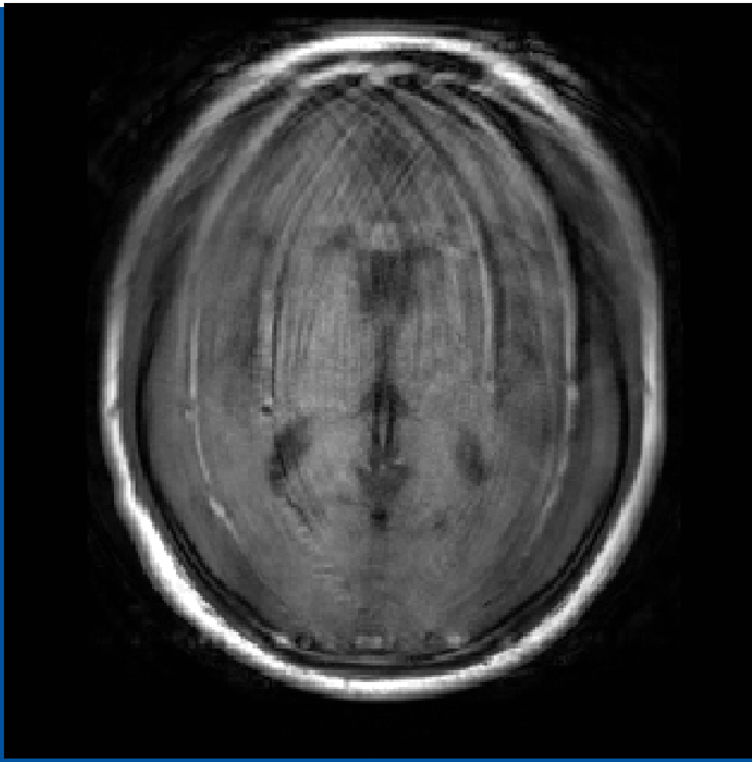

- Motion artifacts propagate mainly in the phase-encoding direction. Motion between phase encoding steps will corrupt the phase-encoding, resulting in ghosts
- Signal sampling in the read-out direction is usually faster than physiological motion and may produce only some spatial blurring

What to do about it?

- Fixation
  - Breath hold
- Fast imaging, cine MRI
- Respiratory gating, cardiac gating etc.
- Navigators, Propeller/MultiVane

Motion correction with a Propeller sequence

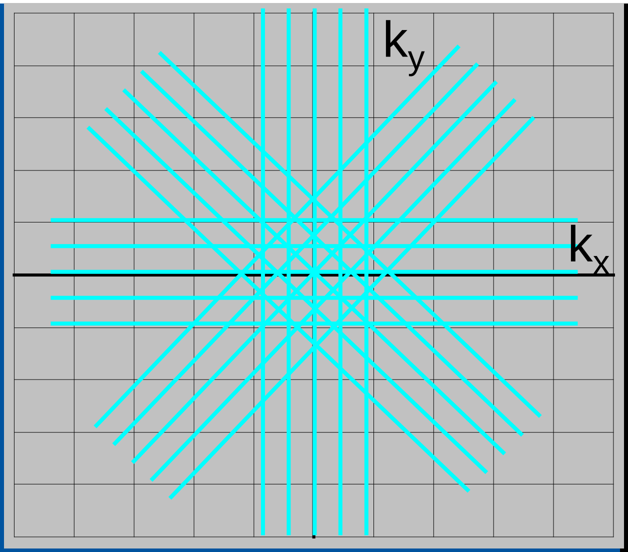

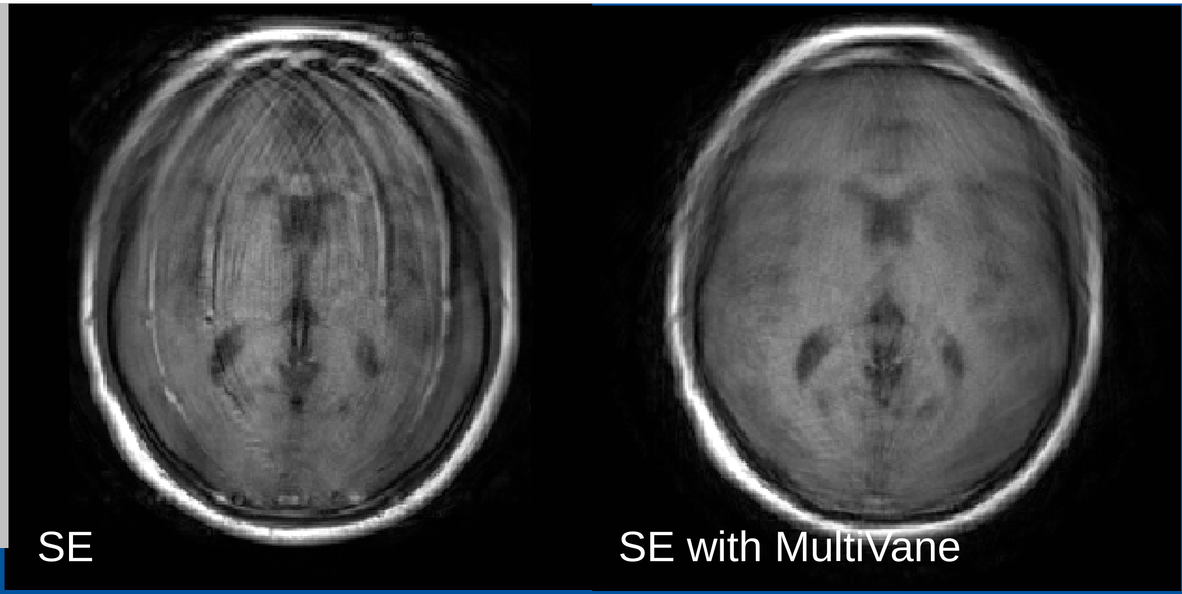

- Sample a set of lines in k-space repeatedly at a different orientation
  - The central part is sampled each time, allowing for a phase correction of the signal
  - The outer part of k-space is sampled only by one of the vanes

Propeller sequence: Eye movement

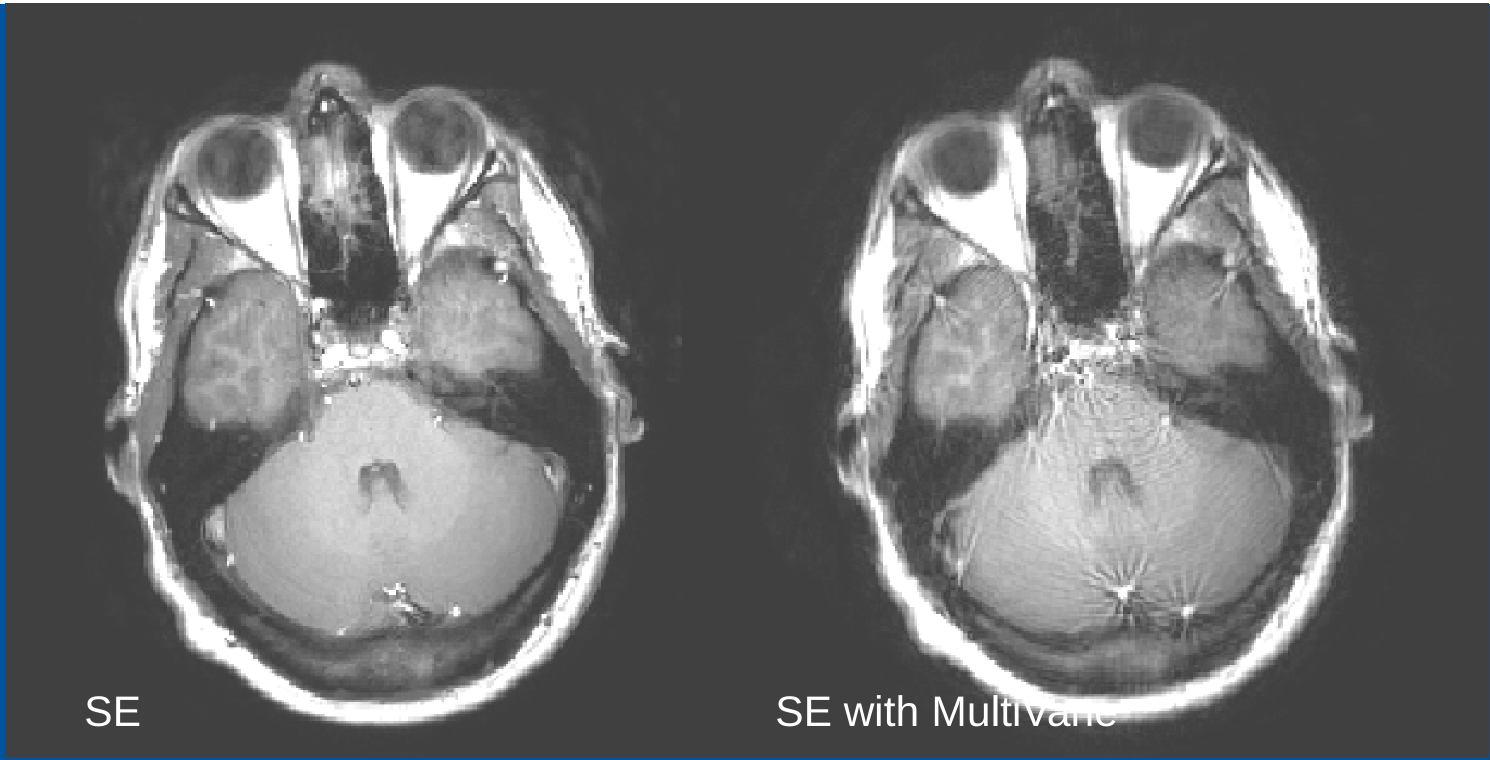

- The MultiVane sequence in a Philips 3T achieva scanner reduces the ghosting artifact around the eyes
- Near blood vessels ‘streak’ artifacts show up, due to undersampling of the outer part of k-space

bSSFP artifact

- Balanced Steady State Free Precession

  also known as:

  – bTFE, bFFE (Philips)
  – trueFISP (Siemens)
  – FIESTA (GE)

- Steady state depends on T_1 and T_2
- Spins from many excitations create a steady state of precessing spins
- B0 distortions (susceptibility) result in spins that are off-resonance and don't see the RF pulses. Thus they don't produce a signal

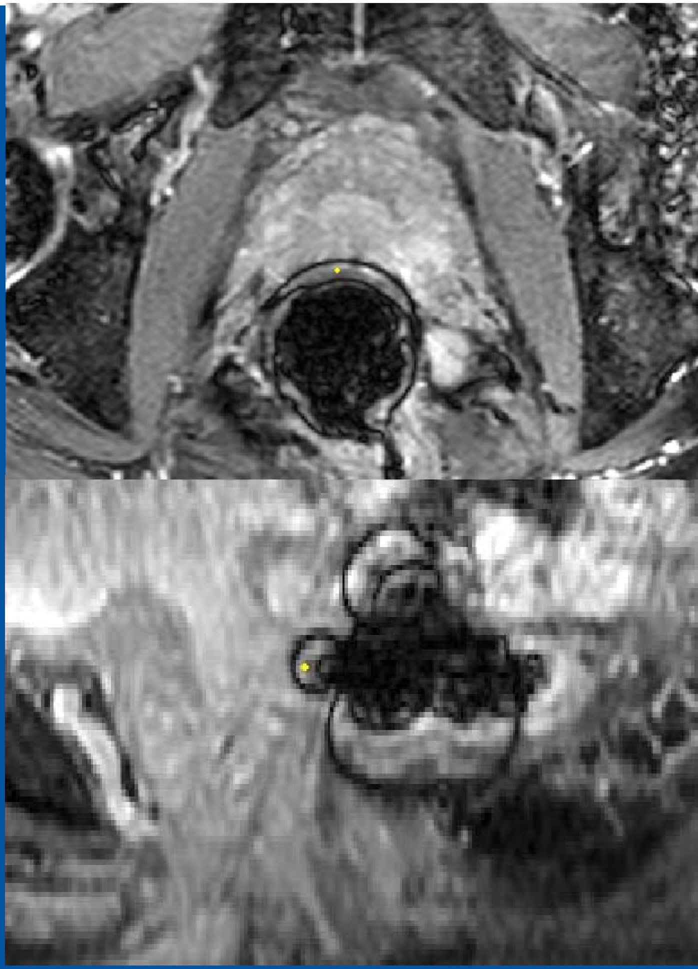

bSSFP artifacts at rectum prostate interface

bSSFP artifact

Artifact:

- A periodic pattern of dark bands in the image

What to do about it:

- Avoid metal, as much as you can
- Minimize pockets of air if possible
- Optimize shimming
- Change the center frequency f_0 (multiple series with shifted f_0)

EPI artifacts

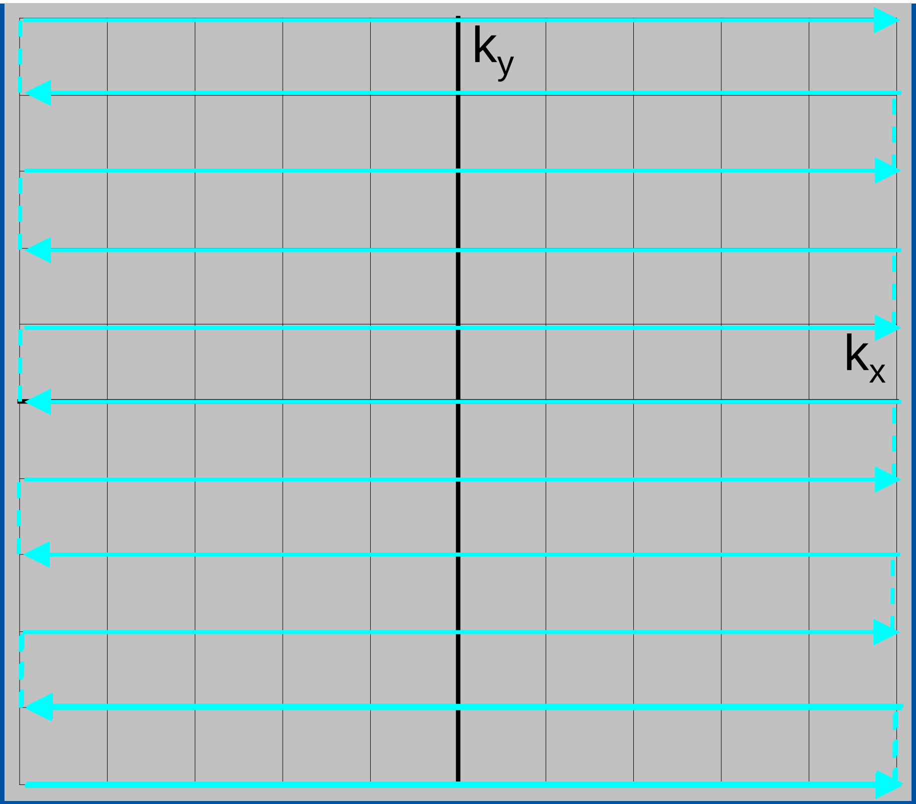

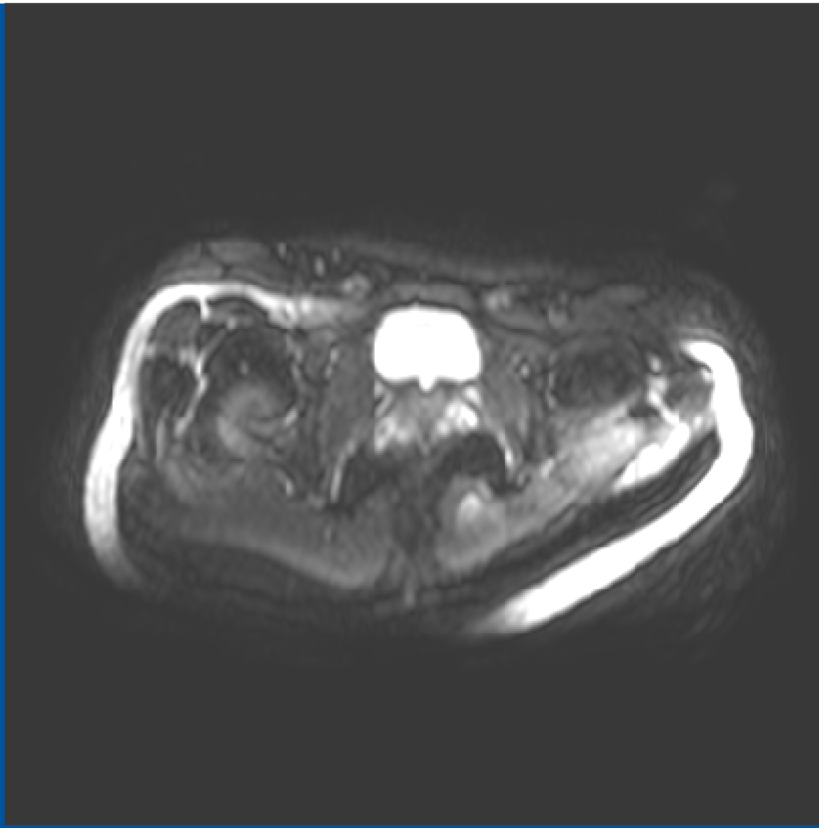

- Very fast switching of gradients because all phase-encoding is done within one read-out
- A very narrow band width is used to collect the data rapidly (example BW = 42 Hz per pixel)
- Therefore very sensitive to B_0 distortions

EPI artifact

Artifact:

- Geometrical distortion

What to do about it:

- Optimize shimming
- Use multi-shot EPI, rather than single shot

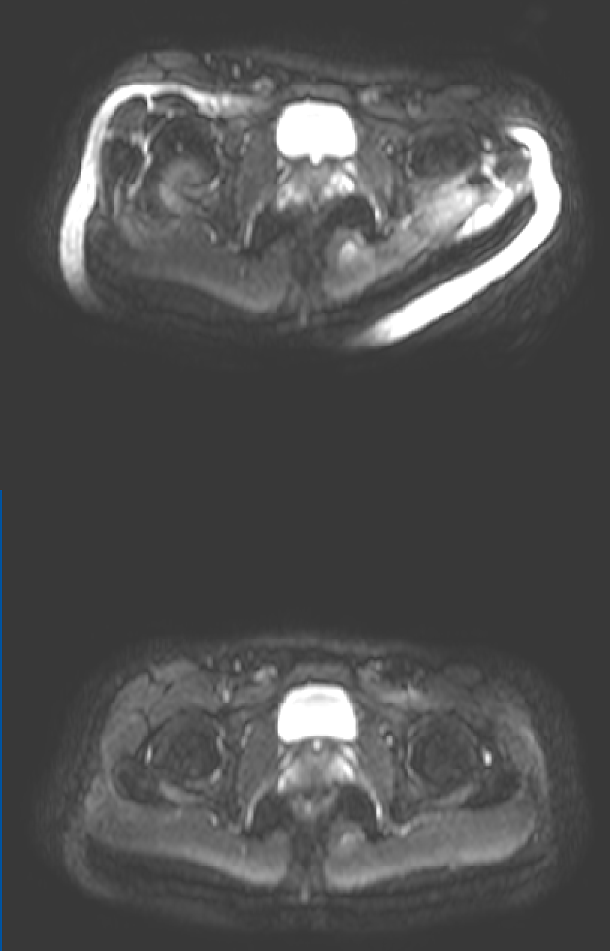

Geometrical artifacts

Artifact	axis	remedy
Fold-over (aliasing)	phase encoding	increase FOV
Ringing (truncation)	both	reduce voxel size
Susceptibility	read-out	increase BW
Water-fat shift	read-out	increase BW
Motion (ghosting)	phase encoding	reduce motion gating fast scanning

Practical consequences

- The geometrical accuracy of MR images tends to be worse towards the edges of the field of view
- Field distortions due to susceptibility differences are larges near interfaces (body contour, air pockets)
- Devices used during interventions (brachytherapy) make cause artifacts

Practical consequences

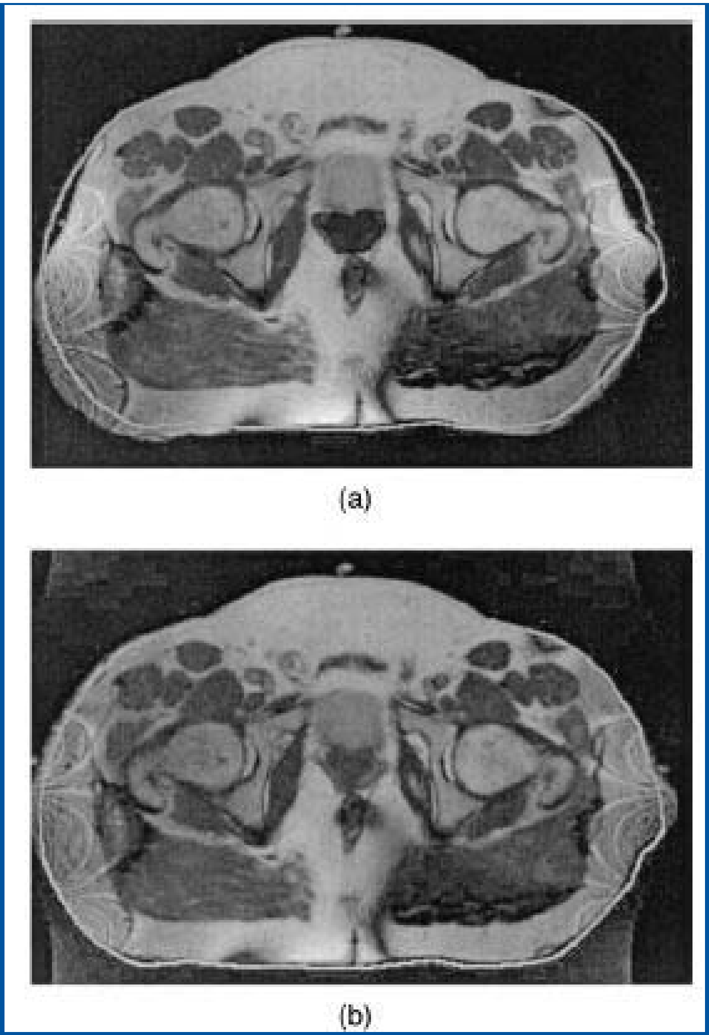

Mah et al. 2002 Int. J. Radiat. Oncol. Biol. Phys. 53 (3), 757-765

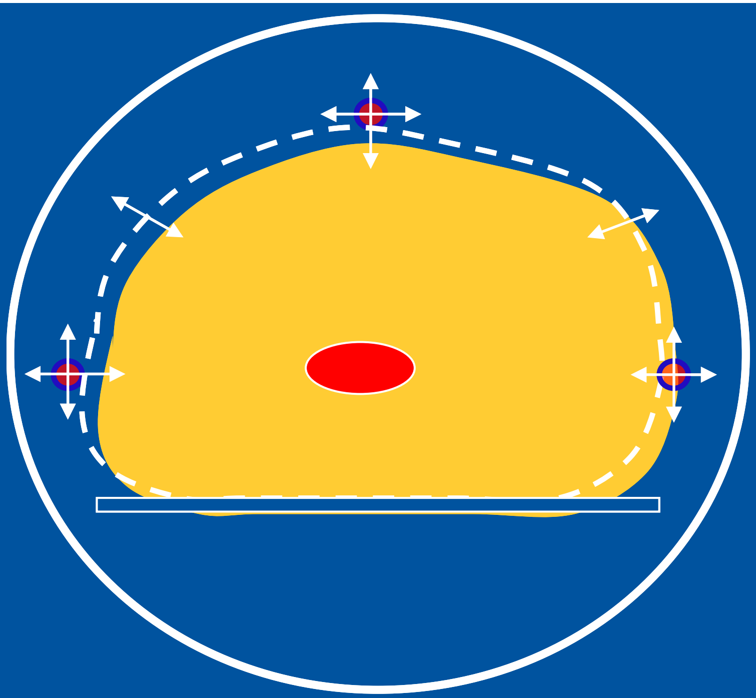

Largest distortions at the edges of the MR bore

Markers on the skin not reliable as reference for beam setup

➔ Registration of planning CT and MRI

MRI-guided interventions: needles

Spin echo images of needles (18G/1.3 mm) in a 1.5 T B0 field

0 degrees with respect to Bo field

Titanium

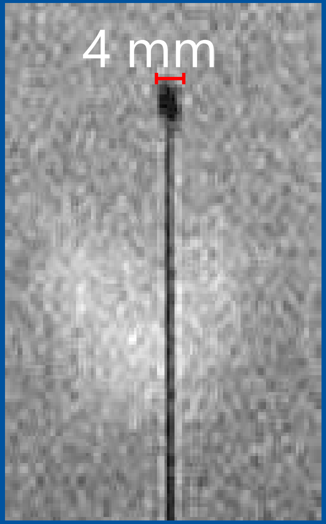

Stainless steel

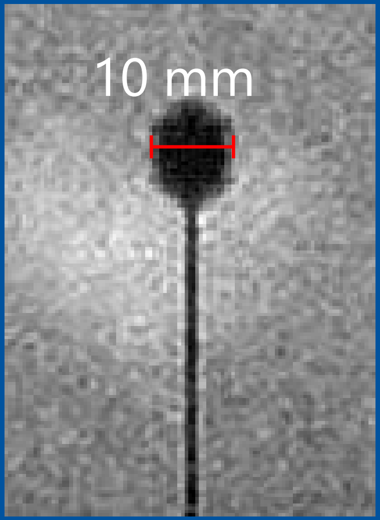

Plastic

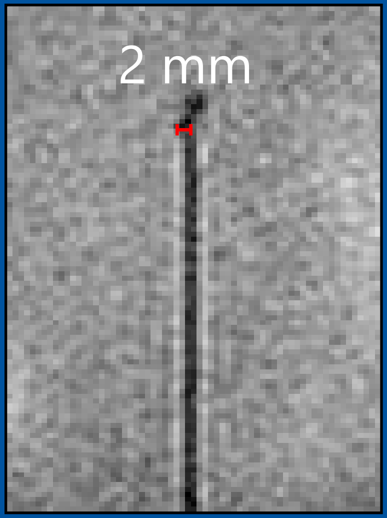

40 degrees

Titanium

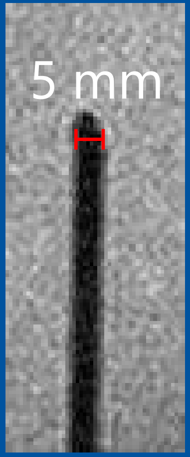

Stainless steel

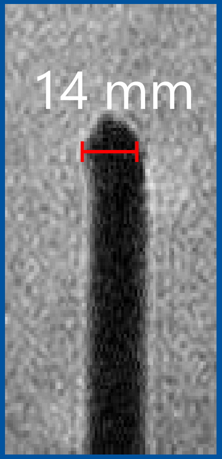

Distortions depend on material, shape and orientation

Summary 1

- Many reasons exists for artifacts in images
  - Erroneous sampling of k-space
    - Aliasing
    - Ringing
  - Magnetic field errors
    - Gradient artifacts
    - Susceptibility artifacts
    - Water-fat shift

- Geometrical artifacts show up in a particular direction
  - Phase encoding direction: aliasing
  - Read-out direction: susceptibility, water-fat shift

- Dephasing results in signal loss in gradient echo sequences

Summary 2

- Characterizing geometrical distortions can be done with a phantom
  - Avoid inducing additional susceptibility artifacts
  - Distortions depend on specific sequence

- Geometrical accuracy tends to deteriorate towards the body contour and tends to be good in the center of the body
  - Localization of external markers may be inaccurate

- Many possibilities exist to avoid artifacts or to minimize their impact. It is important to be aware of possible artifacts

‘Every drawback has a benefit’

Artifacts are often exploited to create new contrast mechanisms

Artifact	MRI technique
Susceptibility	Dynamic Susceptibility Contrast MRI
	Blood Oxygen Level Dependent (BOLD) MRI
Water-fat shift	DIXON (separation of water and fat imaging)
	MRI spectroscopy
In-flow artifacts	MR angiography
….	

Acknowledgments

Thanks for many slides and help in preparing these lectures:

- Gary Liney
- Rien Moerland
- Alexis Kotte
- Marielle Phillipens

Positron Emission Tomography

Physics – Image Reconstruction, Contouring

ESTRO Teaching Course on Advanced Imaging Technologies

September 18 - 22, 2016 in Florence, Italy

Daniela Thorwarth
Section for Biomedical Physics,
University Hospital for Radiation Oncology, Tübingen

Eberhard-Karls-Universität
UKT
Universitätsklinikum Tübingen

PET Image Formation

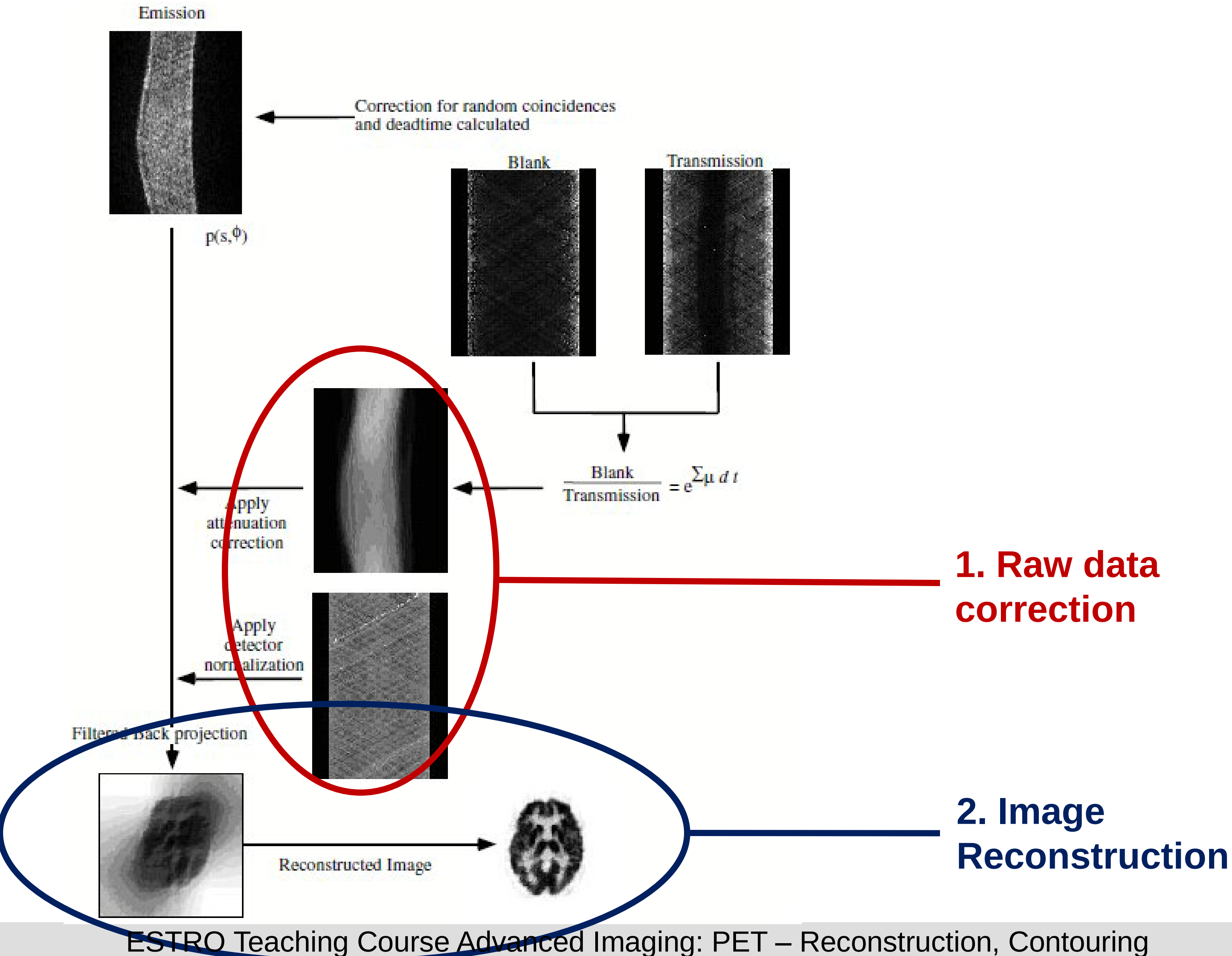

Random Correction

- Randoms: $R_{ab} = 2\tau \cdot N_a N_b \propto N^2$

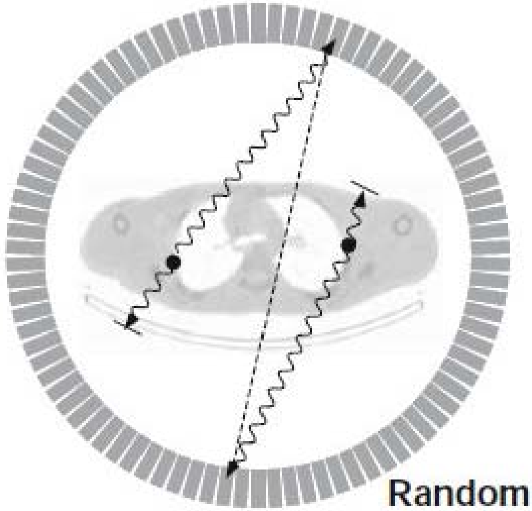

<u>*Correction Methods:*</u>

- Tail Fitting
  - Estimate random distribution in the object by fitting the tails outside the object
- Estimation from Single Rates
  - Direct determination from single rates N_a and N_b
- Delayed Coincidence Channel Estimation
  - Data stream containing signals from one channel is delayed for several times the coincidence window
  - Removal of all annihilation events
  - Any coincidences detected are random
  - Subtraction from coincidences in the prompt channel

Normalization

- LORs have different sensitivities
- Individual correction factor for each LOR

Correction Methods:

- Direct Normalization
  - Illumination of all possible LORs with planar or rot. line source
  - Long scan times necessary
  - Sources must have very uniform activity distribution

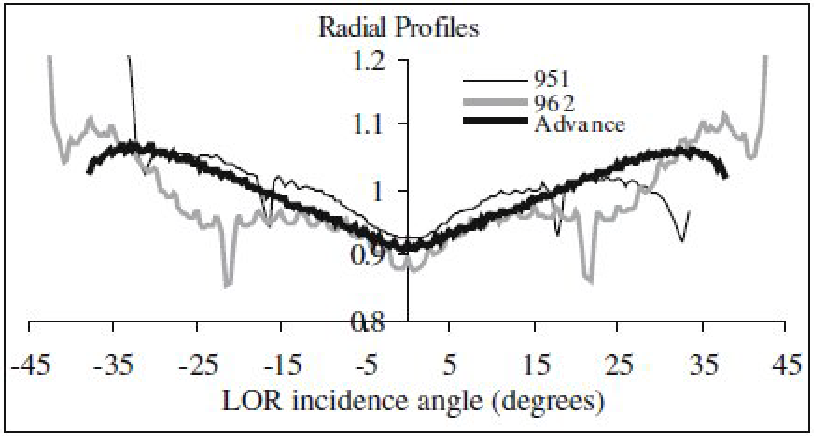

Mean radial geometric profiles for three block-detectors. Asymmetry due to the fact that centre of rotation of sources not coincident with center of detector ring (from [2]).

- Component-based Model for Normalization

Dead Time Correction

- Measurement of dead time with 'decaying source'
  - Uniform source (^{18}F, ^{11}C) of known activitiy
  - Measurements of singles, prompt and random coincidence rates

- Construction of look-up tables for dead time correction factors

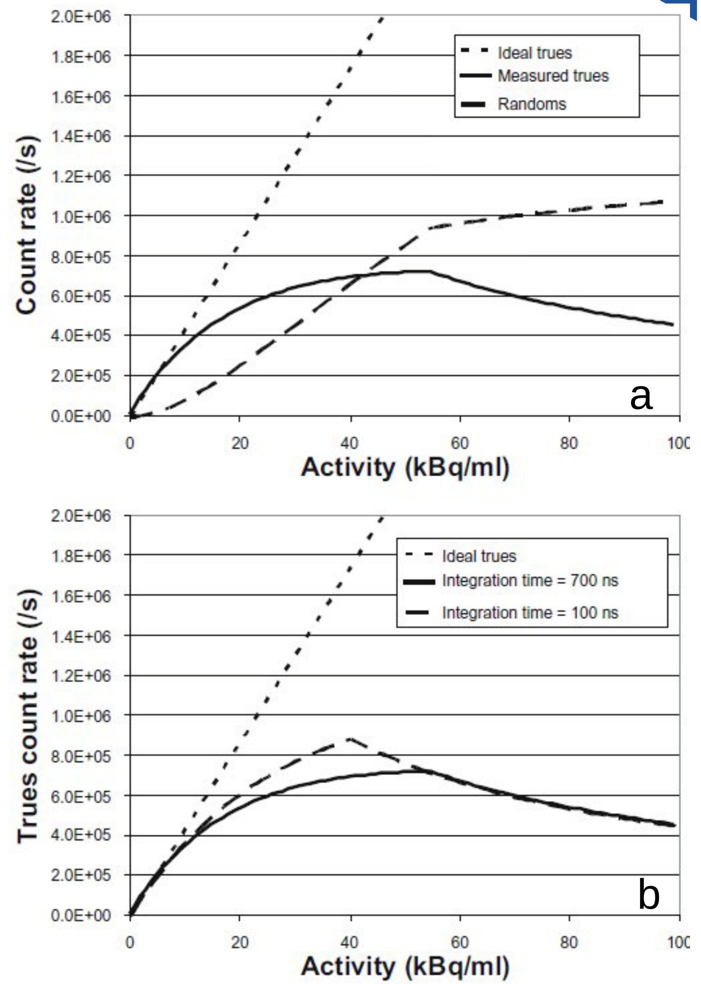

(a) Effect of dead time on count rate linearity.
(b) Effect of shortening the signal integration time (from [2]).

Scatter Correction

- Most likely: Compton scattering
- Compton equation $$E_{sc} = \frac{E}{1+\frac{E}{m_0c^2}(1-\cos\Omega)}$$
  - Relates photon energy before (*E*) and after scattering (E_{sc}) to scattering angle *Ω*
  - m_0c^2: resting energy of electron before scattering

<u>*Correction strategies:*</u>

- Fitting scatter tails
- Direct measurement
- Dual energy window methods
- Multiple energy window methods
- Simulation-based methods

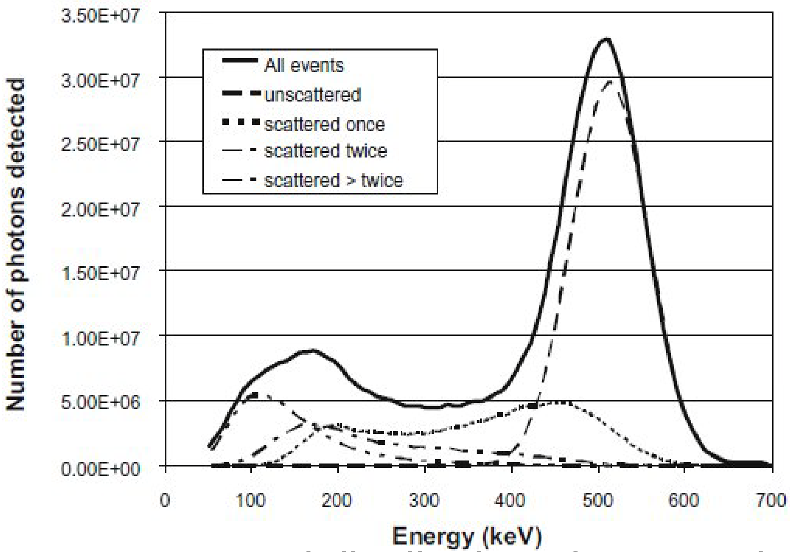

Spectral distribution of scattered 511 keV photons [2].

Improved image quality due to random and scatter correction

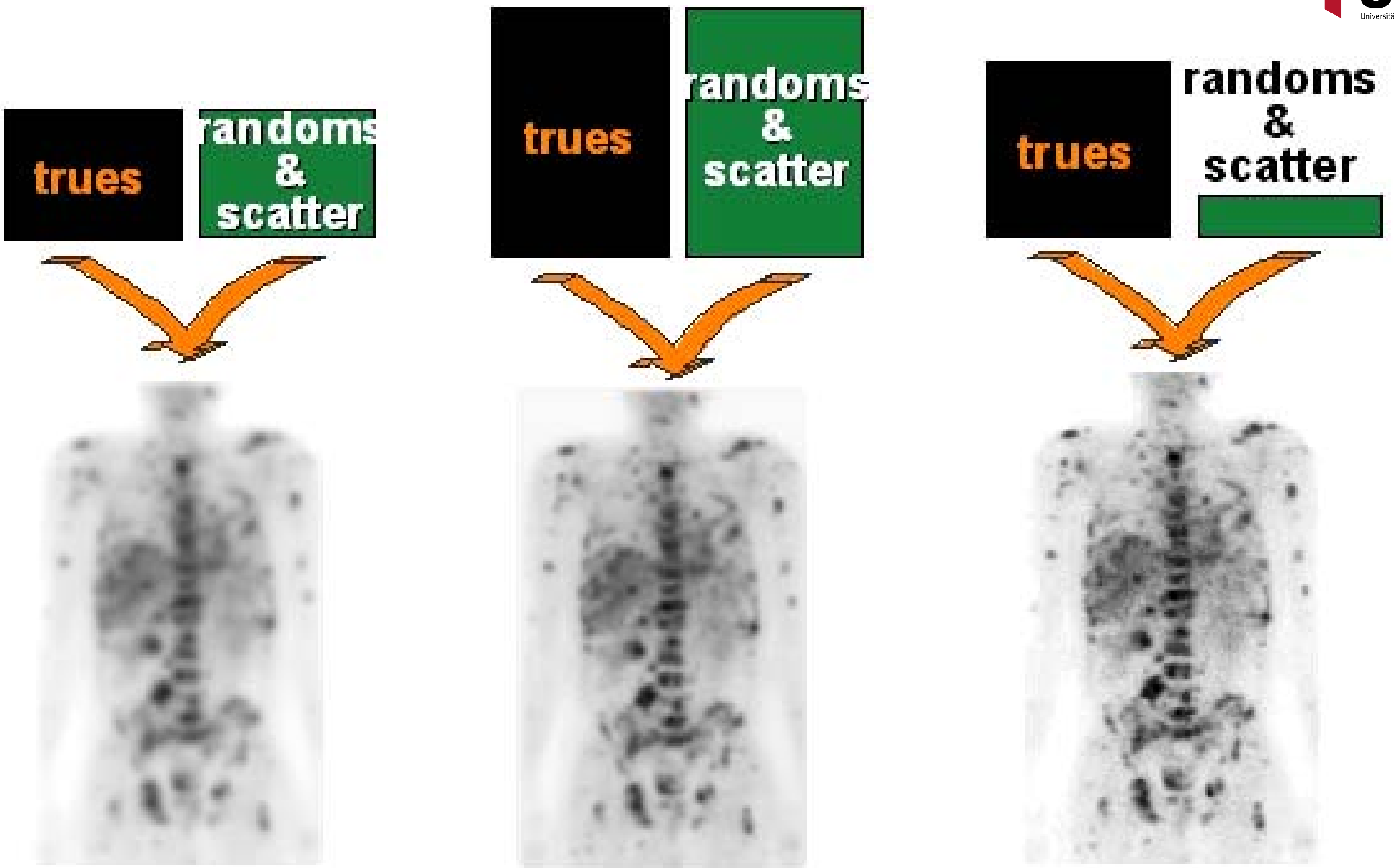

Attenuation Correction

Probability P_1 for quant γ_1 to reach a detector:

$$P_1 = k_1 \cdot e^{-\int_{x}^{x_O} \mu(x)dx}$$

Accordingly P_2 for quant γ_2:

$$P_2 = k_2 \cdot e^{-\int_{x_u}^{x} \mu(x)dx}$$

Probability for a coincidence event:

$$P_{tot} = P_1 \cdot P_2 = k_1 \cdot k_2 \cdot e^{-\int_{x_u}^{x_O} \mu(x)dx}$$

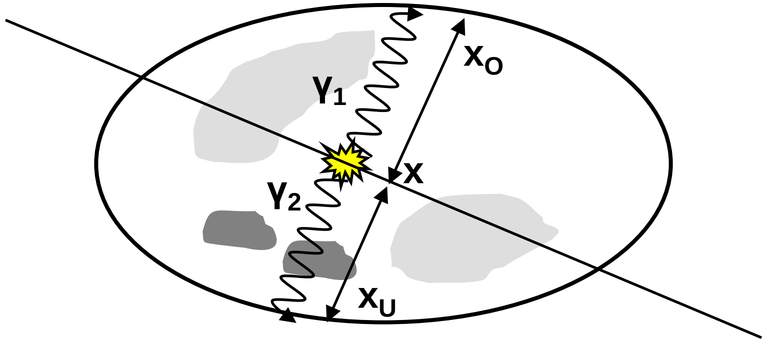

Accurate attenuation correction is possible if the line integral $\int_{x_u}^{x_o} \mu(x)dx$ can be obtained from a transmission measurement.

CT is used for attenuation correction!

CT-based attenuation correction

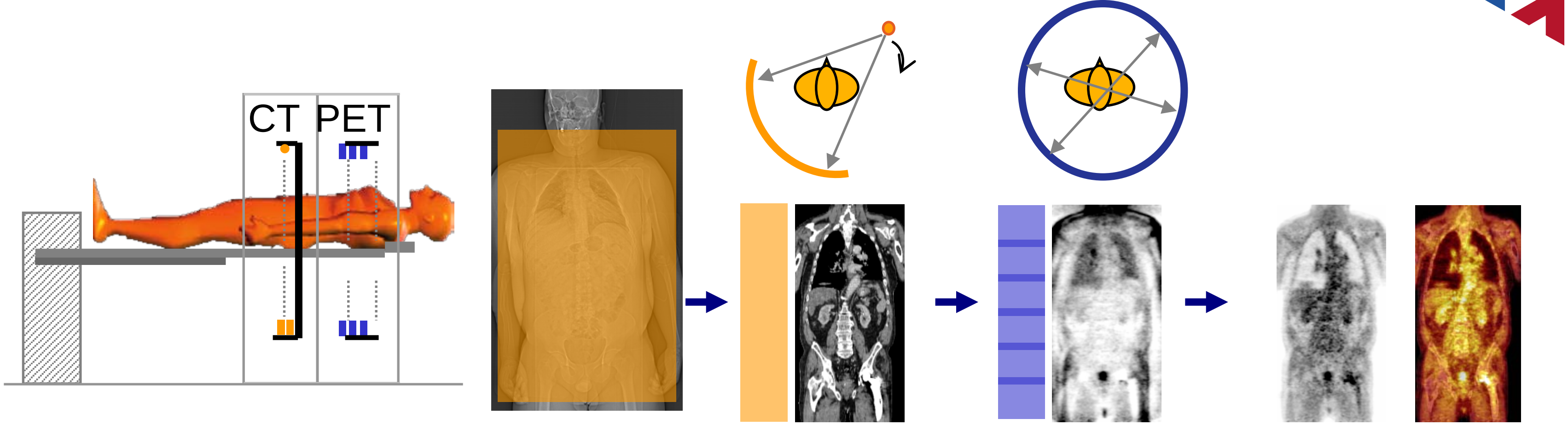

(a) $^{68}Ge/^{68}Ga$ positron source (b) ^{137}Cs gamma-ray source (c) 120 kVp x-ray source

CT-transmission imaging: fast, low noise, not affected by emission.

Kinahan et al, Sem Nucl Med 2003.

Artifacts due to CT-based attenuation correction

Breathing…

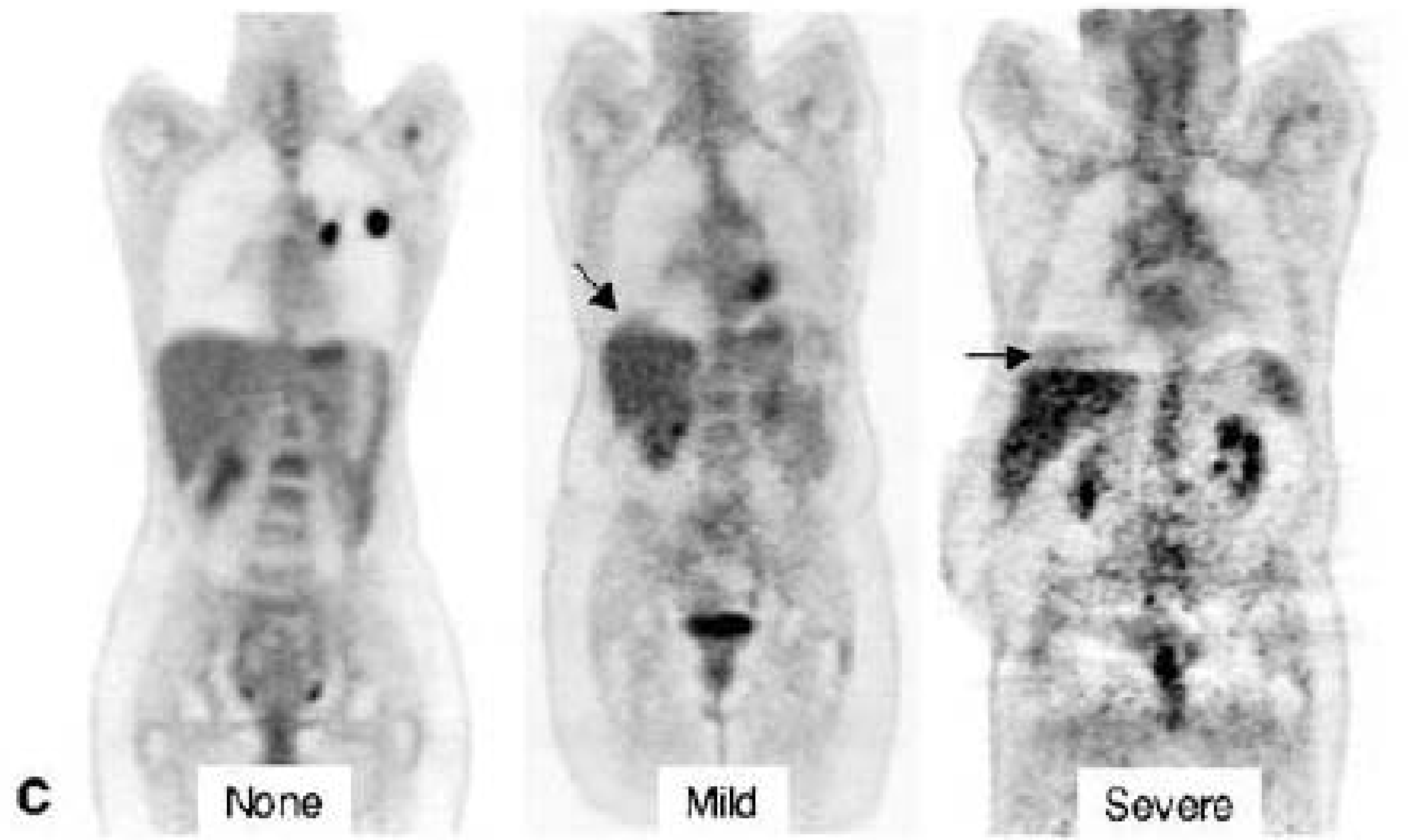

Beyer et al, EJNMMI 2005; 32: 1429-1439.

...and their consequences

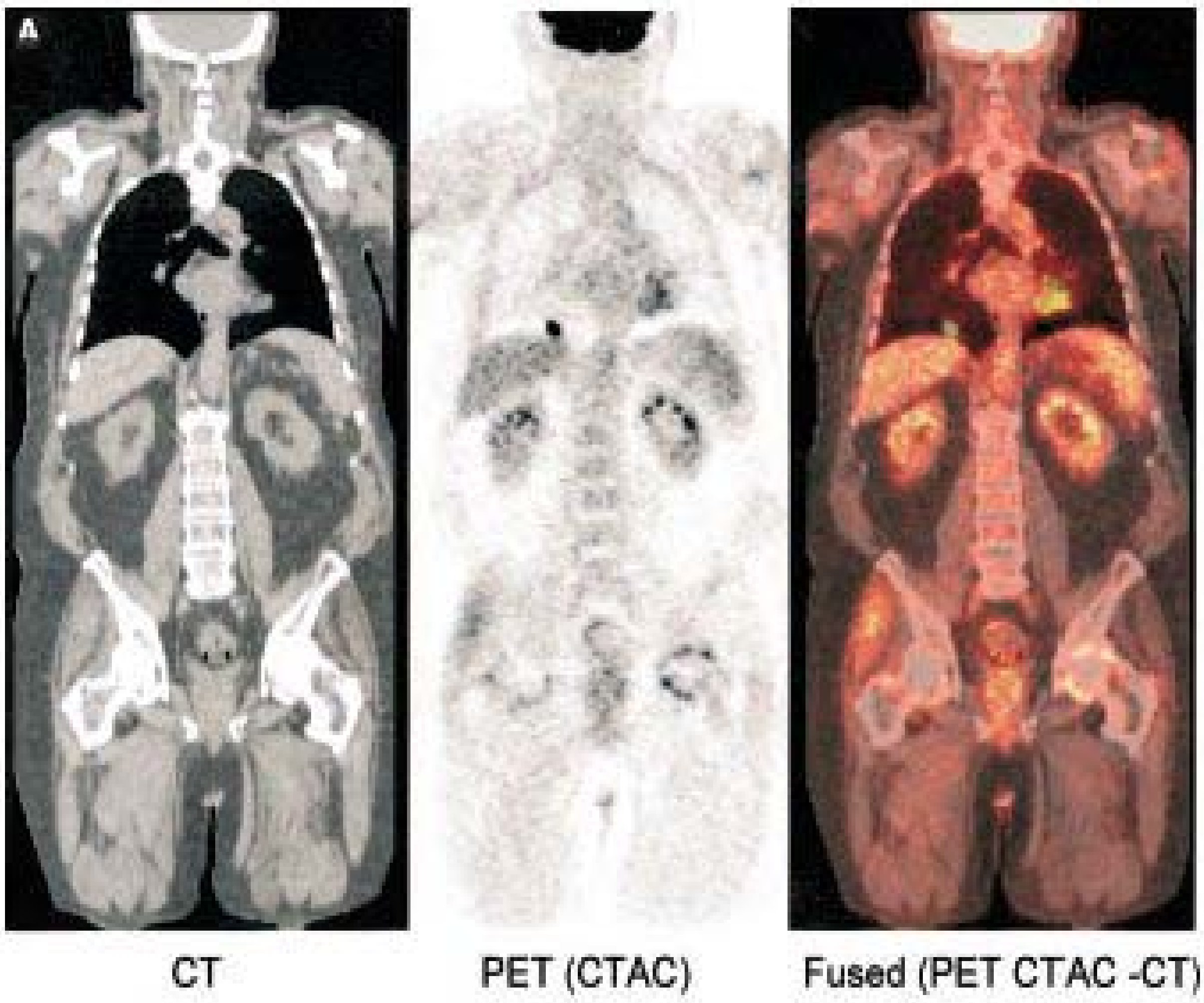

Osmann et al, JNM 2003; 44: 240-243.

FIGURE 2. Coronal (A) and transaxial (B) PET/CT fusion images of 70-y-old man with colon cancer and MRI-proven liver metastases (arrow) but no lung lesions. Lesion is seen in right lung base, but no lung lesion is seen on CT; on both NAC and GeAC images without CT fusion, lesion was correctly localized to liver. Fused (PET CTAC-CT) – PET CTAC fused with CT; fused (PET GeAC-CT) – PET GeAC fused with CT.

4D-PET/CT

- Respiratory organ or lesion motion induces degradation effects on PET/CT data
- 4D-PET/CT acquisition improves image quality and quantitative accuracy

Breathing Signal:

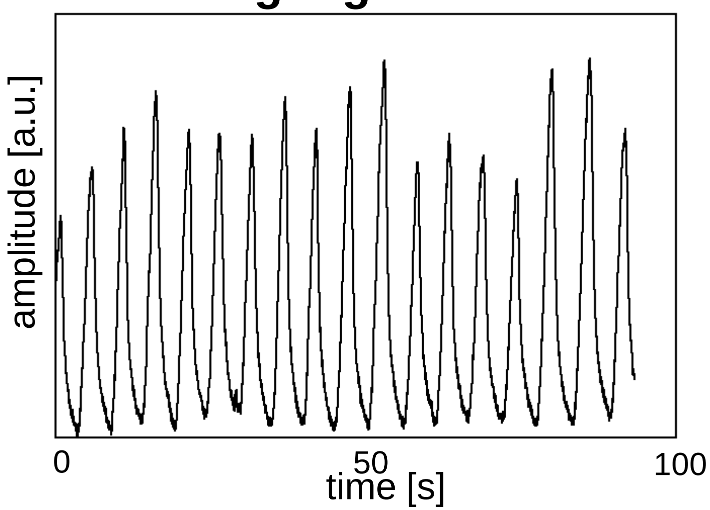

PET acquisition time:

$$T = N_p \cdot t$$

- Respiratory monitoring synchronized to 4D-PET and 4D-CT
  - Pressure sensor
  - Spirometry system, …
- 4D-PET
  - Preferentially recorded in 3D mode
  - data sorted into different phases of the breathing cycle
    - Prospective sorting
    - Retrospective (list mode acq.)
- 4D-CT for phase-sensitive attenuation correction!

4D-PET/CT vs. 3D-PET/CT

Aristophanous et al, IJROBP 2012; 82(1): e99-105.

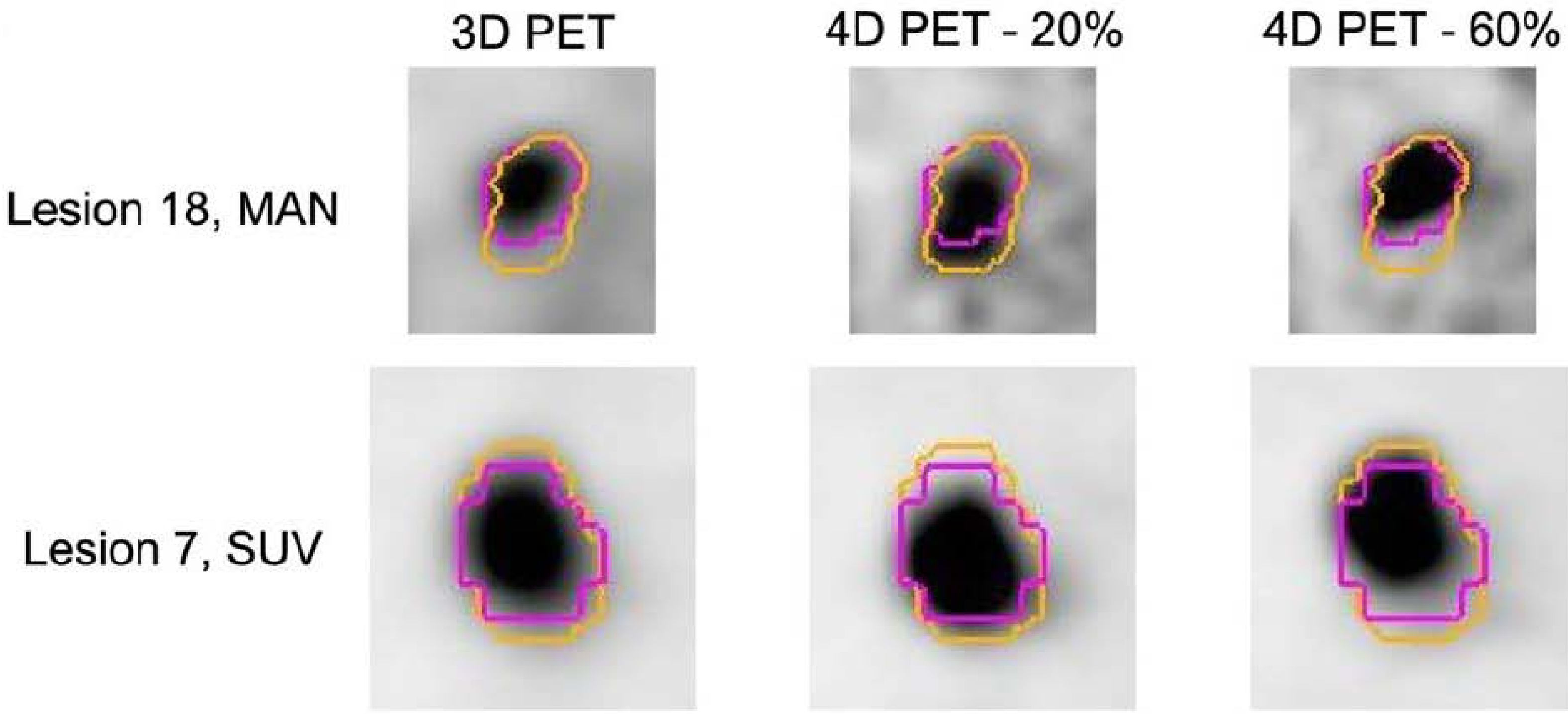

- Comparison of PET-based GTV contouring on 3D- vs. 4D PET (different phases: 20%, 60%)
- RT volumes contoured on 4D-PET (orange) were larger than 3D-PET volumes (pink)

Image Reconstruction

sinogram ***Reconstructed image***

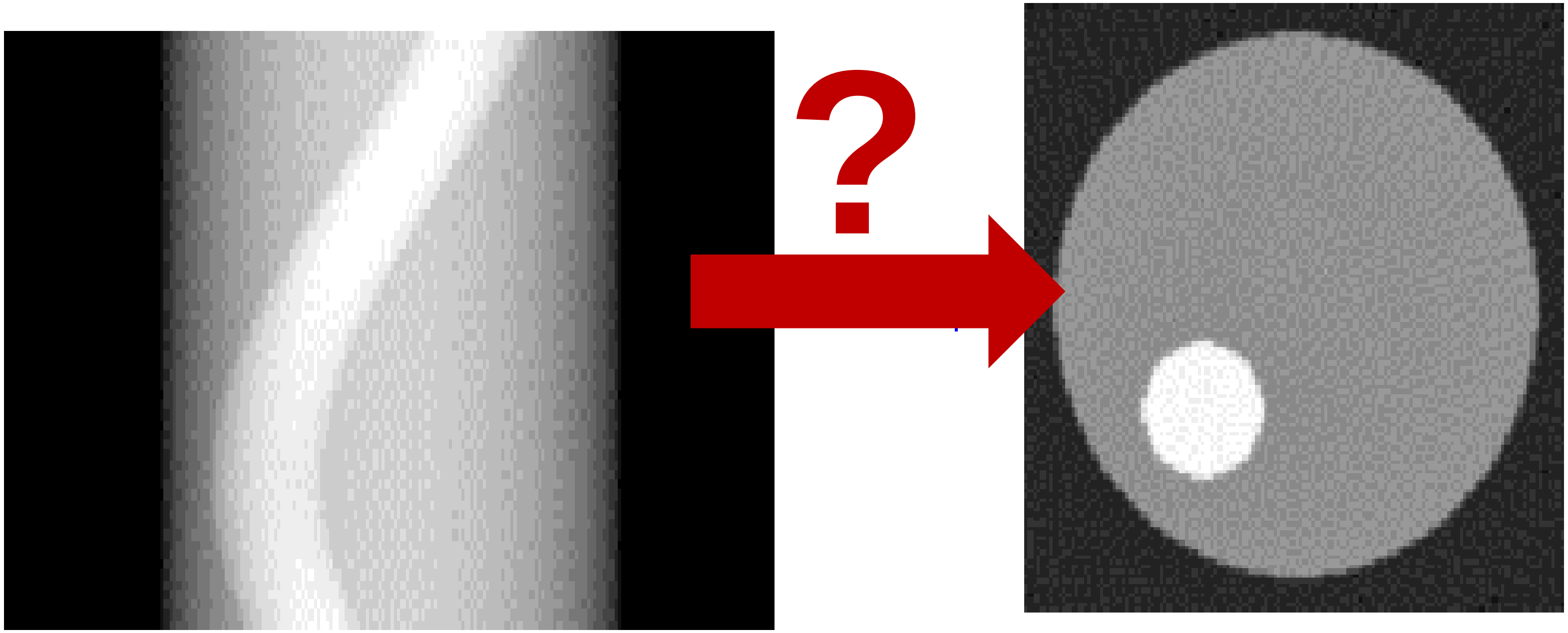

1. Filtered Backprojection
2. Iterative Reconstruction Methods

Analogue to CT reconstruction: Filtered Backprojection

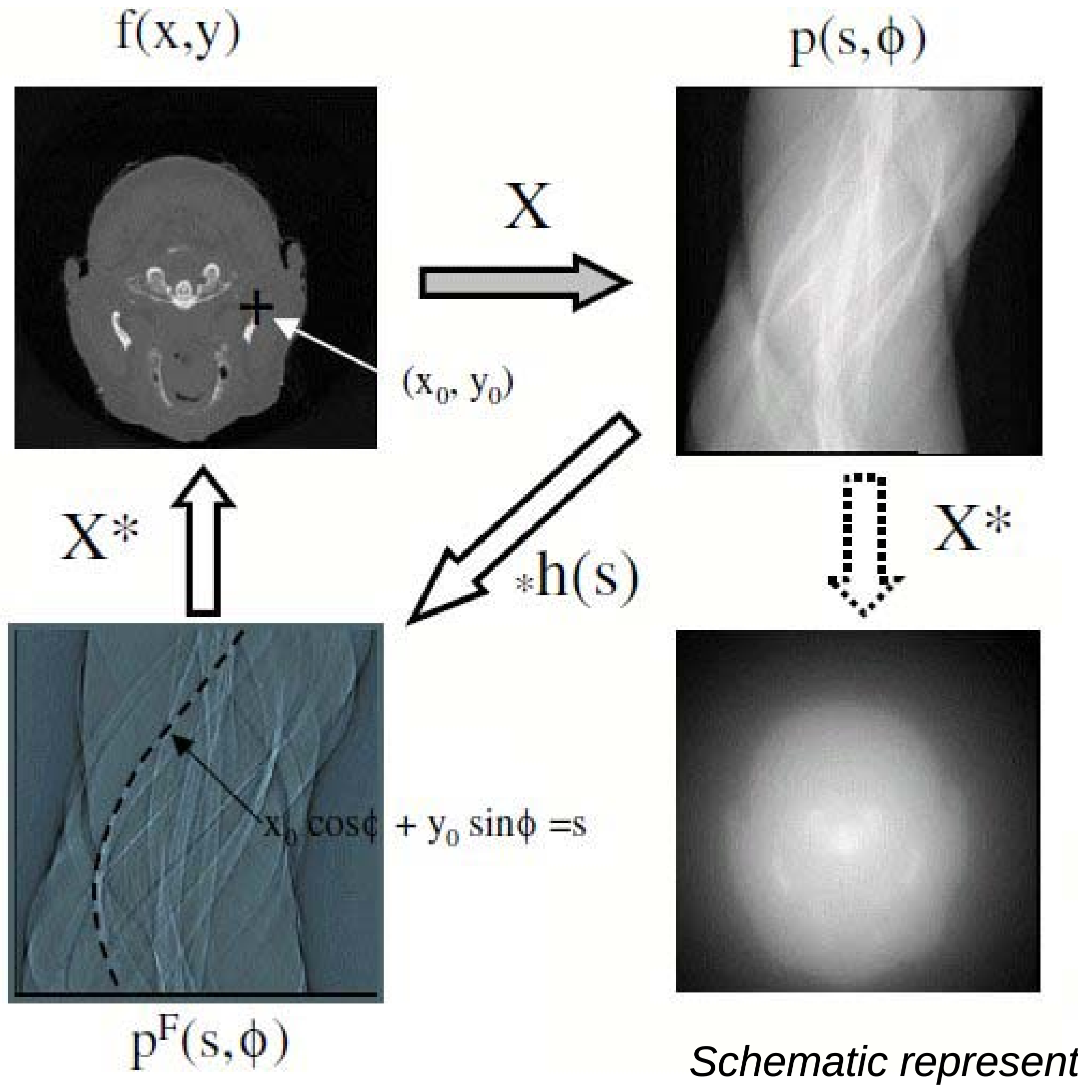

Schematic representation of FBP [1].

- Works well for lower noise environment of brain
- Not optimal for whole-body imaging

Fourier Slice Theorem

The Fourier transform of the projection equals the Fourier transform of the density distribution along a line in polar coordinates.

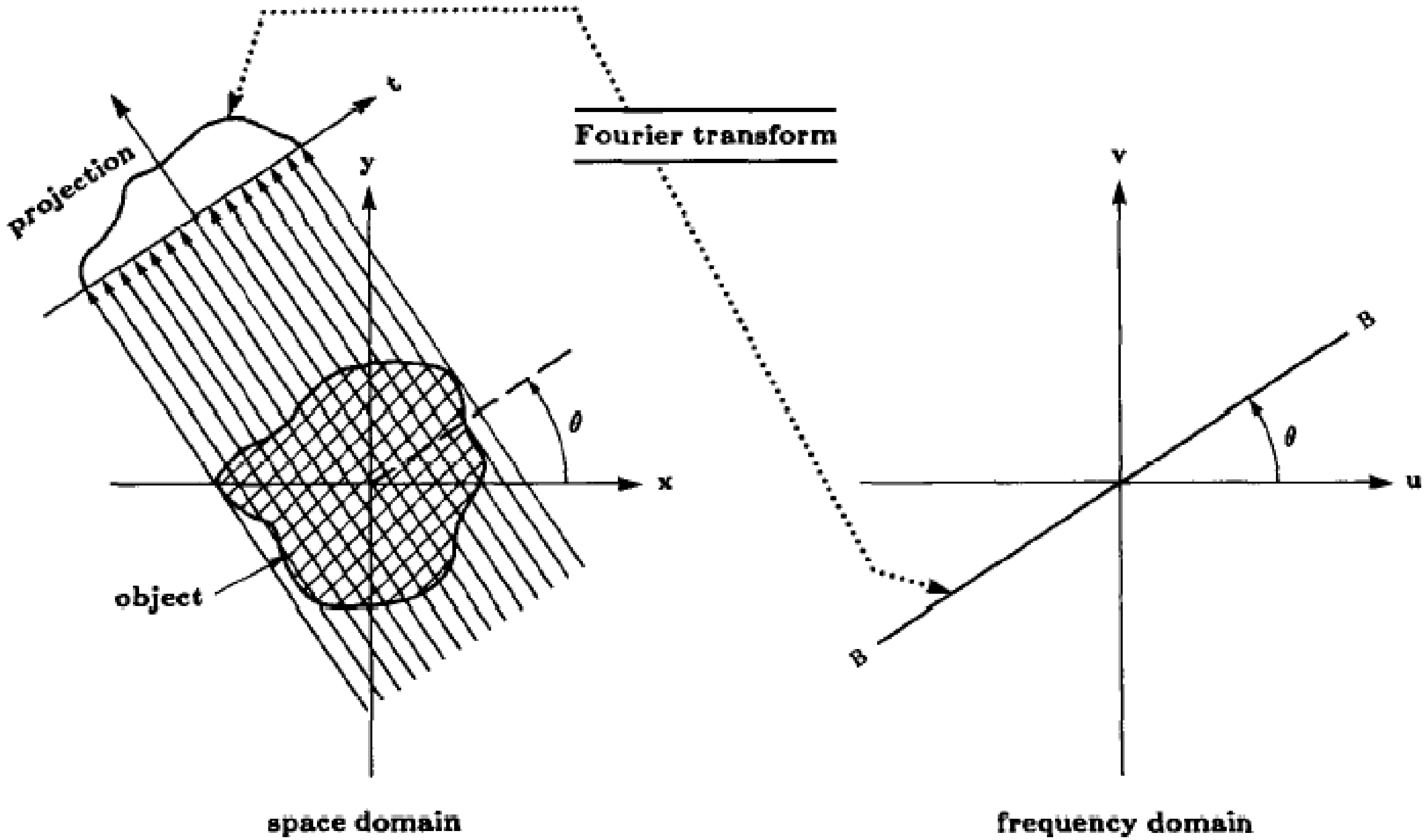

Filtered Backprojection (FBP)

Projection:

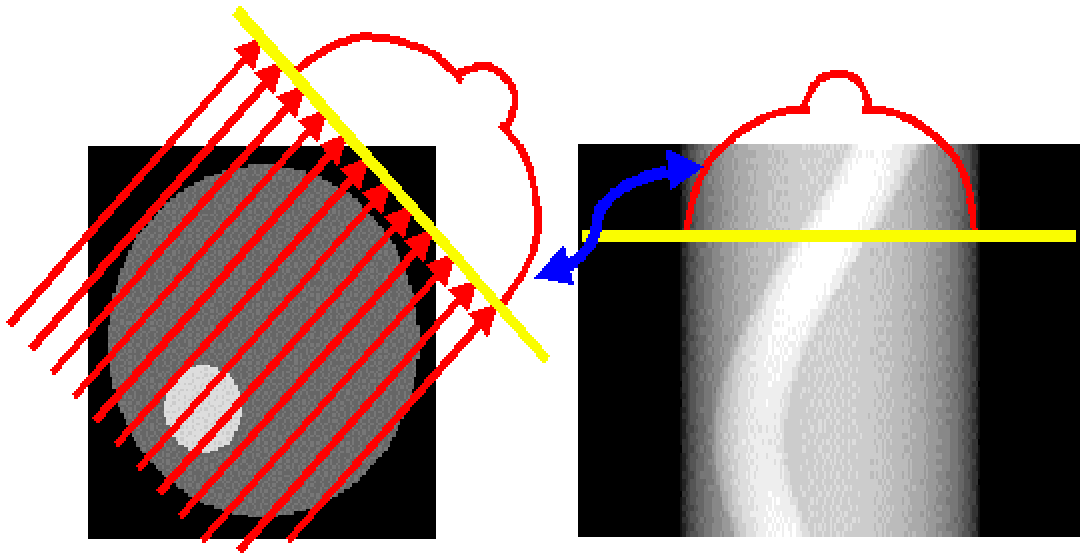

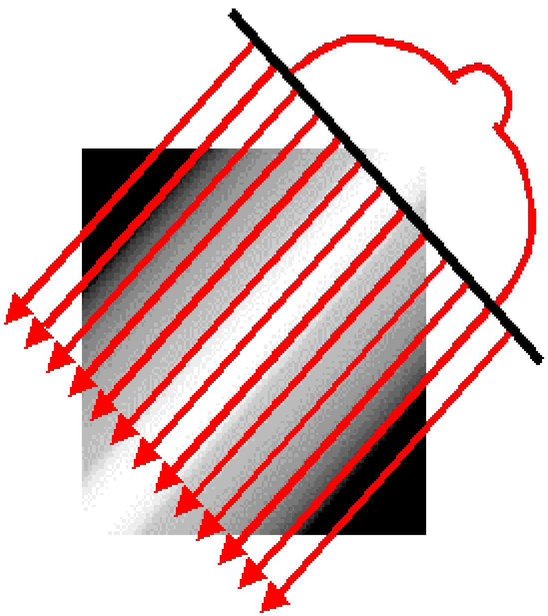

and Backprojection

Note: Blurring effect of line integration!

Filtered Backprojection FBP

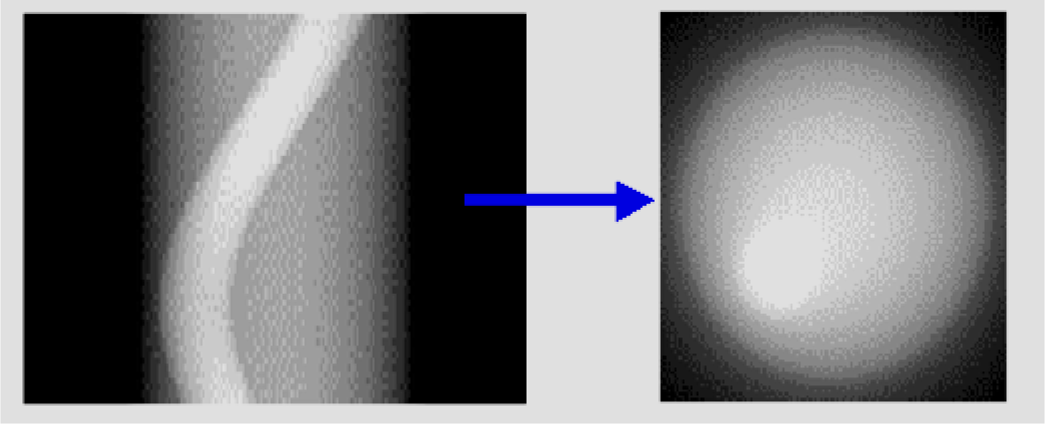

- Backprojection of all projections yields a blurred image.
- Unblurring Operation = convolution with an edge enhancing filter
- 1D-convolution of the sinogram with a ramp filter that enhances high frequencies (Linearity of projection operation allows to convolve projection data with a filter!)

Filtered Backprojection

To increase edge definition, the projections are convolved with an edge enhancement filter:

filtered Sinogram

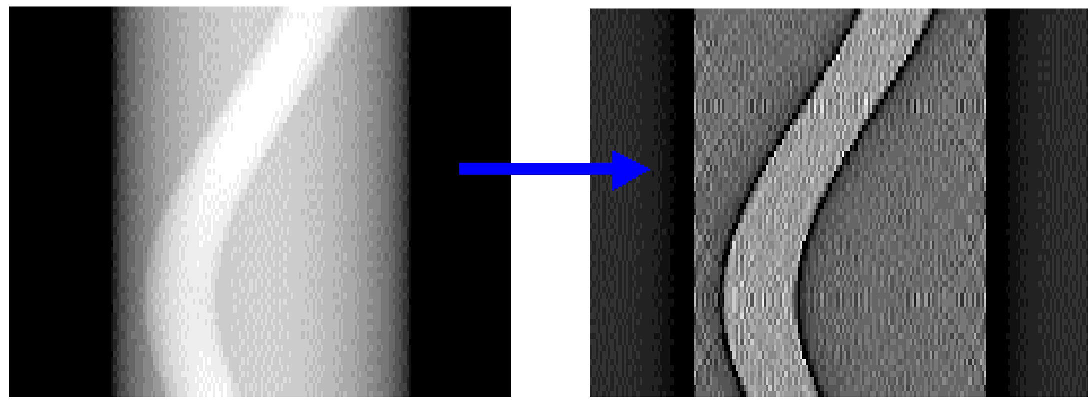

filtered Backprojection

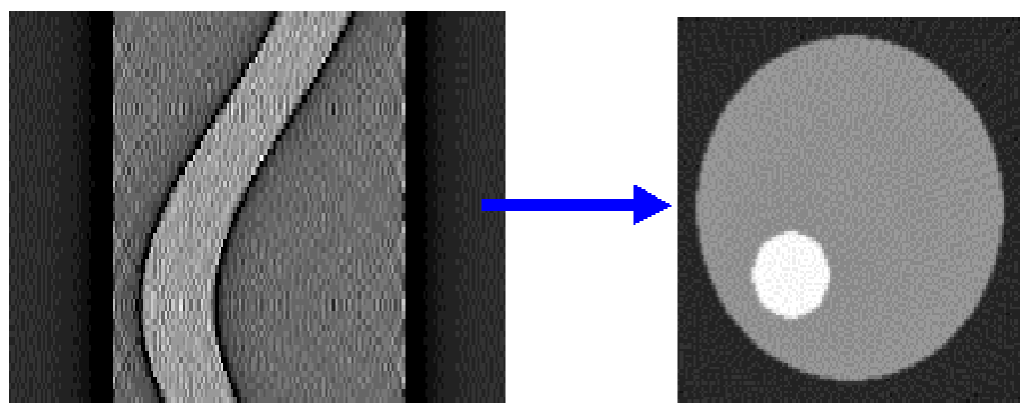

Iterative reconstruction: ML-EM

- Iterative reconstruction
  - Discrete representation of data and image
- **Expectation maximization (EM)** algorithm offers determination of **maximum likelihood (ML)** estimate of the image

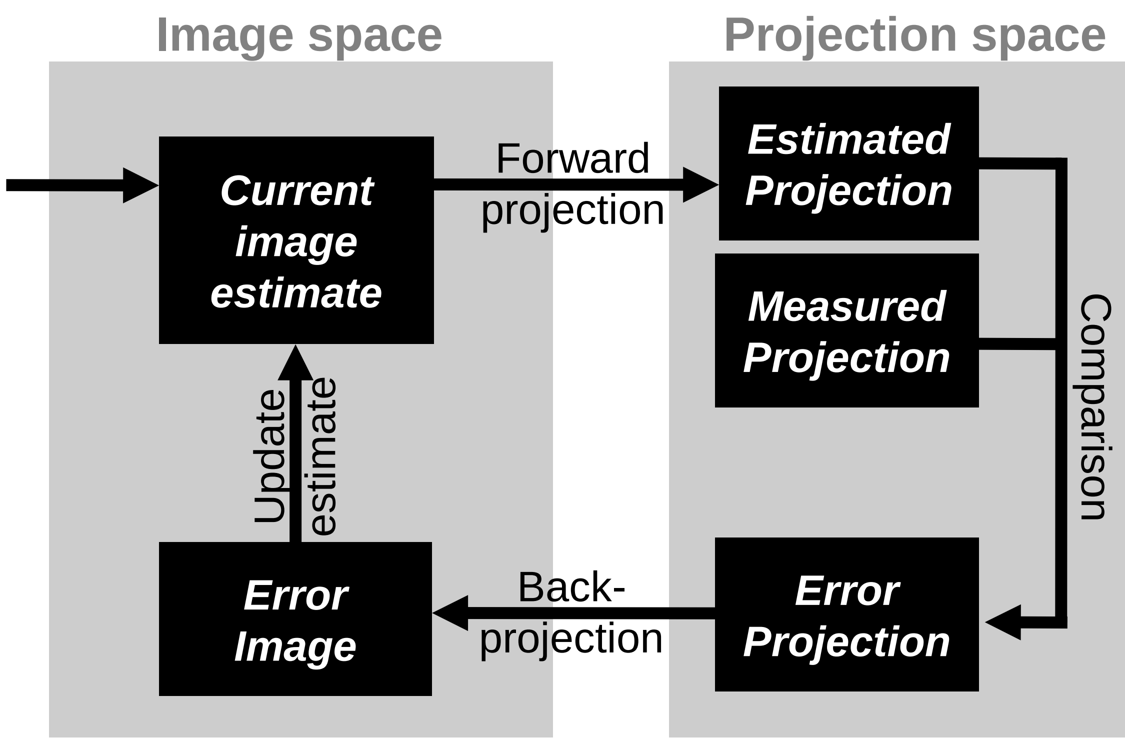

ML-EM: noisy data introduce instabilities

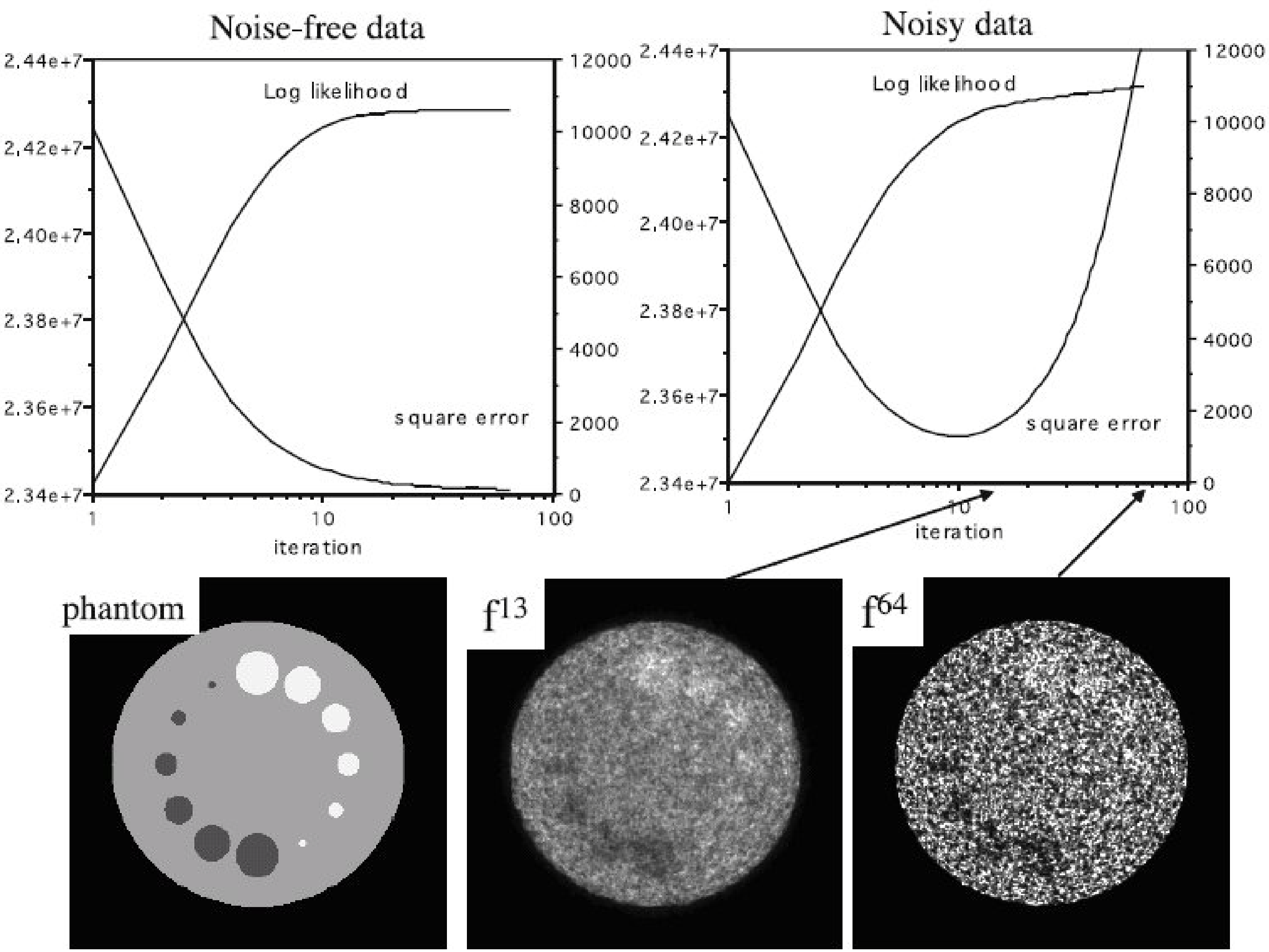

2D reconstruction of math. phantom with ML-EM. Poisson log-likelihood and square reconstruction error with regard to reference image versus number of iterations [1].

OSEM (ordered subset EM)

- Accelerated version of ML-EM
- LOR data are partitioned in *S* disjoint subsets

$$J_1, \ldots, J_S \subset [1, \ldots, N_{LOR}]$$

- Commonly, projections are divided into subsets with different views, or azimuthal angles
- ML-EM algorithm for data from one subset only
- Each subset processed in well-defined order
- Convergence accelerated by factor ≈ *S*

OSEM (ordered subset EM)

image ***profile*** ***histogram***

2 iterations, **4 s**ubsets:

2 iterations, **8 s**ubsets:

4 iterations, **8 s**ubsets:

8 iterations, **8 s**ubsets:

8 iterations, **16 s**ubsets:

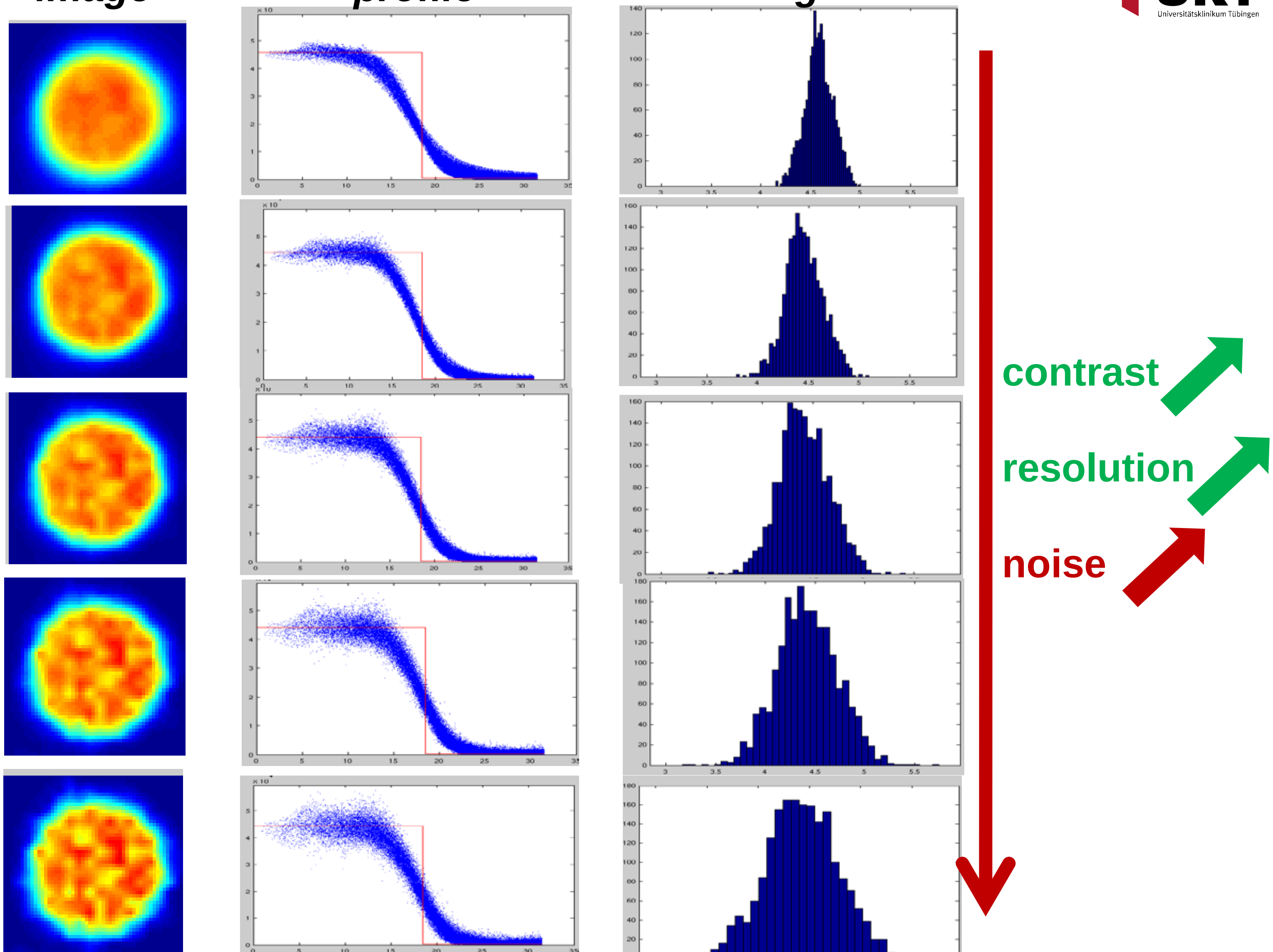

3D Iterative Reconstruction

- Fully 3D PET measurements and reconstruction
- Increasing computational demands
- Rebinning 3D data into 2D transaxial slices

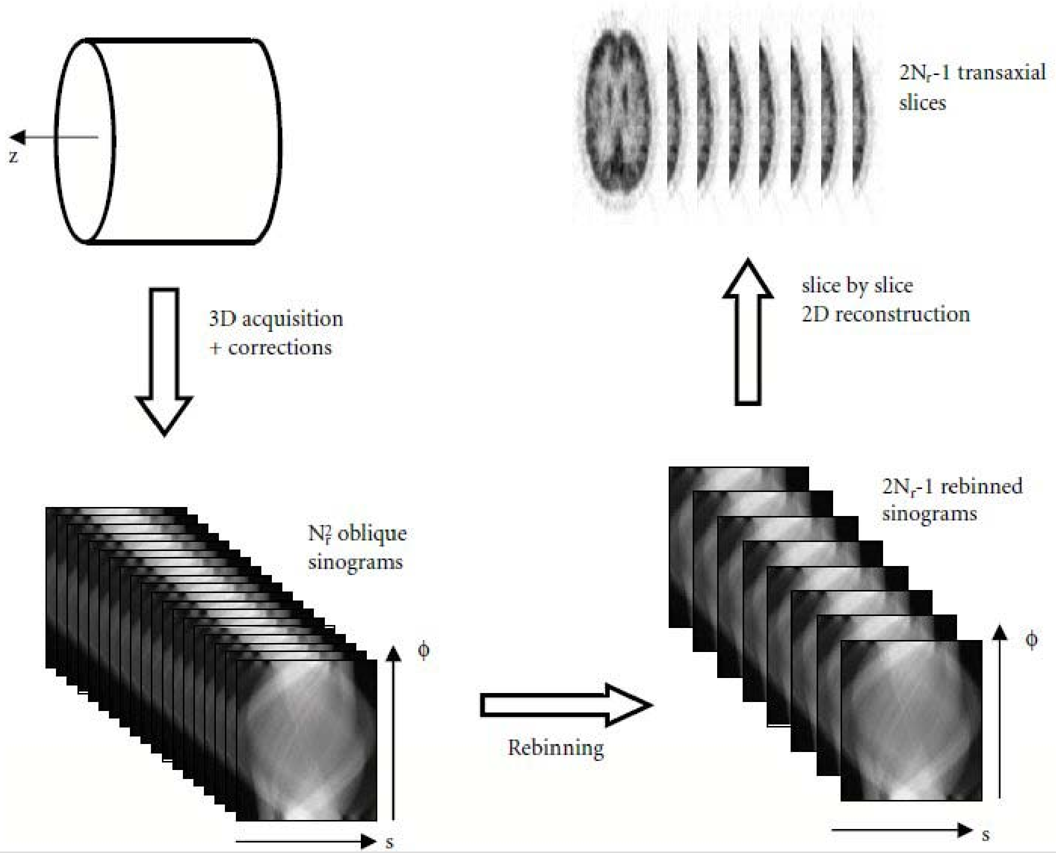

Time-of-Flight (TOF) PET

- Difference in flight time of photons is registered

$$\Delta t = \frac{2\Delta x}{c}$$

- Probability of event occurrence is limited to a certain area along the LOR

- Better SNR
  - Especially in the abdomen / heavy patients

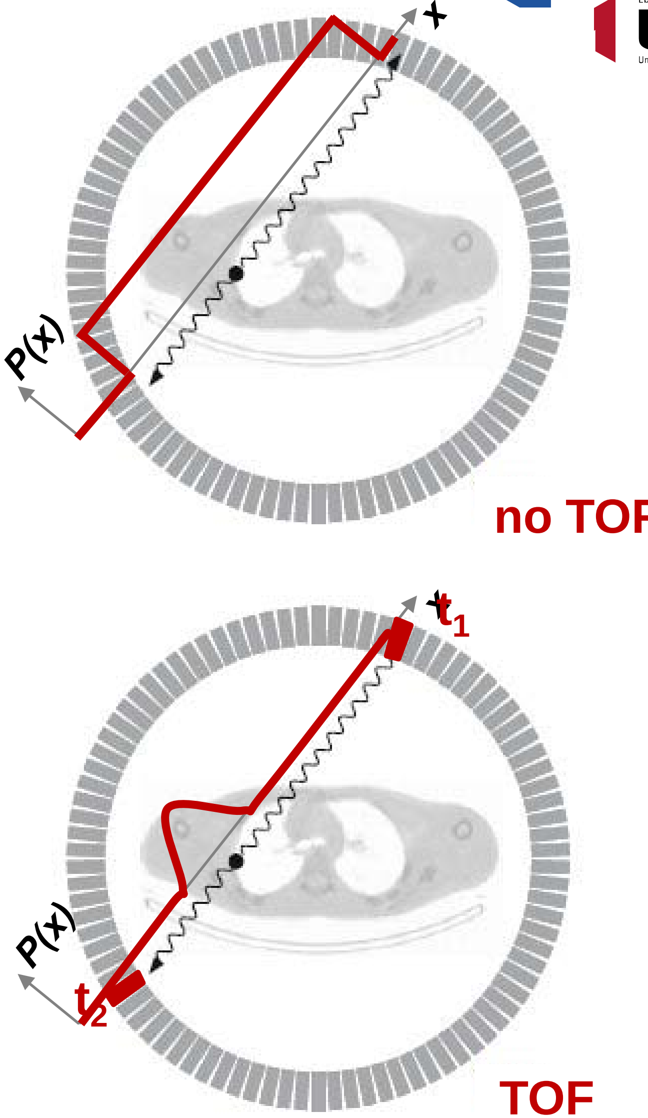

Resolution Modeling - PSF

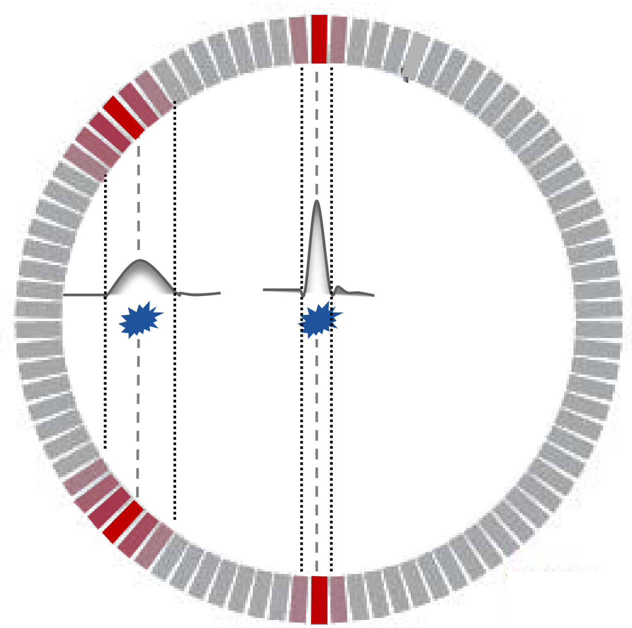

- Deconvolution of local **point-spread functions (PSF)** during iterative reconstruction
- Enhanced resolution
- Reduction of blurring and distortions

Iterative reconstruction with resolution modeling

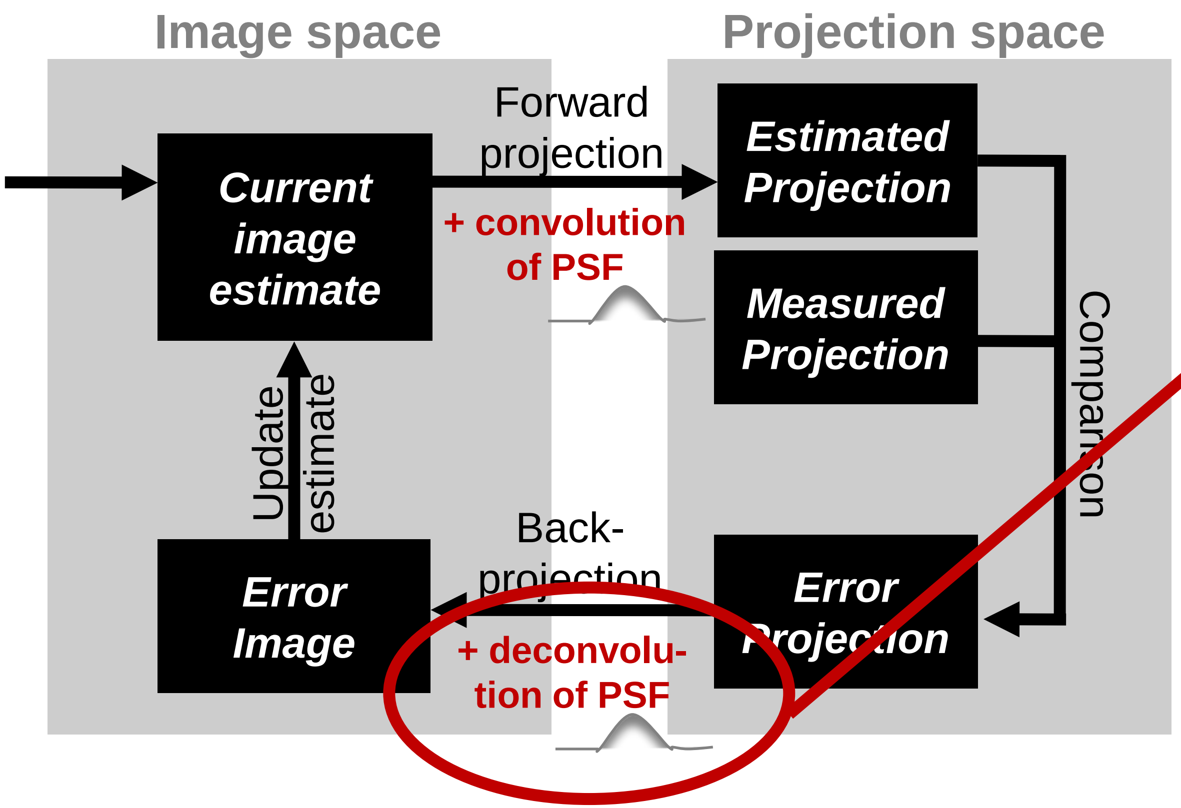

- May introduce Gibbs-artifacts
- Not necessarily activity conservation

Improvement of PET/CT Image Quality

[18F]-FDG PET study performed on a PET-only BGO system:

[18F]-FDG PET study performed on a state-of-the art PET/CT system:

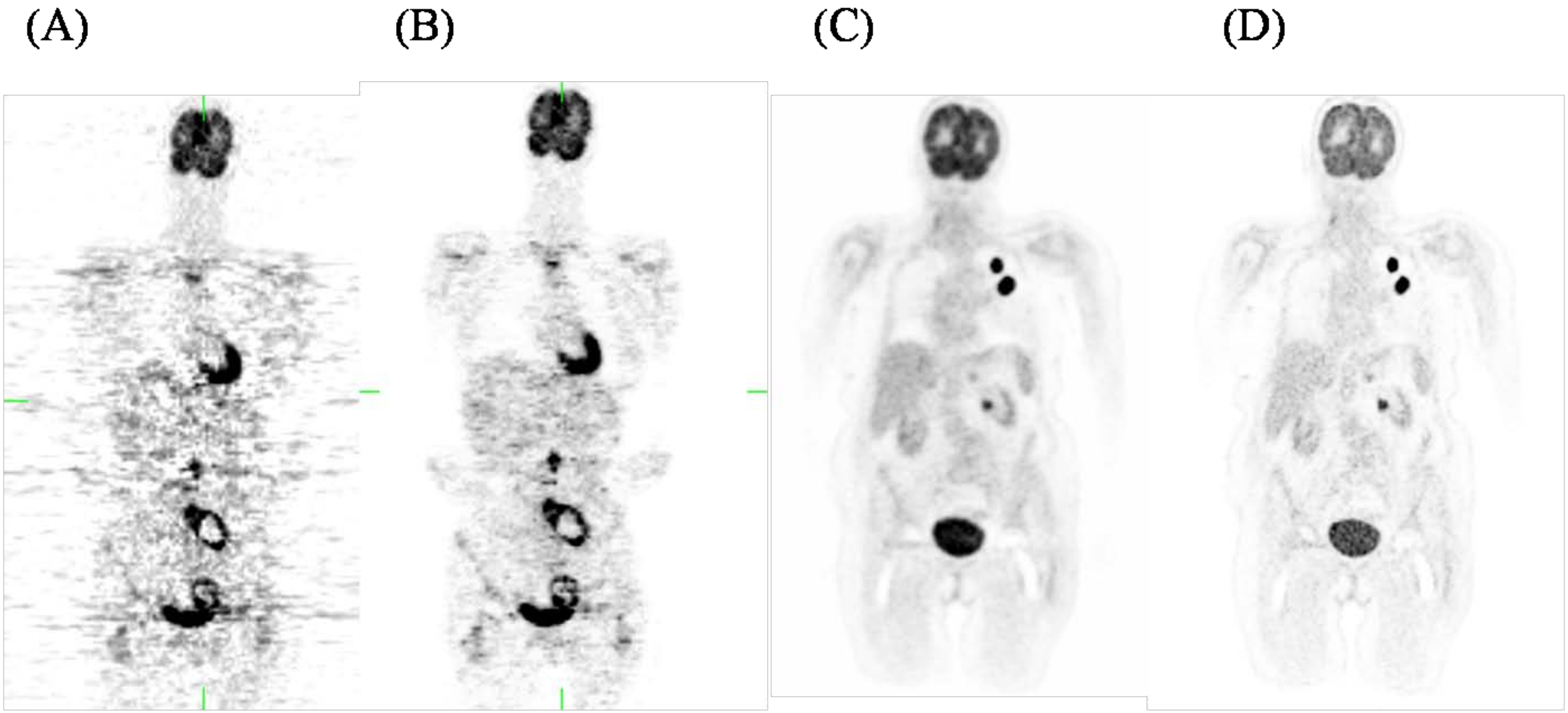

FBP Reconstruction

Iterative Reconstruction

Iterative Reconstruction

TOF+PSF Iterative Reconstruction

Coutesy R. Boellaard, Amsterdam

Summary: Reconstruction

- Today, iterative reconstruction (IR) algorithms are standard on all PET/CT systems
- Superior image quality when compared to filtered back projection
- Iteratively reconstructed images are characterized by
  - number of iterations and subsets
  - matrix and voxel size
  - image zoom
  - image smoothing, smoothing filter size or kernel (FWHM).
- IR methods employing a sufficient number of iterations and subsets to ensure sufficient amount of convergence are preferred.
- Reconstructed with and without AC recommended to allow inspection of AC artifacts.

Quantitative analysis of PET images

Tracer uptake is frequently quantified by the

Standardized uptake value (SUV)

$$SUV = \frac{C}{A} w$$

with *C:* tumor/voxel activity concentration [Bq/ml]

A: injected activity [Bq]

w: body weight [g]

!!! *SUV=1 means that the tracer is equally distributed in the whole body*

Radiotherapy target volume delineation (TVD) based on PET

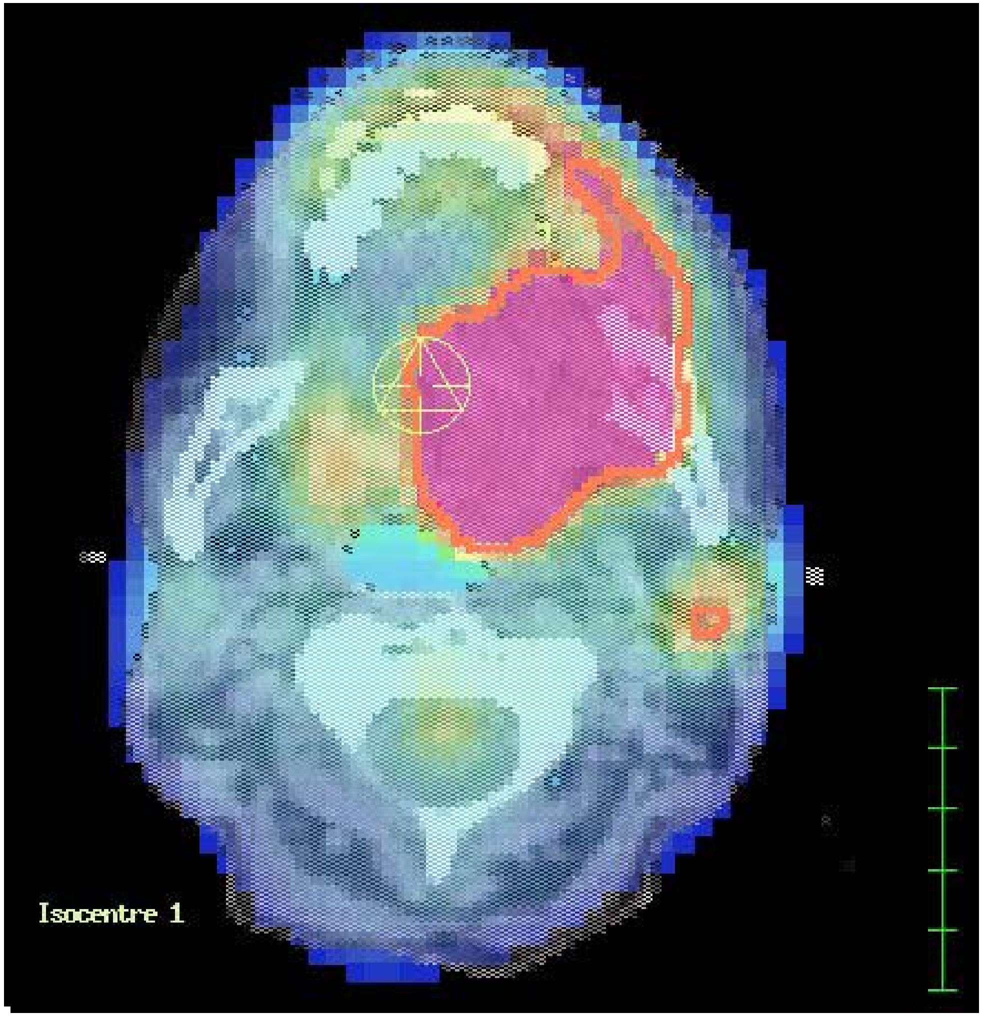

Floor of mouth carcinoma, 45 y, w

- Most commonly used for TVD: [^{18}F]FDG
- Image Registration / Patient Positioning very important issue
- **Which is the correct theshold to use?**

Absolute Thresholding

PET image

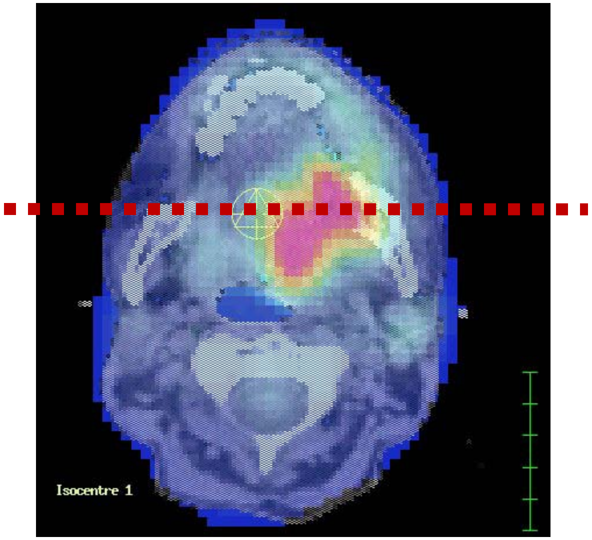

Line profile

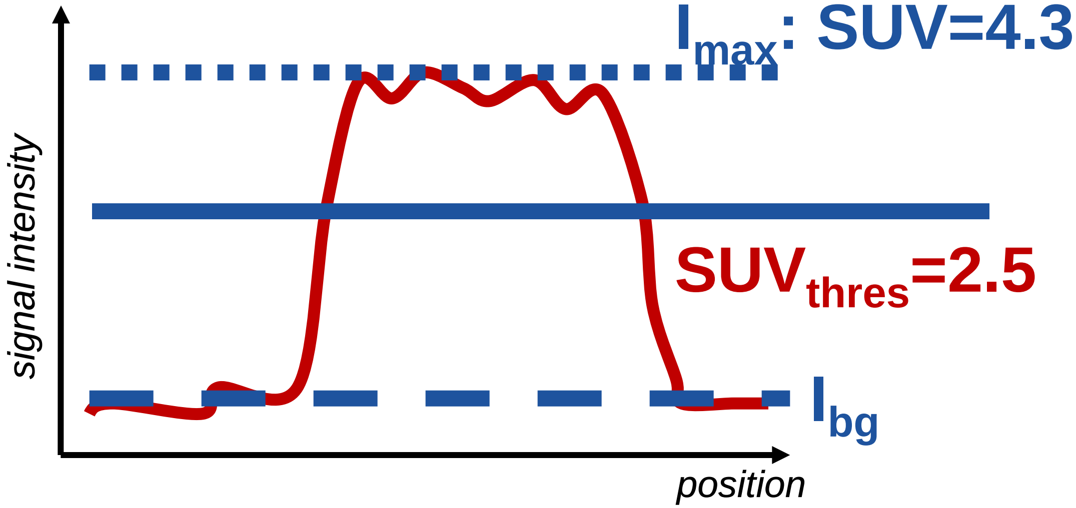

- Fix SUV-threshold of 2.0/2.5
- Easy to implement
- Often fails when the physiologic background activity lies above the threshold
- Absolute SUVs are strongly influenced by various technical factors (scan protocol, image acquisition, reconstruction, scanner calibration, etc.)

Relative Thresholding

PET image

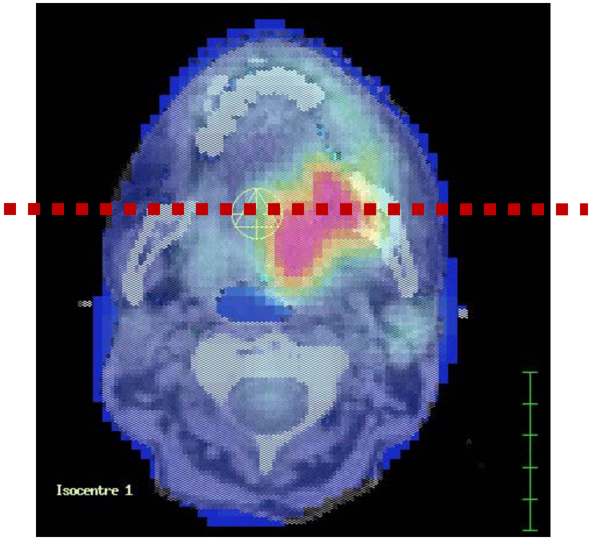

Line profile

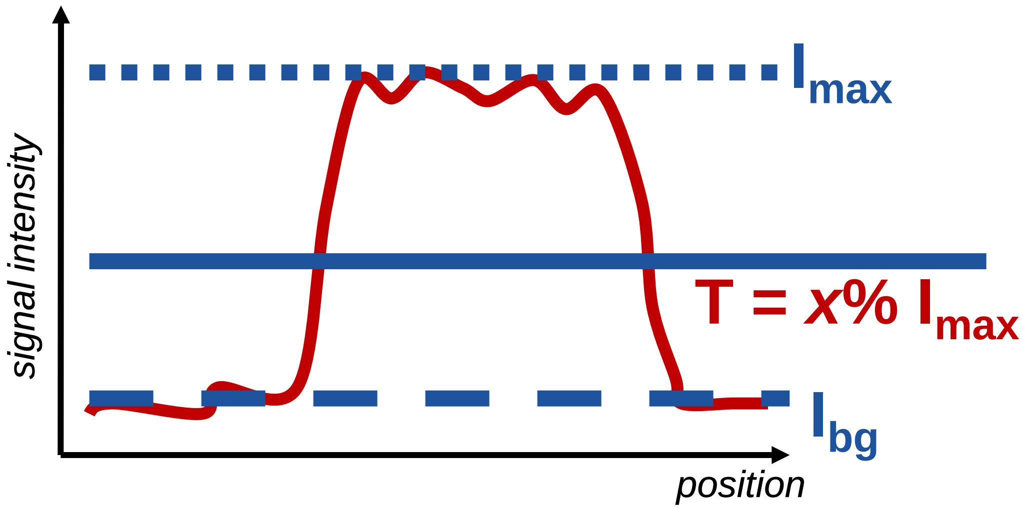

- Relative Threshold *T*, depending on the max. intensity
- Commonly used: *x*=42% (40-50%)
- Easy to implement
- Calibration with phantom measurements possible
- Frequently used in clinical routine

Iterative Thresholding

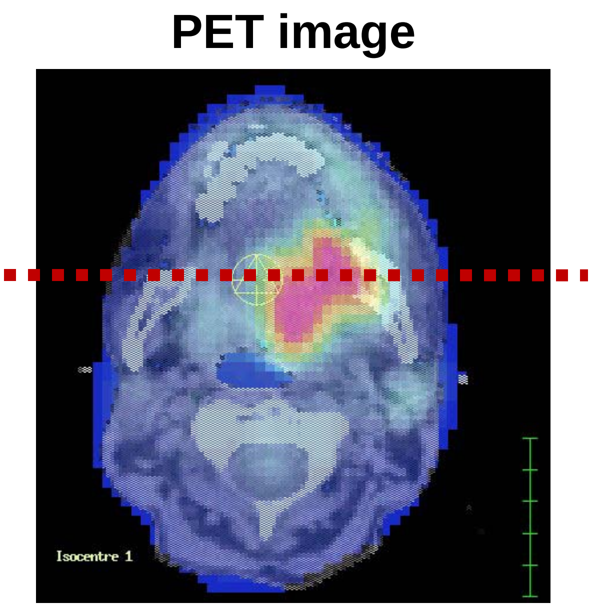

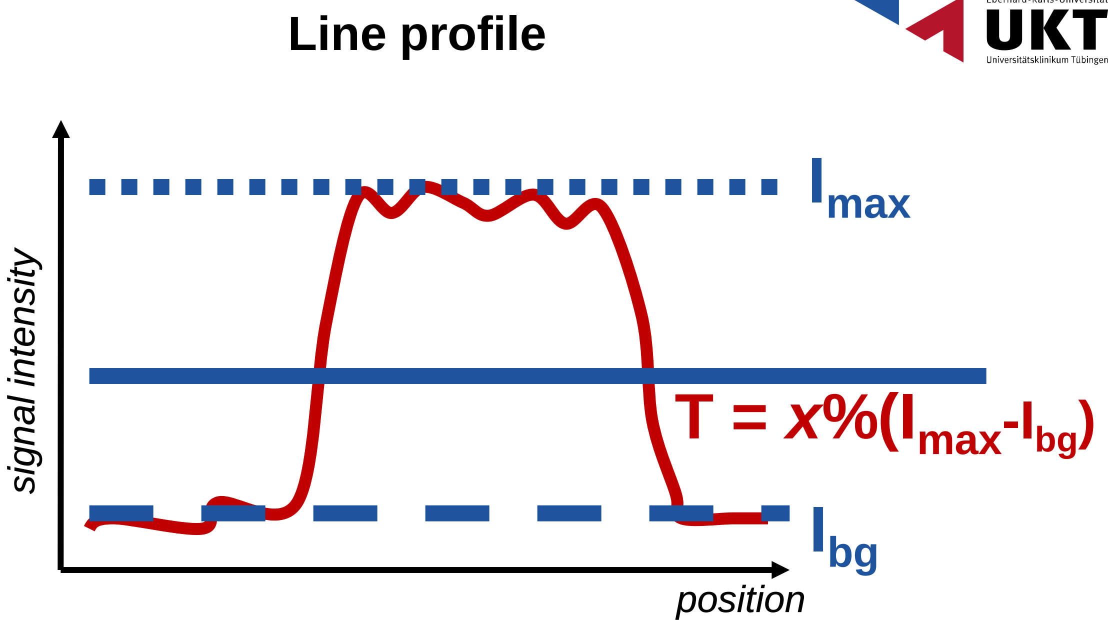

- Background-subtracted relative threshold level
- Adjustable threshold *x*
- Iterative approach based on phantom measurements

Source-to-Background Algorithms

PET image

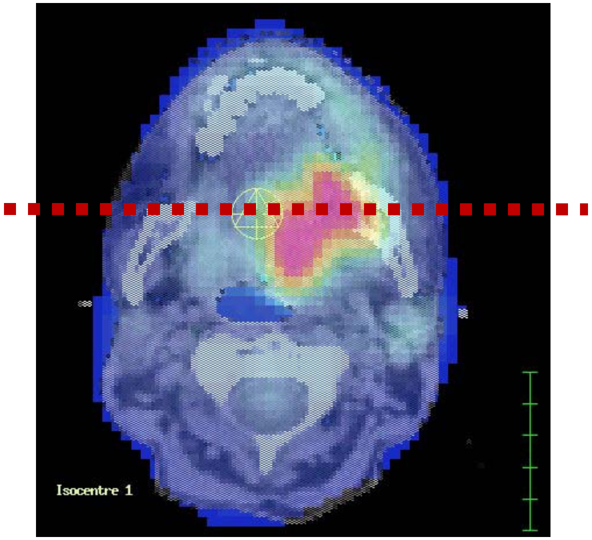

Line profile

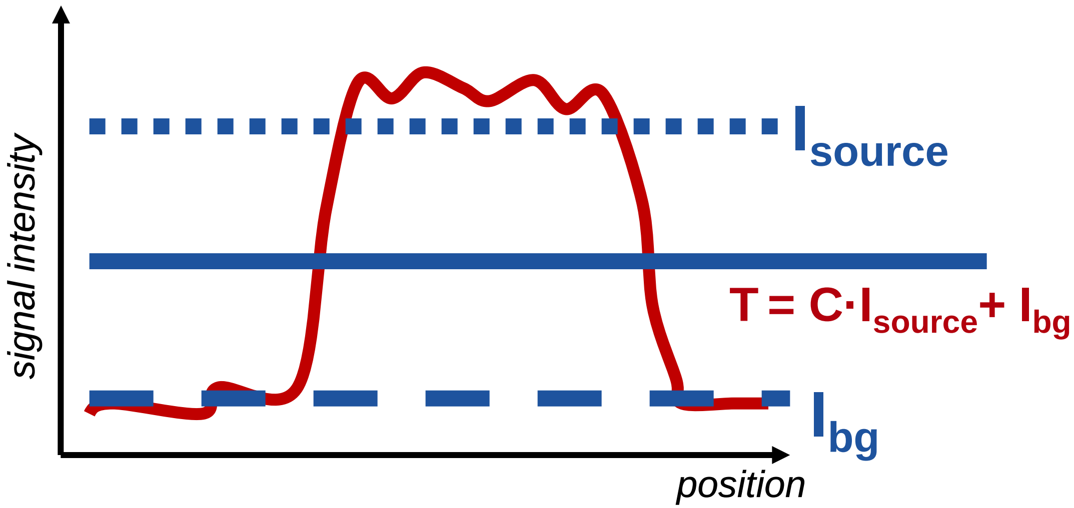

- Constant C determined from phantom measurements
- Works very well for quasi-spherical lesions
- *Value of C depending of different factors:*
  - *Lesion size and shape*
  - *Scanner type and calibration*
  - *Reconstruction protocol*
  - *Image analysis software*

Schaefer et al, EJNMMI 2008; 35(11): 1989-99.

Comparison of different contouring approaches

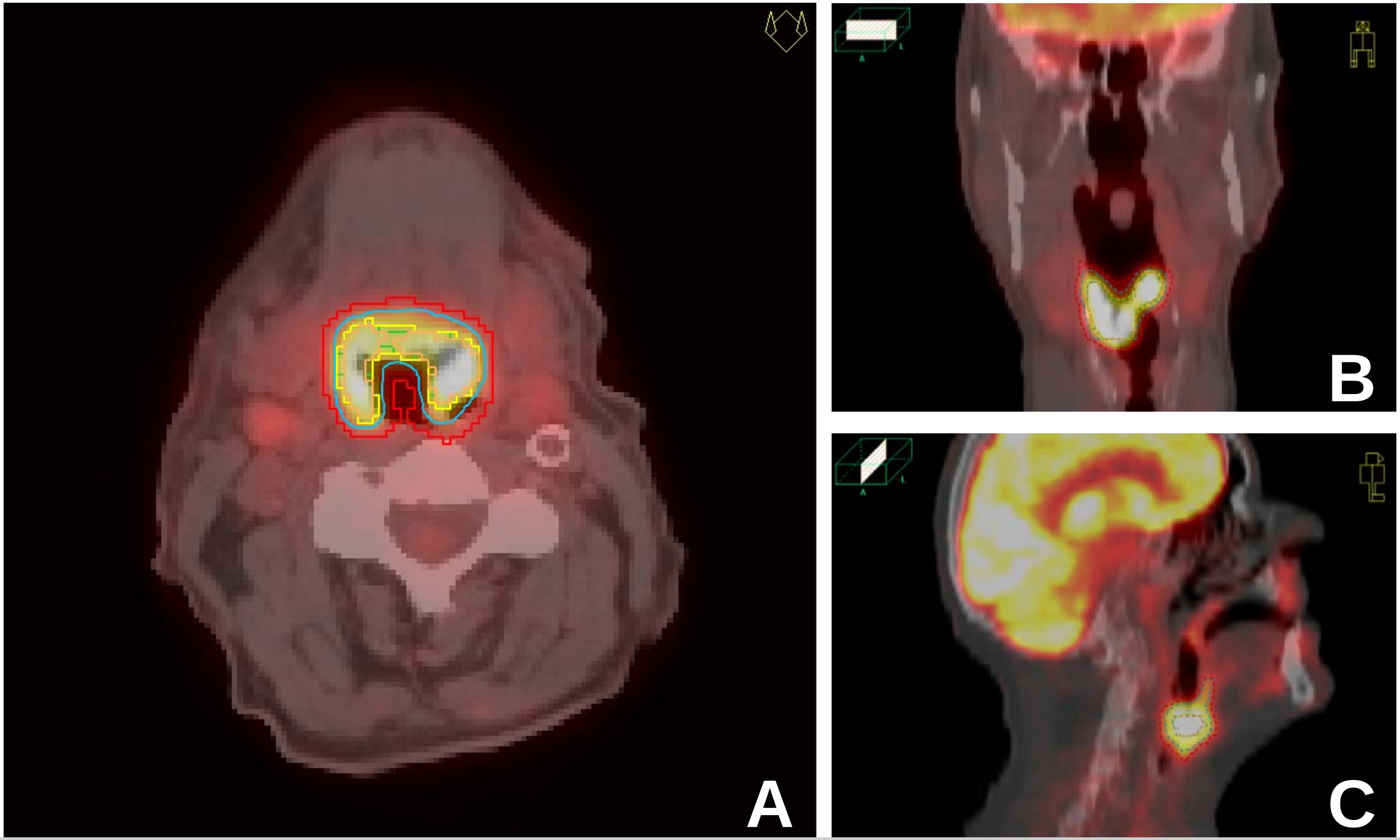

Contours created with different segmentation algorithms: manual delineation (21.8 ccm), absolute threshold SUV=2.5 (35.0 ccm), relative threshold 42% of maximum PET intensity (11.5 ccm), adaptive thresholding (10.6 ccm), source-to-background based algorithm of Schaefer *et al* (13.0 ccm)

Gradient-based auto-contouring

1. Image processing

- **Denoising** by bilateral edge-preserving filter

Fig. 2 Axial PET images from a patient with a hypopharyngeal tumour. On the *left panel*, the PET image corresponds to the raw image reconstructed with 3D OSEM algorithm. The application of the bilateral filter and the deconvolution algorithm restored the intensity gradient (*right panel*) in comparison with the classical 4-mm Gaussian filter (*middle panel*)

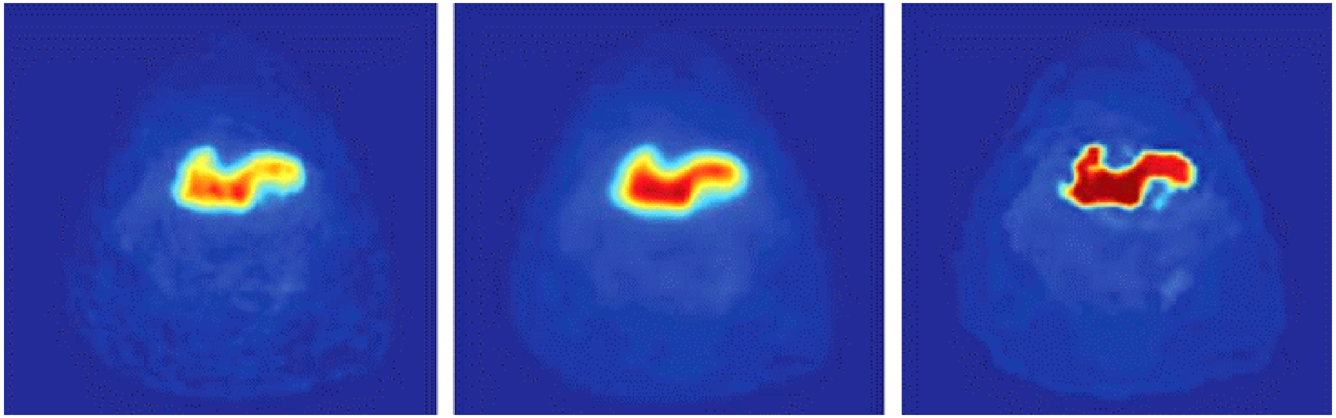

Geets et al, EJNMMI 2007; 34: 1427-1438.

Gradient-based auto-segmentation

2. Gradient-based segmentation

- Derive a gradient-intensity image:
  Plains & Plateaus → Mountain chains & Valleys
- Crest detection by applying Watershed Transformation
- Cluster analysis

PET image

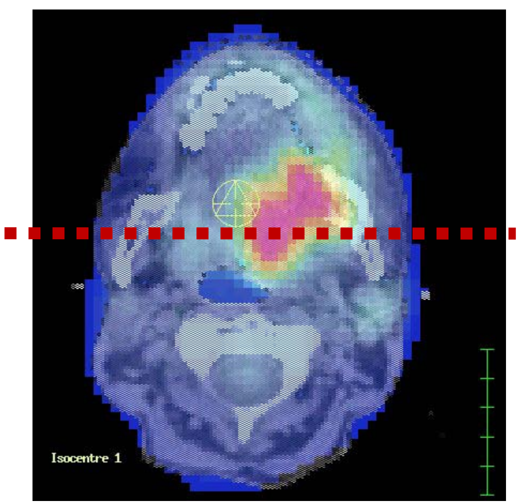

Line profile

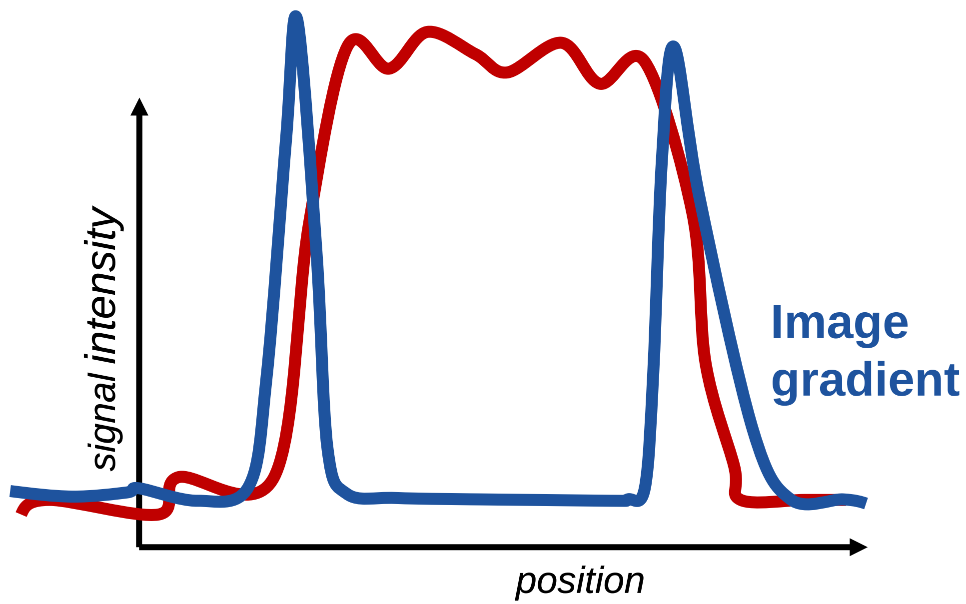

Gradient-based segmentation improves target volume definition in NSCLC

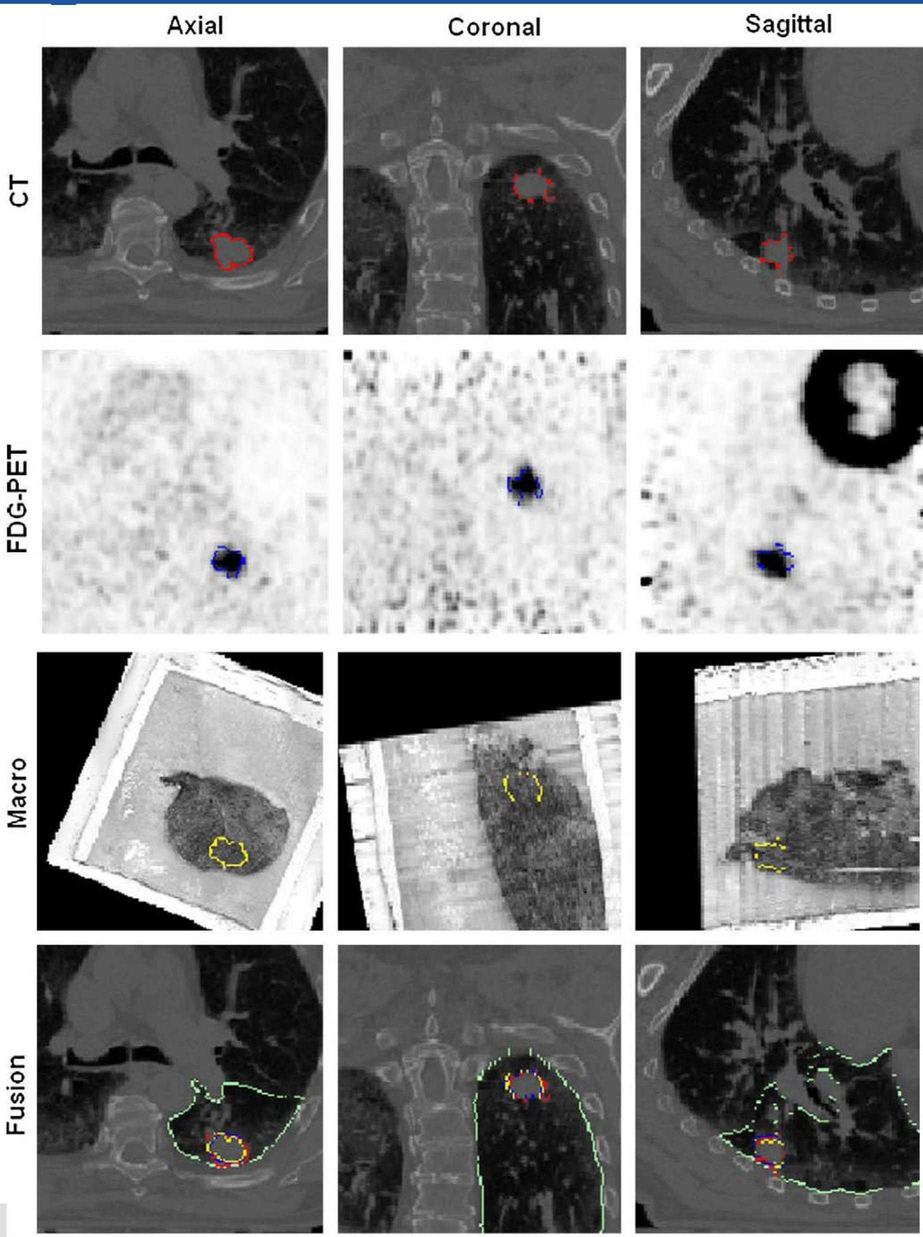

Wanet M et al. Radiother Oncol 2011;98:117-25.

- N=10 NSCLC patients
- GTV delineation on CT±PET
- Comparison with surgical specimen
- PET yields more robust delineation in poorly defined tumors
- Gradient based seg. outper-formed threshold method in terms of accuracy and robustness

Activity Recovery, Partial Volume Effect: The Smaller the Volume, the Darker it Appears

^{68}Ga Phantom measurements:

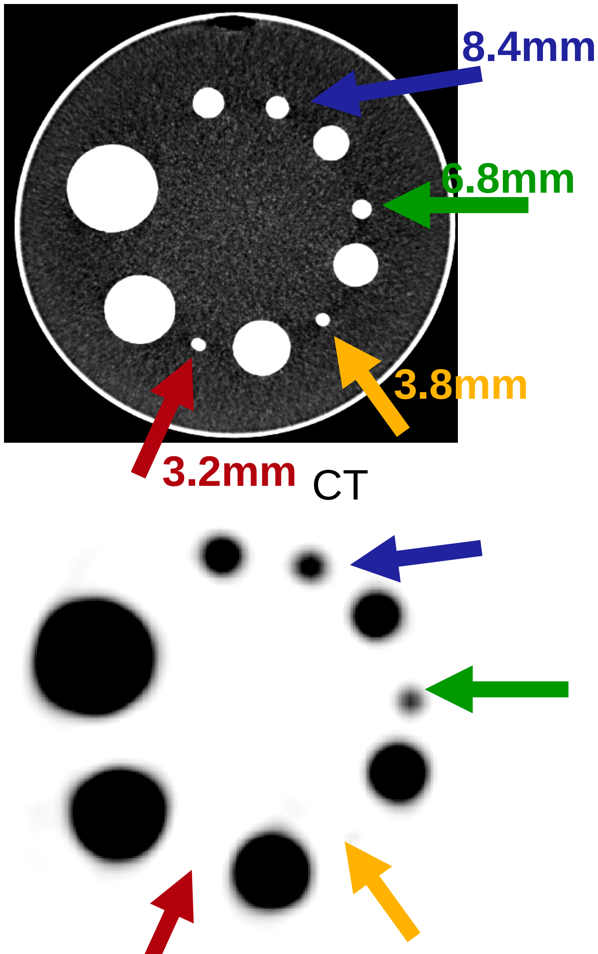

PET, contrast 1:0

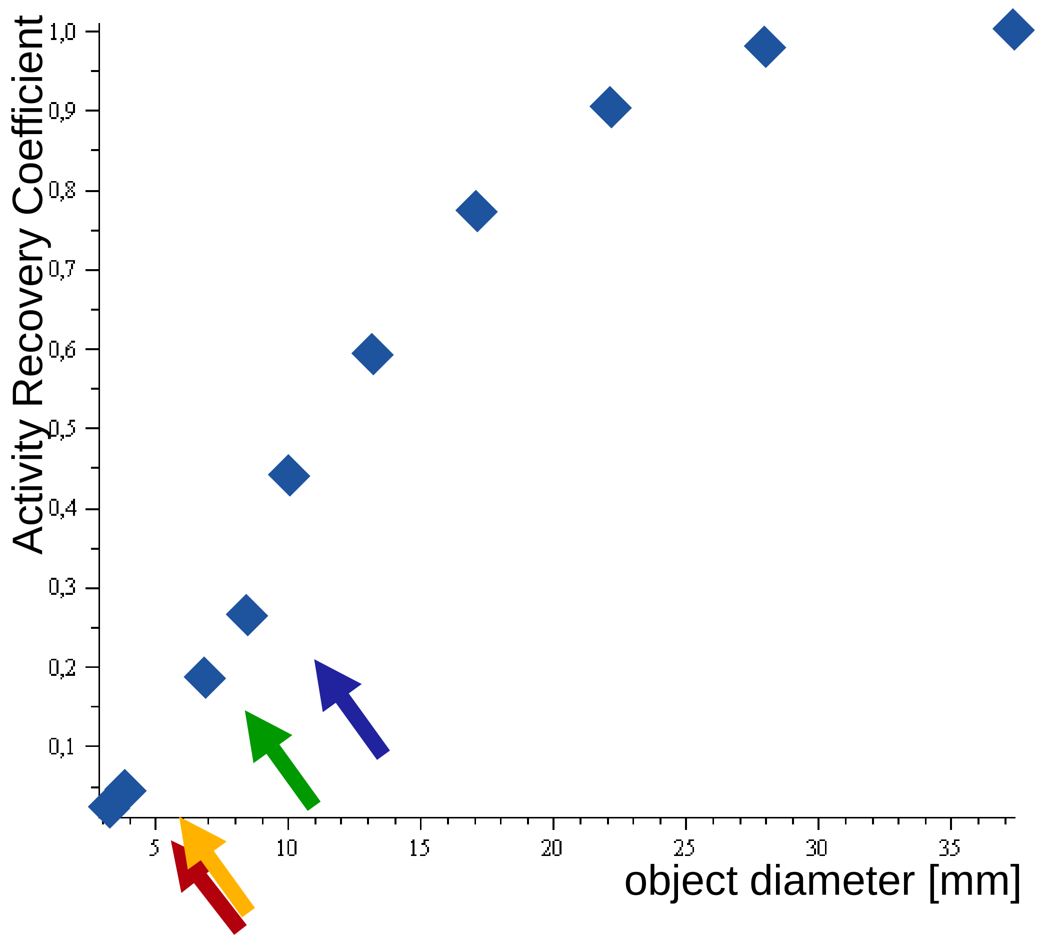

Influence of PET reconstruction

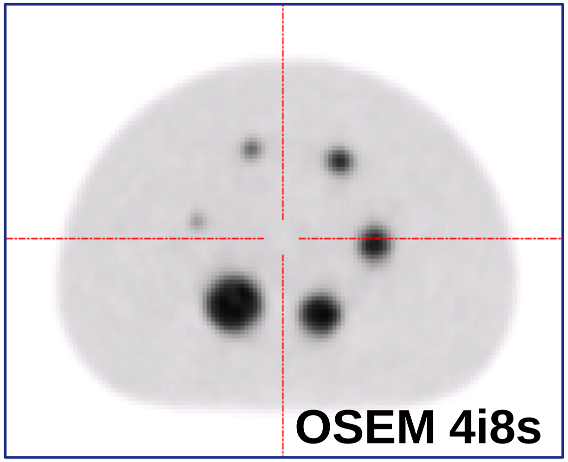

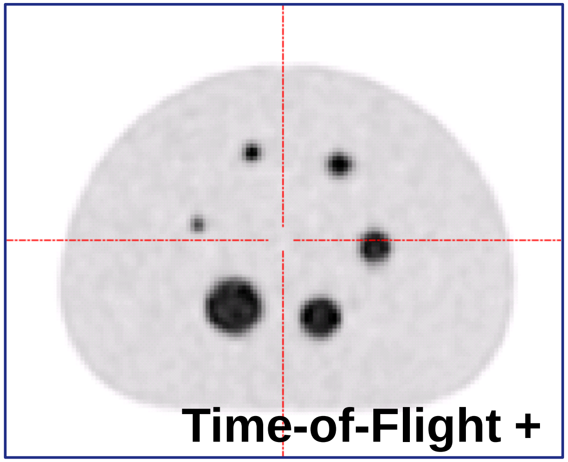

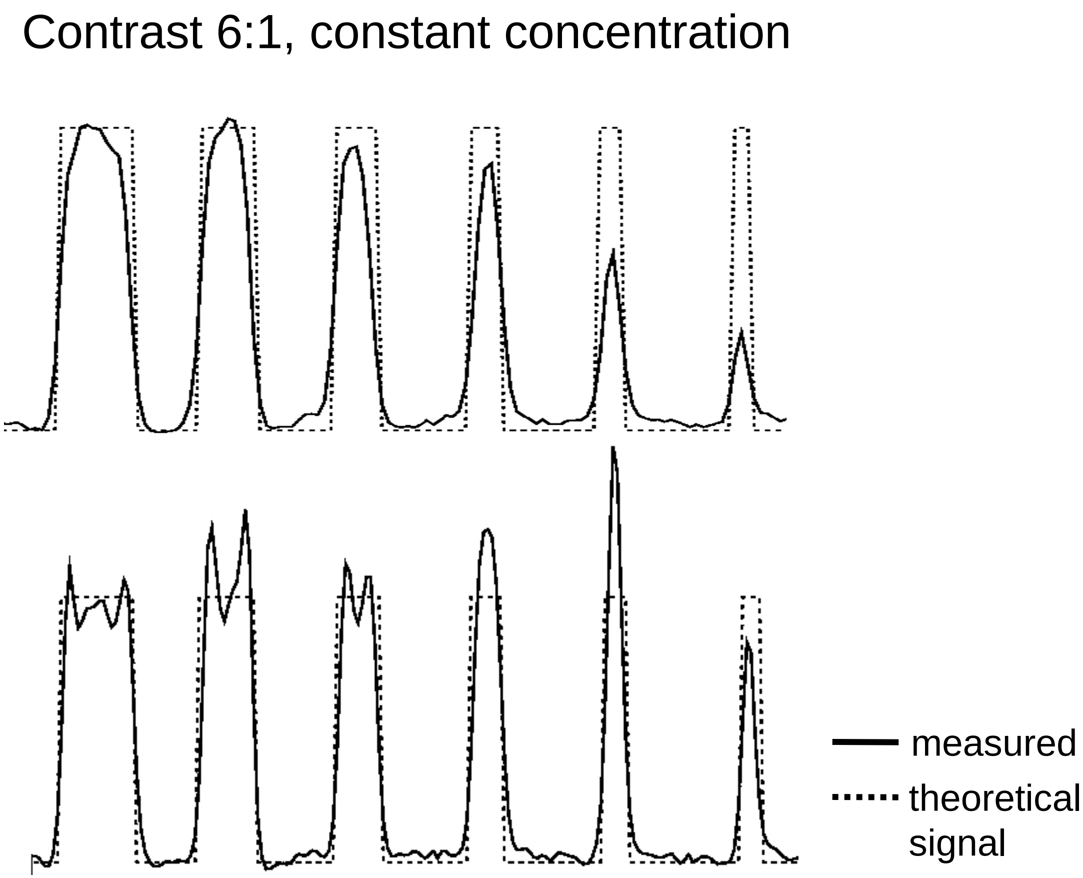

Effect of reconstruction on PET-based contouring

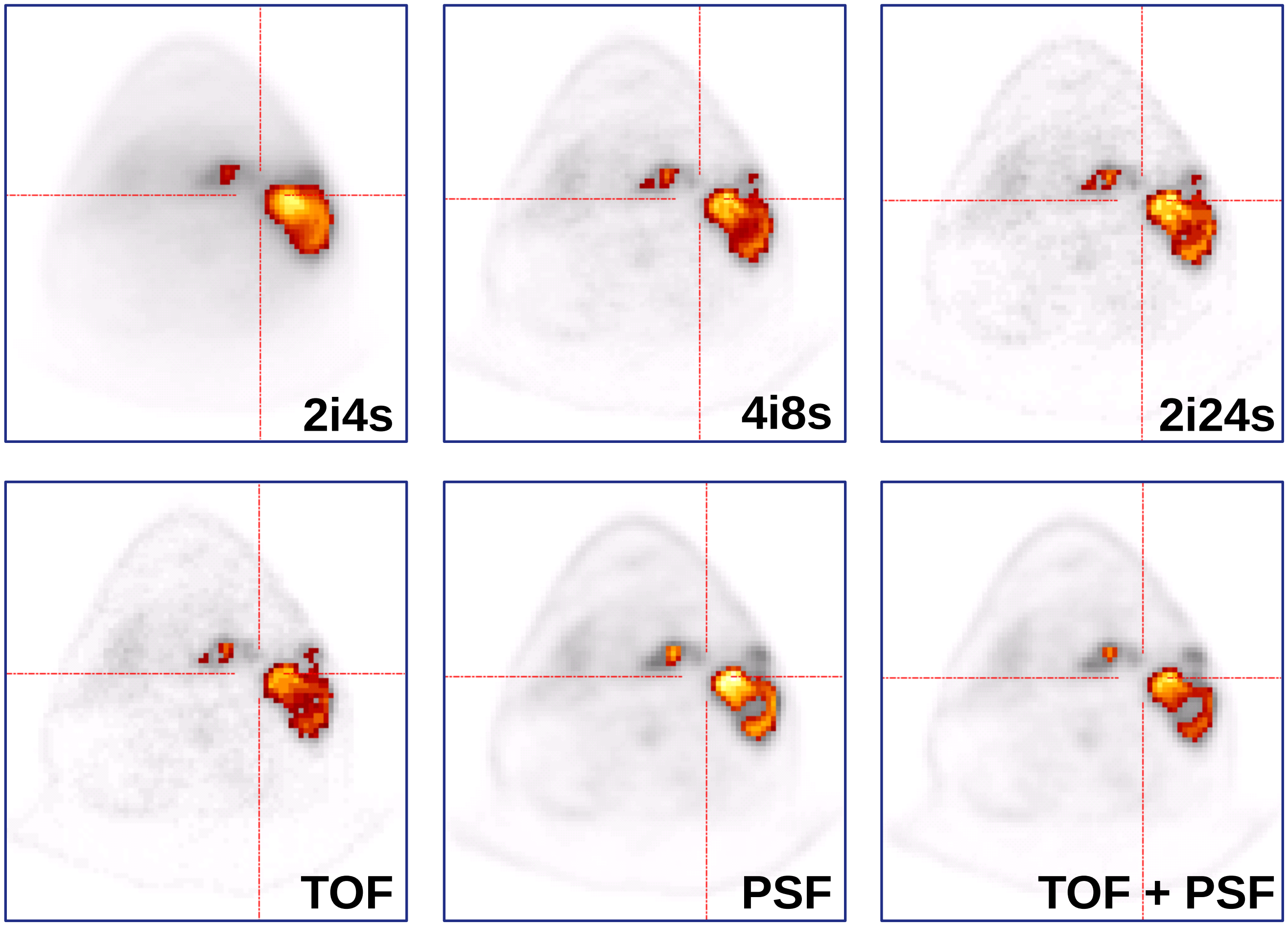

Threshold:
40% SUV_{max}

Comparison of auto-contouring methods with „intelligent“ manual delineation

Bayne M et al. Int J Radiother Oncol Biol Phys 2010; 77: 1151-7.

- GTVs contoured by 6 experts using a **highly standardized protocol**
- Autocontouring with SUV=2.5, 3.5, 4.0, and 40% SUV_{max}
- Automatic delineations differed widely
- Visual contouring protocol gave reproducible results

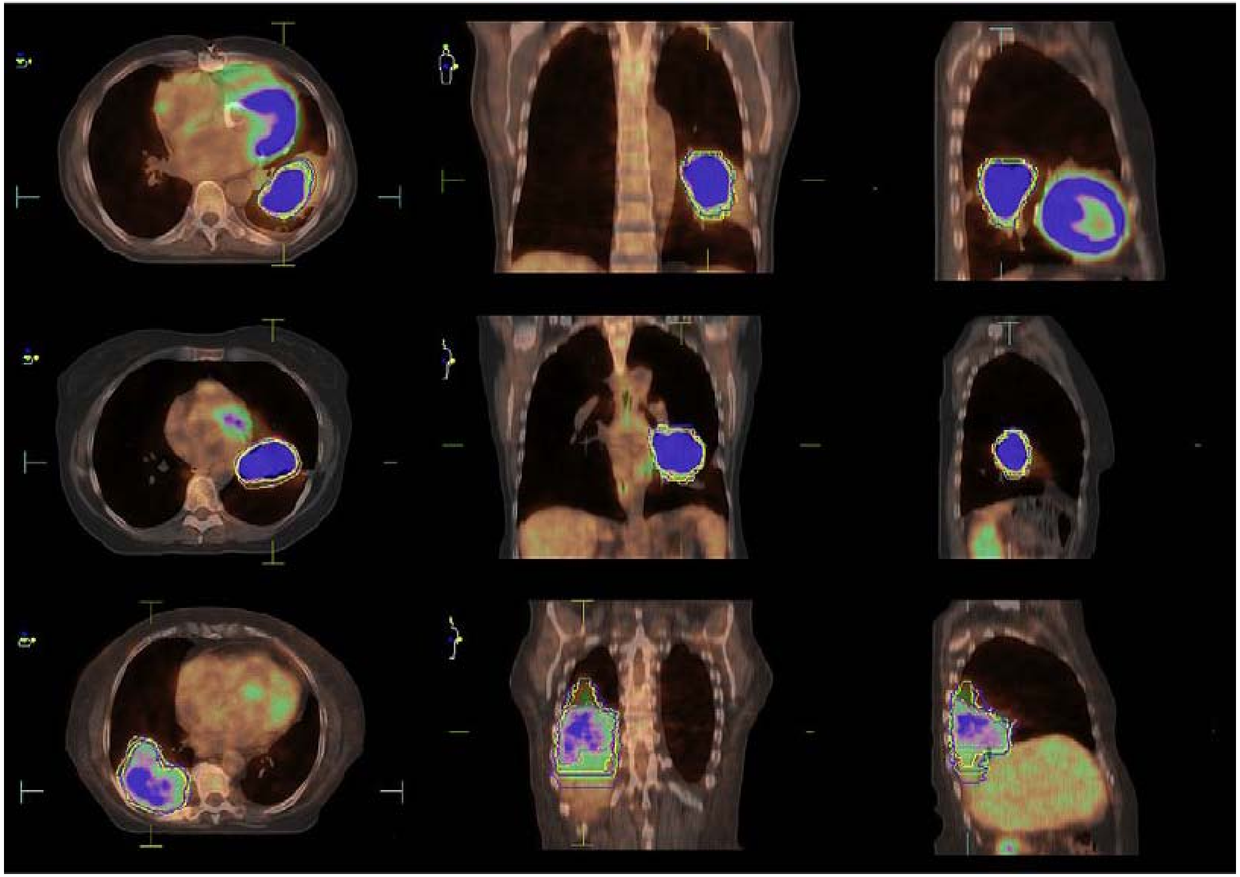

EARL: Standardization of clinical PET scanners

Guideline of the EANM (European Assoc. of Nuclear Medicine:

"FDG PET and PET/CT: EANM procedure guideline for tumour PET imaging: version 1.0." (Boellaard R et al, EJNMMI 2010; 37(1):181-200)

Objectives of EARL:

- to provide a minimum standard of PET/CT scanner performance in order to harmonise the acquisition and interpretation of PET scans
- ensure similar performance of PET/CT systems within a multicentre setting
- characterisation of imaging site by continuing quality control, making it highly eligible as a participant in multicentre studies
- high quality of routine patient examinations

EARL: Multicenter QC and calibration

- Calibration
  - Minimum allowable deviation: +/- 10%

- SUV recovery
  - For SUV_{max}
  - For SUV_{mean}

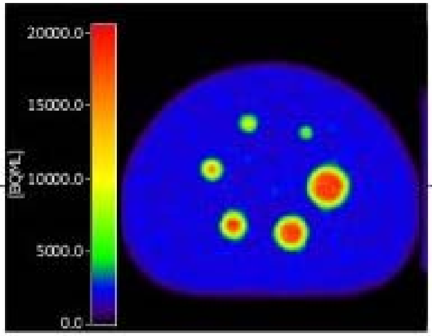

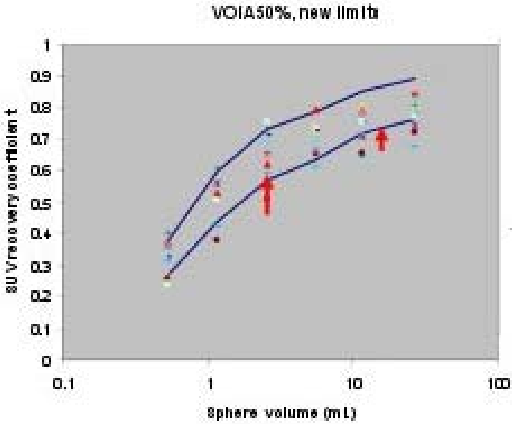

http://www.earl.eanm.org

Summary / Conclusion

- For quantitative PET imaging, raw data correction is necessary
  - Random, scatter and dead time correction
  - Normalization
  - Attenuation correction with CT!
- Image reconstruction
  - FBP, ML-EM, OSEM, 3D-reconstruction protocols
- Automatic contouring algorithms for RT
  - Absolute / relative thresholding
  - Iterative thresholding
  - Source-to-background
  - Gradient-based algorithm

Literature

[1] M Defrise, PE Kinahan, CJ Michel. Image Reconstruction. In: Positron Emission Tomography: Basic Science and Clinical Practice. Editors: PE Valk, DL Bailey, DW Townsend, MN Maisey. Springer London 2003, pp. 63-91.

[2] SR Meikle, RD Badawi. Quantitative Techniques in PET. In: Positron Emission Tomography: Basic Science and Clinical Practice. Editors: PE Valk, DL Bailey, DW Townsend, MN Maisey. Springer London 2003, pp. 93-126.

[3] DW Townsend. Multimodality imaging of structure and function. Phys Med Biol 2008; 53: R1-R39.

[4] JA Lee. Segmentation of positron emission tomography images: Some recommendations for target volume delineation in radiation oncology. Radiother Oncol 2010; 96: 302-307. Review.

[5] D. Thorwarth, A. Schaefer. Functional radiotherapy target volume delineation on the basis of Positron Emission Tomography and the correlation to histopathology. *QJNMMI 2010; 54(5):490-499.*

Applications: MRI in Brain

Cynthia Ménard, M.D.

Goal – MRI Simulation

- To develop a better ‘simulation procedure’ …(using MRI)

- Build ideal patient model for radiotherapy planning (using MRI)?
  - Accurate and precise depiction of target and organ boundaries (reduce observer uncertainty, enable autosegmentation) — **MRI**
  - Representative of therapy conditions (+ motion) — **F, CT**
  - Geometrically accurate — **CT**
  - Inform on tissue composition / dose attenuation — **CT**
  - Bridge to online guidance tools — **F, CT**
  - Predictive of response (guide dose prescriptions) — **MRI**

MRI Simulator

_DSC0408

VARIAN medical systems

IMRIS

CHUM

2009-2012

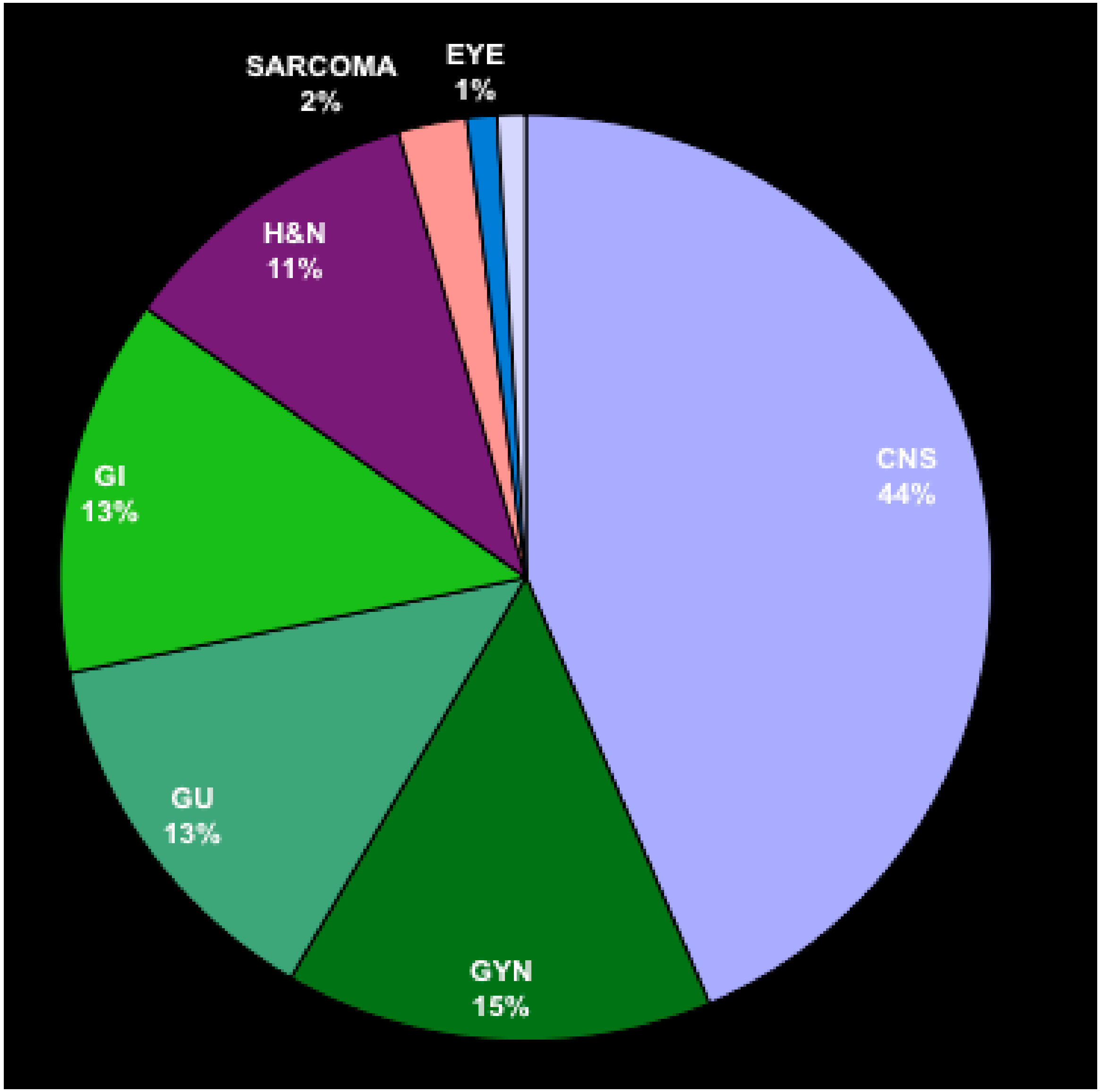

CHUM

Consensus recommendations for a standardized Brain Tumor Imaging Protocol in clinical trials

Benjamin M. Ellingson, Martin Bendszus, Jerrold Boxerman, Daniel Barboriak, Bradley J. Erickson, Marion Smits, Sarah J. Nelson, Elizabeth Gerstner, Brian Alexander, Gregory Goldmacher, Wolfgang Wick, Michael Vogelbaum, Michael Weller, Evanthia Galanis, Jayashree Kalpathy-Cramer, Lalitha Shankar, Paula Jacobs, Whitney B. Pope, Dewen Yang, Caroline Chung, Michael V. Knopp, Soonme Cha, Martin J. van den Bent, Susan Chang, W.K. Al Yung, Timothy F. Cloughesy, Patrick Y. Wen, Mark R. Gilbert, and the Jumpstarting Brain Tumor Drug Development Coalition Imaging Standardization Steering Committee

UCLA Neuro-Oncology Program and UCLA Brain Tumor Imaging Laboratory (BTIL), David Geffen School of Medicine, University of California – Los Angeles, Los Angeles, California (B.M.E., T.F.C.); Department of Radiological Sciences, David Geffen School of Medicine, University of California – Los Angeles, Los Angeles, California (B.M.E., W.B.P.); Department of Neuroradiology, Heidelberg University Hospital, Heidelberg, Germany (M.B.); Department of Diagnostic Imaging, Warne Alpert Medical School, Brown University, Providence, Rhode Island (J.B.); Department of Neuroradiology, Duke University School of Medicine, Durham, North Carolina (D.B.); Department of Radiology, Mayo Clinic, Rochester, Minnesota (B.J.E.); Department of Radiology, Erasmus MC University, Rotterdam, Netherlands (M.S.); Department of Radiology and Biomedical Imaging, University of California – San Francisco, San Francisco, California (S.J.N., S.C.); Department of Neurology, Massachusetts General Hospital, Harvard Medical School, Boston, Massachusetts (E.G.); Center for Neuro-Oncology, Dana-Farber/Brigham and Women's Cancer Center, Harvard Medical School, Boston, Massachusetts (B.A., P.Y.W.); Medical and Scientific Affairs, ICON Medical Imaging, Warrington, Pennsylvania (G.G., D.Y.); Department of Neurooncology, National Center of Tumor Disease, University Clinic Heidelberg, Heidelberg, Germany (W.W.); Department of Neurological Surgery, Brain Tumor and Neuro-Oncology Center, Cleveland Clinic, Cleveland, Ohio (M.V.); Department of Neurology, University Hospital Zurich, Zurich, Switzerland (M.W.); Division of Medical Oncology, Department of Oncology, Mayo Clinic, Rochester, Minnesota (E.G.); Martinos Center for Biomedical Imaging, Massachusetts General Hospital and Harvard Medical School, Boston, Massachusetts (J.K.-C.); Division of Cancer Treatment and Diagnosis, National Cancer Institute (NCI), Bethesda, Maryland (L.S., P.J.); Department of Radiation Oncology, University of Toronto and Princess Margaret Hospital, Toronto, Ontario, Canada (C.C.); Wright Center for Innovation in Biomedical Imaging, Division of Imaging Science, Wexner Medical Center, Ohio State University, Columbus, Ohio (M.V.K.); Department of Neuro-Oncology, Erasmus MC Cancer Institute, Rotterdam, Netherlands (M.J.v.d.B.); Department of Neurological Surgery, University of California – San Francisco, San Francisco, California (S.C., S.C.); Department of Neuro-Oncology, Division of Cancer Medicine, The University of Texas MD Anderson Cancer Center, Houston, Texas (W.K.A.Y.); Department of Neurology, David Geffen School of Medicine, University of California – Los Angeles, Los Angeles, California (T.F.C.); Neuro-Oncology Branch, National Cancer Institute (NCI), Bethesda, Maryland (M.R.G.); Adult Brain Tumor Consortium (ABTC) (B.M.E., E.G., P.Y.W.); Ivy Consortium for Early Phase Clinical Trials (B.M.E., S.J.N.); American College of Radiology Imaging Network (ACRIN) (B.M.E., J.B., D.B.); European Organisation for Research and Treatment of Cancer (EORTC) (M.B., M.S., W.W., M.J.v.d.B.); Alliance for Clinical Trials in Oncology (B.J.E., E.G.); RSNA Quantitative Imaging Biomarker Alliance (QIBA) (B.M.E., D.B., G.G., B.J.E., M.V.K.); American Society of Neuroradiology (ASNR) (B.M.E., J.B., D.B., B.J.E., W.B.P.); American Society of Functional Neuroradiology (ASFNR) (J.B.); Radiation Therapy Oncology Group (RTOG) (M.V., M.R.G.)

Corresponding Author: Benjamin M. Ellingson, PhD, Radiological Sciences, David Geffen School of Medicine at UCLA, 924 Westwood Blvd, Suite 650, Los Angeles CA 90095 (bellingson@mednet.ucla.edu).

See the editorial by Sul and Krainak, on pages 1179–1180.

Table 3. Recommended 1.5T protocol

	3D T1w Pre	Ax 2D FLAIR	Ax 2D DWI	Contrast Injection[a]	Ax 2D T2w	3D T1w Post[b]
Sequence	IR-GRE[d,e]	TSE[c]	EPI[f]		TSE[c]	IR-GRE[d,e]
Plane	Sagittal/axial	Axial	Axial		Axial	Sagittal/axial
Mode	3D	2D	2D		2D	3D
TR [ms]	2100[g]	>6000	>5000		>3500	2100[g]
TE [ms]	Min	100–140	Min		100–120	Min
TI [ms]	1100[h]	2200				1100[h]
Flip angle	10°–15°	90°/≥160°	90°/180°		90°/≥160°	10°–15°
Frequency	≥172	≥256	128		≥256	≥172
Phase	≥172	≥256	128		≥256	≥172
NEX	≥1	≥1	≥1		≥1	≥1
FOV	256 mm	240 mm	240 mm		240 mm	256 mm
Slice thickness	≤1.5 mm	≤4 mm	≤4 mm		≤4 mm	≤1.5 mm
Gap/spacing	0	0	0		0	0
Diffusion options[i]			$b = 0$, 500, and 1000 s/mm^2 ≥3 directions			
Parallel imaging	No	Up to 2x	Up to 2x		Up to 2x	No
Scan time (approximate)	5–10 min	4–5 min	3–5 min		3–5 min	5–10 min

Abbreviations: 3D, 3-dimensional; A/P, anterior to posterior; ADC, apparent diffusion coefficient; Ax, axial; DWI, diffusion-weighted imaging; EPI, echo-planar imaging; FLAIR, fluid-attenuated inversion recovery; FOV, field of view; IR-GRE, inversion-recovery gradient-recalled echo; MPRAGE, magnetization prepared rapid gradient-echo; NEX, number of excitations or averages; R/L, right to left; TSE, turbo spin-echo.

[a]0.1 mmol/kg or up to 20 cc (single, full dose) of MR contrast.

[b]Postcontrast 2D axial T1-weighted images should be collected with identical parameters to precontrast 2D axial T1-weighted images.

[c]TSE = turbo spin-echo (Siemens & Philips) is equivalent to FSE (fast spin-echo; GE, Hitachi, Toshiba).

[d]IR-GRE = inversion-recovery gradient-recalled echo sequence is equivalent to MPRAGE = magnetization prepared rapid gradient-echo (Siemens and Hitachi) and the inversion recovery spoiled gradient-echo (IR-SPGR or Fast SPGR with inversion activated or BRAVO; GE), 3D turbo field echo (TFE; Philips), or 3D fast field echo (3D Fast FE; Toshiba).

[e]A 3D acquisition without inversion preparation will result in different contrast compared with MPRAGE or another IR-prepped 3D T1-weighted sequences and therefore should be avoided.

[f]In the event of significant patient motion, a radial acquisition scheme may be used (eg, BLADE [Siemens], PROPELLER [GE], MultiVane [Philips], RADAR [Hitachi], or JET [Toshiba]); however, this acquisition scheme can cause significant differences in ADC quantification and therefore should be used only if EPI is not an option.

[g]For Siemens and Hitachi scanners. GE, Philips, and Toshiba scanners should use a TR = 5–15 milliseconds for similar contrast.

[h]For Siemens and Hitachi scanners. GE, Philips, and Toshiba scanners should use a TI = 400–450 milliseconds for similar contrast.

[i]Older model MR scanners that are not capable of >2 *b*-values should use $b = 0$ and 1000 s/mm^2.

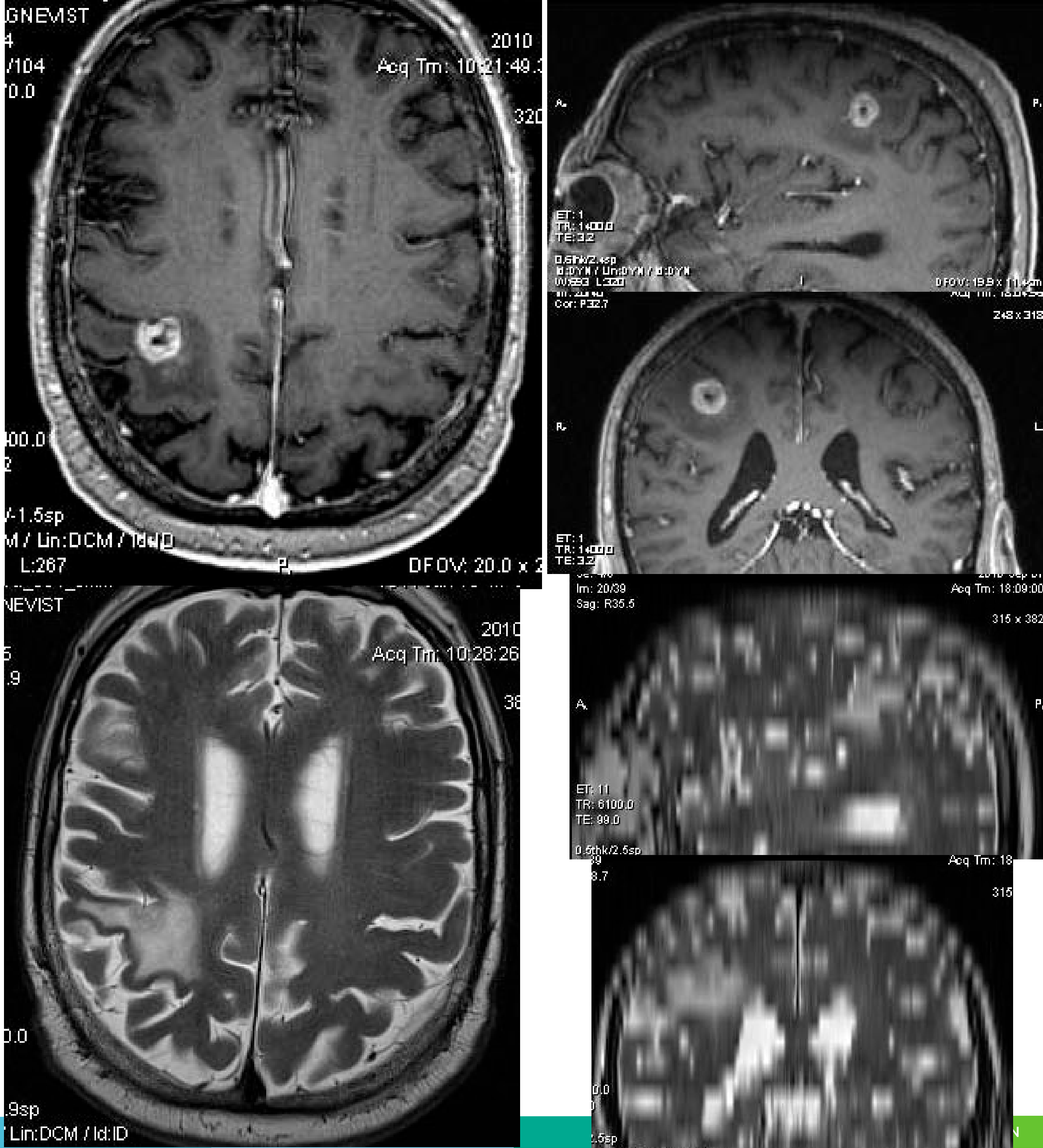

3D

1.5mm slice thickness

2D

3mm slice thickness

Tissue Contrast

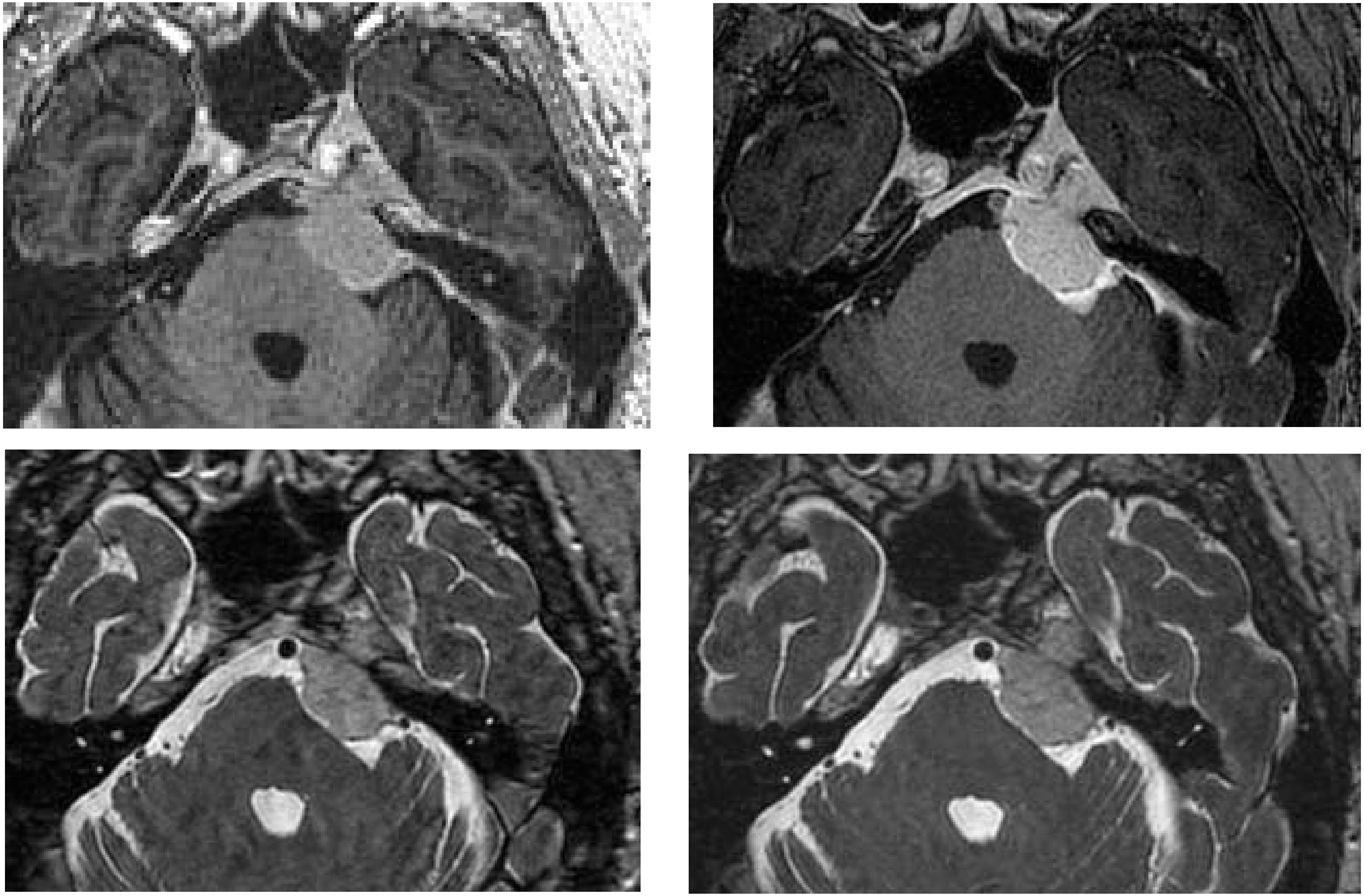

MacFadden et al., IJROBP 76:5:1472-1479, 2010


H
L

Imaging Coils

GE

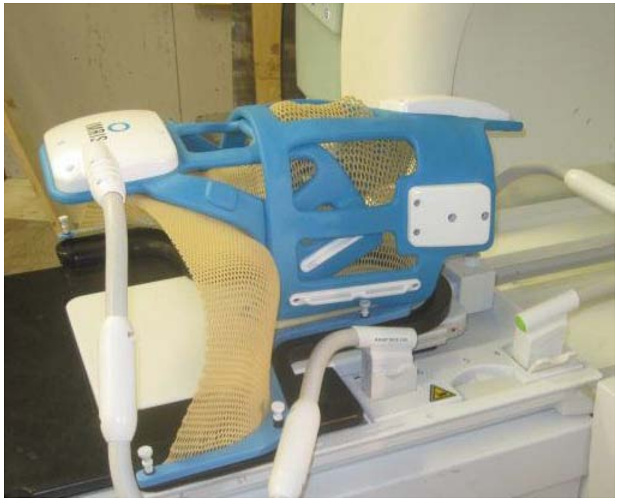

IMRIS

SIEMENS

MR-only simulation
MR imaging of cortical bone with Ultra-short TE

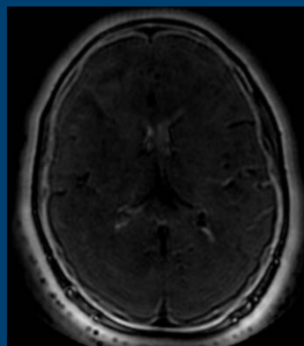

TE – short (~100 μs)

-

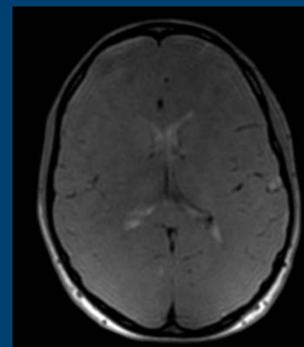

TE – long (~ 2 ms)

=

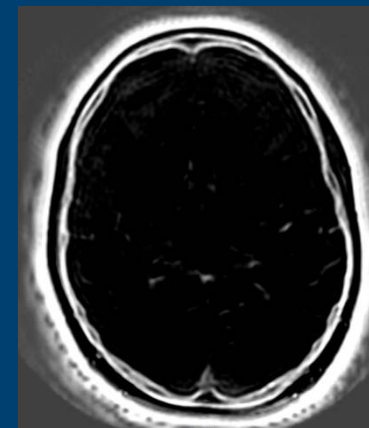

Cortical bone visualization

DRRs generated from MR images

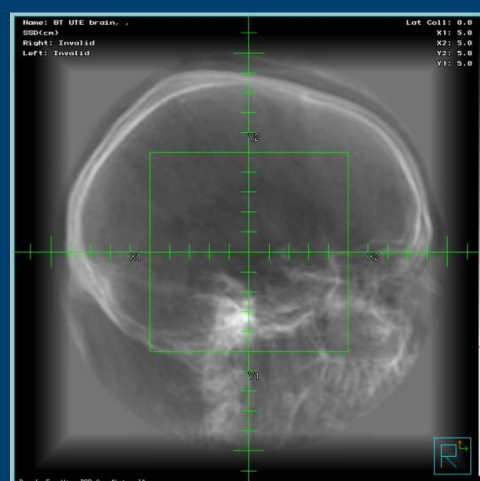

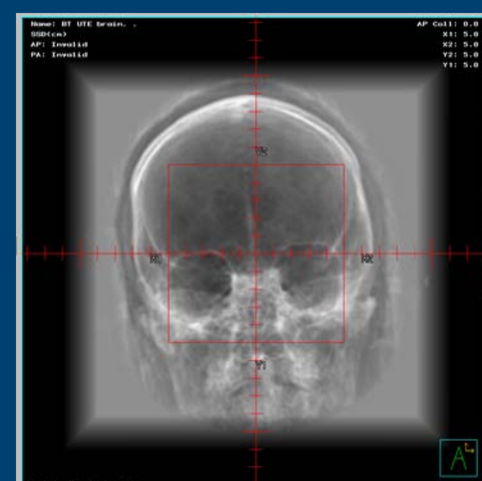

Philips Research

MR-Only Simulation

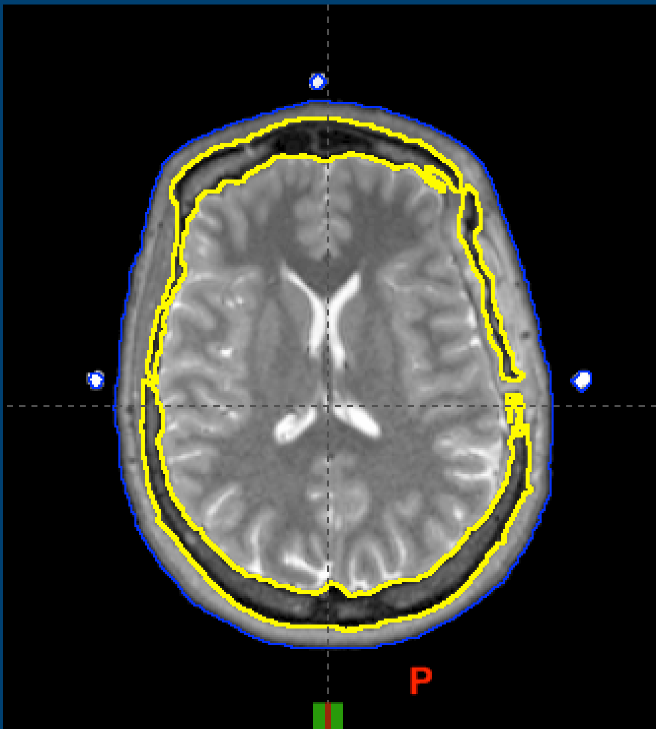

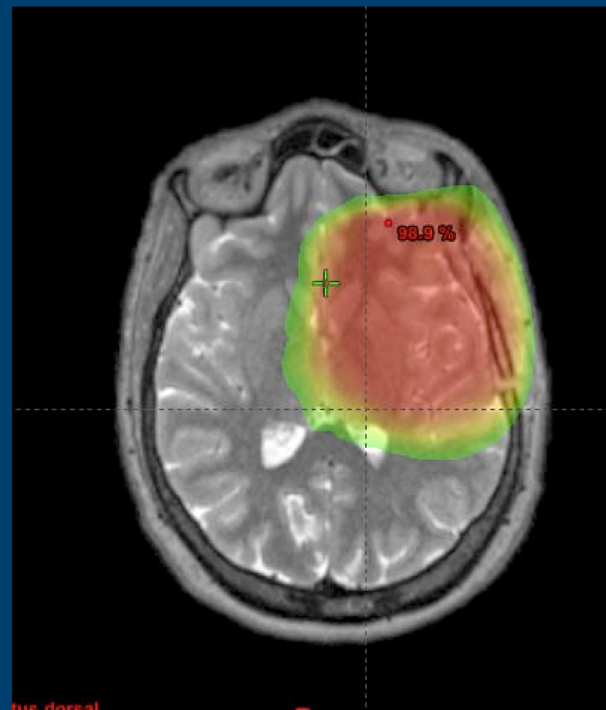

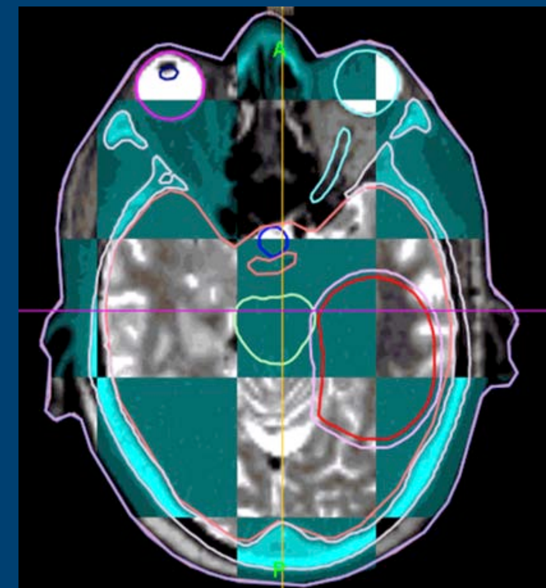

- Imaging
- Bone segmentation
- Body contour segmentation
- Density override

- Dose calculation

- IGRT
- Dose re-calculation

CHUM

Delineation – Visible Tumor

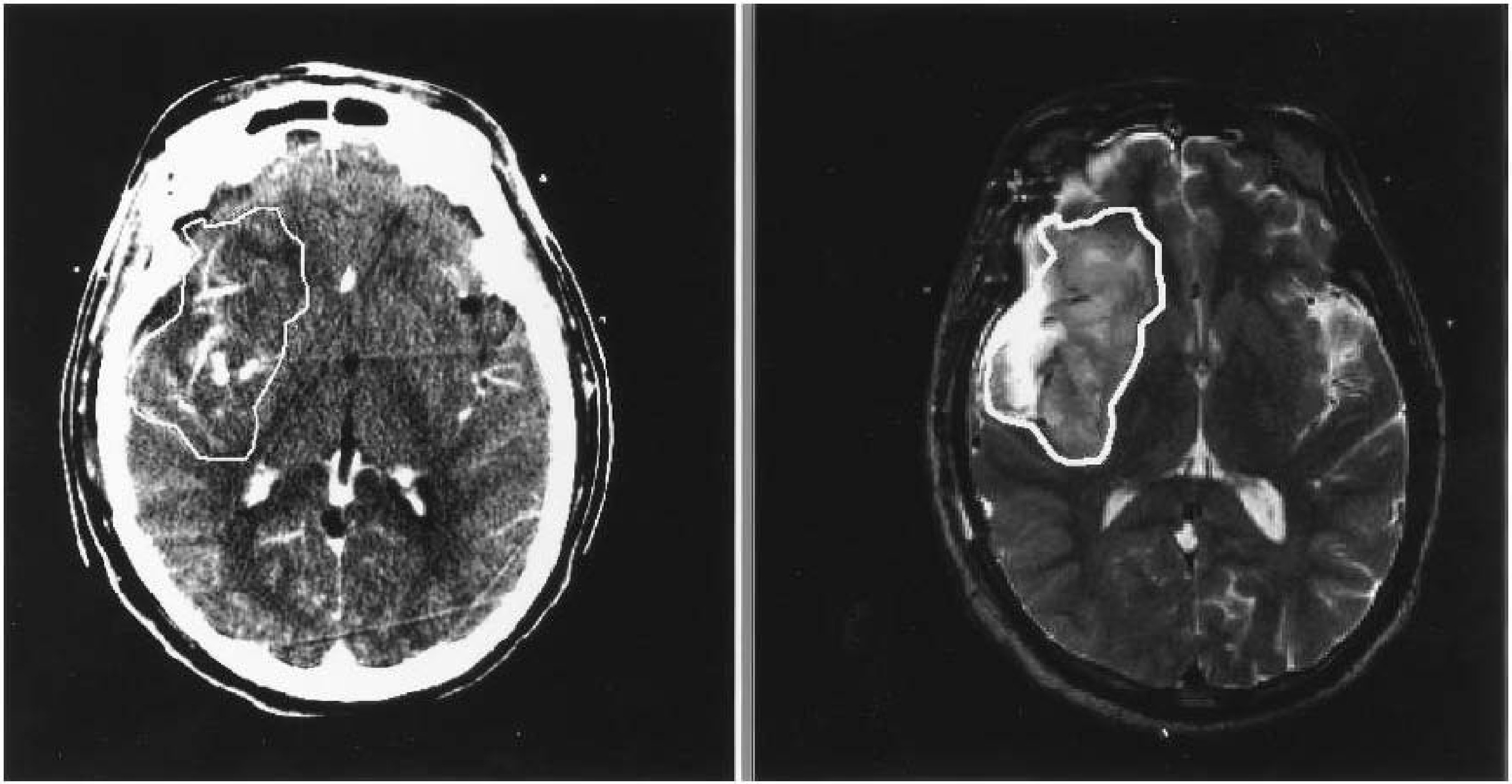

Ten Haken et al., Radiot Oncol, 1992

Khoo et al., IJROBP 2000

Aoyama et al., IJROBP 2001

Delineation – MRSI

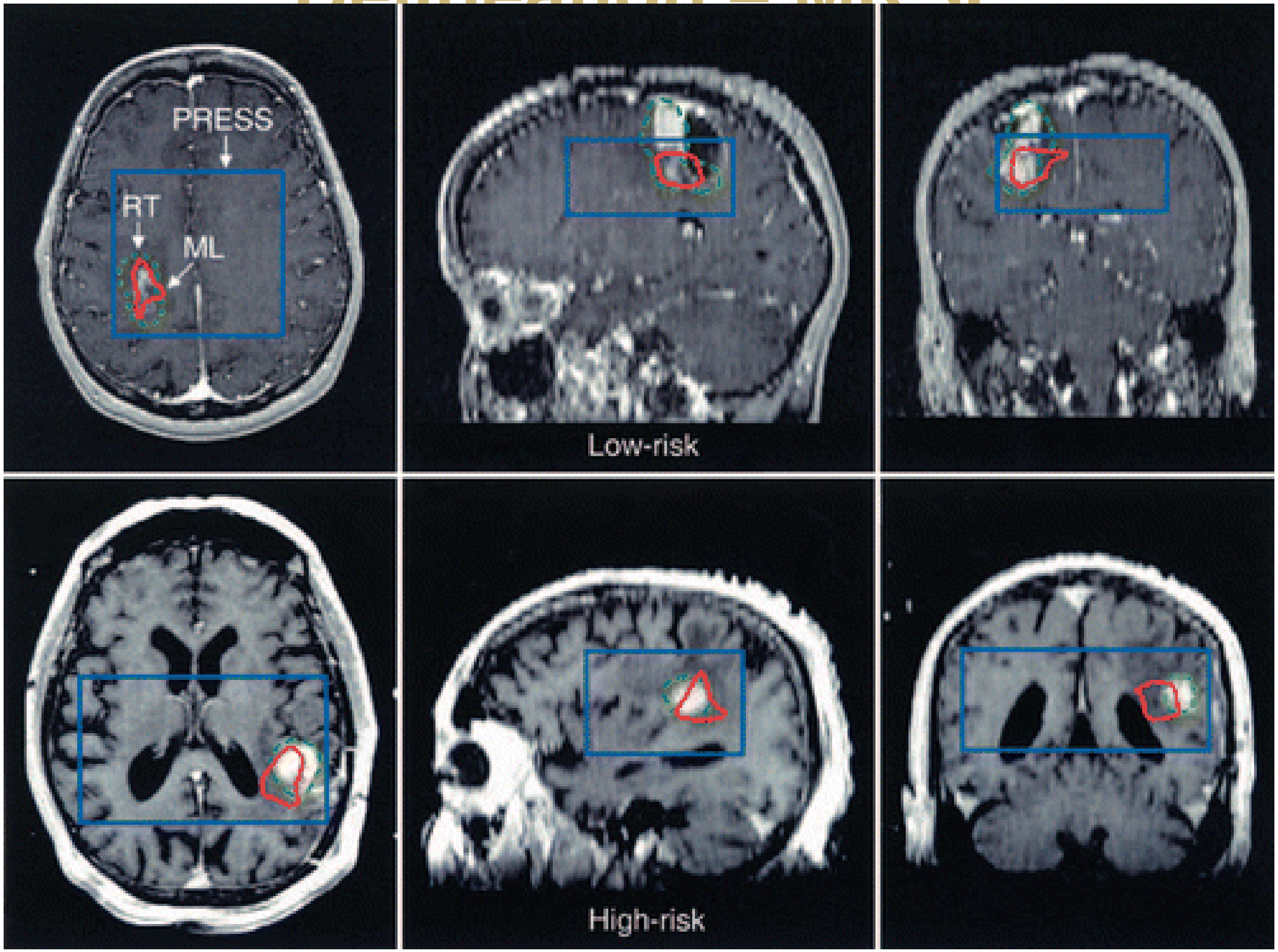

Chan et al, J Neurosurg, 2004

MRSI – Predicting Site of Recurrence

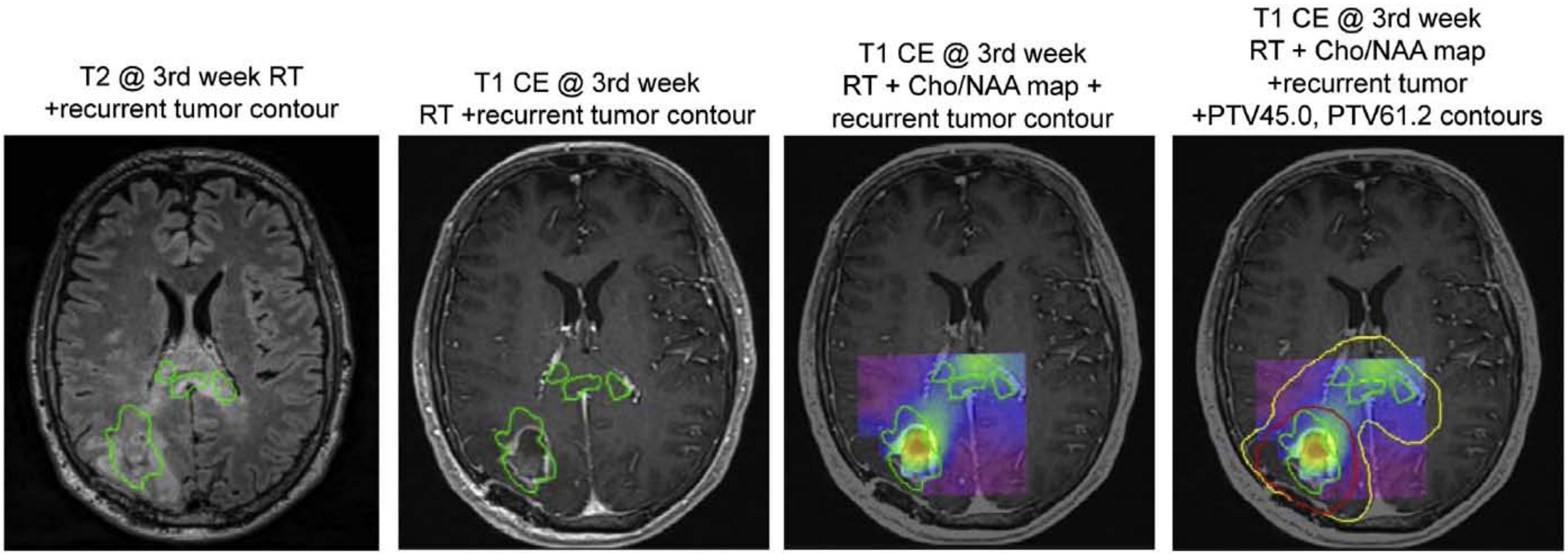

Muruganadham et al., 2014, IJROBP

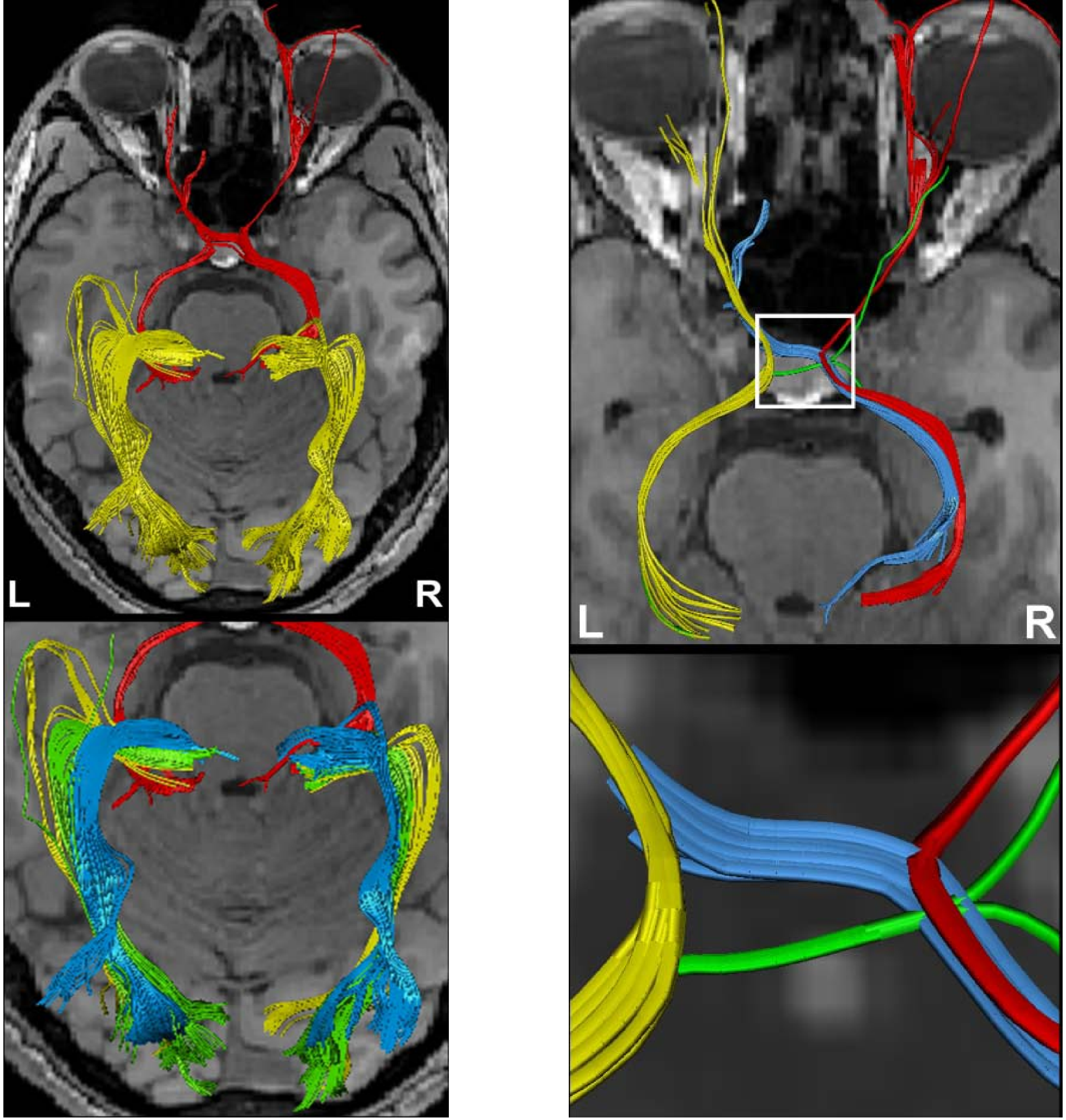

Hofer et al., Front Neur 4: 15, 2010

CHUM

FA map for CTV delineation

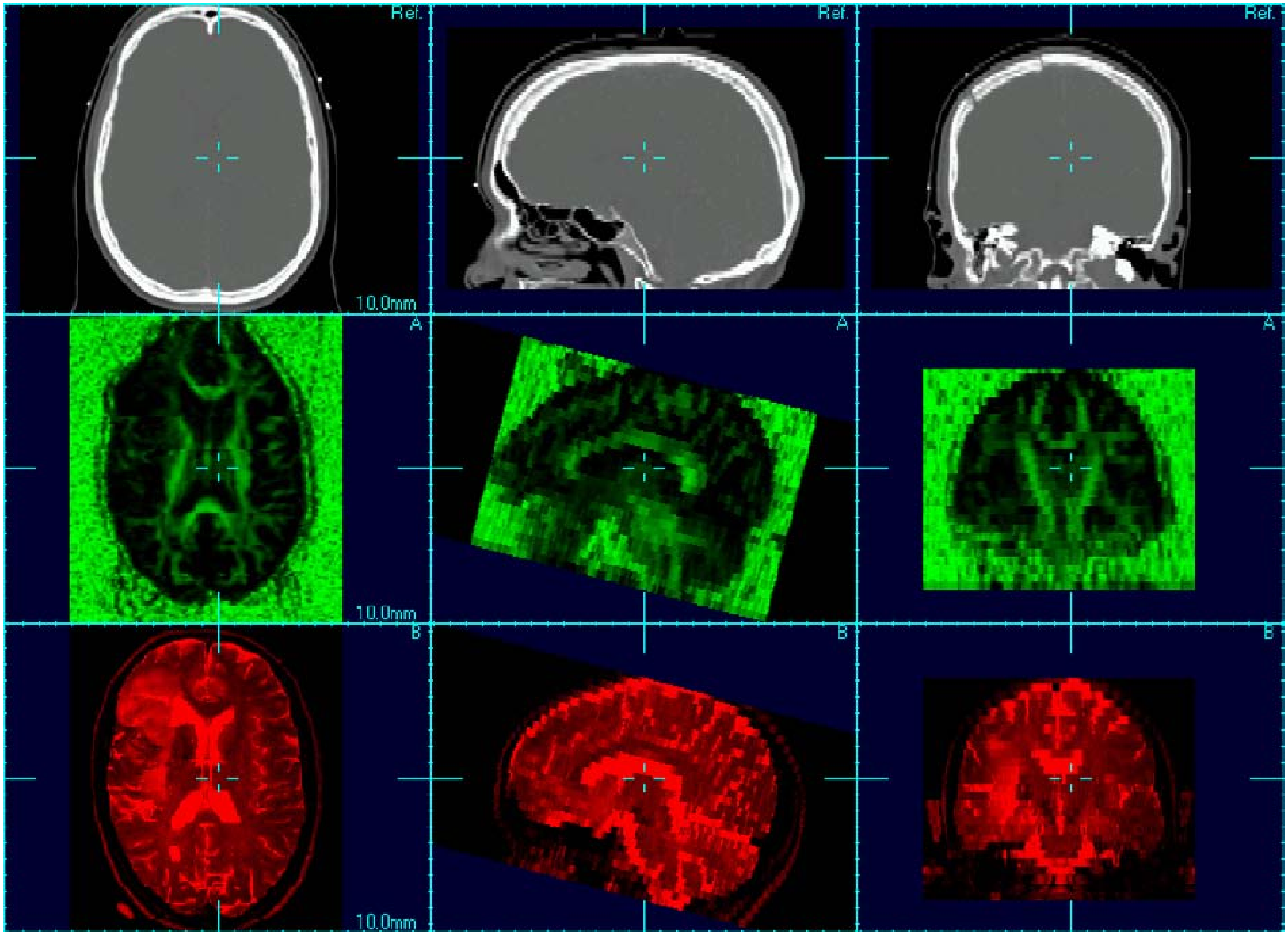

Jena et al., Clin Oncol 2005

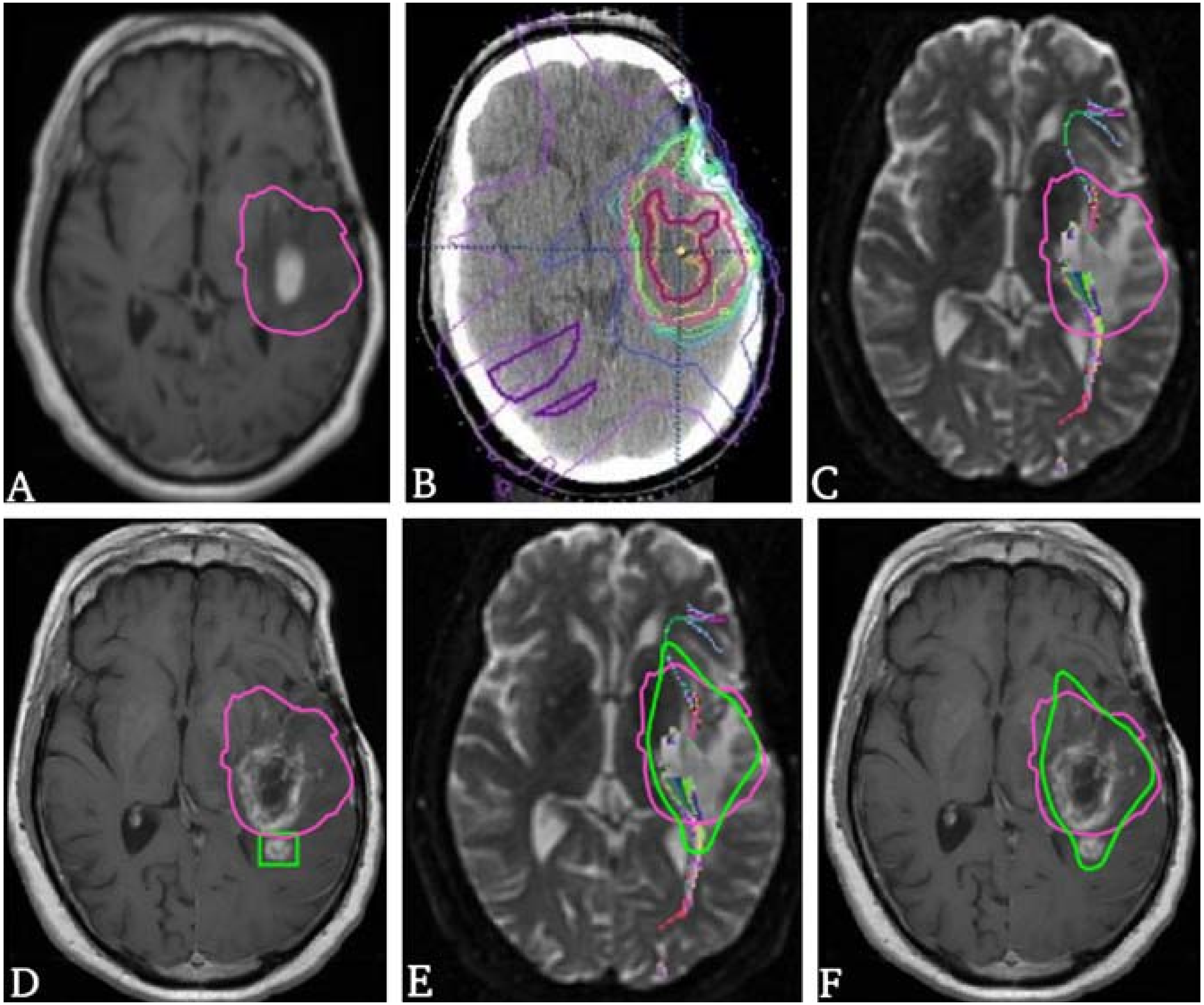

Krishnan et al., IJROBP, 2008;

Berberat et al., Strahlenther Oncol 2014

Optic Radiation – SRS Injury

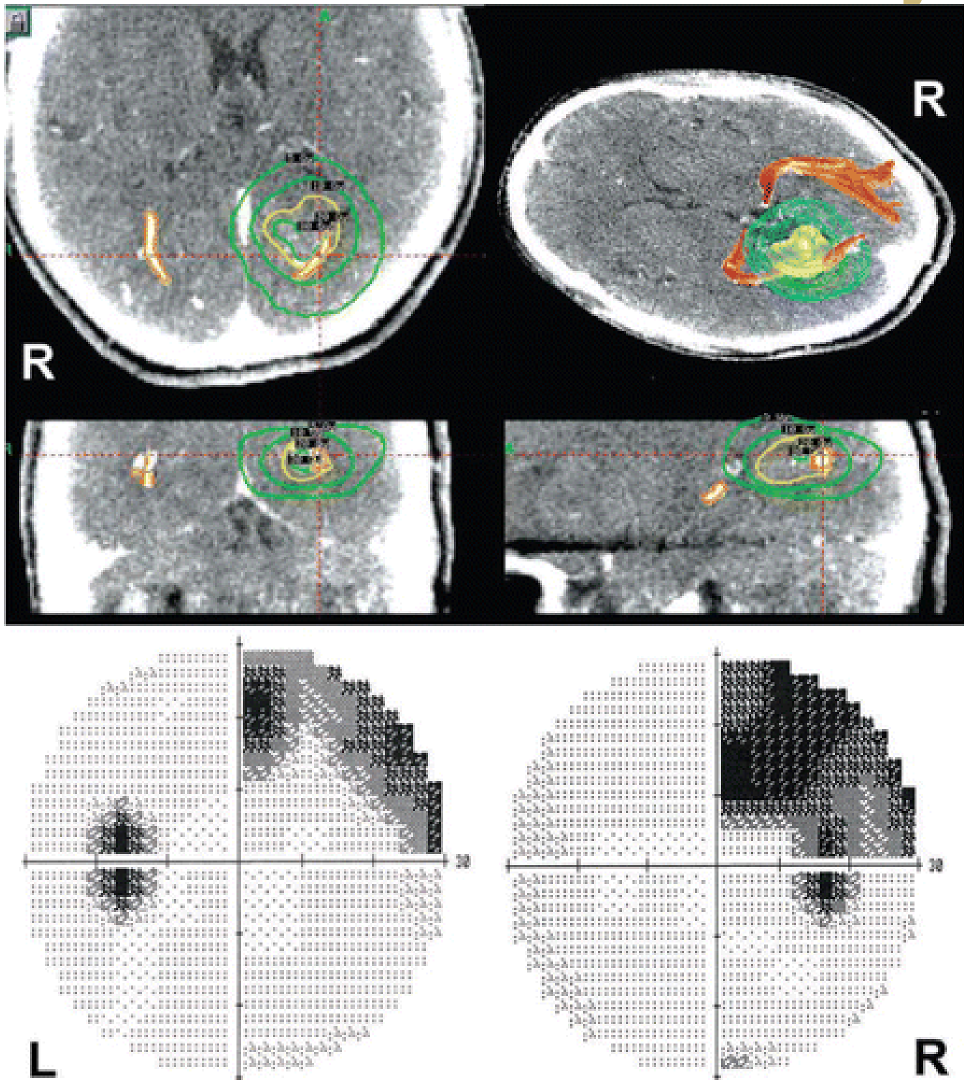

Maruyama et al, J Neurosurg, 2007

DTI – OAR Sparing

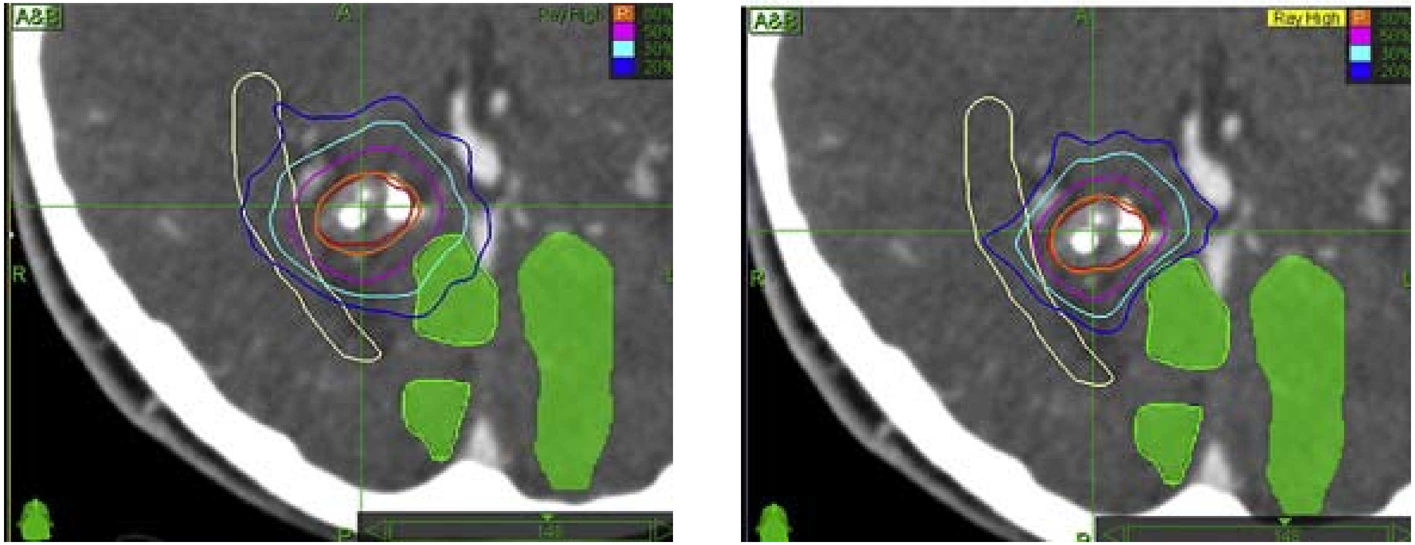

Pantelis et al, IJROBP, 2010

Atlas-based Segmentation

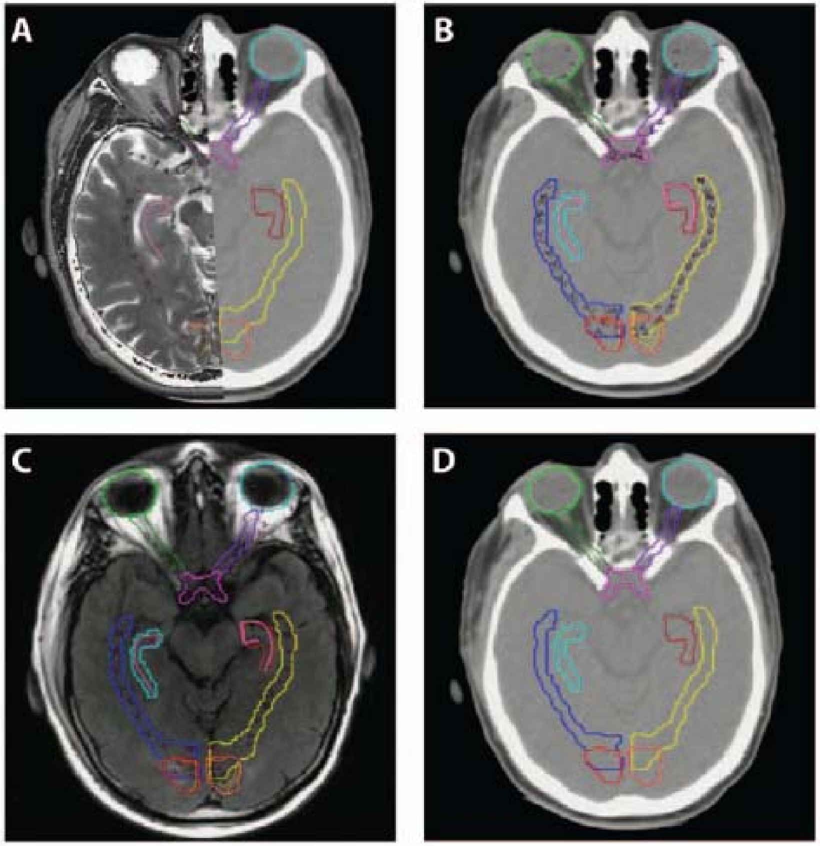

Figure 3. Identification of cryptic critical structures. In A) the overlay of the Anatom-E atlas and planning CT is illustrated. In B), the atlas image has been turned off, leaving the structures alone superimposed on the planning CT. Panel C shows the overlay with the pre-treatment MRI, and Panel D depicts the atlas images turned off, with the resultant contours on the planning CT.
doi:10.1371/journal.pone.0032098.g003

Weksberg et al., 2012, PLoS One

Stereotactic Reference - Deviation

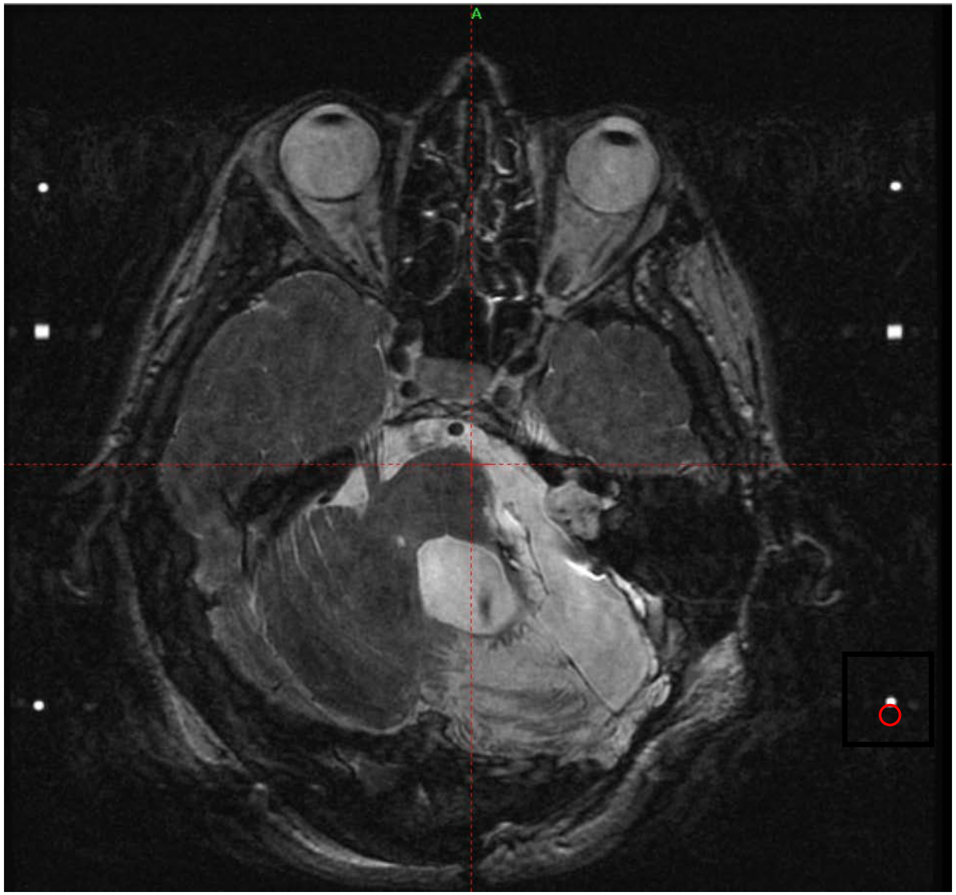

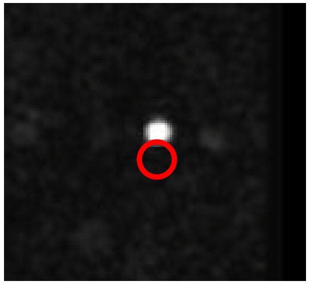

📖Zhang et al. PMB 55:22:6601-6615, 2010

Displacement of IAC

3T T2 FRFSE

CT

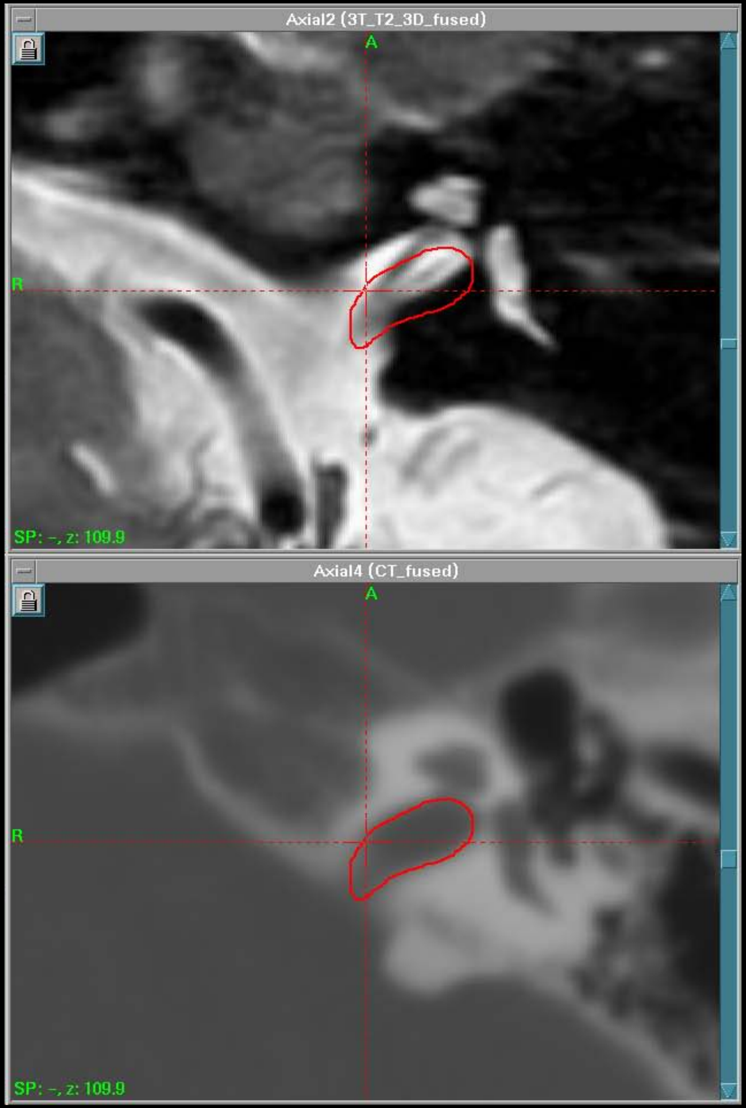

Zhang et al. PMB 55:22:6601-6615, 2010

Stereotactic Reference Deviation (T2)

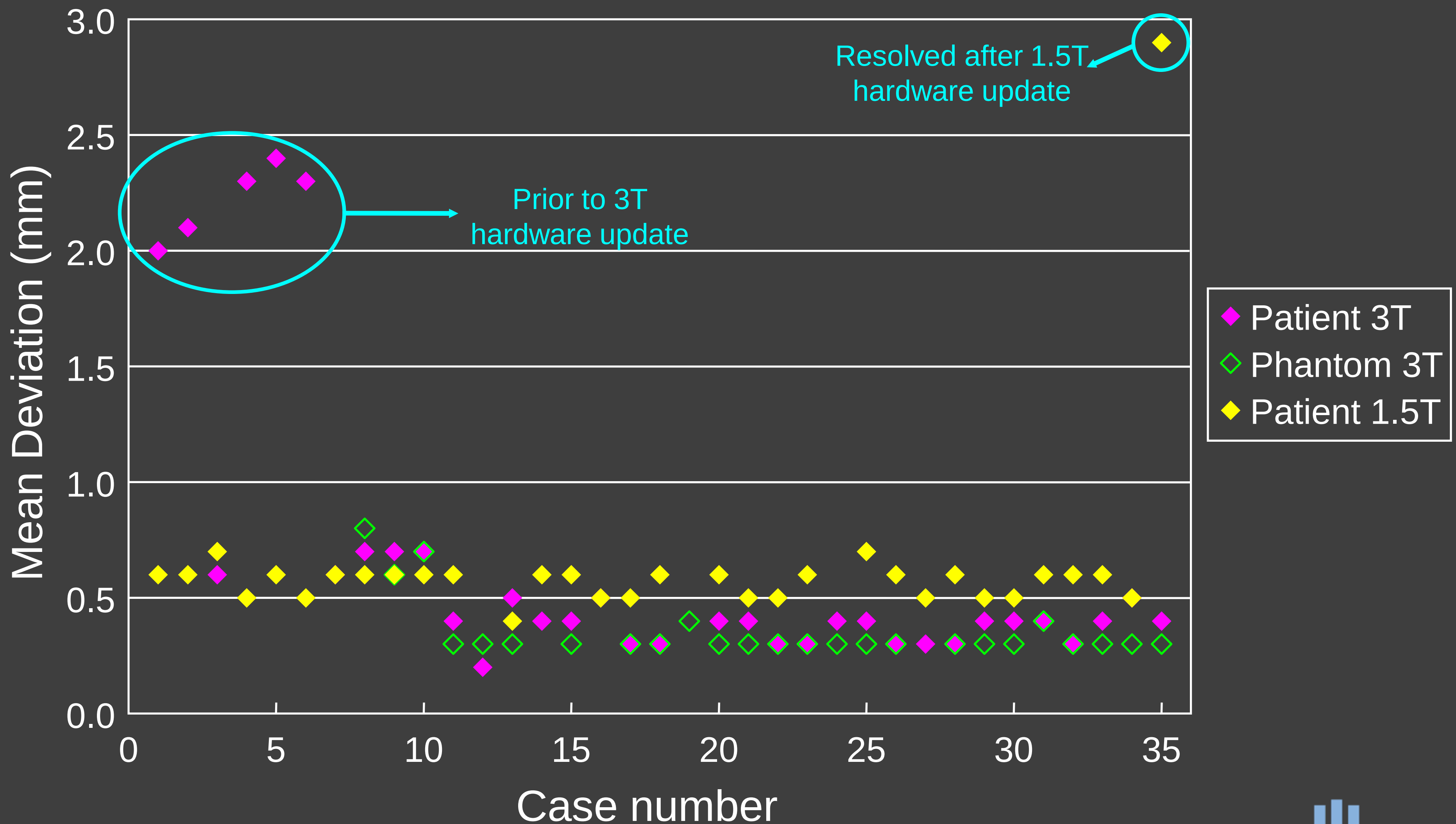

Zhang et al. PMB 55:22:6601-6615, 2010

CHUM

Stereotactic Reference Deviation (T1)

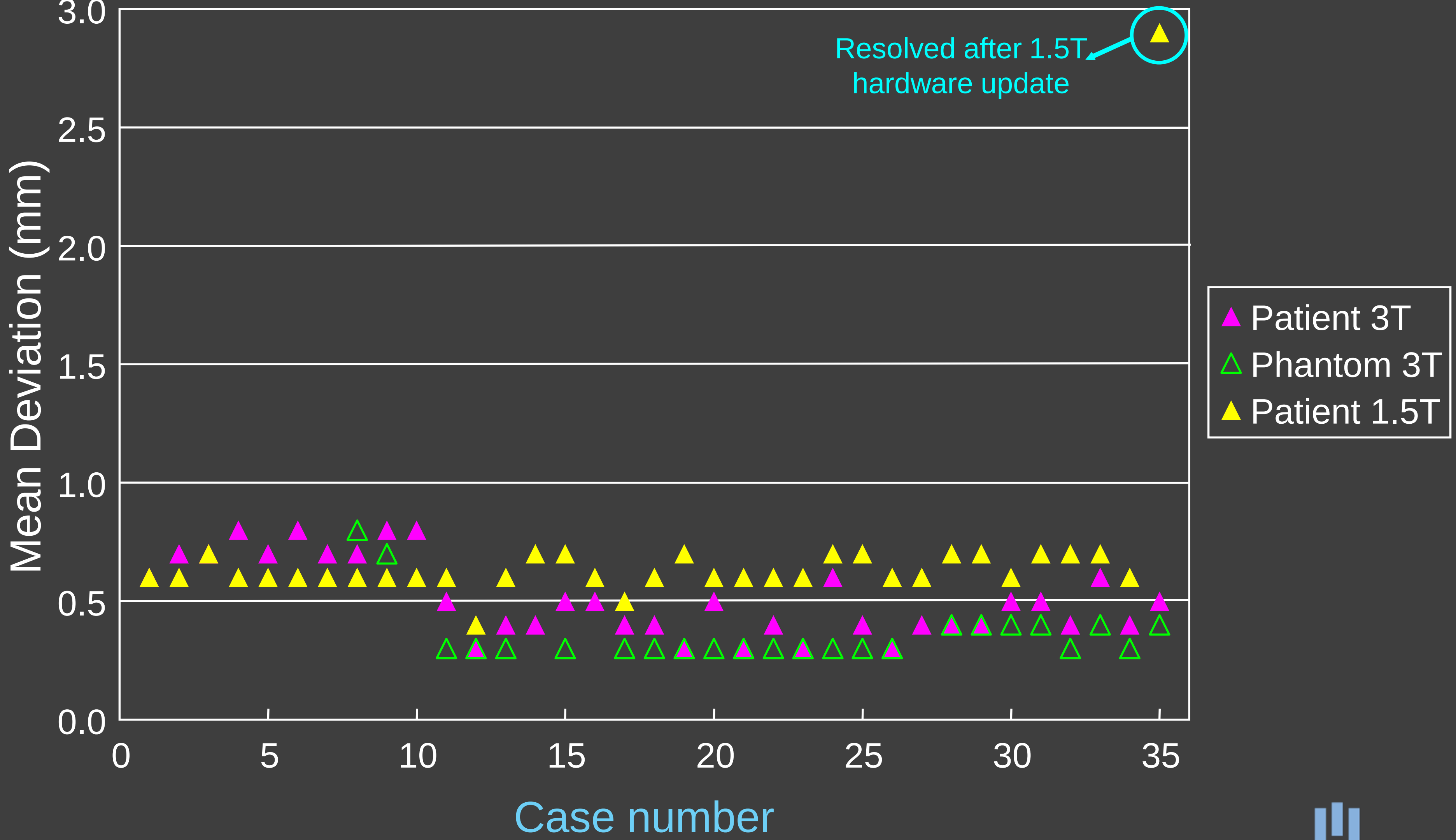

📖Zhang et al. PMB 55:22:6601-6615, 2010

Stereotactic Reference Deviation (Mean)

3T: Patient vs. Phantom

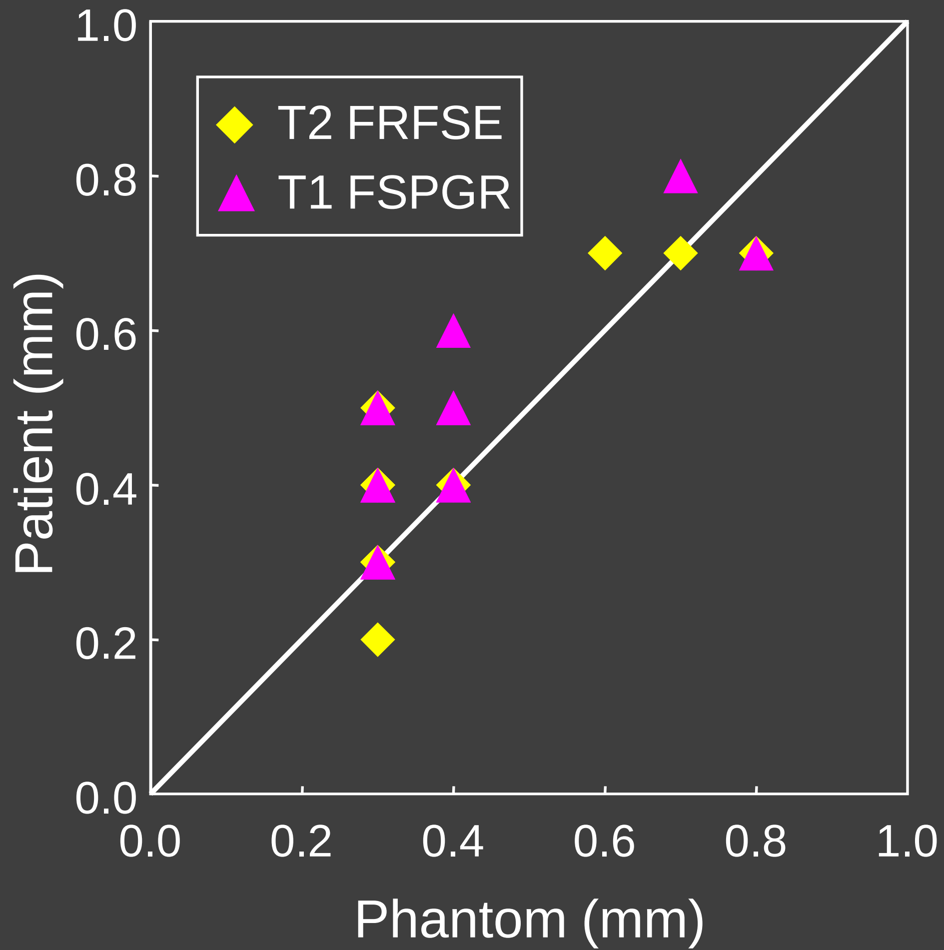

3T vs. 1.5T (Patient)

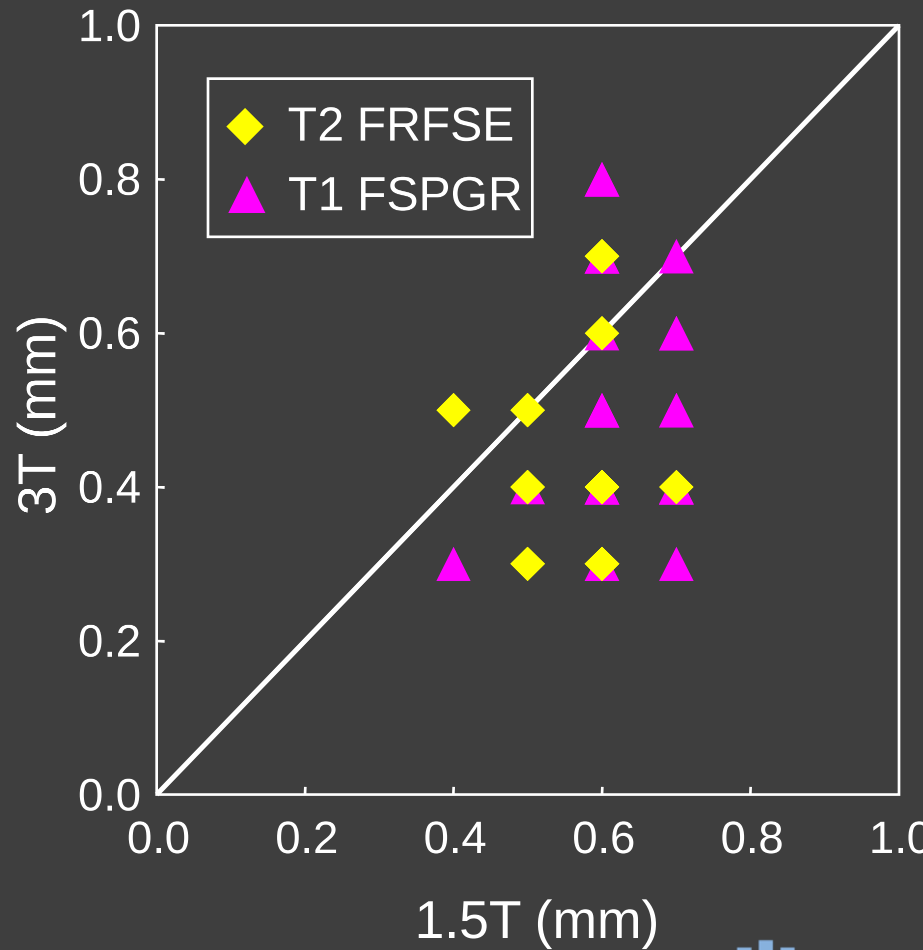

Zhang et al. PMB 55:22:6601-6615, 2010

Phantom: Internal Deviation (3T)

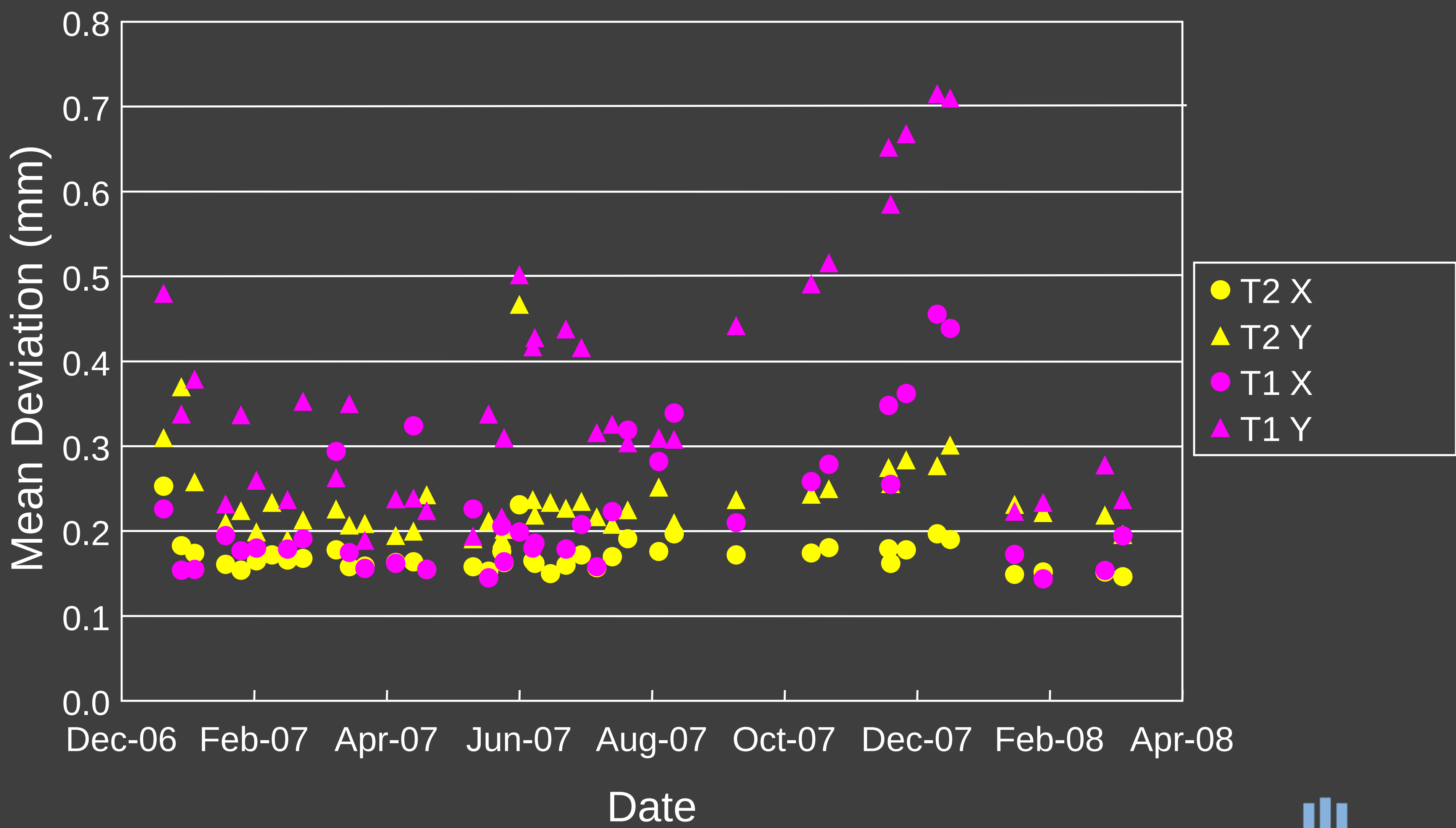

Zhang et al. PMB 55:22:6601-6615, 2010

Clinical - Anatomic Landmark Displacement Relative to CT (16 Patients)

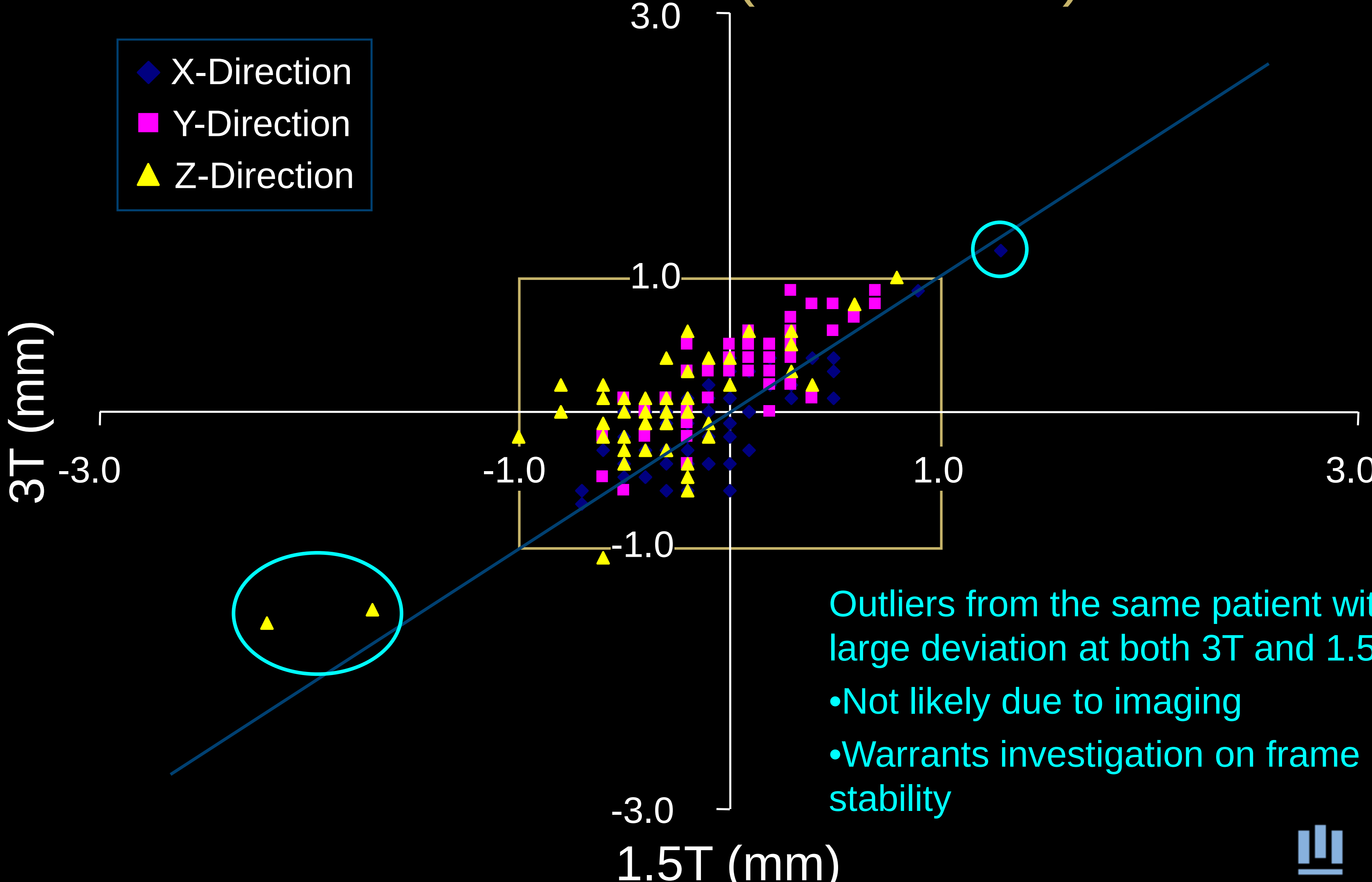

Outliers from the same patient with large deviation at both 3T and 1.5T

- Not likely due to imaging
- Warrants investigation on frame stability

Zhang et al. PMB 55:22:6601-6615, 2010

Hemorhagic Metastasis

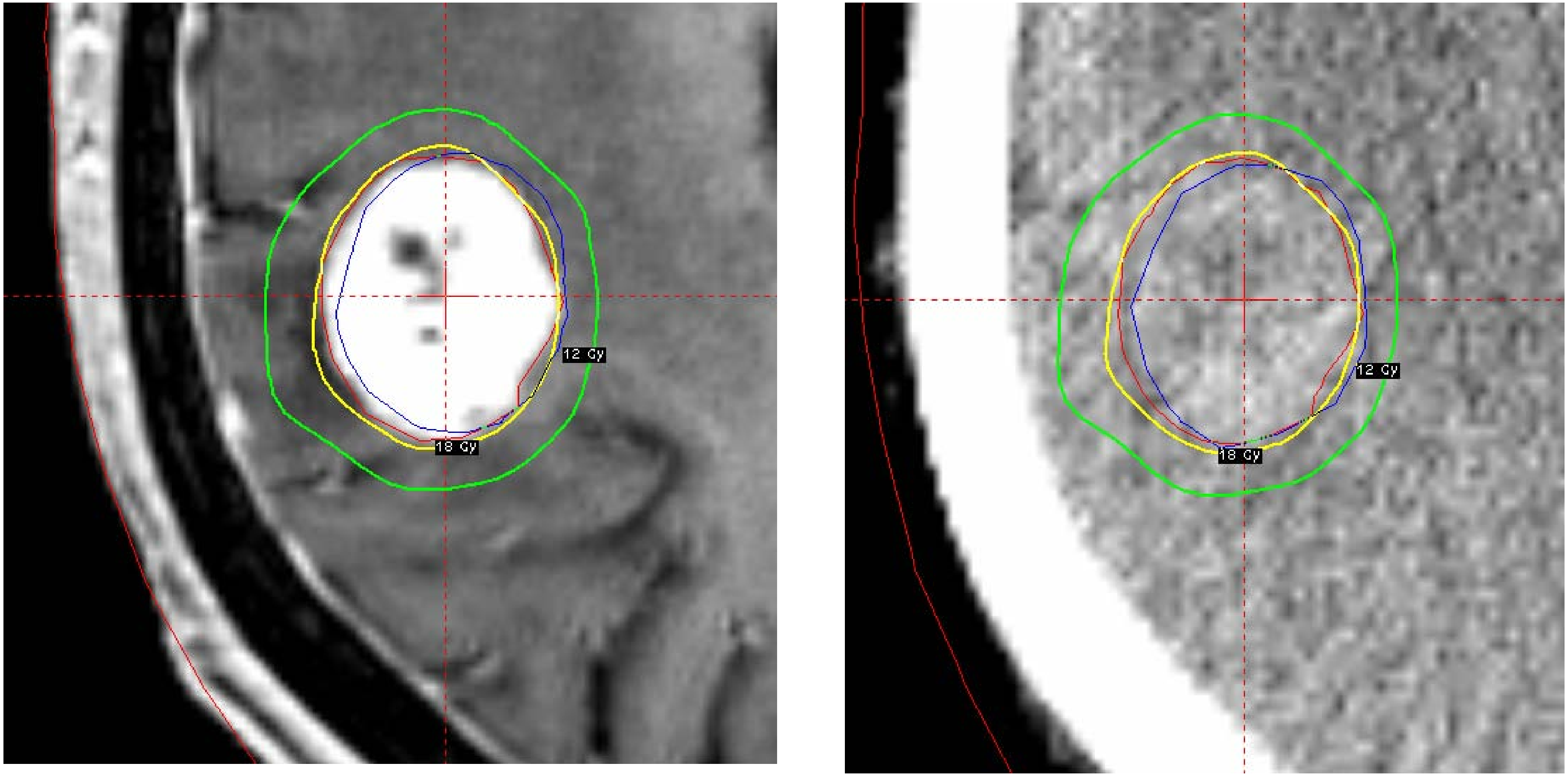

Chung et al., ISRS, 2011

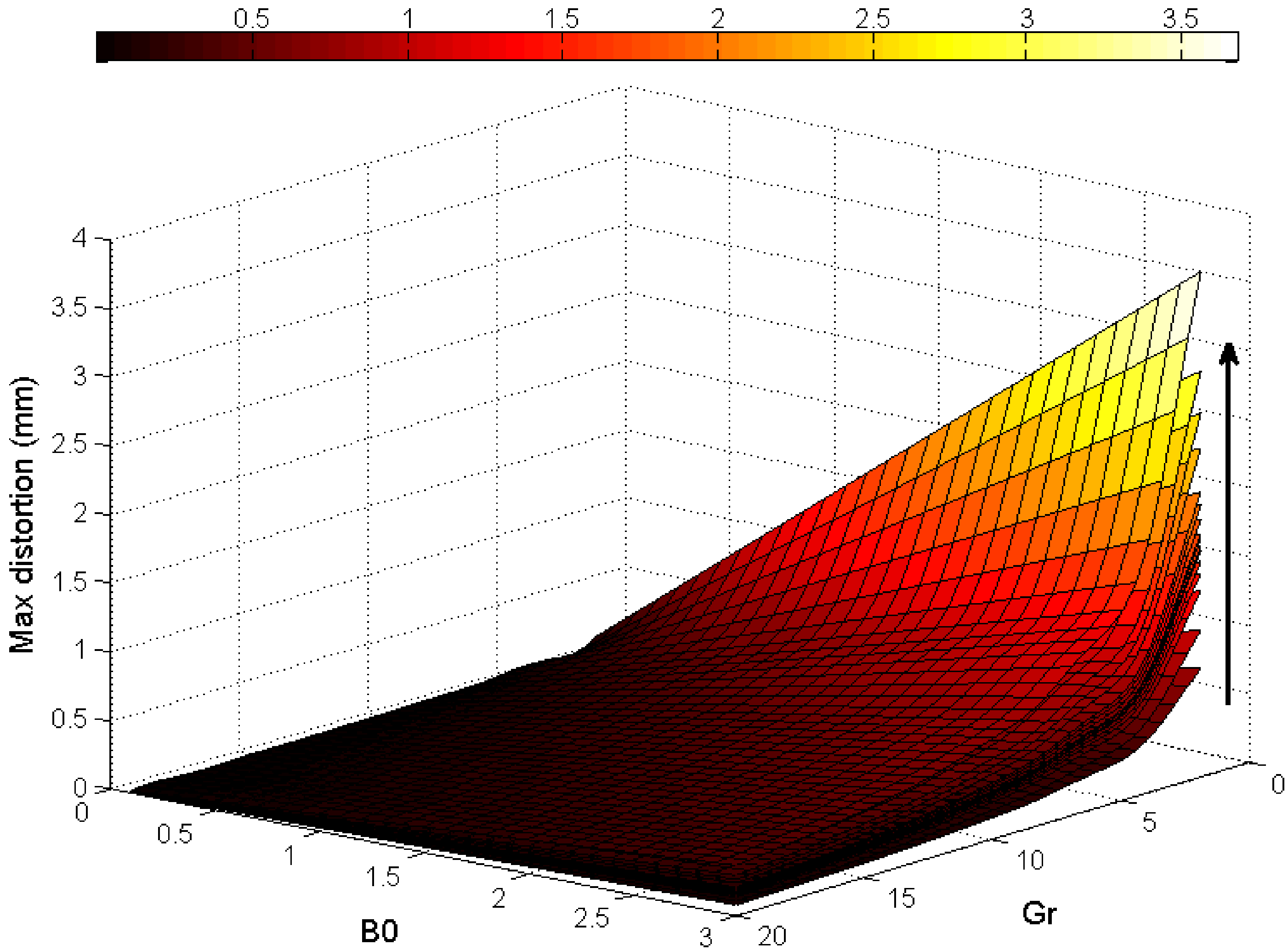

Stanescu et al., 2011

Example – Clinical readout-segmented-DWI at 3 T

→ RESOLVE (Works-in-Progress, Siemens Medical Systems)

T2w image | RESOLVE ADC | Standard ADC

3T IMRIS Verio

1.5x1.5x3-mm voxels in 20 slices

4 b-values (0, 100, 600, 1000 s/mm^2), 3 diffusion directions

Geometry – Key Points

- 1. System or scanner-related: B0 inhomogeneity, gradient non-linearities
  - Correction: with grid phantom + image processing software
  - Issues of system drift, system upgrades…

- 2. Patient or device-induced: susceptibility or chemical shift (fat)
  - Correction: a) numerical sims (our approach) and exp by acquiring additional image data with diff parameters (e.g., reversed gradient).
  - Magnitude: a few mm depending on the interface, worst for air-soft tissue.
  - distortion ~ Gr/Bo; where Gr is the readout gradient strength and B0 main magnetic field.

Issues mitigated by individual CT reference check!

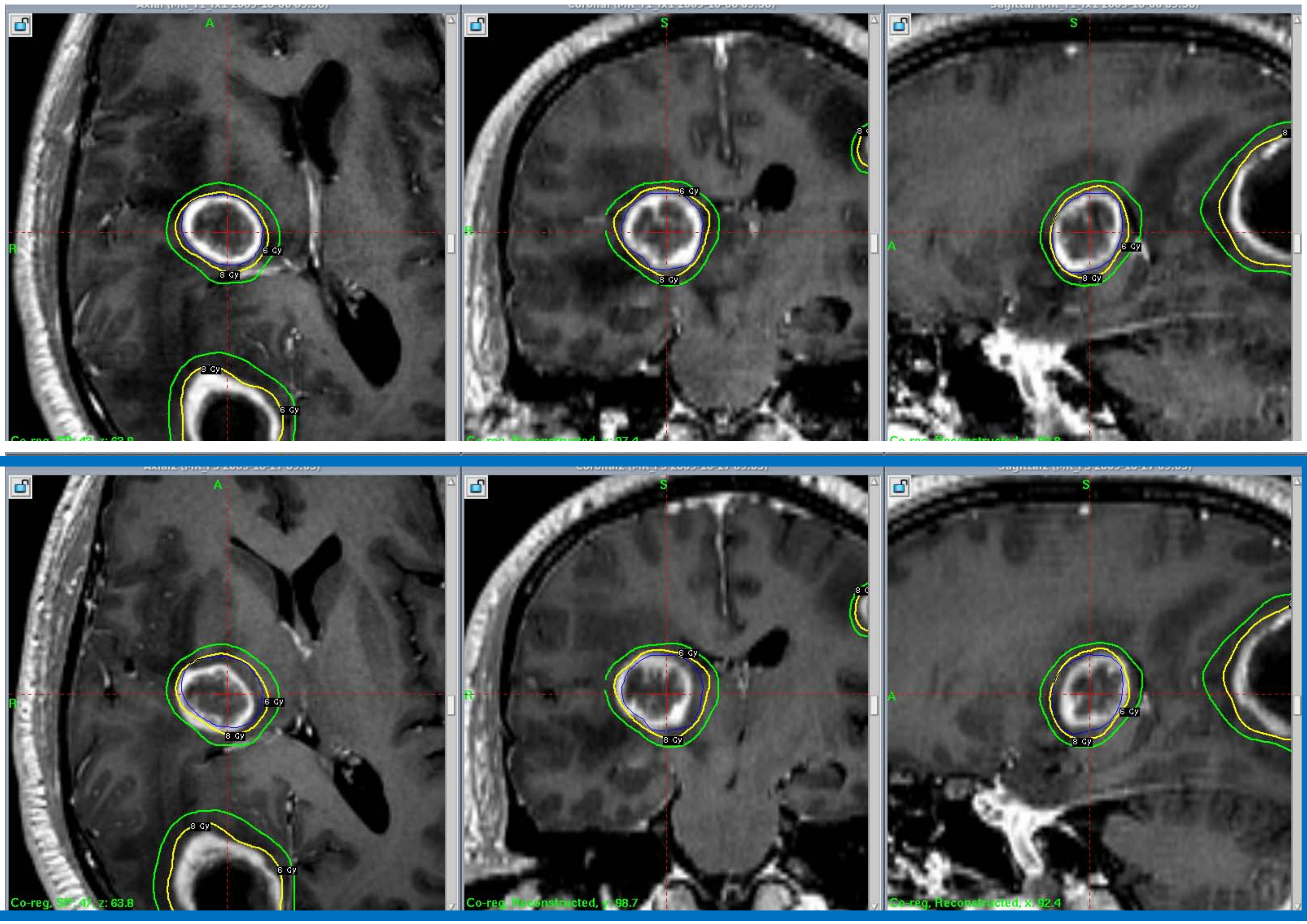

MRI at day 21 overlaid with the original plan

Cho et al., submitted

CHUM

Tumor Geometry ROC for 2y OS

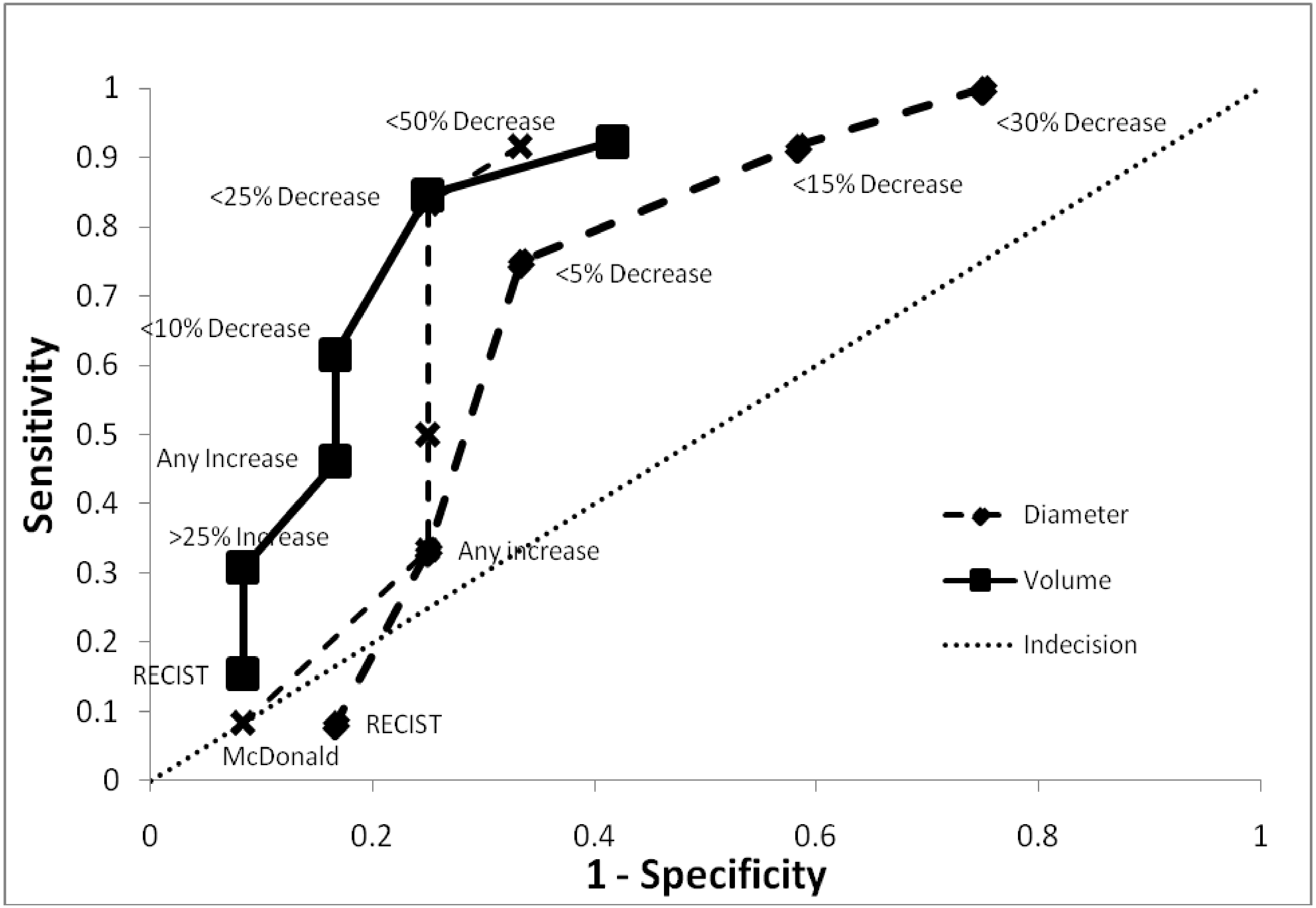

Gladwish et al., Radiat Oncol 2011

MRSI – Predicting Response

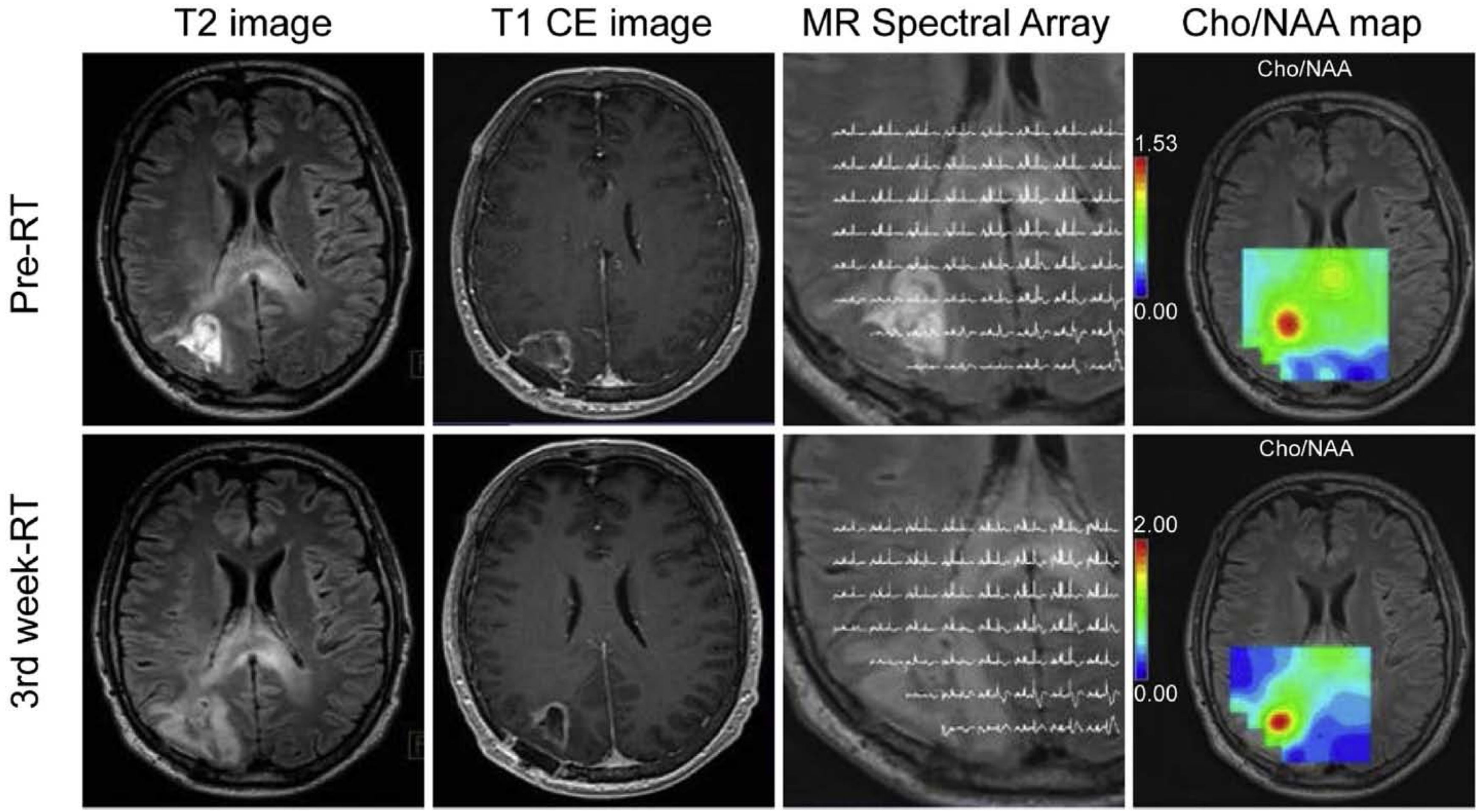

Fig. 2. A 52-year-old man with GBM and disease progression at last follow-up shows an increase in tumor metabolic status at 3 weeks of radiation therapy (RT) (tumor Cho/NAA ratio = voxel-based choline/N-acetylaspartate ratios [Cho/NAA] mean ± standard error 1.33 ± 0.59 to 2.13 ± 0.95). Note that the scaling for the spectroscopy for the pre-RT images and third-week RT images are different and automatically assigned within the spectroscopy software. MR = magnetic resonance.

Muruganadham et al., 2014, IJROBP

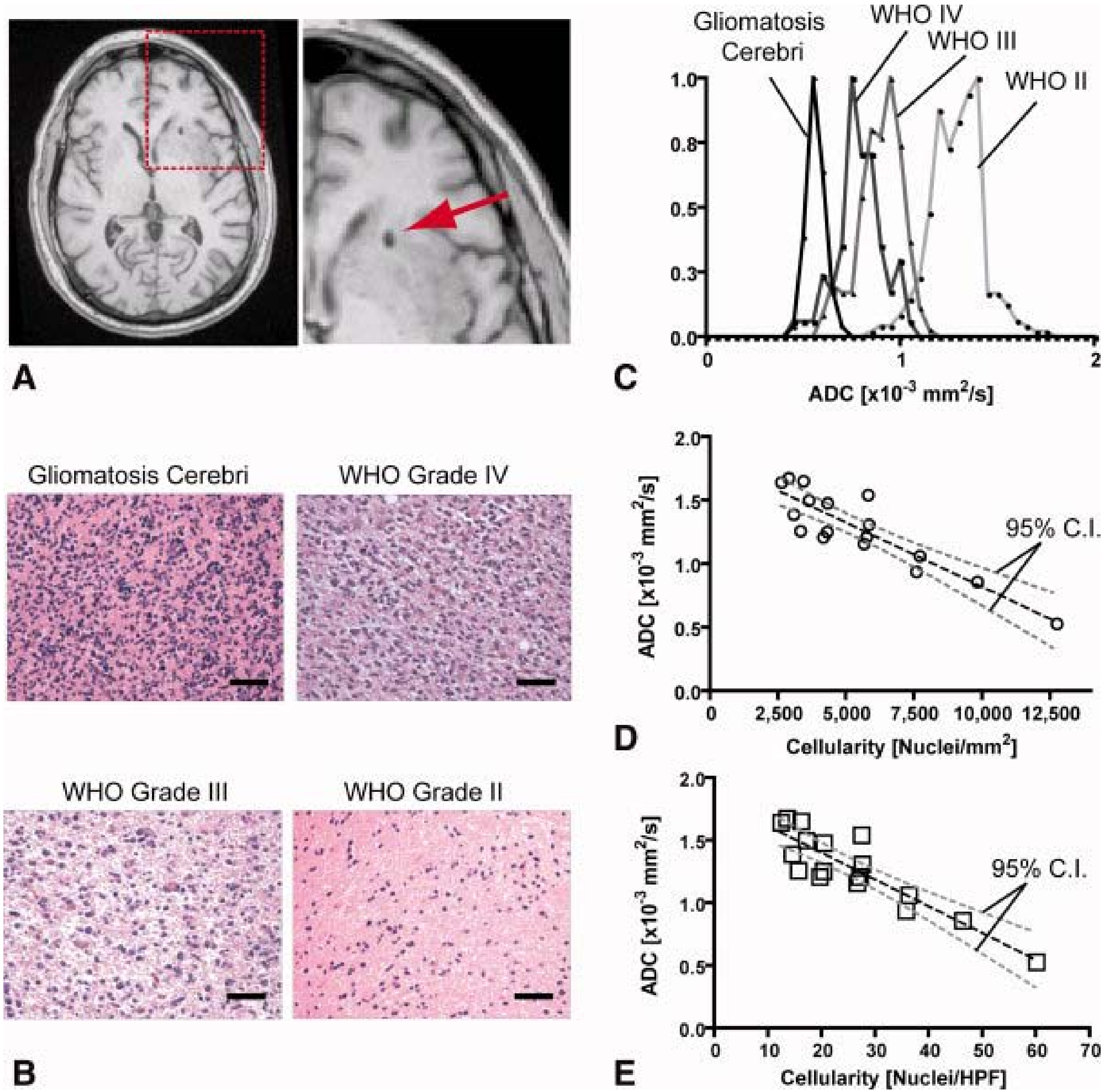

Ellingson et al., JMRI 31:538-548 (2010)

CHUM

ADC Response

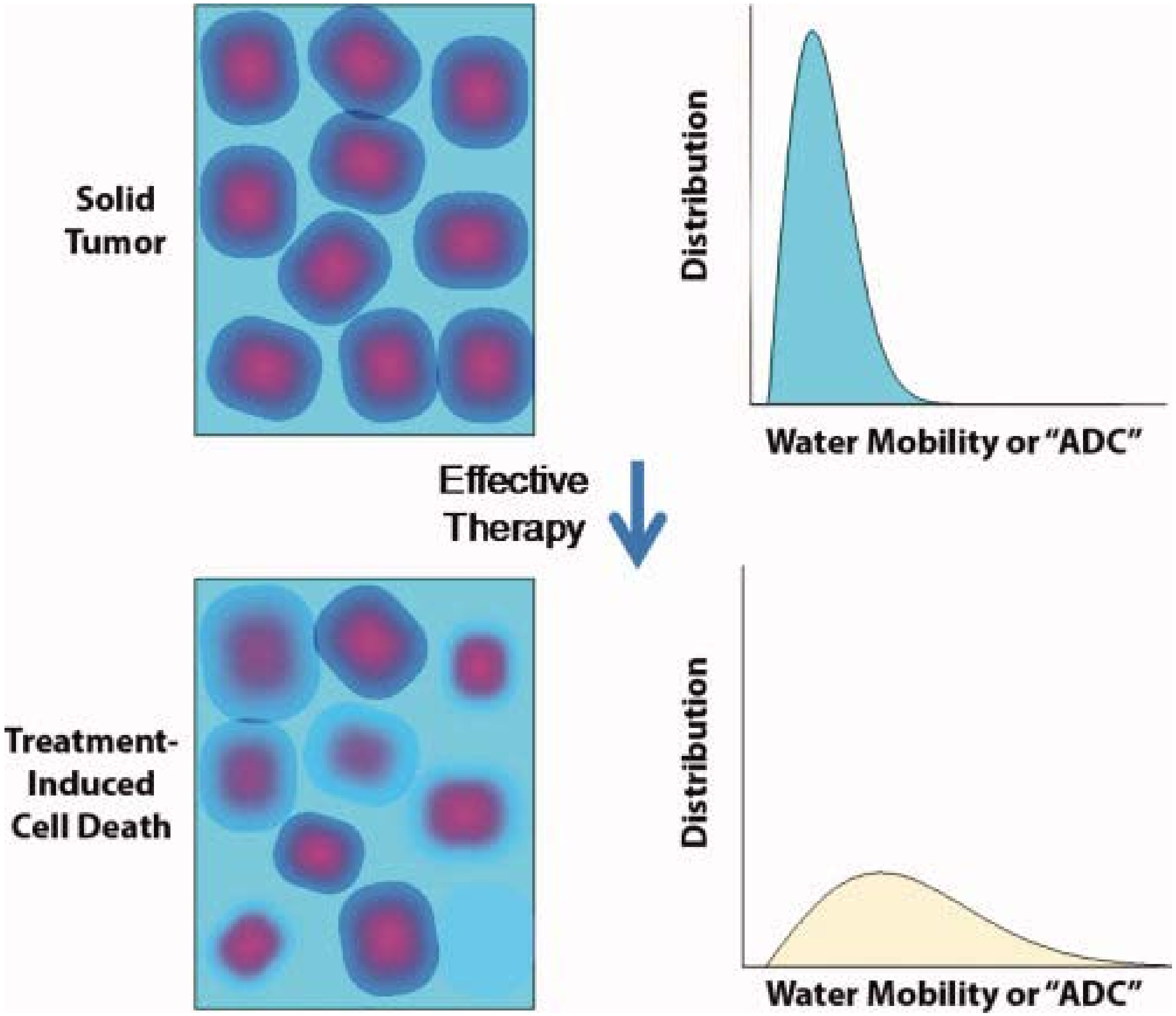

📖 Thoeny et al., JMRI 32:2-16, 2010

ADC Dynamics

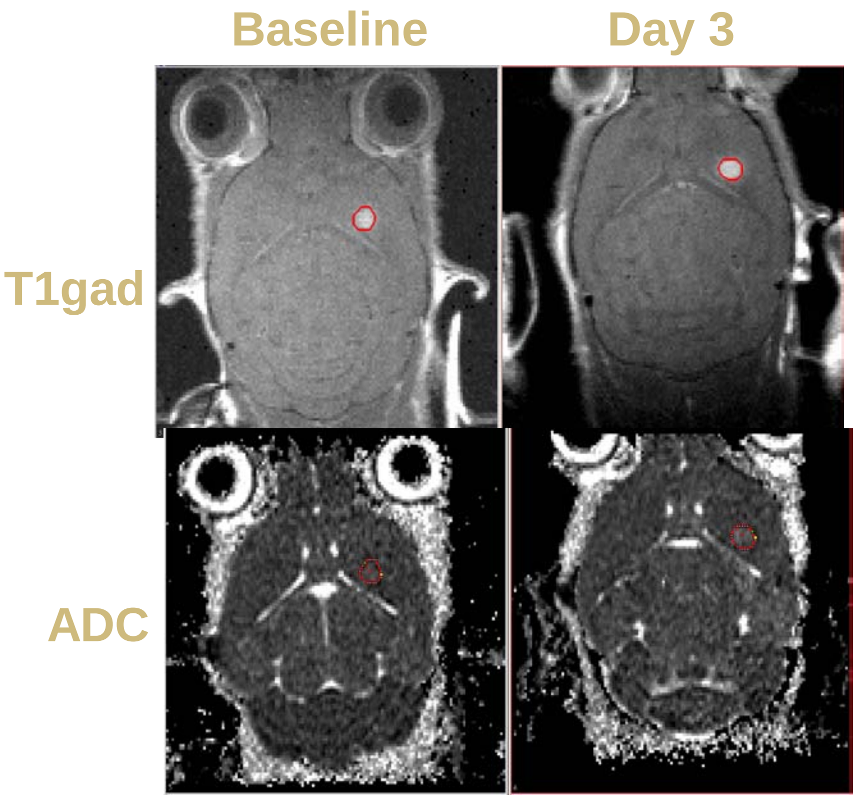

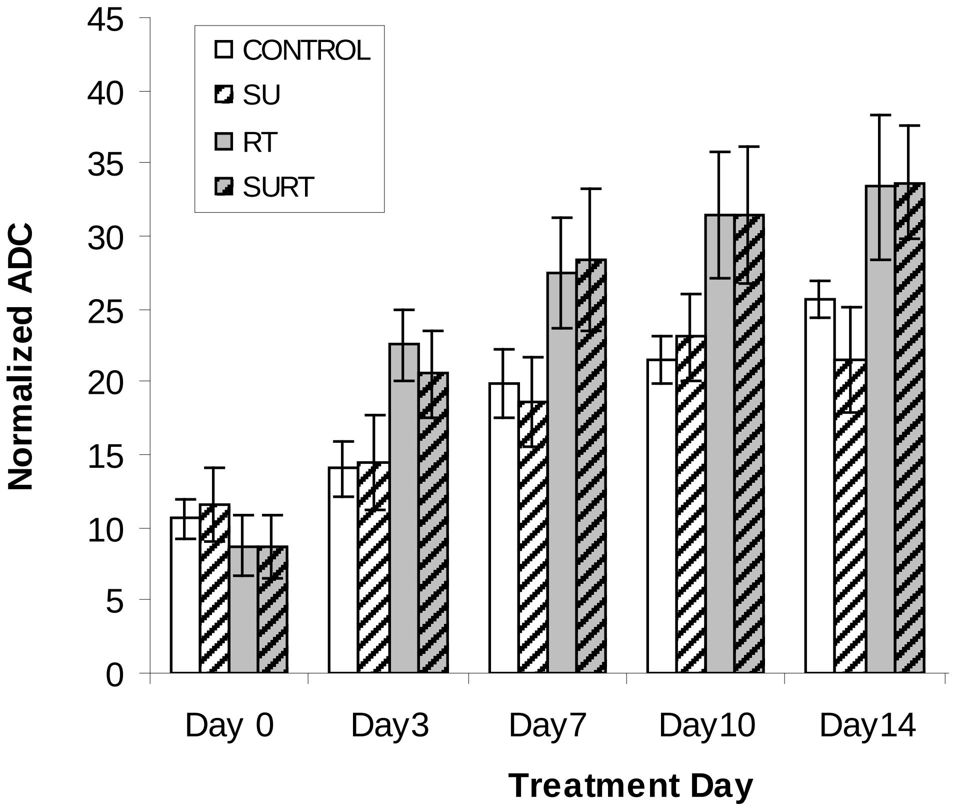

Chung et al., IJROBP, 2012

ADC Response vs Tumor Growth Rate

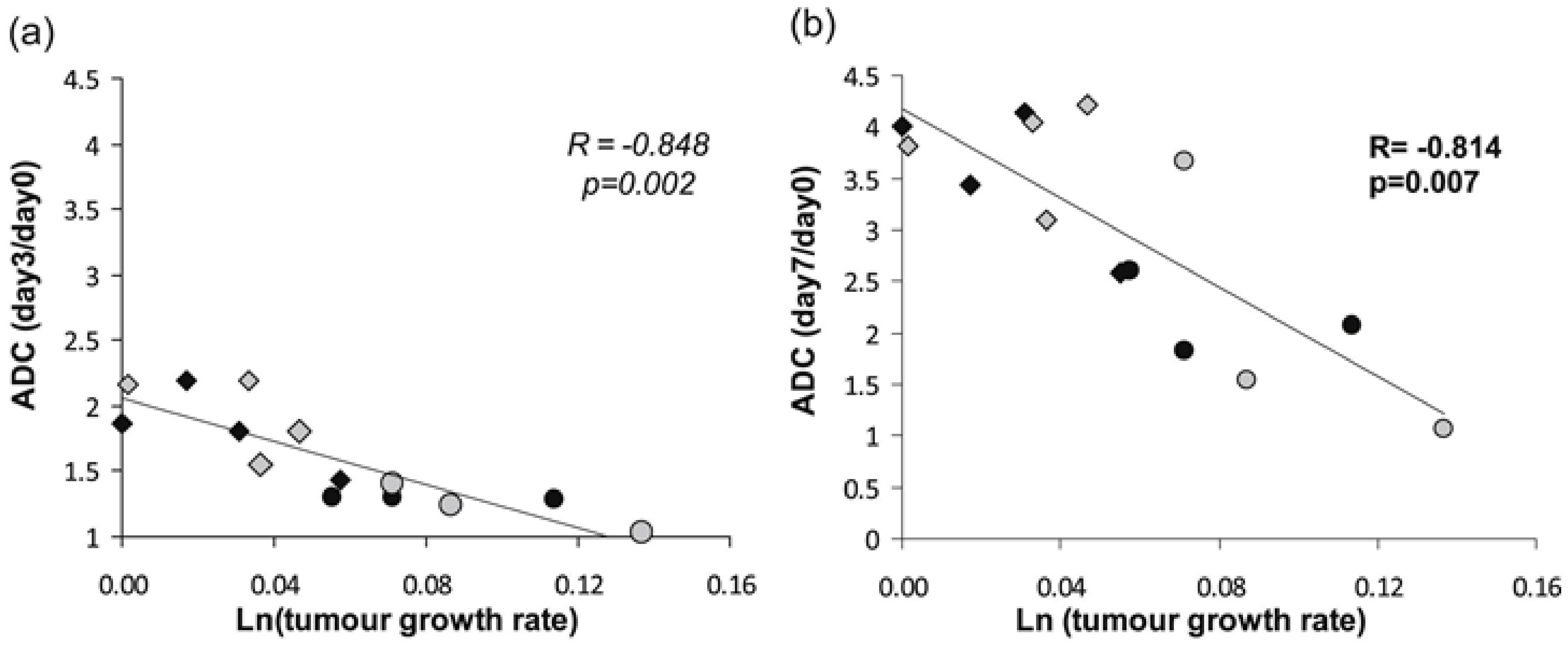

Chung et al., IJROBP, 2012

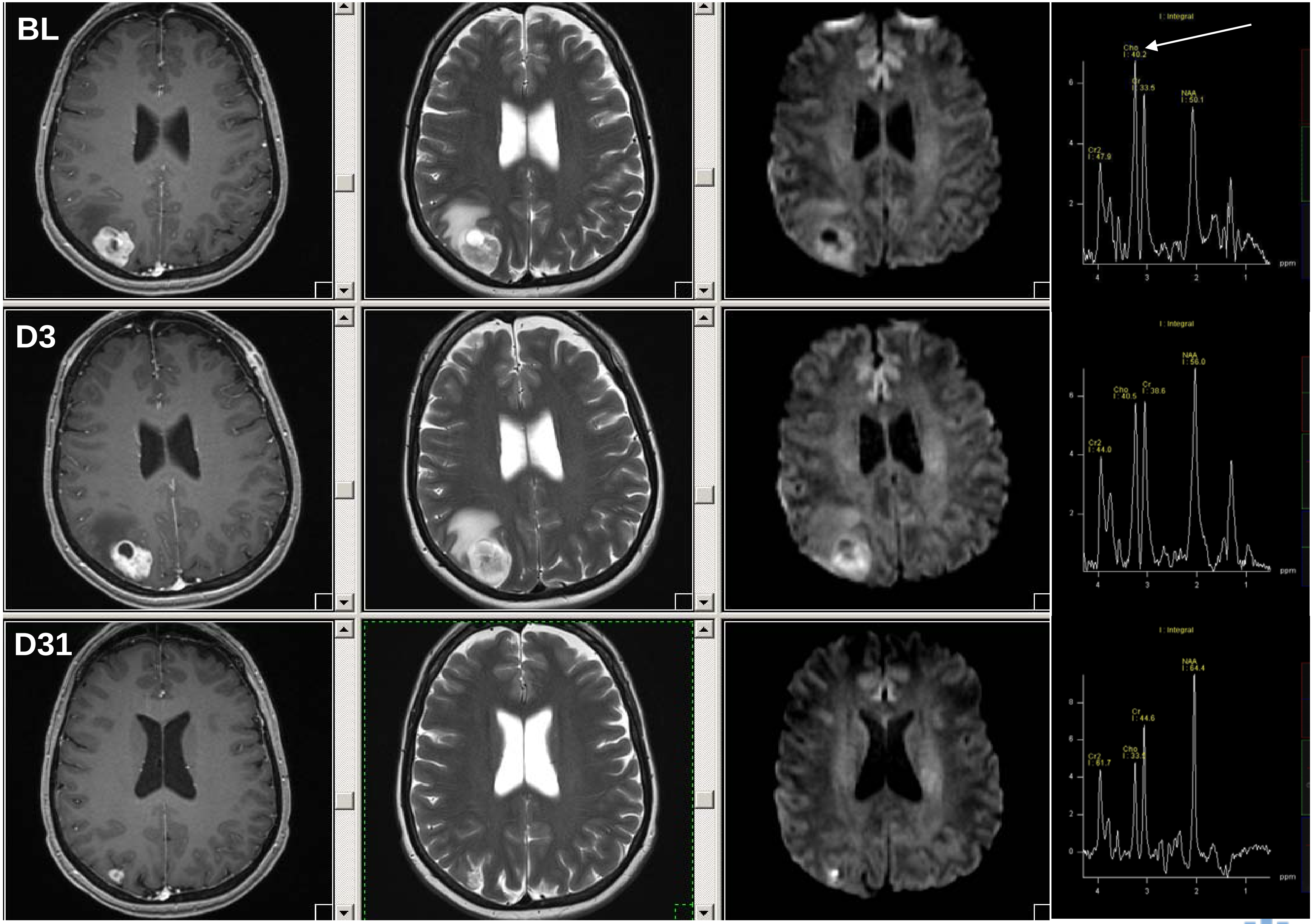

📖 Menard et al., Chapter in Technical Basis of RT

CHUM

QUALITÉ | INTÉGRITÉ | INNOVATION | COLLABORATION | PERFORMANCE

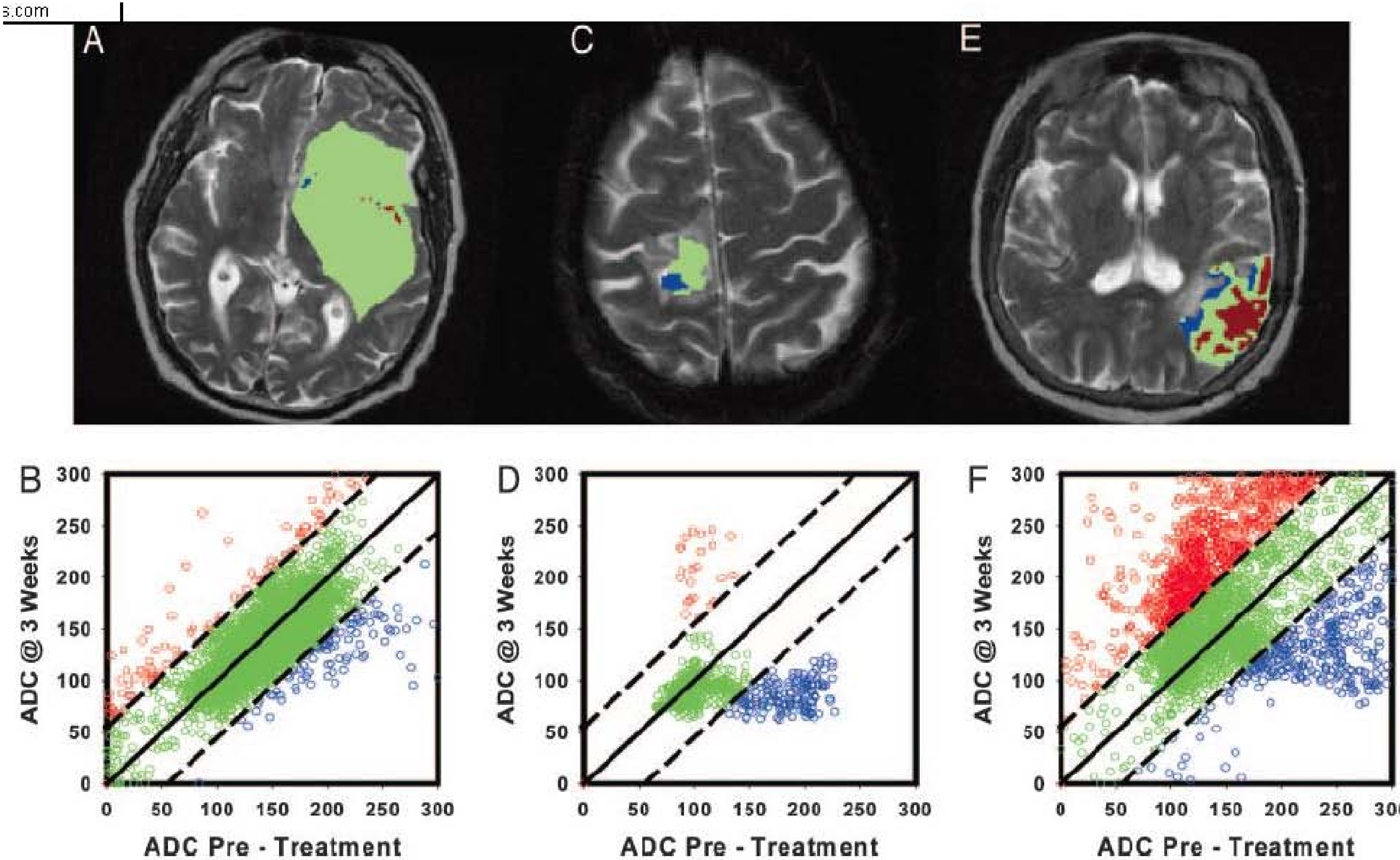

Moffat et al.

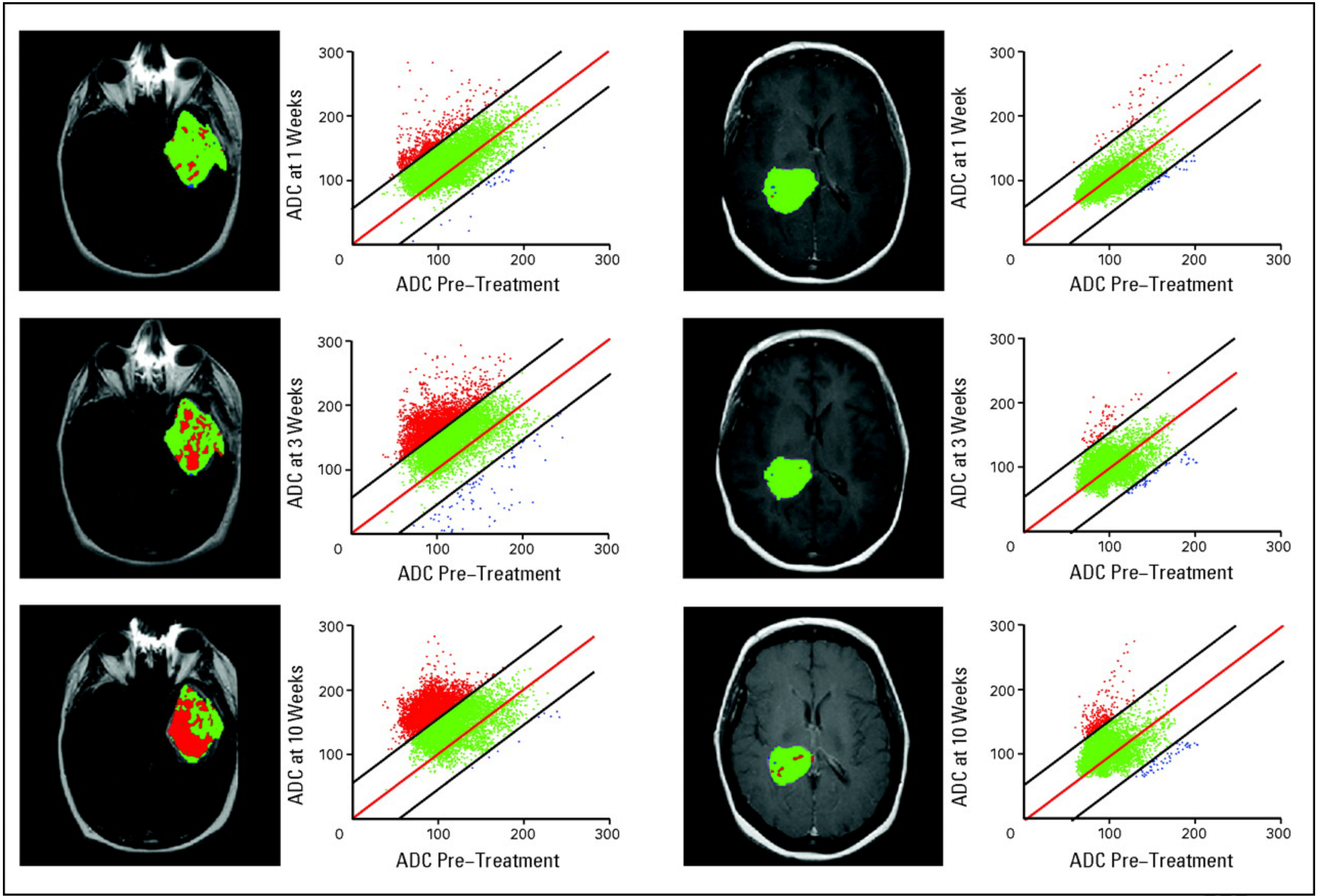
ADC at 1 Weeks
ADC at 3 Weeks
ADC at 10 Weeks
ADC at 1 Week
ADC Pre–Treatment
0
100
200
300

Diffusion Abnormality Index

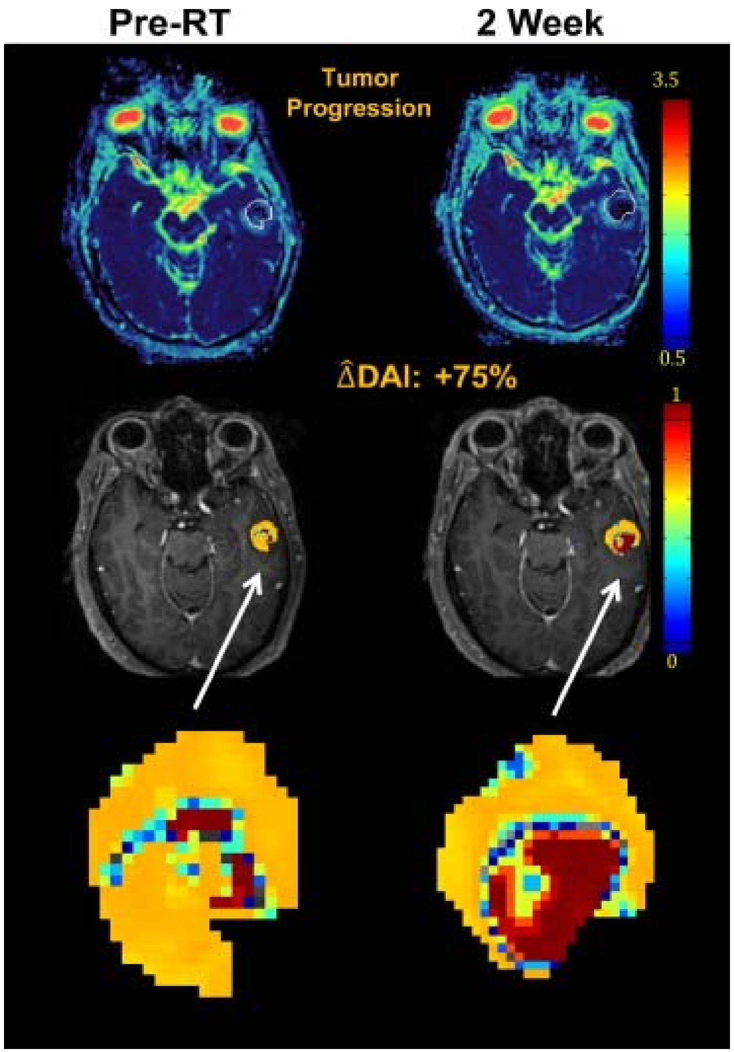

Tsien et al., Sem in Rad Oncol 2014

Voxel Correspondence

- The FDM approach assumes equivalent geometric and biological voxel correspondences between pre- and post-therapy images
- Dynamic tumor morphology confounds this assumption

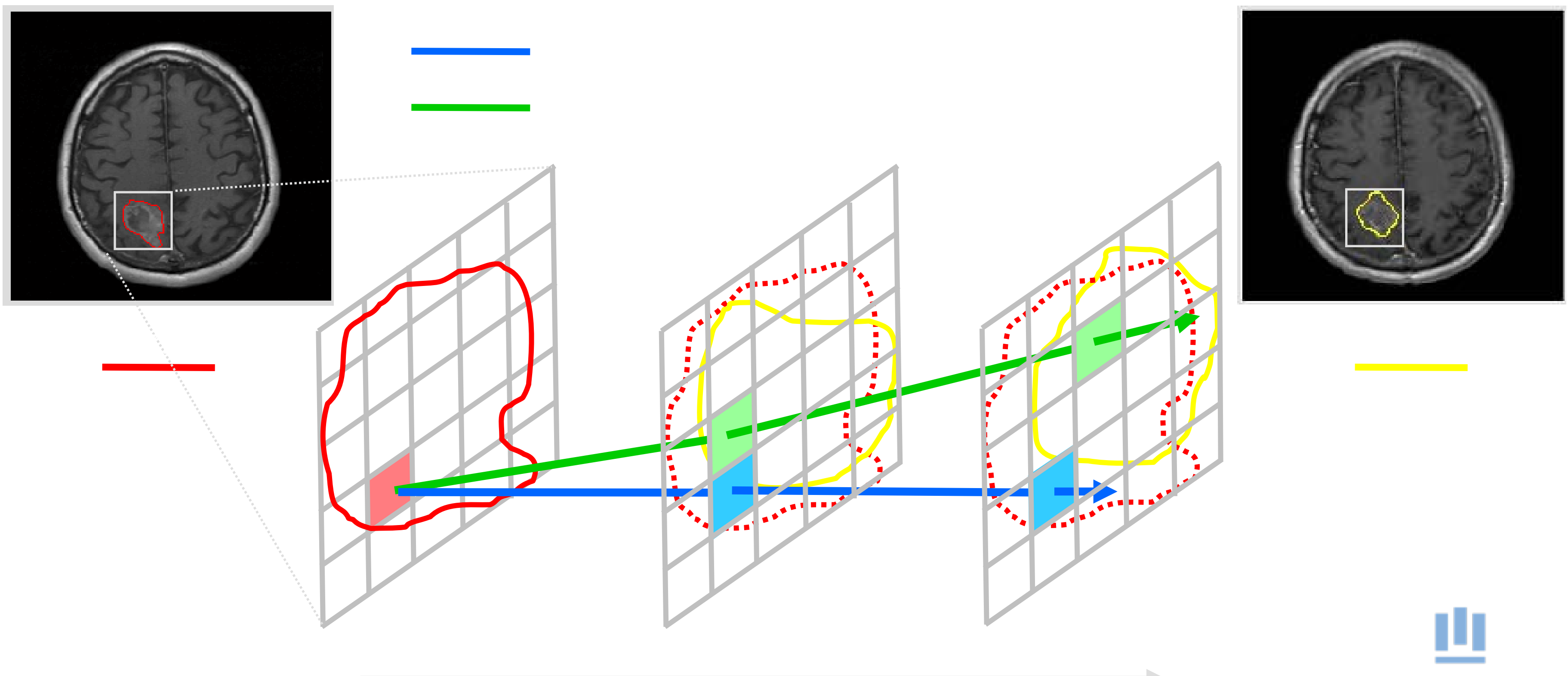

Hoisak et al.

Registration: ADC → (T2 → T1)

-using normalized mutual information

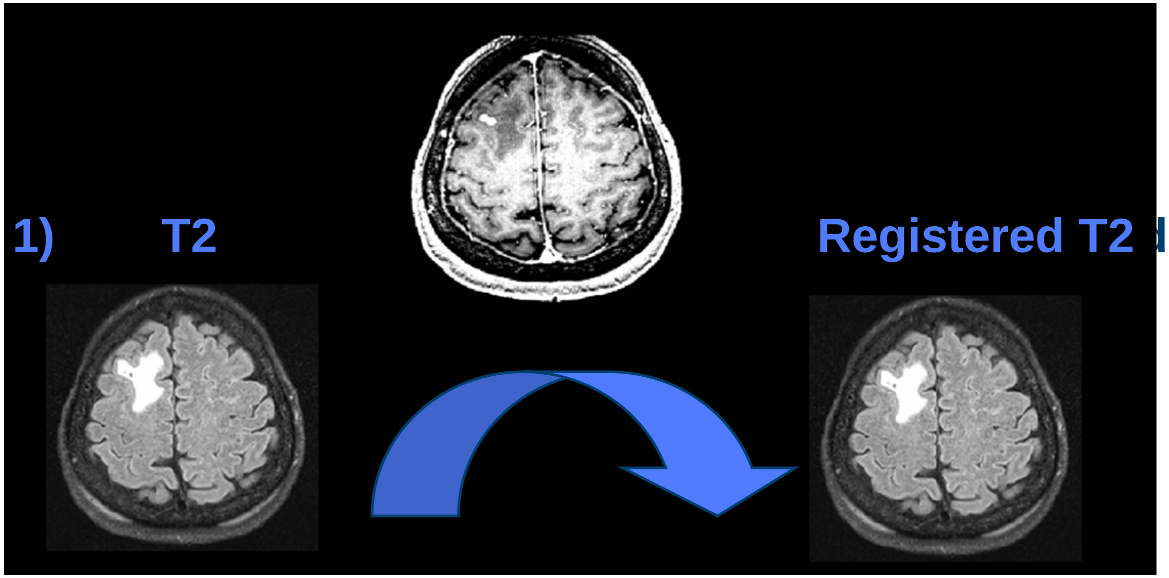

DTI in RT

- Several studies track FA and diffusivities longitudinally post-RT in normal appearing white matter
- Early DTI changes now being related to functional consequences

<u>DTI & radiation effects</u> <u>DTI & late cognitive decline</u>

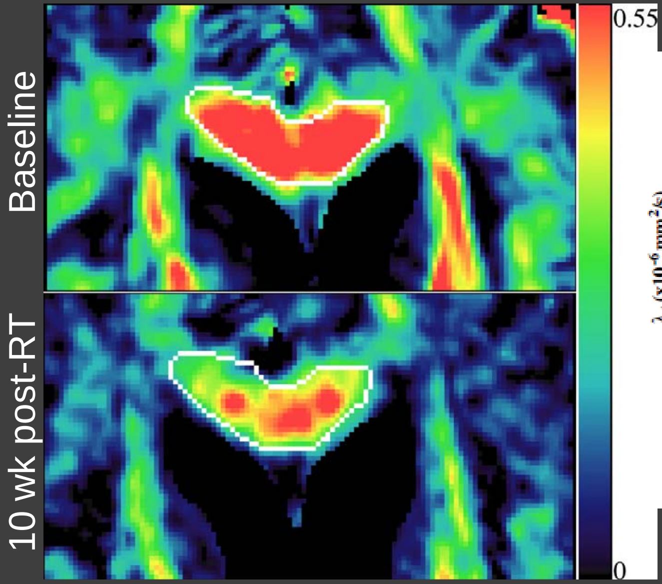

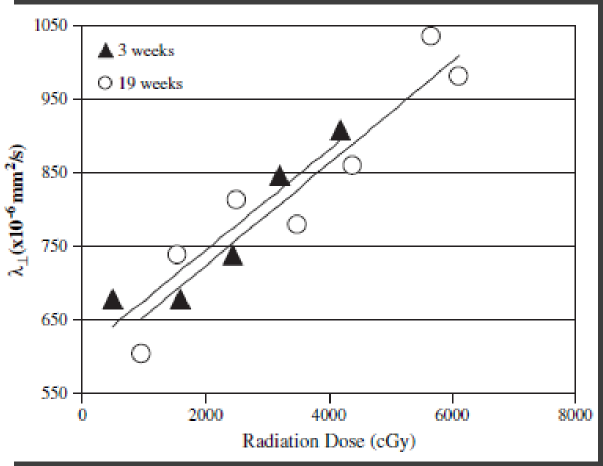

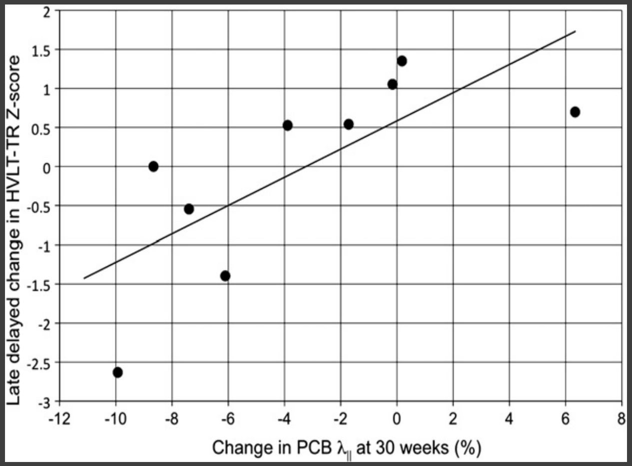

Nagesh, IJROBP, 2008; Chapman, IJROBP, 2012

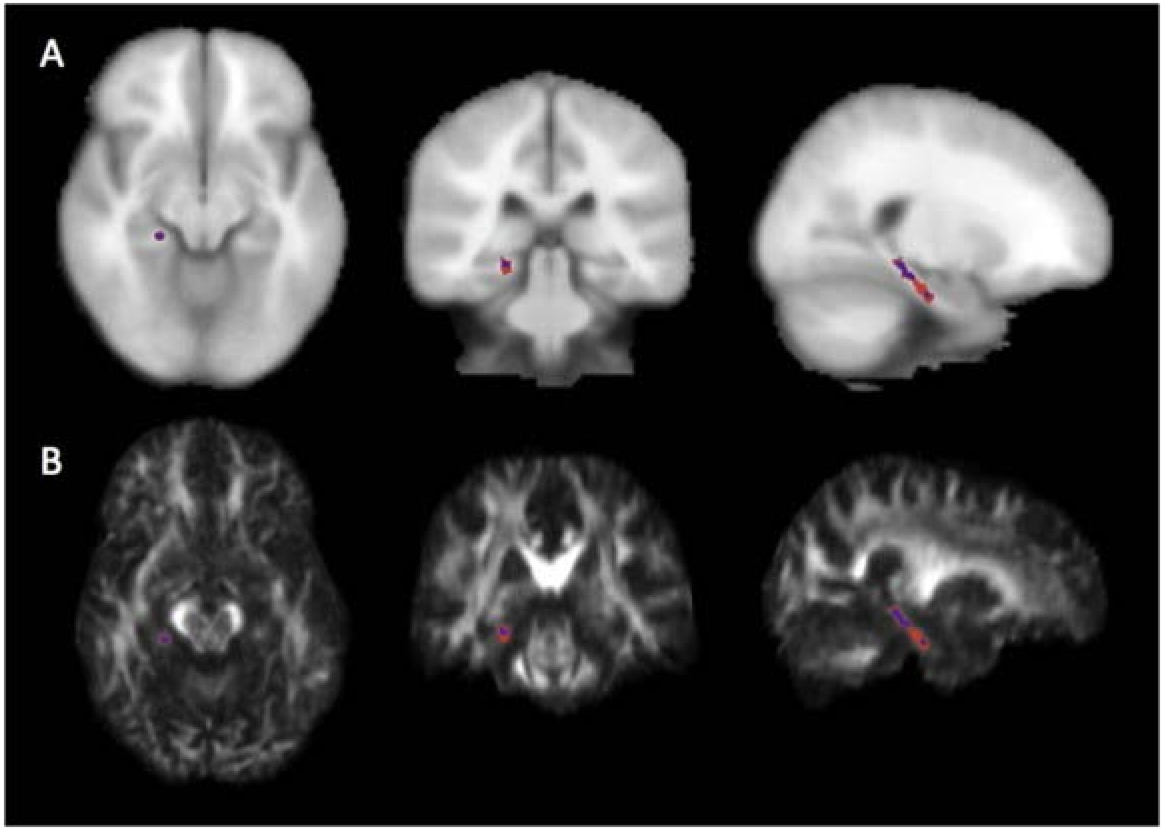

Chapman et al., 2016

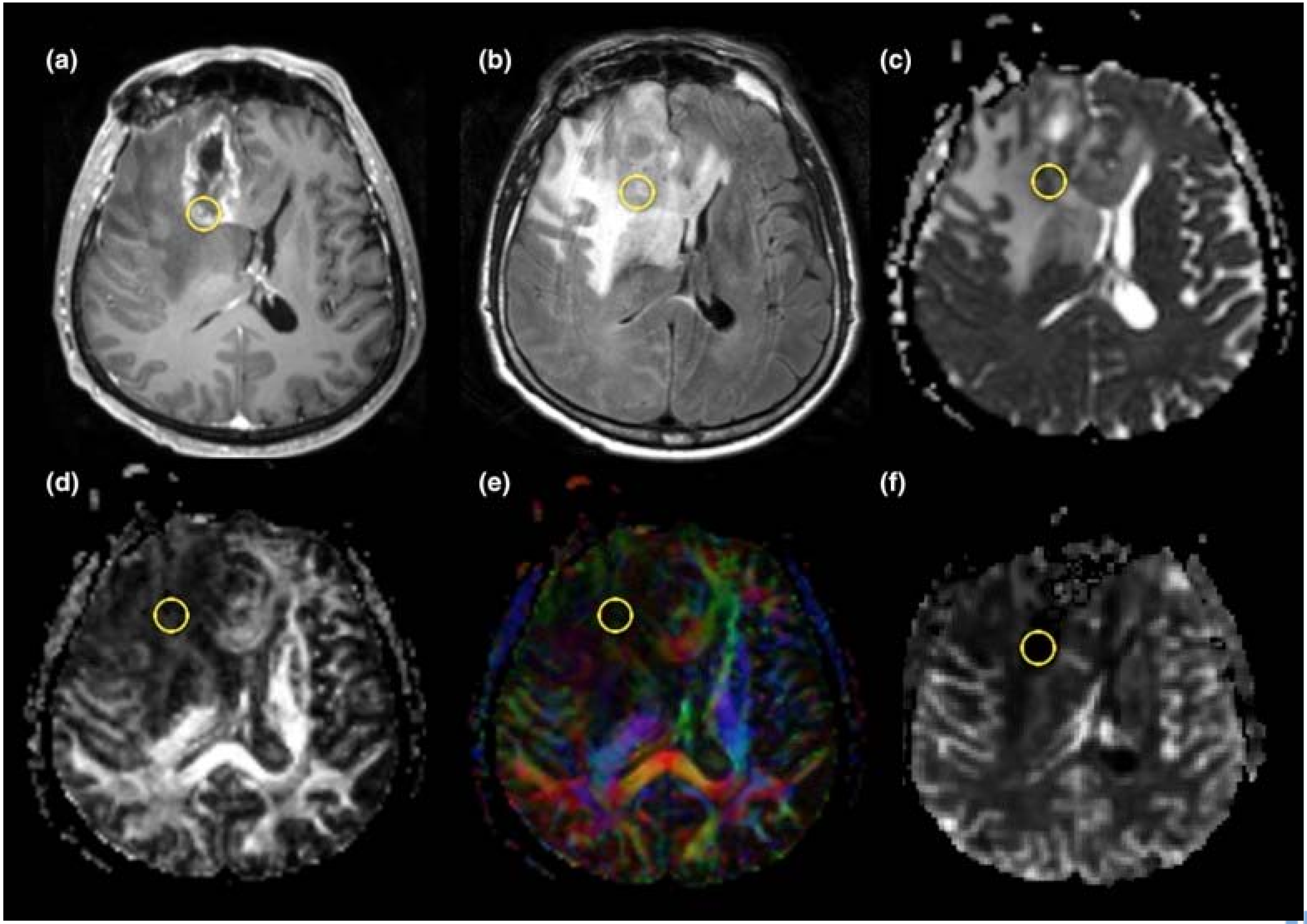

Masch et al, Academic Radiology 2016

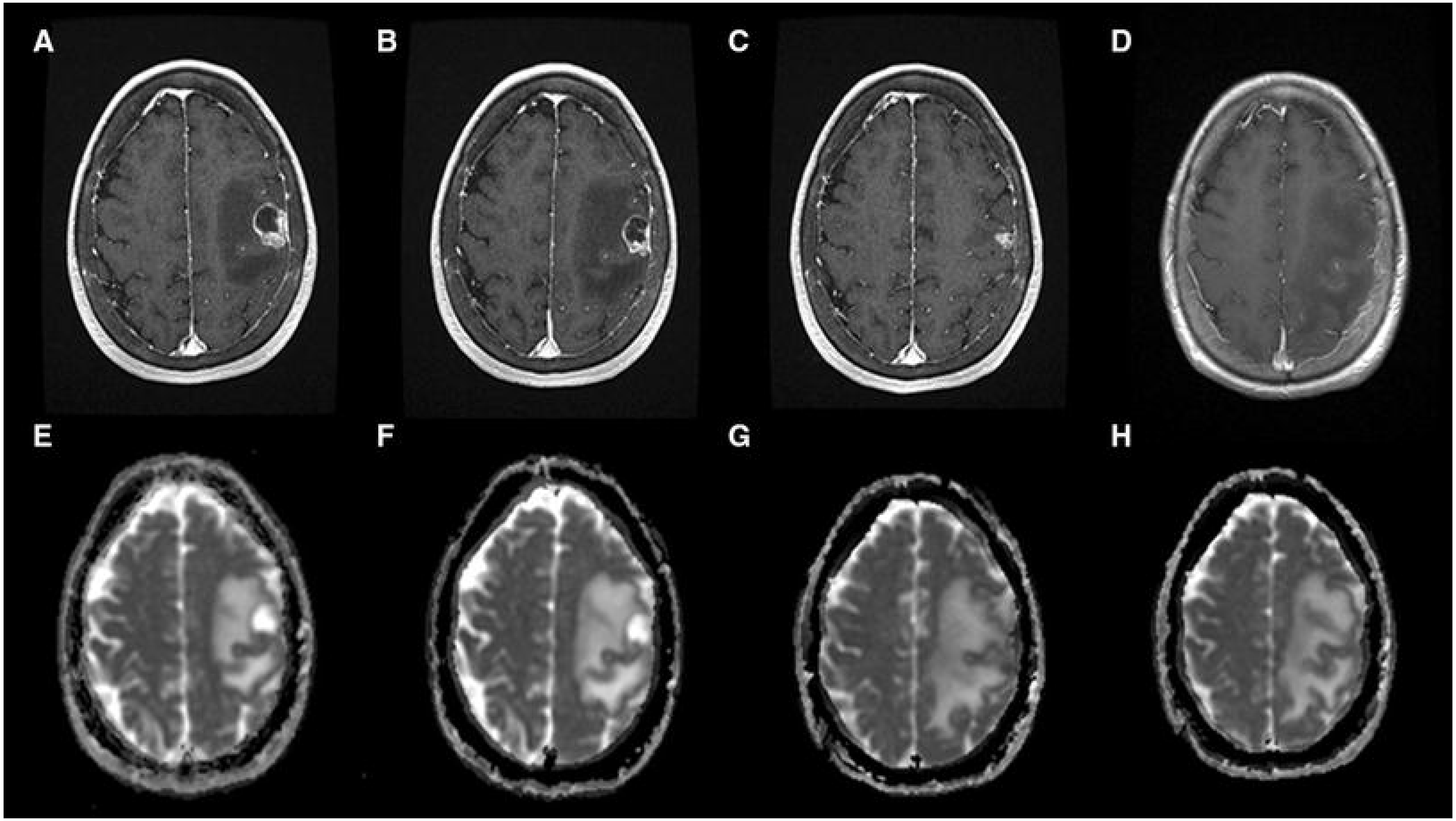

Jakubovic et al., Clin Exp Met 2016

Parametric Response Map

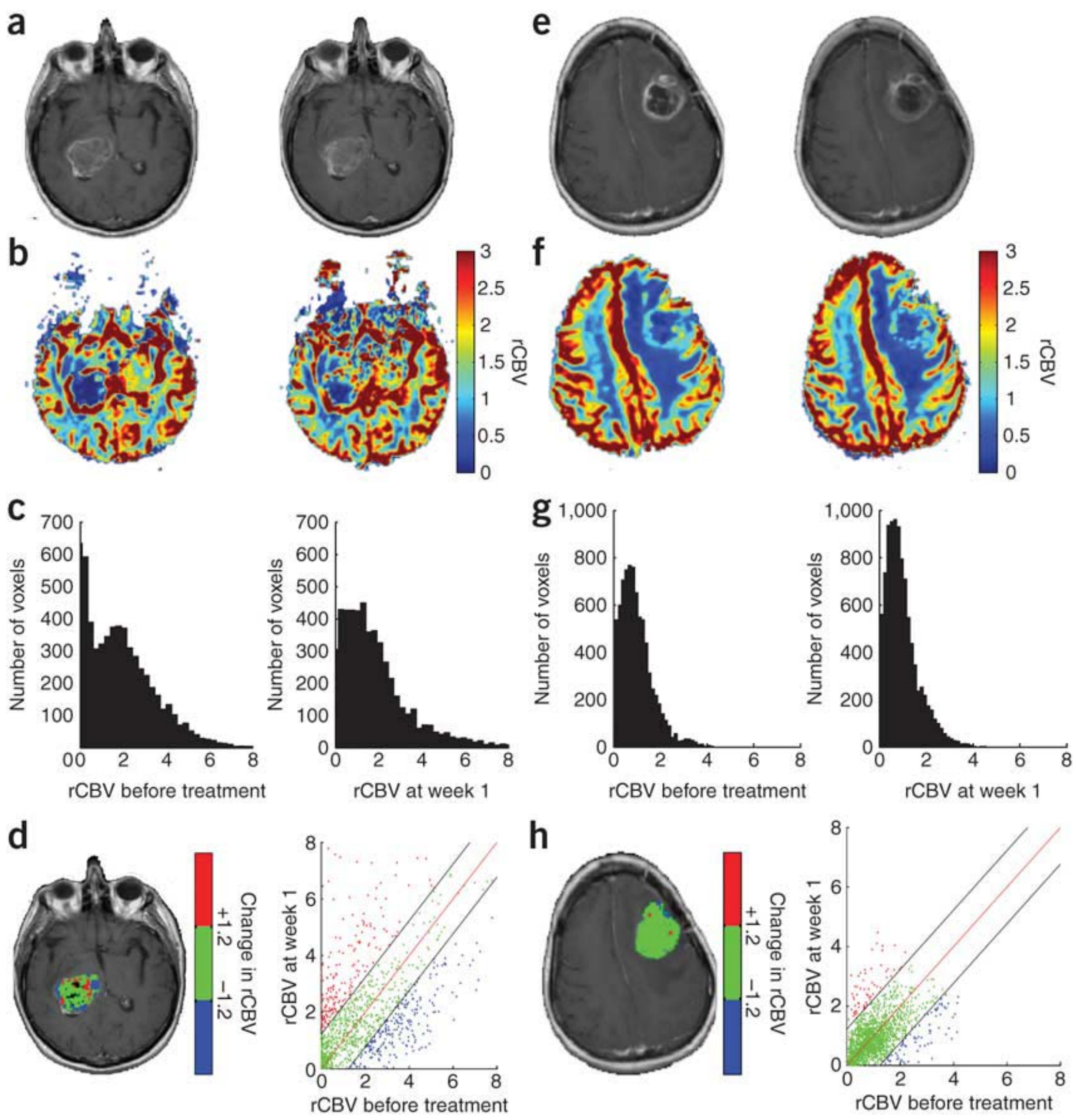

Galban et al., Nat Med, 2009

Radionecrosis - Structure

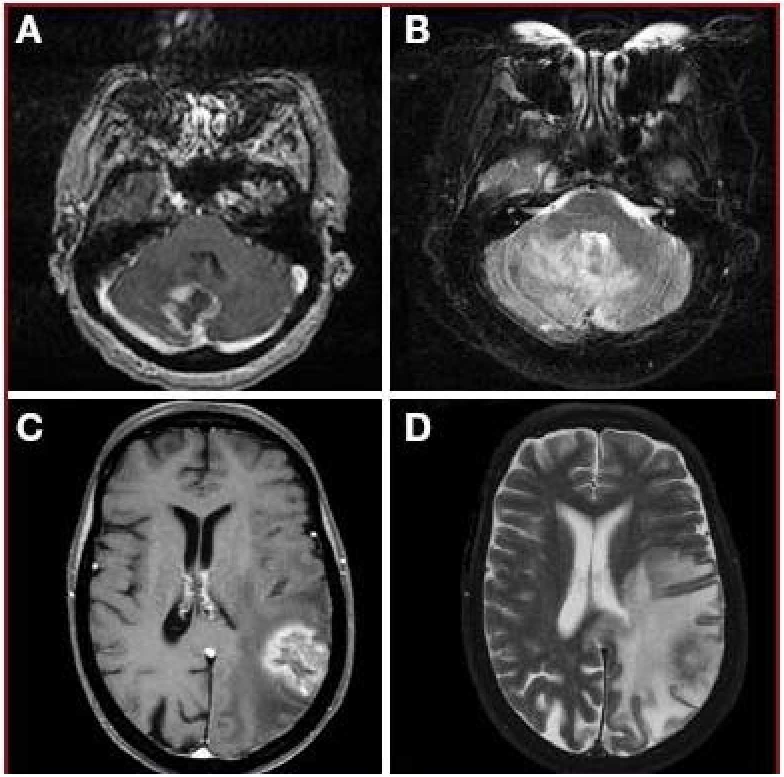

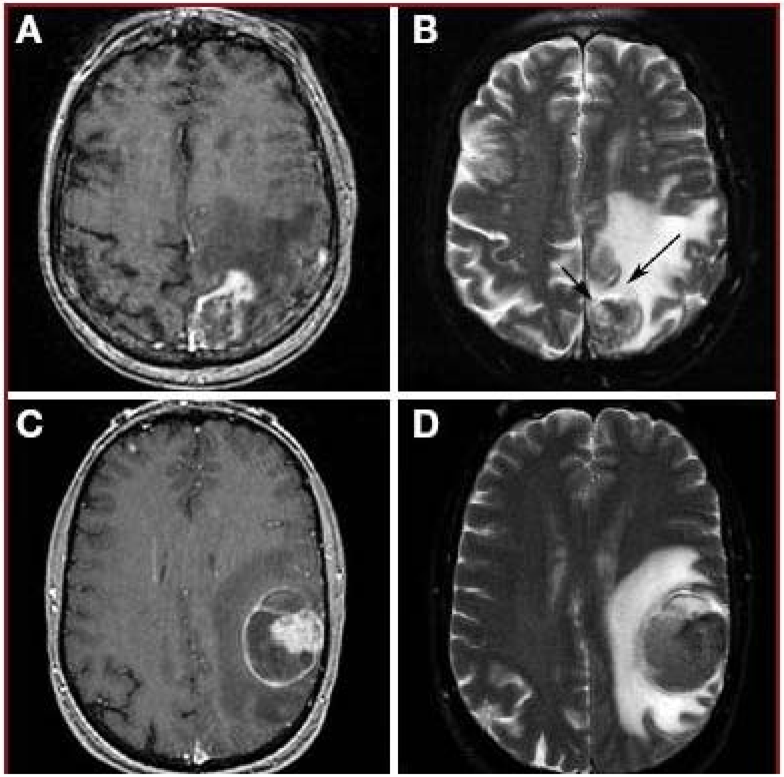

Kano et al., Neurosurg, 2010

Radionecrosis - DSC

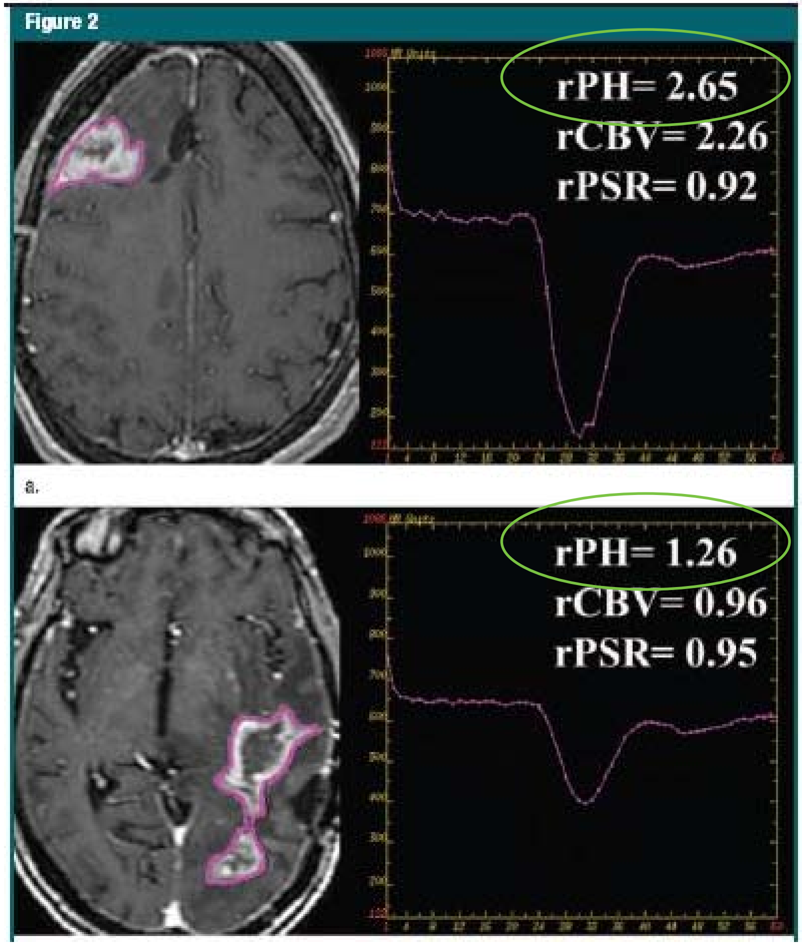

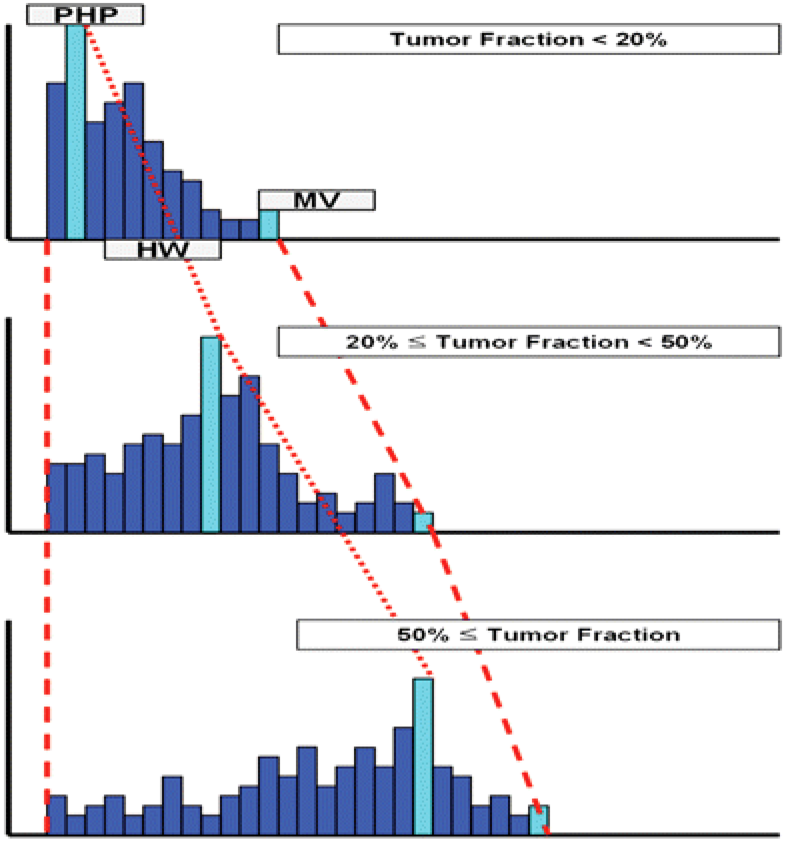

Barajas et al., Radiology 253(2), 2009; Kim et al., Radiology 256(3), 2010; Alexiou et al., MRI 2014; Larsen et al., Neuroradiology 2013

Acknowledgements

- Laura Dawson
- Normand Laperriere
- Barbara-Ann Millar
- Messeret Tamerou
- Bei-Bei Zhang
- Derek MacFadden
- Warren Foltz
- Teodor Stanescu

- Caroline Chung
- Jeremy Hoisak
- Young-Bin Cho
- Anna Simeonov
- Gelareh Zadeh
- David Jaffray
- Walter Kurcharczyk

Applications: MRI in Prostate

Cynthia Ménard, M.D.

CHUM

MRI – Target Delineation

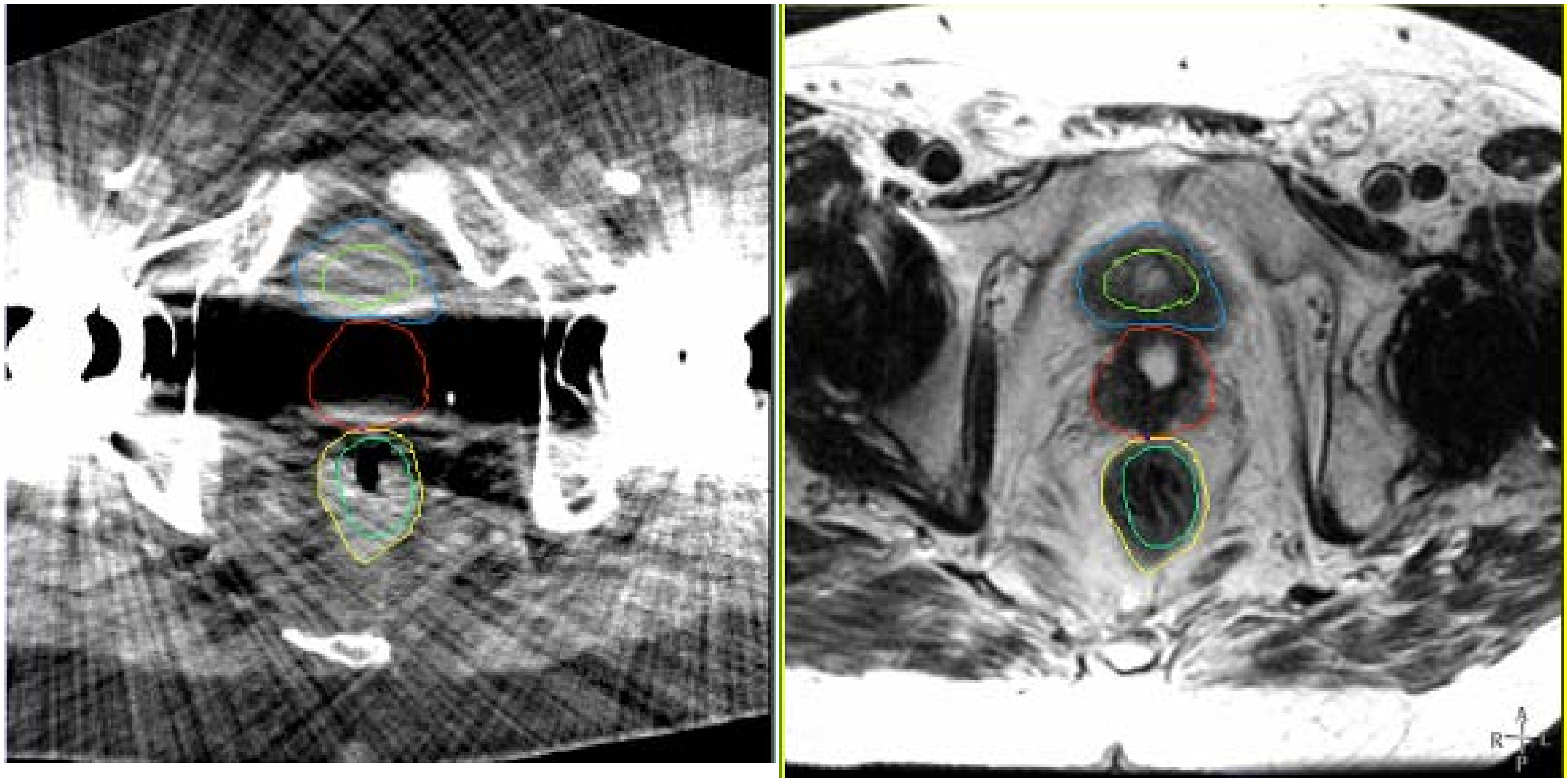

Rosewall et al., Radiother Oncol. 2009 Mar;90(3):325-30.

MRI Integration Improves Prostate Delineation Accuracy?

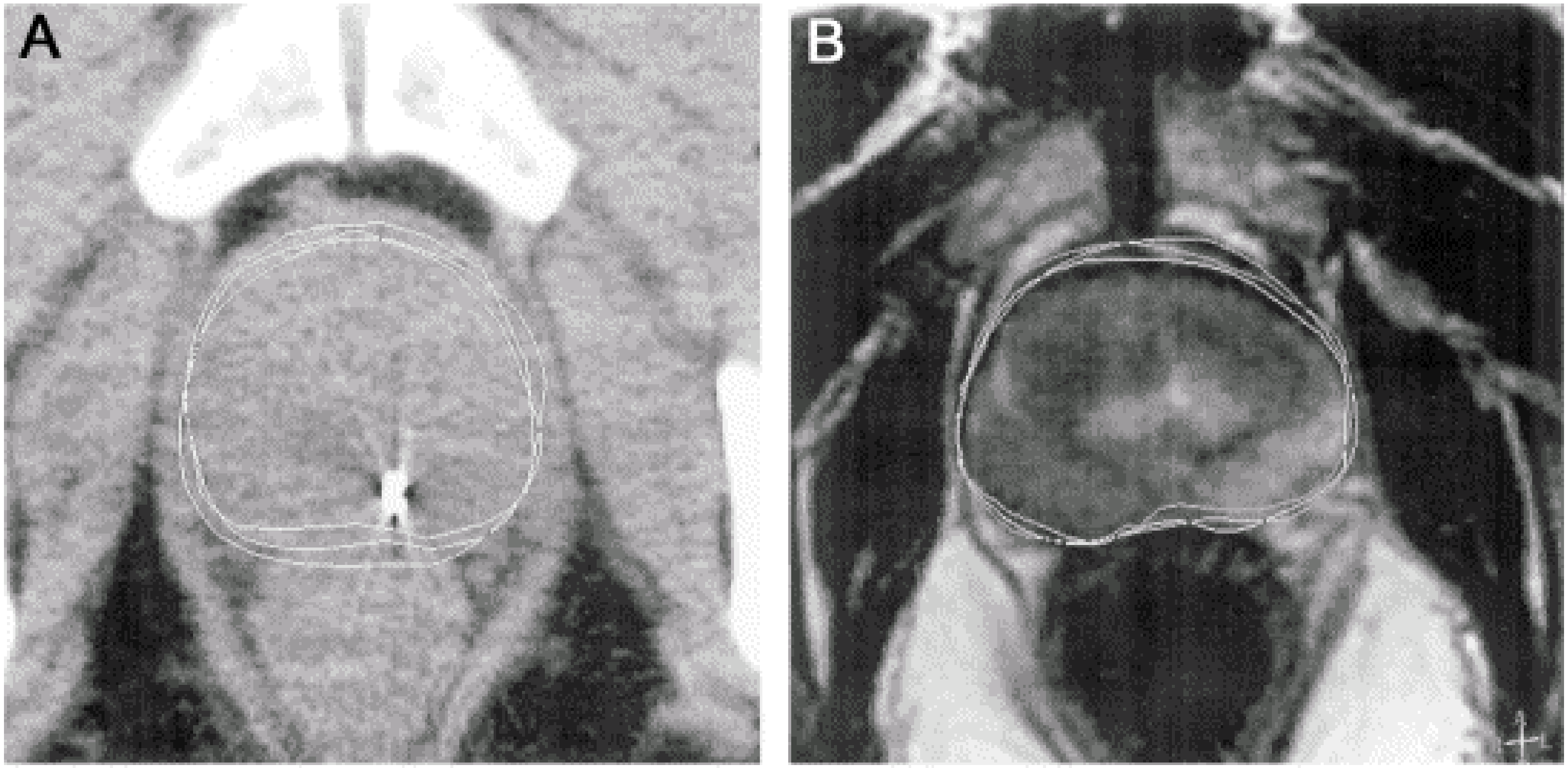

- 🕮 Milosevic et al., Radiother Oncol, 1998
- 🕮 Wachter, et al., Strahlenther Onkol, 2002
- 🕮 Parker et al, Radiot Oncol, 2003
- 🕮 Villeirs et al., Int J Radiat Oncol Biol Phys, 2004
- 🕮 Villeirs et al., Strahlenther Onkol, 2005
- 🕮Nyholm et al., Radiat Oncol 2013

CHUM

Learning Curve

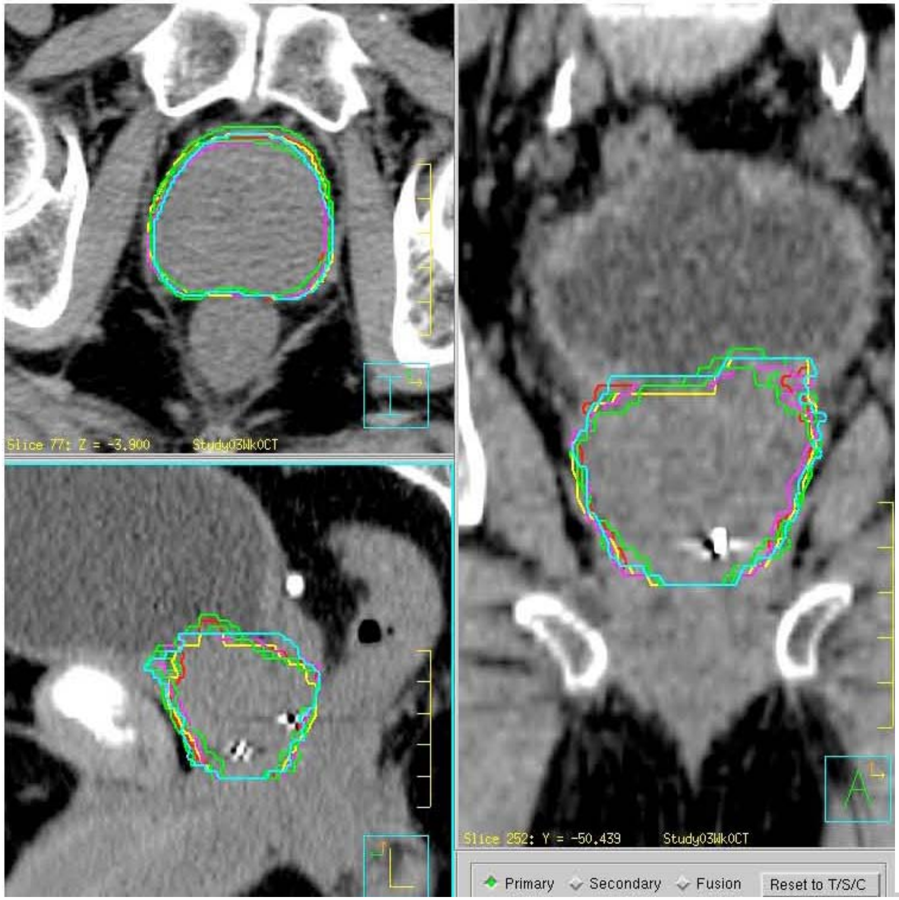

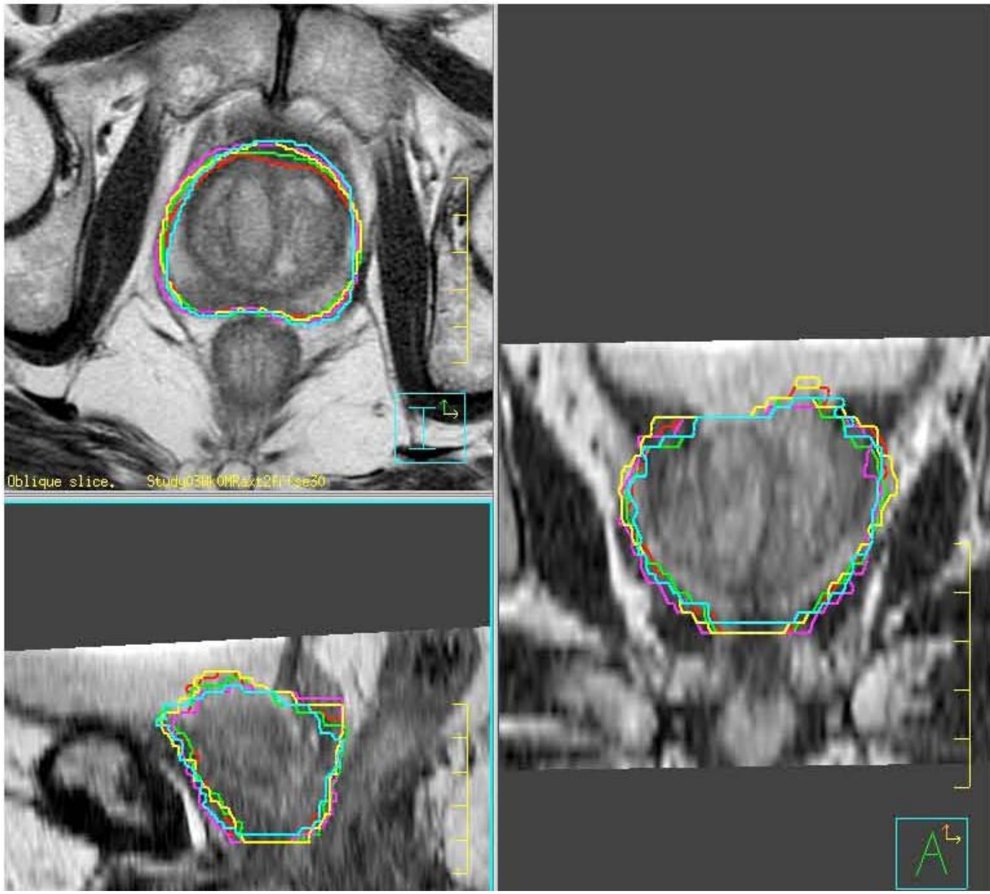

CT

MRI

📖 Craig et al.

CHUM

Autosegmentation

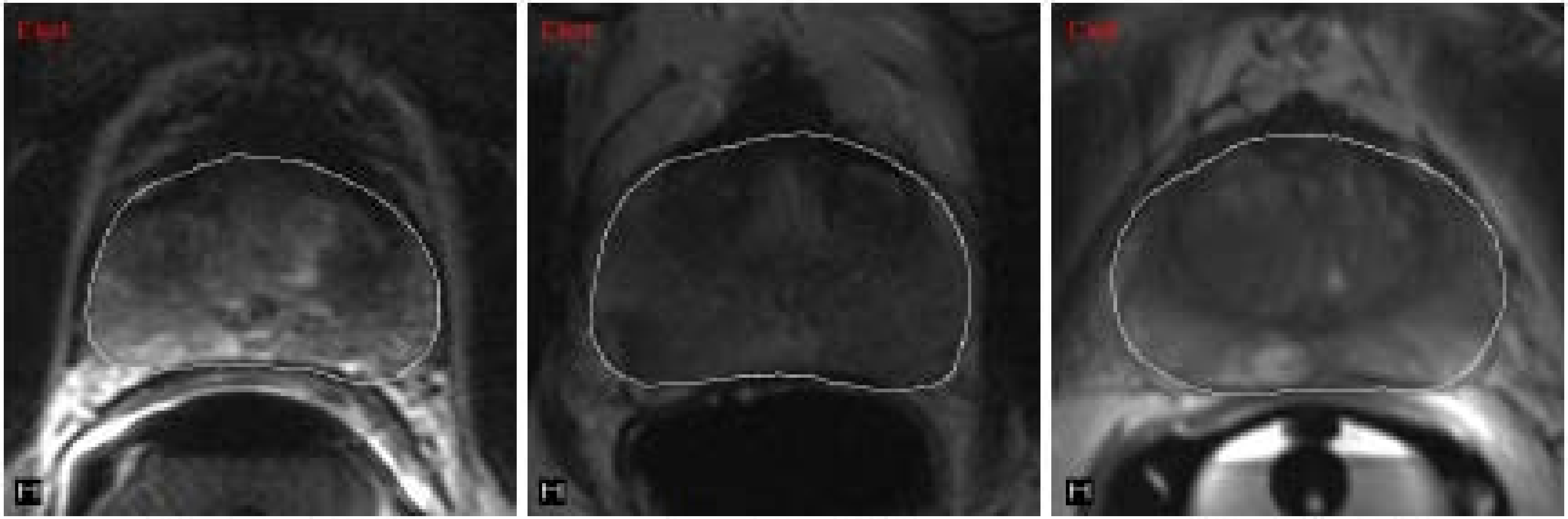

Fig. 5. Qualitative results on axial slices of 3 unseen PROMISE12 challenge cases.

Litgens et al., Med Imag Anal 2014

Smaller CTV

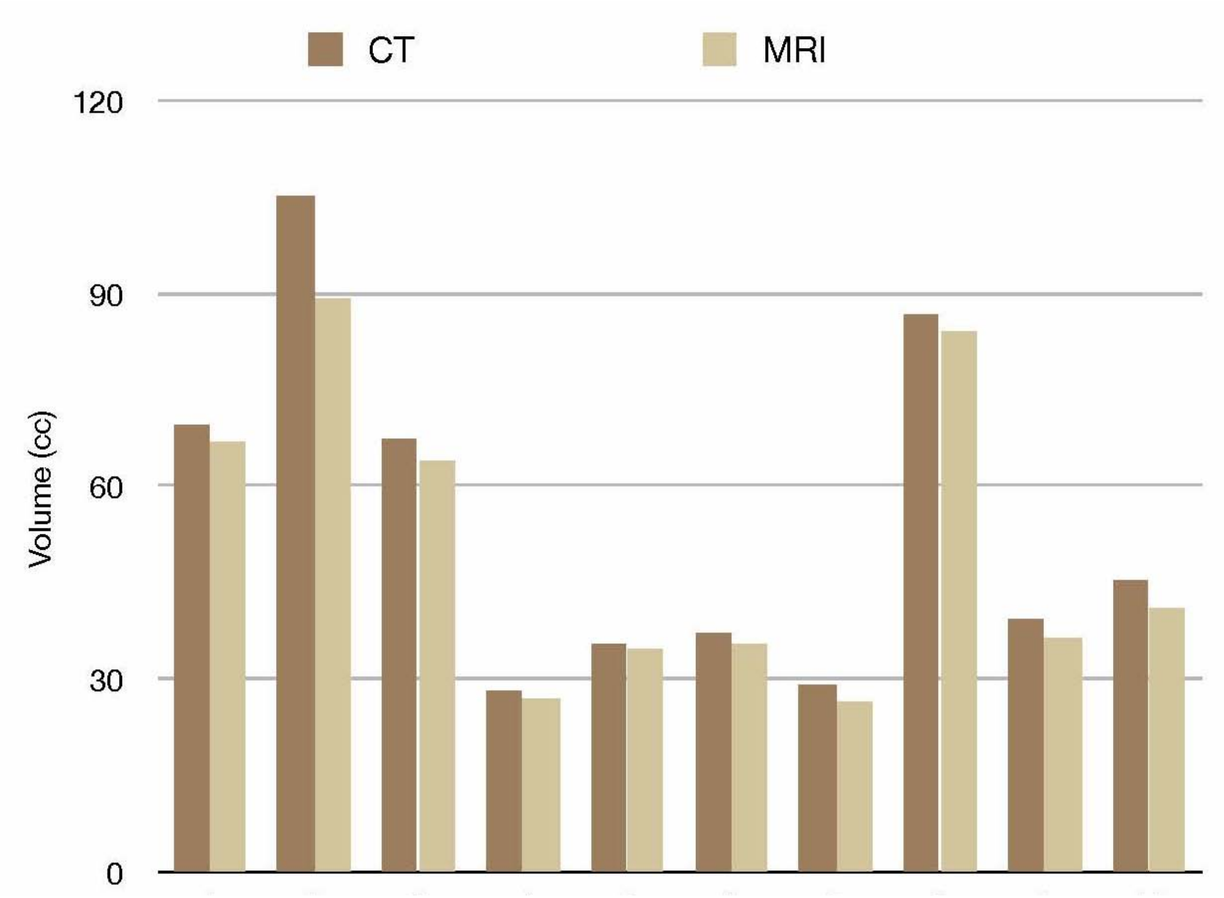

Roach, M., 3rd, et al., Int J Radiat Oncol Biol Phys, 1996
Kagawa, K., et al., Int J Radiat Oncol Biol Phys, 1997
Debois et al., Int J Radiat Oncol Biol Phys, 1999
Rasch, C., et al., Int J Radiat Oncol Biol Phys, 1999
Smith, W.L., et al., Int J Radiat Oncol Biol Phys, 2007

Better Dosimetry

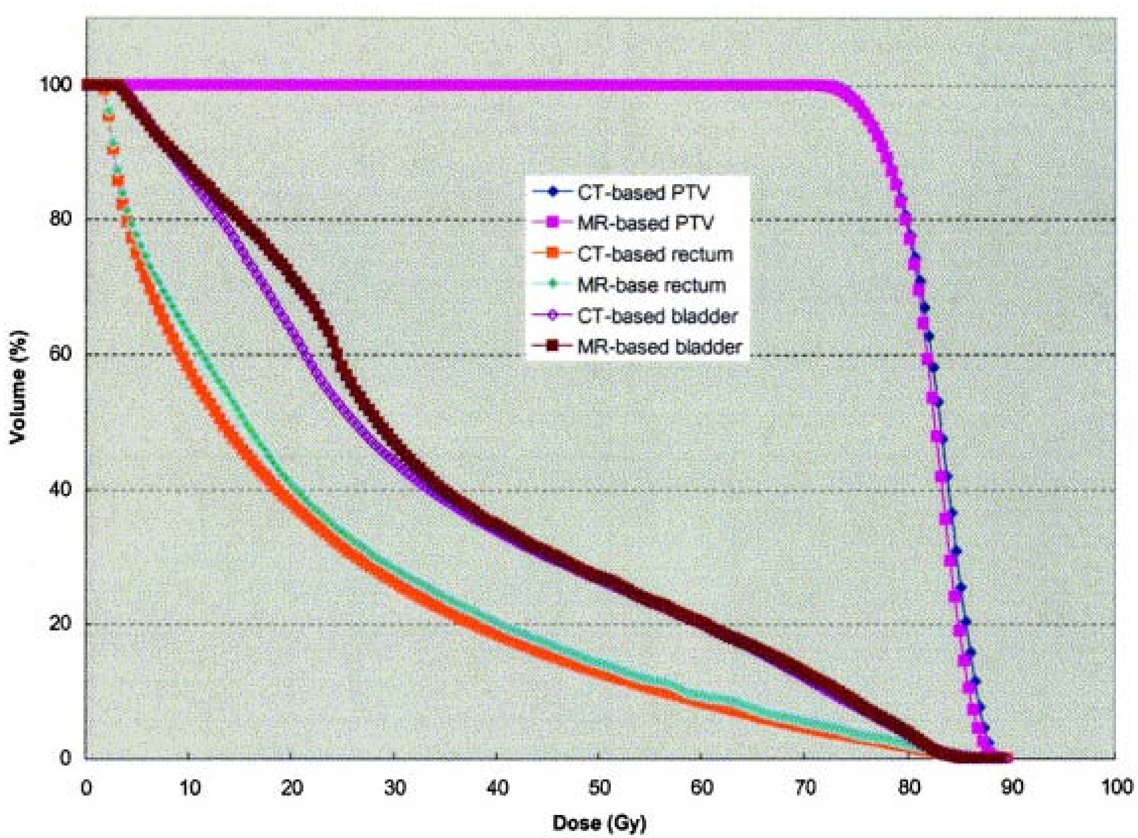

(b)

- 🕮 Sannazzari, G.L., et al., Br J Radiol, 2002.
- 🕮 Chen et al., 2004
- 🕮 Buyyounouski, M.K., et al., Int J Radiat Oncol Biol Phys, 2004
- 🕮 McLaughlin, P.W., et al., Int J Radiat Oncol Biol Phys, 2005

CHUM

Better Outcomes?

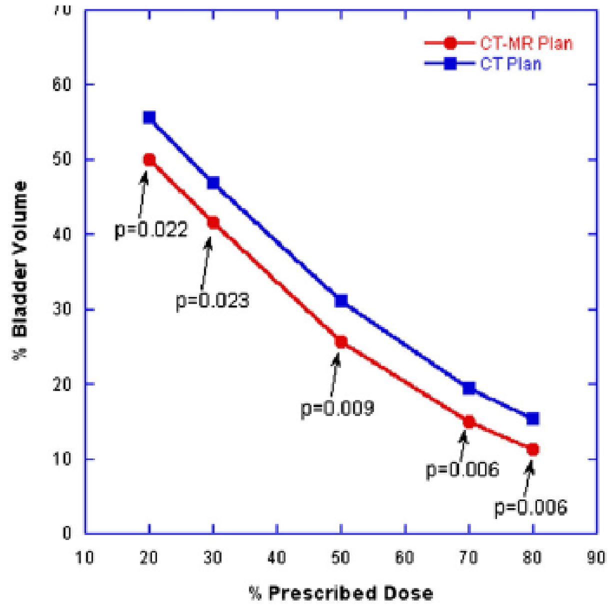

e6 A.N. Ali et al Practical Radiation Oncology: January-March 2013

Table 4 Comparison of acute rectal and GU toxicity rates for CT-MRI and CT-based plans

Acute toxicity type	Plan	Acute grade 0		Acute grade 1		Acute grade 2		*P* value
		No.	%	No.	%	No.	%	
For all patients								
GU	CT-MRI	7	25	7	25	14	50	.024 [a]
	CT	4	7.5	11	20.8	38	71.7	
Rectal	CT-MRI	11	39.3	8	28.6	9	32.1	.495 [a]
	CT	17	32.1	15	28.3	21	39.6	
For those patients without lymph nodes treated								
GU	CT-MRI	4	26.7	3	20.0	8	53.3	.211 [a]
	CT	3	10.0	6	20.0	21	70.0	
Rectal	CT-MRI	6	40.0	5	33.3	4	26.7	.599 [a]
	CT	12	40.0	5	16.7	13	43.3	

CT, computed tomography; GU, genitourinary; MRI, magnetic resonance imaging.
[a] Mantel-Haenszel χ^2 test.

Better Outcomes?

Table IV. Late overall rectal and urinary toxicity.

	MRI (n = 73)		CT (n = 72)		
Grade	n	%	n	%	p-value
Rectal					
0	46	63	39	54.1	0.4
1	26	35.6	30	41.7	
2	1	1.4	3	4.2	
Urinary					
0	29	39.7	25	34.7	0.5
1	32	43.8	38	52.8	
2	12	16.4	9	12.5	

Sander et al., Acta Oncol 2014

How To: An Approach

- Determine guidance / registration strategy up front

- Clarify Imaging Objectives
  1. Prostate Boundary (CTV)
  2. Implanted Markers (Guidance/registration surrogate)
  3. Tumor-Dense Regions (GTV)

- Manage Prostate Motion
  – Must not assume stable prostate geometry b/w acquisitions
  – Trade off spatial resolution / acquisition time
  – Repeat acquisition if motion blurring present
  – +/- antiperistaltic agent + bowel prep
  – Consider ERC

📖 Yanke et al, 1991

CT-MRI Registration

- Kagawa et al., IJROBP (1997) - BONE
- Parker et al, Radiot Oncol 66 (2003) 217–224 – FM GRE
- Huisman et al., Radiology (2005) – FM GRE
- vanLin et al., IJROBP (2006) - GRE

Image Registration

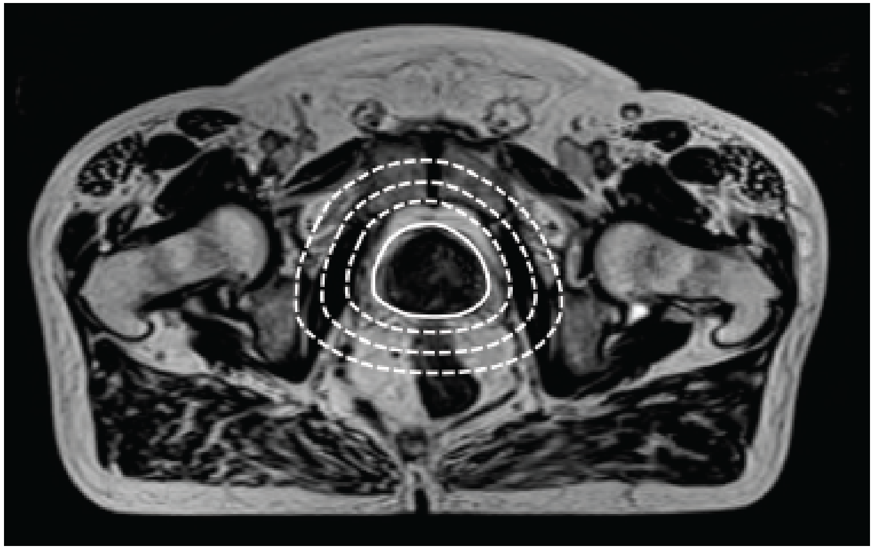

Figure 1 Registration volumes. The figure demonstrates an MR image with the different registration volumes RV_0 (solid line), RV_1, RV_2 and RV_3 (dotted lines).

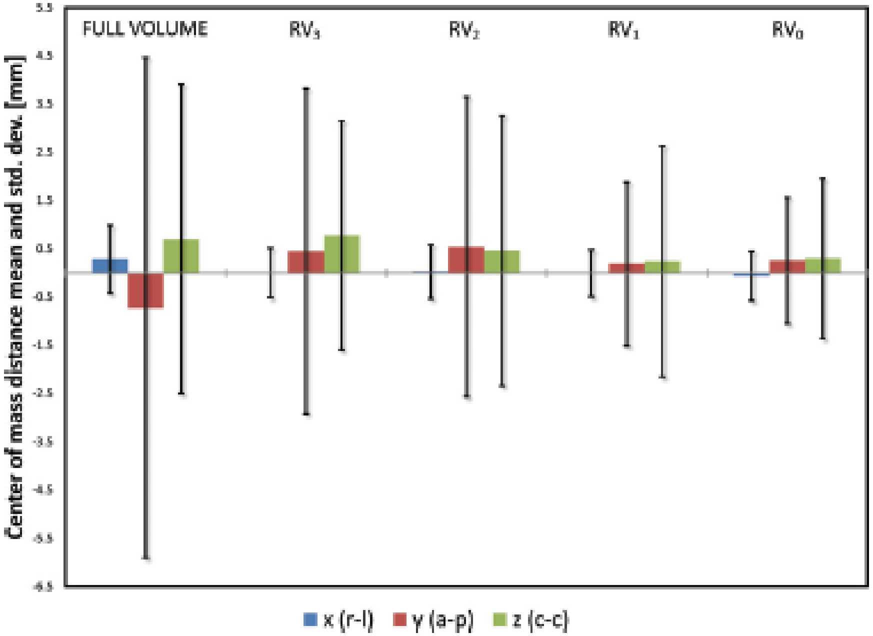

Figure 2 Registration results. Center of mass standard deviations

📖 Jonsson et al., Radiat Oncol 2011

Automated CT-MRI registration

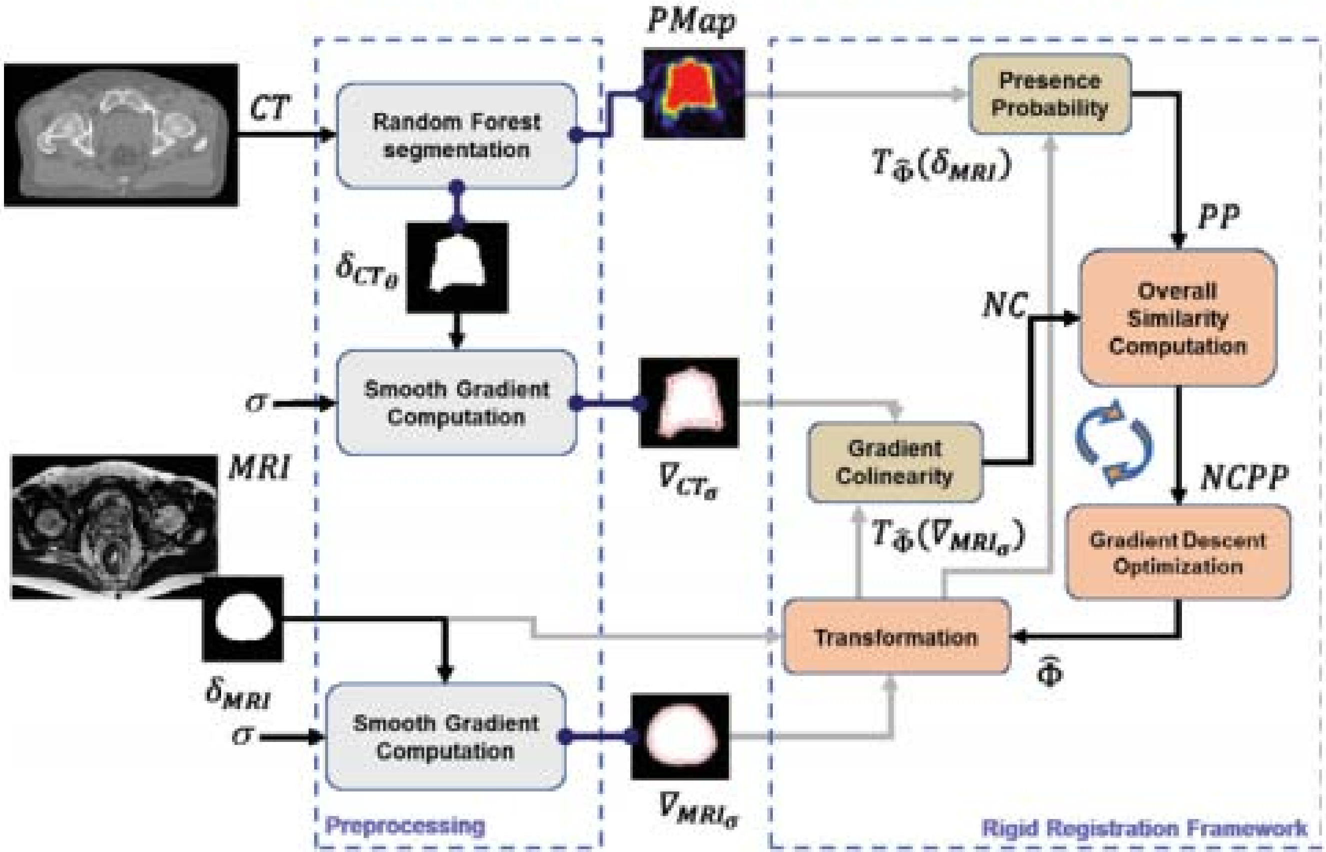

Fig. 3: Overall workflow for the proposed registration method.

Commandeur et al., IEEE J Biomed Health Inform 2016

Dual-Echo TSE, SPACE

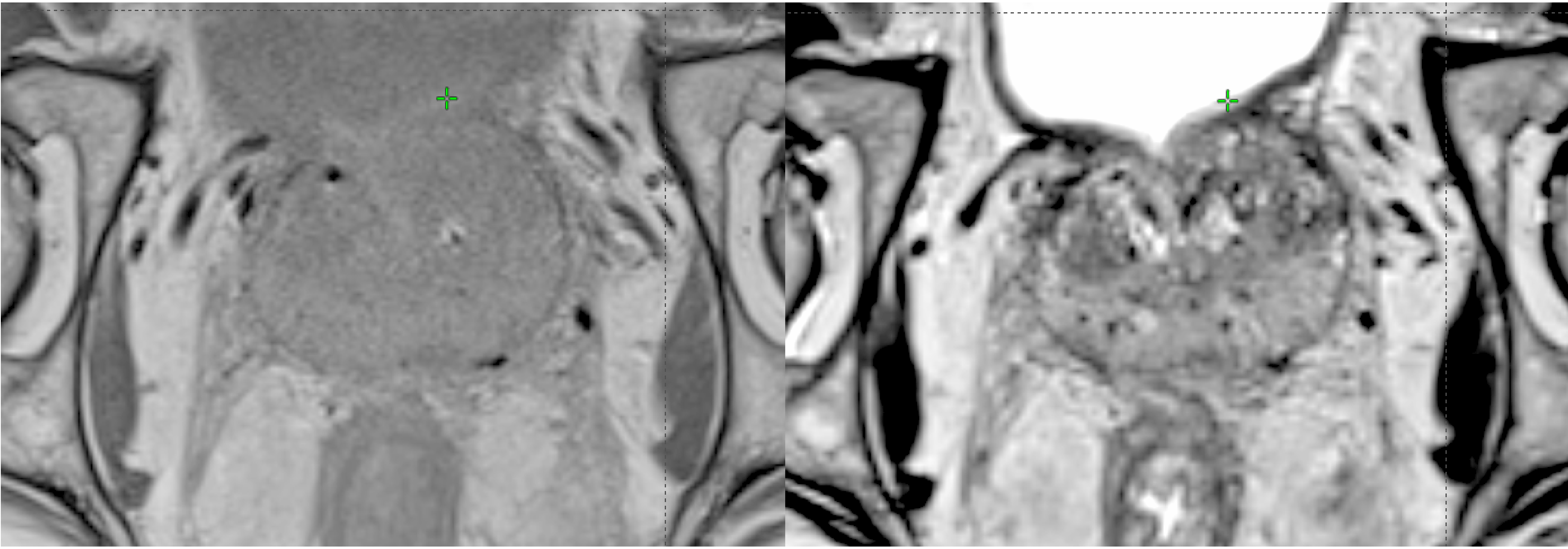

CHUM

Result

Position accuracy - Simulation

Accuracy the spatial position of gold markers in MR images

The charts below shows position deviations when switching the frequency encoding direction in the image plane is depicted for the 2D and 3D sequence.

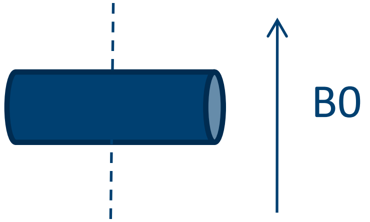

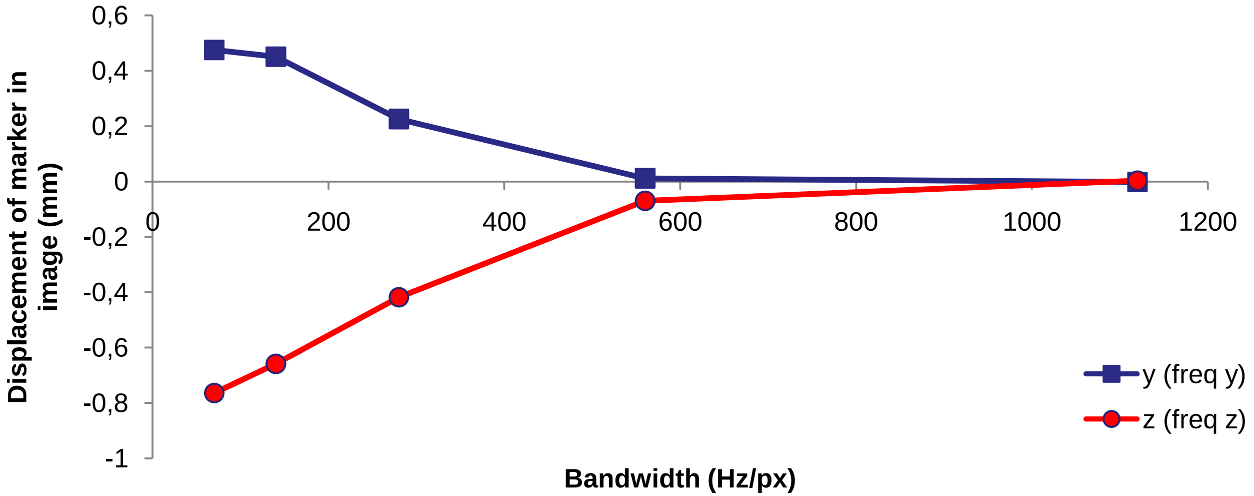

Tufve Nyholm, Umeå University Hospital, Sweden

Motion and Image Quality

3mmFSE | ssfp | T2prep | GRE | 2mmFSE

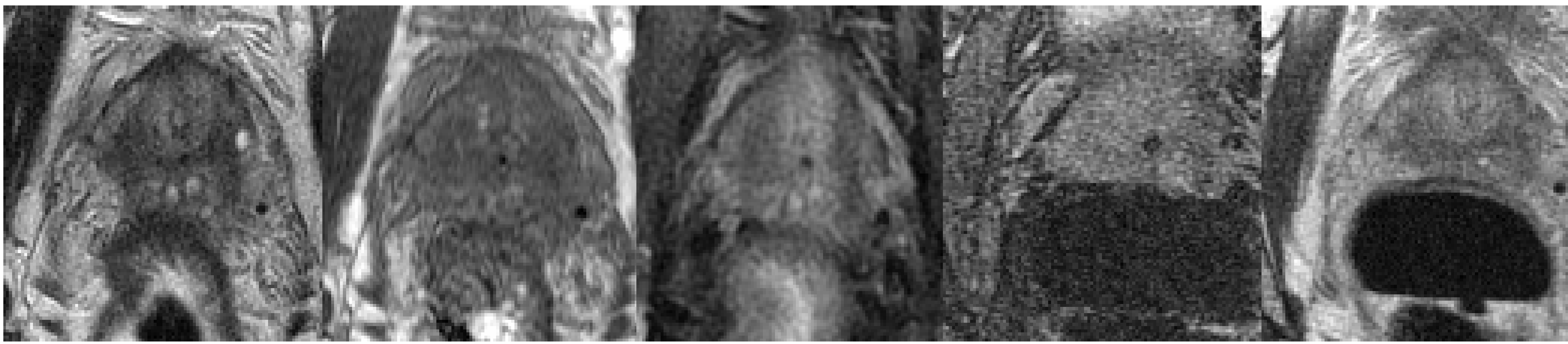

Deformable Registration

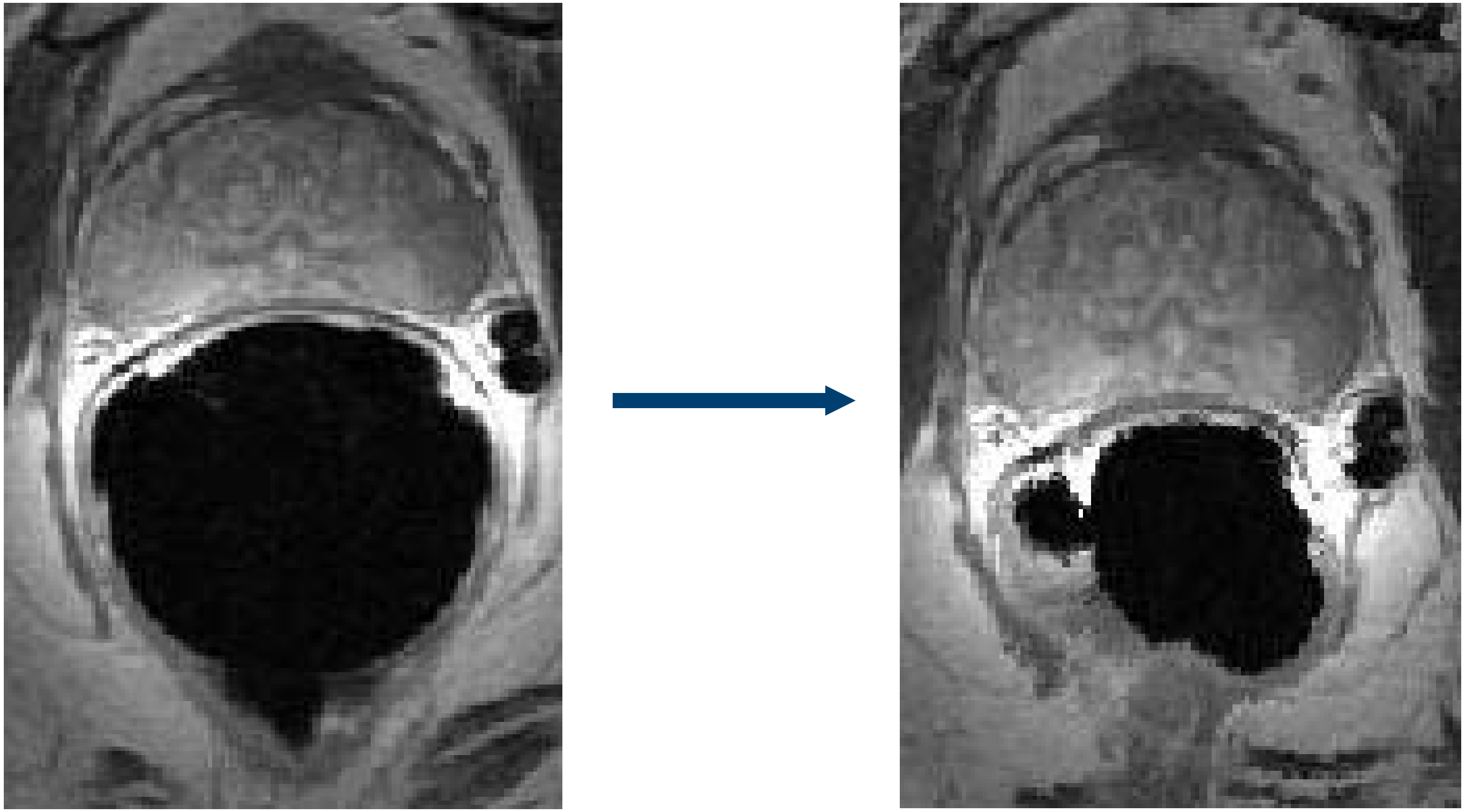

Hensel et al. IJROBP 68(5) 2007

Registration

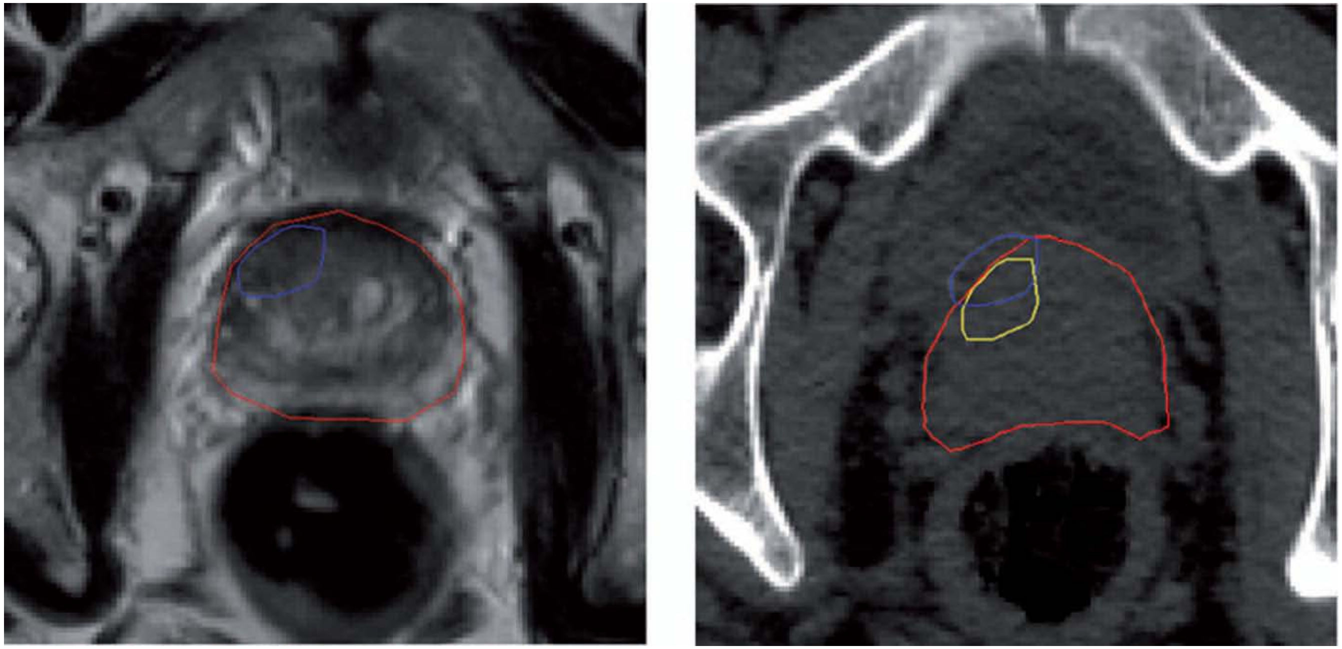

Figure 2. Left: Section of a T2-weighted MR image showing the prostate (red) and focal lesion (blue). Right: Section of the planning CT image with prostate (red) and rigidly registered focal contour (blue), which lies outside of the prostate volume. The result of non-rigidly registering the focal lesion (yellow) using the same deformation pattern that the prostate has undergone between MR and CT acquisition places the focal lesion inside the prostate.

Published in: Yang Feng; Daniel Welsh; Kim McDonald; Linda Carruthers; Kun Cheng; Dean Montgomery; Jessica Lawrence; David J. Argyle; Stephen McLaughlin; Duncan B. McLaren; William H. Nailon; *Acta Oncologica* **2015,** 54, 1543-1550.
DOI: 10.3109/0284186X.2015.1063782

Pelvis

CHUM

MRSeries™ Positioning Devices

MRSeries products are MRI compatible in 1.5 and 3T environments. All indexable MRSeries products are three-pin compatible.

The following MRI overlay options are available:

MRI Overlay for:	Dimensions	Part Number
Philips Panorama, 50cm wide	214 x 50 x 2.2cm	MTM3400
Philips Panorama, 40cm wide	214 x 40 x 2.2cm	MTM3401
GE Signa	208 x 50 x 4.8cm	MTM3300
GE Wide Bore	213.4 x 53 x 6.2cm	MTM3301
Siemens Magnetom Avanto, Magnetom Espree, Magnetom Symphony A Tim System, Magnetom Trio A Tim System	187 x 50 x 2.2cm	MTM3000
Siemens Magnetom Verio	187 x 50 x 2.2cm	MTM3001

Three-Pin Lok-Bars™

Three-Pin Lok-Bars allow you to index MRI compatible devices to your MRI couchtop. They also help prevent non-MRI compatible devices from being used on an MRI machine.

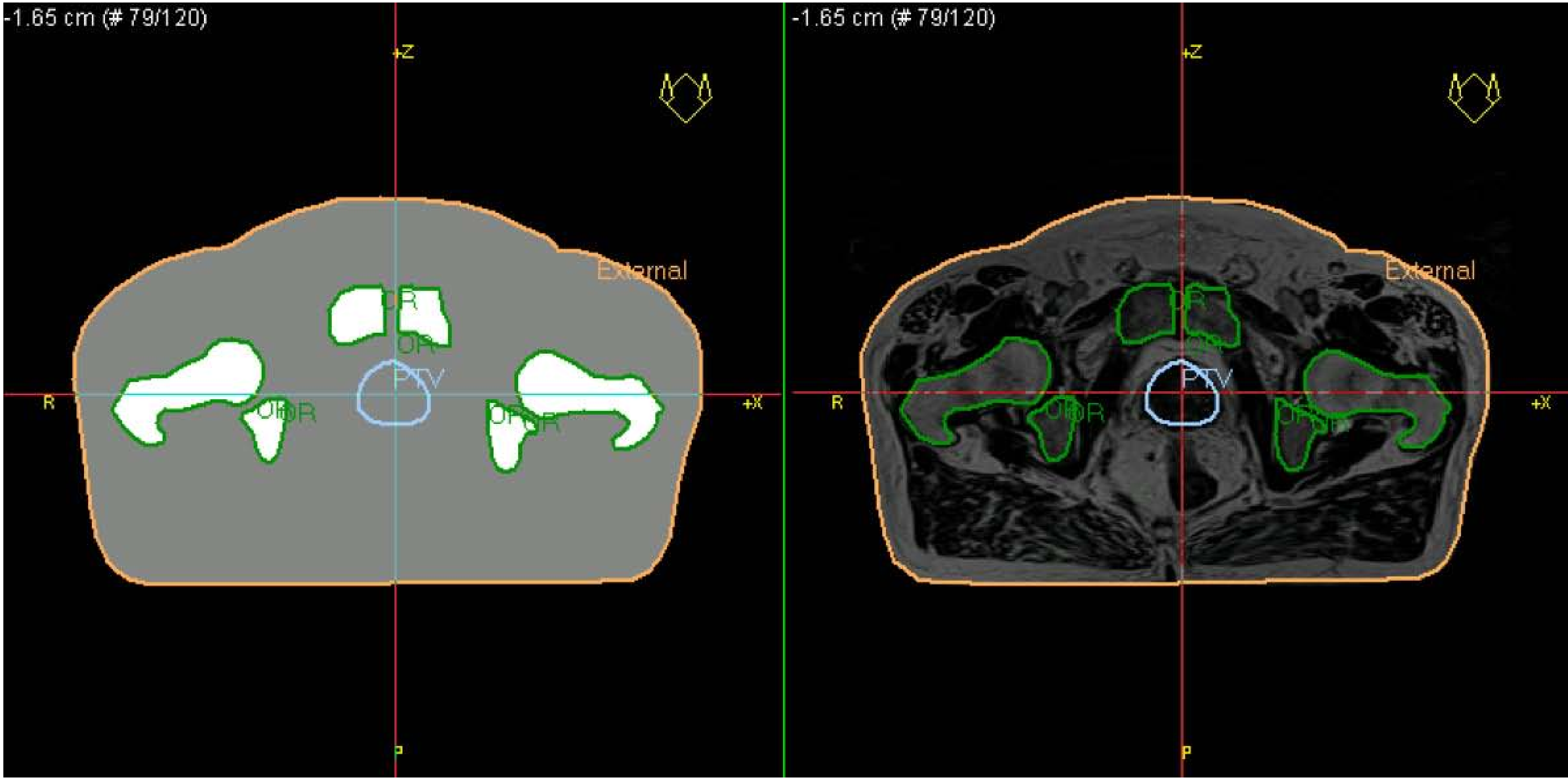

Synthetic CT and MR image. The synthetic CT with assigned mass densities (left) and the MR image on which it was based (right).
Jonsson *et al. Radiation Oncology* 2010 **5**:62

CHUM

Pseudo-CT (pCT)

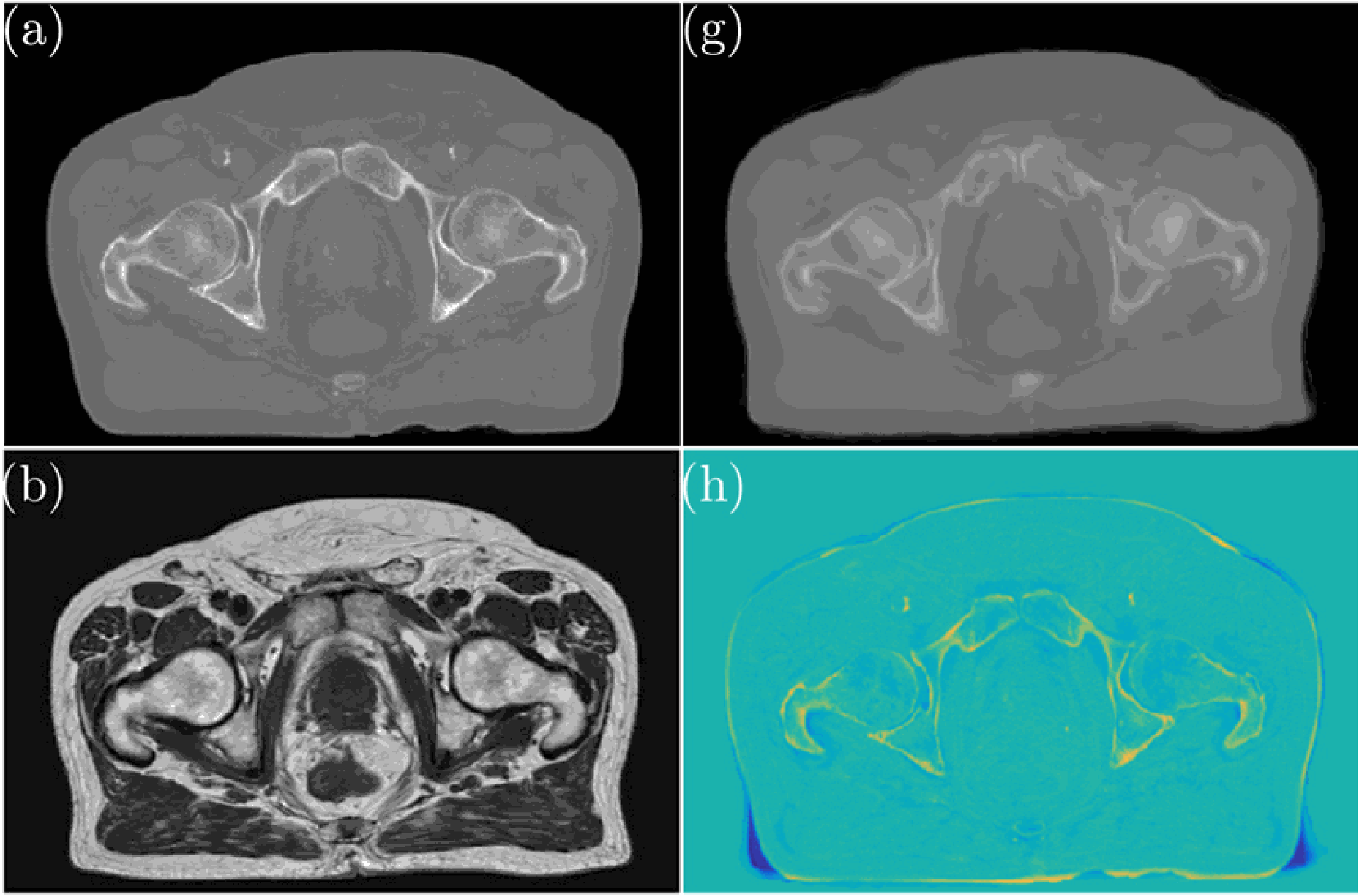

Andreasen et al., Med Phys 2016

sCT (substitute CT) – multi Atlas

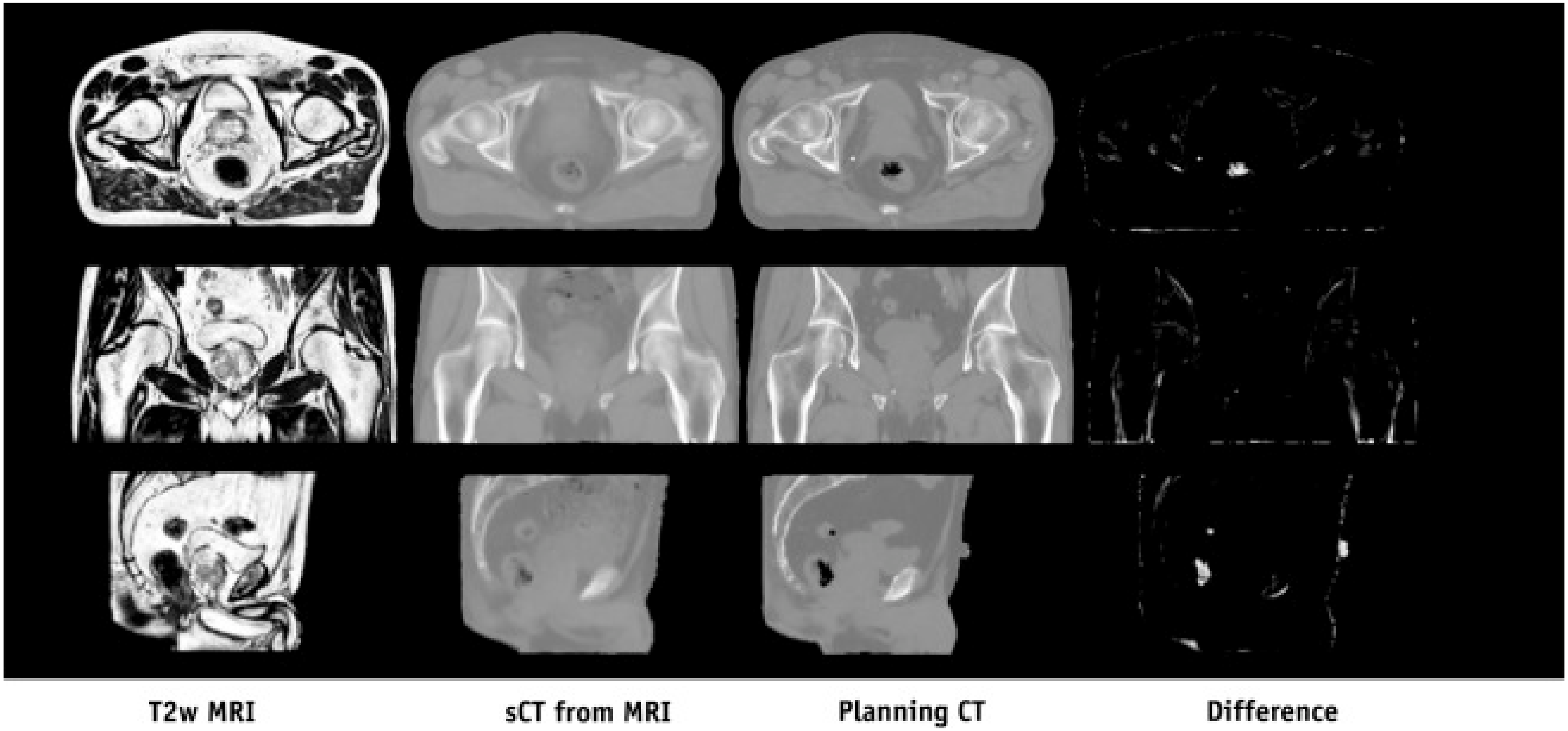

Dowling et al., IJROBP 2015

Statistical Decomposition Algorithm (Spectronic)

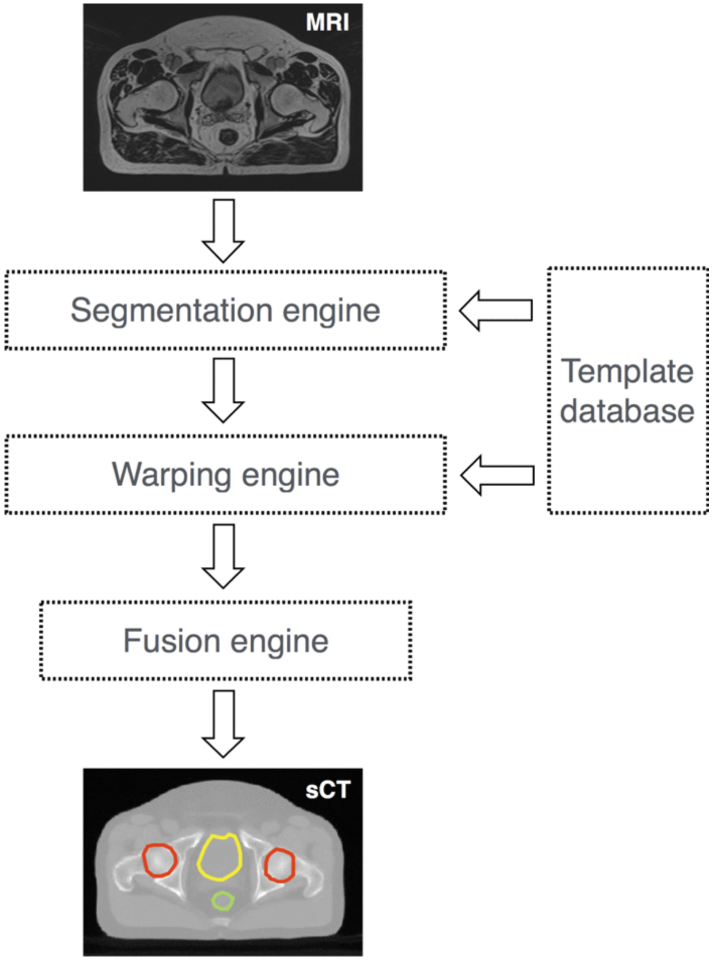

Siversson et al., 2015

Paradigm Shift

- Need to further improve *radio*-therapeutic ratio in prostate cancer

- Cancer outcomes related to gross tumor-bearing sub-regions

- Approach → Tumor-targeting

- Need → Accurate technique

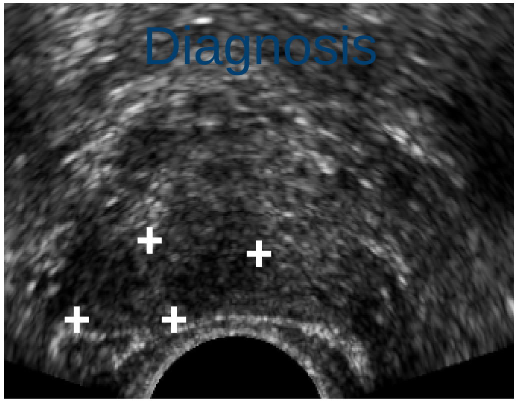

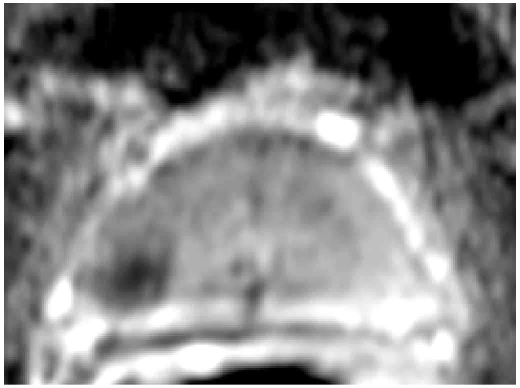

📖Pucar *et al.* IJROBP 69(1) 2007

📖Joseph *et al.* IJROBP 73(3) 2009

📖Arrayeh et al. IJROBP 82(5) 2012

Imaging Tumours

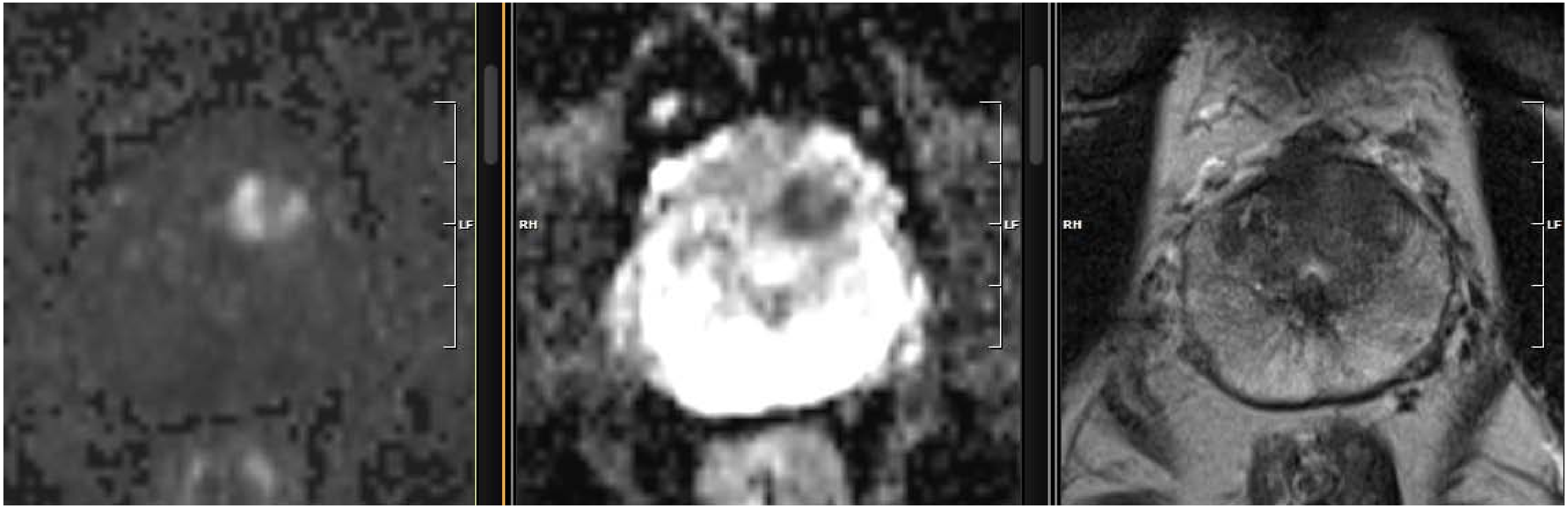

PIRADS v2.0, ACR, 2015

Diffusion techniques

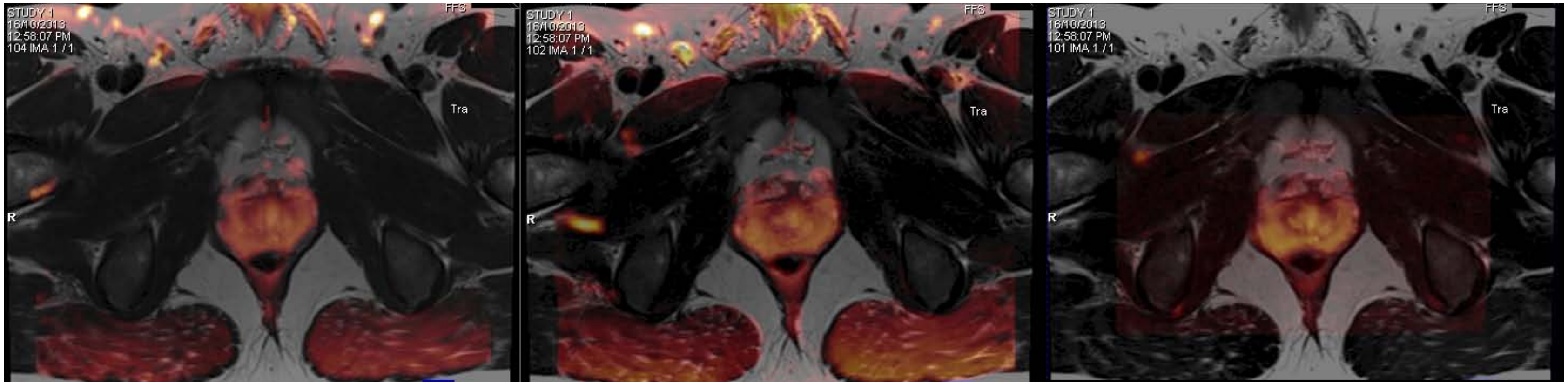

EPI RESOLVE ZoomIT+EPI

GP Liney et al Br J Radiol 2015; 88:20150034.

- Normal volunteer study

Diffusion Imaging - Geometry

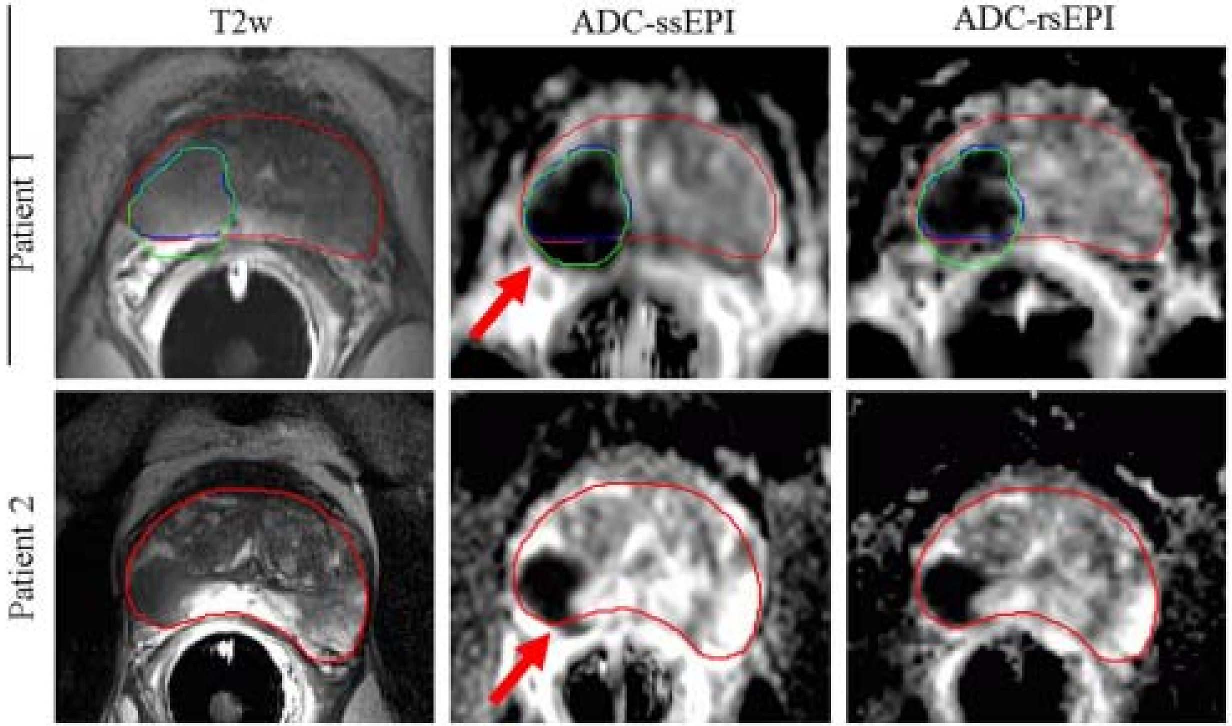

Fig. 3. ADC geometric performance in vivo applied to prostate cancer for two patients, demonstrating extension of disease outside of the anatomic posterior boundary of the prostate in ADC-ssEPI but not with ADC-rsEPI (shown by the red arrow). The red contour is the anatomic prostate boundary defined on T_2-weighted images, copied across all images. In the top row, the green contour demarcates the tumor boundary in ADC-ssEPI and the blue contour demarcates the tumor boundary in ADC-rsEPI. The tumor contours are left off the bottom row images to improve tumor visualization relative to the posterior anatomic boundary.

Foltz et al. Radiother Oncol 2015

Cancer is Not Confided to the Prostate Gland

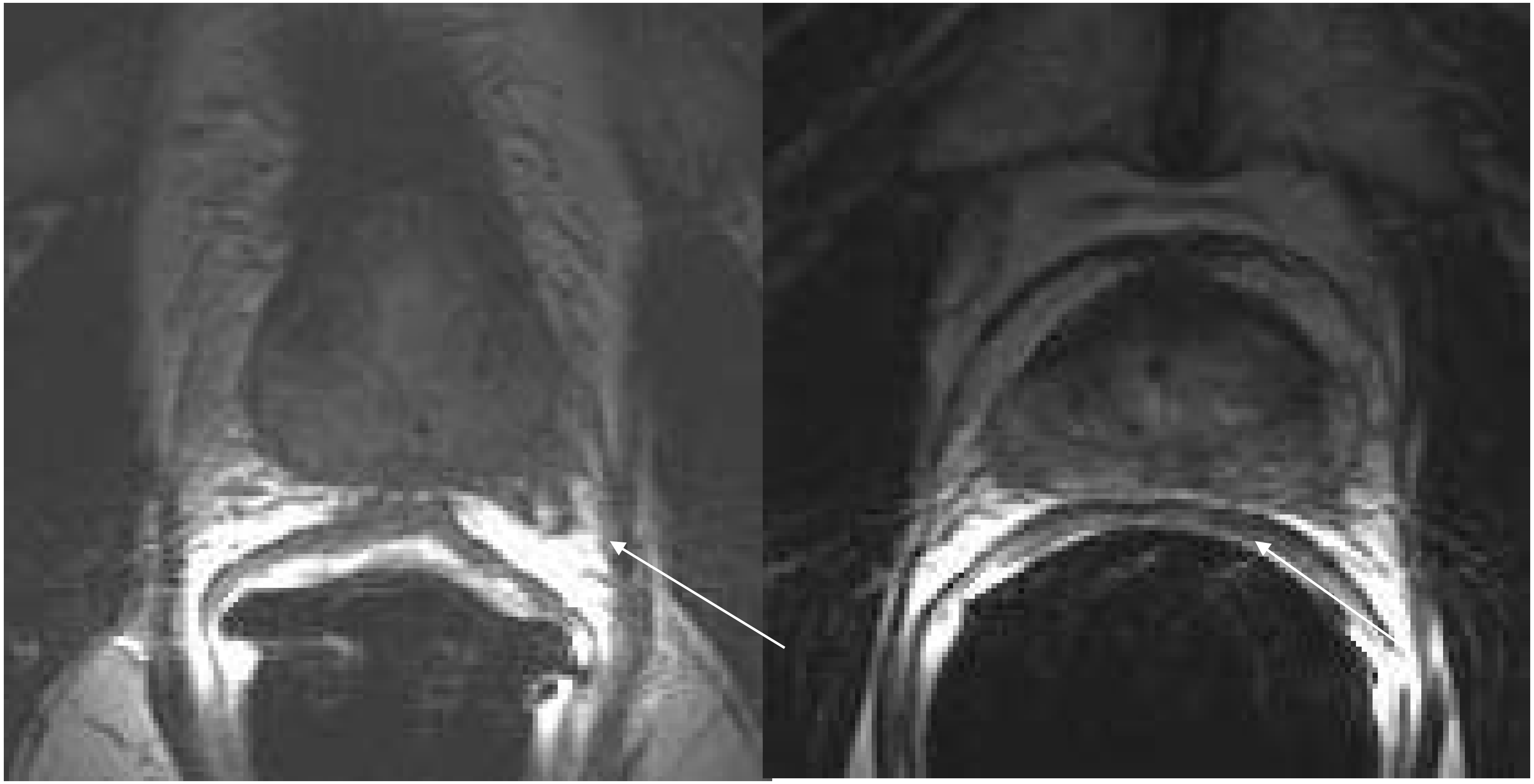

Courtesy P. Choyke

Independent Predictive Factor

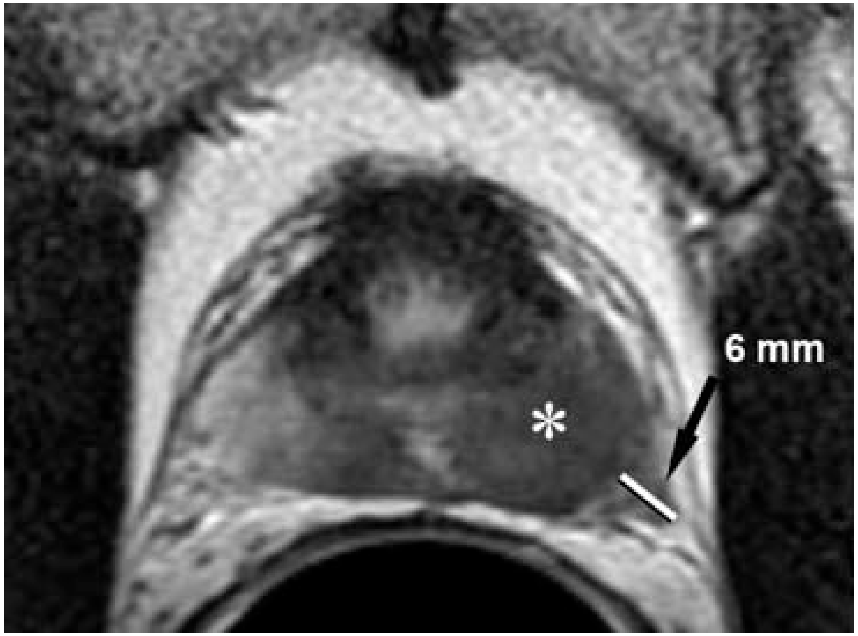

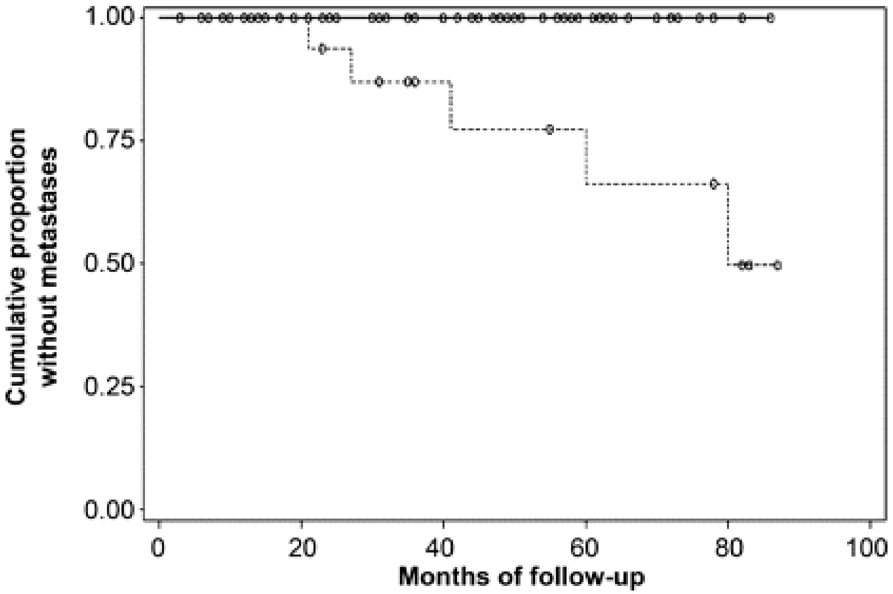

📖Nguyen et al. IJROBP 59(2) 2004

📖McKenna et al. Radiology 247(1) 2008

📖Westphalen et al. Radiology 261(2) 2011

ECE and Brachytherapy

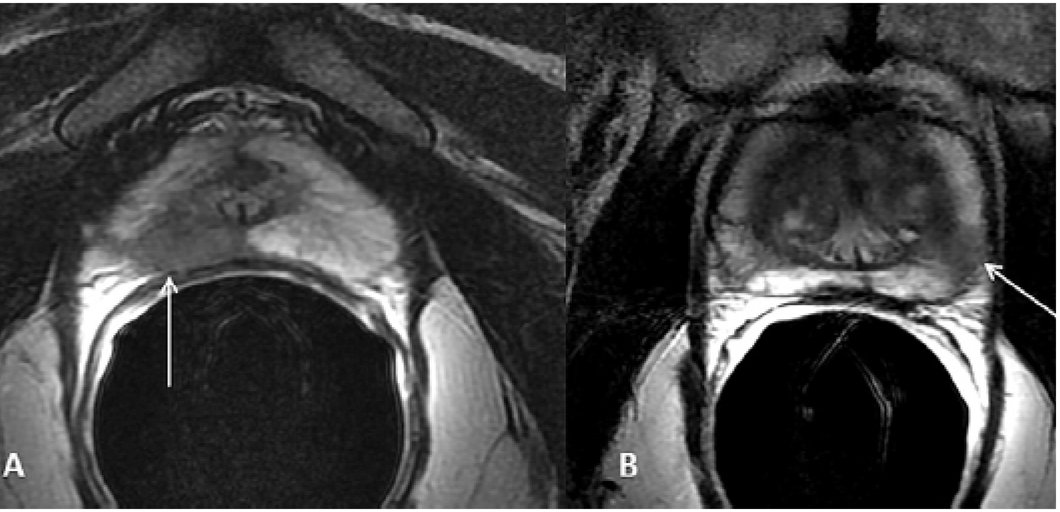

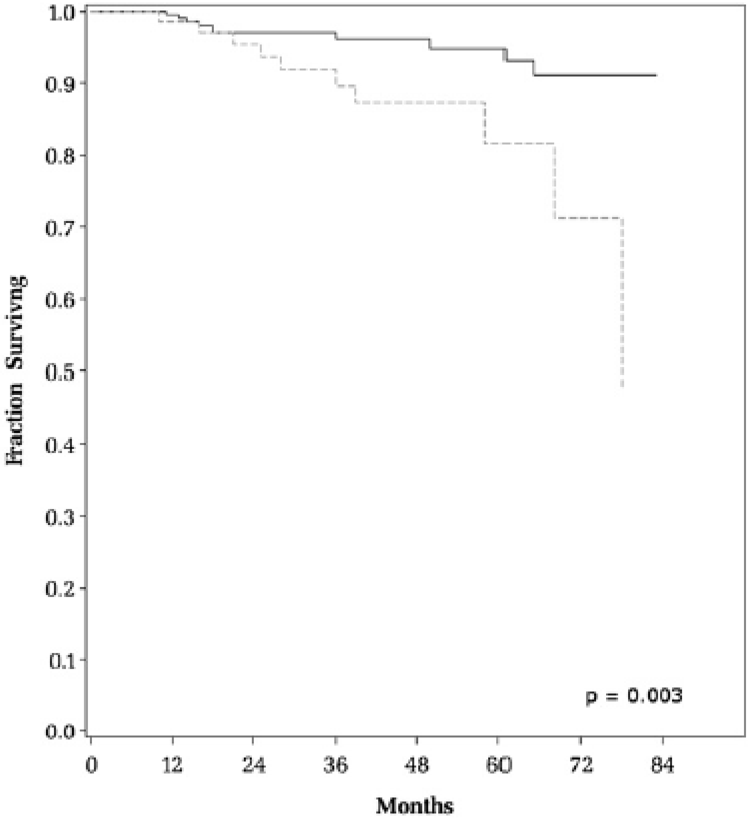

Number at Risk

No ECE	207	173	119	74	55	38	29
ECE	69	55	42	24	13	6	2

Riaz et al, Int J Radiat Oncol Biol Phys 2012

Local Failure

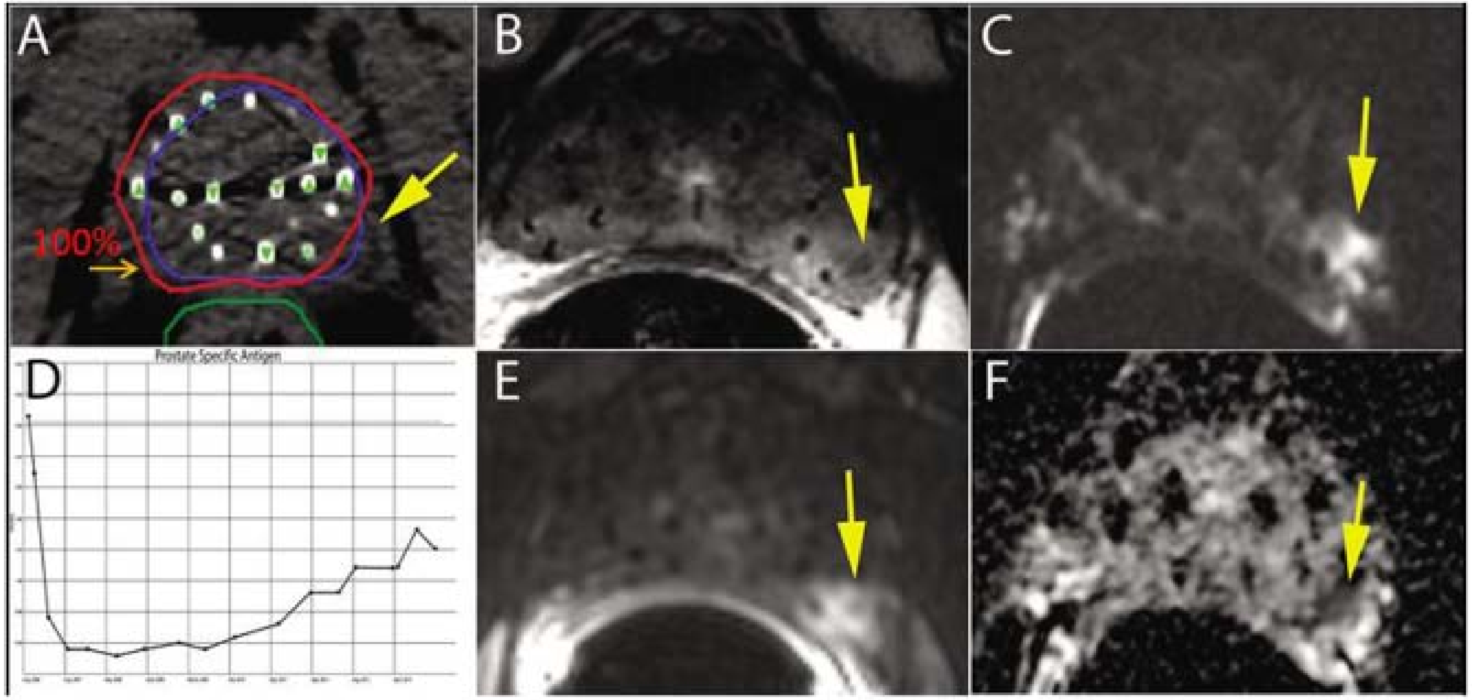

Figure 5 A 75-year-old male presented with a small nodule at the left base of the gland (ie, clinical T2a), PSA of 6 ng/mL, and Gleason Score (GS) of 7 (3 + 4) and was treated with a prostate brachytherapy implant alone to 144 Gy with 125-I (A). Postimplant dosimetry demonstrated a V100 = 97% and a D90 = 177 Gy; however, the left midgland was not covered with the 100% isodose line (A). The patient's PSA reached a nadir of 0.3 ng/mL 18 months after the implant. At 6 years after treatment, he had a PSA of 2.3 ng/mL with a PSA doubling time greater than 12 months (D). Multiparametric 1.5T MRI including T2W (B), DWI (C), DCE (E), and ADC maps (F) localized the recurrence at the left midgland. Metastatic workup showed negative result. Biopsy of the left midgland confirmed adenocarcinoma with a GS of 7 (4 + 3). ADC, apparent diffusion coefficient. (Color version of figure is available online.)

Tanderup et al., Sem Rad Oncol 2014

Impact on stage

Table 3. Number of patients with extracapsular extension or seminal vesicle invasion incorporated into target volumes

Initial risk group	Extracapsular extension, *n* (%)		Seminal vesicle invasion, *n* (%)	
	Conventional clinical T-staging	Additional MRI T-staging	Conventional clinical T-staging	Additional MRI T-staging
Low (*n* = 7)	0 (0)	1 (14)	0 (0)	0 (0)
Intermediate (*n* = 31)	0 (0)	4 (13)	0 (0)	5 (16)
High/very high (*n* = 77)	37 (48)	41 (53)	3 (4)	16 (21)
Total (*n* = 115)	37 (32)	46 (40)	3 (3)	21 (18)

Chang JMIRO 2014

CHUM

Volume of Tumor Burden on MRI and Radiotherapy Outcomes

Variable	Metastatic failure*	
	HR (95% CI)	p
Clinical		
Pretreatment PSA value	1.06 (0.99–1.13)	0.12
Gleason score	1.14 (0.45–2.87)	0.78
Percentage of positive biopsies	1.08 (0.98–1.19)	0.10
D'Amico risk category	1.02 (0.99–1.04)	0.23
MRI/MRSI		
MRI tumor size	1.12 (1.02–1.2)	0.01†
MRI tumor stage*	0.34 (0.24–0.49)	0.99
Seminal vesicle invasion at MRI	11.49 (3.23–40.88)	0.0002†
Volume of malignant metabolism at MRSI	1.53 (1.08–2.16)	0.02†

Joseph et al. IJROBP 2008

CHUM

Contouring Variability

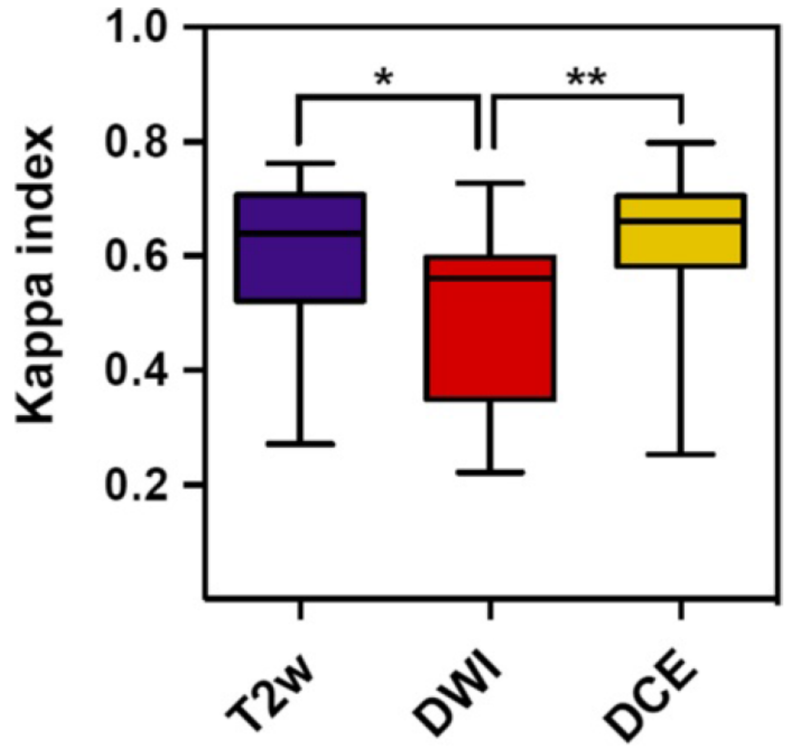

Figure 3 KI-T2w and KI-DCE was significantly higher than KI-DWI, *p = 0.01 (CI: 0.02-0.18) and **p = 0.0027 (CI: 0.2-0.04), respectively.

Rischke et al., Radia Oncol, 2013

CHUM

Figure 4

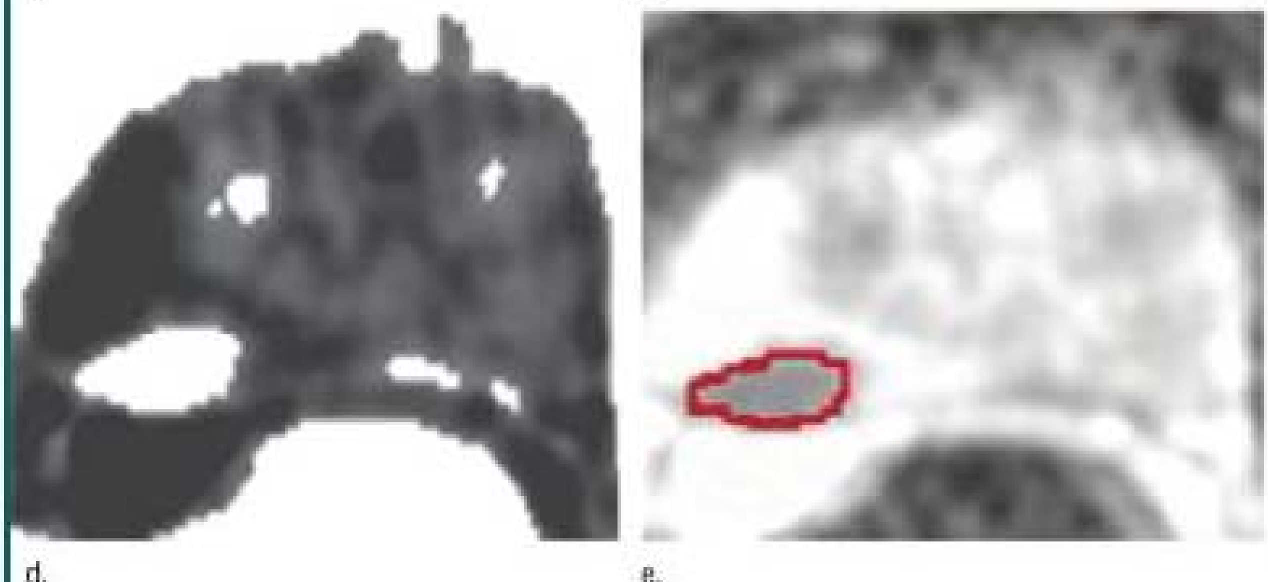

Figure 4: Data from 66-year-old patient with prostate cancer: presurgical PSA, 5.52 ng/mL (5.52 μg/L); clinical stage, T1C; surgical Gleason score, 3 + 4; and pathologic tumor volume, 4.77 cm^3. Whole-mount step-section histopathologic map shows prostate gland. (a) Only one (of 12) slices shown; tumor was present on seven slices. (b) Closest transverse T2-weighted image corresponding to matching pathologic slice. (c) ADC map of slice in b. (d) Mask generated from voxels that satisfy cluster requirements (ADC cutoff, 0.0016 mm^2/sec). (e) ROI containing the voxel cluster that satisfies all criteria (ADC cutoff, 0.0016 mm^2/sec). Tumor volume was 5.11 cm^3 measured on T2-weighted images and 4.81 cm^3 on combined T2-weighted and DW MR images.

Mazaheri Y et al. Radiology 2009;252:449-457

Scatterplots of tumor volume measurements made on basis of MR images (T2-weighted and combined T2-weighted and DW MR images) versus histopathologic measurements

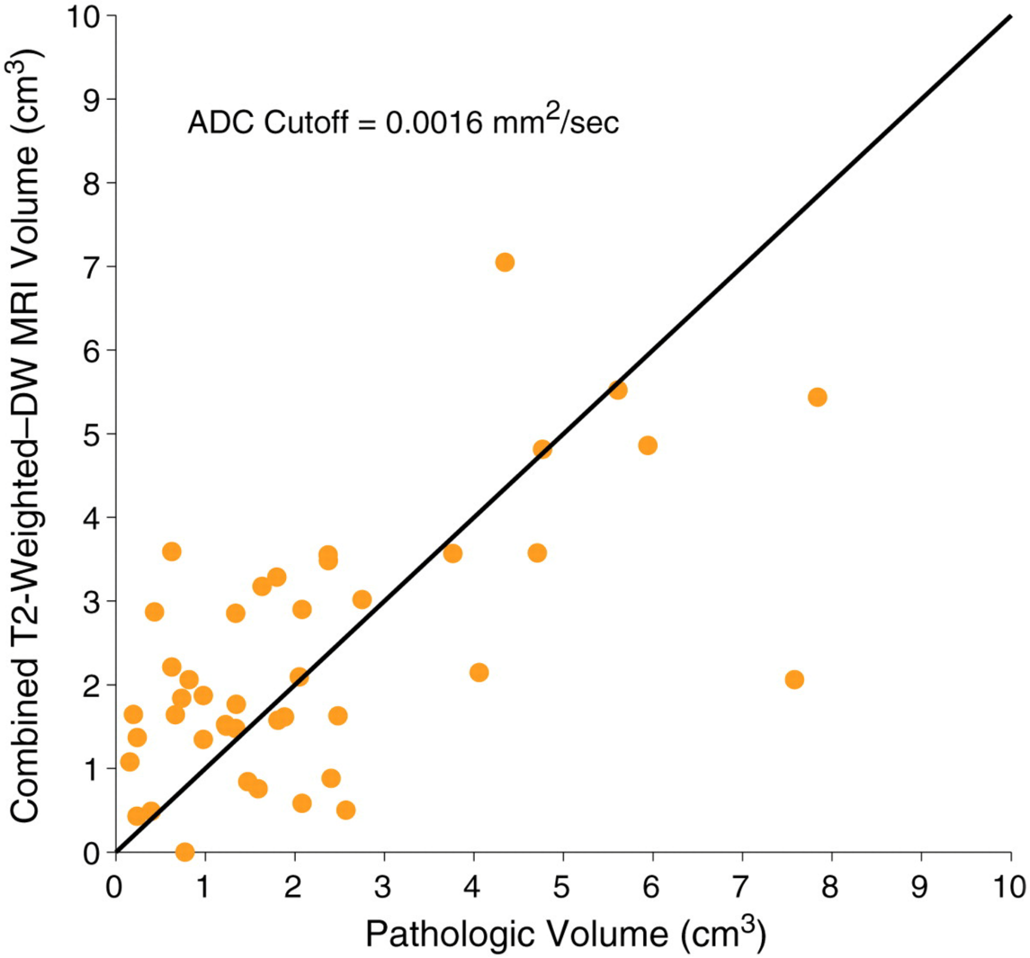

Mazaheri Y et al. Radiology 2009;252:449-457

Radiology

CHUM

Box-and-whisker plot of ADCs of tumor lesions for three Gleason grades from 60 cancer lesions in 42 patients

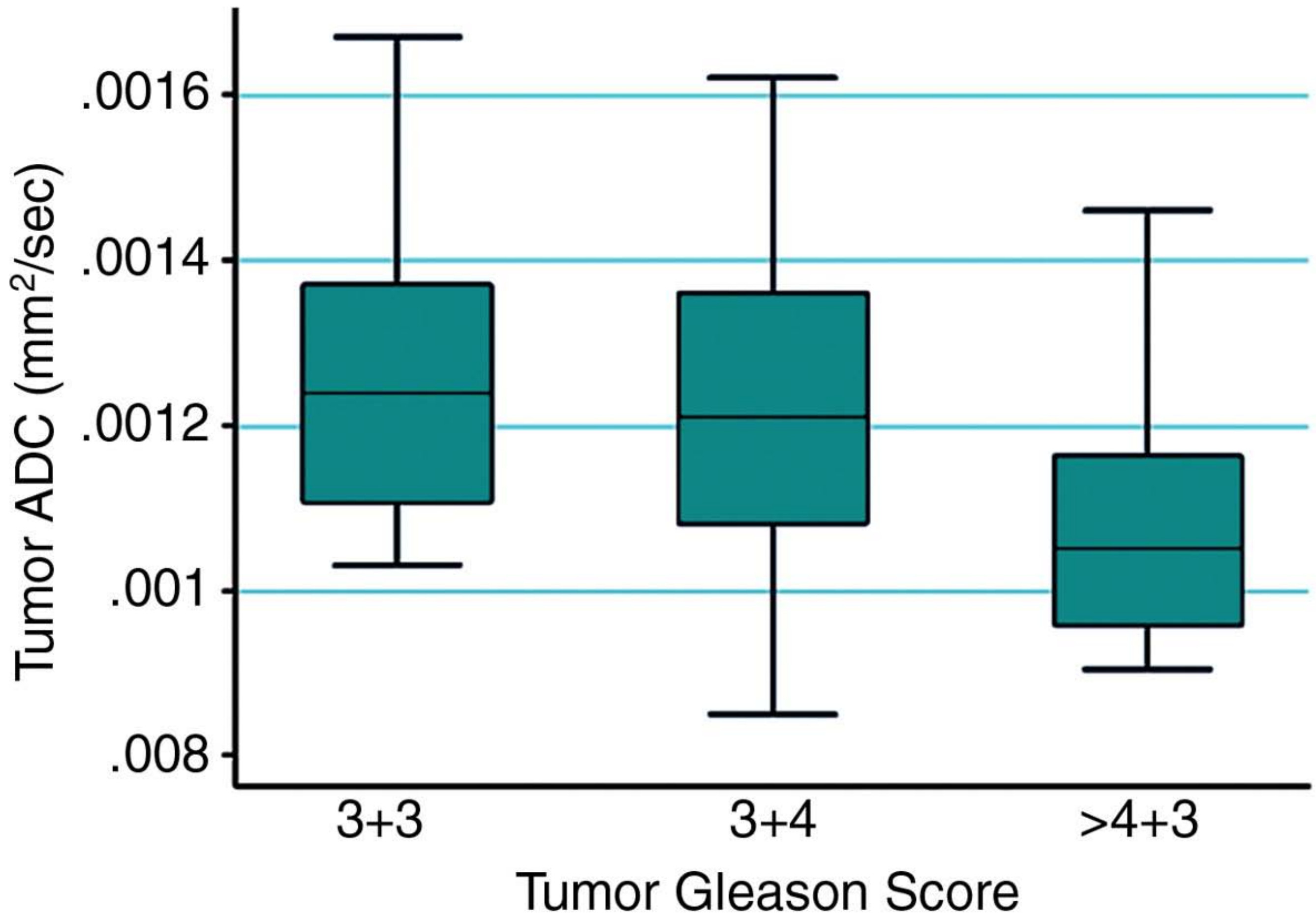

Mazaheri Y et al. Radiology 2009;252:449-457

Radiology

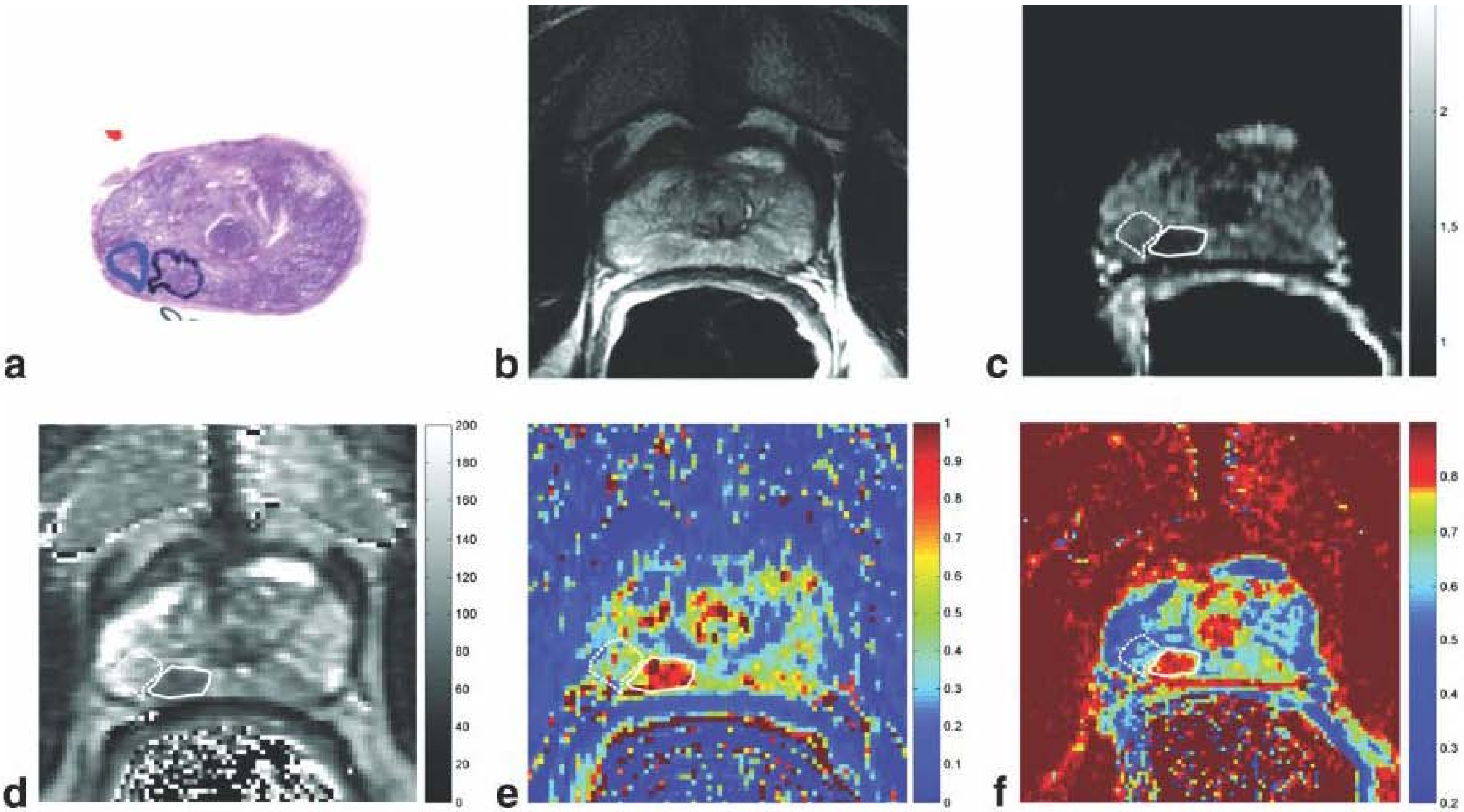

Langer et al. JMRI 2009

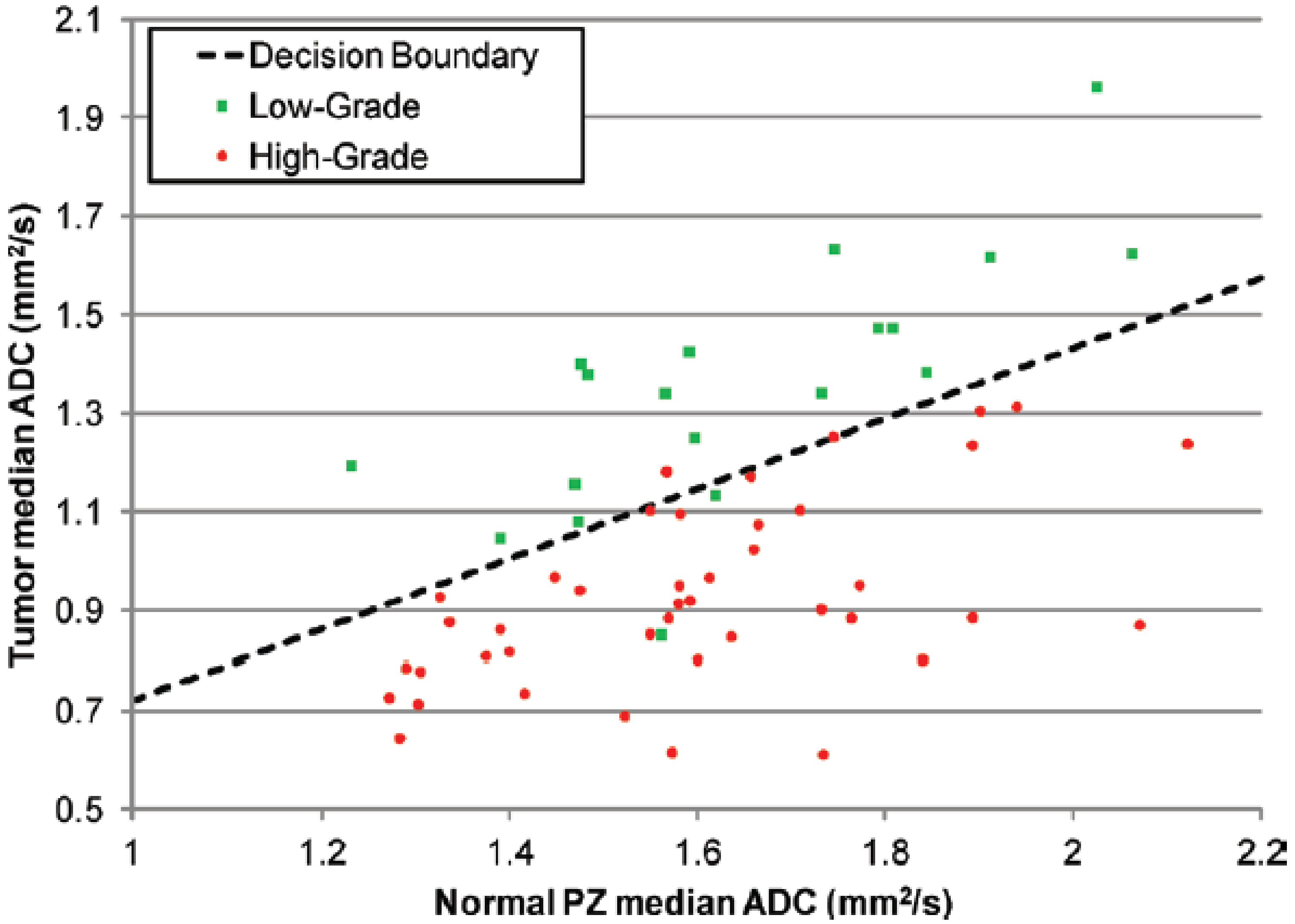

Litjens et al. Radiology 2012

Neo-adjuvant Hormones

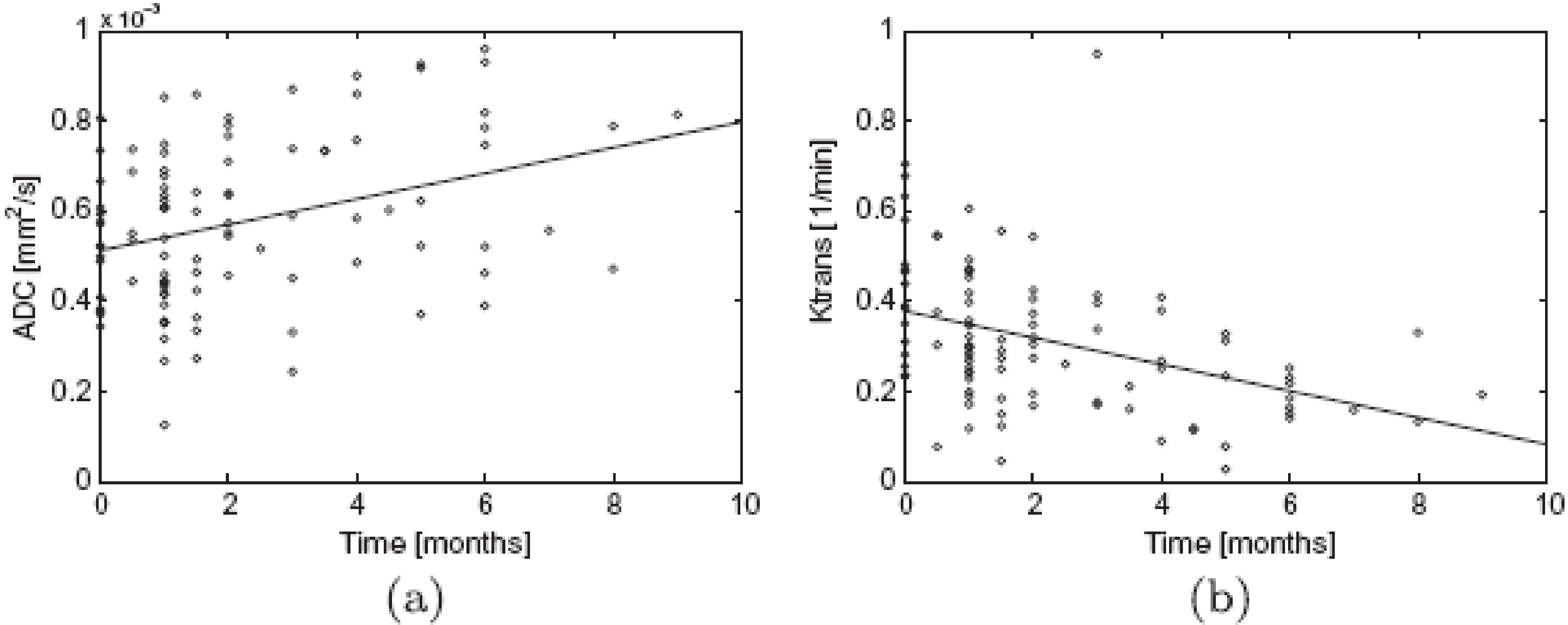

📖 Groenendaal et al., Radiother Oncol 2012

CHUM

Probability Maps – Path Validation

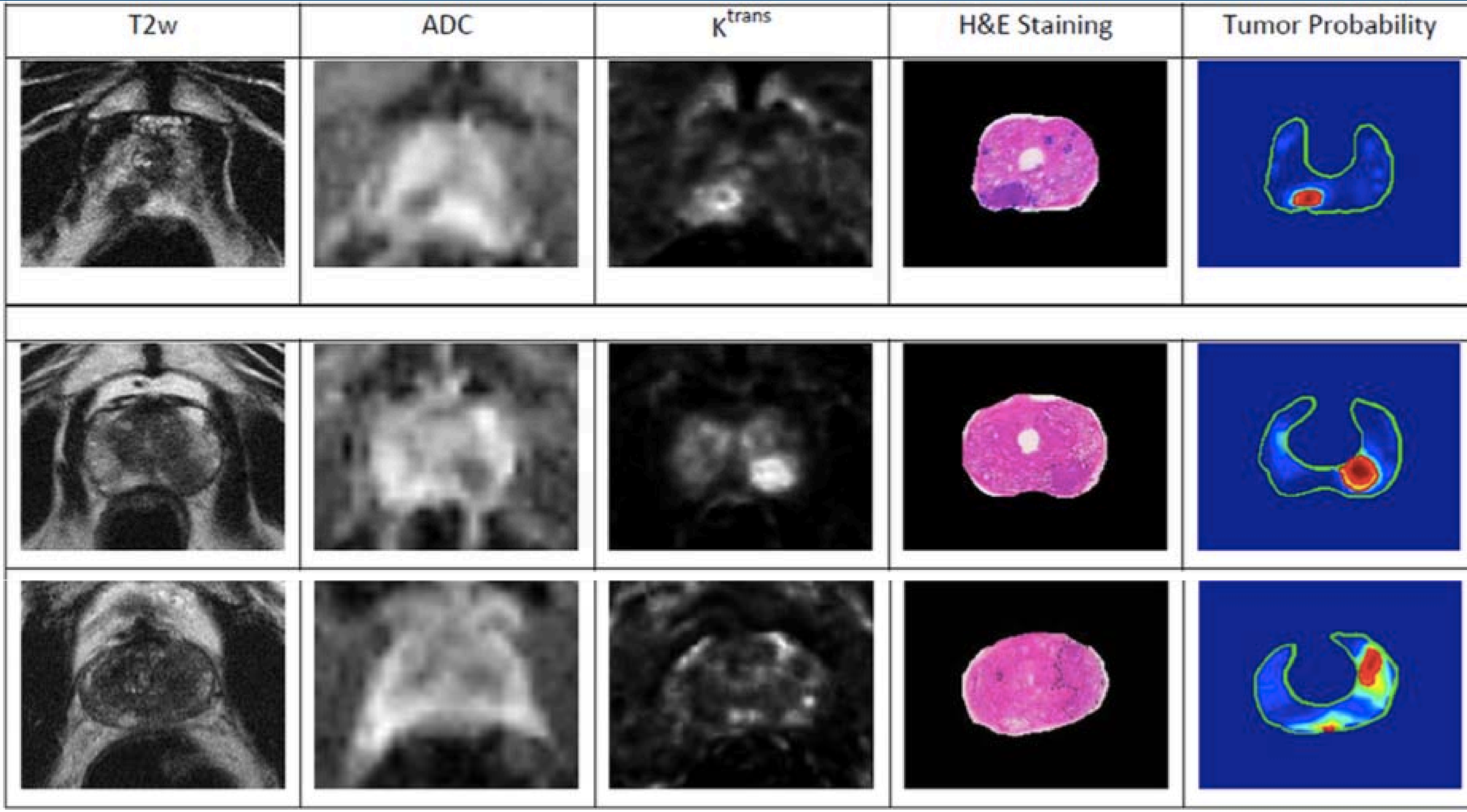

Dinh et al., Physica Medica 2016

Voxel-Based Correspondence

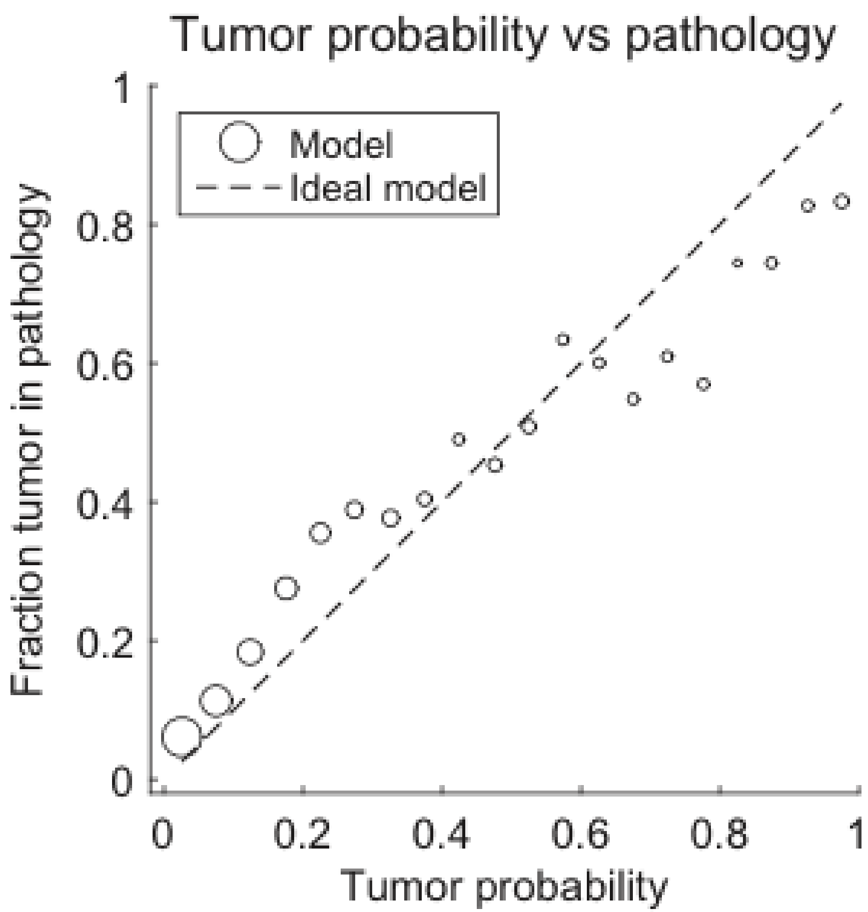

📖 Dinh et al., Physica Medica 2016

‘Wisdom of the crowd’

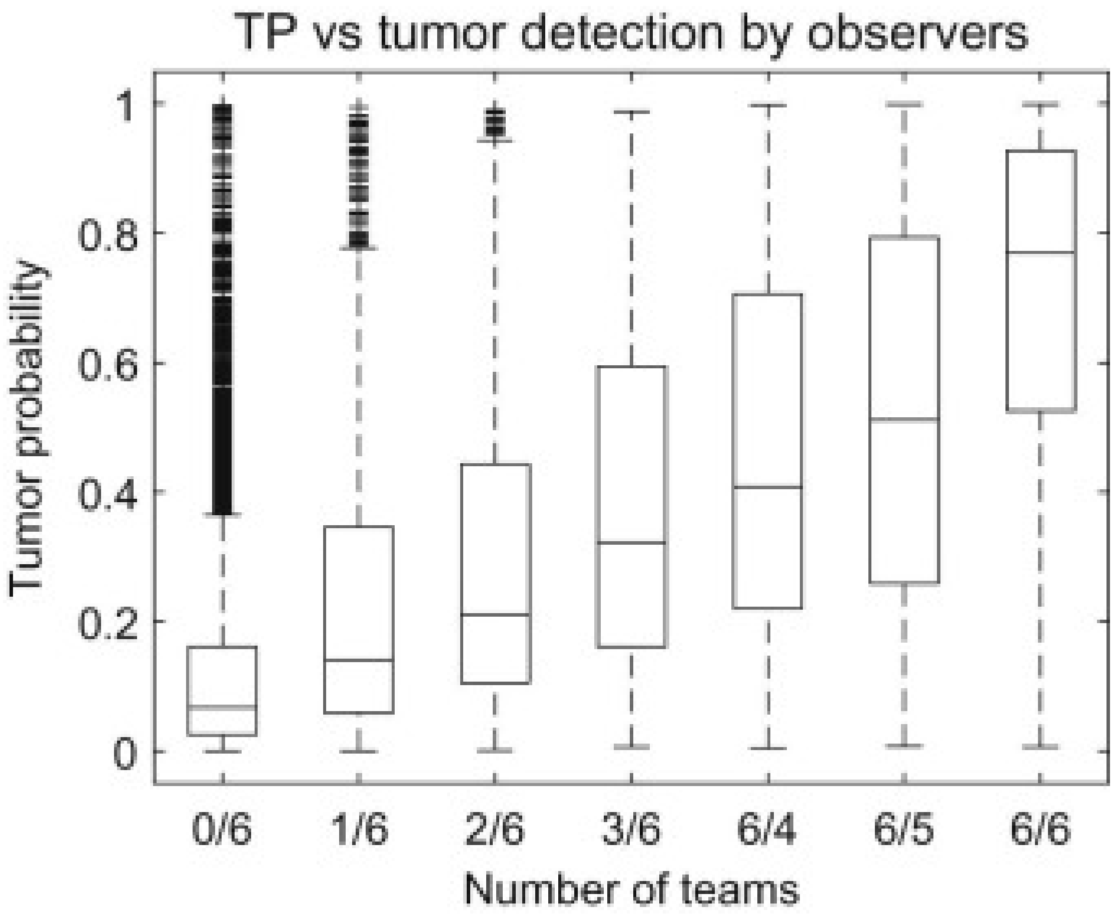

📖 Dinh et al., Physica Medica 2016

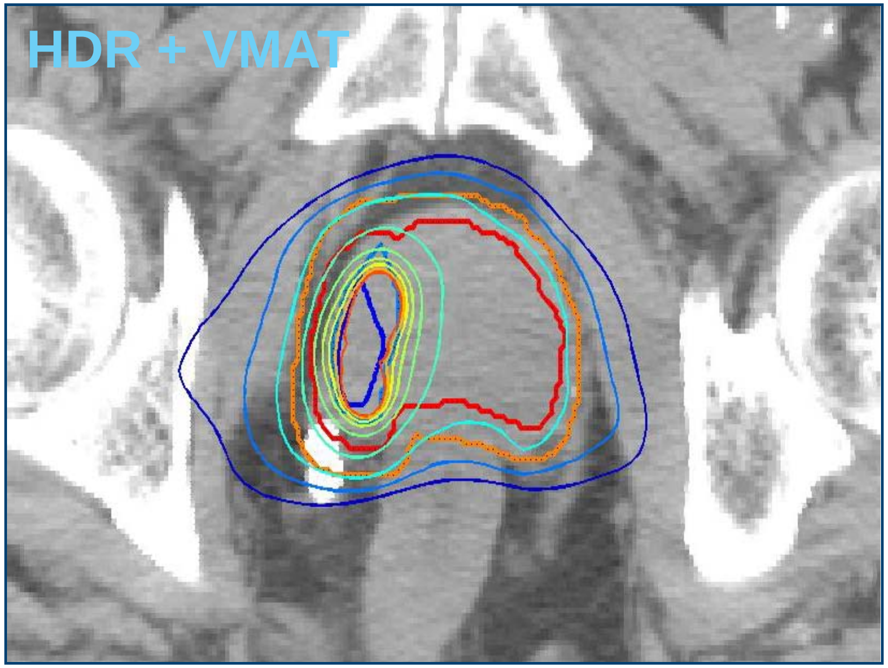

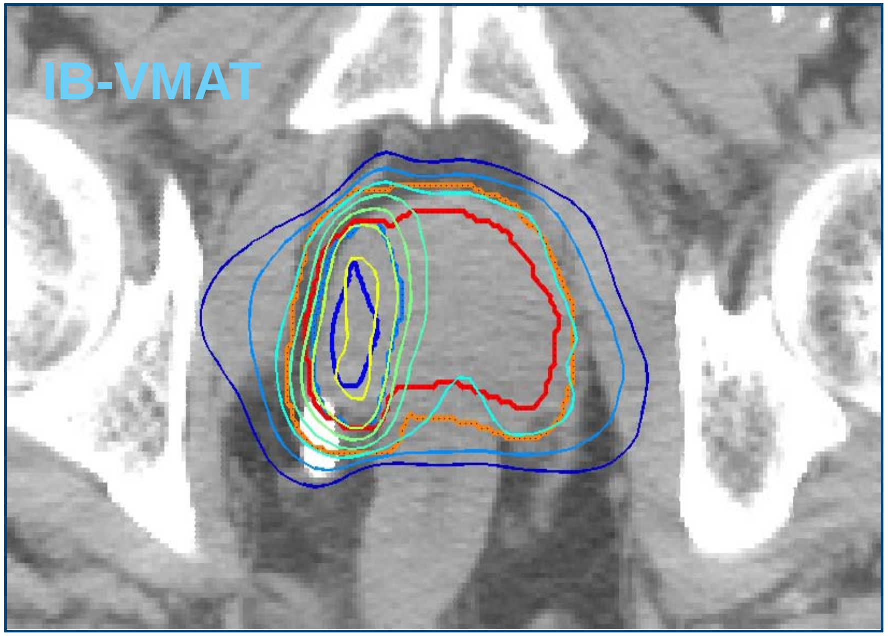

Dose (EQD2 [Gy])

50
60
70
80
90
100
110
120
130

Structures

GTV
CTV
PTV(GTV)
PTV(CTV)

CHUM

Dosimetry Literature

- +++ publications
- Absolute modeled TCP achieved by SIB ranged from 2-15% and generally achieved with similar or small increase to NTCP rectum
- Ability to dose escalate was anatomy dependent; lesions within 5mm of rectal wall were difficult to dose escalate
- TCP/NTCP calculations highly dependent on accuracy of GTV delineation
- Ability to boost independent of technique (fixed field IMRT vs. VMAT; sequential vs. SIB) when considering the effects of intra-fraction motion

Systematic Review – Tumor Boost

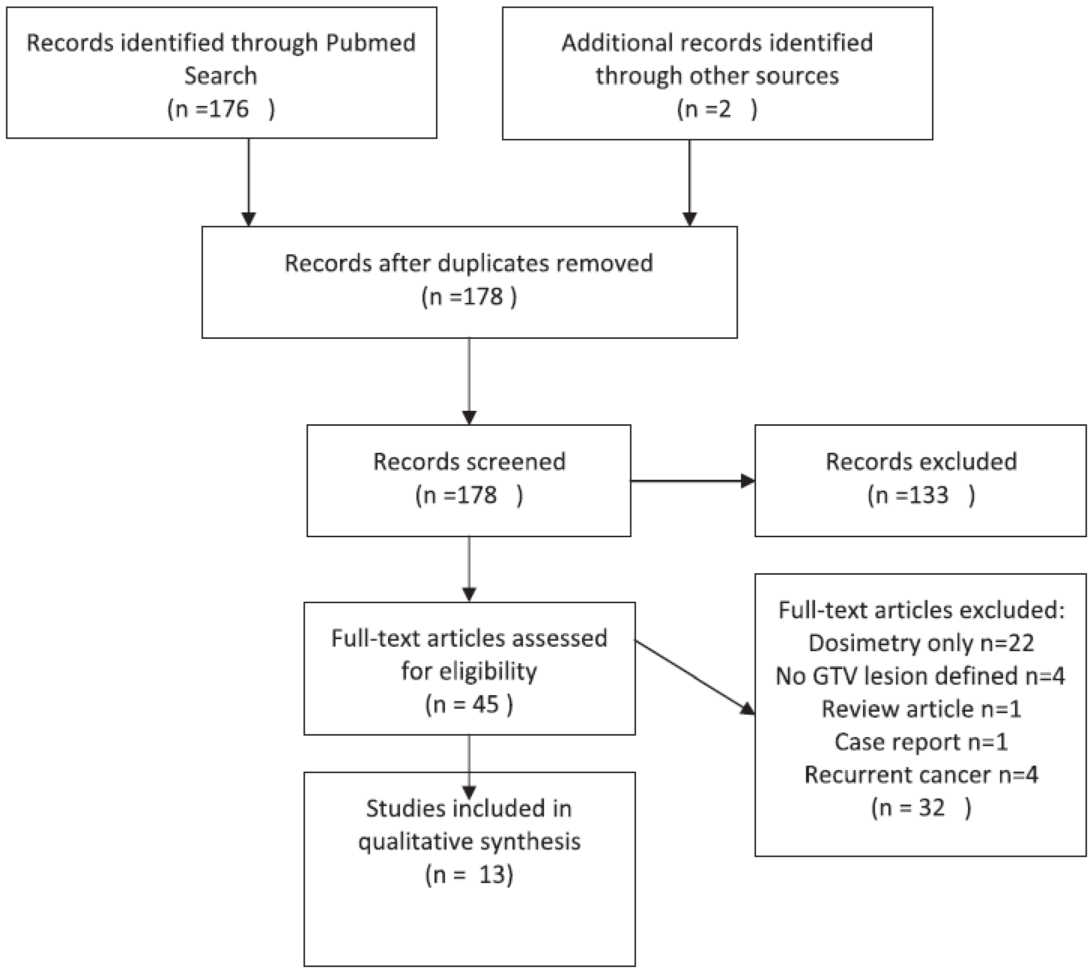

Bauman et al., Radiotherapy & Oncology 2013

Systematic Review

- Thirteen papers describing 11 unique patient series and 833 patients in total were identified.
- Methods and details of GTV definition and treatment varied substantially between series.
- GTV boosts were on average 8 Gy (range 3–35 Gy) for external beam, or 150% for brachytherapy (range 130–155%) and GTV volumes were small (<10 ml).
- Reported toxicity rates were low and may reflect the modest boost doses, small volumes and conservative DVH constraints employed in most studies.

📖 Bauman et al., Radiotherapy & Oncology 2013

Caution in De-escalation

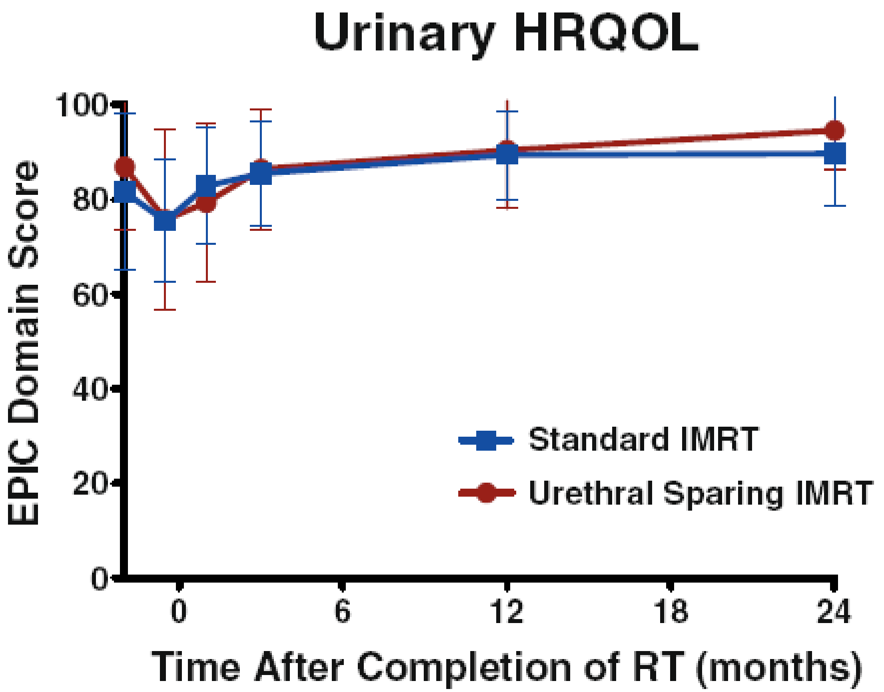

Figure 4 Urinary HRQOL by EPIC Urinary Domain Summary Score after Urethral Sparing IMRT and Standard IMRT.

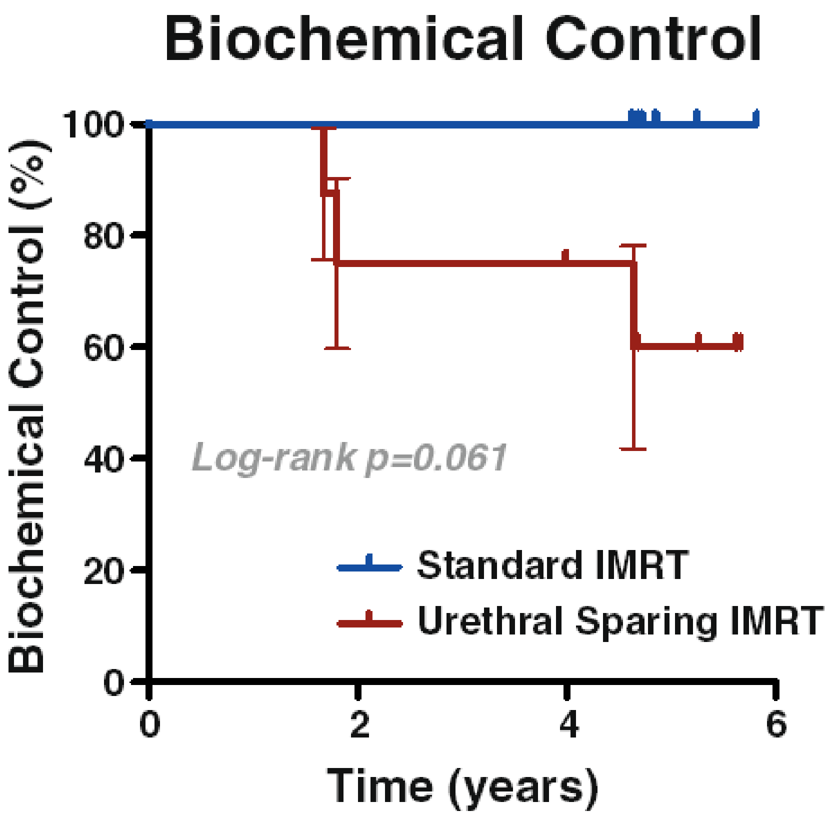

Figure 5 Biochemical Control after Urethral Sparing IMRT and Standard IMRT.

Vainshtein et al., Radiat Oncol 2012

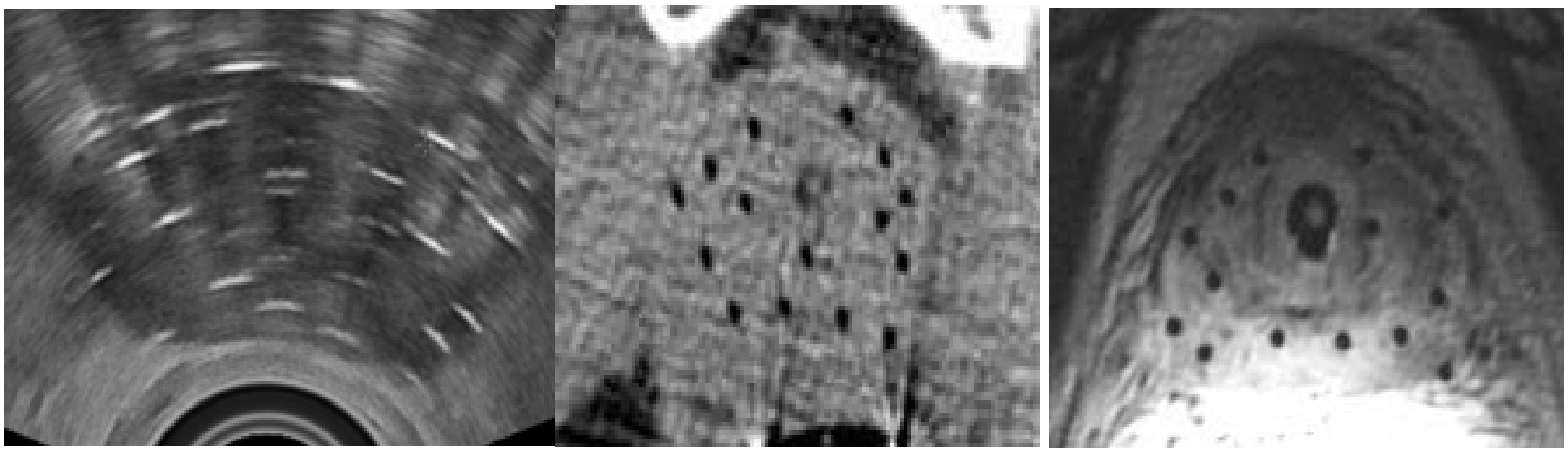

Atalar et al.

Real-Time TRUS-only Workflow

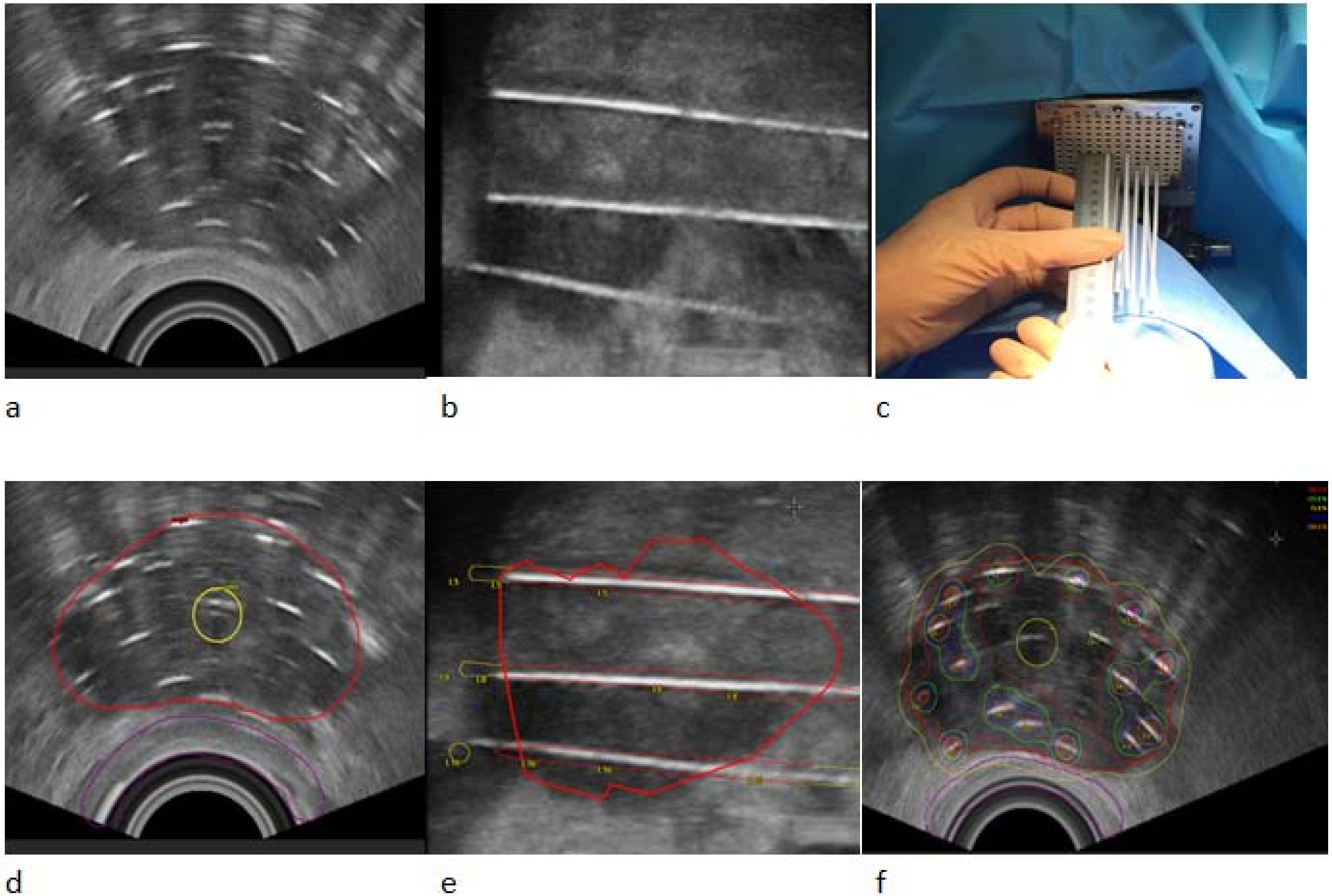

Lauche et al., 2016

First - MRI for LDR Post-Planning - 1997

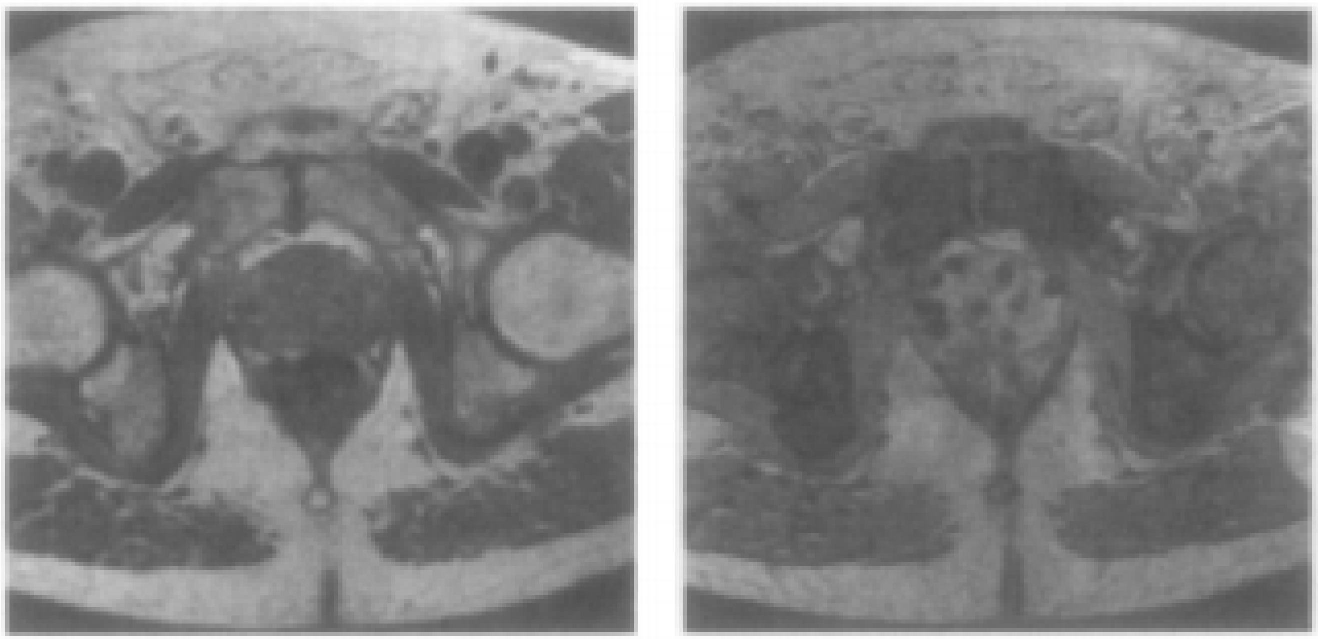

Fig. 1. Transversal spin-echo (left) and gradient-echo (right) image of the prostate. I-125 seeds are depicted as signal voids.

📖 Moerland et al. Int J Radiat Oncol Biol Phys 1997

Prostate Post-Plan

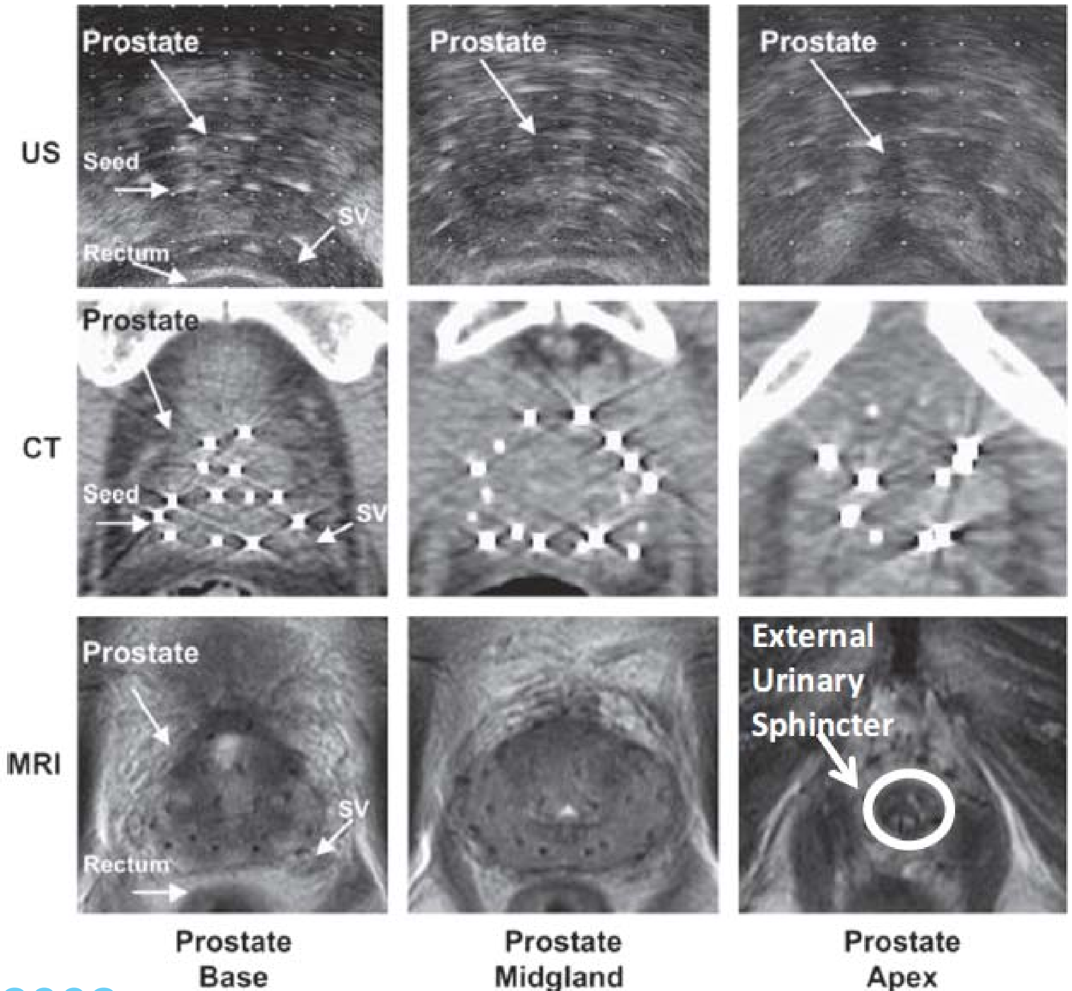

Frank et al., 2008

MRI Post-Plan

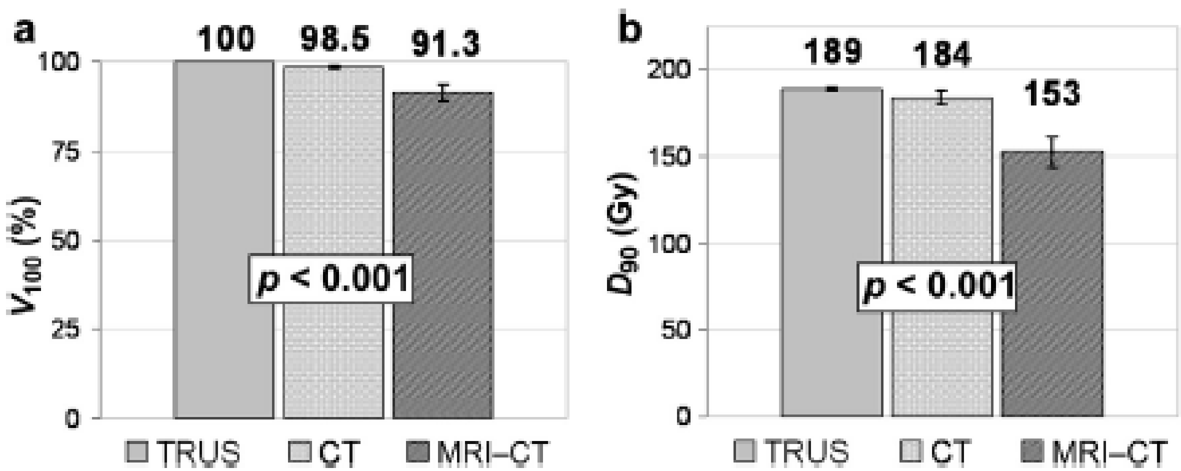

Fig. 2. Mean V_{100} values (a) and D_{90} values (b) for the whole prostate, calculated by using TRUS, postimplant CT alone, and postimplant MRI–CT fusion (MRI–CT). The MRI–CT fusion scan revealed significantly lower mean D_{90} and V_{100} values compared with the TRUS scans obtained before implantation and standard dosimetry based on CT alone ($p < 0.001$). Vertical bars represent 95% confidence intervals. TRUS = transrectal ultrasonography.

📖 Brown et al., Brachytherapy 2013

📖 Dinkla et al., Acta Oncol 2013

CHUM

Dosimetric Innacuracies - Quality

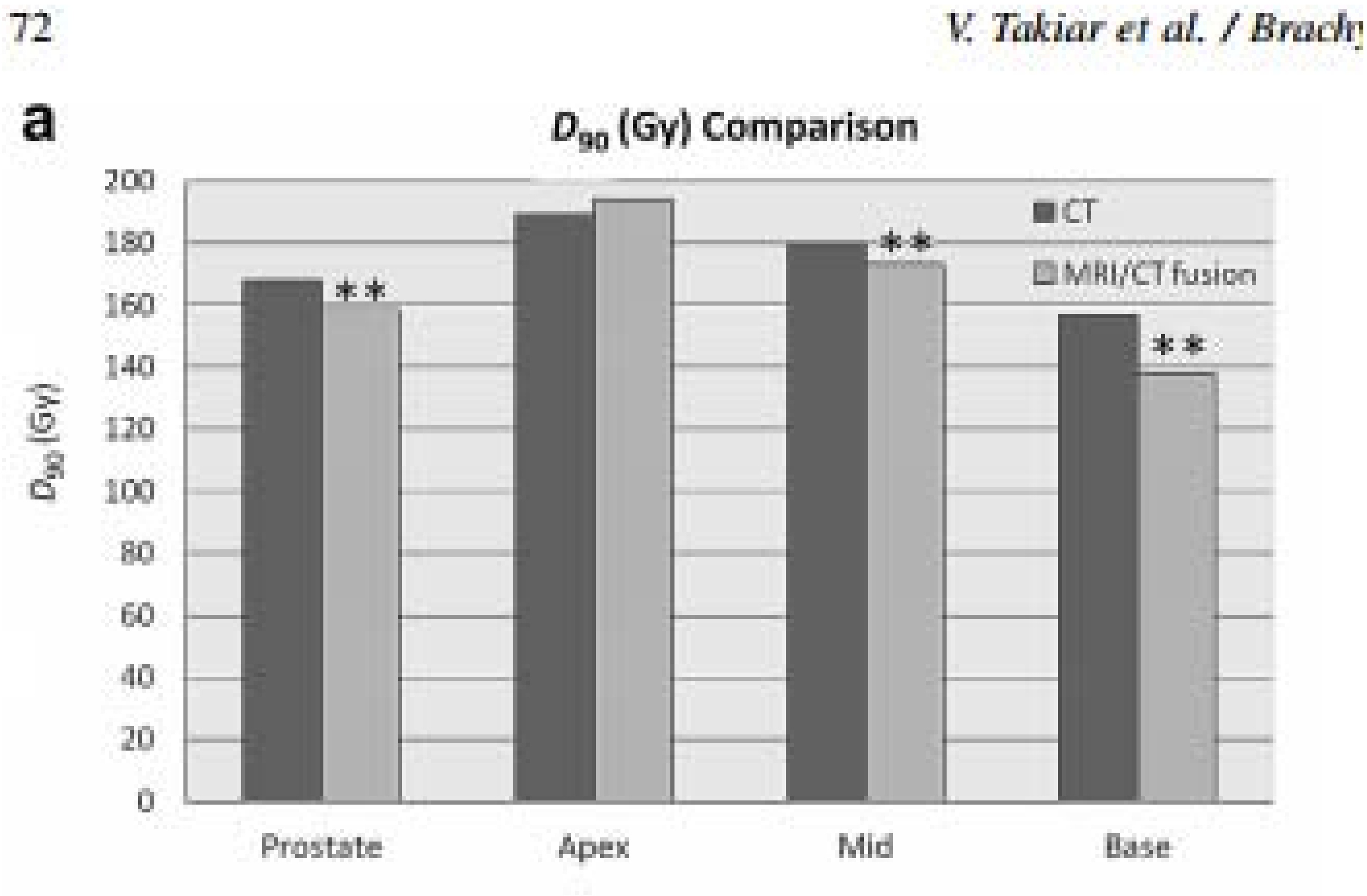

📖 Takiar et al. Brachytherapy 2014

CHUM

MRI - GEC/ESTRO 2005 → 2013

- T2 weighted MR images will provide optimal anatomical definition *but T1 weighted images will provide more accurate catheter reconstruction*
- CTV + plus any macroscopic extracapsular disease or seminal vesicle involvement identified on diagnostic images expanded by 3 mm to encompass potential microscopic disease
- GTV may be defined, CTV subvolumes may be defined

📖 Hoskin et al. Radiot Oncol 2013

Computational Integration of diagnostic MRI to Online TRUS

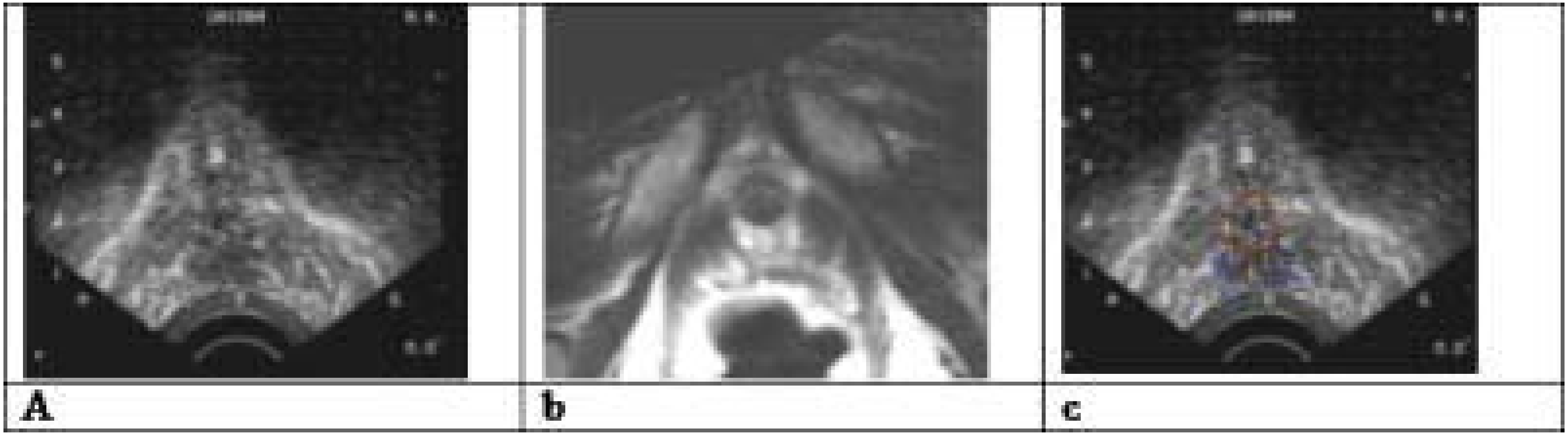

📖 Reynier et al. 2004

Registration to TRUS

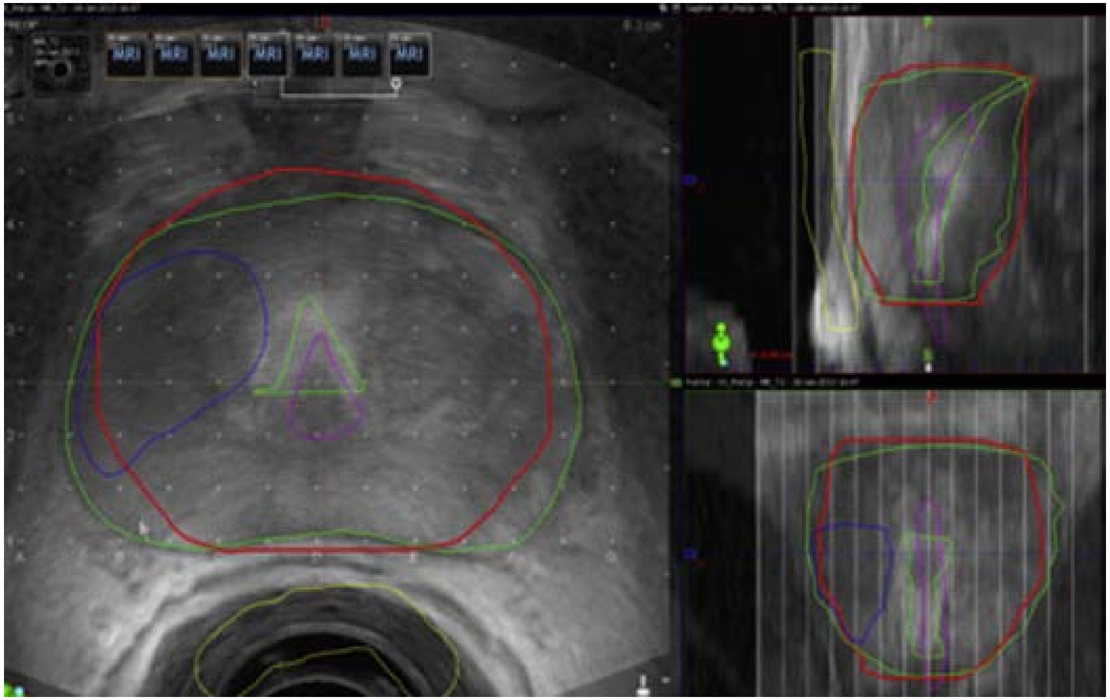

Fig. 2. Three-way fusion of eMRI, intraoperative TRUS, and preoperative TRUS (eMRI prostate, green; TRUS prostate, red; and DIL, blue). Note slight deformation of prostate by endorectal coil. eMRI = endorectal MRI; TRUS = transrectal ultrasound; DIL = dominant...

Juanita Crook, Ana Ots, Miren Gaztañaga, Matt Schmid, Cynthia Araujo, Michelle Hilts, Deidre Batchelar, Brent Parker, François Bachand, Marie-Pierre Milette

Ultrasound-planned high-dose-rate prostate brachytherapy: Dose painting to the dominant intraprostatic lesion

Brachytherapy, Volume 13, Issue 5, 2014, 433–441

SLICER

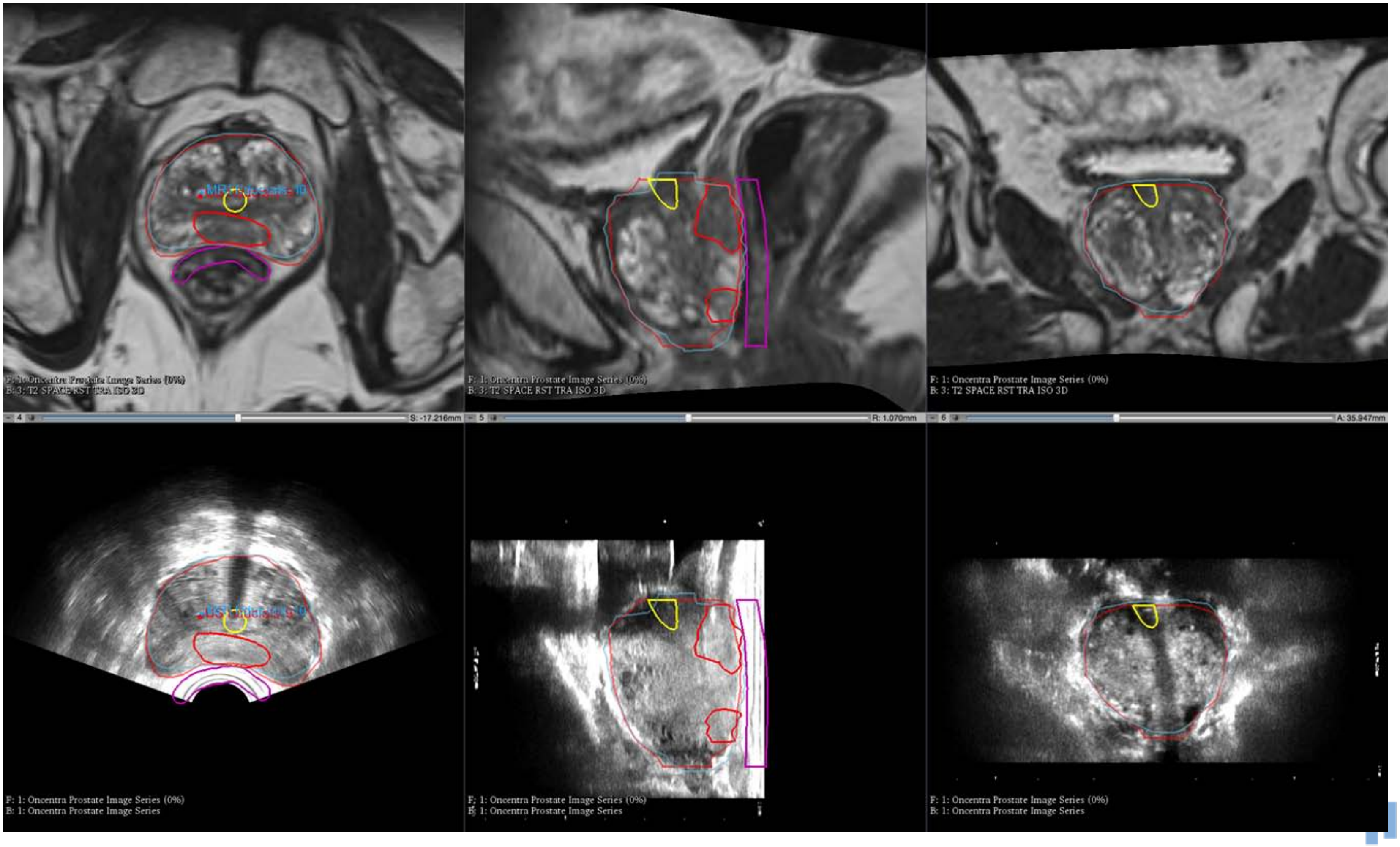
F: 1: Oncentra Prostate Image Series (0%)
B: 3: T2 SPACE RST TRA ISO 3D
S: -17.216mm
F: 1: Oncentra Prostate Image Series (0%)
B: 3: T2 SPACE RST TRA ISO 3D
R: 1.070mm
F: 1: Oncentra Prostate Image Series (0%)
B: 3: T2 SPACE RST TRA ISO 3D
A: 35.947mm
F: 1: Oncentra Prostate Image Series (0%)
B: 1: Oncentra Prostate Image Series
F: 1: Oncentra Prostate Image Series (0%)
B: 1: Oncentra Prostate Image Series
F: 1: Oncentra Prostate Image Series (0%)
B: 1: Oncentra Prostate Image Series

CHUM

High-field MRI-only Workflow (HDR)

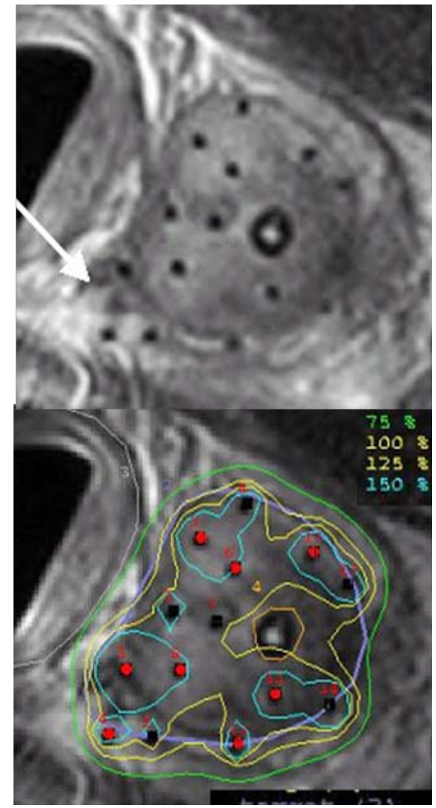

📖 Ménard and Susil et al. 2004

CHUM

InVivo – Philips – Sentinelle Endocoil Array

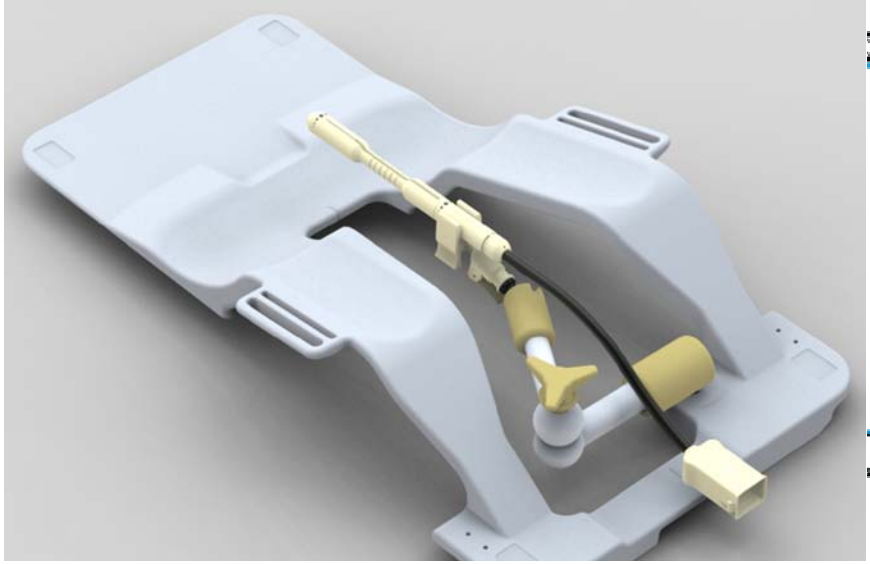

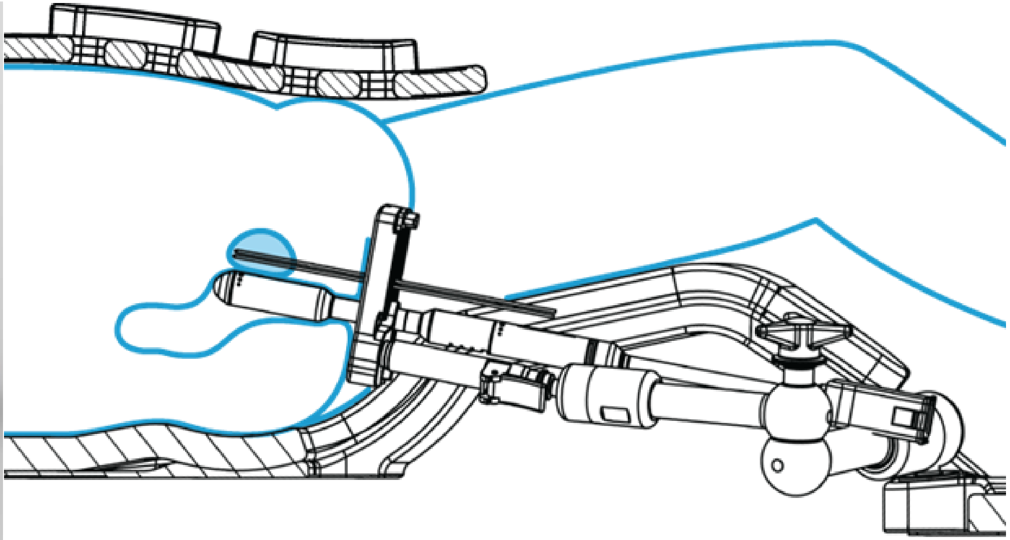

CHUM

- Set-up – median 25 min
- Imaging + catheter insertion – median 100 min
- Overall sedation 4.0 hours (2.1-6.9)

Registration to high-field MRI

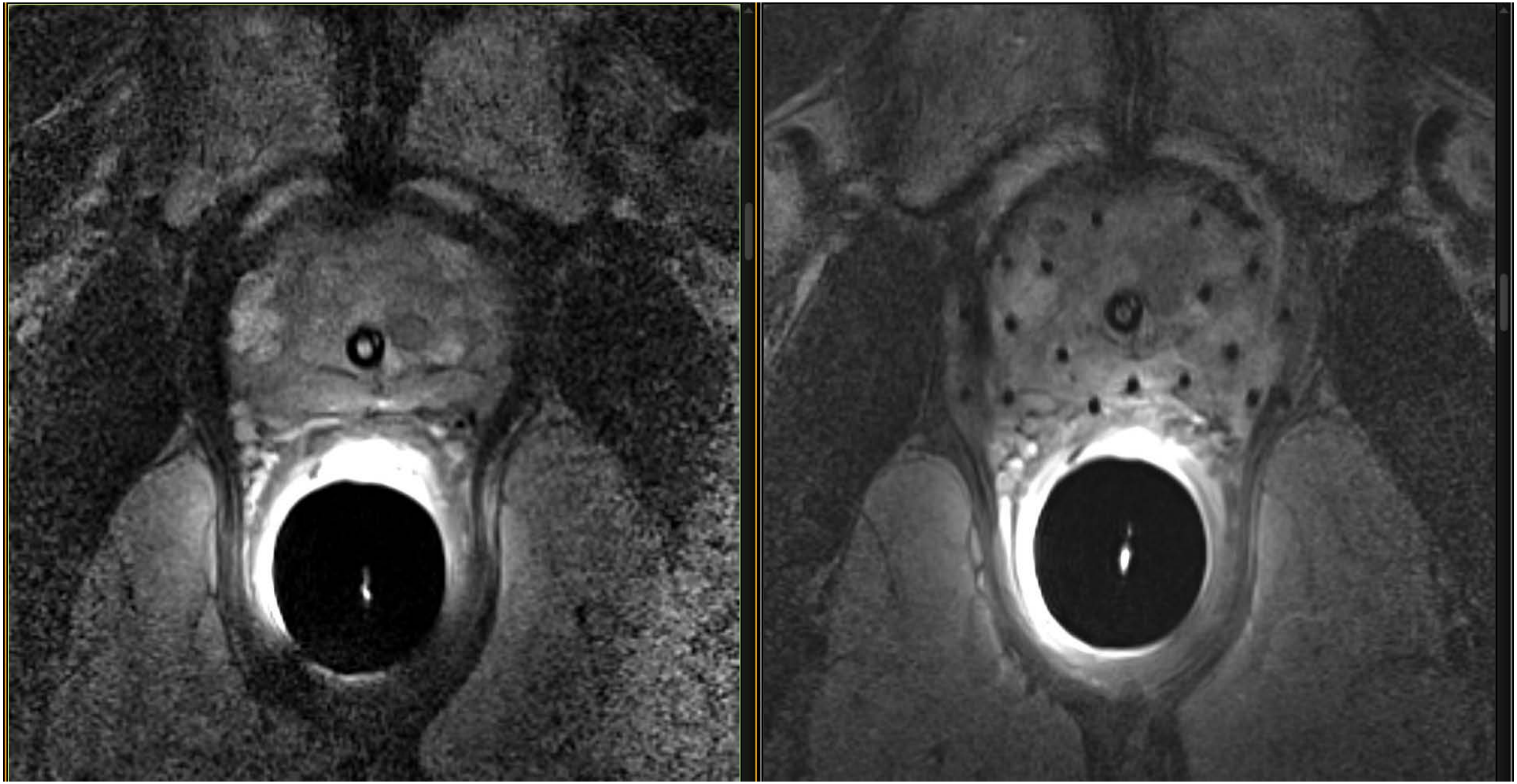


0.10 cm
0.10 cm
Patient

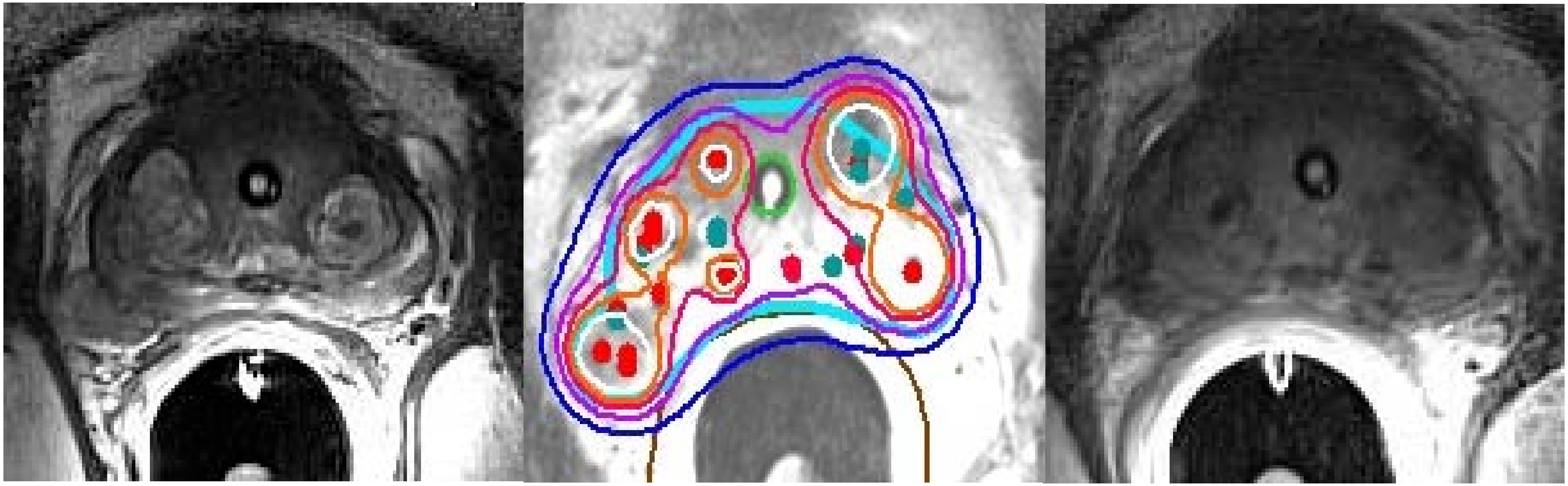

CHUM

Needle Guidance – Anterior Tumours

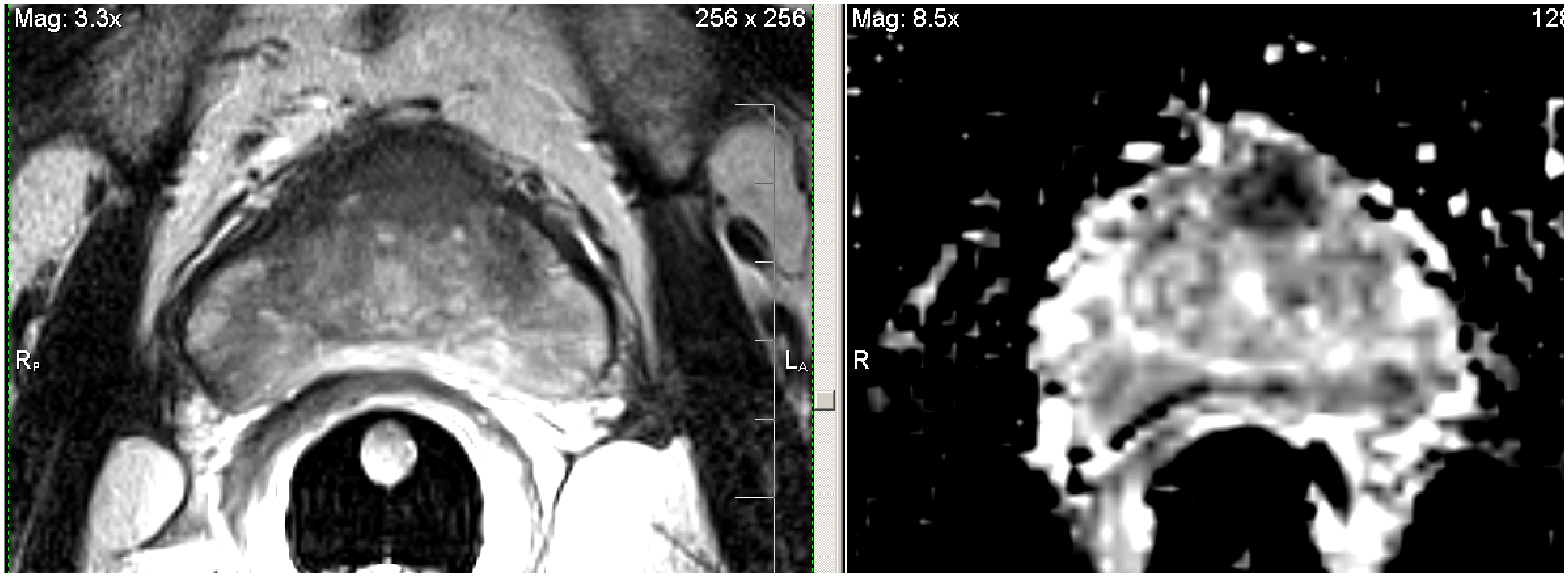

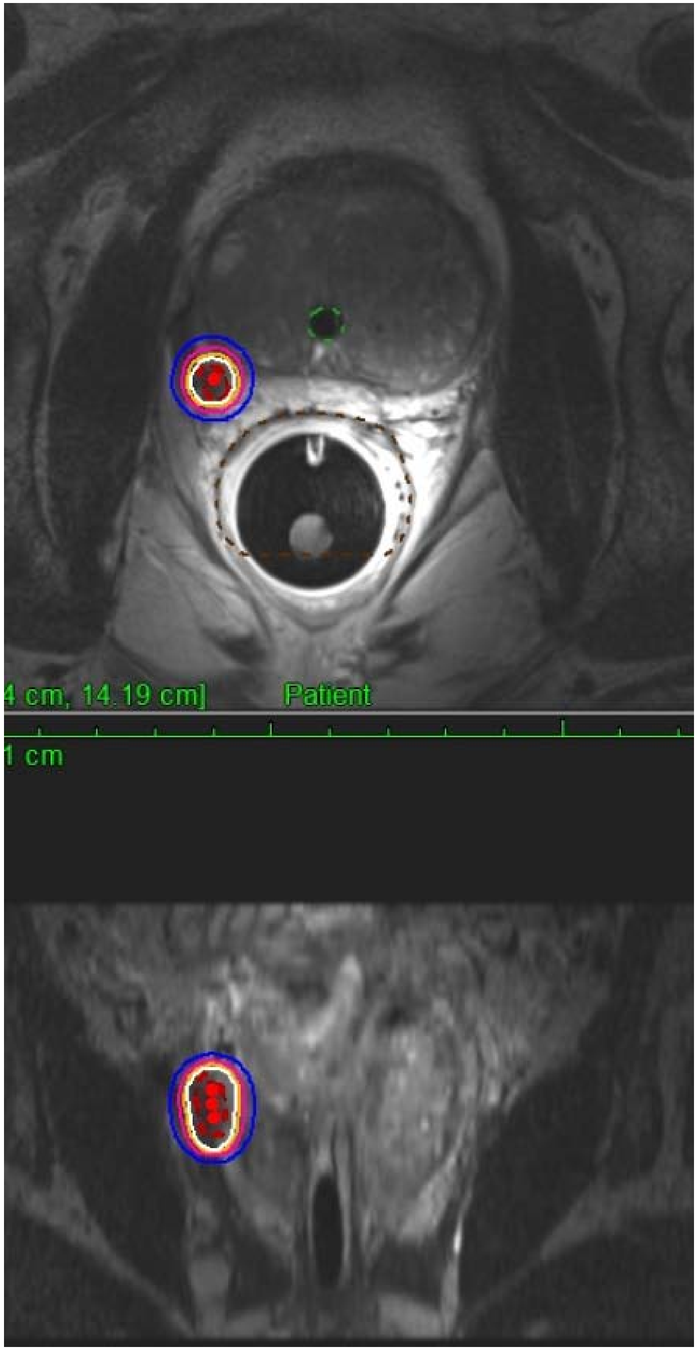
4 cm, 14.19 cm]
Patient
1 cm

Mechatronic Robot – Princess Margaret

UMCU robot
first clinical version

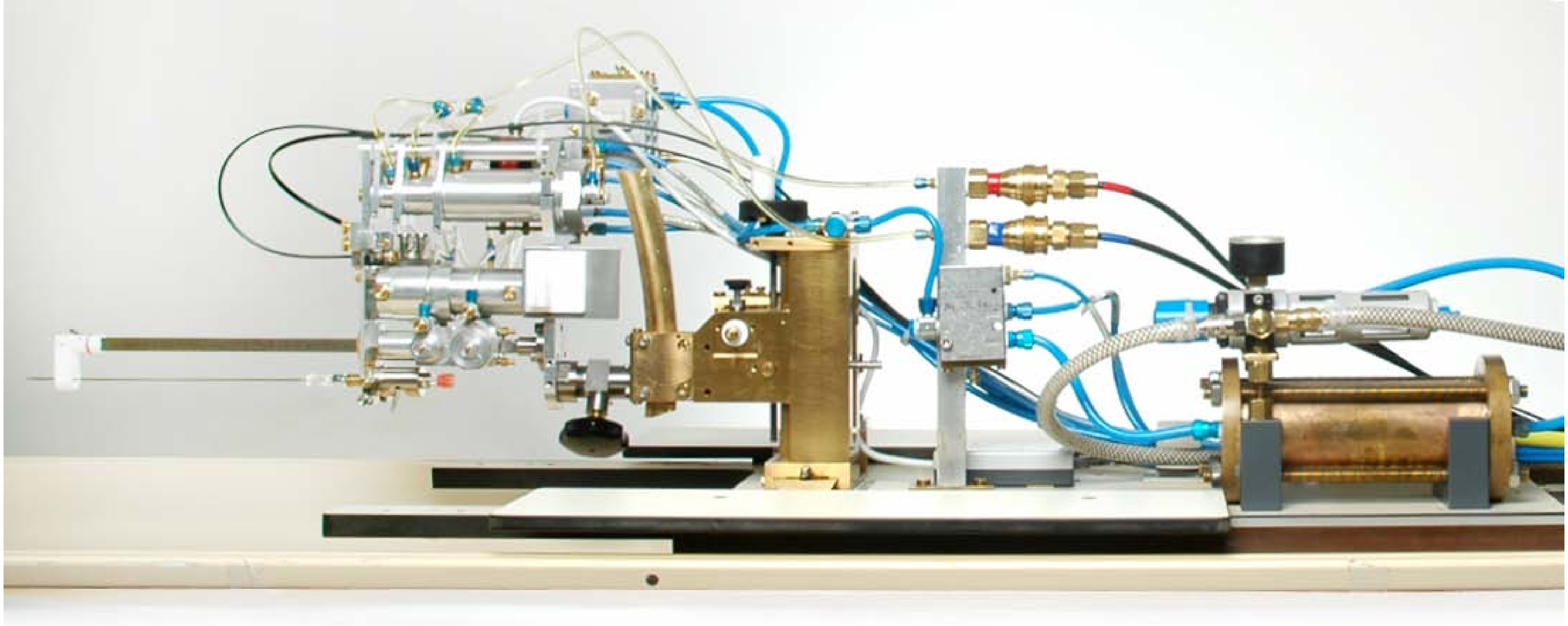

CHUM

Tracking Coils

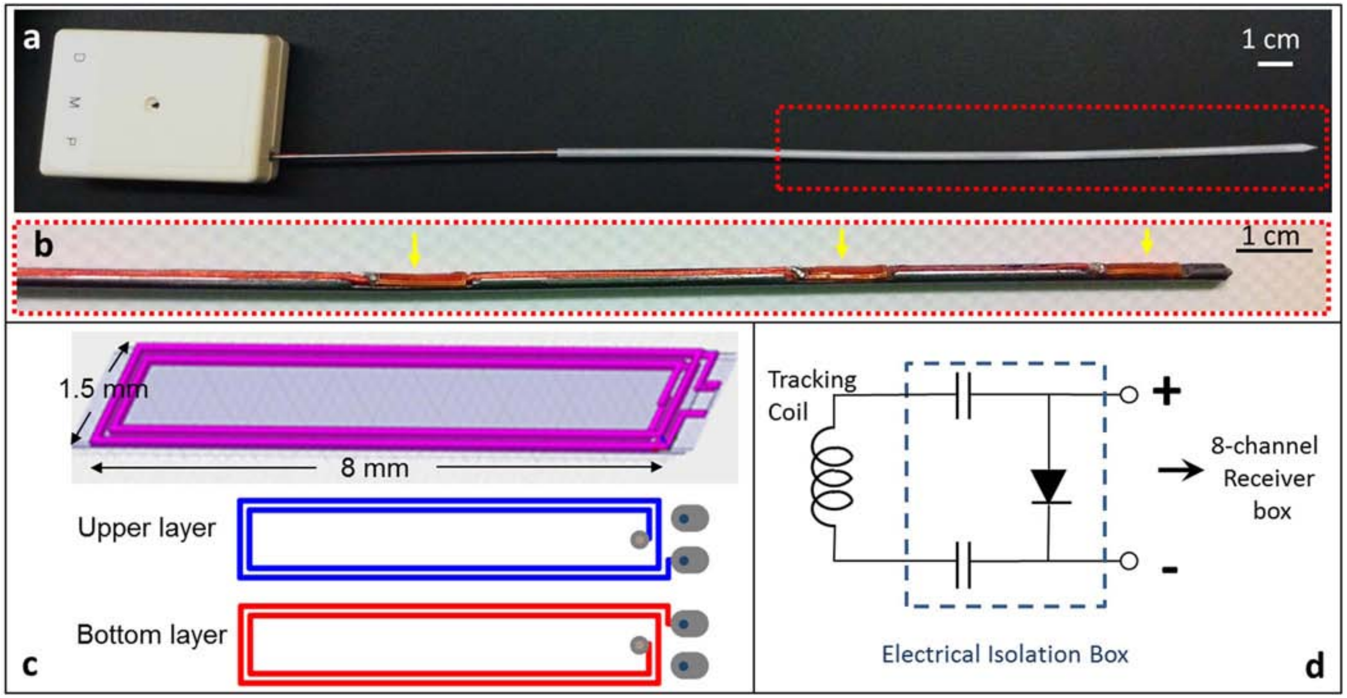

Schmidt et al., Magn Reson Med 2015

Acknowledgements

- Laura Dawson
- Masoom Haider
- Peter Chung
- Robert Bristow
- Michael Milosevic
- Padraig Warde
- Charles Catton
- Gerard Morton
- Danny Vespirini
- Mary Gospodarowicz
- Andrew Bayley
- Saibish Elan
- Juanita Crook
- Ants Toi
- Marco van Vulpen
- Warren Foltz
- Douglas Iupati
- Jessy Abed
- Jenny Lee
- Supriya Chopra
- Denis Suljendic
- Julia Publicover
- Anna Kirilova
- Akbar Beiki
- John Jezioranski
- Iris Elliott
- Axel Krieger
- Dave Gallop
- Bernadeth Lao
- Debbie Tsuji
- Uulke van der Heider
- David Jaffray

APPLICATIONS:
PET/MRI IN HEAD & NECK

Piet Dirix MD, PhD
Dpt. of Radiation Oncology, Iridium Cancer Network
Associate Professor, University of Antwerp
www.iridiumkankernetwerk.be

PET/MRI in radiotherapy for HNC

Diagnosis & Staging → Planning → Re-planning → Response assessment → Follow-up

1. GTV delineation
2. CTV selection
3. Early response assessment
4. Dose-painting on a BTV
5. Follow-up
6. Organ-sparing
7. Pitfalls

Head and neck cancer (HNC)

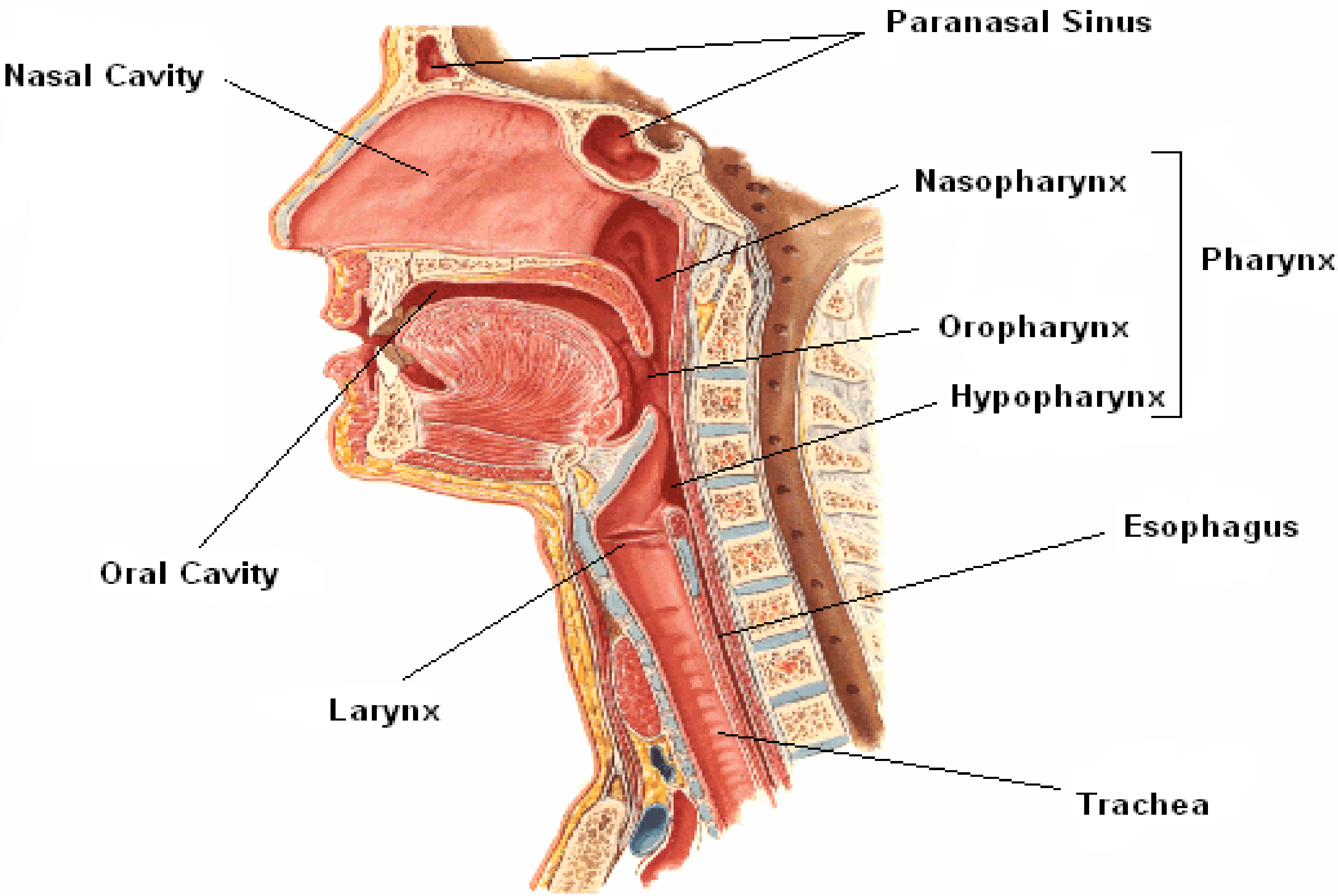

Current standard: concomitant CRT

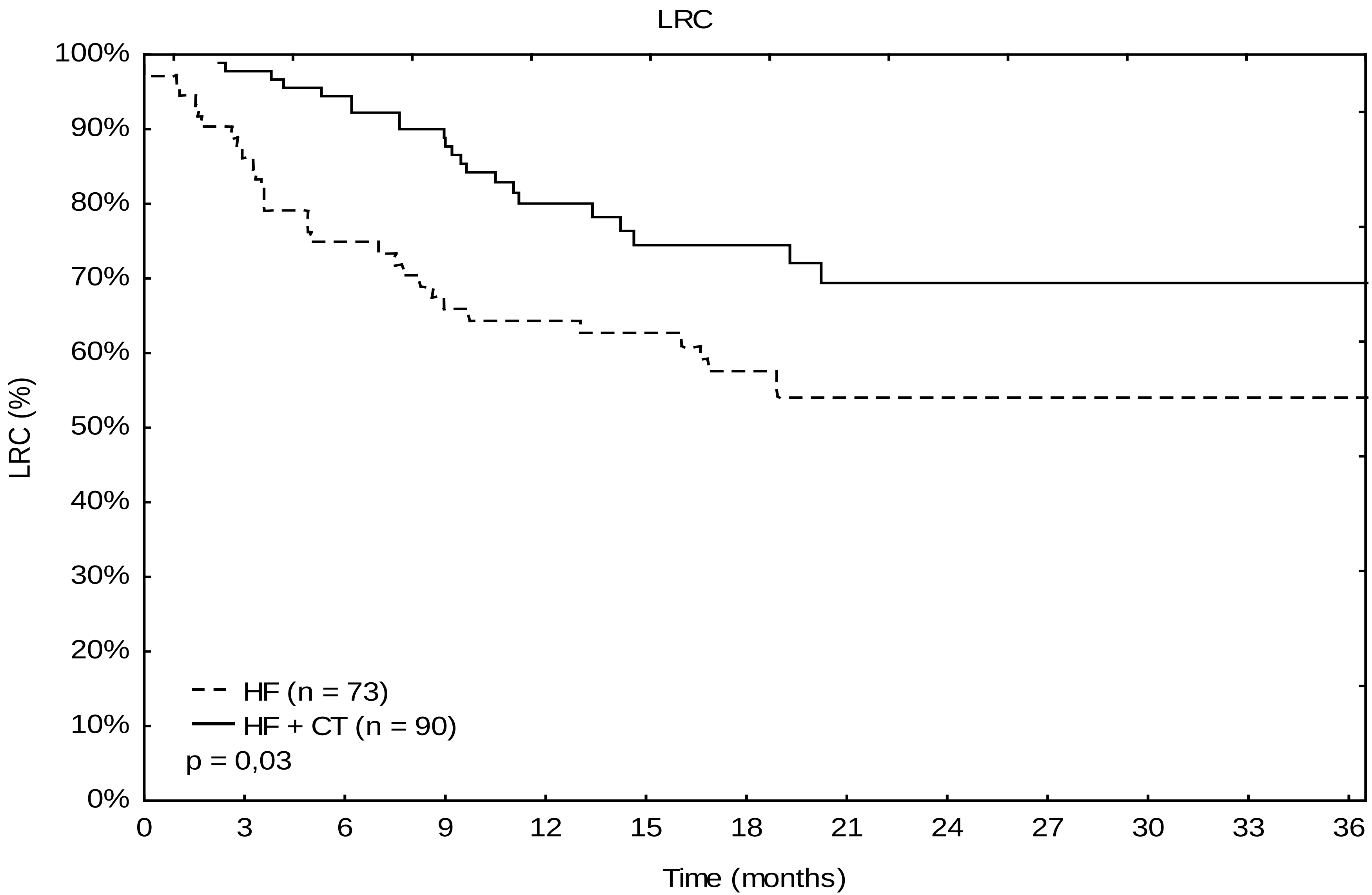

Nuyts S. et al. Int J Radiat Oncol Biol Phys 2009.

Towards a higher conformality

2D-RT → 1990 → 3D-CRT → 2000 → IMRT → 2010 → VMAT

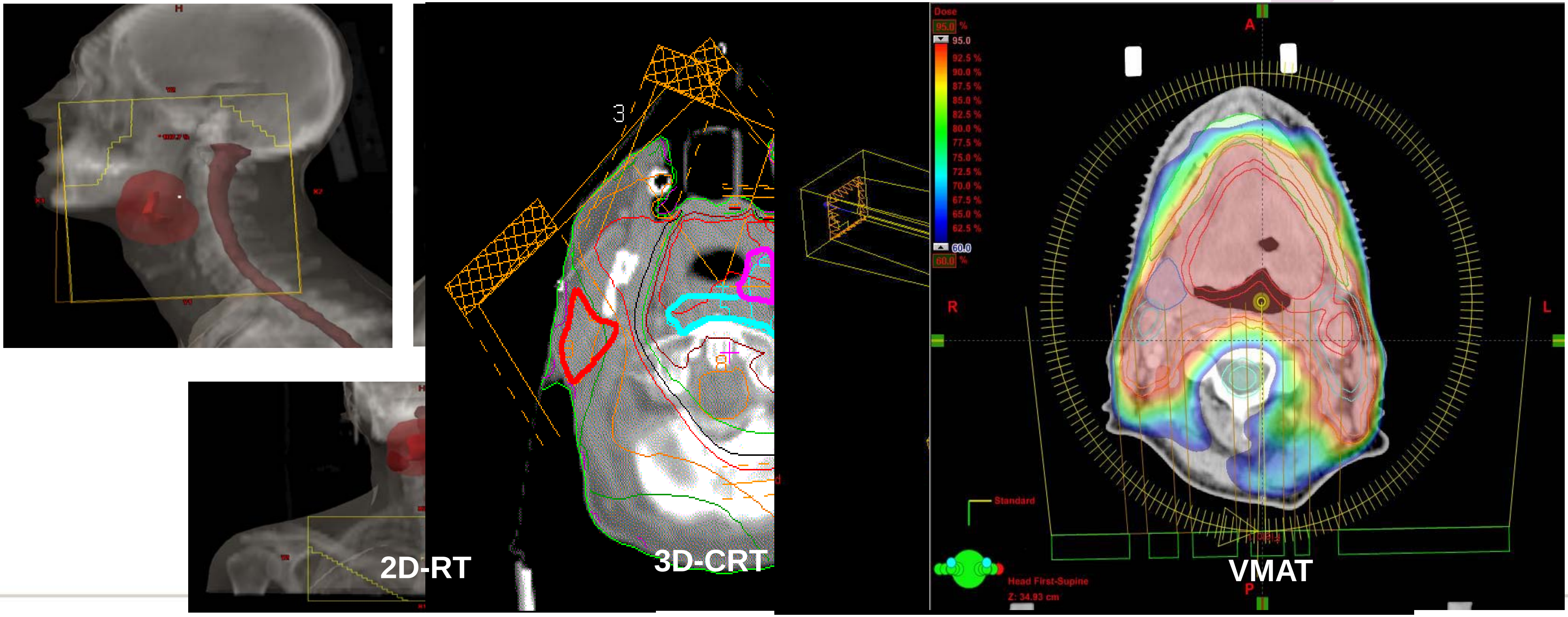

1. GTV delineation becomes critical

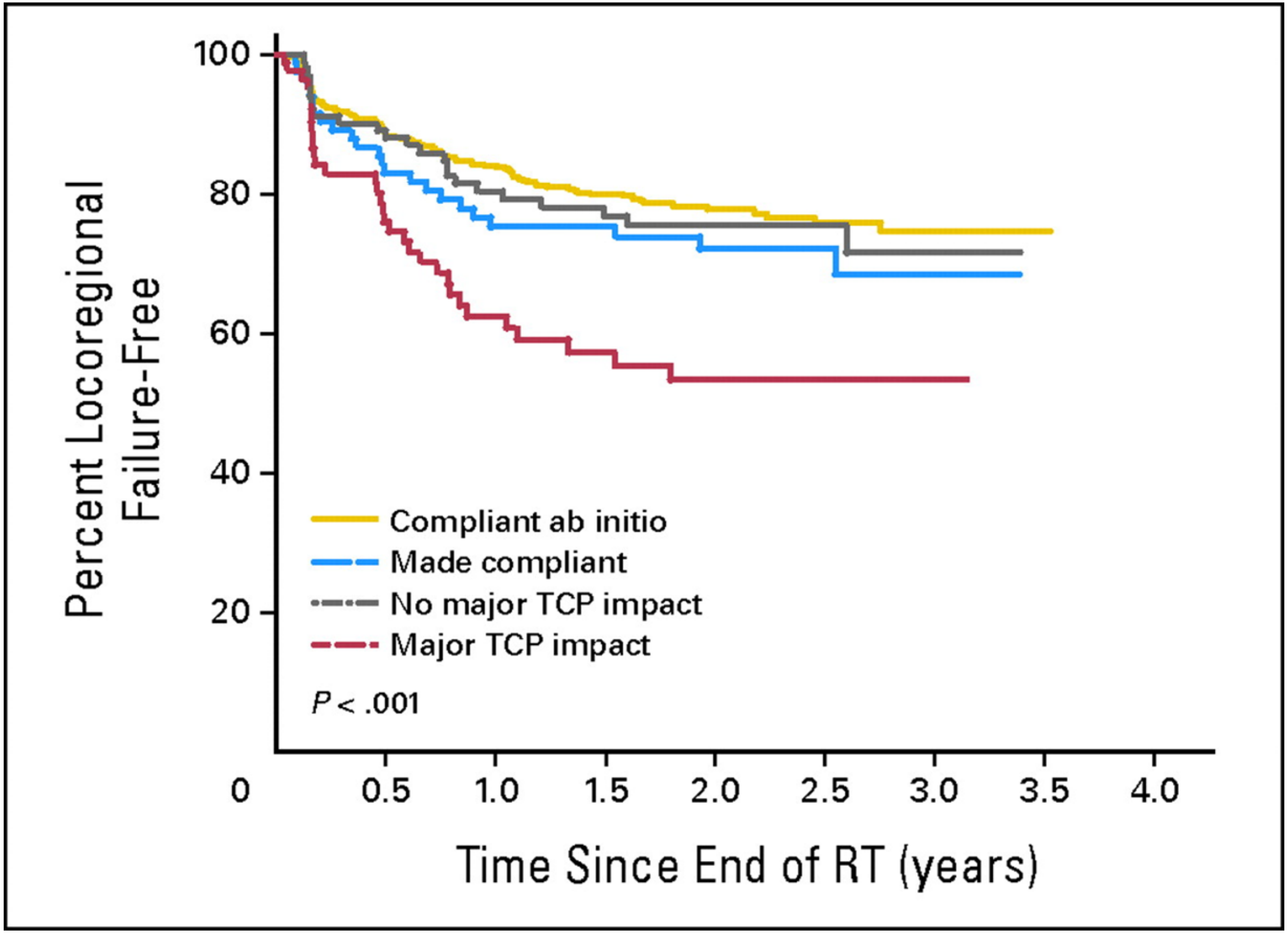

Peters L.J. et al. J Clin Oncol 2010.

Is imaging reliable?

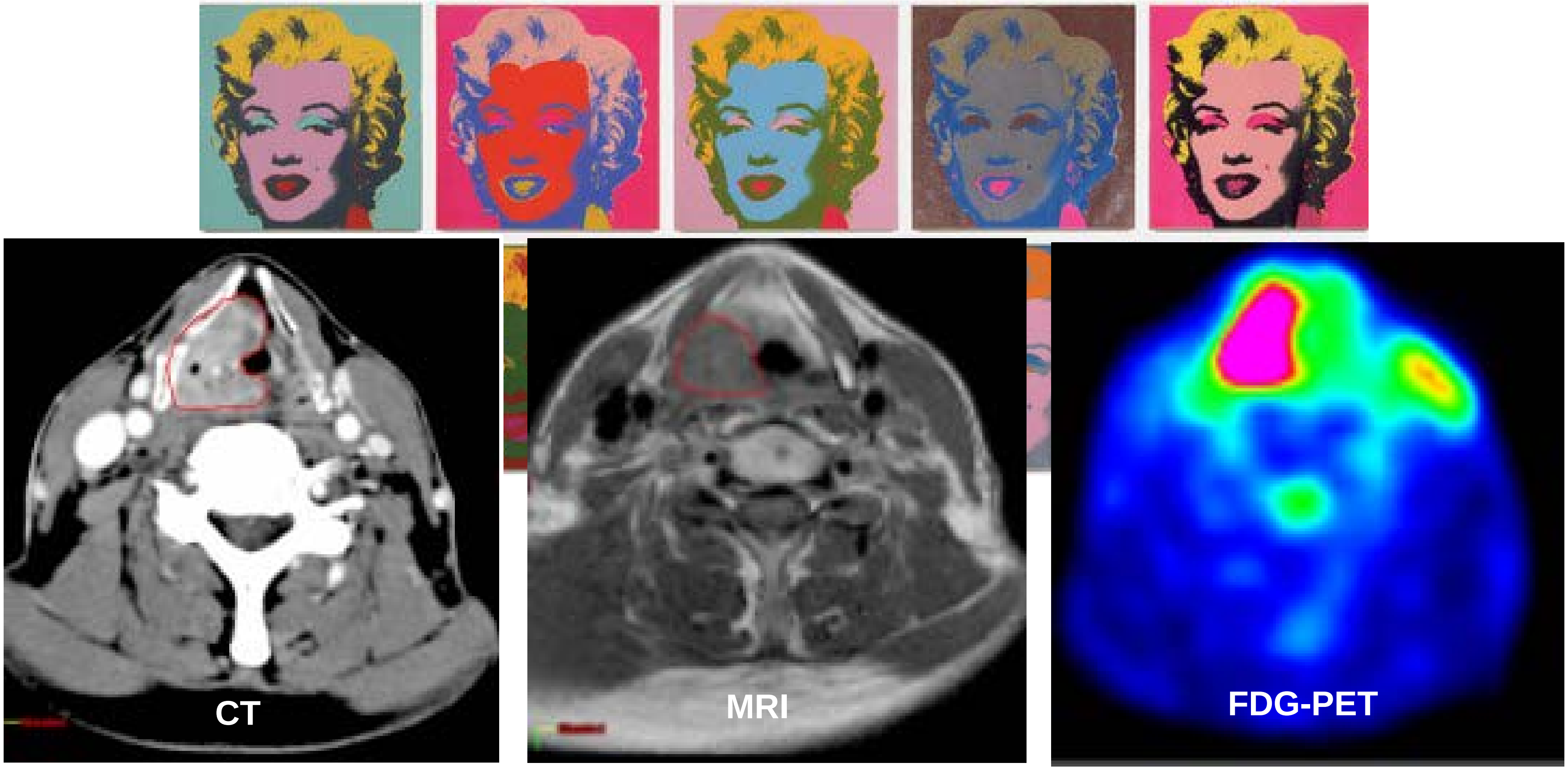

Imaging provides several different representations of 1 ground truth (i.e. pathology)…

Large intra/inter-observer variability on CT

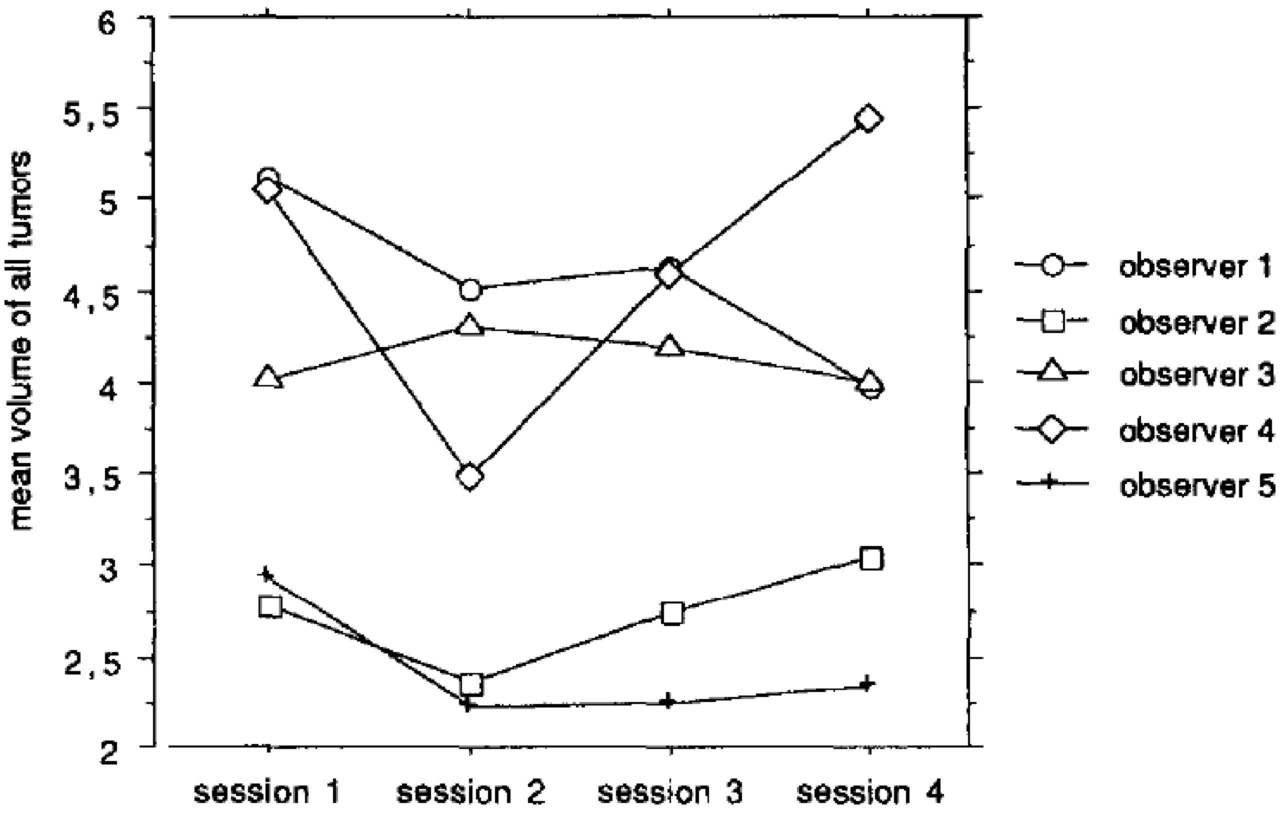

Fig. 1. Graph showing the interaction of the mean volume of all tumors (ml) and the four measurement sessions.

Hermans R. et al. Int J Radiat Oncol Biol Phys 1998.

CT vs. MRI: advantages

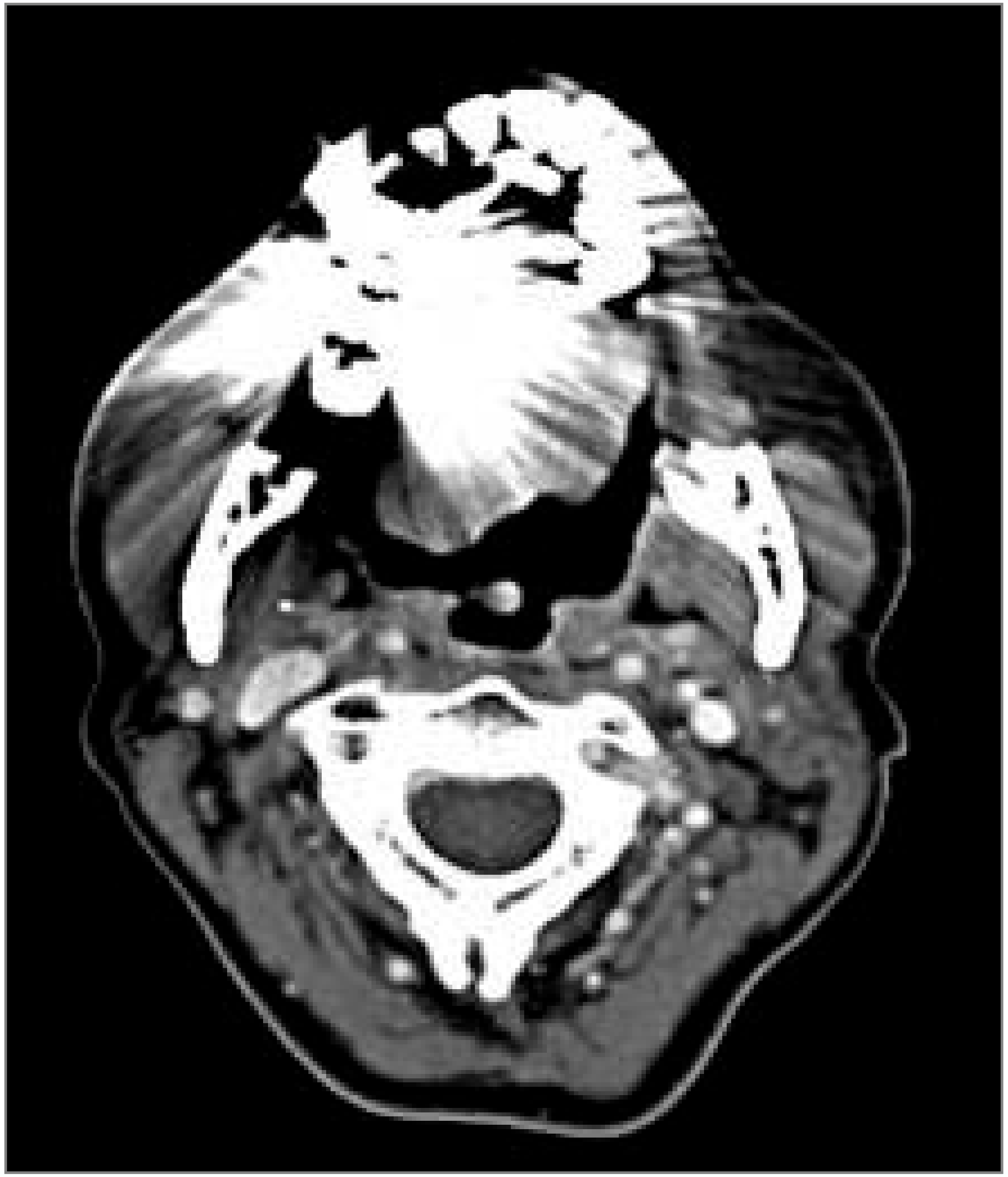

Images courtesy of Prof. R. Hermans.

CT vs. MRI: disadvantages



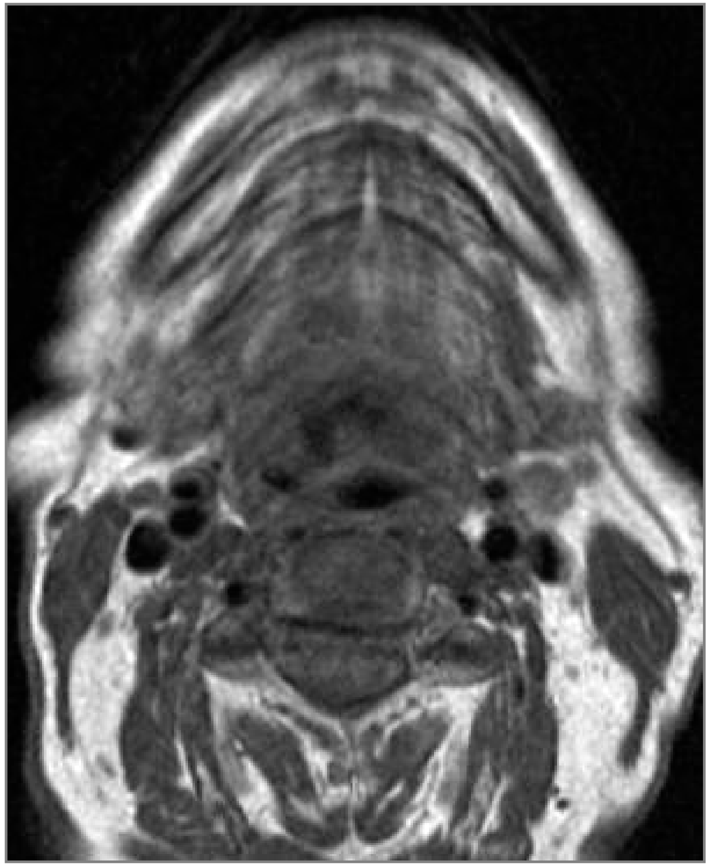

Images courtesy of Prof. R. Hermans.

MRI in treatment position

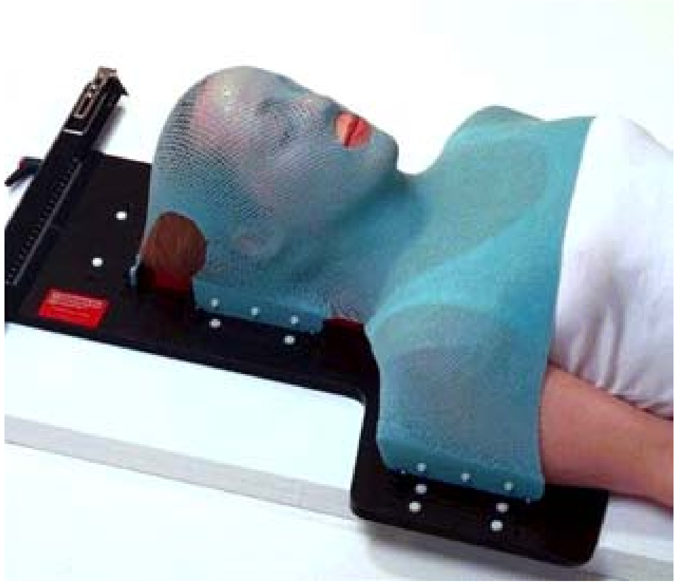

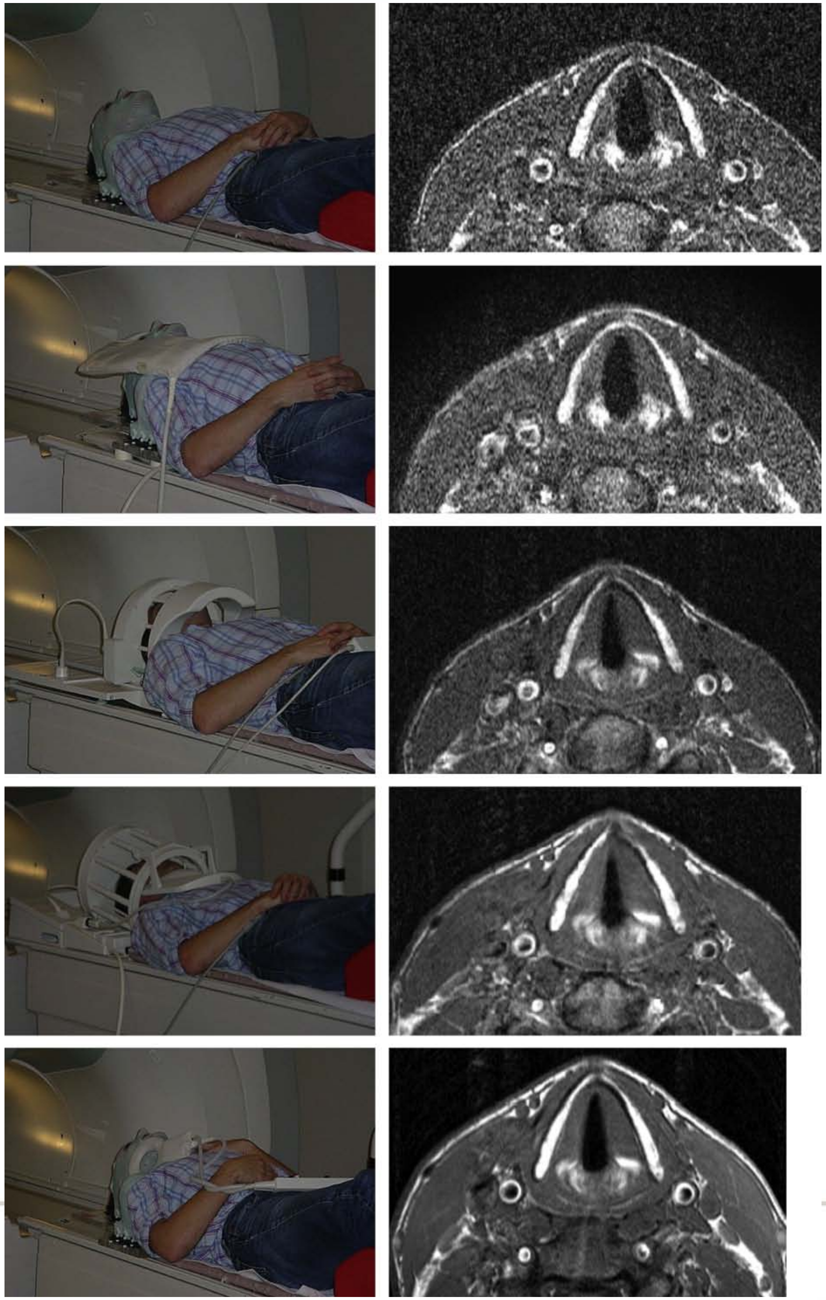

Verduijn G.M. et al. Int J Radiat Oncol Biol Phys 2009.
Webster G.J. et al. Br J Radiol 2009.
Ahmed M. et al. Radiother Oncol 2010.

MRI for nasopharyngeal cancer (NPC)

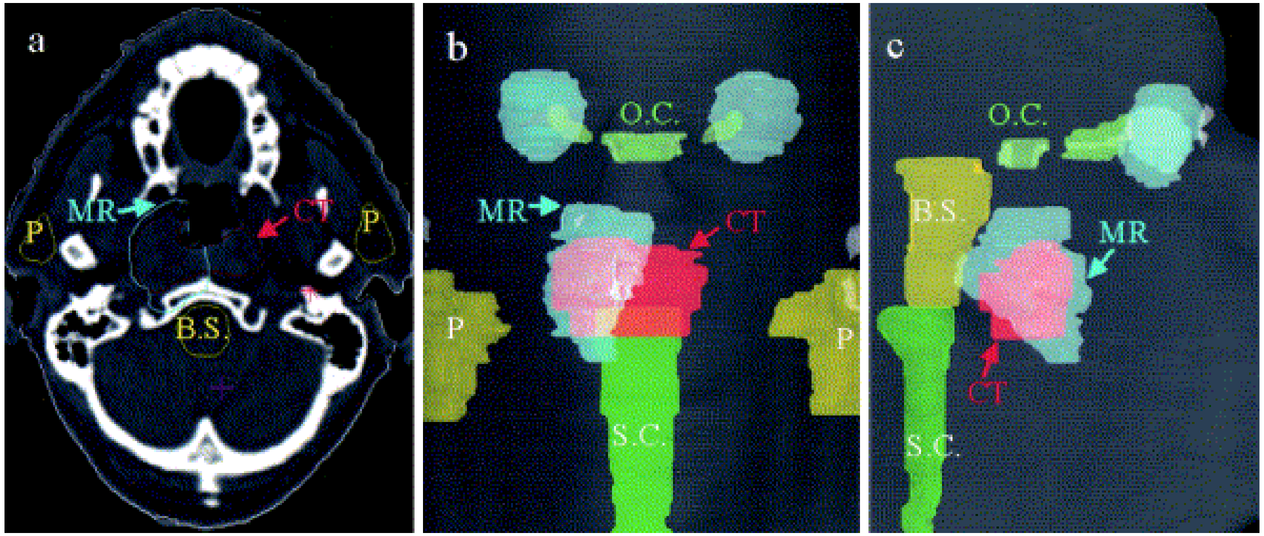

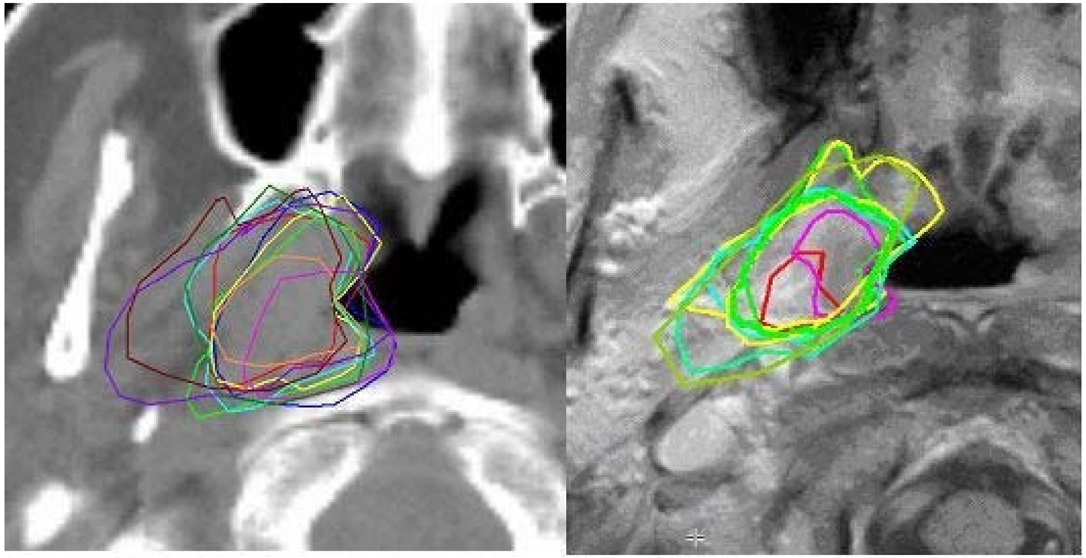

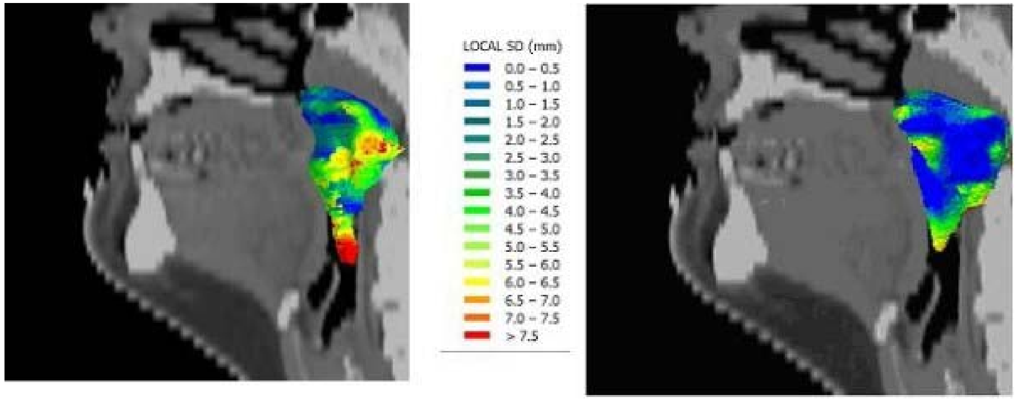

Emami B. et al. Int J Radiat Oncol Biol Phys 2003.
Rasch C. et al. Radiat Oncol 2010.

MRI for sinonasal cancer (SNC)

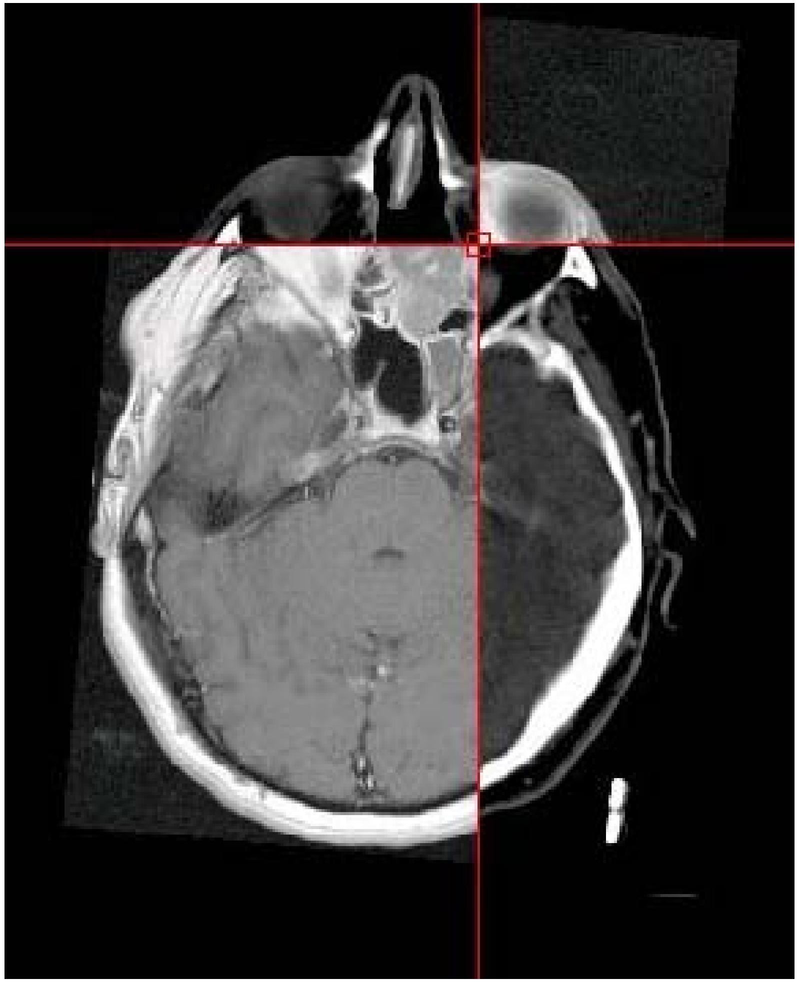

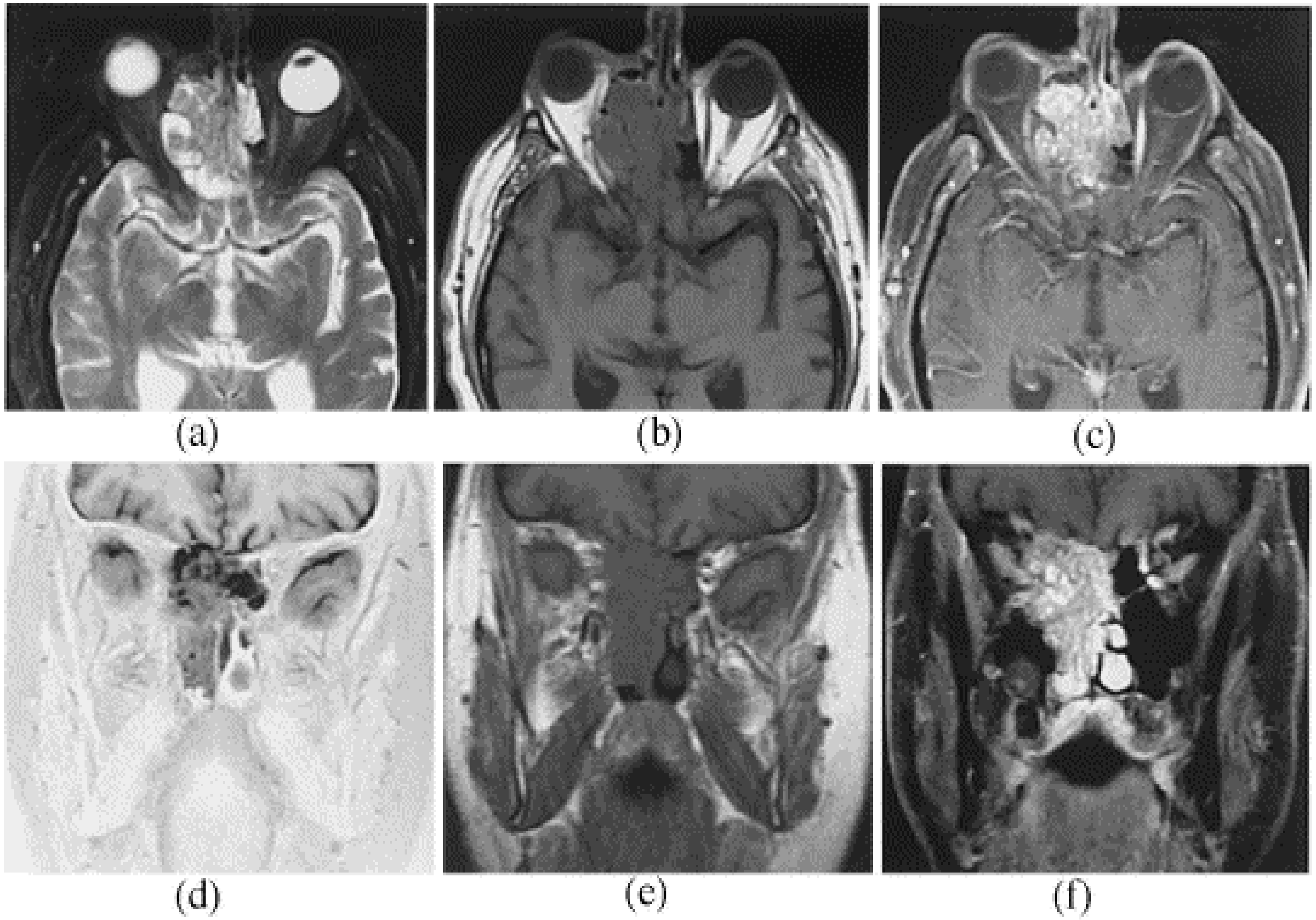

Sievers K. W. et al. Eur J Radiol 2000.
Dirix P. et al. Int J Radiat Oncol Biol Phys 2010.

MRI for all base of skull tumors!

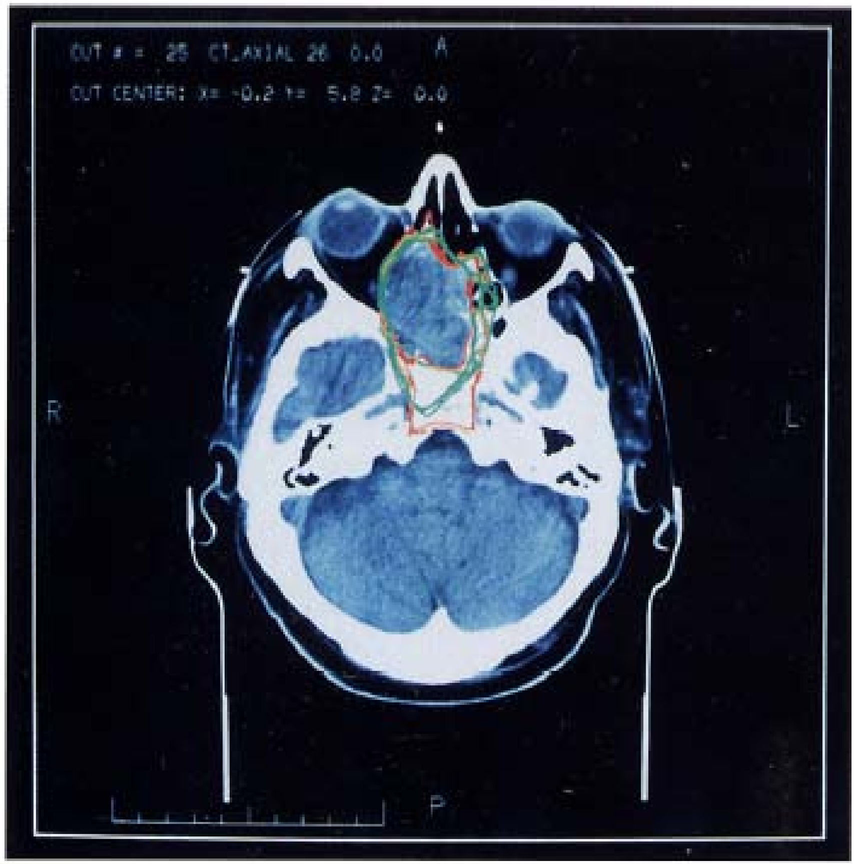

Fig. 2. The axial CT scan of patient 1 (ethmoid tumor). In red, the four contours as outlined on this scan by the four observers; in green, the contours outlined on axial MRI. Note the difference in the posterior border; on the CT either the clivus is entirely included in the Gross Tumor Volume or not at all.

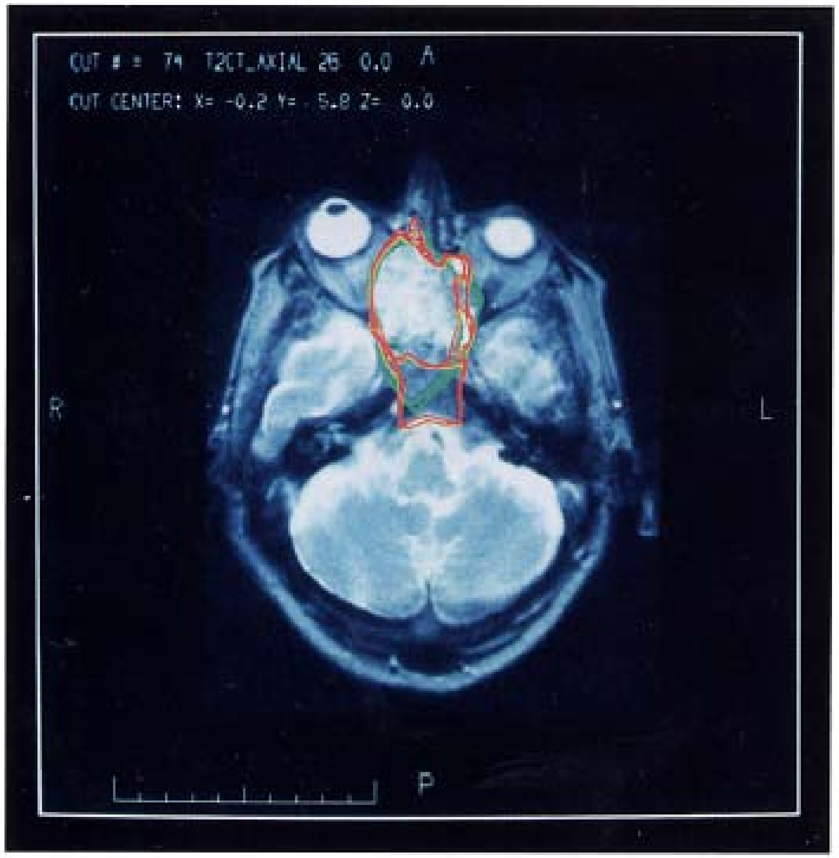

Fig. 3. The axial MRI scan of patient 1 (ethmoid tumor), resampled to fit the CT scan of Fig. 2. The contours outlined in the CT scan are red; the contours drawn on this axial MRI are green. On the CT scan, the observers outlined either the whole clivus as tumor or did not include the clivus at all in their Gross Tumor Volume. On the MRI, half of the clivus was included in the GTV.

Rasch C. et al. Int J Radiat Oncol Biol Phys 1997.

MRI for oropharyngeal cancer (OPC)

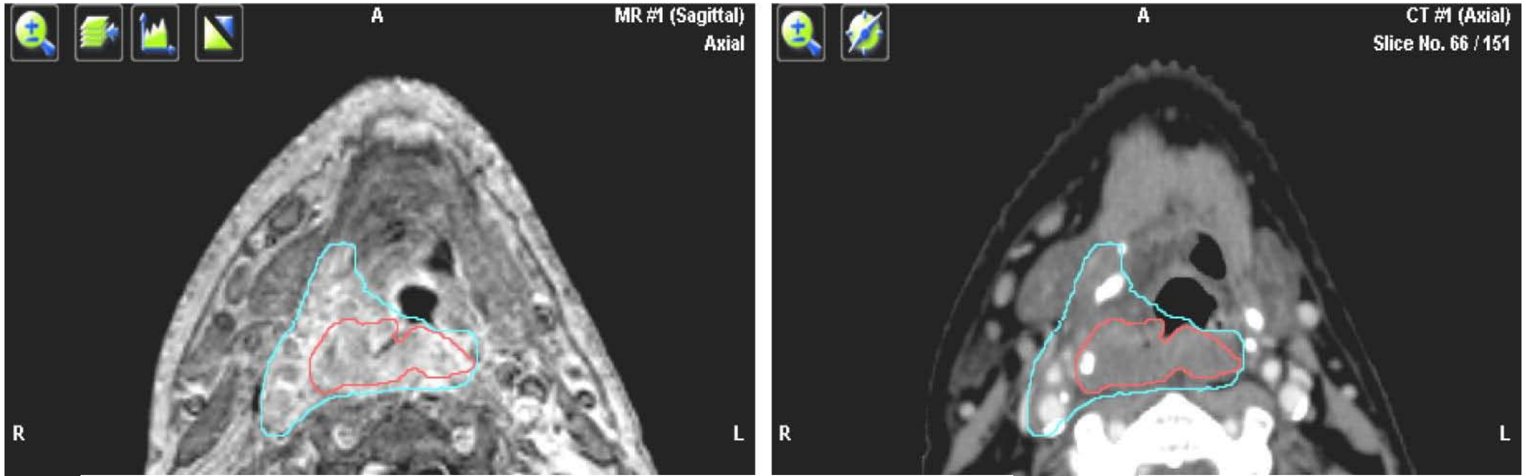

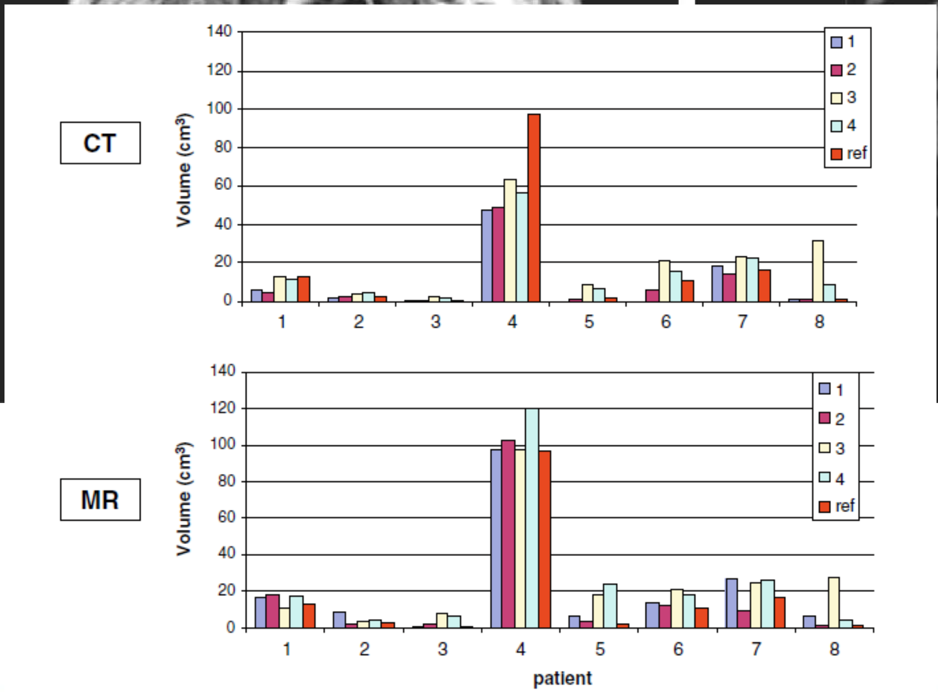

Table 1
MRI and CT volumes for GTV, CTV and PTV and OAR. A difference between CT GTV and MRI GTV was detected. This difference was confirmed to be significant following the assessment of volumes delineated by other clinicians ($p = 0.003$).

Mean volume units in cm^3 (SEM)	Mean volume on MR (cm^3) ± SE	Mean volume on CT (cm^3) ± SE	VOI	p value
GTV primary	22.2 (11.1)	9.5 (5.9)	0.34	0.05
GTV primary for all clinicians	24.6 (5.7)	14.4 (3.1)	N/A	0.003
GTV primary and lymph nodes	30.2	16.2	0.5	0.05
GTV primary and lymph nodes for all clinicians	30.8 (8)	18.5 (4)	N/A	0.01
GTV nodes only	5.8 (1.3)	5.8 (1.1)	N/A	0.9
CTV	301.2 (28.9)	309.5 (27.7)	0.9	0.23
PTV	448	452	0.9	0.6
Nodal CTV	53.8	53.9	0.6	1
Nodal PTV	131	125	0.8	0.5
Parotid volumes ($n = 16$)	26.1 ± 1.9	22.9 ± 2.2	0.7	0.01
Brainstem ($n = 8$)	24.8 ± 1.2	30.2 ± 2.2	0.8	0.002
Spinal cord ($n = 8$)	7.3 ± 0.5	11.9 ± 1.1	0.7	0.002

Ahmed M. et al. Radiother Oncol 2010.

MRI for hypopharyngo-laryngeal cancer (1)

Table 1. Signal-to-noise ratio (SNR) and contrast-to-noise ratio (CNR) values of MR images of the larynx for various receiver coils

Receiver coil	SNR (vocal cord)	CNR (cord/thyroid)
Integrated transmit/ receiver body coil	3.4	5.9
Four-channel phased-array coil	4.6	5.9
Quadrature head coil	6.2	12.3
Multi-element head-and-neck coil with neck coverage	15.4	27.2
Two-element flexible surface coil (11-cm diameter)	19.8	43.4
Two-element flexible surface coil at 3.0 T (11-cm diameter)*	16.9	42.7

* CNR and SNR for magnetic field strength of 3.0 T. All other values are determined for a field strength of 1.5 T.

Verduijn G. M. et al. Int J Radiat Oncol Biol Phys 2010.

MRI for hypopharyngo-laryngeal cancer (2)

Table 3
Inter-observer and inter-modality (i.e. CT-based against MRI-based GTVs for every single observer) variability for laryngeal/hypopharyngeal tumors ($n=10$)

	CT		MRI		Inter-modality variability*
	Volume (ml)	SEM	Volume (ml)	SEM	
Observer 1	18.1	5.8	19.3	4.9	***
Observer 2	20.7	6.1	21.5	5.7	$P=0.76$
Observer 3	20.9	5.8	20.0	4.7	$P=0.75$
Observer 4	19.3	5.9	22.1	5.6	$P=0.44$
Observer 5	21.9	6.1	21.8	5.3	$P=0.99$
Inter-observer variability**	$P=0.29$		$P=0.16$		

*P-values assessed by paired t-test or Wilcoxon rank test. **P-values assessed by ANOVA. ***Not assessed as CT-based and MR-based volume delineation was performed by two different radiologists (see Materials and Methods for explanation).

Table 4
Inter-observer and inter-modality (i.e. CT-based against MRI-based volume for every single observer) variability for parotid glands ($n=20$)

	CT		MR		Inter-modality variability*
	Volume (ml)	SD	Volume (ml)	SD	
Observer 1	34.8	9.6	30.6	12.3	$P<0.001$
Observer 2	29.4	8.7	27.9	9.5	$P=0.11$
Observer 3	26.8	9.3	20.4	8.0	$P<0.001$
Inter-observer variability**	$P<0.001$		$P<0.001$		

*P-values assessed by paired t-test or Wilcoxon rank test. **P-values assessed by ANOVA.

Geets X. et al. Radiother Oncol 2005.

PET/MRI for hypopharyngo-laryngeal cancer (3)

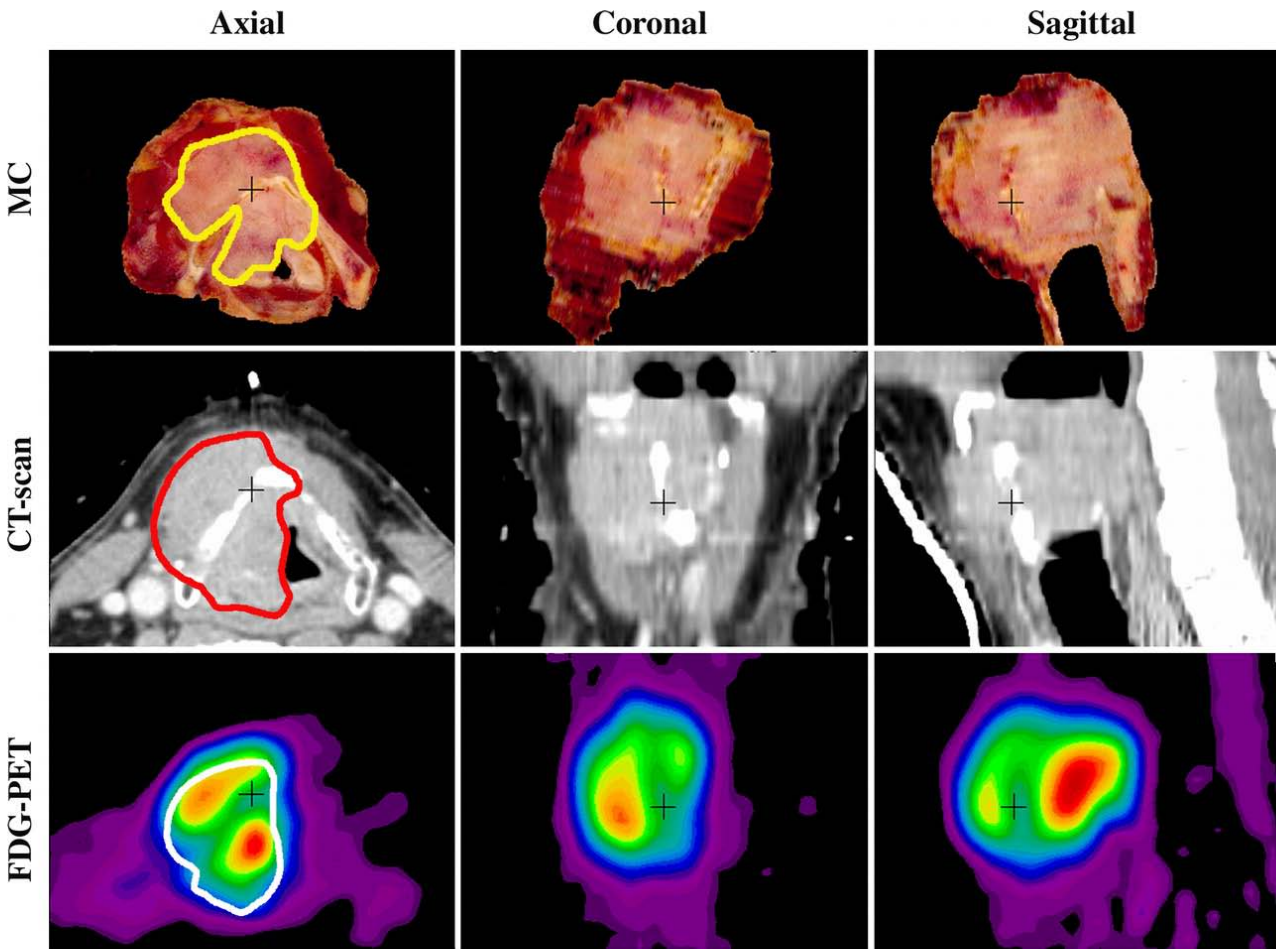

- In 9 laryngectomy patients: PET was most accurate modality.
- However, no modality depicted superficial tumor extension.

Daisne JF. et al. Radiology 2004.

Caution with FDG-PET for GTV delineation

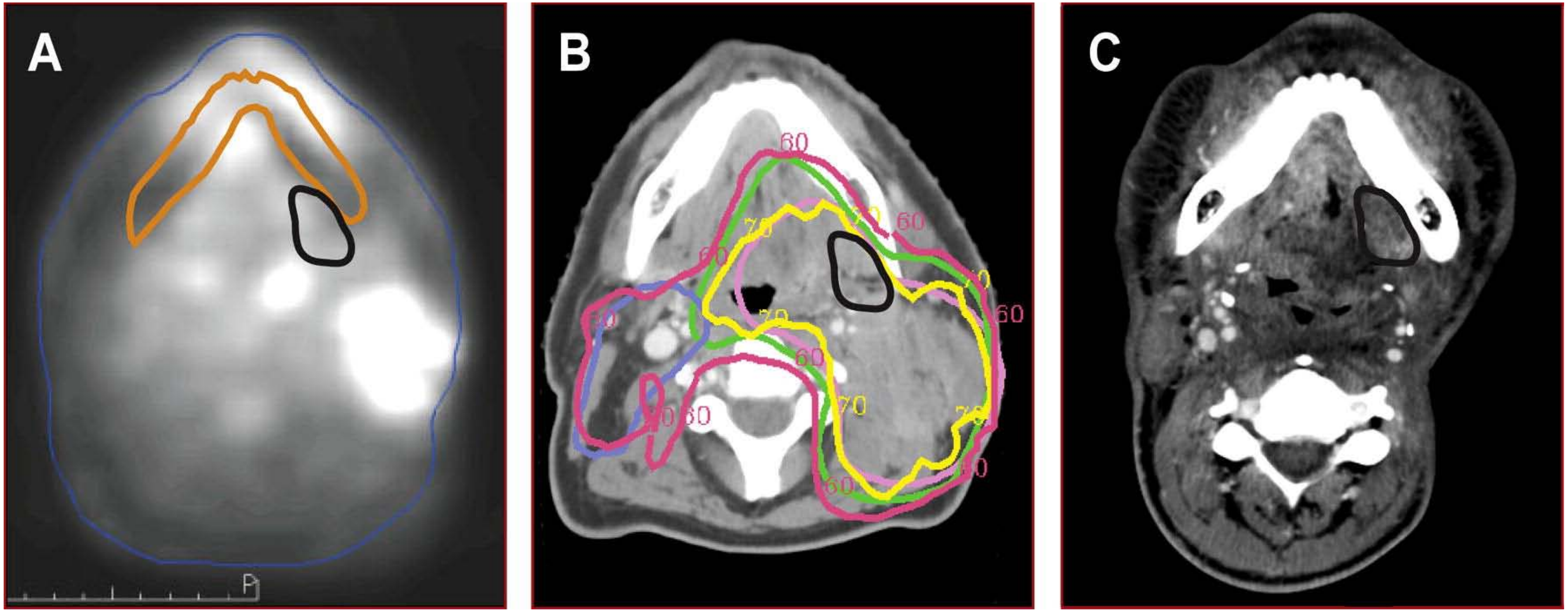

- Local in-field recurrences can occur outside the PET-GTV.
- FDG-PET is not suitable as an exclusive modality for GTV delineation.
- Inherently low spatial resolution functional imaging such as FDG-PET should not be used as a surrogate for anatomical imaging.
- Functional imaging indicates tumor biology (proliferation, hypoxia,…), rather than the exact tumor extension.

Soto D. et al. Radiother Oncol 2008.

ESTRO School

Belgian prospective trial on PET delineation

Table 3
Volume comparison.

Volumes	PET (mean cm^3)	CT (mean cm^3)	*p*
GTV			
All patients	28.8	40.4	<0.01
Larynx and hypopharynx	9.9	15.8	0.03
Oropharynx and oral cavity	32.6	45.5	<0.01
Lille	38.9	49.7	0.01
Brussels	22.0	34.3	<0.01
Namur	30.3	41.7	0.05
CTV T 70			
All patients	53.5	73.1	<0.01
Larynx and hypopharynx	22.4	28.9	0.05
Oropharynx and oral cavity	61.0	83.7	<0.01
Lille	68.9	94.9	0.02
Brussels	44.1	60.8	<0.01
Namur	63.8	84.6	0.03
CTV T 50			
All patients	109.1	118.8	0.01
Larynx and hypopharynx	55.7	45.4	0.05
Oropharynx and oral cavity	121.9	136.4	<0.0005
Lille	185.4	191.0	0.3
Brussels	77.6	89.0	0.03
Namur	114.8	124.0	0.2
PTV T 70			
All patients	94.6	124.7	<0.0001
Larynx and hypopharynx	50.1	64.2	0.046
Oropharynx and oral cavity	105.2	139.3	<0.01
Lille	105.5	137.5	0.02
Brussels	83.1	113.4	<0.01
Namur	116.0	143.9	0.03
PTV T 50			
All patients	189.7	202.6	0.02
Larynx and hypopharynx	113.7	100.4	0.1
Oropharynx and oral cavity	207.9	227.1	<0.01
Lille	286.2	286.4	0.7
Brussels	142.8	163.6	0.02
Namur	217.6	221.7	0.5

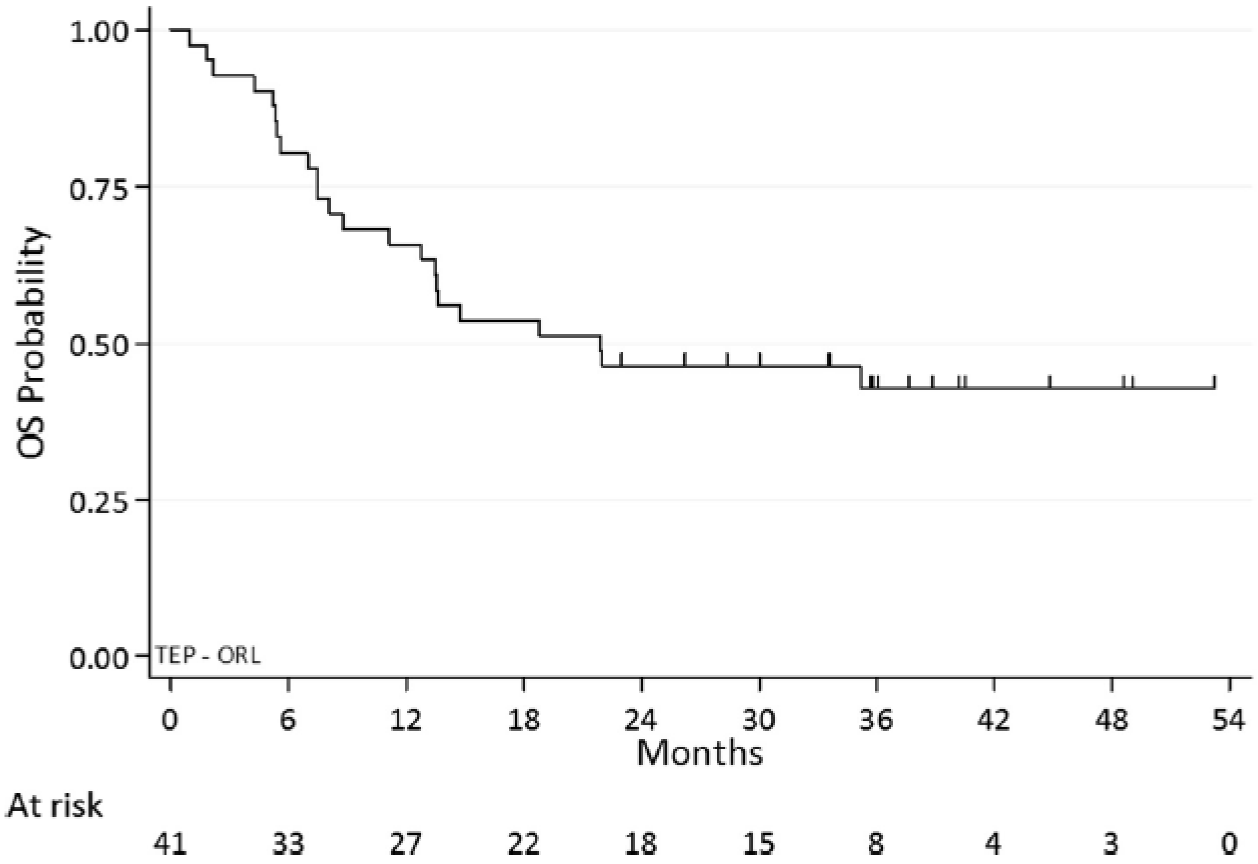

No marginal recurrences (in the CTV-CT but outside the CTV-PET) were observed.

Leclerc M. et al. Radiother Oncol 2015.

2. Highly conformal RT: LN staging is crucial

avoid geographic miss & regional recurrence

optimize organ-sparing e.g. salivary glands, swallowing structures

FDG-PET/CT

Comparison Between CT and FDG-PET for Nodal Staging

Site	Sensitivity		Specificity	
	CT (%)	FDG-PET (%)	CT (%)	FDG-PET (%)
Head and neck cancer	36-86	50-96	56-100	88-100

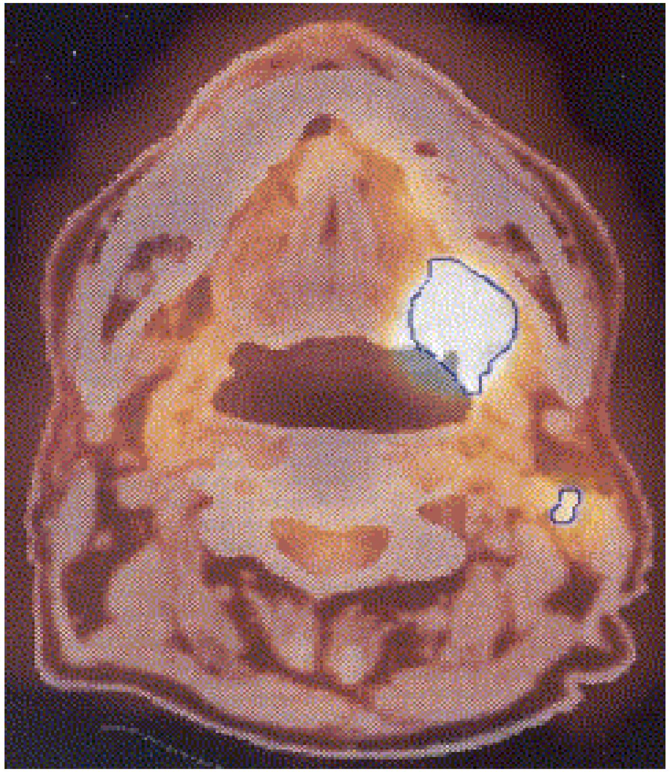

Sensitivity: FN because limited spatial resolution (0.5 cm)

Specificity: FP due to inflammation

Very promising, especially PET/CT, but not yet standard.

Grégoire V. et al. Semin Radiat Oncol 2006.

Materials and Methods

- **33 patients with advanced HNSCC planned for surgery with neck dissection:**

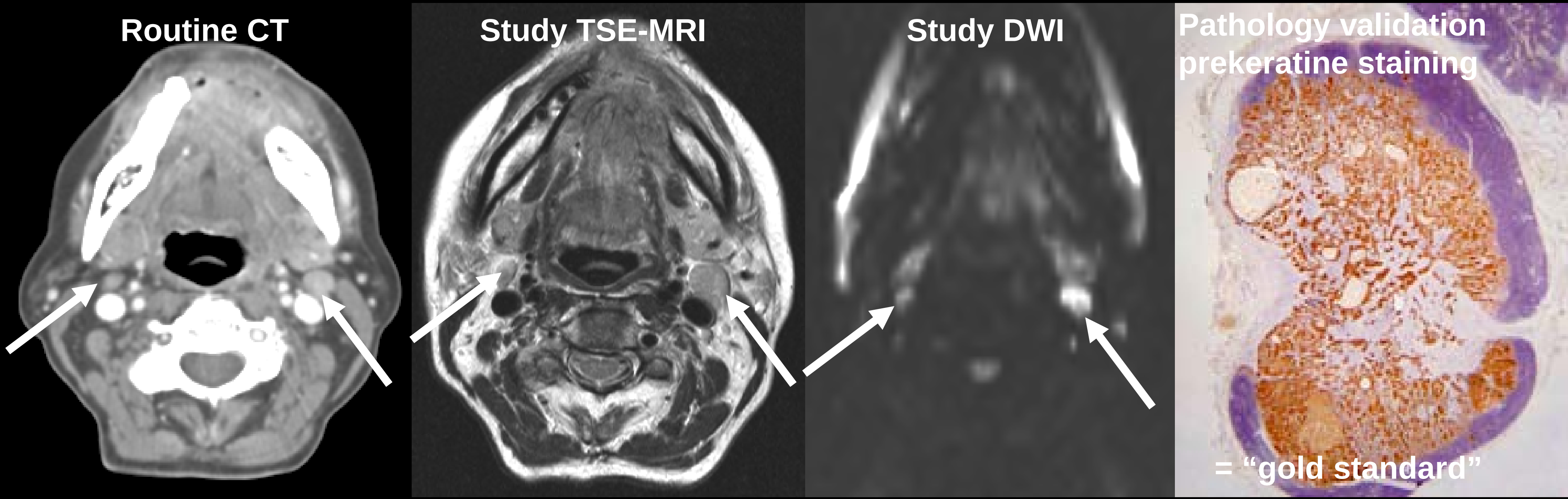

- **Radiotherapy planning study:**

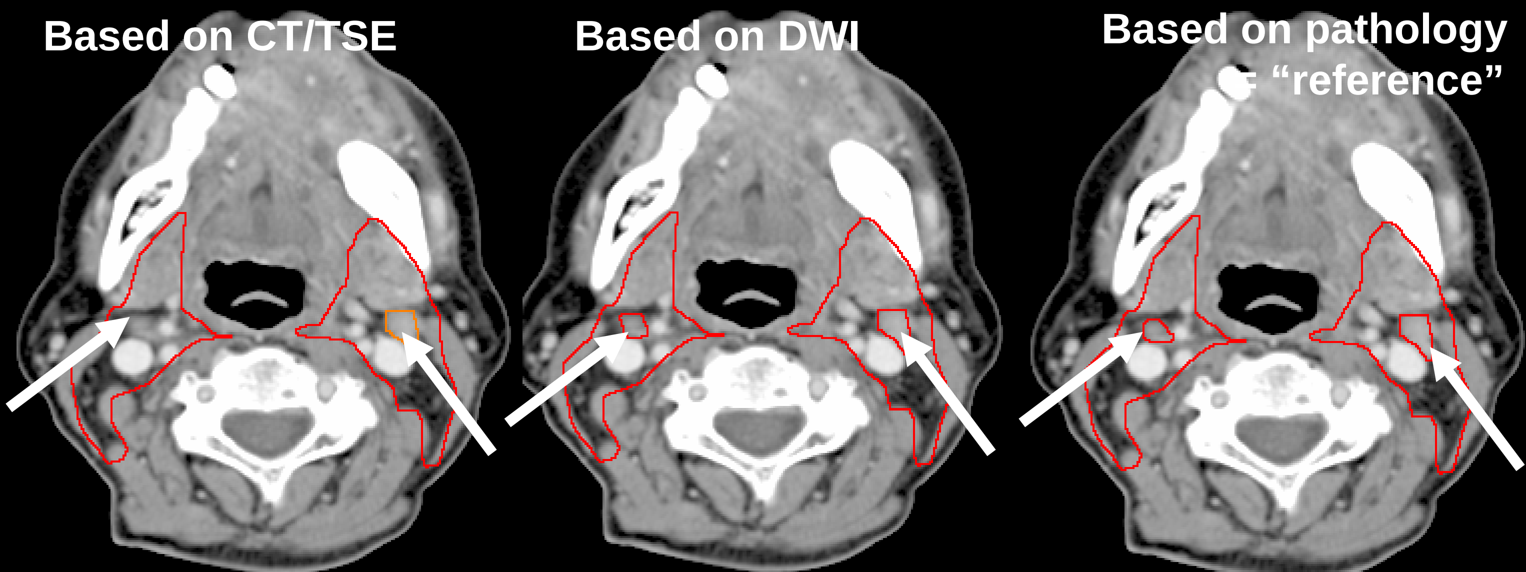

Results (1)

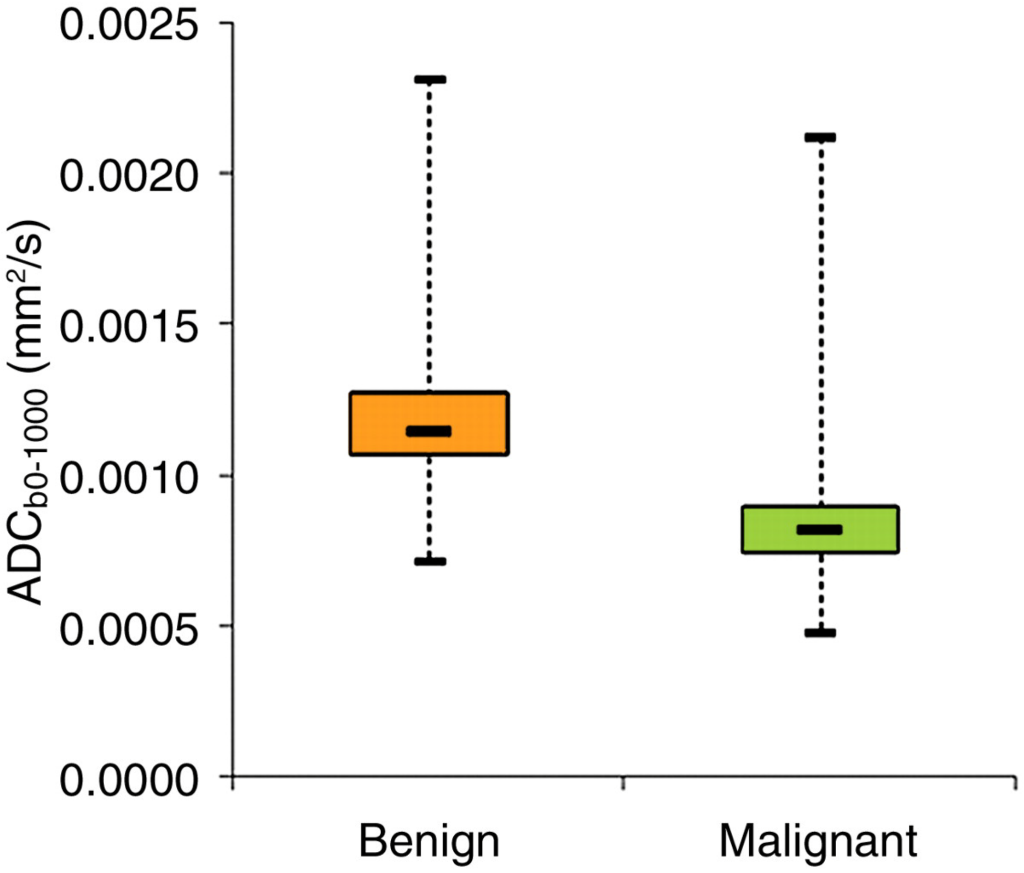

198 LN could be evaluated:

153 benign LN:
ADC = 0.00119 ± 0.00022 mm^2/sec

45 malignant LN:
ADC = 0.00085 ± 0.00027 mm^2/sec

$p < 0.0001$

Cut-off ADC value: 0.00094 mm^2/sec

Vandecaveye V. et al. Radiology 2009.

Results (2)

Nodal staging agreement between imaging results & pathology findings			
Modality	Kappa	95% CI	McNemar's test
CT/TSE	0.56	0.16 - 0.96	P = 0.019
DWI	0.97	0.84 - 1.00	

Sensitivity of 89% & specificity of 97% per LN.

DWI allows the radiation oncologist to very closely approach the true nodal target volume:

- **Dose-escalation (~ PPV of 91%)?**
- **Organ-sparing (~ NPV of 97%)?**

Preliminary results, require confirmation in a larger group…

Dirix P. et al. Int J Radiat Oncol Biol Phys 2010.

Clinical example of DWI for LN staging

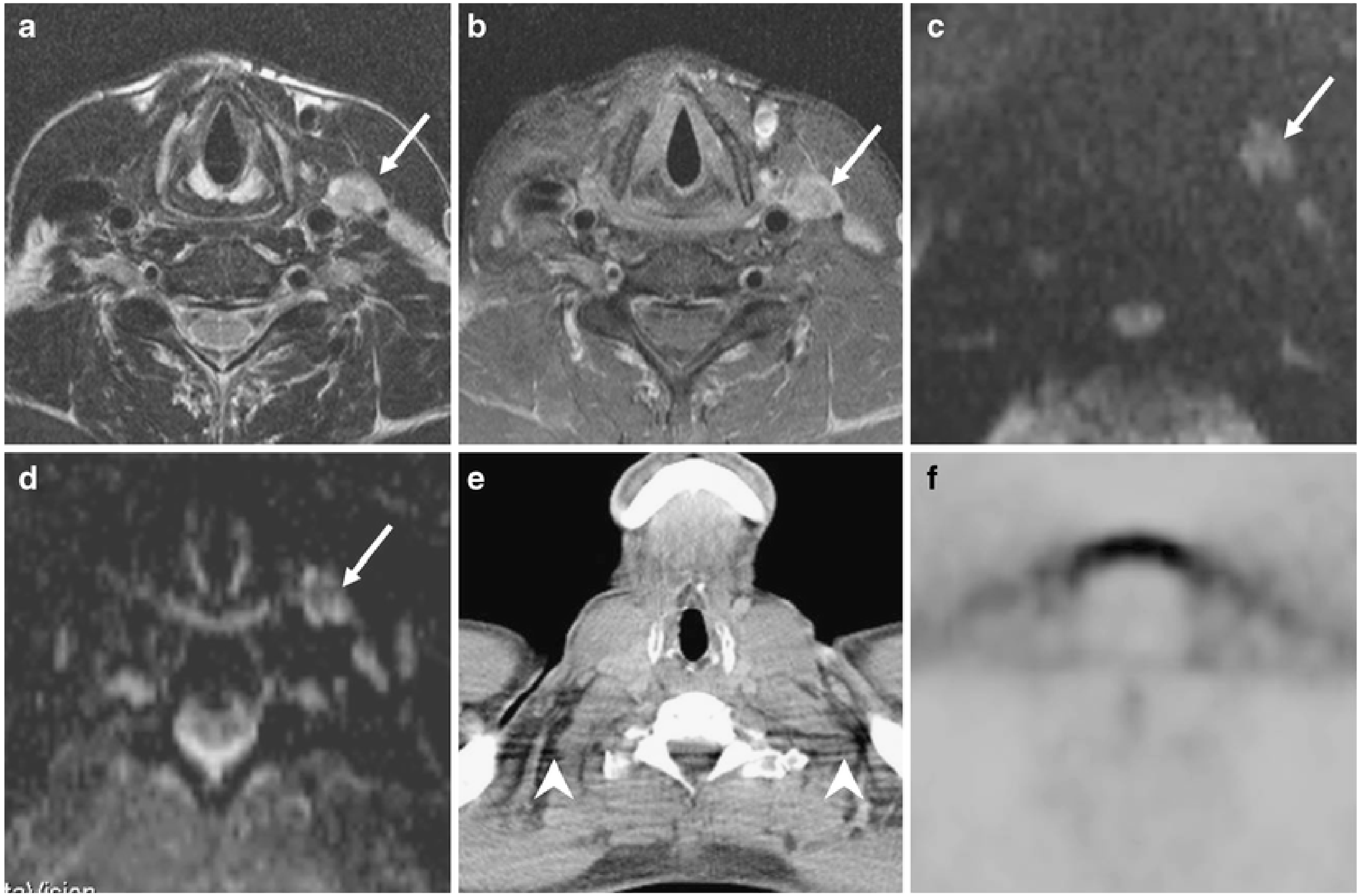

Images courtesy of Dr. V. Vandecaveye.

Similar results at Maastricht University

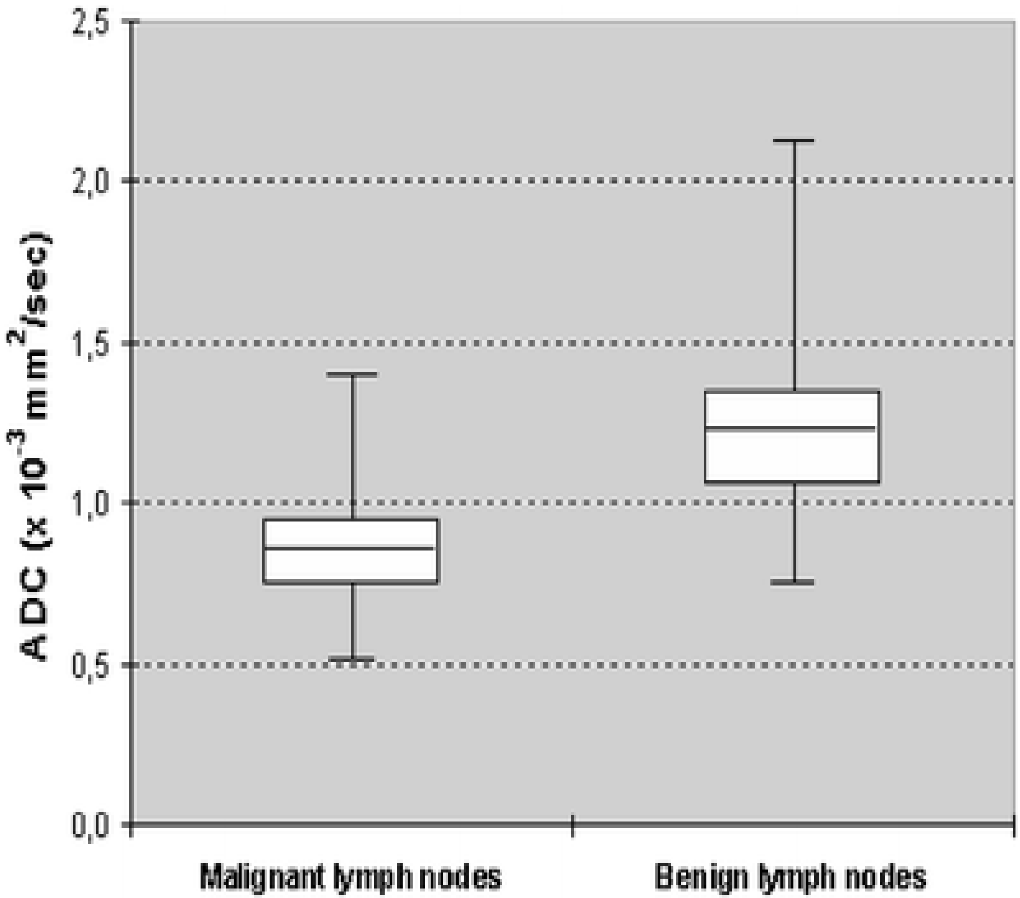

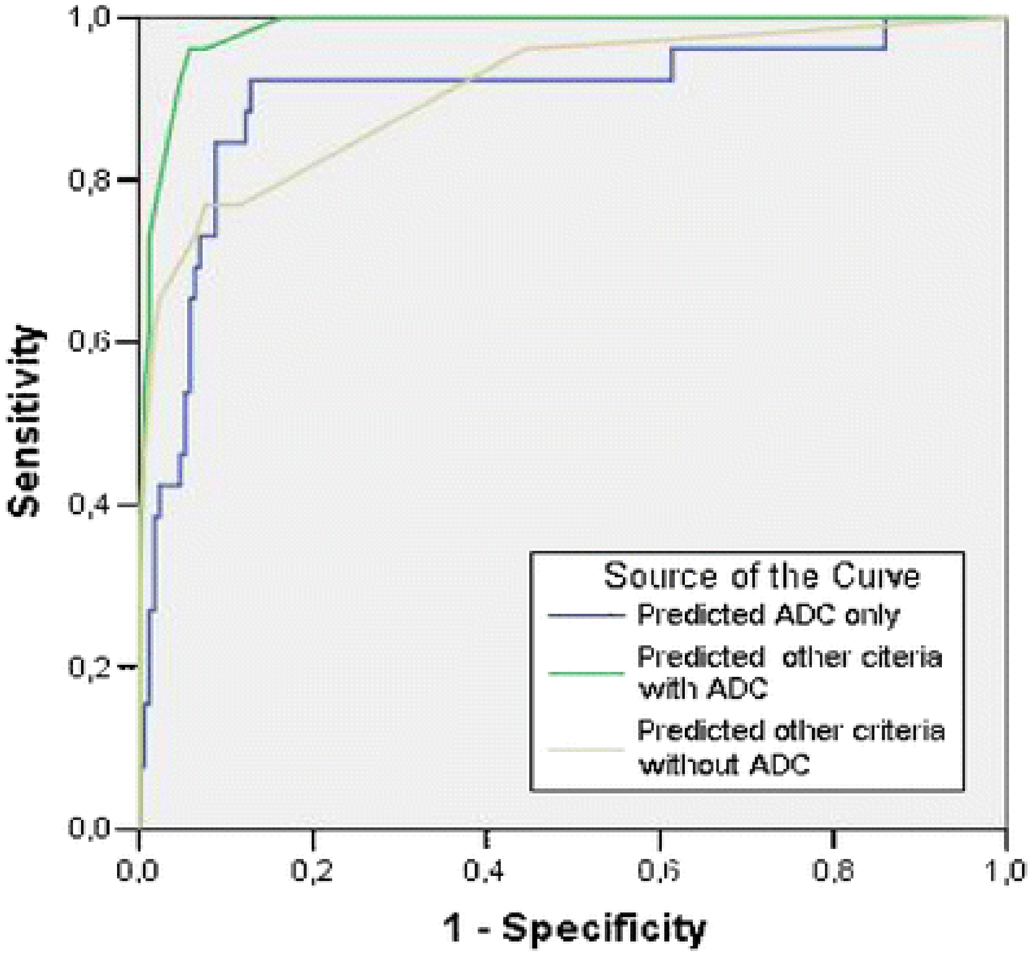

ADC cut-off: 0.0001 mm^2/sec: sensitivity 92% and specificity 84%

de Bondt R.B.J. et al. Neuroradiology 2009.

ESTRO School

All reported results for ADC-based nodal staging

Study	Lesion size (cm)	Mean ADC N+ (x 10^{-3} mm^2/sec)	Mean ADC N- (x 10^{-3} mm^2/sec)	p-value	Threshold (x 10^{-3} mm^2/sec)	Sens (%)	Spec (%)
Wang et al. *Radiology 2001*	> 1.0	1.13 ± 0.43	1.56 ± 0.51	0.002	1.22	84	91
Sumi et al. *J Neuroradiol 2003*	> 1.0	0.41 ± 0.11	0.30 ± 0.06	< 0.01	0.4	52	97
Abdel Razek et al. *Eur Radiol 2006*	0.9 – 1.5	1.09 ± 0.11	1.64 ± 0.16	< 0.04	1.38	98	88
Sumi et al. *AJR 2006*	> 1.0	1.17 ± 0.45	0.63 ± 0.10	< 0.001	0.74	86	94
Vandecaveye et al. *Radiology 2009*	0.4 – 1.5	0.85 ± 0.27	1.19 ± 0.22	< 0.0001	0.94	84	94
de Bondt et al. *Neuroradiology 2009*	0.5 – 3.0	0.85 ± 0.19	1.2 ± 0.24	< 0.05	1.0	92	84
Holzapfel et al. *Eur J Radiol 2009*	> 1.0	0.78 ± 0.09	1.24 ± 0.16	< 0.05	1.02	100	87
Perrone et al. *Eur J Radiol 2011*	NA	0.85	1.45	< 0.01	1.03	100	93

Lambrecht M. et al. Expert Rev Anticancer Ther 2010.

Towards dose de-escalation on the elective neck?

200 patients included

Arm A	Arm B
(NID2Gy 40 Gy)	(NID2Gy 50 Gy)
96 patiens *	97 patients *

Study Arm

Control Arm

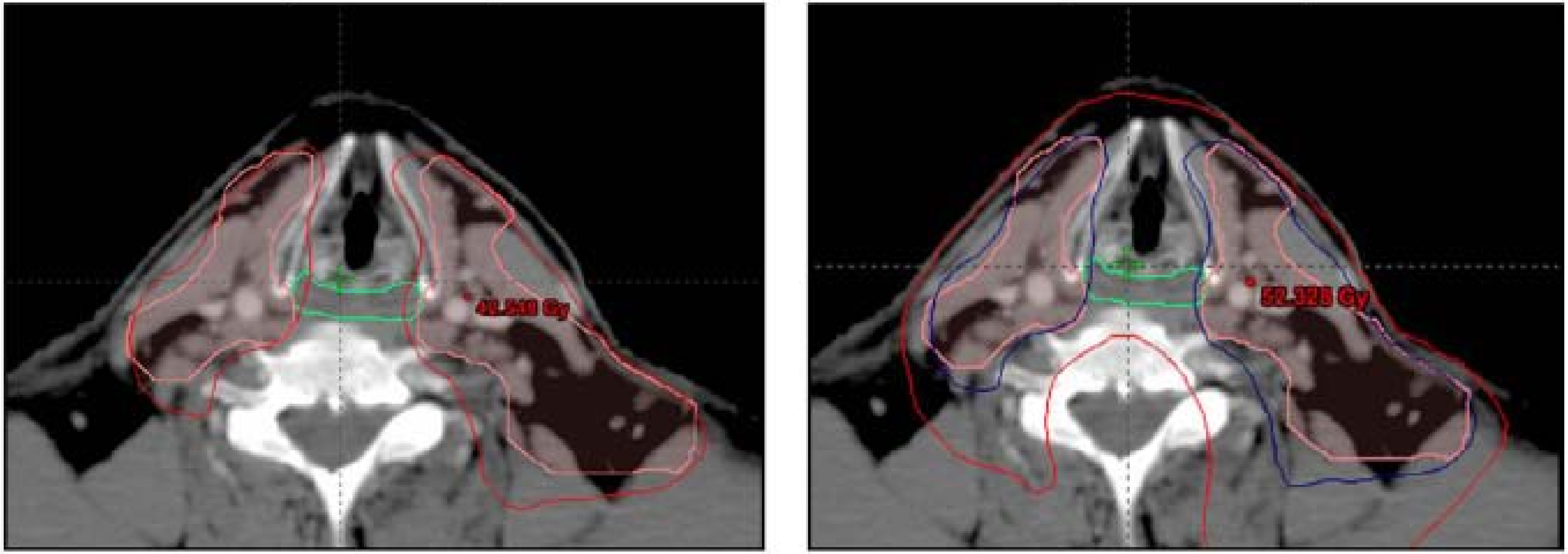

Microscopic tumor burden is probably low in cN0 neck on FDG-PET & DWI, and could be sterilized with lower doses than used to be necessary when only CT was used.

Nuyts S. et al. Radiother Oncol 2013.

Significantly less acute dysphagia

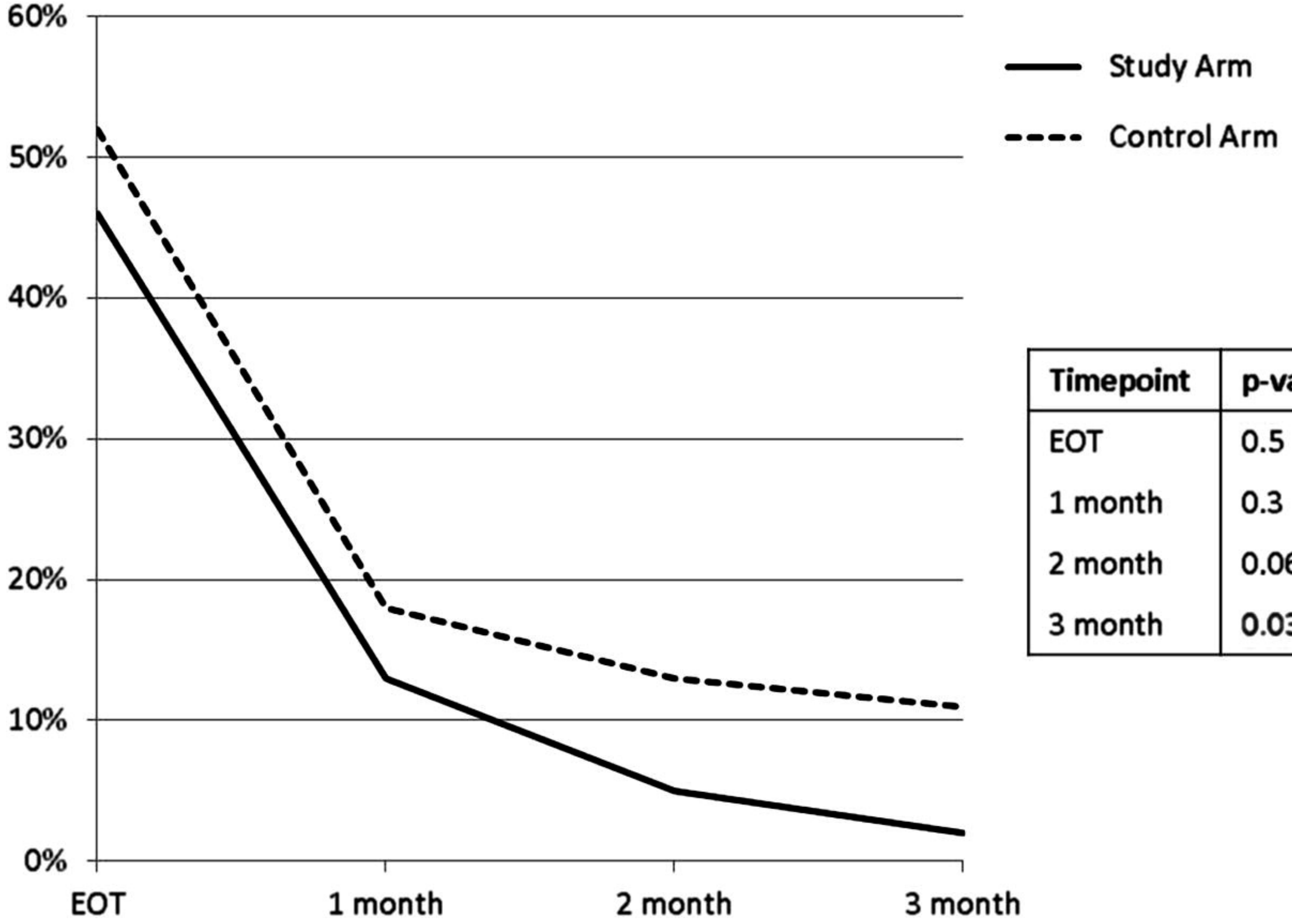

Timepoint	p-value
EOT	0.5
1 month	0.3
2 month	0.06
3 month	0.03

Nuyts S. et al. Radiother Oncol 2013.

Regional recurrences

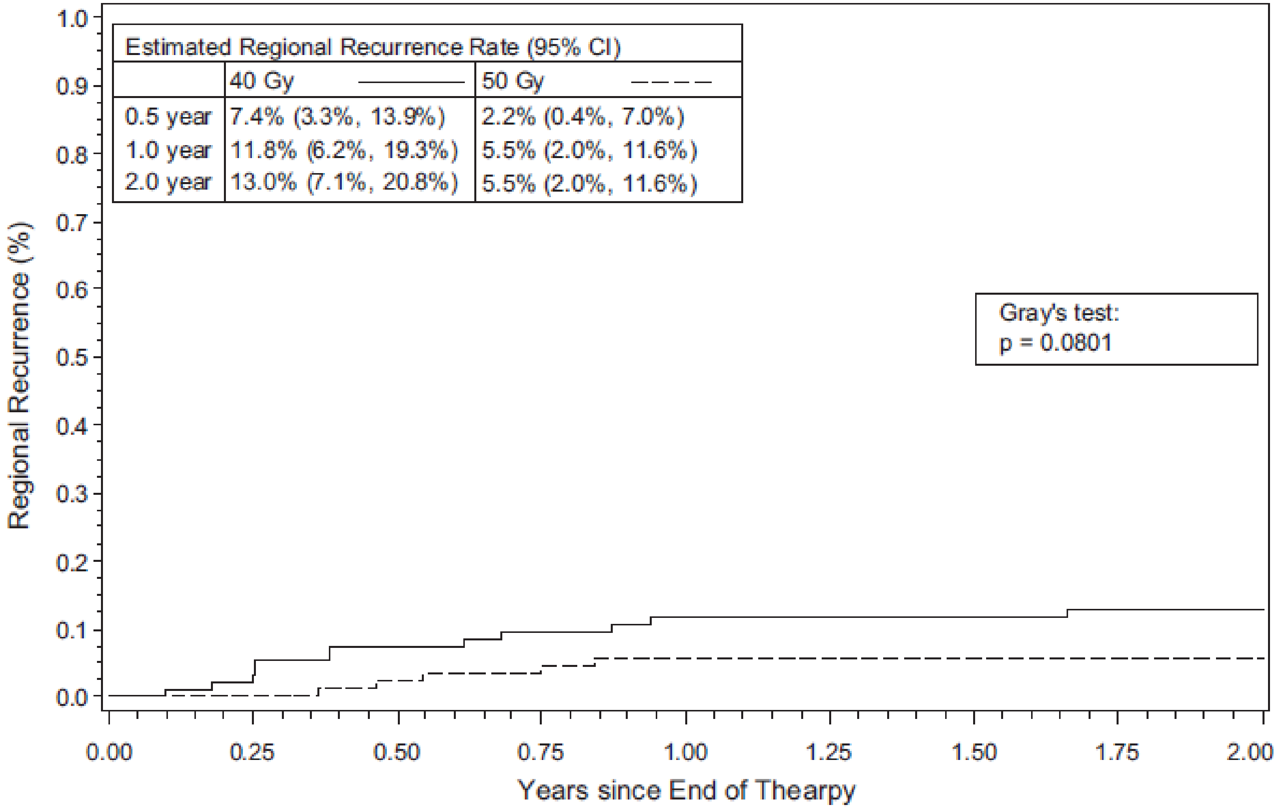

Number at risk

40 Gy	95	89	82	73	67	65	61	58
50 Gy	94	90	85	79	73	70	67	64

Table 5
Site of the regional recurrences.

Recurrence	40 Gy ARM	50 Gy ARM
GTV lymph node	6	5
PTV lymph node	1	0
Outside planning volume	2	0
PTV elective	2	1

Nevens D. et al. Radiother Oncol 2016.

FDG-PET at 8 weeks after RT

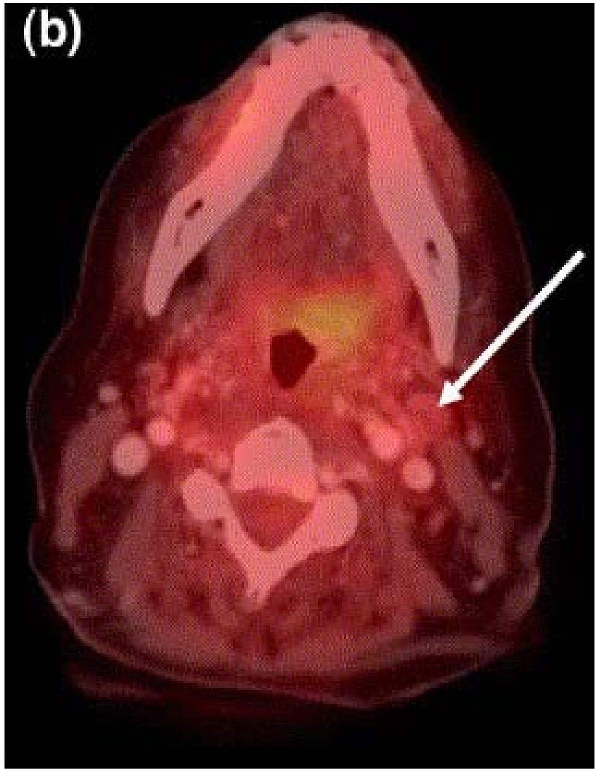

	FDG-PET/CT	CT
Sensitivity (%)	76.9	92.3
Specificity (%)*	93.3	46.7
Positive predictive value (%)†	90.9	60
Negative predictive value (%)	82.4	87.5
Accuracy (%)	85.7	67.9

Promising, applicability mainly limited by the number of false negatives.

Andrade R. et al. Int J Radiat Oncol Biol Phys 2006.

DWI as a response biomarker (1)

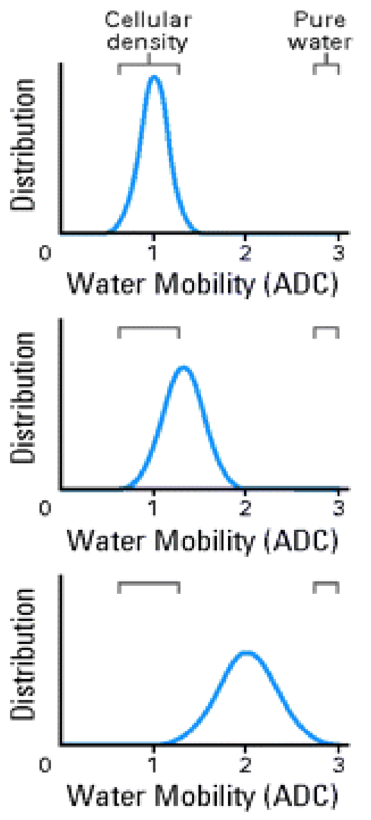

Hamstra D.A. et al. J Clin Oncol 2007.

DWI as a response biomarker (2)

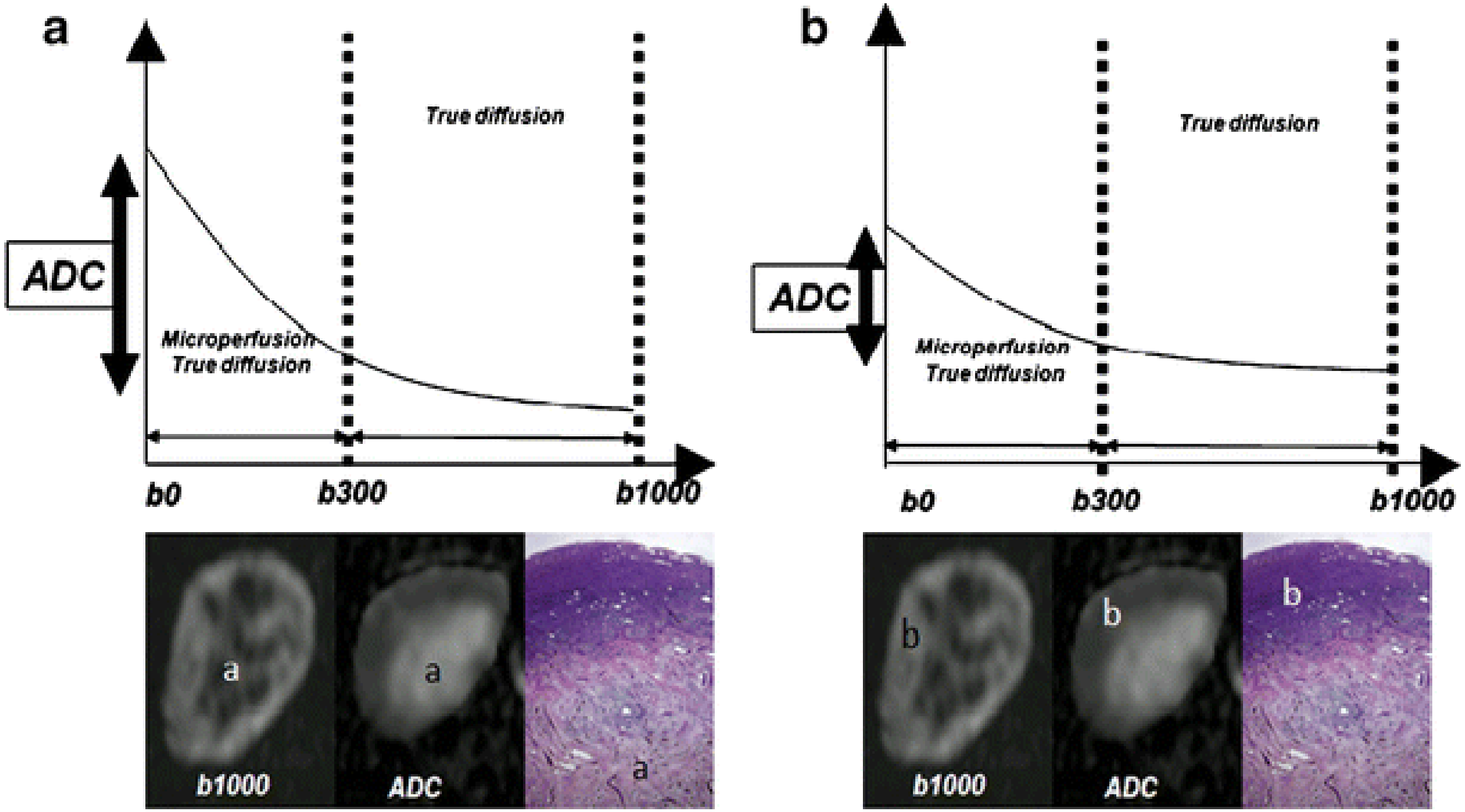

Vandecaveye V. et al. Neuroradiology 2010.

Materials and Methods

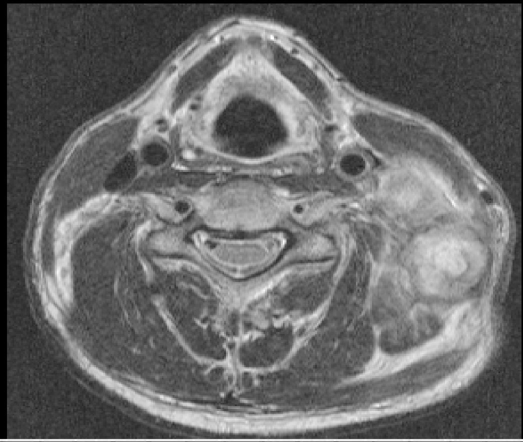

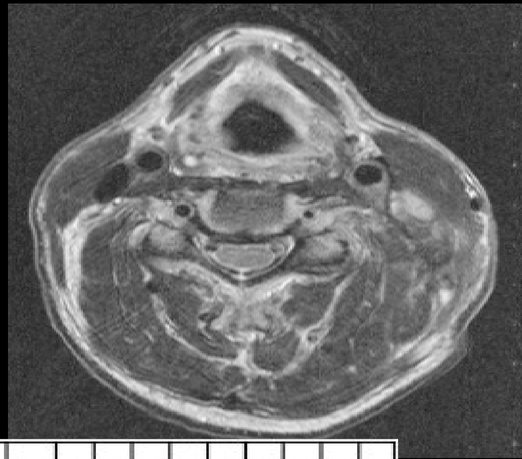

DAY	1	2	3	4	5	8	9	10	11	12	15	16	17	18	19	22	23	24	25	26	29	30	31	32	33	36	37	38	39	40
DOSE	2	2	2	2	2	2	2	2	2	2	2	2	2	2	2	2	2	2	2	2	1.6	1.6	1.6	1.6	1.6	1.6	1.6	1.6	1.6	1.6
																					1.6	1.6	1.6	1.6	1.6	1.6	1.6	1.6	1.6	1.6
TOTAL					10					20					30					40		46.4			56					72

Cx (cisplatinum 100 mg/m^2) on day 1 and 22.

= primary field

= boost

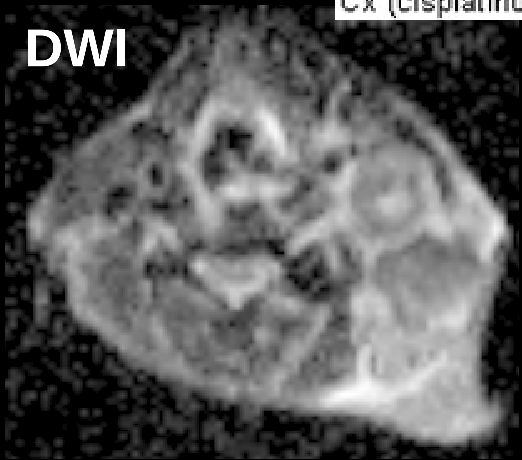

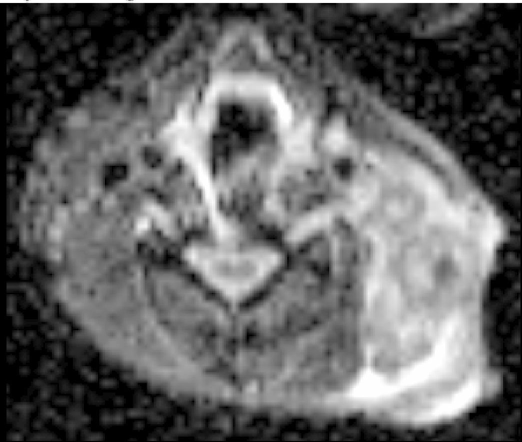

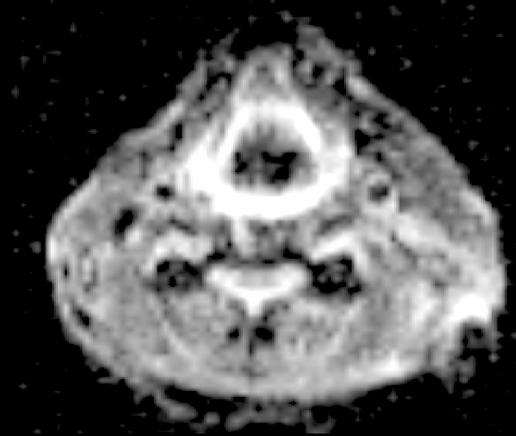

before RT **days 10 and 24** **3 weeks after RT**

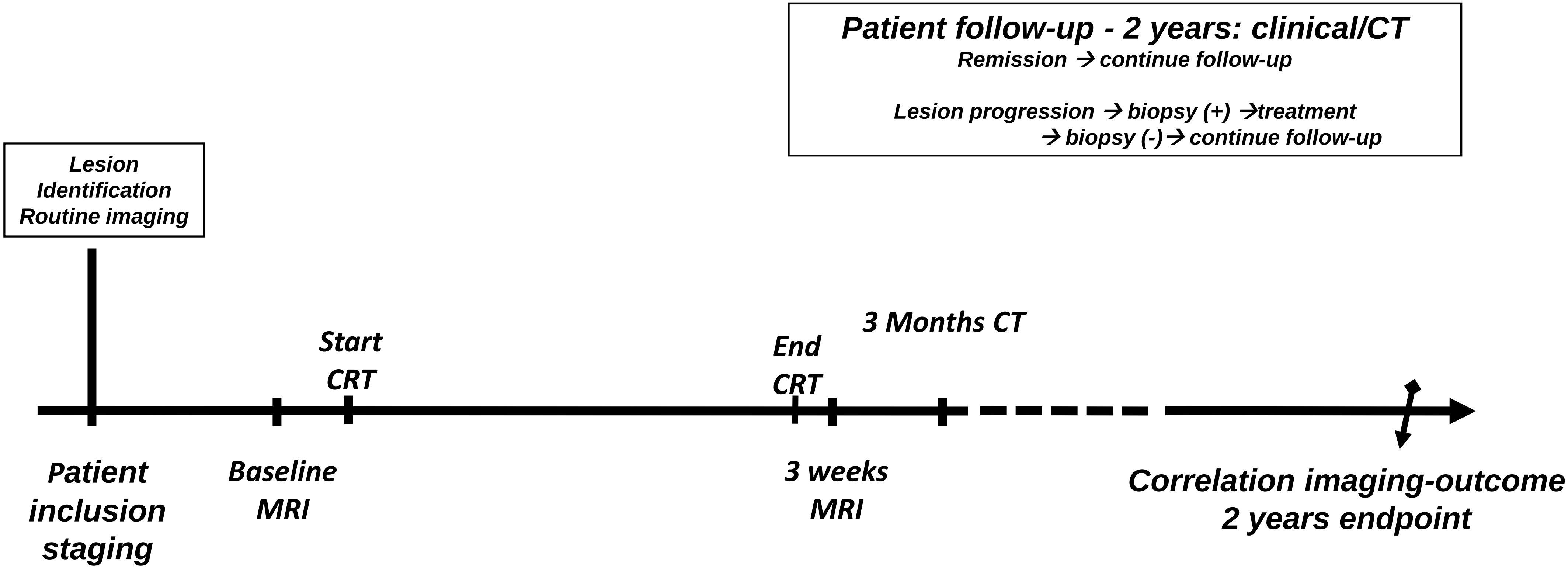
Patient follow-up - 2 years: clinical/CT
Remission → continue follow-up
Lesion progression → biopsy (+) →treatment
→ biopsy (-)→ continue follow-up
Lesion Identification Routine imaging
Start CRT
End CRT
3 Months CT
Patient inclusion staging
Baseline MRI
3 weeks MRI
Correlation imaging-outcome 2 years endpoint

Results (1): DWI during CRT

At 2 weeks

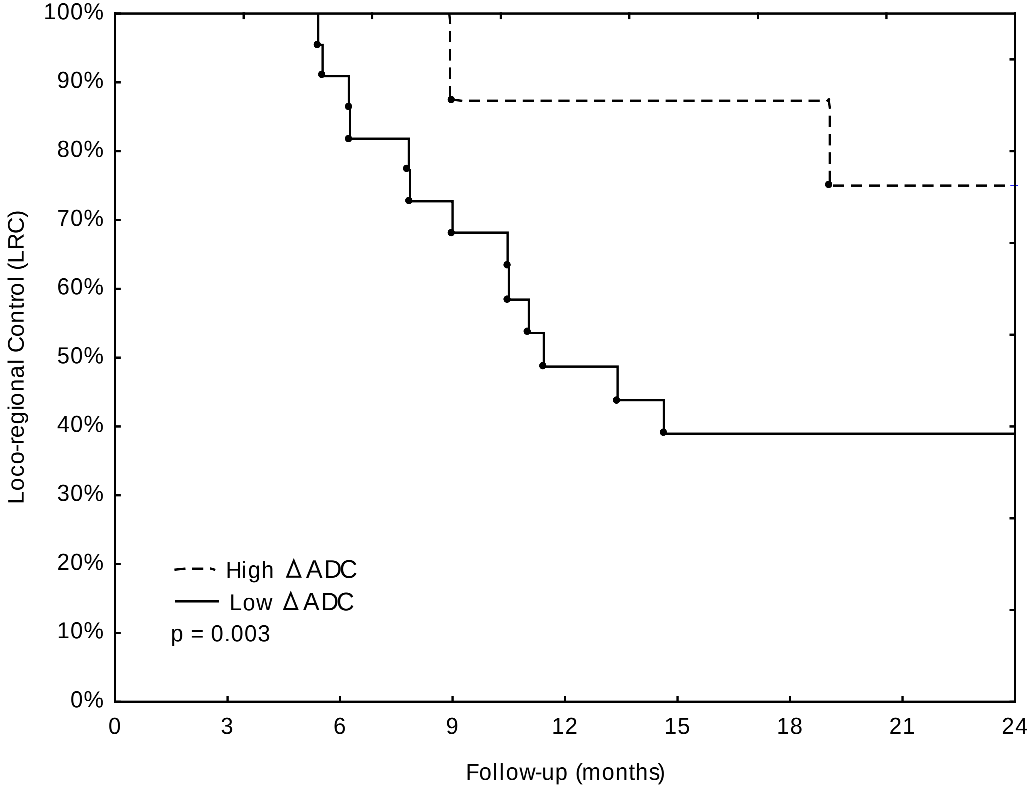

%ΔADC = (ADC 2w – ADC base) / ADC base

At 4 weeks

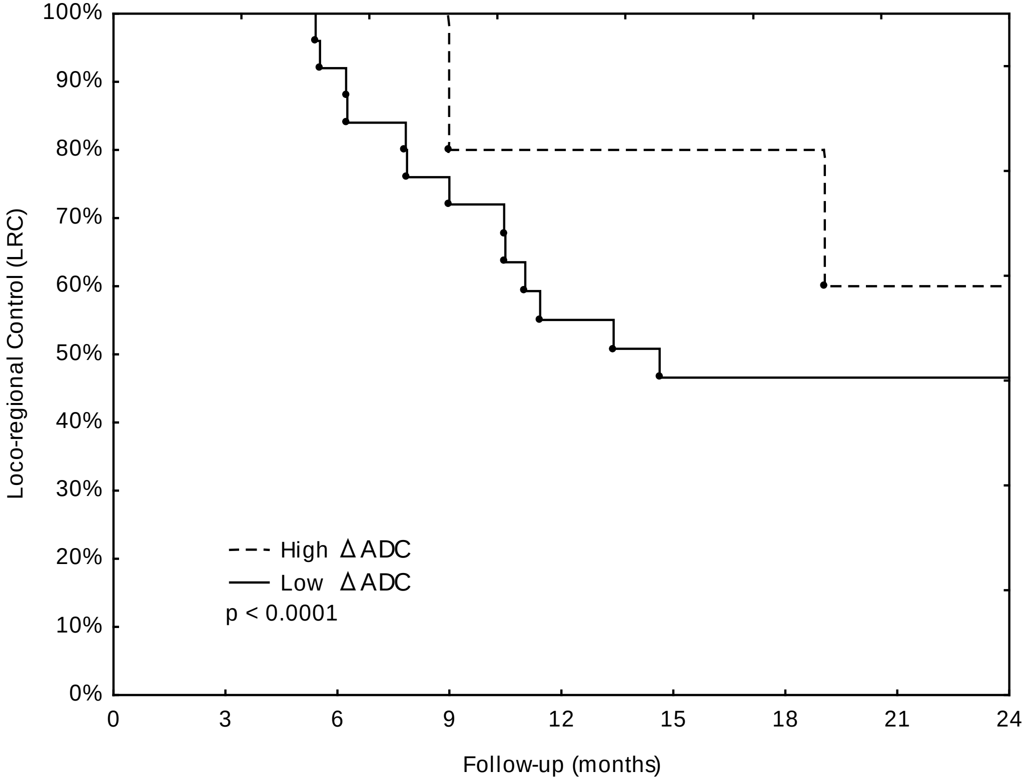

%ΔADC = (ADC 4w – ADC base) / ADC base

Dirix P. et al. J Nucl Med 2009.
Vandecaveye V. et al. Eur Radiol 2010.

Results (2): DWI at 3 weeks after CRT

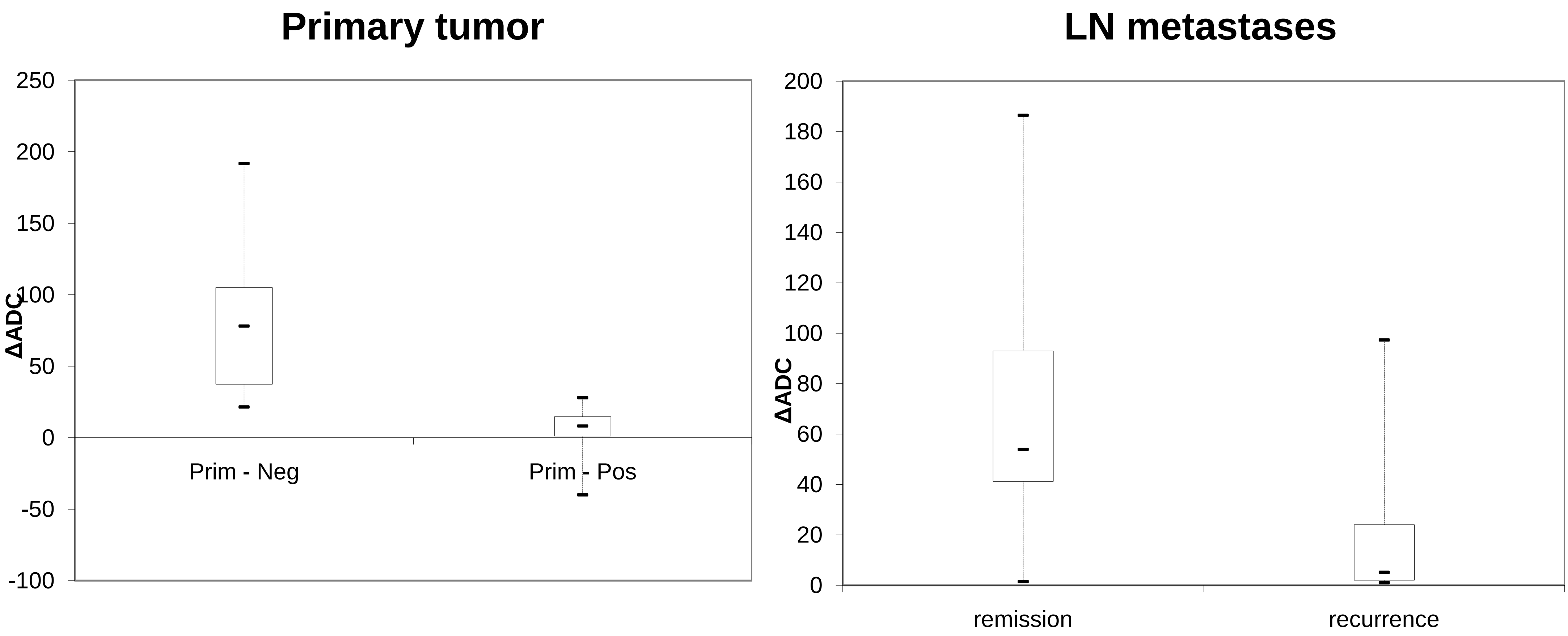

%ΔADC = (ADC 9w – ADC base) / ADC base

Vandecaveye V. et al. Int J Radiat Oncol Biol Phys 2012.

ESTRO School

Visual representation of ΔADC within the tumor

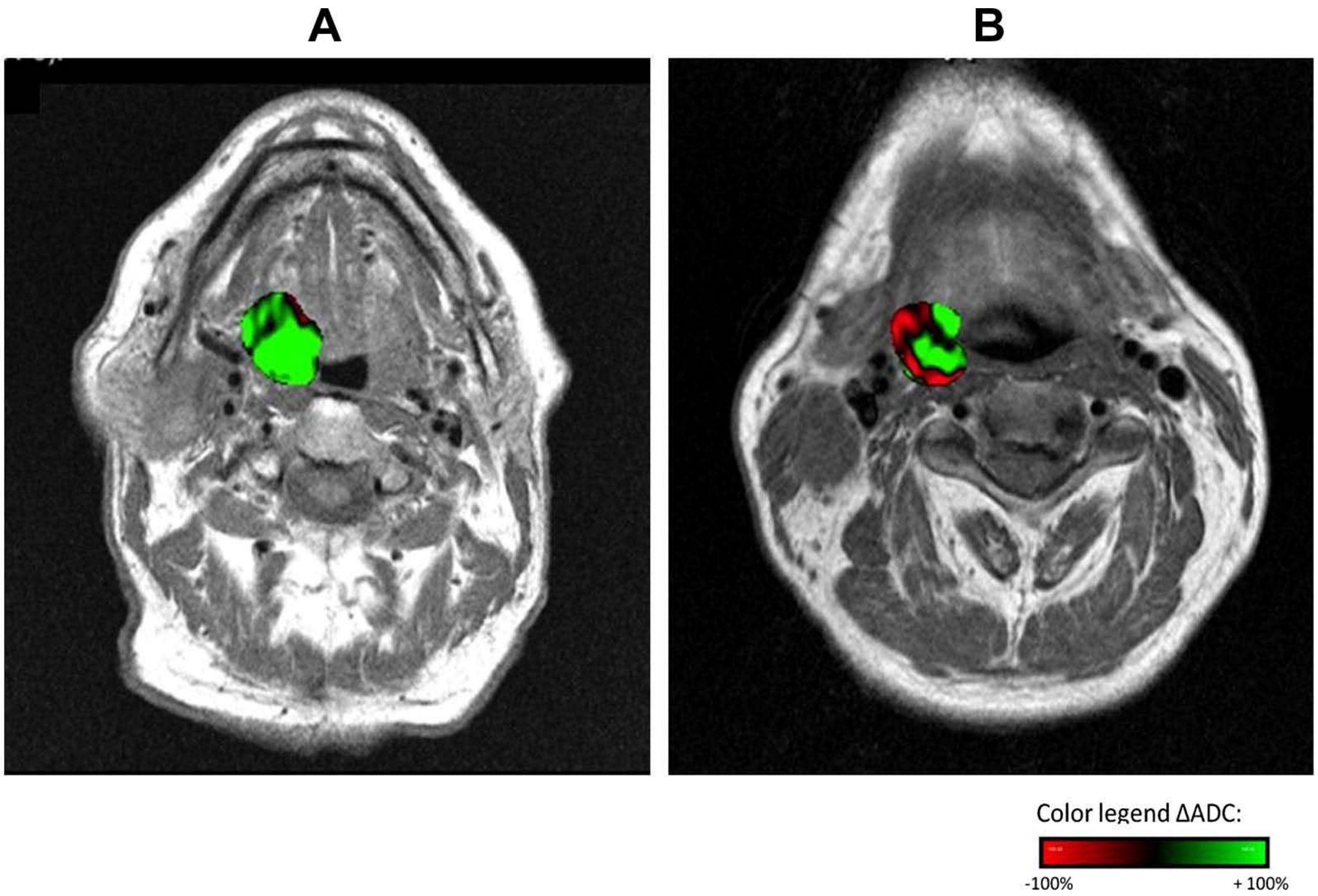

%ΔADC = (ADC 2w – ADC base) / ADC base

Lambrecht M. et al. Radiother Oncol 2014.

Clinical example of DWI for response assessment (1)

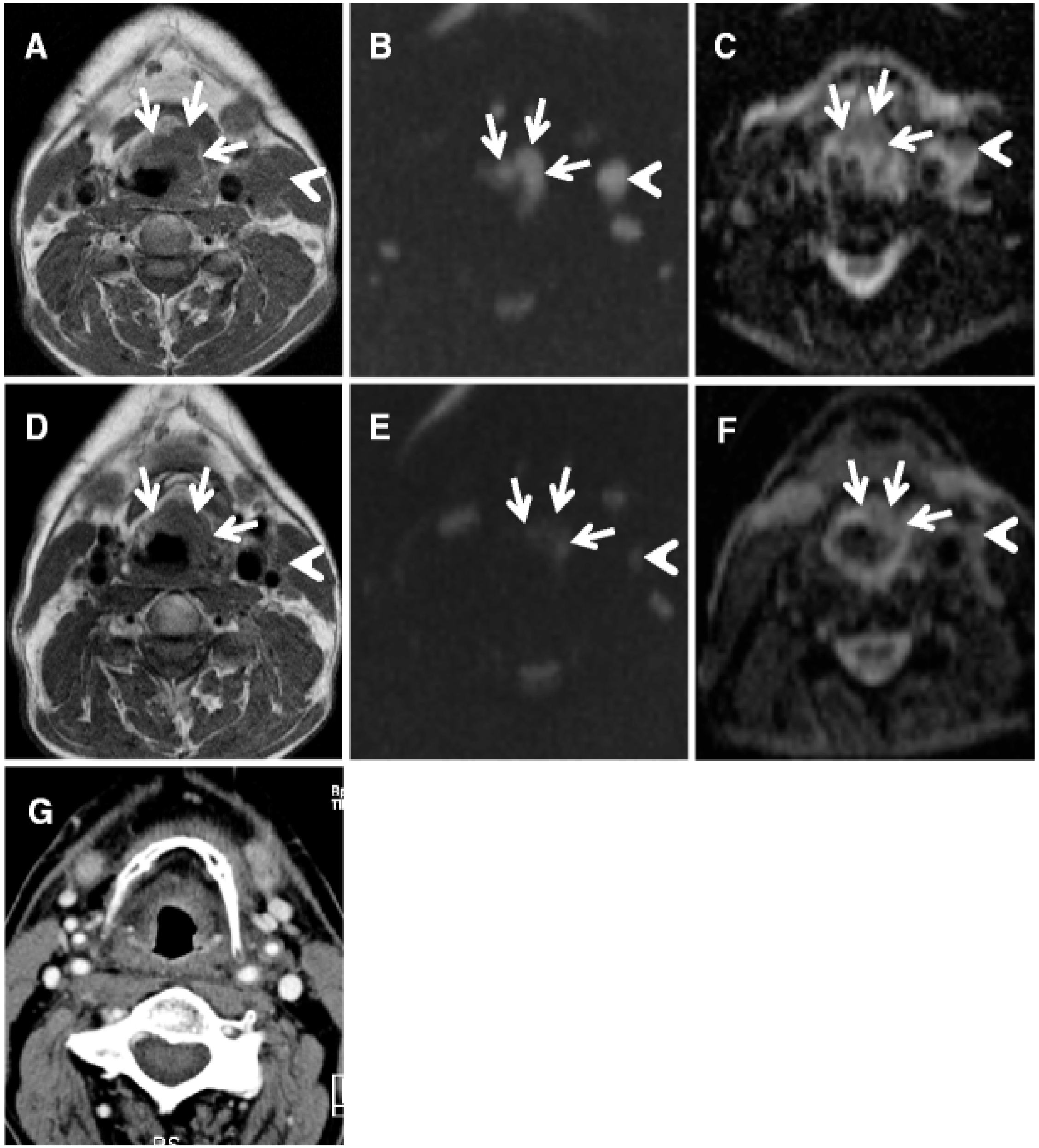

Images courtesy of Prof. V. Vandecaveye.

Clinical example of DWI for response assessment (2)

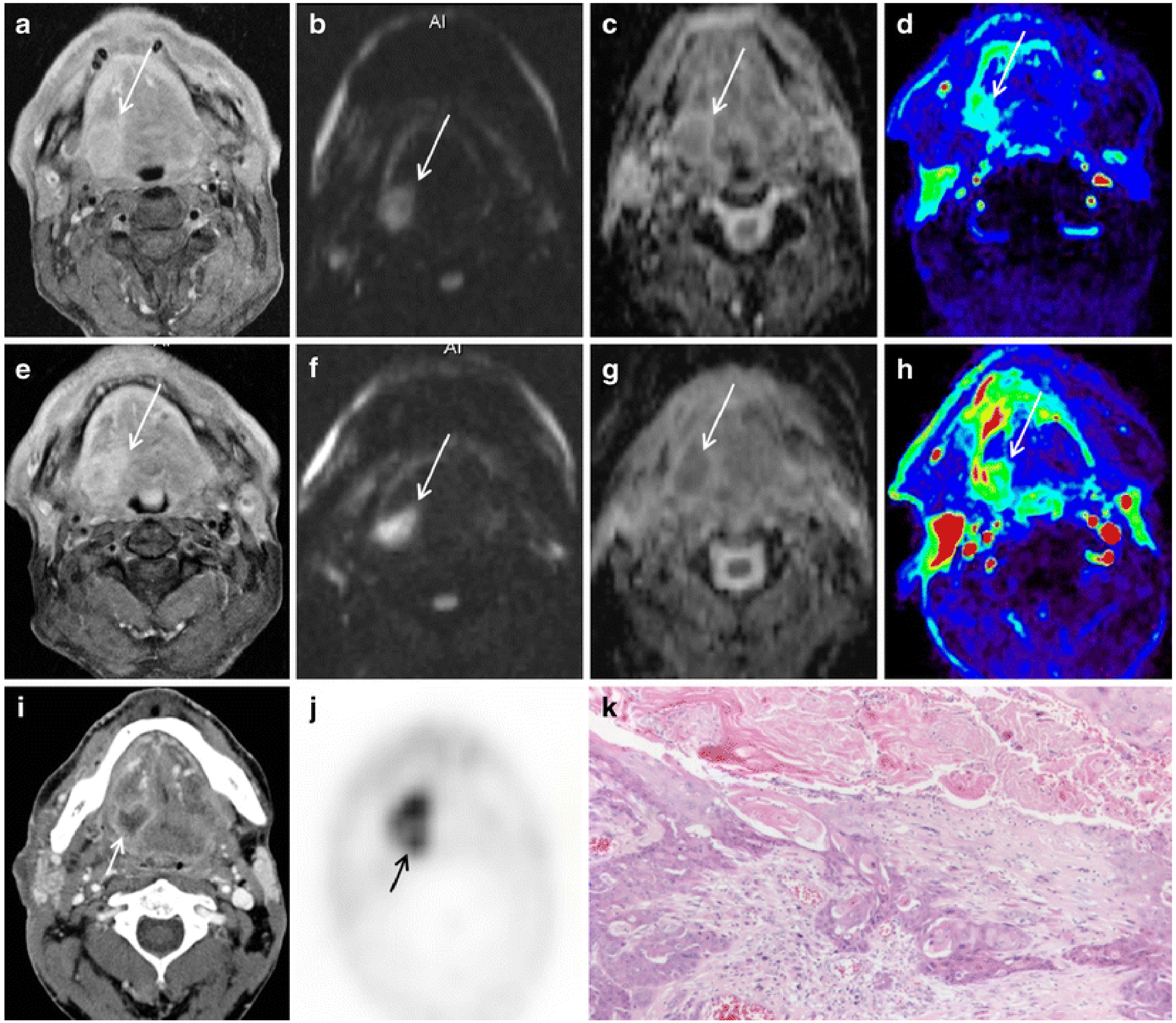

Images courtesy of Prof. V. Vandecaveye.

Clinical example of DWI for response assessment (3)

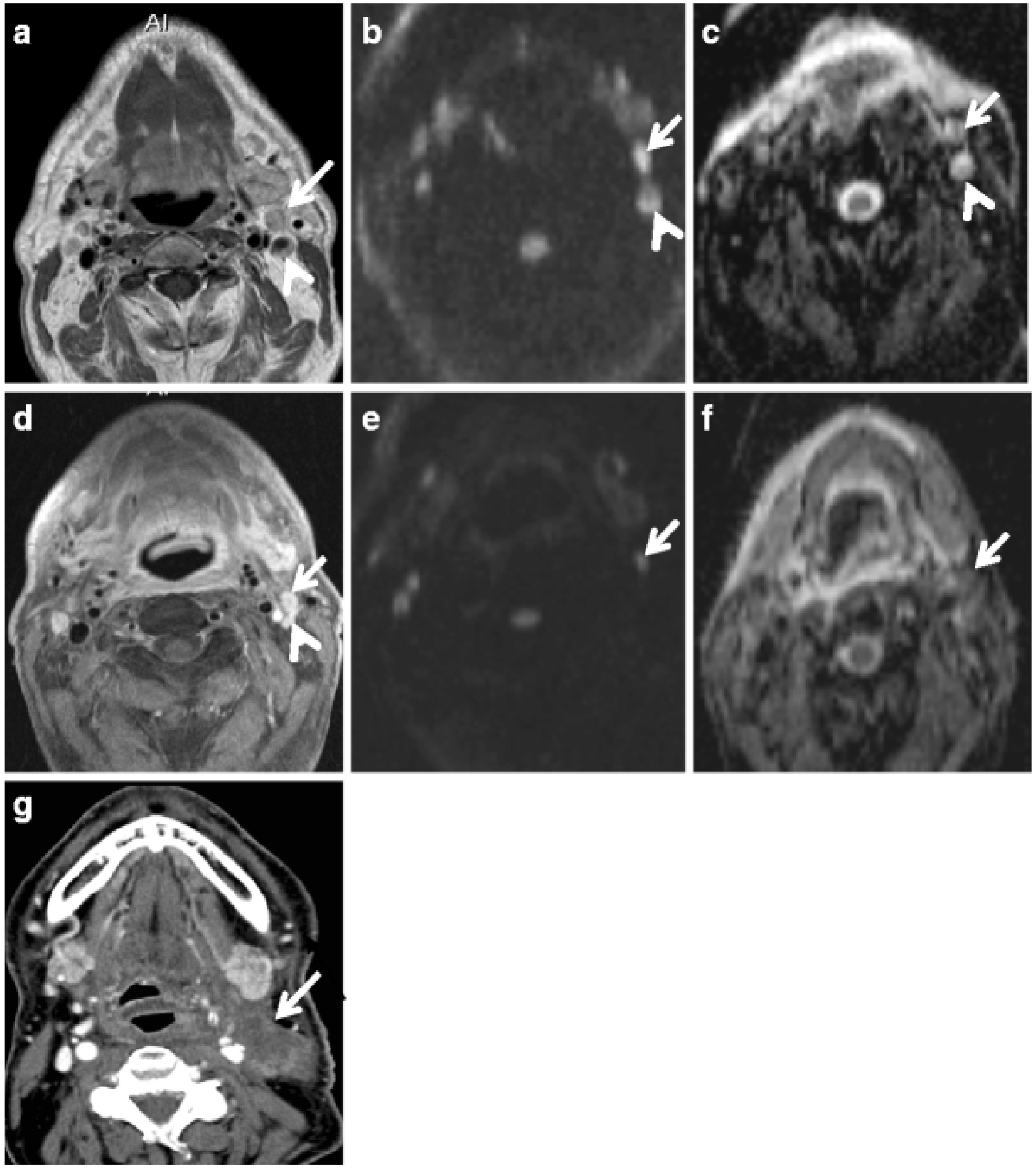

Images courtesy of Prof. V. Vandecaveye.

Similar results at the University of Pennsylvania

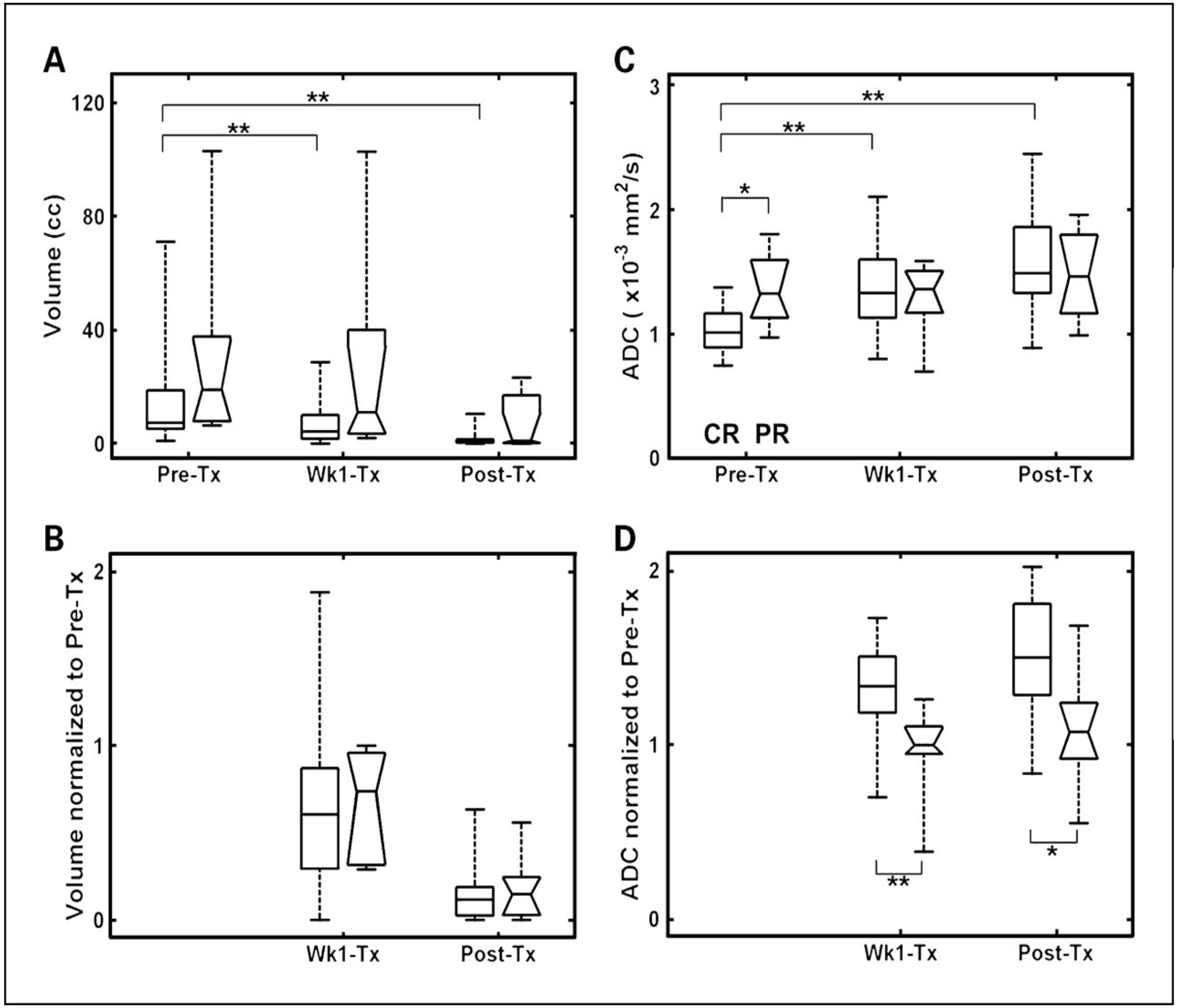

Variable	Cutoff value	Sensitivity (%)	Specificity (%)	AUC*
Pre-Tx	1.11×10^{-3} mm^2/s	65 (44, 82)	86 (42, 99)	0.80 (0.62, 0.99)
Wk1-Tx/Pre-Tx	1.11	86 (64, 96)	83 (36, 99)	0.88 (0.74, 1.00)
Post-Tx/Pre-Tx	1.11	82 (56, 95)	80 (30, 99)	0.80 (0.57, 1.00)

Kim S. et al. Clin Cancer Res 2009.

Similar results at the University of Michigan

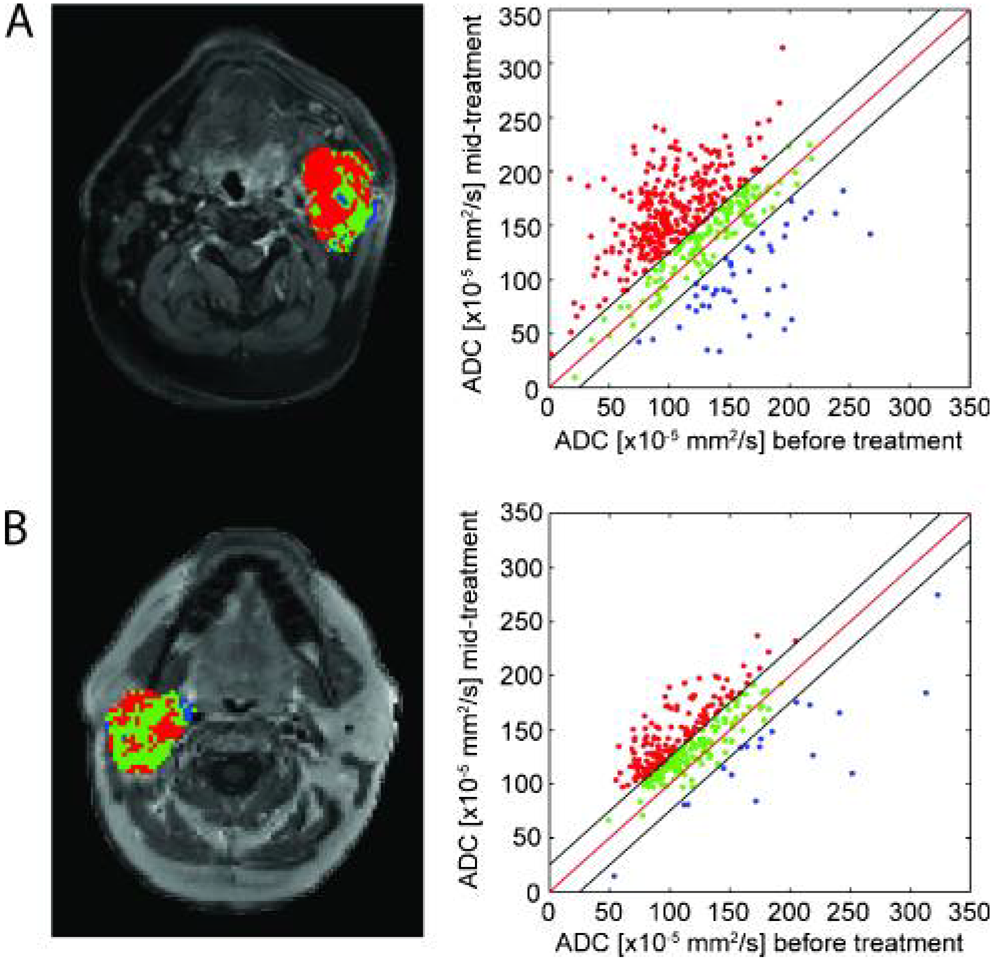

Early Response of Volume and Tumor ADC Values at 3 Weeks after Treatment Initiation.

	Volume [cm³] (SEM)		ADC [x10⁻⁵ mm²/sec] (SEM)	
	Pretreatment	Midtreatment	Pretreatment	Midtreatment
Primary	**28.8 (9.5)**	**19.3 (7.2)**	145.8 (11.3)	163.3 (10.6)
Lymph nodes	**43.7 (9.9)**	**29.6 (10.2)**	**122.5 (5.0)**	**153.4 (5.1)**
CR	**30.6 (5.9)**	**18.2 (5.4)**	**133.5 (7.7)**	**162.9 (6.3)**
PR	**57.8 (22.3)**	**47.1 (19.7)**	132.7 (8.6)	141.5 (9.5)

Galbán C.J. et al. Transl Oncol 2009.

Similar results at the Prince of Wales Hospital (Hong Kong)

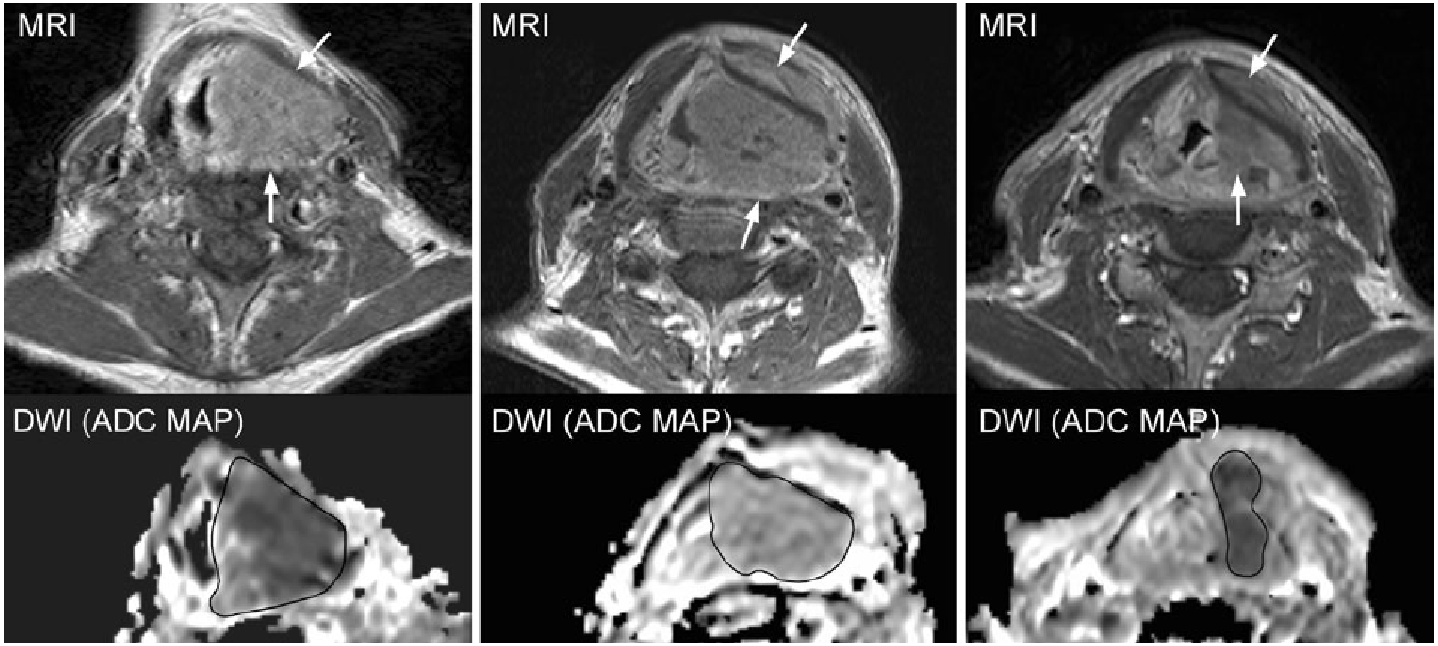

Table 3 DWI in 20 patients with a residual post-treatment mass: accuracy of ADC for distinguishing between a residual cancer and a benign post-treatment mass by using a fall in ADC in the early or later phase of treatment to indicate locoregional failure

	TP *n*	TN *n*	FP *n*	FN *n*	Sens %	Spec %	NPV %	PPV %	Accuracy %
6 months	7	12	1	0	100	92	100	88	95
12 months	7	11	1	1	88	92	92	88	90
Total duration of study	8	10	0	2	80	100	83	100	90

TP true positive, *TN* true negative, *FP* false positive, *FN* false negative, *Sens* sensitivity, *Spec* specificity, *NPV* negative predictive value, *PPV* positive predictive value

King A. D. et al. Transl Oncol 2009.

ESTRO School

DCE-MRI for early response assessment

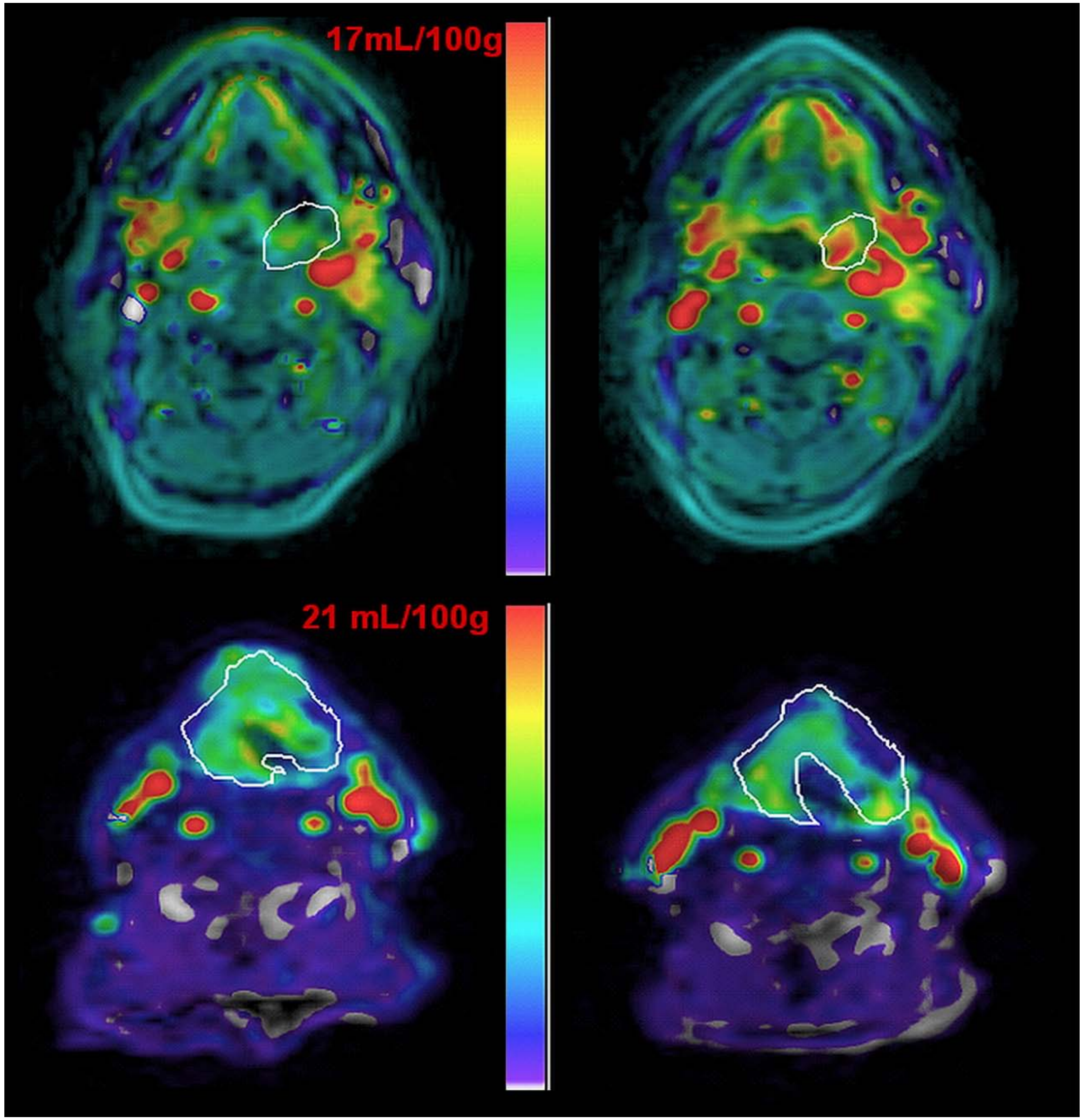

Cao Y. et al. Int J Radiat Oncol Biol Phys 2008.

4. Towards a biological target volume (BTV)?

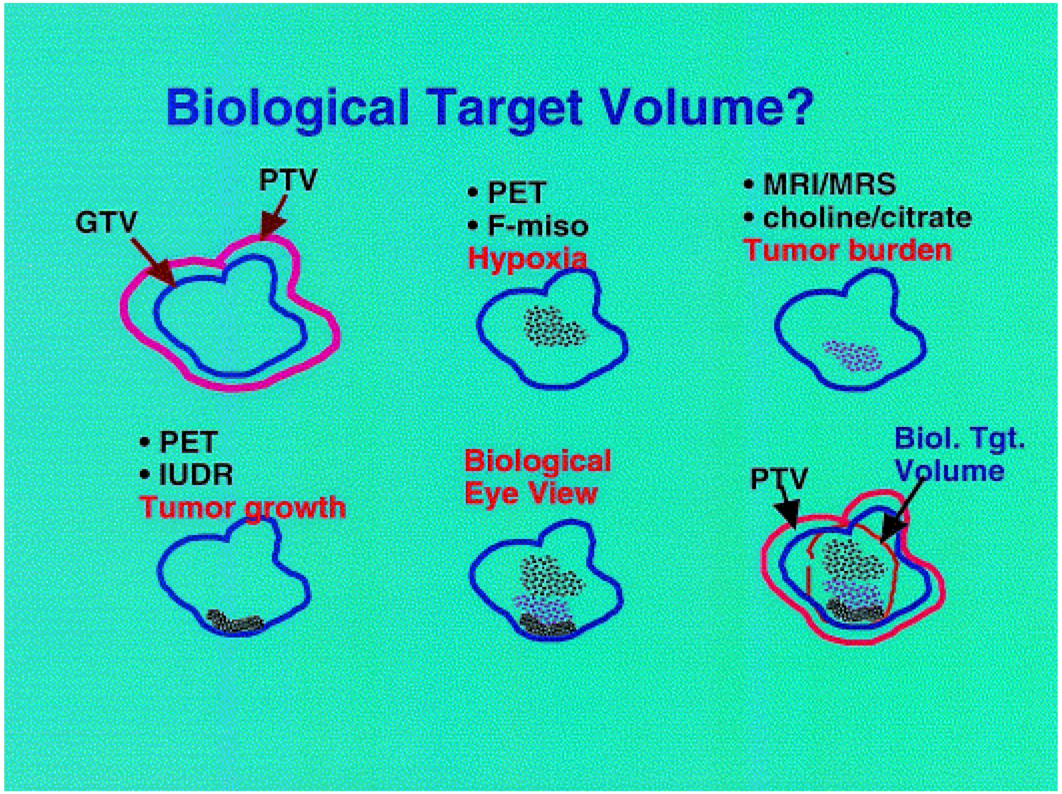

- BTV derived from functional/biological imaging guides customized dose delivery to various parts of the treatment volume.
- = “dose-painting” or “dose-sculpting”.

Ling C. et al. Int J Radiat Oncol Biol Phys 2000.

FDG-PET

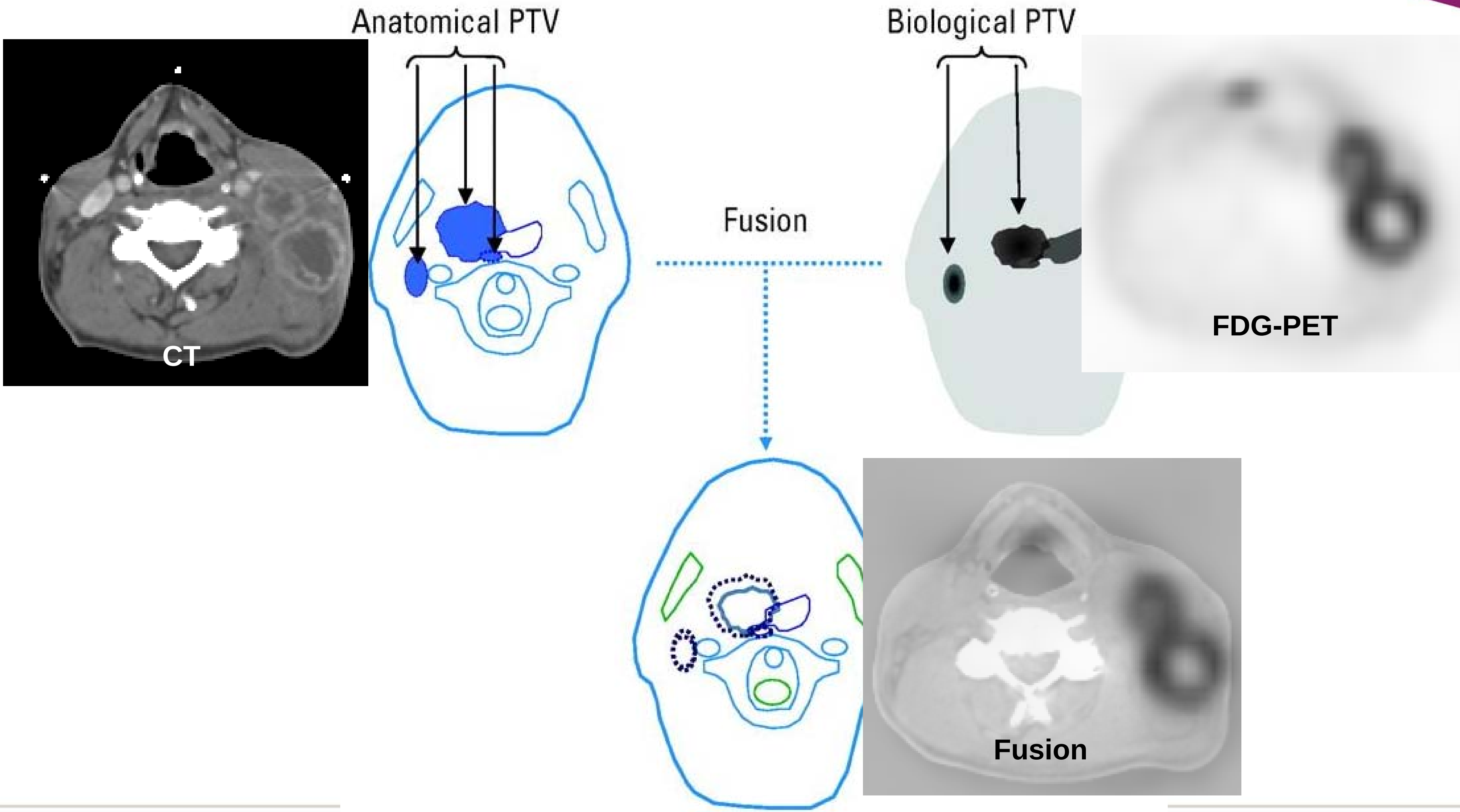

Galvin J. & De Neve W. J Clin Oncol 2007.

UZ Gent Phase I trial

Prescription-dose levels to the PTVs

PTV	Dose per fraction (Gy)		Total dose (Gy)	NID_{2Gy} (Gy)
	Fractions 1–10	Fractions 11–32		
PTV_{PET} = level I of dose escalation	2.5	2.16	72.5	78.2
PTV_{PET} = level II of dose escalation	3.0*	2.16	77.5	86.7
PTV_{69} = macroscopic tumor + enlarged lymph nodes	2.16	2.16	69.1	72.5
PTV_{66} = resected lymph nodes with capsule rupture	2.06	2.06	65.9	67.2
PTV_{62} = resected lymph nodes without capsule rupture	1.94	1.94	62.1	60.9
PTV_{56} = elective lymph nodes	1.75	1.75	56.0	51.1

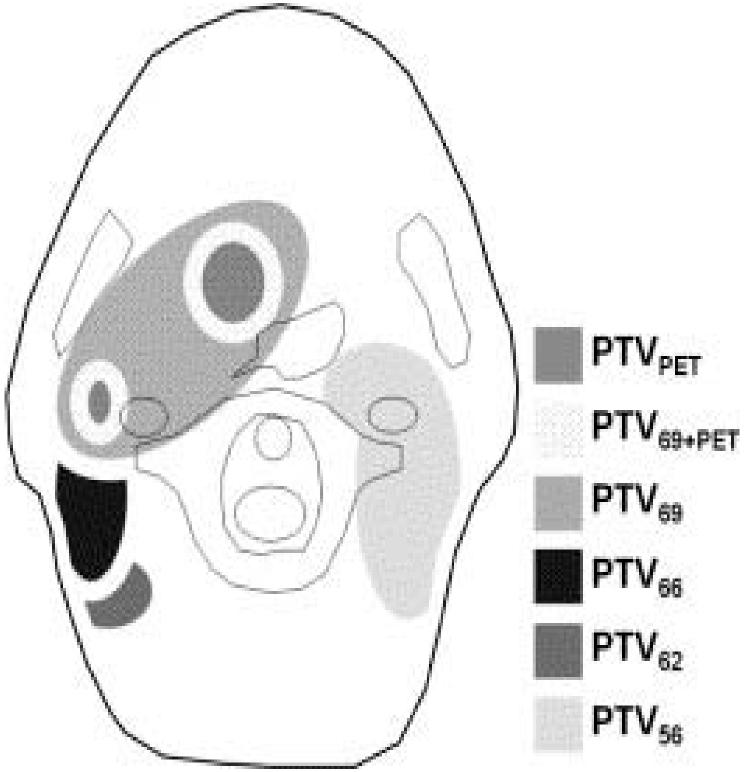

- **23 pts dose level I (5.7 Gy), 18 pts dose level II (14.2 Gy) in first 10 fractions.**
- **2 cases of DLT at dose level I (grade 4 dermitis & dysphagia).**
- **1 toxic death at dose level II (not RT-related?).**
- **In 4 of 9 relapsed patients, the site of relapse was in the PTV-PET.**
- **PET-guided dose escalation appears to be well-tolerated?**

Madani I. et al. Int J Radiat Oncol Biol Phys 2007.
Duprez F. et al. Int J Radiat Oncol Biol Phys 2011.

Pretreatment ADC of the primary lesion

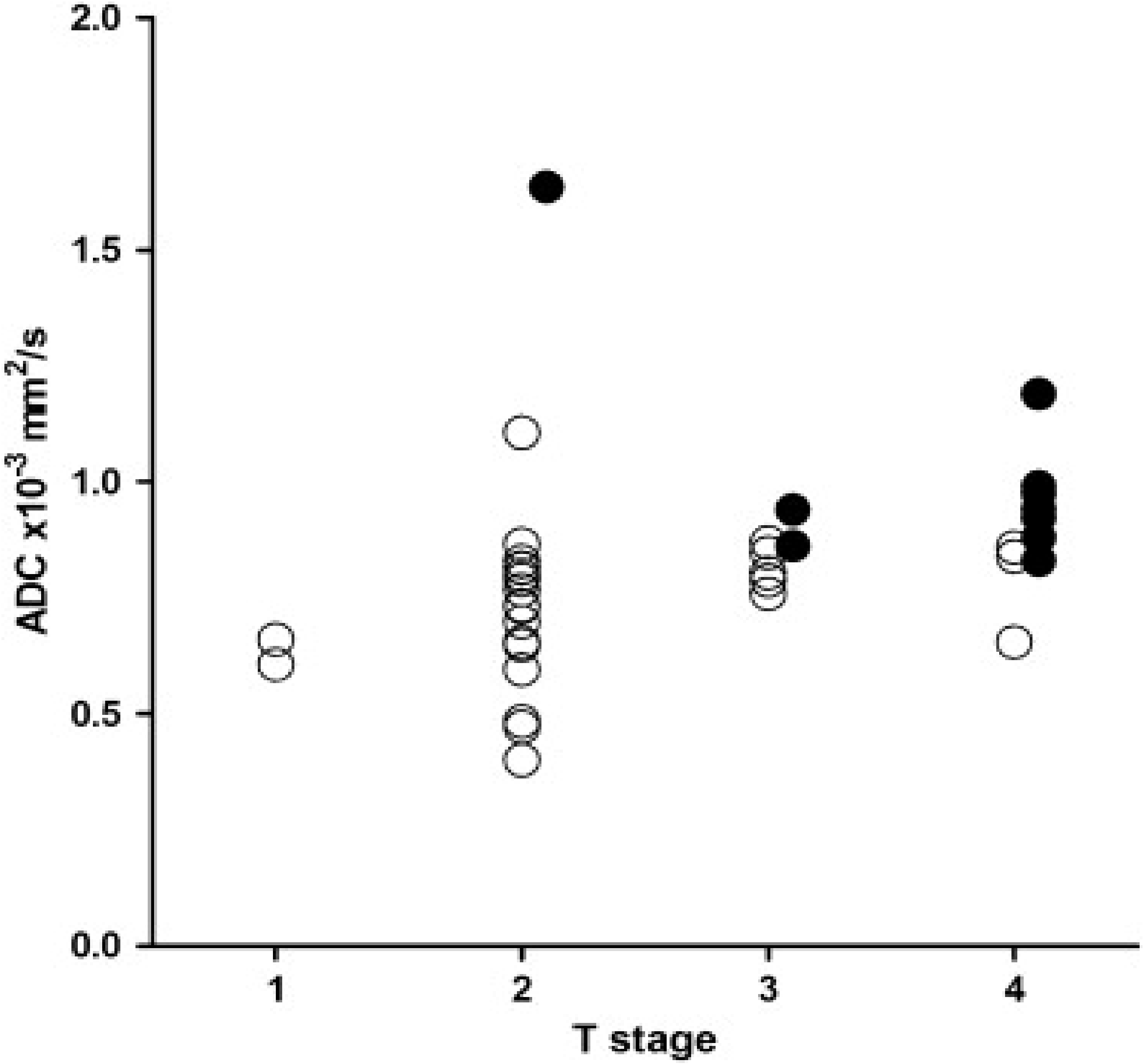

Hatakenaka M. et al. Int J Radiat Oncol Biol Phys 2011.

ADC$_{high}$ before RT correlates with outcome

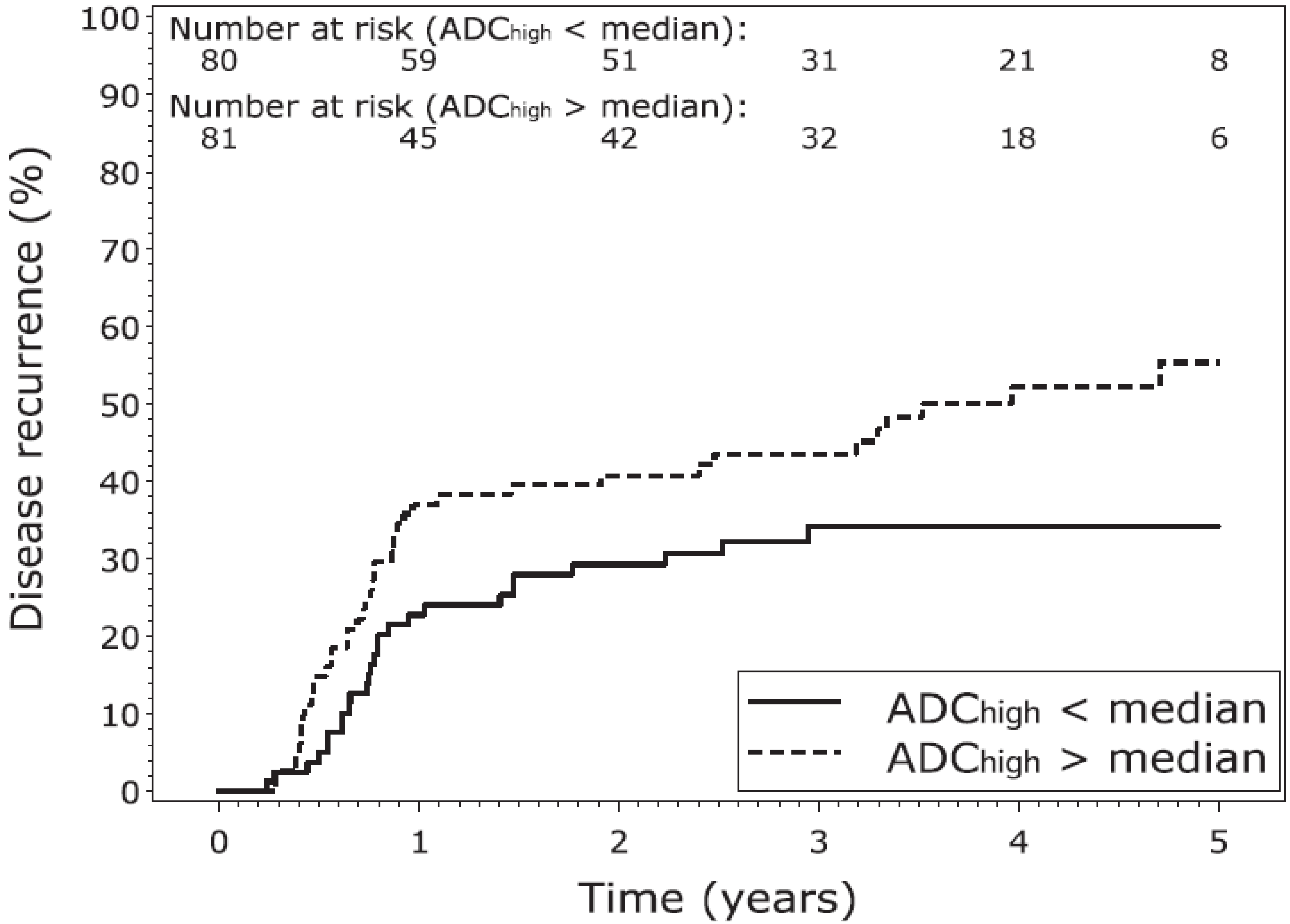

Lambrecht M. et al. Radiother Oncol 2014.

Multivariable prognostic model

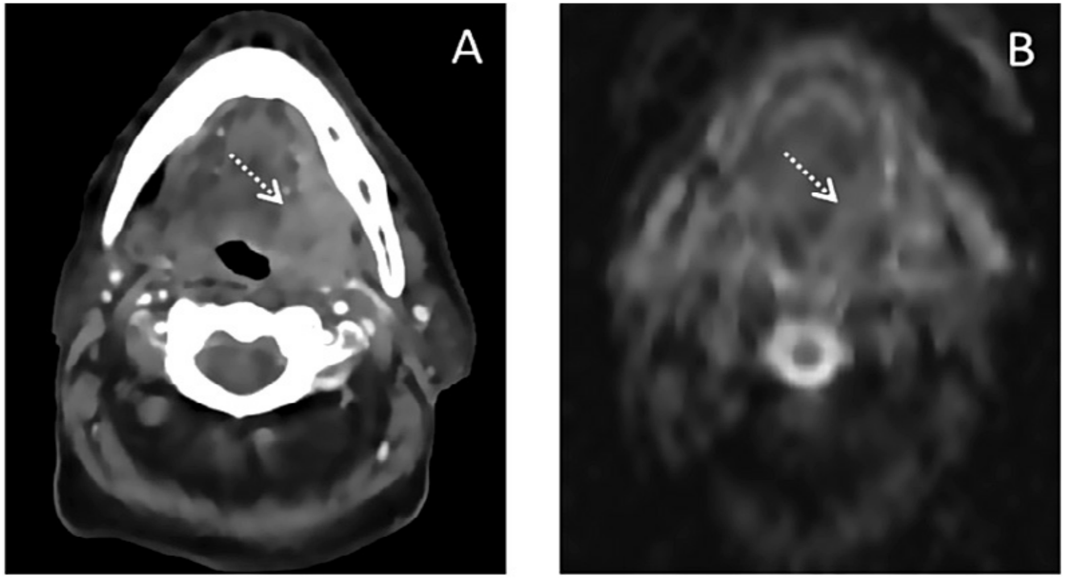

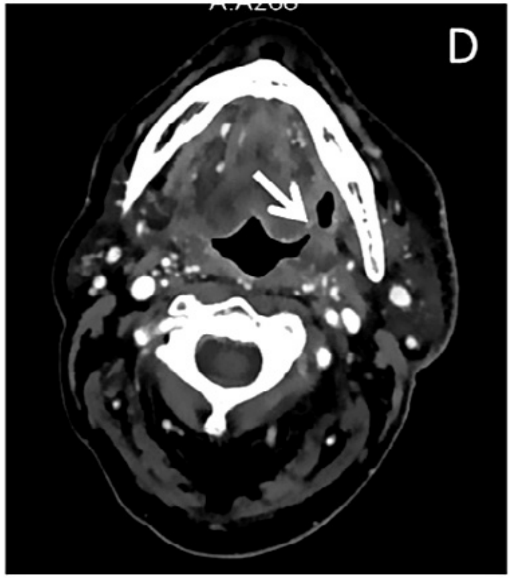

C

Age	:	56
Location		Oropharynx
Tumour Volume		0,3 dl:
Nodal Volume		0,05 dl:
ADC_{high} value		11 x10^{-4} mm²/s:
Recurrence probability:		**42%**

Lambrecht M. et al. Radiother Oncol 2014.

ESTRO School

FDG-PET & DWI contain different info

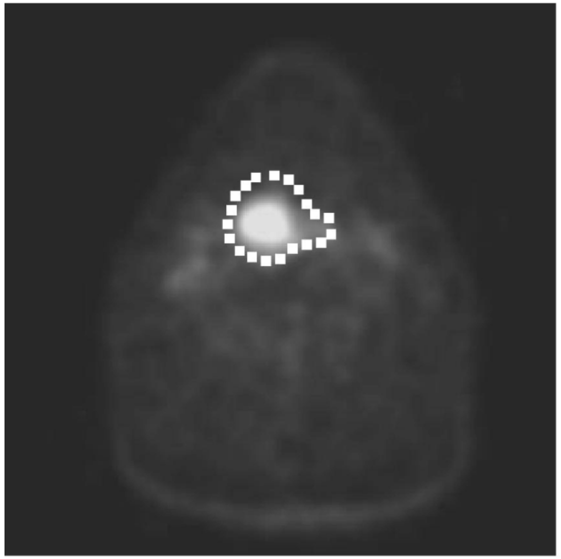

(a)

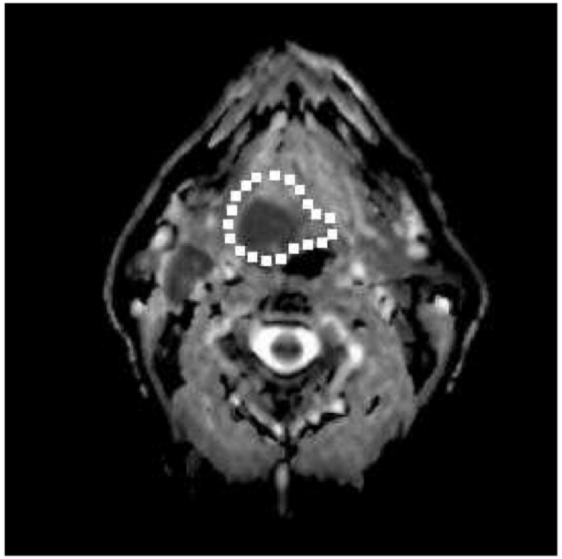

(b)

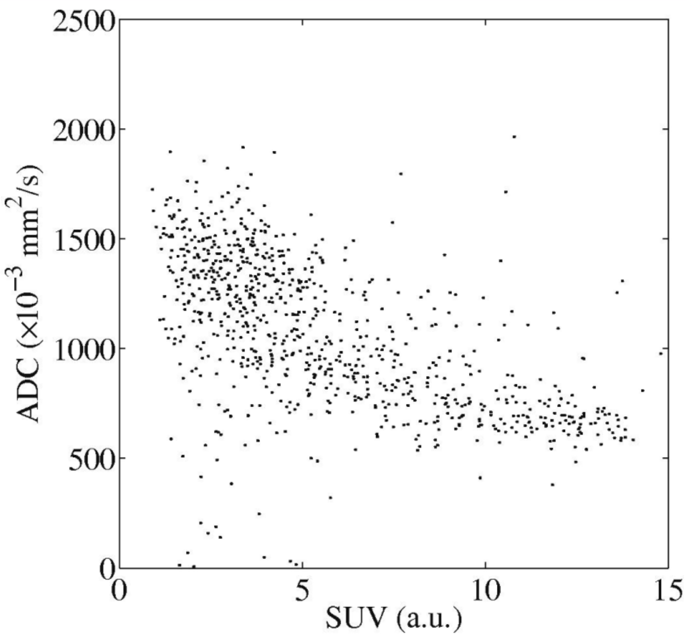

(c)

Table 2
Overlap of the different targets with the $SUV_{50\%max}$-target.

	Volume (ml)		Overlap (%)	
	Average	Range	Average	Range
$SUV_{50\%max}$	7.7	1.3–30.6	–	–
$SUV_{60\%max}$	5.1	0.9–22.5	100	100– 100
$SUV_{40\%max}$	11.2	2.1–38.3	67.9	51.1–80.2
$ADC_{<mean}$	18.4	2.7–61.2	30.2	8.0–68.1
$ADC_{<mean-SD}$	4.6	0.9–12.4	27.0	3.9–72.5
$ADC_{>mean}$	16.3	3.0–57.5	18.6	0.7–56.3

Houweling A.C. et al. Radiother Oncol 2013.

ESTRO School

Combination of both can be valuable

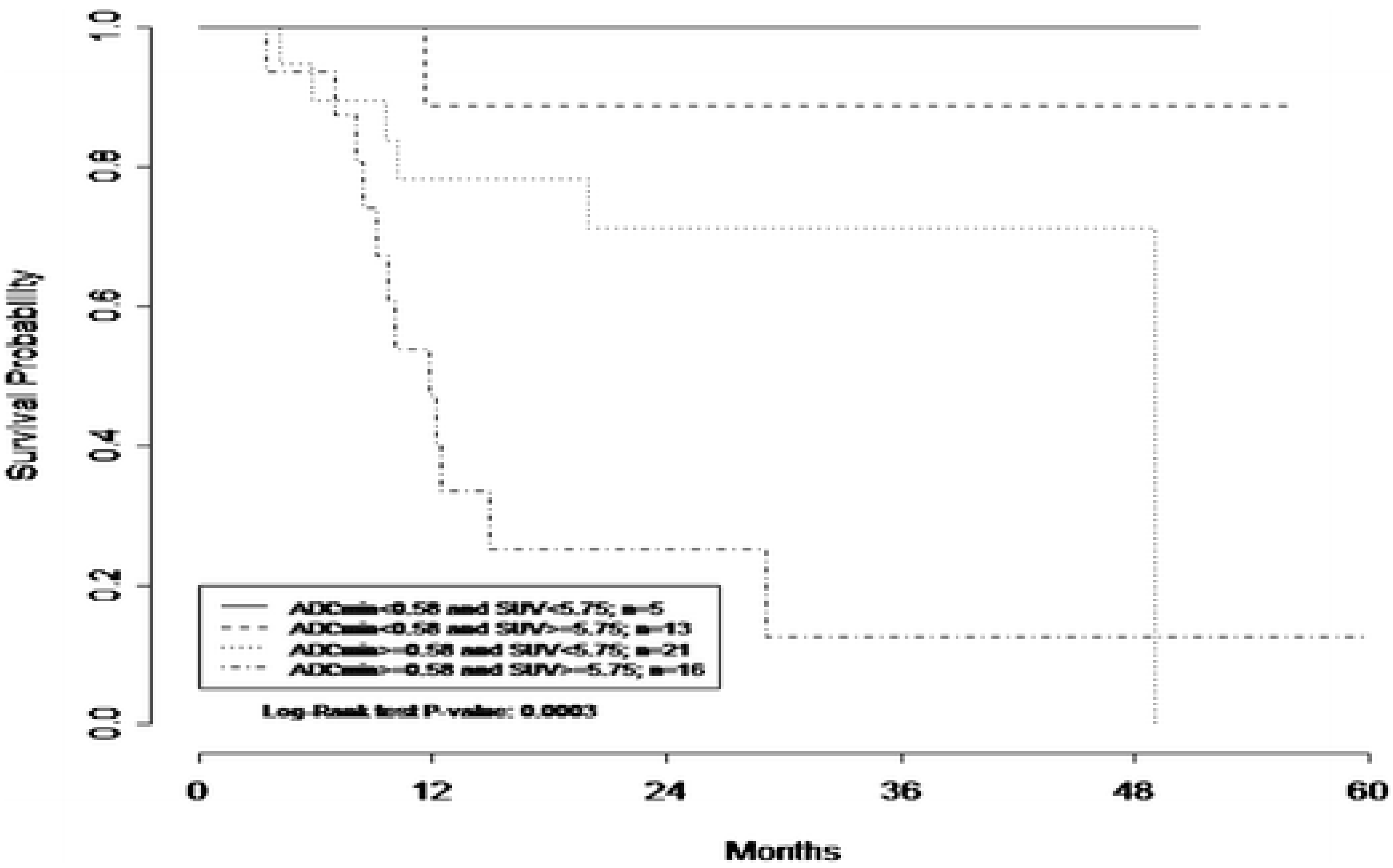

Preda L. et al. Eur Radiol 2016.

Pathology validation study

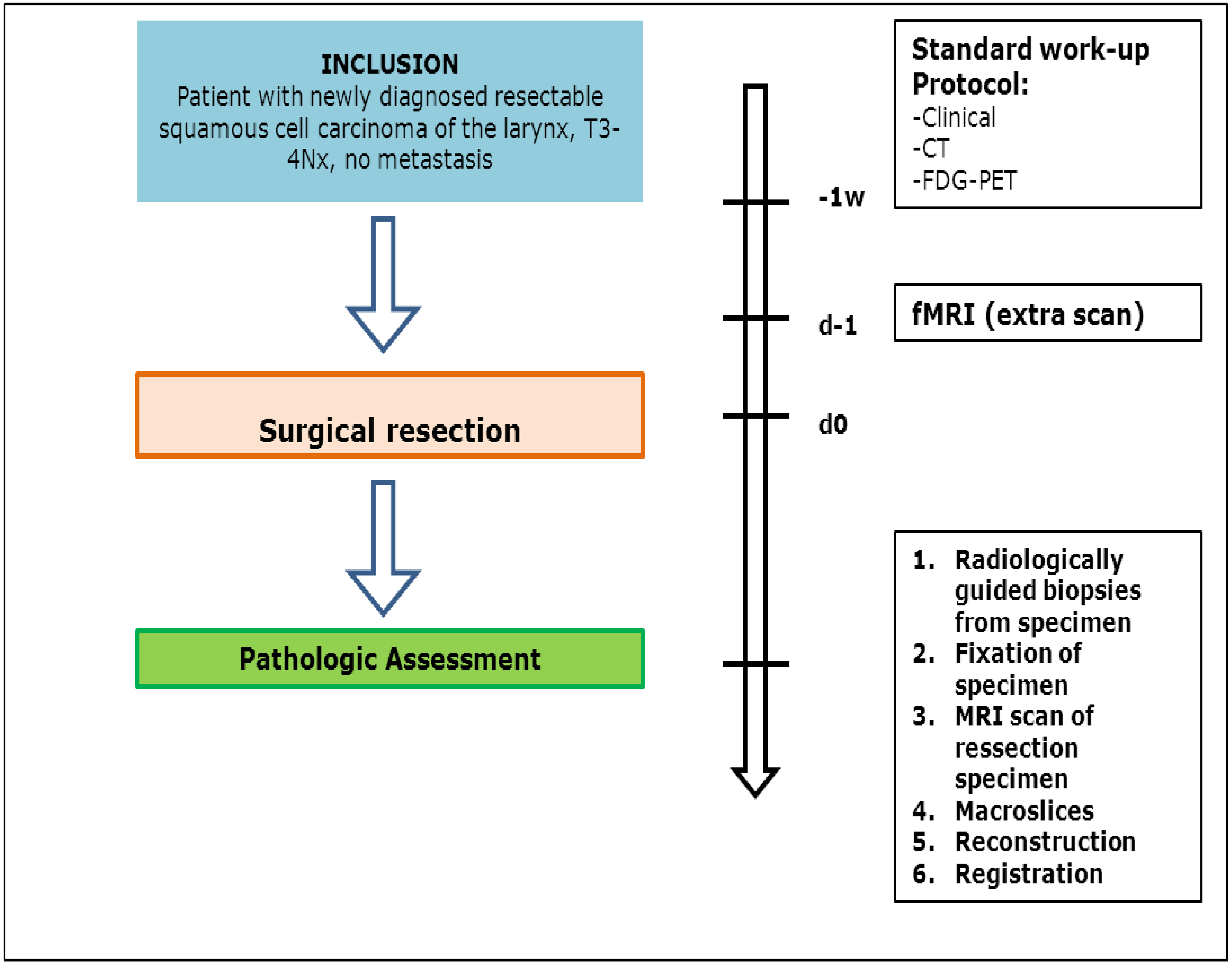

Slide courtesy of Dr. D. Nevens

Pathology validation study

± 5mm

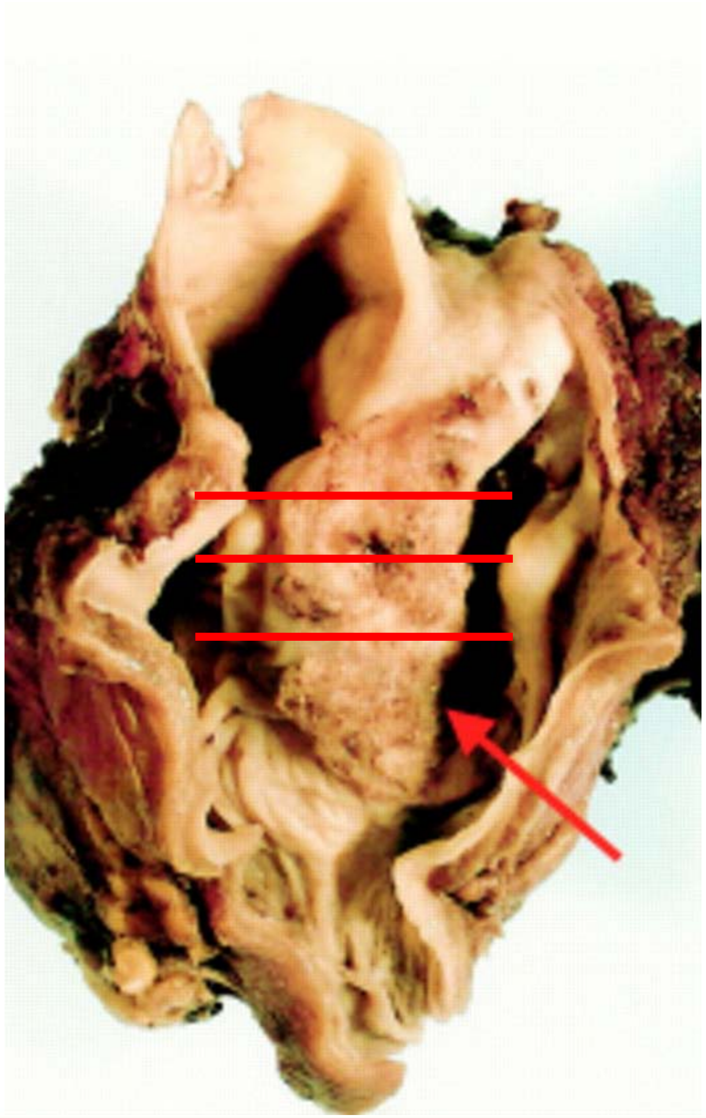

Slide courtesy of Dr. D. Nevens

Pathology validation study

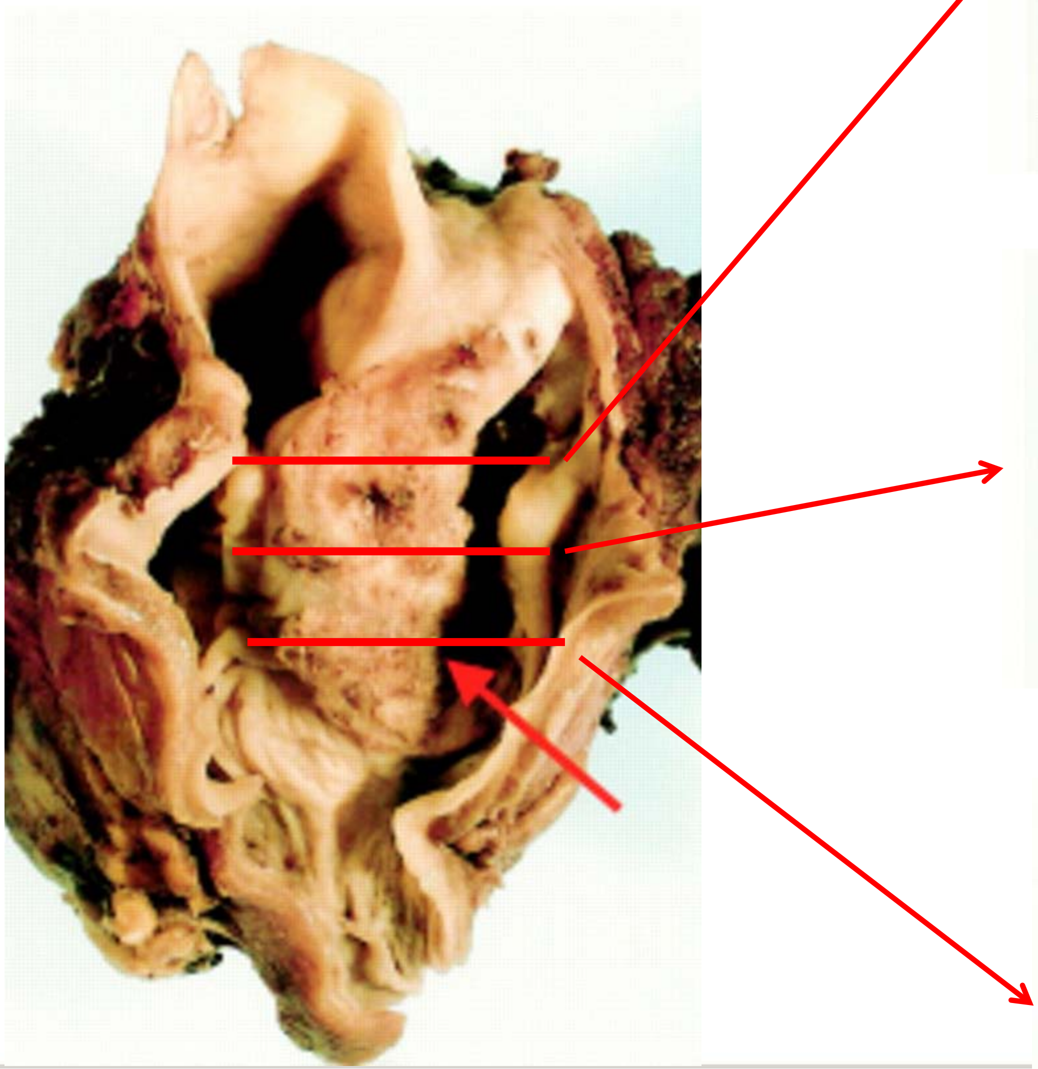

Slide courtesy of Dr. D. Nevens

Association between ADC and pathology (1)

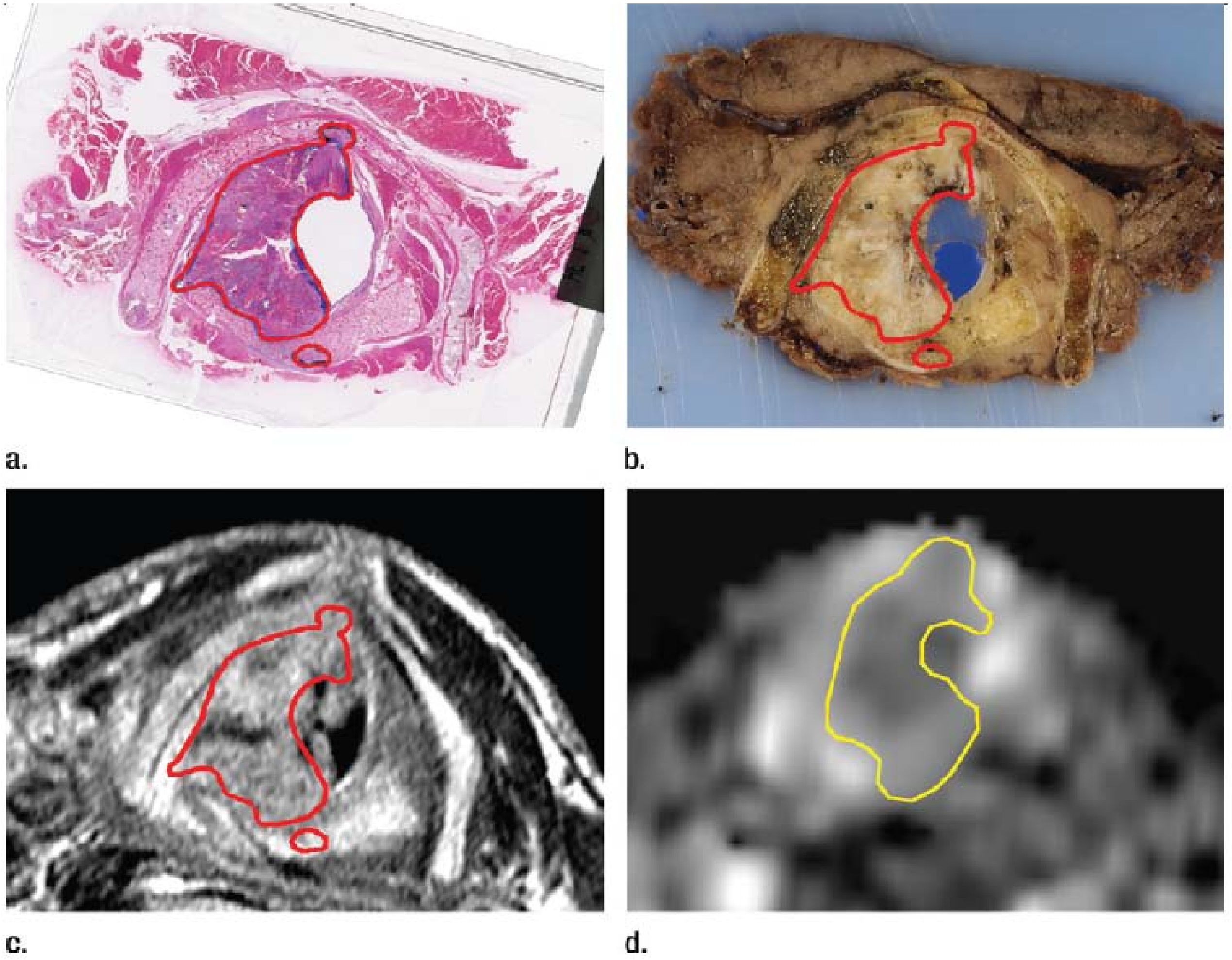

Driessen J.P. et al. Radiology 2015.

Association between ADC and pathology (2)

Figure 5

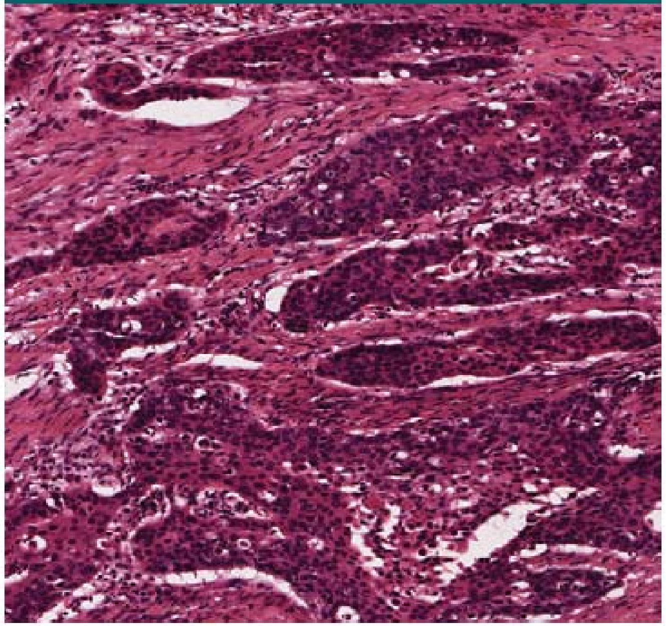

Figure 5: Digitized whole-mount H-E section (original magnification, ×10) of a T3 hypopharyngeal carcinoma. The tumor shows an intermediate CD of 6188 cells per square millimeter, 38% nuclear area, 38% stromal area, NC ratio of 1.59, and intermediate ADC of 1.19×10^{-3} mm^2/sec.

Figure 6

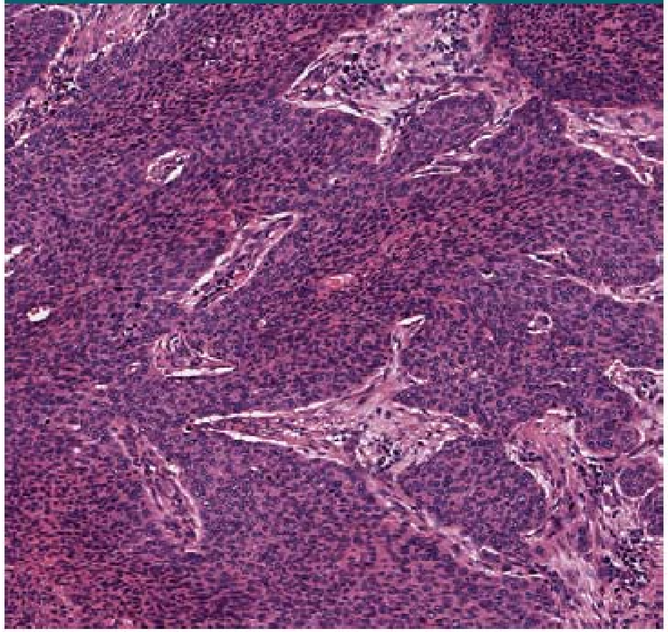

Figure 6: Digitized whole-mount H-E section (original magnification, ×10) of a T4a laryngeal carcinoma. The tumor shows a high CD of 8050 cells per square millimeter, 65% nuclear area, 18% stromal area, NC ratio of 4.14, and low ADC of 0.96×10^{-3} mm^2/sec.

Driessen J.P. et al. Radiology 2015.

All reported results for DWI & response assessment

Study	n	During CRT	After CRT	Correlation	Results
Kim et al. *Clin Cancer Res 2009*	33	1w	2w	Response after CRT	Baseline ADC of responders was significantly lower. A significant increase in ADC was observed in responders within 1 week of CRT which remained until after CRT.
Galban et al. *Transl Oncol 2009*	15	3w	-	6-month LC	Significant differences in ADC were observed between patients with different outcomes.
Vandecaveye et al. *Eur Radiol 2010*	30	2w & 4w	-	2-year LRC	The ΔADC 2 and 4 weeks after the start of CRT was significantly lower in lesions with recurrence.
King et al. *Eur Radiol 2010*	50	2w	6w	2-year LRC	A significant correlation was found between local failure and post-treatment ADC but not pre- or intra-treatment ADC.
Hatakenaka et al. *IJROBP 2011*	38	-	-	2-year LC	Baseline ADC of responders was significantly lower.
Vandecaveye et al. *IJROBP 2012*	29	-	3w	2-year LRC	The ΔADC of lesions with later recurrence was significantly lower.
Srinivasan et al. *JCAT 2012*	17	-	-	2-year outcome	Baseline ADC of responders was significantly lower.
King et al. *Radiology 2013*	30	2w	-	2-year LC	Baseline ADC showed no correlation with local failure. During treatment, primary tumors showed a significantly lower ΔADC for local failure.

Dirix P. et al. Seminars in Radiation Oncology 2014.

Initial K^{trans} predicts outcome

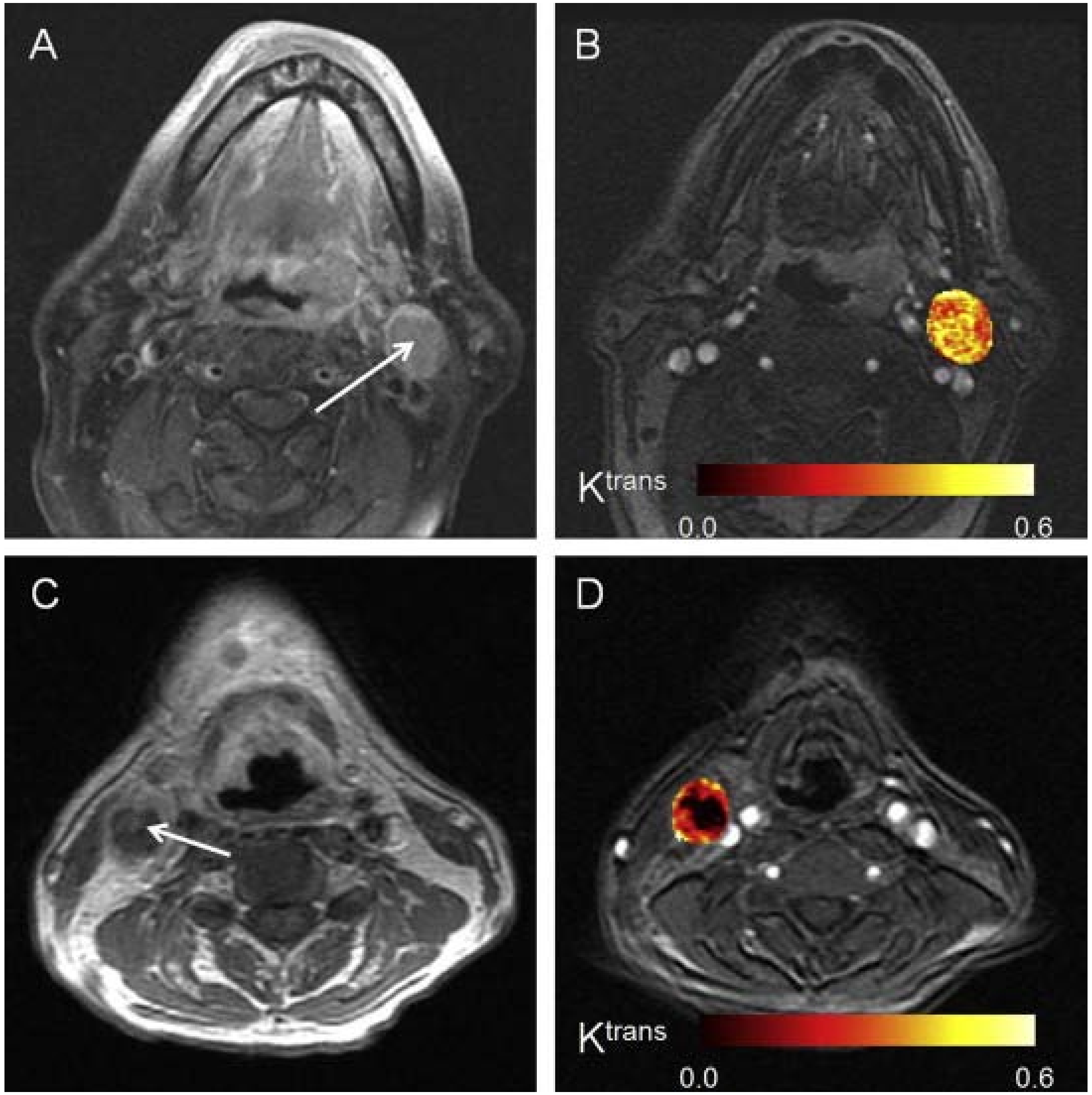

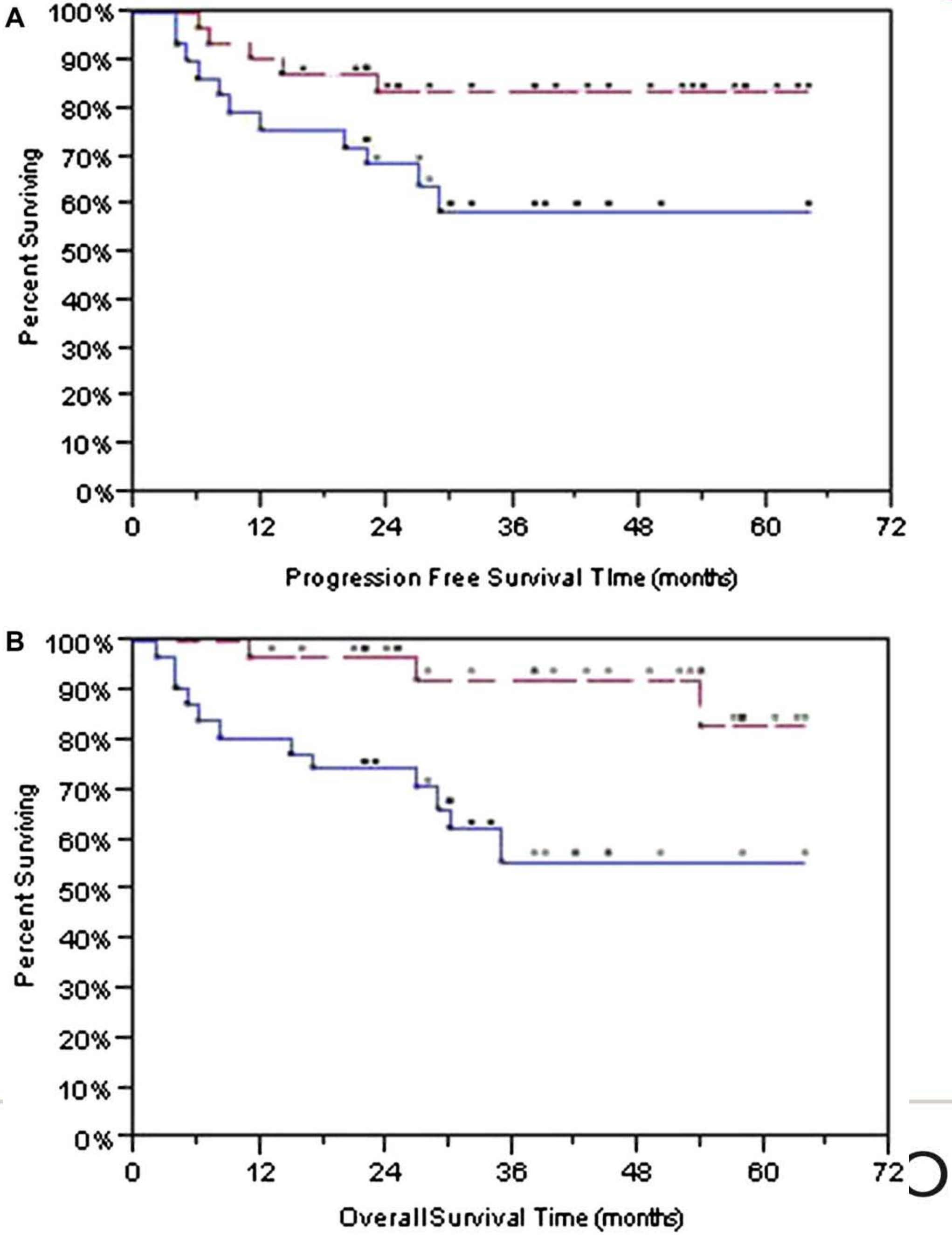

Shukla-Dave A. et al. Int J Radiat Oncol Biol Phys 2012.

Repeated imaging during RT

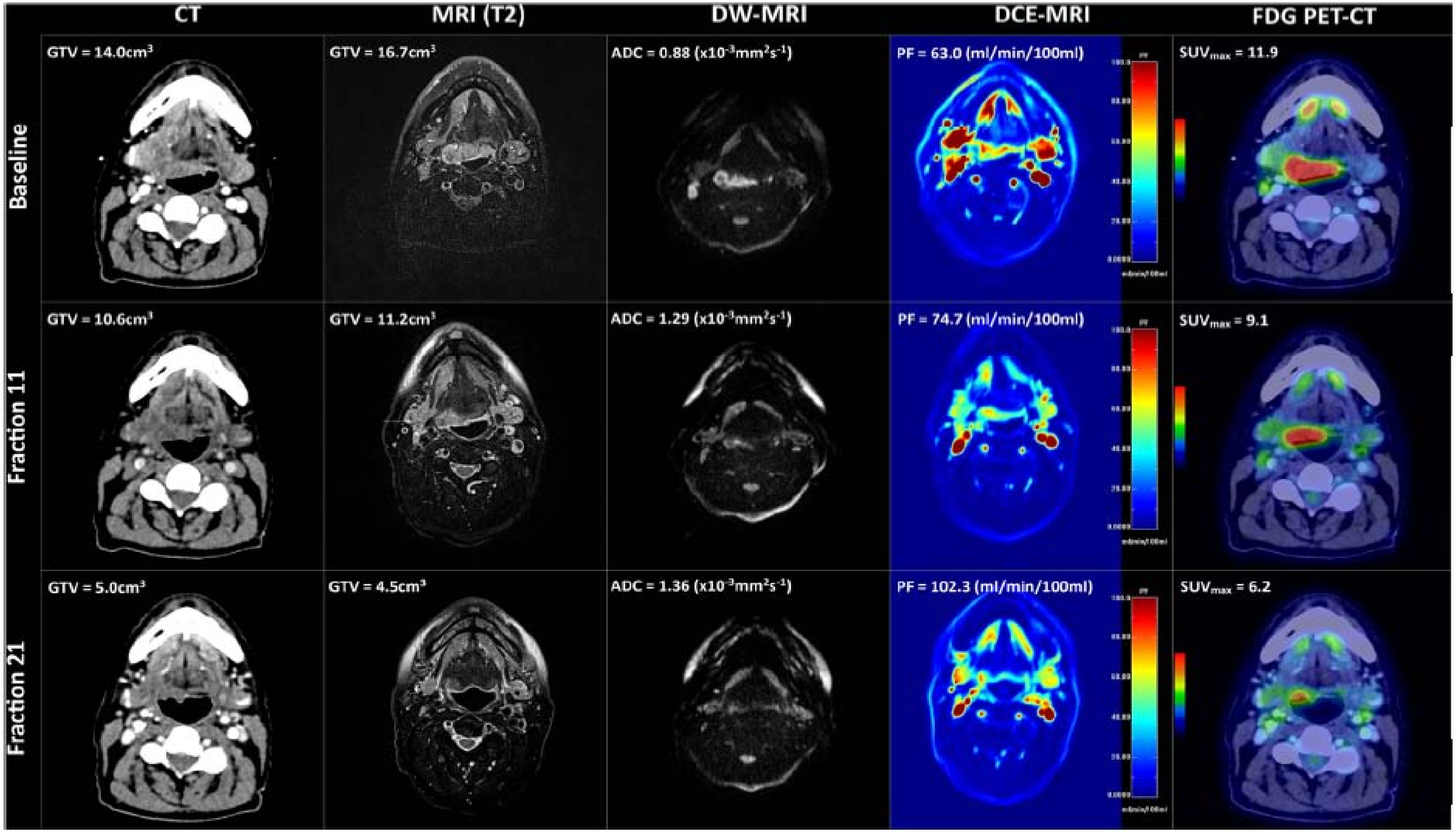

Subesinghe M. et al. BMC cancer 2015.

Ideally on an MRI-RT machine?

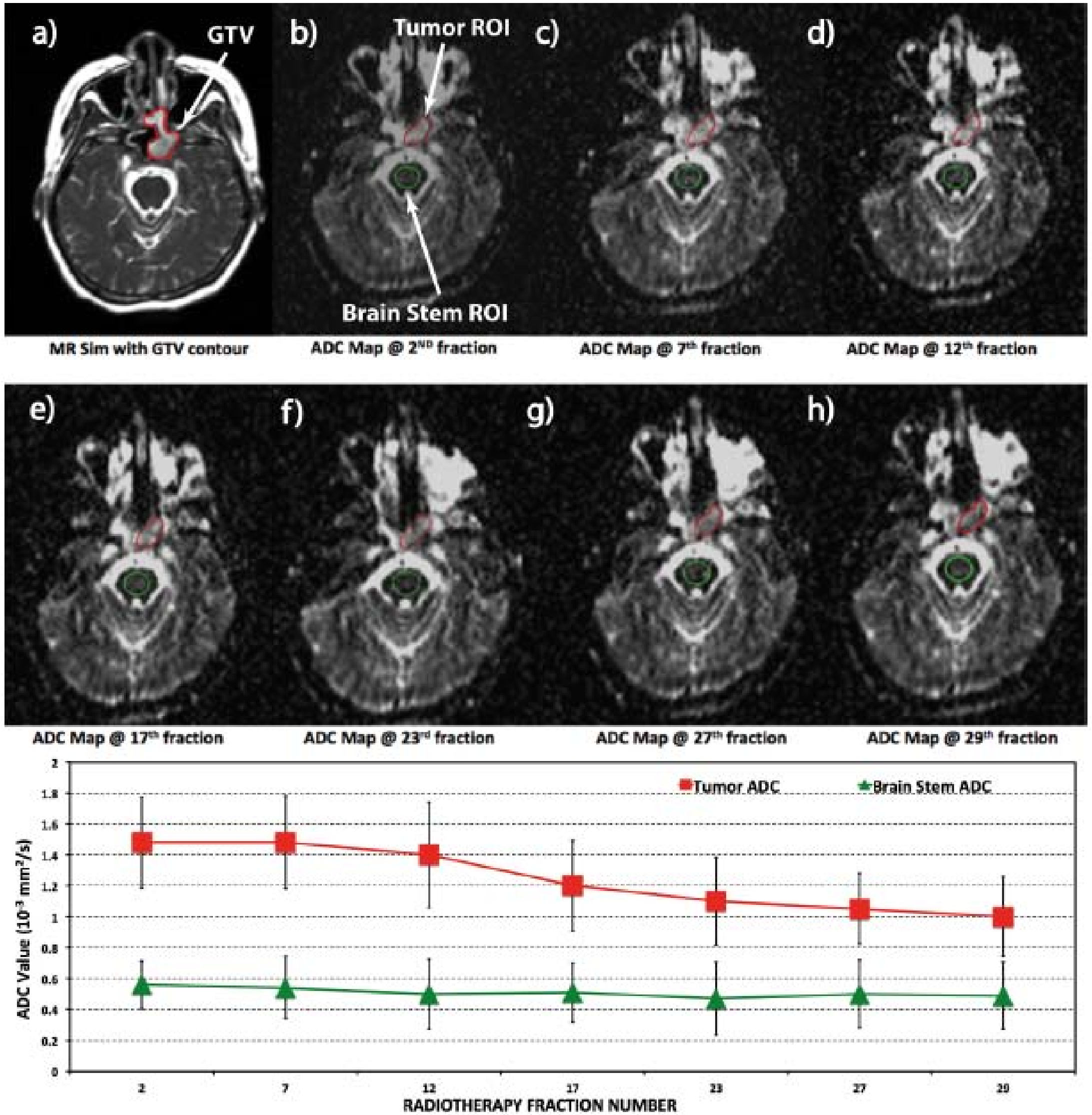

Yang Y. et al. Med Phys 2016.

ESTRO School

5. DWI during follow-up

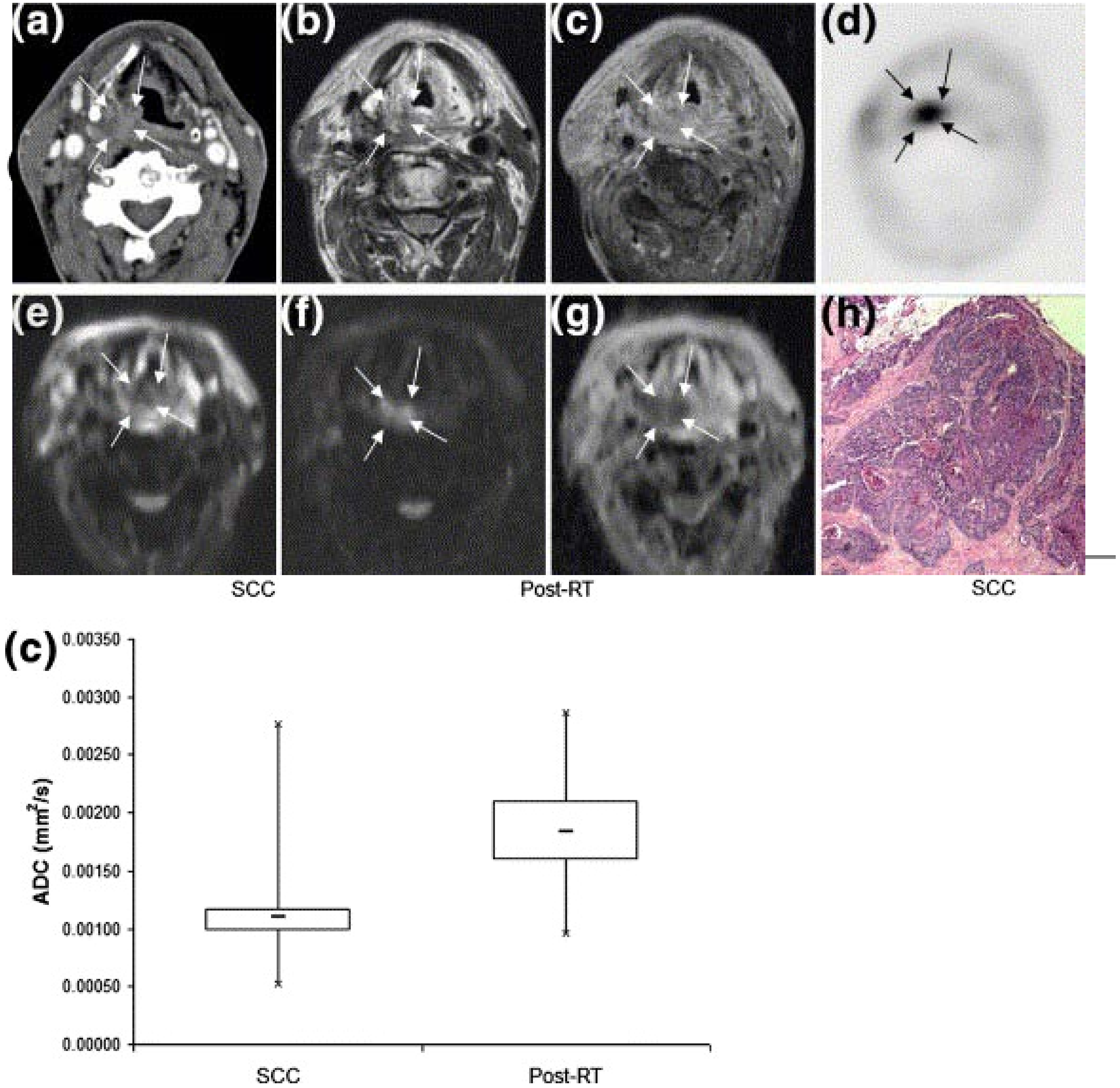

DW-MRI	B0(*)	B1000(†)	ADC(‡)
True-positives at tissue subsite	49	53	70
False-positives at tissue subsite	67	49	7
True-negatives at tissue subsite	104	122	164
False-negatives at tissue subsite	25	21	4
Sensitivity (%)	66.2	71.6	94.6
Specificity (%)	60.8	71.3	95.9
Accuracy (%)	62.4	71.4	95.5

Vandecaveye V. et al. Int J Radiat Oncol Biol Phys 2007.

Clinical example of DWI during follow-up

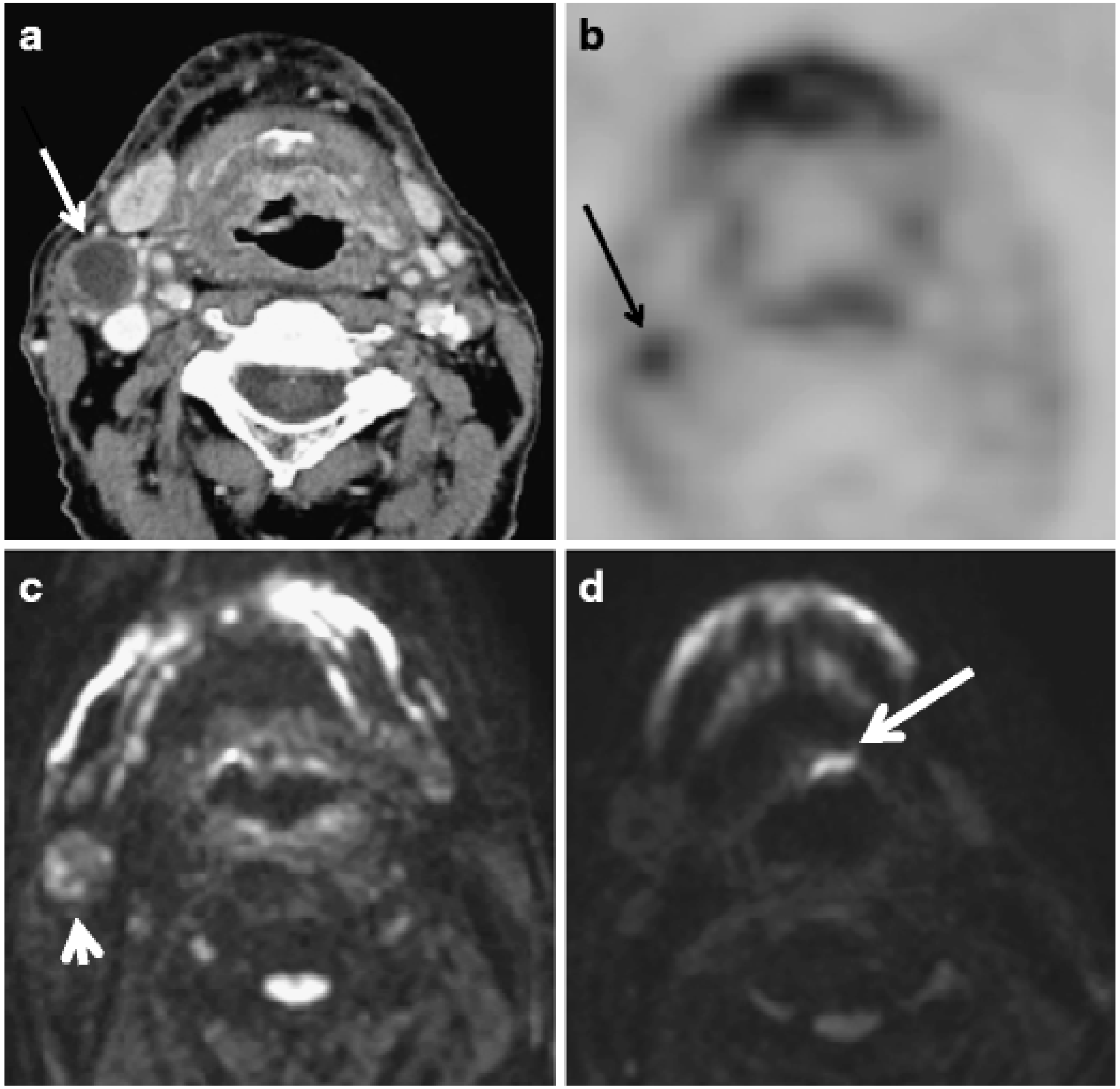

Images courtesy of Prof. V. Vandecaveye

Similar results at Mansoura University (Egypt)

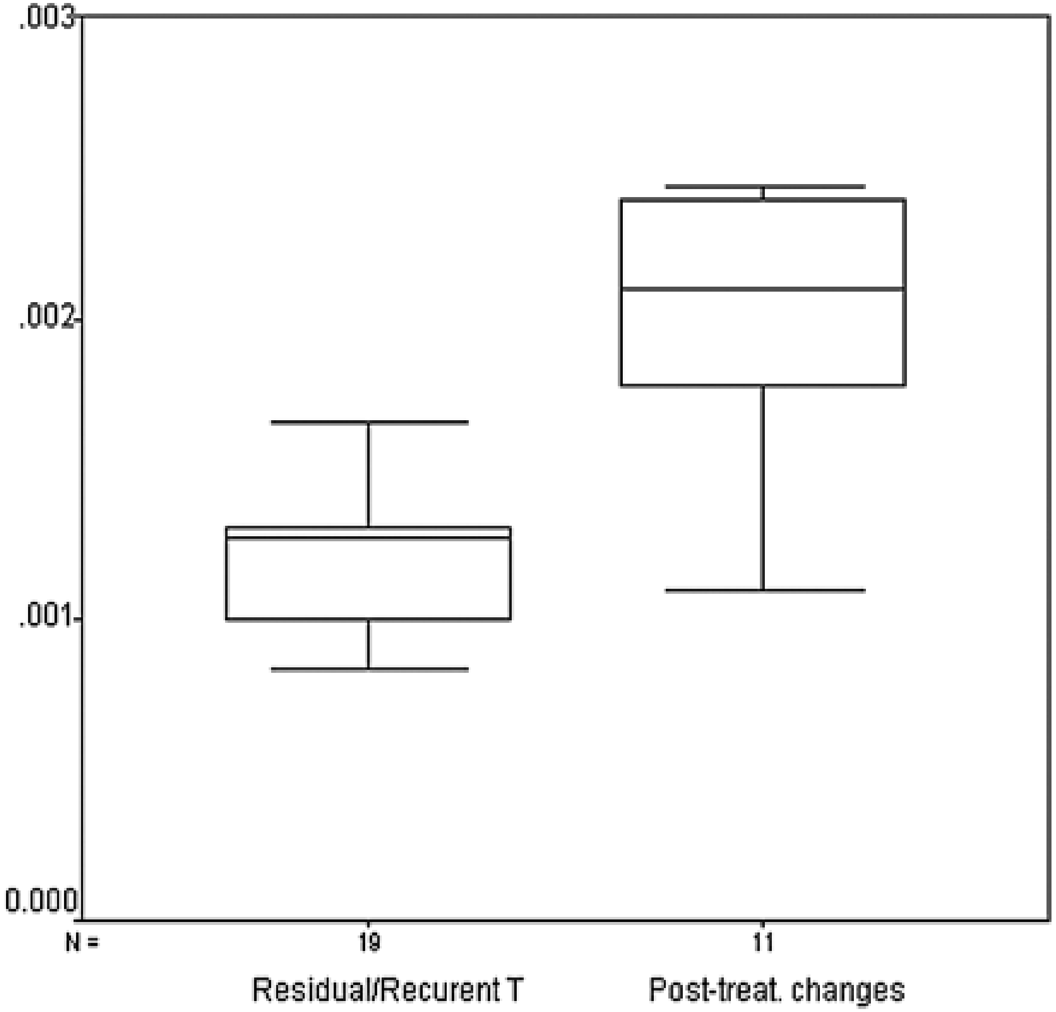

Variable	Range of ADC Value	Mean ADC Value
Residual or recurrent tumor	(0.83–1.65) x 10^{-3} mm^2/s	1.17 ± 0.33 x 10^{-3} mm^2/s
Posttreatment changes	(1.10–2.44) x 10^{-3} mm^2/s	2.07 ± 0.25 x 10^{-3} mm^2/s

Threshold of ADC Value (x10^{-3} mm^2/s)	Sensitivity % (*n*/*N*)	Specificity % (*n*/*N*)	Accuracy %	Positive Predictive Value % (*n*/*N*)	Negative Predictive Value % (*n*/*N*)
≤1.00	37 (7/19)	100 (11/11)	60	100 (7/7)	47 (11/23)
≤1.30	84 (16/19)	90 (10/11)	87	94 (16/17)	76 (10/13)
≤1.50	89 (16/19)	73 (9/11)	83	85 (17/20)	80 (8/10)
≤2.00	100 (19/19)	45 (5/11)	80	76 (19/25)	100 (5/5)
≤2.40	100 (19/19)	9 (1/11)	66	65 (19/29)	100 (1/1)

Abdel Razek A. A. et al. AJNR Am J Neuroradiol 2007.

DCE during follow-up

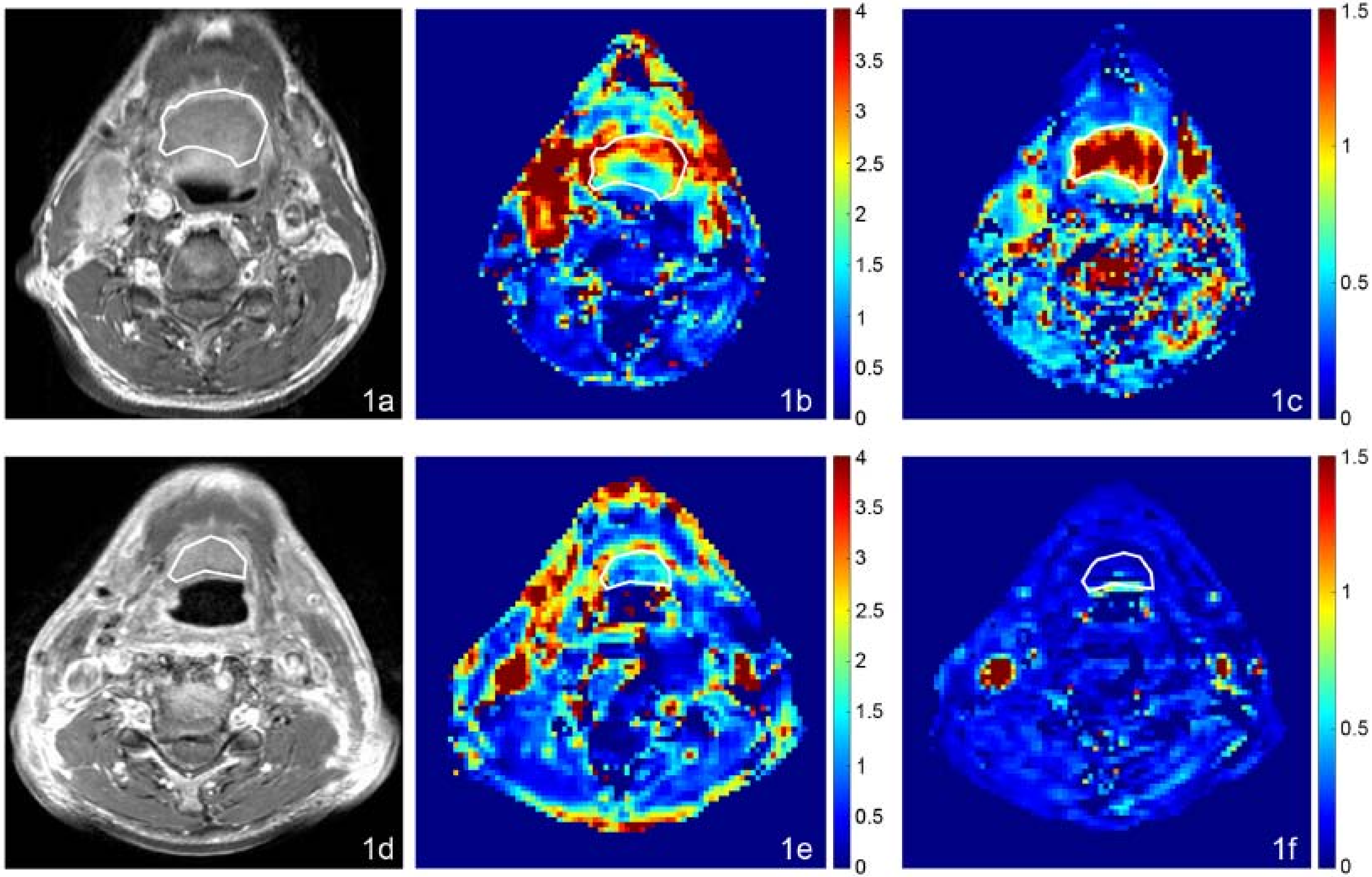

Pre-treatment DCE-MRI did not predict which SCC sites would fail treatment, but post-treatment DCE-MRI showed potential for identifying residual masses that had failed treatment.

King A. et al. Plos One 2016.

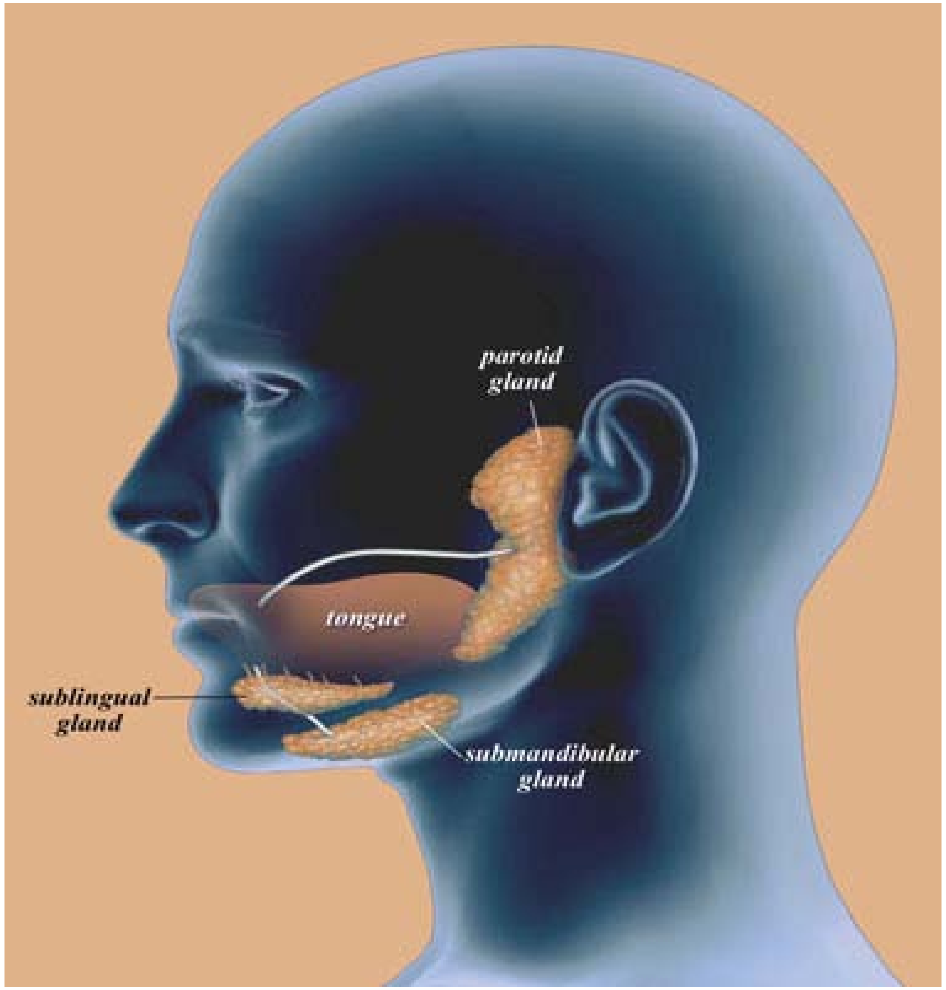

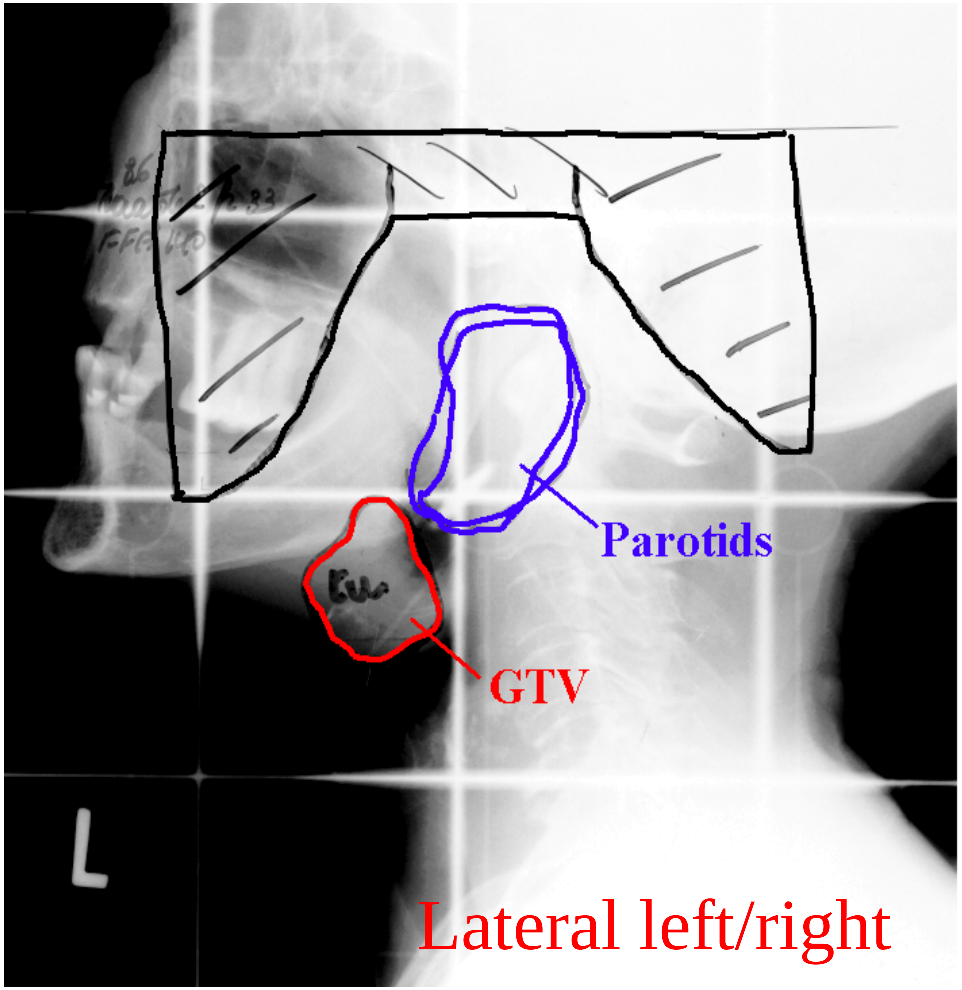

Xerostomia is one of the most common complications of RT for HNC.

Dirix P. et al. Cancer 2006.
Dirix P. et al. Lancet Oncol 2010.

DWI: non-invasive evaluation of salivary gland function

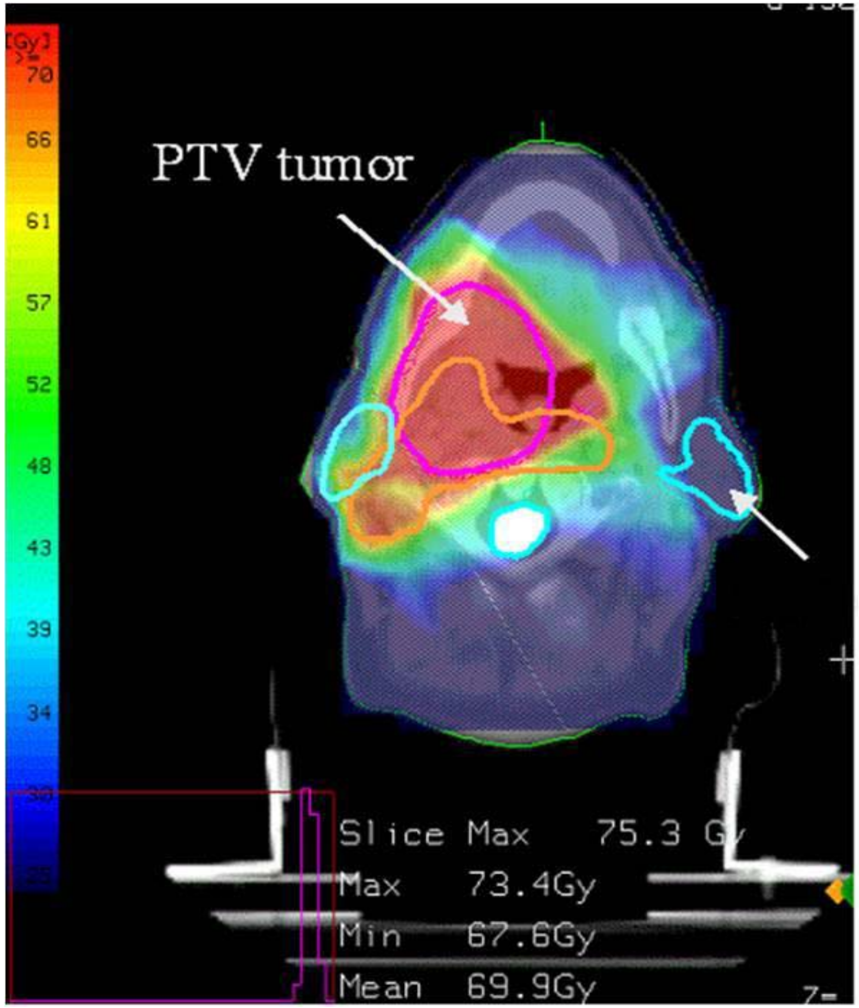

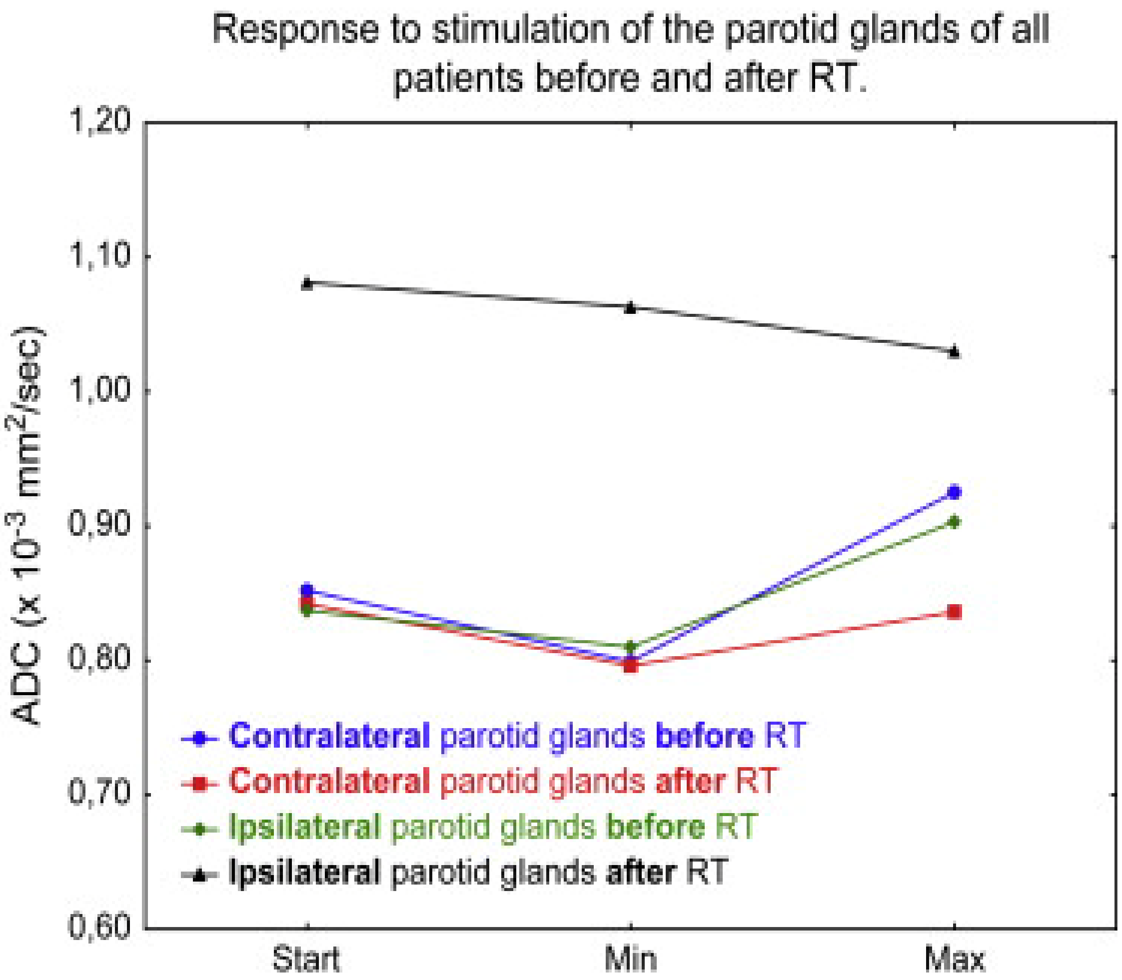

Dirix P. et al. Int J Radiat Oncol Biol Phys 2007.

DWI: non-invasive evaluation of salivary gland function

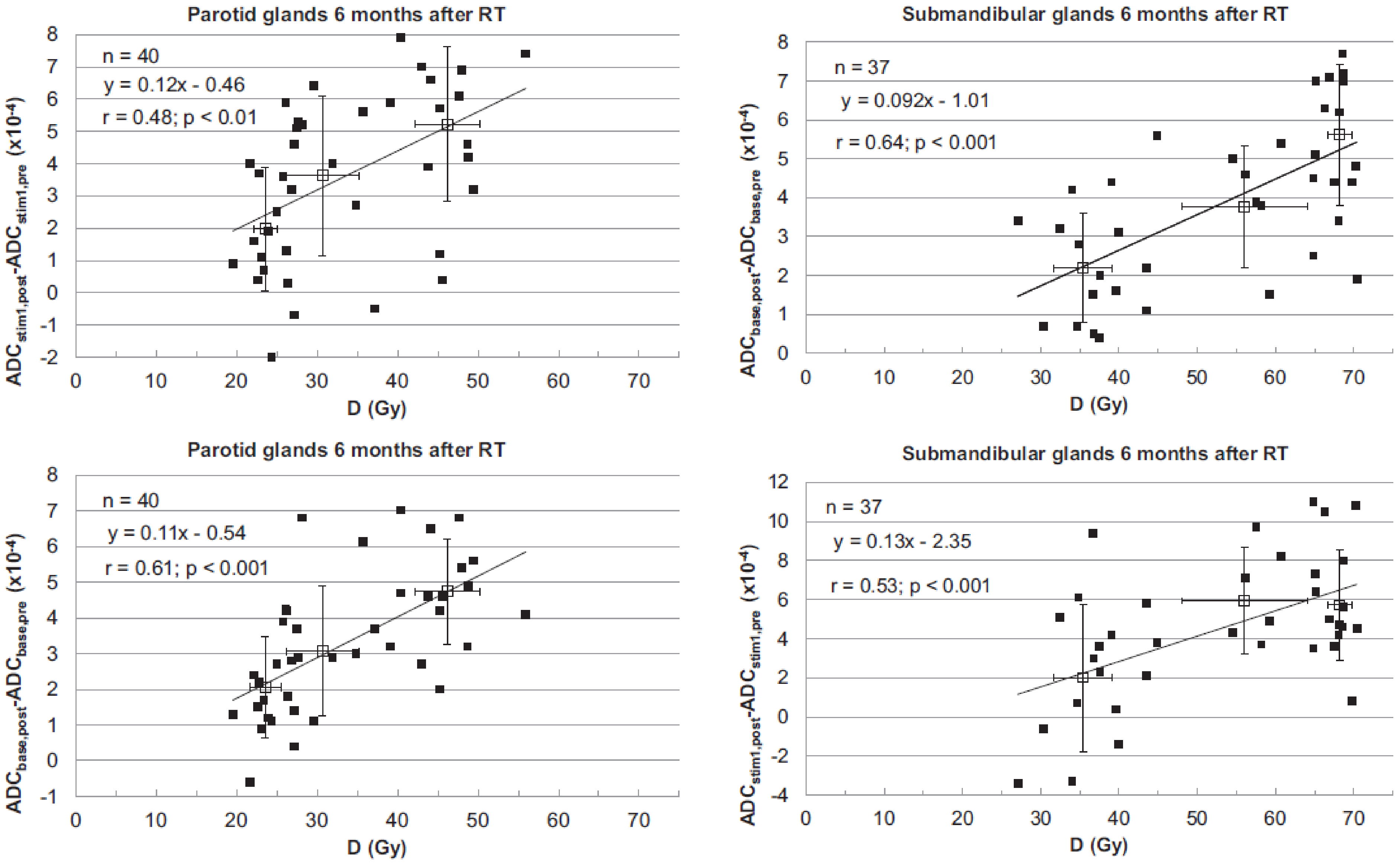

Loimu V. et al. Radiother Oncol 2016.

7. Pitfalls of DWI

Rapid evolution of body imaging protocols

Divergence among and between vendors on data measurements/analysis and lack of transparency on how measurements are made

No accepted standards for measurements and analysis

Multiple data acquisition protocols depending on body part and usage of data

Qualitative to quantitative assessments

Lack of understanding of DW-MRI at a microscopic level

Multiexponential decay components which affect the calculated ADC values

Incomplete validation and documentation of reproducibility

Divergent nomenclature and symbols

Lack of multicenter working methodologies, accepted quality assurance (QA) standards, and physiologically realistic phantoms

Padhani A.R. et al. Neoplasia 2009.

Registration (1)

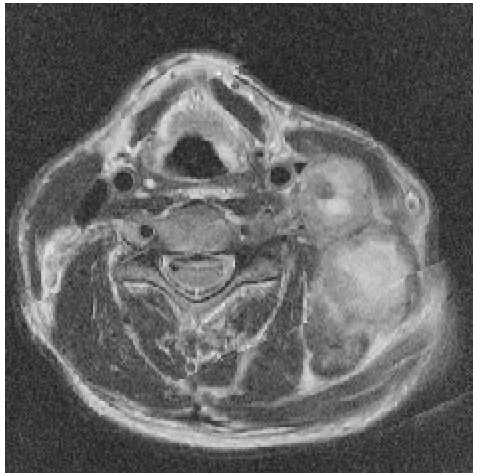

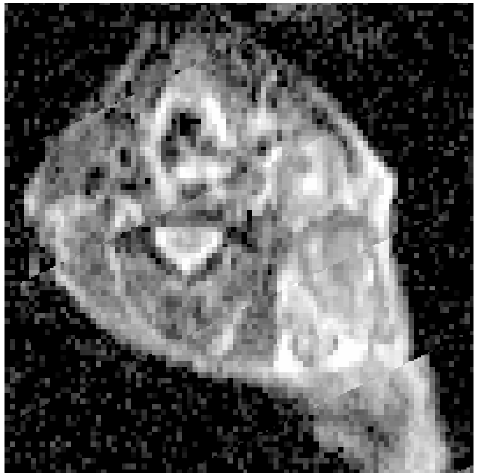

▲

Non-rigid registration needed for distortion

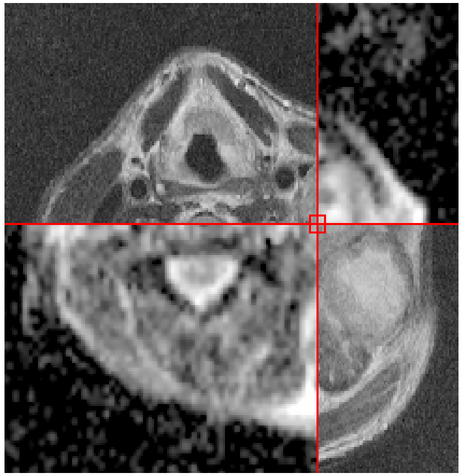

Registration (2)

	Mean error	SD	Median error	Maximal error
Original SSD	7.78 mm	4.15 mm	7.10 mm	20.26 mm
Final SSD	2.10 mm	1.39 mm	1.83 mm	6.53 mm

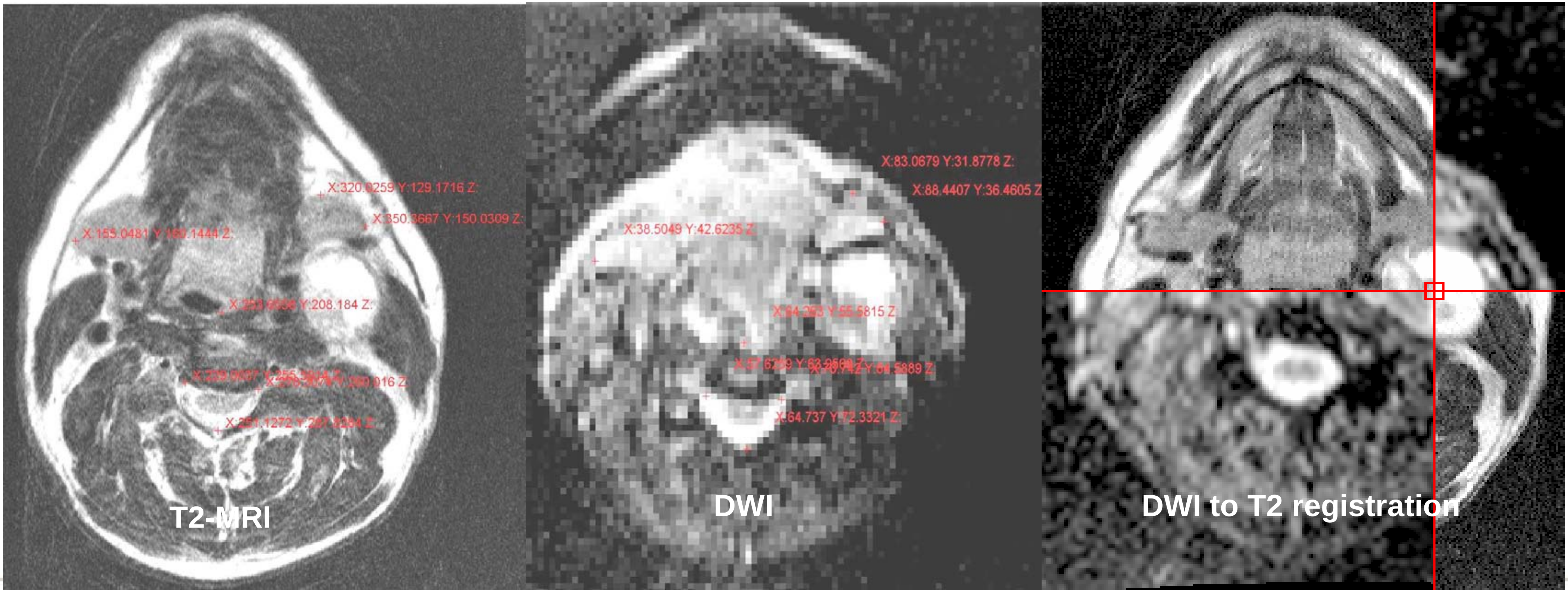

Registration (3)

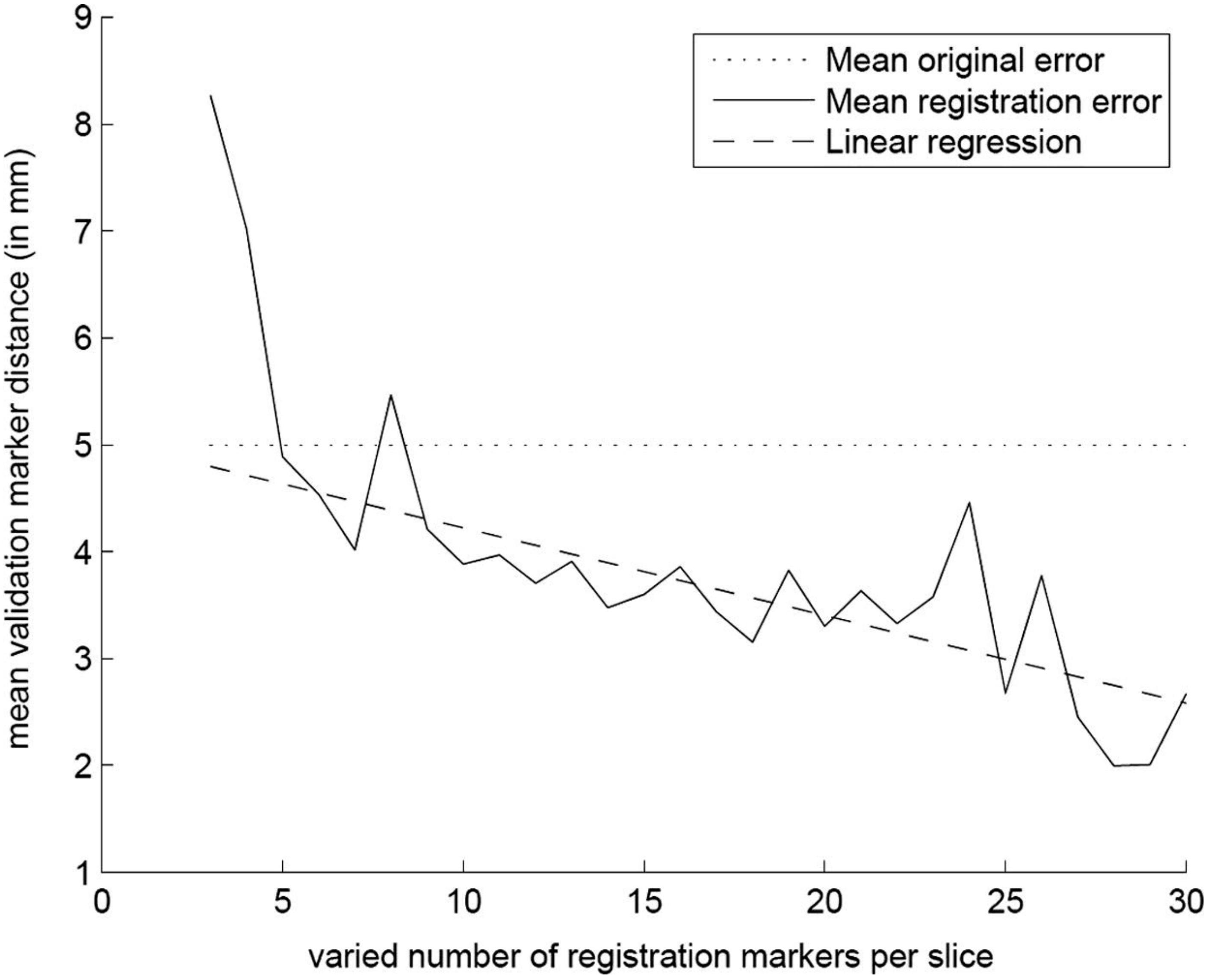

Lambrecht M. et al. Radiother Oncol 2014.

Conclusions

- **Important role for anatomical MRI, especially in base of skull and oropharyngeal cancer.**
- **DWI and DCE-MRI could guide dose-painting and early response assessment.**
- **Standardisation of technique (b-values), interpretation, and registration.**

Table 1 Key themes emerging from preclinical and clinical data on diffusion MRI in cancer.

Key themes	Strength of evidence*
Apparent diffusion coefficient (ADC) maps generated with low b-values are dominated by diffusion-related flow information	3
ADC maps provide information on the cellularity of tissues that can be used for lesion characterization	3
Pretherapy ADC maps may indicate the outcome of therapy	2
There is a transient decrease in ADC at the start of therapy that probably represents cellular swelling	1
Therapy-induced increases in ADC coincide with the onset of cell lysis and necrosis, and changes in ADC values predict clinical outcome for some tumors	4/2
Apoptotic cell removal and/or repopulation by resistant cells may cause decreases in ADC at the end of therapy	3

*Strength of evidence scale (1–5): weak–moderate–substantial–firm–definite (scale based on authors' perceptions of the literature used for this Review).

Patterson D.M. et al. Nat Clin Pract Oncol 2008.

Introduction to Computed Tomography

Francesco Pisana

German Cancer Research Center (DKFZ), Heidelberg, Germany

Index of Contents

- **Introduction:**
  - Overview and components
  - History
- **Physics:**
  - X-ray generation
  - X-ray attenuation
  - X-ray detection
- **Image reconstruction:**
  - Filtered back-projection
  - Algebraic reconstructions
- **Noise and artifacts:**
  - Noise
  - Motion artifacts
  - Beam hardening artifacts
- **Dose and image quality:**
  - mAs modulation
  - kV selection

Overview and Components

Computed tomography shows the spatial distribution of X-ray attenuation in our body.

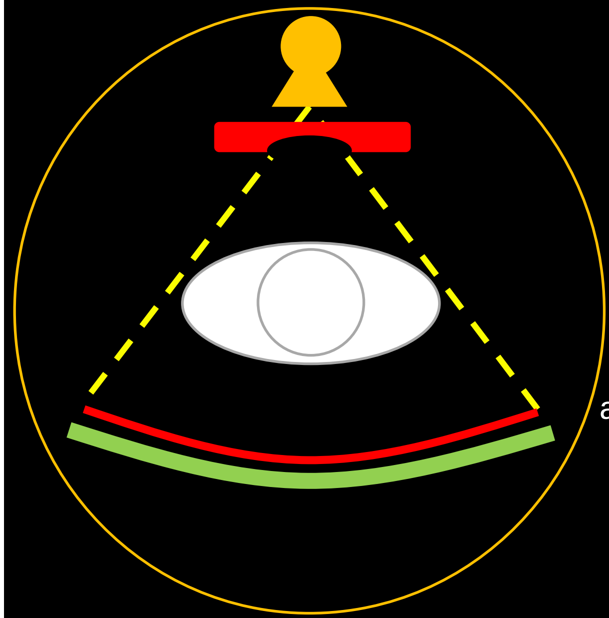

Overview and Components

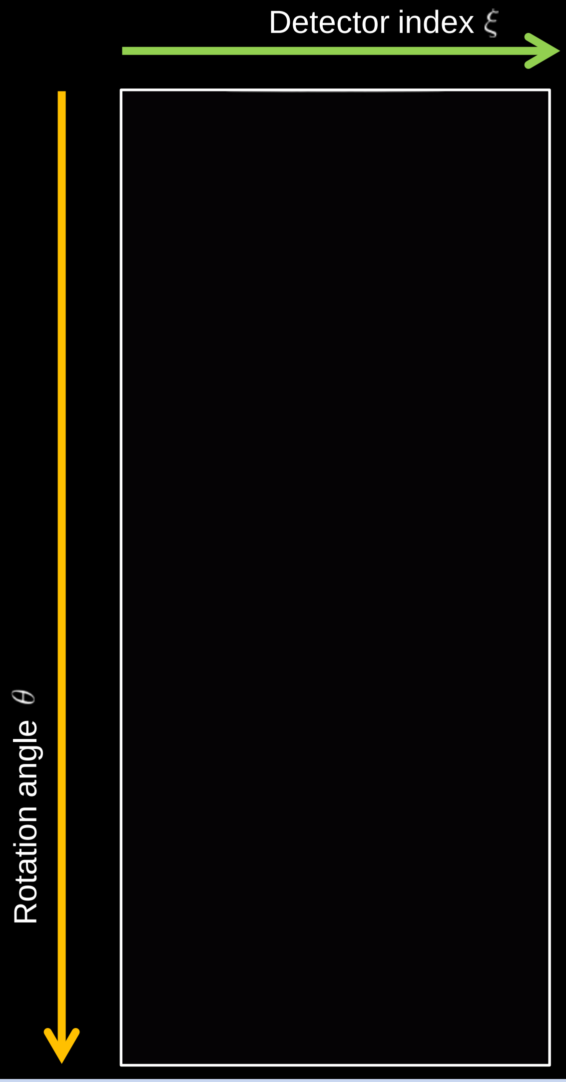

Sinogram

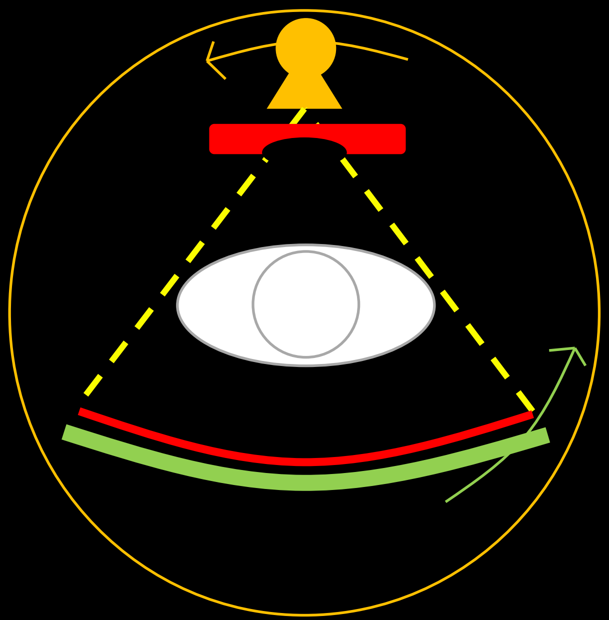

History

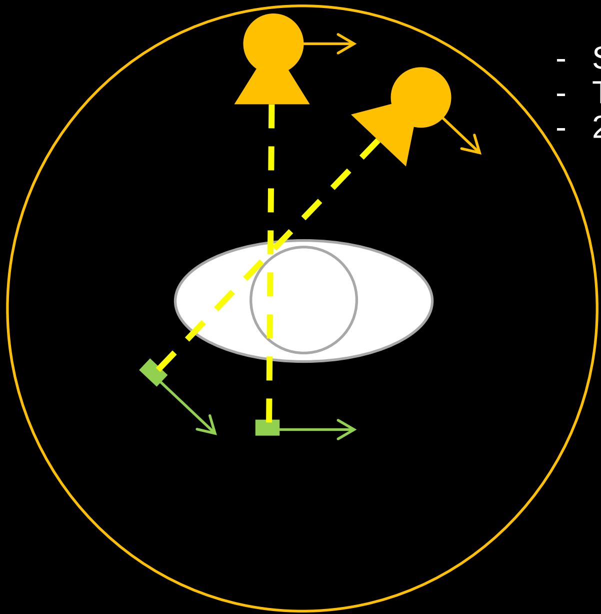

- Single detector
- Translation + rotation
- 20-30 min

- Multi-detector
- Translation + rotation
- 2 min

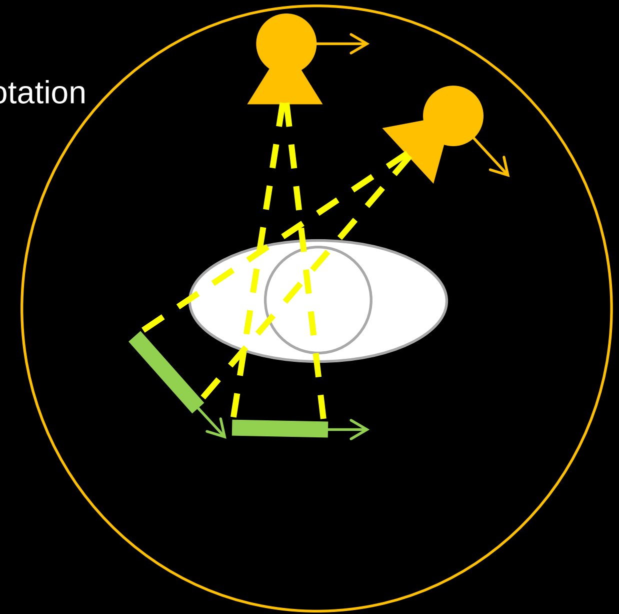

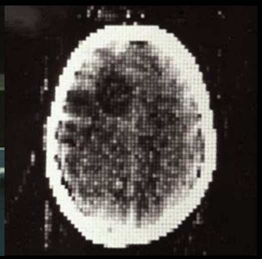

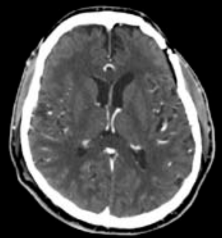

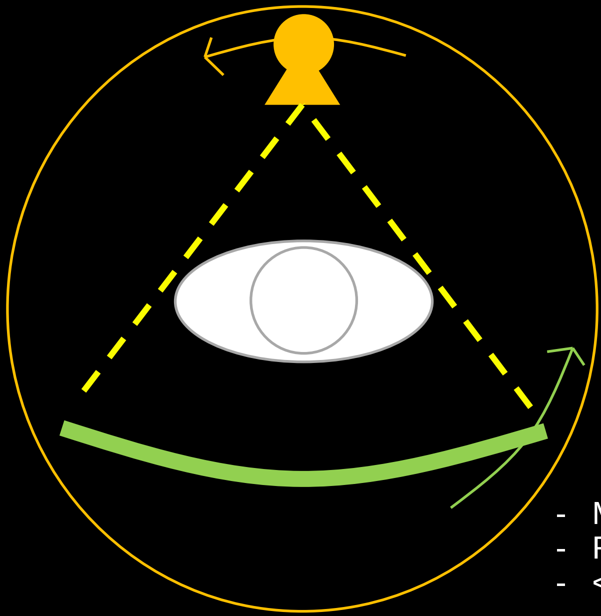

- Multi-detector
- Rotation
- < 1 s

- Full multi-detector ring stationary
- Tube rotation
- < 1 s

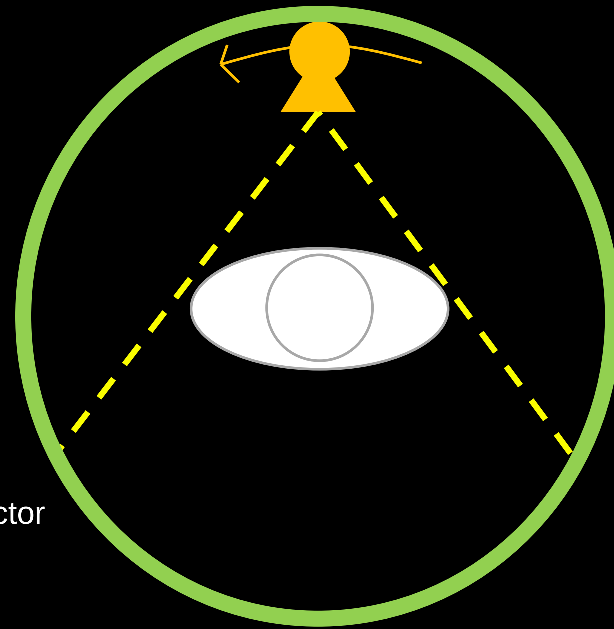

Detector Coverage Along z-axis

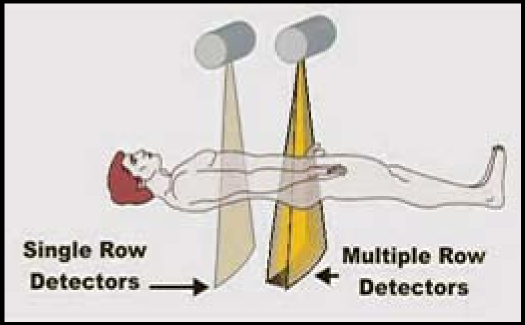

Pitch value:

$$\text{pitch} = \frac{\text{Table movement in one rotation}}{\text{Coverage}}$$

Nowadays CT

Procedure:
Transcatheter aortic valve implantation (TAVI)

Patient age: 80 years

Tube voltage: 80 kV
Current: 340 ref mAs/rot

Rotation time: 0.25 s
Pitch: 3.2
Slice thickness: 0.75 mm
Scan length: 557 mm
Scan time: 0.76 s
Scan speed: 737 mm/s

Kernel : B40
Recon: ADMIRE 3

CTDIvol: 2.7 mGy
DLP: 162 mGy·cm
Effective dose: 2.3 mSv

Case information

Axial slices, *C* = 0 HU, *W* = 1500 HU

Volume Rendering

Index of Contents

- **Introduction:**
  - Overview and components
  - History
- **Physics:**
  - X-ray generation
  - X-ray attenuation
  - X-ray detection
- **Image reconstruction:**
  - Filtered back-projection
  - Algebraic reconstructions
- **Noise and artifacts:**
  - Noise
  - Motion artifacts
  - Beam hardening artifacts
- **Dose and image quality:**
  - mAs modulation
  - kV selection

X-ray Spectrum Generation

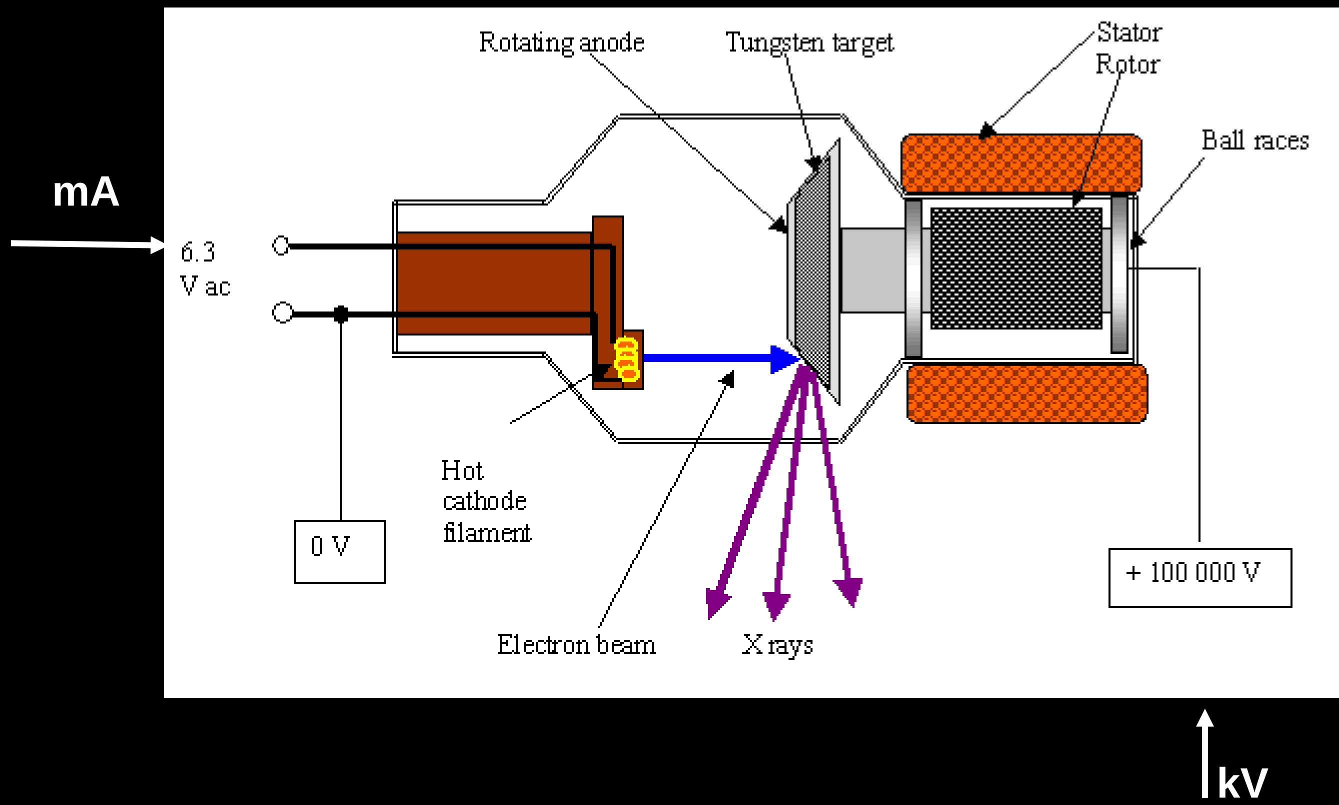

X-ray Spectrum Generation

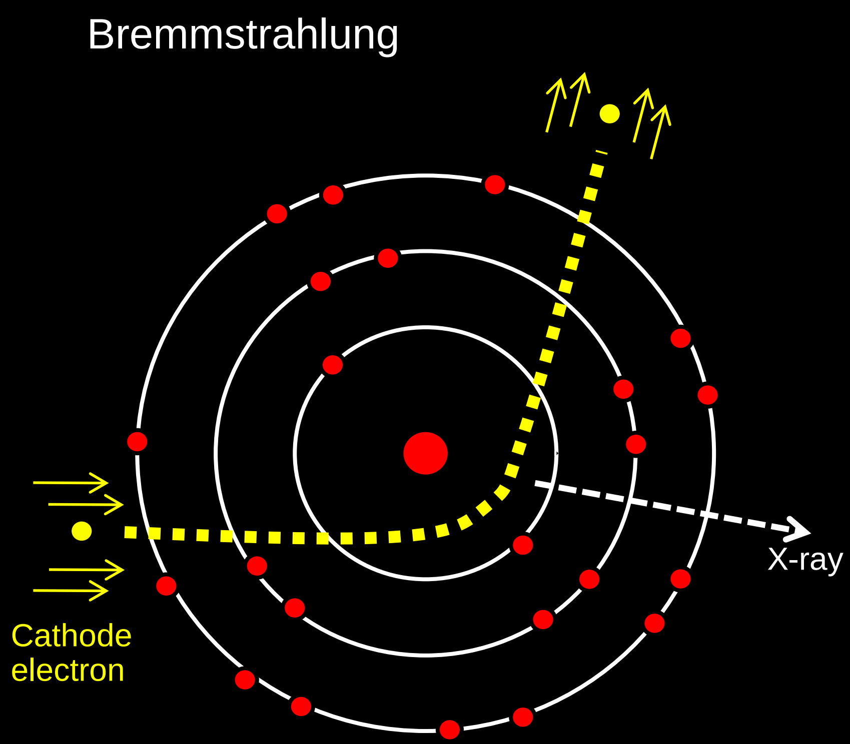

Energy of photons eV =
electron charge (e) · Voltage (V)

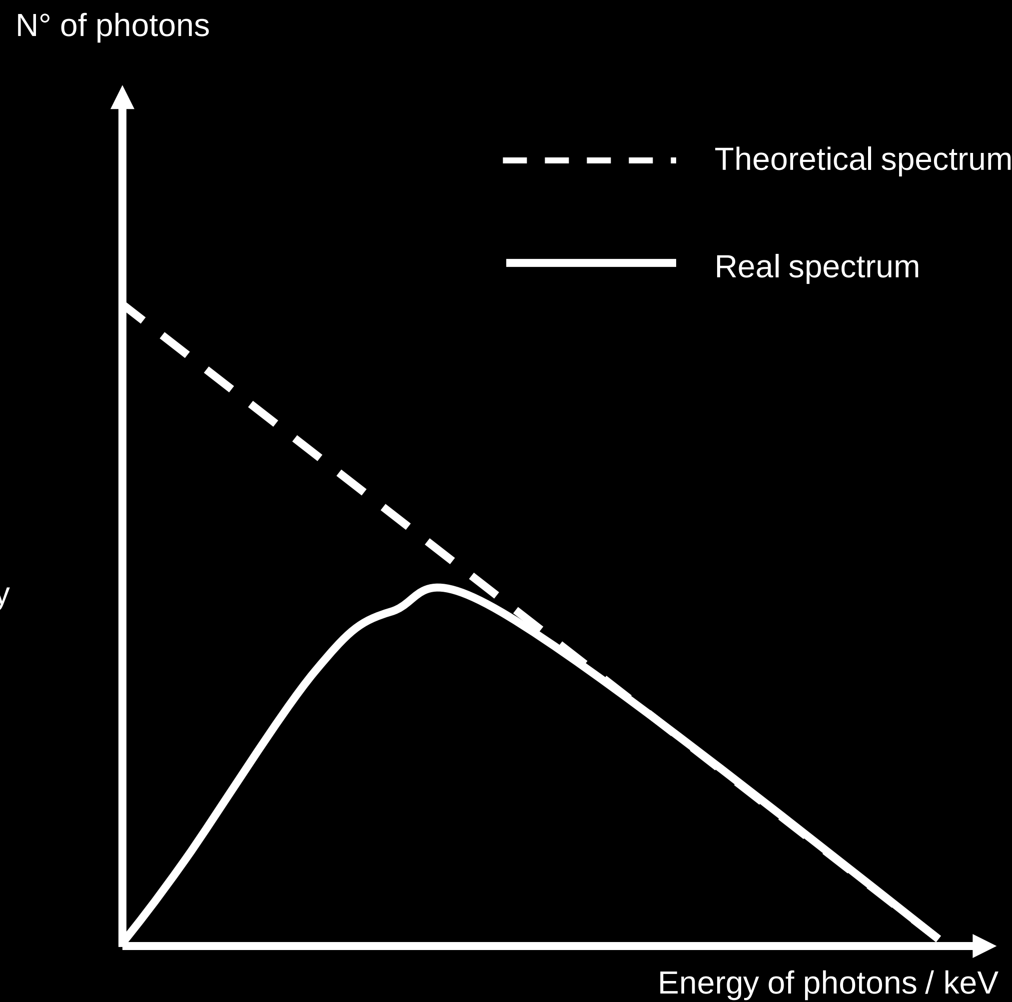

X-ray Spectrum Generation

Characteristic radiation

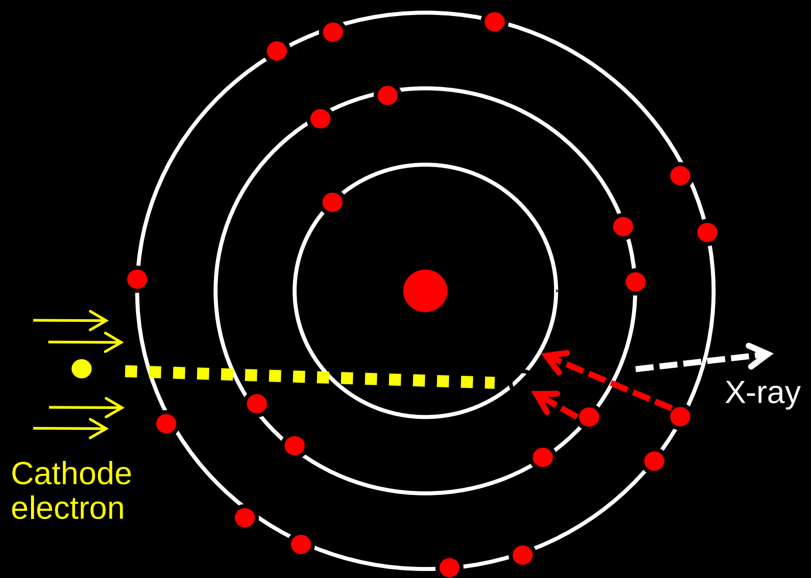

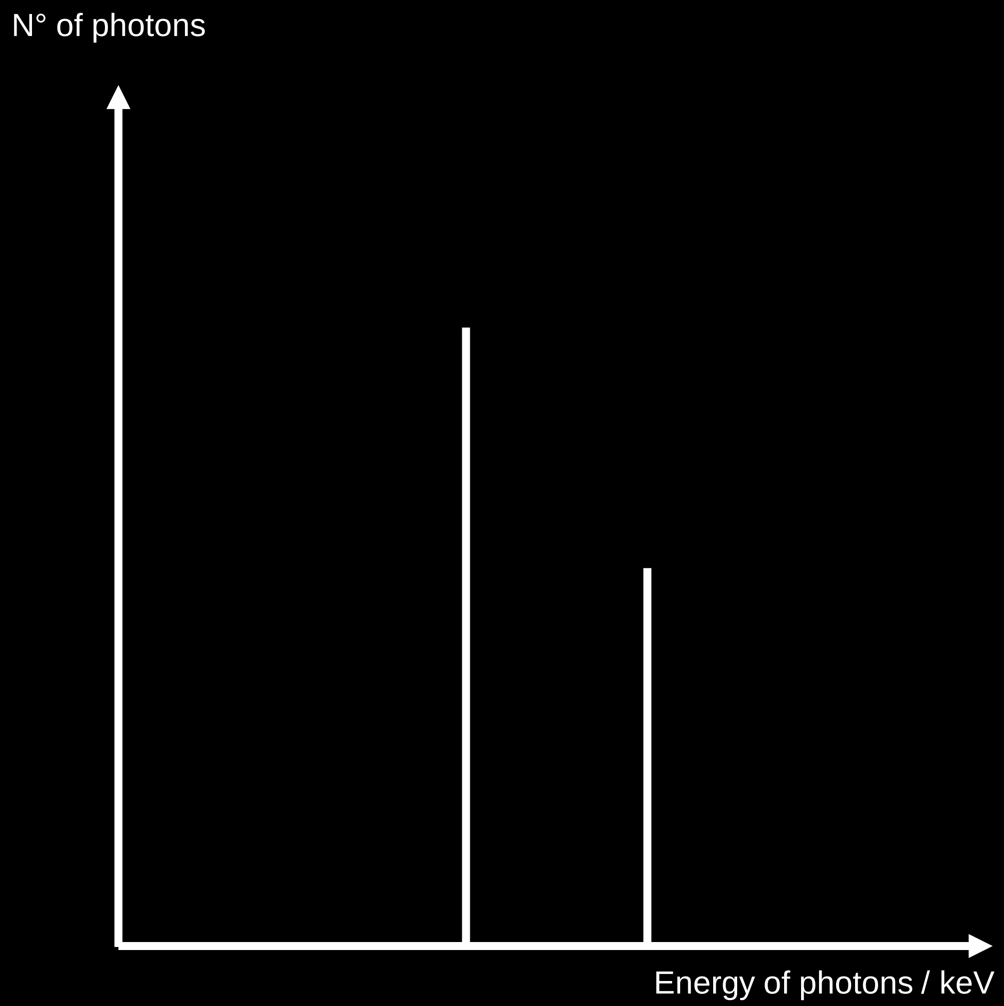

X-ray Spectrum Generation

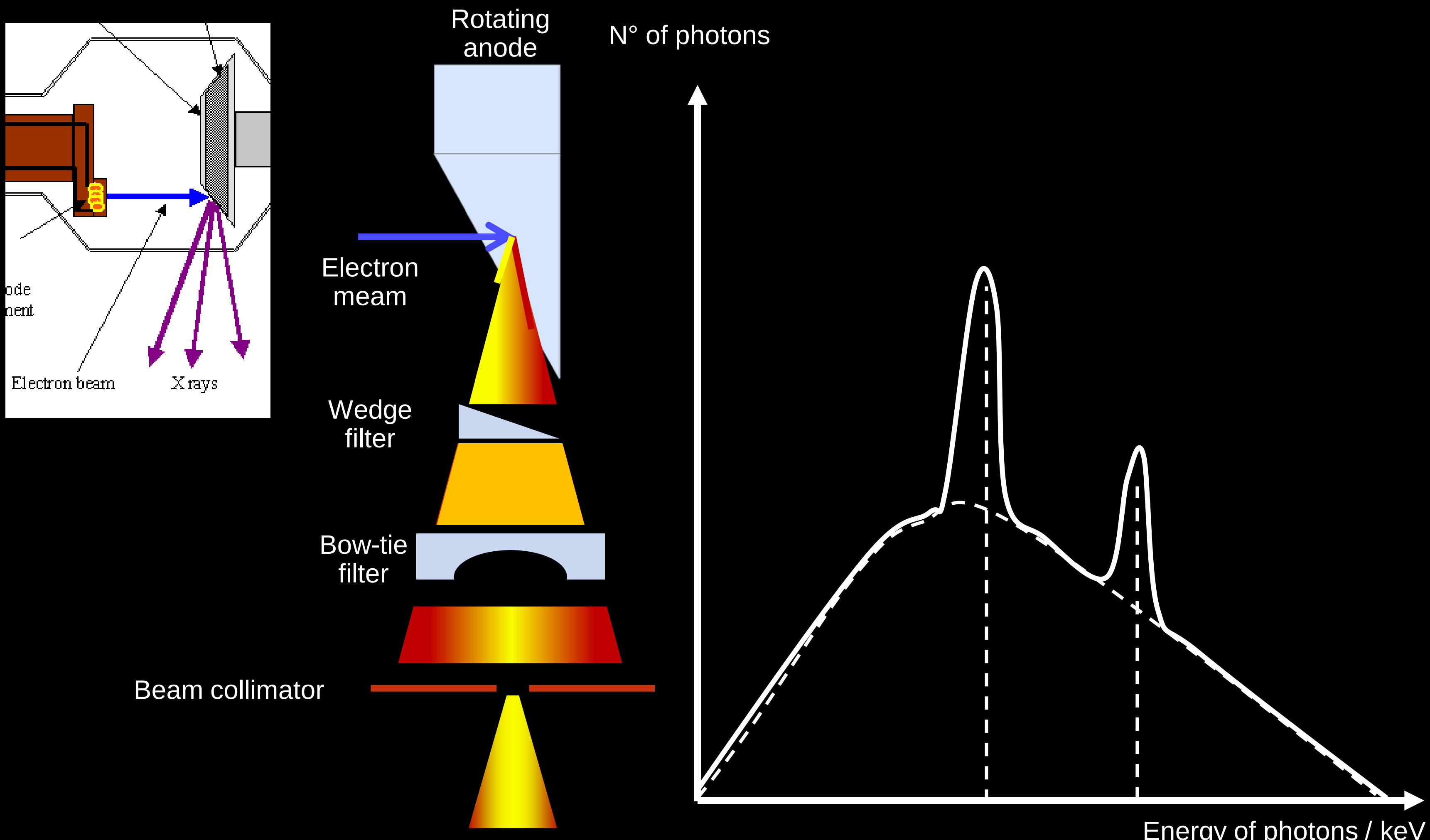

dkfz.

X-ray Spectrum Generation

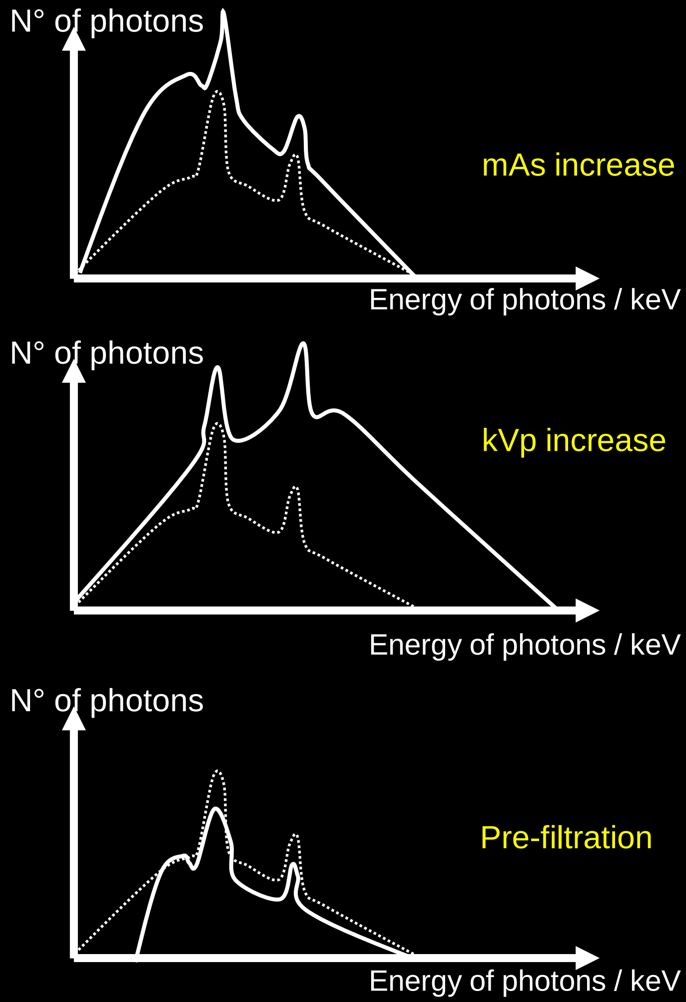

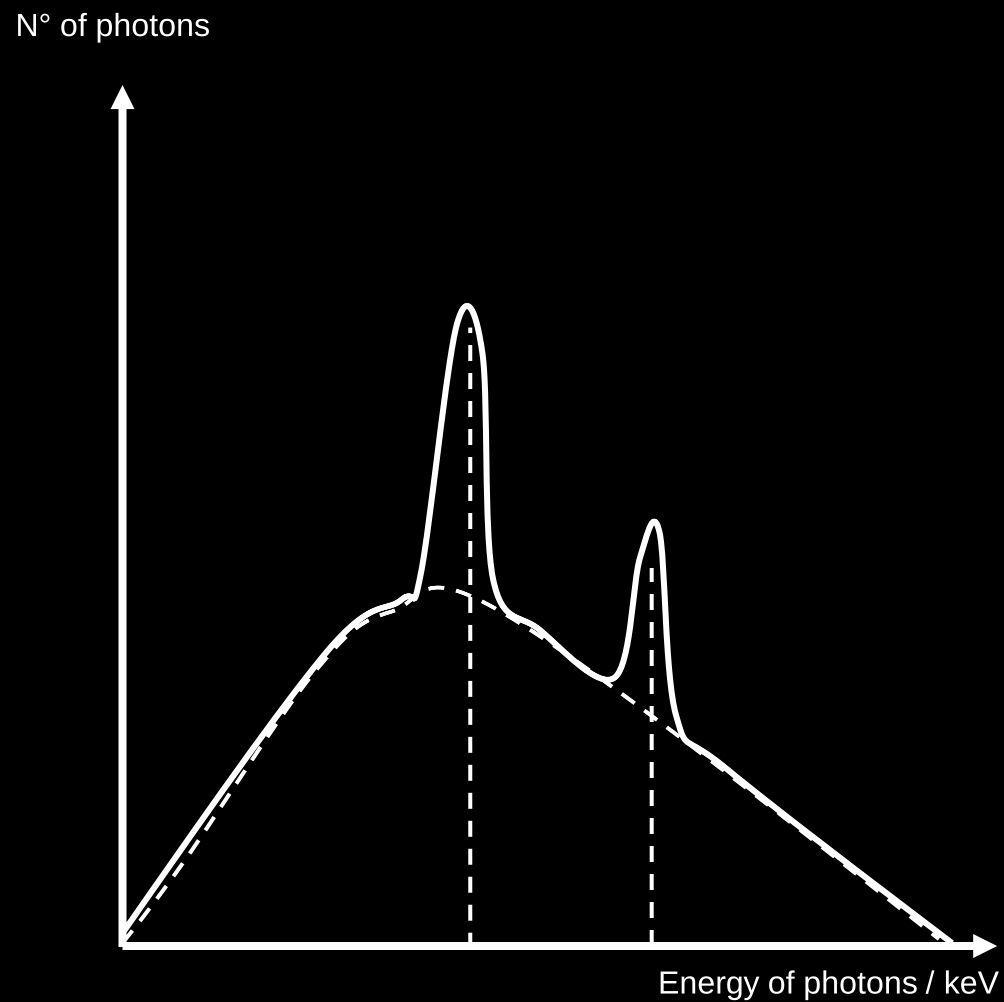

X-ray Attenuation

- Beer's law:

$$I = I_0\, e^{-\int_0^{\mathrm{keVp}} \int_0^L \mu(x,\mathrm{E}) dx\, dE}$$

Used for filtered back-projection: $I = I_0\, e^{-\int_0^L \mu(x) dx}$

- Attenuation coefficient:

$$\mu_x(E) = x_{\mathrm{R}}\, f_{\mathrm{R}}(E) + x_{\mathrm{P}}\, f_{\mathrm{P}}(E) + x_{\mathrm{C}}\, f_{\mathrm{C}}(E) + x_{\mathrm{PP}}\, f_{\mathrm{PP}}(E)$$

$$\mu_x(E) \sim \rho_x \frac{\mathrm{N_A}}{A_x} Z_x^4 f_{\mathrm{P}}(E) + \rho_x \frac{\mathrm{N_A}}{A_x} Z_x f_{\mathrm{C}}(E)$$

$$\mu_x(E) \sim \rho_x \frac{\mathrm{N_A}}{A_x} Z_x \left(Z_x^3 \frac{1}{E^3} + f_{\mathrm{KN}}(E) \right)$$

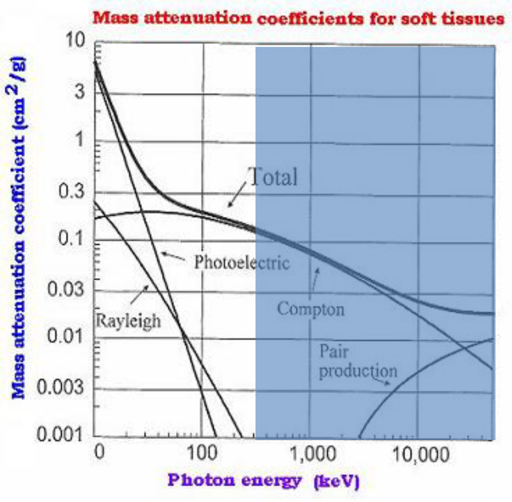

Where f_{KN} is the Klein-Nishina function

X-ray Detection

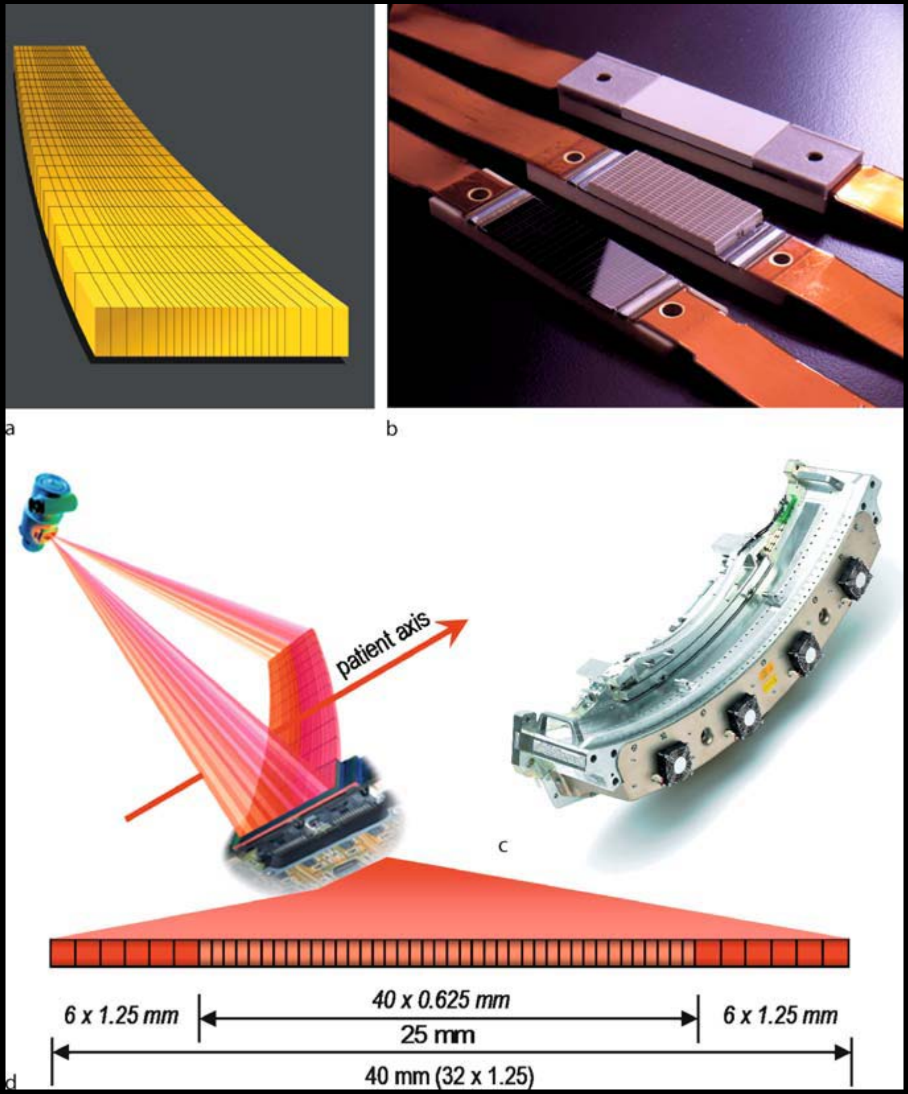

X-ray Detection

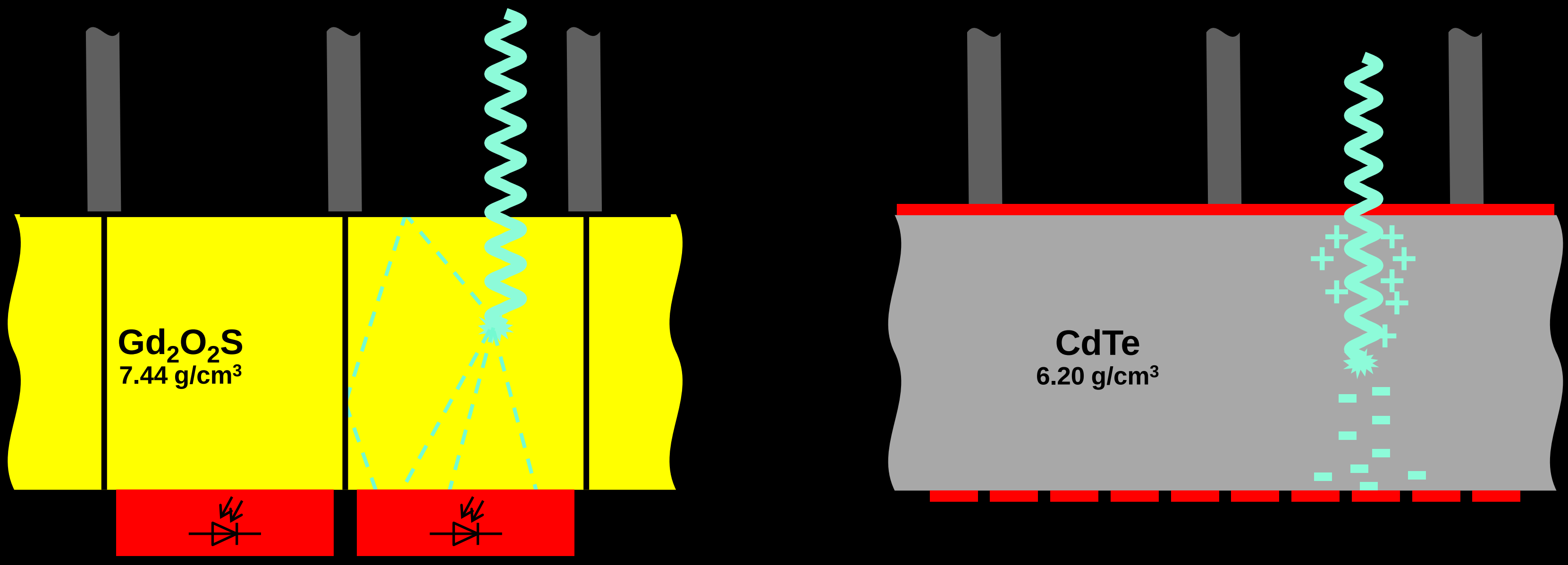

X-ray Detection

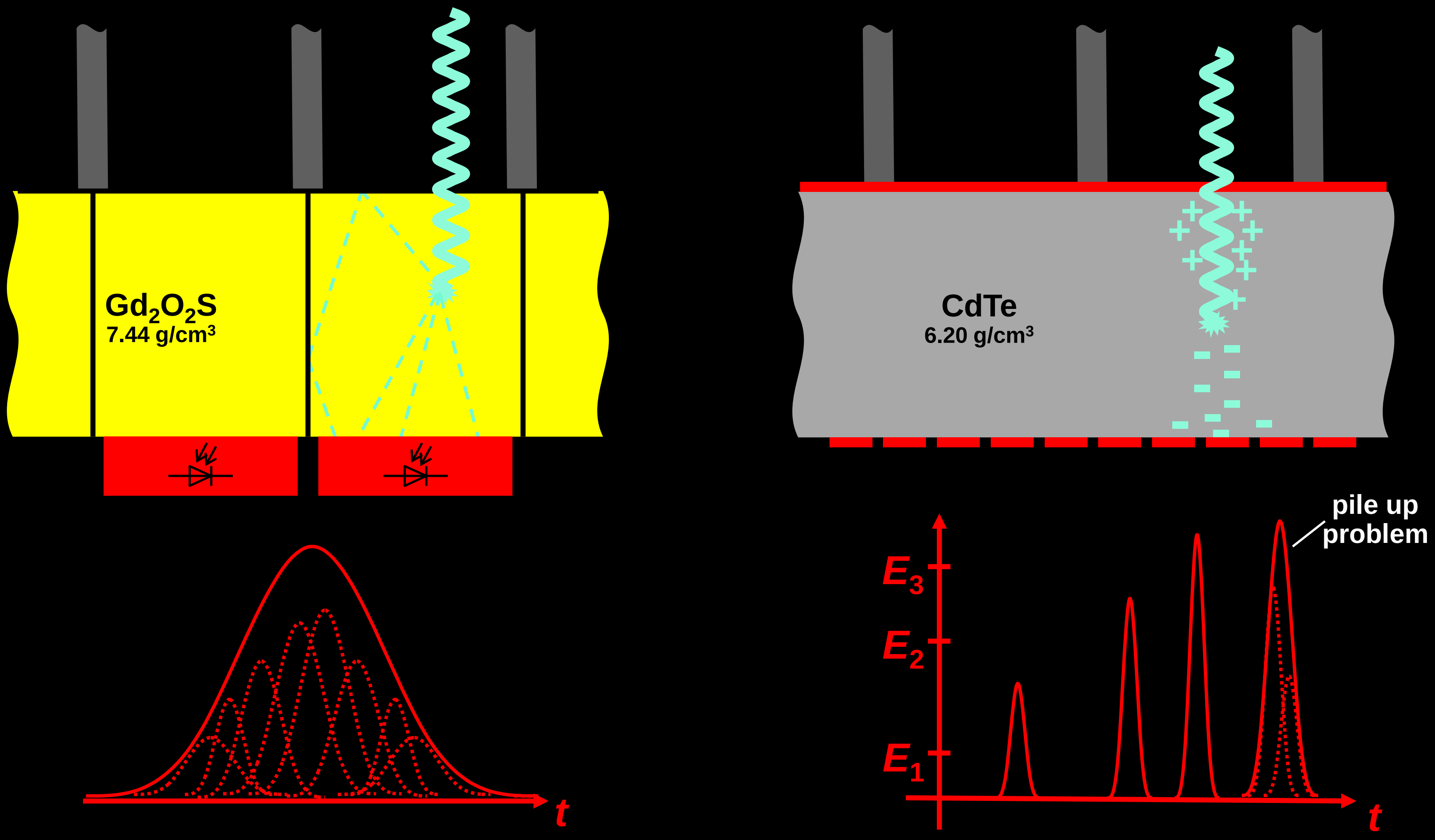

Index of Contents

Sinogram Creation

Rebinning:

All projections from different angles are re-sorted in such a way to be parallel.

This means only the central projection is considered for each view angle theta, while all the others are parallel to it and come from different rotation steps.

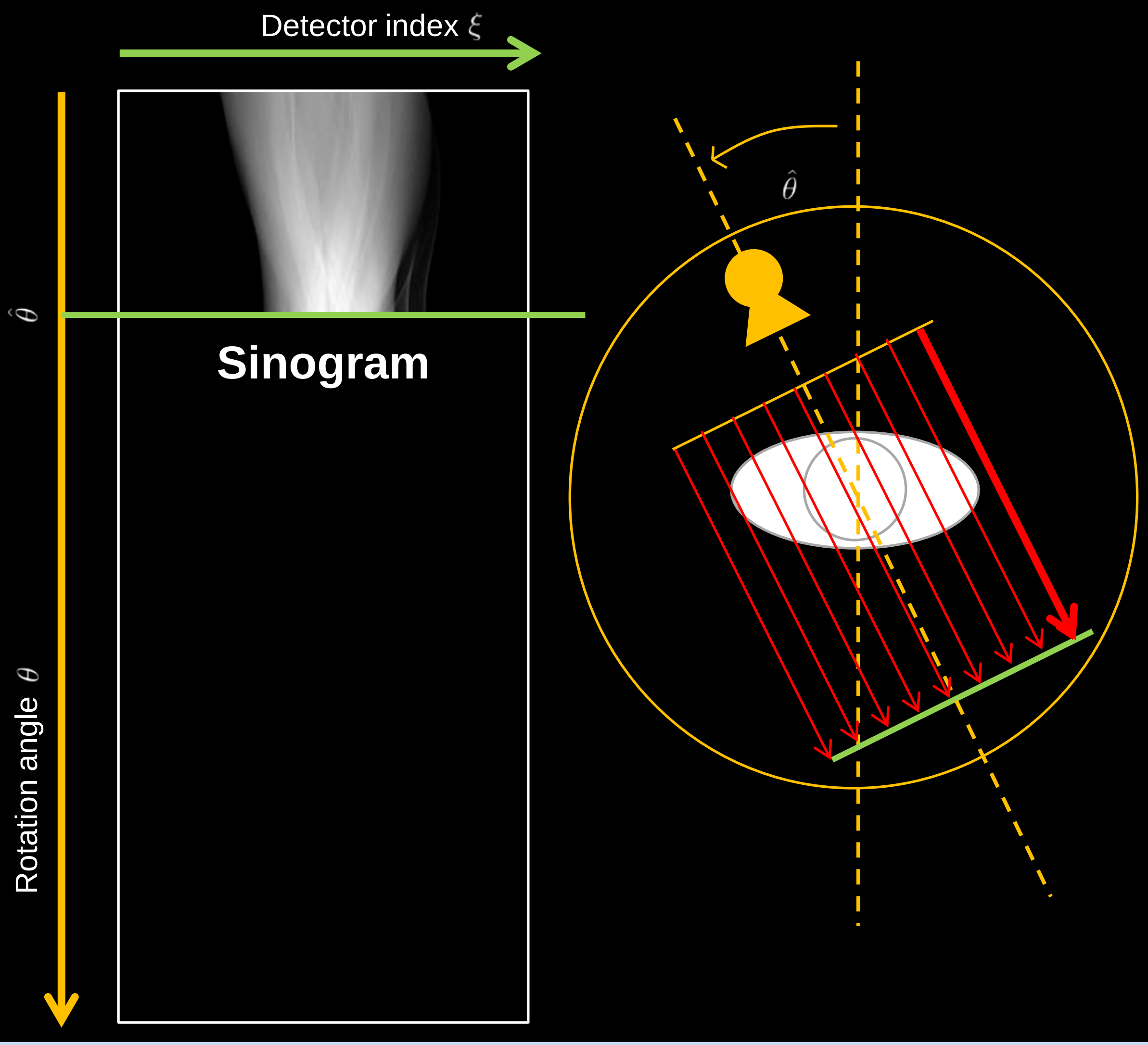

Sinogram Creation

Rebinning:

All projections from different angles are re-sorted in such a way to be parallel.

This means only the central projection is considered for each view angle theta, while all the others are parallel to it and come from different rotation steps.

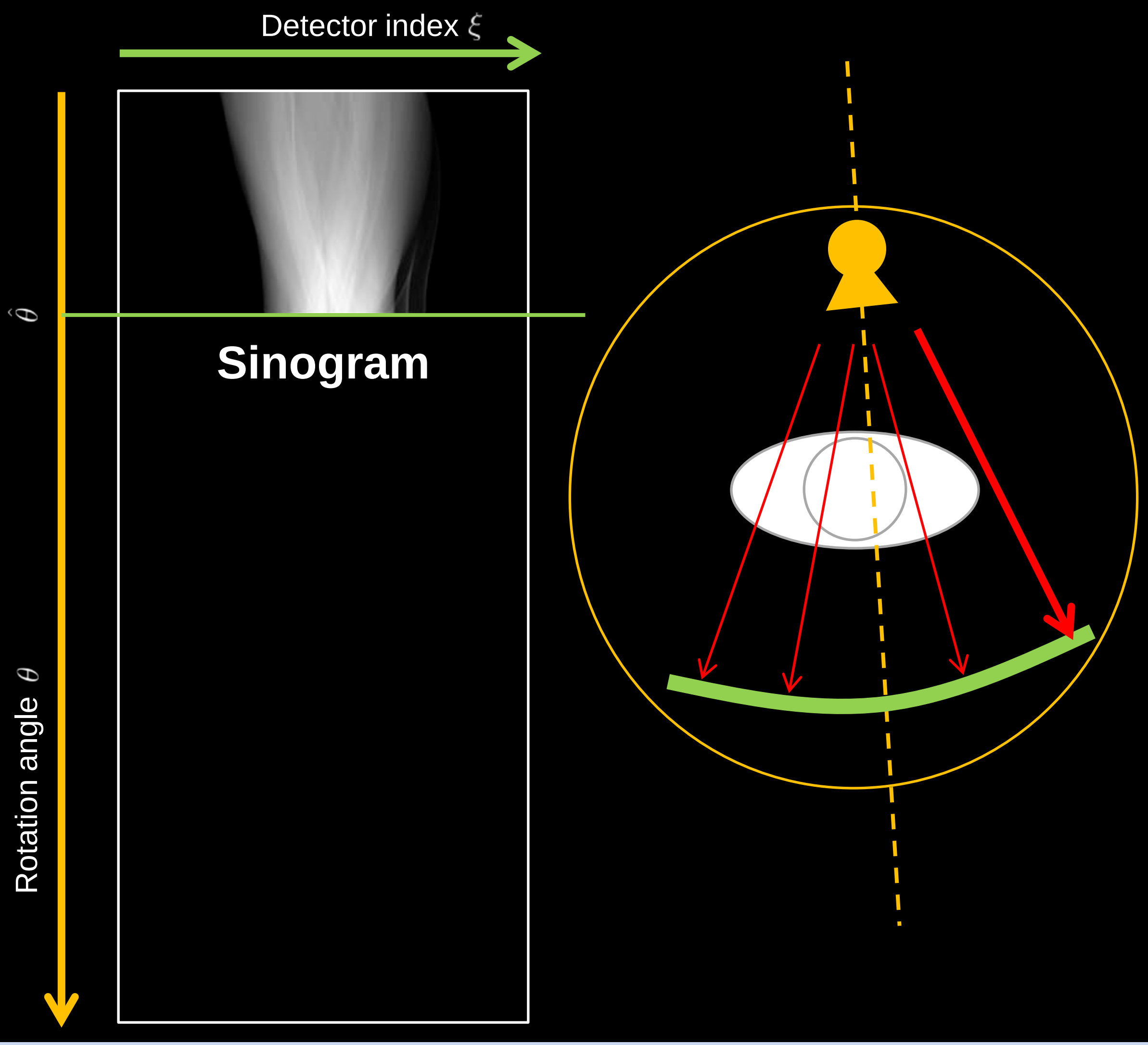

Sinogram Creation

- Lambert-Beer law is considered with some semplifications:

$$I(\theta,\xi) = I_0(\theta,\xi)\, e^{-\int_0^L \mu(\xi,\eta)d\eta}$$

- Each detector ξ measures the attenuated intensity along the direction θ.

- Since for each angle and detector only the structures along that path are responsible for the attenuation, the coordinates x and y can be expressed as:

$$\xi = x\cos(\theta) + y\sin(\theta)$$
$$\eta = -x\sin(\theta) + y\cos(\theta)$$

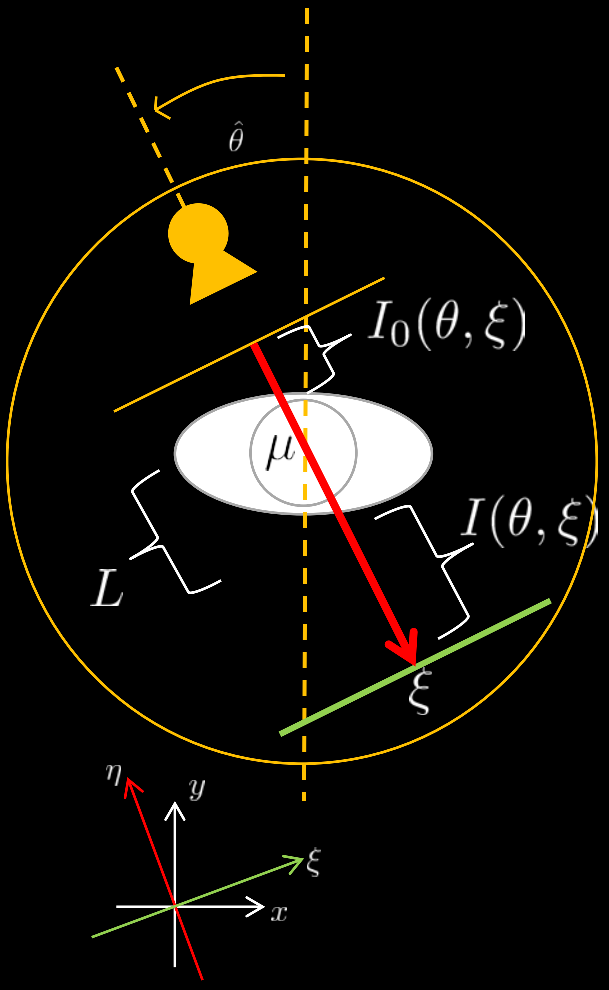

Sinogram Creation

From the intensity domain, it is convenient to move to projections domain, via division and negative log operation:

$$I(\theta,\xi) = I_0(\theta,\xi)\, e^{-\int_0^L \mu(\xi,\eta)d\eta}$$

$$\frac{I(\theta,\xi)}{I_0(\theta,\xi)} = e^{-\int_0^L \mu(\xi,\eta)d\eta}$$

$$-\ln\left(\frac{I(\theta,\xi)}{I_0(\theta,\xi)}\right) = \int_0^L \mu(\xi,\eta)d\eta = p(\theta,\xi) = p_\theta(\xi)$$

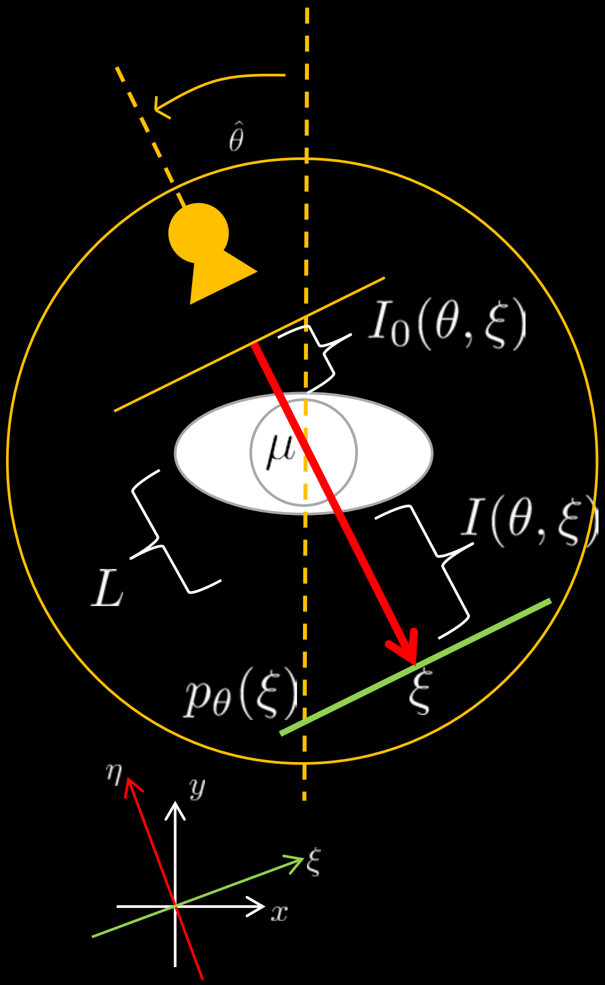

Sinogram Creation

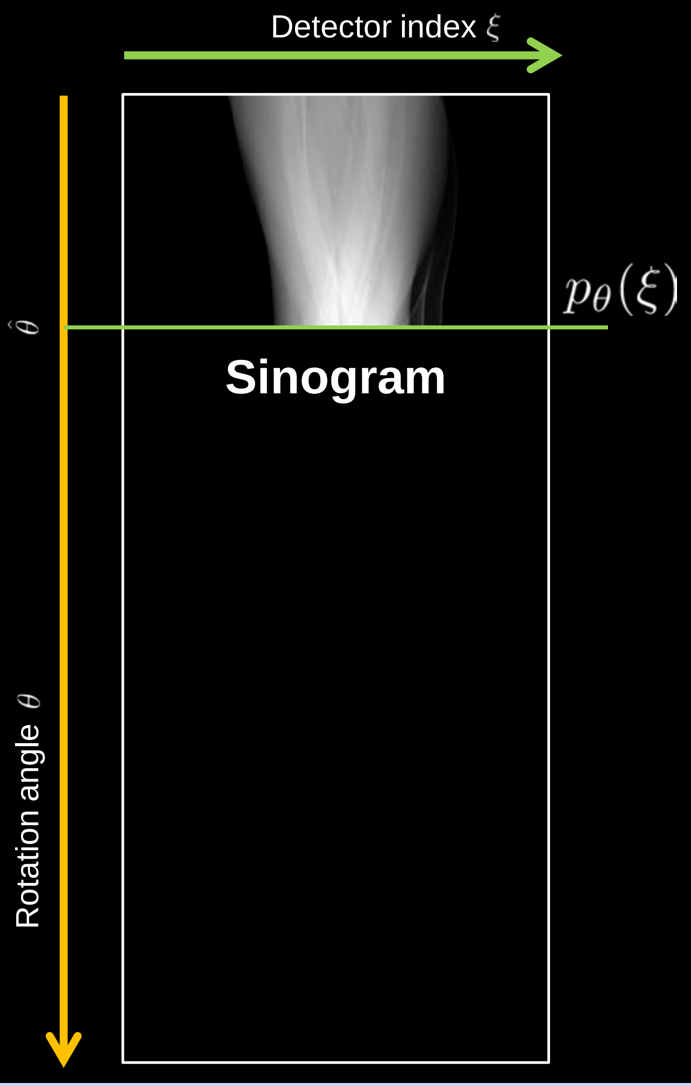

The sinogram is the collection of projections for each detector, for each angle (from 0 to π).

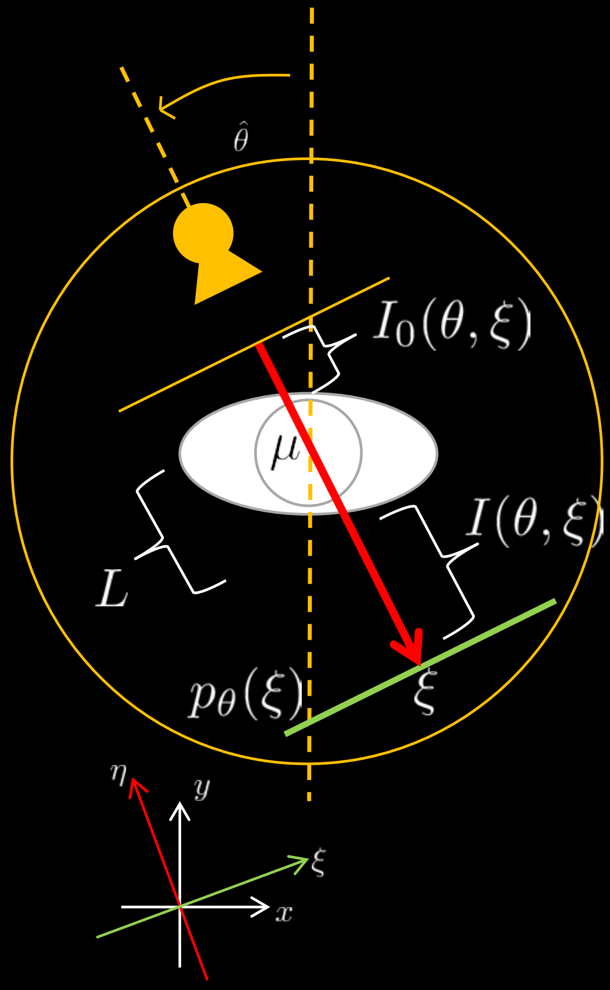

Sinogram Creation

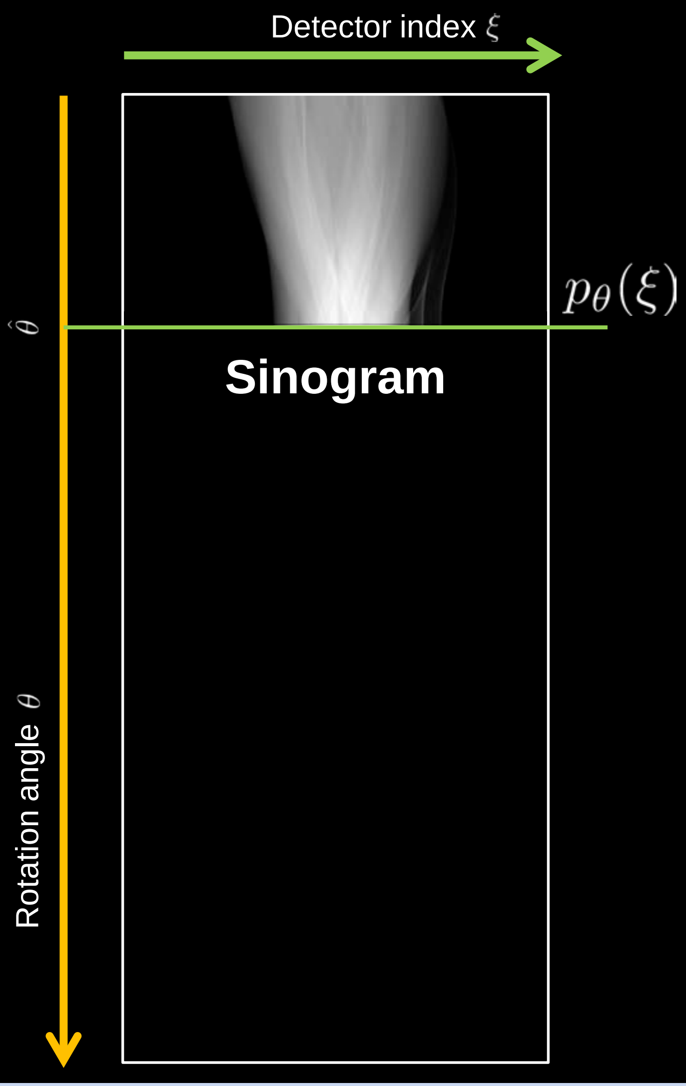

The sinogram is the collection of projections for each detector, for each angle (from 0 to π).

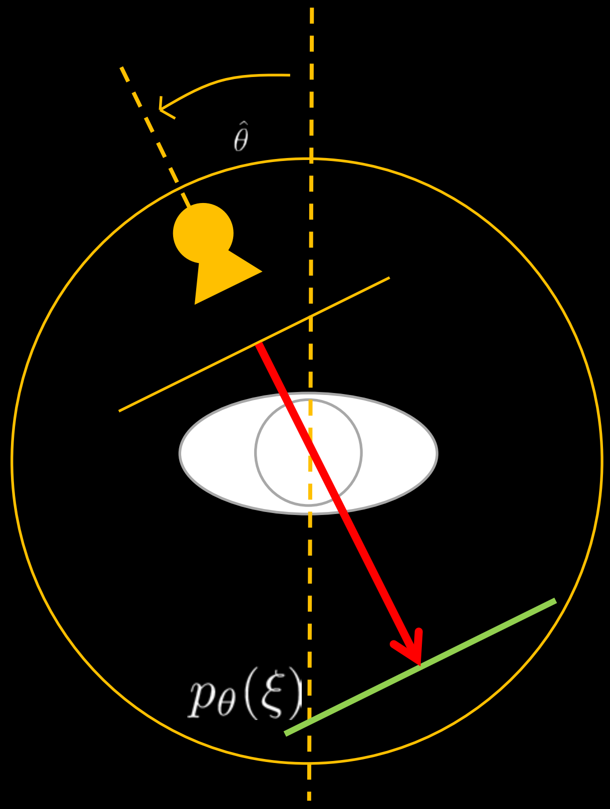

Sinogram Creation

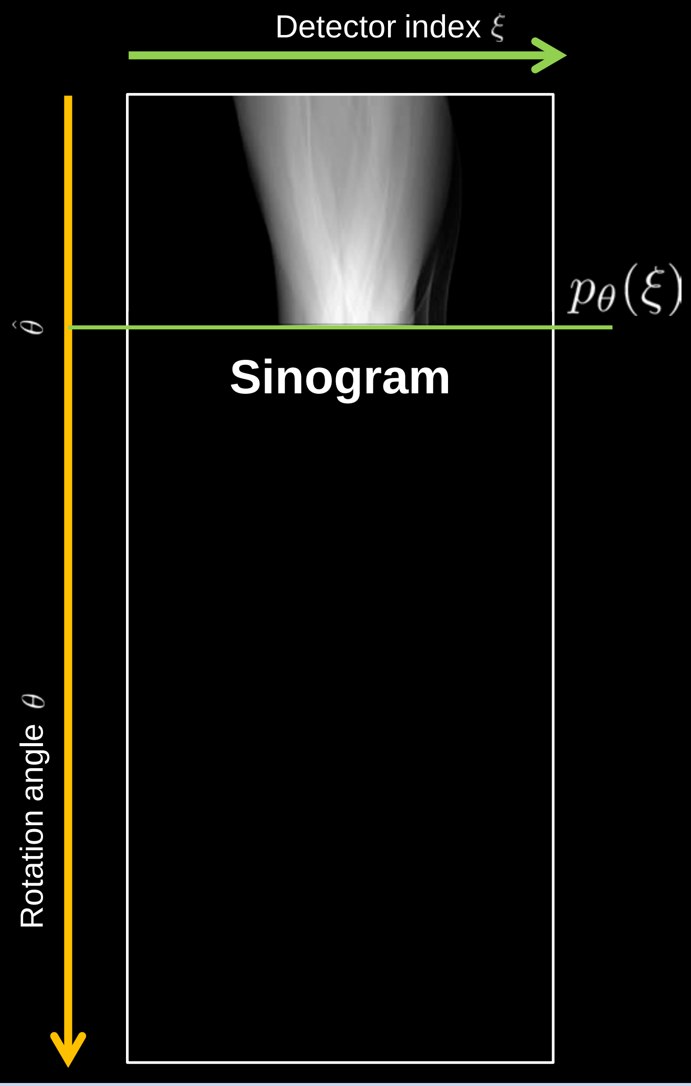

The sinogram is the collection of projections for each detector, for each angle (from 0 to π).

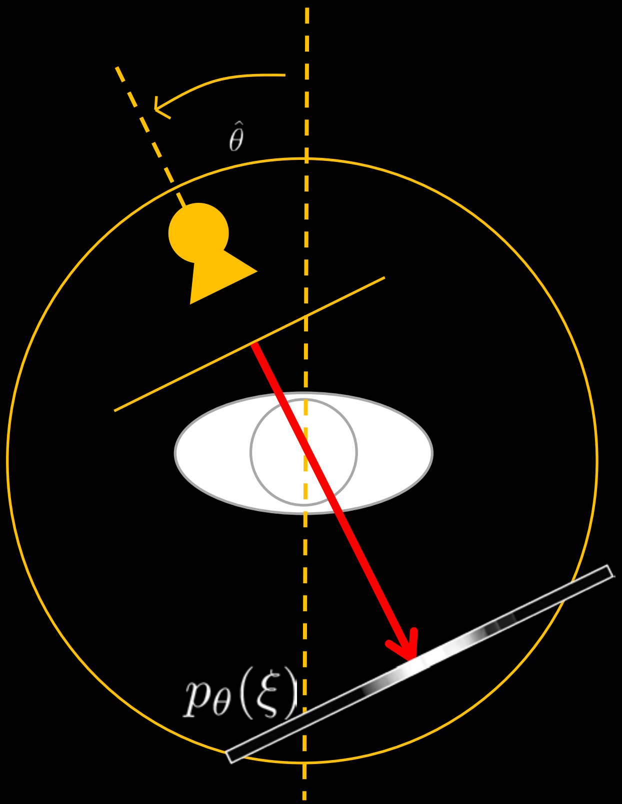

Slice Theorem

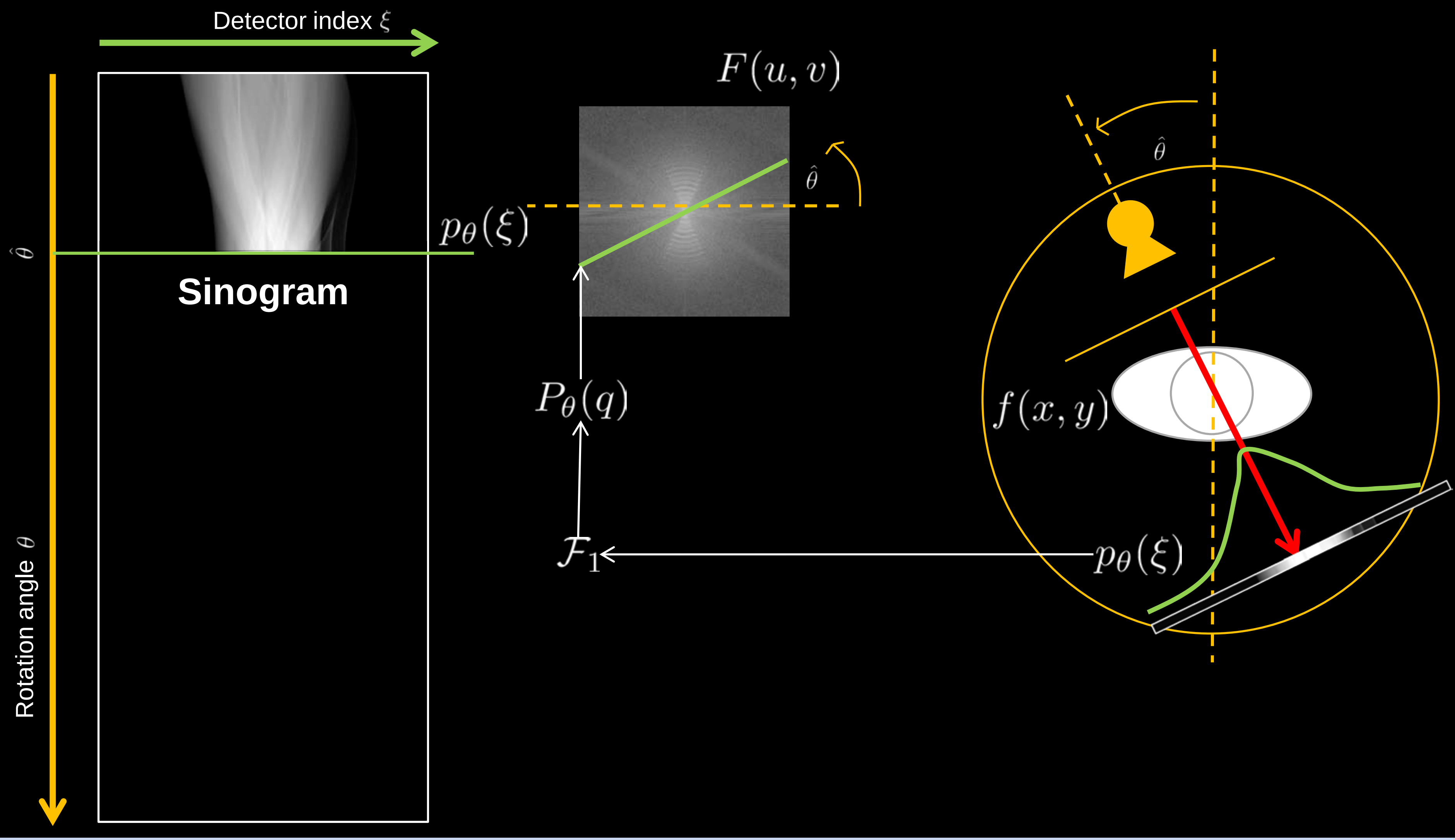

Backprojection

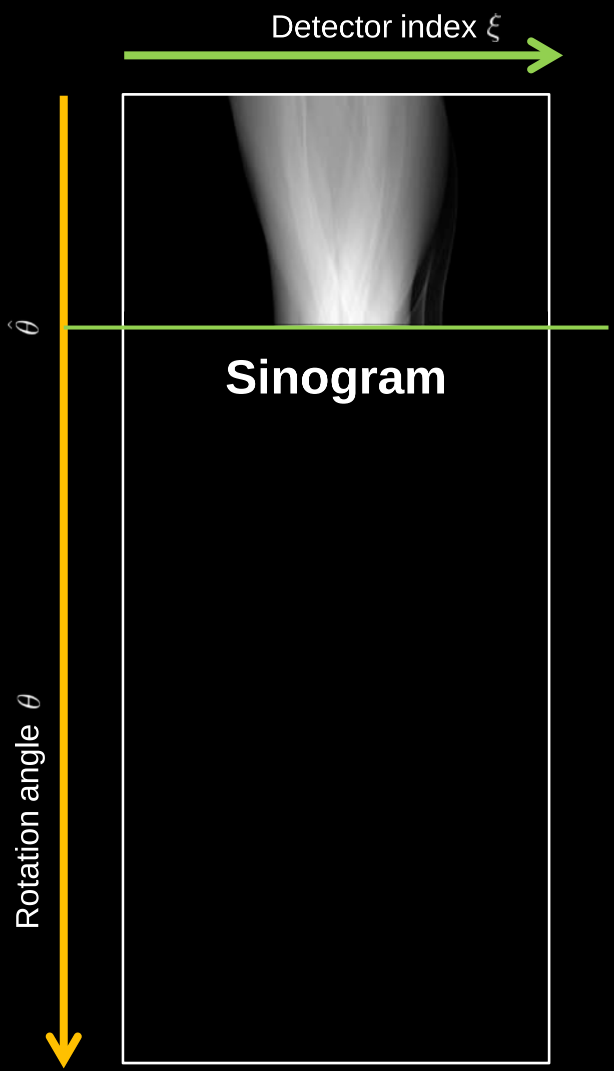

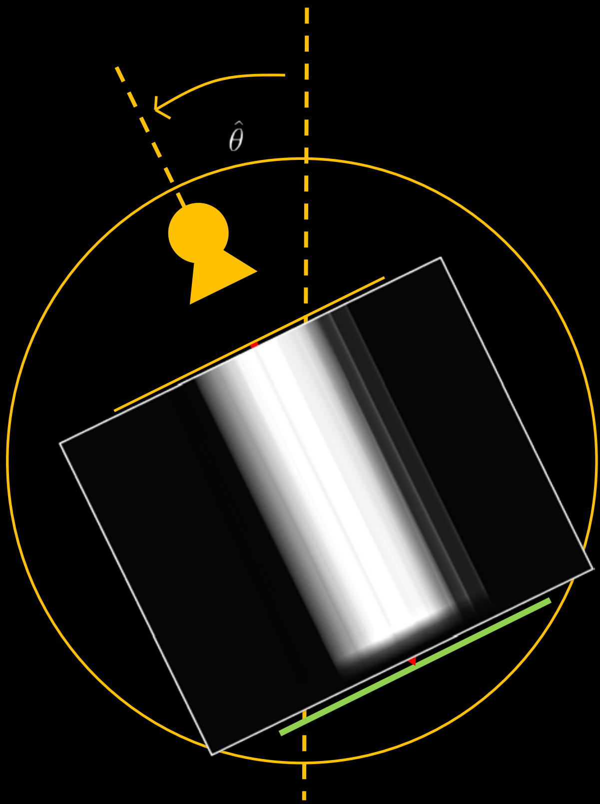

Backprojection

Developing the mathematics behind, one can see that via simple back-projection a different image is obtained, which does not correspond to the inital one (for example positive values are assigned also to pixels outside of the object).

It turns out that a simple back-projection results in:

$$g(x,y) = f(x,y) * h(x,y)$$

which means the original image is convolved with a point spread function h(x,y).

Backprojection

Simple backprojection

Filtered Backprojection

For inverse Fourier transform we have:

$$f(x,y) = \int_{-\infty}^{\infty}\int_{-\infty}^{\infty} F(u,v)e^{2\pi i(xu+yv)}dudv$$

We saw from slice theorem, that for $u = q\cos(\theta)$ and $v = q\sin(\theta)$, we have that F(u,v) equals $P_\vartheta(q)$.

We can move to polar coordinates and re-write

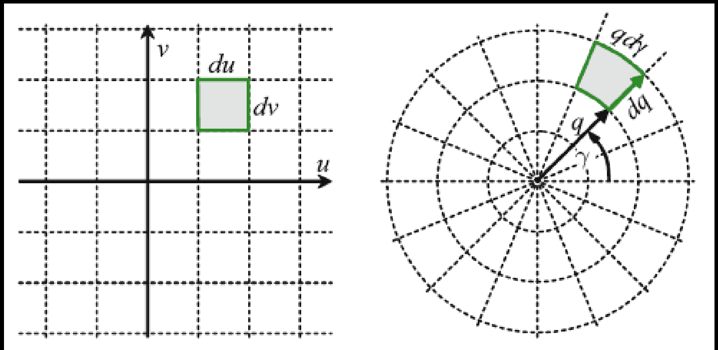

$$f(x,y) = \int_{0}^{2\pi}\int_{-\infty}^{\infty} F(q\cos(\theta), q\sin(\theta))e^{2\pi i(xq\cos(\theta)+yq\sin(\theta))}q\,dq\,d\theta$$

which can be re-written as:

$$f(x,y) = \int_{0}^{\pi}\int_{-\infty}^{\infty} P_\theta(q)e^{2\pi i q\xi}|q|\,dq\,d\theta$$

Filtered Backprojection

$$f(x,y) = \int_0^{\pi} \int_{-\infty}^{\infty} P_\theta(q) e^{2\pi i q \xi} |q| \, dq \, d\theta = f(x,y) = \int_0^{\pi} \int_{-\infty}^{\infty} P_\theta(q) e^{2\pi i q \xi} |q| \, dq \;\; d\theta$$

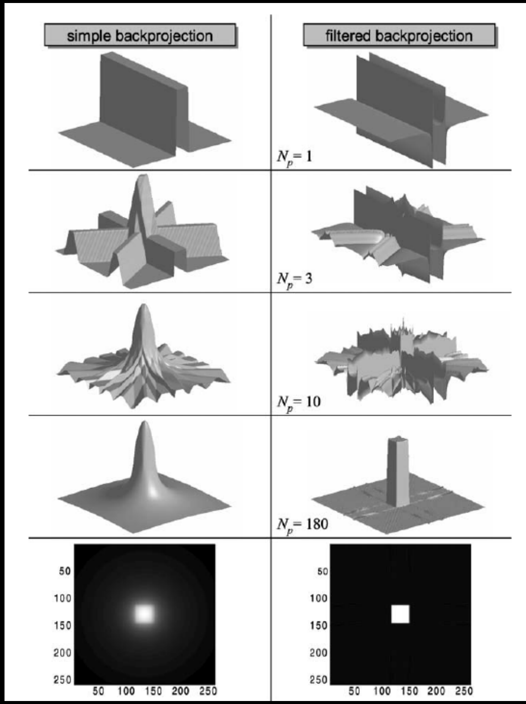

Filtered Backprojection

Simple backprojection

Filtered backprojection

Filtered Backprojection

With FBP, not so much can be optimized, except for the reconstruction kernel, which can be chosen to control the Modulation Transfer Function (i.e. the spatial frequency response of the algorithm).

Smooth kernels reduce noise and spatial frequency.

Sharp kernels allow to see more fine structures, but introduce more noise in the image.

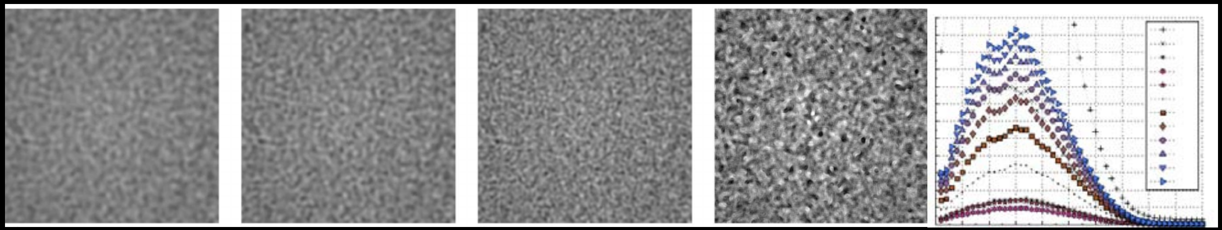

MTFs

Furthermore:

- all approximation done to solve the inverse problem might generate artifacts,
- to reconstruct an image, the rotation must be at least 180° plus fan angle.

Algebraic Reconstructions

Algebraic reconstructions are much more flexible, but significantly slower. They approach the problem as a set of linear equations to be solved.

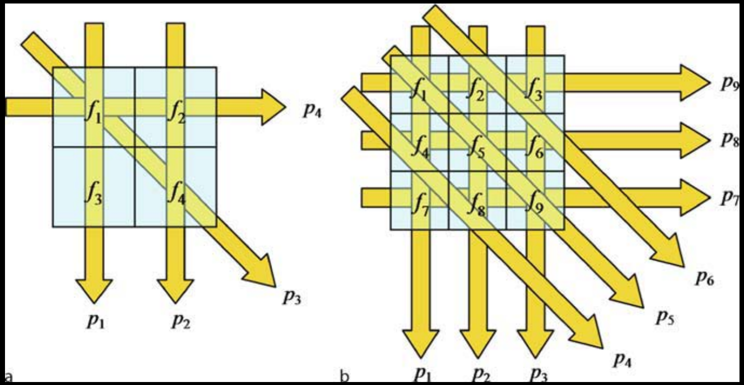

$$\begin{cases} w_{1,1}f(1) + w_{1,2}f(2) + \cdots + w_{1,N}f(N) = p_1 \\ \vdots \\ w_{M,1}f(1) + w_{M,2}f(2) + \cdots + w_{M,N}f(N) = p_M \end{cases}$$

Where:

- $f(i)$ are the unknowns, i.e. the values of the image for each voxel $1 \leq i \leq N$
- $w(i,j)$ are the coefficients which are known and derived from system's geometry. They indicate how much each voxel i „falls" into the path of that specific projection $1 \leq j \leq M$
- p_j are the measured projections.

Algebraic Reconstructions

$$\begin{cases} w_{1,1}f(1) + w_{1,2}f(2) + \cdots + w_{1,N}f(N) = p_1 \\ \vdots \\ w_{M,1}f(1) + w_{M,2}f(2) + \cdots + w_{M,N}f(N) = p_M \end{cases}$$

In a matrix form we can write:

$$\boldsymbol{A} \cdot \boldsymbol{f} = \boldsymbol{p}$$

Where $\boldsymbol{A} = \begin{pmatrix} w(1,1) & \cdots & w(N,1) \\ \vdots & \vdots & \vdots \\ w(1,M) & \cdots & w(N,M) \end{pmatrix}$ $\quad \boldsymbol{f} = \begin{pmatrix} f(1) \\ \vdots \\ f(N) \end{pmatrix}$ $\quad \boldsymbol{p} = \begin{pmatrix} p_1 \\ \vdots \\ p_M \end{pmatrix}$

Normally the pseudo-solution is found as:

$$\boldsymbol{f}^* = \arg\min_{\boldsymbol{f}} \|\boldsymbol{A} \cdot \boldsymbol{f} - \boldsymbol{p}\|_2^2$$

Algebraic Reconstructions

The algorithm is very flexible and allows, for example, to weight each projection according to how reliable it is, remembering that when very few photons are measured, the signal to noise ratio of the projection decreases.

This variation of the algorithm is known as penalized weighted least suqare error (PWLS):

$$\boldsymbol{f}^* = \arg\min_{\boldsymbol{f}} \left((\boldsymbol{A} \cdot \boldsymbol{f} - \boldsymbol{p})^T \boldsymbol{W}^{-1} (\boldsymbol{A} \cdot \boldsymbol{f} - \boldsymbol{p}) \right)$$

Where the matrix W is a diagonal matrix containing the weights for each projection.

Algebraic Reconstructions

- Total variation:

$$f^* = \arg\min_{f} \|A \cdot f - p\|_2^2 + \lambda \|\nabla f\|_1$$

- Nuclear norm (for correlated images):

$$f^* = \arg\min_{f} \|A \cdot f - p\|_2^2 + \lambda \|f\|_*$$

- Prior-induce similarity:

$$f^* = \arg\min_{f} \|A \cdot f - p\|_2^2 + \lambda \|R(f - g)\|_2$$

- Dicitionary based:

$$f^* = \arg\min_{f} \|A \cdot f - p\|_2^2 + \lambda \|f - Dc\|_2^2$$

Index of Contents

- **Introduction:**
  - Overview and components
  - History
- **Physics:**
  - X-ray generation
  - X-ray attenuation
  - X-ray detection
- **Image reconstruction:**
  - Filtered back-projection
  - Algebraic reconstructions
- **Noise and artifacts:**
  - Noise
  - Motion artifacts
  - Beam hardening artifacts
- **Dose and image quality:**
  - mAs modulation
  - kV selection

Noise

Theoretically, the number of photons that reach the detectors can be described as a cascade of Bernoulli distribution, describing the probability that a photon is emitted or not, absorbed from the patient or not, detected or not etc. This cascade can be approximated with a Poisson distribution and hence we can write:

$$n \sim \mathcal{P}(N, N) \qquad \mathrm{SNR} = \frac{N}{\sqrt{N}} = \sqrt{N}$$

The noise is theoretically uncorrelated, but the cross-talk between adjacent detectors, the logarithmic operation to obtain the sinogram, and especially the filtering of the sinogram and backprojection operations make such that the noise is spatially correlated in image domain.

Motion Artifacts

Some of the possible ways to solve this issue are:

- Improving scan speed
- Instructing the patient
- Acquiring data with less than 180° of rotation. This would generate other types of artifacts (namely truncation artifacts) since the data are incomplete, but these new artifacts might be easier to correct for.
- Reduce entropy in selected regions of the image

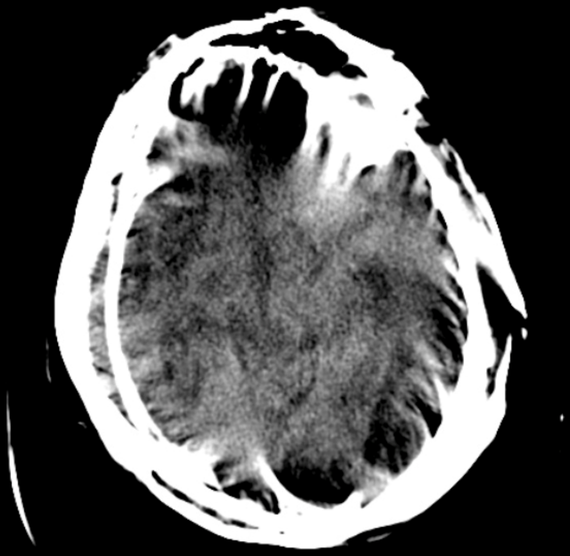

Beam Hardening Artifacts

$$I = I_0\, e^{-\int_0^{\mathrm{keVp}} \int_0^L \mu(x,\mathrm{E})dx\, dE} \longrightarrow I = I_0\, e^{-\int_0^L \mu(x) dx}$$

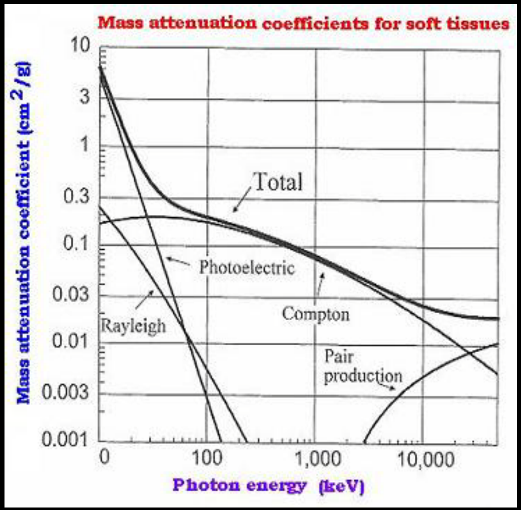

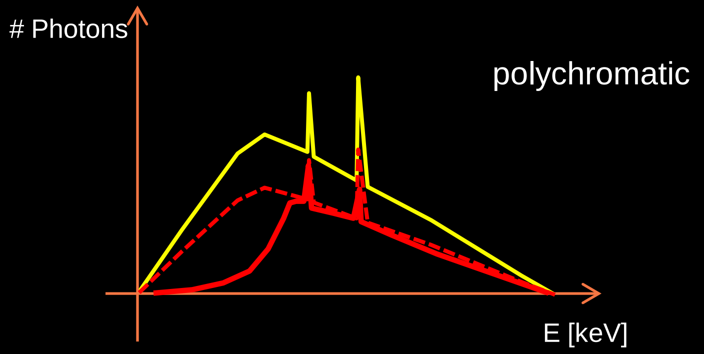

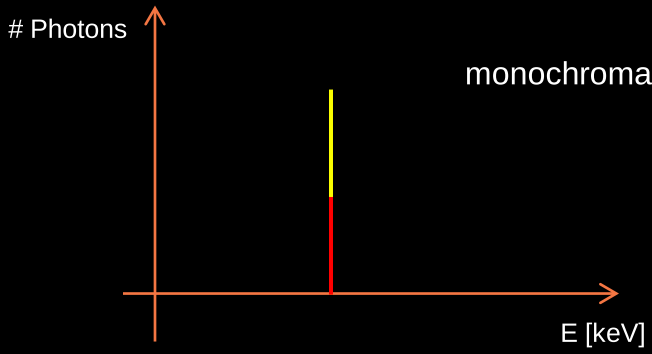

Beam Hardening Artifacts

Common ways to correct for these artifacts consist in:

- Segmenting the metal or high attenuating objects in the image (which are the main responsible of the artifacts, since the inhomogeneity in the absorption due to the energy is maximum when highly attenuating objects are met).
- Identifying all the affected projections, i.e. those projections that have passed throught these objects.
- Replacing the affected projection with some sort of interpolation of the non-affected adjacent ones.

These types of algorithms are normally iterative: small improvements are done in each iteration,

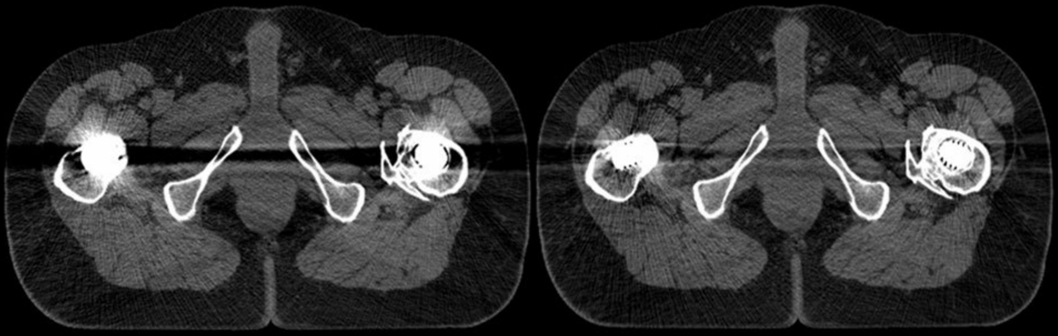

original corrected

Index of Contents

- **Introduction:**
  - Overview and components
  - History
- **Physics:**
  - X-ray generation
  - X-ray attenuation
  - X-ray detection
- **Image reconstruction:**
  - Filtered back-projection
  - Algebraic reconstructions
- **Noise and artifacts:**
  - Noise
  - Motion artifacts
  - Beam hardening artifacts
- **Dose and image quality:**
  - mAs modulation
  - kV selection

CTDI

CTDI measures the dose absorbed by the phantom in one tube rotation, without any table movement.

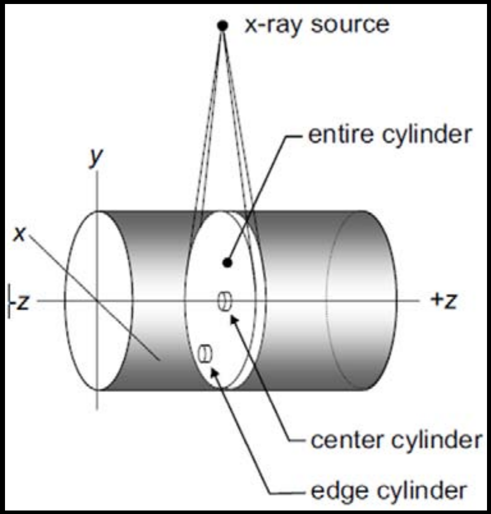

CTDI

Absorbed dose:

1 Gy = 1J/Kg

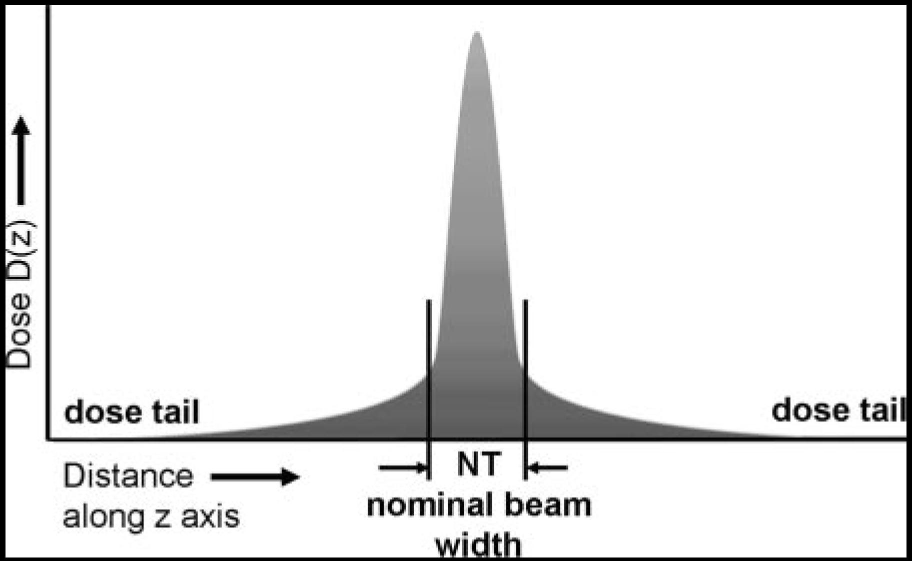

CTDI

CTDI definiton:

$$\text{CTDI} = \frac{1}{NT}\int_{-\infty}^{\infty} D(z)dz$$

CTDI measures the entire dose along z-axis (integral along z), accumulated in the phantom in one tube rotation, without any table movement. The result is normalized by the beam nominal width, (i.e. detectors coverage: NT)

N = number of detectros

T = single detector´s width

CTDI

CTDI measurement:

We cannot measure an integral from -∞ to +∞.

Plus, we need a reference standardized value.

10cm sensors are used.

So the dose accumulated in the phantom in a distance from -50 mm to +50 mm from the center is measured

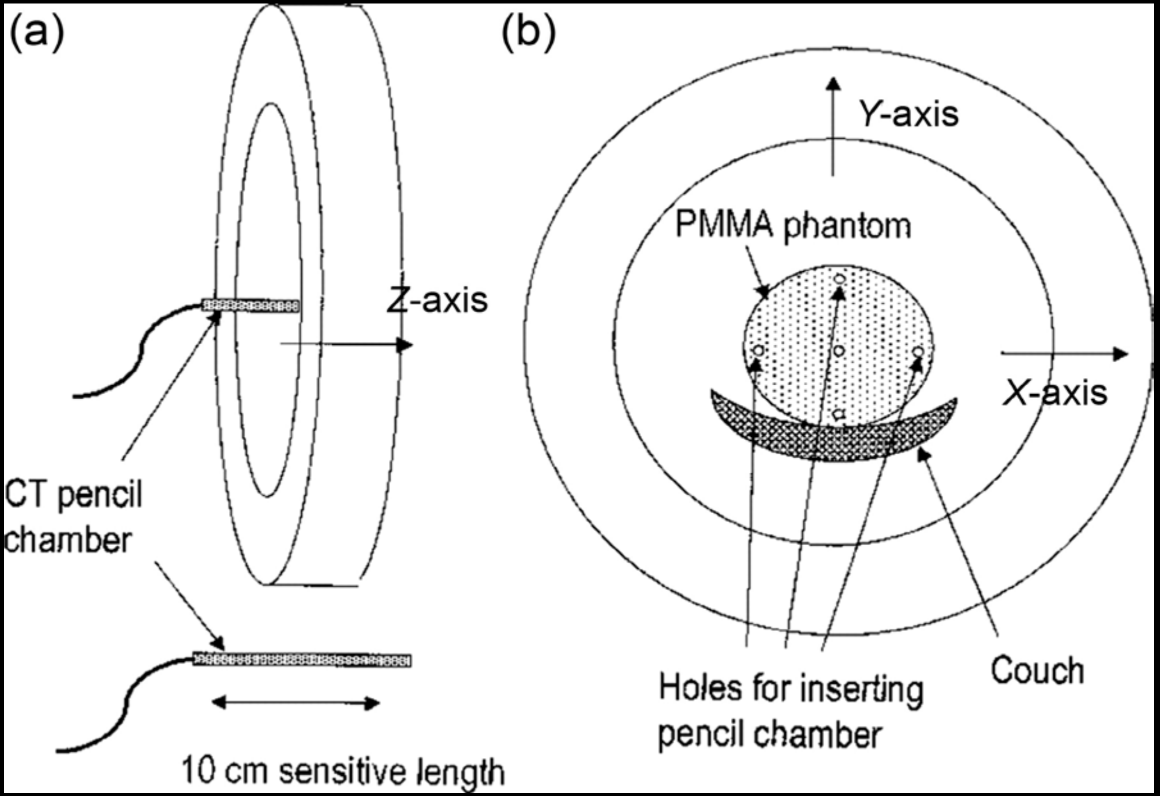

CTDI

CTDI_{100}

Unsing sensors of 100 mm, we define CTDI_{100} like:

$$\mathrm{CTDI}_{100} = \frac{1}{NT} \int_{-50}^{50} D(z)dz$$

CTDI

$CTDI_w$

The dose accumulated will be different in the center and in the periphery of the phantom.

Sensors are positioned both in the center and in the periphery.

The absorbed dose, will be calculated as a weighted average of central and peripheral measured values:

$$\mathrm{CTDI}_w = \frac{1}{3}\mathrm{CTDI}_{100}^{\mathrm{central}} + \frac{2}{3}\mathrm{CTDI}_{100}^{\mathrm{peripheral}}$$

CTDI

$CTDI_{vol}$

Now we have to take into account the fact that the table (for spiral examinations) is actually moving. We define $CTDI_{vol}$ as:

$$\mathrm{CTDI}_{\mathrm{vol}} = \frac{\mathrm{CTDI}_w}{\mathrm{pitch}}$$

$CTDI_{vol}$ reflects the dose that a 32 cm or 16 cm water phantom would absorb with the specific scan settings.

Patient size plays an important role in estimating the effectively absorbed dose and should be taken into account.

One way of doing it is to calculate the effective diameter of the patient and estimate the aborbed dose via a proportion with the diameter of the phantom.

Effective dose is calculated as DLP*w, where the weight w depends on the body region and the DLP is the CTDI multiplied by the scan lenght.

Form DLP to Effective Dose

Normalised values of effective dose per dose-length product (DLP) over various body regions and (standard) patient age[1]:

Region of body	Effective dose per DLP (mSv (mGy cm)$^{-1}$) by age				
	0 [a]	1y [a]	5y [a]	10y [a]	Adult [b]
Head & neck	0.013	0.0085	0.0057	0.0042	0.0031
Head	0.011	0.0067	0.004	0.0032	0.0021
Neck	*0.017*	*0.012*	*0.011*	*0.0079*	*0.0059*
Chest	*0.039*	*0.026*	*0.018*	*0.013*	0.014
Abdomen & pelvis	*0.049*	*0.03*	*0.02*	*0.015*	0.015
Trunk	*0.044*	*0.028*	*0.019*	*0.014*	0.015

[a] All data normalised to CTDIw in the standard head CT dosimetry phantom (∅16 cm).

[b] Data for the head & neck regions normalised to CTDIw in the standard head CT dosimetry phantom(∅16 cm); data for other regions normalised to CTDIw in the standard body CT dosimetry phantom (∅32 cm).

mAs Modulation

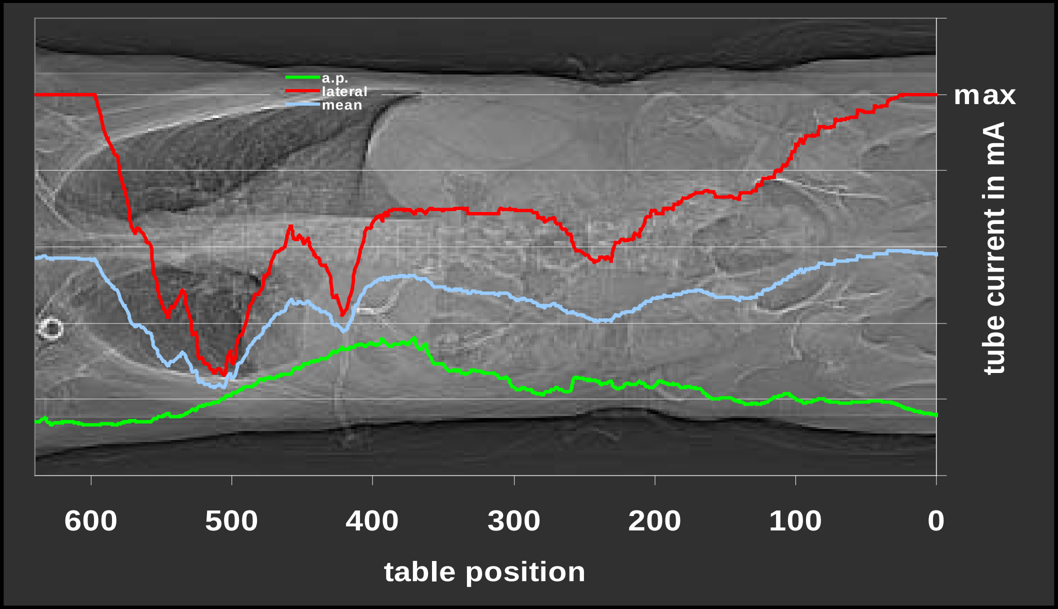

kVp Automatic Selection

Reference kV	=	120kV
Reference mAs	=	210 mAs
Slider position	=	Tissue with contrast (TOI)

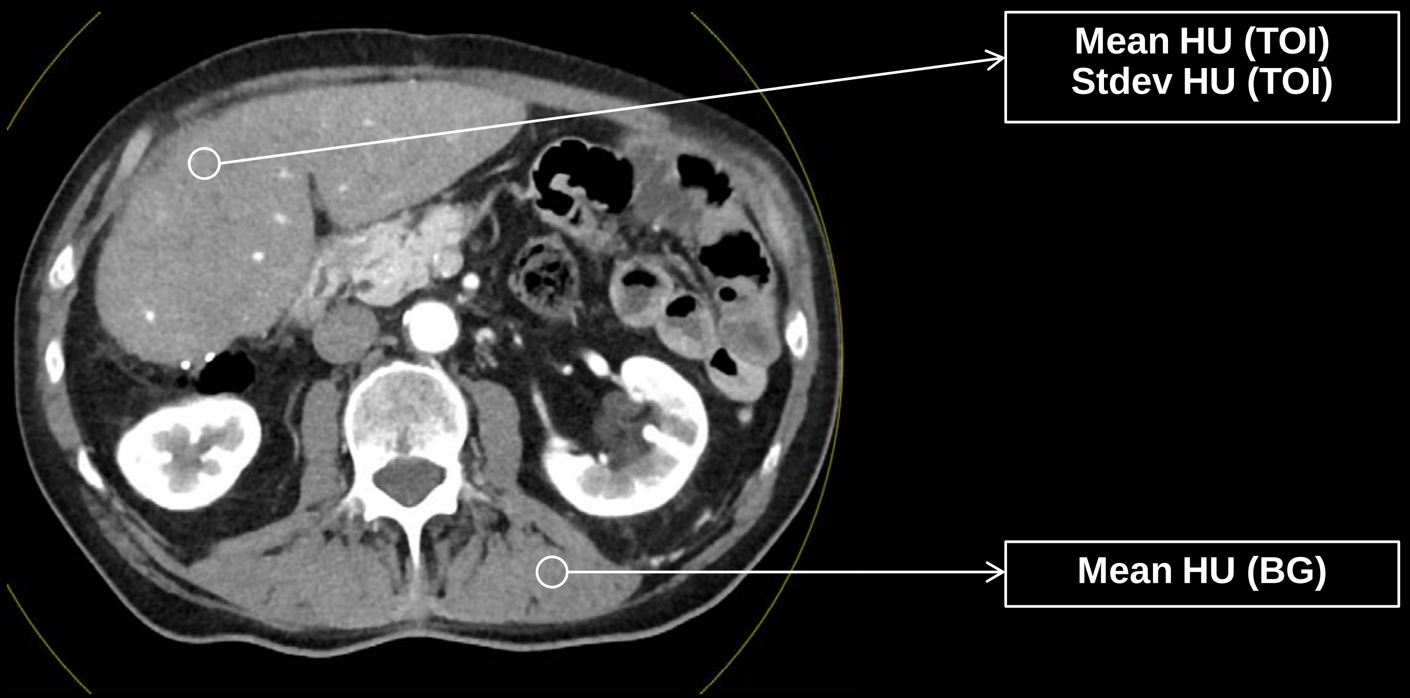

kVp Automatic Selection

$$\mathrm{CNR} = \frac{|\hat{\mu}_1 - \hat{\mu}_2|}{\sqrt{\sigma_1^2 + \sigma_2^2}}$$

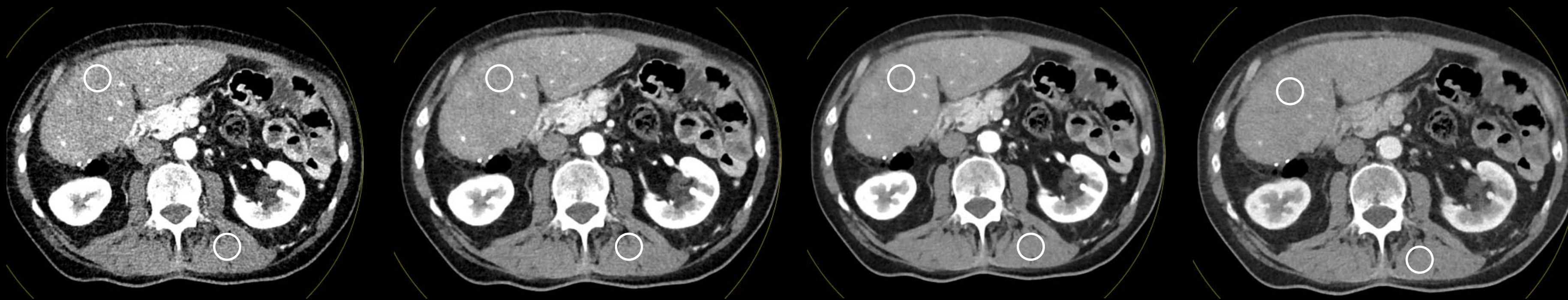

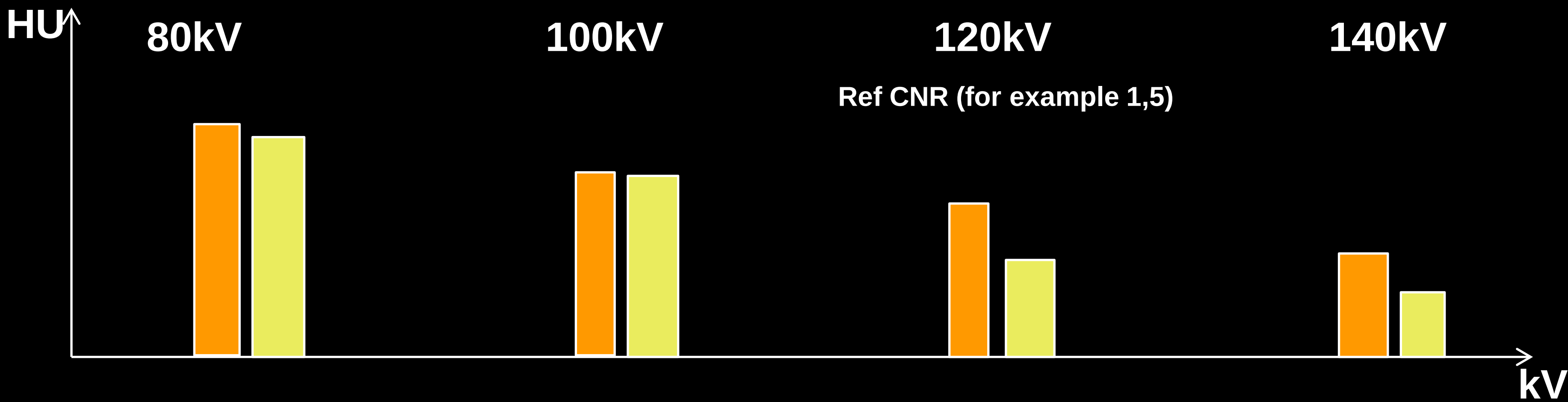

kVp Automatic Selection

mAs adaptation

$$\mathrm{CNR} = \frac{|\hat{\mu}_1 - \hat{\mu}_2|}{\sqrt{\sigma_1^2 + \sigma_2^2}}$$

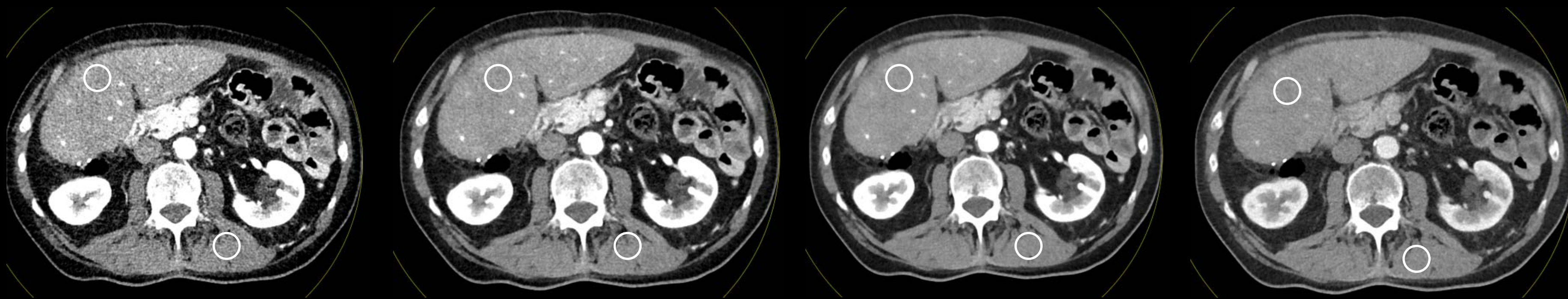

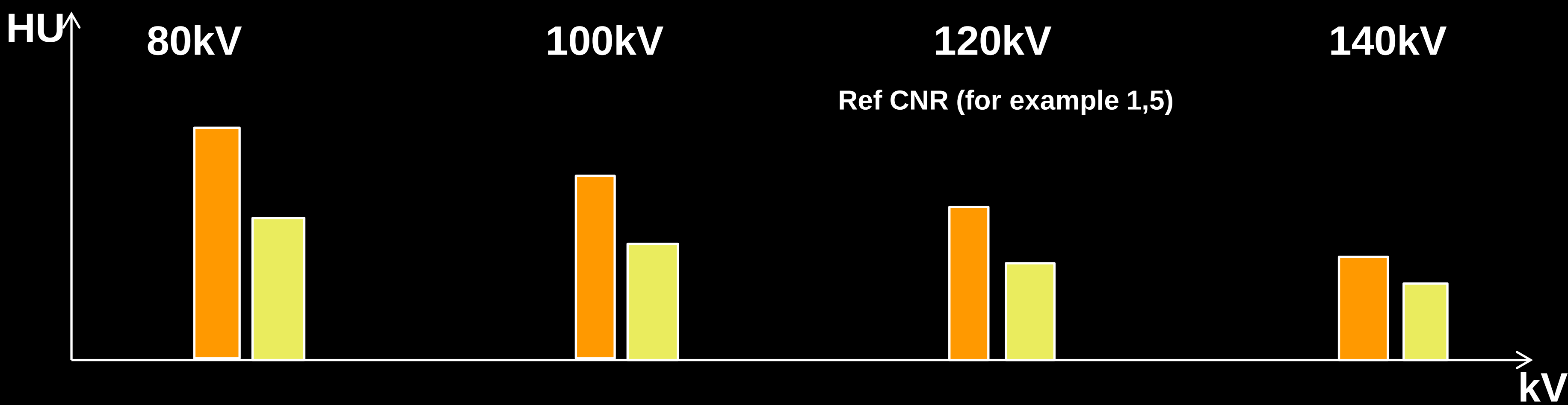

kVp Automatic Selection

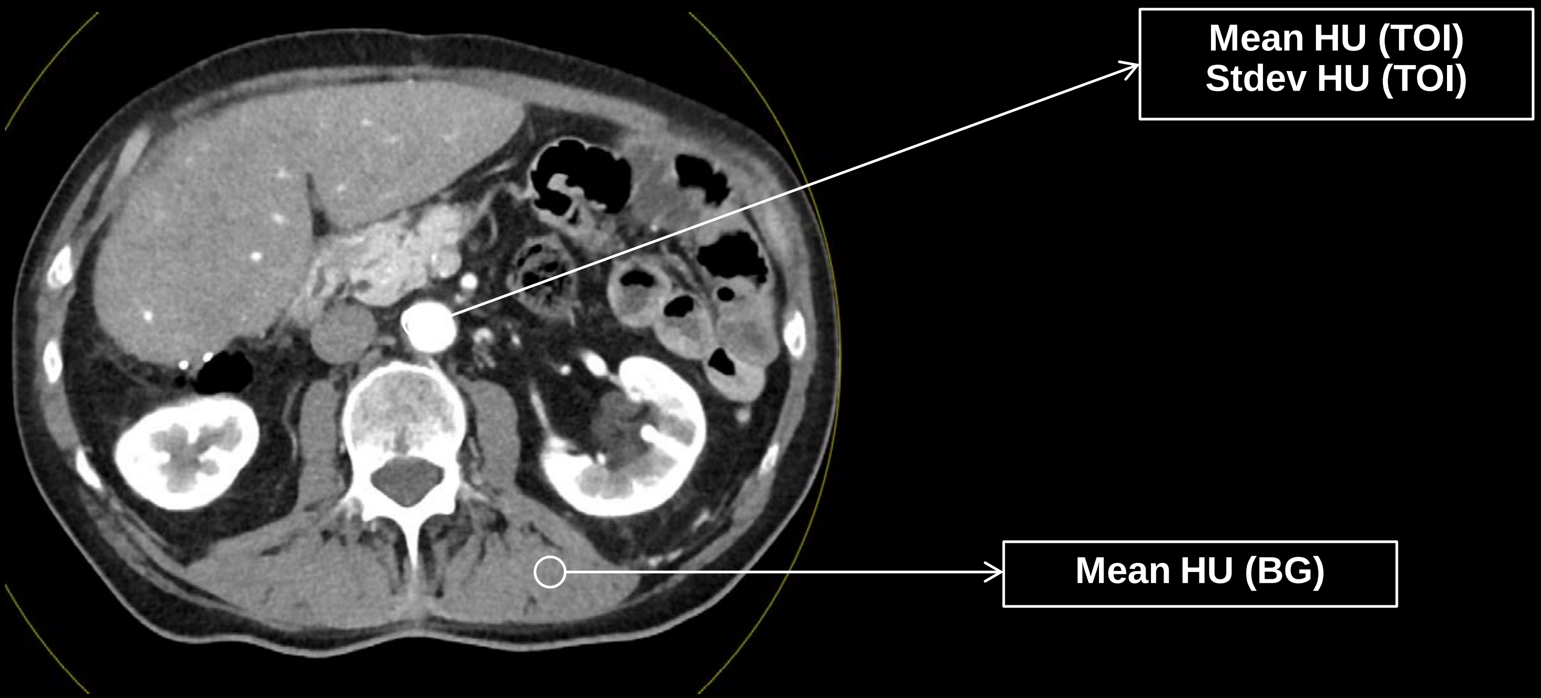

dkfz.

kVp Automatic Selection

$$\text{CNR} = \frac{|\hat{\mu}_1 - \hat{\mu}_2|}{\sqrt{\sigma_1^2 + \sigma_2^2}}$$

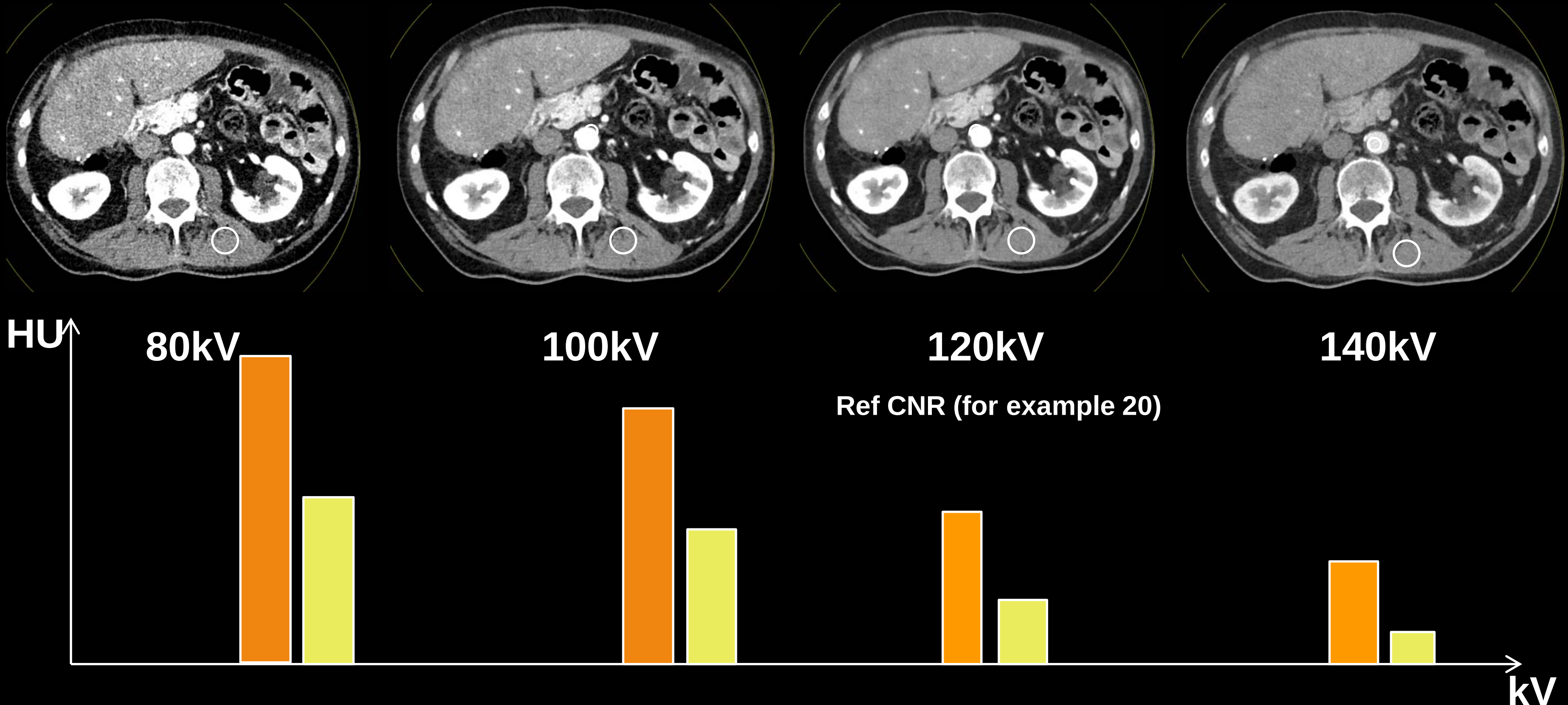

kVp Automatic Selection

mAs adaptation

$$\mathrm{CNR} = \frac{|\hat{\mu}_1 - \hat{\mu}_2|}{\sqrt{\sigma_1^2 + \sigma_2^2}}$$

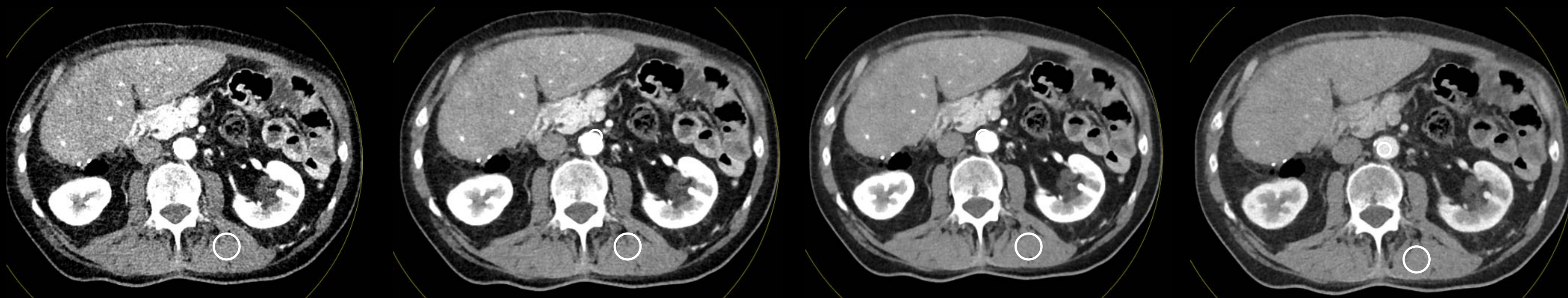

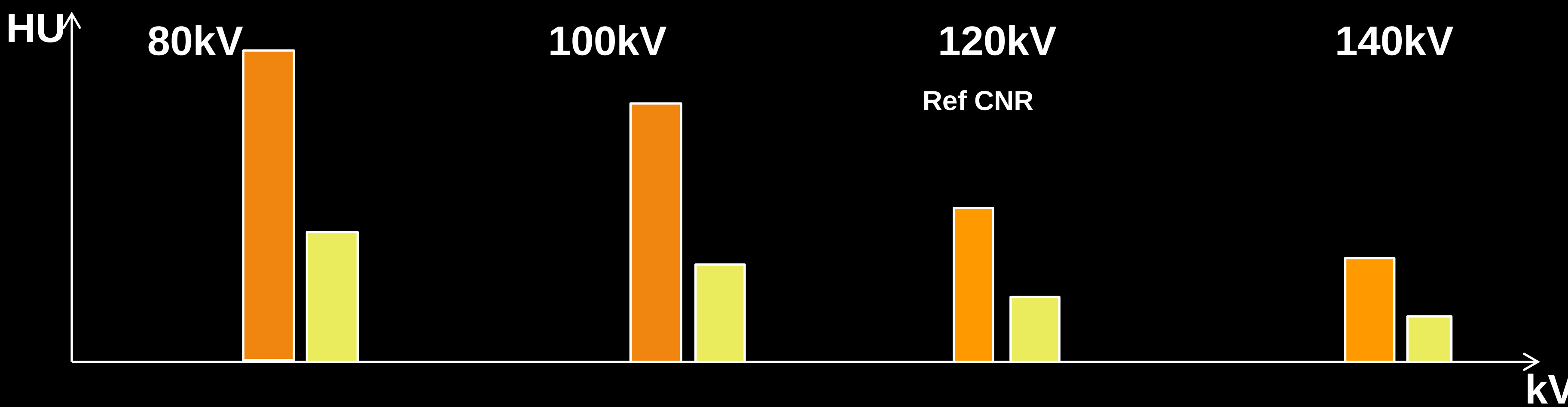

Further reading

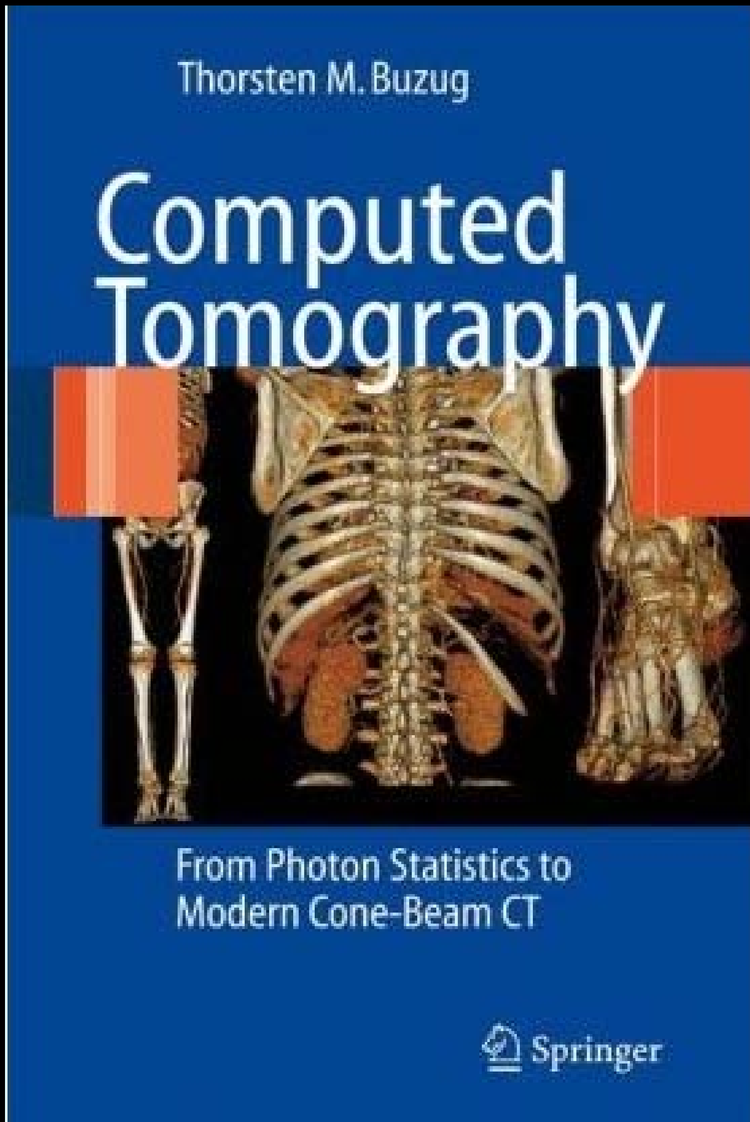

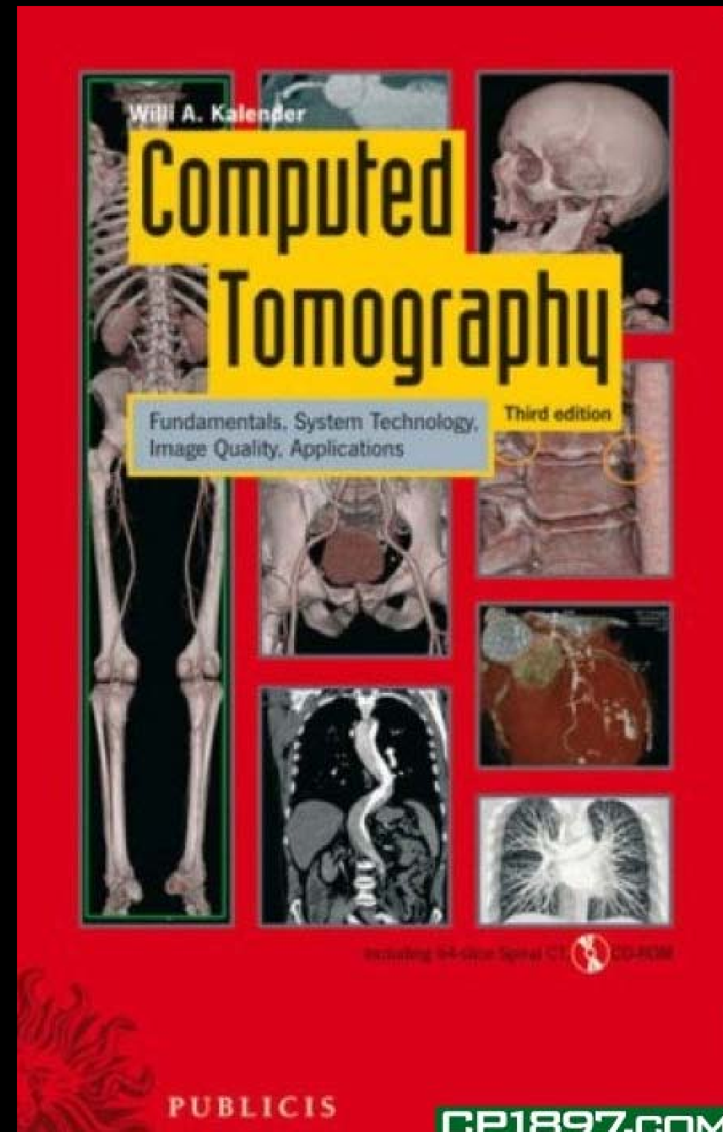

Which one of the follwoing statements is <u>true</u> regarding the algebraic reconstruction techniques in CT?

A. They always need projections acquired from a rotation of (180 + fan angle) degrees.
B. They are normally faster compared to filtered back-projection.
C. They are normally composed by a data fidelity term and an image domain function called regularizer.
D. They are more keen to artifacts respect to filtered back-projection.

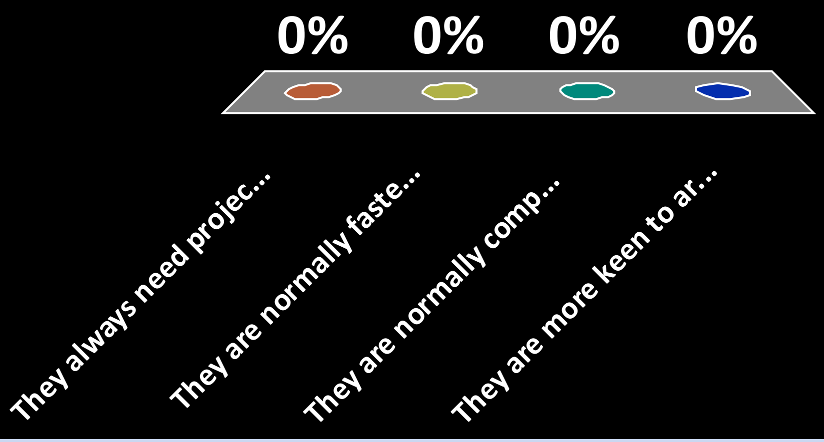

dkfz.

Which one of the follwoing statements is <u>false</u> regarding photon counting (PC) detectors in CT?

A. PC detectors can potentially allow for spectral CT without significant dose increase.

B. PC detectors might suffer from pile up and charge sharing effects when the same photon is detected from adjacent detector pixels.

C. The response time is much shorter compared to conventional energy integrating (EI) detectors.

D. The anti-scatter grid is no longer necessary, due to the much finer pixelization of the PC detectors.

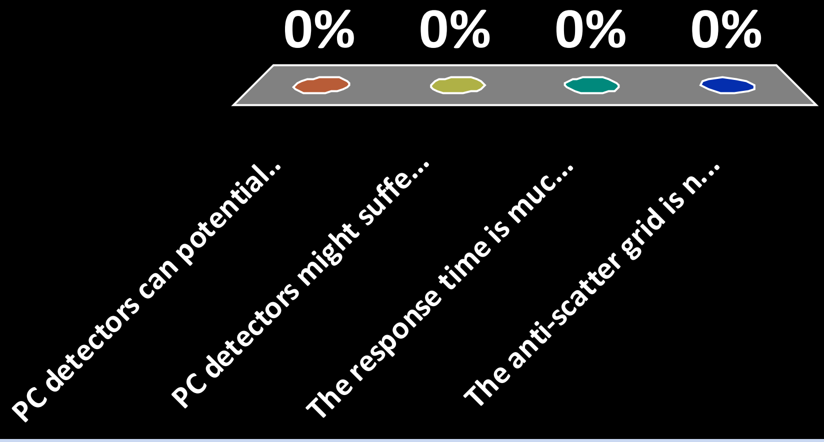

Enter Question Text

A. Increasing the mAs value would result in higher number of X-ray photons, but without affecting the energy spectrum.
B. Increasing the kVp values would shift the X-ray spectrum towards lower energies.
C. Increasing the mAs value would result in higher energy X-ray photons.
D. Incresing the kVp values would result in higher contrast between soft tissue structures.

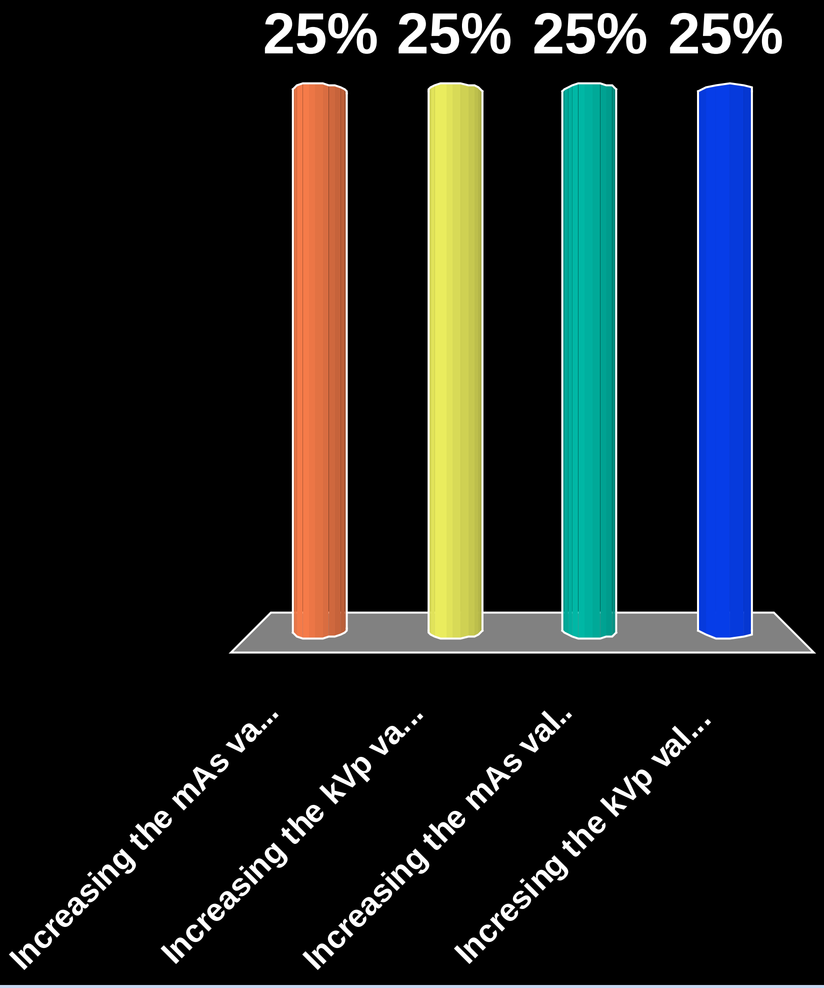

Advanced CT Applications

Cardiac CT and DE CT

Francesco Pisana

German Cancer Research Center (DKFZ), Heidelberg, Germany

DEUTSCHES KREBSFORSCHUNGSZENTRUM IN DER HELMHOLTZ-GEMEINSCHAFT

Cardiac CT

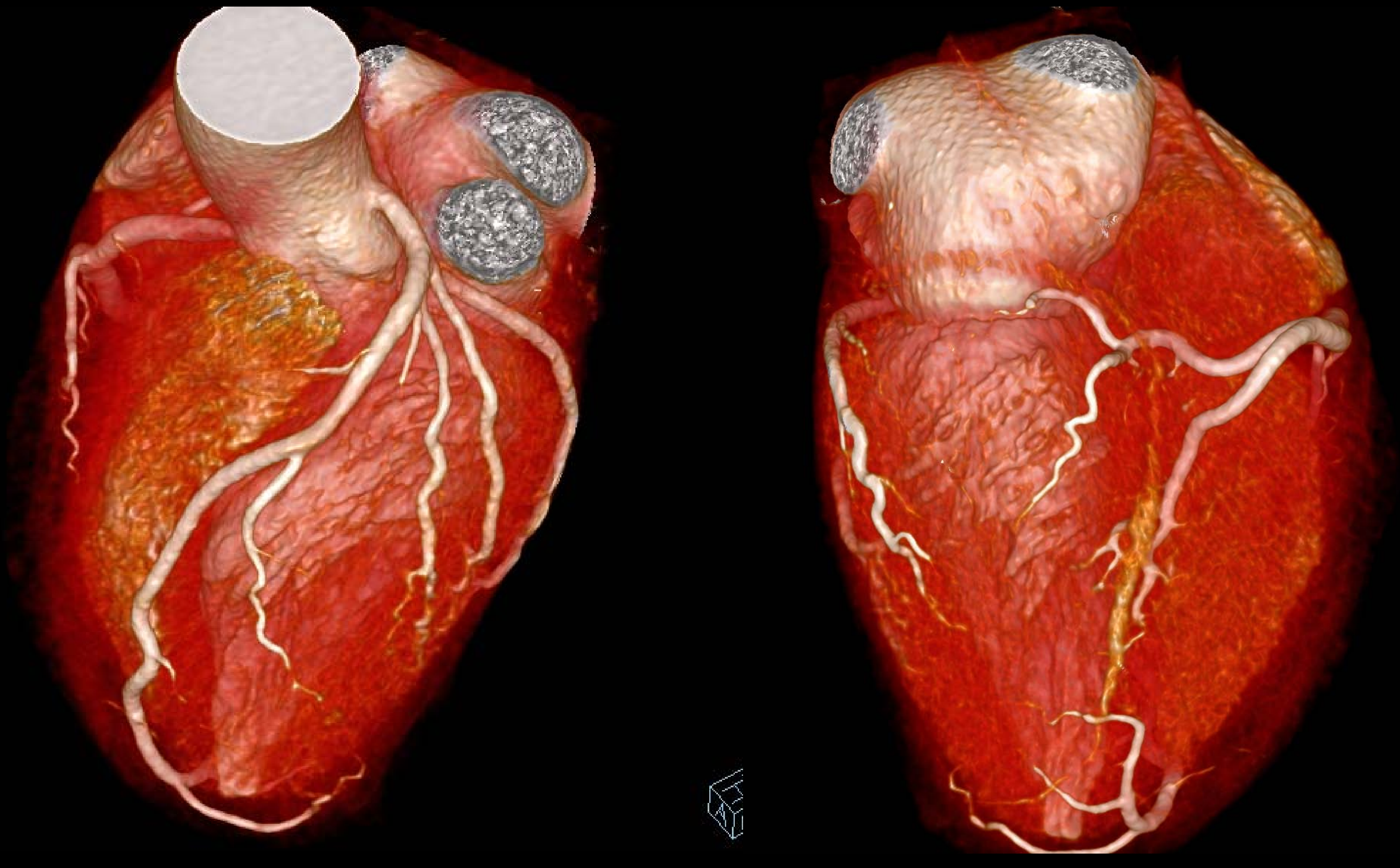

Prospective Triggering

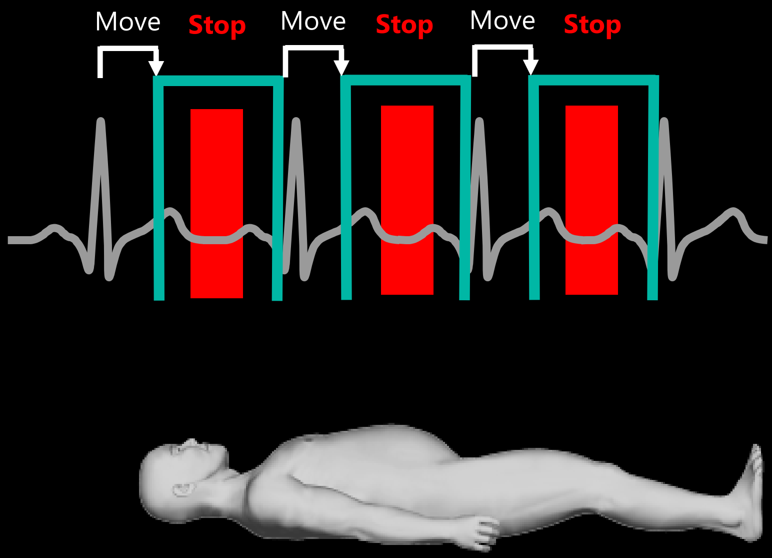

Prospective Triggering

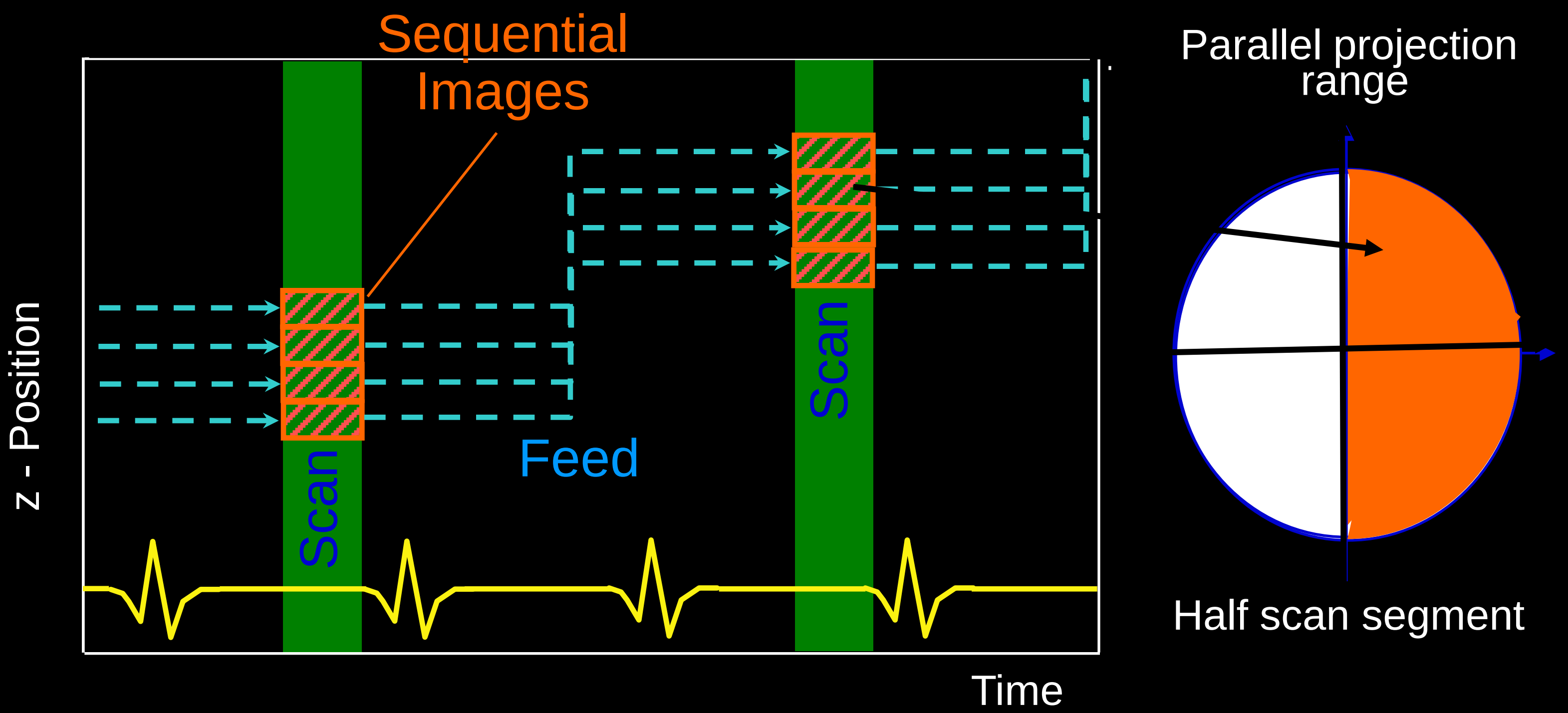

- Temporal resolution half the rotation time $T_{rot}/2$
- Sequential volume coverage

Prospective Triggering

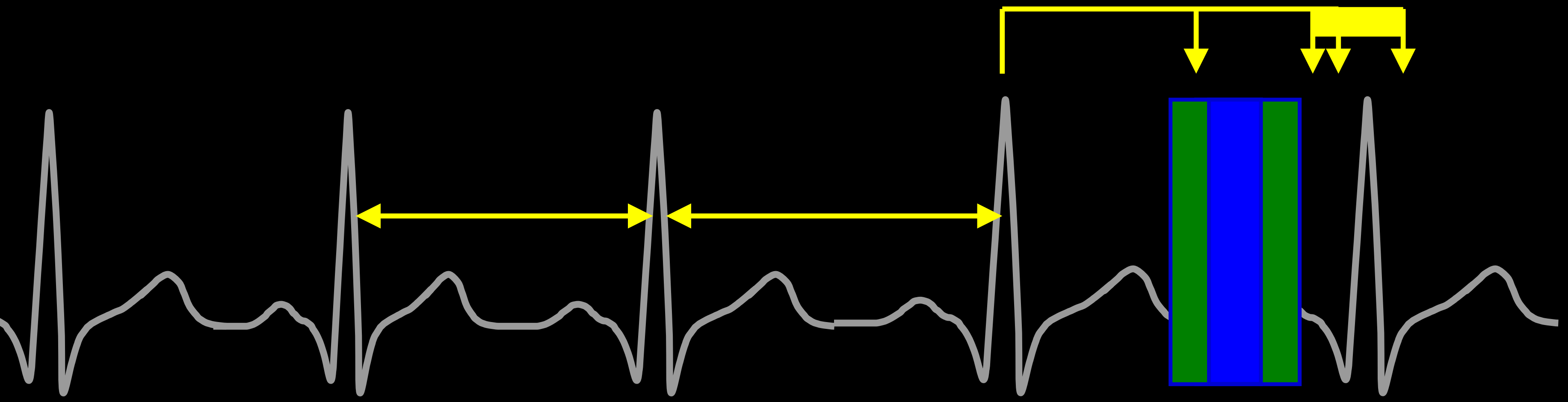

Retrospective Gating

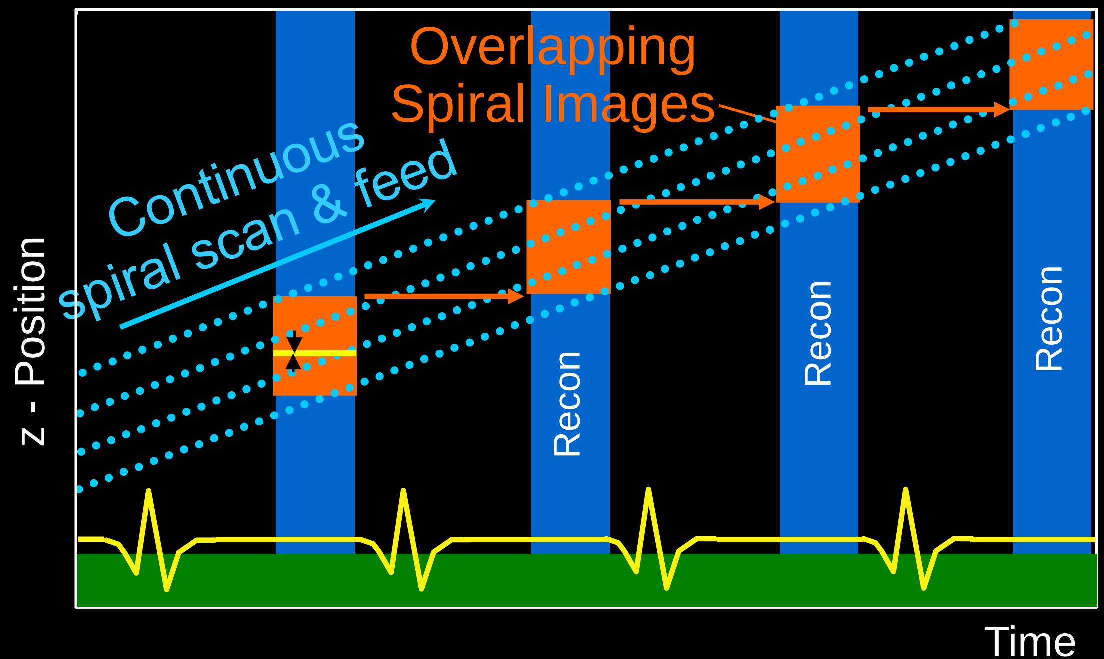

Retrospective Gating

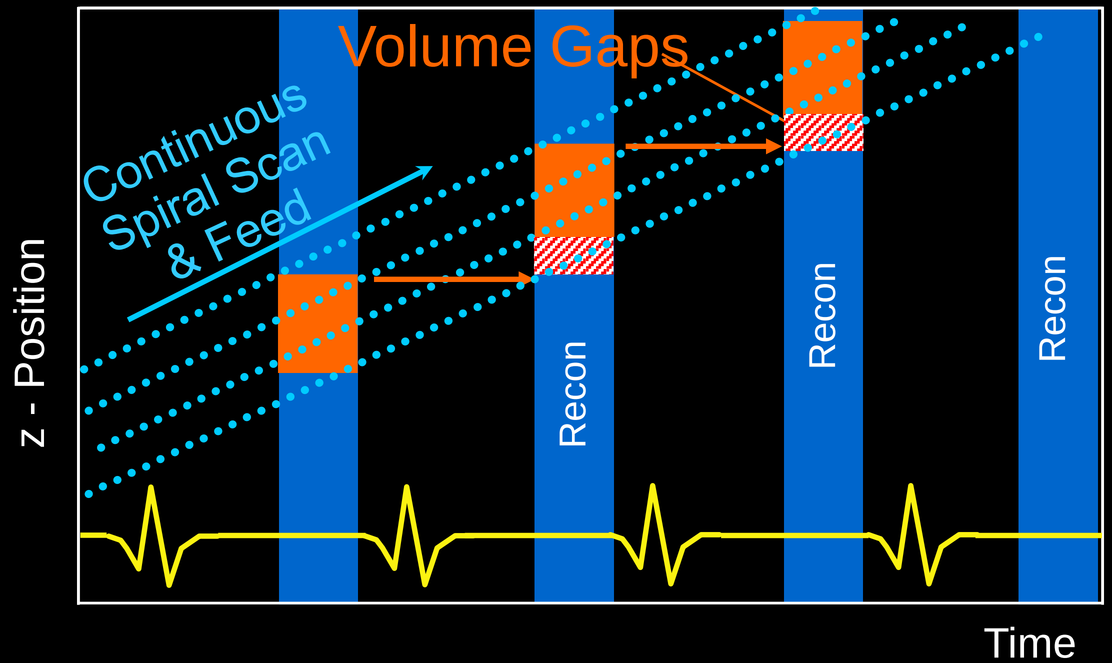

- Heart rate limits the pitch for continuous volume coverage
- Pitch < $\frac{HR}{60}$ * Rotation time

Flash Scan

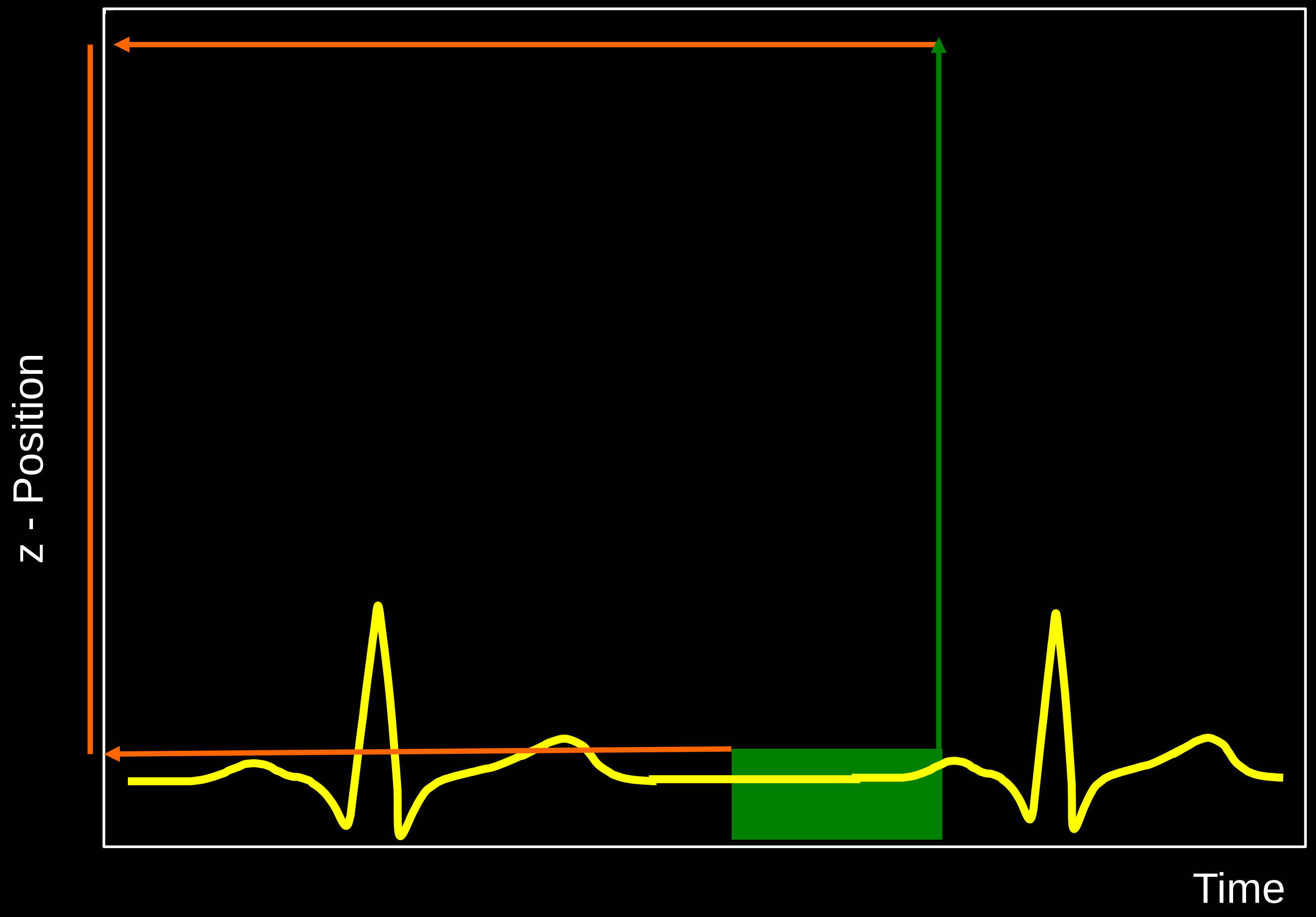

Flash Spiral

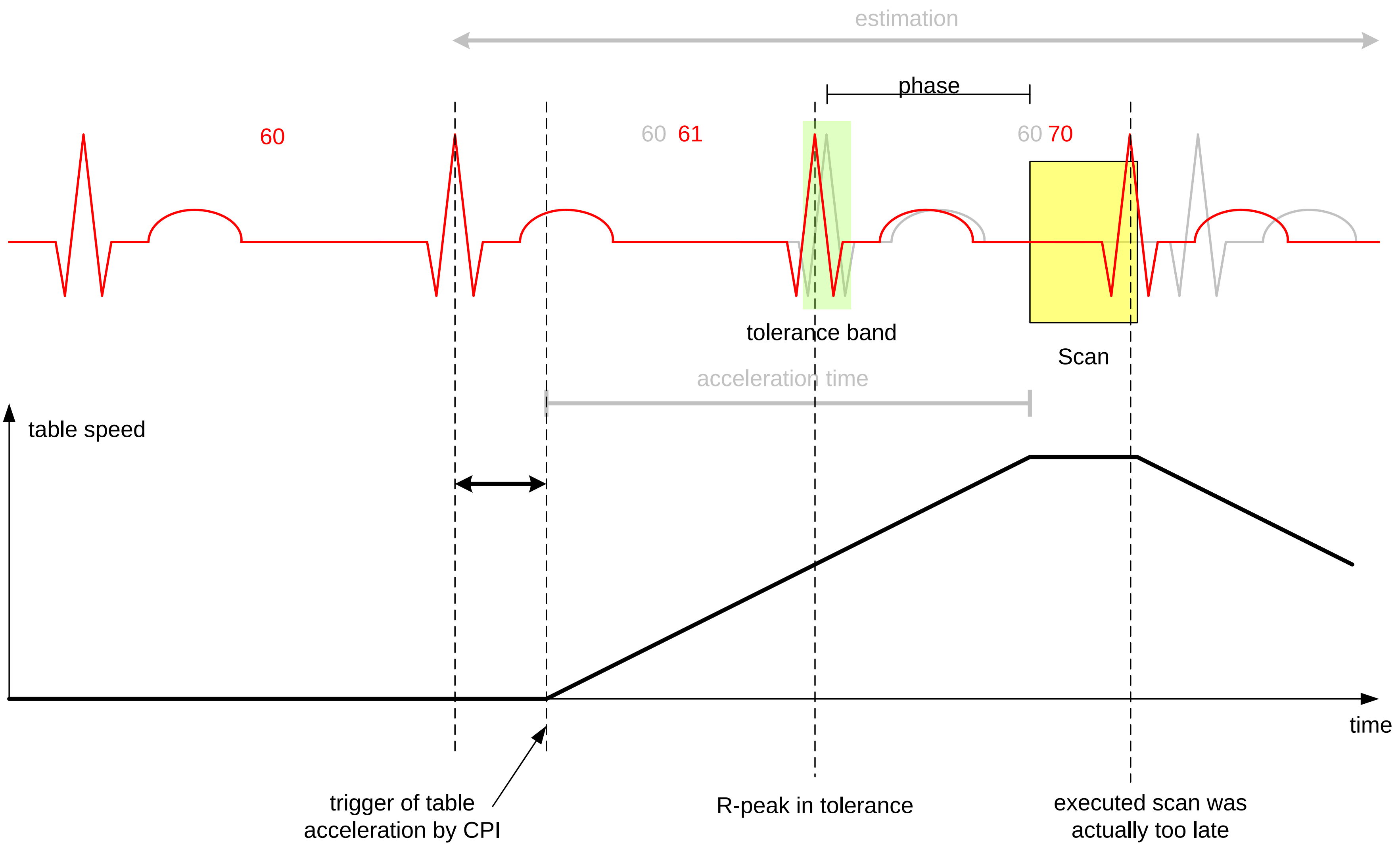

X-Ray Dose

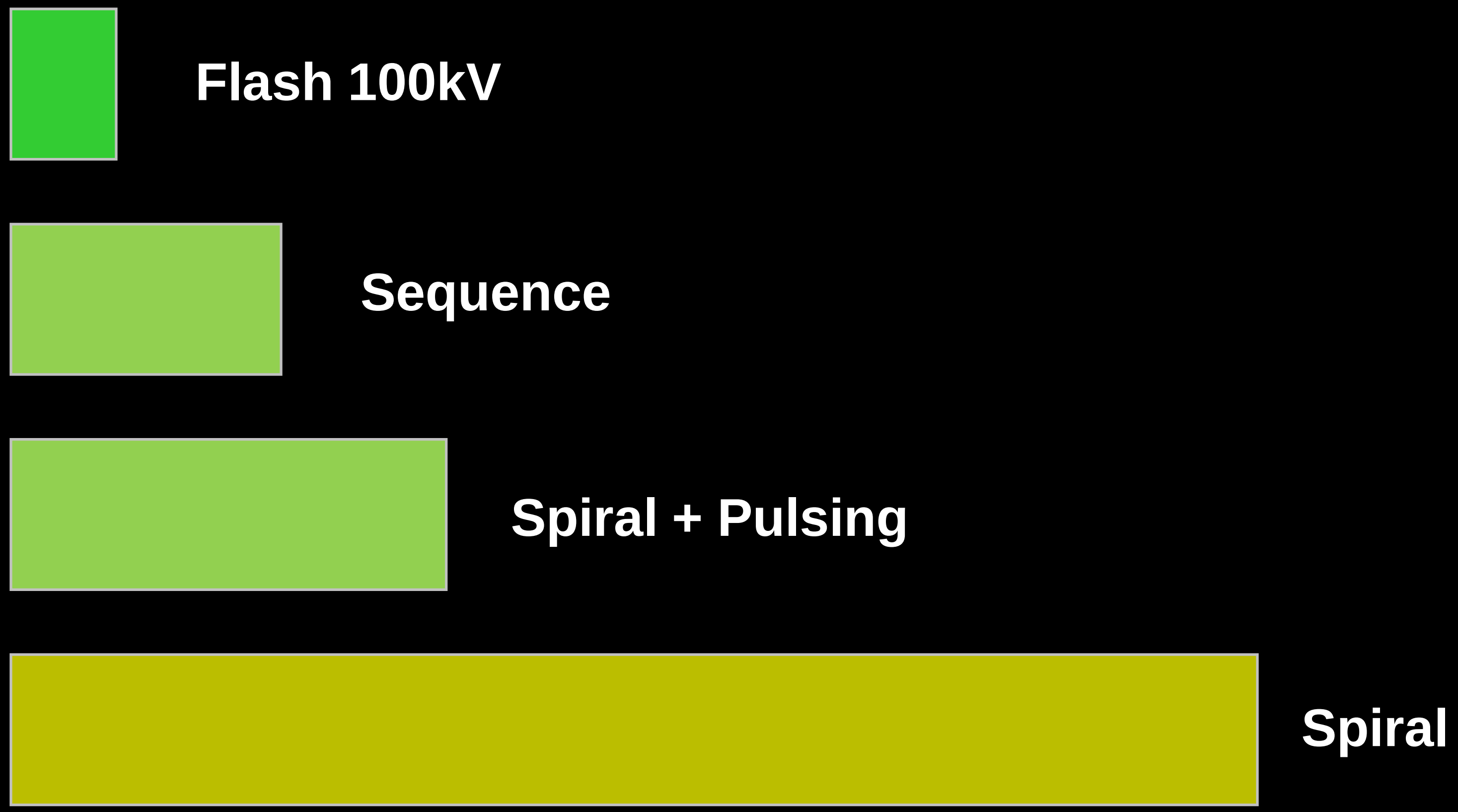

Dual Energy CT

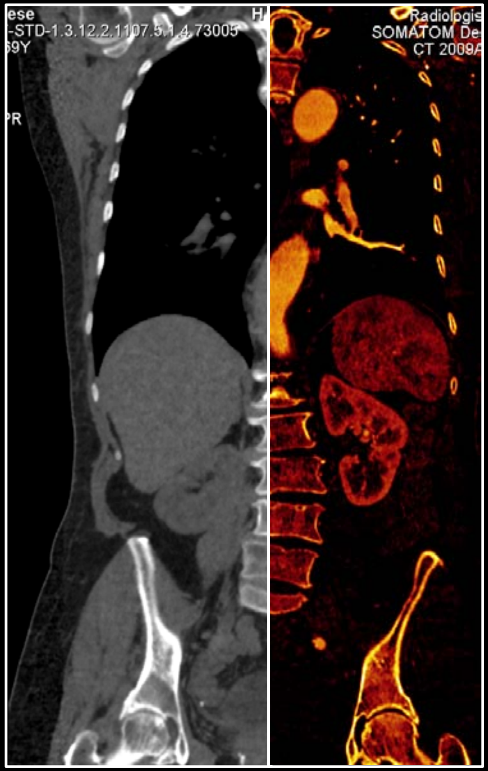

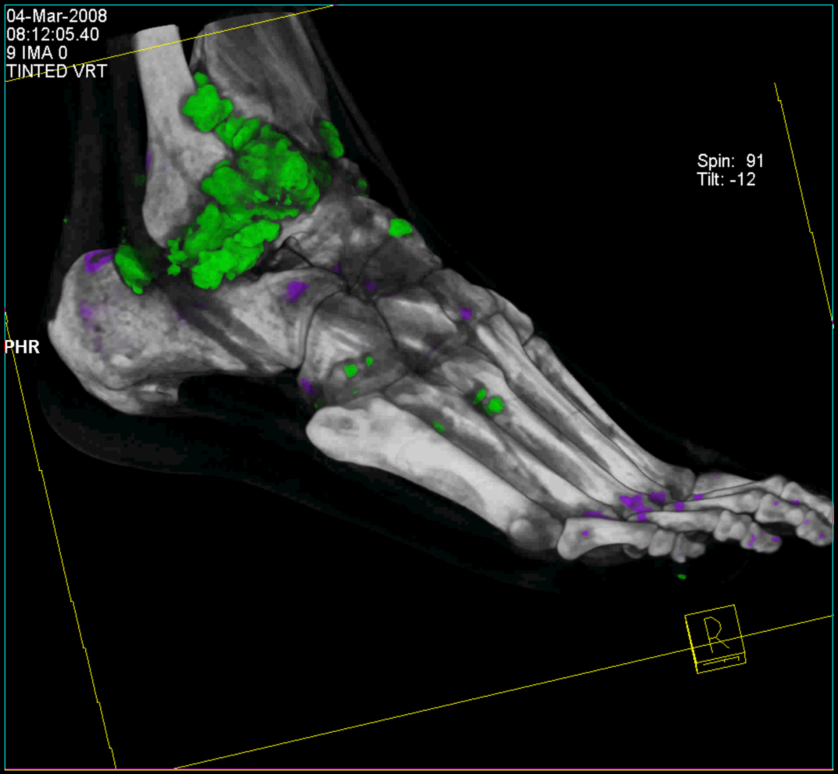

dkfz.

Index of Contents

- **Introduction:**
  - X-ray attenuation
  - DE principles and technical solutions
- **Clinical applications and protocol optimization:**
  - Material classification
  - Material quantification (decomposition)
  - Pseudo-monoenergetic images
  - Electron density and effective atomic number images
  - Metal artifacts reduction

Index of Contents

- **Introduction:**
  - X-ray attenuation
  - DE principles and technical solutions
- **Clinical applications and protocol optimization:**
  - Material classification
  - Material quantification (decomposition)
  - Pseudo-monoenergetic images
  - Electron density and effective atomic number images
  - Metal artifacts reduction

X-ray Attenuation

- Beer's law:

$$I = I_0\, e^{-\int_0^{\mathrm{keVp}} \int_0^{L} \mu(x,\mathrm{E})dx\, dE}$$

- Attenuation coefficient:

$$\mu_x(E) = x_\mathrm{R}\, f_\mathrm{R}(E) + x_\mathrm{P}\, f_\mathrm{P}(E) + x_\mathrm{C}\, f_\mathrm{C}(E) + x_\mathrm{PP}\, f_\mathrm{PP}(E)$$

$$\mu_x(E) \sim \rho_x \frac{\mathrm{N_A}}{A_x} Z_x^4 f_\mathrm{P}(E) + \rho_x \frac{\mathrm{N_A}}{A_x} Z_x f_\mathrm{C}(E)$$

$$\mu_x(E) \sim \rho_x \frac{\mathrm{N_A}}{A_x} Z_x \left(Z_x^3 \frac{1}{E^3} + f_\mathrm{KN}(E) \right)$$

Where fKN is the Klein-Nishina function

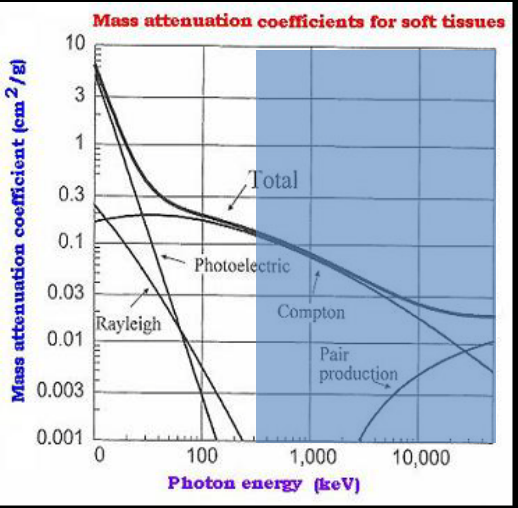

X-ray Attenuation

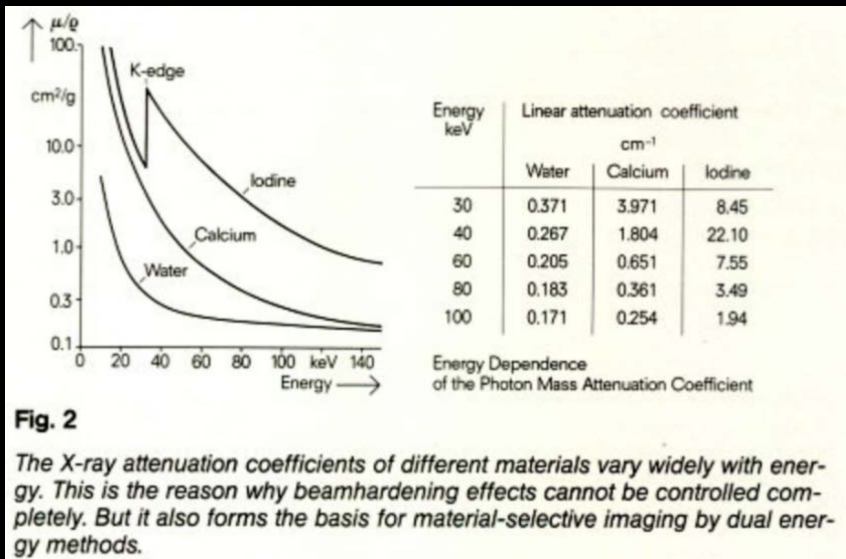

Energy keV	Linear attenuation coefficient cm⁻¹		
	Water	Calcium	Iodine
30	0.371	3.971	8.45
40	0.267	1.804	22.10
60	0.205	0.651	7.55
80	0.183	0.361	3.49
100	0.171	0.254	1.94

Energy Dependence of the Photon Mass Attenuation Coefficient

Fig. 2

The X-ray attenuation coefficients of different materials vary widely with energy. This is the reason why beamhardening effects cannot be controlled completely. But it also forms the basis for material-selective imaging by dual energy methods.

Kalender WA et al. Radiology 164:419-423, 1987

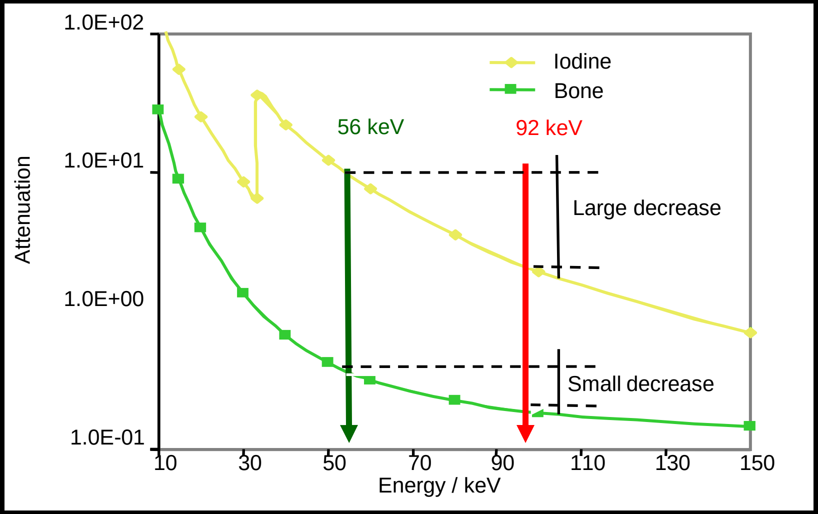

$$\mathrm{D.E.I.}_x = \frac{\mu_x(E_1) - \mu_x(E_2)}{\mu_x(E_1) + \mu_x(E_2)}$$

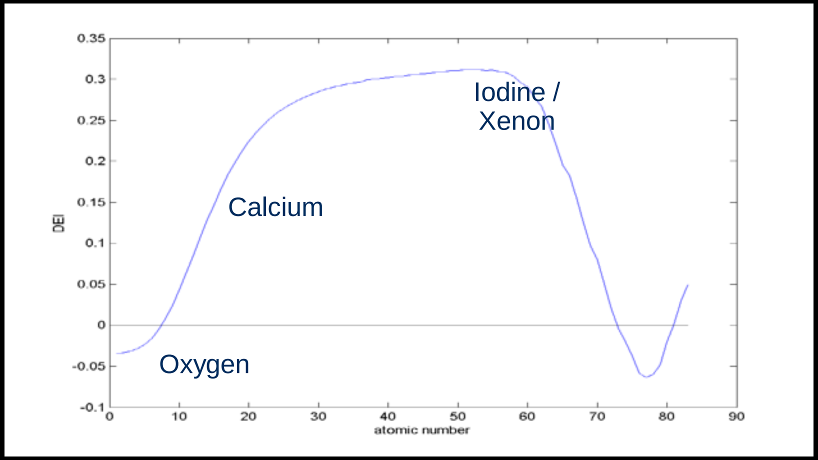

Index of Contents

- Introduction:
  - X-ray attenuation
  - DE principles and technical solutions
- Clinical applications and protocol optimization:
  - Material classification
  - Material quantification (decomposition)
  - Pseudo-monoenergetic images
  - Electron density and effective atomic number images
  - Metal artifacts reduction

DE Principles

- Basic assumptions.
  - Noise
  - Motion
  - Artifacts
- K-edge.
- Materials with “DE properties”.

DE Principles

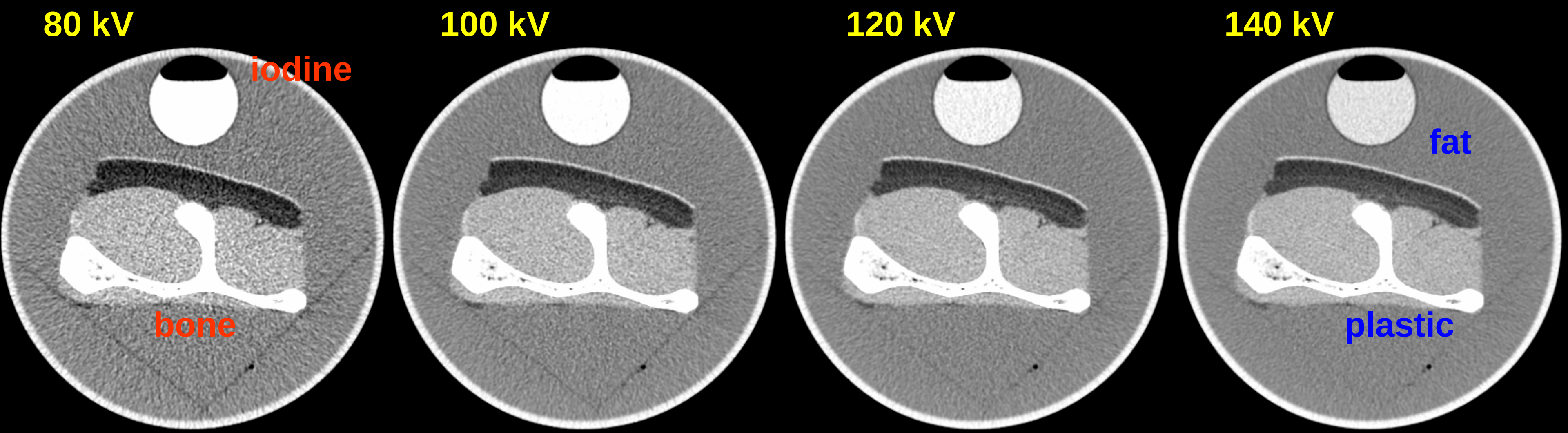

Technical Implementation

- In the clinic:
  - Multiple scans at different spectra mid-range
  - Dual source CT (DSCT), generations 2, and 3
    high-end
  - Fast tube voltage switching high-end
  - Dual layer sandwich detectors high-end
  - Split filter mid-range
- First prototypes:
  - Photon counting detectors (two or more energy bins)
    high-end?

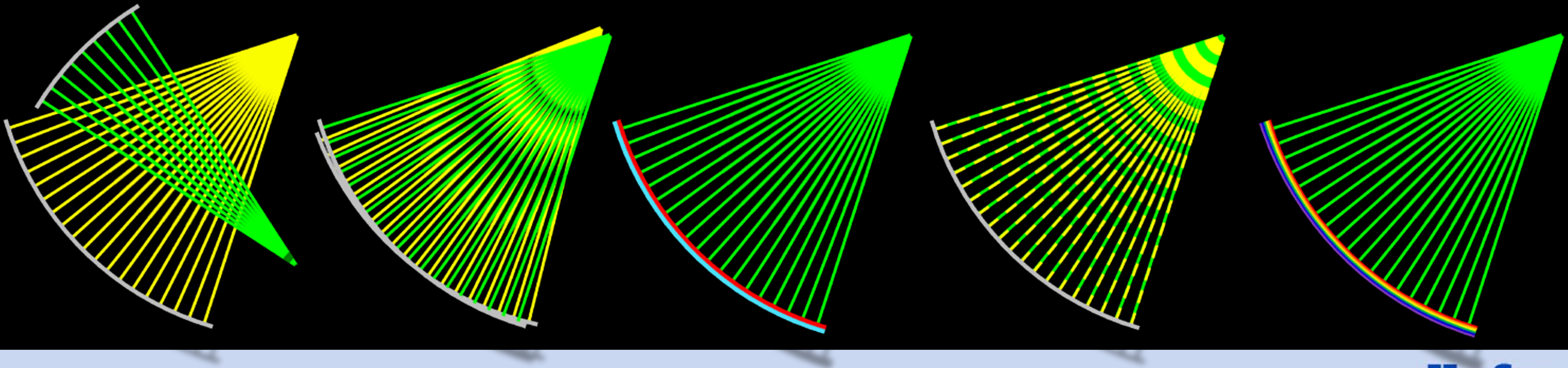

Technical Implementation

- DECT approaches in the clinic:
  - Dual source DECT (Siemens)

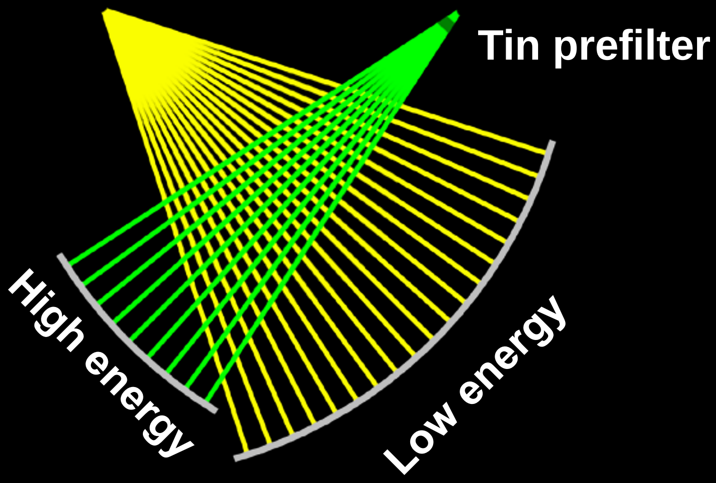

Siemens Somatom Force

Technical Implementation

- DECT approaches in the clinic:
  - Dual source DECT (Siemens)
  - Fast tube voltage switching (GE)

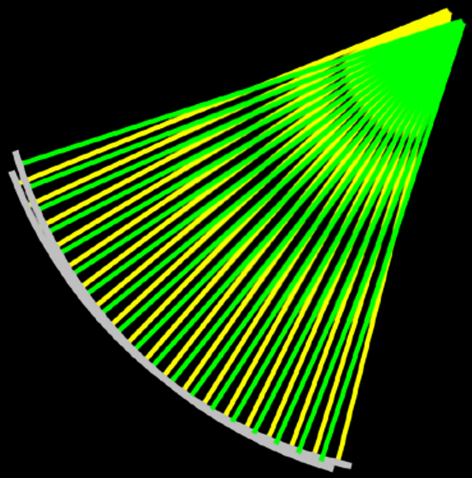

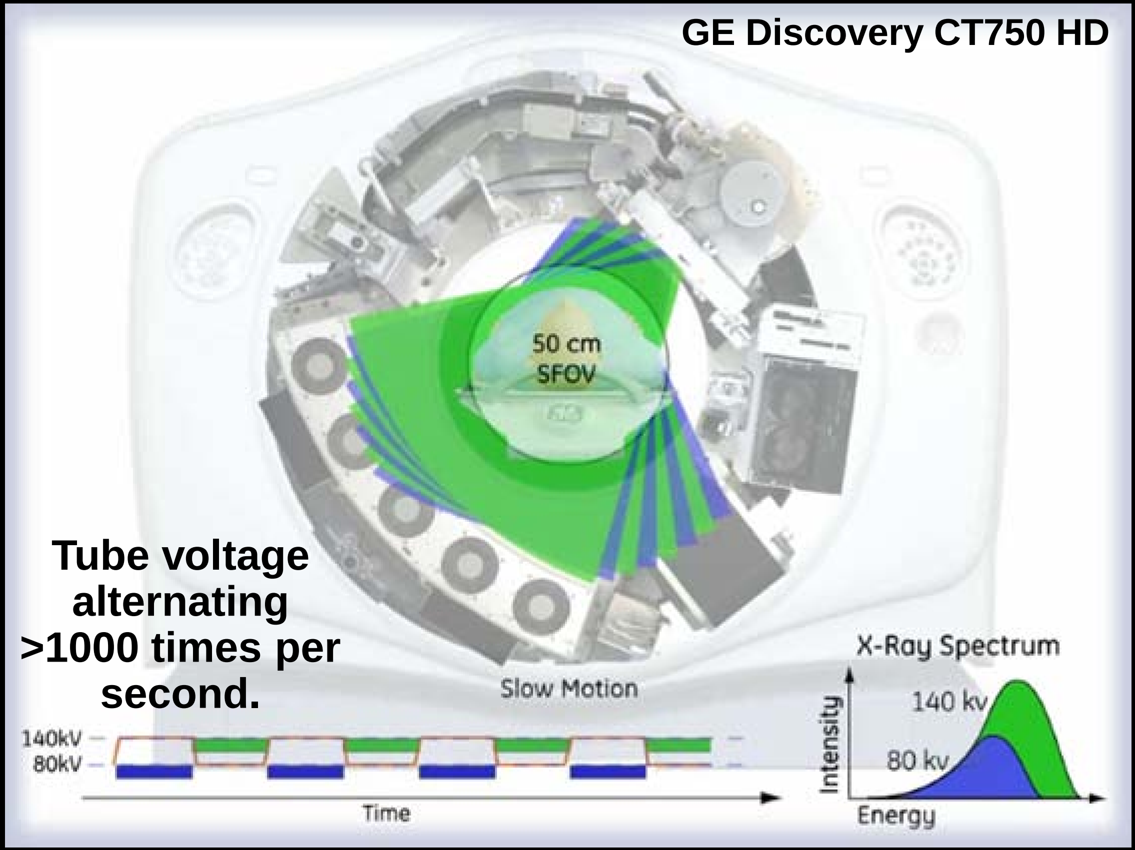

Technical Implementation

- DECT approaches in the clinic:
  - Dual source DECT (Siemens)
  - Fast tube voltage switching (GE)

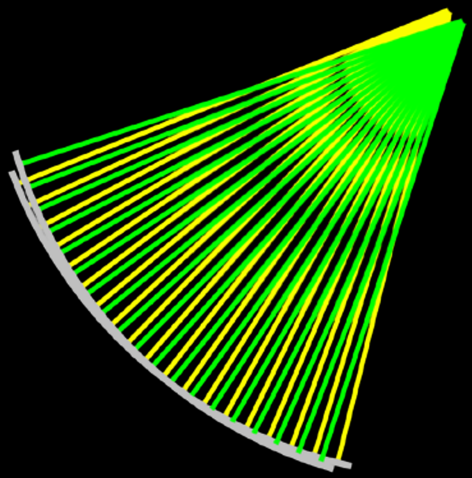

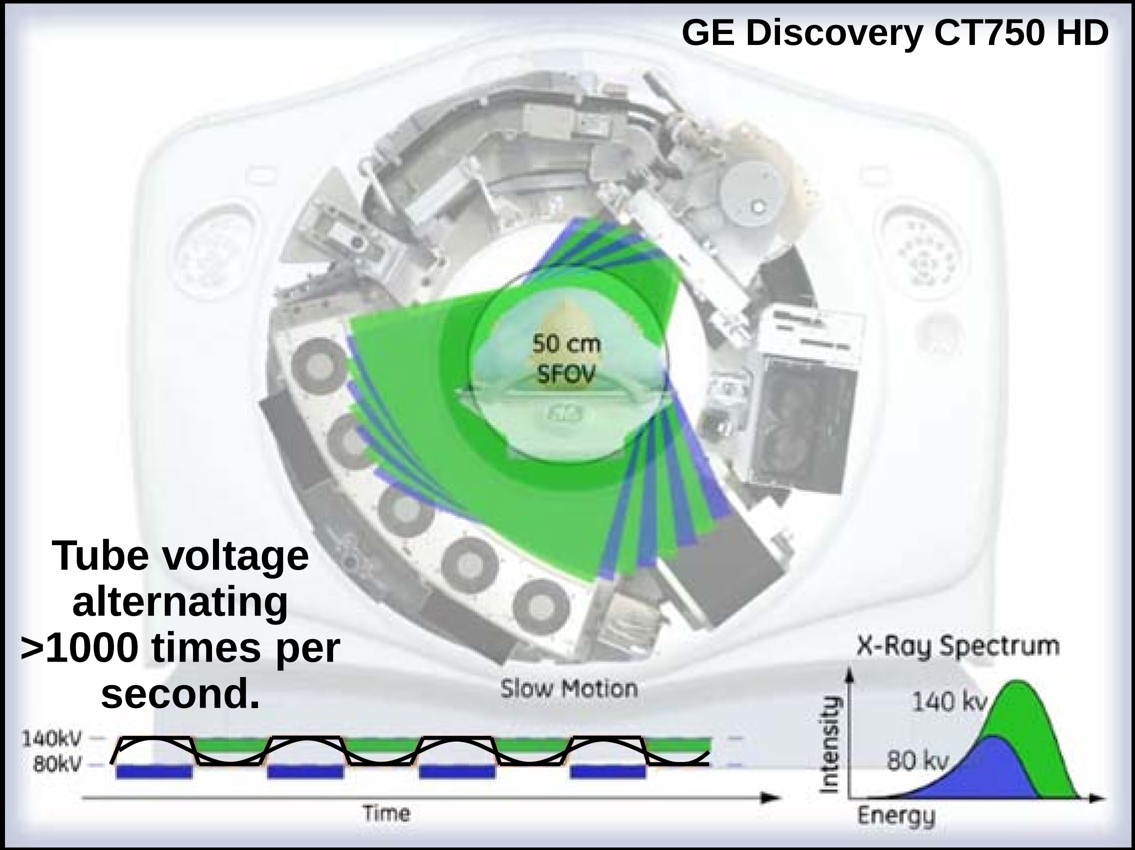

Technical Implementation

- DECT approaches in the clinic:
  - Dual source DECT (Siemens)
  - Fast tube voltage switching (GE)
  - Dual layer (sandwich) detector (Philips)

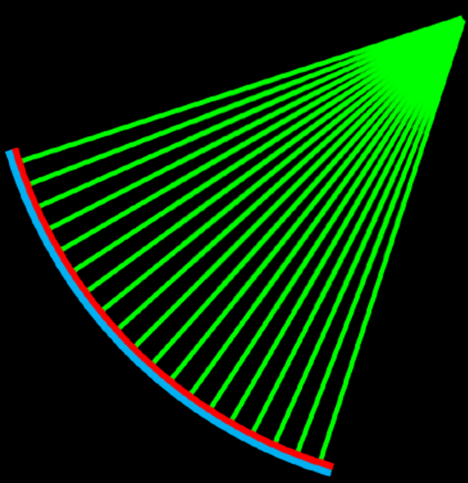

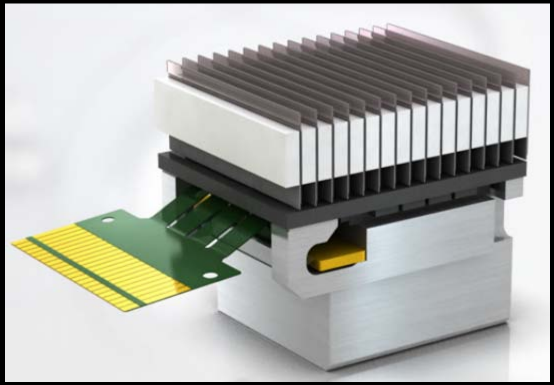

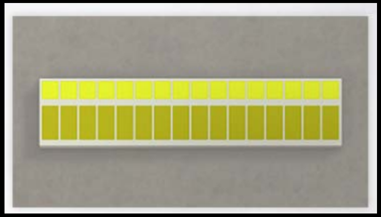

Philips IQon

Technical Implementation

- DECT approaches in the clinic:
  - Dual source DECT (Siemens)
  - Fast tube voltage switching (GE)
  - Dual layer (sandwich) detector (Philips)
  - Split filter (Siemens)

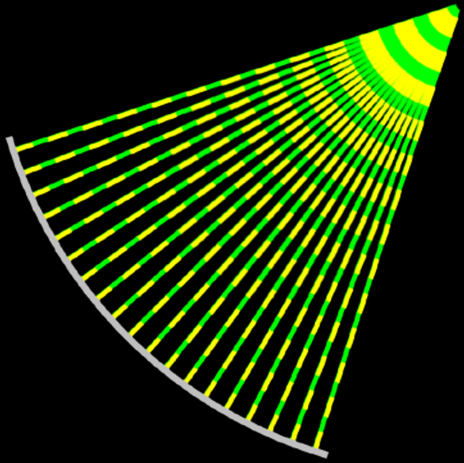

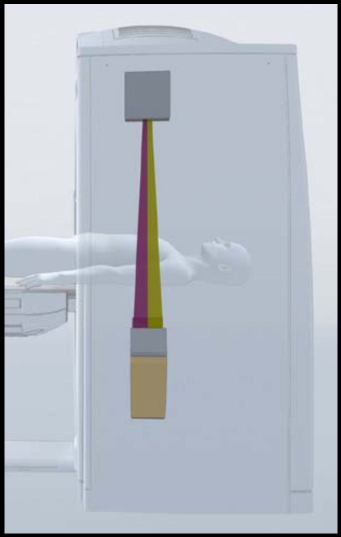

Siemens Definition Edge TwinBeam

Technical Implementation

- DECT approaches in the clinic:
  - Dual source DECT (Siemens)
  - Fast tube voltage switching (GE)
  - Dual layer (sandwich) detector (Philips)
  - Split filter (Siemens)
- First prototype systems
  - Photon counting detector, multiple energy bins

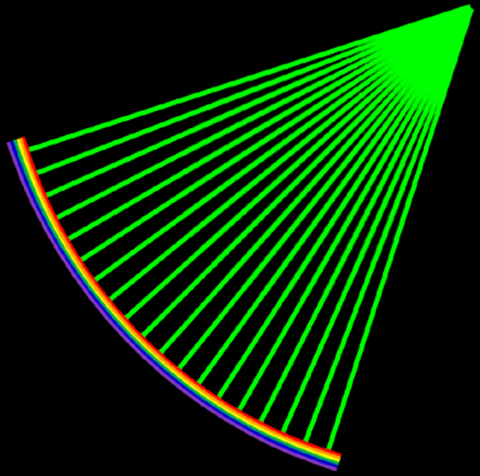

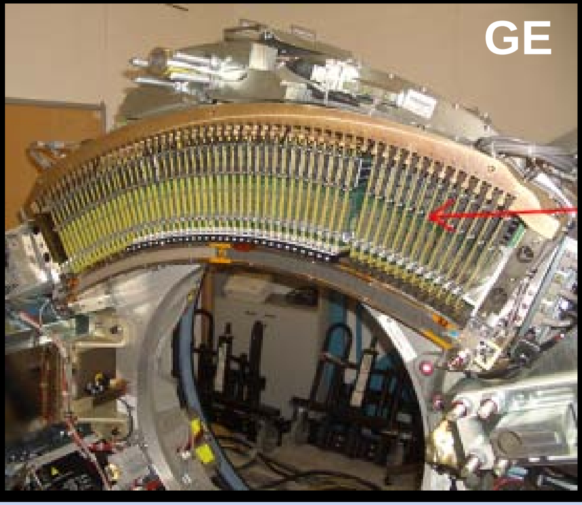

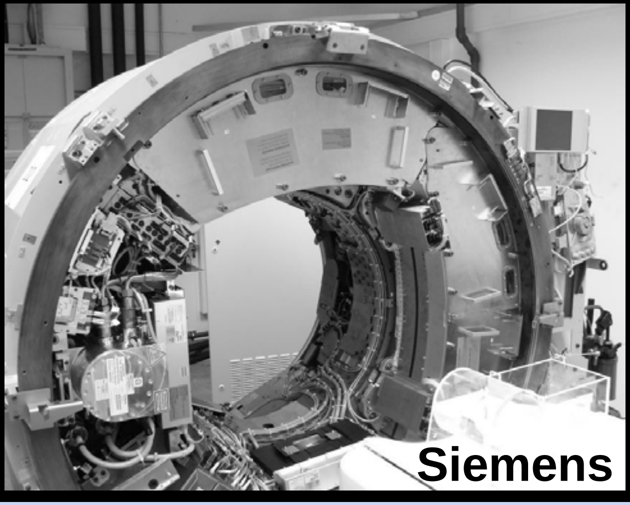

Spectral Separation

Used in
- Siemens‘ 1st generation DSCT

80 kV / 140 kV

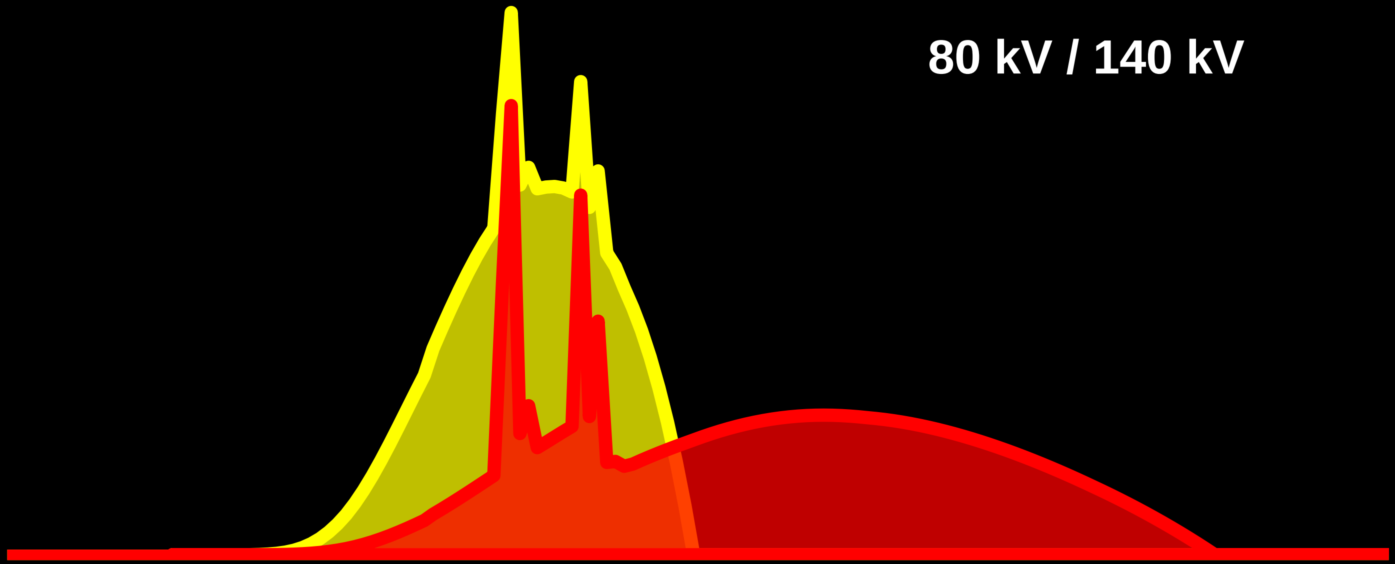

Spectra as seen after having passed a 32 cm water layer.

Faby S and Kachelrieß M.: “Performance of today’s dual energy CT and future multi energy CT in virtual non-contrast imaging and in iodine quantification: A simulation study”, *Med Phys* **42**, 4349 (2015);

Spectral Separation

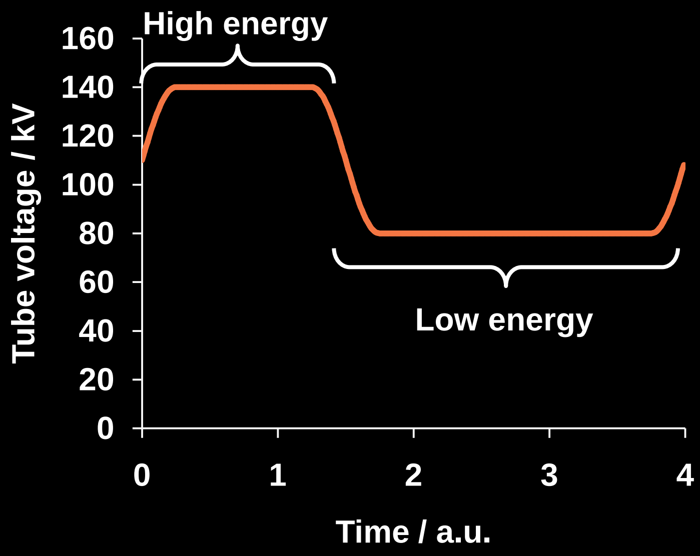

Used in
- GE‘s fast tube voltage switching CT

80 kV / 140 kV

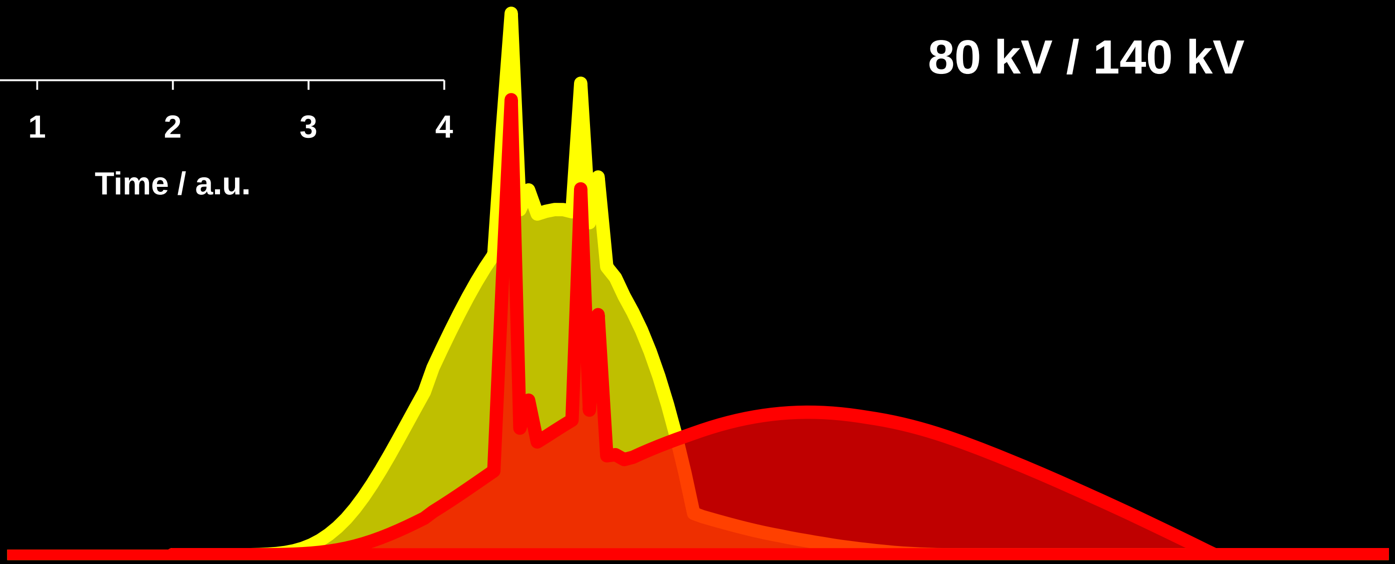

Spectra as seen after having passed a 32 cm water layer.

Faby S and Kachelrieß M.: “Performance of today’s dual energy CT and future multi energy CT in virtual non-contrast imaging and in iodine quantification: A simulation study”, *Med Phys* **42**, 4349 (2015);

Spectral Separation

Used in
- Siemens‘ 2nd generation DSCT

80 kV / $\mathrm{Sn}_{0.4\ \mathrm{mm}}$140 kV

Spectra as seen after having passed a 32 cm water layer.

Faby S and Kachelrieß M.: “Performance of today’s dual energy CT and future multi energy CT in virtual non-contrast imaging and in iodine quantification: A simulation study”, *Med Phys* **42**, 4349 (2015);

Spectral Separation

Used in
- **Siemens‘ 3rd generation DSCT**

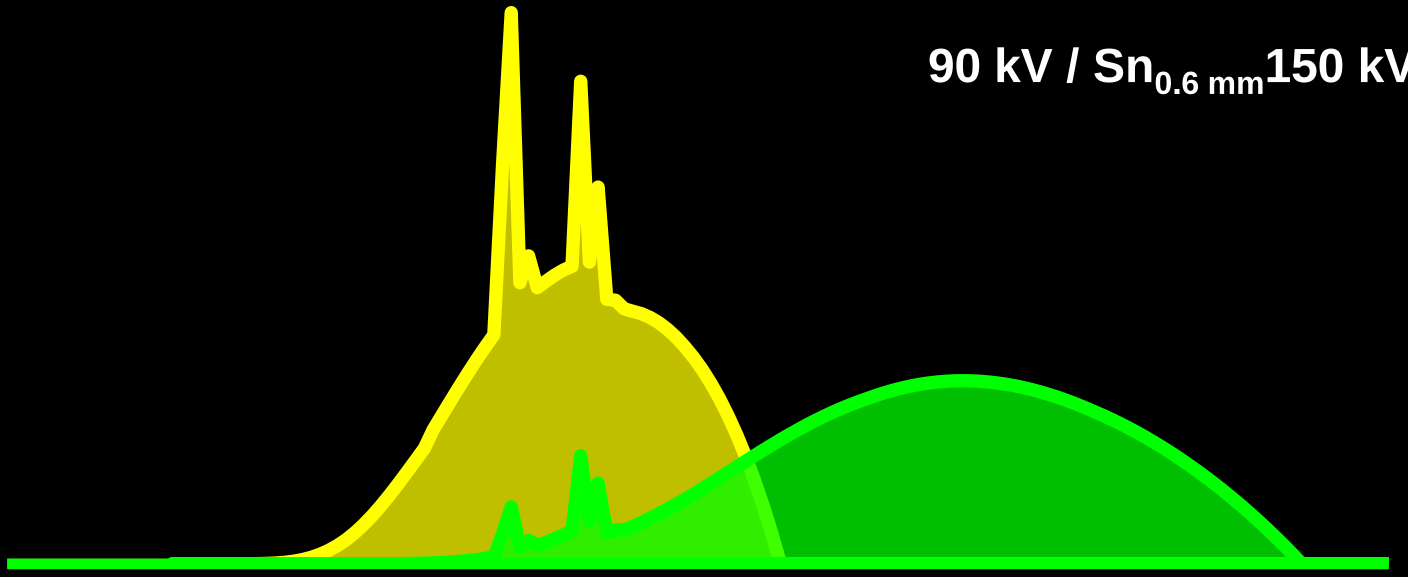

Spectra as seen after having passed a 32 cm water layer.

Faby S and Kachelrieß M.: “Performance of today’s dual energy CT and future multi energy CT in virtual non-contrast imaging and in iodine quantification: A simulation study”, *Med Phys* **42**, 4349 (2015);

Spectral Separation

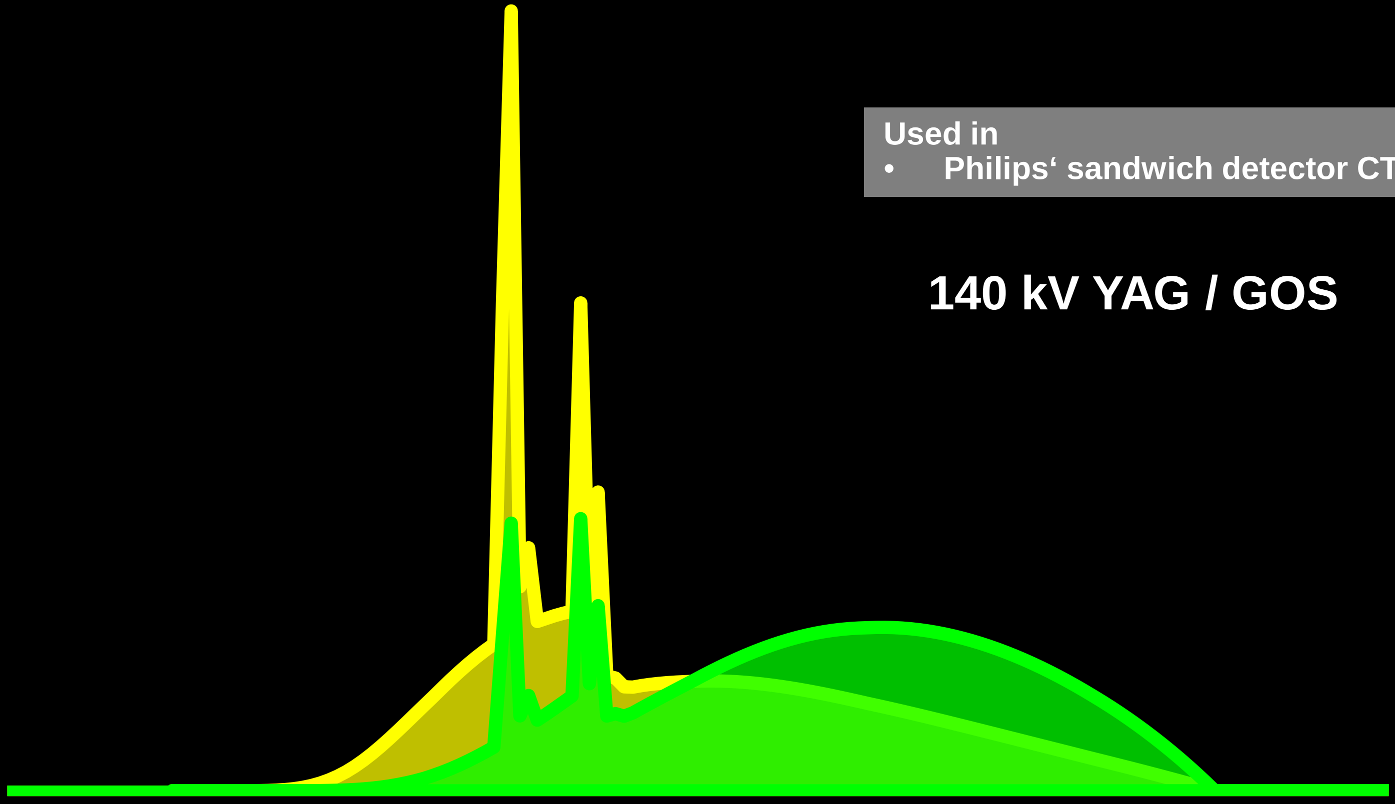

Used in
- Philips‘ sandwich detector CT

140 kV YAG / GOS

Spectra as seen after having passed a 32 cm water layer.

Faby S and Kachelrieß M.: “Performance of today’s dual energy CT and future multi energy CT in virtual non-contrast imaging and in iodine quantification: A simulation study”, *Med Phys* **42**, 4349 (2015);

Spectral Separation

Used in
- **Siemens‘ split filter DSCT**

Spectra as seen after having passed a 32 cm water layer.

Faby S and Kachelrieß M.: “Performance of today’s dual energy CT and future multi energy CT in virtual non-contrast imaging and in iodine quantification: A simulation study”, *Med Phys* **42**, 4349 (2015);

Spectral Separation

PC 140 kV (2 Bins)

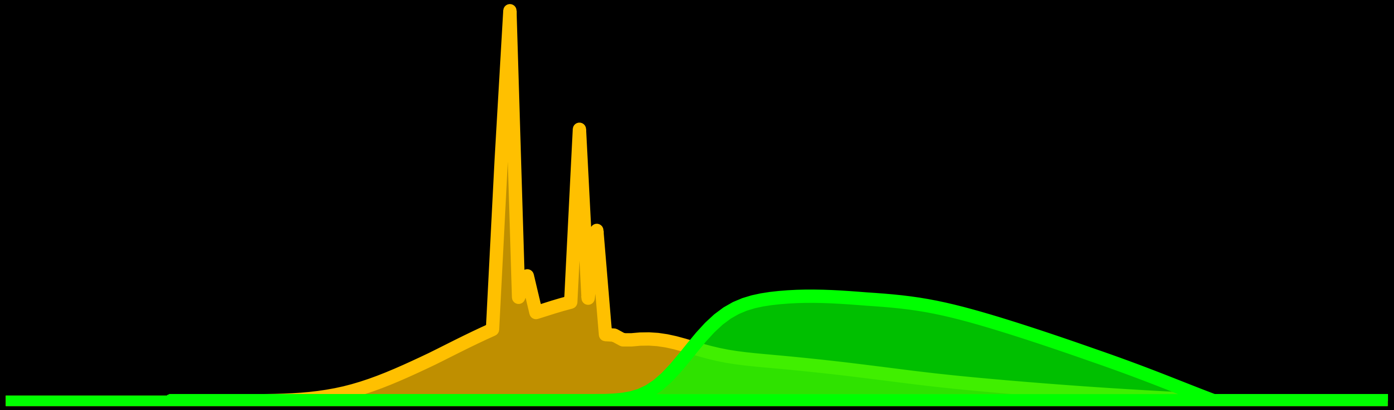

Spectra as seen after having passed a 32 cm water layer.

Faby S and Kachelrieß M.: “Performance of today’s dual energy CT and future multi energy CT in virtual non-contrast imaging and in iodine quantification: A simulation study”, *Med Phys* **42**, 4349 (2015);

Index of Contents

- **Introduction:**
  - X-ray attenuation
  - DE principles and technical solutions
- **Clinical applications and protocol optimization:**
  - Material classification
  - Material quantification (decomposition)
  - Pseudo-monoenergetic images
  - Electron density and effective atomic number images
  - Metal artifacts reduction

Material Classification

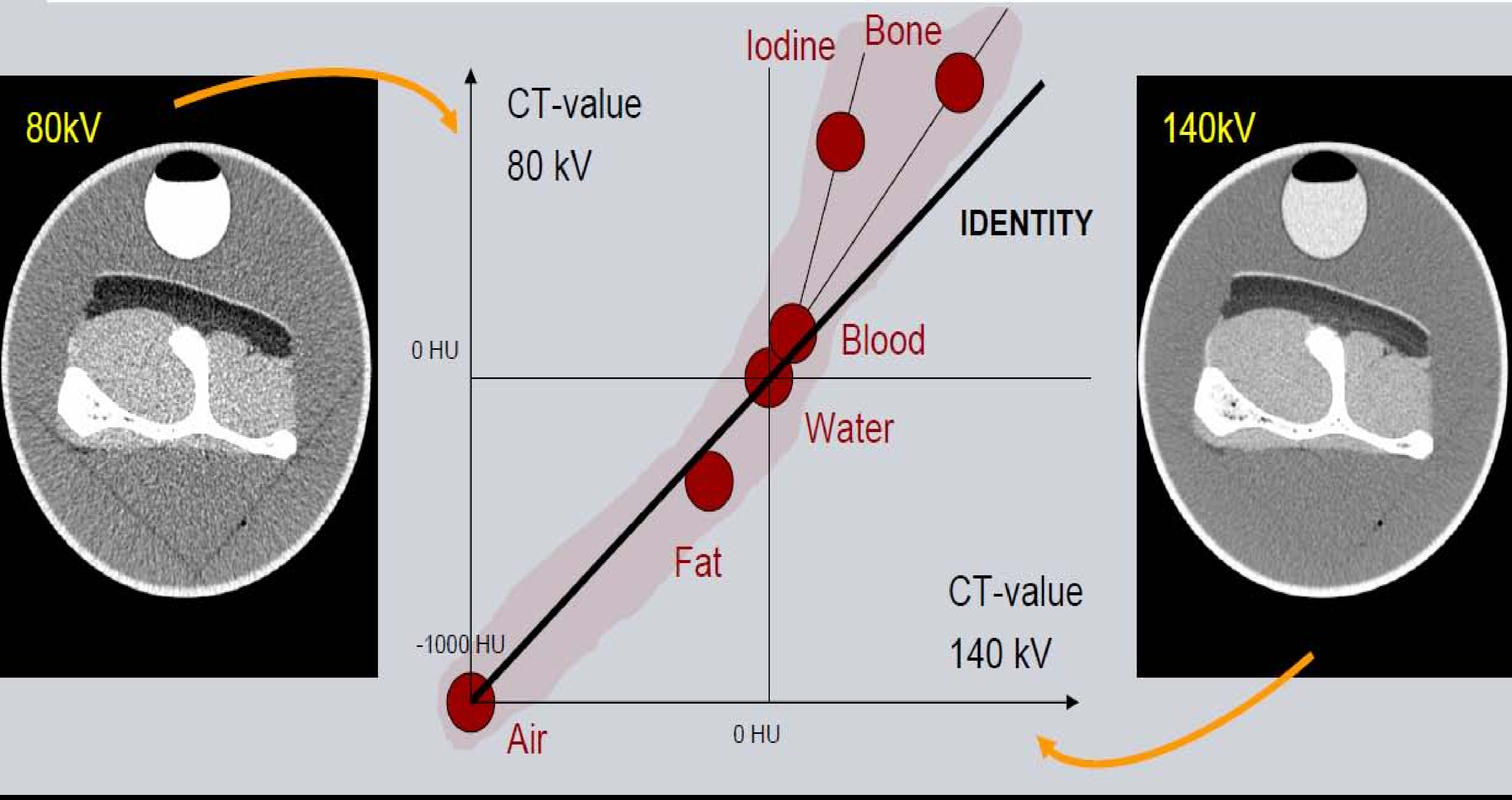

Material Classification

Bone Removal

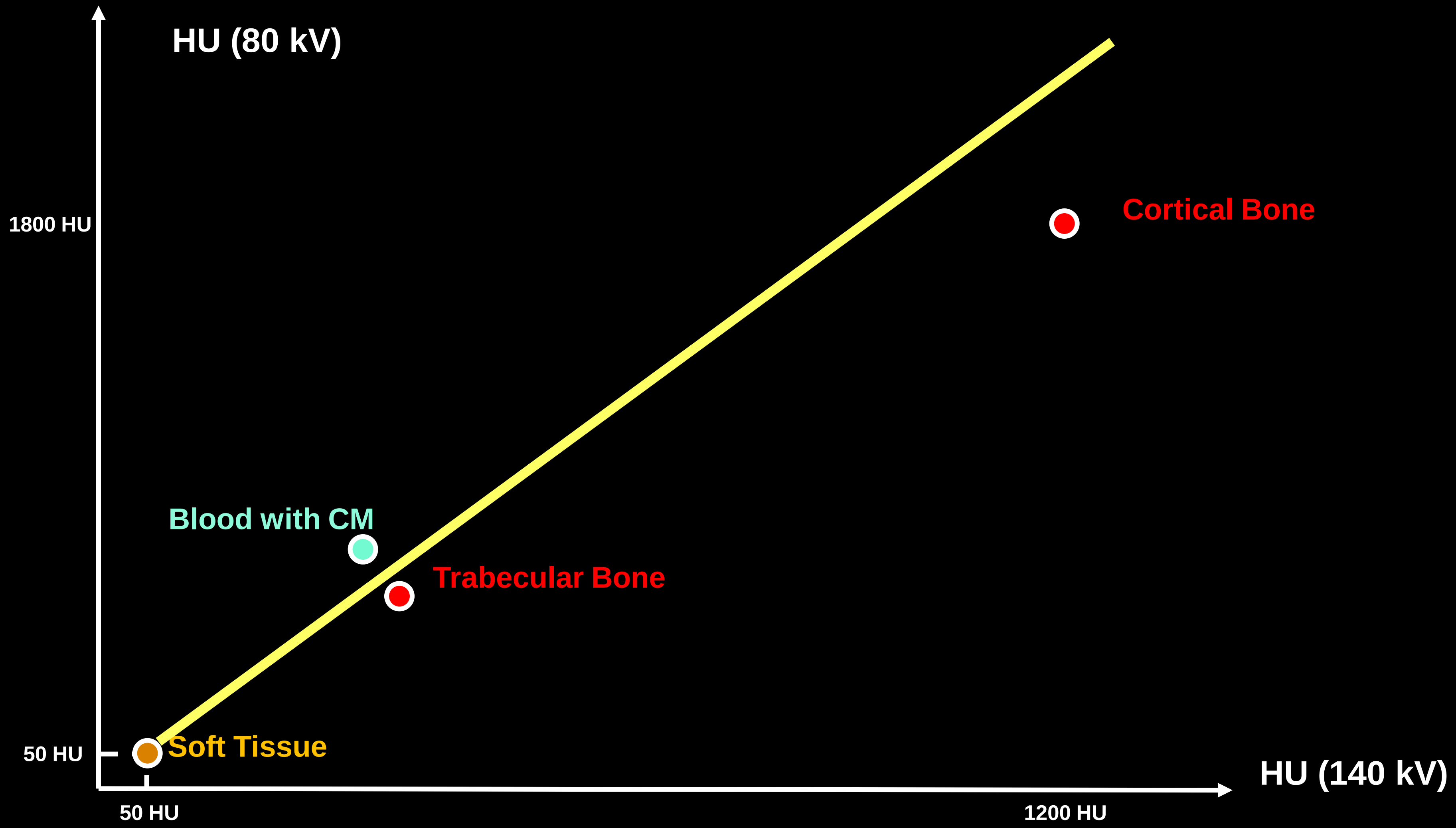

Material Classification

Bone Removal

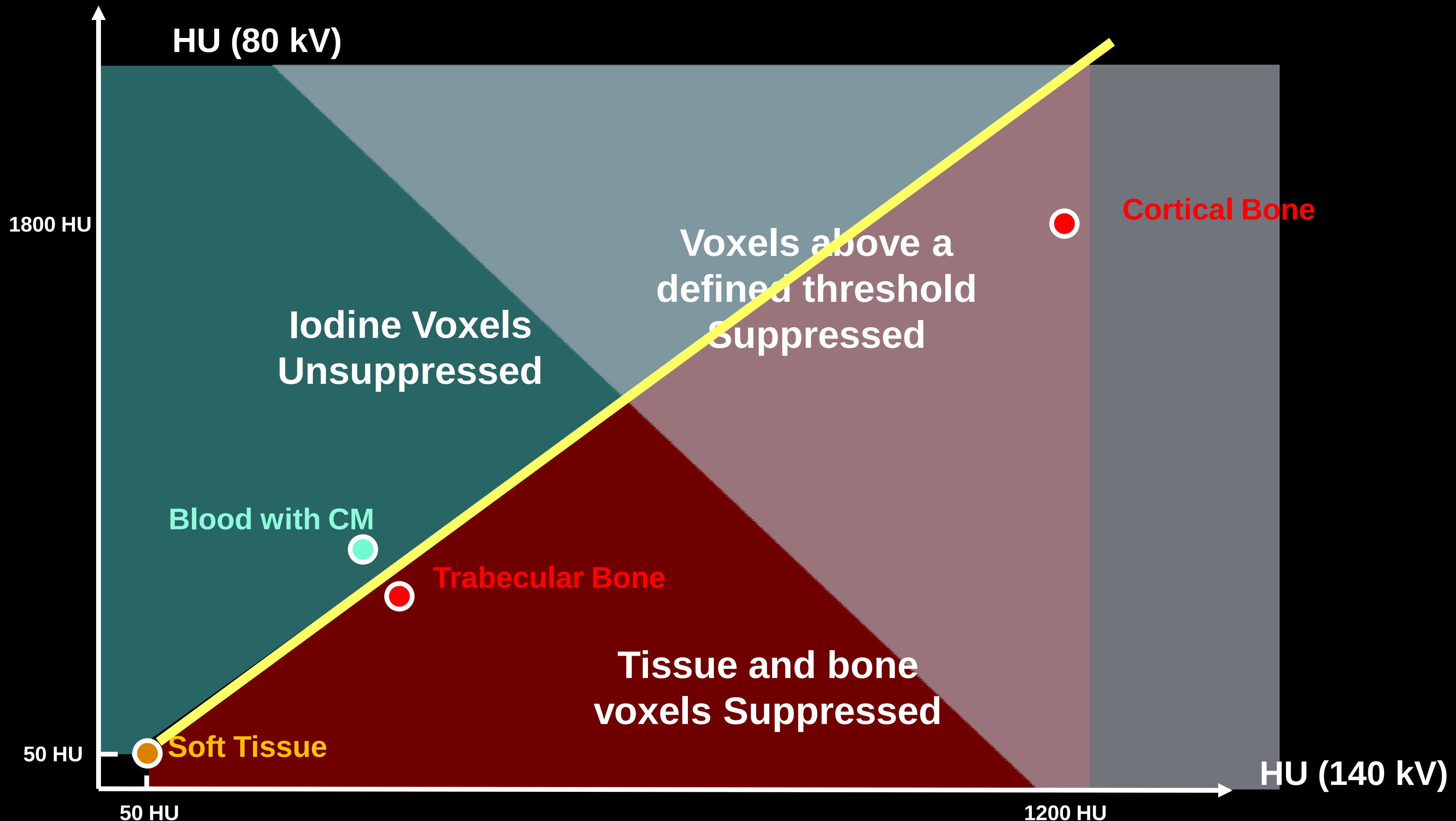

dkfz.

Material Classification

Bone Removal

Dual energy CT
plaque-removal

Digital subtraction
angiography

Material Classification

Kidney Stones

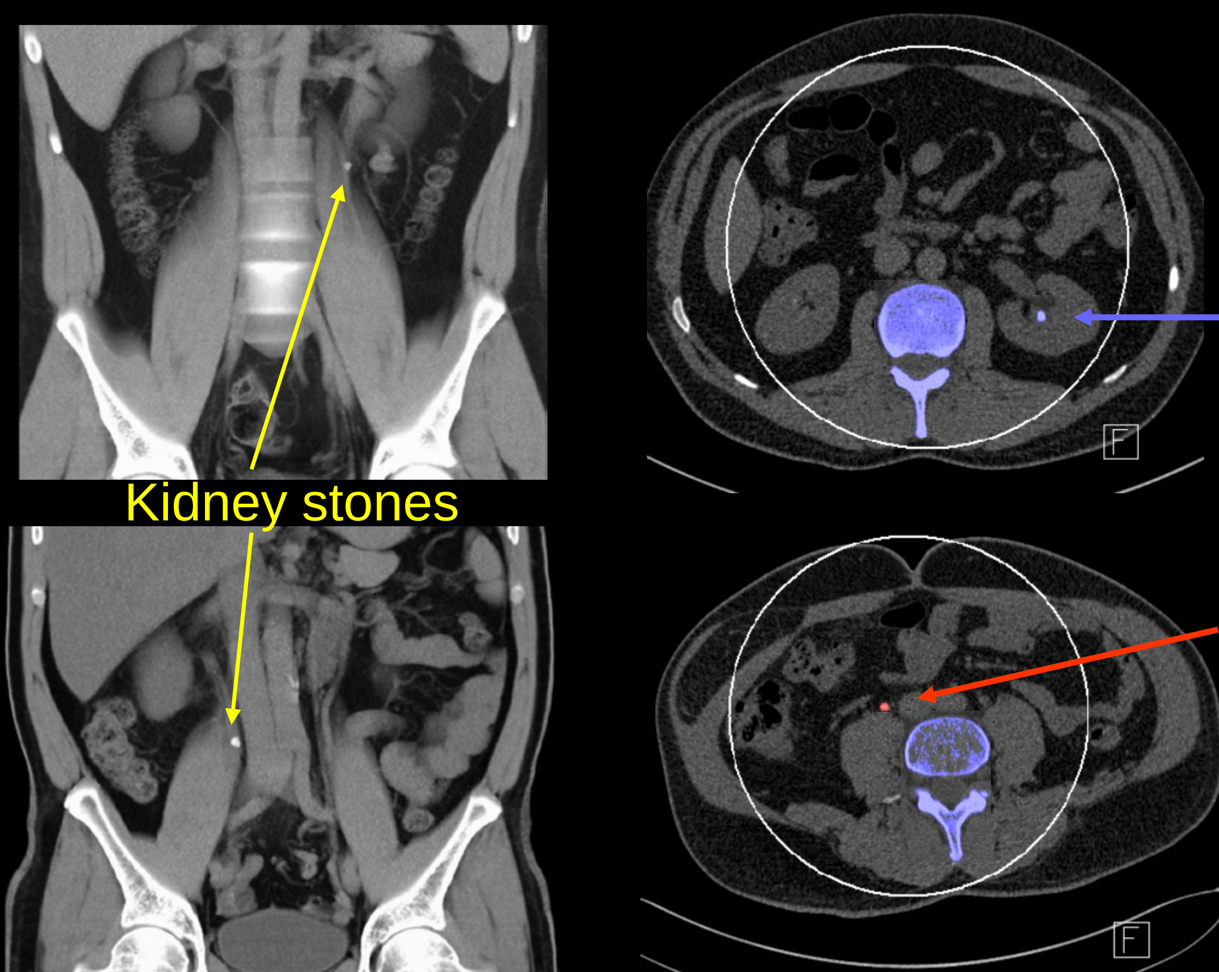

Different
therapy options!

Material Classification

Gout

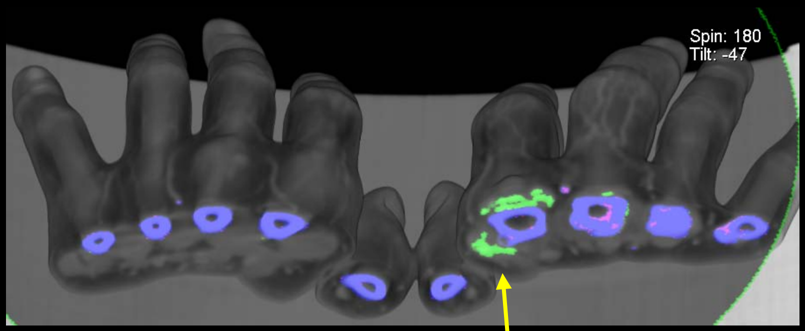

Uric acid-crystals

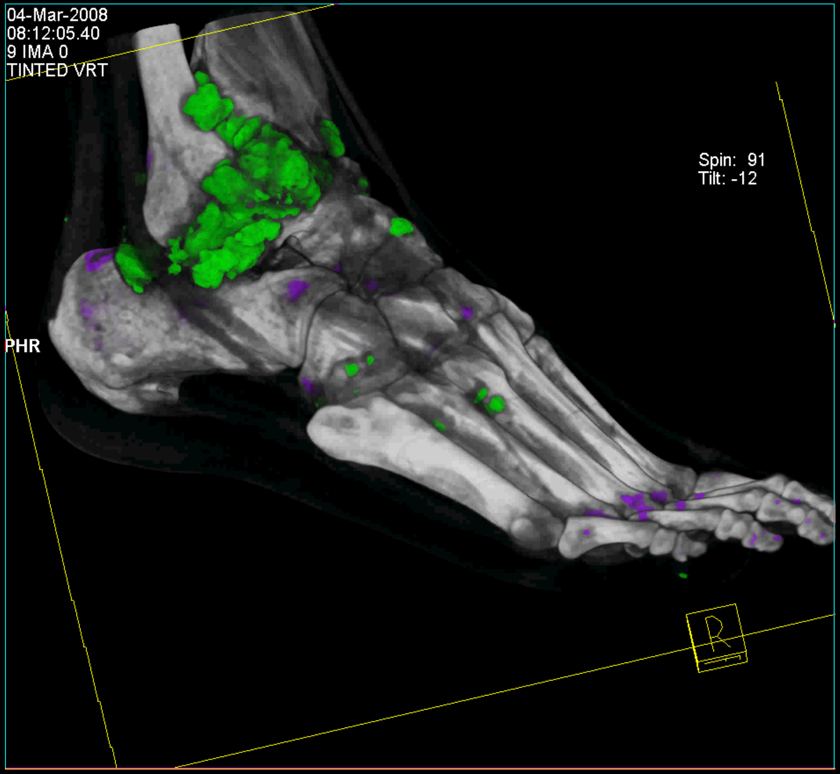

→ Differential diagnosis of gout

Index of Contents

- **Introduction:**
  - X-ray attenuation
  - DE principles and technical solutions
- **Clinical applications and protocol optimization:**
  - Material classification
  - Material quantification (decomposition)
  - Pseudo-monoenergetic images
  - Electron density and effective atomic number images
  - Metal artifacts reduction

Material Quantification

Liver VNC

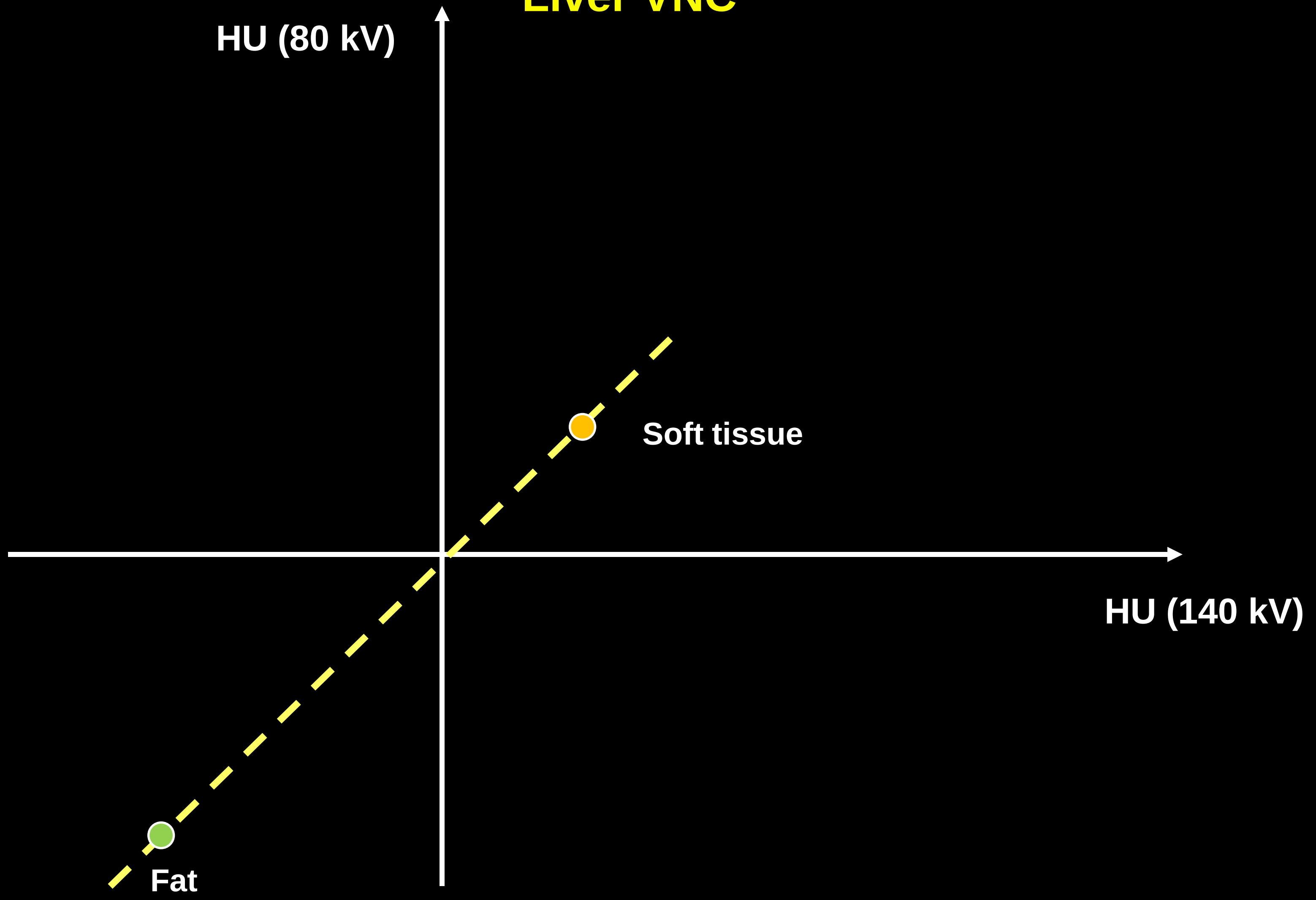

Material Quantification

Liver VNC

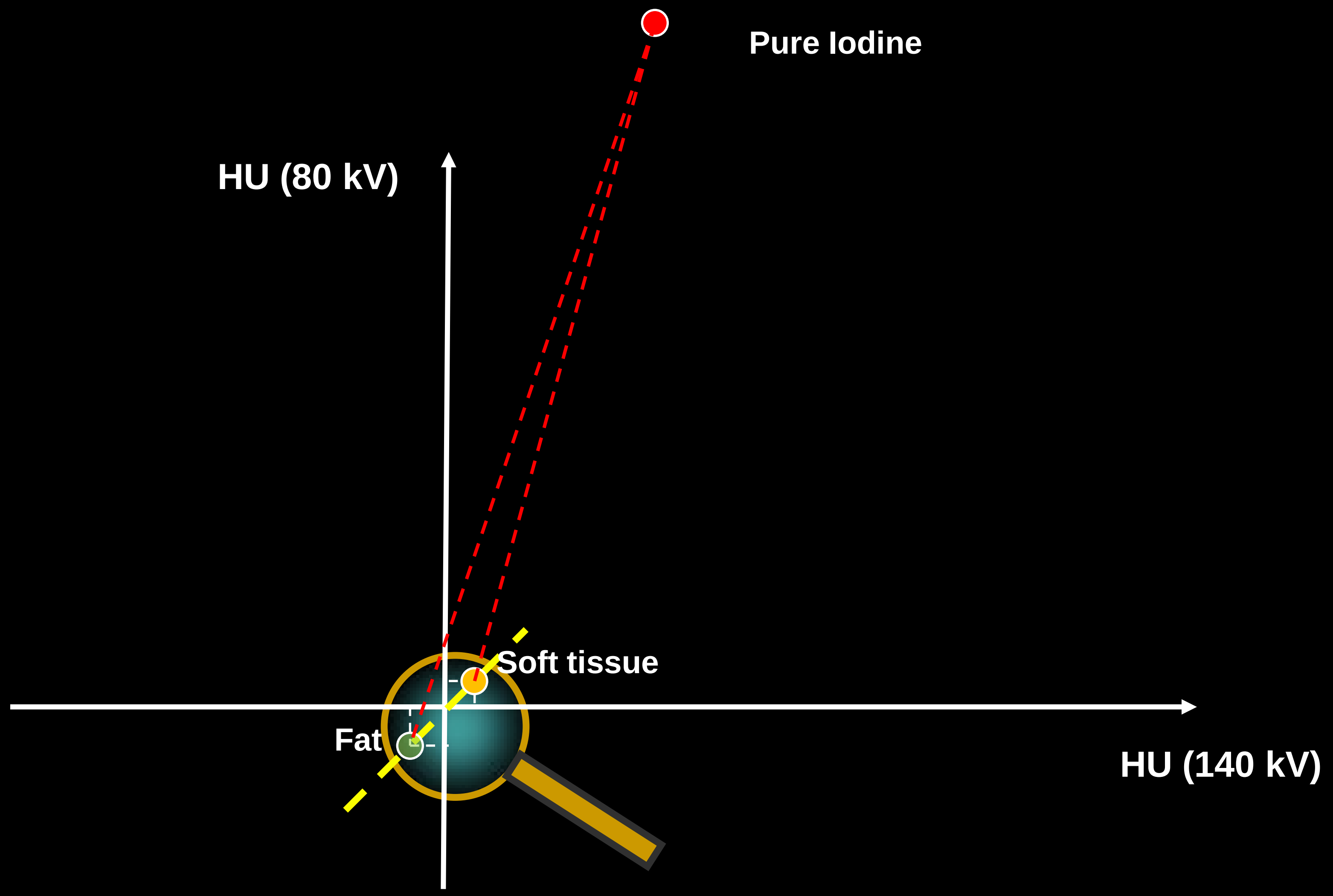

Material Quantification

Liver VNC

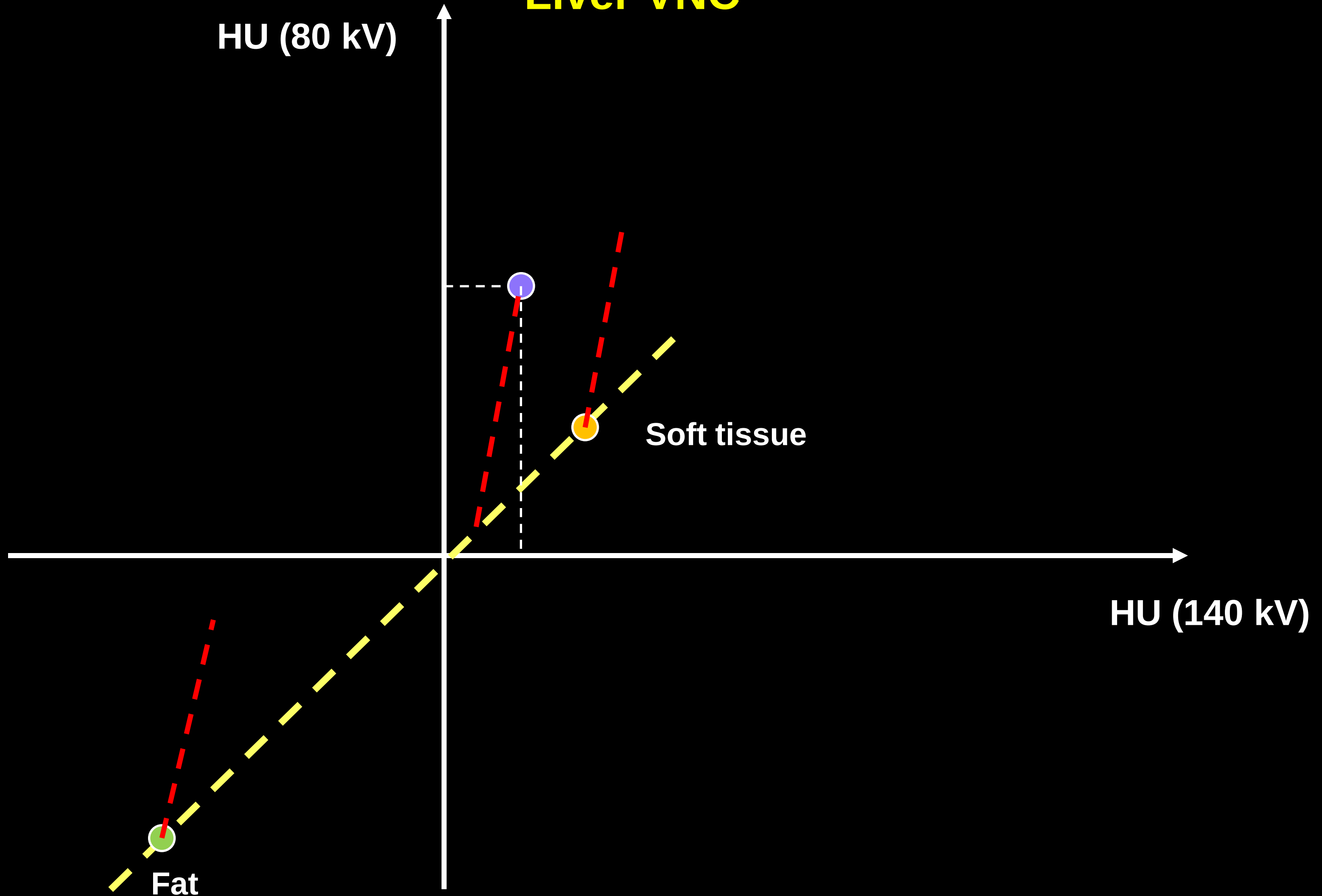

Material Quantification

Liver VNC

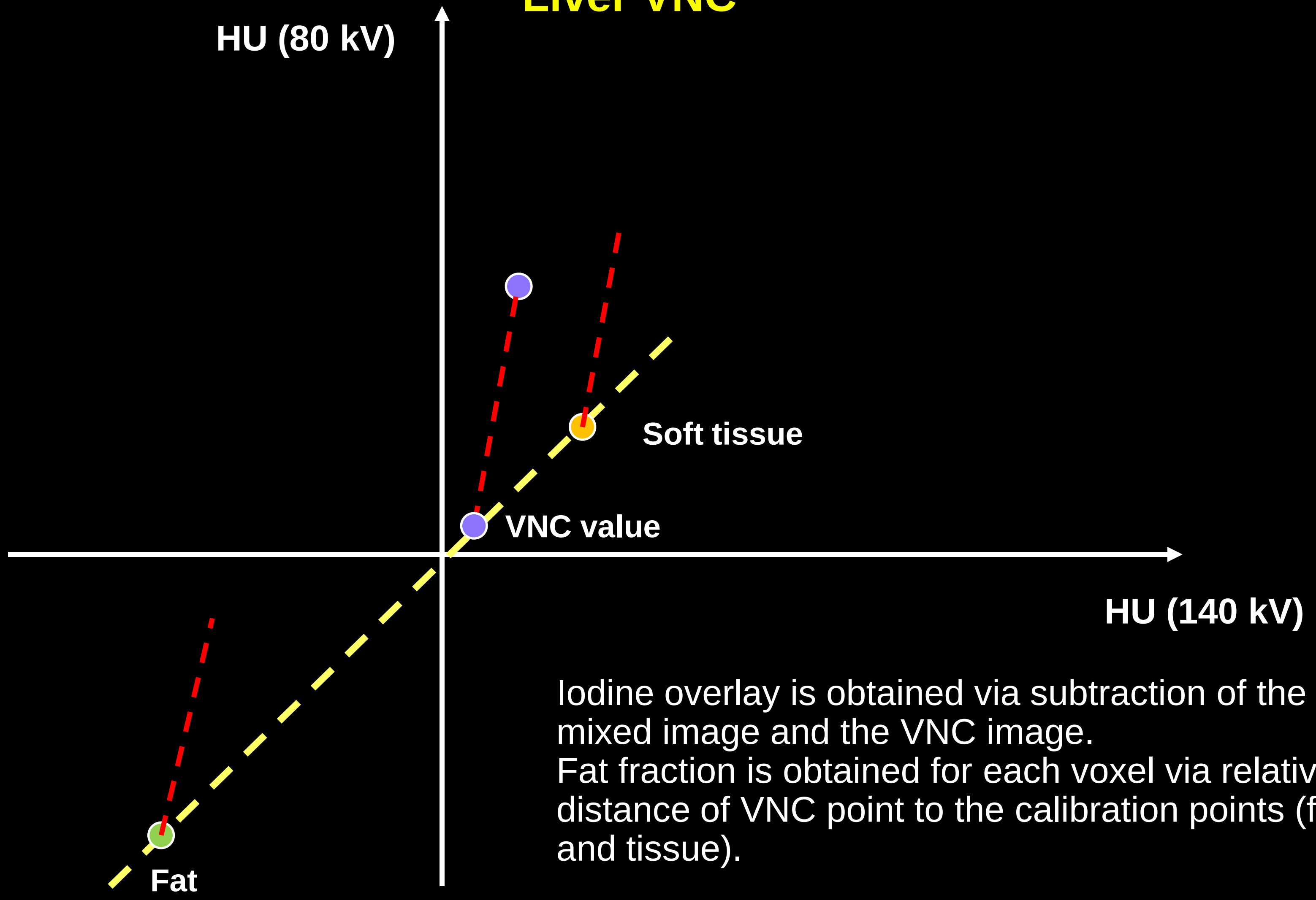

Iodine overlay is obtained via subtraction of the mixed image and the VNC image.
Fat fraction is obtained for each voxel via relative distance of VNC point to the calibration points (fat and tissue).

Material Quantification

Problem in Presence of a 4th Material (i.e. Calcium)

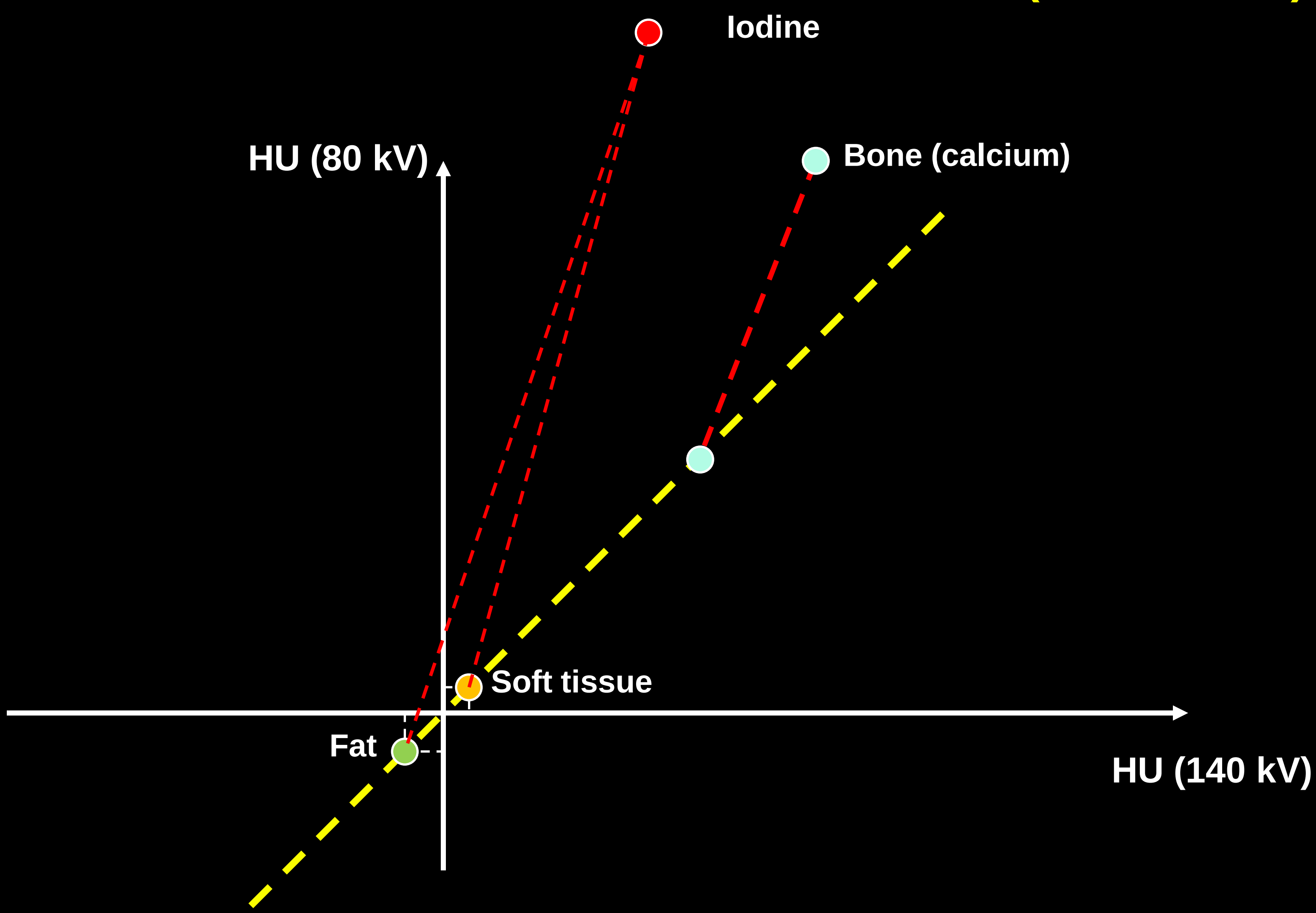

Material Quantification

Liver VNC

Other quantification application are possible changing:

- Calibration materials (for example air and soft tissue for lung iodine enhancement)
- Material to be quantified (for example calcium instead of iodine, VNCa)

Single DECT Scan

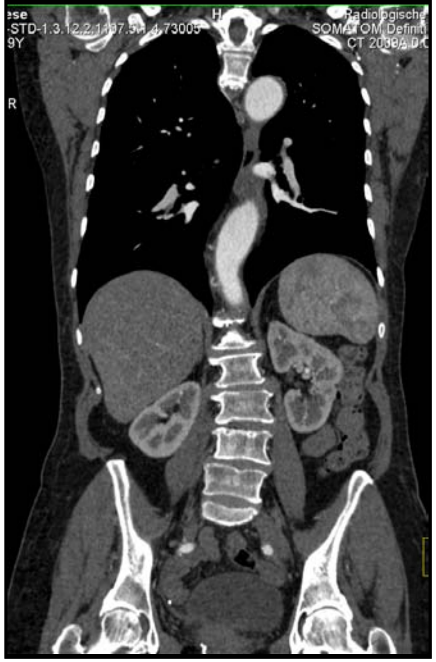

Mixed image

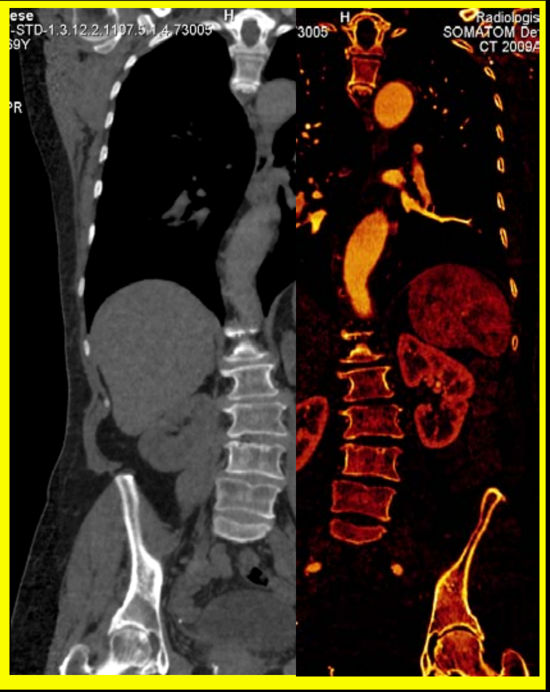

Virtual non-contrast and iodine image

Material Quantification

Other Applications

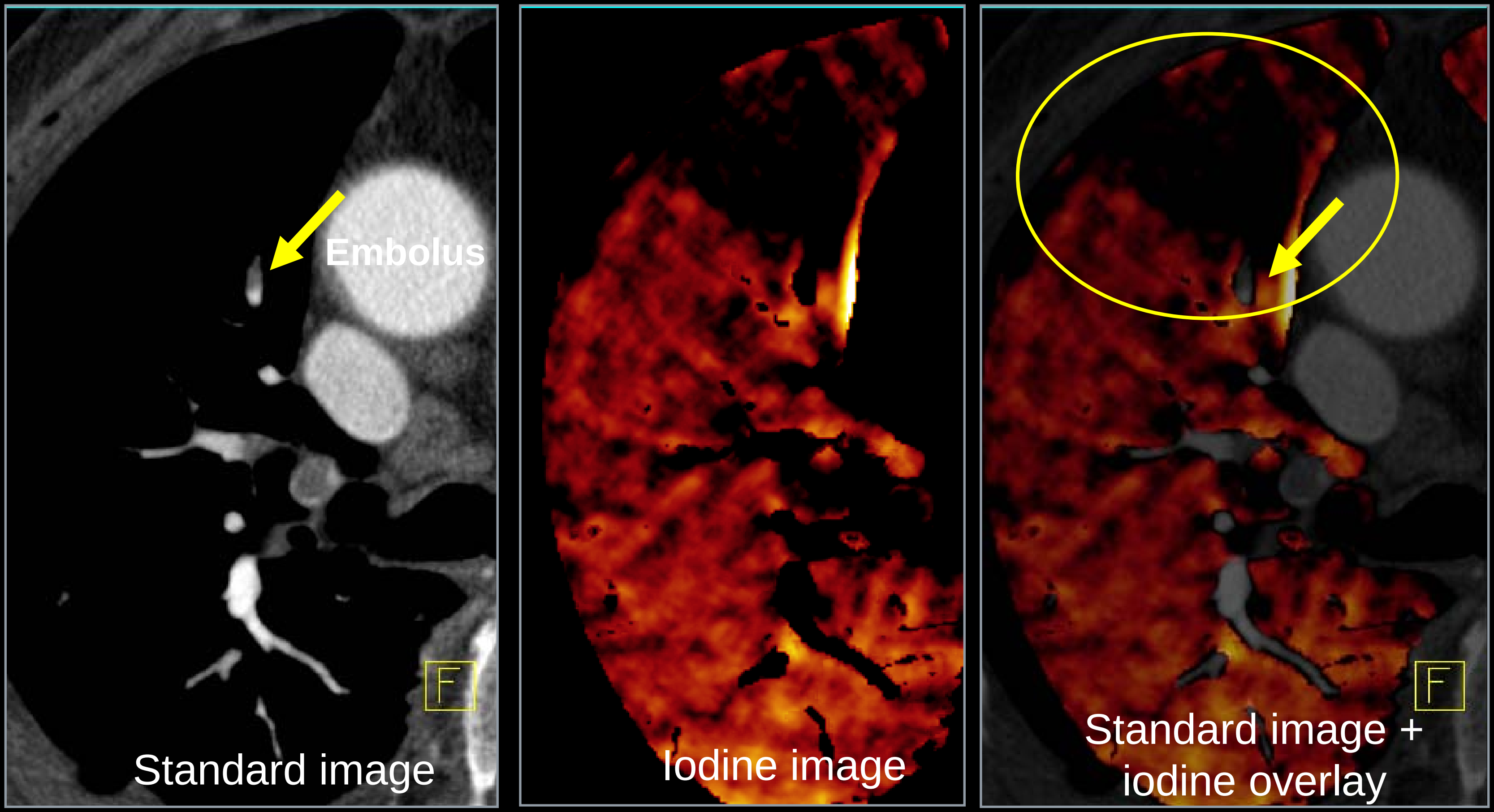

Material Quantification

Other Applications

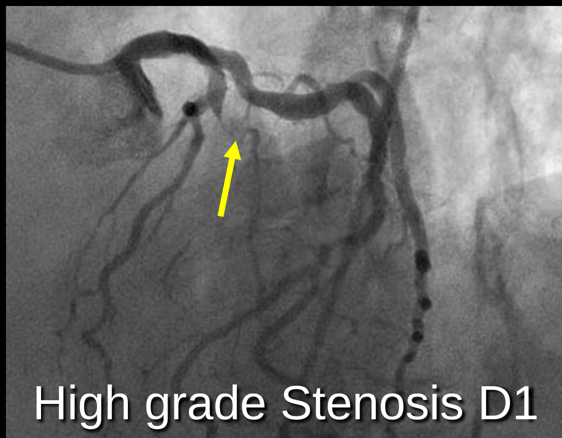

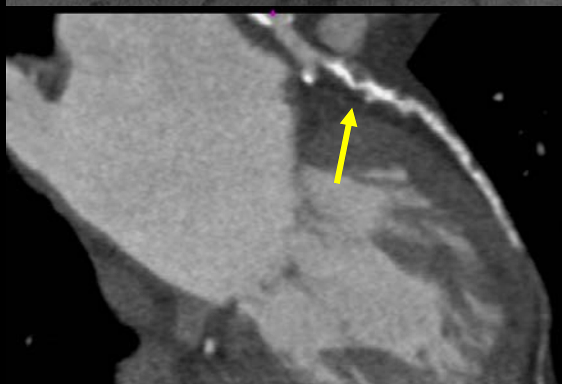

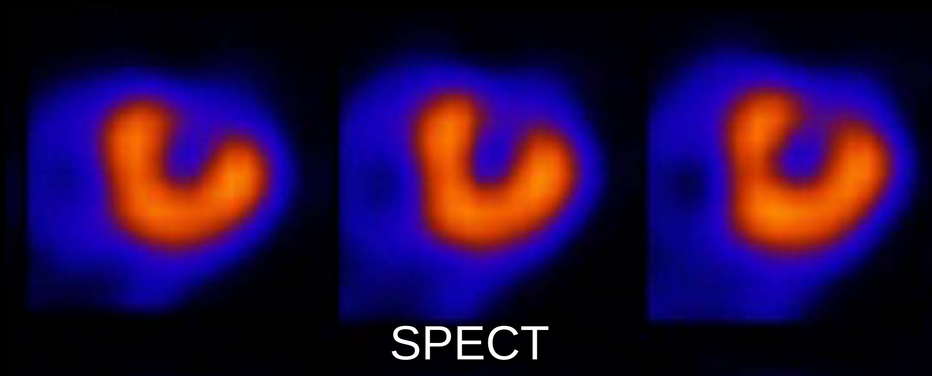

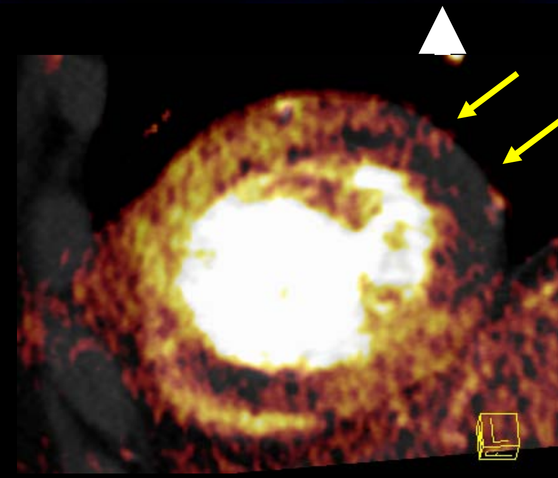

Material Quantification

Other Applications

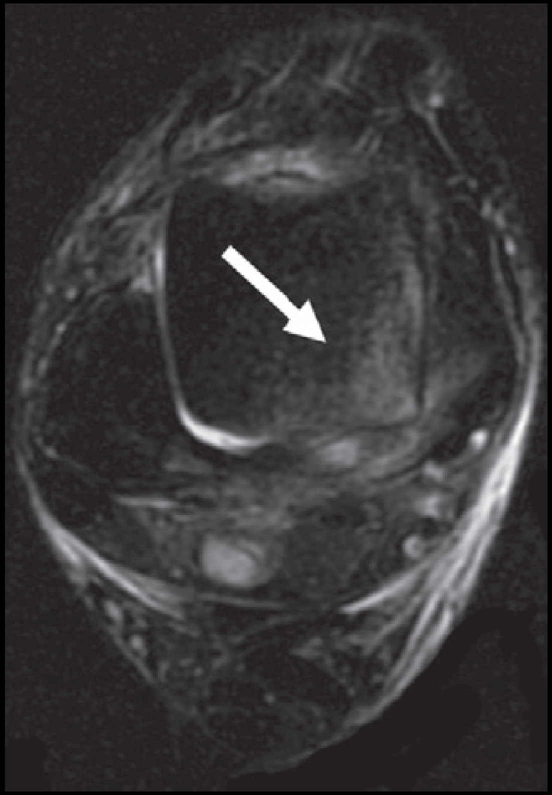

MR

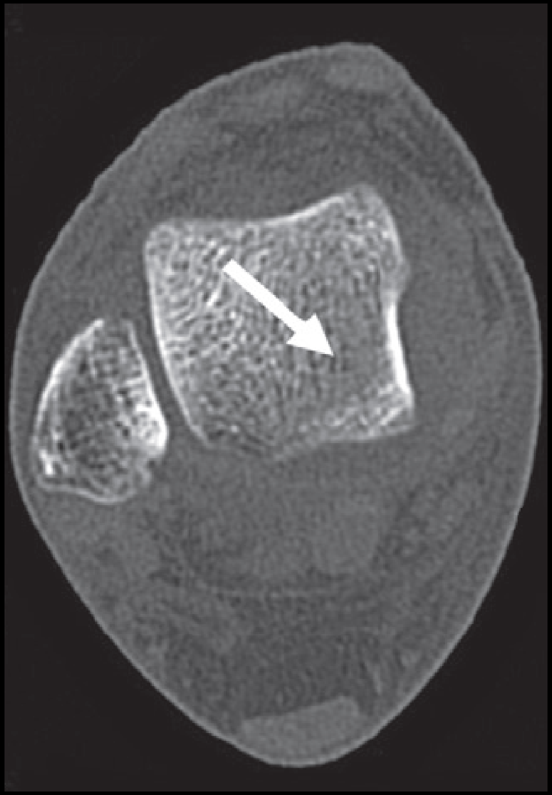

DE mixed CT
(equivalent to SE 120 kV)

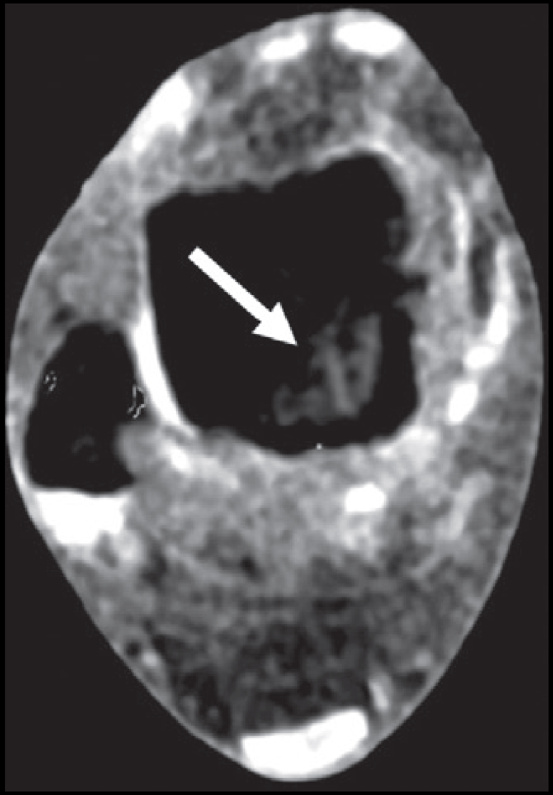

VNCa

Calcium has weak DE properties. VNCa works fine for small body regions.

R. Guggemberger et al.: "Diagnostic Performance of Dual-Energy CT for the Detection of Traumatic Bone Marrow Lesions in the Ankle: Comparison with MR Imaging". *Radiology* **264**, (2012)

Index of Contents

- **Introduction:**
  - X-ray attenuation
  - DE principles and technical solutions
- **Clinical applications and protocol optimization:**
  - Material classification
  - Material quantification (decomposition)
  - Pseudo-monoenergetic images
  - Electron density and effective atomic number images
  - Metal artifacts reduction

Pseudo-Monoenergetic Images

Attenuation coefficient for a material x:

$$\mu_x(E) = x_\mathrm{P}\, f_\mathrm{P}(E) + x_\mathrm{C}\, f_\mathrm{C}(E)$$

Attenuation coefficient for materials y and z:

$$\mu_y(E) = y_\mathrm{P}\, f_\mathrm{P}(E) + y_\mathrm{C}\, f_\mathrm{C}(E)$$

$$\mu_z(E) = z_\mathrm{P}\, f_\mathrm{P}(E) + z_\mathrm{C}\, f_\mathrm{C}(E)$$

y and z are called “basis material”. They have to be chosen in such a way that their photoelectric and Compton cross-sections (y_P, z_P and y_C, z_C respectively) are known.

Pseudo-Monoenergetic Images

Direct Method

$$\mu_x(E) = x_\mathrm{P}\, f_\mathrm{P}(E) + x_\mathrm{C}\, f_\mathrm{C}(E)$$

$$\begin{cases} \mu_x(E_\mathrm{low}) = x_\mathrm{P}\, f_\mathrm{P}(E_\mathrm{low}) + x_\mathrm{C}\, f_\mathrm{C}(E_\mathrm{low}) \\ \mu_x(E_\mathrm{high}) = x_\mathrm{P}\, f_\mathrm{P}(E_\mathrm{high}) + x_\mathrm{C}\, f_\mathrm{C}(E_\mathrm{high}) \end{cases}$$

Unknown: x_P, x_C

Known: $f_P(E), f_C(E) \quad \forall E$

Measured: $\mu_x(E_\mathrm{low}), \mu_x(E_\mathrm{high})$

Pseudo-Monoenergetic Images

Material Basis Method (more robust)

$$\mu_x(E) = x_\mathrm{P}\, f_\mathrm{P}(E) + x_\mathrm{C}\, f_\mathrm{C}(E)$$

$$\begin{cases} \mu_y(E) = y_\mathrm{P}\, f_\mathrm{P}(E) + y_\mathrm{C}\, f_\mathrm{C}(E) \\ \mu_z(E) = z_\mathrm{P}\, f_\mathrm{P}(E) + z_\mathrm{C}\, f_\mathrm{C}(E) \end{cases} \rightarrow$$

$$f_P(E) = g_1(\mu_y(E), \mu_z(E))$$

$$f_C(E) = g_2(\mu_y(E), \mu_z(E))$$

Pseudo-Monoenergetic Images

Material Basis Method (more robust)

$$\mu_x(E) = x_\mathrm{P}\, f_\mathrm{P}(E) + x_\mathrm{C}\, f_\mathrm{C}(E)$$

$$f_P(E) = g_1(\mu_y(E), \mu_z(E))$$

$$f_C(E) = g_2(\mu_y(E), \mu_z(E))$$

$$\begin{cases} \mu_x(E_\mathrm{low}) = a_y\, \mu_y(E_\mathrm{low}) + a_z\, \mu_z(E_\mathrm{low}) \\ \mu_x(E_\mathrm{high}) = a_y\, \mu_y(E_\mathrm{high}) + a_z\, \mu_z(E_\mathrm{high}) \end{cases}$$

$$\mu_x(E) = a_y\, \mu_y(E) + a_z\, \mu_z(E)$$

Pseudo-Monoenergetic Images

Solving the system and expressing everything in CT values, if one of the two basis material is water, we obtain:

$$\mathrm{HU}_x(E) = (1 - \alpha(E))\,\mathrm{HU}_x(E_{\mathrm{low}}) + \alpha(E)\,\mathrm{HU}_x(E_{\mathrm{high}})$$

Pseudo-Monoenergetic Images

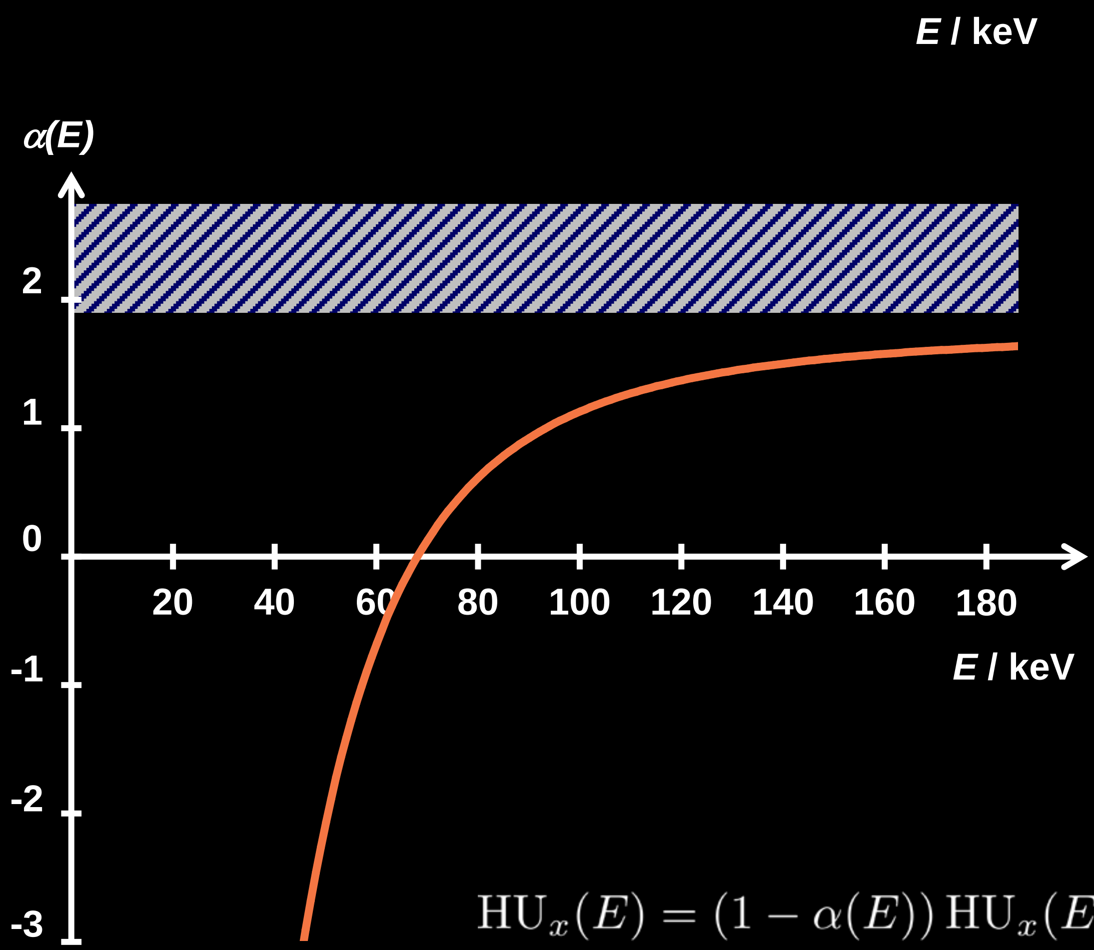

$$\mathrm{HU}_x(E) = (1-\alpha(E))\,\mathrm{HU}_x(E_{\mathrm{low}}) + \alpha(E)\,\mathrm{HU}_x(E_{\mathrm{high}})$$

Index of Contents

- **Introduction:**
  - X-ray attenuation
  - DE principles and technical solutions
- **Clinical applications and protocol optimization:**
  - Material classification
  - Material quantification (decomposition)
  - Pseudo-monoenergetic images
  - Electron density and effective atomic number images
  - Metal artifacts reduction

Electron Density and Effective Atomic Number Images

Direct Method

$$\mu_x(E) \sim \rho_x \frac{\mathrm{N_A}}{A_x} Z_x \left(Z_x^3 \frac{1}{E^3} + f_{\mathrm{KN}}(E) \right)$$

- ρ_x, density of the element $\left[\frac{g}{m^3}\right]$ → unknown
- N_A , Avogadro number: number of atoms needed to have A grams of an element of atomic mass A → known
- A_x , atomic mass of the element $[\mathrm{a.m.u.}](\sim g)$ → unknown
- Z_x , average atomic number of the voxel (i.e. number of electrons of the element) → unknown

Electron Density and Effective Atomic Number Images

Direct Method

Electron density is defined as the number of electrons in one unit of volume:

$$\rho_e = \frac{n}{m^3} = \frac{g}{m^3}\frac{n}{g} = \frac{g}{m^3}\left(n_e\frac{n_a}{g}\right) = \rho Z\frac{N_A}{A}$$

↓

$$\mu_x(E) \sim \rho_x\frac{\mathrm{N_A}}{A_x}Z_x\left(Z_x^3\frac{1}{E^3} + f_{\mathrm{KN}}(E)\right)$$

$$\mu_x(E) \sim \rho_{e_x}\left(Z_x^3\frac{1}{E^3} + f_{\mathrm{KN}}(E)\right)$$

Electron Density and Effective Atomic Number Images

Material Basis Method (more robust)

$$\mu_x(E) = a_y\,\mu_y(E) + a_z\,\mu_z(E)$$

Pseudo-monoenergetic formula

$$\rho_{e_x} = a_y\,\rho_{e_y} + a_z\,\rho_{e_z}$$

Electron density formula (does not depend on energy)

Electron Density and Effective Atomic Number Images

Material Basis Method (more robust)

$$\hat{\rho}_{e_x} = \frac{\rho_{e_x}}{\rho_{e_w}} = a_w \frac{\rho_{e_w}}{\rho_{e_w}} + a_i \frac{\rho_{e_i}}{\rho_{e_w}} = a_w + a_i \hat{\rho}_{e_i}$$

$$Z_x = \left[\left(\frac{a_w}{a_w + a_i \hat{\rho}_{e_i}} Z_w \right)^n + \left(\frac{a_i \hat{\rho}_{e_i}}{a_w + a_i \hat{\rho}_{e_i}} Z_i \right)^n \right]^{\frac{1}{n}}$$

Index of Contents

- **Introduction:**
  - X-ray attenuation
  - DE principles and technical solutions
- **Clinical applications and protocol optimization:**
  - Material classification
  - Material quantification (decomposition)
  - Pseudo-monoenergetic images
  - Electron density and effective atomic number images
  - Metal artifacts reduction

DE for Metal Artifacts Reduction

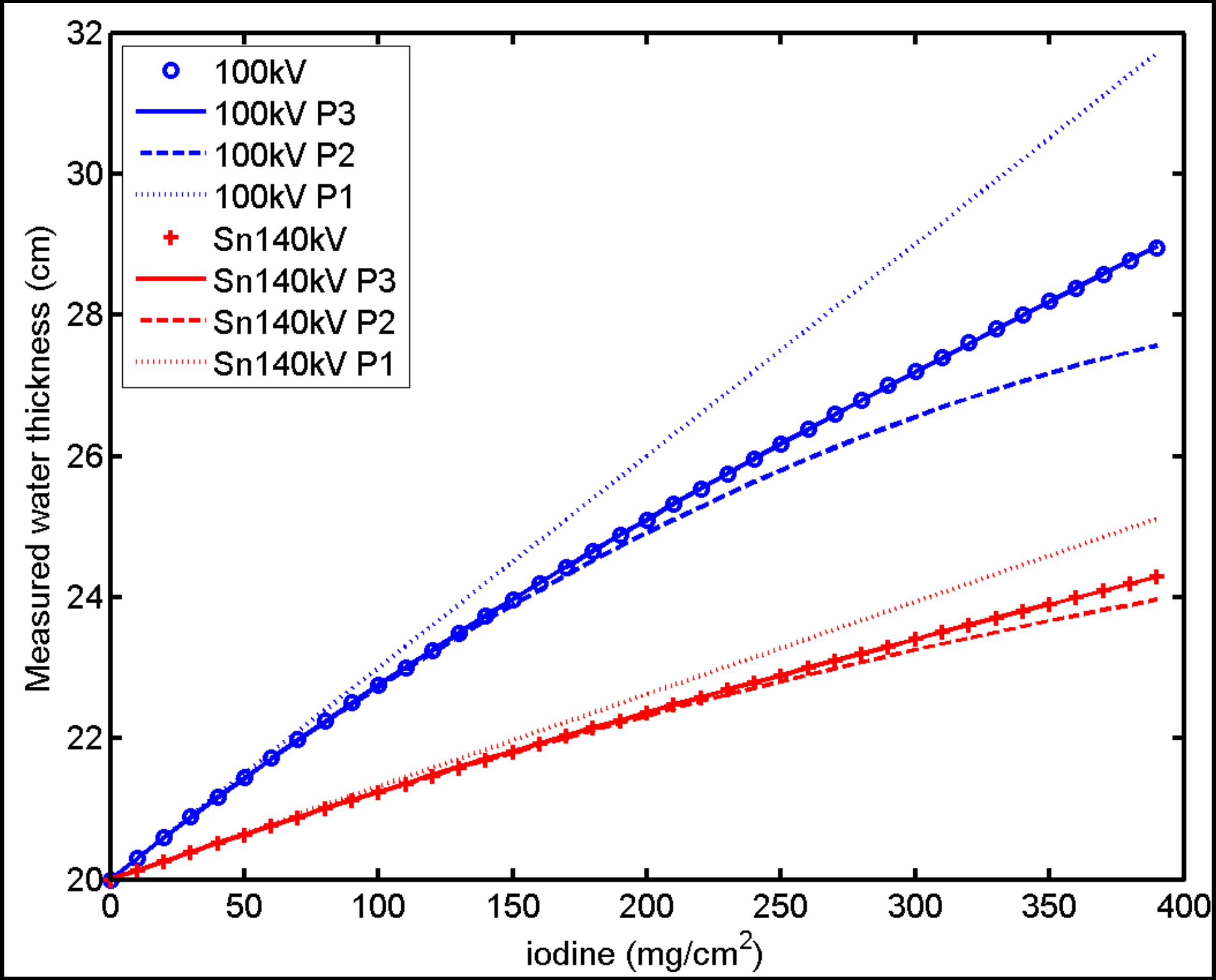

$$D = W + \alpha_1 \delta$$

$$D = W + \alpha_1 \delta + \alpha_2 \delta^2 + \alpha_3 \delta^3$$

$$D = W + \alpha_1 \delta + \alpha_2 \delta^2$$

DE for Metal Artifacts Reduction

$$I_{recon} = I_s + a_1 \cdot I_1 + a_2 \cdot I_2 + a_3 \cdot I_3$$

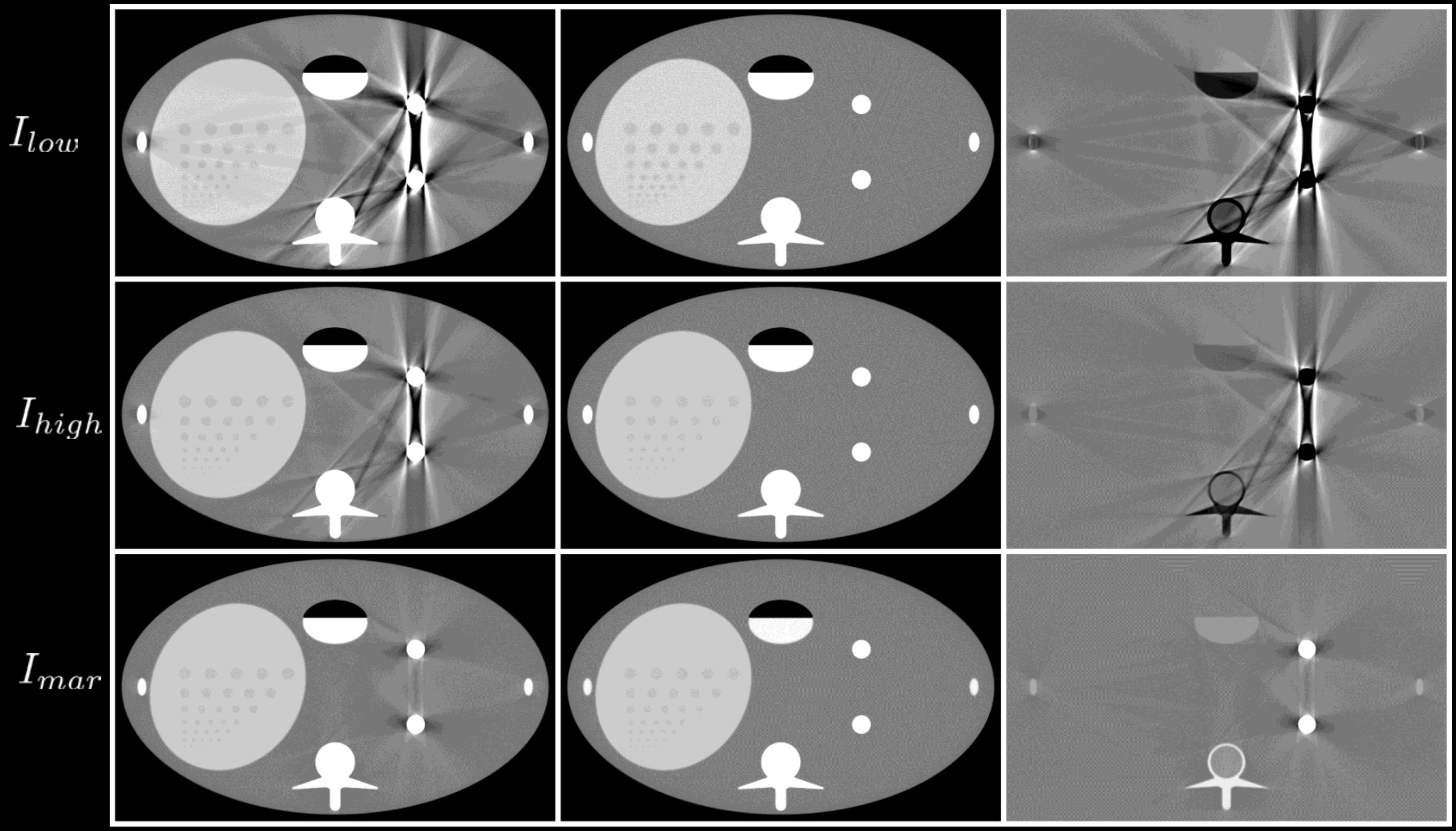

Dual Energy Metal Artifact Reduction
(linear combination plus noise reduction with mono+)

50 keV | 80 keV | 160 keV

Courtesy of Prof. Michael Lell, Friedrich-Alexander University Erlangen-Nürnberg

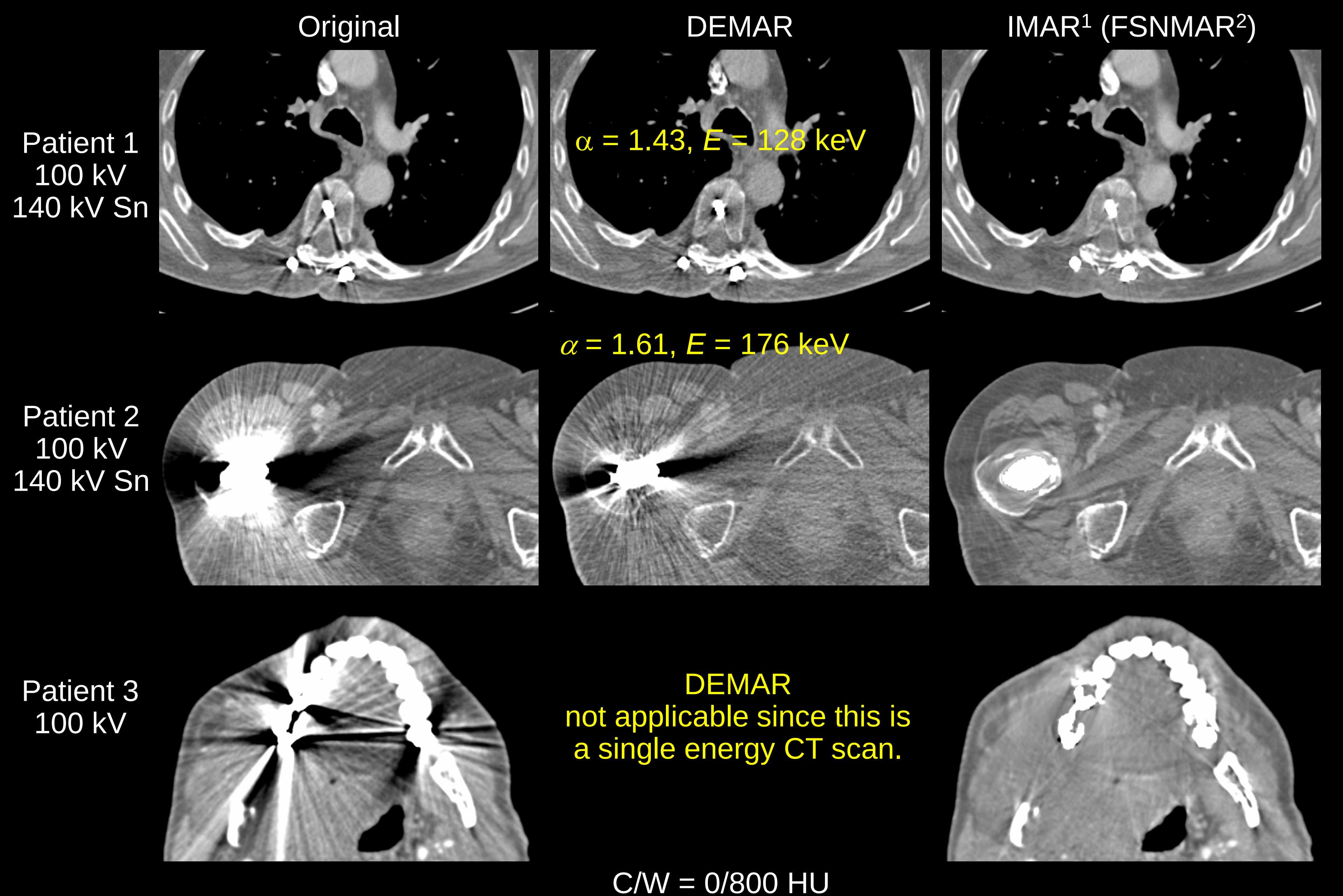

[1]Iterative metal artifact reduction (IMAR) is the Siemens product implementation of FSNMAR.
[2]Frequency split normalized metal artifact reduction: Meyer, Kachelrieß. MedPhys 39(4), 2012.

dkfz.

Positron Emission Tomography

Tracers and applications

ESTRO Teaching Course on Advanced Imaging Technologies

September 18 - 22, 2016 in Florence, Italy

Daniela Thorwarth
Section for Biomedical Physics,
University Hospital for Radiation Oncology, Tübingen

Eberhard-Karls-Universität
UKT
Universitätsklinikum Tübingen

Possibilities for Functional Imaging in Radiotherapy

Glucose Metabolism (unspecific)

- **[^{18}F]FDG**
- Citrate MR spectroscopy, Phosphate spectroscopy

Amino acids (protein synthesis)

- **[^{11}C]MET, [^{18}F]FET**

Choline (cell membrane synthesis)

- **[^{11}C]Choline, [^{18}F]Choline**
- MR spectroscopy

Proliferation (DNA generation)

- **[^{18}F]FLT**

Hypoxia (Radiation resistance/general aggressiveness)

- **[^{18}F]FMISO, [^{18}F]FAZA, [^{18}F]EF3/-5, [^{64}Cu]ATSM**, T2*w MR,

Receptors (tumour specific traits)

- **[^{68}Ga]DOTATOC**

Vascularity

- [^{18}F]Galacto RGD, DCE MR, DW MR

Radionuclides for diagnostic applications

Nuclid	γ-Energy [keV]	Half life	Radioactive decay (max. β+-Energy)	Production
^{11}C	511	20,3 min	β+ (0,97 MeV)	cyclotron
^{13}N	511	9,93 min	β+ (1,2 MeV)	cyclotron
^{15}O	511	124 s	β+ (1,74 MeV)	cyclotron
^{18}F	511	109 min	β+ (0,64 MeV) EC	cyclotron
^{81m}Kr	190	13 s	IT	
^{99m}Tc	140	6,03 h	IT	
^{123}I	159	13 h	EC	cyclotron
^{133}Xe	81 31(Cs-Kα)	5,3 d	β-	nuclear reactor

Max. β+-energy determines mean free path length of β+ !

Production of radionuclides in a nuclear reactor

Production of artificial isotopes by collision of photons or ions with high energies with stable isotopes.

- Nuclear fission

$$^{235}_{92}U + ^{1}_{0}n \rightarrow ^{236}_{92}U \rightarrow ^{99}_{42}Mo + ^{133}_{50}Sn + 4^{0}_{0}n$$

- Neutron collision

$$^{98}_{42}Mo + ^{1}_{0}n \rightarrow ^{99}_{42}Mo + \gamma$$

$$^{98}_{42}Mo(n,\gamma)^{99}_{42}Mo$$

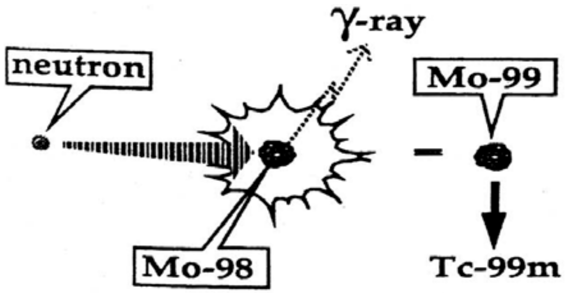

... in the cyclotron

- Use of accelerator, i.e. cyclotron for radionuclide generation
- Kinetic energy of the particle has the be high (~10MeV), to overcome Coulomb barrier of nuclei.
- Production of most used [18F]FDG!

$$^{18}_{8}O + p \rightarrow ^{18}_{9}F + n$$

$$^{18}_{8}O(p,n)^{18}_{9}F$$

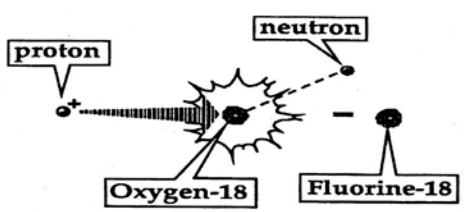

Cyclotron (schematic)

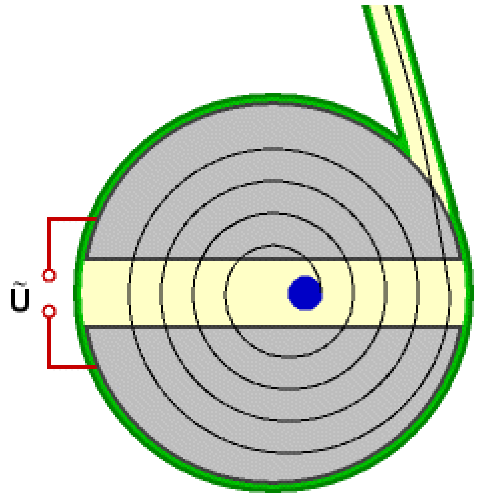

Cyclotron for production of diagnostic radionuclides

… in the radionuclide generator

- widely used to produce certain radioisotopes in the clinic
- Involves a relatively long-lived radioisotope which decays into the isotope of interest

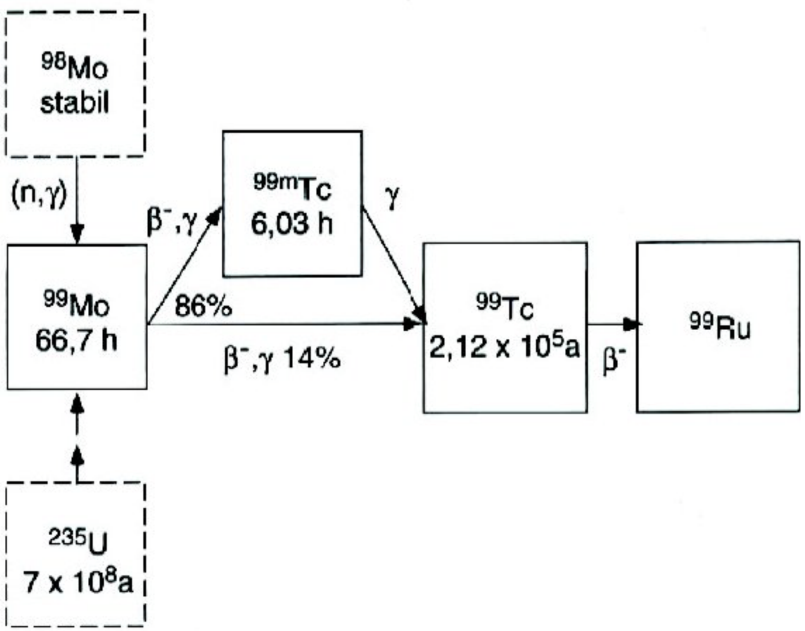

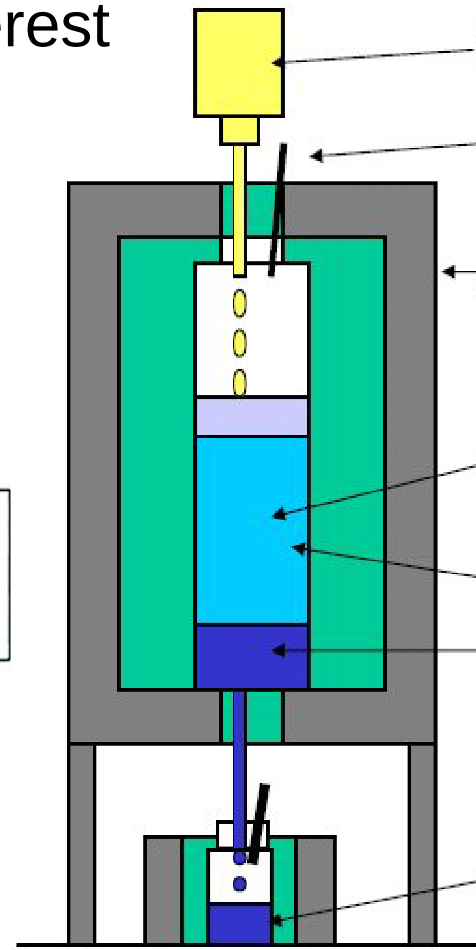

Radioactive equilibrium between ^{99}Mo and ^{99m}Tc builds up again after each elution

[^{18}F]FDG for target delineation and LN staging

The introduction of PET/CT is establishing FDG PET as the new standard for diagnosis and staging of several diseases

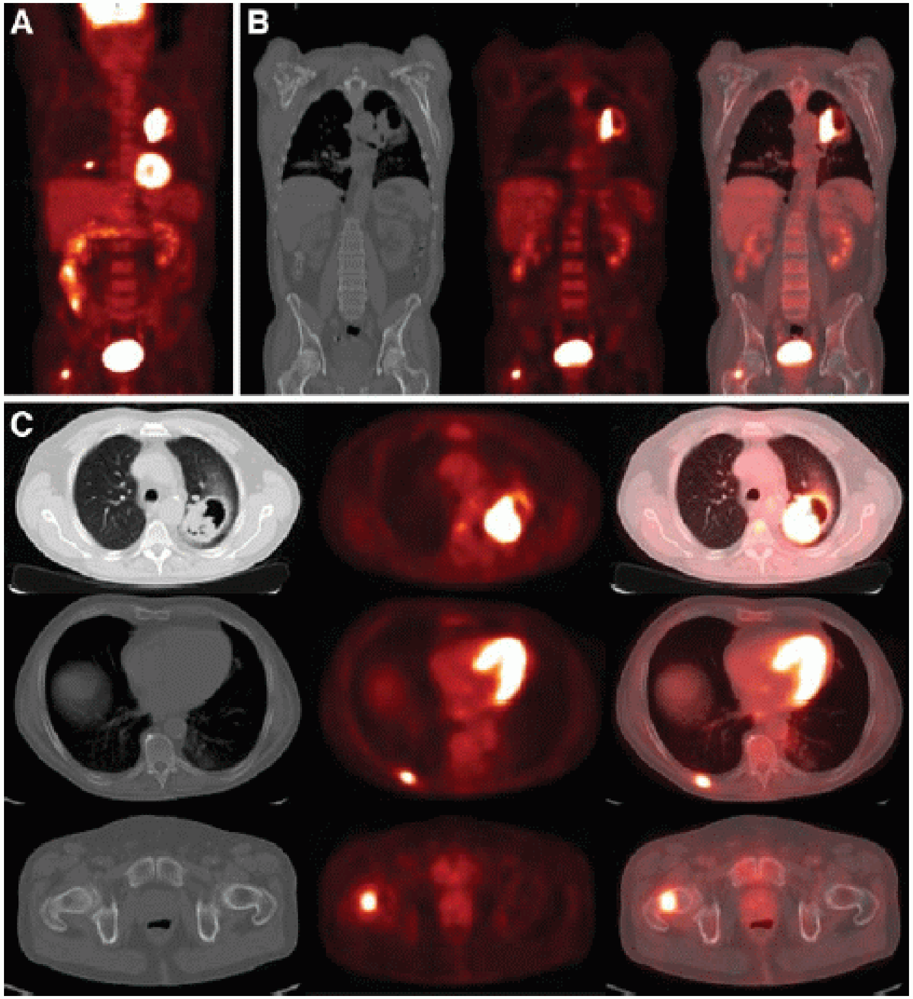

FIGURE 8. Lung cancer with osseous metastases. Hypermetabolic cavitary lung mass is seen in left upper lobe (A–C). Maximum-intensity-projection image (A) demonstrates additional lesions in contralateral thorax and hip. Additional focus of hypermetabolism is seen in right femoral neck (A–C) and corresponds to subtle lytic lesion on CT. Axial images (C) show hypermetabolism in right posterior 8th rib without osseous changes on CT.

Bunyaviroch, Coleman, JNM (2006)

FDG PET/CT improves consistency of GTV delineation in NSCLC

- N=30 NSCLC patients were contoured with and without fused PET/CT data.
- Mean variation of GTV with combined modalities was significantly lower than with CT alone.

Caldwell C et al. Int J Radiat Oncol Biol Phys 2001; 51: 923-31.

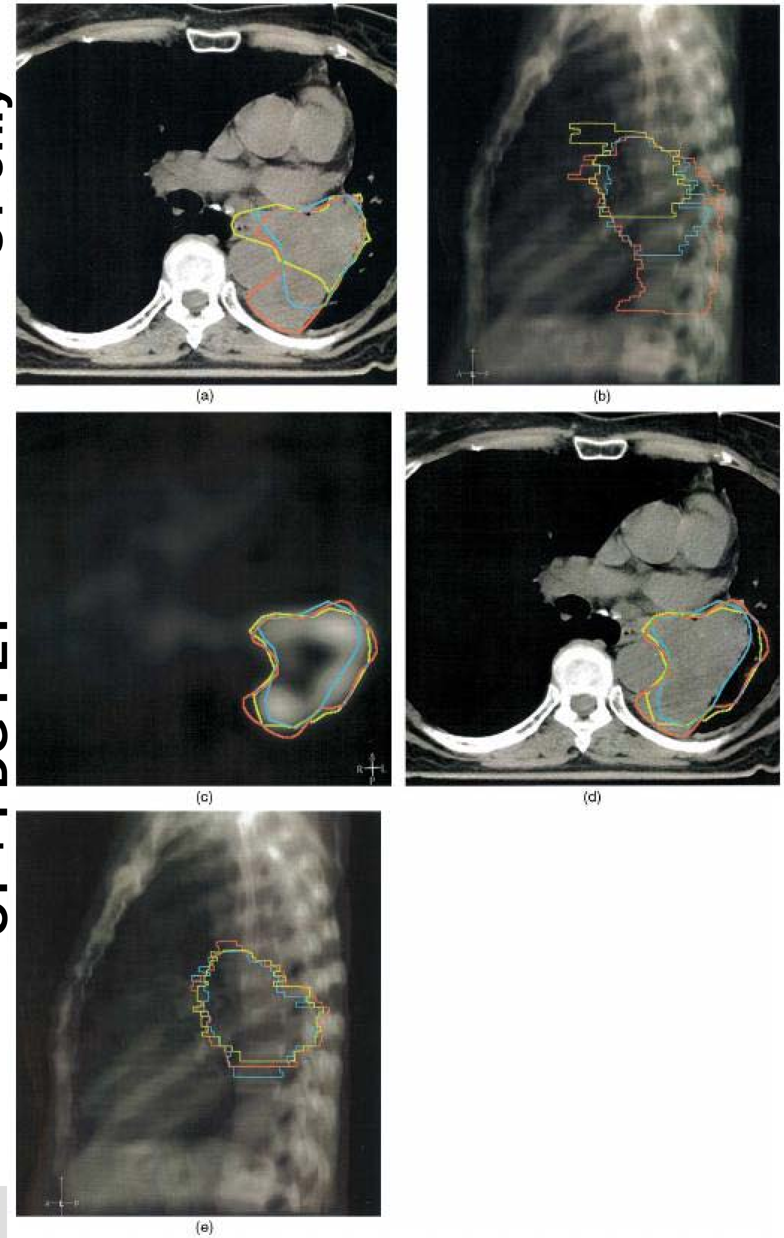

CT only

CT + FDG PET

FDG PET/CT improves consistency of GTV delineation in NSCLC

In **12/30**, respectively **23/30** patients all three observers‘ volumes were within the standard deviation.

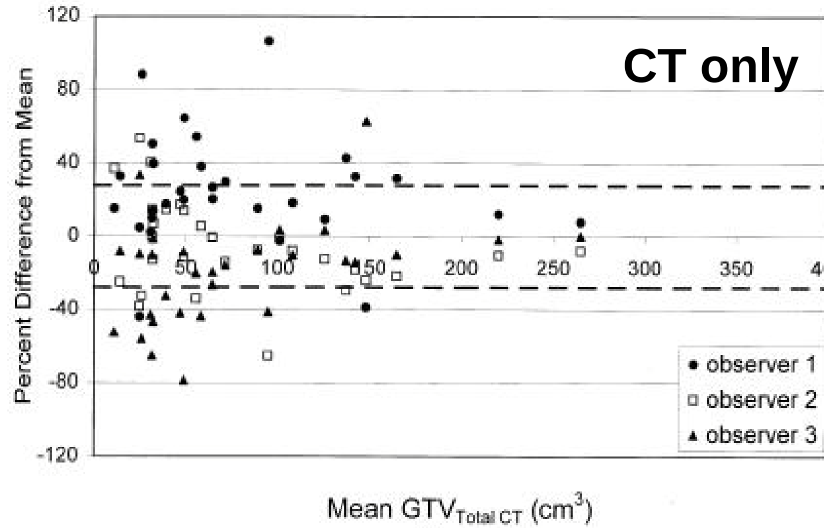

(a)

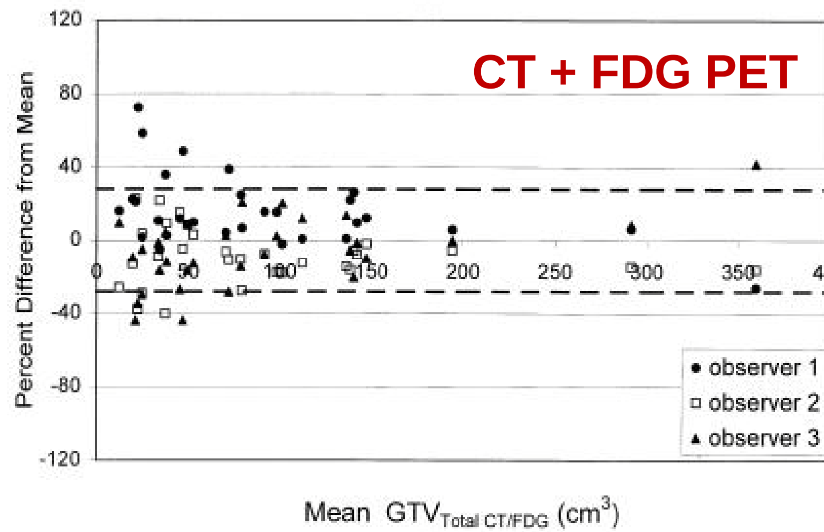

(b)

Caldwell C et al. Int J Radiat Oncol Biol Phys 2001; 51: 923-31.

[^{18}F]FDG PET/CT to assess tumor volume during RT

Feng M et al. IJROBP 2009; 73(4): 1228-34.

- Tumour delineation on PET with manually adj. threshold
- Using mid-RT PET volumes, tumour dose can be escalated

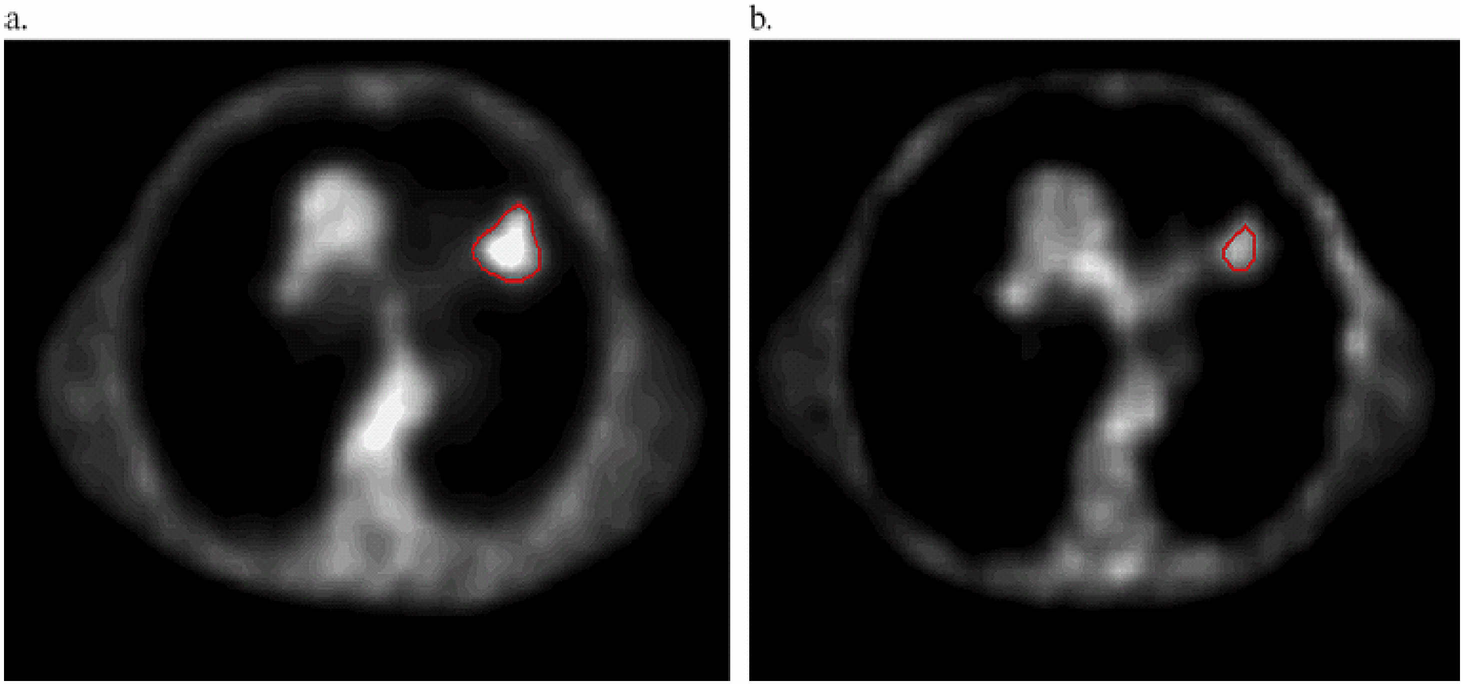

Fig. 4. An example of the change in positron emission tomography tumor volume between pretreatment (a) and after 40–50 Gy during the course of radiation therapy (b).

Response Prediction by Quantitative Assessment of Glucose Use

Weber W et al. J Clin Oncol 2003; 21: 2651-7.

- FDG PET before and after first cycle of CT (n=57)
- Metabolic response = reduction of SUV by more than 20%
- SUV reduction predictive for therapy outcome

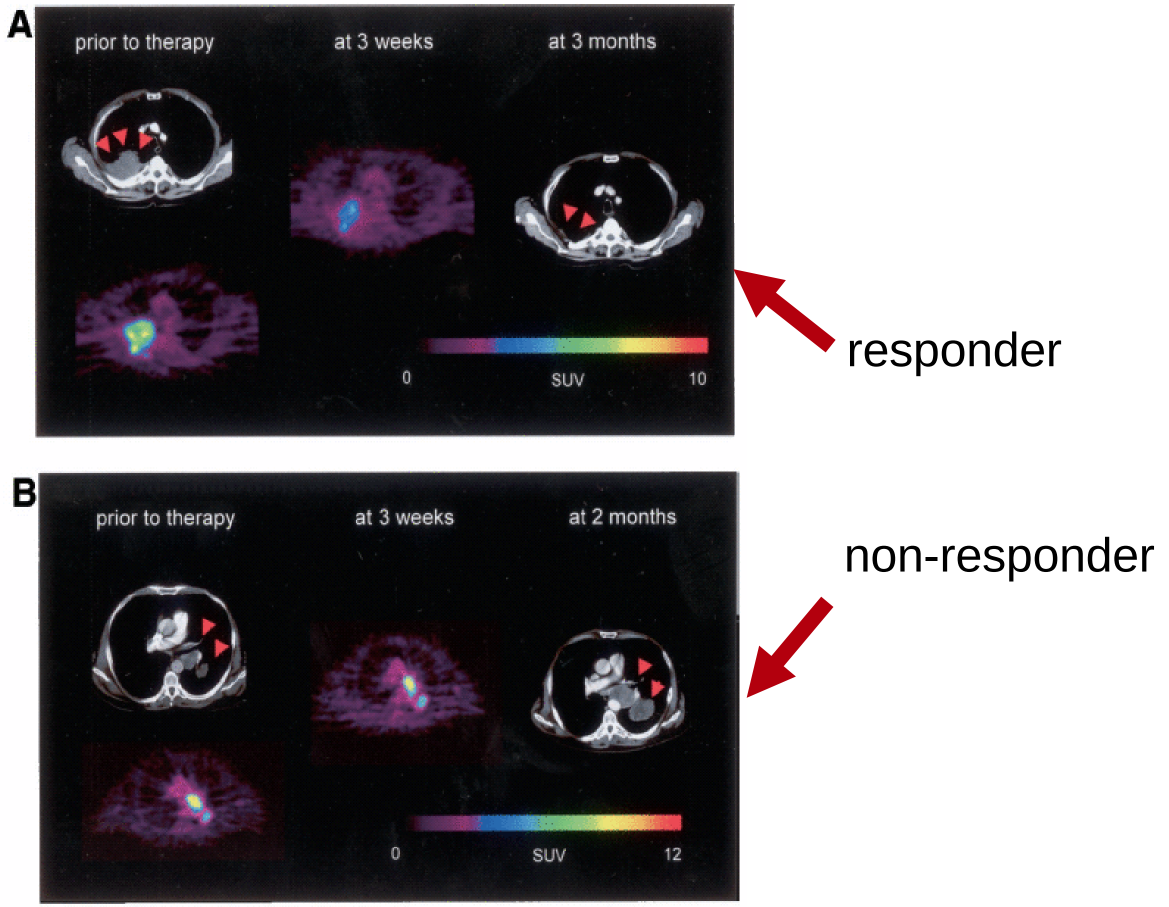

Fig 1. Fluorodeoxyglucose (FDG) positron emission tomography and computed tomography scans of a responding (A) and a nonresponding tumor (B). In the responding tumor, there is a 61% decrease in FDG uptake 3 weeks after initiation of chemotherapy. In contrast, tumor FDG uptake is almost unchanged in the nonresponding tumor.

Therapy monitoring with FDG-PET in HNC

Gregoire V et al. J Nucl Med 2007; 48: 68S-77S.

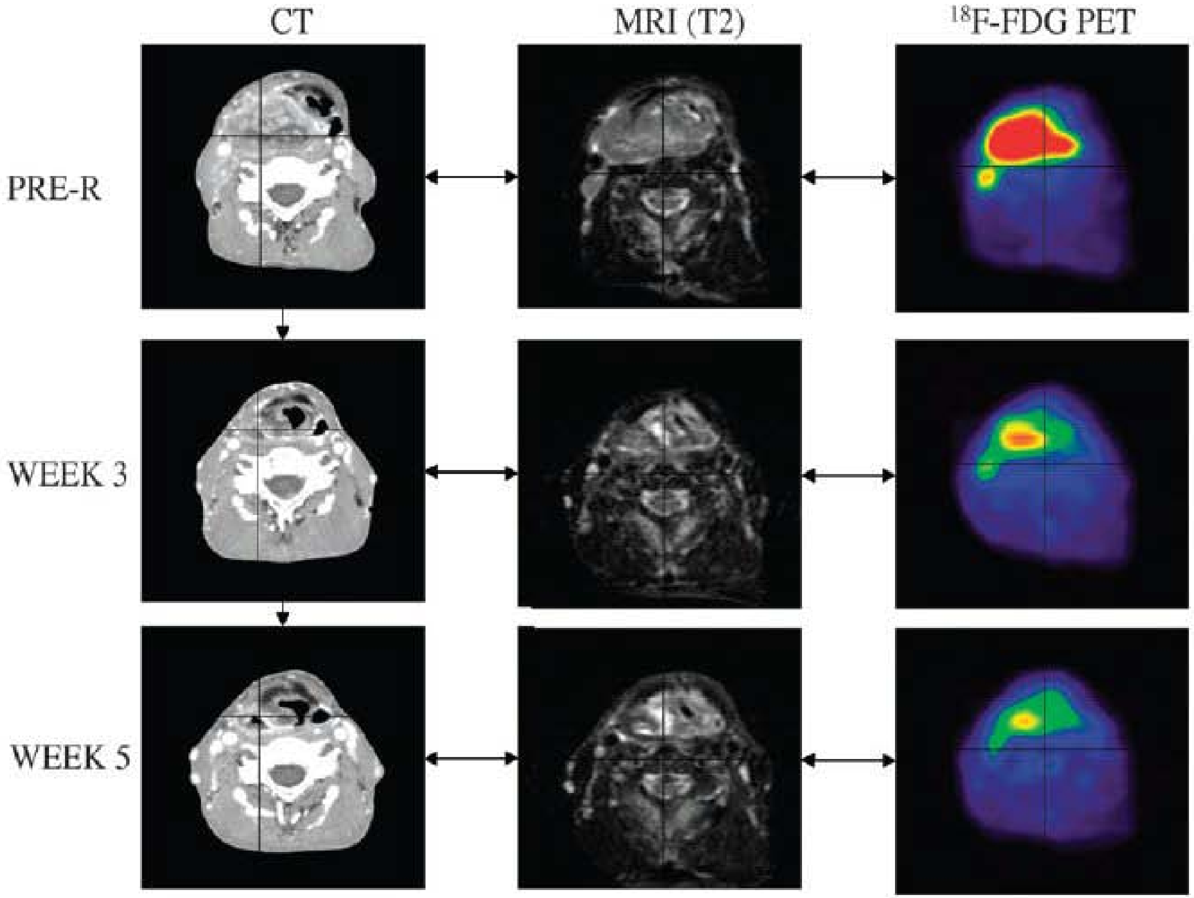

FIGURE 5. Patient with T4 N3 M0 squamous cell carcinoma of right piriform sinus. CT, MRI (T2-weighted fat suppression), and ^{18}F-FDG PET were performed before treatment (PRE-R) and during wk 3 (26 Gy) and wk 5 (46 Gy) of treatment with chemoradiotherapy. Three sets of images were coregistered by use of semiautomatic tool based on isocontouring. Substantial reduction in tumor volume and metabolic activity can be observed throughout treatment.

Treatment Monitoring with FDG PET

- **FDG PET can provide reliable long-term prognostic information**
- **Potential treatment stratification based on metabolic response**
- **FDG PET may be used to guide additional therapy**

Specific criteria for PET image analysis and response evaluation still need to be developed and validated!

FDG PET/CT imaging techniques and imaging protocols require standardization!

[^{11}C]MET / [^{18}F]FET / [^{18}F]FLT for Brain Lesions

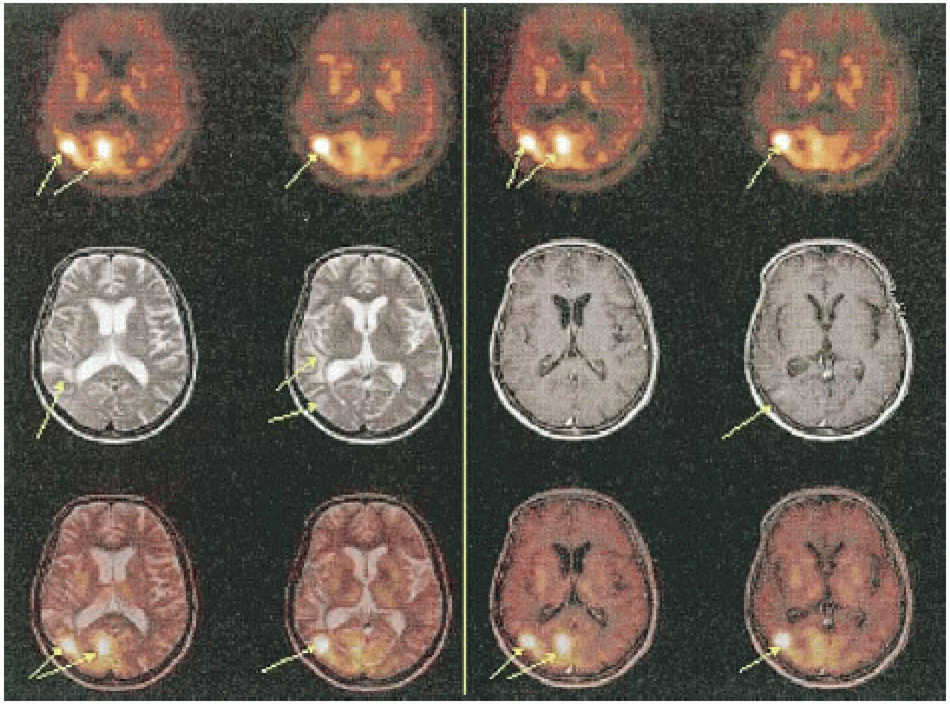

Fig. 4. Glioblastoma. L-(methyl-11C)-labeled methionine-positron emission tomography (MET-PET), T_2-weighted magnetic resonance imaging (MRI), T_1-weighted MRI with Gd, and PET/MRI fusion images. Yellow arrows indicate hyperintensity areas on T_2-weighted MRI, Gd enhancement on T_1-weighted MRI, and pathologic MET uptake on PET. Note, intensive MET uptake outside of changes seen on MRI.

Grosu IJROBP (2005)

MET-PET appears to have the highest specificity and sensitivity for malignant brain tumours

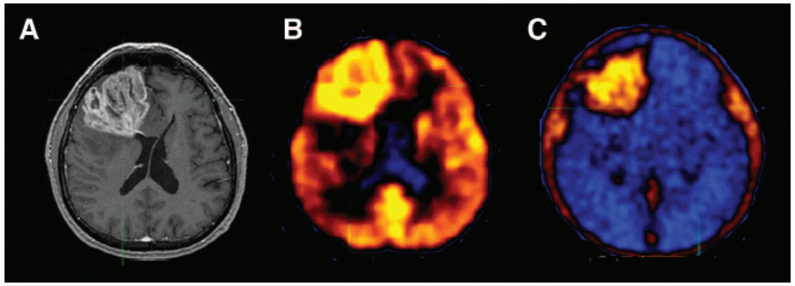

T1MR FDG FLT

Chen et al. JNM (2005)

Dynamic Imaging: [18F]-FET PET
Staging by Tracer Kinetics

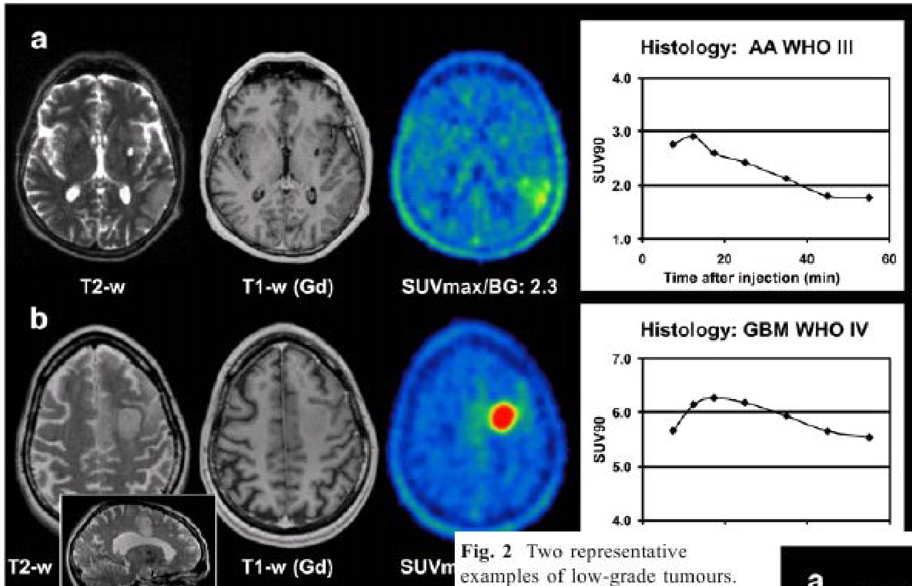

Fig. 3 Two representative examples of high-grade tumours. Both studies show circumscribed hyperintense lesions in T2-weighted MRI, without, however, relevant pathologic contrast enhancement on T1-weighted MRI. MR diagnosis was low-grade astrocytoma in (**a**) and pseudotumoural multiple sclerosis plaque in (**b**), due to the irradiation into the corpus callosum. FET uptake is high in (**b**) but only moderate

Uptake kinetics allow separation of high grade and low grade glioma.

Fig. 2 Two representative examples of low-grade tumours. Both studies show circumscribed hyperintense lesions in T2-weighted MRI with pathologic contrast enhancement on T1-weighted MRI in small parts of the tumour, which was suspicious for malignant transformation, and increased FET uptake (see SUVmax/BG ratios). Dynamic evaluation shows in both cases increasing SUV90 values until the end of acquisition. **a** Thirty-seven-year-old man with histopathological diagnosis of an oligoastrocytoma WHO II. **b** Thirty-two-year-old man with histopathological diagnosis of an astrocytoma WHO II

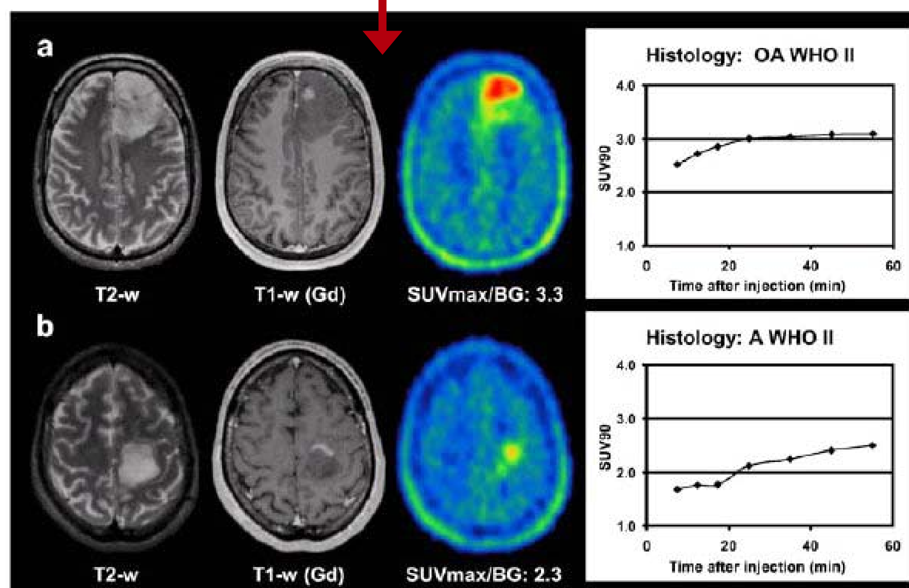

Pöpperl G et al.
EJNMMI 2007; 34(12): 1933-1942.

Proliferation Imaging with [^{18}F]FLT PET

Reversible binding in the tumour, irreversible binding in bone marrow

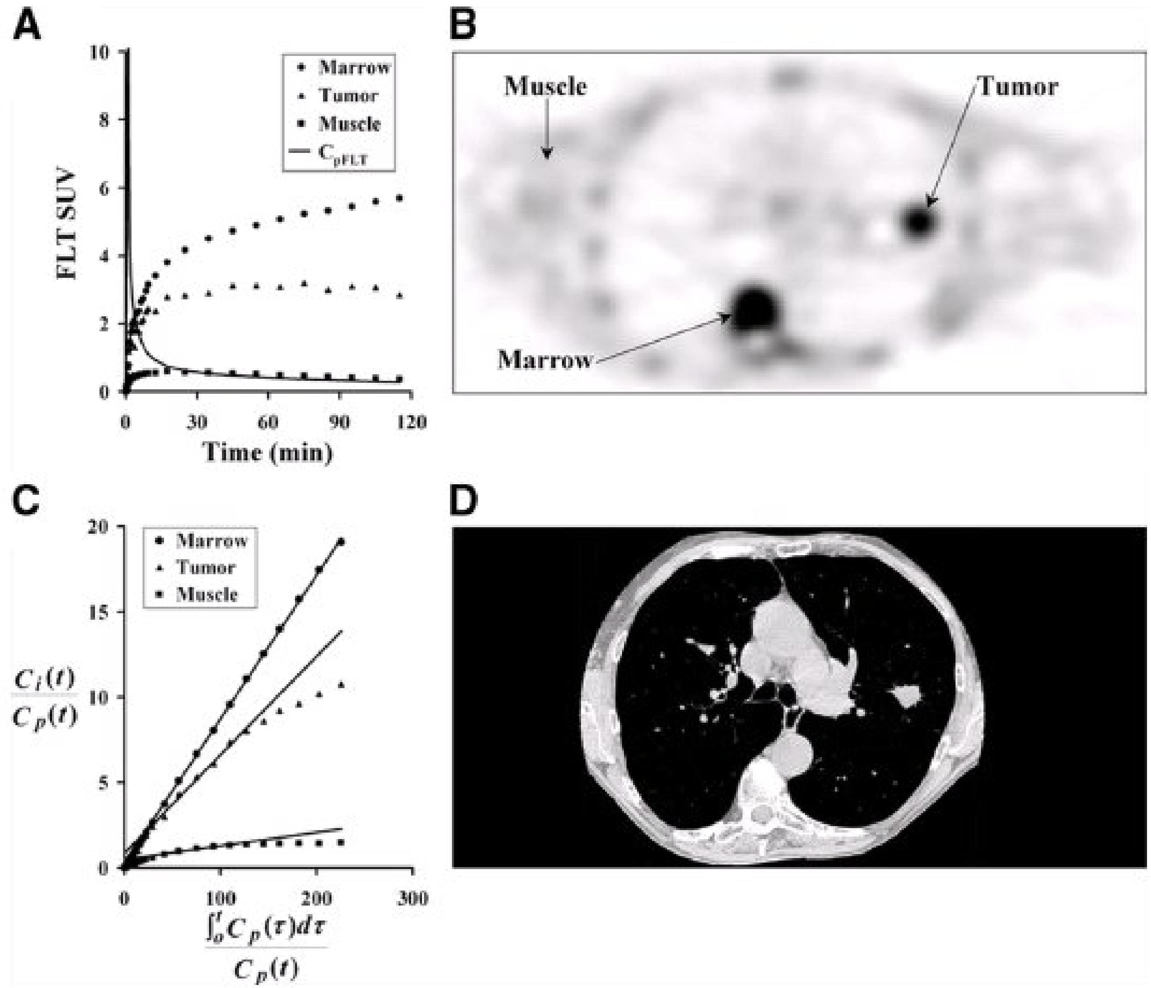

FIGURE 3. Three tissue types were investigated for FLT uptake. (A) Example of patient tissue time–activity curves decay corrected to time of injection. (B) Patient PET image acquired 30–60 min after injection of 118.4 MBq FLT. (C) Graphical analysis plot of normalized tissue uptake vs. normalized time for marrow, tumor, and muscle. (D) CT image close to PET image slice provides information for ROI placement and determination of recovery coefficients for tumor regions. Patient's arms are not in field of view for standard CT protocol.

Muzi M et al. J Nucl Med 2005; 46(2): 274-282.

Imaging Cellular Proliferation during RT

Everitt S et al. IJROBP 2009; 75(4):1098-104.

- FLT uptake can monitor biologic tumour response
- FLT might be used for response-adapted RT

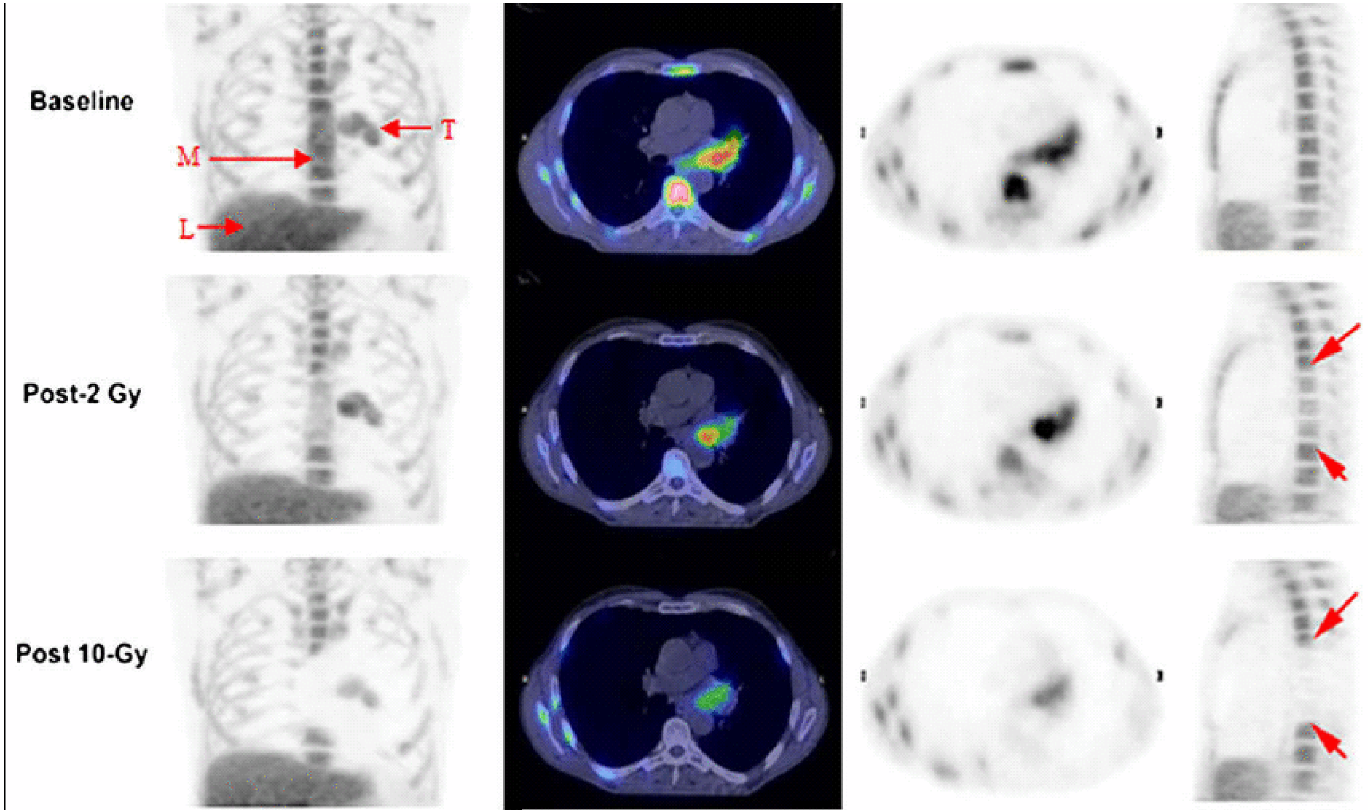

Fig. 4. Serial images of the patient designated as Case 1, demonstrating the distribution of ^{18}F-3′-deoxy-3′-fluoro-L-thymidine (^{18}F-FLT PET) in tumor and bone marrow at three time points: baseline before commencement of therapy (top row), 20 h after administration of 2 Gy (middle row), and 72 h after 10 Gy (bottom row). Red arrows in the right-hand column denote the upper and lower boundaries of the radiation fields. L = liver; M = bone marrow; T = tumor.

Dose Painting Hypothesis I: Direct Dose at Tumour Cell Foci

Cell density $\rho(x_i)$ (or proliferation rate) is spatially variable:

$$F = \frac{1}{N}\sum_{i=1}^{N} \rho_i \exp(-\alpha D_i)$$

requires a formula that relates image intensity to $\rho(x_i)$.

Alternatively, define one or multiple nested functional PTVs.

Both concepts may redistribute dose in the target volume, i.e. ***reduce the dose in some parts*** *to gain the possibility* ***to increase it in others****.*

FLT PET does not discriminate between reactive and metastatic lymph nodes

Troost EGC et al. J Nucl Med 2007; 48: 726-35.

- [18F]-FLT PET before surgical tumour resection with lymph node dissection (n=10 HNC)
- 9/10 patients had FLT-positive lymph nodes, but only 3 of them had histologically proven metastases

Utility of [18F]-FLT PET for response assessment of small metastatic nodes is unclear!

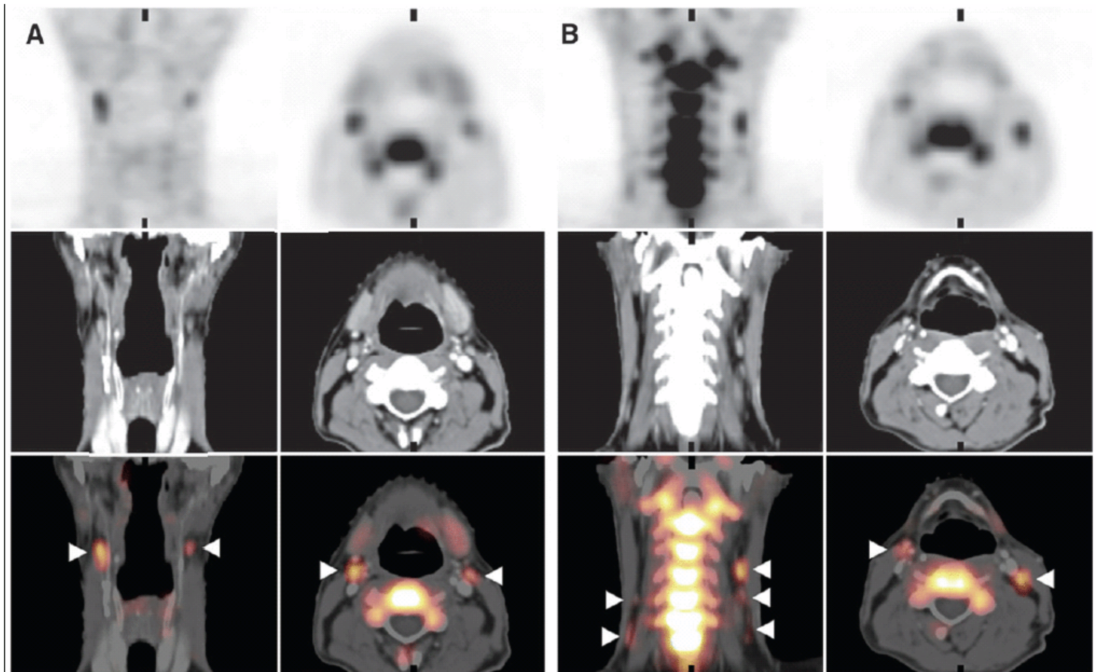

FIGURE 1. [18]F-FLT PET/CT images of patient 9 (pT2pN0M0 oral cavity carcinoma). Top panels show PET images, middle panels show CT images, and bottom panels show fusion of both image modalities. Cervical lymph nodes with increased [18]F-FLT uptake are found bilaterally in level II (A, arrowheads) and in levels III and IV (B, arrowheads). All lymph nodes detected with [18]F-FLT in this example were false-positive for metastasis, due to uptake in proliferating B-lymphocytes in reactive germinal centers.

From Functional Imaging to Dose Painting

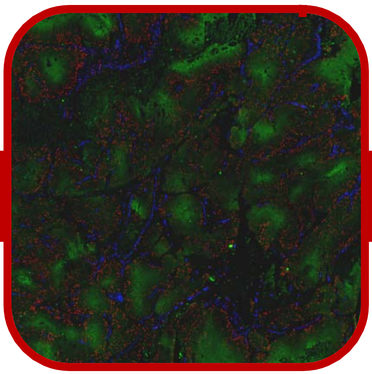

biology

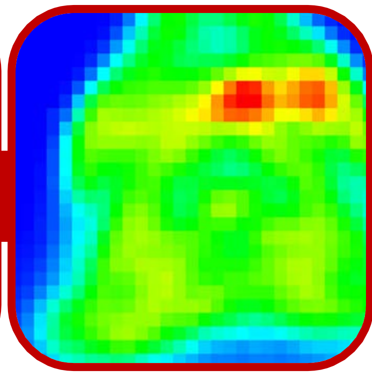

Imaging physics / resolution

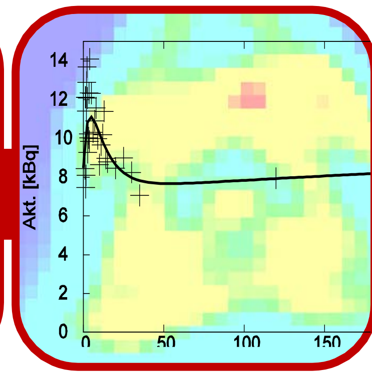

Image analysis / parameter interpretation

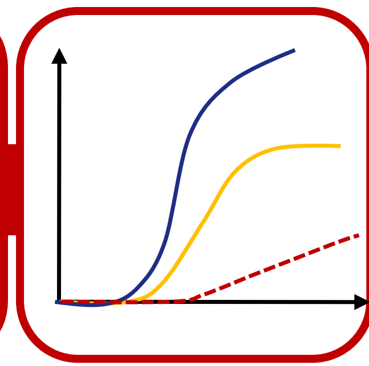

Prescription function

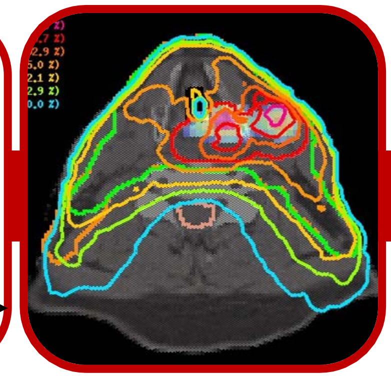

Technical feasibility

Hypoxia Imaging with [^{18}F]FMISO

Dirix P et al. J Nucl Med 2009; 50(7): 1020-7.

- Sequential PET (FDG, FMISO) and MRI (T1, T2, DCE, DW) were performed before, during and after RT
- FMISO PET (T/B and hypoxic volume) before and during RT were prognostic for therapy outcome

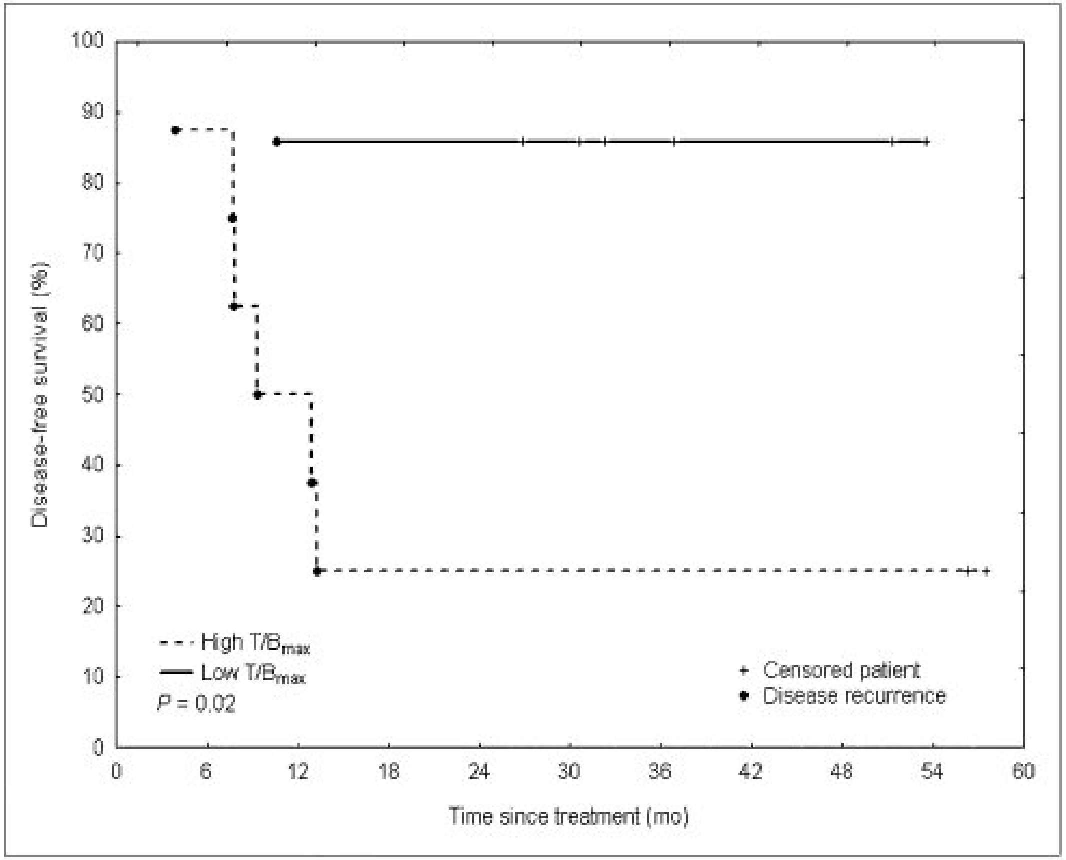

FIGURE 3. Actuarial disease-free survival according to T/B$_{max}$ during radiotherapy (n = 15). High T/B$_{max}$ is defined as a value greater than or equal to median of 1.17.

Hypoxia PET Imaging with FMISO

Zips D et al. Radiother Oncol 2012;105(1):21-8.

- N=25 HNC patients
- FMISO PET/CT in week 0, 1, 2, and 5
- Different imaging parameters evaluated @ 4h pi
  - HV (T/Bg: 1.4, 1.6, 1.8, 2.0)
  - TBR_{max}
  - SUV_{max}
- Correlation with LPFS in week 2

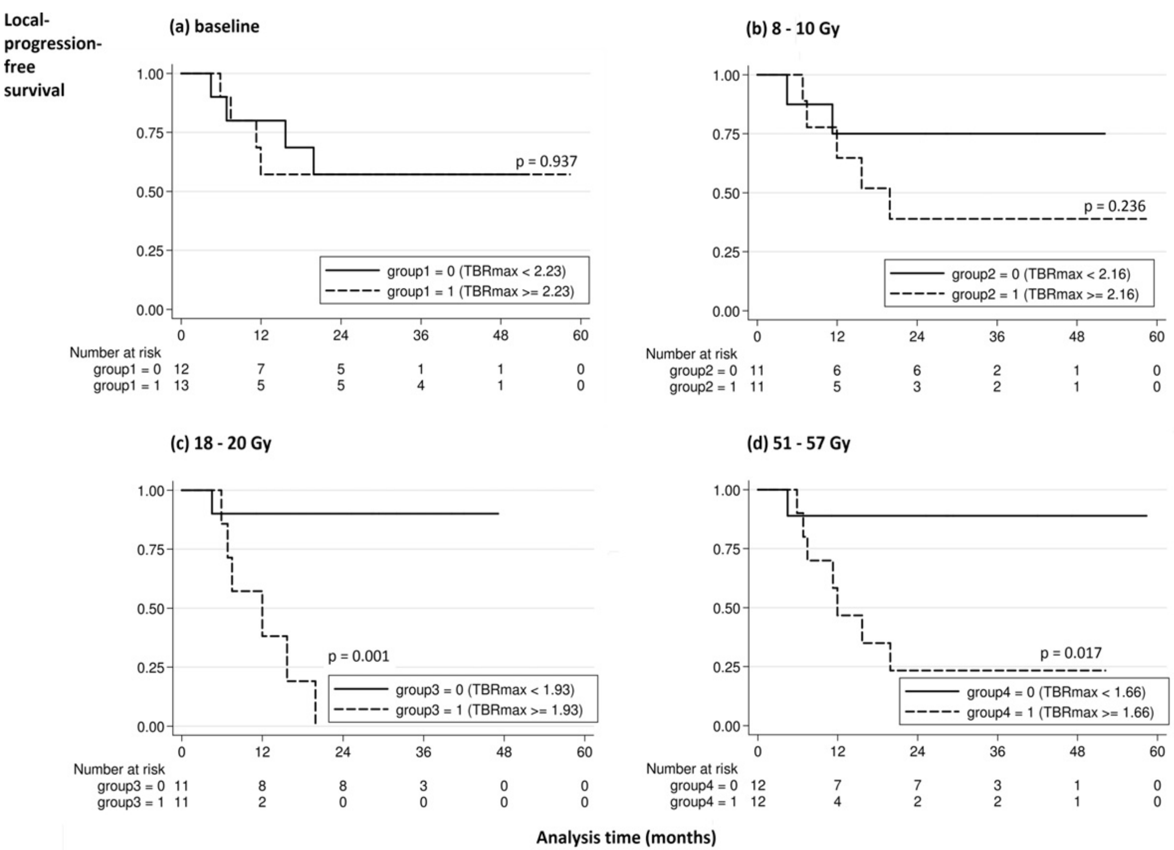

Hypoxia PET Imaging with FAZA

Mortensen LS et al. Radiother Oncol 2012;105(1):14-20.

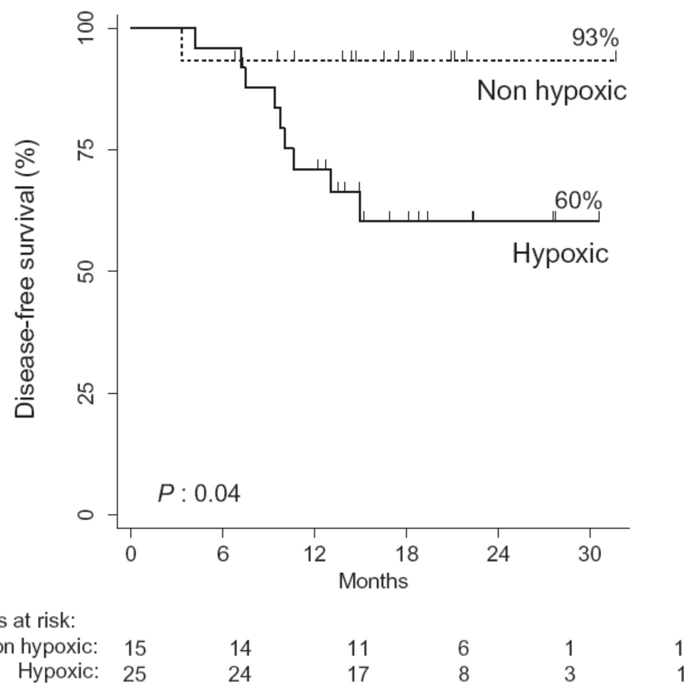

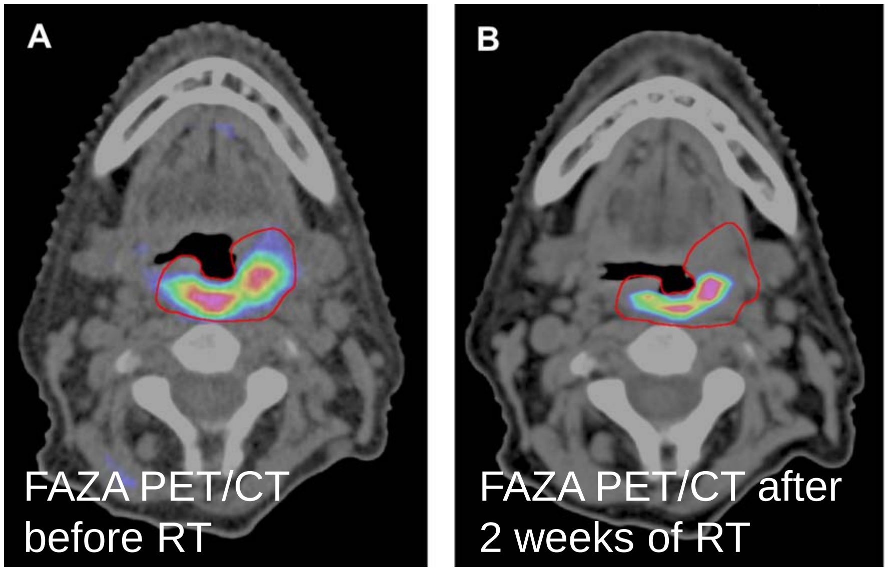

- N=40 HNC
- FAZA PET/CT in week 0 and 2
- $HV_{TMR1.4}$ evaluated @ 2h pi
- Prognostic potential for detection of hypoxia in HNSCC

Hypoxia Imaging with DCE-MRI

Halle C et al. Cancer Res 2012;72(20):5285-95.

- N=78 cervix patients
- Analysis of gene expression set and DCE-MRI
- Significant correlation between A_{Brix} and hypoxia gene sets
- Independent validation (n=109)
- DCE-MRI for identification of chemoradioresistance

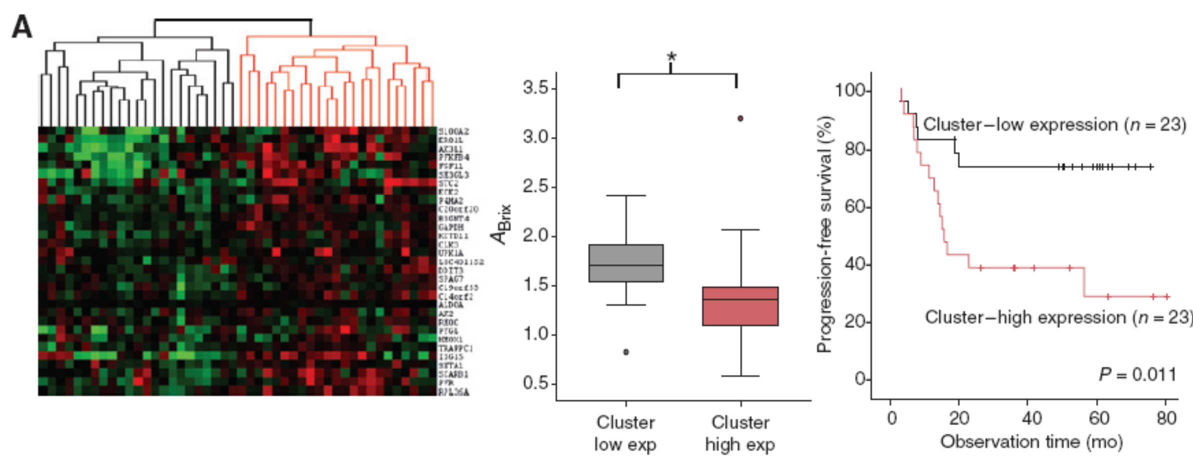

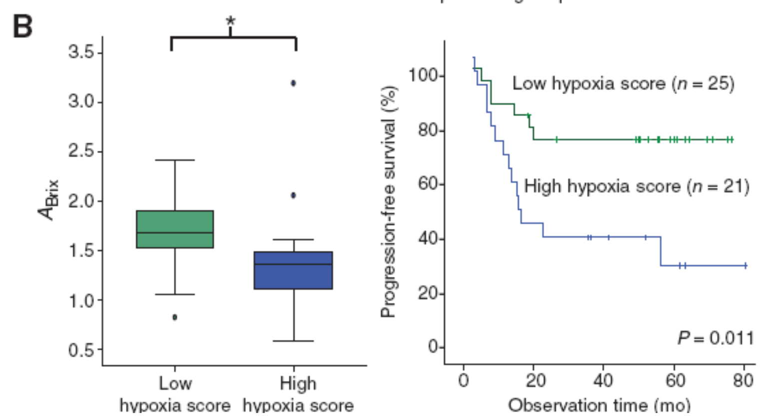

Patients grouped according to DCE-MRI hypoxia score.

Dose Painting Hypotheses II: direct Dose at Insensitive Cells

Cell sensitivity $\alpha(x_i)$ is spatially variable:

$$F = \frac{1}{N}\sum_{i=1}^{N} \rho \exp(-\alpha_i D_i)$$

requires a formula that relates image intensity to $\alpha(x_i)$.

The requirements on understanding the image are high.
Here, an uncertainty in $\alpha(x_i)$ influences the dose ***linearly****,*
while in ***situation I only logarithmically****.*

The sensitivity map $\alpha(x_i)$ provides the basis for
Dose Painting By Numbers (DPBN).

Dose Painting based on dynamic FMISO PET: Phase II trial in Tübingen

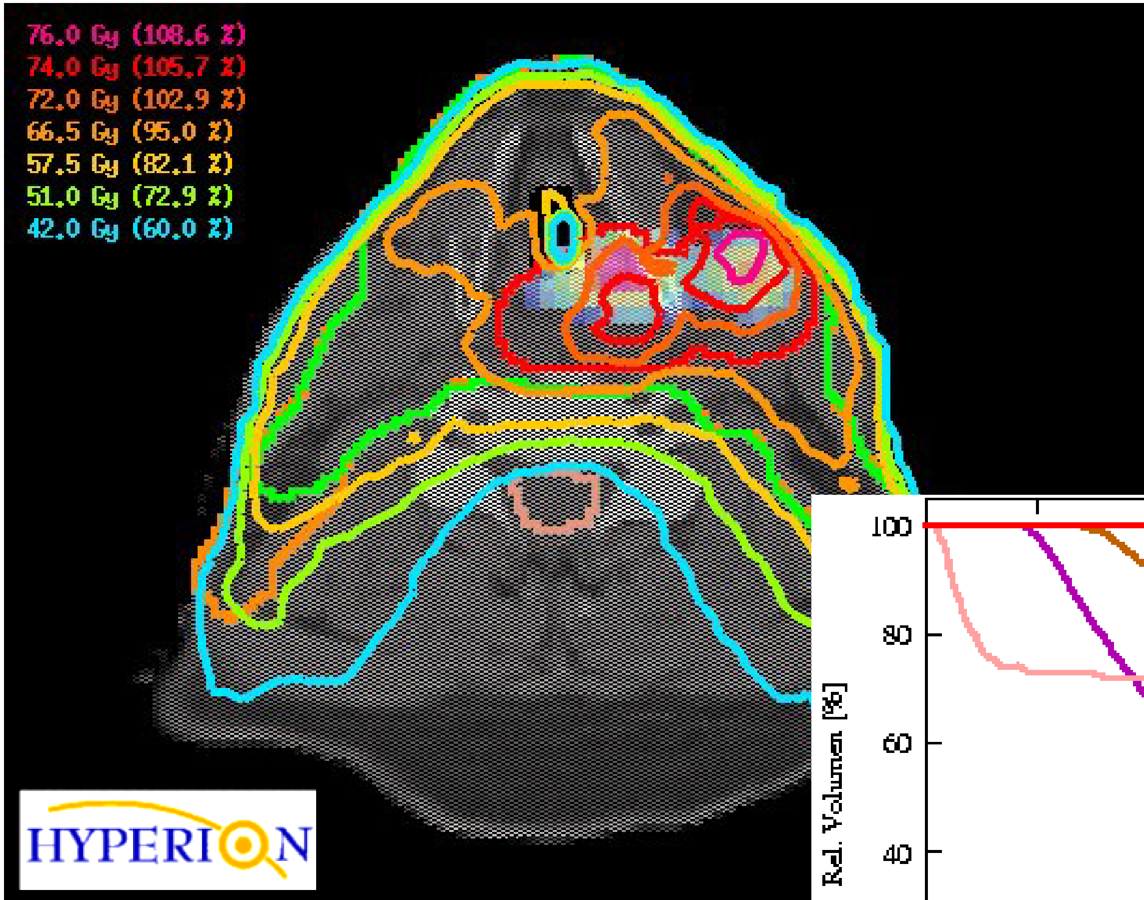

IMRT treatment plan 70/77 Gy

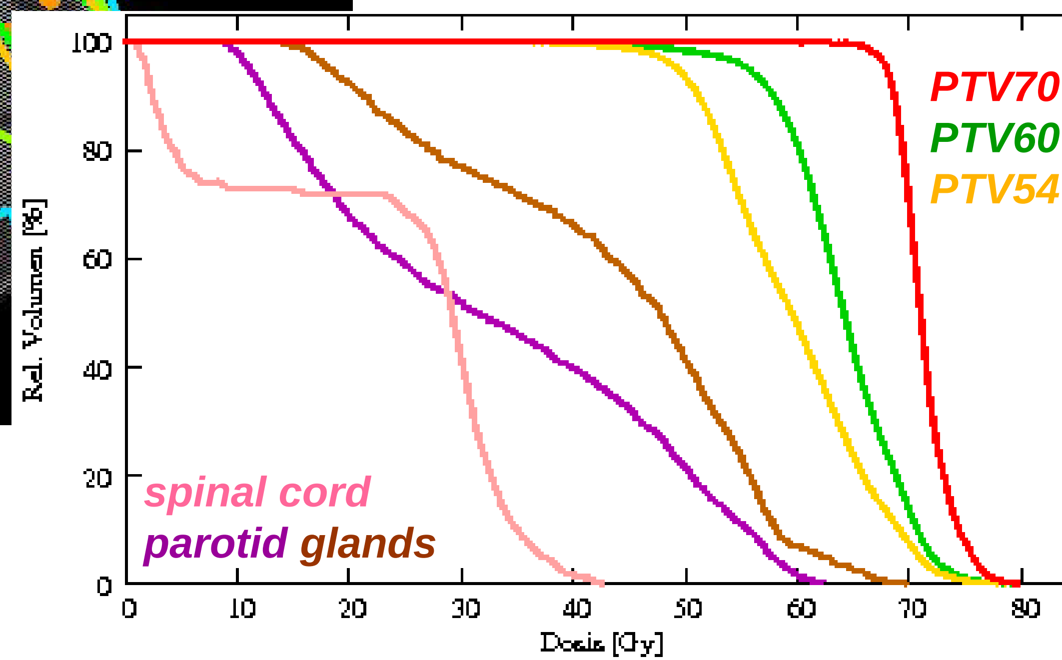

Hypoxia dose painting (HDP) in HNC: A randomized phase II trial in Tübingen

Aims
- Feasibility and toxicity of PET-based HDP
- Prospective validation of a hypoxia TCP model

Imaging
- Planning CT + FDG PET/CT
- Dynamic FMISO PET/CT in treatment position
- Additional FMISO PET/MR aimed for
- Second dyn. FMISO PET/CT after approx. 2 weeks of RT

Therapy
- Randomization of hypoxic patients in 2 arms:
  - **Arm 1: Standard IMRT** - 70 Gy in 35 fx
  - **Arm 2: HDP** - homogeneous dose escalation of 10% in hypoxic tumor areas defined on dynamic FMISO PET/CT data

Results of a planned interim analysis

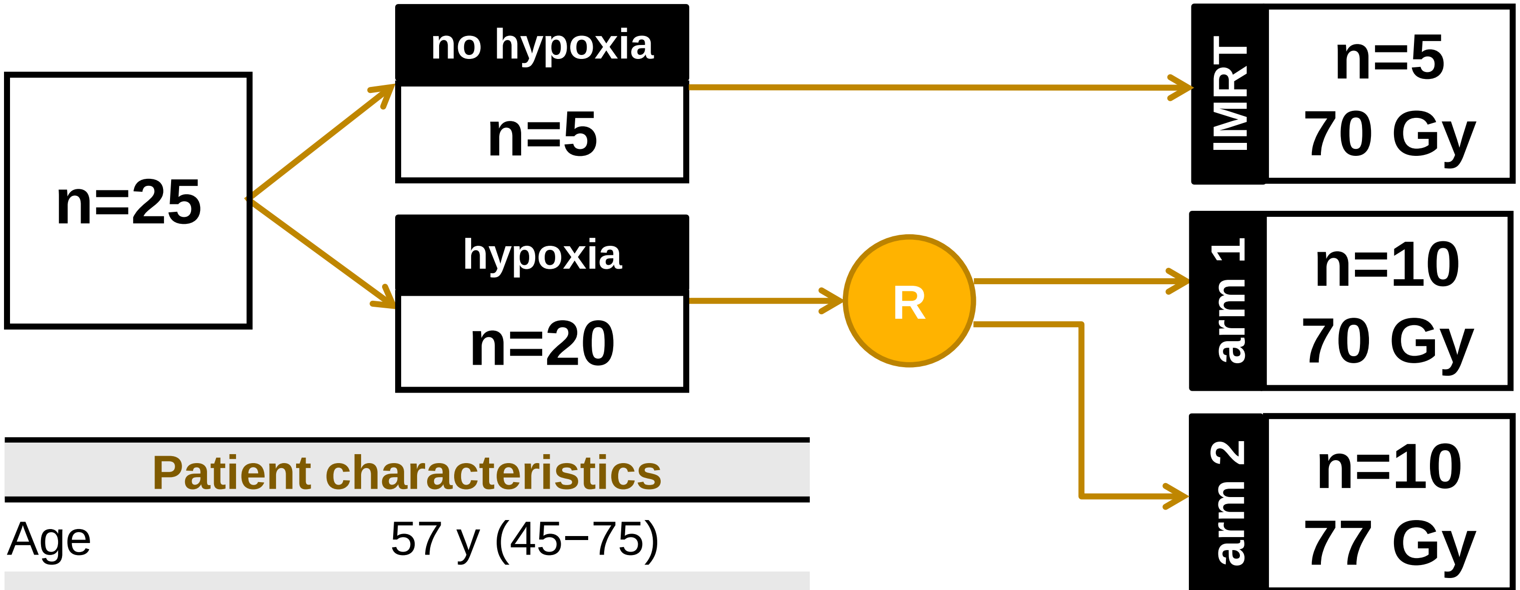

Patient characteristics	
Age	57 y (45−75)
Gender (m / f)	19 / 6
Site (oro / hypo / both)	13 / 6 / 6
p16 (− / + / n.a.)	21 / 3 / 1
T stage (T2 / T3 / T4)	2 / 12 / 11
GTV (total)	73 cm^3 (23-342)

- **9 LF** (all in hypoxic group: 6 in arm 1, 3 in arm 2)
- Median follow-up time: 27 months

Baseline dyn. FMISO PET is prognostic for loco-regional control

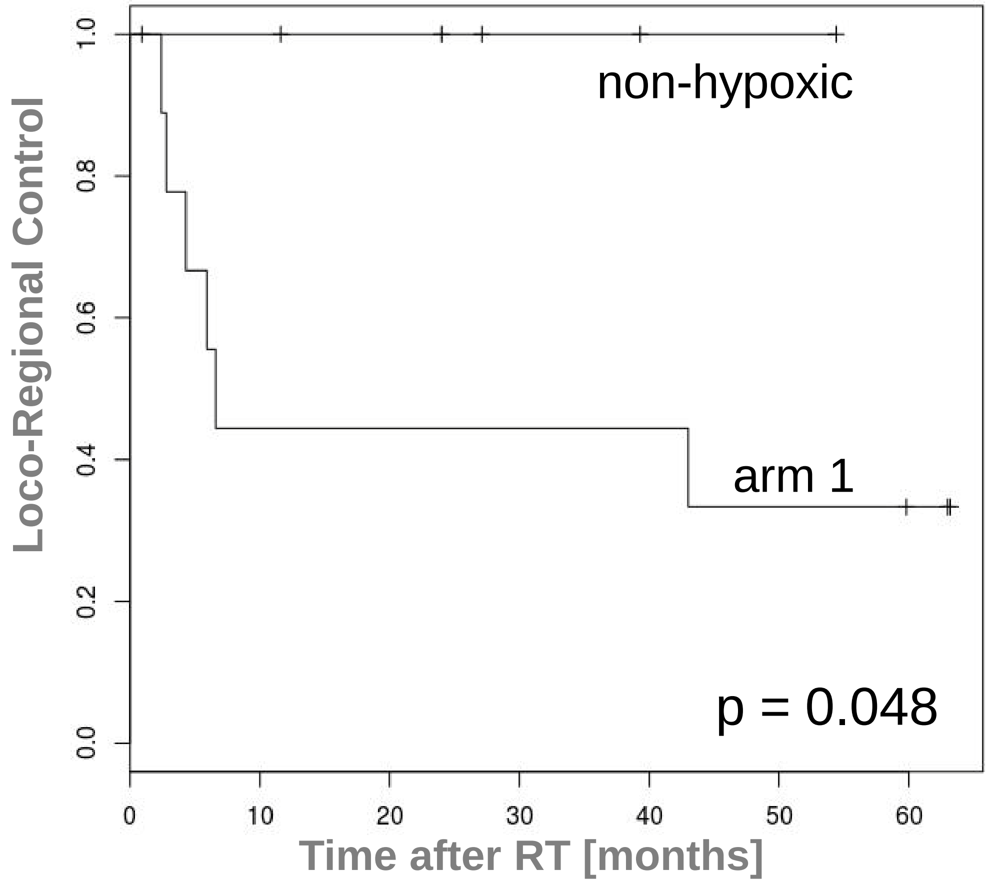

LRC rates

Arm 1: 32 %
Arm 2: 67 %
Non-hyp: 100 %

FDG PET based dose painting study in lung cancer

- PET-boost trial
- Randomizes between escalating the whole primary tumor or the high FDG uptake area (>50% SUV_{max})

Van Elmpt W et al. Radiother Oncol 2012;104(1): 67-71.

PET-boost trial scheme:

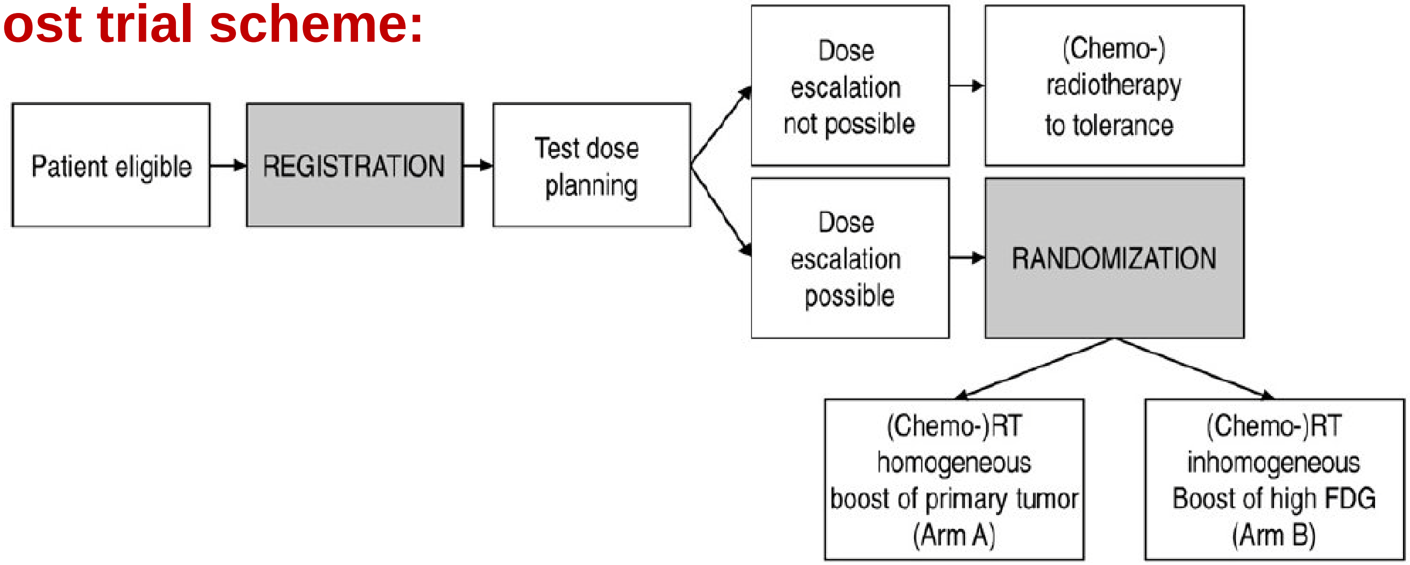

New multimodality imaging perspective: Combined PET/MRI

Combined PET/MR:

- Integrated Design
- Simultaneous PET and MR

MR specification:

- 3T static magnetic field
- 60 cm bore size
- Spatial resolution < 1-3 mm

PET detector:

- Detector crystal: LSO
- MR-compatible PET components
- Size of detector element: 4 x 4 x20 mm

Siemens Biograph mMR

PET/CT vs. PET/MR: PET performance

	PET/MR (mMR)*	PET/CT (mCT)**
Detector material	LSO	LSO
Detector block size (mm)	4 x 4 x 20	4 x 4 x 20
Ring diameter (cm)	65.6	84.2
Axial FOV (cm)	25.8	21.8
Energy window (keV)	430 - 610	435 - 650
Coincidence window (ns)	5.9	4.1
Spatial resolution (mm)	FWHM, 4.3	FWHM, 4.4

** Delso et al. JNM 2011*   *** Jakoby et al. PMB 2011*

PET/CT vs. PET/MR: practical aspects

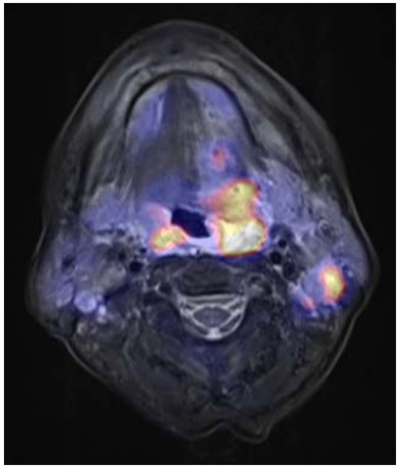
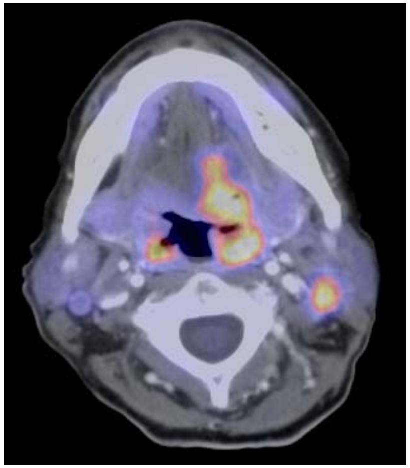

Duration of examination	45 – 60 min	~ 40 min
Image acquisition	simultaneous	sequential
Intrinsic registration	+	+
Radiation exposure	~ 7 mSv	27 - 32 mSv
Attenuation correction	MR-based	CT-based

Limitations of combined PET/MR

- Image fusion of planning CT and PET/MR
  - No tools for RT specific patient positioning available for mMR.
  - Deformable Registration?!

- MR-based attenuation correction of PET data
  - Segmentation approach based on Dixon-MR-sequence

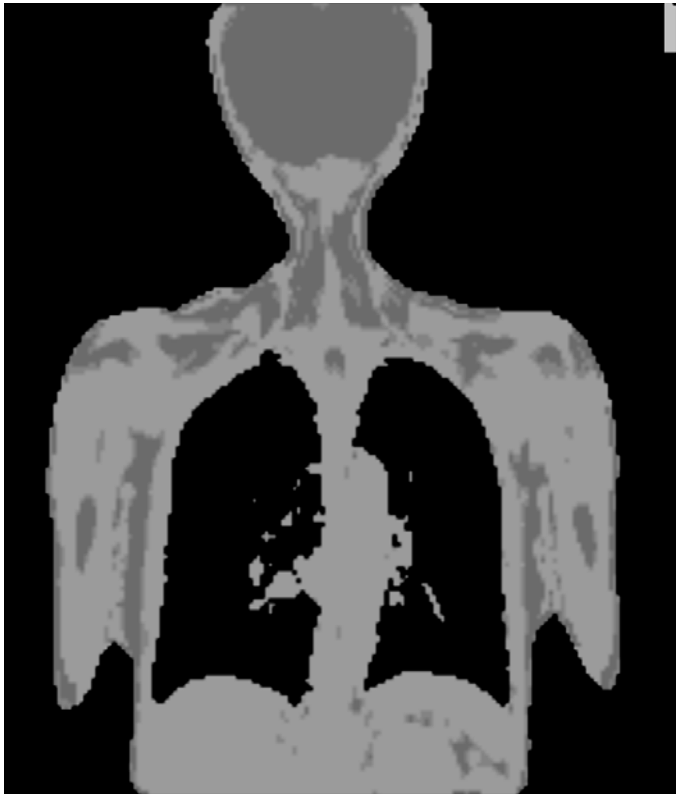

μ-map for PET attenuation correction derived from Dixon-sequence

Future prospects: Hypoxia imaging using PET/MRI

Eberhard-Karls-Universität UKT Universitätsklinikum Tübingen

FMISO PET/MR

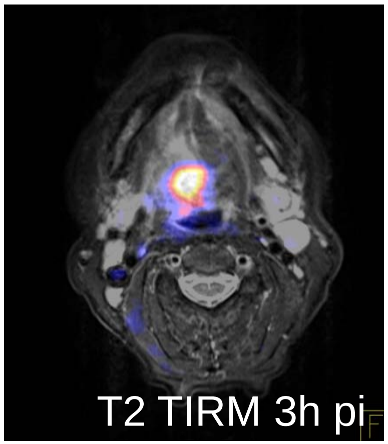

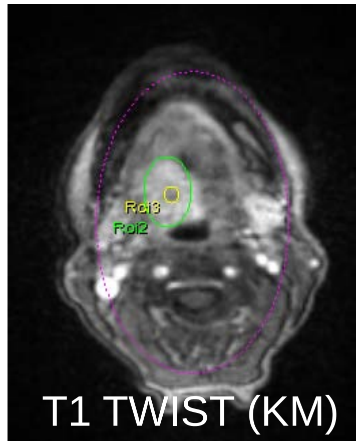

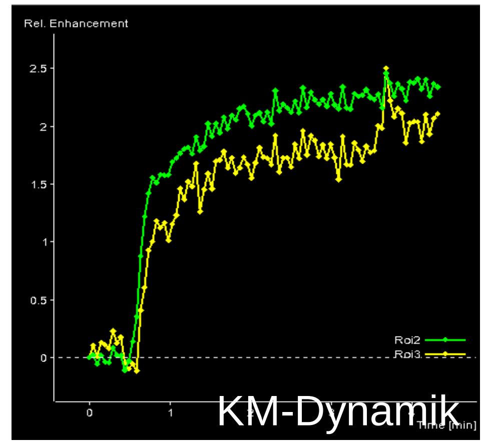

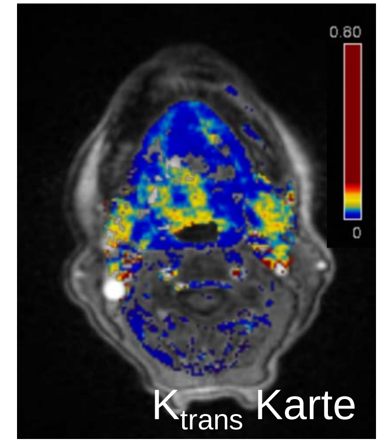

FMISO PET/CT

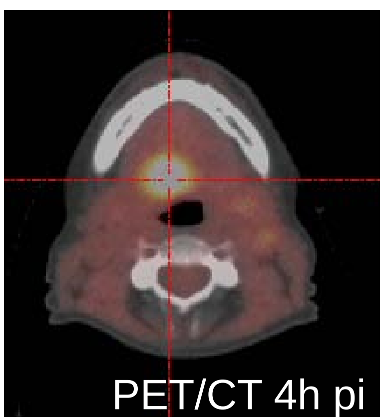

<u>PET/MR Protocol:</u>

- PET Acquisition of 30 min (ca. 3h pi)
- fast diagnostic MR-Protocol
- DCE
- DW

Summary / Conclusion

- PET/CT imaging for RT with various tracers
  - Patient Stratification
  - Target Volume Delineation
  - Hypoxia and Proliferation Imaging for individually directed Dose Escalation ("Dose Painting")
- Reliable interpretation of PET data requires
  - Established imaging protocols
  - Certified calibration and quality control procedures
  - Tracer quantification
- Before dose painting trials can be started
  - Tracer evaluation and
  - Detailed Outcome / Failure Analysis are necessary!
- Multiparametric Imaging

EBERHARD KARLS UNIVERSITÄT TÜBINGEN

MEDIZINISCHE FAKULTÄT

Sektion Biomedizinische Physik

UNIVERSITÄTS KLINIKUM TÜBINGEN

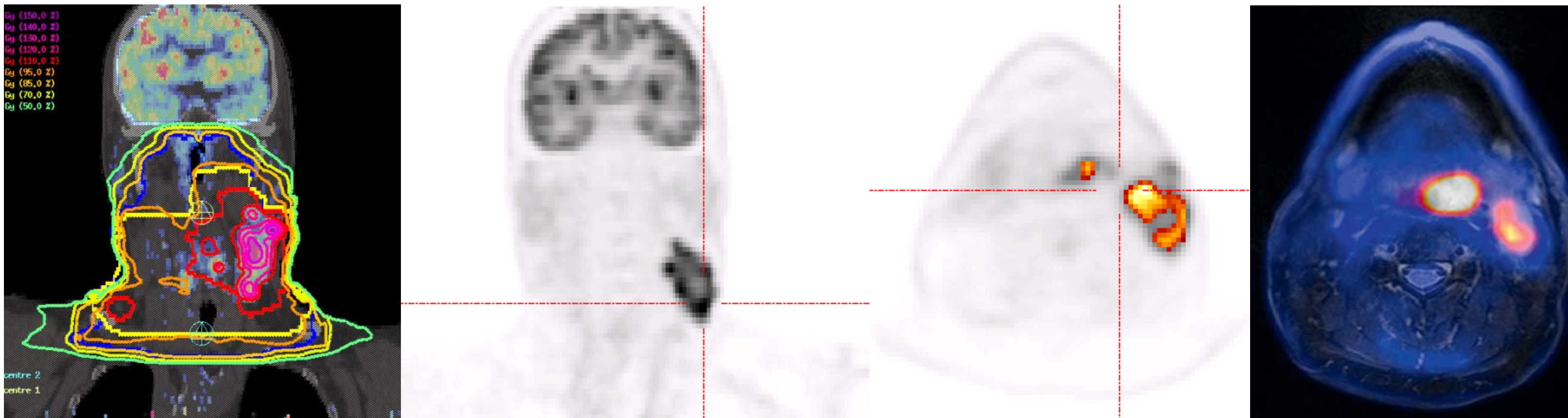

Recommendations for the integration of FDG PET/CT into radiotherapy treatment planning

ESTRO teaching course on advanced imaging

September 18 - 22, 2016 in Florence, Italy

Daniela Thorwarth

Section for Biomedical Physics, University Hospital for Radiation Oncology Tübingen

Integration of FDG-PET/CT into external beam radiation therapy planning

Technical aspects and recommendations on methodological approaches

D. Thorwarth[1]; T. Beyer[2,3]; R. Boellaard[4]; D. De Ruysscher[5]; A. Grgic[6]; J. A. Lee[7]; U. Pietrzyk[8,9]; B. Sattler[10]; A. Schaefer[6]; W. van Elmpt[5]; W. Vogel[11]; W. J. G. Oyen[12]; U. Nestle[13]

[1]University Hospital for Radiation Oncology, Section for Biomedical Physics, Eberhard-Karls University Tübingen, Germany; [2]University Hospital for Radiology, Imaging Science Institute Tübingen, Germany; [3]cmi-experts, Zürich, Switzerland; [4]University Medical Centre, Department of Nuclear Medicine & PET Research, Amsterdam, The Netherlands; [5]Department of Radiation Oncology (MAASTRO), GROW – School for Oncology and Developmental Biology, Maastricht University Medical Centre, The Netherlands; [6]Department of Nuclear Medicine, Saarland University Medical Center, Homburg/Saar, Germany; [7]Center of Molecular Imaging and Experimental Radiotherapy, Université Catholique de Louvain, Brussels, Belgium; [8]Institute of Neurosciences and Medicine – Medical Imaging Physics (INM-4), Research Center Jülich, Germany; [9]Faculty of Mathematics and Natural Sciences, University of Wuppertal, Germany; [10]Department of Nuclear Medicine, University Hospital Leipzig, Germany; [11]Departments of Nuclear Medicine and Radiation Oncology, The Netherlands Cancer Institute – Antoni van Leeuwenhoek ziekenhuis (NKI-AVL), Amsterdam; [12]Department of Nuclear Medicine, Radboud University Nijmegen Medical Centre, The Netherlands; [13]University Hospital for Radiation Oncology Freiburg, Germany

Nuklearmedizin 2012; 51: 140-153.

A joint project of the German working group for Nuclear Medicine and Radiation Therapy and the EANM.

Potential of PET in radiotherapy (RT) treatment planning (TP)

- PET allows imaging of functional and molecular characteristics
- Complementary to anatomical information obtained by CT and MRI
- **More precise definition of the target volume is possible!**

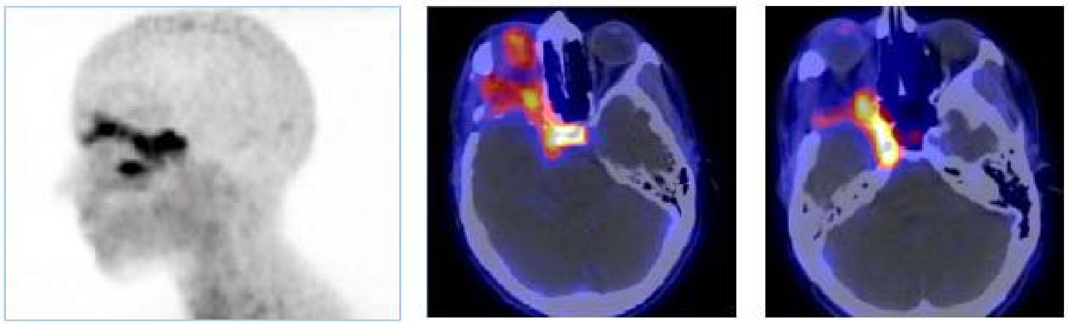

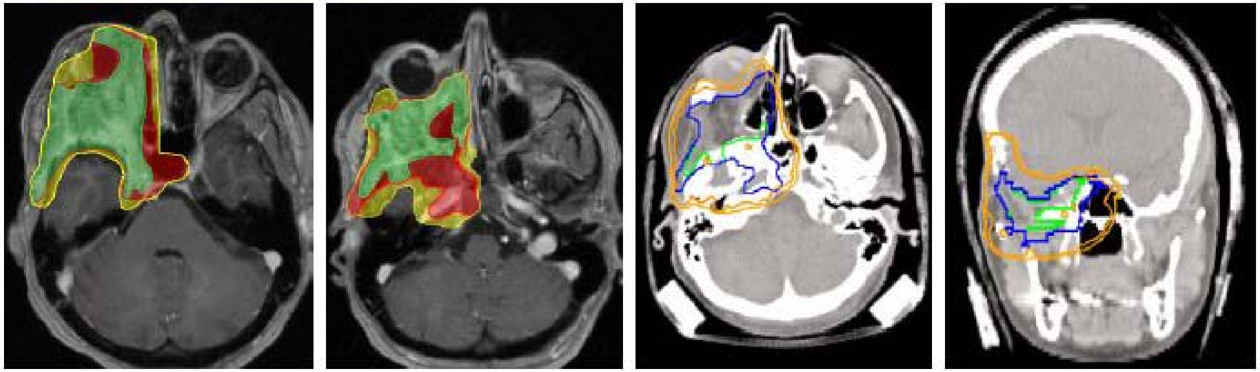

***Gehler B** et al.*
Radiat Oncol 2009

PET in RT TP

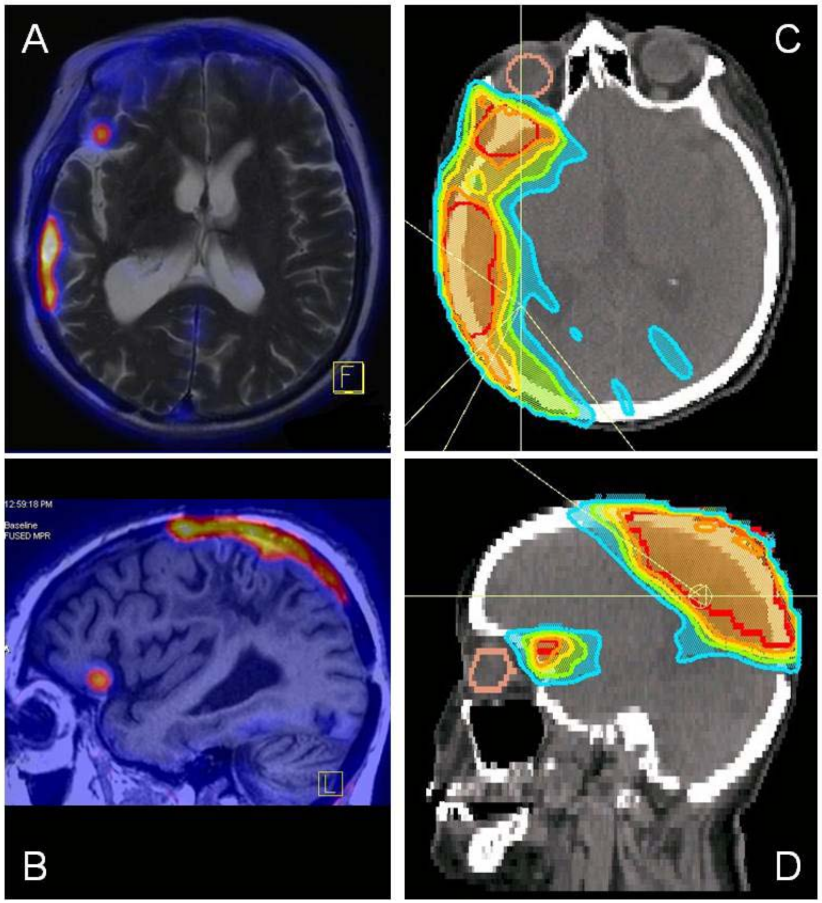

University Hospital Tübingen: PET/MR

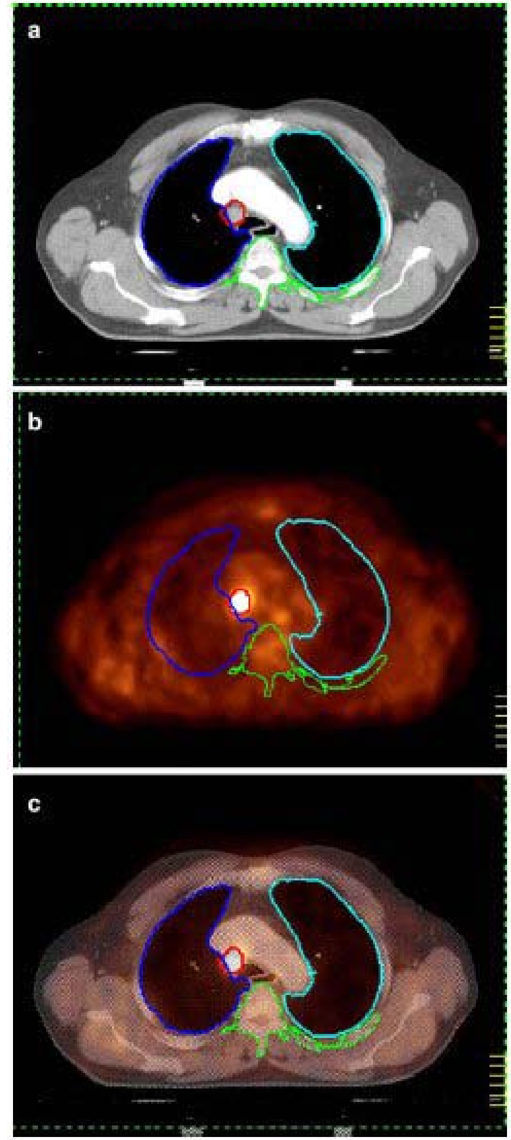

***Nestle** et al.*
EJNMMI 2007

Practical recommendations for using PET/CT in RT

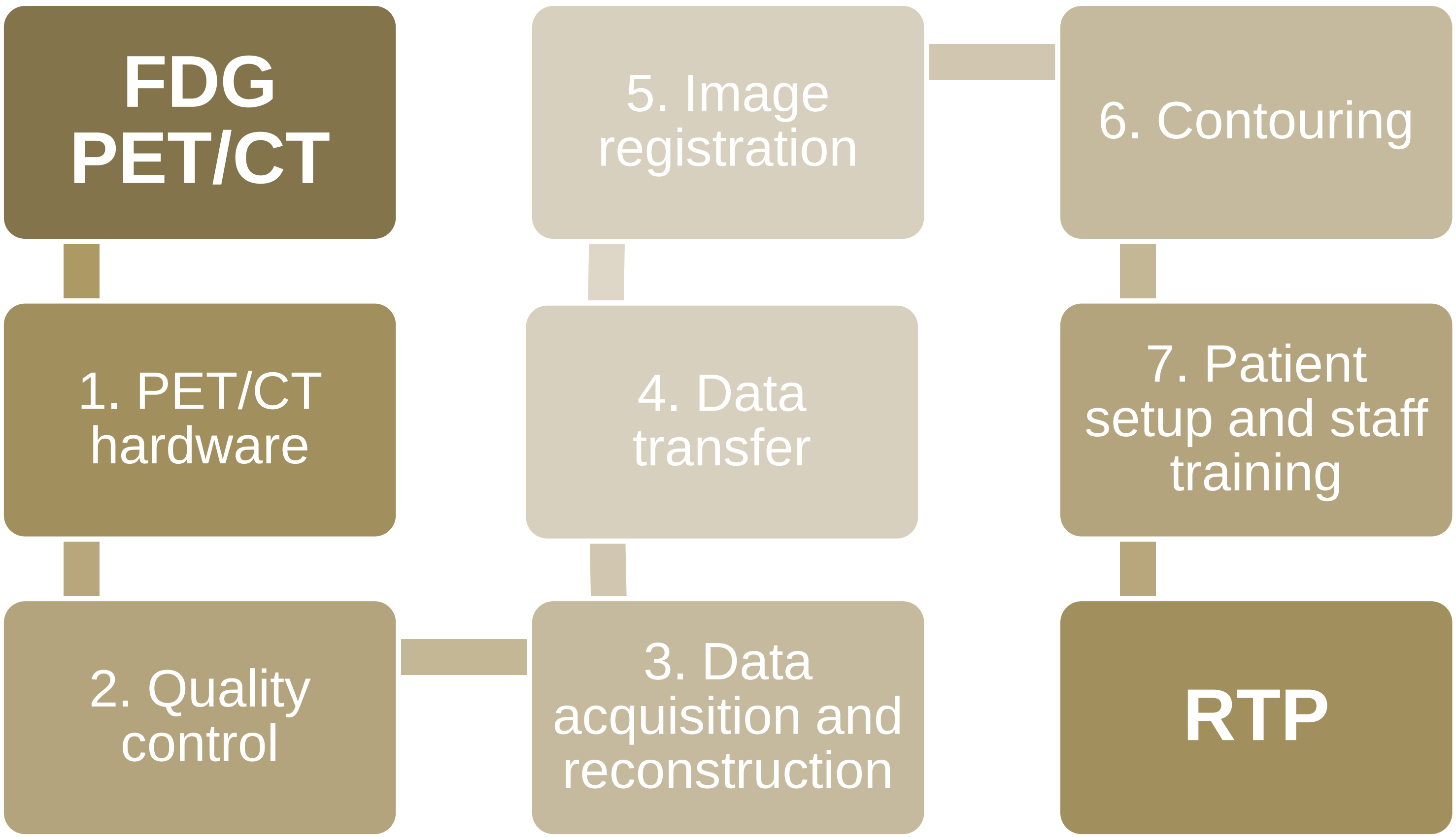

1. PET/CT hardware

Dedicated PET/CT hardware for RT requirements:

- Flat table top
- Positioning aids and devices fixated to the flat RT table
- Increased gantry diameter (up to 85 cm)
- RT laser systems

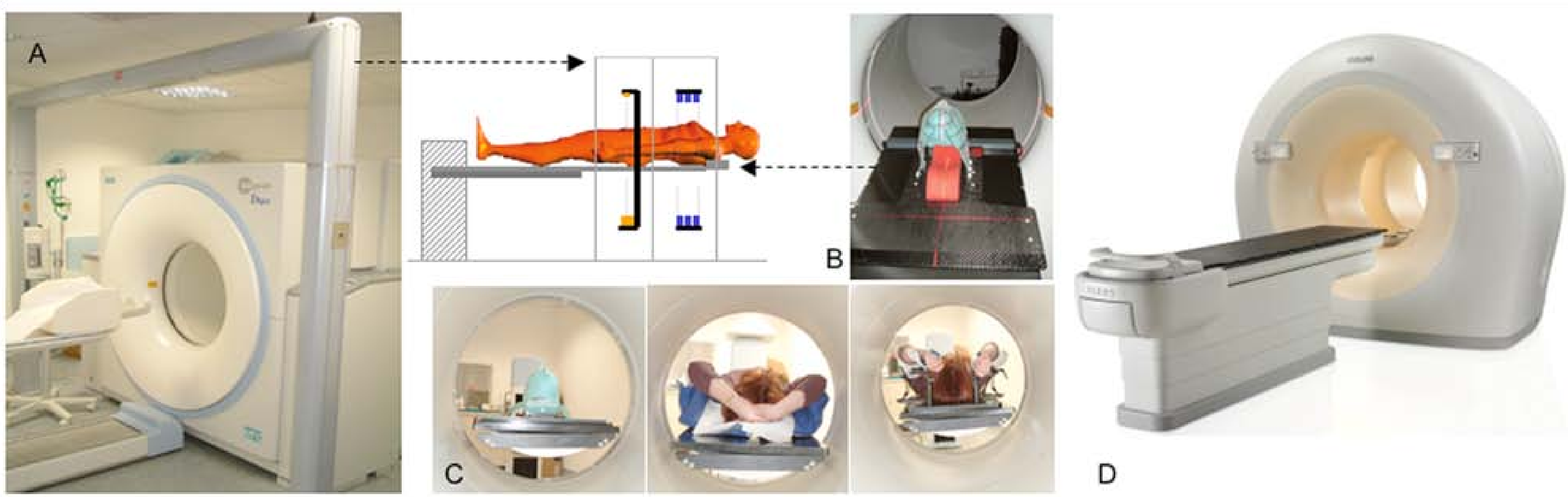

***Thorwarth** et al. Nuklearmedizin 2012 (courtesy T. Beyer)*

1. PET/CT Hardware

Recommendations:

- Combined PET/CT systems and certified RTP hardware accessories should be used for RT TP purposes.
- A PET/CT-guided RT workflow should be defined and managed in close collaboration with the responsible radiation oncology team.

2. Quality control, calibration

- Quality control (QC) and system calibration of PET/CT are prerequisites for accurate and reproducible PET-guided RT TP.
- QC is required
  - During installation (acceptance test)
  - After maintenance service
  - On a regular basis
- QC necessary for the individual components of the system and dedicated to the dual-modality concept:
  - CT system
  - PET components
  - PET/CT alignment
  - RT specific aspects

2a. QC of the CT system

- QC for the CT system have to follow European standards:
  - IEC 61223-2-6 (2006)
  - IEC 61223-3-5 (2004)
- CT QC measurements include
  - Noise levels in uniform areas (air, water)
  - Mean CT numbers (in Hounsfield units, HU)
  - Uniformity
  - Slice thickness
  - Spatial resolution (modulation transfer function, MTF)
  - Accuracy of table positioning
- In case of 4D PET/CT, quality assurance procedures for 4D are useful.

2b. QC of the PET system

- Periodic measurements recommended for
  - Transaxial resolution
  - Imaging Scale
  - Documentation unit
- Routine PET QC measurements
  - Buseman Sokole et al, EJNMMI 2010; 37: 662-71.
  - Buseman Sokole et al, EJNMMI 2010; 37: 672-81.
- QC of PET components consists of
  - Check of coincidence sensitivity and detector normalization
  - Normalization calibration (conversion factor for activity conc.)
  - Certification of imaging properties that describes the results of mandatory data correction (e.g. randoms, attenuation, scatter).

2c. PET/CT alignment

- QC of the physical alignment of CT and PET component (*off-set*) is required.
- Measured first after installation (during acceptance)
- *off-set* may change after service when CT and PET components were set apart for access to the interior gantry.

2d. RT specific QC aspects

- No standard QC for RT specific PET/CT aspects yet
- QC steps according to RT recommendations should be followed (Mutic et al, Med Phys 2003; 30: 2762-92):
  - Positioning and movement of table top under constant load
  - Table top should not contain any artifact producing objects (screws)
  - Laser geometry and accuracy (via alignment phantom)

2. Quality control, calibration

Recommendations

- Regular QC and calibration of PET/CT hardware is required for PET/CT-guided RT TP. Existing guidelines and recommendations should be followed.
- There is a lack of standard QC procedures for ancillary RT devices. A set of QC measured should be agreed on among expert staff from nuclear medicine, radiology and radiation oncology.
- The full range of service operations must be verified following service access of PET/CT hardware

3. Data acquisition and reconstruction

- Depending on the clinical question (staging, target volume delineation, response assessment) different acquisition protocols and co-axial imaging ranges are used
- For target volume delineation: a limited co-axial imaging range may be acceptable
- Attention must be given to patient positioning
- For follow-up scans and response assessment, the same acquisition protocol should be used in terms of:
  - Patient positioning
  - Imaging range
  - Acquisition parameters
  - Image reconstruction

3a. Image acquisition techniques (thorax scans)

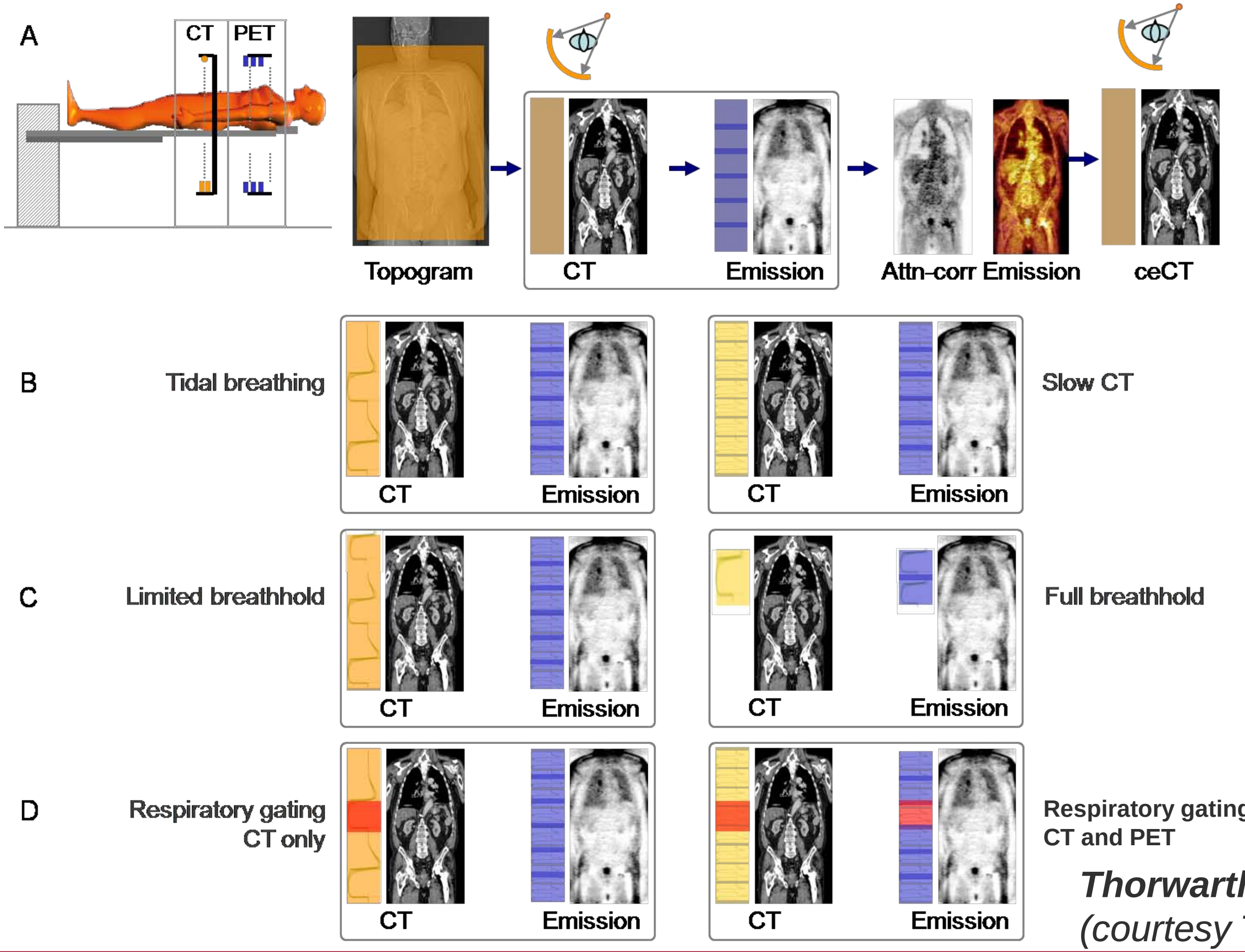

***Thorwarth** et al. Nuklearmedizin 2012 (courtesy T. Beyer)*

3b. PET image reconstruction

- PET/CT reconstruction directly affects detection and delineation of lesions
- Different diagnostic objectives may require different strategies for image quality and quantification
- Image characteristics strongly depend on acquisition protocols
    - patient preparation
    - Injected activity
    - Acquisition time and duration
- Consistent and standardized acquisition protocols and reconstruction methods are absolutely necessary!

3b. PET image reconstruction

- Standard reconstruction today: Iterative methods (eg. OSEM).
- Iterative methods are characterized by:
  - Number of iterations and subsets
  - Matrix and voxel size
  - Image zoom
  - Smoothing kernel
- Sufficient number of iterations and subsets is important to ensure a convergence of the algorithm (product larger than 40).
- Full 3D reconstruction without Fourier rebinning
- PET image reconstruction with and without attenuation correction to check for artifacts due to contrast agents, metal implants and patient motion.

3b. PET image reconstruction

[18F]-FDG PET examination on a PET-only BGO system:

[18F]-FDG PET examination on a state-of-the-art PET/CT system:

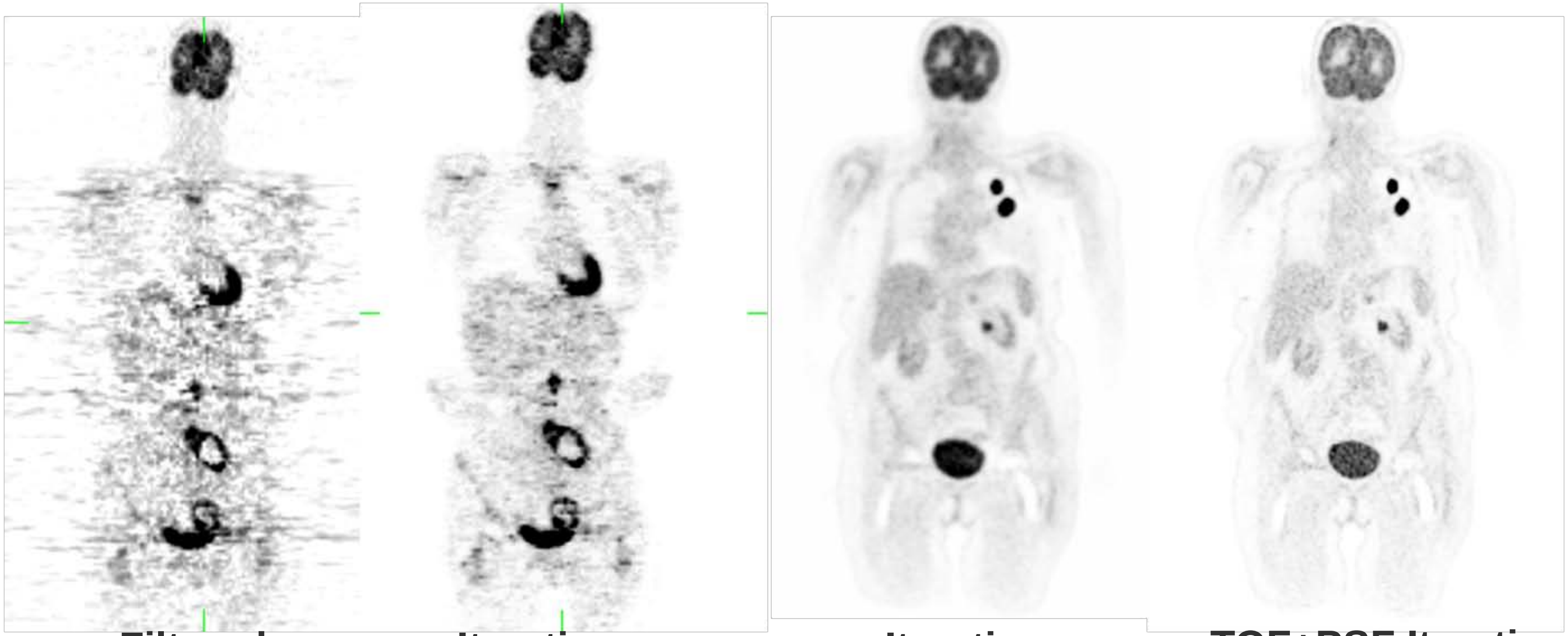

Filtered Backprojection | **Iterative** Reconstruction | **Iterative** Reconstruction | **TOF+PSF Iterative** Reconstruction

Courtesy R. Boellaard, Amsterdam

3. PET data acquisition and image reconstruction

Recommendations

- Image reconstruction should be standardized for PET/CTs use ind RT-planning on an institutional or study level.
- Hardware and software updates must be reported to the cooperating RT-responsibles, they may affect volume delineation.
- For standard RT planning purposes, 3D PET/CT imaging following limited breath hold or tidal breathing is sufficient. 4D PET/CT acquisitions may be useful to complement 4D-CT information on the magnitude of tumor motion.
- Artifacts may be induced by metal implants or contrast agents. Relevant artifacts should be reported by the nuclear medicine specialists.

4. Data transfer / treatment planning system (TPS)

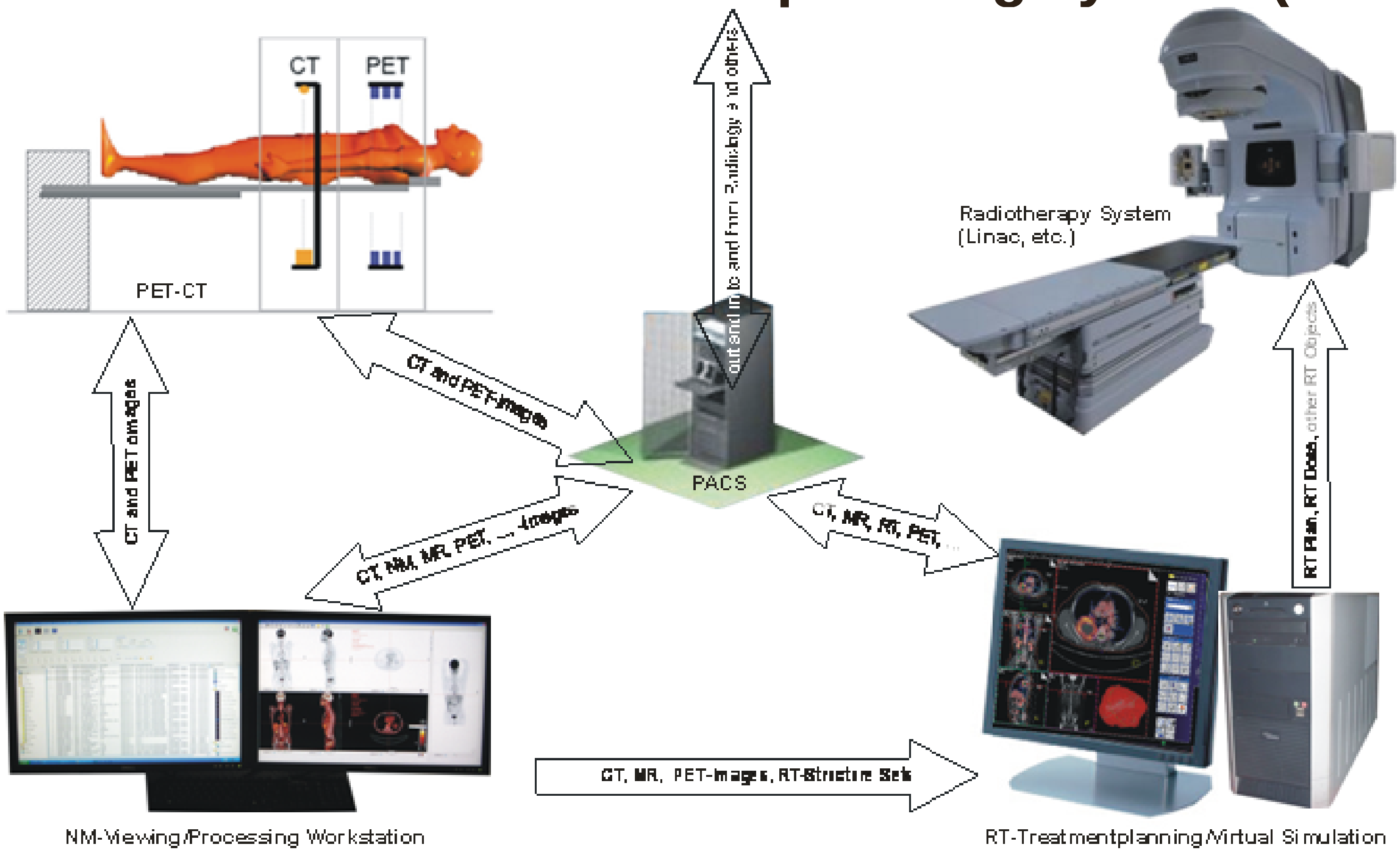

Courtesy W. van Elmpt, Maastricht

4. Data transfer / TPS

Recommendations

- Set-up and verify DICOM path between image acquisition console and RT TP workstation.
- Verify the alignment of PET/CT data prior to using them for RT TP.
- Implement a routine to visually or manually check the consistency of the data when transferring the data from PET/CT to the TPS.
- Establish a routine workflow for communication of diagnostic findings and pre-defined tumor volumes between PET/CT and radiation oncology departments.

5. Image fusion / registration

- Co-registration of image data (CT, MRI, PET/CT, …) is essential for image-guided RT.

- Linear / rigid registration:
  - Landmark – based
  - Mutual information

- Non-linear / deformable registration methods:
  - Volume / feature-based algorithms
  - Optical flow methods
  - Demon’s algorithm

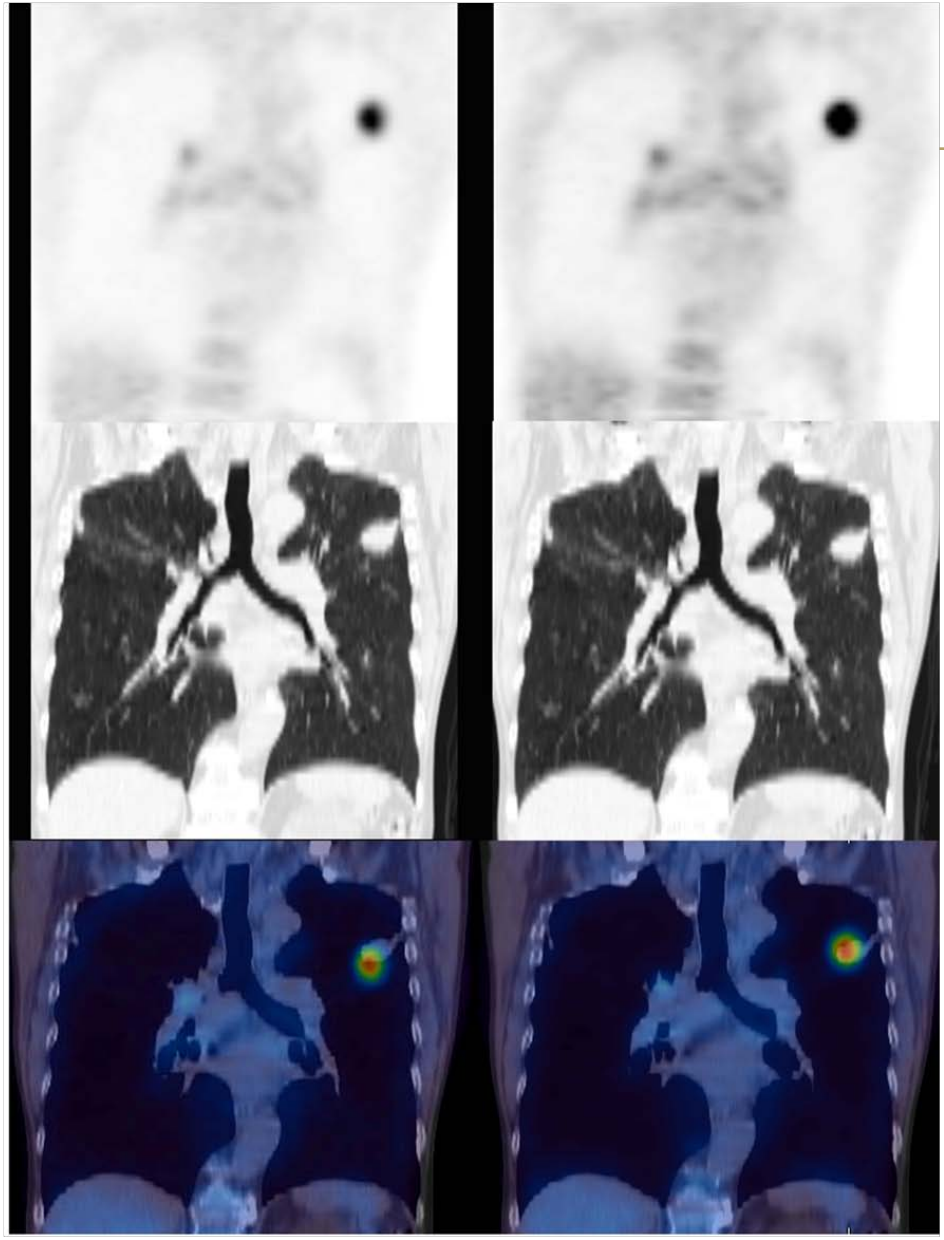
(A) (B)

5. Image fusion / registration

- Often deformable registration would be required to accurately fuse the image data.
- Problem: validation of deformable registration algorithms!

(A) Linear registration of PET and CT.
(B) Non-rigid registration.

Courtesy U. Pietrzyk, Jülich

5. Image fusion / registration

Recommendations

- Image fusion for RT TP demands accurately aligned image volumes.
- For the purpose of RT TP based on PET or PET/CT and CT images at this moment, only linear registration algorithms should be employed clinically.
- The accuracy of co-registration must be checked prior to proceeding with the TP process on the aligned data sets.

6. Image contouring

- Automatic contouring of PET image data seems to be beneficial: objectivity, reproducibility.
- PET has low spatial resolution and high signal-to-noise ratio (SNR)
- Blurred images with partial volume effects (PVE) for small objects.

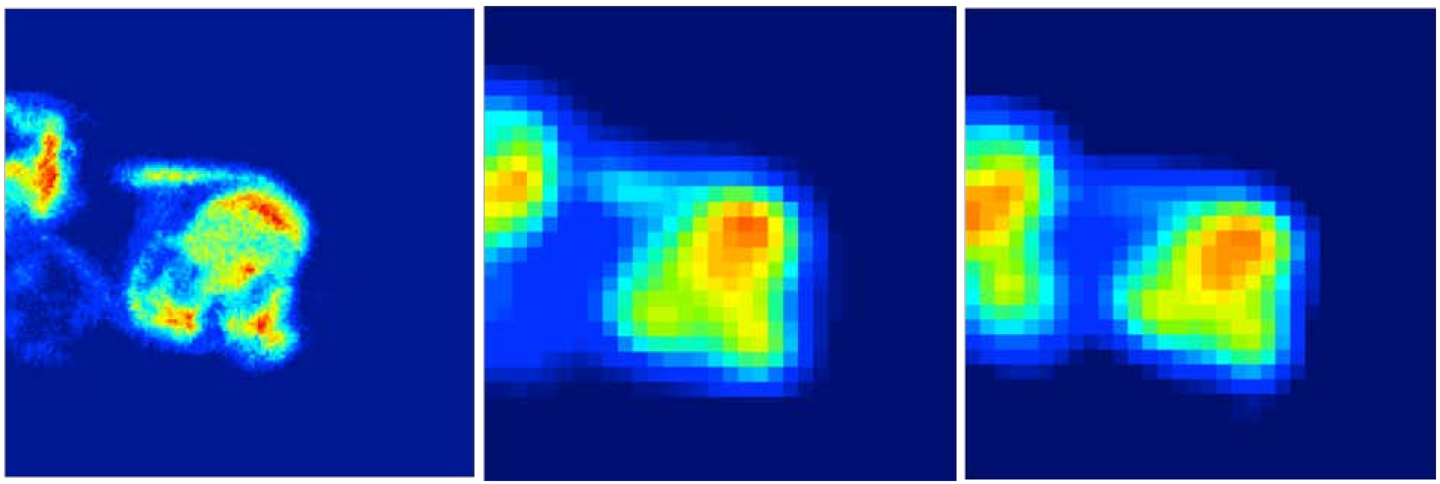

(A) [18F]-FDG autoradiography of a mouse leg bearing a tumour. In order to mimic the limited spatial resolution of PET images (C), the autoradiography image in (A) was blurred with the point-spread function of the PET system used in (C) and resampled to the same voxel size (B). The original PET image is shown in (C).

Courtesy J. Lee, Brussels

6. Image contouring

- Existing automatic contouring algorithms:
  - Thresholding methods
  - Gradient based algorithms
  - Methods including PVE-correction and deconvolution
  - Statistical clustering
- Chosen method has to be validated using PET phantom measurements.

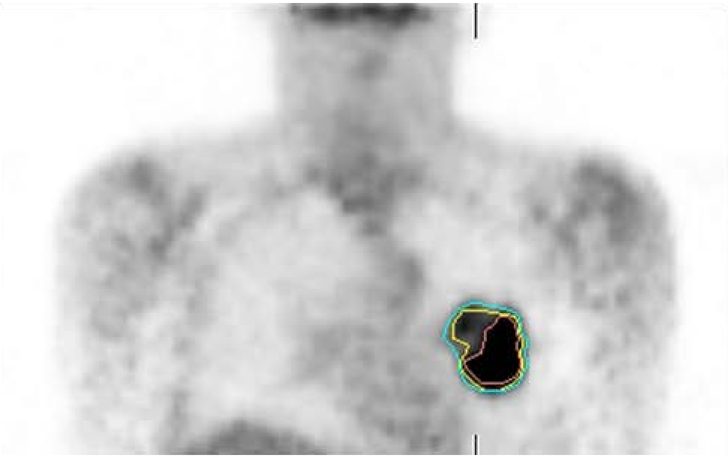

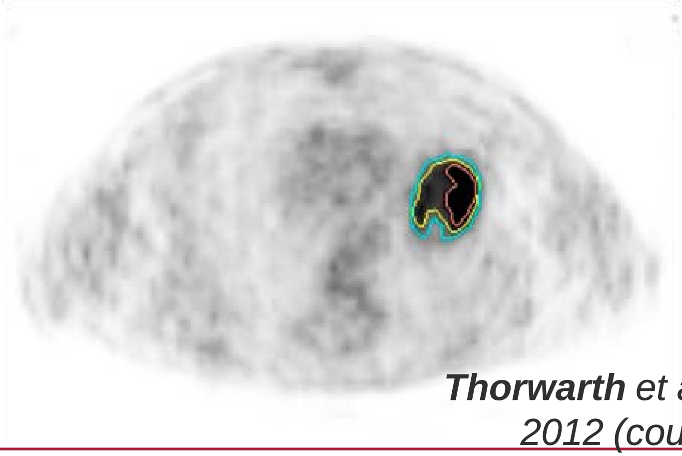

40% SUV_{max} (47 ml)
SUV=2.5 (105 ml)
Adaptive thresholding (77ml)

***Thorwarth** et al. Nuklearmedizin 2012 (courtesy A. Schaefer)*

6. Image contouring

Recommendations

- Any segmentation algorithm chosen for RT TP should provide algorithmic robustness and should be parameterized to the spatial resolution of the PET system in use.
- A validation of the delineation with phantom data should be done.
- In clinical routine, a delineation method needs to be selected and agrees upon among imaging experts and radiation oncologists.
- Contouring should be performed jointly by two experts from radiotherapy and nuclear medicine.

7. Patient set-up / staff training

- Adequately trained PET/CT staff is essential for efficiency, quality and safety.
- Expertise in imaging and radiation oncology is required.
- Staff from both departments should be involved.

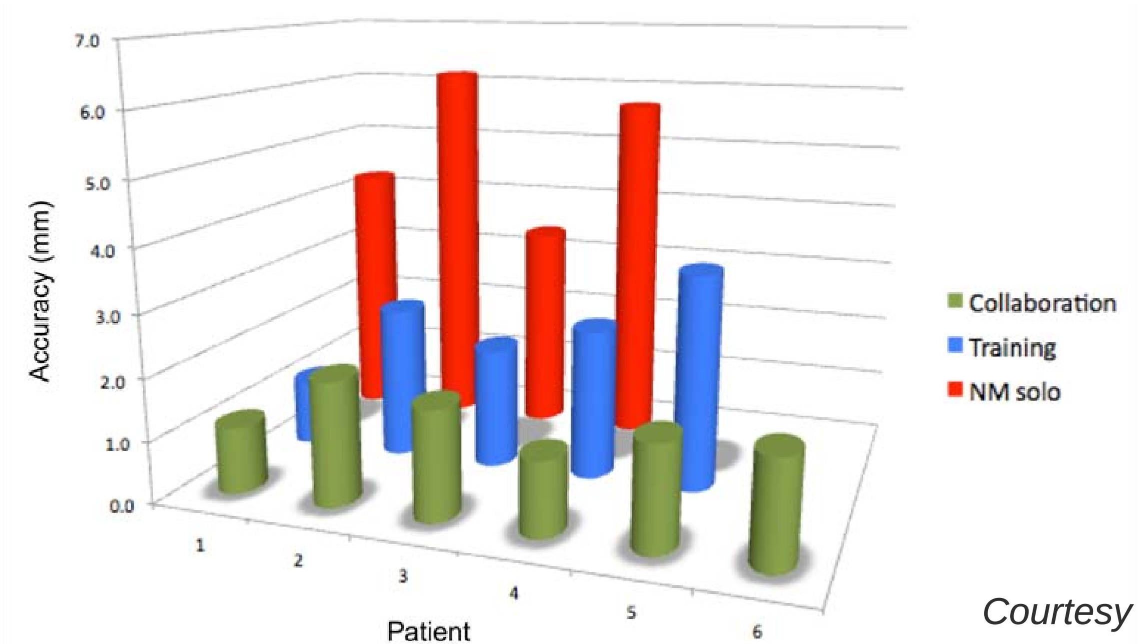

Courtesy W. Vogel, Amsterdam

7b. Radiation exposure

- Approx. 40% of the staff exposure in clinical PET/CT originates from exposure during patient set-up (Seierstad et al, Radiat Prot Dosimetry 2007)
- Complex positioning increases staff exposure
- Staff exposure should be reduced by
  - Patient instructions before tracer injection
  - Adaptation of positioning aids before injection
  - Trained RT staff should be involved during set up to shorten the time needed for patient positioning
  - Use of motorized activity injectors
  - Use of new PET/CT technology that allows less activity to be injected thanks to higher detector sensitivities

7. Patient set-up and staff training

Recommendations

- Adequate staff training for patient positioning with the use of dedicated RT positioning devices is essential for PET/CT-guided RT TP.
- Joint efforts by PET/CT imaging staff and RT technologists are required to yield optimum quality and to reduce staff exposure.
- Relatively increased staff exposure rates should not deter from careful patient positioning.

Conclusion

- PET/CT-guided RT TP requires extensive logistics, patient preparation and hardware, QC and standardization.
- Intensive Communication between specialists and technicians from all involved disciplines is essential.
- When fulfilling these requirements, PET/CT imaging can help to significantly improve RT TP, clinical studies and finally enable for better patient care.

Acknowledgments

- Thomas Beyer (Vienna)
- Ronald Boellaard (Amsterdam)
- Dirk De Ruysscher (Maastricht)
- Aleksandar Grgic (Homburg)
- John Lee (Brussels)
- Uwe Pietrzyk (Jülich)
- Bernhard Sattler (Leipzig)
- Andrea Schaefer (Homburg)
- Wouter van Elmpt (Maastricht)
- Wouter Vogel (Amsterdam, NKI)
- Wim Oyen (Nijmegen)
- Ursula Nestle (Freiburg)

UiO Department of Physics
University of Oslo

Oslo University Hospital

Dynamic CT and PET

Eirik Malinen

Background

- Non-invasive study of physiological and biological function
- Use imaging contrast agents /tracers with different properties
- Monitor uptake of agent in time and space - **4D**
- *NOT* motion management in the following

Dynamic CT

- Sequential CT scans, single-or multi-slice, where temporal resolution may be varied

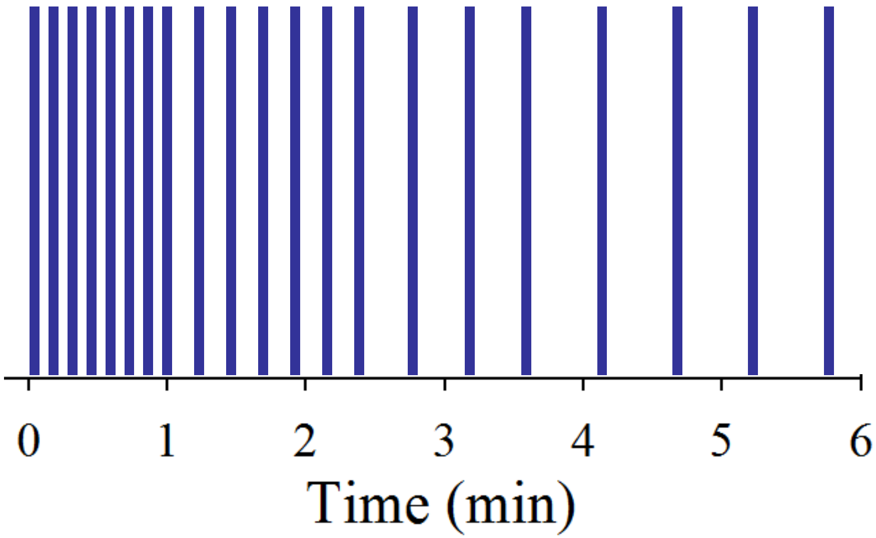

- Acquisition parameters and image reconstruction similar to standard CT

Iodinated contrast agents

Iohexol

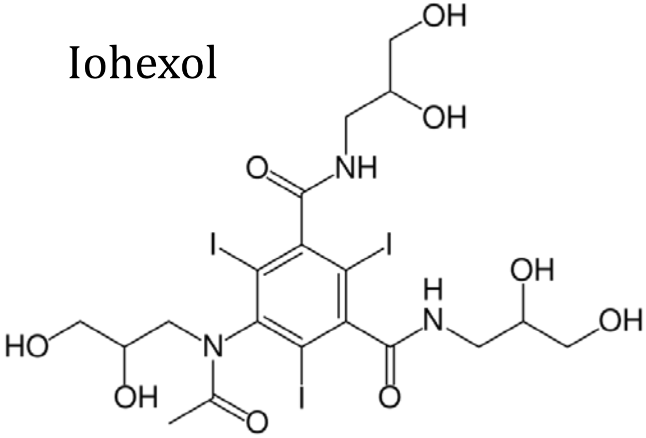

Iodixanol

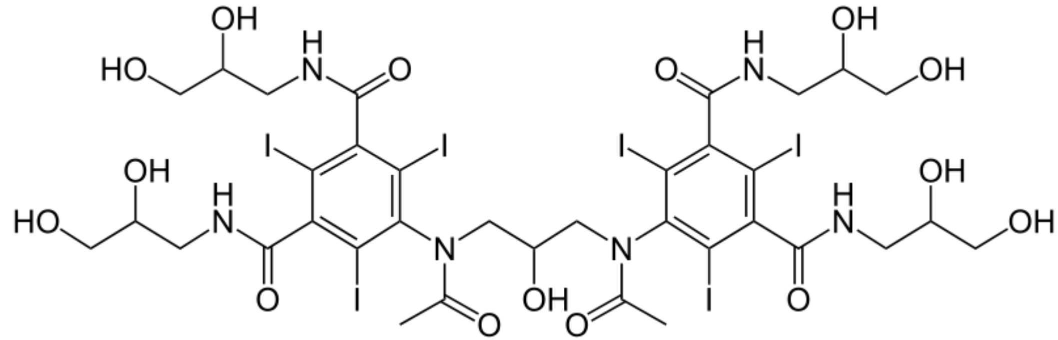

- Injected intravenously
- Linear relationship between concentration and attenuation
- 1 mg/mL of iodine gives 25-35 HU increase

Vessel leakiness in tumors

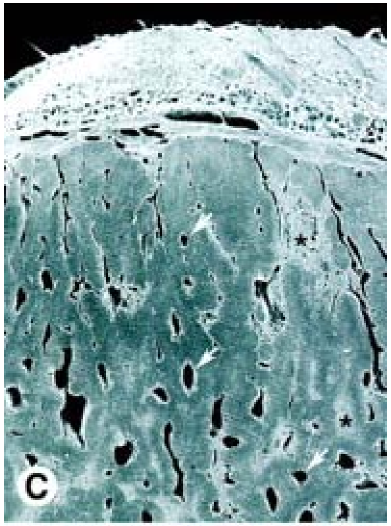

400 µm

Normal

10 µm

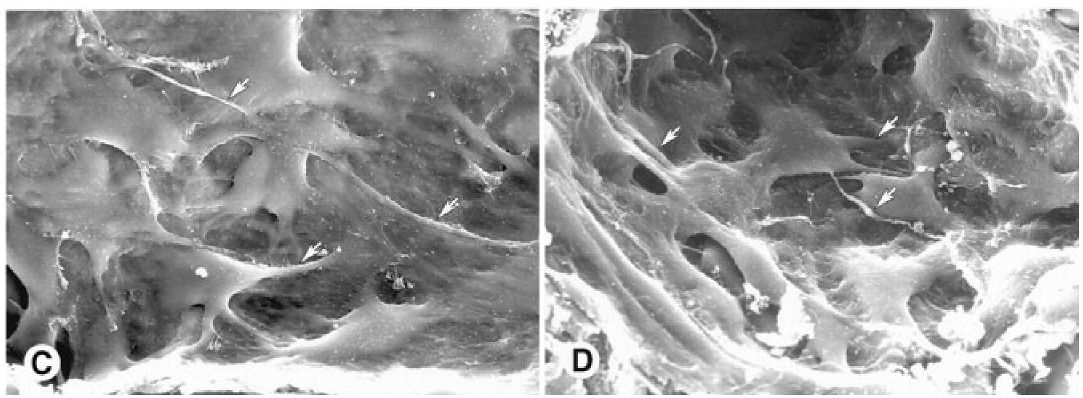

Abnormal

Am J Pathol 2000; 156: 1363–1380

Tissue distribution

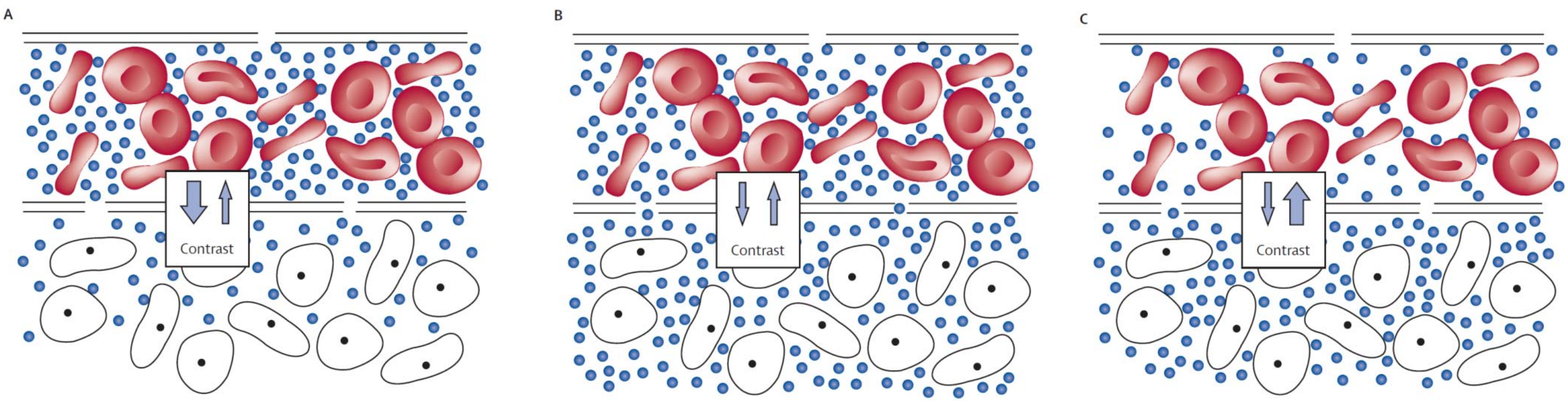

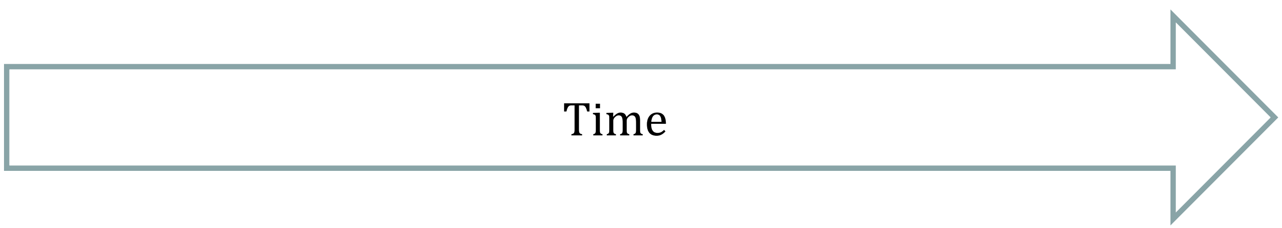

UiO Department of Physics
University of Oslo

Lancet Oncol 2007; 8: 63–74

Oslo University Hospital

Temporal uptake characteristics

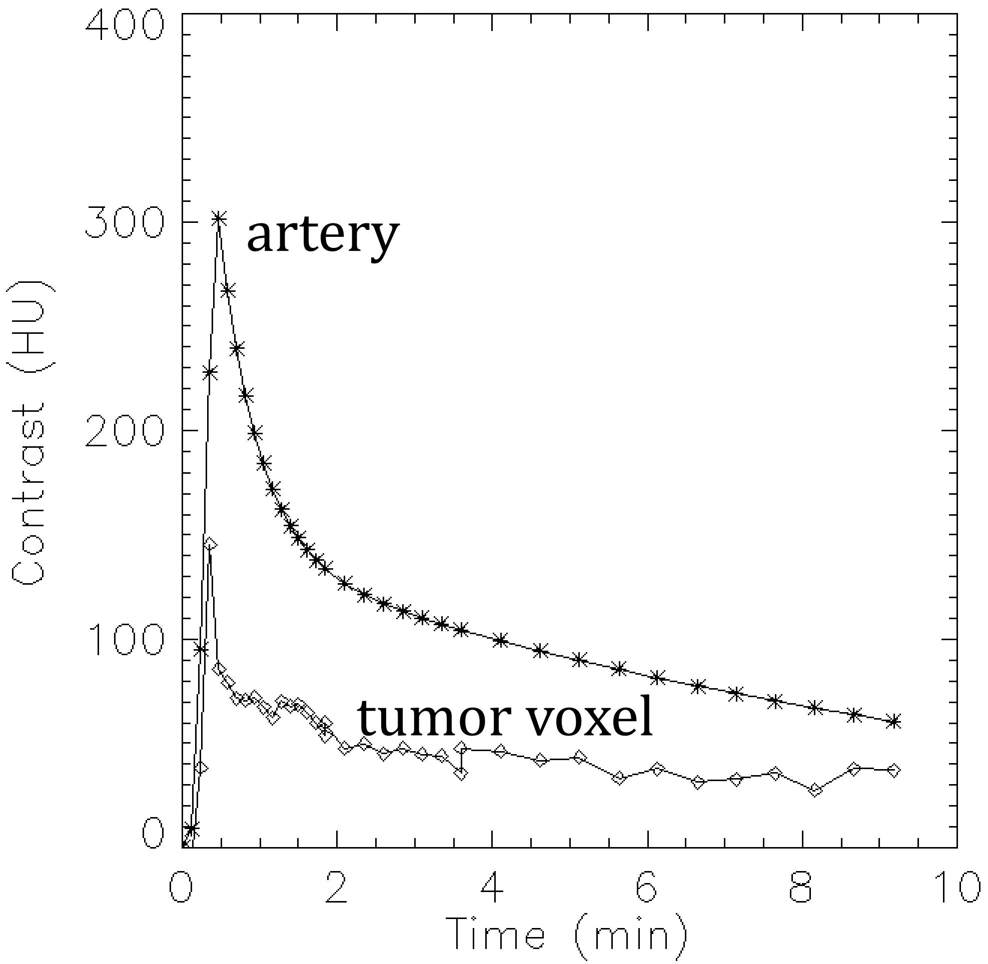

Compartmental modeling

- Fit mathematical models reflecting underlying microenvironment to uptake curves
- Model parameters have biological meaning
- Results in a condensation of the image basis

1-compartment model

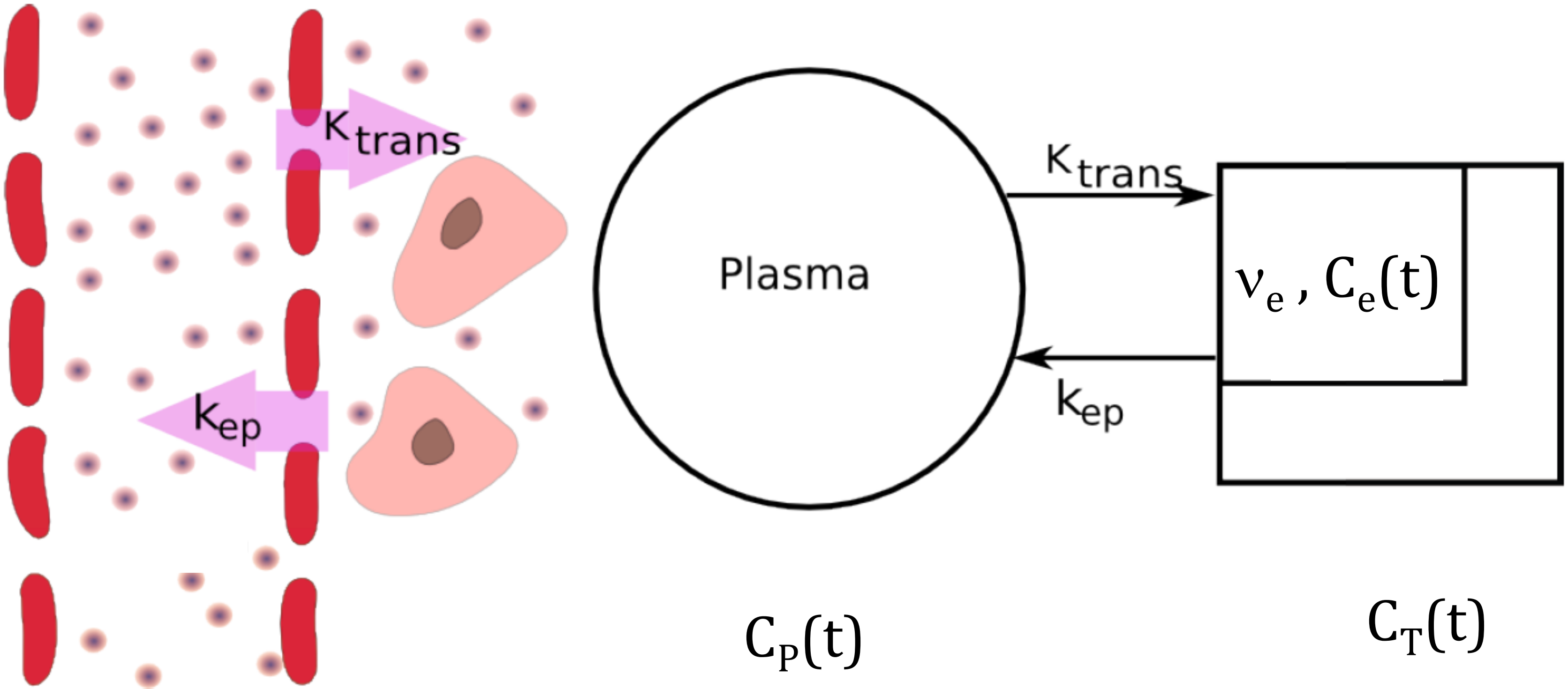

$C_p(t)$: Plasma concentration

$C_T(t)$: Tissue concentration (the measurand)

ν_e: volume fraction of extravascular, extracellular space (EES)

$C_e(t)$: Concentration in EES

1-compartment model

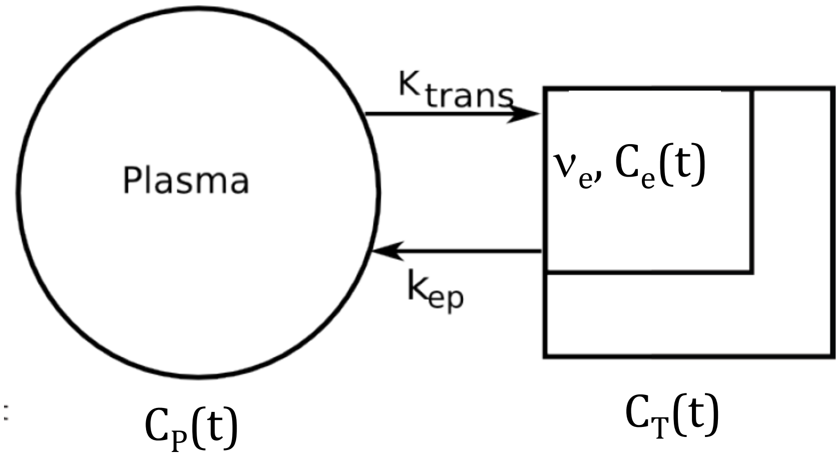

$$C_T = C_e \nu_e$$

$$\frac{dC_T}{dt} = K^{trans}(C_P - C_e)$$

$$\Leftrightarrow \frac{dC_T}{dt} = K^{trans}(C_P - \frac{C_T}{\nu_e})$$

- Solution to differential equation is

$$C_T(t) = K^{trans} \int_0^t C_P(t')e^{-k_{ep}(t-t')}dt' \quad , \; k_{ep} = \frac{K^{trans}}{\nu_e}$$

$$\Leftrightarrow C_T(t) = K^{trans} e^{-k_{ep}t} \otimes C_P(t)$$

- May be fitted to uptake curves by regression

Interpreting K^{trans}

Perfusion under perfusion-limited conditions, permeability surface area product under permeability-limited conditions, or a combination of both!

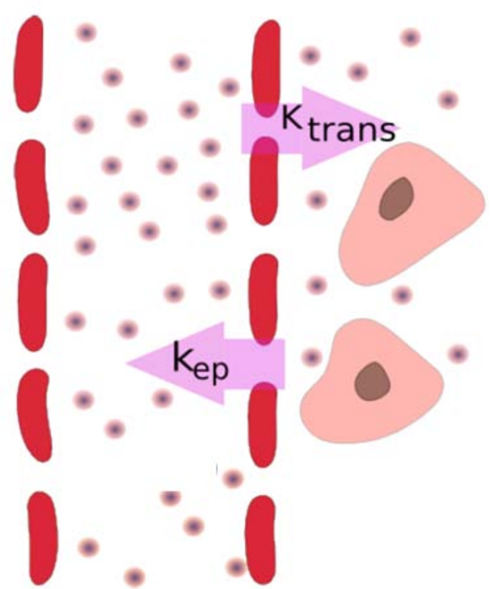

Case study: DCECT of lymphoma patients

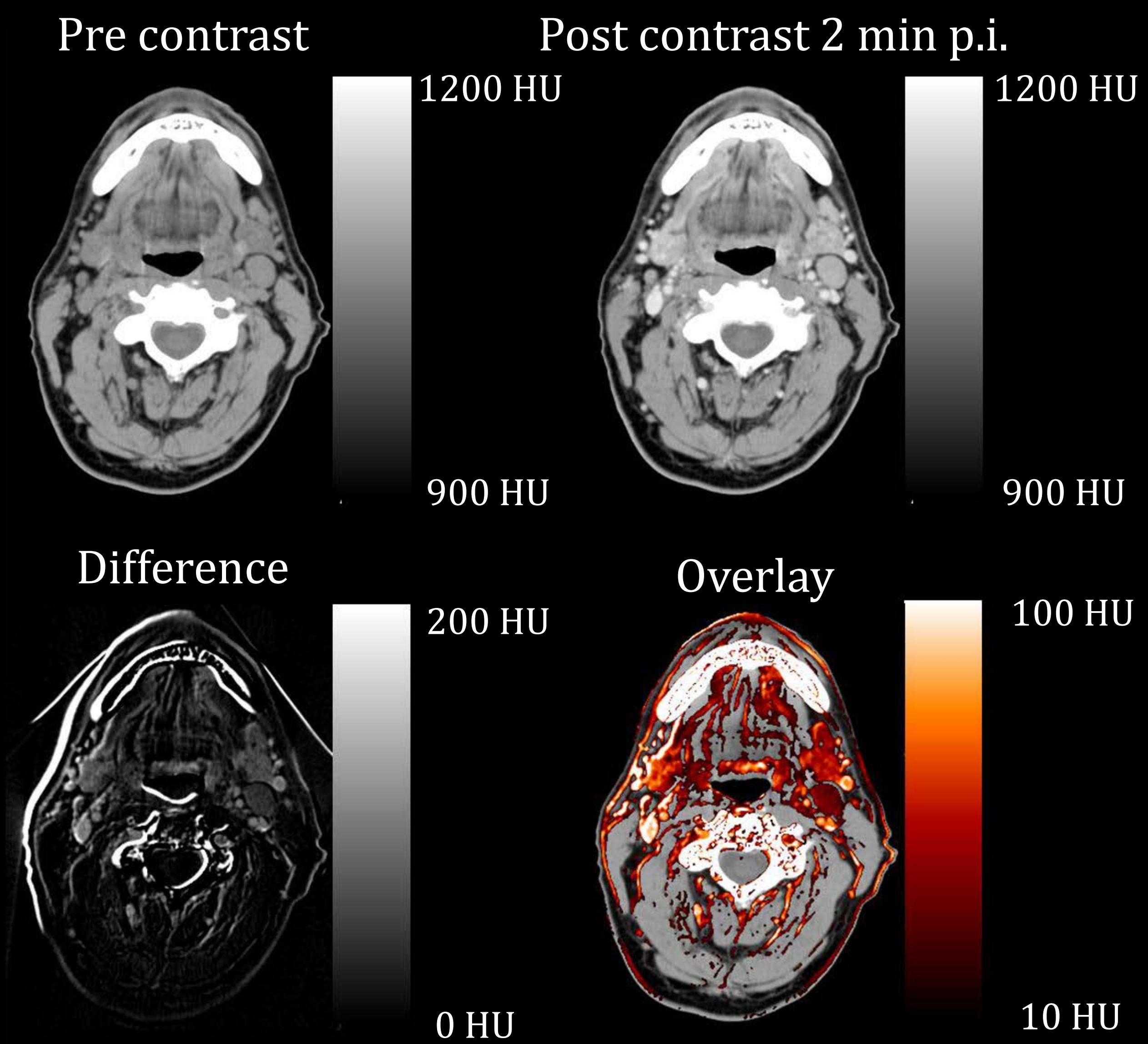

Dynamic image series, overlay

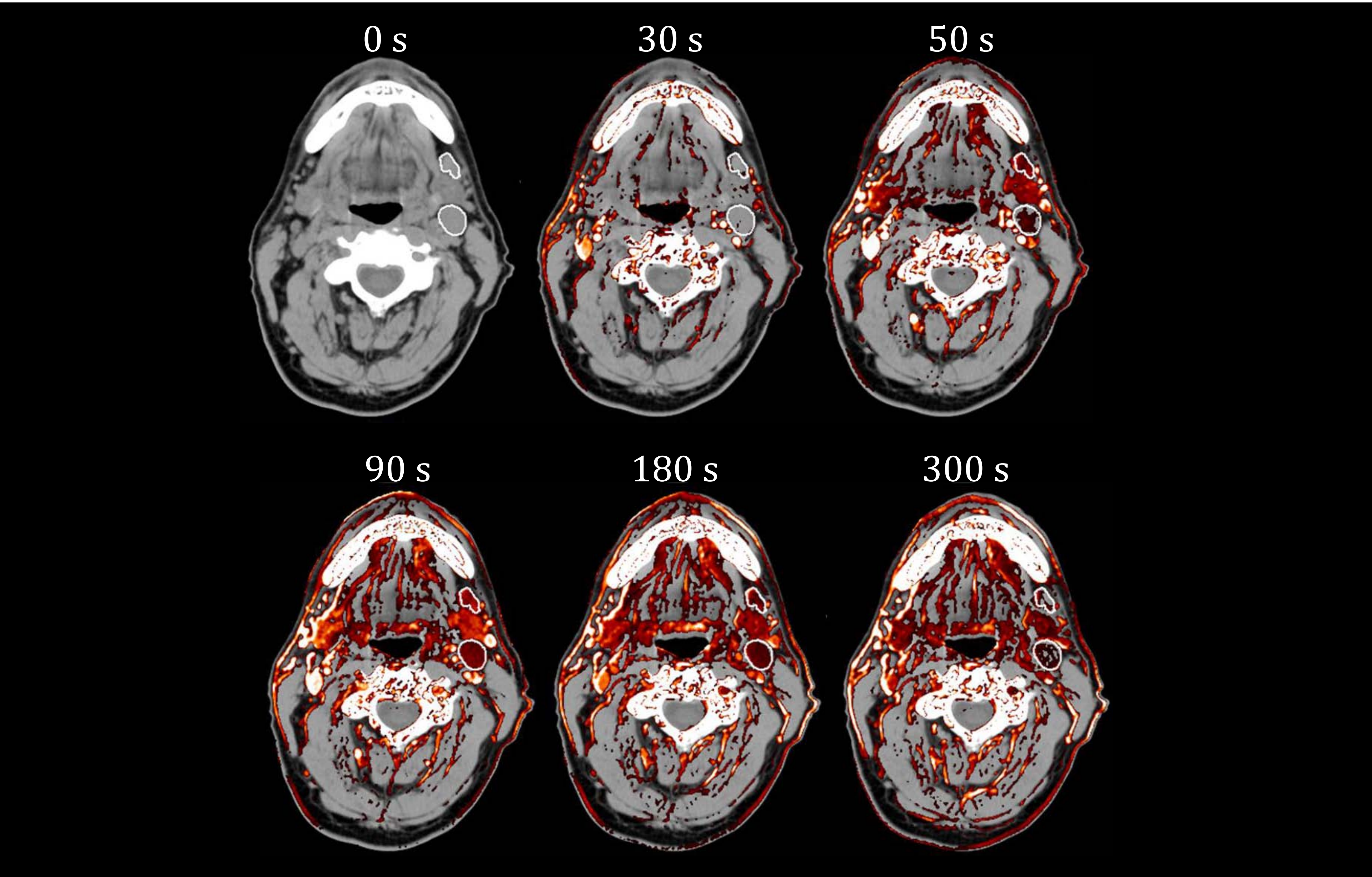

Identifying the artery

Image acquired 70 s p.i.

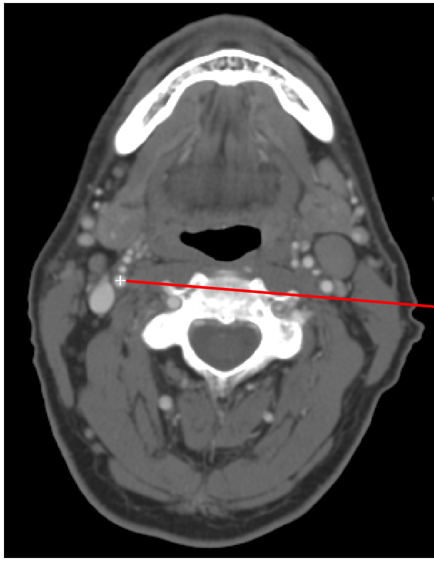

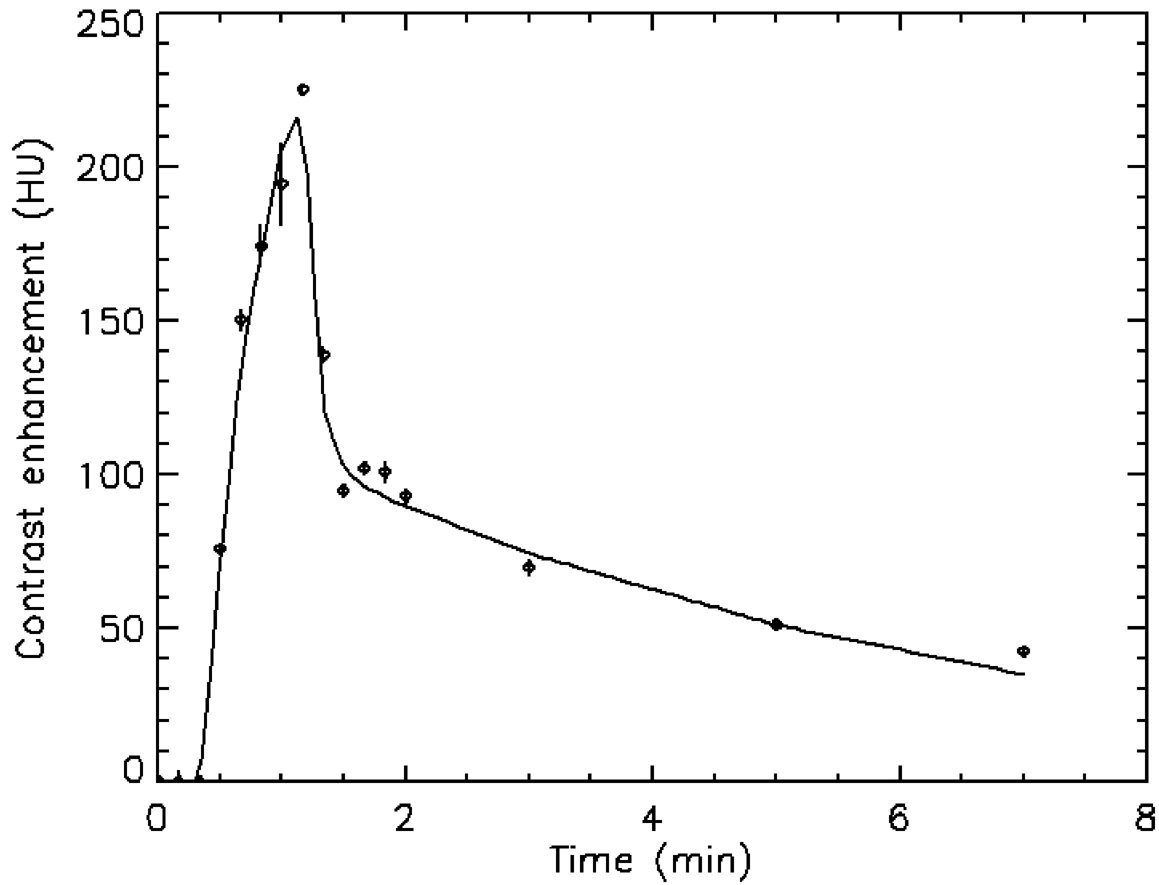

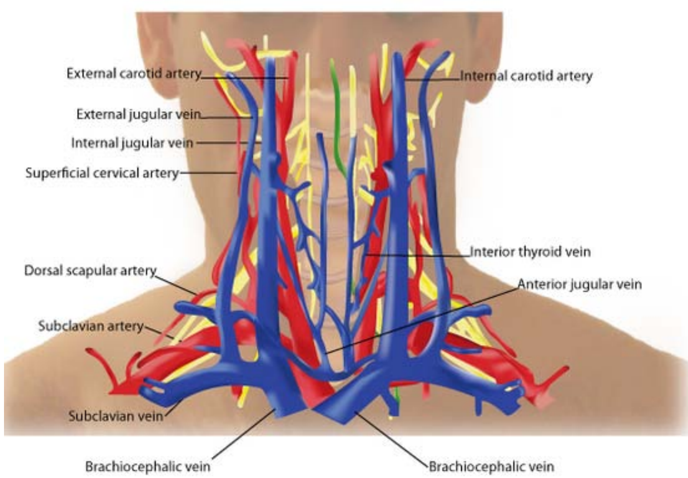

Oslo University Hospital

Voxel-by-voxel analysis

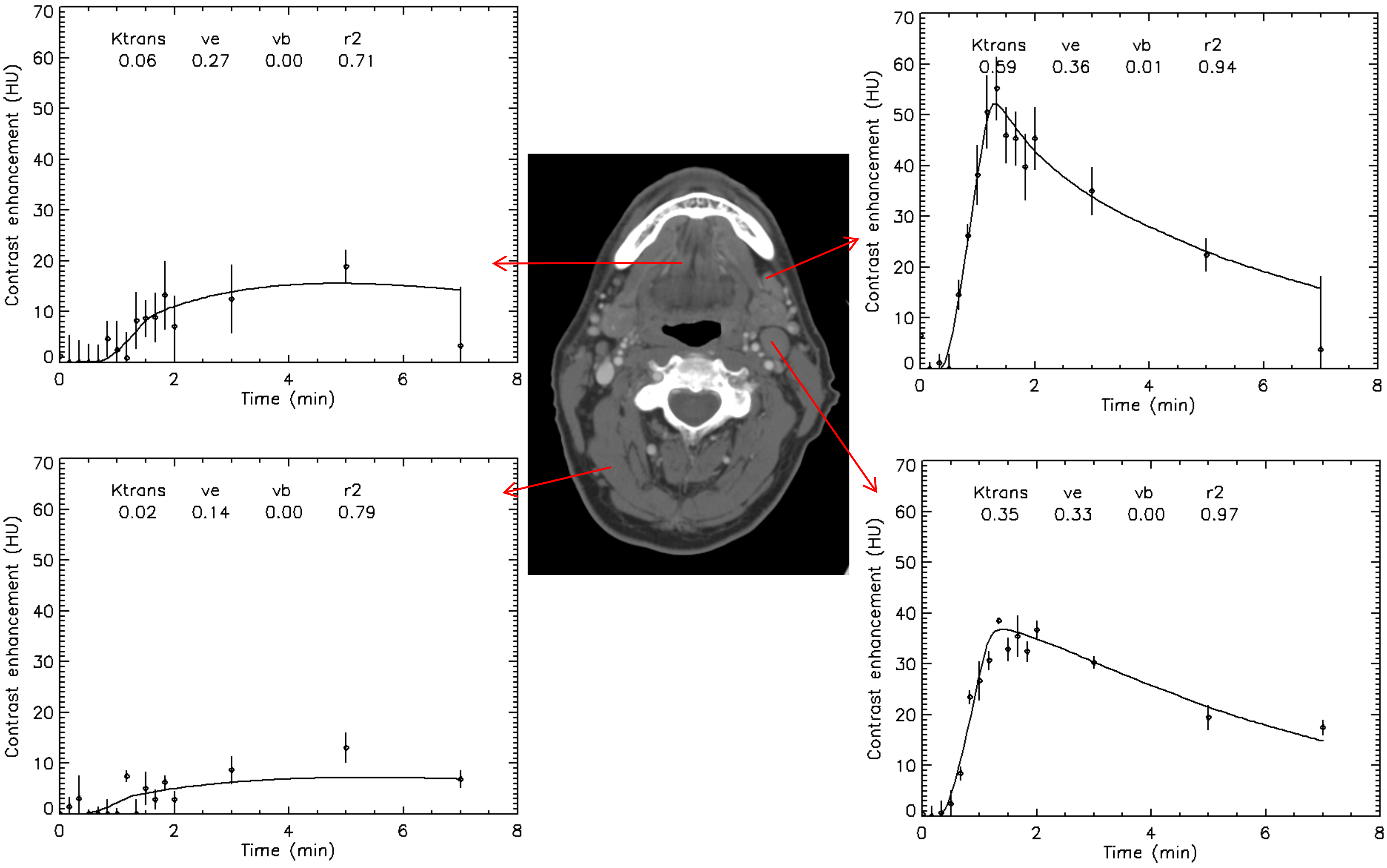

Parametric maps

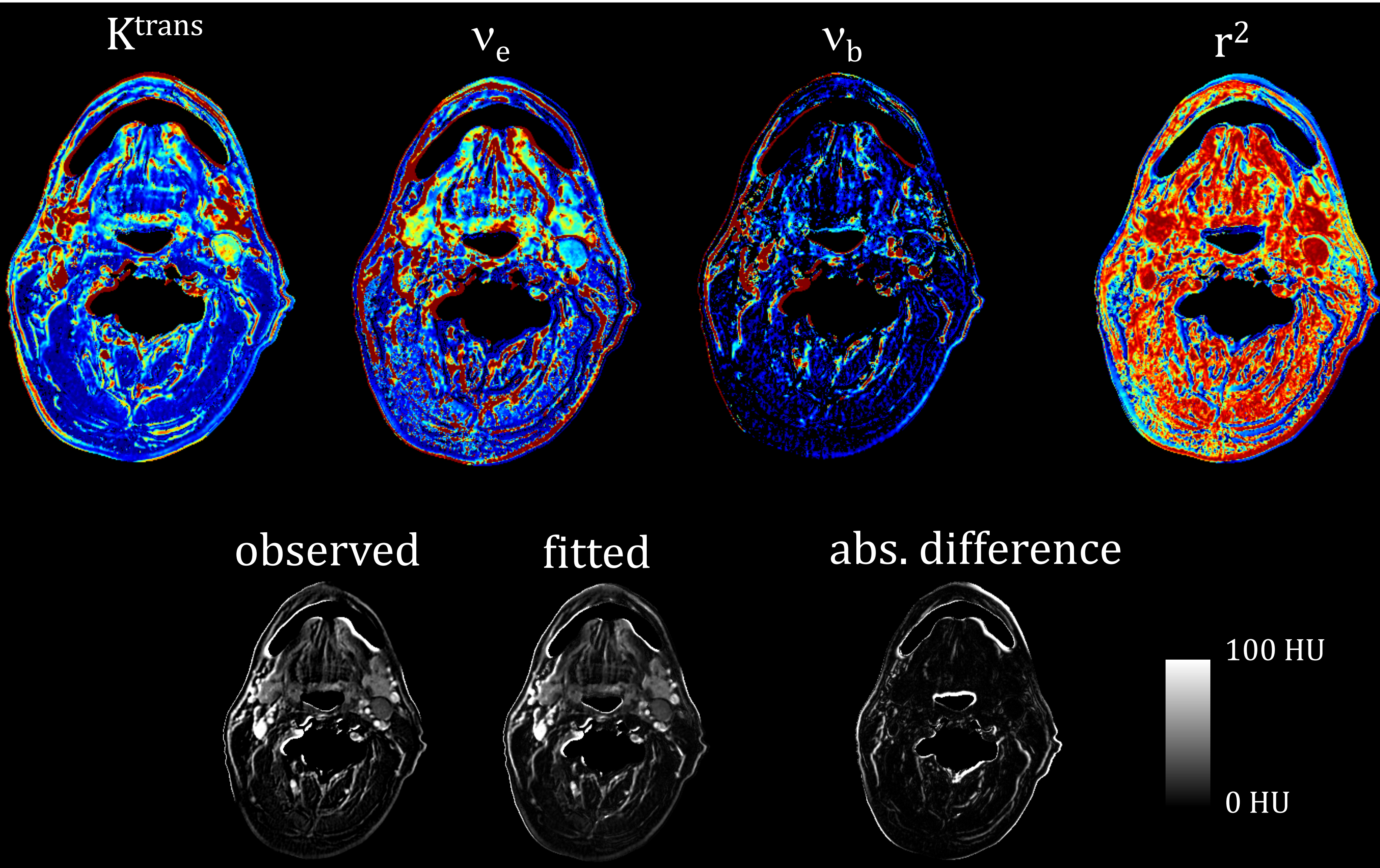

Impact of AIF

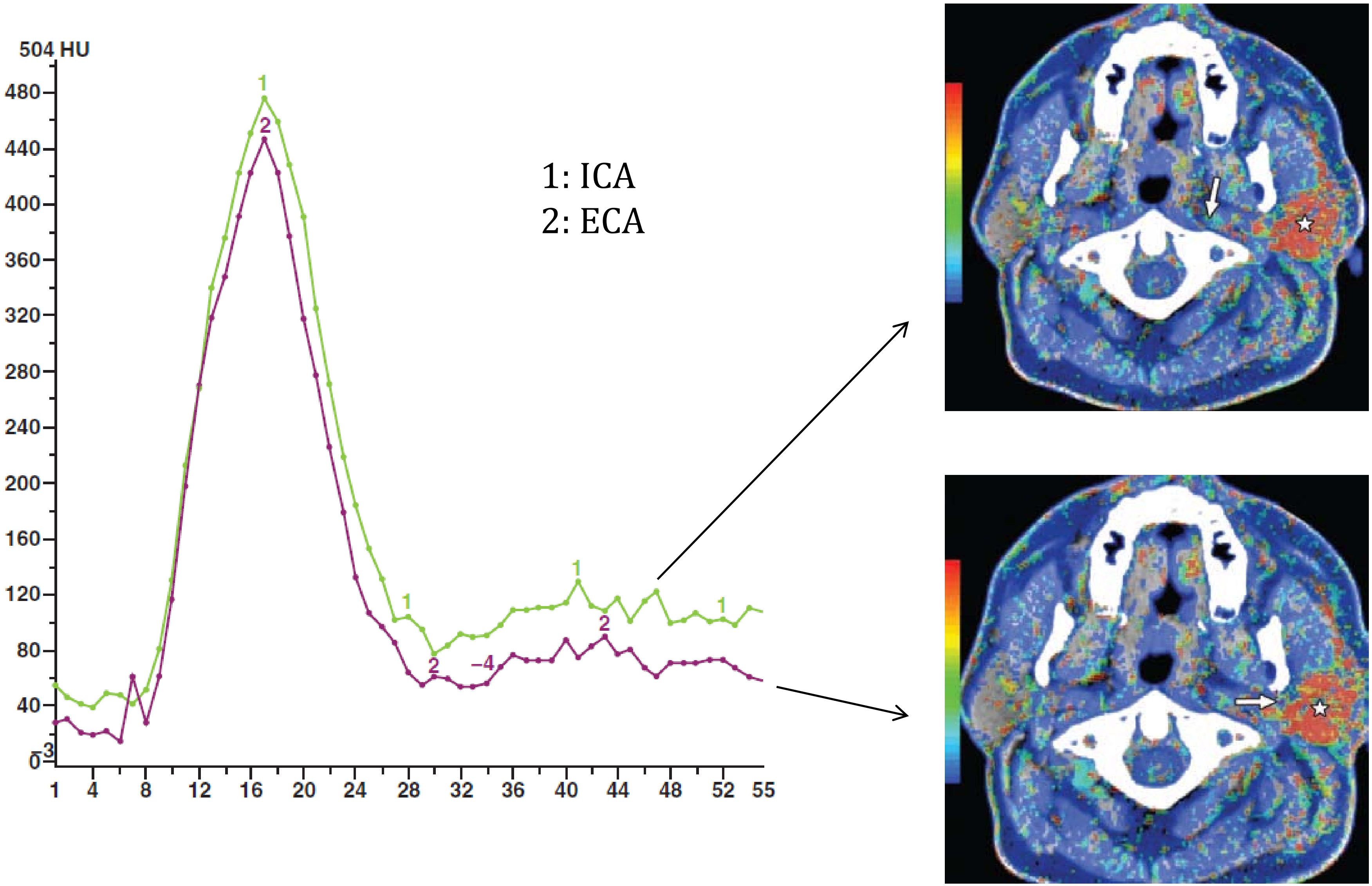

Clinical significance – cervical cancer

Higher perfusion

Higher EES

Lower perfusion

Lower EES

UiO : Department of Physics
University of Oslo

Radiother Oncol 2013; 107: 117-22

Oslo University Hospital

DCE + gene expression

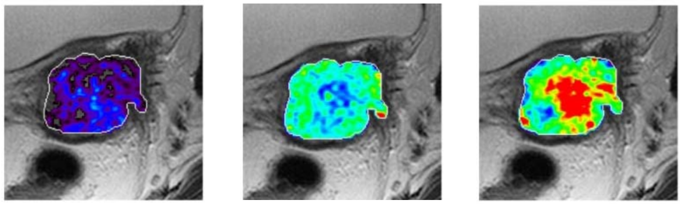

Feature 1 Feature 2 Feature 3

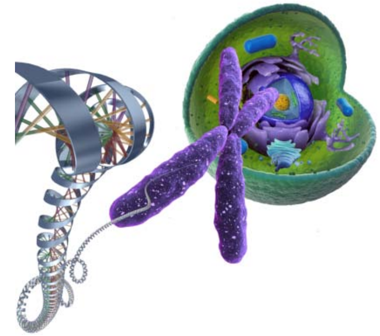

DCEMRI,
Patient 1

DCEMRI,
Patient 2

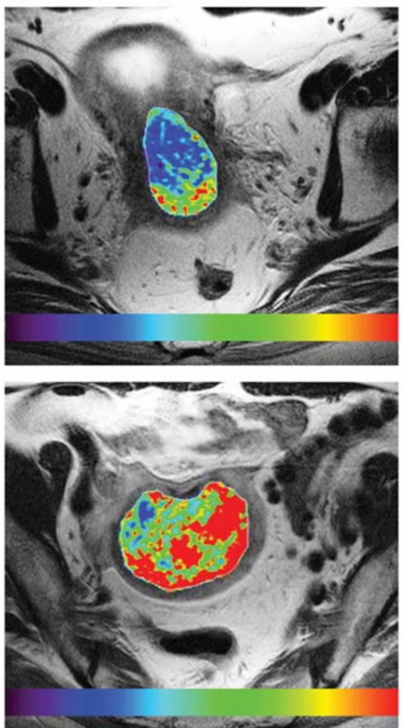

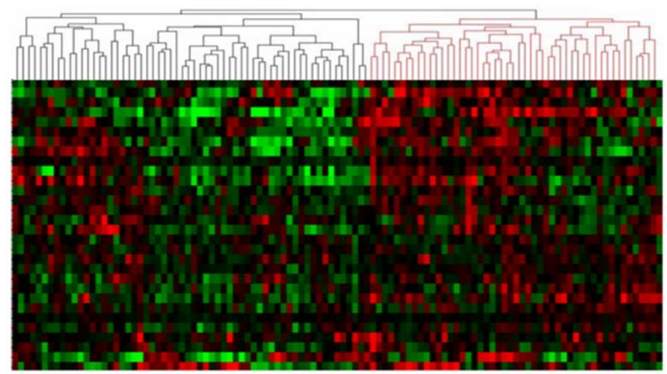

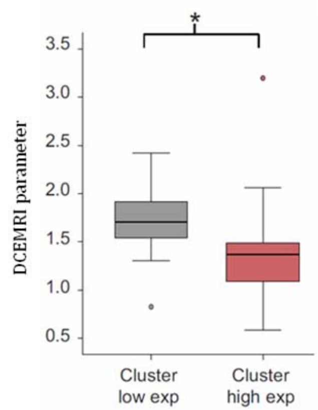

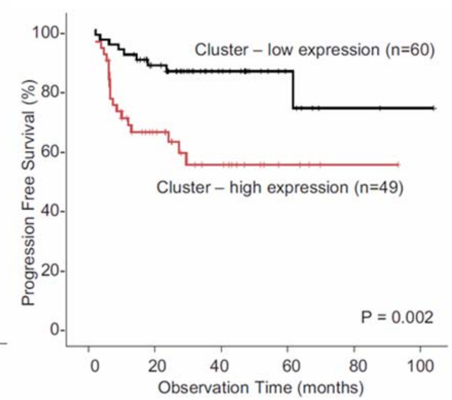

-Cancer Res 2012; 72: 5285-5295 *-Radiother Oncol 2013; 107: 117-22*

Reproducibility…

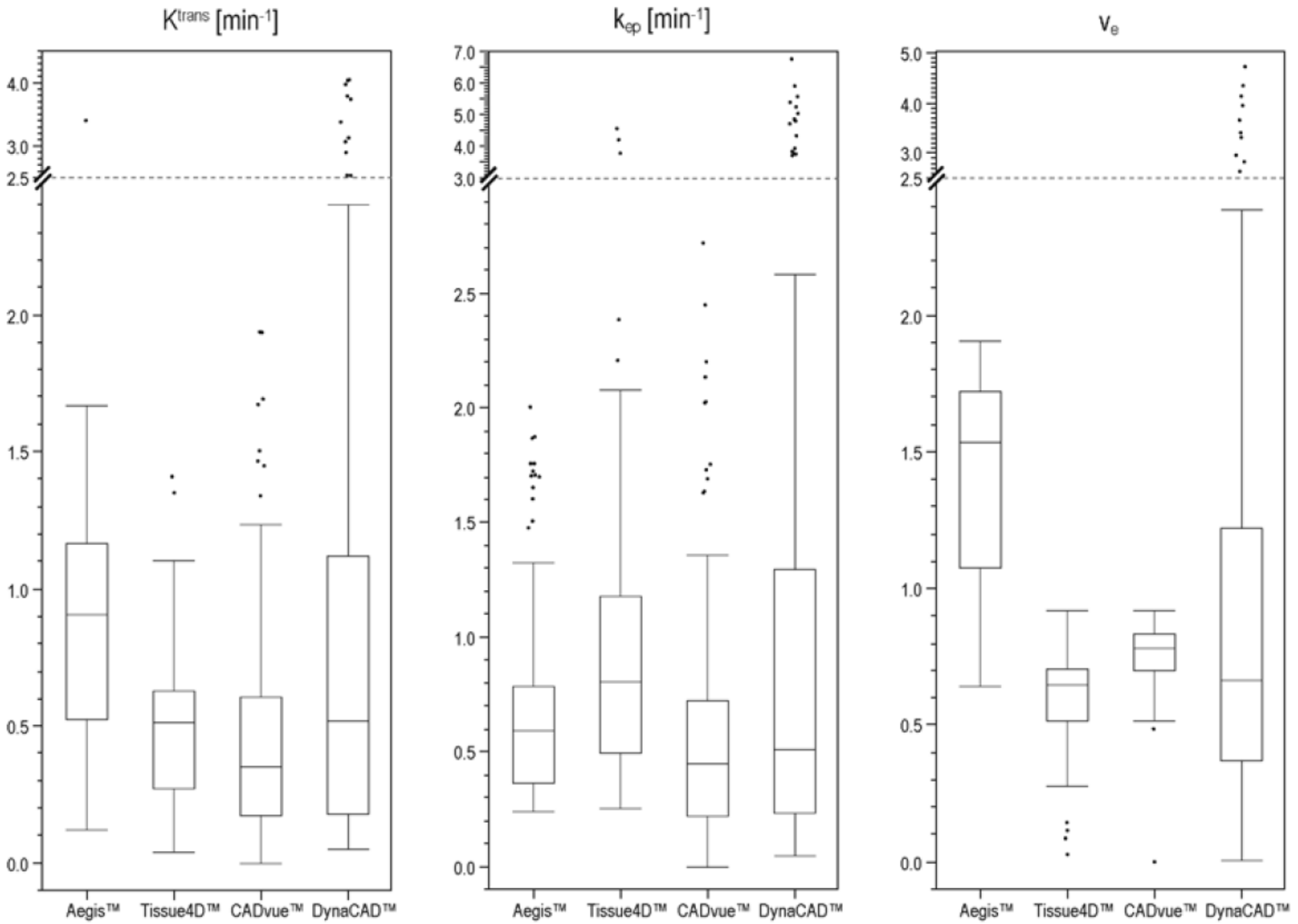

Radiology 2013; 266: 801-

Dynamic FDG-PET

Conventional PET:

- Patient rests for 1 hour after injection
- Produces a ”static” PET image series (3D)

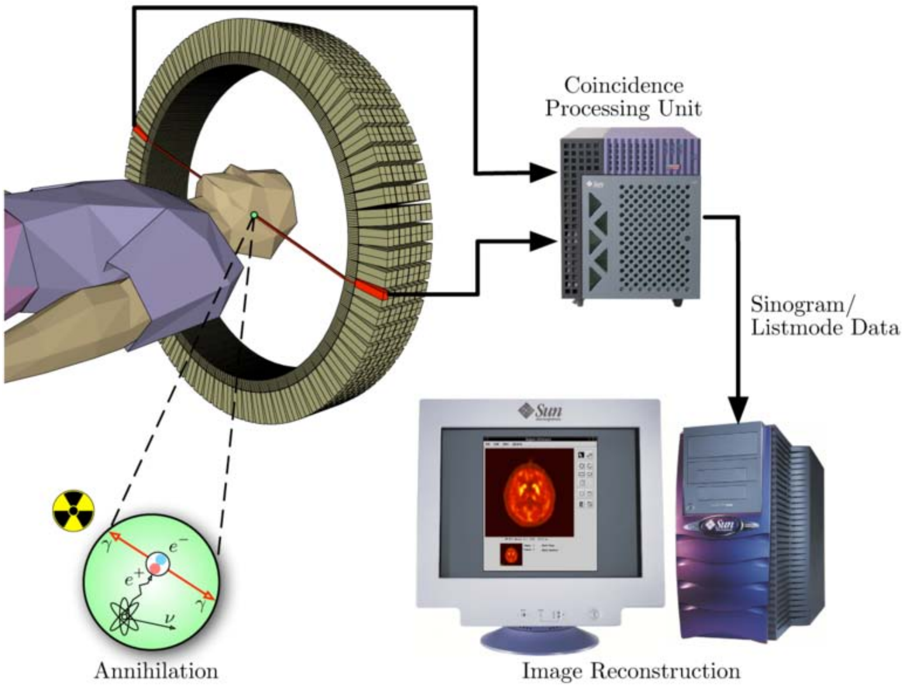

Dynamic PET

- PET-acquisition starts at the time of injection
- Time stamps for each coincidence
- Standard image reconstruction for given time intervals

DICOM header

0008 0020	Study Date	DA	8	20080509
0008 0021	Series Date	DA	8	20080509
0008 0022	Acquisition Date	DA	8	20080509
0008 0023	Image Date	DA	8	20080818
0008 0030	Study Time	TM	14	082049.562000
0008 0031	Series Time	TM	14	084955.953000
0008 0032	Acquisition Time	TM	14	085010.952984
0008 0033	Image Time	TM	14	162430.000000
0008 0050	Accession Number	SH	8	01151304
0008 0060	Modality	CS	2	PT
0018 0050	Slice Thickness	DS	16	2.0000000298023
0020 0032	Image Position (Patient)	DS	38	-341.51951401934\-498.26837193474\-715
0028 0010	Rows	US	2	128
0028 0011	Columns	US	2	128
0028 1053	Rescale Slope	DS	16	3.3176465034485
0018 1072	*Radionuclide Start Time	TM	14	083700.000000
0018 1074	*Radionuclide Total Dose	DS	12	14726000000
0018 1075	Radionuclide Half Life	DS	6	6586.2
0018 1076	Radionuclide Positron Fraction	DS	4	0.97
0054 0081	Number of Slices	US	2	41
0054 0101	Number of Time Slices	US	2	43
0054 1001	Units	CS	4	BQML
0054 1101	Attenuation Correction Method	LO	18	CT-derived mu-map
0054 1102	Decay Correction	CS	6	START
0054 1103	Reconstruction Method	LO	12	OSEM2D 4i8s
0054 1105	Scatter Correction Method	LO	12	Model-based
7FE0 0010	Pixel Data	OW	32768	(binary data)

Tissue distribution

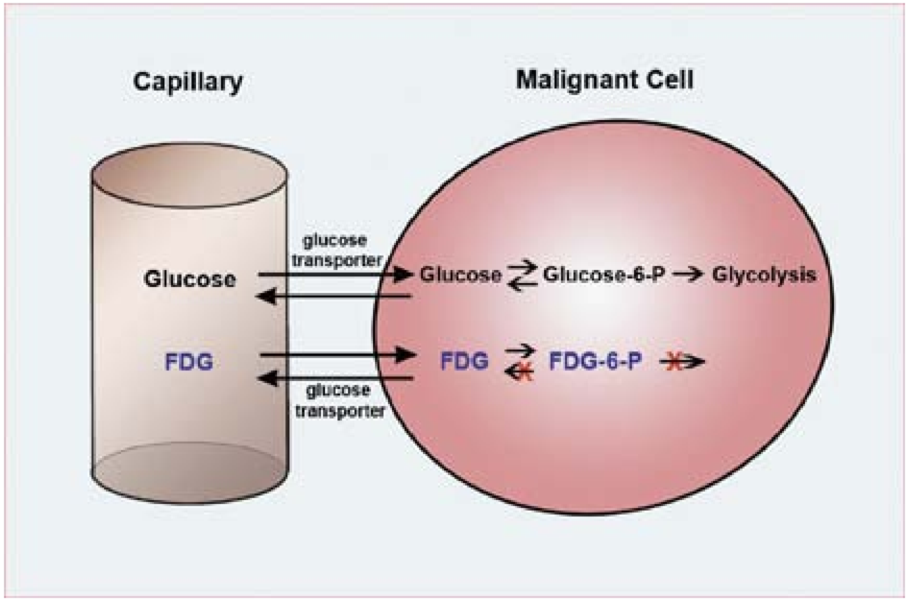

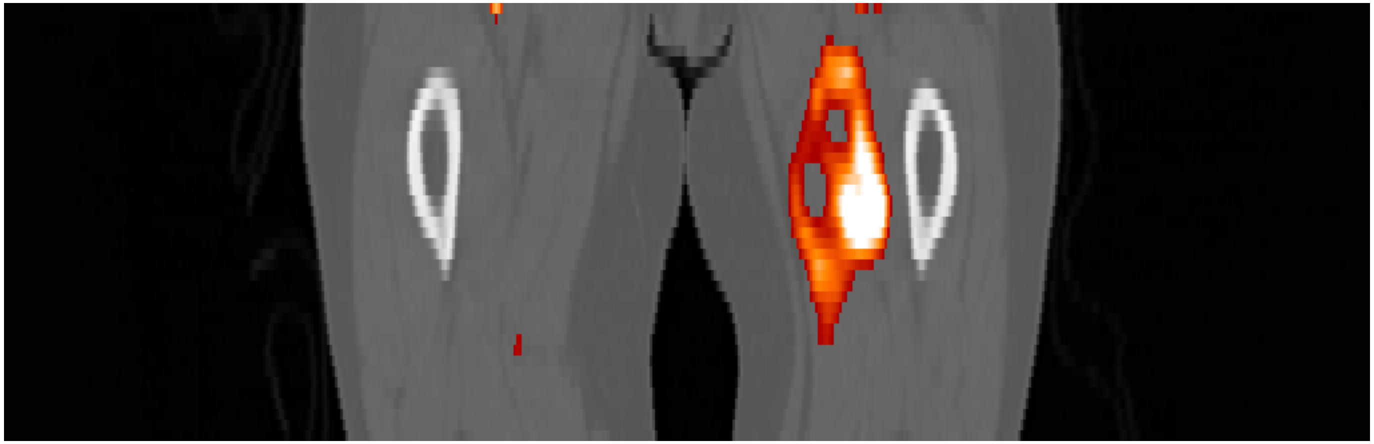

Dynamic FDG-PET

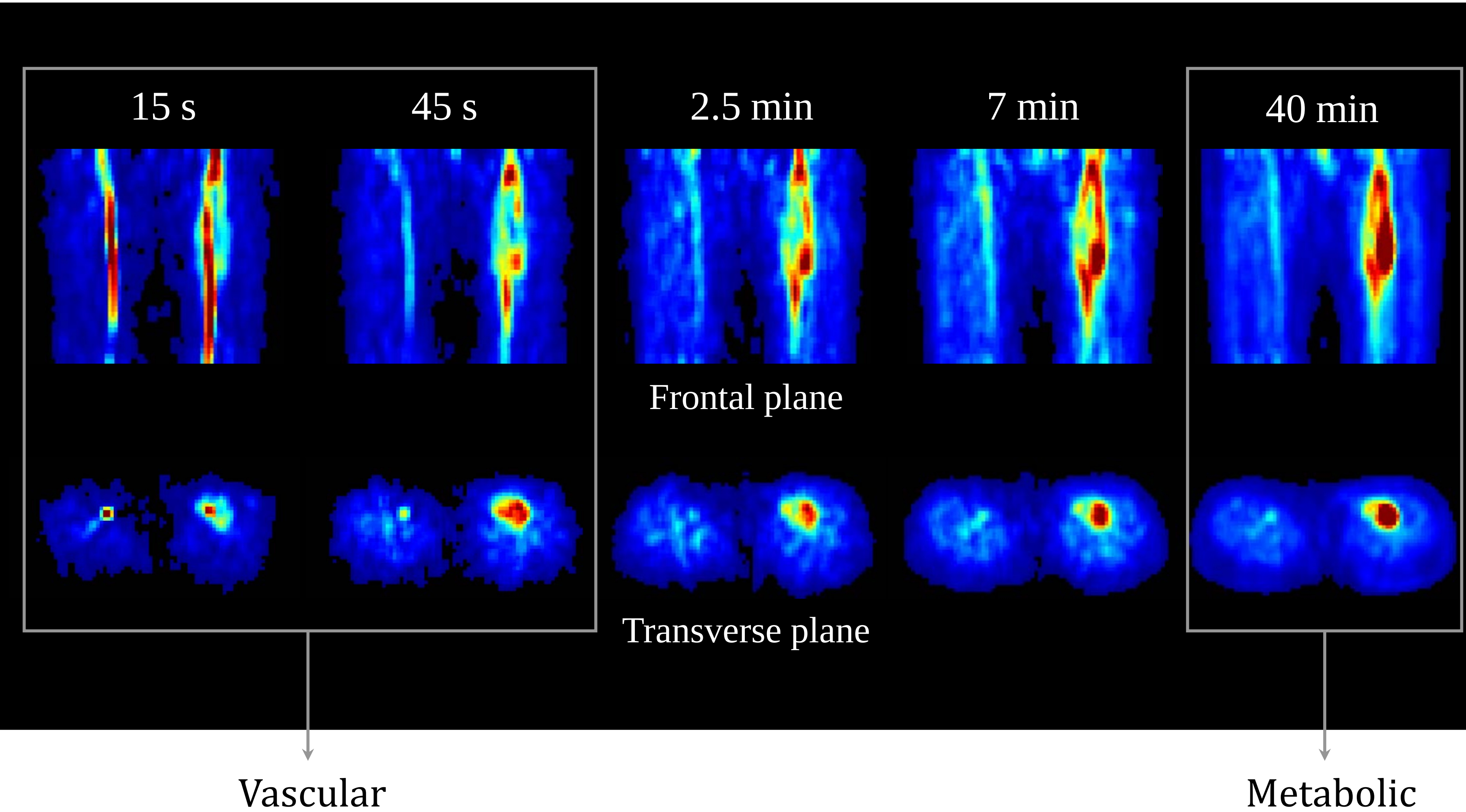

UiO : Department of Physics
University of Oslo

Oslo University Hospital

Temporal characteristics

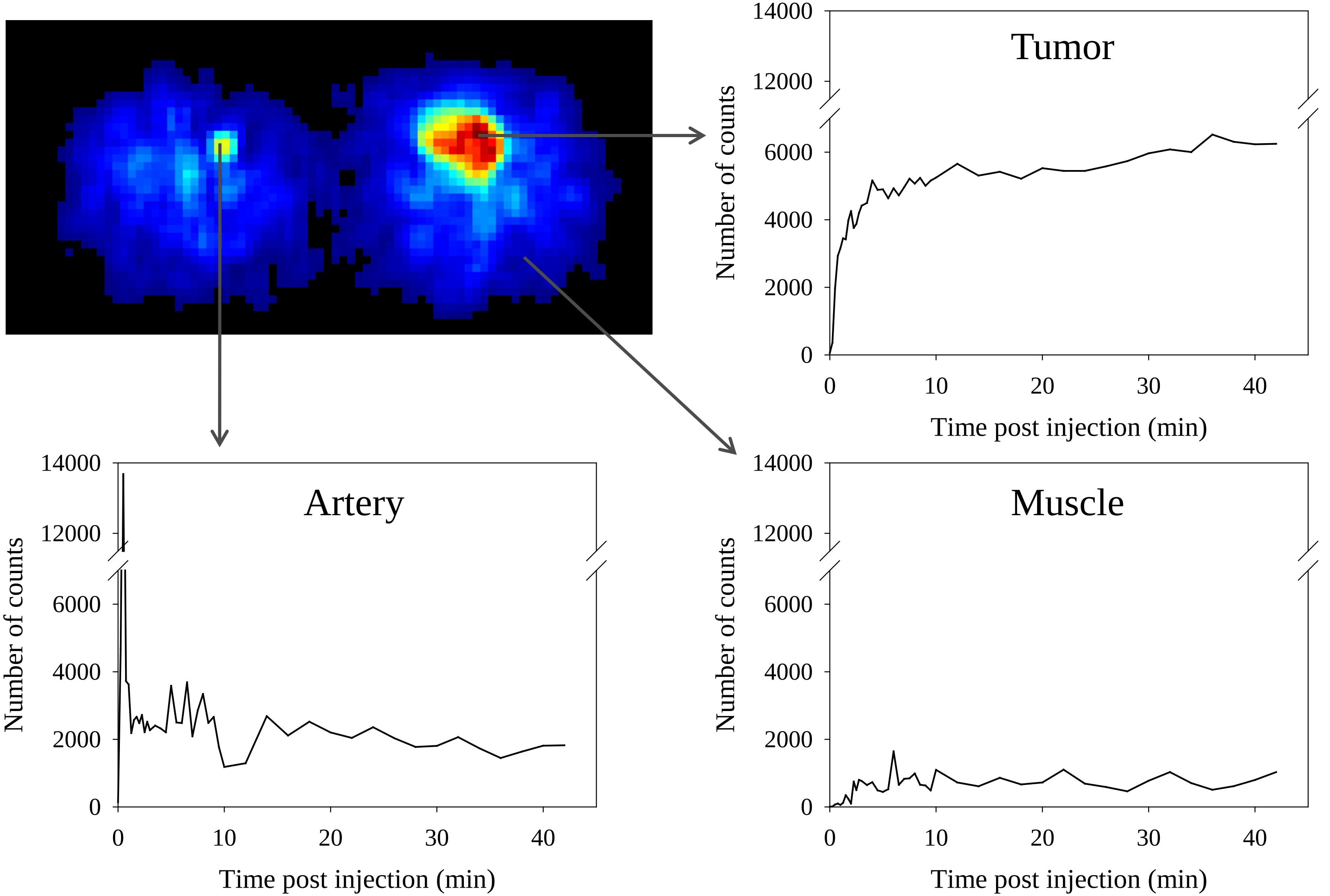

FDG-uptake in sarcomas

- Tumor uptake curves in individual patients

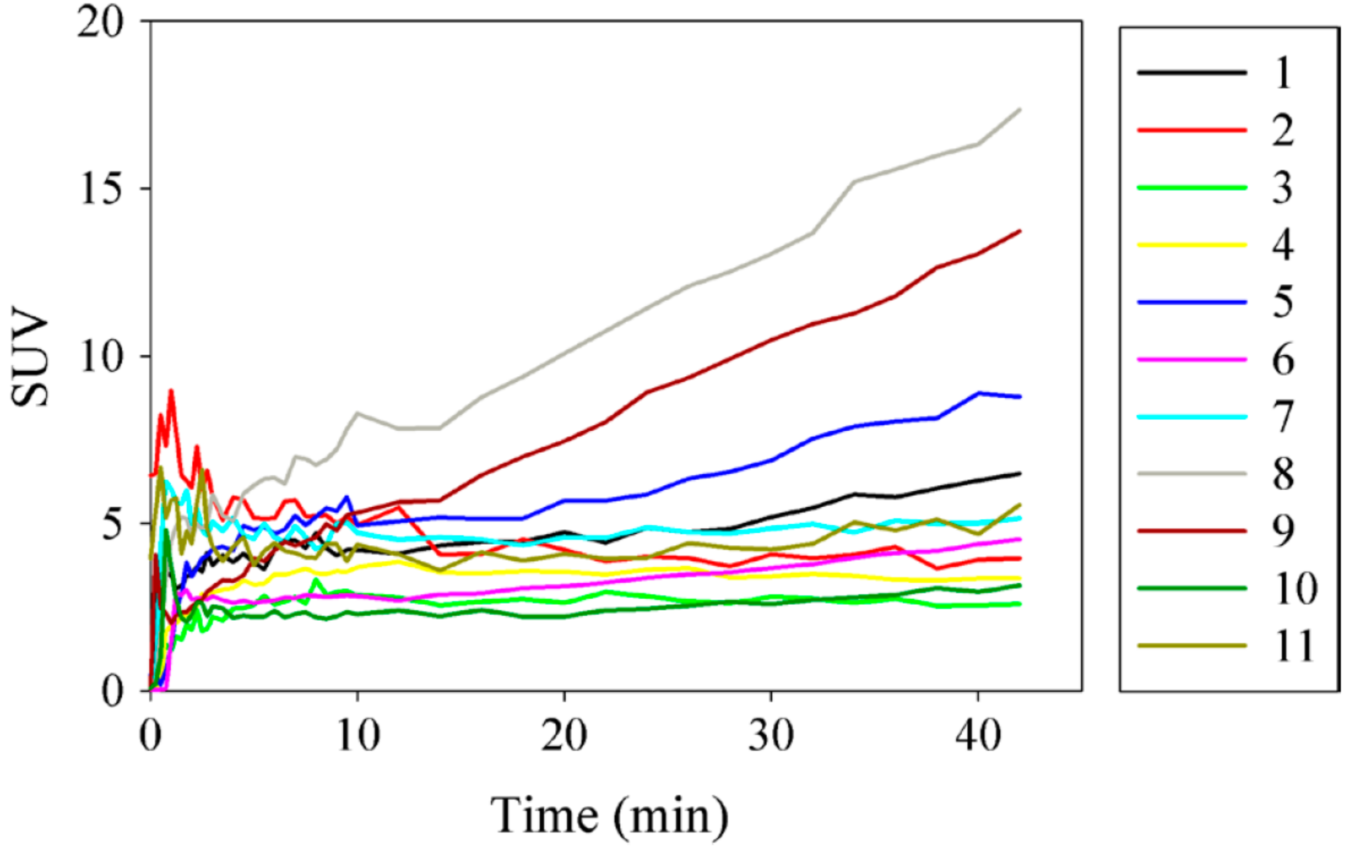

Acta Oncol. 2013 Aug;52(6):1160-7

Perfusion imaging

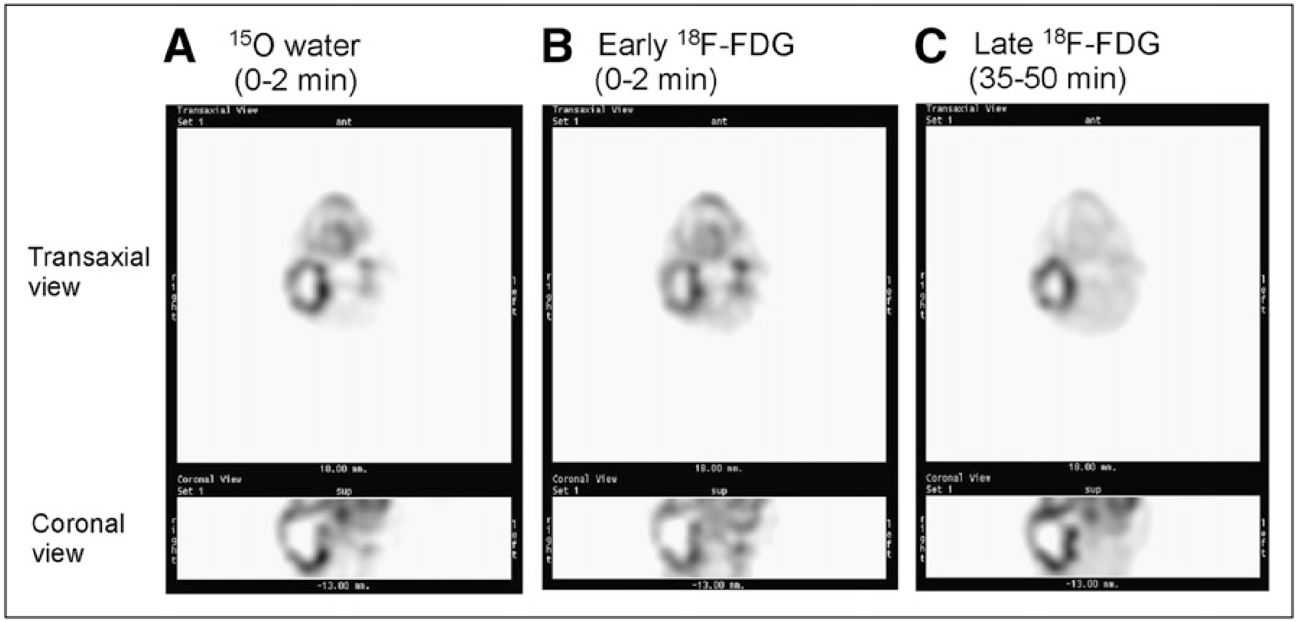

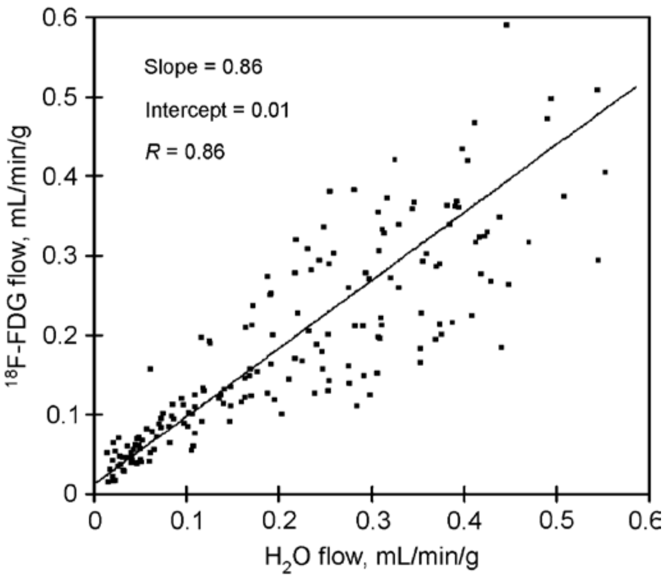

J Nucl Med 2008; 49:517–523

Dogs; DPET and DCECT 1 min p.i.

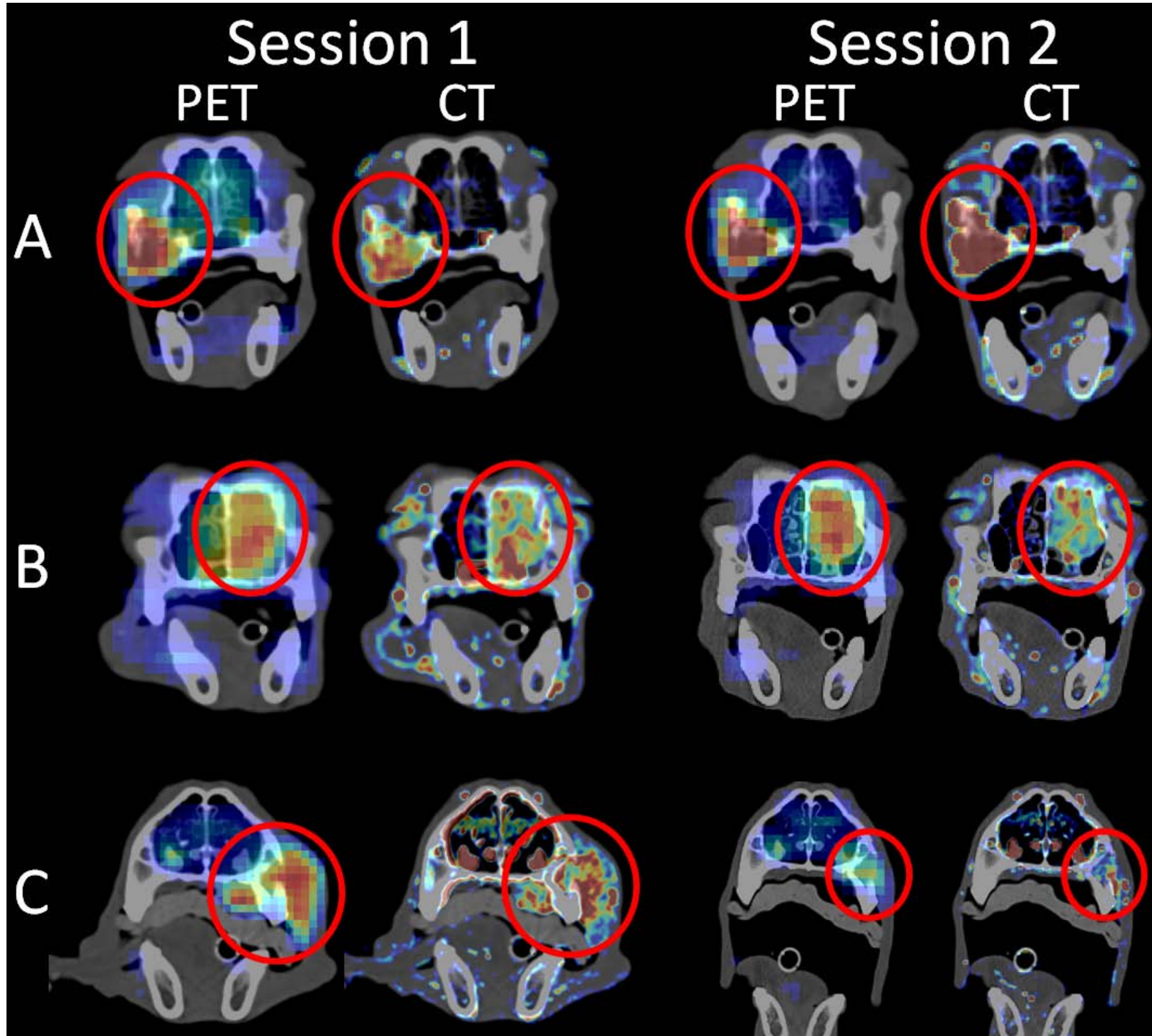

Acta Oncologica, 2011; 50: 873–882

2-compartment modeling

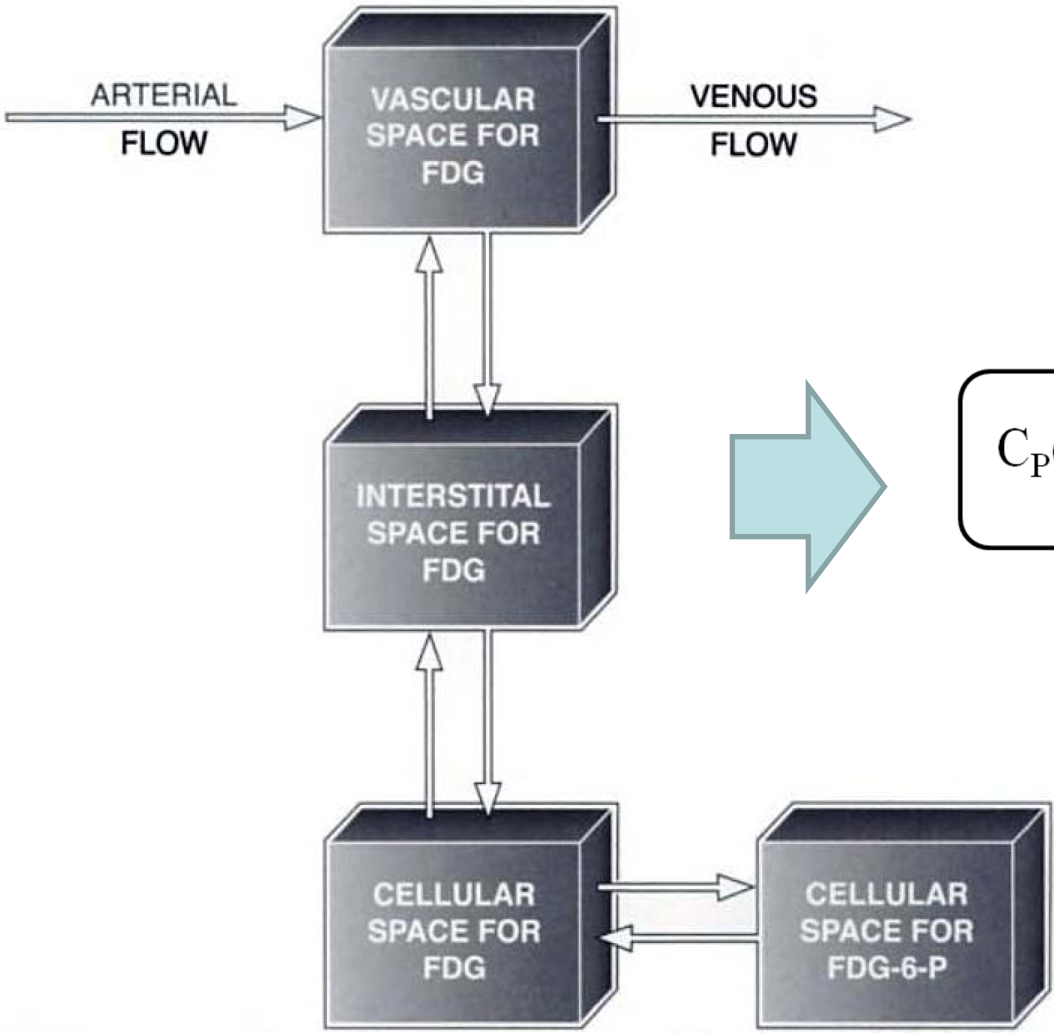

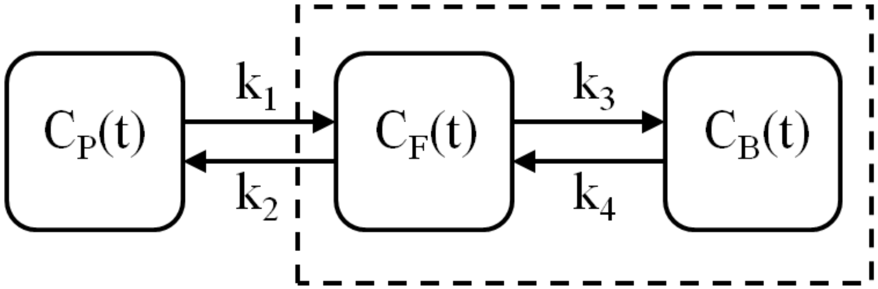

$$C_T(t) = C_F(t) + C_B(t)$$

2-compartment modeling

- Again, a set of differential equations results:

$$\frac{dC_F(t)}{dt} = k_1 C_P(t) - (k_2 + k_3) C_F(t) + k_4 C_B(t)$$

$$\frac{dC_B(t)}{dt} = k_3 C_F(t) - k_4 C_B(t)$$

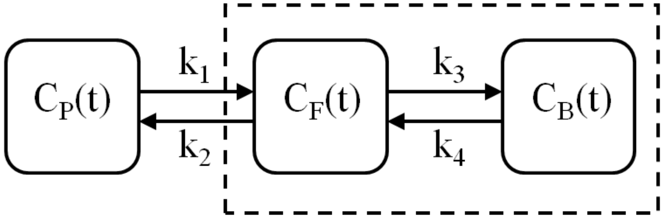

$C_T(t) = C_F(t) + C_B(t)$

- Horrible, but applicable, solution:

$$C_F(t) = \left\{ \frac{k_1}{\alpha_2 - \alpha_1} \left[(k_4 - \alpha_1) e^{-\alpha_1 t} + (\alpha_2 - k_4) e^{-\alpha_2 t} \right] \right\} \otimes C_P(t)$$

$$C_B(t) = \left\{ \frac{k_1 k_3}{\alpha_2 - \alpha_1} \left[e^{-\alpha_1 t} - e^{-\alpha_2 t} \right] \right\} \otimes C_P(t)$$

$$\alpha_1, \alpha_2 = \frac{k_2 + k_3 + k_4}{2} \mp \frac{\sqrt{(k_2 + k_3 + k_4)^2 - 4 k_2 k_4}}{2}$$

Model analysis

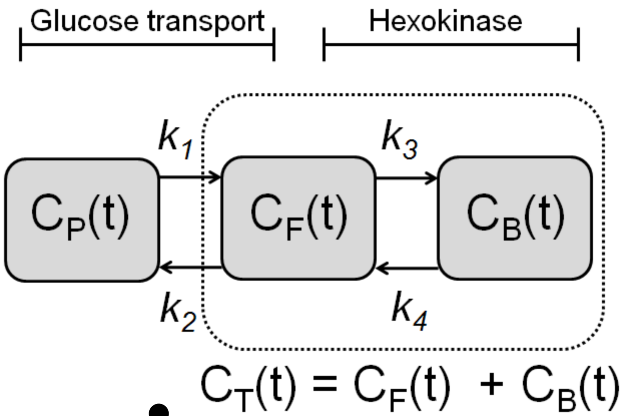

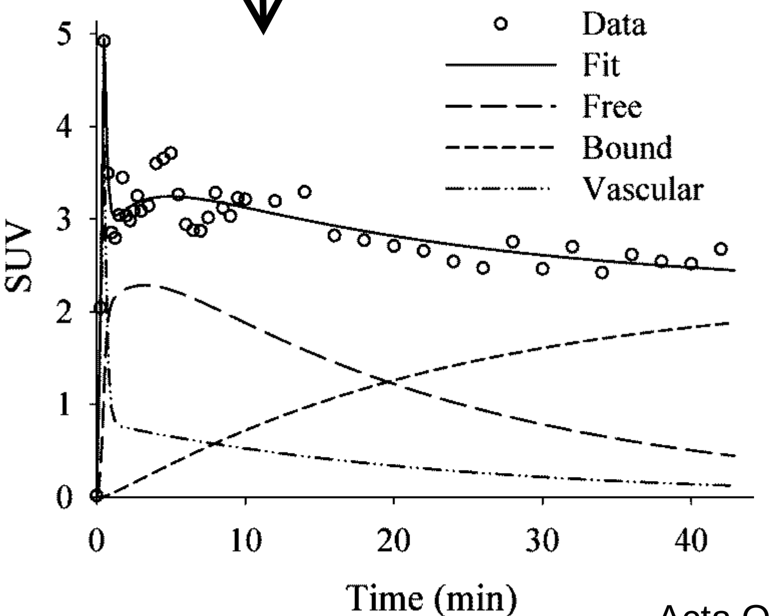

$K_1 = 0.20$
$k_2 = 0.40$
$k_3 = 0.037$
$\nu_p = 0.16$
$MR_{FDG} = 0.016$
$r^2 = 0.89$

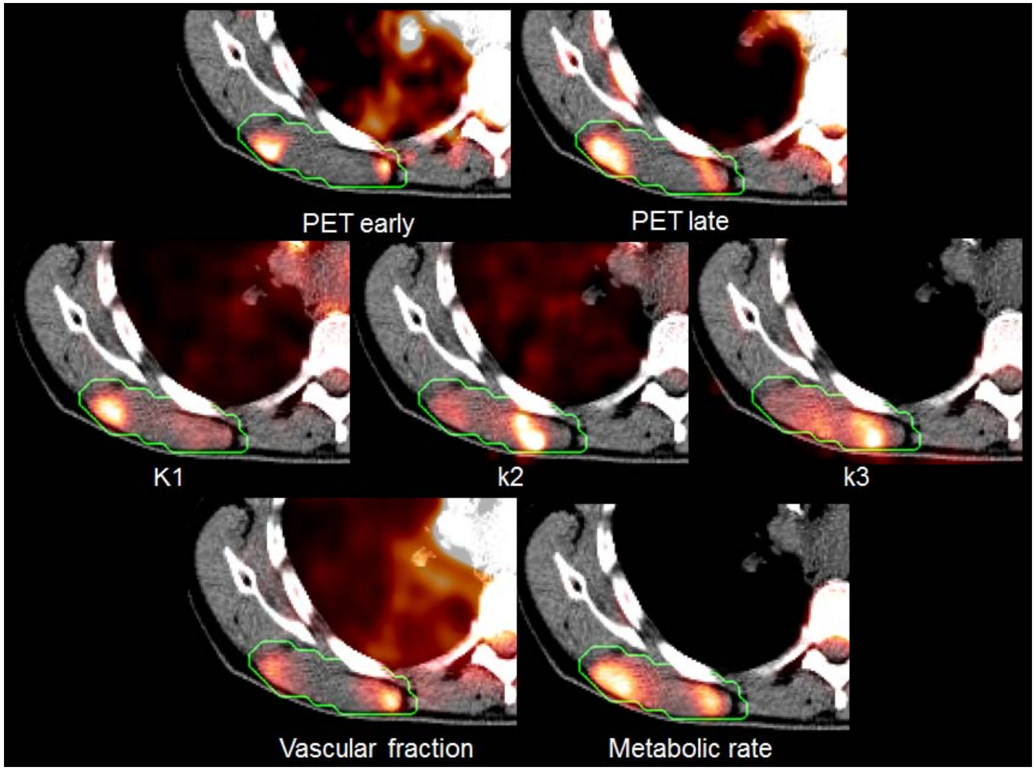

Acta Oncol. 2013 Aug;52(6):1160-7

Oslo University Hospital

Dose painting simulations

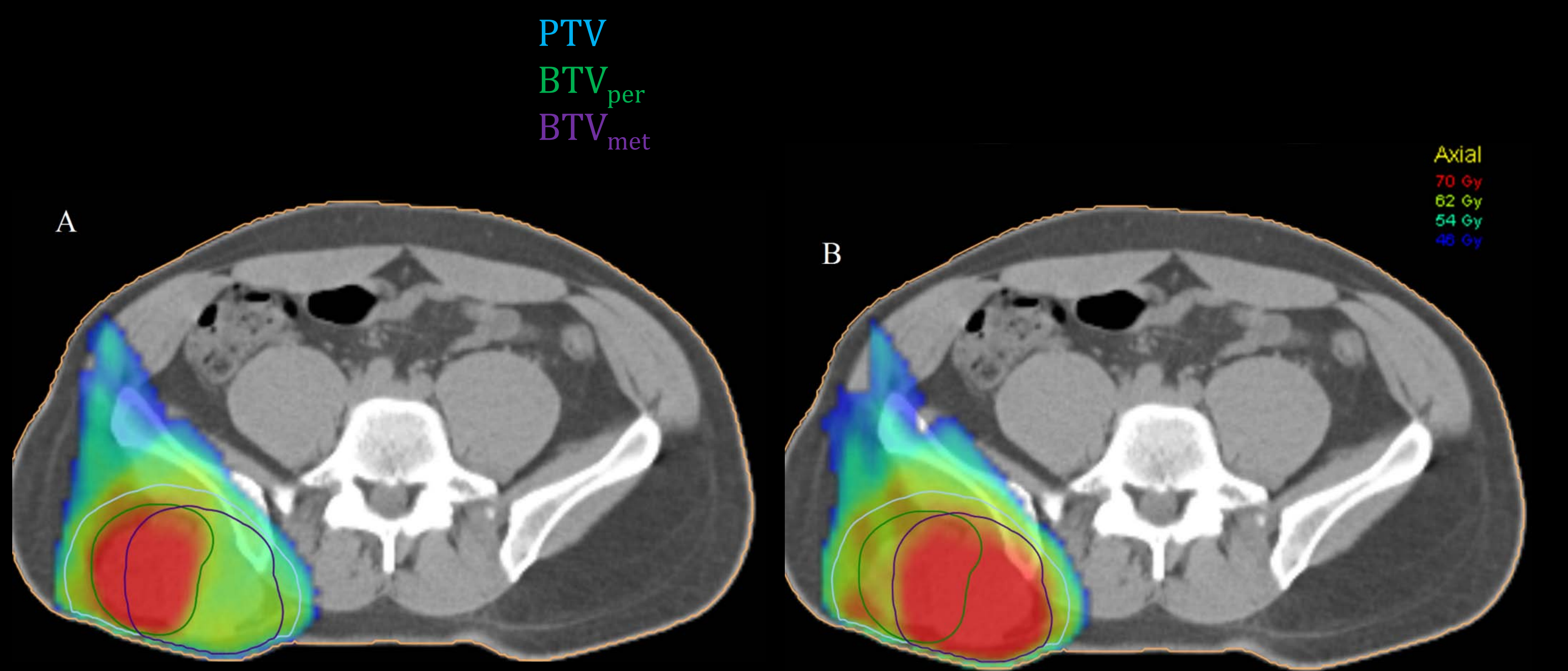

Thank you for your attention!

MRI Physics: Fast Scanning, Volume Sequences

A/Prof Gary Liney

21st September 2016

ESTRO Imaging for Physicists

ESTRO School

Introduction

- MRI slow technique (compared to CT)
- Desirable to cover anatomy as quick as possible
  - ✓Patient comfort
  - ✓Reduce artefacts
  - ✓Image physiological

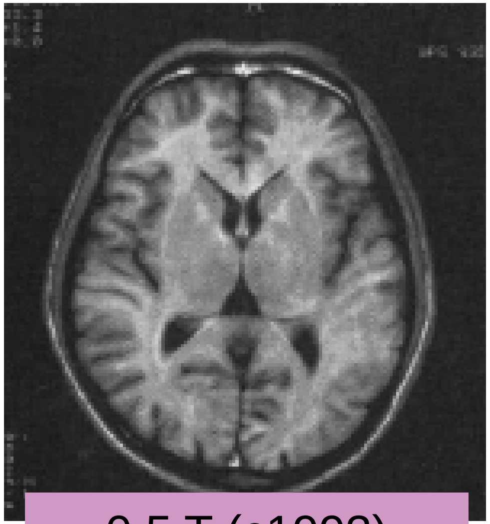

0.5 T (c1993)
32 x 4 mm in 5 min

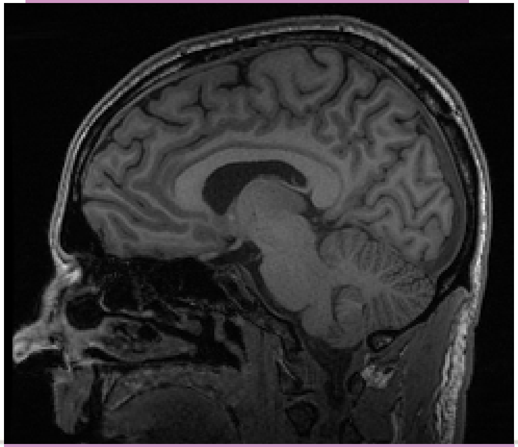

3.0 T (2010)
148 x 1 mm in 3.5 min

How Do We Go Faster?

Things to Consider…

- Higher Fields
  Trade-off higher SNR for scan time
- Ultra-fast Imaging
- Reconstruction Speeds
  Become significant when dealing with huge volumetric datasets

Some ‘Fast’ Terminology?

Terms you will hear…

- Multi or single-shot

  Related to number of TRs required to acquire FULL k-space

- Partial k-space

  Speed up image sequence by NOT acquiring complete k-space

- Partial <u>and</u> Reduced Flip

  Less than 90 ° flip angles and less than 180° refocusing pulses respectively

- Echo Train

  Closely spaced signal echoes (with a certain *echo spacing*) within one TR

- Parallel Imaging

  Use of multi-coil sensitivities to speed up image acquisition

Ultra-fast Imaging

- Rapid and/or single-shot sequences
  e.g. FSPGR, ssFSE, EPI
- Reduced k-space acquisitions
  e.g HASTE
- Hardware/Post-processing reconstruction methods
  e.g. Parallel imaging

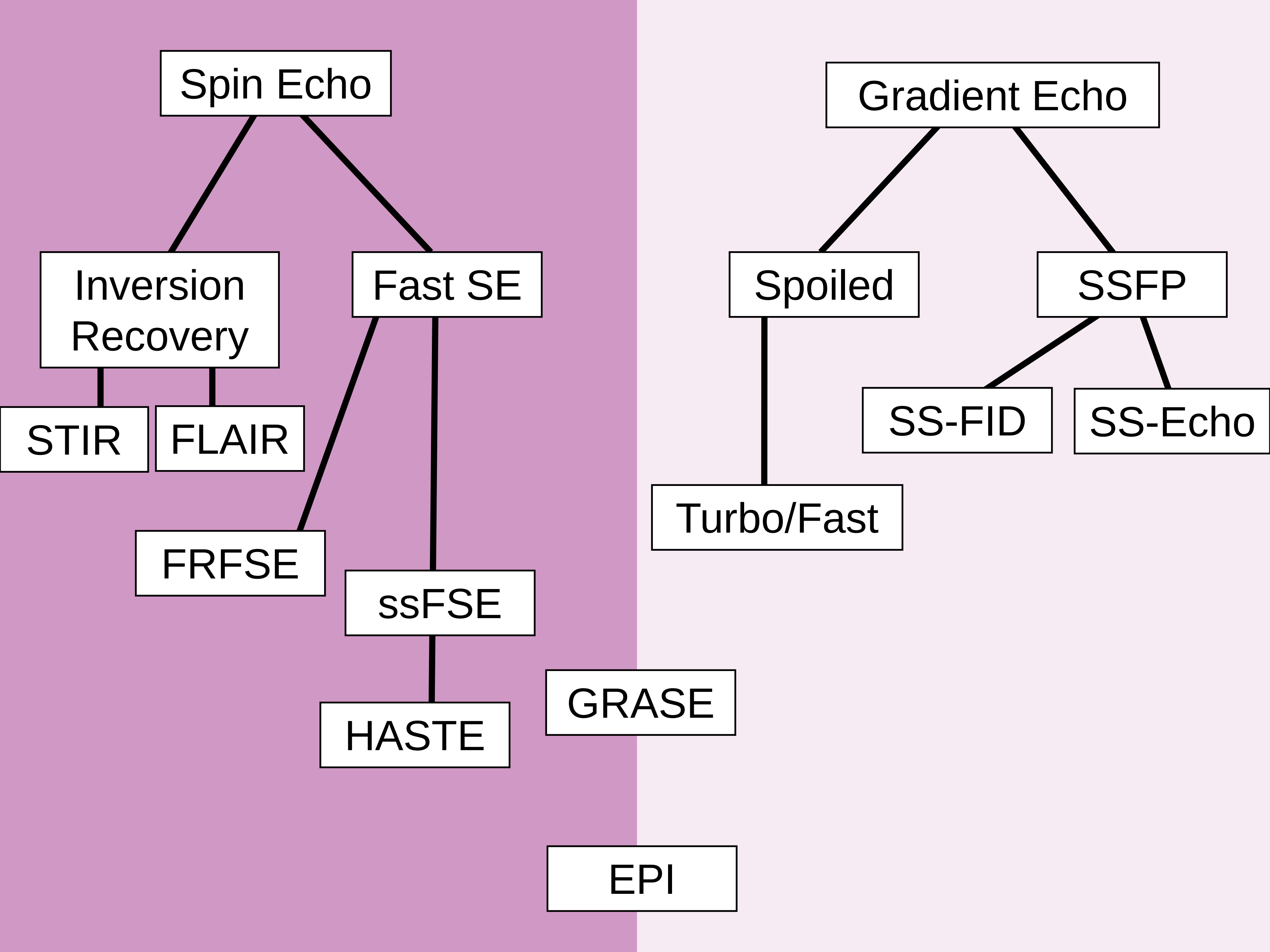
Spin Echo
Inversion Recovery
Fast SE
STIR
FLAIR
FRFSE
ssFSE
HASTE
GRASE
EPI
Gradient Echo
Spoiled
SSFP
SS-FID
SS-Echo
Turbo/Fast

Spin-echoes…

- T_2-weighted essentially limited by long TR
- Increase speed by:
  - ✓ Segmented k-space
  - ✓ Acquire more than one line of k-space per TR
  - ✓ Partial k-space
  - ✓ Acquire less than full k-space

Segmented k-space

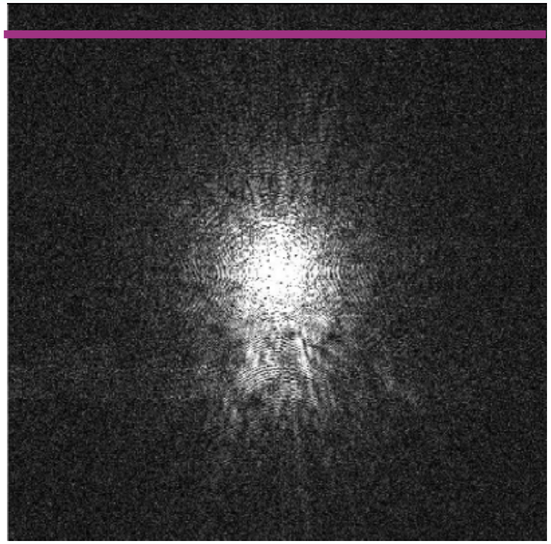

Scan time = **(TR× N_{AV} × N_{PE})**

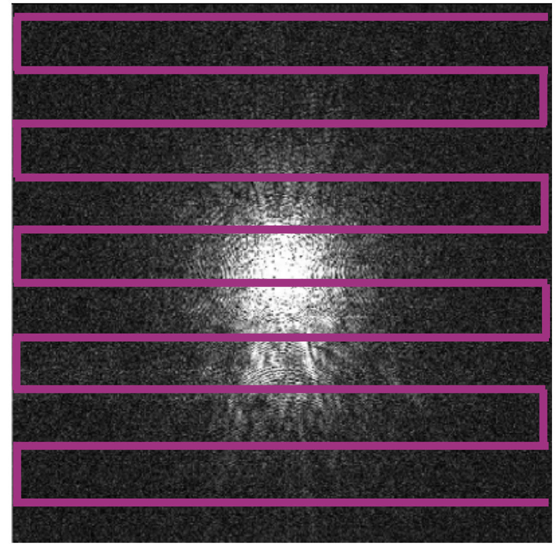

Scan time = **TR**

Single shot

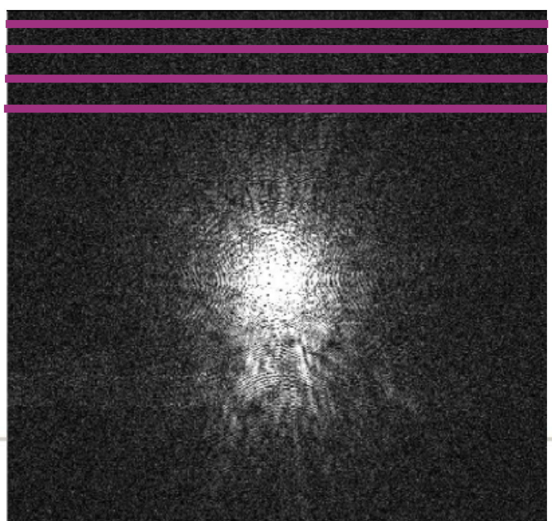

Scan time = **(TR× N_{AV} × N_{PE})/ETL**

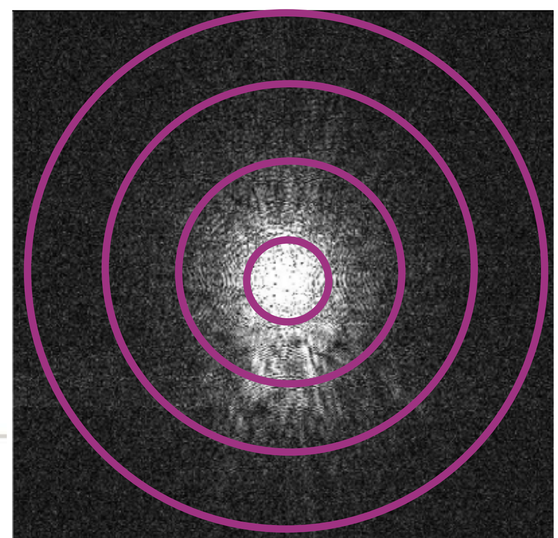

Fast Spin Echo (Turbo Spin Echo)

- Multiple SEs but individually phase encoded
- Scan time reduced by ETL (‘Turbo factor’)
- Effective TE
- Image quality trade-off:

  Blurring with excessive ETL & ESP

  Characteristic bright fat

FSE
TSE
RARE

Scan time = $(TR \times N_{AV} \times N_{PE})/ETL$

FSE (TSE)

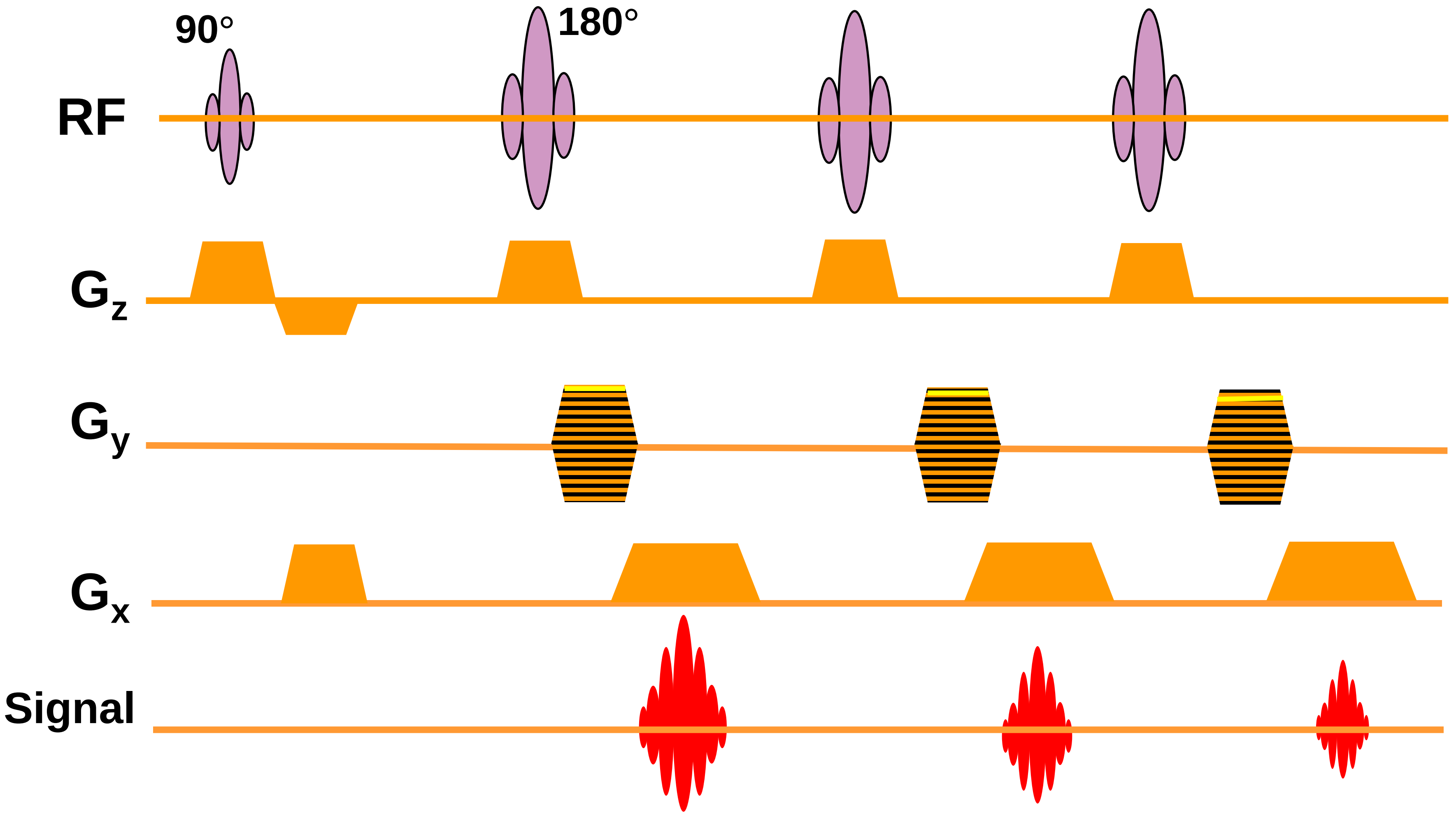

Example: Prostate

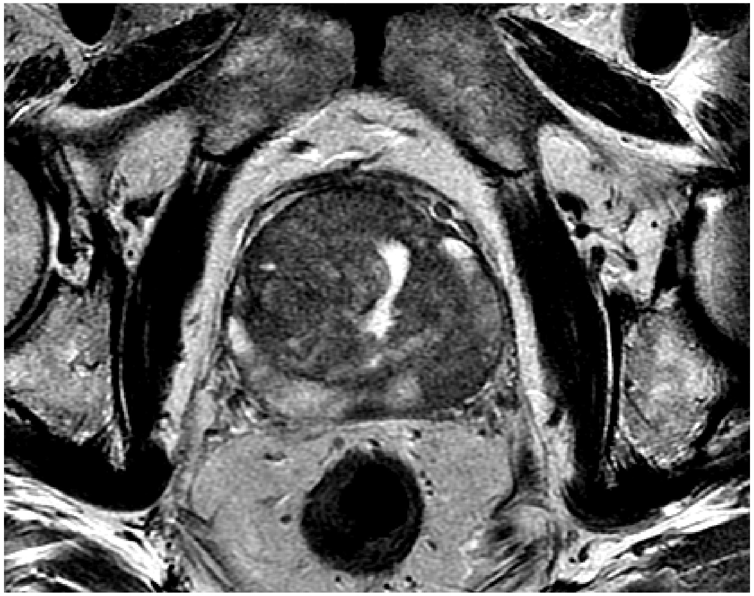

FSE extensively used in prostate: here axial and coronal planes at 3.0 Tesla without ER coil

Partial k-Space

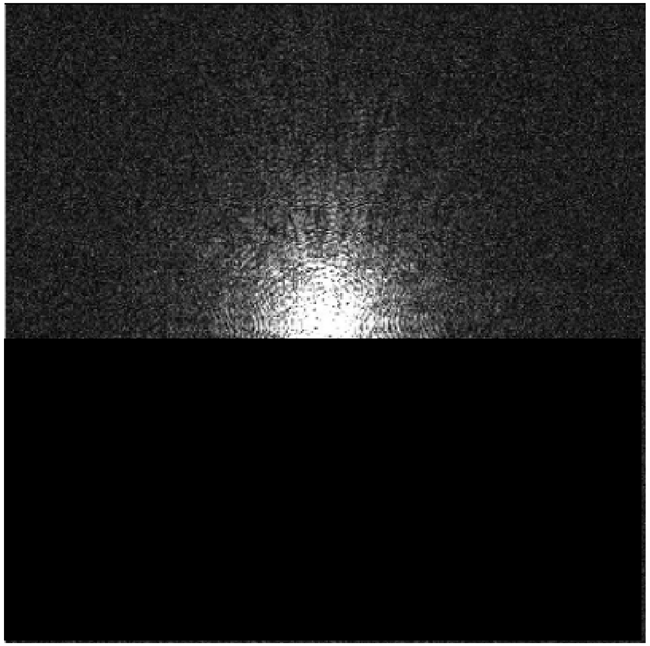

Partial Fourier/ Fractional NEX

- Half of phase encoding
- **Reduced scan time**
- Other reduction fractions possible

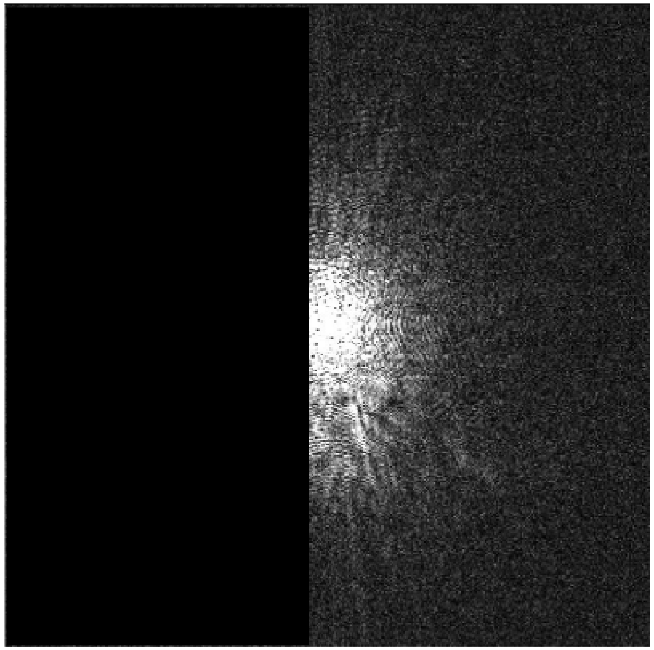

Partial Echo

- Half of echo
- Reduced minimum TE
- No effect on scan time

ssFSE and HASTE

- Single shot FSE all k-space in one TR
- HASTE
  - Single shot AND partial k-space
  - Just over half k-space acquired
- Image quality degraded
- Useful for high T_2 (volumetric) imaging where resolution not too important
  - MRCP exam (right)

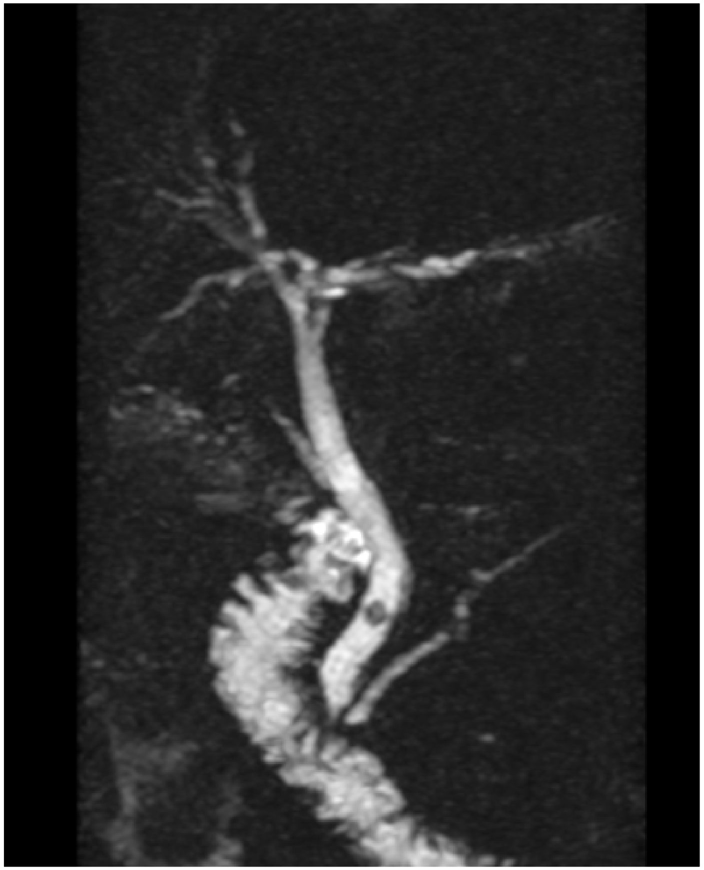

MIP from ssFSE
(TE/TR = 260 ms/12 s)

Driven Equilibrium

- Use -90° RF to force recovery
- T_2-weighting in shorter TR
- High fluid signal in short scan
- Used in abdomen

21 s FRFSE breathold scan in normal liver

FRFSE
DRIVE
RESTORE
T2Plus

Echo Planar Imaging (EPI)

- Implemented by Mansfield (1977)
- Single-shot (can be run multi-shot)
  - Scan time = TR
- Blipped, spiral and constant versions
- Inherently noisy
- Acquired at limited resolution (e.g. 64 or 128)
- Can be SE or GRE based
- Widespread use in fMRI

EPI

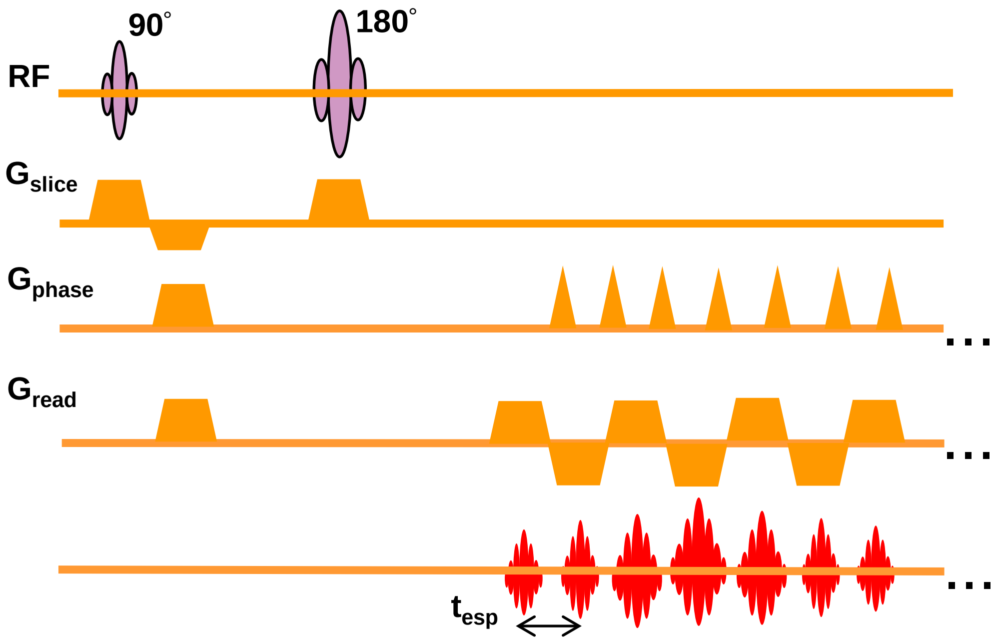

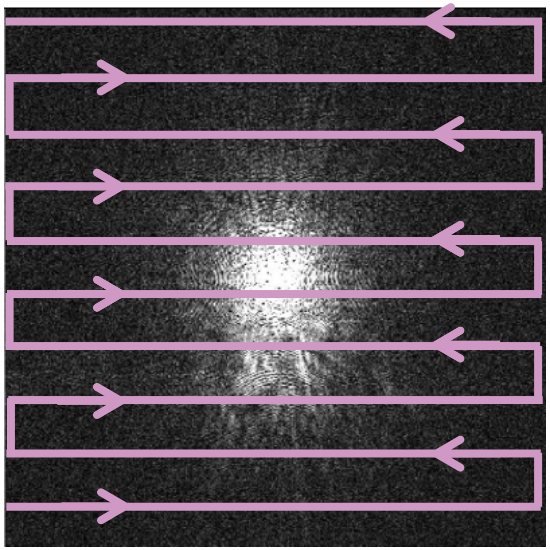

$$\Delta \nu_{phase} = \frac{N_{shot}}{t_{esp}}$$

Effective 'phase-encoding' bandwidth

(e.g. 1 ms $t_{esp} \Rightarrow$ 1 kHz)

EPI

Prone to artefacts:

- N/2 ghosting (switching between lines)
- Distortions (eddy currents)
- Large chemical shift requires fat suppression
- Huge susceptibility effects along PE

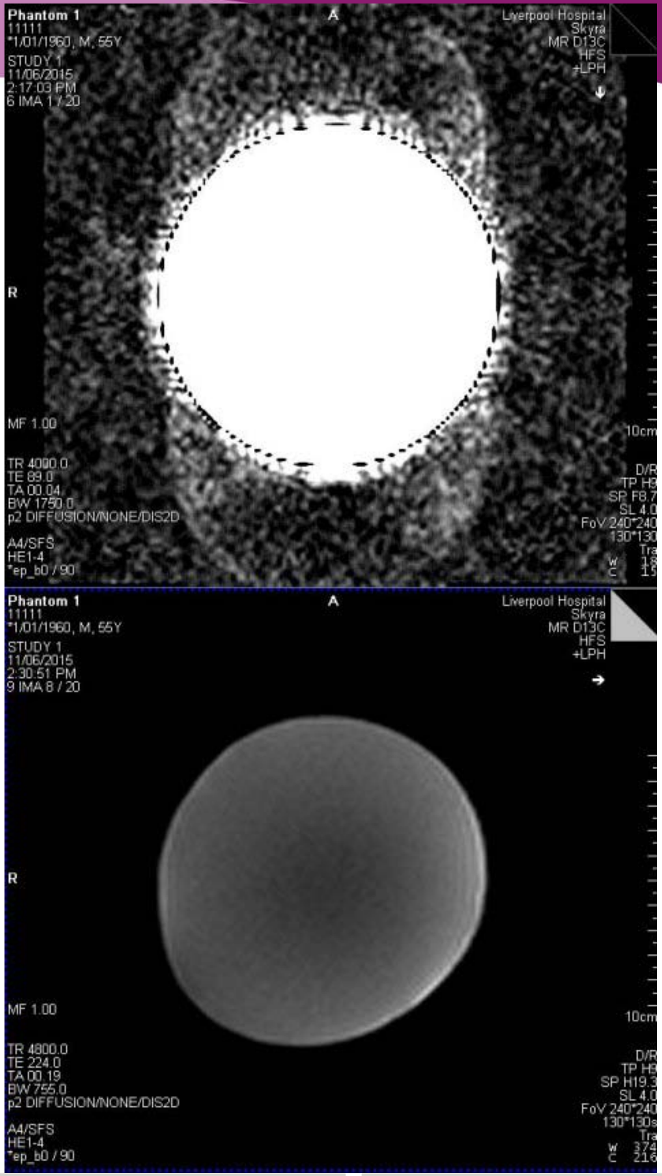

EPI with B_0 Correction

Non corrected

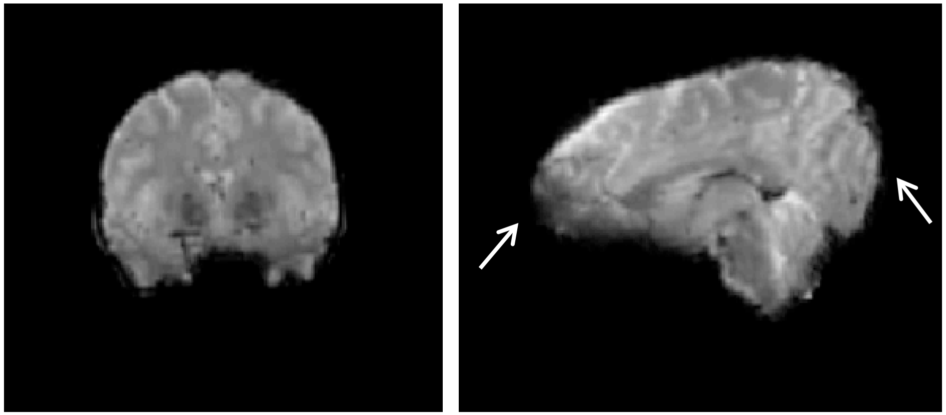

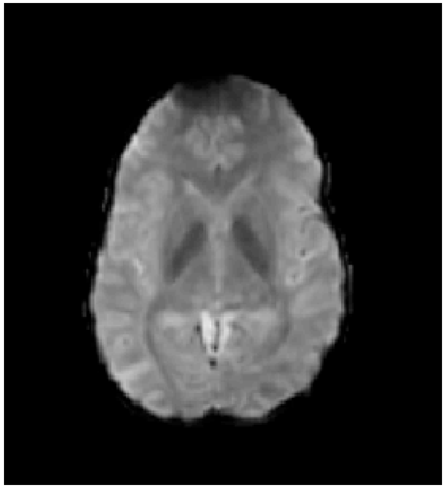

Susceptibility effects are particularly noticeable in frontal and occipital lobes.

Corrected

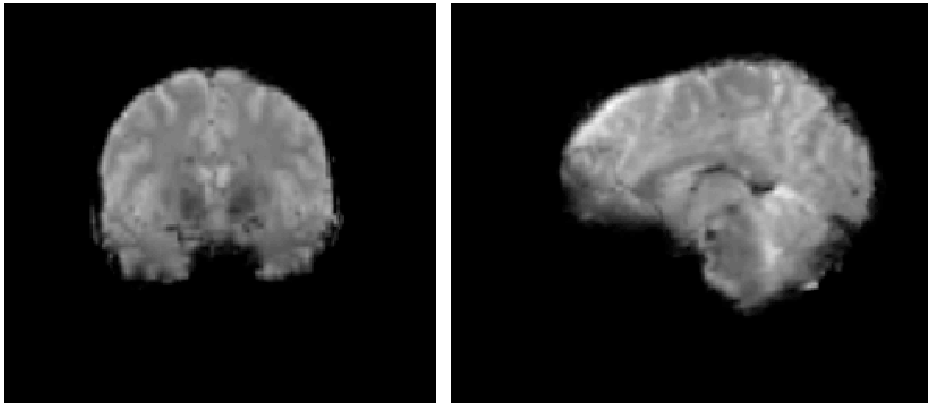

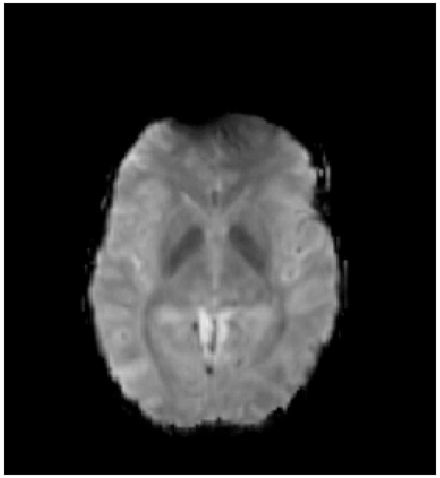

Courtesy of Roberto Garcia-Alvarez, GE Healthcare

GRASE

- Hybrid sequence
- Gradient And Spin Echo
- Also known as TurboGSE
- Multiple spin-echoes and gradient echoes at each spin-echo
  - ‘Gradient’ AND ‘Turbo’ factors to consider
- Each echo phase encoded

$$\text{Scan time} = (TR \times N_{AV} \times N_{PE}) / (N_{GRE} \times N_{SE})$$

GRASE (TGSE)

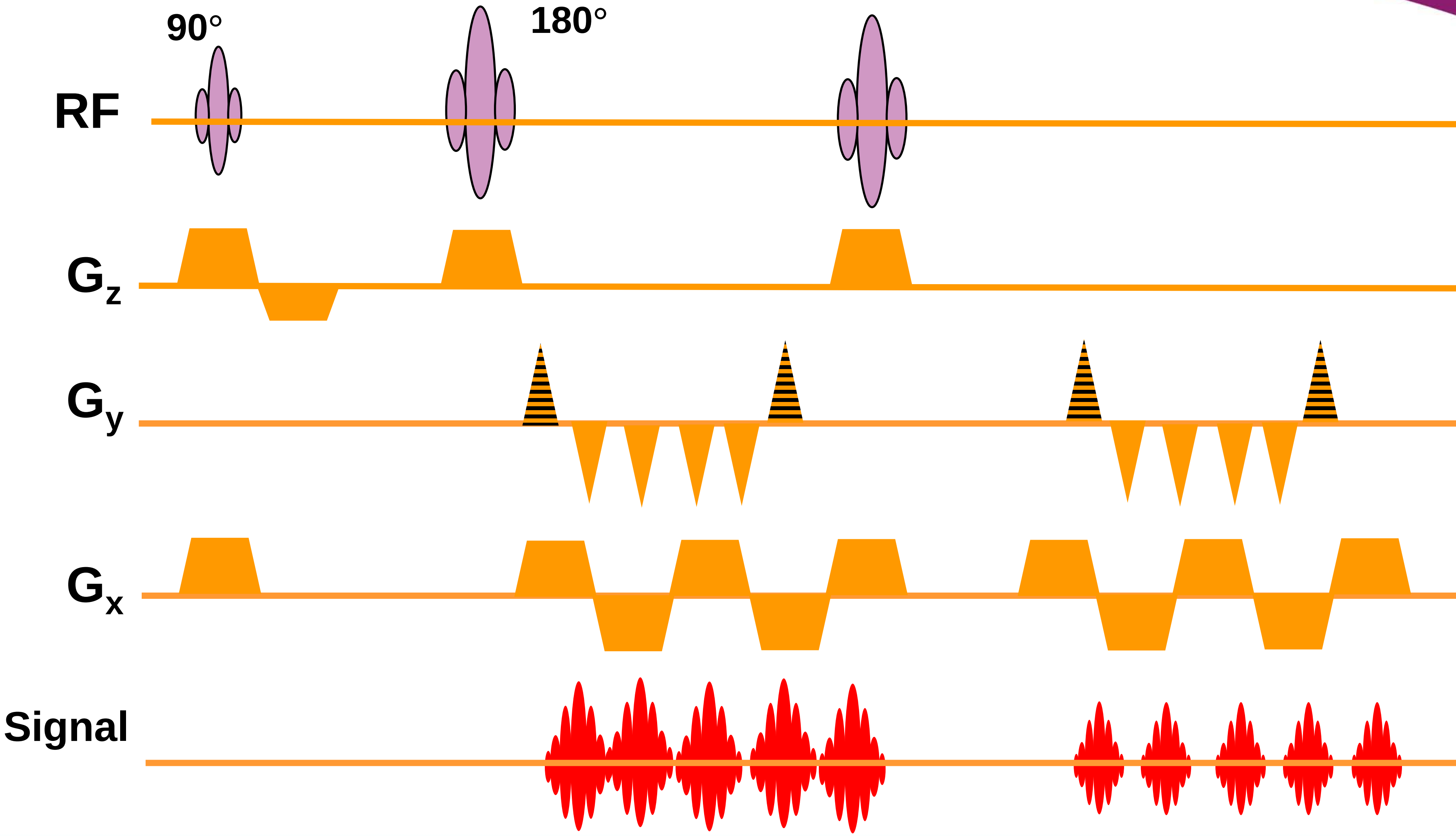

TGSE in Prostate

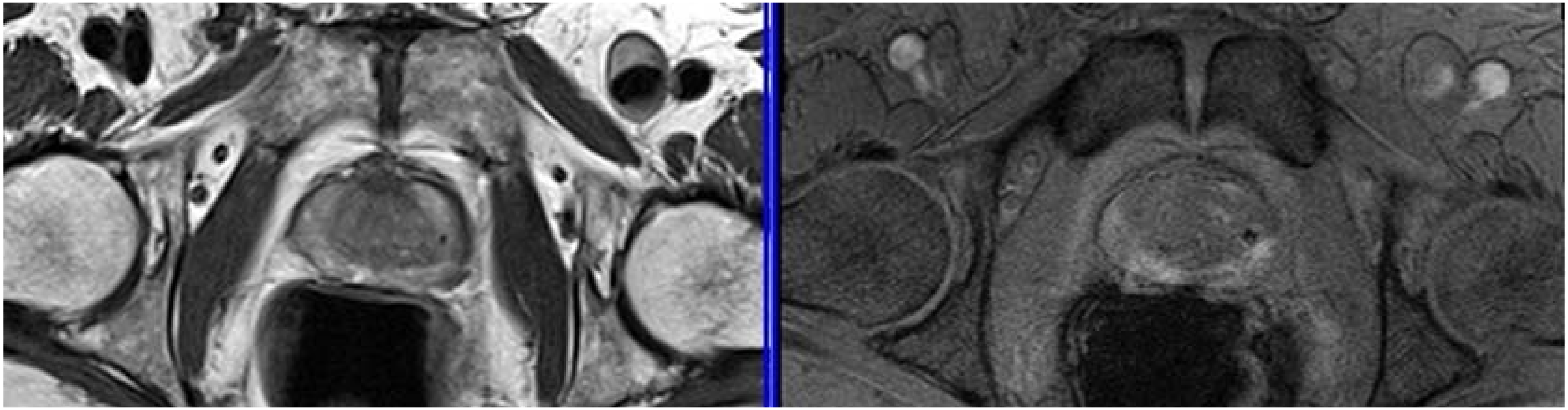

TGSE GE

- TGSE in prostate with gold seeds compared to GE
- T_2-w contrast and seed visualisation in one sequence

Gradient-echoes…

- Inherently fast due to lack of 180° and short TR
- Partially excite using reduced flip (Ernst) angle
  - Not restricted by relaxation
- If we further reduce TR…
  - Steady-state magnetisation when TR << T_2

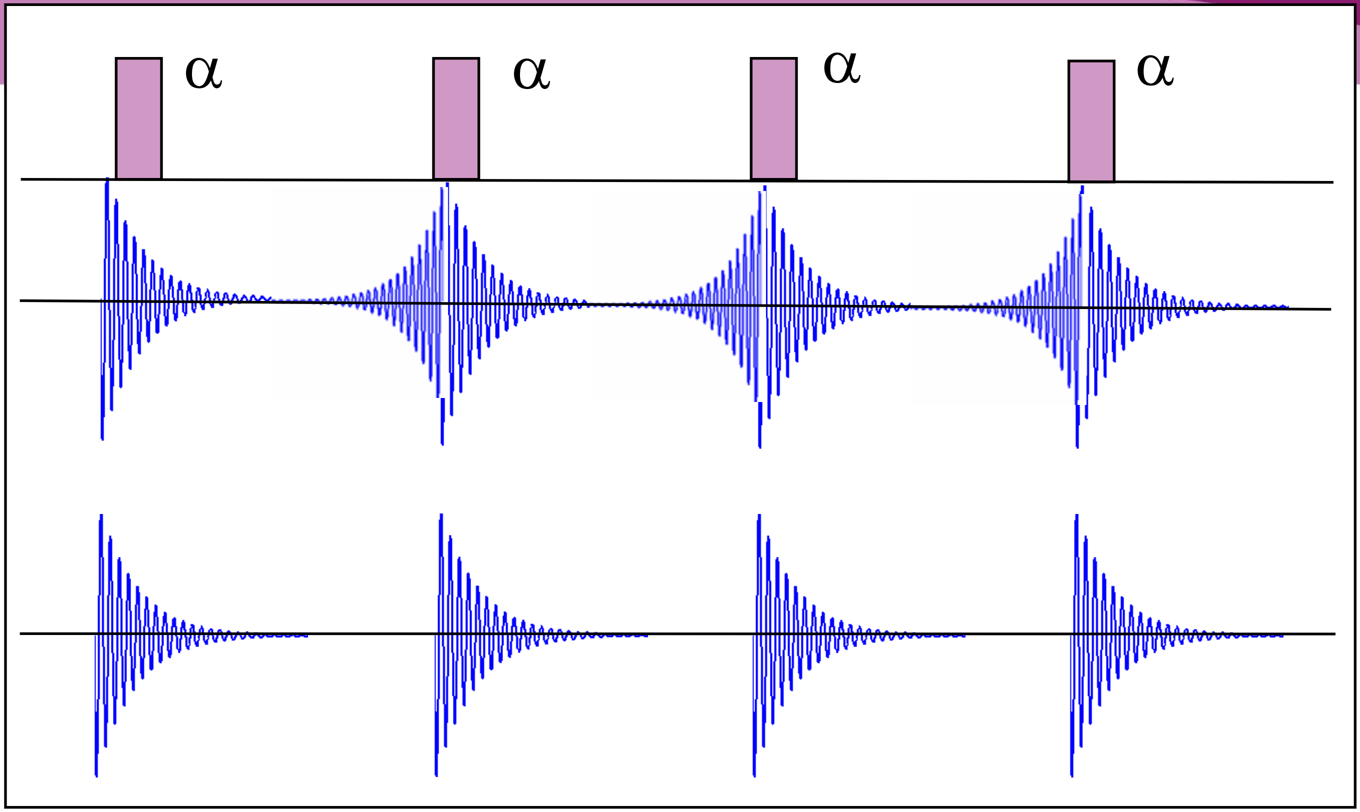

- Rapid successive RF pulses
- Refocus residual transverse magnetisation into ‘Hahn’ echoes
- Using or destroying these alters contrast

Steady State Sequences

- Spoiling (or 'incoherent steady state')
  - Removes residual transverse signal
  - Use RF (or gradient) spoiling
    - RF phase angle increased to produce net cancellation of transverse magnetization
  - Incomplete spoiling leads to 'FLASH-bands'

FLASH (Turbo-FLASH)
SPGR (FSPGR)
RF-FAST

$$S \propto \frac{\sin\alpha\left[1-\exp\left(-TR/T_1\right)\right]\exp\left(-TE/T_2^{*}\right)}{1-\cos\alpha\exp\left(-TR/T_1\right)}$$

Steady State Sequences

- Rewinding (SS-FID)
  - Maintains coherent transverse magnetisation
  - FISP, GRASS rewind phase encoding only
  - 'True' FISP or bFFE rewind all 3 gradient directions

    Have to additionally phase cycle RF (ROAST)

FAST
FISP
GRASS
bFFE/bSSFP
FIESTA

- Time Reversed sequences (SS-Echo)
  - PSIF
  - Use (Hahn) echo -essentially T_2-weighted

CE-FAST
PSIF
SSFP

Signals depend on:
flip angle, T_1/T_2

Steady-State Sequences

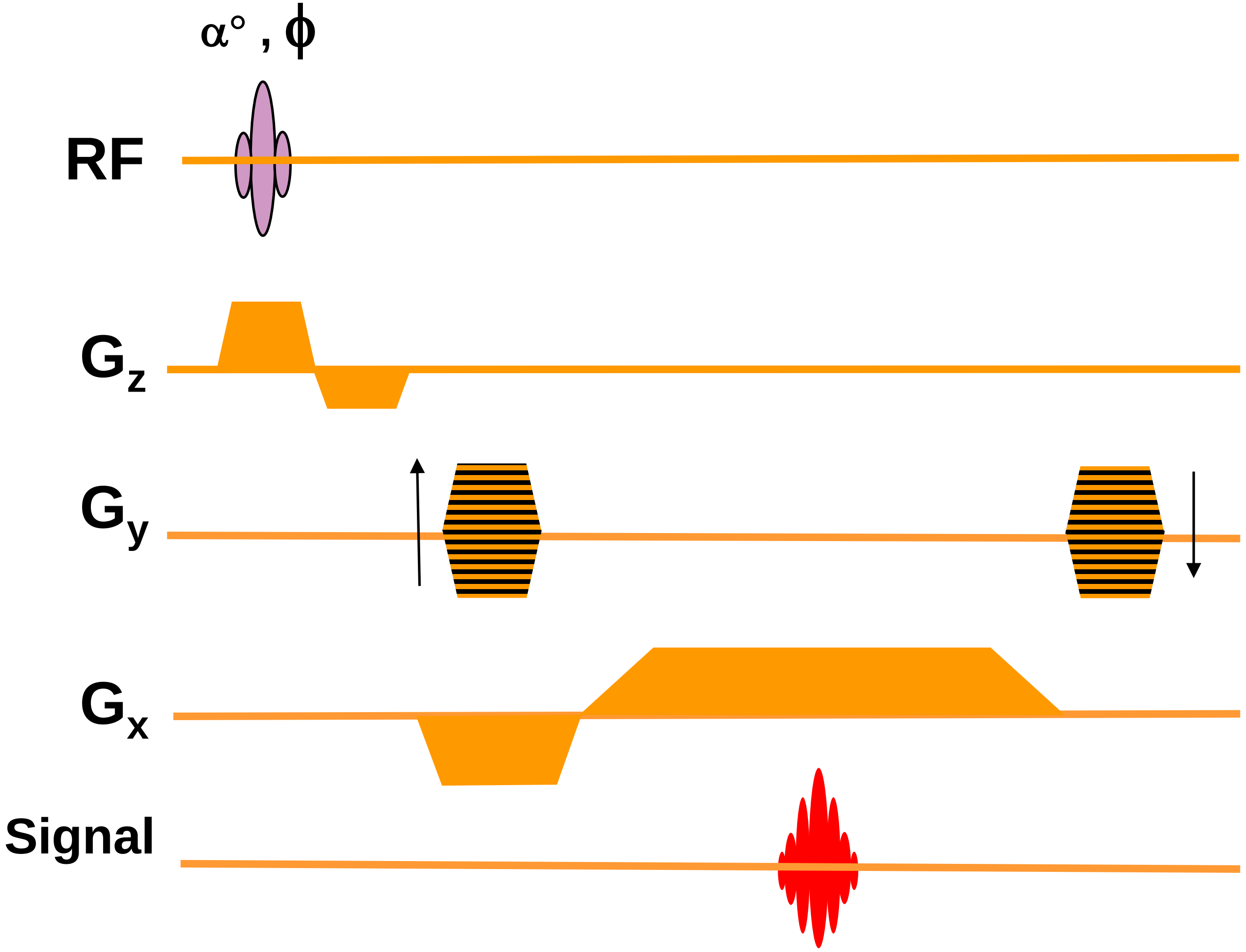

<u>RF spoiled:</u>
phase (ϕ) is increased

Example: Fast GRE

- 2D FSPGR dynamic scan used to obtain good temporal resolution (10-15s)

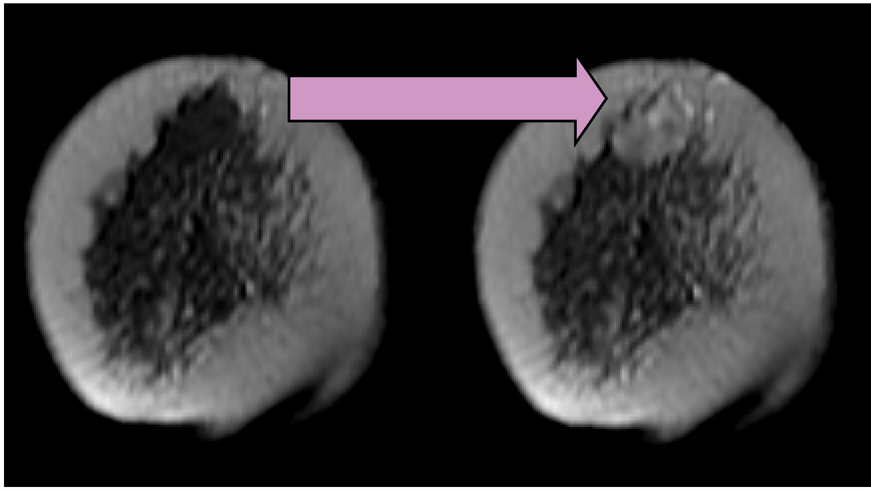

- 3D VIBRANT dynamic sequence provides good spatial resolution and reasonable temporal resolution (30-45s)

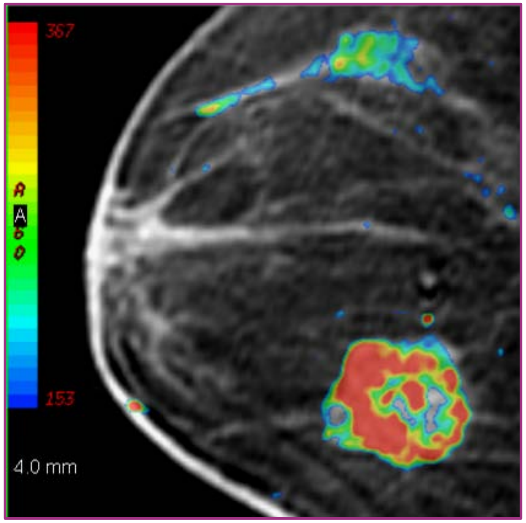

ESTRO School

Example: TrueFISP

Real time free breathing TrueFISP

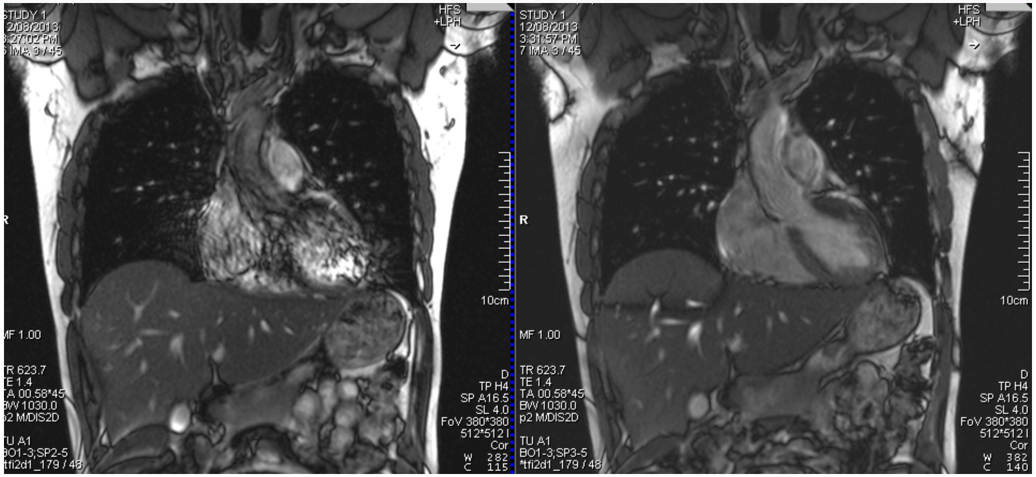

Reduced artefacts with cardiac shim

(right) Lung tumour motion

ESTRO School

Gradient-Speed Limit

G.t × pixel width = constant

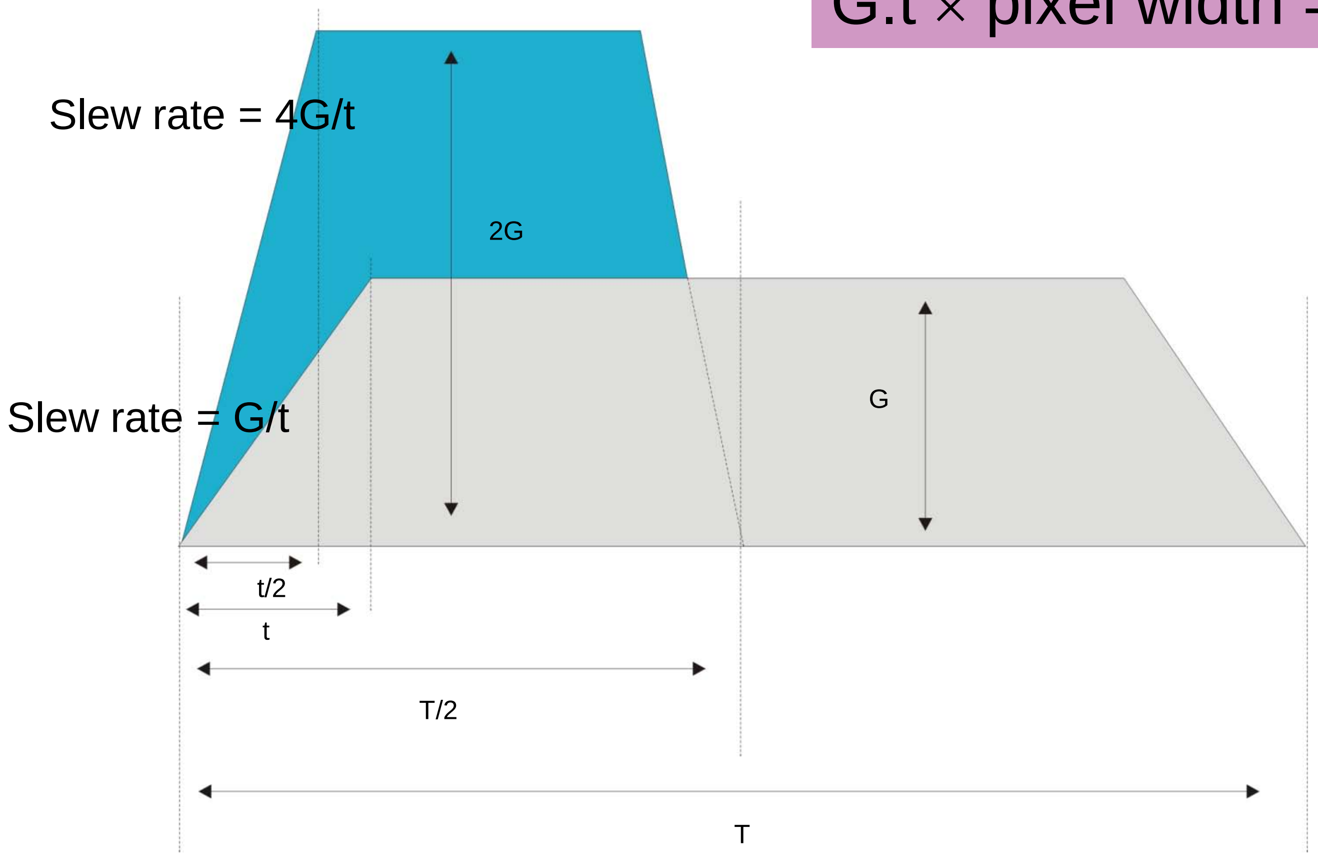

Gradients can be made to run faster

<u>but</u>

Physiological limit = PNS

Parallel Imaging = ‘Coil Encoding’

- Acquire fewer k-space lines
  - ✓ Speed up scanning
- Use Coil Arrays to:

Unwrap aliased images (image space) ‘SENSE’ -like

OR

Generate missing lines (k-space) ‘SMASH’ -like

Scan time = $(TR \times N_{AV} \times N_{PE})/R$

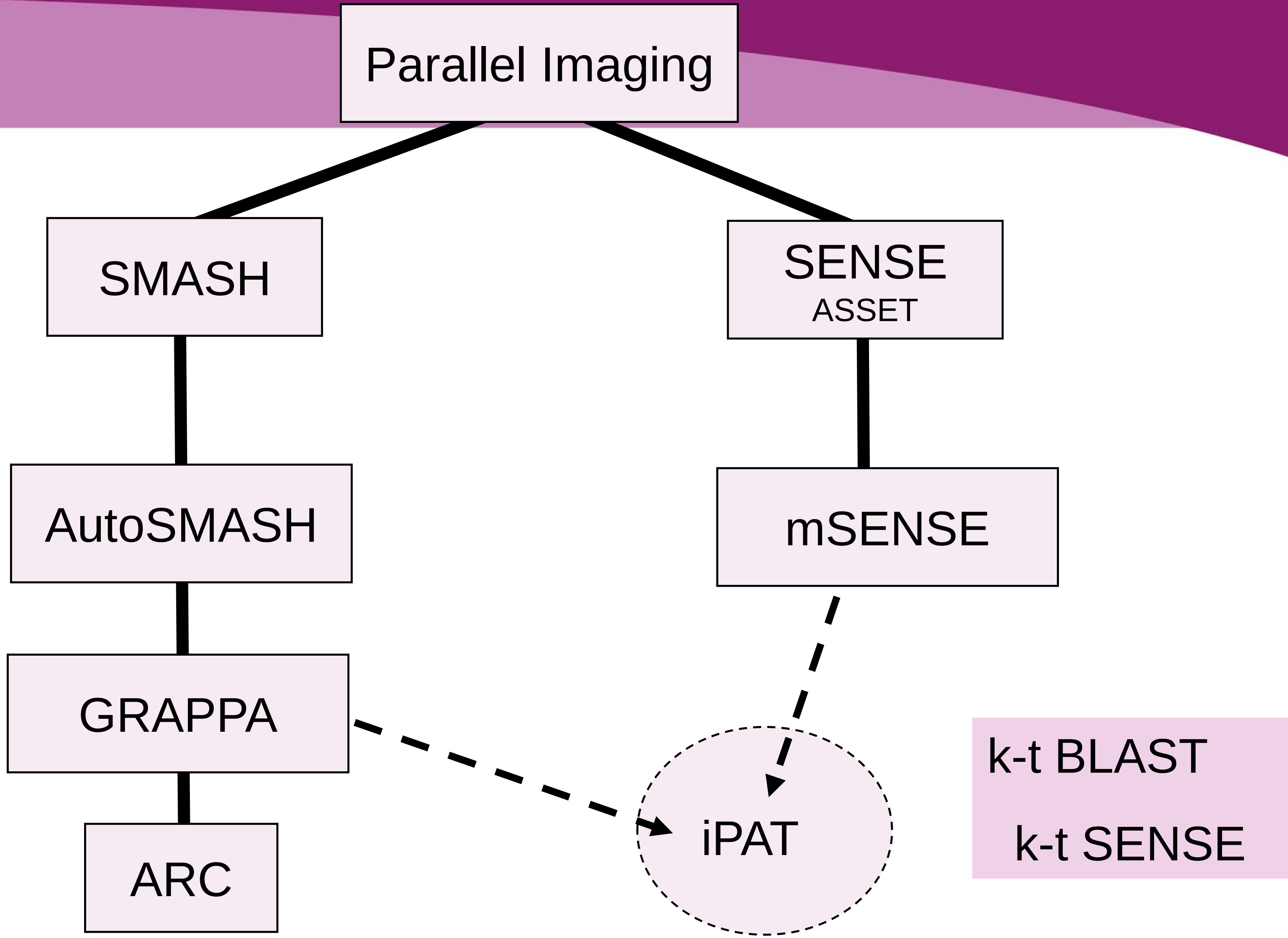
Parallel Imaging
SMASH
SENSE
ASSET
AutoSMASH
mSENSE
GRAPPA
ARC
iPAT
k-t BLAST
k-t SENSE

Multi-Coil Arrays

Signal strength from one coil with respect to another provides alternative localisation method

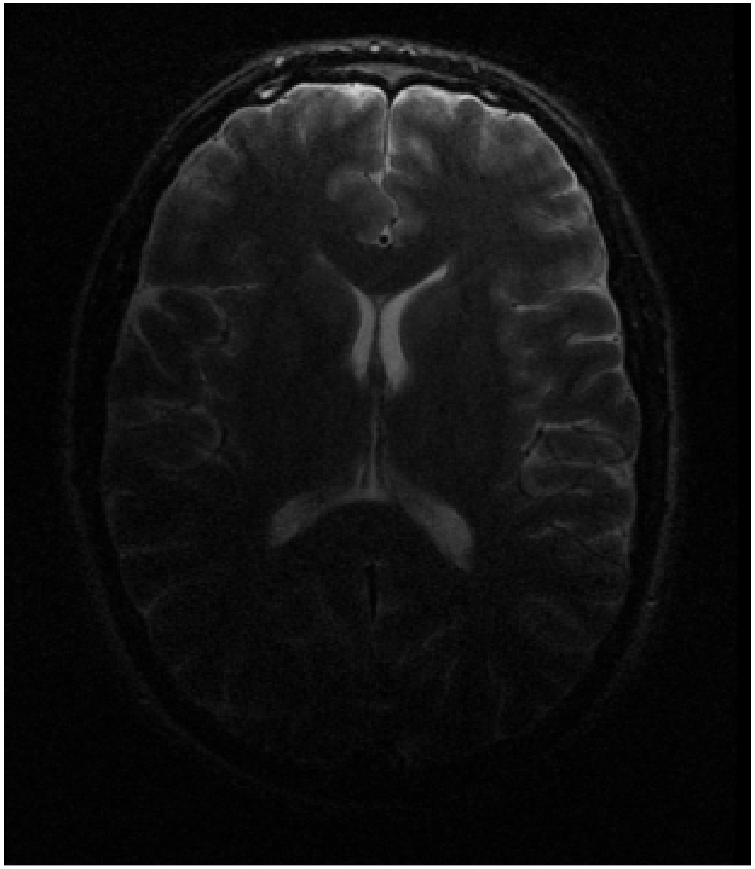

Parallel Imaging

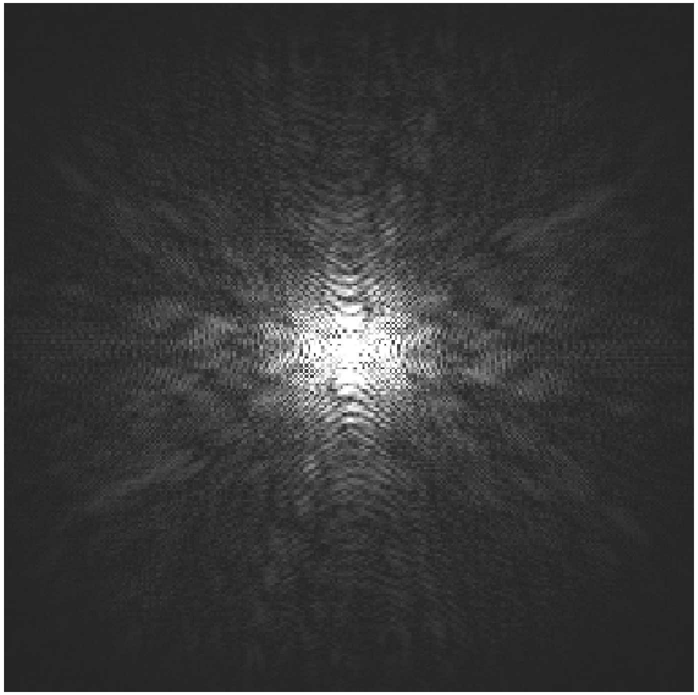

Full k-space

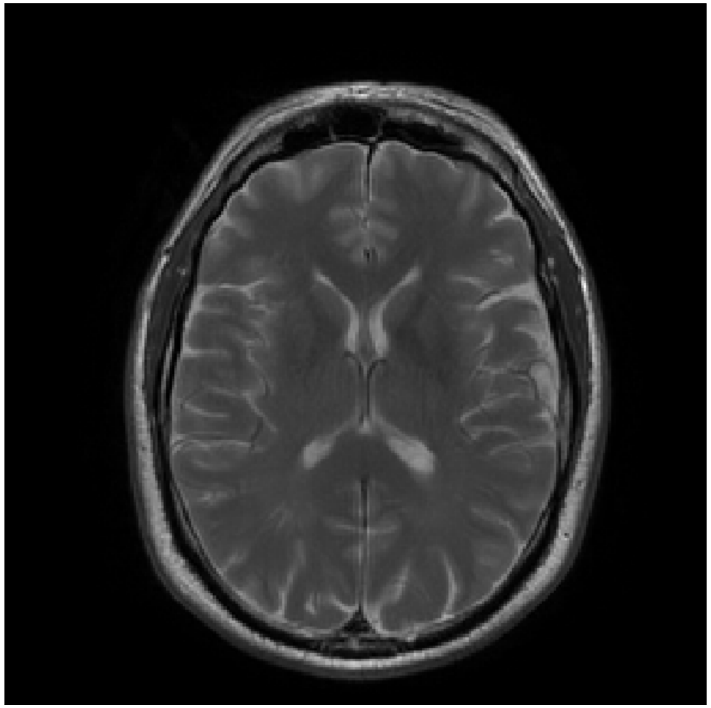

Whole image

Parallel Imaging

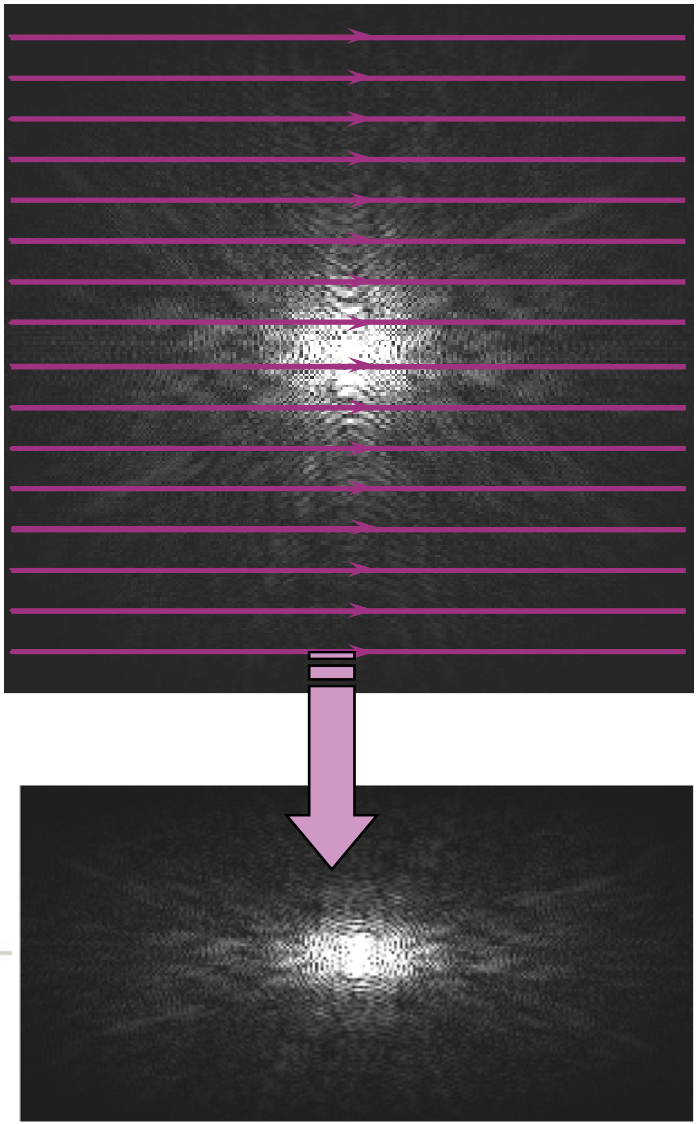

Missing every other line
Speeds up scan (x2) but
Results in aliasing

SENSE

- SENSitivity Encoding
- Commercially implemented by Philips
- Other Implementations:
  - ASSET (GE), SPEEDER (Toshiba), RAPID (Hitachi)
- Apply knowledge of coil sensitivity profiles to calculate aliased signal component
- Can be applied in through-plane phase encoding (3D)
- Reduction Factor = 1 to number of coils (+non integers)
- Cannot handle inherent aliasing (FOV must encompass object)

Where $\Delta y = FOV_{rec}/R$

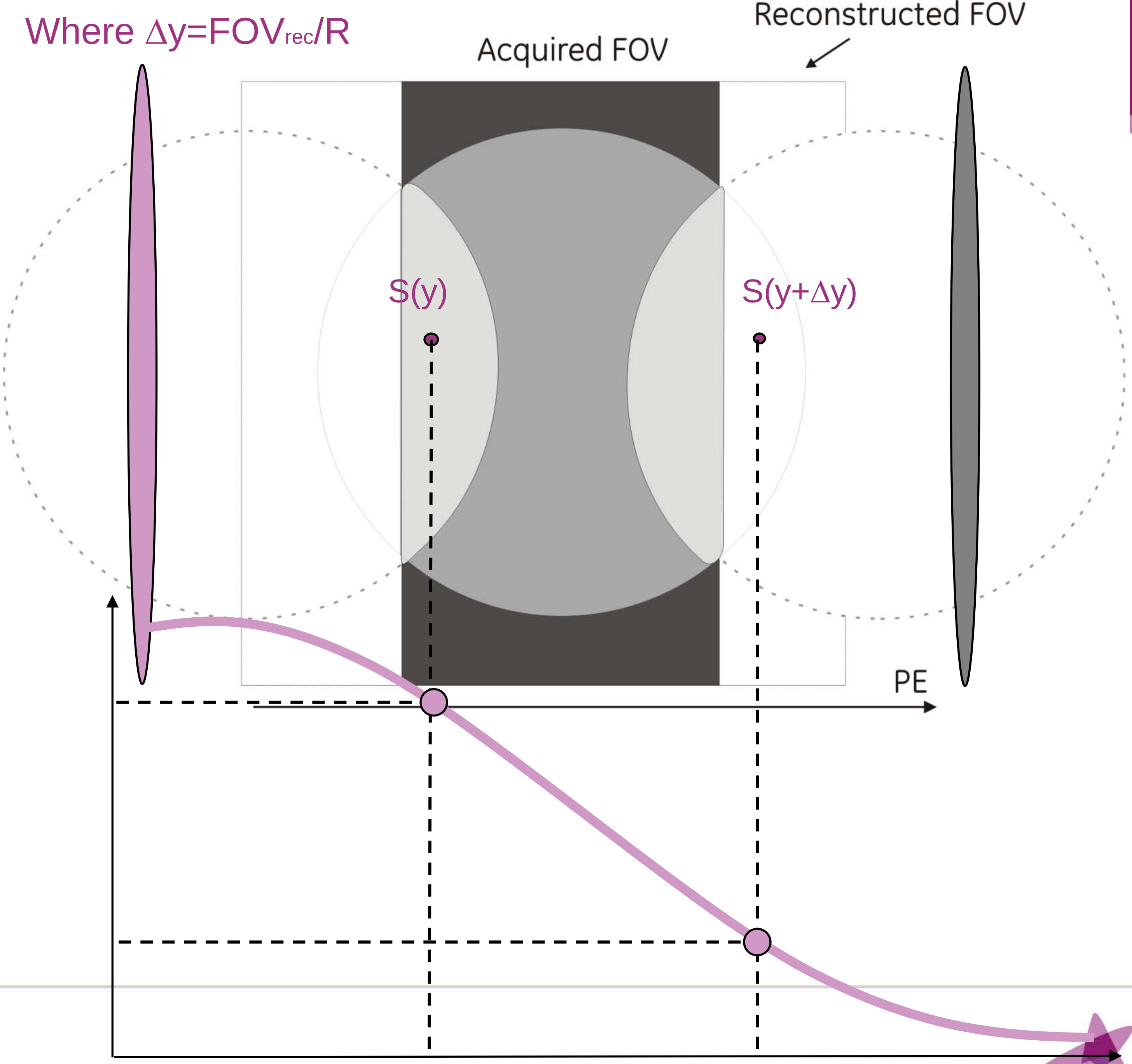

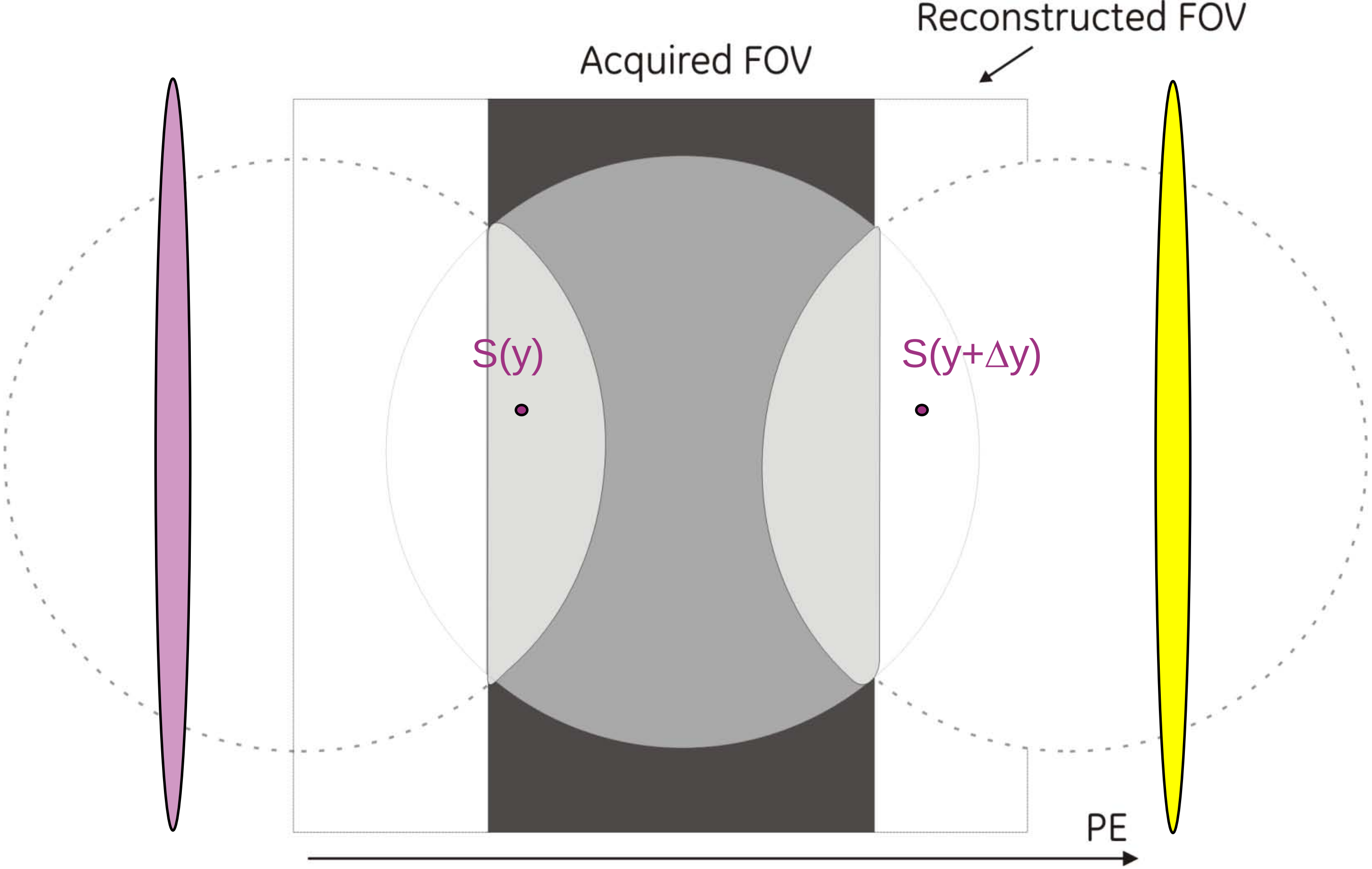

$$I(y)_1 = C_1(y)S(y) + C_1(y + FOV_{rec}/R)\,S(y + FOV_{rec}/R)$$

$$I(y)_2 = C_2(y)S(y) + C_2(y + FOV_{rec}/R)\,S(y + FOV_{rec}/R)$$

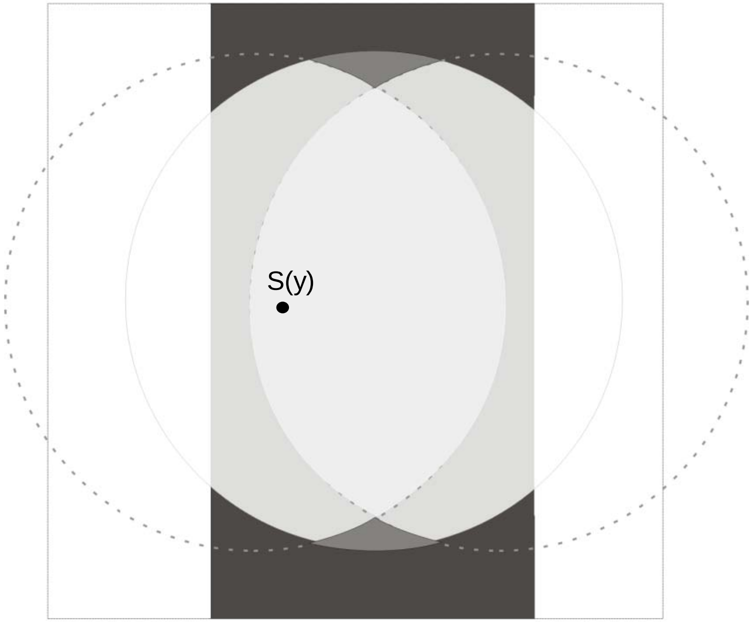

$$I_j(x,y)=\sum_{n=0}^{n_A-1} C_j(x,y+n\Delta Y)\, S(x,y+n\Delta Y)$$

$$I_j(y)=C_j(y)\,S(y)+C_j(y+\Delta Y)\,S(y+\Delta Y)+\ldots+C_j(y+(n_A-1)\Delta Y)\,S(y+(n_A-1)\Delta Y)$$

$$\begin{pmatrix} I_1(x,y)\\ I_2(x,y)\\ .\\ .\\ .\\ I_L(x,y)\end{pmatrix}_{L\,x\,1}=\begin{pmatrix} C_1(x,y) & C_1(x,y+\Delta Y) & . & . & . & C_1(x,y+(n_A-1)\Delta Y)\\ C_2(x,y) & C_2(x,y+\Delta Y) & . & . & . & C_2(x,y+(n_A-1)\Delta Y)\\ . & & . & & & .\\ . & & & . & & .\\ . & & & & . & .\\ C_L(x,y) & C_L(x,y+\Delta Y) & & & & C_L(x,y+(n_A-1)\Delta Y)\end{pmatrix}_{L\,x\,n_A}\begin{pmatrix} S(x,y)\\ S(x,y+\Delta Y)\\ .\\ .\\ .\\ S(x,y+(n_A-1)\Delta Y)\end{pmatrix}_{n_A\,x\,1}$$

$$I=C\;S$$

SENSE

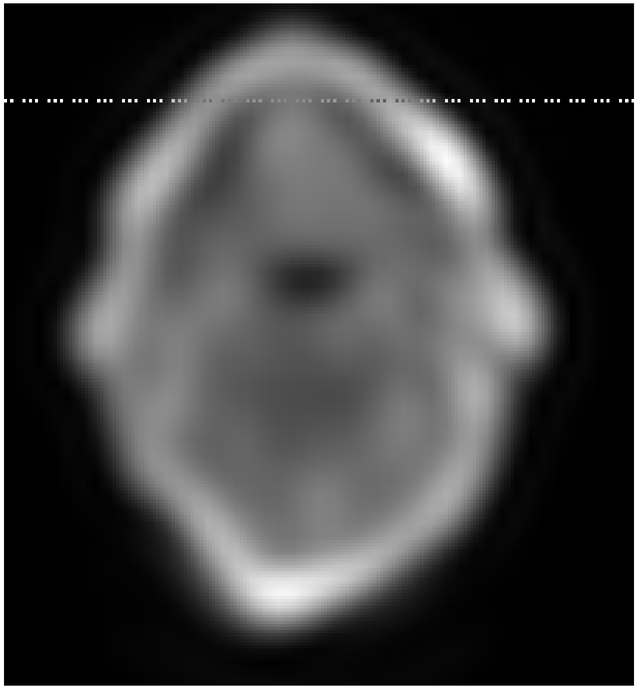

- Calibration scan (sensitivity maps) required
- Typically 20 s
- single scan only
- Relies on no patient motion between calibration and speed-up scans

$$SNR' = \frac{SNR}{g\sqrt{R}}$$

mSENSE

- Modified SENSE
  - Auto calibration lines
- Central k-space fully sampled
- Extracted to give sensitivity map
- No motion/registration problems
- Do not get full speed-up

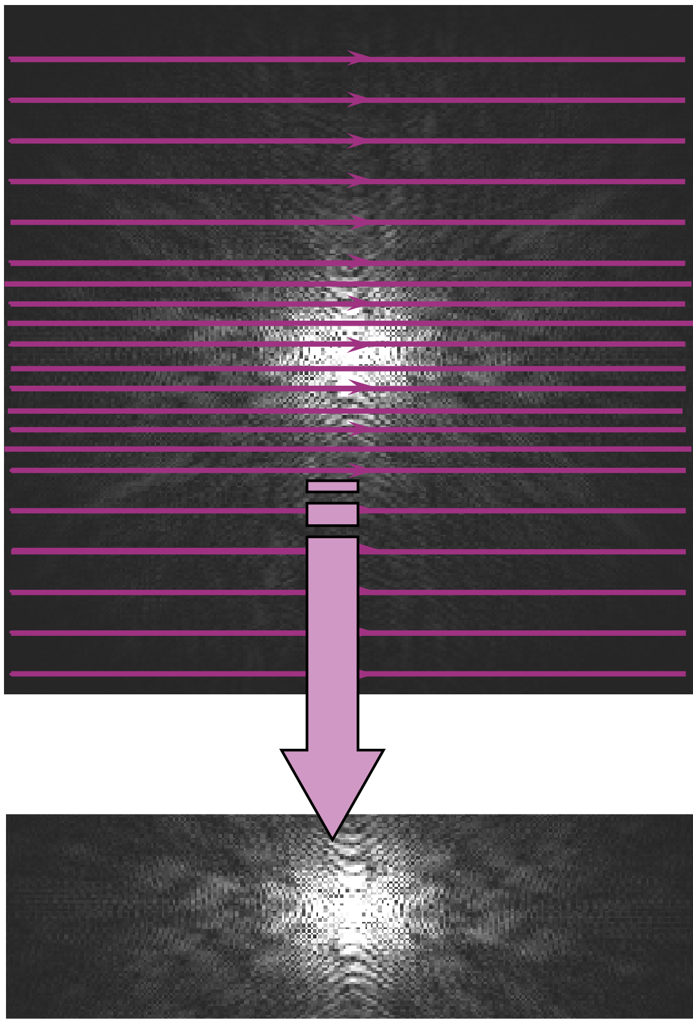

SMASH

- SiMultaneous Acquisition of Spatial Harmonics
- First parallel imaging technique
  - Generate virtual k-space lines from spatial response of coil sensitivity
  - Combining elements to produce required sinusoidal variations
- Weighted coil sensitivities used
  - Determine coil sensitivity profiles
- In practice very restricting on coil design, empirical self-calibration is used

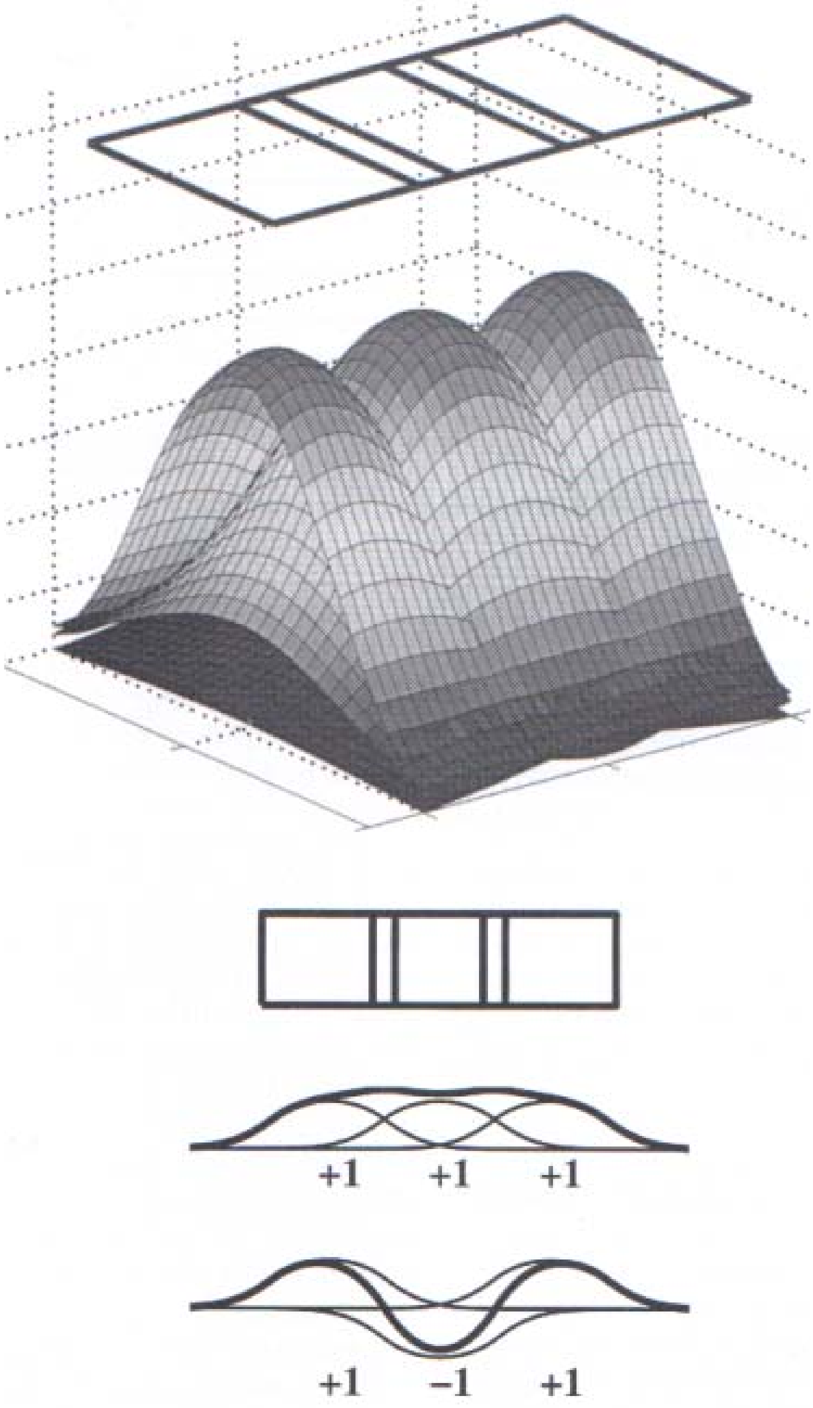

Re-create sinusoidal
Signal variation from
'missing'
phase encoding

<u>Also self calibration:</u>

AutoSMASH

GRAPPA

ARC

Example: Brain

- 3D BRAVO sequence acquired with ARC
- 0.9 × 0.9 × 1.2 mm resolution
- 148 images in 3.5 mins
- Used as high resolution registration scan in fMRI

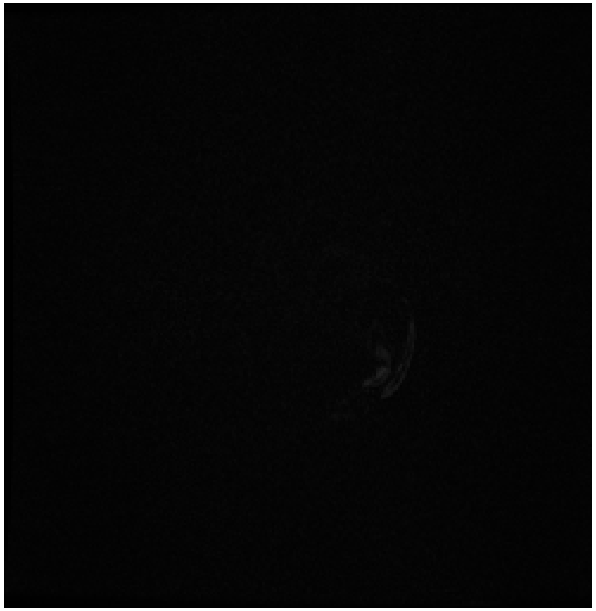

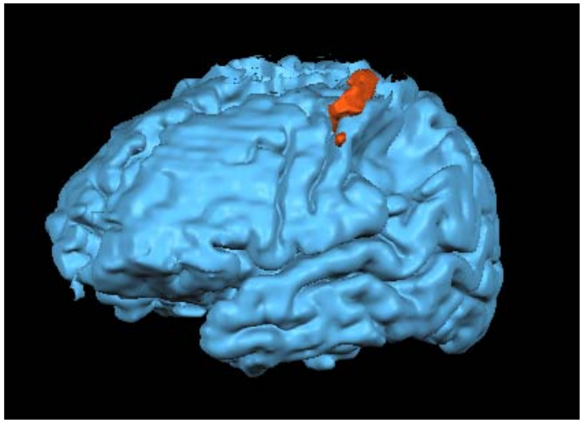

Key-hole Imaging

- Acquire full k-space once
- Rapidly acquire centre (key-hole) of k-space thereafter
- Fill-in missing data from first scan
- Very useful in dynamic scans

•TRICKS
•TRAQ
•TRAK
•TWIST
•Freeze Frame

Key-hole Imaging

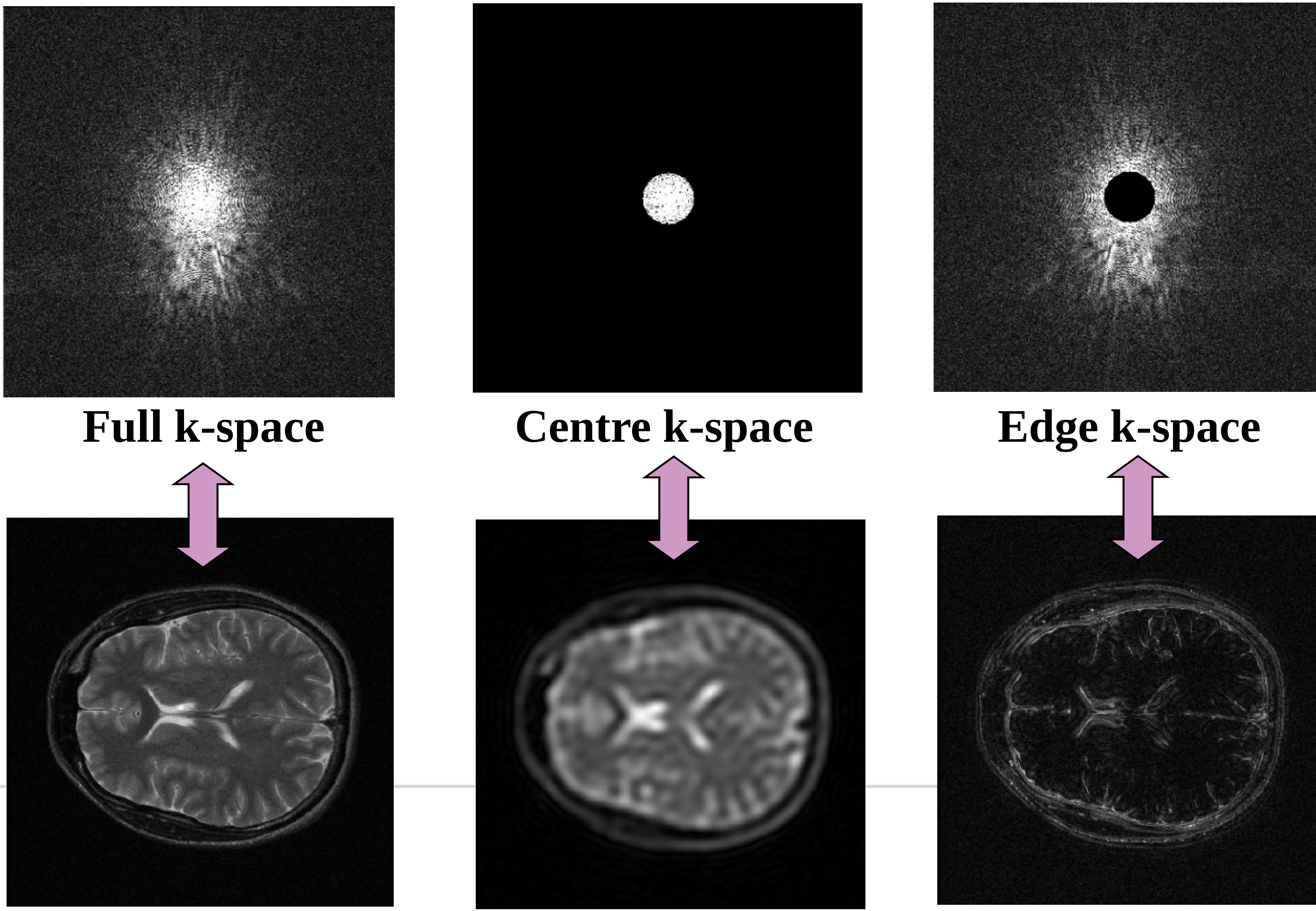

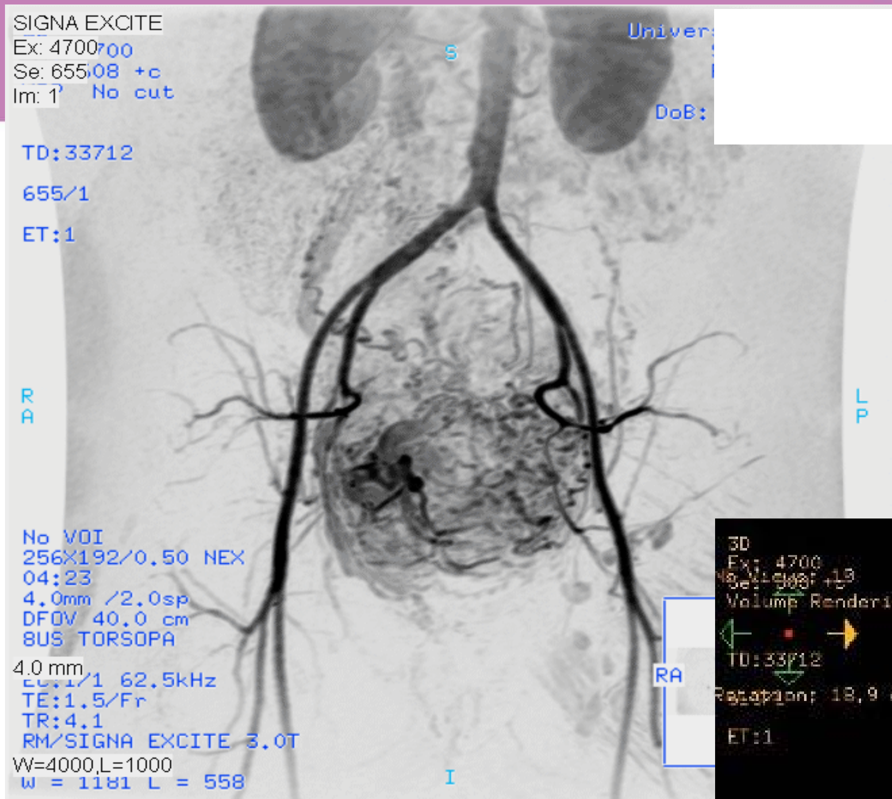
SIGNA EXCITE
Ex: 4700
Se: 655
Im: 1
No cut
TD:33712
655/1
ET:1
R
A
L
P
No VOI
256X192/0.50 NEX
04:23
4.0mm /2.0sp
DFOV 40.0 cm
8US TORSOPA
4.0 mm
TE:1.5/Fr
TR:4.1
RM/SIGNA EXCITE 3.0T
W=4000,L=1000
W = 1181 L = 558

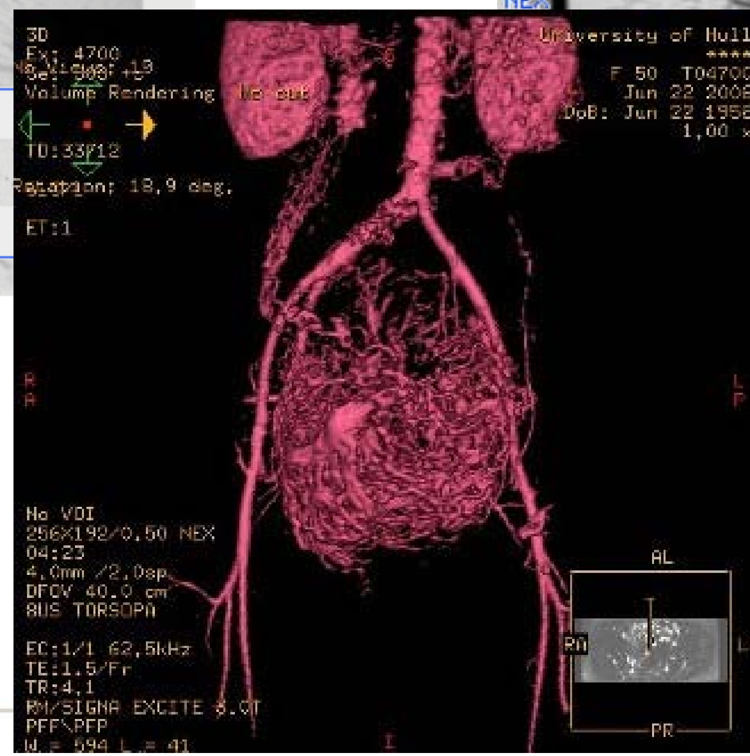
3D
Ex: 4700
Volume Rendering
University of Hull
F 50 T04700
Jun 22 2006
DoB: Jun 22 1956
TD:33712
Rotation: 18.9 deg.
ET:1
No VOI
256X192/0.50 NEX
04:23
4.0mm /2.0sp
DFOV 40.0 cm
8US TORSOPA
EC:1/1 62.5kHz
TE:1.5/Fr
TR:4.1
RM/SIGNA EXCITE 3.0T
PFF\PFP
W = 594 L = 41
AL
RA
LP
PR

TRICKS

Recent Developments

Faster scans, increased volume…

Whole Body Screening

- Fast scanning, moving table
- Continuous scanning + simultaneous reconstruction (Siemens TIM CT)

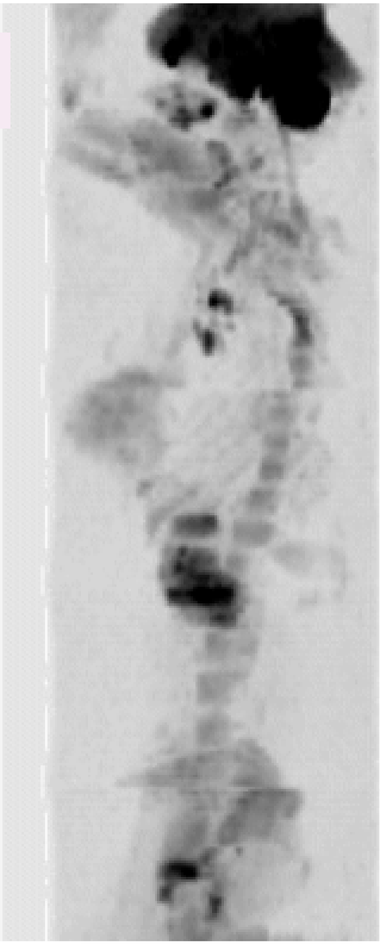

Sydney 2017

www.mrinrt2017.com

5th MR in RT Symposium 2017

ESTRO School

Pulse sequences in this talk

ARC: Auto calibrating Reconstruction with Cartesian sampling
ASSET: Array SenSitive Encoding Technique
bFFE: Balanced Fast Field Echo
BLAST: Broad use Linear Acquisition Speed-up Technique
BRAVO: BRAin Volume
bSSP: Balanced Steady State Free Precession
CE-FAST: Contrast Enhanced FAST
DIET: Delayed Interval Echo Train
DRIVE: DRIVEn equilibrium
EPI: Echo Planar Imaging
FAST: Fourier Acquisition STeady state
FIESTA: Fast Imaging Employing Steady State
FISP: Fast Imaging with Steady state Precession
FLAIR: Fluid Attenuated Inversion Recovery
FLASH: Fast Low Angle Snap sHot
FRFSE: Fast Recovery FSE
FSE: Fast Spin Echo
FSPGR: Fast Spoiled Gradient Echo
GRAPPA: GeneRalised Autocalibarting Partially Parallel Acquisition

RO
School

GRASE:	Gradient And Spin Echo
GRASS:	Gradient Recalled Acquisition Steady State
HASTE:	HAlf fourier Single-shot Turbo spin Echo
iPAT:	Integrated Parallel Acquisition Technique
mSENSE:	Modified SENSE
PSIF:	Not an acronym (reverse of FISP)
RAPID:	Not an acronym
RARE:	Rapid Acquisition with Relaxation Enhancement
RESTORE:	Not an acronym
SENSE:	SENSitivity Encoding
SMASH:	SiMultaneous Acquisition of Spatial Harmonics
SPEEDER:	Not an acronym
SSFP:	Steady State Free Precession
STIR:	Short Tau Inversion Recovery
T2Plus:	Not an acronym
TGSE:	Turbo Gradient Spin Echo
TRAQ:	Time Resolved AcQuisition
TRICKS:	Time Resolved Imaging with Contrast KineticS
TWIST:	Time resolved angiography With Interleaved Stochastic Trajectories
TrueFISP:	FISP with rewinding in each direction
VIBRANT:	Volume Imaging for BReast AssessmeNT

VÄSTERBOTTENS LÄNS LANDSTING

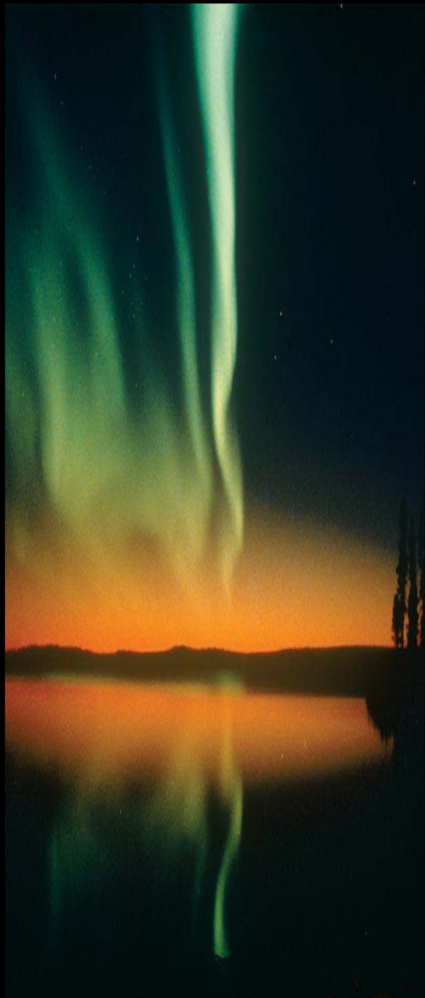

Health risks associated with MR

Tufve Nyholm

UMEÅ UNIVERSITET

Mechanical risks

Be very careful about what you bring into a MR room!

Accidents

http://www.medicalnewstoday.com/releases/139552.php

“The failure to report projectile accidents is one reason why many experts believe that the FDA's data may represent only 1% of the actual number of MRI accidents that occur, suggesting that the frequency and variety of accidents is far greater than is widely believed by the industry. ”

- In 2001, Michael Colombini, 6, was killed while undergoing an MRI when an oxygen tank flew out of the hands of an anesthesiologist toward the machine, hitting him in the head.
- In 2003, a New Mexico woman sued a Los Alamos hospital, claiming the magnetic pull of an MRI caused an oxygen tank to hit her in the back.
- In 1992, a 74-year-old woman hemorrhaged and died after an aneurysm clip in her brain shifted while she was on a table preparing for an MRI.

Demonstration of the powerful magnetic field of a clinical 1.5 Tesla MR scanner

Part IV - Patient bed

by
G. Starck, B. Vikhoff-Baaz, K. Lagerstrand,
E. Forssell-Aronsson och S. Ekholm

SAHLGRENSKA
UNIVERSITY HOSPITAL

2004


Demonstration of the powerful magnetic field
of a clinical 1.5 Tesla MR scanner
Part II - Oxygen bottle
by
G. Starck, B. Vikhoff-Baaz, K. Lagerstrand,
E. Forssell-Aronsson och S. Ekholm
SAHLGRENSKA
UNIVERSITY HOSPITAL
2004

Heating

- **The Internet Journal of World Health and Societal Politics ISSN: 1540-269X**
  MRI Safety at 3T versus 1.5T

“There was an incident reported to the FDA of a patient receiving blistered burns to the left thumb and left thigh that was touching the side of the bore, the incident occurred because the MRI operator input an inaccurate patient weight resulting in an incorrect SAR value (FDA 1997). “

Transdermal patches

Displacement and Heating

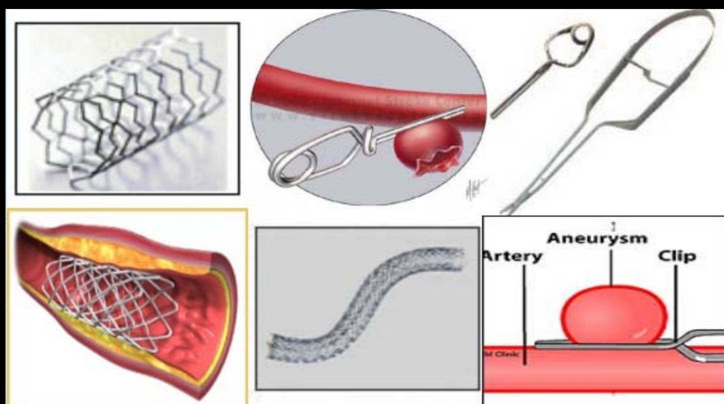

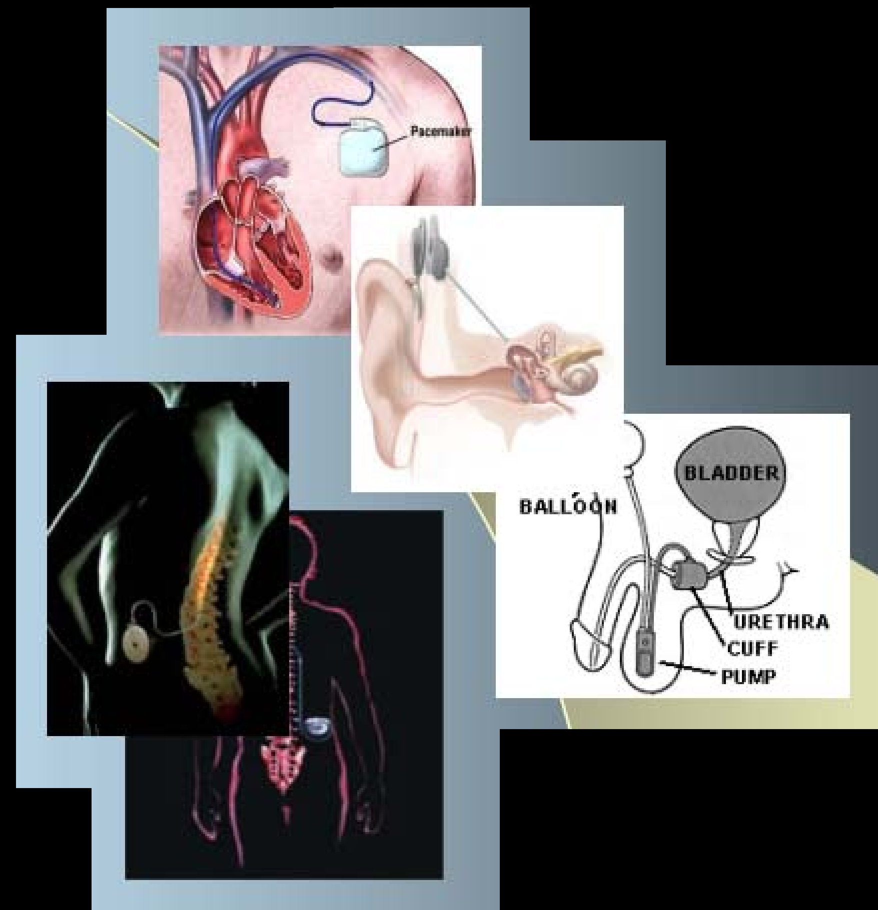

Medical inplants

- Electrical interference
- Mechanical force
- Heating

- Image distortions

Do you see the artifact?

Some tattoo ink used in radiotherapy may be suboptimal..

Courtesy: Christian Gustavsson, Lund

Long and short term effects

Some history:

2004/40/EC Directive on Protecting Workers from Exposure to Electromagnetic Fields (EMF Directive)

- Original version did limit the possibilities to perform medical MR examinations.

- The current version which has been approved by the parliament make an exception for MRI in medicine and research.

WHO grades

- **Group 1:** carcinogenic (X-rays, UVA, UVB, UVC, Arsenic, Asbestos,….)
- **Group 2A: probably** carcinogenic (Akrylamid, Diesel exhaust, Cisplatin, …)
- **Group 2B: possibly carcinogenic** (Coffee , Lead, Titanium dioxid,..)
- **Group 3: Not possible to classify** (Cholesterol, Sulfites, …)
- **Group 4: Probably not carcinogenic** (caprolactam- a substance used in nylon.)

www.iarc.fr

WHO grades (update june 2016)

- **Group 1:** carcinogenic (X-rays, UVA, UVB, UVC, Arsenic, Asbestos,….)
- **Group 2A: probably** carcinogenic (Akrylamid, Diesel exhaust, Cisplatin, …)
- **Group 2B: possibly carcinogenic** (Coffee, Lead, Titanium dioxid,..)
- **Group 3: Not possible to classify** (Cholesterol, Sulfites, …)
- **Group 4: Probably not carcinogenic** (caprolactam- a substance used in nylon.)

www.iarc.fr

Static magnetic field

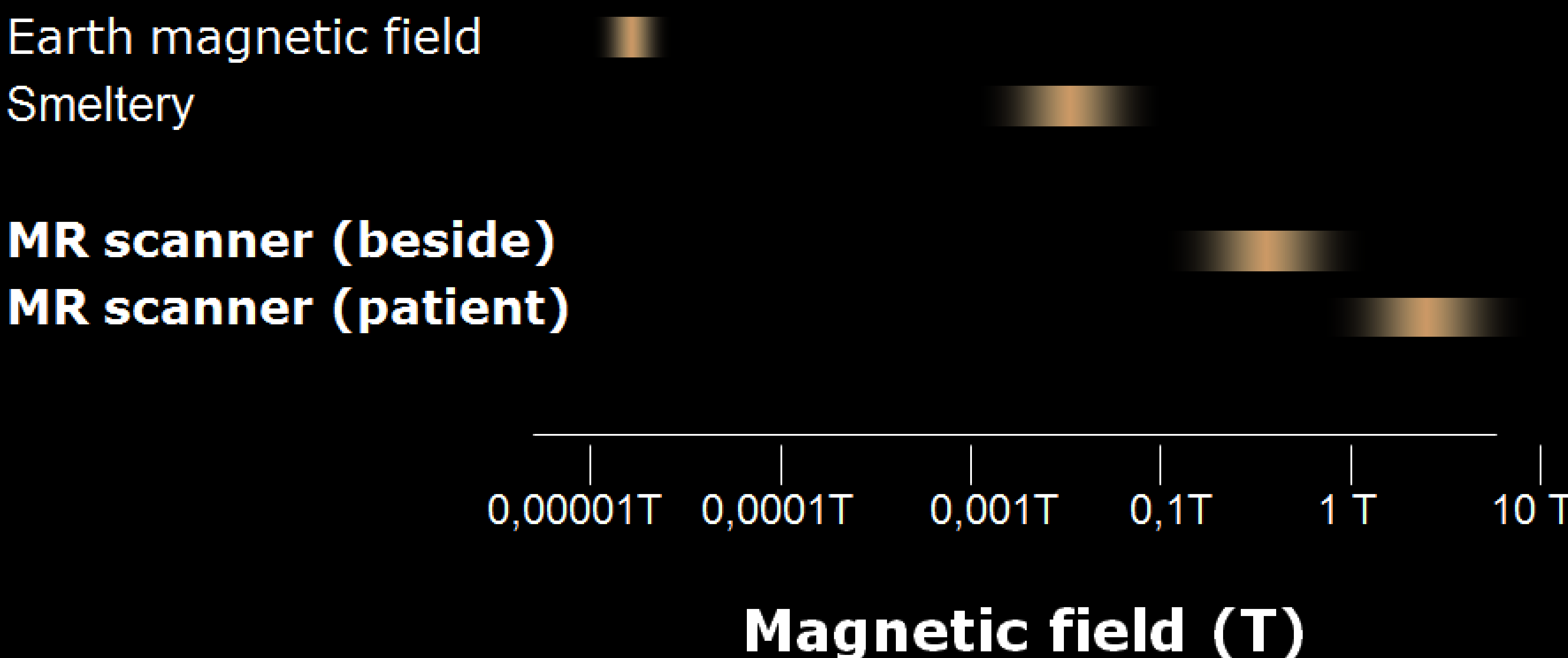

Health risk
(static fields)

- Acute
  - Dizziness
  - Nausea
- Long term effects
  - No worry about long term effects

Local survey of problems

- 59 people working with MR scanning in northen sweden
- 13 reported MR related problems
  - All worked with 3T scanners
- Instructions:
  - Move slower
  - Avoid to be close to the scanner if not nessisary

Gradient field – low frequency

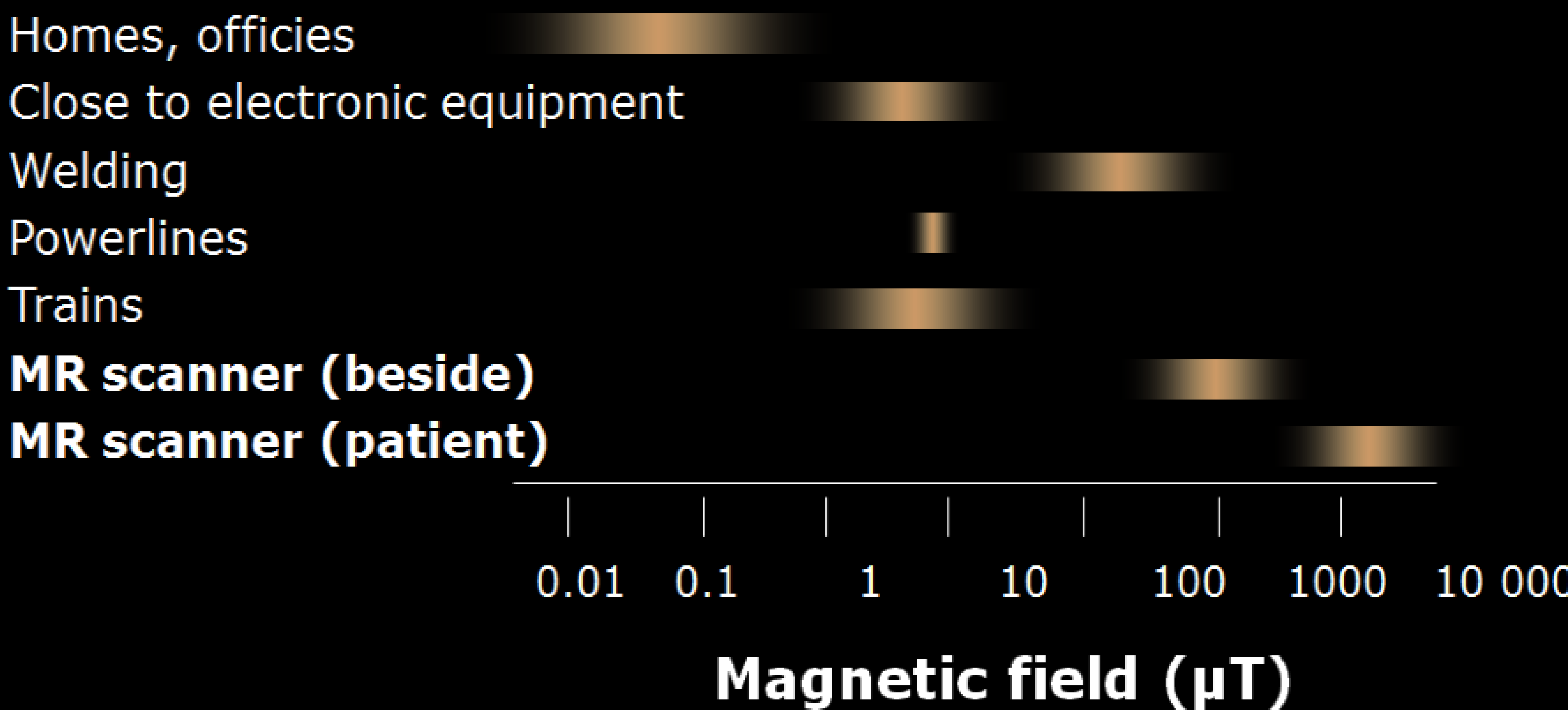

Health risks
Low frequency magnetic fields

- Acute
  - Nerve stimulation (peripheral and central)
- Late effects
  - Possibly carcinogenic (WHO grade 2B)

The International Agency for Research on Cancer (IARC)

"Human health population studies showing weak evidence of an association with childhood leukemia; and a large database of laboratory study results showing inadequate evidence of an association with cancer in animals"

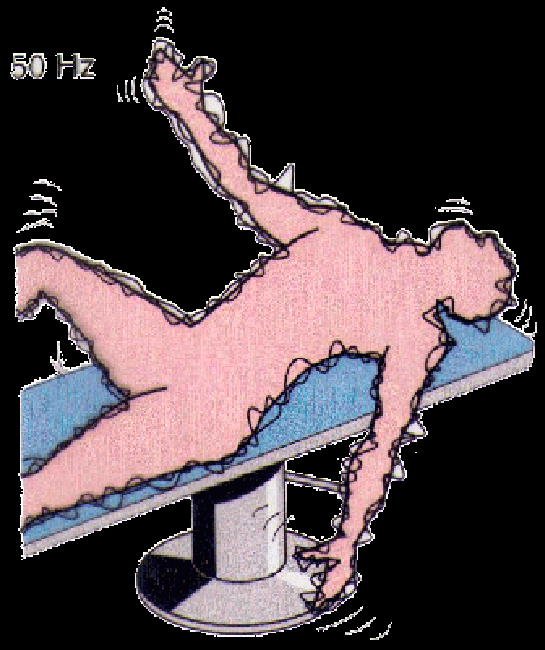

Peripheral nerve excitation

- Unusual but sometime reported by patients when using fast gradients (second level controlled)

Central nerve excitation

- Should never happen!

Radio frequent EMF

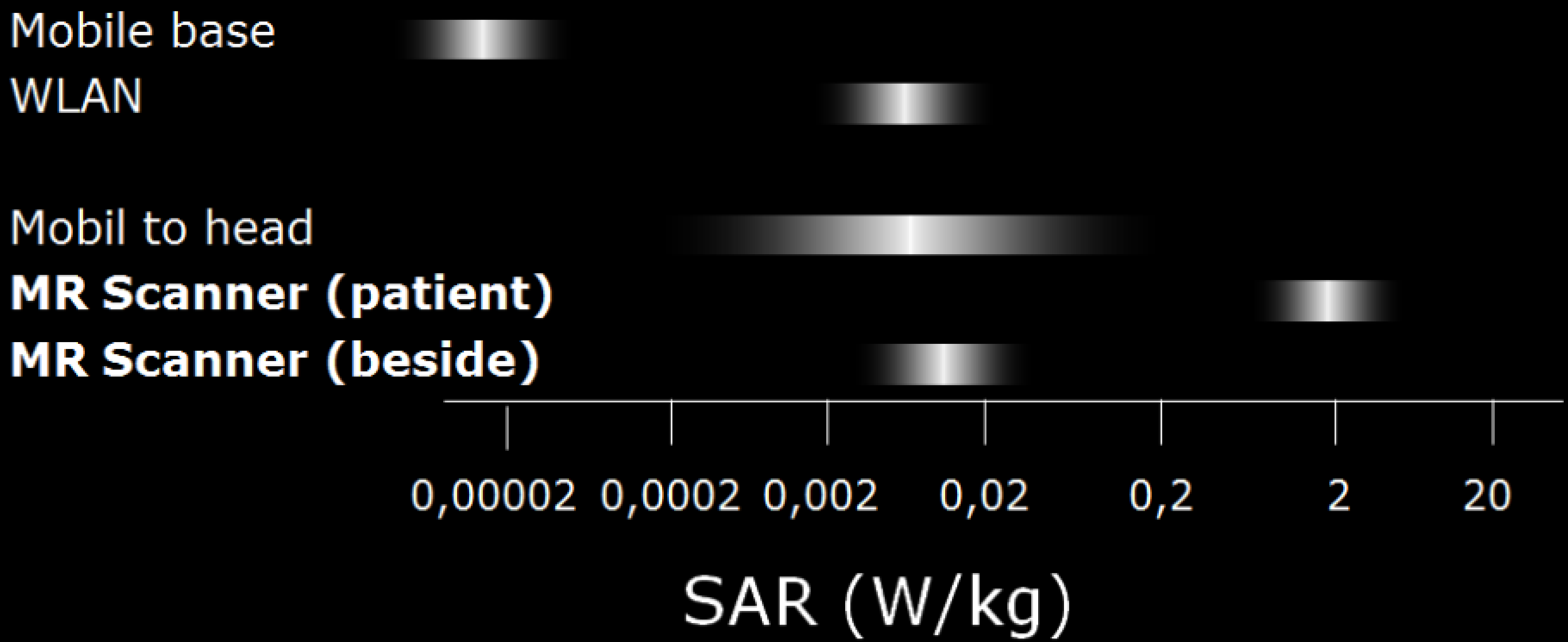

Radio frequent fields

- Acute
  - Heating
- Late effects
  - Possibly carcinogenic (WHO grade 2B)

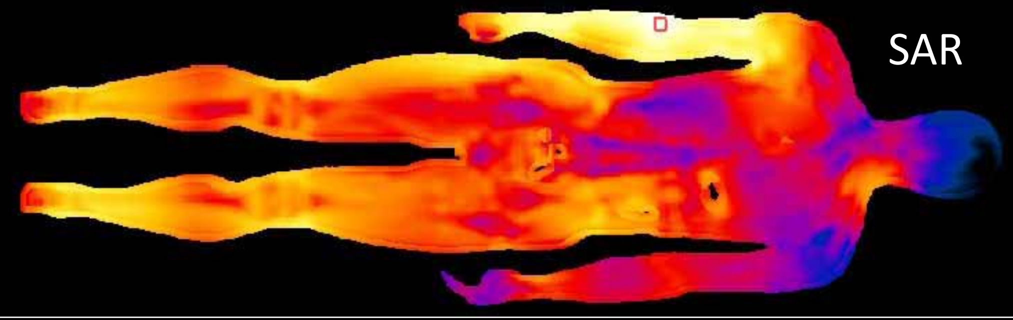

SAR

Capstick et al 2007

The International Agency for Research on Cancer (IARC)

"the evidence, while still accumulating, is strong enough to support a conclusion and the 2B classification. The conclusion means that there could be some risk, and therefore we need to keep a close watch for a link between cell phones and cancerrisk."

Whole body heating

- Normal mode
  - Max 0.5 degrees increase
- First level controlled
  - Max 1.0 degrees increase
- Second level controlled
  - More than 1.0 degrees increase

Burn injuries

- Risk for problems in second level controlled
- Large uncertainties in calculations for 7T scanners
- Avoid usage of carbon fiber equipment

Lack of knowleadge

- There are animal studies finding increased risk for cancer, but more that do not see any increased risk.
- The DNA damage mechanism is unknown
- Very few studies using actual MR sequences
- Two studies see effects on lymphocytes (Simi et al 2008, Lee et al 2011) – the quality of these has been questioned.

Recommened reading:

http://monographs.iarc.fr/ENG/Monographs/vol80/mono80.pdf

Thank you!

- Courtesy Jonna Wilen, Umeå

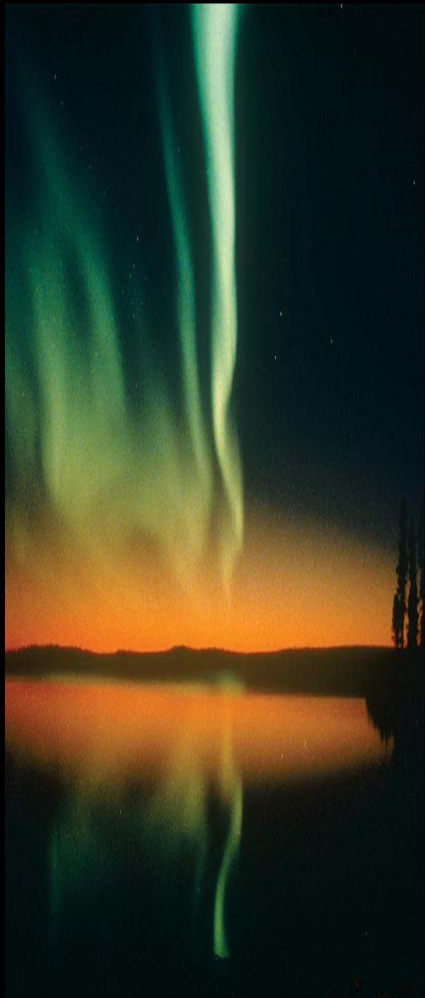

In-room imaging and MR planning

Tufve Nyholm

Overview of the lecture

- MR only treatment planning
- Cone beam CT
- In-room MR

Imaging in radiotherapy

Right dose
Right place

- Target definition
- Treatment planning
- Dose calculation
- Positioning

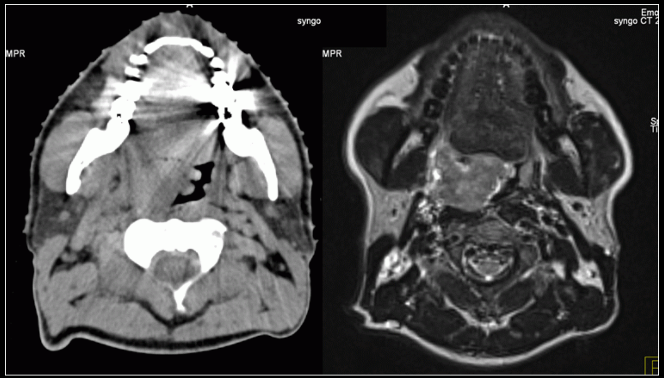

Workflow

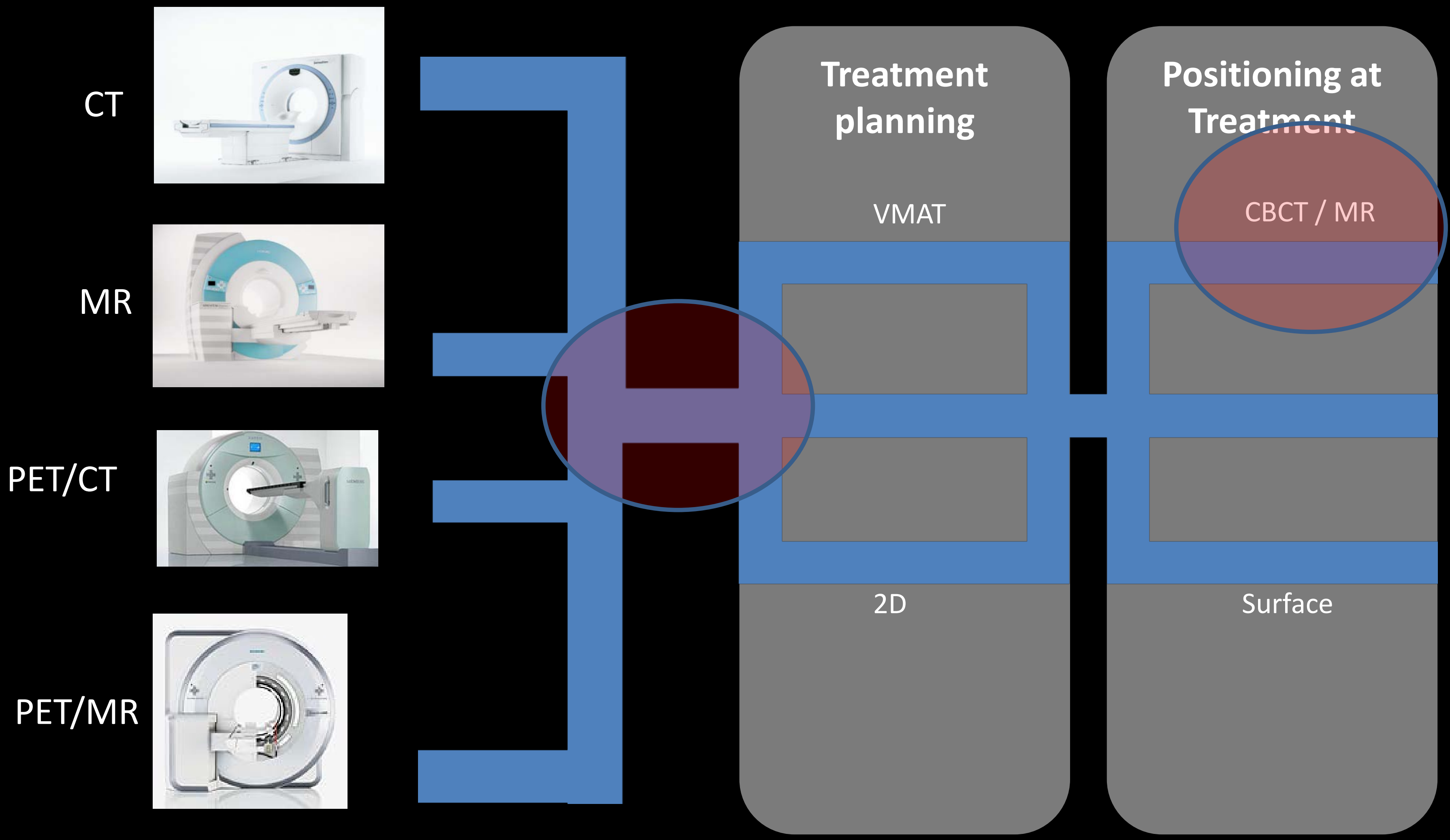
CT
MR
PET/CT
PET/MR
Treatment planning
VMAT
2D
Positioning at Treatment
CBCT / MR
Surface

Why is MR needed in radiotherapy

Imporved soft t

artifacts

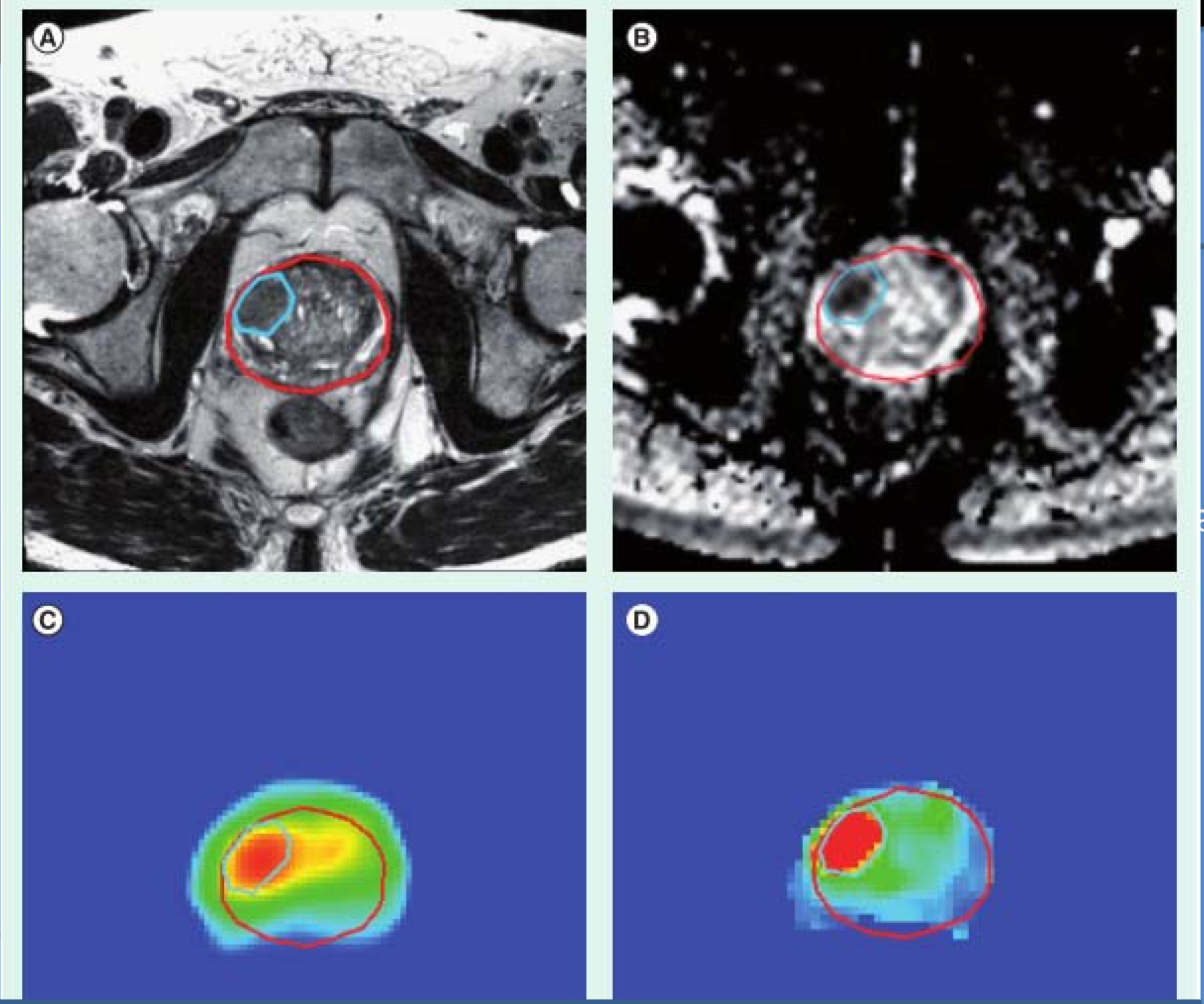

Van der Heide et al.
Future Medicin (2011)

CT/MR workflow

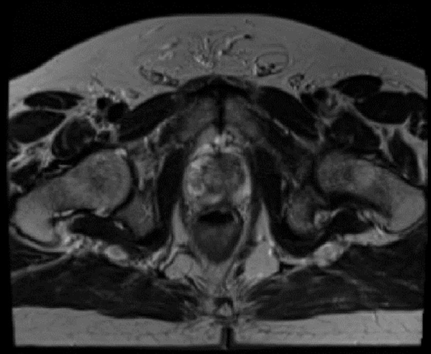

Images

Registration /
Target definition

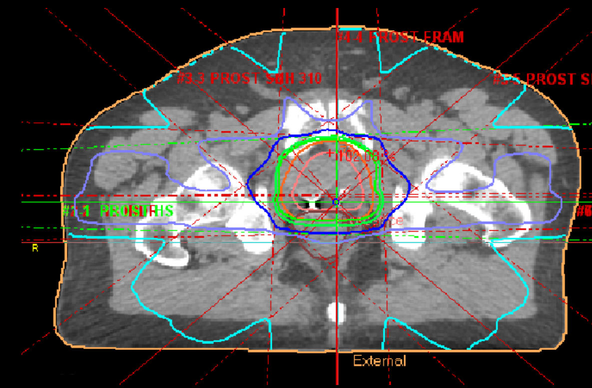

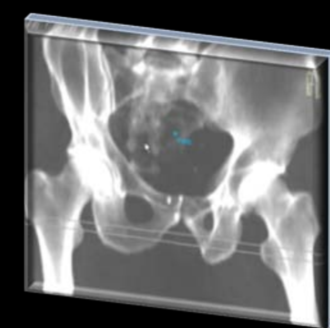

Treatment planning

Problem

Registration

RESULTS OFA MULTI-INSTITUTIONAL BENCHMARK TEST FOR CRANIAL CT/MR IMAGE REGISTRATION
Ulin et al.
Int. J. Radiation Oncology Biol. Phys., Vol. 77, No. 5, pp. 1584–1589, 2010

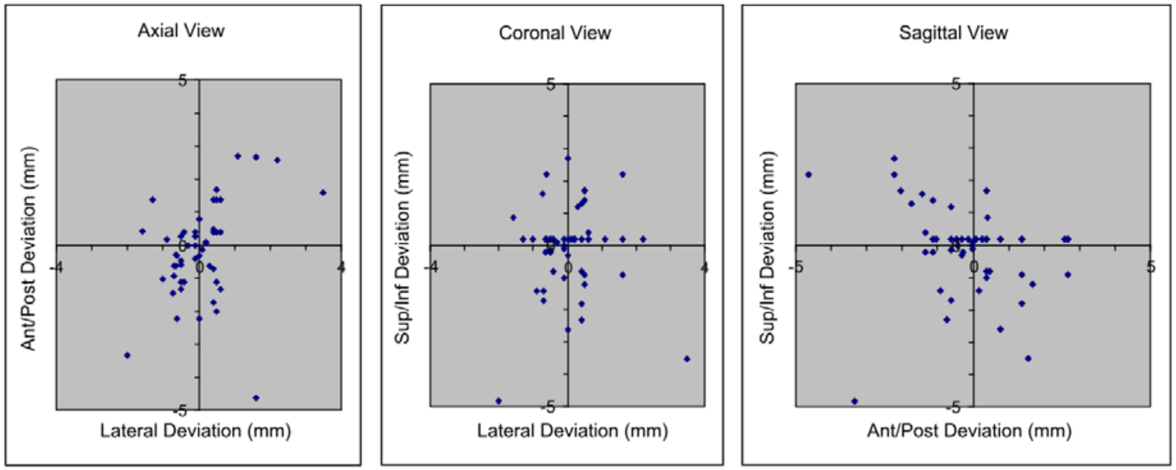

Fig. 6. Distribution of results in the axial, coronal, and sagittal planes relative to the true center of the target. Ant/Post = anterior/posterior.

Method
MR and CT examination of head case was sent to 45 clinics for registration

Result
Standard deviation: 2.2 mm

Switch from CT based to MR based workflow

Imaging

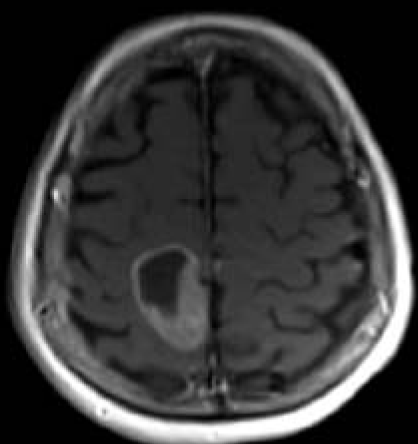

Target definition

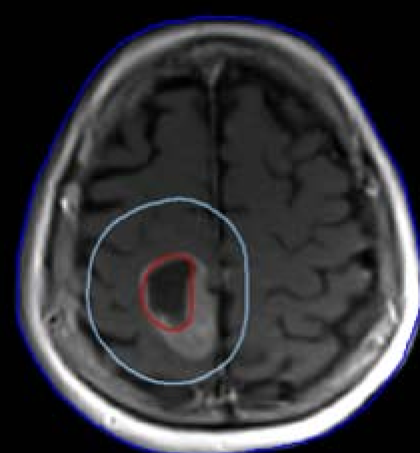

Treatment planning

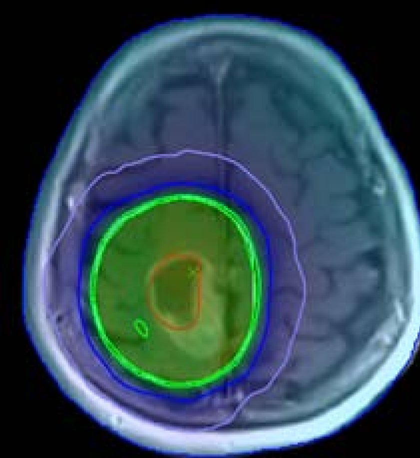

How?

Dose calculation

Positioning reference

MR

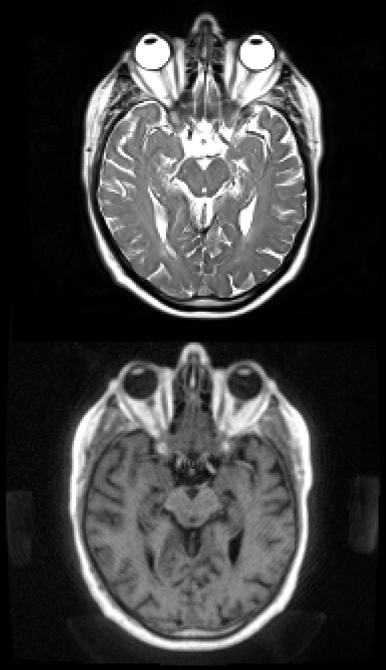

CT equivalent

MR signal

T2w

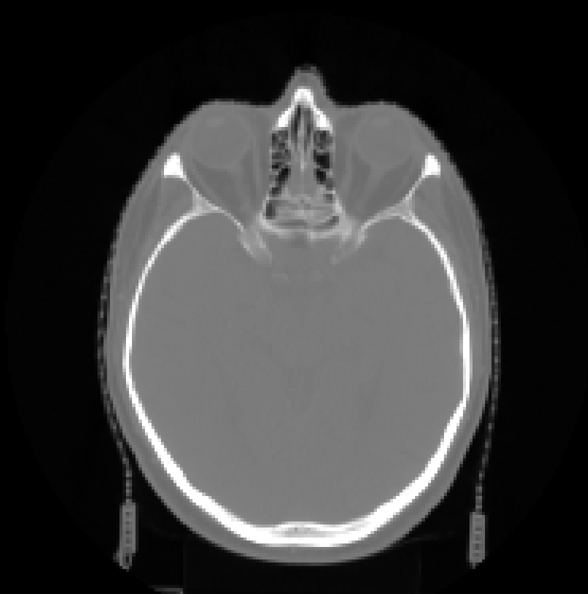

CT

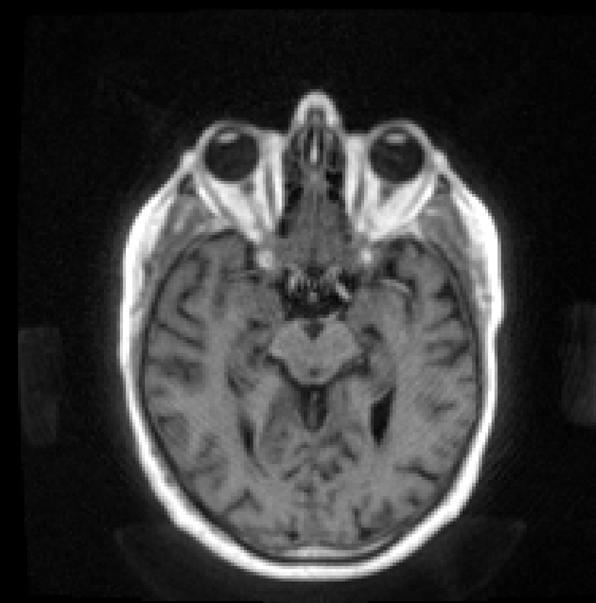

UTE, ZTE
(Ultra short echo time,
Zero echo time)

2 commercial solutions at the moment

- Phillips MRCAT
- Spectronics MRI-Planer

Many other solutions suggested in literature

Spectronics MRI-Planner

Evaluation of accuracy – ongoing study

MRI Only workflow

Clinical workflow

MriPlanner

SPECTRONIC MEDICAL

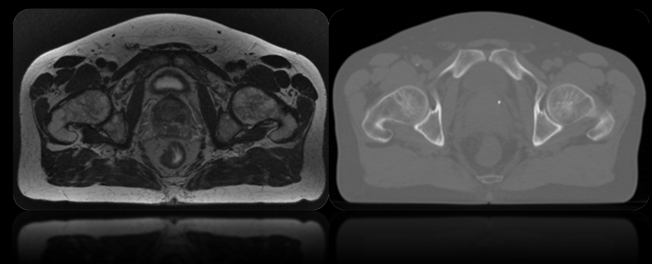

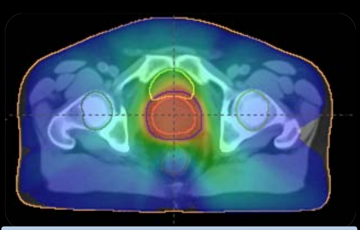

Synthetic CT - sCT

170 patients

- Three university hospitals
- Two vendors
- Two field strengths (1.5T and 3T)
- Different clinical routines

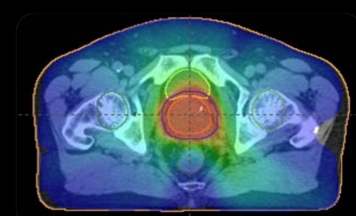

Conventional CT

REGION SKANE

Courtesy: Emilia Persson

Body contour correction

- Correction of differences due to repositioning between MR and CT
  - CT Body contour as reference
  - sCT and CT rigidly registered on bone
  - sCT with a corrected body was created
  - CT treatment plan transferred to the corrected sCT

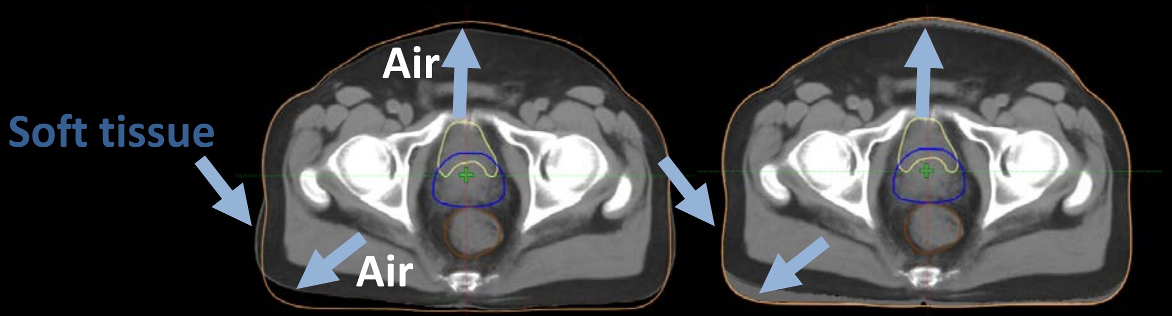

sCT without body correction vs. sCT with body correction

Courtesy: Emilia Persson

Results – Body contour correction

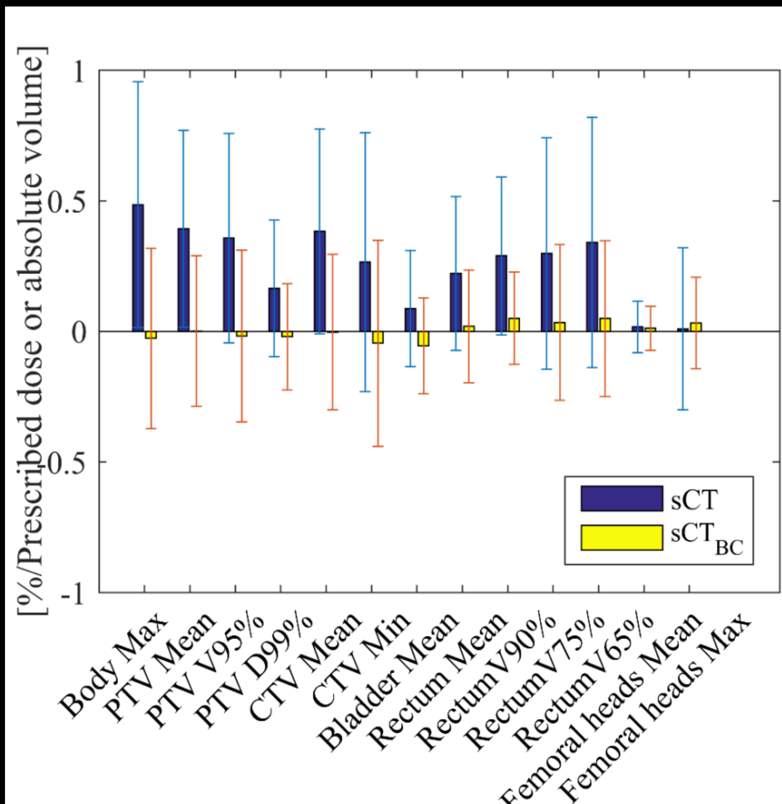

Prescribed 78 Gy

- Mean doses t

0.4±0.4%→ 0.0

- Overall correc

< 0.05%±0.4% (1

Courtesy: Emilia Persson

MRCAT Source Image Acquisition

MR Image Acquisition

Echo 1

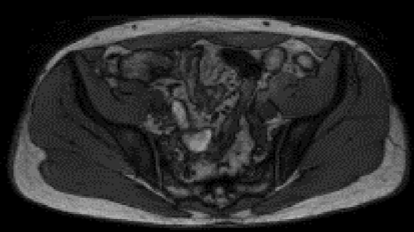

Echo 2

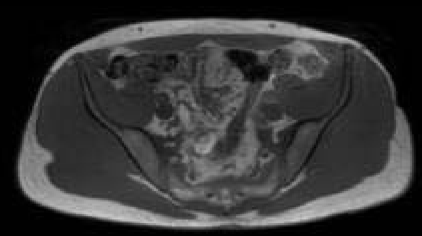

Dixon Reconstruction

In-Phase

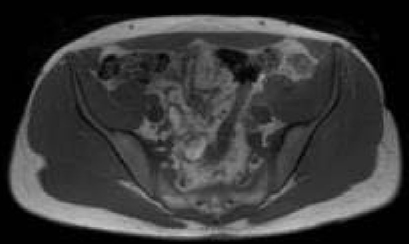

Water

Fat

- 3D FFE 2-echo, full body contour large volume scan is acquired in less than three minutes.

Field-of-View (AP-LR-HF):

M: 350 x 451 x 300 mm^3

L: 368 x 552 x 300 mm^3

- 2-point Dixon reconstruction is used to generate the following 3D image sets:
  1. In-phase
  2. Water-only
  3. Fat-only

Courtesy: Neelam Tyagi

Philips; white paper Kohler et al 2015

MRCAT Algorithm Overview

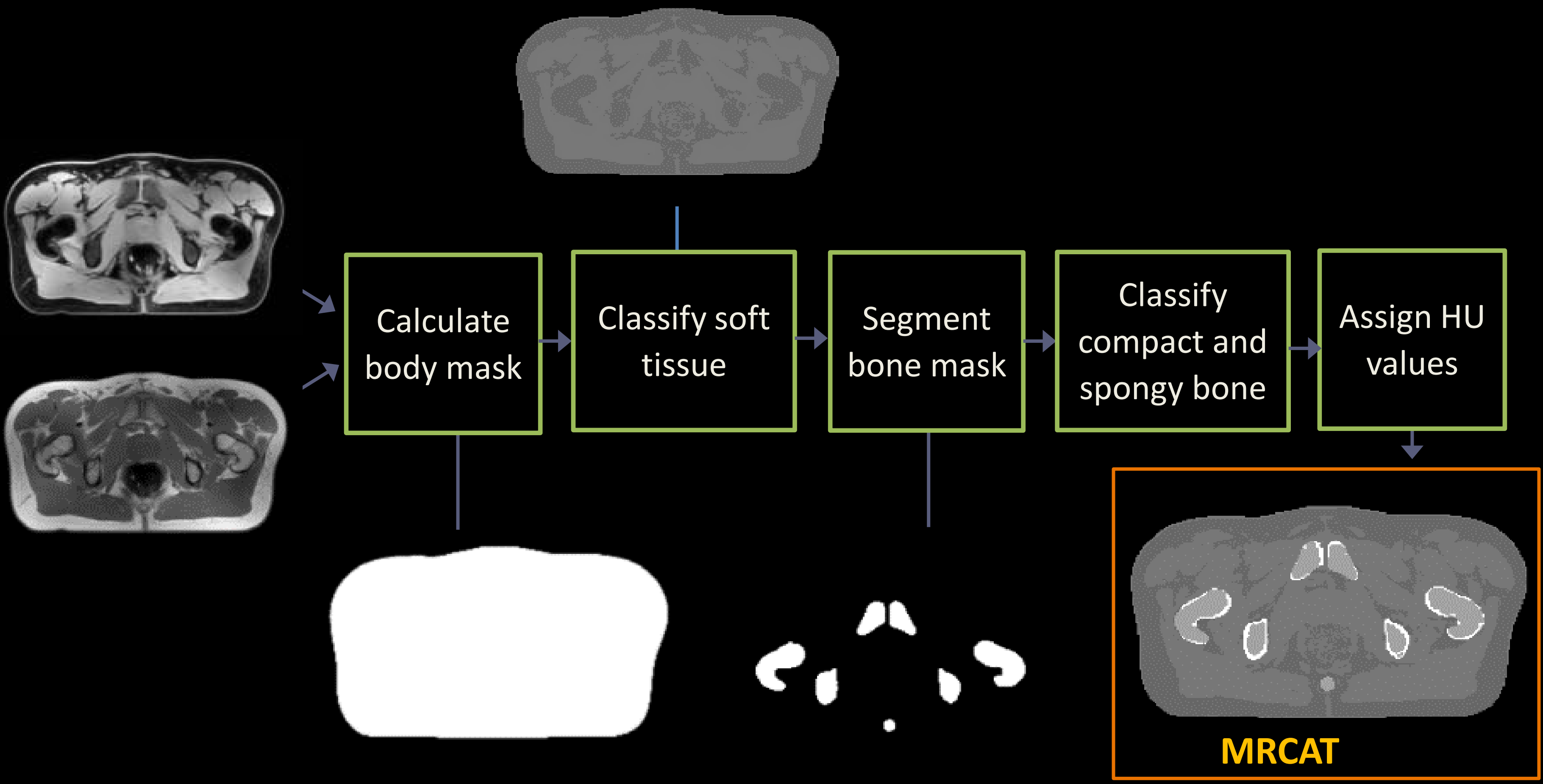

Courtesy: Neelam Tyagi

Philips; white paper Kohler et al 2015

Dosimetric Validation (% dose difference) (MRCAT – defCT)

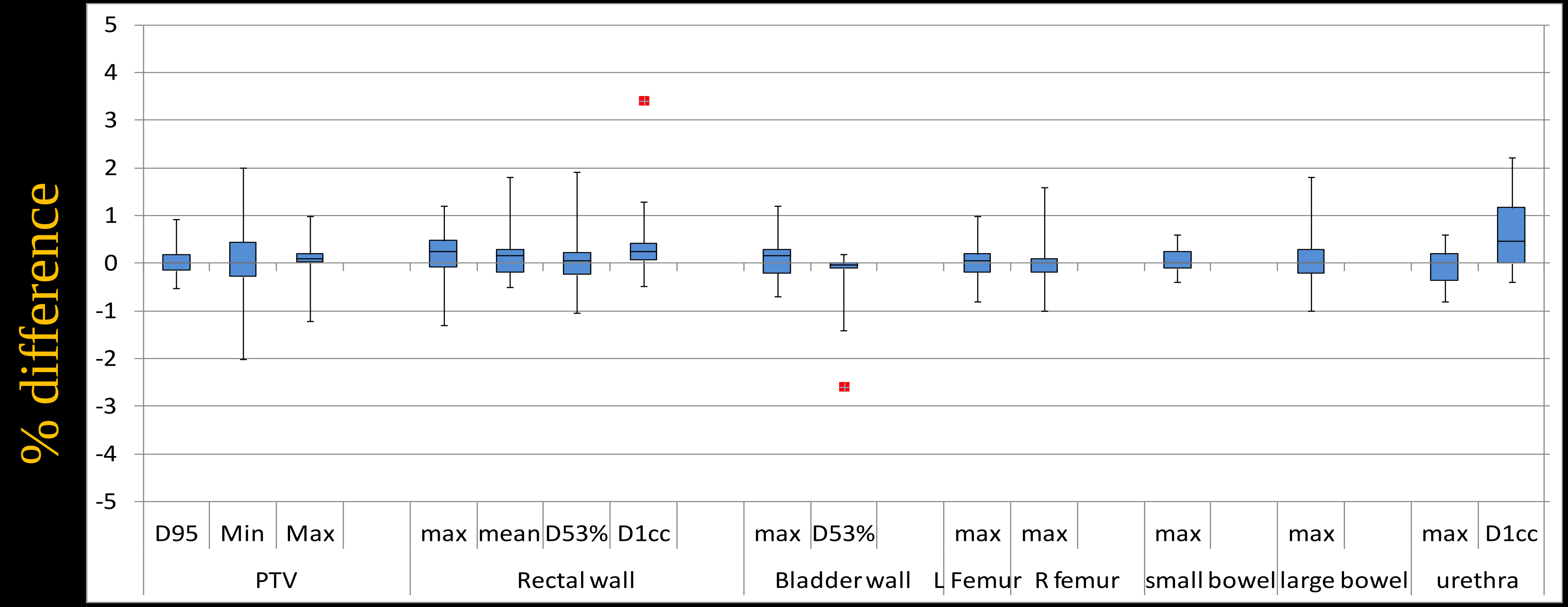

Analysis based on 20 patients

Courtesy: Neelam Tyagi

Other proposed methods

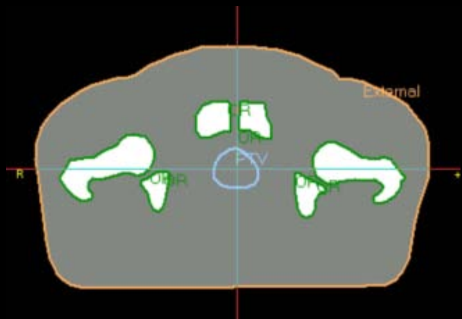

Manual delineation

UTE or ZTE

Registration based methods, Voxel by voxel conversion, Patches etc etc … and combinations

An Atlas-Based Electron Density Mapping Method for Magnetic Resonance Imaging (MRI)-Alone Treatment Planning and Adaptive MRI-Based Prostate Radiation Therapy

Jason /
Olivier
Chris V

IOP PUBLISHING PHYSICS IN MEDICINE AND BIOLOGY
Phys. Med. Biol. 58 (2013) 8419–8435 doi:10.1088/0031-9155/58/23/8419

CT substitute derived from MRI sequences with ultrashort echo time

Adam Johansson,[a)] Mikael Karlsson, and Tufve Nyholm
Department of Radiation Sciences, Umeå University, Umeå, Sweden

…enerating synthetic CT
…head and neck for
radiation therapy

MR-based atte…
using deforma…

Eduard

Dosimetric evaluation o…
planning for prostate ca…

MRI-based treatment plan simulation and adaptation for ion radiotherapy using a classification-based approach

Christopher M Rank[1*], Christoph Tremmel[1], Nora Hünemohr[1], Armin M Nagel[2], Oliver Jäkel[1,3] and Steffen Greilich[1]

MRI-Based Attenuation Correctio…
Systems: A 4-Class Tissue Segmen…
a Combined Ultrashort-Echo-Time…

Yannick Berke…
Felix M. Motta…
and Volkmar S…

brain tumours

Treatment planning of intracranial targets on MRI derived substitute CT data

Joakim H. Jonsson[a,*], Adam Johansson[a], Karin Söderström[b], Thomas Asklund[b], Tufve Nyholm[a]
[a] Radiation Physics; [b] Oncology, Department of Radiation Sciences, Umeå University, Sweden

Matthias Hofm…
Michael Brady…

PHYSICS CONTRIBUTION

MRI-BASED TREATMENT PLANNING FOR …
VERIFICATION FOR PR…

LILI CHEN, PH.D., ROBERT A. PRICE, JR., PH.D., L…
LIHONG QIN, PH.D., SHAWN MCNEELEY, M.S., C-M CHA…
AND ALAN POLLACK, PH.D., M.D.

ORIGINAL ARTICLE

Automatic, three-segment, MR-based attenuation correction for whole-body PET/MR data

V. Schulz · I. Torres-Espallardo · S. Renisch · Z. Hu · N. Ojha · P. Börnert · M. Perkuhn · T. Niendorf · W. M. Schäfer · H. Brockmann · T. Krohn · A. Buhl · R. W. Günther · F. M. Mottaghy · G. A. Krombach

Summary (MR-only)

- Main benefits
  - No registration
  - No need for the CT examination
- Commercial solutions are now on the market
  - Only male pelvis (prostate)
- There are promising solutions described also for intra-cranial tumors

- Technical aspects
  - The dose calculation is insensitive and probably the least problem
  - Use for positioning is difficult to verify
  - Potential error sources and QA measures needs to be identified

Imaging in the treatment room

Purpose

Hit the target, i.e. localize the target within the body eigher before the irradiation or continously during the treatment.

Means

- 2D MV or kV systems, optical systems, 3D MV or kV systems, MR
- Information (images) from the planning is typically used as referece
- Markers or patient anatomy can be used to calculate an offset

Cone beam CT

For 4-slice CT scanners an ideal fan beam geometry can be assumed during the reconstruction. For cone angles above around 2-4 degrees reconstruction adapted to the cone beam should be used (Feldkamp algorithm, 1984).

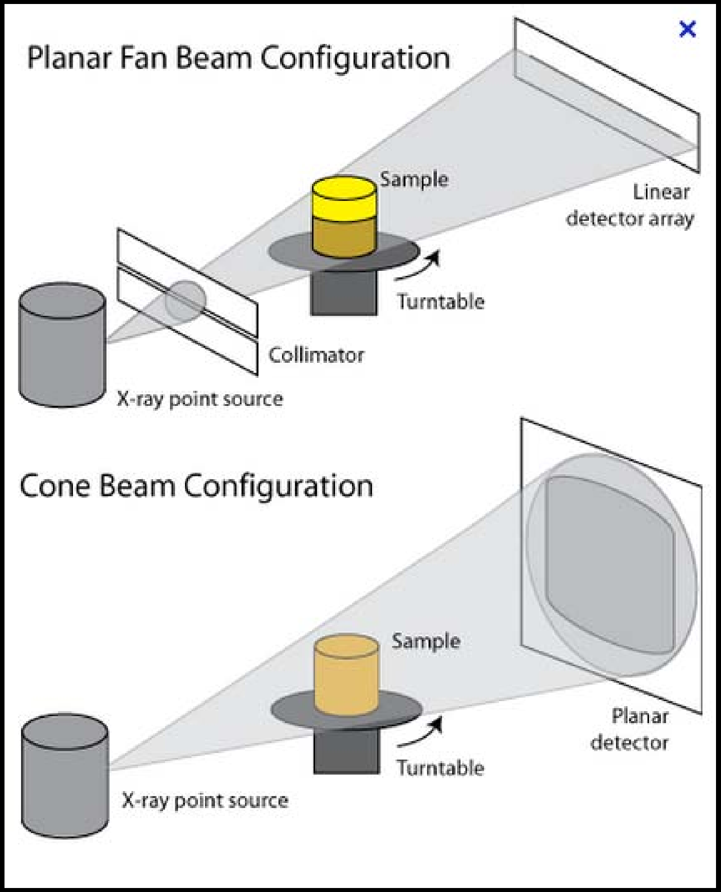

Richard Ketcham, University of Texas at Austin

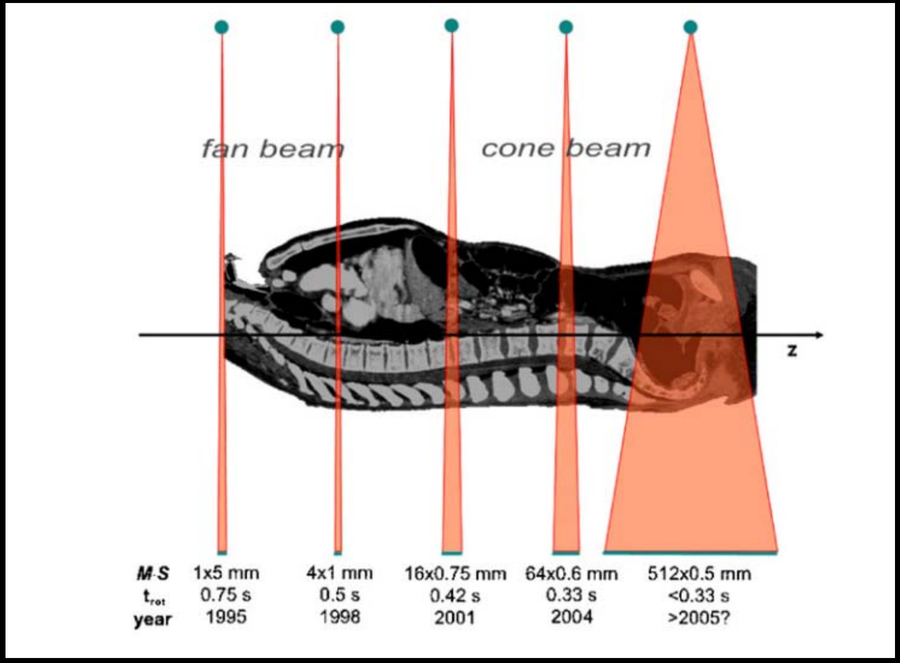

Flat-detector computed tomography (FD-CT)
Kalender et al. Eur Radiol (2007)

Cone beam CT

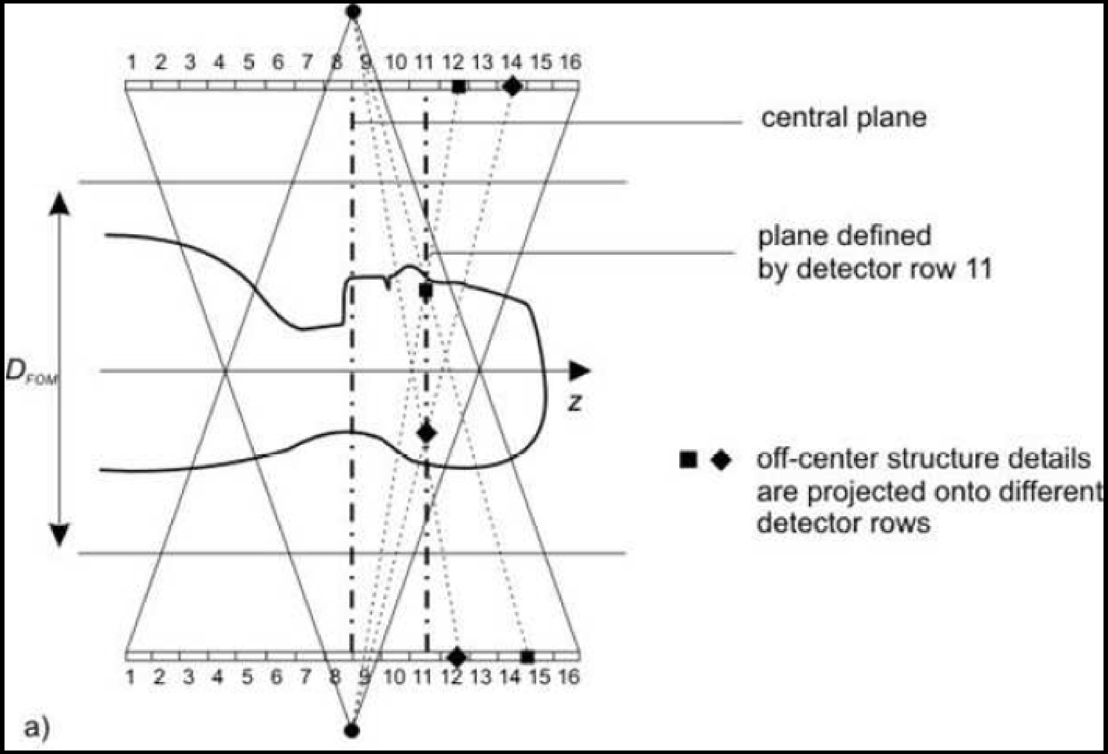

The cone-beam problem in CT: a single off-center detector row does not yield data representing details of solely one object slice. The larger the cone beam angle, the greater are potential inconsistencies in the data.

W.A. Kalender, Computed Tomography, 2005

Comparison CBCT and CT

FPD CT scanners are inferior to CT scanners with regard to:

- Output of the x-ray tube, output is higher for CT scanners (noise)
- Axial coverage (field of view), coverage is better for CT scanners
- Rotation speed, CT scanners rotate faster
- Quality of the detector, CT scanner detectors have better performance

FPD CT scanners are superior to CT scanners with regard to:

- Spatial resolution (voxel size, not so much in radiotherapy)
- Z-axis coverage

Scatter artifacts in CBCT

- Reduction of image contrast
- Increased image noise
- Non-uniformity artifacts (Cupping)

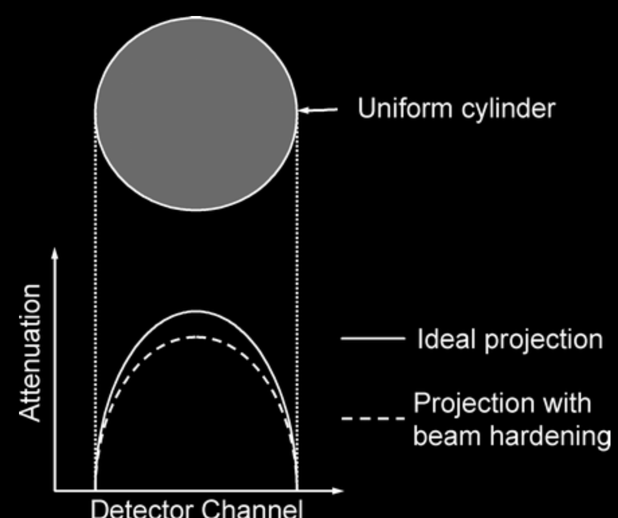

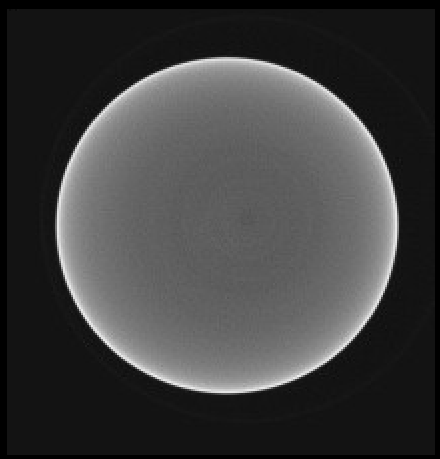

Corrected

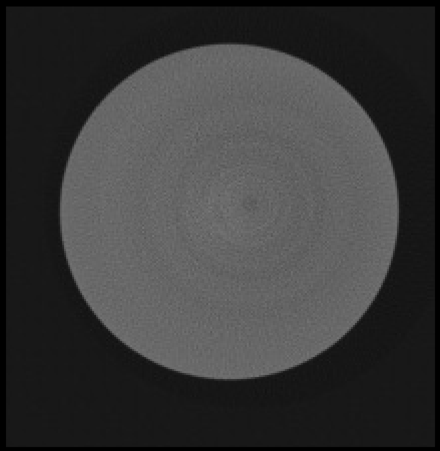

Barrett J F , Keat N Radiographics 2004;24:1679-1691

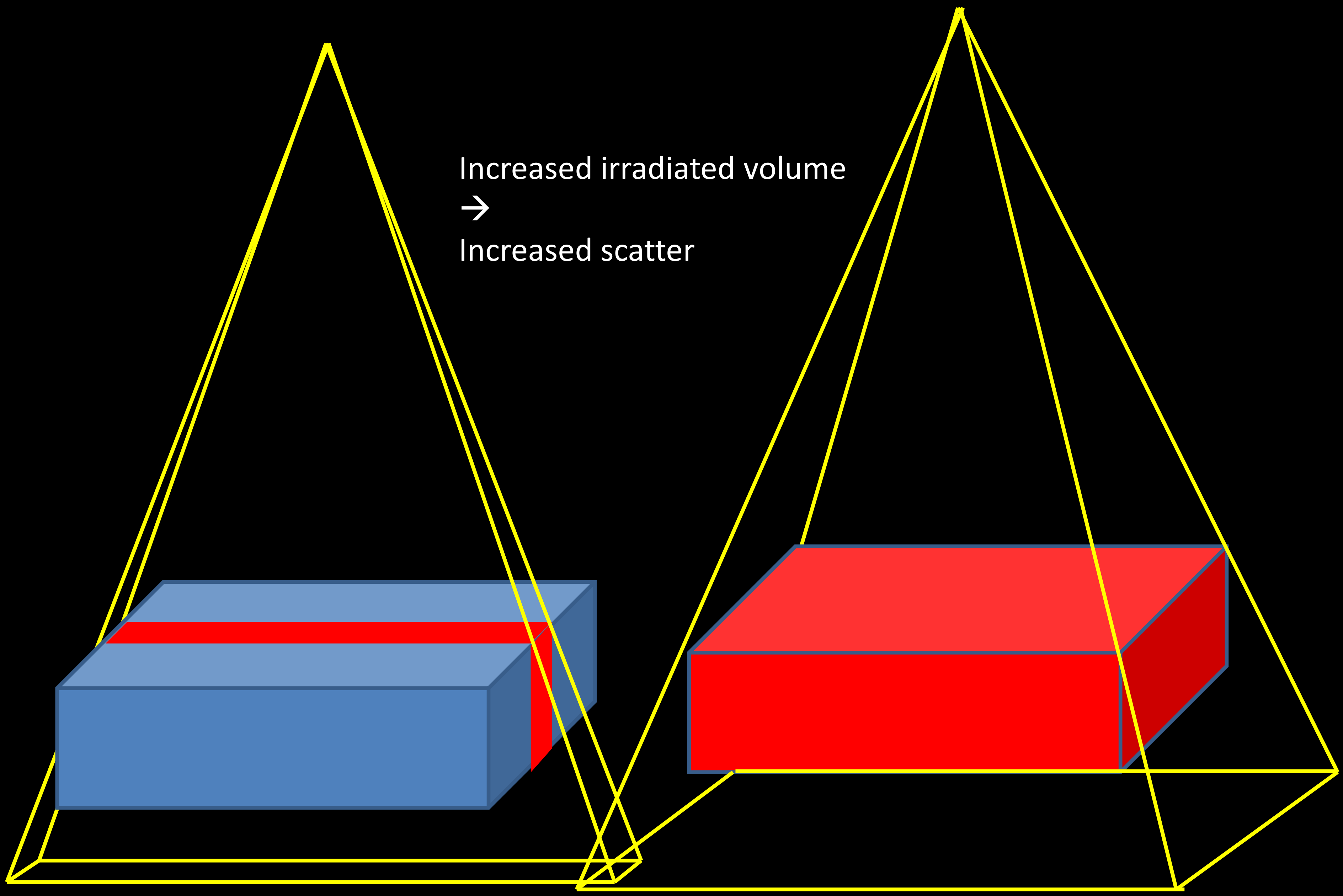
Increased irradiated volume
→
Increased scatter

Dealing with scatter

- Avoidance
  - Limit the field of view
  - Grids
  - Distance between patient and detector
- Correction

Not corrected for scatter
Corrected for beam hardning

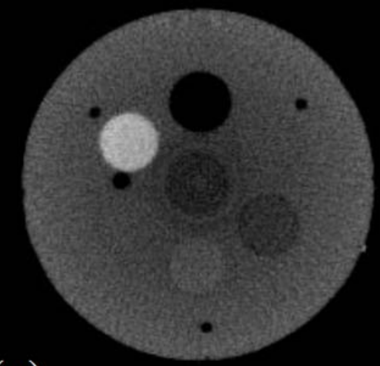

(a)

Corrected for scatter
and beam hardning

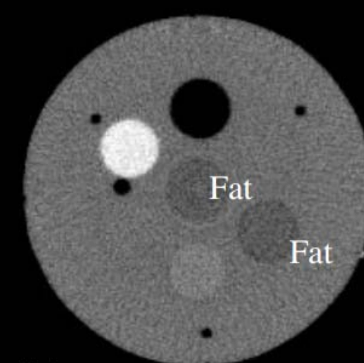

(b)

Correction of scatter in megavoltage cone-beam CT
Spies et al. Phys. Med. Biol 2001

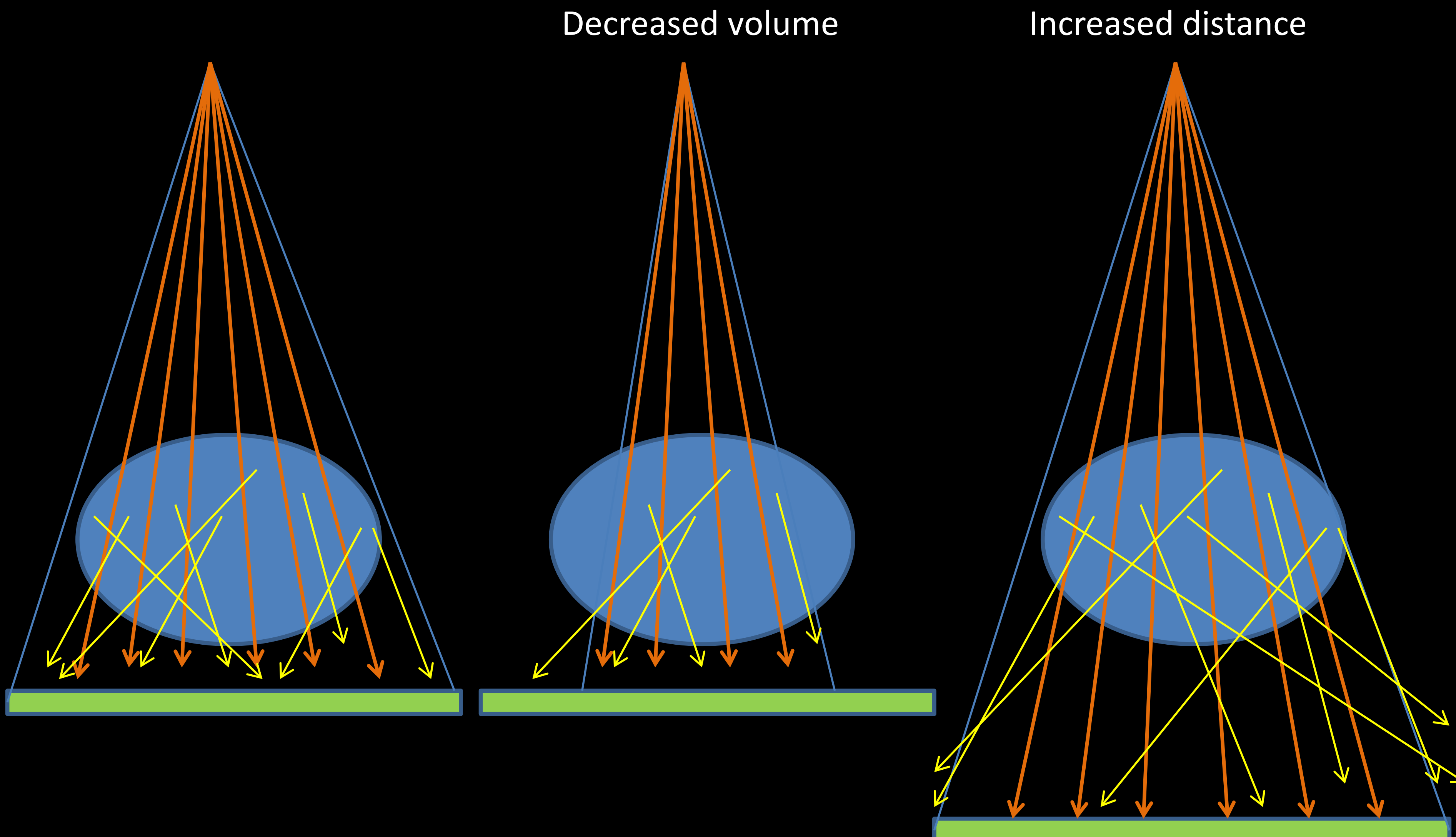
Decreased volume
Increased distance

Correction

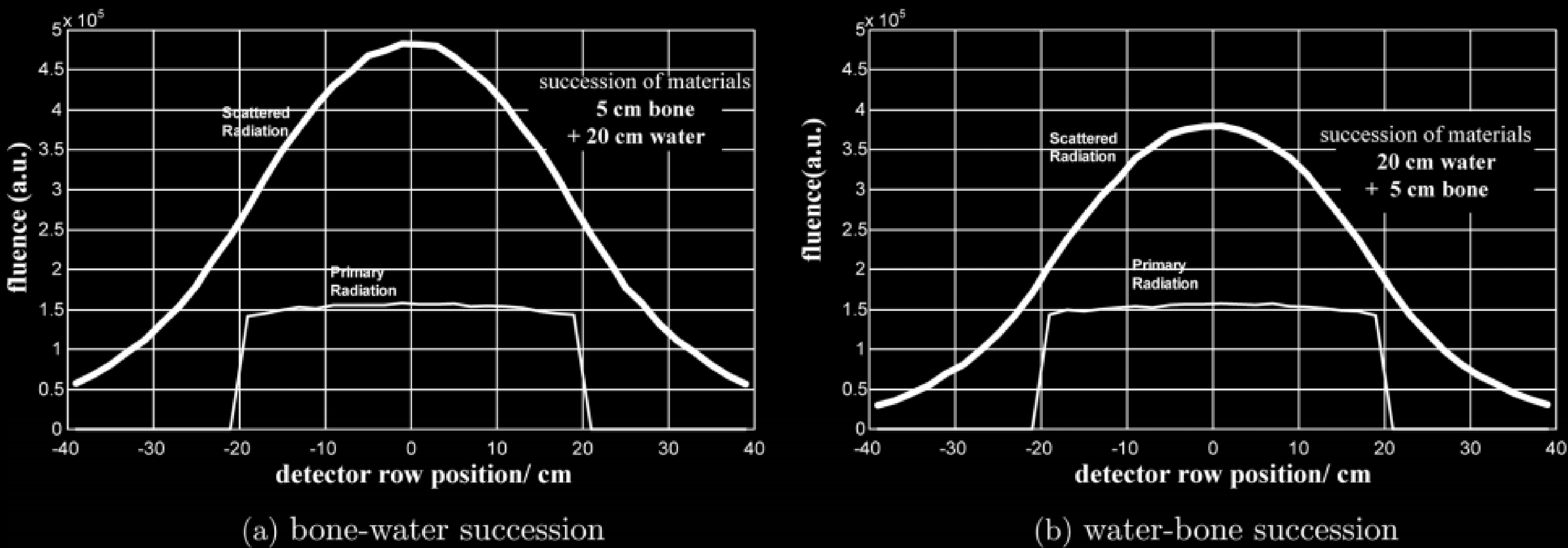

FIG. 4. Scatter dependency on material succession along the ray. Monte Carlo simulation. Phantom: two slabs, 5 cm bone and 20 cm water. Acquisition: X-ray spectrum at 70 kV, field-size 40×30 cm^2, no antiscatter grid. Plots show scatter and primary fluence in central line at the detector. (a) *SPR* in center is 25% higher than in (b).

Ruhrnschopf et al. , Med Phys 2011

Dealing with scatter

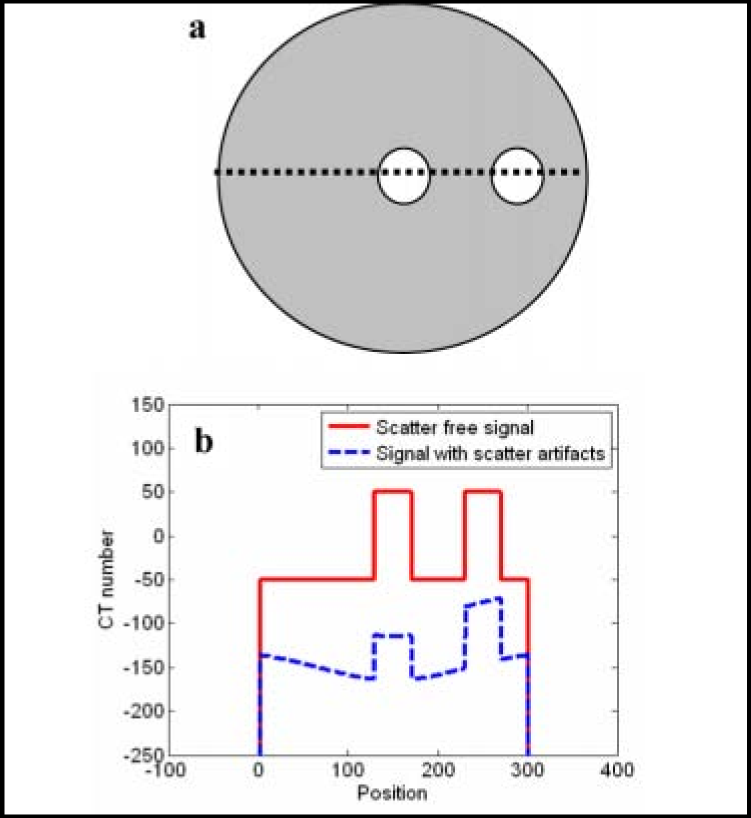

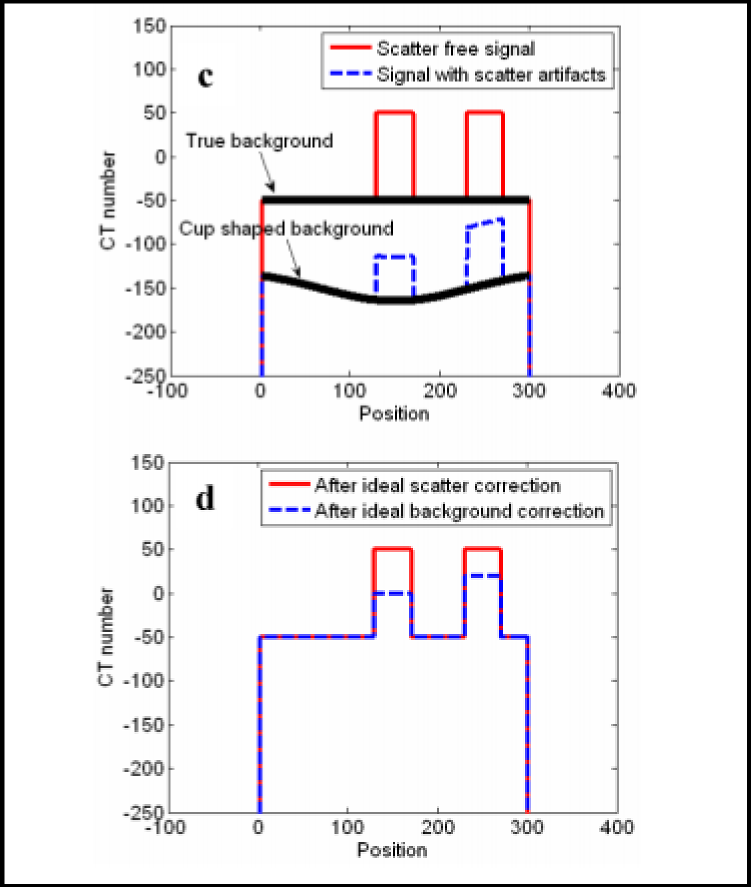

Altunbas et al. Med Phys 2007

Scatter reduction with grid

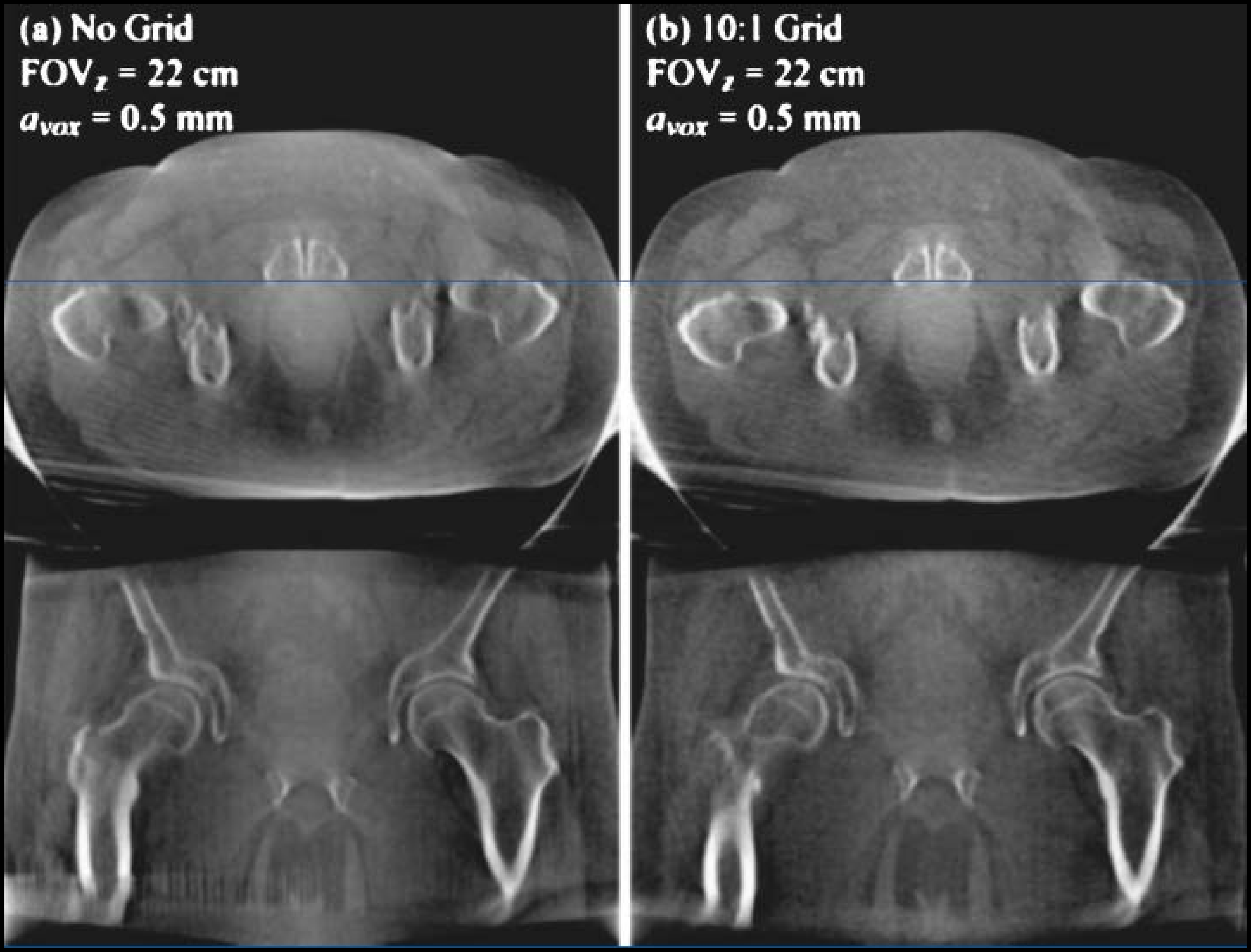

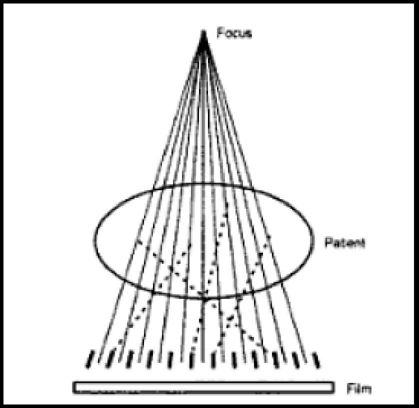

Encyclopaedia of Medical Imaging; Petterson ed.

Siewerdsen et al. 2004. Med. Phys. 31:3506-3520

Other artifacts

- Ghosting – Detector after-glow from previous exposure
- Aliasing – Undersamplig of voxels far from the source due to the cone shape of the beam
  - Cause the commonly seen lines from the center to the peripheral part of the image
- Patient motion
- Non-ideal gantry rotation
  - Variation in gantry rotation speed
  - Sag of detector and/or X-ray source

Schulze et al. 2011

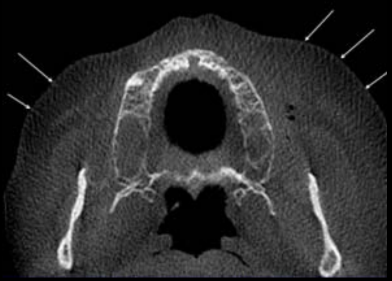

Not corrected

Corrected

Rit et al. 2008

QA of CBCT

- Alignment of kV and MV lines
  - verify isocenter 3D agreement
  - verify registration and alignment process
- Image quality
  - monitor image quality parameters
  - watch for degradation
- Patient dose
  - measure base value (surrogates: air dose, HVL)
  - monitor changes

Recommended reading:
Commissioning experience with cone beam computed tomography for image-guided radiation therapy
Lehmann et al. Journal of applied clinical physics 2007

Clinical use of electronic portal imaging: Report of AAPM Radiation Therapy Committee Task Group 58

AAPM Medical Physics Practice Guideline 2.a: Commissioning and quality assurance of X-ray–based image-guided radiotherapy systems

Penta Guide

Catphan

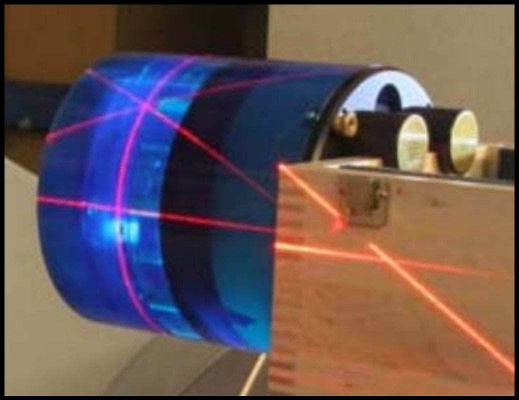

Clinical application

Benefits of CBCT compared to 2D x-Ray imaging

- Match in 3D
- See anatomical changes
- Visual verification of target coverage

Drawbacks

- Not as easy to include the imaging dose in the treatment plan
  - Could be more than 1 Gy for a 30 fraction treatment
- Time
  - Both acquisition and reconstruction takes time

But MRI has potential to provide better soft tissue contrast, real time imaging without any dose, so why not go for that?

Accelerator in magnetic field

- Easiest solution is to not use an accelerator

http://www.viewray.com

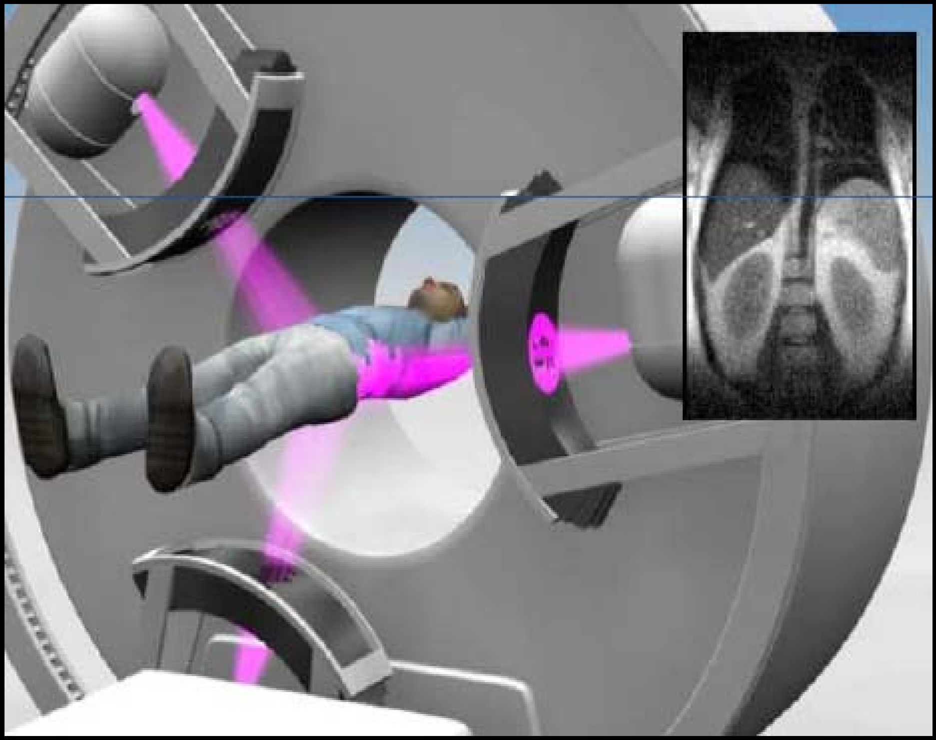

Viewray
0.3T superconducting
3 cobolt sources
Clinical in 2011

Accelerator in magnetic field

- Other solution is to use a fix geometry

Edmonton, Stanford/Sydney Passive shielding with rigid configuration

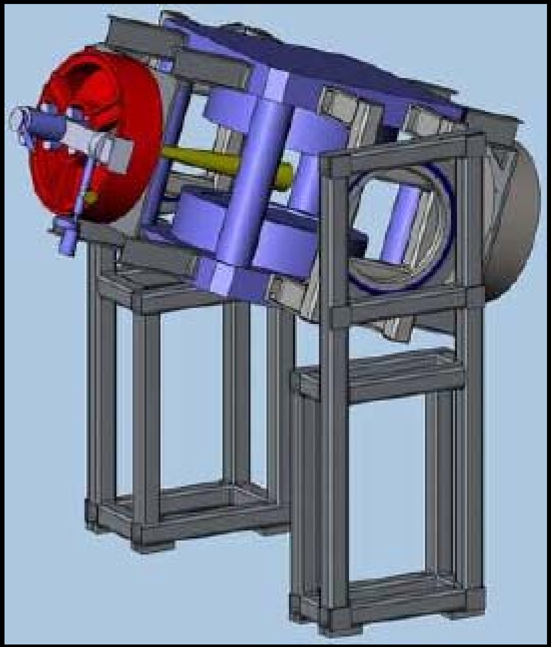

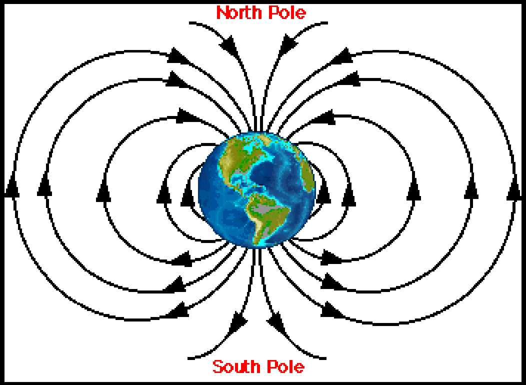

Wachowicz et al. Med Phys 2012

Accelerator in magnetic field

- Last posibility is to place the accelerator where there is ”no” field

UTRECHT
6 MV Linac
1.5 T MRI

Linac mounted in ring around MRI

Modify active shielding to create a ‘safe spot’ for the electron gun

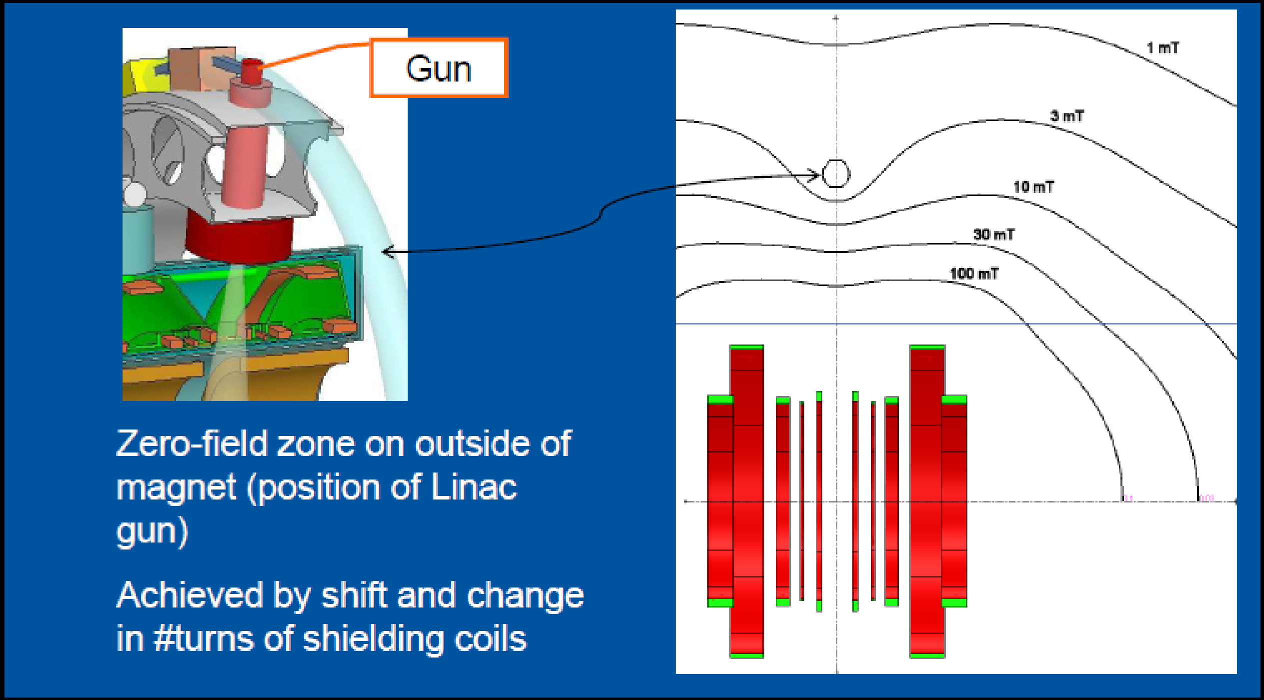

Principal of active shielding

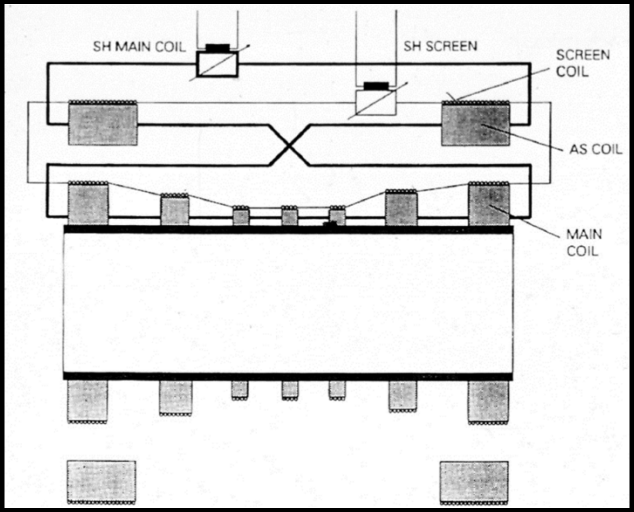

Courtasy Jerry Allison

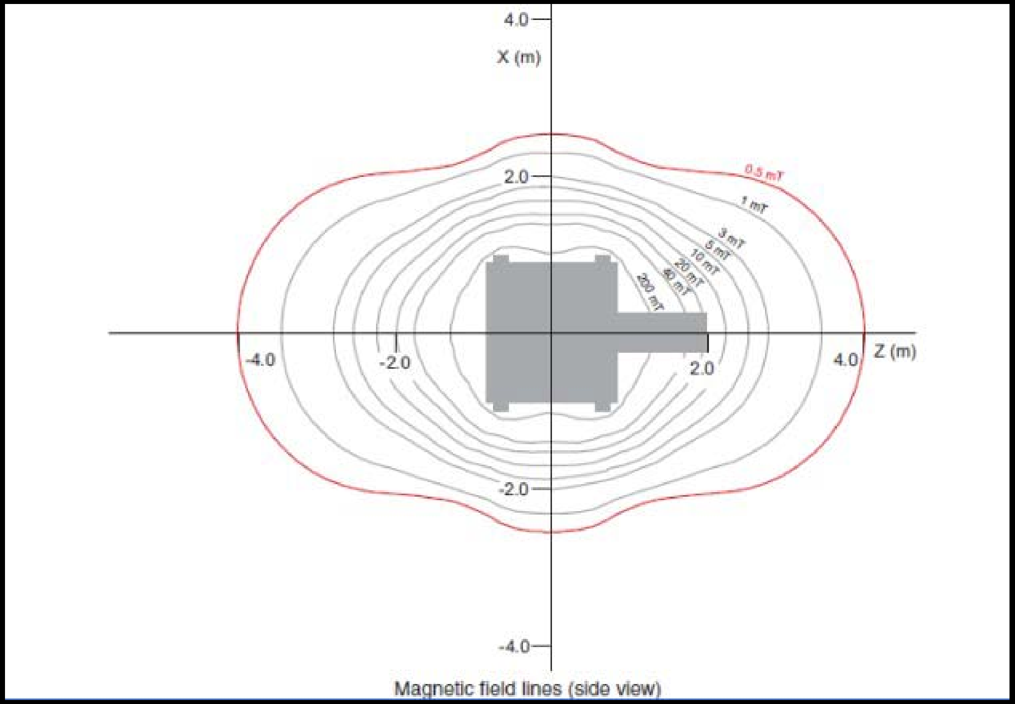

http://mriforyou.blogspot.se/2009/08/introduction-to-mr-safety-part-i.html

- Worlds first activly shieled magnet 1986
- First 1.5 T activly shielded magnet 1989
- First 3 T activly shielded magnet 1997

Principal of active shielding

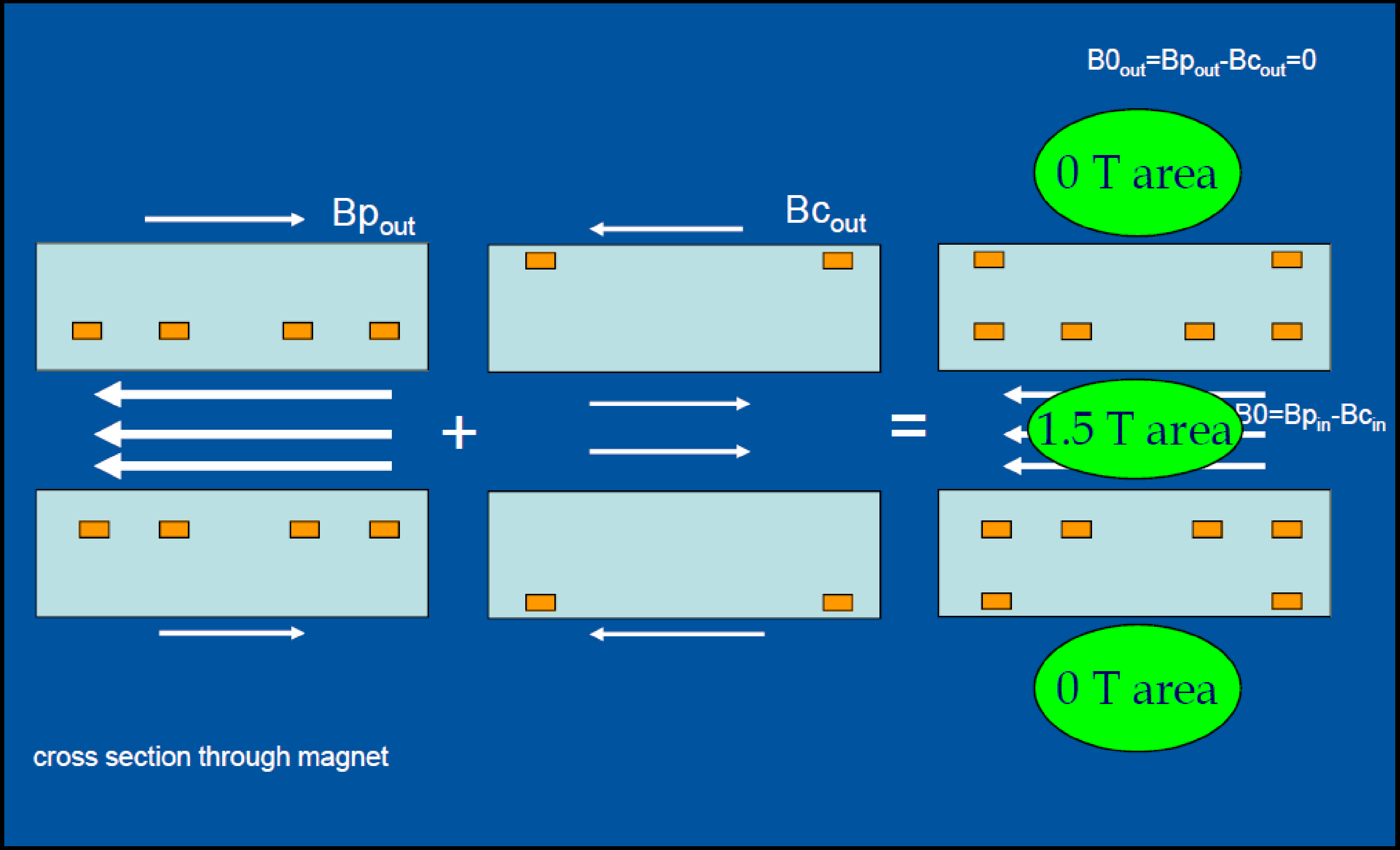

RF from linac disturbing the MR

- Do not image and irradiate at the same time
- Shield the RF
- Place the linac outside the RF cage

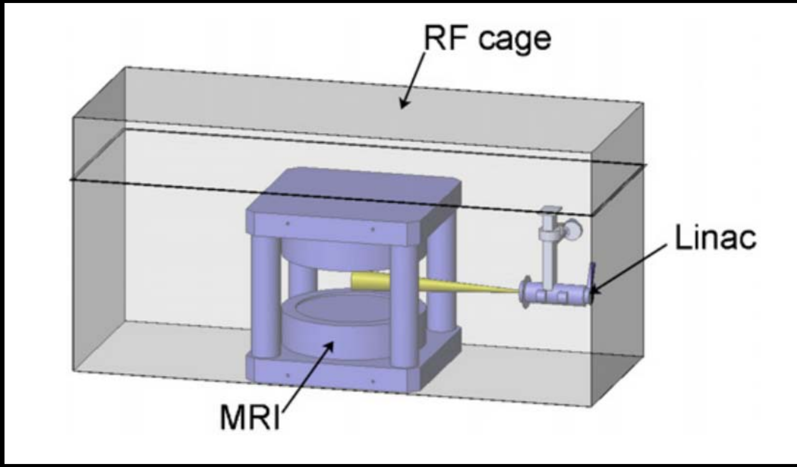

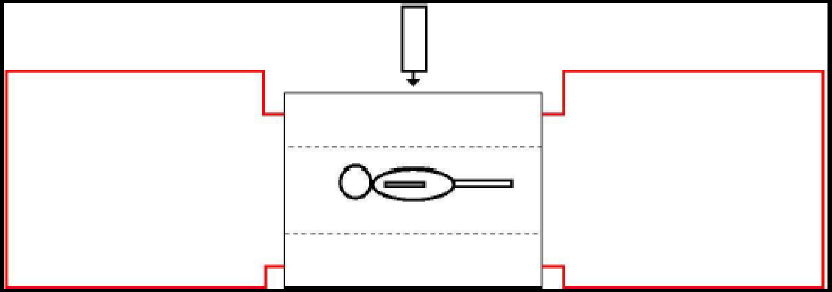

Edmonton

Utrecht

Lamey et al. Phys. Med. Biol. 2010

Courtasy: Jan Lagendijk

Dosimetry with magnetic field

- The Lorenz force affect charged particles in a magnetic field

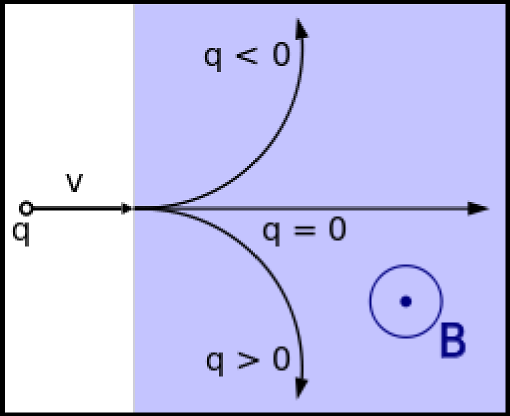

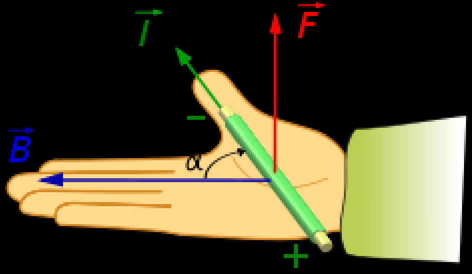

Right hand role

Dosimetry with magnetic field

- Radiation perpendicular to the magnetic field

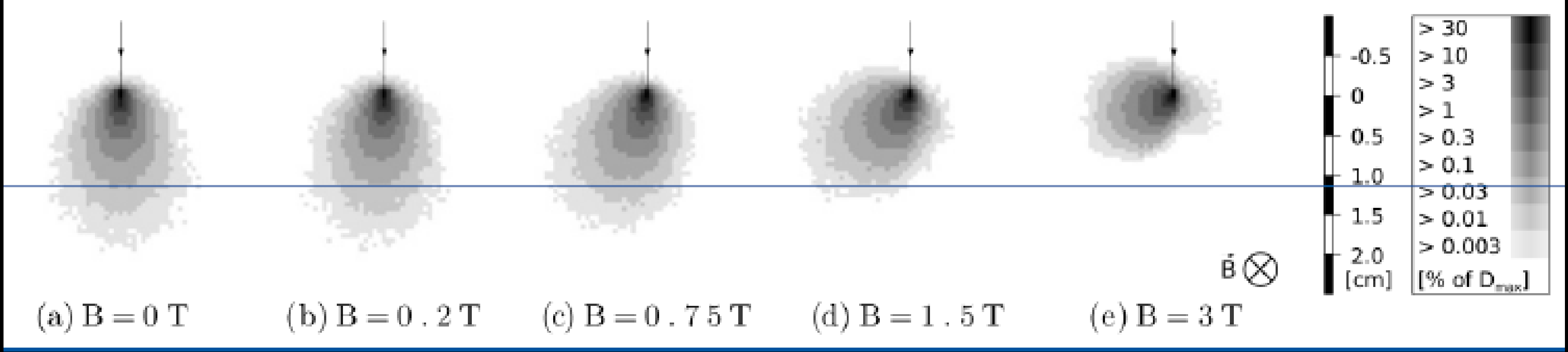

From Raaijmakers et al., 2008

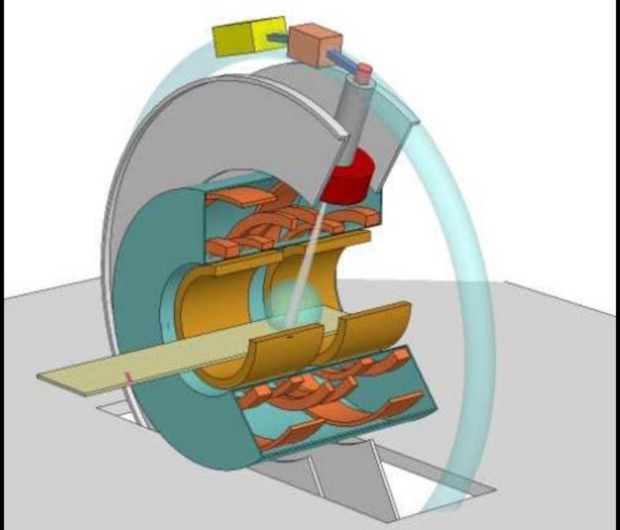

Utrecht

Can be dealt with:
See series of publications from Raaijmakers et al.

Dosimetry with magnetic field

- Radiation parallel to the magnetric field

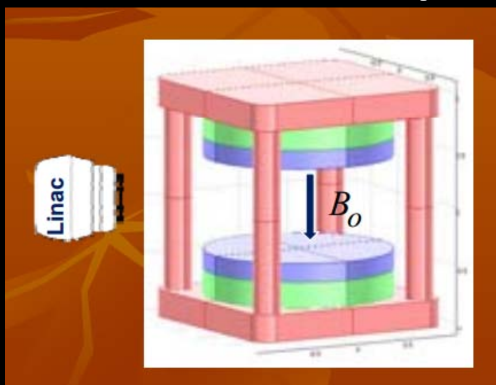

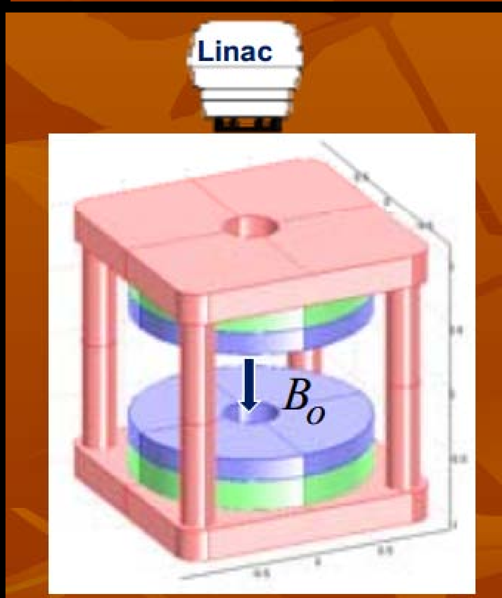

Electrons thats gets an perpendicular component will move in a spiral trajectrory

20MeV

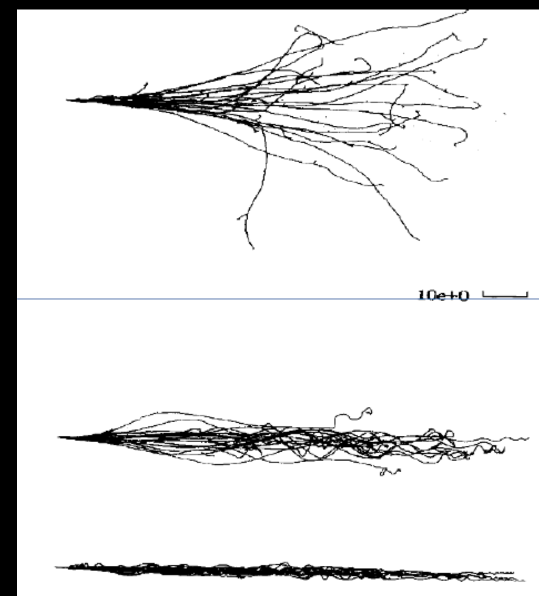

From Bielajew, Med Phys 20(4) 1993

Real-Time MR-Guided Radiotherapy: Integration of a Low-Field MR System
B Fallone et al. **51st AAPM Annual Meeting**

Potential with MR guided radiotherapy

- Soft tissue contrast for position verification
  - Inter-fraction
  - Dose escalation
  - Improve current RT

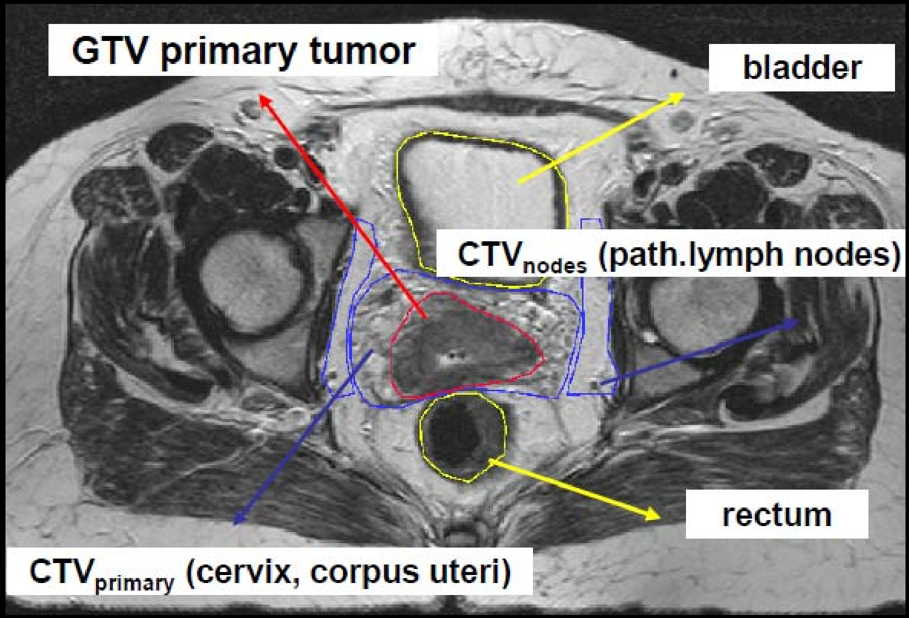

Courtesy U. v. d. Heide

Potential with MR guided radiotherapy

New RT indications – Real time tracking

- Body stereotaxy
- GTV ablation

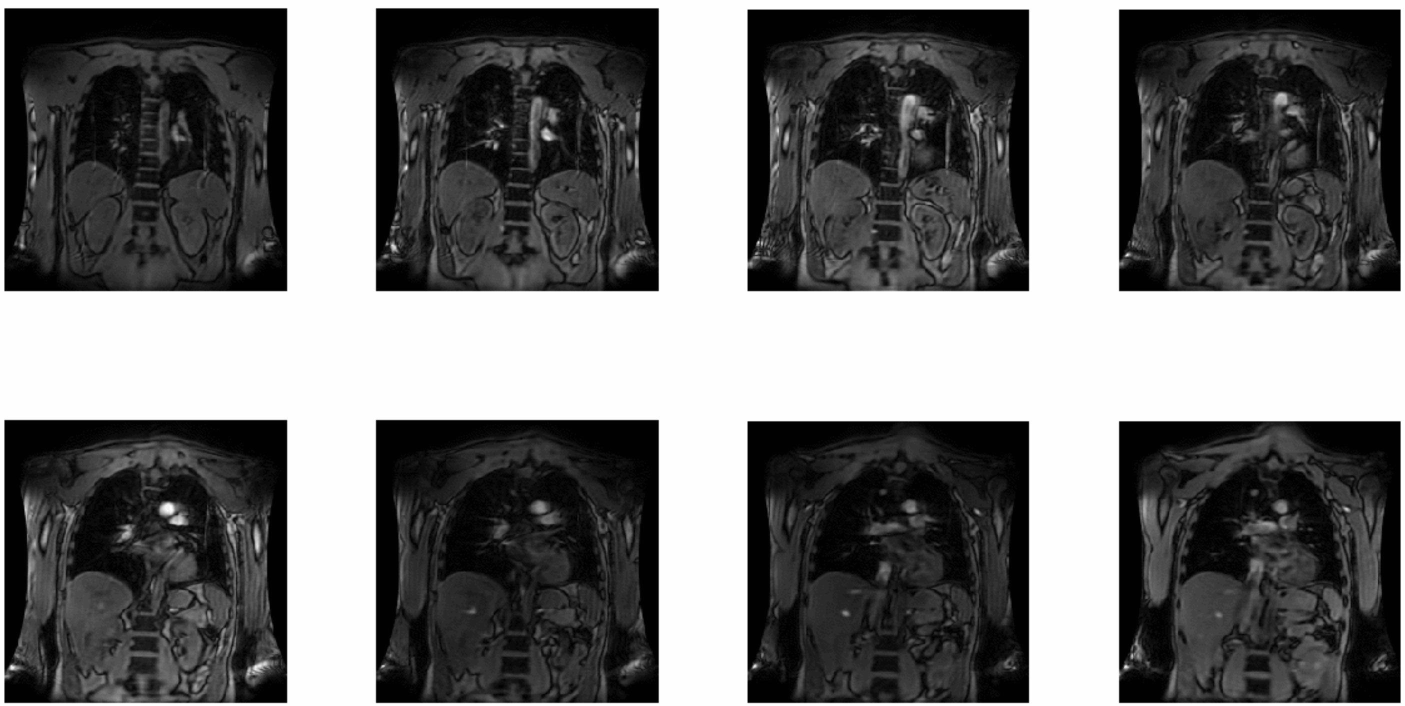

Courtesy **Bjorn Stemkens**

When to do what

Target definition	Treatment planning	Positioning	
CT/PET-CT	CT	CBCT/2D x-ray	Lung, Breast, Bone metastasis, Head/Neck?
MR/PET-MR	MR	CBCT/2D x-ray	Pelvis, Brain, Head/Neck?
MR	CT	CBCT/2D x-ray	What we often do today
MR/PET-MR	MR	MR	Adomen, Pelvis

Plan the treatment on the primary information source for the target defintion

Thank you!

Acknowledgments

Uulke Van der Heide

Bjorn Stemkens

Emilia Persson

Neelam Tyagi